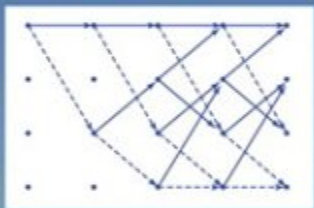


# COMMUNICATION SYSTEMS ENGINEERING

SECOND EDITION



John G. Proakis  
Masoud Salehi

# COMMUNICATION SYSTEMS ENGINEERING

**John G. Proakis**

**Masoud Salehi**

**2nd Ed.**



Upper Saddle River, New Jersey 07458

To Felia, George, and Elena.

—John G. Proakis

To Fariba, Omid, Sina, and my parents.

—Masoud Salehi

**Library of Congress Cataloging-in-Publication Data**

CIP data available on file.

Vice President and Editorial Director, ECS: *Marcia J. Horton*

Publisher: *Tom Robbins*

Editorial Assistant: *Jody McDonnell*

Vice President and Director of Production and Manufacturing, ESM: *David W. Riccardi*

Executive Managing Editor: *Vince O'Brien*

Managing Editor: *David A. George*

Production Editor: *Chanda Wakefield*

Director of Creative Services: *Paul Belfanti*

Creative Director: *Carole Anson*

Art Director: *Jayne Conte*

Art Editor: *Greg Dulles*

Manufacturing Manager: *Trudy Piscioti*

Manufacturing Buyer: *Lynda Castillo*

Marketing Manager: *Holly Stark*

Marketing Assistant: *Karen Moon*



© 2002 by Prentice-Hall, Inc.  
Upper Saddle River, New Jersey

All rights reserved. No part of this book may be reproduced, in any form or by any means without permission in writing from the publisher.

*Printed in the United States of America*

10 9 8 7 6 5 4 3 2 1

ISBN 0-13-061793-8

Pearson Education Ltd., *London*

Pearson Education Australia Pty. Ltd., *Sydney*

Pearson Education Singapore, Pte. Ltd.

Pearson Education North Asia Ltd., *Hong Kong*

Pearson Education Canada, Inc., *Toronto*

Pearson Educación de México, S.A. de C.V.

Pearson Education—Japan, *Tokyo*

Pearson Education Malaysia, Pte. Ltd.

# *Contents*

<b>PREFACE</b>	<b><i>xi</i></b>
<b>1 INTRODUCTION</b>	<b>1</b>
1.1 Historical Review	1
1.2 Elements of an Electrical Communication System	4
1.2.1 <i>Digital Communication System</i> ,	7
1.2.2 <i>Early Work in Digital Communications</i> ,	10
1.3 Communication Channels and Their Characteristics	12
1.4 Mathematical Models for Communication Channels	19
1.5 Organization of the Book	22
1.6 Further Reading	23
<b>2 FREQUENCY DOMAIN ANALYSIS OF SIGNALS AND SYSTEMS</b>	<b>24</b>
2.1 Fourier Series	24
2.1.1 <i>Fourier Series for Real Signals: the Trigonometric Fourier Series</i> ,	29
2.2 Fourier Transforms	31
2.2.1 <i>Fourier Transform of Real, Even, and Odd Signals</i> ,	35

2.2.2	<i>Basic Properties of the Fourier Transform, 36</i>	
2.2.3	<i>Fourier Transform for Periodic Signals, 39</i>	
2.3	Power and Energy 40	
2.3.1	<i>Energy-Type Signals, 41</i>	
2.3.2	<i>Power-Type Signals, 42</i>	
2.4	Sampling of Bandlimited Signals 45	
2.5	Bandpass Signals 49	
2.6	Further Reading 57	
	Problems 57	
<b>3</b>	<b><i>ANALOG SIGNAL TRANSMISSION AND RECEPTION</i></b>	<b>70</b>
3.1	Introduction to Modulation 70	
3.2	Amplitude Modulation (AM) 71	
3.2.1	<i>Double-Sideband Suppressed Carrier AM, 71</i>	
3.2.2	<i>Conventional Amplitude Modulation, 78</i>	
3.2.3	<i>Single-Sideband AM, 81</i>	
3.2.4	<i>Vestigial-Sideband AM, 85</i>	
3.2.5	<i>Implementation of AM Modulators and Demodulators, 88</i>	
3.2.6	<i>Signal Multiplexing, 94</i>	
3.3	Angle Modulation 96	
3.3.1	<i>Representation of FM and PM Signals, 97</i>	
3.3.2	<i>Spectral Characteristics of Angle-Modulated Signals, 101</i>	
3.3.3	<i>Implementation of Angle Modulators and Demodulators, 107</i>	
3.4	Radio and Television Broadcasting 115	
3.4.1	<i>AM Radio Broadcasting, 115</i>	
3.4.2	<i>FM Radio Broadcasting, 116</i>	
3.4.3	<i>Television Broadcasting, 120</i>	
3.5	Mobile Radio Systems 128	
3.6	Further Reading 131	
	Problems 131	
<b>4</b>	<b><i>RANDOM PROCESSES</i></b>	<b>144</b>
4.1	Probability and Random Variables 144	
4.2	Random Processes: Basic Concepts 159	
4.2.1	<i>Description of Random Processes, 162</i>	
4.2.2	<i>Statistical Averages, 164</i>	
4.2.3	<i>Stationary Processes, 166</i>	
4.2.4	<i>Random Processes and Linear Systems, 174</i>	

- 4.3 Random Processes in the Frequency Domain 177
  - 4.3.1 *Power Spectrum of Stochastic Processes*, 177
  - 4.3.2 *Transmission over LTI Systems*, 183
- 4.4 Gaussian and White Processes 186
  - 4.4.1 *Gaussian Processes*, 186
  - 4.4.2 *White Processes*, 188
- 4.5 Bandlimited Processes and Sampling 192
- 4.6 Bandpass Processes 194
- 4.7 Further Reading 201
  - Problems 202

## **5 EFFECT OF NOISE ON ANALOG COMMUNICATION SYSTEMS**

217

- 5.1 Effect of Noise on Linear-Modulation Systems 217
  - 5.1.1 *Effect of Noise on a Baseband System*, 218
  - 5.1.2 *Effect of Noise on DSB-SC AM*, 218
  - 5.1.3 *Effect of Noise on SSB AM*, 220
  - 5.1.4 *Effect of Noise on Conventional AM*, 221
- 5.2 Carrier-Phase Estimation with a Phase-Locked Loop (PLL) 225
  - 5.2.1 *The Phase-Locked Loop (PLL)*, 226
  - 5.2.2 *Effect of Additive Noise on Phase Estimation*, 229
- 5.3 Effect of Noise on Angle Modulation 234
  - 5.3.1 *Threshold Effect in Angle Modulation*, 244
  - 5.3.2 *Pre-emphasis and De-emphasis Filtering*, 248
- 5.4 Comparison of Analog-Modulation Systems 251
- 5.5 Effects of Transmission Losses and Noise in Analog Communication Systems 252
  - 5.5.1 *Characterization of Thermal Noise Sources*, 253
  - 5.5.2 *Effective Noise Temperature and Noise Figure*, 254
  - 5.5.3 *Transmission Losses*, 257
  - 5.5.4 *Repeaters for Signal Transmission*, 258
- 5.6 Further Reading 261
  - Problems 261

## **6 INFORMATION SOURCES AND SOURCE CODING**

267

- 6.1 Modeling of Information Sources 268
  - 6.1.1 *Measure of Information*, 269
  - 6.1.2 *Joint and Conditional Entropy*, 271

- 6.2 Source-Coding Theorem 273
- 6.3 Source-Coding Algorithms 276
  - 6.3.1 *The Huffman Source-Coding Algorithm*, 276
  - 6.3.2 *The Lempel-Ziv Source-Coding Algorithm*, 280
- 6.4 Rate-Distortion Theory 282
  - 6.4.1 *Mutual Information*, 283
  - 6.4.2 *Differential Entropy*, 284
  - 6.4.3 *Rate-Distortion Function*, 285
- 6.5 Quantization 290
  - 6.5.1 *Scalar Quantization*, 291
  - 6.5.2 *Vector Quantization*, 300
- 6.6 Waveform Coding 302
  - 6.6.1 *Pulse-Code Modulation (PCM)*, 302
  - 6.6.2 *Differential Pulse-Code Modulation (DPCM)*, 307
  - 6.6.3 *Delta Modulation ( $\Delta M$ )*, 310
- 6.7 Analysis-Synthesis Techniques 312
- 6.8 Digital Audio Transmission and Digital Audio Recording 316
  - 6.8.1 *Digital Audio in Telephone Transmission Systems*, 317
  - 6.8.2 *Digital Audio Recording*, 319
- 6.9 The JPEG Image-Coding Standard 323
- 6.10 Further Reading 327
  - Problems 327

## **7 DIGITAL TRANSMISSION THROUGH THE ADDITIVE WHITE GAUSSIAN NOISE CHANNEL**

340

- 7.1 Geometric Representation of Signal Waveforms 341
- 7.2 Pulse Amplitude Modulation 345
- 7.3 Two-dimensional Signal Waveforms 350
  - 7.3.1 *Baseband Signals*, 350
  - 7.3.2 *Two-dimensional Bandpass Signals—Carrier-Phase Modulation*, 354
  - 7.3.3 *Two-dimensional Bandpass Signals—Quadrature Amplitude Modulation*, 357
- 7.4 Multidimensional Signal Waveforms 360
  - 7.4.1 *Orthogonal Signal Waveforms*, 360
  - 7.4.2 *Biorthogonal Signal Waveforms*, 365
  - 7.4.3 *Simplex Signal Waveforms*, 366
  - 7.4.4 *Binary-Coded Signal Waveforms*, 367

- 7.5 Optimum Receiver for Digitally Modulated Signals in Additive White Gaussian Noise 370
  - 7.5.1 Correlation-Type Demodulator, 370
  - 7.5.2 Matched-Filter-Type Demodulator, 375
  - 7.5.3 The Optimum Detector, 381
  - 7.5.4 Demodulation and Detection of Carrier-Amplitude Modulated Signals, 386
  - 7.5.5 Demodulation and Detection of Carrier-Phase Modulated Signals, 388
  - 7.5.6 Demodulation and Detection of Quadrature Amplitude Modulated Signals, 396
  - 7.5.7 Demodulation and Detection of Frequency-Modulated Signals, 398
- 7.6 Probability of Error for Signal Detection in Additive White Gaussian Noise 405
  - 7.6.1 Probability of Error for Binary Modulation, 405
  - 7.6.2 Probability of Error for M-ary PAM, 408
  - 7.6.3 Probability of Error for Phase-Coherent PSK Modulation, 413
  - 7.6.4 Probability of Error for DPSK, 417
  - 7.6.5 Probability of Error for QAM, 418
  - 7.6.6 Probability of Error for M-ary Orthogonal Signals, 423
  - 7.6.7 Probability of Error for M-ary Biorthogonal Signals, 428
  - 7.6.8 Probability of Error for M-ary Simplex Signals, 429
  - 7.6.9 Probability of Error for Noncoherent Detection of FSK, 430
  - 7.6.10 Comparison of Modulation Methods, 432
- 7.7 Performance Analysis for Wireline and Radio Communication Channels 436
  - 7.7.1 Regenerative Repeaters, 437
  - 7.7.2 Link Budget Analysis for Radio Channels, 438
- 7.8 Symbol Synchronization 442
  - 7.8.1 Early-Late Gate Synchronizers, 443
  - 7.8.2 Minimum Mean-Square-Error Method, 445
  - 7.8.3 Maximum-Likelihood Methods, 448
  - 7.8.4 Spectral Line Methods, 449
  - 7.8.5 Symbol Synchronization for Carrier-Modulated Signals, 451
- 7.9 Further Reading 452
  - Problems 453

## **8 DIGITAL TRANSMISSION THROUGH BANDLIMITED AWGN CHANNELS**

**474**

- 8.1 Digital Transmission through Bandlimited Channels 474
  - 8.1.1 Digital PAM Transmission through Bandlimited Baseband Channels, 478
  - 8.1.2 Digital Transmission through Bandlimited Bandpass Channels, 480



- 8.2 The Power Spectrum of Digitally Modulated Signals 482
  - 8.2.1 *The Power Spectrum of the Baseband Signal*, 483
  - 8.2.2 *The Power Spectrum of a Carrier-Modulated Signal*, 488
- 8.3 Signal Design for Bandlimited Channels 490
  - 8.3.1 *Design of Bandlimited Signals for Zero ISI—The Nyquist Criterion*, 492
  - 8.3.2 *Design of Bandlimited Signals with Controlled ISI—Partial Response Signals*, 497
- 8.4 Probability of Error in Detection of Digital PAM 499
  - 8.4.1 *Probability of Error for Detection of Digital PAM with Zero ISI*, 500
  - 8.4.2 *Symbol-by-Symbol Detection of Data with Controlled ISI*, 501
  - 8.4.3 *Probability of Error for Detection of Partial Response Signals*, 504
- 8.5 Digitally Modulated Signals with Memory 507
  - 8.5.1 *Modulation Codes and Modulation Signals with Memory*, 508
  - 8.5.2 *The Maximum-Likelihood Sequence Detector*, 521
  - 8.5.3 *Maximum-Likelihood Sequence Detection of Partial Response Signals*, 525
  - 8.5.4 *The Power Spectrum of Digital Signals with Memory*, 530
- 8.6 System Design in the Presence of Channel Distortion 534
  - 8.6.1 *Design of Transmitting and Receiving Filters for a Known Channel*, 535
  - 8.6.2 *Channel Equalization*, 538
- 8.7 Multicarrier Modulation and OFDM 556
  - 8.7.1 *An OFDM System Implemented via the FFT Algorithm*, 557
- 8.8 Further Reading 560
  - Problems 561

## **9 CHANNEL CAPACITY AND CODING**

**576**

- 9.1 Modeling of Communication Channels 576
- 9.2 Channel Capacity 579
  - 9.2.1 *Gaussian Channel Capacity*, 583
- 9.3 Bounds on Communication 586
  - 9.3.1 *Transmission of Analog Sources by PCM*, 590
- 9.4 Coding for Reliable Communication 591
  - 9.4.1 *A Tight Bound on Error Probability of Orthogonal Signals*, 592
  - 9.4.2 *The Promise of Coding*, 595
- 9.5 Linear Block Codes 601
  - 9.5.1 *Decoding and Performance of Linear Block Codes*, 606
  - 9.5.2 *Burst-Error-Correcting-Codes*, 614
- 9.6 Cyclic Codes 615
  - 9.6.1 *The Structure of Cyclic Codes*, 615

- 9.7 Convolutional Codes 623
  - 9.7.1 *Basic Properties of Convolutional Codes*, 624
  - 9.7.2 *Optimum Decoding of Convolutional Codes—The Viterbi Algorithm*, 629
  - 9.7.3 *Other Decoding Algorithms for Convolutional Codes*, 634
  - 9.7.4 *Bounds on Error Probability of Convolutional Codes*, 634
- 9.8 Complex Codes Based on Combination of Simple Codes 638
  - 9.8.1 *Product Codes*, 639
  - 9.8.2 *Concatenated Codes*, 640
  - 9.8.3 *Turbo Codes*, 640
  - 9.8.4 *The BCJR Algorithm*, 642
  - 9.8.5 *Performance of Turbo Codes*, 644
- 9.9 Coding for Bandwidth-Constrained Channels 646
  - 9.9.1 *Combined Coding and Modulation*, 647
  - 9.9.2 *Trellis-Coded Modulation*, 649
- 9.10 Practical Applications of Coding 655
  - 9.10.1 *Coding for Deep-Space Communications*, 656
  - 9.10.2 *Coding for Telephone-Line Modems*, 657
  - 9.10.3 *Coding for Compact Discs*, 658
- 9.11 Further Reading 661
  - Problems 661

## 10 WIRELESS COMMUNICATIONS

674

- 10.1 Digital Transmission on Fading Multipath Channels 674
  - 10.1.1 *Channel Models for Time-Variant Multipath Channels*, 676
  - 10.1.2 *Signal Design for Fading Multipath Channels*, 684
  - 10.1.3 *Performance of Binary Modulation in Frequency Nonselective Rayleigh Fading Channels*, 686
  - 10.1.4 *Performance Improvement Through Signal Diversity*, 689
  - 10.1.5 *Modulation and Demodulation on Frequency Selective Channels—The RAKE Demodulator*, 694
  - 10.1.6 *Multiple Antenna Systems and Space-Time Codes*, 697
- 10.2 Continuous Carrier-Phase Modulation 702
  - 10.2.1 *Continuous-Phase FSK (CPFSK)*, 702
  - 10.2.2 *Continuous-Phase Modulation (CPM)*, 711
  - 10.2.3 *Spectral Characteristics of CPFSK and CPM Signals*, 715
  - 10.2.4 *Demodulation and Detection of CPM Signals*, 720
  - 10.2.5 *Performance of CPM in AWGN and Rayleigh Fading Channels*, 726
- 10.3 Spread-Spectrum Communication Systems 729
  - 10.3.1 *Model of a Spread-Spectrum Digital Communication System*, 730
  - 10.3.2 *Direct-Sequence Spread-Spectrum Systems*, 731
  - 10.3.3 *Some Applications of DS Spread-Spectrum Signals*, 742

10.3.4	<i>Effect of Pulsed Interference and Fading</i> , 746	
10.3.5	<i>Generation of PN Sequences</i> , 748	
10.3.6	<i>Frequency-Hopped Spread Spectrum</i> , 752	
10.3.7	<i>Synchronization of Spread-Spectrum Systems</i> , 758	
10.4	Digital Cellular Communication Systems 766	
10.4.1	<i>The GSM System</i> , 766	
10.4.2	<i>CDMA System Based on IS-95</i> , 768	
10.5	Further Reading 774	
	Problems 775	
	<b>APPENDIX A: THE PROBABILITY OF ERROR FOR MULTICHANNEL RECEPTION OF BINARY SIGNALS</b>	<b>782</b>
	<b>REFERENCES</b>	<b>785</b>
	<b>INDEX</b>	<b>794</b>

# *Preface*

The objective of this book is to provide an introduction to the basic principles in the analysis and design of communication systems. It is primarily intended for use as a text for a first course in communications, either at a senior level or at a first-year graduate level.

## **BROAD TOPICAL COVERAGE**

Although we have placed a very strong emphasis on digital communications, we have provided a review of important mathematical foundational topics and a solid introduction to analog communications. The major topics covered are:

- A review of frequency domain analysis of signals and systems, and the characterization of random processes (*Chapters 2 and 4*)
- An introduction to analog signal transmission and reception (*Chapters 3 and 5*)
- An introduction to digital communications (*Chapters 6–10*)

## **EMPHASIS ON DIGITAL COMMUNICATIONS**

Our motivation for emphasizing digital communications is due to the technological developments that have occurred during the past five decades. Today, digital communication systems are in common use and generally carry the bulk of our daily information transmission through a variety of communications media, such as wireline telephone channels, microwave radio, fiber optic channels, and satellite channels. We are currently witnessing an explosive growth in the development of personal communication systems

and ultrahigh speed communication networks, which are based on digital transmission of the information, whether it is voice, still images, or video. We anticipate that, in the near future, we will witness a replacement of the current analog AM and FM radio and television broadcast by digital transmission systems.

The development of sophisticated, high-speed digital communication systems has been accelerated by concurrent developments in inexpensive high speed integrated circuits (IC) and programmable digital signal processing chips. The developments in Microelectronic IC fabrication have made possible the implementation of high-speed, high precision A/D converters, of powerful error-correcting coders/decoders, and of complex digital modulation techniques. All of these technological developments point to a continuation in the trend toward increased use of digital communications as a means for transmitting information.

## OVERVIEW OF THE TEXT

It is assumed that students using this book have a basic understanding of linear system theory, both continuous and discrete, including a working knowledge of Fourier series and Fourier transform techniques. Chapter 2 provides a review of basic material on signals and systems and establishes the necessary notation used in subsequent chapters. It is also assumed that students have had a first course in probability. Such courses are currently required in many undergraduate electrical engineering and computer engineering programs. Chapter 4 provides a review of probability and random processes to the extent that is necessary for a first course in communications.

Chapter 3 treats modulation and demodulation of analog signals. This treatment includes *amplitude modulation (AM)*, *frequency modulation (FM)*, and *phase modulation (PM)*. Radio and television broadcasting and mobile radio cellular systems are discussed as examples of analog communication systems. Chapter 5 continues the treatment of analog communication systems by analyzing the effect of additive noise in the demodulation of AM, FM, and PM signals. The phase-locked loop, which is used for estimating the phase of a sinusoidal carrier in both analog and digital communication systems is also described in Chapter 5. The chapter concludes with a treatment of the effect of transmission losses and the characterization of noise sources in communication systems.

A logical beginning in the introduction of digital communication systems analysis and design is the characterization of information sources and source encoding. Chapter 6 is devoted to this topic. In this chapter we introduce the reader to the modeling of information sources, both discrete and continuous (analog), and the basic mathematical concepts of entropy and mutual information. Our discussion of source encoding for discrete sources includes the Huffman coding algorithm and the Lempel-Ziv algorithm. For the case of analog sources, we treat both scalar and vector quantization and describe the common waveform-coding techniques, namely, PCM, DPCM, and DM. We also describe the LPC-based source modeling method. As practical examples of the source-coding methods described in this chapter we cite the digital speech transmission systems

in the telephone plant, the digital audio recording systems as embodied in the compact disc (CD) player and the JPEG image-coding standard.

Digital modulation and demodulation techniques are described in Chapter 7. Binary and nonbinary modulation methods are described based on a geometric representation of signals, and their error-rate performance is evaluated and compared. This chapter also describes symbol synchronization methods for digital communication systems.

Chapter 8 treats digital transmission through bandlimited AWGN channels. In this chapter we derive the power-spectral density of linearly modulated baseband signals and consider the problem of signal design for a bandlimited channel. We show that the effect of channel distortion is to introduce intersymbol interference (ISI), which can be eliminated or minimized by proper signal design. The use of linear and nonlinear adaptive equalizers for reducing the effect of ISI is also described.

Chapter 9 treats the topic of channel coding and decoding. The capacity of a communication channel is first defined, and the capacity of the Gaussian channel is determined. Linear block codes and convolutional codes are introduced and appropriate decoding algorithms are described. The benefits of coding for bandwidth constrained channels are also described. The final section of this chapter presents three practical applications of coding.

The last chapter of this book treats topics in wireless communications. First, we consider the characterization of fading multipath channels and describe the effects of such channels on wireless digital communication systems. The design of signals that are effective in mitigating this type of channel distortion is also considered. Second, we describe the class of continuous-phase modulated signals, which are especially suitable for digital communication in wireless channels. Finally, we treat the class of spread-spectrum signals, which are suitable for multi-user wireless communication systems.

## EXAMPLES AND HOMEWORK PROBLEMS

We have included a large number of carefully chosen examples and homework problems. The text contains over 180 worked-out examples and over 480 problems. Examples and problems range from simple exercises to more challenging and thought-provoking problems. A Solutions Manual is available free to all adopting faculty, which is provided in both typeset form and as a diskette formatted in  $\text{\LaTeX}$ . Solutions are not available for sale to students. This will enable instructors to print out solutions in any configuration easily.

## COURSE OPTIONS

This book can serve as a text in either a one- or two-semester course in communication system. An important consideration in the design of the course is whether or not the students have had a prior course in probability and random processes. Another important consideration is whether or not analog modulation and demodulation techniques are to be covered. Here, we outline three scenarios. Others are certainly possible.

1. A one-term course in analog and digital communication: Selected review sections from Chapters 2 and 4, all of chapters 3, 5, 7, and 8, and selections from chapters 6, 9, and 10.
2. A one-term course in digital communication: Selected review sections from Chapters 2 and 4, and Chapters 6–10.
3. A two-term course sequence on analog and digital communications:
  - (a) Chapters 2–6 for the first course.
  - (b) Chapters 7–10 for the second course.

We wish to thank Gloria Doukakis for her assistance in the preparation of the manuscript.

*John Proakis*  
Adjunct Professor,  
University of California at San Diego  
and Professor Emeritus,  
*Masoud Salehi*  
Northeastern University

# *Introduction*

Every day, in our work and in our leisure time, we come in contact with and use a variety of modern communication systems and communication media, the most common being the telephone, radio, television, and the Internet. Through these media we are able to communicate (nearly) instantaneously with people on different continents, transact our daily business, and receive information about various developments and events of note that occur all around the world. Electronic mail and facsimile transmission have made it possible to rapidly communicate written messages across great distances.

Can you imagine a world without telephones, radio, and TV? Yet, when you think about it, most of these modern-day communication systems were invented and developed during the past century. Here, we present a brief historical review of major developments within the last two hundred years that have had a major role in the development of modern communication systems.

## 1.1 HISTORICAL REVIEW

**Telegraphy and Telephony.** One of the earliest inventions of major significance to communications was the invention of the electric battery by Alessandro Volta in 1799. This invention made it possible for Samuel Morse to develop the electric telegraph, which he demonstrated in 1837. The first telegraph line linked Washington with Baltimore and became operational in May 1844. Morse devised the variable-length binary code given in Table 1.1, in which letters of the English alphabet were represented by a sequence of dots and dashes (code words). In this code, more frequently occurring letters are represented by short code words, while letters occurring less frequently are represented by longer code words.



TABLE 1.1 MORSE CODE

A	· —	N	— ·		
B	— ···	O	— — — —		
C	— · — ·	P	— · — ·		
D	— ···	Q	— — · —	1	· — — — —
E	·	R	— · ·	2	·· — — —
F	·· — ·	S	·· ·	3	·· — — —
G	— — — ·	T	—	4	···· —
H	····	U	·· —	5	···· ·
I	··	V	·· — —	6	— ··· ·
J	· — — — —	W	·· — —	7	— — — · ·
K	— · — —	X	— · · —	8	— — — · ·
L	· — · ·	Y	— · — — —	9	— — — — ·
M	— — —	Z	— — — · ·	0	— — — — —
(a) Letters				(b) Numbers	
<hr/>					
Period (·)	· — · — · — ·	Wait sign (AS)	· — · · ·		
Comma (,)	— — — · — — —	Double dash (break)	— — · — —		
Interrogation (?)	·· — — — ·	Error sign	·· · · · · ·		
Quotation Mark (")	· — · — · — ·	Fraction bar (/)	— · — · —		
Colon (:)	— — — · · ·	End of message (AR)	· — · — ·		
Semicolon (;)	— · — · — ·	End of transmission (SK)	·· · — · —		
Parenthesis ( )	— · — — — ·				
(c) Punctuation and Special Characters					

The *Morse code* was the precursor to the variable-length source-coding methods that are described in Chapter 6. It is remarkable that the earliest form of electrical communications that was developed by Morse, namely *telegraphy*, was a binary digital communication system in which the letters of the English alphabet were efficiently encoded into corresponding variable-length code words having binary elements.

Nearly forty years later, in 1875, Émile Baudot developed a code for telegraphy in which each letter was encoded into fixed-length binary code words of length 5. In the *Baudot code* the binary code elements have equal length and are designated as mark and space.

An important milestone in telegraphy was the installation of the first transatlantic cable in 1858 that linked the United States and Europe. This cable failed after about four weeks of operation. A second cable was laid a few years later and became operational in July 1866.

*Telephony* came into being with the invention of the telephone in the 1870s. Alexander Graham Bell patented his invention of the telephone in 1876, and in 1877 established the Bell Telephone Company. Early versions of telephone communication systems were relatively simple and provided service over several hundred miles. Significant advances in the quality and range of service during the first two decades of the twentieth century resulted from the invention of the carbon microphone and the induction coil.

The invention of the triode amplifier by Lee De Forest in 1906 made it possible to introduce signal amplification in telephone communication systems and, thus, to allow for telephone signal transmission over great distances. For example, transcontinental telephone transmission became operational in 1915.

Two world wars and the Great Depression during the 1930s must have been a deterrent to the establishment of transatlantic telephone service. It was not until 1953, when the first transatlantic cable was laid, that telephone service became available between the United States and Europe.

Automatic switching was another important advance in the development of telephony. The first automatic switch, developed by Strowger in 1897, was an electromechanical step-by-step switch. This type of switch was used for several decades. With the invention of the transistor, electronic (digital) switching became economically feasible. After several years of development at the Bell Telephone Laboratories, a digital switch was placed in service in Illinois in June 1960.

During the past thirty years there have been numerous significant advances in telephone communications. Fiber optic cables are rapidly replacing copper wire in the telephone plant and electronic switches have replaced the old electromechanical systems.

**Wireless Communications.** The development of wireless communications stems from the works of Oersted, Faraday, Gauss, Maxwell, and Hertz. In 1820, Oersted demonstrated that an electric current produces a magnetic field. On August 29, 1831, Michael Faraday showed that an induced current is produced by moving a magnet in the vicinity of a conductor. Thus, he demonstrated that a changing magnetic field produces an electric field. With this early work as background, James C. Maxwell in 1864 predicted the existence of electromagnetic radiation and formulated the basic theory that has been in use for over a century. Maxwell's theory was verified experimentally by Hertz in 1887.

In 1894, a sensitive device that could detect radio signals, called the *coherer*, was used by its inventor Oliver Lodge to demonstrate wireless communication over a distance of 150 yards at Oxford, England. Guglielmo Marconi is credited with the development of *wireless telegraphy*. Marconi demonstrated the transmission of radio signals at a distance of approximately 2 kilometers in 1895. Two years later, in 1897, he patented a radio telegraph system and established the Wireless Telegraph and Signal Company. On December 12, 1901, Marconi received a radio signal at Signal Hill in Newfoundland, which was transmitted from Cornwall, England, a distance of about 1700 miles.

The invention of the vacuum tube was especially instrumental in the development of radio communication systems. The vacuum diode was invented by Fleming in 1904 and the vacuum triode amplifier was invented by De Forest in 1906, as previously indicated. The invention of the triode made radio broadcast possible in the early part of the twentieth century. *Amplitude modulation (AM)* broadcast was initiated in 1920 when radio station KDKA, Pittsburgh, went on the air. From that date, AM radio broadcasting grew rapidly across the country and around the world. The *superheterodyne AM radio receiver*, as we know it today, was invented by Edwin Armstrong during World War I. Another significant development in radio communications was the invention

of *Frequency modulation (FM)*, also by Armstrong. In 1933, Armstrong built and demonstrated the first FM communication system. However, the use of FM was slow to develop compared with AM broadcast. It was not until the end of World War II that FM broadcast gained in popularity and developed commercially.

The first television system was built in the United States by V. K. Zworykin and demonstrated in 1929. Commercial television broadcasting began in London in 1936 by the British Broadcasting Corporation (BBC). Five years later the Federal Communications Commission (FCC) authorized television broadcasting in the United States.

**The Past Fifty Years.** The growth in communications services over the past fifty years has been phenomenal. The invention of the transistor in 1947 by Walter Brattain, John Bardeen, and William Shockley; the integrated circuit in 1958 by Jack Kilby and Robert Noyce; and the laser by Townes and Schawlow in 1958, have made possible the development of small-size, low-power, low-weight, and high-speed electronic circuits which are used in the construction of satellite communication systems, wideband microwave radio systems, and lightwave communication systems using fiber optic cables. A satellite named Telstar I was launched in 1962 and used to relay TV signals between Europe and the United States. Commercial satellite communication services began in 1965 with the launching of the Early Bird satellite.

Currently, most of the wireline communication systems are being replaced by fiber optic cables which provide extremely high bandwidth and make possible the transmission of a wide variety of information sources, including voice, data, and video. Cellular radio has been developed to provide telephone service to people in automobiles, buses, and trains. High-speed communication networks link computers and a variety of peripheral devices literally around the world.

Today we are witnessing a significant growth in the introduction and use of personal communications services, including voice, data, and video transmission. Satellite and fiber optic networks provide high-speed communication services around the world. Indeed, this is the dawn of the modern telecommunications era.

There are several historical treatments in the development of radio and telecommunications covering the past century. We cite the books by McMahan, entitled *The Making of a Profession—A Century of Electrical Engineering in America* (IEEE Press, 1984); Ryder and Fink, entitled *Engineers and Electronics* (IEEE Press, 1984); and S. Millman, Ed., entitled *A History of Engineering and Science in the Bell System—Communications Sciences (1925–1980)* (AT & T Bell Laboratories, 1984).

## 1.2 ELEMENTS OF AN ELECTRICAL COMMUNICATION SYSTEM

Electrical communication systems are designed to send messages or information from a source that generates the messages to one or more destinations. In general, a communication system can be represented by the functional block diagram shown in Figure 1.1. The information generated by the source may be of the form of voice (speech source), a picture (image source), or plain text in some particular language, such as English, Japanese, German, French, etc. An essential feature of any source that generates infor-

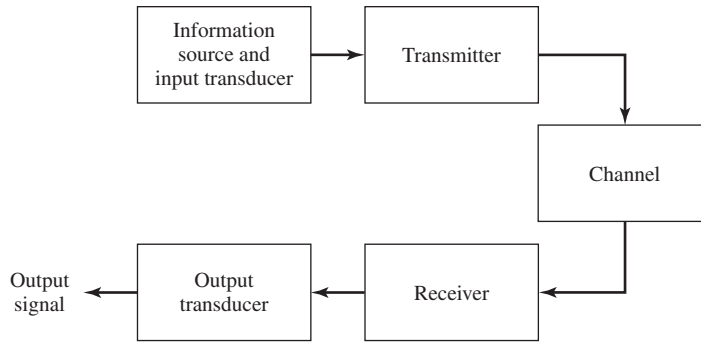


**Figure 1.1** Functional block diagram of a communication system.

mation is that its output is described in probabilistic terms; i.e., the output of a source is not deterministic. Otherwise, there would be no need to transmit the message.

A transducer is usually required to convert the output of a source into an electrical signal that is suitable for transmission. For example, a microphone serves as the transducer that converts an acoustic speech signal into an electrical signal, and a video camera converts an image into an electrical signal. At the destination, a similar transducer is required to convert the electrical signals that are received into a form that is suitable for the user; e.g., acoustic signals, images, etc.

The heart of the communication system consists of three basic parts, namely, the *transmitter*, the *channel*, and the *receiver*. The functions performed by these three elements are described next.

**The Transmitter.** The transmitter converts the electrical signal into a form that is suitable for transmission through the physical channel or transmission medium. For example, in radio and TV broadcast, the Federal Communications Commission (FCC) specifies the frequency range for each transmitting station. Hence, the transmitter must translate the information signal to be transmitted into the appropriate frequency range that matches the frequency allocation assigned to the transmitter. Thus, signals transmitted by multiple radio stations do not interfere with one another. Similar functions are performed in telephone communication systems where the electrical speech signals from many users are transmitted over the same wire.

In general, the transmitter performs the matching of the message signal to the channel by a process called *modulation*. Usually, modulation involves the use of the information signal to systematically vary either the amplitude, frequency, or phase of a sinusoidal carrier. For example, in AM radio broadcast, the information signal that is transmitted is contained in the amplitude variations of the sinusoidal carrier, which is the center frequency in the frequency band allocated to the radio transmitting station. This is an example of *amplitude modulation*. In FM radio broadcast, the information signal that is transmitted is contained in the frequency variations of the sinusoidal carrier. This is an example of *frequency modulation*. *Phase modulation (PM)* is yet a third method for impressing the information signal on a sinusoidal carrier.

In general, carrier modulation such as AM, FM, and PM is performed at the transmitter, as indicated above, to convert the information signal to a form that matches the characteristics of the channel. Thus, through the process of modulation, the information signal is translated in frequency to match the allocation of the channel. The choice of the type of modulation is based on several factors, such as the amount of bandwidth allocated, the types of noise and interference that the signal encounters in transmission over the channel, and the electronic devices that are available for signal amplification prior to transmission. In any case, the modulation process makes it possible to accommodate the transmission of multiple messages from many users over the same physical channel.

In addition to modulation, other functions that are usually performed at the transmitter are filtering of the information-bearing signal, amplification of the modulated signal, and in the case of wireless transmission, radiation of the signal by means of a transmitting antenna.

**The Channel.** The communications channel is the physical medium that is used to send the signal from the transmitter to the receiver. In wireless transmission, the channel is usually the atmosphere (free space). On the other hand, telephone channels usually employ a variety of physical media, including wirelines, optical fiber cables, and wireless (microwave radio). Whatever the physical medium for signal transmission, the essential feature is that the transmitted signal is corrupted in a random manner by a variety of possible mechanisms. The most common form of signal degradation comes in the form of additive noise, which is generated at the front end of the receiver, where signal amplification is performed. This noise is often called *thermal noise*. In wireless transmission, additional additive disturbances are man-made noise, and atmospheric noise picked up by a receiving antenna. Automobile ignition noise is an example of man-made noise, and electrical lightning discharges from thunderstorms is an example of atmospheric noise. Interference from other users of the channel is another form of additive noise that often arises in both wireless and wireline communication systems.

In some radio communication channels, such as the ionospheric channel that is used for long range, short-wave radio transmission, another form of signal degradation is multipath propagation. Such signal distortion is characterized as a nonadditive signal disturbance which manifests itself as time variations in the signal amplitude, usually called fading. This phenomenon is described in more detail in Section 1.3.

Both additive and nonadditive signal distortions are usually characterized as random phenomena and described in statistical terms. The effect of these signal distortions must be taken into account on the design of the communication system.

In the design of a communication system, the system designer works with mathematical models that statistically characterize the signal distortion encountered on physical channels. Often, the statistical description that is used in a mathematical model is a result of actual empirical measurements obtained from experiments involving signal transmission over such channels. In such cases, there is a physical justification for the mathematical model used in the design of communication systems. On the other hand, in some communication system designs, the statistical characteristics of the channel

may vary significantly with time. In such cases, the system designer may design a communication system that is robust to the variety of signal distortions. This can be accomplished by having the system adapt some of its parameters to the channel distortion encountered.

**The Receiver.** The function of the receiver is to recover the message signal contained in the received signal. If the message signal is transmitted by carrier modulation, the receiver performs *carrier demodulation* in order to extract the message from the sinusoidal carrier. Since the signal demodulation is performed in the presence of additive noise and possibly other signal distortion, the demodulated message signal is generally degraded to some extent by the presence of these distortions in the received signal. As we shall see, the fidelity of the received message signal is a function of the type of modulation, the strength of the additive noise, the type and strength of any other additive interference, and the type of any nonadditive interference.

Besides performing the primary function of signal demodulation, the receiver also performs a number of peripheral functions, including signal filtering and noise suppression.

### 1.2.1 Digital Communication System

Up to this point we have described an electrical communication system in rather broad terms based on the implicit assumption that the message signal is a continuous time-varying waveform. We refer to such continuous-time signal waveforms as *analog signals* and to the corresponding information sources that produce such signals as *analog sources*. Analog signals can be transmitted directly via carrier modulation over the communication channel and demodulated accordingly at the receiver. We call such a communication system an *analog communication system*.

Alternatively, an analog source output may be converted into a digital form and the message can be transmitted via digital modulation and demodulated as a digital signal at the receiver. There are some potential advantages to transmitting an analog signal by means of digital modulation. The most important reason is that signal fidelity is better controlled through digital transmission than analog transmission. In particular, digital transmission allows us to regenerate the digital signal in long-distance transmission, thus eliminating effects of noise at each regeneration point. In contrast, the noise added in analog transmission is amplified along with the signal when amplifiers are used periodically to boost the signal level in long-distance transmission. Another reason for choosing digital transmission over analog is that the analog message signal may be highly redundant. With digital processing, redundancy may be removed prior to modulation, thus conserving channel bandwidth. Yet a third reason may be that digital communication systems are often cheaper to implement.

In some applications, the information to be transmitted is inherently digital; e.g., in the form of English text, computer data, etc. In such cases, the information source that generates the data is called a *discrete (digital) source*.

In a digital communication system, the functional operations performed at the transmitter and receiver must be expanded to include message signal discretization at

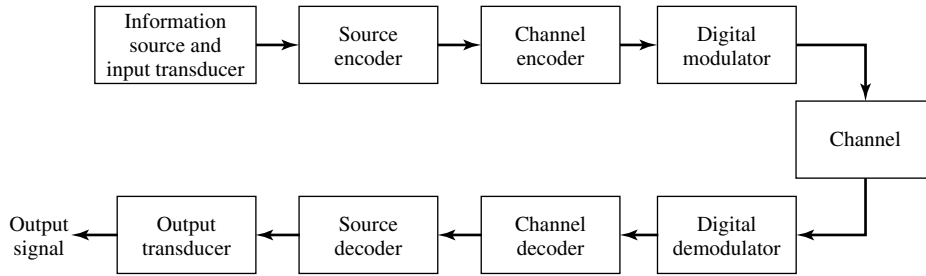


**Figure 1.2** Basic elements of a digital communication system.

the transmitter and message signal synthesis or interpolation at the receiver. Additional functions include redundancy removal, and channel coding and decoding.

Figure 1.2 illustrates the functional diagram and the basic elements of a digital communication system. The source output may be either an analog signal, such as audio or video signal, or a digital signal, such as the output of a computer which is discrete in time and has a finite number of output characters. In a digital communication system, the messages produced by the source are usually converted into a sequence of binary digits. Ideally, we would like to represent the source output (message) by as few binary digits as possible. In other words, we seek an efficient representation of the source output that results in little or no redundancy. The process of efficiently converting the output of either an analog or a digital source into a sequence of binary digits is called *source encoding* or *data compression*. We shall describe source-encoding methods in Chapter 6.

The sequence of binary digits from the source encoder, which we call the *information sequence* is passed to the *channel encoder*. The purpose of the channel encoder is to introduce, in a controlled manner, some redundancy in the binary information sequence which can be used at the receiver to overcome the effects of noise and interference encountered in the transmission of the signal through the channel. Thus, the added redundancy serves to increase the reliability of the received data and improves the fidelity of the received signal. In effect, redundancy in the information sequence aids the receiver in decoding the desired information sequence. For example, a (trivial) form of encoding of the binary information sequence is simply to repeat each binary digit  $m$  times, where  $m$  is some positive integer. More sophisticated (non-trivial) encoding involves taking  $k$  information bits at a time and mapping each  $k$ -bit sequence into a unique  $n$ -bit sequence, called a *code word*. The amount of redundancy introduced by encoding the data in this manner is measured by the ratio  $n/k$ . The reciprocal of this ratio, namely,  $k/n$ , is called the rate of the code or, simply, the *code rate*.

The binary sequence at the output of the channel encoder is passed to the *digital modulator*, which serves as the interface to the communications channel. Since nearly all of the communication channels encountered in practice are capable of transmitting electrical signals (waveforms), the primary purpose of the digital modulator is to map

the binary information sequence into signal waveforms. To elaborate on the point, let us suppose that the coded information sequence is to be transmitted one bit at a time at some uniform rate  $R$  bits/s. The digital modulator may simply map the binary digit 0 into a waveform  $s_0(t)$  and the binary digit 1 into a waveform  $s_1(t)$ . In this manner, each bit from the channel encoder is transmitted separately. We call this *binary modulation*. Alternatively, the modulator may transmit  $b$  coded information bits at a time by using  $M = 2^b$  distinct waveforms  $s_i(t)$ ,  $i = 0, 1, \dots, M - 1$ , one waveform for each of the  $2^b$  possible  $b$ -bit sequences. We call this *M-ary modulation* ( $M > 2$ ). Note that a new  $b$ -bit sequence enters the modulator every  $b/R$  seconds. Hence, when the channel bit rate  $R$  is fixed, the amount of time available to transmit one of the  $M$  waveforms corresponding to a  $b$ -bit sequence is  $b$  times the time period in a system that uses binary modulation.

At the receiving end of a digital communications system, the *digital demodulator* processes the channel-corrupted transmitted waveform and reduces each waveform to a single number that represents an estimate of the transmitted data symbol (binary or  $M$ -ary). For example, when binary modulation is used, the demodulator may process the received waveform and decide on whether the transmitted bit is a 0 or a 1. In such a case, we say the *demodulator has made a binary decision*. As one alternative, the demodulator may make a ternary decision; that is, it decides that the transmitted bit is either a 0 or 1 or it makes no decision at all, depending on the apparent quality of the received signal. When no decision is made on a particular bit, we say that *the demodulator has inserted an erasure in the demodulated data*. Using the redundancy in the transmitted data, the decoder attempts to fill in the positions where erasures occurred. Viewing the decision process performed by the demodulator as a form of quantization, we observe that binary and ternary decisions are special cases of a demodulator that quantizes to  $Q$  levels, where  $Q \geq 2$ . In general, if the digital communications system employs  $M$ -ary modulation, where  $m = 0, 1, \dots, M - 1$  represent the  $M$  possible transmitted symbols, each corresponding to  $b = \log_2 M$  bits, the demodulator may make a  $Q$ -ary decision, where  $Q \geq M$ . In the extreme case where no quantization is performed,  $Q = \infty$ .

When there is no redundancy in the transmitted information, the demodulator must decide which of the  $M$  waveforms was transmitted in any given time interval. Consequently  $Q = M$ , and since there is no redundancy in the transmitted information, no discrete channel decoder is used following the demodulator. On the other hand, when there is redundancy introduced by a discrete channel encoder at the transmitter, the  $Q$ -ary output from the demodulator occurring every  $b/R$  seconds is fed to the decoder, which attempts to reconstruct the original information sequence from knowledge of the code used by the channel encoder and the redundancy contained in the received data.

A measure of how well the demodulator and encoder perform is the frequency with which errors occur in the decoded sequence. More precisely, the average probability of a bit-error at the output of the decoder is a measure of the performance of the demodulator-decoder combination. In general, the probability of error is a function of the code characteristics, the types of waveforms used to transmit the information over the channel, the transmitter power, the characteristics of the channel; i.e., the amount of noise, the nature of the interference, etc., and the method of demodulation and decoding. These items and their effect on performance will be discussed in detail in Chapters 7–9.



As a final step, when an analog output is desired, the source decoder accepts the output sequence from the channel decoder and, from knowledge of the source-encoding method used, attempts to reconstruct the original signal from the source. Due to channel-decoding errors and possible distortion introduced by the source encoder and, perhaps, the source decoder, the signal at the output of the source decoder is an approximation to the original source output. The difference or some function of the difference between the original signal and the reconstructed signal is a measure of the distortion introduced by the digital communications system.

## 1.2.2 Early Work in Digital Communications

Although Morse is responsible for the development of the first electrical digital communication system (telegraphy), the beginnings of what we now regard as modern digital communications stem from the work of Nyquist (1924), who investigated the problem of determining the maximum signaling rate that can be used over a telegraph channel of a given bandwidth without intersymbol interference. He formulated a model of a telegraph system in which a transmitted signal has the general form

$$s(t) = \sum_n a_n g(t - nT)$$

where  $g(t)$  represents a basic pulse shape and  $\{a_n\}$  is the binary data sequence of  $\{\pm 1\}$  transmitted at a rate of  $1/T$  bits/sec. Nyquist set out to determine the optimum pulse shape that was bandlimited to  $W$  Hz and maximized the bit rate  $1/T$  under the constraint that the pulse caused no intersymbol interference at the sampling times  $k/T$ ,  $k = 0, \pm 1, \pm 2, \dots$ . His studies led him to conclude that the maximum pulse rate  $1/T$  is  $2W$  pulses/sec. This rate is now called the *Nyquist rate*. Moreover, this pulse rate can be achieved by using the pulses  $g(t) = (\sin 2\pi Wt)/2\pi Wt$ . This pulse shape allows the recovery of the data without intersymbol interference at the sampling instants. Nyquist's result is equivalent to a version of the sampling theorem for band-limited signals, which was later stated precisely by Shannon (1948). The sampling theorem states that a signal  $s(t)$  of bandwidth  $W$  can be reconstructed from samples taken at the Nyquist rate of  $2W$  samples/sec using the interpolation formula

$$s(t) = \sum_n s\left(\frac{n}{2W}\right) \frac{\sin 2\pi W(t - n/2W)}{2\pi W(t - n/2W)}$$

In light of Nyquist's work, Hartley (1928) considered the issue of the amount of data that can be transmitted reliably over a bandlimited channel when multiple amplitude levels are used. Due to the presence of noise and other interference, Hartley postulated that the receiver can reliably estimate the received signal amplitude to some accuracy, say  $A_\delta$ . This investigation led Hartley to conclude that there is a maximum data rate that can be communicated reliably over a bandlimited channel, when the maximum signal amplitude is limited to  $A_{\max}$  (fixed power constraint) and the amplitude resolution is  $A_\delta$ .

Another significant advance in the development of communications was the work of Wiener (1942) who considered the problem of estimating a desired signal waveform  $s(t)$  in the presence of additive noise  $n(t)$ , based on observation of the received signal  $r(t) = s(t) + n(t)$ . This problem arises in signal demodulation. Wiener determined the linear filter whose output is the best mean-square approximation to the desired signal  $s(t)$ . The resulting filter is called the *optimum linear (Wiener) filter*.

Hartley's and Nyquist's results on the maximum transmission rate of digital information were precursors to the work of Shannon (1948a,b) who established the mathematical foundations for information theory and derived the fundamental limits for digital communication systems. In his pioneering work, Shannon formulated the basic problem of reliable transmission of information in statistical terms, using probabilistic models for information sources and communication channels. Based on such a statistical formulation, he adopted a logarithmic measure for the information content of a source. He also demonstrated that the effect of a transmitter power constraint, a bandwidth constraint, and additive noise can be associated with the channel and incorporated into a single parameter, called the *channel capacity*. For example, in the case of an additive white (spectrally flat) Gaussian noise interference, an ideal bandlimited channel of bandwidth  $W$  has a capacity  $C$  given by

$$C = W \log_2 \left( 1 + \frac{P}{WN_0} \right) \text{ bits/s}$$

where  $P$  is the average transmitted power and  $N_0$  is the power-spectral density of the additive noise. The significance of the channel capacity is as follows: If the information rate  $R$  from the source is less than  $C$  ( $R < C$ ), then it is theoretically possible to achieve reliable transmission through the channel by appropriate coding. On the other hand if  $R > C$ , reliable transmission is not possible regardless of the amount of signal processing performed at the transmitter and receiver. Thus, Shannon established basic limits on communication of information and gave birth to a new field that is now called *information theory*.

Initially, the fundamental work of Shannon had a relatively small impact on the design and development of new digital communications systems. In part, this was due to the small demand for digital information transmission during the decade of the 1950s. Another reason was the relatively large complexity and, hence, the high cost of digital hardware required to achieve the high efficiency and the high reliability predicted by Shannon's theory.

Another important contribution to the field of digital communications is the work of Kotelnikov (1947) which provided a coherent analysis of the various digital communication systems based on a geometrical approach. Kotelnikov's approach was later expanded by Wozencraft and Jacobs (1965).

The increase in the demand for data transmission during the last three decades, coupled with the development of more sophisticated integrated circuits, has led to the development of very efficient and more reliable digital communications systems. In the course of these developments, Shannon's original results and the generalization

of his results on maximum transmission limits over a channel and on bounds on the performance achieved, have served as benchmarks relative to which any given communications system design is compared. The theoretical limits derived by Shannon and other researchers that contributed to the development of information theory serve as an ultimate goal in the continuing efforts to design and develop more efficient digital communications systems.

Following Shannon's publications came the classic work of Hamming (1950) on error detecting and error-correcting codes to combat the detrimental effects of channel noise. Hamming's work stimulated many researchers in the years that followed and a variety of new and powerful codes were discovered, many of which are used today in the implementation of modern communication systems.

### 1.3 COMMUNICATION CHANNELS AND THEIR CHARACTERISTICS

As indicated in our preceding discussion, the communication channel provides the connection between the transmitter and the receiver. The physical channel may be a pair of wires that carry the electrical signal, or an optical fiber that carries the information on a modulated light beam, or an underwater ocean channel in which the information is transmitted acoustically, or free space over which the information-bearing signal is radiated by use of an antenna. Other media that can be characterized as communication channels are data storage media, such as magnetic tape, magnetic disks, and optical disks.

One common problem in signal transmission through any channel is additive noise. In general, additive noise is generated internally by components such as resistors and solid-state devices used to implement the communication system. This is sometimes called *thermal noise*. Other sources of noise and interference may arise externally to the system, such as interference from other users of the channel. When such noise and interference occupy the same frequency band as the desired signal, its effect can be minimized by proper design of the transmitted signal and its demodulator at the receiver. Other types of signal degradations that may be encountered in transmission over the channel are signal attenuation, amplitude and phase distortion, and multipath distortion.

The effects of noise may be minimized by increasing the power in the transmitted signal. However, equipment and other practical constraints limit the power level in the transmitted signal. Another basic limitation is the available channel bandwidth. A bandwidth constraint is usually due to the physical limitations of the medium and the electronic components used to implement the transmitter and the receiver. These two limitations result in constraining the amount of data that can be transmitted reliably over any communications channel. Shannon's basic results relate the channel capacity to the available transmitted power and channel bandwidth.

Next, we describe some of the important characteristics of several communication channels.

**Wireline Channels.** The telephone network makes extensive use of wire lines for voice signal transmission, as well as data and video transmission. Twisted-pair wire-

lines and coaxial cable are basically guided electromagnetic channels which provide relatively modest bandwidths. Telephone wire generally used to connect a customer to a central office has a bandwidth of several hundred kilohertz (KHz). On the other hand, coaxial cable has a usable bandwidth of several megahertz (MHz). Figure 1.3 illustrates the frequency range of guided electromagnetic channels which includes waveguides and optical fibers.

Signals transmitted through such channels are distorted in both amplitude and phase and further corrupted by additive noise. Twisted-pair wireline channels are also prone to crosstalk interference from physically adjacent channels. Because wireline channels carry a large percentage of our daily communications around the country and

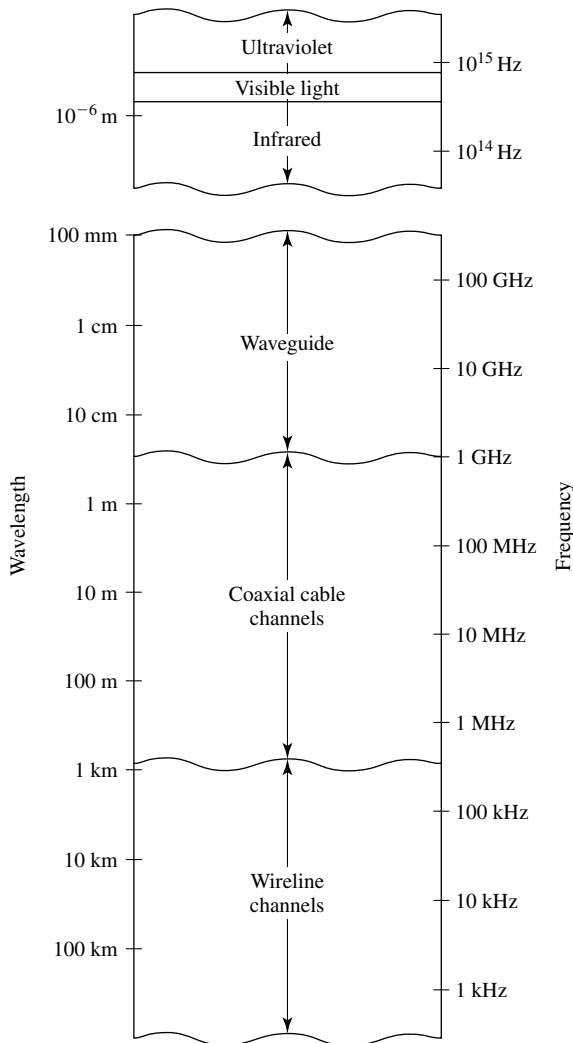


**Figure 1.3** Frequency range for guided wireline channels.

the world, much research has been performed on the characterization of their transmission properties and on methods for mitigating the amplitude and phase distortion encountered in signal transmission. In Chapter 8, we describe methods for designing optimum transmitted signals and their demodulation, including the design of *channel equalizers* that compensate for amplitude and phase distortion.

**Fiber Optic Channels.** Optical fibers offer the communications system designer a channel bandwidth that is several orders of magnitude larger than coaxial cable channels. During the past decade optical fiber cables have been developed which have a relatively low signal attenuation and highly reliable photonic devices have been developed for signal generation and signal detection. These technological advances have resulted in a rapid deployment of optical fiber channels both in domestic telecommunication systems as well as for transatlantic and transpacific communications. With the large bandwidth available on fiber optic channels it is possible for the telephone companies to offer subscribers a wide array of telecommunication services, including voice, data, facsimile, and video.

The transmitter or modulator in a fiber optic communication system is a light source, either a light-emitting diode (LED) or a laser. Information is transmitted by varying (modulating) the intensity of the light source with the message signal. The light propagates through the fiber as a light wave and is amplified periodically (in the case of digital transmission, it is detected and regenerated by repeaters) along the transmission path to compensate for signal attenuation. At the receiver, the light intensity is detected by a photodiode, whose output is an electrical signal that varies in direct proportion to the power of the light impinging on the photodiode.

It is envisioned that optical fiber channels will replace nearly all wireline channels in the telephone network in the next few years.

**Wireless Electromagnetic Channels.** In radio communication systems, electromagnetic energy is coupled to the propagation medium by an *antenna* which serves as the radiator. The physical size and the configuration of the antenna depend primarily on the frequency of operation. To obtain efficient radiation of electromagnetic energy, the antenna must be longer than 1/10 of the wavelength. Consequently, a radio station transmitting in the AM frequency band, say at 1 MHz (corresponding to a wavelength of  $\lambda = c/f_c = 300$  m) requires an antenna of at least 30 meters.

Figure 1.4 illustrates the various frequency bands of the electromagnetic spectrum. The mode of propagation of electromagnetic waves in the atmosphere and in free space may be subdivided into three categories, namely, ground-wave propagation, sky-wave propagation, and line-of-sight (LOS) propagation. In the VLF and ELF frequency bands, where the wavelengths exceed 10 km, the earth and the ionosphere act as a waveguide for electromagnetic wave propagation. In these frequency ranges, communication signals practically propagate around the globe. For this reason, these frequency bands are primarily used to provide navigational aids from shore to ships around the world. The channel bandwidths available in these frequency bands are relatively small (usually from 1–10% of the center frequency), and hence, the information that is transmitted through

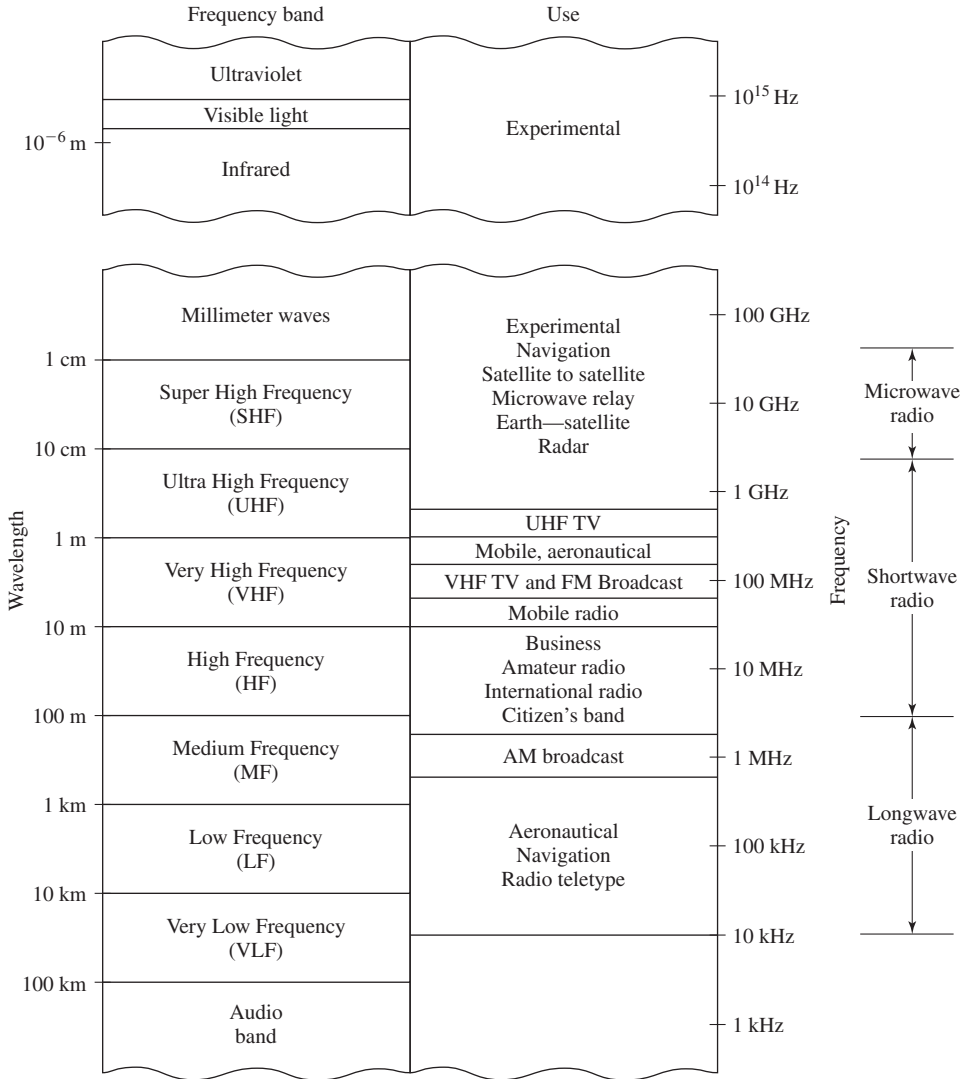


**Figure 1.4** Frequency range for wireless electromagnetic channels. (Adapted from Carlson, Sec. Ed.; © 1975 McGraw-Hill. Reprinted with permission of the publisher.)

these channels is relatively slow speed and, generally, confined to digital transmission. A dominant type of noise at these frequencies is generated from thunderstorm activity around the globe, especially in tropical regions. Interference results from the many users of these frequency bands.

Ground-wave propagation, illustrated in Figure 1.5, is the dominant mode of propagation for frequencies in the MF band (0.3–3 MHz). This is the frequency band

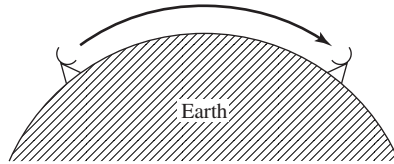


**Figure 1.5** Illustration of ground-wave propagation.

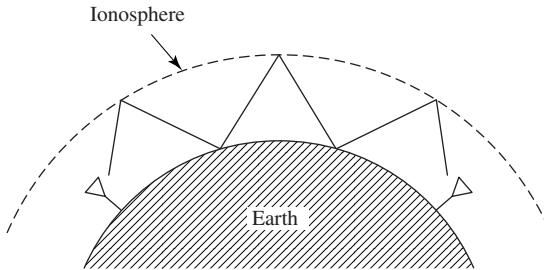


**Figure 1.6** Illustration of sky-wave propagation.

used for AM broadcasting and maritime radio broadcasting. In AM broadcast, the range with ground-wave propagation of even the more powerful radio stations is limited to about 100 miles. Atmospheric noise, man-made noise, and thermal noise from electronic components at the receiver are dominant disturbances for signal transmission of MF.

Sky-wave propagation, as illustrated in Figure 1.6, results from transmitted signals being reflected (bent or refracted) from the ionosphere, which consists of several layers of charged particles ranging in altitude from 30–250 miles above the surface of the earth. During the daytime hours, the heating of the lower atmosphere by the sun causes the formation of the lower layers at altitudes below 75 miles. These lower layers, especially the D-layer serve to absorb frequencies below 2 MHz, thus, severely limiting sky-wave propagation of AM radio broadcast. However, during the night-time hours the electron density in the lower layers of the ionosphere drops sharply and the frequency absorption that occurs during the day time is significantly reduced. As a consequence, powerful AM radio broadcast stations can propagate over large distances via sky-wave over the F-layer of the ionosphere, which ranges from 90–250 miles above the surface of the earth.

A frequently occurring problem with electromagnetic wave propagation via sky-wave in the HF frequency range is *signal multipath*. Signal multipath occurs when the transmitted signal arrives at the receiver via multiple propagation paths at different delays. Signal multipath generally results in intersymbol interference in a digital communication system. Moreover, the signal components arriving via different propagation paths may add destructively, resulting in a phenomenon called *signal fading*, which most people have experienced when listening to a distant radio station at night, when sky-wave is the dominant propagation mode. Additive noise at HF is a combination of atmospheric noise and thermal voice.

Sky-wave ionospheric propagation ceases to exist at frequencies above approximately 30 MHz, which is the end of the HF band. However, it is possible to have

ionospheric scatter propagation at frequencies in the range of 30–60 MHz, resulting from signal scattering from the lower ionosphere. It is also possible to communicate over distances of several hundred miles by use of tropospheric scattering at frequencies in the range of 40–300 MHz. Troposcatter results from signal scattering due to particles in the atmosphere at altitudes of 10 miles or less. Generally, ionospheric scatter and tropospheric scatter involve large signal propagation losses and require a large amount of transmitter power and relatively large antennas.

Frequencies above 30 MHz propagate through the ionosphere with relatively little loss and make satellite and extraterrestrial communications possible. Hence, at frequencies in the VHF band and higher, the dominant mode of electromagnetic propagation is line-of-sight (LOS) propagation. For terrestrial communication systems, this means that the transmitter and receiver antennas must be in direct LOS with relatively little or no obstruction. For this reason television stations transmitting in the VHF and UHF frequency bands mount their antennas on high towers in order to achieve a broad coverage area.

In general, the coverage area for LOS propagation is limited by the curvature of the earth. If the transmitting antenna is mounted at a height  $h$  feet above the surface of the earth, the distance to the radio horizon, assuming no physical obstructions such as a mountains, is approximately  $d = \sqrt{2h}$  miles. For example, a TV antenna mounted on a tower of 1000 ft in height provides a coverage of approximately 50 miles. As another example, microwave radio relay systems used extensively for telephone and video transmission at frequencies above 1 GHz have antennas mounted on tall towers or on the top of tall buildings.

The dominant noise limiting the performance of communication systems in the VHF and UHF frequency ranges is thermal noise generated in the receiver front end and cosmic noise picked up by the antenna. At frequencies in the SHF band above 10 GHz, atmospheric conditions play a major role in signal propagation. Figure 1.7 illustrates the signal attenuation in dB/mile due to precipitation for frequencies in the range of 10–100 GHz. We observe that heavy rain introduces extremely high propagation losses that can result in service outages (total breakdown in the communication system).

At frequencies above the EHF band, we have the infrared and visible light regions of the electromagnetic spectrum which can be used to provide LOS optical communication in free space. To date, these frequency bands have been used in experimental communication systems, such as satellite-to-satellite links.

**Underwater Acoustic Channels.** Over the past few decades, ocean exploration activity has been steadily increasing. Coupled with this increase in ocean exploration is the need to transmit data, collected by sensors placed underwater, to the surface of the ocean. From there it is possible to relay the data via a satellite to a data collection center.

Electromagnetic waves do not propagate over long distances underwater, except at extremely low frequencies. However, the transmission of signals at such low frequencies is prohibitively expensive because of the large and powerful transmitters required. The attenuation of electromagnetic waves in water can be expressed in terms of the *skin*



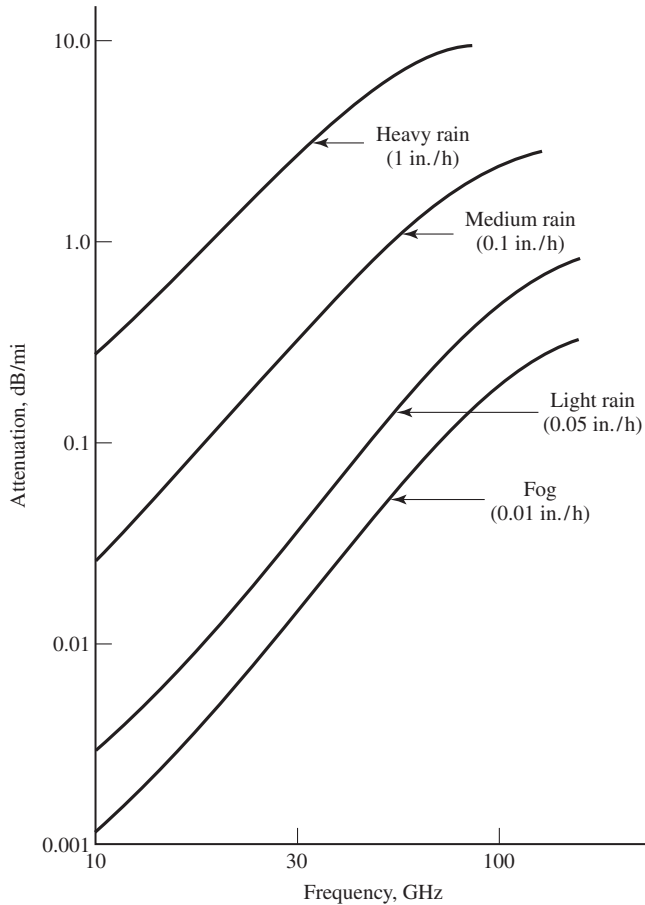


**Figure 1.7** Signal attenuation due to precipitation. (From Ziemer and Tranter (1990); © Houghton Mifflin Reprinted with permission of the publisher.)

*depth*, which is the distance a signal is attenuated by  $1/e$ . For sea water, the skin depth  $\delta = 250/\sqrt{f}$ , where  $f$  is expressed in Hz and  $\delta$  is in meters. For example, at 10 kHz, the skin depth is 2.5 m. In contrast, acoustic signals propagate over distances of tens and even hundreds of kilometers.

A shallow water acoustic channel is characterized as a multipath channel due to signal reflections from the surface and the bottom of the sea. Due to wave motion, the signal multipath components undergo time-varying propagation delays which result in signal fading. In addition, there is frequency-dependent attenuation, which is approximately proportional to the square of the signal frequency.

Ambient ocean acoustic noise is caused by shrimp, fish, and various mammals. Near harbors, there is also man-made acoustic noise in addition to the ambient noise.

In spite of this hostile environment, it is possible to design and implement efficient and highly reliable underwater acoustic communication systems for transmitting digital signals over large distances.

**Storage Channels.** Information storage and retrieval systems constitute a very significant part of our data-handling activities on a daily basis. Magnetic tape, including digital audio tape and video tape, magnetic disks used for storing large amounts of computer data, and optical disks used for computer data storage, music (compact disks), and video are examples of data storage systems that can be characterized as communication channels. The process of storing data on a magnetic tape or a magnetic or optical disk is equivalent to transmitting a signal over a telephone or a radio channel. The readback process and the signal processing involved in storage systems to recover the stored information is equivalent to the functions performed by a receiver in a telephone or radio communication system to recover the transmitted information.

Additive noise generated by the electronic components and interference from adjacent tracks is generally present in the readback signal of a storage system, just as is the case in a telephone or a radio communication system.

The amount of data that can be stored is generally limited by the size of the disk or tape and the density (number of bits stored per square inch) that can be achieved by the write/read electronic systems and heads. For example, a packing density of  $10^9$  bits/sq. in. has been recently demonstrated in an experimental magnetic disk storage system. (Current commercial magnetic storage products achieve a much lower density.) The speed at which data can be written on a disk or tape and the speed at which it can be read back is also limited by the associated mechanical and electrical subsystems that constitute an information storage system.

Channel coding and modulation are essential components of a well-designed digital magnetic or optical storage system. In the readback process, the signal is demodulated and the added redundancy introduced by the channel encoder is used to correct errors in the readback signal.

## 1.4 MATHEMATICAL MODELS FOR COMMUNICATION CHANNELS

In the design of communication systems for transmitting information through physical channels, we find it convenient to construct mathematical models that reflect the most important characteristics of the transmission medium. Then, the mathematical model for the channel is used in the design of the channel encoder and modulator at the transmitter and the demodulator and channel decoder at the receiver. Next, we provide a brief description of the channel models that are frequently used to characterize many of the physical channels that we encounter in practice.

**The Additive Noise Channel.** The simplest mathematical model for a communication channel is the additive noise channel, illustrated in Figure 1.8. In this model the transmitted signal  $s(t)$  is corrupted by an additive random noise process

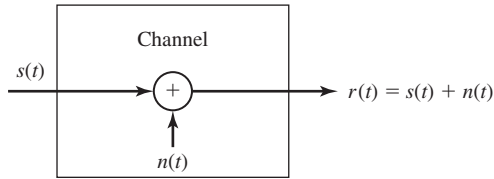


**Figure 1.8** The additive noise channel.

$n(t)$ . Physically, the additive noise process may arise from electronic components and amplifiers at the receiver of the communication system, or from interference encountered in transmission, as in the case of radio signal transmission.

If the noise is introduced primarily by electronic components and amplifiers at the receiver, it may be characterized as thermal noise. This type of noise is characterized statistically as a *Gaussian noise process*. Hence, the resulting mathematical model for the channel is usually called the *additive Gaussian noise channel*. Because this channel model applies to a broad class of physical communication channels and because of its mathematical tractability, this is the predominant channel model used in our communication system analysis and design. Channel attenuation is easily incorporated into the model. When the signal undergoes attenuation in transmission through the channel, the received signal is

$$r(t) = as(t) + n(t) \quad (1.4.1)$$

where  $a$  represents the attenuation factor.

**The Linear Filter Channel.** In some physical channels such as wireline telephone channels, filters are used to ensure that the transmitted signals do not exceed specified bandwidth limitations and, thus, do not interfere with one another. Such channels are generally characterized mathematically as linear filter channels with additive noise, as illustrated in Figure 1.9. Hence, if the channel input is the signal  $s(t)$ , the

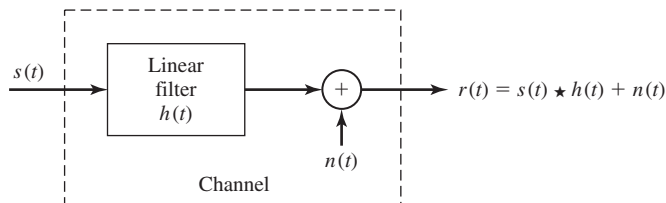


**Figure 1.9** The linear filter channel with additive noise.

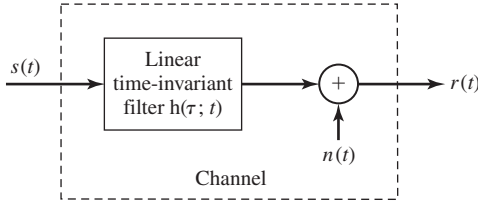


**Figure 1.10** Linear time-variant filter channel with additive noise.

channel output is the signal

$$\begin{aligned} r(t) &= s(t) \star h(t) + n(t) \\ &= \int_{-\infty}^{+\infty} h(\tau) s(t - \tau) d\tau + n(t) \end{aligned} \quad (1.4.2)$$

where  $h(t)$  is the impulse response of the linear filter and  $\star$  denotes convolution.

**The Linear Time-Variant Filter Channel.** Physical channels such as underwater acoustic channels and ionospheric radio channels which result in time-variant multipath propagation of the transmitted signal may be characterized mathematically as time-variant linear filters. Such linear filters are characterized by time-variant channel impulse response  $h(\tau; t)$  where  $h(\tau; t)$  is the response of the channel at time  $t$ , due to an impulse applied at time  $t - \tau$ . Thus,  $\tau$  represents the “age” (elapsed time) variable. The linear time-variant filter channel with additive noise is illustrated Figure 1.10. For an input signal  $s(t)$ , the channel output signal is

$$\begin{aligned} r(t) &= s(t) \star h(\tau; t) + n(t) \\ &= \int_{-\infty}^{+\infty} h(\tau; t) s(t - \tau) d\tau + n(t) \end{aligned} \quad (1.4.3)$$

A good model for multipath signal propagation through physical channels, such as the ionosphere (at frequencies below 30 MHz) and mobile cellular radio channels, is a special case of Equation (1.4.3) in which the time-variant impulse response has the form

$$h(\tau; t) = \sum_{k=1}^L a_k(t) \delta(\tau - \tau_k) \quad (1.4.4)$$

where the  $\{a_k(t)\}$  represent the possibly time-variant attenuation factors for the  $L$  multipath propagation paths. If Equation (1.4.4) is substituted into Equation (1.4.3), the received signal has the form

$$r(t) = \sum_{k=1}^L a_k(t) s(t - \tau_k) + n(t) \quad (1.4.5)$$

Hence, the received signal consists of  $L$  multipath components, where each component is attenuated by  $\{a_k\}$  and delayed by  $\{\tau_k\}$ .

The three mathematical models described above adequately characterize a large majority of physical channels encountered in practice. These three channel models are used in this text for the analysis and design of communication systems.

## 1.5 ORGANIZATION OF THE BOOK

Before we embark on the analysis and design of communication systems, we provide a brief review of basic frequency-domain characteristics of signals and linear systems in Chapter 2. Emphasis is placed on the Fourier series and the Fourier transform representation of signals and the use of transforms in linear systems analysis. The process of sampling a bandlimited analog signal is also considered.

In Chapter 3, we treat the modulation and demodulation of analog signals. This chapter provides detailed description of amplitude modulation (AM), frequency modulation (FM), and phase modulation (PM). As examples of analog signal transmission and reception, we consider radio and television broadcasting, and mobile radio cellular communication systems.

In Chapter 4, we present a review of the basic definitions and concepts in probability and random processes. These topics are particularly important in our study of electrical communications, because information sources produce random signals at their output and communication channels generally corrupt the transmitted signals in a random manner, through the addition of noise and other channel distortion. Special emphasis is placed on Gaussian random processes, which provide mathematically tractable models for additive noise disturbances. Both time domain and frequency domain representations of random signals are presented.

Chapters 5 provides a treatment of the effects of additive noise in the demodulation of amplitude modulated (AM) and angle modulated (FM, PM) analog signals and a comparison of these analog signal modulations in terms of their signal-to-noise ratio performance. Also discussed in this chapter is the problem of estimating the carrier phase using a phase-locked loop (PLL). Finally, we describe the characterization of thermal noise and the effect of transmission losses in analog communication systems.

The remainder of the book is focused on digital communication systems. Chapter 6 is devoted to the modeling and characterization of information sources and source coding. In this chapter, we introduce a measure for the information content of a discrete source and describe two algorithms, the Huffman algorithm and the Lempel-Ziv algorithm, for efficient encoding of the source output. The major part of the chapter is devoted to the problem of encoding the outputs of analog sources. Several waveform-encoding methods are described, including pulse-code modulation (PCM), differential PCM, and delta modulation (DM). We also describe a model-based approach to analog source encoding, based on linear prediction. As practical examples of the theory presented in this chapter, we consider digital audio recording systems, digital audio transmission in telephone systems, and the JPEG image-coding standard.

Chapter 7 treats modulation methods for digital signal transmission through an additive white Gaussian noise channel. Various types of binary and nonbinary

modulation methods are described based on a geometric representation of signals and their performance is evaluated in terms of the probability of error. A link budget analysis for radio communication systems is also described. The final topic of this chapter is focused on signal synchronization methods for digital communication systems.

In Chapter 8, we consider the problem of digital communication through bandlimited, additive white Gaussian noise channels. In particular, we describe the design of bandlimited signal waveforms for such channels and the spectral characteristics of digitally modulated signals. Digitally modulated signals with memory, their modulation, and their spectral characteristics are also described. The effect of channel distortion on the transmitted signals is characterized in terms of intersymbol interference (ISI), and the design of adaptive equalizers for suppressing ISI is described.

Channel coding and decoding is the topic of Chapter 9. In this chapter, we describe the concept of channel capacity, and derive the capacity of an additive white Gaussian noise channel. Linear block codes and convolutional codes are considered for enhancing the performance of a digital communication system in the presence of additive noise. Decoding algorithms for both block codes and convolutional codes are also described. The final topic of this chapter provides a treatment of trellis-coded modulation, which is widely used in the implementation of high speed modems.

The last chapter of the book, Chapter 10, focuses on topics dealing with wireless communications. We begin by characterizing channel fading and multipath effects in wireless communication systems and describe the design of signals that are effective in mitigating these channel distortions. Then, we describe the class of continuous-phase modulated signals, which are especially suitable for digital communications in wireless channels due to their constant amplitude and narrow bandwidth characteristics. Finally, we treat the class of spread-spectrum signals, which are suitable for multi-user wireless communication systems. As examples of practical wireless communication systems, we briefly describe two digital cellular communication systems, the pan European GSM system and the North-American IS-95 CDMA system.

In an introductory book of this level, we have not attempted to provide a large number of references to the technical literature. However, we have included in each chapter several supplementary references for further reading, including textbooks and basic or tutorial treatments of important topics. References are cited by giving the author's name, with the year of publication in parentheses; e.g., Nyquist (1924).

## 1.6 FURTHER READING

We have already cited several historical treatments of radio and telecommunications during the past century. These include the book by McMahan (1984), Ryder and Fink (1984), and Millman (1984). The classical works of Nyquist (1924), Hartley (1928), Kotelnikov (1947), Shannon (1948), and Hamming (1950) are particularly important because they lay the groundwork of modern communication systems engineering.

# 2

## *Frequency Domain Analysis of Signals and Systems*

In this chapter, we review the basics of *signals* and *linear systems* in the frequency domain. The motivation for studying these fundamental concepts stems from the basic role they play in modeling various types of communication systems. In particular signals are used to transmit the information over a communication channel. Such signals are usually called *information-bearing signals*.

In the transmission of an information-bearing signal over a communication channel, the shape of the signal is changed, or *distorted*, by the channel. In other words, the output of the communication channel, which is called the *received signal*, is not an exact replica of the channel input due to the channel distortion. The communication channel is an example of a *system*; i.e., an entity that produces an output signal when excited by an input signal. A large number of communication channels can be modeled closely by a subclass of systems called *linear systems*. Linear systems are a large subclass of systems which arise naturally in many practical applications and are rather easy to analyze. We have devoted this entire chapter to the study of the basics of signals and linear systems in the frequency domain.

### **2.1 FOURIER SERIES**

The analysis of signals and linear systems in the frequency domain is based on representation of signals in terms of the frequency variable and this is done through employing Fourier series and Fourier transforms. Fourier series is applied to periodic signals whereas the Fourier transform can be applied to periodic and nonperiodic signals.

**Theorem 2.1.1. [Fourier Series]** Let the signal  $x(t)$  be a periodic signal with period  $T_0$ . If the following conditions (known as the Dirichlet conditions) are satisfied

1.  $x(t)$  is absolutely integrable over its period; i.e.,

$$\int_0^{T_0} |x(t)| dt < \infty,$$

2. The number of maxima and minima of  $x(t)$  in each period is finite,
3. The number of discontinuities of  $x(t)$  in each period is finite,

then  $x(t)$  can be expanded in terms of the complex exponential signals  $\{e^{j2\pi \frac{n}{T_0} t}\}_{n=-\infty}^{+\infty}$  as

$$x_{\pm}(t) = \sum_{n=-\infty}^{+\infty} x_n e^{j2\pi \frac{n}{T_0} t} \quad (2.1.1)$$

where

$$x_n = \frac{1}{T_0} \int_{\alpha}^{\alpha+T_0} x(t) e^{-j2\pi \frac{n}{T_0} t} dt \quad (2.1.2)$$

for some arbitrary  $\alpha$  and

$$x_{\pm}(t) = \begin{cases} x(t) & \text{if } x(t) \text{ is continuous at } t \\ \frac{x(t^+) + x(t^-)}{2} & \text{if } x(t) \text{ is discontinuous at } t \end{cases} \quad (2.1.3)$$

■

Some observations concerning this theorem are in order.

- The coefficients  $x_n$  are called the Fourier series coefficients of the signal  $x(t)$ . These are, in general, complex numbers.
- The parameter  $\alpha$  in the limits of the integral is arbitrary. It can be chosen to simplify computation of the integral. Usually  $\alpha = 0$  or  $\alpha = -T_0/2$  are good choices.
- For all practical purposes,  $x_{\pm}(t)$  equals  $x(t)$ . From now on, we will use  $x(t)$  instead of  $x_{\pm}(t)$  but will keep in mind that the Fourier series expansion, at points of discontinuity of  $x(t)$ , gives the midpoint between right and left limits of the signal.
- The Dirichlet conditions are only sufficient conditions for the existence of the Fourier series expansion. For some signals that do not satisfy these conditions, we can still find the Fourier series expansion.
- The quantity  $f_0 = \frac{1}{T_0}$  is called the *fundamental frequency* of the signal  $x(t)$ . We observe that the frequencies of the complex exponential signals are multiples of this fundamental frequency. The  $n$ th multiple of the fundamental frequency (for positive  $n$ 's) is called the  $n$ th *harmonic*.



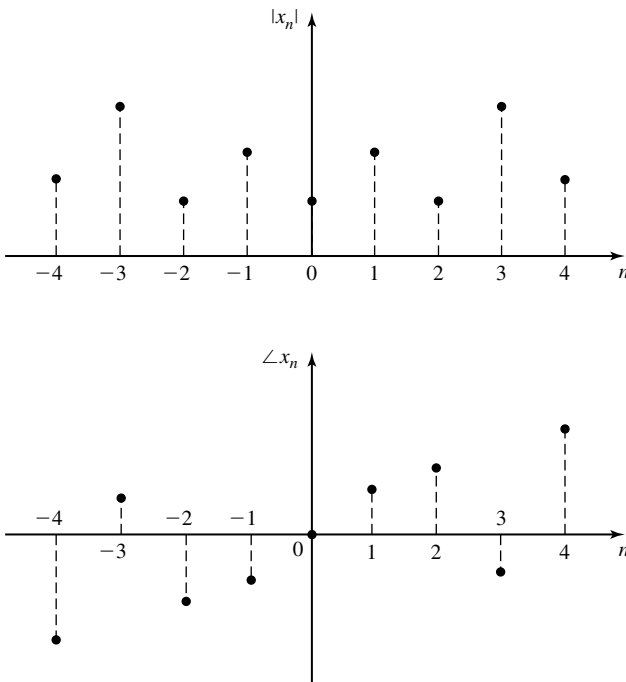
- Conceptually this is a very important result. It states that the periodic signal  $x(t)$  can be described by the period  $T_0$  (or fundamental frequency  $f_0$ ) and the sequence of complex numbers  $\{x_n\}$ ; i.e., to describe  $x(t)$  it is sufficient to specify a *countable* set of (in general complex) numbers. This is a considerable reduction in complexity for describing  $x(t)$ , since to define  $x(t)$  for all  $t$ , we have to specify its values on an *uncountable* set of points.
- The Fourier series expansion can be expressed in terms of the angular frequency  $\omega_0 = 2\pi f_0$ , by

$$x_n = \frac{\omega_0}{2\pi} \int_{\alpha}^{\alpha + \frac{2\pi}{\omega_0}} x(t) e^{-jn\omega_0 t} dt \quad (2.1.4)$$

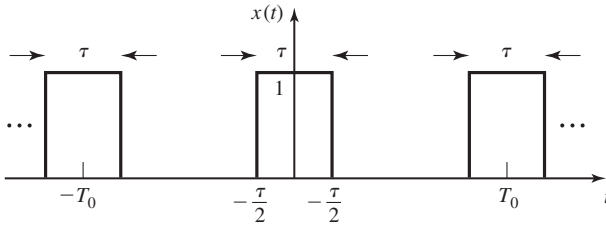
and

$$x(t) = \sum_{n=-\infty}^{+\infty} x_n e^{jn\omega_0 t} \quad (2.1.5)$$

- In general,  $x_n = |x_n|e^{j\angle x_n}$ .  $|x_n|$  gives the magnitude of the  $n$ th harmonic and  $\angle x_n$  gives its phase. Figure 2.1 shows a graph of the magnitude and phase of various harmonics in  $x(t)$ . This type of graph is called the *discrete spectrum* of the periodic signal  $x(t)$ .



**Figure 2.1** The discrete spectrum of  $x(t)$ .

Figure 2.2 Periodic signal  $x(t)$ .**Example 2.1.1**

Let  $x(t)$  denote the periodic signal depicted in Figure 2.2 and described analytically by

$$x(t) = \sum_{n=-\infty}^{+\infty} \Pi\left(\frac{t - nT_0}{\tau}\right) \quad (2.1.6)$$

where

$$\Pi(t) = \begin{cases} 1, & |t| < \frac{1}{2} \\ \frac{1}{2}, & |t| = \frac{1}{2} \\ 0, & \text{otherwise} \end{cases}$$

is a rectangular pulse. Determine the Fourier series expansion for this signal.

**Solution** We first observe that the period of the signal is  $T_0$  and

$$\begin{aligned} x_n &= \frac{1}{T_0} \int_{-\frac{T_0}{2}}^{+\frac{T_0}{2}} x(t) e^{-jn\frac{2\pi t}{T_0}} dt \\ &= \frac{1}{T_0} \int_{-\frac{\tau}{2}}^{+\frac{\tau}{2}} 1 e^{-jn\frac{2\pi t}{T_0}} dt \\ &= \frac{1}{T_0} \frac{T_0}{-jn2\pi} [e^{-jn\frac{\pi\tau}{T_0}} - e^{+jn\frac{\pi\tau}{T_0}}] \\ &= \frac{1}{\pi n} \sin\left(\frac{n\pi\tau}{T_0}\right) \\ &= \frac{\tau}{T_0} \operatorname{sinc}\left(\frac{n\tau}{T_0}\right) \end{aligned} \quad (2.1.7)$$

where we have used the definition of the sinc function  $\operatorname{sinc}(t) = \sin(\pi t)/(\pi t)$ . Therefore,

$$x(t) = \sum_{n=-\infty}^{+\infty} \frac{\tau}{T_0} \operatorname{sinc}\left(\frac{n\tau}{T_0}\right) e^{jn\frac{2\pi t}{T_0}} \quad (2.1.8)$$

A graph of the Fourier series coefficients for is shown in Figure 2.3.

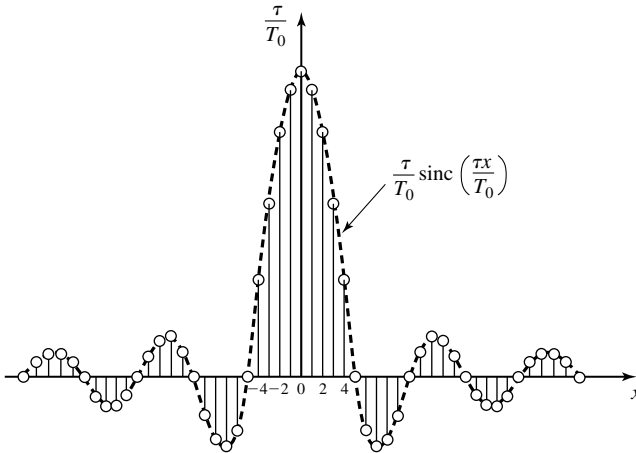


**Figure 2.3** The discrete spectrum of the rectangular pulse train.

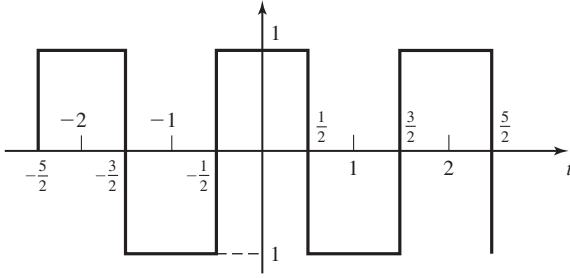
### Example 2.1.2

Determine the Fourier series expansion for the signal  $x(t)$  shown in Figure 2.4 and described by

$$x(t) = \sum_{n=-\infty}^{+\infty} (-1)^n \Pi(t - n) \quad (2.1.9)$$

**Solution** Here  $T_0 = 2$  and it is convenient to choose  $\alpha = -\frac{1}{2}$ . Then,

$$\begin{aligned} x_n &= \frac{1}{2} \int_{-\frac{1}{2}}^{\frac{3}{2}} x(t) e^{-jn\pi t} dt \\ &= \frac{1}{2} \int_{-\frac{1}{2}}^{\frac{1}{2}} e^{-jn\pi t} dt - \frac{1}{2} \int_{\frac{1}{2}}^{\frac{3}{2}} e^{-jn\pi t} dt \\ &= -\frac{1}{j2\pi n} [e^{-j\frac{n\pi}{2}} - e^{j\frac{n\pi}{2}}] - \frac{1}{-j2\pi n} [e^{-jn\frac{3\pi}{2}} - e^{-jn\frac{\pi}{2}}] \\ &= \frac{1}{n\pi} \sin\left(\frac{n\pi}{2}\right) - \frac{1}{n\pi} e^{-jn\pi} \sin\left(\frac{n\pi}{2}\right) \\ &= \frac{1}{n\pi} (1 - \cos(n\pi)) \sin\left(\frac{n\pi}{2}\right) \\ &= \begin{cases} \frac{2}{n\pi} & n = 4k + 1 \\ -\frac{2}{n\pi} & n = 4k + 3 \\ 0 & n \text{ even} \end{cases} \end{aligned}$$

Figure 2.4 Signal  $x(t)$ .

From these values of  $x_n$  we have the following Fourier series expansion for  $x(t)$

$$\begin{aligned}
 x(t) &= \frac{2}{\pi}(e^{j\pi t} + e^{-j\pi t}) - \frac{2}{3\pi}(e^{j3\pi t} + e^{-j3\pi t}) + \frac{2}{5\pi}(e^{j5\pi t} + e^{-j5\pi t}) - \dots \\
 &= \frac{4}{\pi} \cos(\pi t) - \frac{4}{3\pi} \cos(3\pi t) + \frac{4}{5\pi} \cos(5\pi t) - \dots \\
 &= \frac{4}{\pi} \sum_{k=0}^{\infty} \frac{(-1)^k}{2k+1} \cos(2k+1)\pi t
 \end{aligned} \tag{2.1.10}$$

### 2.1.1 Fourier Series for Real Signals: the Trigonometric Fourier Series

If the signal  $x(t)$  is a real signal satisfying the conditions of the Fourier series theorem, then there exist alternative ways to expand the signal. For real  $x(t)$ , we have

$$\begin{aligned}
 x_{-n} &= \frac{1}{T_0} \int_{\alpha}^{\alpha+T_0} x(t) e^{j2\pi \frac{n}{T_0} t} dt \\
 &= \left[ \frac{1}{T_0} \int_{\alpha}^{\alpha+T_0} x(t) e^{-j2\pi \frac{n}{T_0} t} dt \right]^* \\
 &= x_n^*
 \end{aligned} \tag{2.1.11}$$

This means that for a real, periodic  $x(t)$ , the positive and negative coefficients are conjugates. Hence,  $|x_n|$  has even symmetry and  $\angle x_n$  has odd symmetry with respect to the  $n = 0$  axis. An example of the discrete spectrum for a real signal is shown in Figure 2.5.

From  $x_{-n} = x_n^*$  it follows that if we denote  $x_n = \frac{a_n - jb_n}{2}$ , then  $x_{-n} = \frac{a_n + jb_n}{2}$  and therefore, for  $n \geq 1$ ,

$$x_n e^{j2\pi \frac{n}{T_0} t} + x_{-n} e^{-j2\pi \frac{n}{T_0} t} = \frac{a_n - jb_n}{2} e^{j2\pi \frac{n}{T_0} t} + \frac{a_n + jb_n}{2} e^{-j2\pi \frac{n}{T_0} t} \tag{2.1.12}$$

$$= a_n \cos\left(2\pi \frac{n}{T_0} t\right) + b_n \sin\left(2\pi \frac{n}{T_0} t\right) \tag{2.1.13}$$

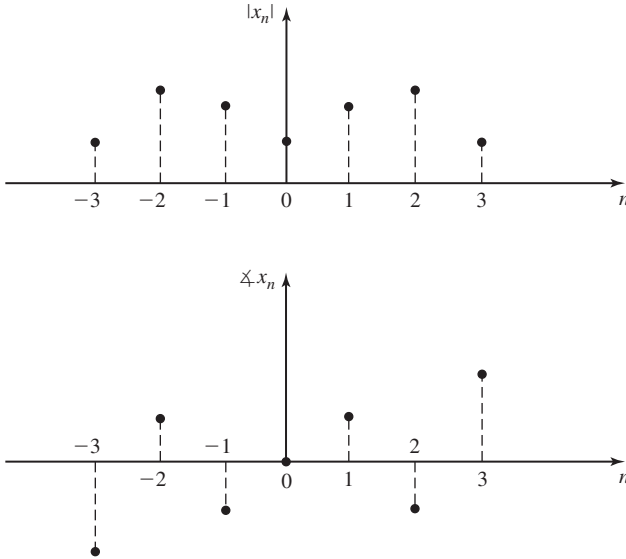


**Figure 2.5** Discrete spectrum of a real-valued signal.

Since  $x_0$  is real and given as  $x_0 = \frac{a_0}{2}$ , we conclude that

$$x(t) = \frac{a_0}{2} + \sum_{n=1}^{\infty} \left[ a_n \cos \left( 2\pi \frac{n}{T_0} t \right) + b_n \sin \left( 2\pi \frac{n}{T_0} t \right) \right] \quad (2.1.14)$$

This relation, which only holds for a real periodic signal  $x(t)$ , is called the *trigonometric Fourier series expansion*. To obtain  $a_n$  and  $b_n$ , we have

$$x_n = \frac{a_n - jb_n}{2} = \frac{1}{T_0} \int_{\alpha}^{\alpha+T_0} x(t) e^{-j2\pi \frac{n}{T_0} t} dt,$$

and, therefore,

$$\frac{a_n - jb_n}{2} = \frac{1}{T_0} \int_{\alpha}^{\alpha+T_0} x(t) \cos \left( 2\pi \frac{n}{T_0} t \right) dt - \frac{j}{T_0} \int_{\alpha}^{\alpha+T_0} x(t) \sin \left( 2\pi \frac{n}{T_0} t \right) dt$$

From this we obtain

$$a_n = \frac{2}{T_0} \int_{\alpha}^{\alpha+T_0} x(t) \cos \left( 2\pi \frac{n}{T_0} t \right) dt \quad (2.1.15)$$

$$b_n = \frac{2}{T_0} \int_{\alpha}^{\alpha+T_0} x(t) \sin \left( 2\pi \frac{n}{T_0} t \right) dt \quad (2.1.16)$$

There exists still a third way to represent the Fourier series expansion of a real signal. Noting that

$$x_n e^{j2\pi \frac{n}{T_0} t} + x_{-n} e^{-j2\pi \frac{n}{T_0} t} = 2|x_n| \cos\left(2\pi \frac{n}{T_0} t + \angle x_n\right) \quad (2.1.17)$$

we have

$$x(t) = x_0 + 2 \sum_{n=1}^{\infty} |x_n| \cos\left(2\pi \frac{n}{T_0} t + \angle x_n\right) \quad (2.1.18)$$

In summary, for a real periodic signal  $x(t)$ , we have three alternative ways to represent the Fourier series expansion

$$x(t) = \sum_{n=-\infty}^{+\infty} x_n e^{j2\pi \frac{n}{T_0} t} \quad (2.1.19)$$

$$= \frac{a_0}{2} + \sum_{n=1}^{\infty} \left[ a_n \cos\left(2\pi \frac{n}{T_0} t\right) + b_n \sin\left(2\pi \frac{n}{T_0} t\right) \right] \quad (2.1.20)$$

$$= x_0 + 2 \sum_{n=1}^{\infty} |x_n| \cos\left(2\pi \frac{n}{T_0} t + \angle x_n\right) \quad (2.1.21)$$

where the corresponding coefficients are obtained from

$$x_n = \frac{1}{T_0} \int_{\alpha}^{\alpha+T_0} x(t) e^{-j2\pi \frac{n}{T_0} t} dt = \frac{a_n}{2} - j \frac{b_n}{2} \quad (2.1.22)$$

$$a_n = \frac{2}{T_0} \int_{\alpha}^{\alpha+T_0} x(t) \cos\left(2\pi \frac{n}{T_0} t\right) dt \quad (2.1.23)$$

$$b_n = \frac{2}{T_0} \int_{\alpha}^{\alpha+T_0} x(t) \sin\left(2\pi \frac{n}{T_0} t\right) dt \quad (2.1.24)$$

$$|x_n| = \frac{1}{2} \sqrt{a_n^2 + b_n^2} \quad (2.1.25)$$

$$\angle x_n = -\arctan\left(\frac{b_n}{a_n}\right) \quad (2.1.26)$$

## 2.2 FOURIER TRANSFORMS

The Fourier transform is the extension of the Fourier series to the general class of signals (periodic and nonperiodic). Here, as in Fourier series, the signals are expressed in terms of complex exponentials of various frequencies, but these frequencies are not discrete. Hence, in this case, the signal has a *continuous spectrum* as opposed to a discrete spectrum.

We can formally state the Fourier transform theorem as follows.

**Theorem 2.2.1. [Fourier Transform]** If the signal  $x(t)$  satisfies certain conditions known as the Dirichlet conditions, namely,

1.  $x(t)$  is absolutely integrable on the real line; i.e.,

$$\int_{-\infty}^{+\infty} |x(t)| dt < \infty,$$

2. The number of maxima and minima of  $x(t)$  in any finite interval on the real line is finite,
  3. The number of discontinuities of  $x(t)$  in any finite interval on the real line is finite,
- then, the Fourier transform (or Fourier integral) of  $x(t)$ , defined by

$$X(f) = \int_{-\infty}^{+\infty} x(t)e^{-j2\pi ft} dt \quad (2.2.1)$$

exists and the original signal can be obtained from its Fourier transform by

$$x_{\pm}(t) = \int_{-\infty}^{+\infty} X(f)e^{j2\pi ft} df \quad (2.2.2)$$

where  $x_{\pm}(t)$  is defined as in Theorem 2.1.1. ■

We make the following observations concerning the Fourier transform.

- $X(f)$  is in general a complex function. Its magnitude  $|X(f)|$  and phase  $\angle X(f)$  represent the amplitude and phase of various frequency components in  $x(t)$ . The function  $X(f)$  is sometimes referred to as the *spectrum*<sup>†</sup> of the signal  $x(t)$ .
- To denote that  $X(f)$  is the Fourier transform of  $x(t)$ , the following notation is frequently employed

$$X(f) = \mathcal{F}[x(t)]$$

To denote that  $x(t)$  is the *inverse Fourier transform* of  $X(f)$ , the following notation is used

$$x(t) = \mathcal{F}^{-1}[X(f)]$$

Sometimes the following notation is used as a shorthand for both relations

$$x(t) \Leftrightarrow X(f)$$

- If the variable in the Fourier transform is chosen to be  $\omega$  rather than  $f$ , then we have

$$X(\omega) = \int_{-\infty}^{+\infty} x(t)e^{-j\omega t} dt$$

<sup>†</sup>Sometimes  $X(f)$  is referred to as *voltage spectrum*, as opposed to *power spectrum* to be defined later.

and

$$x(t) = \frac{1}{2\pi} \int_{-\infty}^{+\infty} X(\omega) e^{j\omega t} d\omega$$

- The Fourier transform and the inverse Fourier transform relations can be written as

$$\begin{aligned} x(t) &= \int_{-\infty}^{+\infty} \left[ \int_{-\infty}^{+\infty} x(\tau) e^{-j2\pi f\tau} d\tau \right] e^{j2\pi ft} df \\ &= \int_{-\infty}^{+\infty} \left[ \int_{-\infty}^{+\infty} e^{j2\pi f(t-\tau)} df \right] x(\tau) d\tau \end{aligned} \quad (2.2.3)$$

On the other hand,

$$x(t) = \int_{-\infty}^{+\infty} \delta(t - \tau) x(\tau) d\tau \quad (2.2.4)$$

where  $\delta(t)$  is the unit impulse, which is defined as a signal that is zero everywhere except at  $t = 0$  and has unit area. Comparing Equation (2.2.3) with Equation (2.2.4), we obtain

$$\delta(t - \tau) = \int_{-\infty}^{+\infty} e^{j2\pi f(t-\tau)} df \quad (2.2.5)$$

or, in general,

$$\delta(t) = \int_{-\infty}^{+\infty} e^{j2\pi ft} df \quad (2.2.6)$$

Hence, the spectrum of  $\delta(t)$  is equal to unity over all frequencies.

### Example 2.2.1

Determine the Fourier transform of the signal  $\Pi(t)$ .

**Solution** We have

$$\begin{aligned} \mathcal{F}[\Pi(t)] &= \int_{-\infty}^{+\infty} \Pi(t) e^{-j2\pi ft} dt \\ &= \int_{-\frac{1}{2}}^{+\frac{1}{2}} e^{-j2\pi ft} dt \\ &= \frac{1}{-j2\pi f} [e^{-j\pi f} - e^{j\pi f}] \\ &= \frac{\sin \pi f}{\pi f} \\ &= \text{sinc}(f) \end{aligned} \quad (2.2.7)$$



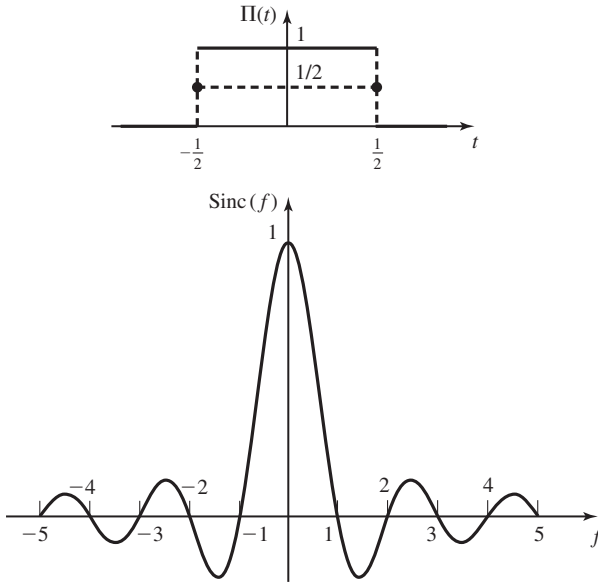


**Figure 2.6**  $\Pi(t)$  and its Fourier transform.

Therefore,

$$\mathcal{F}[\Pi(t)] = \text{sinc}(f)$$

Figure 2.6 illustrates the Fourier transform relationship for this signal.

### Example 2.2.2

Find the Fourier transform of an impulse signal  $x(t) = \delta(t)$ .

**Solution** The Fourier transform can be obtained by

$$\begin{aligned} \mathcal{F}[\delta(t)] &= \int_{-\infty}^{+\infty} \delta(t) e^{-j2\pi ft} dt \\ &= 1 \end{aligned} \tag{2.2.8}$$

where we have used the sifting property of  $\delta(t)$ .<sup>†</sup> This shows that all frequencies are present in the spectrum of  $\delta(t)$  with unity magnitude and zero phase. The graphs of  $x(t)$  and its Fourier transform are given in Figure 2.7. Similarly from the relation

$$\int_{-\infty}^{+\infty} \delta(f) e^{j2\pi ft} dt = 1$$

we conclude that

$$\mathcal{F}[1] = \delta(f)$$

<sup>†</sup>The sifting property of  $\delta(t)$  states that  $\int_{-\infty}^{\infty} x(t)\delta(t - t_0) dt = x(t_0)$ .

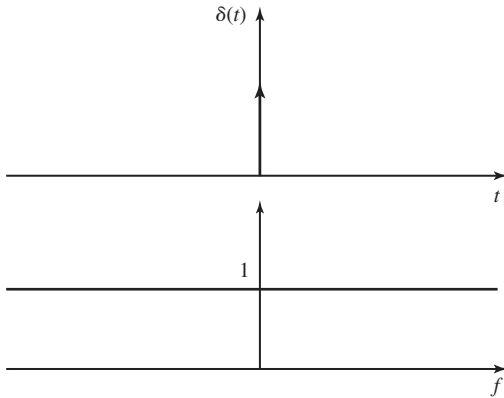


**Figure 2.7** Impulse signal and its spectrum.

### 2.2.1 Fourier Transform of Real, Even, and Odd Signals

The Fourier transform relation can be written in general as

$$\begin{aligned}\mathcal{F}[x(t)] &= \int_{-\infty}^{+\infty} x(t)e^{-j2\pi ft} dt \\ &= \int_{-\infty}^{+\infty} x(t) \cos(2\pi ft) dt - j \int_{-\infty}^{+\infty} x(t) \sin(2\pi ft) dt\end{aligned}$$

For real  $x(t)$ , both integrals

$$\int_{-\infty}^{+\infty} x(t) \cos(2\pi ft) dt$$

and

$$\int_{-\infty}^{+\infty} x(t) \sin(2\pi ft) dt$$

are real and therefore denote the real and imaginary parts of  $X(f)$ , respectively. Since cosine is an even function and sine is an odd function, we see that for real  $x(t)$  the real part of  $X(f)$  is an even function of  $f$  and the imaginary part is an odd function of  $f$ . Therefore, in general, for real  $x(t)$ , the transform  $X(f)$  is a Hermitian function

$$X(-f) = X^*(f)$$

This is equivalent to the following relations:

$$\operatorname{Re}[X(-f)] = \operatorname{Re}[X(f)]$$

$$\operatorname{Im}[X(-f)] = -\operatorname{Im}[X(f)]$$

$$|X(-f)| = |X(f)|$$

$$\angle X(-f) = -\angle X(f)$$

Typical plots of  $|X(f)|$  and  $\angle X(f)$  for a real  $x(t)$  are given in Figure 2.8.

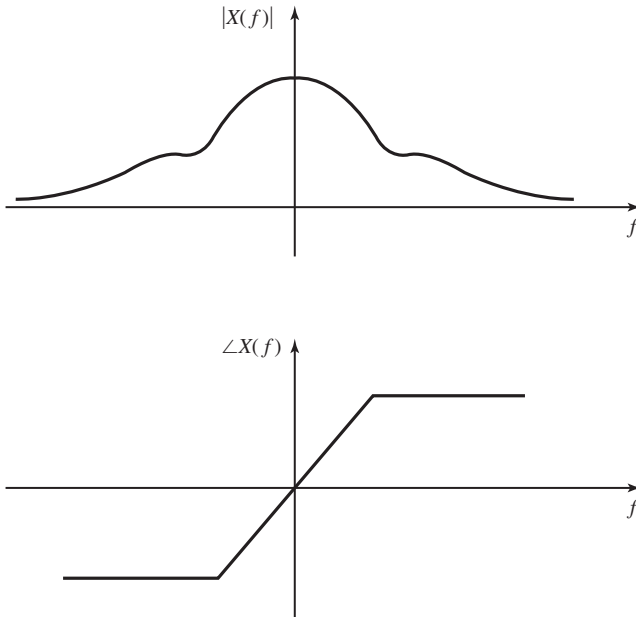


**Figure 2.8** Magnitude and phase of the spectrum of a real signal.

If in addition to being real,  $x(t)$  is an even signal, then the integral

$$\int_{-\infty}^{+\infty} x(t) \sin(2\pi ft) dt$$

vanishes because the integrand is the product of an even and odd signal and, therefore, odd. Hence, the Fourier transform  $X(f)$  will be real and even. Similarly if  $x(t)$  is real and odd, the real part of its Fourier transform vanishes and  $X(f)$  will be imaginary and odd.

### 2.2.2 Basic Properties of the Fourier Transform

In this section, we summarize the basic properties of the Fourier transform.

**Linearity Property.** The Fourier transform operation is linear. That is, if  $x_1(t)$  and  $x_2(t)$  are signals possessing Fourier transforms  $X_1(f)$  and  $X_2(f)$ , respectively, the Fourier transform of  $\alpha x_1(t) + \beta x_2(t)$  is  $\alpha X_1(f) + \beta X_2(f)$ , where  $\alpha$  and  $\beta$  are two arbitrary (real or complex) scalars.

**Duality Property.** If

$$X(f) = \mathcal{F}[x(t)]$$

then

$$x(f) = \mathcal{F}[X(-t)]$$

and

$$x(-f) = \mathcal{F}[X(t)]$$

**Time Shift Property.** A shift of  $t_0$  in the time origin causes a phase shift of  $-2\pi f t_0$  in the frequency domain. In other words,

$$\mathcal{F}[x(t - t_0)] = e^{-j2\pi f t_0} \mathcal{F}[x(t)]$$

**Scaling Property.** For any real  $a \neq 0$ , we have

$$\mathcal{F}[x(at)] = \frac{1}{|a|} X\left(\frac{f}{a}\right) \quad (2.2.9)$$

**Convolution Property.** If the signals  $x(t)$  and  $y(t)$  both possess Fourier transforms, then

$$\mathcal{F}[x(t) \star y(t)] = \mathcal{F}[x(t)] \cdot \mathcal{F}[y(t)] = X(f) \cdot Y(f) \quad (2.2.10)$$

**Modulation Property.** The Fourier transform of  $x(t)e^{j2\pi f_0 t}$  is  $X(f - f_0)$ , and the Fourier transform of

$$x(t) \cos(2\pi f_0 t)$$

is

$$\frac{1}{2}X(f - f_0) + \frac{1}{2}X(f + f_0)$$

**Parseval's Property.** If the Fourier transforms of the signals  $x(t)$  and  $y(t)$  are denoted by  $X(f)$  and  $Y(f)$ , respectively, then

$$\int_{-\infty}^{\infty} x(t)y^*(t) dt = \int_{-\infty}^{\infty} X(f)Y^*(f) df \quad (2.2.11)$$

**Rayleigh's Property.** If  $X(f)$  is the Fourier transform of  $x(t)$ , then

$$\int_{-\infty}^{\infty} |x(t)|^2 dt = \int_{-\infty}^{\infty} |X(f)|^2 df$$

**Autocorrelation Property.** The (time) autocorrelation function of the signal  $x(t)$  is denoted by  $R_x(\tau)$  and is defined by

$$R_x(\tau) = \int_{-\infty}^{\infty} x(t)x^*(t - \tau) dt \quad (2.2.12)$$

The autocorrelation property states that

$$\mathcal{F}[R_x(\tau)] = |X(f)|^2 \quad (2.2.13)$$

**Differentiation Property.** The Fourier transform of the derivative of a signal can be obtained from the relation

$$\mathcal{F}\left[\frac{d}{dt}x(t)\right] = j2\pi f X(f) \quad (2.2.14)$$

**Integration Property.** The Fourier transform of the integral of a signal can be determined from the relation

$$\mathcal{F} \left[ \int_{-\infty}^t x(\tau) d\tau \right] = \frac{X(f)}{j2\pi f} + \frac{1}{2} X(0) \delta(f) \quad (2.2.15)$$

**Moments Property.** If  $\mathcal{F}[x(t)] = X(f)$ , then  $\int_{-\infty}^{\infty} t^n x(t) dt$ , the  $n$ th moment of  $x(t)$ , can be obtained from the relation

$$\int_{-\infty}^{\infty} t^n x(t) dt = \left( \frac{j}{2\pi} \right)^n \frac{d^n}{df^n} X(f) \Big|_{f=0} \quad (2.2.16)$$

Table 2.1 gives a collection of frequently used Fourier transform pairs.

**TABLE 2.1** TABLE OF FOURIER TRANSFORMS

Time Domain ( $x(t)$ )	Frequency Domain ( $X(f)$ )
$\delta(t)$	1
1	$\delta(f)$
$\delta(t - t_0)$	$e^{-j2\pi f t_0}$
$e^{j2\pi f_0 t}$	$\delta(f - f_0)$
$\cos(2\pi f_0 t)$	$\frac{1}{2} \delta(f - f_0) + \frac{1}{2} \delta(f + f_0)$
$\sin(2\pi f_0 t)$	$-\frac{1}{2j} \delta(f + f_0) + \frac{1}{2j} \delta(f - f_0)$
$\Pi(t) = \begin{cases} 1, &  t  < \frac{1}{2} \\ \frac{1}{2}, & t = \pm \frac{1}{2} \\ 0, & \text{otherwise} \end{cases}$	$\text{sinc}(f)$
$\text{sinc}(t)$	$\Pi(f)$
$\Lambda(t) = \begin{cases} t + 1, & -1 \leq t < 0 \\ -t + 1, & 0 \leq t < 1 \\ 0, & \text{otherwise} \end{cases}$	$\text{sinc}^2(f)$
$\text{sinc}^2(t)$	$\Lambda(f)$
$e^{-\alpha t} u_{-1}(t), \alpha > 0$	$\frac{1}{\alpha + j2\pi f}$
$t e^{-\alpha t} u_{-1}(t), \alpha > 0$	$\frac{1}{(\alpha + j2\pi f)^2}$
$e^{-\alpha t }$	$\frac{2\alpha}{\alpha^2 + (2\pi f)^2}$
$e^{-\pi t^2}$	$e^{-\pi f^2}$
$\text{sgn}(t) = \begin{cases} 1, & t > 0 \\ -1, & t < 0 \\ 0, & t = 0 \end{cases}$	$1/(j\pi f)$
$u_{-1}(t)$	$\frac{1}{2} \delta(f) + \frac{1}{j2\pi f}$
$\delta'(t)$	$j2\pi f$
$\delta^{(n)}(t)$	$(j2\pi f)^n$
$\frac{1}{t}$	$-j\pi \text{sgn}(f)$
$\sum_{n=-\infty}^{n=+\infty} \delta(t - nT_0)$	$\frac{1}{T_0} \sum_{n=-\infty}^{n=+\infty} \delta\left(f - \frac{n}{T_0}\right)$

### 2.2.3 Fourier Transform for Periodic Signals

In this section, we extend the results already obtained to develop methods for finding the Fourier transform of periodic signals. We have already included the Fourier transform for some periodic signals (see Table 2.1). These include  $e^{j2\pi f_0 t}$ ,  $\cos(2\pi f_0 t)$ ,  $\sin(2\pi f_0 t)$ , and  $\sum_{n=-\infty}^{+\infty} \delta(t - nT_0)$ . The common property of the Fourier transform of all these periodic signals is that the Fourier transform consists of impulse functions in the frequency domain. We will show in this section that this property holds for all periodic signals and in fact there exists a close relationship between the Fourier transform of a periodic signal and the Fourier series representation of the signal.

Let  $x(t)$  be a periodic signal with period  $T_0$ , satisfying the Dirichlet conditions. Let  $\{x_n\}$  denote the Fourier series coefficients corresponding to this signal. Then

$$x(t) = \sum_{n=-\infty}^{\infty} x_n e^{j2\pi \frac{n}{T_0} t}$$

By taking the Fourier transform of both sides and using the fact that

$$\mathcal{F}[e^{j2\pi \frac{n}{T_0} t}] = \delta\left(f - \frac{n}{T_0}\right)$$

we obtain

$$X(f) = \sum_{n=-\infty}^{\infty} x_n \delta\left(f - \frac{n}{T_0}\right) \quad (2.2.17)$$

From this relation we observe that the Fourier transform of a periodic signal  $x(t)$  consists of a sequence of impulses in frequency at multiples of the fundamental frequency of the periodic signal. The weights of the impulses are just the Fourier series coefficients of the periodic signal. This relation gives a shortcut for computing Fourier series coefficients of a signal using the properties of the Fourier transform. If we define the truncated signal  $x_{T_0}(t)$  as

$$x_{T_0}(t) = \begin{cases} x(t) & -\frac{T_0}{2} < t \leq \frac{T_0}{2} \\ 0, & \text{otherwise} \end{cases} \quad (2.2.18)$$

we see that

$$x(t) = \sum_{n=-\infty}^{\infty} x_{T_0}(t - nT_0) \quad (2.2.19)$$

Noting that  $x_{T_0}(t - nT_0) = x_{T_0}(t) \star \delta(t - nT_0)$ , we have

$$x(t) = x_{T_0}(t) \star \sum_{n=-\infty}^{\infty} \delta(t - nT_0) \quad (2.2.20)$$

Therefore, using the convolution theorem and Table 2.1, we obtain

$$X(f) = X_{T_0}(f) \left[ \frac{1}{T_0} \sum_{n=-\infty}^{\infty} \delta \left( f - \frac{n}{T_0} \right) \right] \quad (2.2.21)$$

which simplifies to

$$X(f) = \frac{1}{T_0} \sum_{n=-\infty}^{\infty} X_{T_0} \left( \frac{n}{T_0} \right) \delta \left( f - \frac{n}{T_0} \right) \quad (2.2.22)$$

Comparing this result with

$$X(f) = \sum_{n=-\infty}^{\infty} x_n \delta \left( f - \frac{n}{T_0} \right) \quad (2.2.23)$$

we conclude that

$$x_n = \frac{1}{T_0} X_{T_0} \left( \frac{n}{T_0} \right) \quad (2.2.24)$$

This equation gives an alternative way to find the Fourier series coefficients. Given the periodic signal  $x(t)$ , we carry out the following steps to find  $x_n$ :

1. First, we find the truncated signal  $x_{T_0}(t)$ .
2. Then, we determine the Fourier transform of the truncated signal using Table 2.1 and the Fourier transform theorems and properties.
3. Finally, we evaluate the Fourier transform of the truncated signal at  $f = \frac{n}{T_0}$ , to obtain the  $n$ th harmonic and multiply by  $\frac{1}{T_0}$ .

### Example 2.2.3

Determine the Fourier series coefficients of the signal  $x(t)$  shown in Figure 2.2 on page 27.

**Solution** We follow the preceding steps. The truncated signal is

$$x_{T_0}(t) = \Pi \left( \frac{t}{\tau} \right)$$

and its Fourier transform is

$$X_{T_0}(f) = \tau \operatorname{sinc}(\tau f)$$

Therefore,

$$x_n = \frac{\tau}{T_0} \operatorname{sinc} \left( \frac{n\tau}{T_0} \right) \quad (2.2.25)$$

## 2.3 POWER AND ENERGY

The energy and power of a signal are representatives of the energy or power delivered by the signal when the signal is interpreted as a voltage or current source feeding a

1 ohm resistor. The energy content of a signal  $x(t)$ , denoted by  $E_x$ , is defined as

$$E_x = \int_{-\infty}^{\infty} |x(t)|^2 dt$$

and the power content of a signal is

$$P_x = \lim_{T \rightarrow \infty} \frac{1}{T} \int_{-\frac{T}{2}}^{+\frac{T}{2}} |x(t)|^2 dt$$

A signal is energy-type if  $E_x < \infty$  and is power-type if  $0 < P_x < \infty$ . A signal *cannot* be both power- and energy-type because for energy-type signals  $P_x = 0$  and for power-type signals  $E_x = \infty$ . A signal can be neither energy-type nor power-type. An example of such a signal is given in Problem 2.30. However, most of the signals of interest are either energy-type or power-type. All periodic signals (with the exception of  $x(t) \equiv 0$ ) are power-type and have power

$$P_x = \frac{1}{T_0} \int_{\alpha}^{\alpha+T_0} |x(t)|^2 dt$$

where  $T_0$  is the period and  $\alpha$  is any arbitrary real number.

### 2.3.1 Energy-Type Signals

For an energy-type signal  $x(t)$ , we define the autocorrelation function  $R_x(\tau)$  as

$$\begin{aligned} R_x(\tau) &= x(\tau) \star x^*(-\tau) \\ &= \int_{-\infty}^{\infty} x(t)x^*(t-\tau) dt \\ &= \int_{-\infty}^{\infty} x(t+\tau)x^*(t) dt \end{aligned} \quad (2.3.1)$$

By setting  $\tau = 0$  in the definition of the autocorrelation function of  $x(t)$ , we obtain the energy content of it; i.e.,

$$\begin{aligned} \mathcal{E}_x &= \int_{-\infty}^{\infty} |x(t)|^2 dt \\ &= R_x(0) \end{aligned} \quad (2.3.2)$$

Now using the autocorrelation theorem of the Fourier transform (see Section 2.2.2) we find the Fourier transform of  $R_x(\tau)$  to be  $|X(f)|^2$ . Using this result, or equivalently, by employing Rayleigh's theorem, we have

$$\begin{aligned} \mathcal{E}_x &= \int_{-\infty}^{\infty} |x(t)|^2 dt \\ &= \int_{-\infty}^{\infty} |X(f)|^2 df \end{aligned} \quad (2.3.3)$$

This relation gives two methods for finding the energy in a signal. One method uses  $x(t)$ , the time domain representation of the signal, and the other method uses  $X(f)$ , the



frequency representation of the signal.  $\mathcal{G}_x(f) = \mathcal{F}[R_x(\tau)] = |X(f)|^2$  is called *energy spectral density* of the signal  $x(t)$ , and represents the amount of energy per hertz of bandwidth present in the signal at various frequencies.

### 2.3.2 Power-Type Signals

For the class of power-type signals a similar development is possible. In this case we define the *time-average autocorrelation function* of the power-type signal  $x(t)$  as

$$R_x(\tau) = \lim_{T \rightarrow \infty} \frac{1}{T} \int_{-\frac{T}{2}}^{\frac{T}{2}} x(t)x^*(t - \tau) dt \quad (2.3.4)$$

Now, obviously, the power content of the signal can be obtained from

$$\begin{aligned} P_x &= \lim_{T \rightarrow \infty} \frac{1}{T} \int_{-\frac{T}{2}}^{\frac{T}{2}} |x(t)|^2 dt \\ &= R_x(0) \end{aligned} \quad (2.3.5)$$

We define  $\mathcal{S}_x(f)$ , the *power-spectral density* or the *power spectrum* of the signal  $x(t)$  to be the Fourier transform of the time-average autocorrelation function.

$$\mathcal{S}_x(f) = \mathcal{F}[R_x(\tau)] \quad (2.3.6)$$

Subsequently, we will justify this definition. Now we can express the power content of the signal  $x(t)$  in terms of  $\mathcal{S}_x(f)$  by noting that  $R_x(0) = \int_{-\infty}^{\infty} \mathcal{S}_x(f) df$ ; i.e.,

$$\begin{aligned} P_x &= R_x(0) \\ &= \int_{-\infty}^{\infty} \mathcal{S}_x(f) df \end{aligned} \quad (2.3.7)$$

If a power-type signal  $x(t)$  is passed through a filter with impulse response  $h(t)$ , the output is

$$y(t) = \int_{-\infty}^{\infty} x(\tau)h(t - \tau) d\tau$$

and the time-average autocorrelation function for the output signal is

$$R_y(\tau) = \lim_{T \rightarrow \infty} \frac{1}{T} \int_{-\frac{T}{2}}^{\frac{T}{2}} y(t)y^*(t - \tau) dt$$

Substituting for  $y(t)$ , we obtain

$$R_y(\tau) = \lim_{T \rightarrow \infty} \frac{1}{T} \int_{-\frac{T}{2}}^{\frac{T}{2}} \left[ \int_{-\infty}^{\infty} h(u)x(t - u) du \right] \left[ \int_{-\infty}^{\infty} h^*(v)x^*(t - \tau - v) dv \right] dt$$

By making a change of variables  $w = t - u$  and changing the order of integration we obtain

$$\begin{aligned}
 R_y(\tau) &= \int_{-\infty}^{\infty} \int_{-\infty}^{\infty} h(u)h^*(v) \\
 &\quad \times \lim_{T \rightarrow \infty} \frac{1}{T} \int_{-\frac{T}{2}-u}^{\frac{T}{2}+u} [x(w)x^*(u+w-\tau-v) dw] du dv \\
 &\stackrel{\text{a}}{=} \int_{-\infty}^{\infty} \int_{-\infty}^{\infty} R_x(\tau+v-u)h(u)h^*(v) du dv \\
 &\stackrel{\text{b}}{=} \int_{-\infty}^{\infty} [R_x(\tau+v) \star h(\tau+v)] h^*(v) dv \\
 &\stackrel{\text{c}}{=} R_x(\tau) \star h(\tau) \star h^*(-\tau)
 \end{aligned} \tag{2.3.8}$$

where in (a) we have used the definition of  $R_x$  and in (b) and (c) we have used the definition of the convolution integral. Taking the Fourier transform of both sides of this equation, we obtain

$$\begin{aligned}
 \mathcal{S}_y(f) &= \mathcal{S}_x(f)H(f)H^*(f) \\
 &= \mathcal{S}_x(f)|H(f)|^2
 \end{aligned} \tag{2.3.9}$$

We have already seen that periodic signals are power-type signals. For periodic signals, the time-average autocorrelation function and the power spectral density simplify considerably. Let us assume that the signal  $x(t)$  is a periodic signal with period  $T_0$  having the Fourier series coefficients  $\{x_n\}$ . To find the time-average autocorrelation function we have

$$\begin{aligned}
 R_x(\tau) &= \lim_{T \rightarrow \infty} \frac{1}{T} \int_{-\frac{T}{2}}^{\frac{T}{2}} x(t)x^*(t-\tau) dt \\
 &= \lim_{k \rightarrow \infty} \frac{1}{kT_0} \int_{-\frac{kT_0}{2}}^{\frac{kT_0}{2}} x(t)x^*(t-\tau) dt \\
 &= \lim_{k \rightarrow \infty} \frac{k}{kT_0} \int_{-\frac{T_0}{2}}^{\frac{T_0}{2}} x(t)x^*(t-\tau) dt \\
 &= \frac{1}{T_0} \int_{-\frac{T_0}{2}}^{\frac{T_0}{2}} x(t)x^*(t-\tau) dt
 \end{aligned} \tag{2.3.10}$$

This relation gives the time-average autocorrelation function for a periodic signal. If we substitute the Fourier series expansion of the periodic signal in this relation, we obtain

$$R_x(\tau) = \frac{1}{T_0} \int_{-\frac{T_0}{2}}^{\frac{T_0}{2}} \sum_{n=-\infty}^{\infty} \sum_{m=-\infty}^{+\infty} x_n x_m^* e^{j2\pi \frac{m}{T_0} \tau} e^{j2\pi \frac{n-m}{T_0} t} dt \tag{2.3.11}$$

Now using the fact that,

$$\frac{1}{T_0} \int_{-\frac{T_0}{2}}^{\frac{T_0}{2}} e^{j2\pi \frac{n-m}{T_0} t} dt = \delta_{m,n}$$

we obtain

$$R_x(\tau) = \sum_{n=-\infty}^{\infty} |x_n|^2 e^{j2\pi \frac{n}{T_0} \tau} \quad (2.3.12)$$

From this relation we see that the time-average autocorrelation function of a periodic signal is itself periodic with the same period as the original signal, and its Fourier series coefficients are magnitude squares of the Fourier series coefficients of the original signal.

To determine the power-spectral density of a periodic signal, it is enough to find the Fourier transform of  $R_x(\tau)$ . Since we are dealing with a periodic function, the Fourier transform consists of impulses in the frequency domain. This is what we expect because a periodic signal consists of a sum of sinusoidal (or exponential) signals, and therefore the power is concentrated at discrete frequencies (the harmonics). Therefore, the power spectral density of a periodic signal is given by

$$S_x(f) = \sum_{n=-\infty}^{\infty} |x_n|^2 \delta\left(f - \frac{n}{T_0}\right) \quad (2.3.13)$$

To find the power content of a periodic signal, we have to integrate this relation over the whole frequency spectrum. When we do this, we obtain

$$P_x = \sum_{n=-\infty}^{\infty} |x_n|^2 \quad (2.3.14)$$

This relation is known as *Rayleigh's relation* for periodic signals (also see Problem 2.6). If this periodic signal passes through an LTI system with frequency response  $H(f)$ , the output will be periodic, and the power spectral density of the output can be obtained by employing the relation between the power spectral densities of the input and the output of a filter. Thus,

$$\begin{aligned} S_y(f) &= |H(f)|^2 \sum_{n=-\infty}^{\infty} |x_n|^2 \delta\left(f - \frac{n}{T_0}\right) \\ &= \sum_{n=-\infty}^{\infty} |x_n|^2 \left|H\left(\frac{n}{T_0}\right)\right|^2 \delta\left(f - \frac{n}{T_0}\right) \end{aligned} \quad (2.3.15)$$

and the power content of the output signal is

$$P_y = \sum_{n=-\infty}^{\infty} |x_n|^2 \left|H\left(\frac{n}{T_0}\right)\right|^2$$

## 2.4 SAMPLING OF BANDLIMITED SIGNALS

The sampling theorem is one of the most important results in the analysis of signals, which has widespread applications in communications and signal processing. This theorem and the numerous applications that it provides clearly show how much can be gained by employing the frequency domain methods and the insight provided by frequency domain signal analysis. Many modern signal processing techniques and the whole family of digital communication methods are based on the validity of this theorem and the insight provided by it. In fact, this theorem, together with results from signal quantization techniques, provide a bridge that connects the analog world to digital techniques.

The idea leading to the sampling theorem is very simple and quite intuitive. Let us assume that we have two signals  $x_1(t)$  and  $x_2(t)$  as shown in Figure 2.9.  $x_1(t)$  is a smooth signal; it varies very slowly, and its main frequency content is at low frequencies. In contrast,  $x_2(t)$  is a signal with rapid changes due to the presence of the high frequency components. We are to approximate these signals with samples taken at regular intervals  $T_1$  and  $T_2$ , respectively. To obtain an approximation of the original signal we can use,

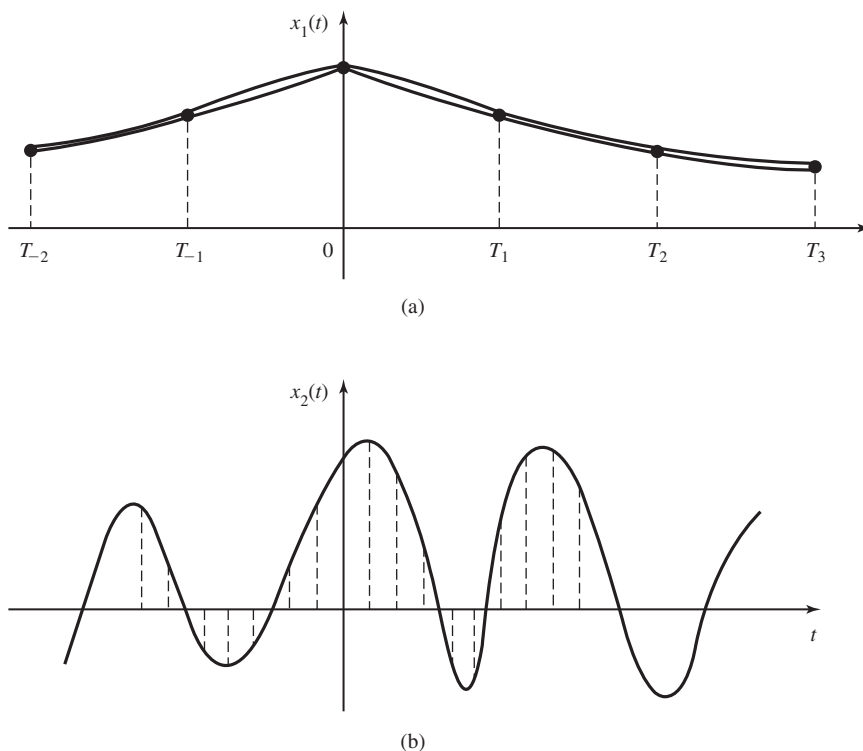


**Figure 2.9** Sampling of signals.

for example, linear interpolation of the sampled values. It is obvious that the sampling interval for the signal  $x_1(t)$  can be much larger than the sampling interval necessary to reconstruct signal  $x_2(t)$  with comparable distortion. This is a direct consequence of the smoothness of the signal  $x_1(t)$  compared to  $x_2(t)$ . Therefore, the sampling interval for the signals of smaller bandwidth can be made larger, or the sampling frequency can be made smaller. The sampling theorem is, in fact, a precise statement of this intuitive reasoning. It basically states that

1. If the signal  $x(t)$  is bandlimited to  $W$ ; i.e., if  $X(f) \equiv 0$  for  $|f| \geq W$ , then it is sufficient to sample at intervals  $T_s = \frac{1}{2W}$ .
2. If we are allowed to employ more sophisticated interpolating signals compared to linear interpolation, we are able to obtain the exact original signal back from the samples as long as the previous condition is satisfied.

As seen here, the importance of the sampling theorem lies in the fact that it provides both a method of reconstruction of the original signal from the sampled values and also gives a precise upper bound on the sampling interval (or equivalently, a lower bound on the sampling frequency) required for distortionless reconstruction.

**Theorem 2.4.1. [Sampling]** Let the signal  $x(t)$  be bandlimited with bandwidth  $W$ ; i.e., let  $X(f) \equiv 0$  for  $|f| \geq W$ . Let  $x(t)$  be sampled at multiples of some basic sampling interval  $T_s$ , where  $T_s \leq \frac{1}{2W}$ , to yield the sequence  $\{x(nT_s)\}_{n=-\infty}^{+\infty}$ . Then it is possible to reconstruct the original signal  $x(t)$  from the sampled values by the reconstruction formula

$$x(t) = \sum_{n=-\infty}^{\infty} 2W'T_s x(nT_s) \text{sinc}[2W'(t - nT_s)] \quad (2.4.1)$$

where  $W'$  is any arbitrary number that satisfies

$$W \leq W' \leq \frac{1}{T_s} - W$$

In the special case where  $T_s = \frac{1}{2W}$ , the reconstruction relation simplifies to

$$x(t) = \sum_{n=-\infty}^{\infty} x(nT_s) \text{sinc}\left(\frac{t}{T_s} - n\right) = \sum_{n=-\infty}^{+\infty} x\left(\frac{n}{2W}\right) \text{sinc}\left[2W\left(t - \frac{n}{2W}\right)\right]$$

*Proof.* Let  $x_\delta(t)$  denote the result of sampling the original signal by impulses at  $nT_s$  time instants. Then

$$x_\delta(t) = \sum_{n=-\infty}^{\infty} x(nT_s) \delta(t - nT_s) \quad (2.4.2)$$

We can write  $x_\delta(t)$  as

$$x_\delta(t) = x(t) \sum_{n=-\infty}^{\infty} \delta(t - nT_s) \quad (2.4.3)$$

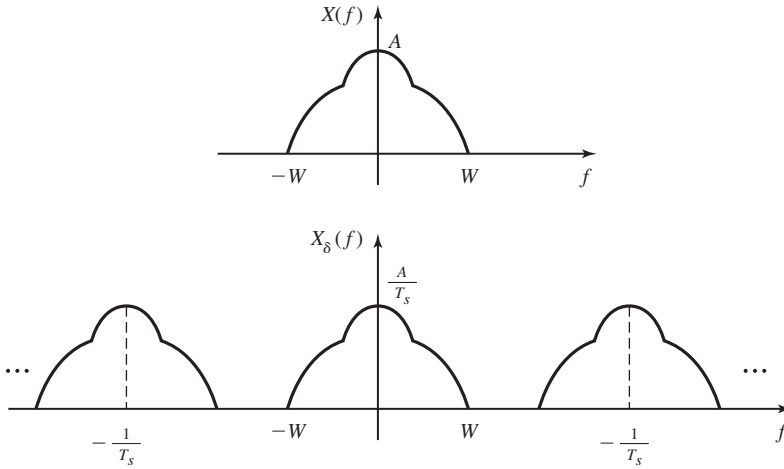


**Figure 2.10** Frequency domain representation of the sampled signal.

Now if we find the Fourier transform of both sides of the above relation and apply the dual of the convolution theorem to the right-hand side, we obtain

$$X_{\delta}(f) = X(f) \star \mathcal{F} \left[ \sum_{n=-\infty}^{\infty} \delta(t - nT_s) \right] \quad (2.4.4)$$

Now using Table 2.1 to find the Fourier transform of  $\sum_{n=-\infty}^{\infty} \delta(t - nT_s)$ , we obtain

$$\mathcal{F} \left[ \sum_{n=-\infty}^{\infty} \delta(t - nT_s) \right] = \frac{1}{T_s} \sum_{n=-\infty}^{\infty} \delta \left( f - \frac{n}{T_s} \right) \quad (2.4.5)$$

By substituting Equation (2.4.5) into Equation (2.4.4), we obtain

$$\begin{aligned} X_{\delta}(f) &= X(f) \star \frac{1}{T_s} \sum_{n=-\infty}^{\infty} \delta \left( f - \frac{n}{T_s} \right) \\ &= \frac{1}{T_s} \sum_{n=-\infty}^{\infty} X \left( f - \frac{n}{T_s} \right) \end{aligned} \quad (2.4.6)$$

where in the last step we have employed the convolution property of the impulse signal.<sup>†</sup> This relation shows that  $X_{\delta}(f)$ , the Fourier transform of the impulse-sampled signal is a replication of the Fourier transform of the original signal at a  $\frac{1}{T_s}$  rate. Figure 2.10 shows this situation.

Now if  $T_s > \frac{1}{2W}$ , then the replicated spectrum of  $x(t)$  overlaps, and reconstruction of the original signal is not possible. This type of distortion that results from under-sampling is known as *aliasing error* or *aliasing distortion*. However, if  $T_s \leq \frac{1}{2W}$ , no

<sup>†</sup>The convolution property of the impulse signal states that  $x(t) \star \delta(t - t_0) = x(t - t_0)$ .

overlap occurs, and by employing an appropriate filter we can reconstruct the original signal back. To obtain the original signal back, it is sufficient to filter the sampled signal by a lowpass filter with frequency response characteristic

1.  $H(f) = T_s$  for  $|f| < W$ .
2.  $H(f) = 0$  for  $|f| \geq \frac{1}{T_s} - W$

For  $W \leq |f| < \frac{1}{T_s} - W$ , the filter can have any characteristics that makes its implementation easy. Of course, one obvious (though not practical) choice is an ideal lowpass filter with bandwidth  $W'$  where  $W'$  satisfies  $W \leq W' < \frac{1}{T_s} - W$ ; i.e.,

$$H(f) = T_s \Pi \left( \frac{f}{2W'} \right) \quad (2.4.7)$$

with this choice we have

$$X(f) = X_s(f) T_s \Pi \left( \frac{f}{2W'} \right) \quad (2.4.8)$$

Taking inverse Fourier transform of both sides, we obtain

$$\begin{aligned} x(t) &= x_s(t) \star 2W'T_s \text{sinc}(2W't) \\ &= \left( \sum_{n=-\infty}^{\infty} x(nT_s) \delta(t - nT_s) \right) \star 2W'T_s \text{sinc}(2W't) \\ &= \sum_{n=-\infty}^{\infty} 2W'T_s x(nT_s) \text{sinc}(2W'(t - nT_s)) \end{aligned} \quad (2.4.9)$$

This relation shows that if we use sinc functions for interpolation of the sampled values, we can reconstruct the original signal perfectly. The sampling rate  $f_s = \frac{1}{T_s}$  is the minimum sampling rate at which no aliasing occurs. This sampling rate is known as the *Nyquist sampling rate*. If sampling is done at the Nyquist rate, then the only choice for the reconstruction filter is an ideal lowpass filter and  $W' = W = \frac{1}{2T_s}$ . Then,

$$\begin{aligned} x(t) &= \sum_{n=-\infty}^{\infty} x \left( \frac{n}{2W} \right) \text{sinc}(2Wt - n) \\ &= \sum_{n=-\infty}^{\infty} x(nT_s) \text{sinc} \left( \frac{t}{T_s} - n \right) \end{aligned} \quad (2.4.10)$$

■

In practical systems, sampling is done at a rate higher than the Nyquist rate. This allows for the reconstruction filter to be realizable and easier to build. In such cases the distance between two adjacent replicated spectra in the frequency domain; i.e.,  $(\frac{1}{T_s} - W) - W = f_s - 2W$ , is known as the *guard band*.

Note that there exists a strong similarity between our development of the sampling theorem and our previous development of the Fourier transform for periodic signals (or

Fourier series). In the Fourier transform for periodic signals, we started with a (time) periodic signal and showed that its Fourier transform consists of a sequence of impulses. Therefore, to define the signal, it was enough to give the weights of these impulses (Fourier series coefficients). In the sampling theorem, we started with an impulse-sampled signal, or a sequence of impulses in the time domain, and showed that the Fourier transform is a periodic function in the frequency domain. Here again, the values of the samples are enough to define the signal completely. This similarity is a consequence of the duality between the time and frequency domains and the fact that both the Fourier series expansion and reconstruction from samples are orthogonal expansions, one in terms of the exponential signals and the other in terms of the sinc functions. This fact will be further explored in the problems.

## 2.5 BANDPASS SIGNALS

In this section, we examine time domain and frequency domain characteristics of a class of signals frequently encountered in communication system analysis. This class of signals is the class of *bandpass* or *narrowband* signals. The concept of bandpass signals is a generalization of the concept of monochromatic signals, and our analysis of the properties of these signals follows that used in analyzing monochromatic signals.

**Definition 2.5.1.** A *bandpass* or *narrowband* signal is a signal  $x(t)$  whose frequency domain representation  $X(f)$  is nonzero for frequencies in a usually small neighborhood of some high frequency  $f_0$ ; i.e.,  $X(f) \equiv 0$  for  $|f - f_0| \geq W$ , where  $W < f_0$ . A *bandpass system* is a system which passes signals with frequency components in the neighborhood of some high frequency  $f_0$ ; i.e.,  $H(f) = 1$  for  $|f - f_0| \leq W$  and highly attenuates frequency components outside of this frequency band. Alternatively, we may say that a bandpass system is one whose impulse response is a bandpass signal.

Note that in the above definition,  $f_0$  need not be the center of the signal bandwidth, or be located in the signal bandwidth at all. In fact, all the spectra shown in Figure 2.11 satisfy the definition of a bandpass signal.

With the above precautions, the frequency  $f_0$  is usually referred to as the *central frequency* of the bandpass signal. A monochromatic signal is a bandpass signal for which  $W = 0$ . A large class of signals used for information transmission, the *modulated signals*, are examples of bandpass signals or at least closely represented by bandpass signals. Throughout this section, we assume that the bandpass signal  $x(t)$  is real valued.

To begin our development of bandpass signals, let us start with the tools used in the analysis of systems or circuits driven by monochromatic (or sinusoidal) signals. Let  $x(t) = A \cos(2\pi f_0 t + \theta)$  denote a monochromatic signal. To analyze a circuit driven by this signal we first introduce the *phasor* corresponding to this signal as  $X = Ae^{j\theta}$ , which contains the information about the amplitude and phase of the signal but does not have any information concerning the frequency of it. To find the output of a linear time invariant circuit driven by this sinusoidal signal, it is enough to multiply the phasor of the excitation signal by the value of the frequency response of the system computed at



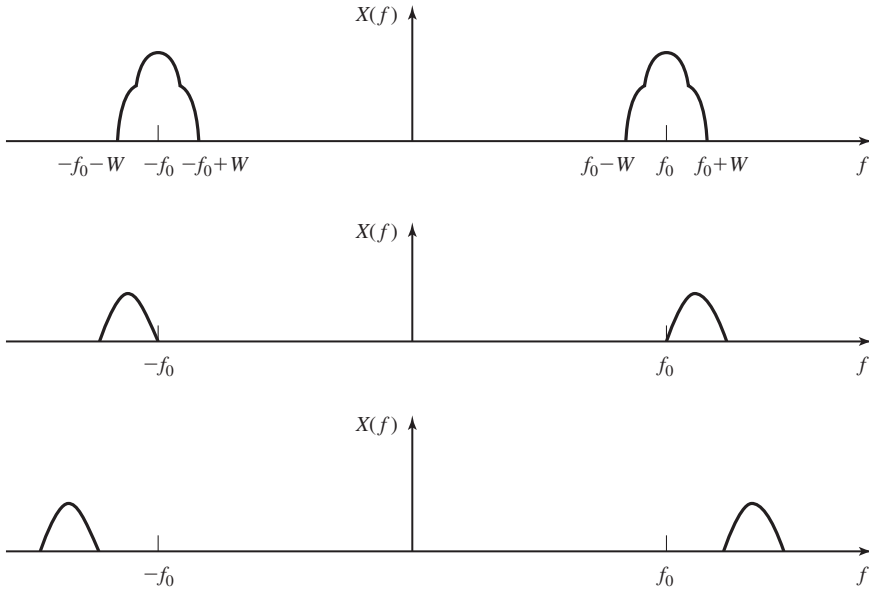


**Figure 2.11** Examples of narrowband signals.

the input frequency to obtain the phasor corresponding to the output. From the output phasor, we can find the output signal by noting that the input and output frequencies are the same. To obtain the phasor corresponding to the input, we first introduce the signal  $z(t)$  as

$$\begin{aligned} z(t) &= Ae^{j(2\pi f_0 t + \theta)} \\ &= A \cos(2\pi f_0 t + \theta) + jA \sin(2\pi f_0 t + \theta) \\ &= x(t) + jx_q(t) \end{aligned}$$

where  $x_q(t) = A \sin(2\pi f_0 t + \theta)$  is a  $90^\circ$  phase shift version of the original signal and the subscript stands for *quadrature*. Note that  $z(t)$  represents a vector rotating at an angular frequency equal to  $2\pi f_0$  as shown in Figure 2.12, and  $X$ , the phasor is obtained from  $z(t)$  by deleting the rotation at the angular frequency of  $2\pi f_0$ , or equivalently by

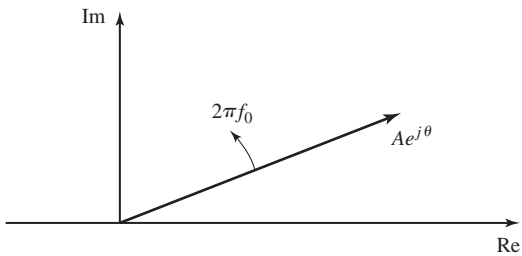


**Figure 2.12** Phasor of a monochromatic signal.

rotating the vector corresponding to  $z(t)$  at an angular frequency equal to  $2\pi f_0$  in the opposite direction, which is equivalent to multiplying by  $e^{-j2\pi f_0 t}$ , or

$$X = z(t)e^{-j2\pi f_0 t}$$

In the frequency domain, this is equivalent to shifting  $Z(f)$  to the left by  $f_0$ . Also note that the frequency domain representation of  $Z(f)$  is obtained by deleting the negative frequencies from  $X(f)$  and multiplying the positive frequencies by 2.

To obtain a parallel development for narrowband signals, we start with a signal corresponding to  $z(t)$ . We define  $z(t)$  for narrowband signals in the same way that  $z(t)$  was defined for monochromatic signals; i.e., by multiplying the positive frequencies in  $X(f)$  by 2 and deleting the negative frequencies. By doing this we have

$$Z(f) = 2u_{-1}(f)X(f) \quad (2.5.1)$$

The signal  $z(t)$  defined by the above relation is called the *analytic signal* corresponding to  $x(t)$ , or *pre-envelope* of  $x(t)$ . To obtain the time domain representation of  $z(t)$ , we first start with finding a signal whose Fourier transform is  $u_{-1}(f)$ . From Table 2.1 we know that

$$\mathcal{F}[u_{-1}(t)] = \frac{1}{2}\delta(f) + \frac{1}{j2\pi f}$$

Applying the duality theorem, we obtain

$$\mathcal{F}\left[\frac{1}{2}\delta(t) + \frac{j}{2\pi t}\right] = u_{-1}(f) \quad (2.5.2)$$

Now, using the convolution theorem, we have

$$\begin{aligned} z(t) &= \left(\delta(t) + \frac{j}{\pi t}\right) \star x(t) \\ &= x(t) + j\frac{1}{\pi t} \star x(t) \\ &= x(t) + j\hat{x}(t) \end{aligned} \quad (2.5.3)$$

where

$$\hat{x}(t) = \frac{1}{\pi t} \star x(t) \quad (2.5.4)$$

Comparing this result with the corresponding monochromatic result

$$z(t) = \underbrace{A \cos(2\pi f_0 t + \theta)}_{x(t)} + j \underbrace{A \sin(2\pi f_0 t + \theta)}_{\hat{x}(t)} \quad (2.5.5)$$

we see that  $\hat{x}(t)$  plays the same role as  $A \sin(2\pi f_0 t + \theta)$ .  $\hat{x}(t)$  is called the *Hilbert transform* of  $x(t)$ . The name “transform” is somewhat misleading because there is no change of domain involved, (as is the case for Fourier, Laplace, and Z transforms, for example). In fact, Hilbert transform is a simple filter (seen from the fact that it can be expressed in terms of a convolution integral). To see what the Hilbert transform does

in the frequency domain we note that

$$\begin{aligned}
 \mathcal{F}\left[\frac{1}{\pi t}\right] &= -j\operatorname{sgn}(f) \\
 &= \begin{cases} -j & f > 0 \\ 0 & f = 0 \\ +j & f < 0 \end{cases} \\
 &= \begin{cases} e^{-j\frac{\pi}{2}} & f > 0 \\ 0 & f = 0 \\ e^{j\frac{\pi}{2}} & f < 0 \end{cases} \\
 &= e^{-j\frac{\pi}{2}\operatorname{sgn}(f)} \tag{2.5.6}
 \end{aligned}$$

This means that the Hilbert transform is equivalent to a  $-\frac{\pi}{2}$  phase shift for positive frequencies and  $+\frac{\pi}{2}$  phase shift for negative frequencies and can be represented by a filter with transfer function  $H(f) = -j\operatorname{sgn}(f)$ . This filter is called a *quadrature filter*, emphasizing its role in providing a  $90^\circ$  phase shift. In the problems, we will investigate some of the most important properties of the Hilbert transform.

To obtain the equivalent of a “phasor” for the bandpass signal we have to shift the spectrum of  $z(t)$ ; i.e.,  $Z(f)$ , to the left by  $f_0$  to obtain a signal denoted by  $x_l(t)$ , which is the *lowpass representation of the bandpass signal*  $x(t)$ . Hence,

$$X_l(f) = Z(f + f_0) = 2u_{-1}(f + f_0)X(f + f_0) \tag{2.5.7}$$

and

$$x_l(t) = z(t)e^{-j2\pi f_0 t} \tag{2.5.8}$$

Figure 2.13 shows  $Z(f)$  and  $X_l(f)$  corresponding to a bandpass signal  $x(t)$ .

As seen  $x_l(t)$  is a lowpass signal, meaning that its frequency components are located around the zero frequency, or  $X_l(f) \equiv 0$  for  $|f| \geq W$  where  $W < f_0$ .  $x_l(t)$  plays the role of the phasor for bandpass signals. In general,  $x_l(t)$  is a complex signal having  $x_c(t)$  and  $x_s(t)$  as its real and imaginary parts respectively; i.e.,

$$x_l(t) = x_c(t) + jx_s(t) \tag{2.5.9}$$

$x_c(t)$  and  $x_s(t)$  are lowpass signals, called *in-phase* and *quadrature* components of the bandpass signal  $x(t)$ . Substituting for  $x_l(t)$  and rewriting  $z(t)$ , we obtain

$$\begin{aligned}
 z(t) &= x(t) + j\hat{x}(t) \\
 &= x_l(t)e^{j2\pi f_0 t} \\
 &= (x_c(t) + jx_s(t))e^{j2\pi f_0 t} \\
 &= (x_c(t) \cos(2\pi f_0 t) - x_s(t) \sin(2\pi f_0 t)) \\
 &\quad + j(x_c(t) \sin(2\pi f_0 t) + x_s(t) \cos(2\pi f_0 t)) \tag{2.5.10}
 \end{aligned}$$

Equating the real and imaginary parts, we have

$$x(t) = x_c(t) \cos(2\pi f_0 t) - x_s(t) \sin(2\pi f_0 t) \tag{2.5.11}$$

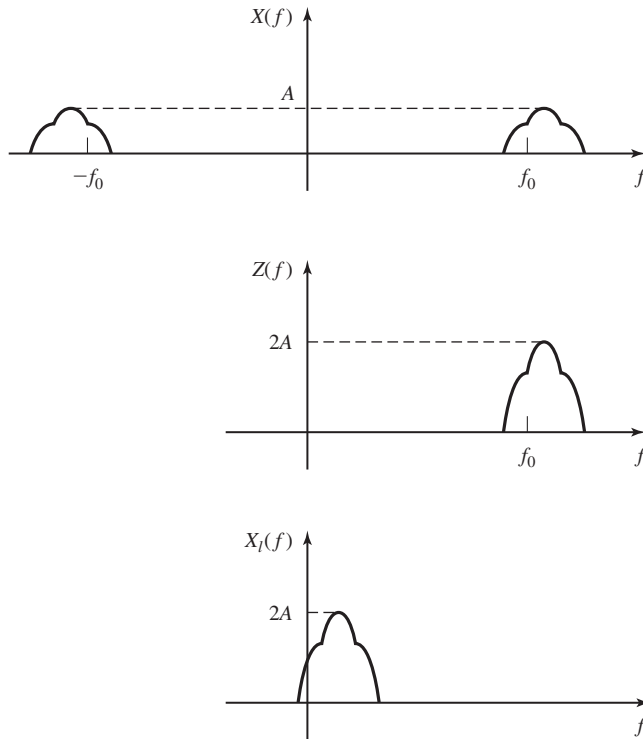


**Figure 2.13**  $Z(f)$  and  $X_I(f)$  corresponding to  $x(t)$ .

and

$$\hat{x}(t) = x_c(t) \sin(2\pi f_0 t) + x_s(t) \cos(2\pi f_0 t) \quad (2.5.12)$$

These relations give  $x(t)$  and  $\hat{x}(t)$  in terms of two lowpass quadrature component signals  $x_c(t)$  and  $x_s(t)$  and are known as *bandpass to lowpass transformation relations*.

If we define  $V(t)$ , the *envelope* of  $x(t)$  as

$$V(t) = \sqrt{x_c^2(t) + x_s^2(t)} \quad (2.5.13)$$

and  $\Theta(t)$ , the *phase* of  $x(t)$ , as

$$\Theta(t) = \arctan \frac{x_s(t)}{x_c(t)} \quad (2.5.14)$$

we can write

$$x_I(t) = V(t)e^{j\Theta(t)} \quad (2.5.15)$$

which looks more like the familiar phasor relation  $X = Ae^{j\theta}$ . The only difference is that in this case the envelope ( $V(t)$ ) and phase ( $\Theta(t)$ ) are both (slowly) time-varying functions. Therefore, in contrast to the monochromatic phasor which has constant

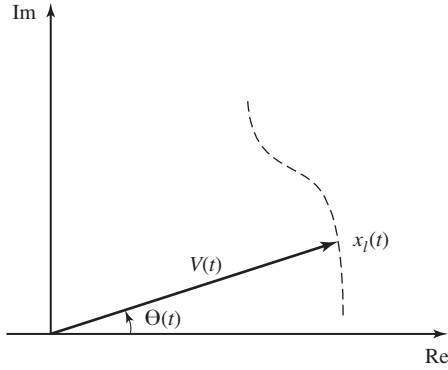


**Figure 2.14** The phasor of a bandpass signal.

amplitude and phase, the envelope and phase of a bandpass signal vary slowly with time, and therefore the vector representation of it moves on a curve in the complex plane (see Figure 2.14).

Substituting  $x_l(t) = V(t)e^{j\Theta(t)}$  in  $z(t)$  in Equation (2.5.10), we obtain

$$\begin{aligned}
 z(t) &= x(t) + j\hat{x}(t) \\
 &= x_l(t)e^{j2\pi f_0 t} \\
 &= V(t)e^{j\Theta(t)}e^{j2\pi f_0 t} \\
 &= V(t)\cos(2\pi f_0 t + \Theta(t)) + jV(t)\sin(2\pi f_0 t + \Theta(t)) \quad (2.5.16)
 \end{aligned}$$

from which we have

$$x(t) = V(t)\cos(2\pi f_0 t + \Theta(t)) \quad (2.5.17)$$

and

$$\hat{x}(t) = V(t)\sin(2\pi f_0 t + \Theta(t)) \quad (2.5.18)$$

These relations show why  $V(t)$  and  $\Theta(t)$  are called the envelope and phase of the signal  $x(t)$ . Figure 2.15 shows the relation between  $x(t)$ ,  $V(t)$ , and  $\Theta(t)$ .

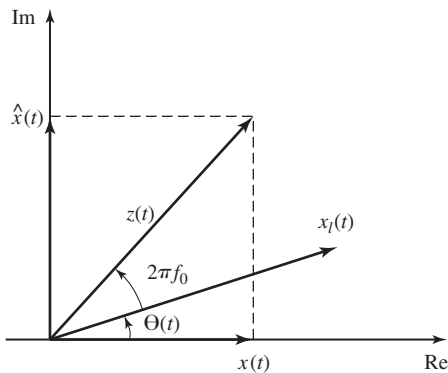


**Figure 2.15** The envelope and phase of a bandpass signal.

**Example 2.5.1**

Show that  $X(f)$  can be written in terms of  $X_I(f)$  as

$$X(f) = \frac{1}{2}[X_I(f - f_0) + X_I^*(-f - f_0)] \quad (2.5.19)$$

**Solution** To obtain  $X(f)$  from  $X_I(f)$ , we do exactly the inverse of what we did to get  $X_I(f)$  from  $X(f)$ . First we shift  $X_I(f)$  to the right by  $f_0$  to get  $Z(f)$ . We have

$$Z(f) = X_I(f - f_0)$$

To get  $X(f)$  from  $Z(f)$ , we have to multiply the positive frequencies by a factor of  $\frac{1}{2}$  and reconstruct the negative frequencies. Since  $x(t)$  is assumed to be real valued, its Fourier transform has Hermitian symmetry (see Section 2.2.1). Therefore, if we write

$$X(f) = X_+(f) + X_-(f)$$

where  $X_+(f)$  denotes the positive frequency part of  $X(f)$  and  $X_-(f)$  denotes the negative frequency part, we have

$$X_-(f) = X_+^*(-f)$$

Since

$$X_+(f) = \frac{1}{2}X_I(f - f_0)$$

we obtain

$$X(f) = \frac{1}{2}[X_I(f - f_0) + X_I^*(-f - f_0)]$$

The relation between the various signals discussed in this section are summarized in Table 2.2.

**Transmission of Bandpass Signals through Bandpass Systems.** In the same way that phasors make analysis of systems driven by monochromatic signals easier, lowpass equivalents of bandpass signals can be employed to find the outputs of bandpass systems driven by bandpass signals. Let  $x(t)$  be a bandpass signal with center frequency  $f_0$ , and let  $h(t)$  be the impulse response of an LTI system. Let us assume that  $h(t)$  is narrowband with the same center frequency as  $x(t)$ . To find  $y(t)$ , the output of the system when driven by  $x(t)$ , we use frequency domain analysis. In the frequency domain, we have  $Y(f) = X(f)H(f)$ . The signal  $y(t)$  is obviously a bandpass signal, and therefore it has a lowpass equivalent  $y_l(t)$ . To obtain  $Y_l(f)$  we have

$$\begin{aligned} Y_l(f) &= 2u_{-1}(f + f_0)Y(f + f_0) \\ &= 2u_{-1}(f + f_0)X(f + f_0)H(f + f_0) \end{aligned} \quad (2.5.20)$$

By writing  $H(f)$  and  $X(f)$  in terms of their lowpass equivalents, we obtain

$$X_l(f) = 2u_{-1}(f + f_0)X(f + f_0)$$

**TABLE 2.2** SUMMARY OF BANDPASS TO LOWPASS TRANSLATION RELATIONS

---


$$\begin{cases}
x(t) = x_c(t) \cos(2\pi f_0 t) - x_s(t) \sin(2\pi f_0 t) \\
\hat{x}(t) = x_c(t) \sin(2\pi f_0 t) + x_s(t) \cos(2\pi f_0 t) \\
x(t) = \operatorname{Re}[x_I(t)e^{j2\pi f_0 t}] \\
\hat{x}(t) = \operatorname{Im}[x_I(t)e^{j2\pi f_0 t}] \\
x(t) = \operatorname{Re}[z(t)] \\
\hat{x}(t) = \operatorname{Im}[z(t)] \\
x(t) = V(t) \cos(2\pi f_0 t + \Theta) \\
\hat{x}(t) = V(t) \sin(2\pi f_0 t + \Theta) \\
x_c(t) = x(t) \cos(2\pi f_0 t) + \hat{x}(t) \sin(2\pi f_0 t) \\
x_s(t) = \hat{x}(t) \cos(2\pi f_0 t) - x(t) \sin(2\pi f_0 t) \\
x_c(t) = \operatorname{Re}[x_I(t)] \\
x_s(t) = \operatorname{Im}[x_I(t)] \\
x_c(t) = \operatorname{Re}[z(t)e^{-j2\pi f_0 t}] \\
x_s(t) = \operatorname{Im}[z(t)e^{-j2\pi f_0 t}] \\
x_c(t) = V(t) \cos \Theta(t) \\
x_s(t) = V(t) \sin \Theta(t) \\
x_I(t) = (x(t) + j\hat{x}(t))e^{-j2\pi f_0 t} \\
x_I(t) = x_c(t) + jx_s(t) \\
x_I(t) = z(t)e^{-j2\pi f_0 t} \\
x_I(t) = V(t)e^{j\Theta(t)} \\
z(t) = x(t) + j\hat{x}(t) \\
z(t) = (x_c(t) + jx_s(t))e^{j2\pi f_0 t} \\
z(t) = x_I(t)e^{j2\pi f_0 t} \\
z(t) = V(t)e^{j(2\pi f_0 t + \Theta(t))} \\
V(t) = \sqrt{x^2(t) + \hat{x}^2(t)} \\
\Theta(t) = \arctan \frac{\hat{x}(t)}{x(t)} - 2\pi f_0 t \\
V(t) = \sqrt{x_c^2(t) + x_s^2(t)} \\
\Theta(t) = \arctan \frac{x_s(t)}{x_c(t)} \\
V(t) = |x_I(t)| \\
\Theta(t) = \angle x_I(t) \\
V(t) = |z(t)| \\
\Theta(t) = \angle z(t) - 2\pi f_0 t
\end{cases}$$


---

and

$$H_I(f) = 2u_{-1}(f + f_0)H(f + f_0)$$

By multiplying these two relations and noting that  $(u_{-1}(f))^2 = u_{-1}(f)$ , we have

$$X_I(f)H_I(f) = 4u_{-1}(f + f_0)X(f + f_0)H(f + f_0)$$

Finally, by substituting in the relation for  $Y_I(f)$ , we obtain

$$Y_I(f) = \frac{1}{2}X_I(f)H_I(f) \quad (2.5.21)$$

or, in time domain, we have

$$y_l(t) = \frac{1}{2}x_l(t) \star h_l(t) \quad (2.5.22)$$

This relation shows that to obtain the output  $y(t)$ , we can carry out the convolution at low frequencies to obtain  $y_l(t)$ , and then transform to higher frequencies using the relation

$$y(t) = \text{Re}[y_l(t)e^{j2\pi f_0 t}] \quad (2.5.23)$$

## 2.6 FURTHER READING

There exist numerous references covering analysis of LTI systems in the time and frequency domain. Oppenheim, Willsky, and Young (1983) contains wide coverage of time and frequency domain analysis of both discrete-time and continuous-time systems. Papoulis (1962) and Bracewell (1965) provide in-depth analysis of the Fourier series and transform techniques. A more advanced treatment of linear systems based on linear operator theory can be found in Franks (1969).

## PROBLEMS

**2.1** Let  $\{\phi_i(t)\}_{i=1}^N$  be an orthogonal set of  $N$  signals; i.e.,

$$\int_{-\infty}^{\infty} \phi_i(t)\phi_j^*(t) dt = \begin{cases} 1, & i \neq j \\ 0, & i = j \end{cases} \quad 1 \leq i, j \leq N$$

and let  $x(t)$  be an arbitrary signal. Let  $\hat{x}(t) = \sum_{i=1}^N \alpha_i \phi_i(t)$  be a linear approximation of  $x(t)$  in terms of  $\{\phi_i(t)\}_{i=1}^N$ . We are interested in finding  $\alpha_i$ 's such that

$$\epsilon^2 = \int_{-\infty}^{\infty} |x(t) - \hat{x}(t)|^2 dt$$

is minimized.

**1.** Show that the minimizing  $\alpha_i$ 's satisfy

$$\alpha_i = \int_{-\infty}^{\infty} x(t)\phi_i^*(t) dt$$

**2.** Show that with the above choice of  $\alpha_i$ 's we have

$$\epsilon_{\min}^2 = \int_{-\infty}^{\infty} |x(t)|^2 dt - \sum_{i=1}^N |\alpha_i|^2$$



**2.2** Determine the Fourier series expansion of the following signals.

1.  $x_1(t) = \sum_{n=-\infty}^{\infty} \Lambda(t - 2n)$
2.  $x_2(t) = \sum_{n=-\infty}^{\infty} \Lambda(t - n)$
3.  $x_3(t) = e^{t-n}$  for  $n \leq t < n + 1$
4.  $x_4(t) = \cos t + \cos 2.5t$
5.  $x_5(t) = \sum_{n=-\infty}^{\infty} \Lambda(t - n)u_{-1}(t - n)$
6.  $x_6(t) = \sum_{n=-\infty}^{\infty} (-1)^n \delta(t - nT)$
7.  $x_7(t) = \sum_{n=-\infty}^{\infty} \delta'(t - nT)$
8.  $x_8(t) = |\cos 2\pi f_0 t|$  (Full-wave rectifier output)
9.  $x_9(t) = \cos 2\pi f_0 t + |\cos 2\pi f_0 t|$  (Half-wave rectifier output)

**2.3** Show that for real  $x(t)$ , we have

$$x_e(t) = \frac{a_0}{2} + \sum_{n=1}^{\infty} a_n \cos\left(2\pi \frac{n}{T_0} t\right)$$

$$x_o(t) = \sum_{n=1}^{\infty} a_n \sin\left(2\pi \frac{n}{T_0} t\right)$$

where  $x_e(t)$  and  $x_o(t)$  denote the even and odd parts of  $x(t)$ , defined as

$$x_e(t) = \frac{x(t) + x(-t)}{2}$$

$$x_o(t) = \frac{x(t) - x(-t)}{2}$$

**2.4** Determine the Fourier series expansion of each of the periodic signals shown in Figure P-2.4. For each signal, also determine the trigonometric Fourier series.

**2.5** Let  $x_n$  and  $y_n$  represent the Fourier Series coefficients of  $x(t)$  and  $y(t)$ , respectively. Assuming the period of  $x(t)$  is  $T_0$ , express  $y_n$  in terms of  $x_n$  in each of the following cases

1.  $y(t) = x(t - t_0)$
2.  $y(t) = x(t)e^{j2\pi f_0 t}$
3.  $y(t) = x(at)$ ,  $a \neq 0$
4.  $y(t) = \frac{d}{dt}x(t)$

**2.6** Let  $x(t)$  and  $y(t)$  be two periodic signals with period  $T_0$ , and let  $x_n$  and  $y_n$  denote the Fourier series coefficients of these two signals. Show that

$$\frac{1}{T_0} \int_{\alpha}^{\alpha+T_0} x(t)y^*(t) dt = \sum_{n=-\infty}^{\infty} x_n y_n^*$$

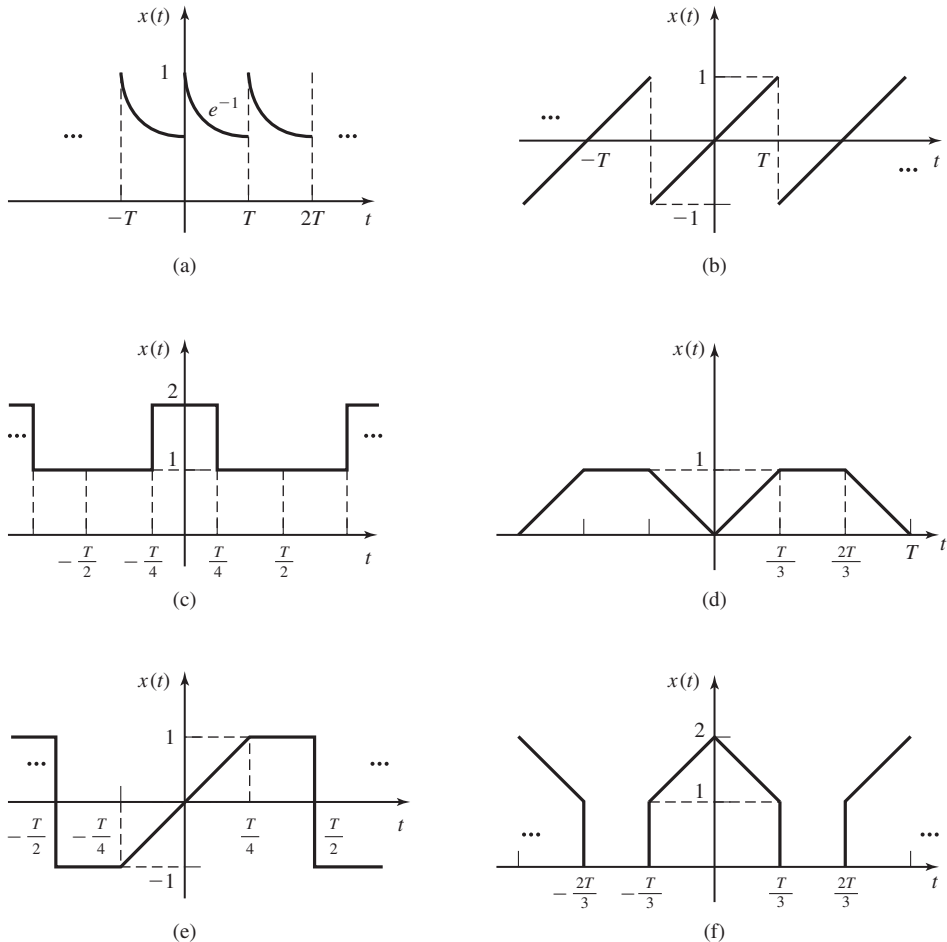


Figure P-2.4

This relation is known as *Parseval's relation* for Fourier series. Show that Rayleigh's relation for periodic signals [see Equation (2.3.14)] is a special case of this relation.

- 2.7** Show that for all periodic physical signals that have finite power, the coefficients of the Fourier series expansion  $x_n$  tend to zero as  $n \rightarrow \infty$ .
- 2.8** Use Parseval's relation in Problem 2.6 to prove the following identity.

$$1 + \frac{1}{3^4} + \frac{1}{5^4} + \cdots + \frac{1}{(2n+1)^4} + \cdots = \frac{\pi^4}{96}$$

**2.9** In this problem, we present the proof of the Cauchy–Schwartz inequality.

1. Show that for nonnegative  $\{\alpha_i\}_{i=1}^n$  and  $\{\beta_i\}_{i=1}^n$ ,

$$\sum_{i=1}^n \alpha_i \beta_i \leq \left[ \sum_{i=1}^n \alpha_i^2 \right]^{\frac{1}{2}} \left[ \sum_{i=1}^n \beta_i^2 \right]^{\frac{1}{2}}$$

What are the conditions for equality?

2. Let  $\{x_i\}_{i=1}^n$  and  $\{y_i\}_{i=1}^n$  be complex numbers. Show that

$$\left| \sum_{i=1}^n x_i y_i^* \right| \leq \sum_{i=1}^n |x_i y_i^*| = \sum_{i=1}^n |x_i| |y_i^*|$$

What are the conditions for equality?

3. From (1) and (2), conclude that

$$\left| \sum_{i=1}^n x_i y_i^* \right| \leq \left[ \sum_{i=1}^n |x_i|^2 \right]^{\frac{1}{2}} \left[ \sum_{i=1}^n |y_i|^2 \right]^{\frac{1}{2}}$$

What are the conditions for equality?

4. Generalize the above results to integrals and prove the Cauchy–Schwartz inequality

$$\left| \int_{-\infty}^{\infty} x(t) y^*(t) dt \right| \leq \left[ \int_{-\infty}^{\infty} |x(t)|^2 dt \right]^{\frac{1}{2}} \left[ \int_{-\infty}^{\infty} |y(t)|^2 dt \right]^{\frac{1}{2}}$$

What are the conditions for equality?

**2.10** Determine the Fourier transform of each of the following signals ( $\alpha$  is positive).

1.  $x(t) = \frac{1}{1+t^2}$
2.  $\Pi(t-3) + \Pi(t+3)$
3.  $\Lambda(2t+3) + \Lambda(3t-2)$
4.  $\text{sinc}^3 t$
5.  $t \text{sinc } t$
6.  $t \cos 2\pi f_0 t$
7.  $e^{-\alpha t} \cos(\beta t)$
8.  $t e^{-\alpha t} \cos(\beta t)$

**2.11** Show that the Fourier transform of  $\frac{1}{2}\delta(t + \frac{1}{2}) + \frac{1}{2}\delta(t - \frac{1}{2})$  is  $\cos(\pi f)$ . Prove the following transform pairs

$$\mathcal{F}[\cos(\pi t)] = \frac{1}{2}\delta\left(f + \frac{1}{2}\right) + \frac{1}{2}\delta\left(f - \frac{1}{2}\right)$$

and

$$\mathcal{F}[\sin(\pi t)] = \frac{j}{2} \delta\left(f + \frac{1}{2}\right) - \frac{j}{2} \delta\left(f - \frac{1}{2}\right)$$

**2.12** Determine the Fourier transform of the signals shown in Figure P-2.12:

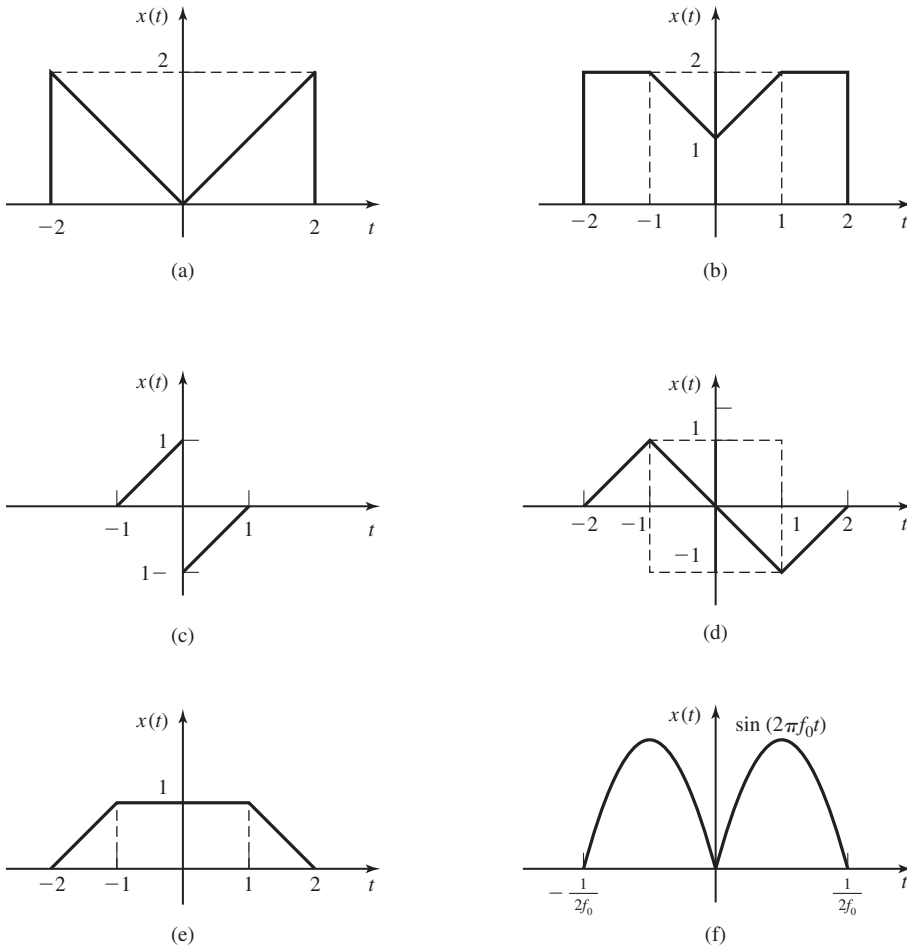


**Figure P-2.12**

**2.13** Prove the scaling property of the Fourier transform.

**2.14** Prove the convolution property of the Fourier transform.

**2.15** Prove the time shift property of the Fourier transform.

**2.16** Prove the Parseval's theorem and conclude Rayleigh's theorem from it.

**2.17** Use the convolution theorem to show that

$$\text{sinc}(t) \star \text{sinc}(t) = \text{sinc}(t)$$

**2.18** Prove that convolution in the frequency domain is equivalent to multiplication in the time domain; that is,

$$\mathcal{F}[x(t)y(t)] = X(f) \star Y(f)$$

**2.19** Let  $x(t)$  be an arbitrary signal and define  $x_1(t) = \sum_{n=-\infty}^{\infty} x(t - nT_0)$ .

1. Show that  $x_1(t)$  is a periodic signal.
2. How can you write  $x_1(t)$  in terms of  $x(t)$  and  $\sum_{n=-\infty}^{\infty} \delta(t - nT_0)$ ?
3. Find the Fourier transform of  $x_1(t)$  in terms of the Fourier transform of  $x(t)$ .

**2.20** Using the properties of the Fourier transform, evaluate the following integrals ( $\alpha$  is positive)

1.  $\int_{-\infty}^{\infty} \text{sinc}^5(t) dt$
2.  $\int_0^{\infty} e^{-\alpha t} \text{sinc}(t) dt$
3.  $\int_0^{\infty} e^{-\alpha t} \text{sinc}^2(t) dt$
4.  $\int_0^{\infty} e^{-\alpha t} \cos(\beta t) dt$

**2.21** A linear time-invariant system with impulse response  $h(t) = e^{-\alpha t} u_{-1}(t)$  is driven by the input  $x(t) = e^{-\beta t} u_{-1}(t)$ . It is assumed that  $\alpha, \beta > 0$ . Using frequency domain analysis, find the output of the system. Is the output power-type or energy-type? Find its power or energy.

**2.22** Let  $x(t)$  be periodic with period  $T_0$ , and let  $0 \leq \alpha < T_0$ . Define

$$x_\alpha(t) = \begin{cases} x(t), & \alpha \leq t < \alpha + T_0 \\ 0, & \text{otherwise} \end{cases}$$

and let  $X_\alpha(f)$  denote the Fourier transform of  $x_\alpha(t)$ . Prove that  $X_\alpha(\frac{n}{T_0})$  is independent of the choice of  $\alpha$ .

**2.23** By computing the Fourier series coefficients for the periodic signal  $\sum_{n=-\infty}^{\infty} \delta(t - nT_s)$ , show that

$$\sum_{n=-\infty}^{\infty} \delta(t - nT_s) = \frac{1}{T_s} \sum_{n=-\infty}^{\infty} e^{jn \frac{2\pi t}{T_s}}$$

Using this result, prove that for any signal  $x(t)$  and any  $T_s$ , the following identity holds

$$\sum_{n=-\infty}^{\infty} x(t - nT_s) = \frac{1}{T_s} \sum_{n=-\infty}^{\infty} X\left(\frac{n}{T_s}\right) e^{jn \frac{2\pi t}{T_s}}$$

From this, conclude the following relation known as *Poisson's sum formula*.

$$\sum_{n=-\infty}^{\infty} x(nT_s) = \frac{1}{T_s} \sum_{n=-\infty}^{\infty} X\left(\frac{n}{T_s}\right)$$

**2.24** Using Poisson's sum formula in Problem 2.23, show that

1.  $\sum_{n=-\infty}^{\infty} \frac{2\alpha}{\alpha^2 + 4\pi^2 n^2} = \sum_{n=-\infty}^{\infty} e^{-\alpha|n|}$  for all  $\alpha > 0$
2.  $\sum_{n=-\infty}^{\infty} \operatorname{sinc}\left(\frac{n}{K}\right) = K$  for all  $K \in \{1, 2, \dots\}$
3.  $\sum_{n=-\infty}^{\infty} \operatorname{sinc}^2\left(\frac{n}{K}\right) = K$  for all  $K \in \{1, 2, \dots\}$

**2.25** The response of an LTI system to  $e^{-\alpha t}u_{-1}(t)$ , ( $\alpha > 0$ ), is  $\delta(t)$ . Using frequency domain analysis techniques find the response of the system to  $x(t) = e^{-\alpha t} \cos(\beta t)u_{-1}(t)$ .

**2.26** Find the output of an LTI system with impulse response  $h(t)$  when driven by the input  $x(t)$  in each of the following cases.

1.  $h(t) = \delta(t) + \delta'(t)$       $x(t) = e^{-\alpha|t|}$ ,     ( $\alpha > 0$ )
2.  $h(t) = e^{-\alpha t}u_{-1}(t)$       $x(t) = e^{-\beta t}u_{-1}(t)$ ,     ( $\alpha, \beta > 0$ )  
(Treat the special case  $\alpha = \beta$  separately.)
3.  $h(t) = e^{-\alpha t} \cos(\beta t)u_{-1}(t)$       $x(t) = e^{-\beta t}u_{-1}(t)$ ,     ( $\alpha, \beta > 0$ )  
(Treat the special case  $\alpha = \beta$  separately.)
4.  $h(t) = e^{-\alpha|t|}u_{-1}(t)$       $x(t) = e^{-\beta t}u_{-1}(t)$ ,     ( $\alpha, \beta > 0$ )  
(Treat the special case  $\alpha = \beta$  separately.)
5.  $h(t) = \operatorname{sinc}(t)$       $x(t) = \operatorname{sinc}^2(t)$

**2.27** Can the response of an LTI system to  $x(t) = \operatorname{sinc}(t)$  be  $y(t) = \operatorname{sinc}^2(t)$ ? Justify your answer.

**2.28** Let the response of an LTI system to  $\Pi(t)$  be  $\Lambda(t)$ .

1. Can you find the response of this system to  $x(t) = \cos 2\pi t$  from the information provided?
2. Show that  $h_1(t) = \Pi(t)$  and  $h_2(t) = \Pi(t) + \cos 2\pi t$  can both be impulse responses of this system, and therefore having the response of a system to  $\Pi(t)$  does not uniquely determine the system.
3. Does the response of an LTI system to  $u_{-1}(t)$  uniquely determine the system? How about the response to  $e^{-\alpha t}u_{-1}(t)$  for some  $\alpha > 0$ ? In general, what conditions must the input  $x(t)$  satisfy so that the system can be uniquely determined by knowing its corresponding output?

**2.29** Classify the following signals into energy-type, power-type, and neither energy-type nor power-type signals. For energy-type and power-type signals, find the energy or the power content of the signal.

1.  $x_1(t) = e^{-t} \cos t u_{-1}(t)$
2.  $x_2(t) = e^{-t} \cos t$

3.  $x_3(t) = \text{sgn}(t)$
4.  $x_4(t) = A \cos 2\pi f_1 t + B \cos 2\pi f_2 t$

**2.30** Using the definition of power-type and energy-type signals,

1. Show that  $x(t) = Ae^{j(2\pi f_0 t + \theta)}$  is a power-type signal and its power content is  $A^2$ .
2. Show that the unit step signal  $u_{-1}(t)$  (the unit step function) is a power-type signal and find its power content.
3. Show that the signal

$$x(t) = \begin{cases} Kt^{-\frac{1}{4}} & t > 0 \\ 0, & t \leq 0 \end{cases}$$

is neither an energy- nor a power-type signal.

**2.31** Determine whether these signals are energy-type or power-type. In each case, find the energy or power-spectral density and also the energy or power content of the signal.

1.  $x(t) = e^{-\alpha t} \cos(\beta t)u_{-1}(t) \quad \alpha, \beta > 0$
2.  $x(t) = \text{sinc}(t)$
3.  $x(t) = \sum_{n=-\infty}^{\infty} \Lambda(t - 2n)$
4.  $x(t) = u_{-1}(t)$
5.  $x(t) = \frac{1}{t}$

**2.32** Find the energy spectral density and the energy content, or power-spectral density and the power content of the output of the following LTI systems when driven by the signals of the previous problem.

1.  $h(t) = e^{-\gamma t}u_{-1}(t)$
2.  $h(t) = \text{sinc}(6t)$
3.  $h(t) = \frac{1}{\pi t}$

**2.33** Show that if  $x_T(t)$  denotes the truncated signal corresponding to the power-type signal  $x(t)$ ; that is,

$$x_T(t) = \begin{cases} x(t) & -\frac{T}{2} < t \leq \frac{T}{2} \\ 0, & \text{otherwise} \end{cases}$$

and if  $\mathcal{S}_{x_T}(f)$  denotes the energy spectral density of  $x_T(f)$ , then  $\mathcal{S}_x(f)$ , the power-spectral density of  $x(t)$ , can be expressed as

$$\mathcal{S}_x(f) = \lim_{T \rightarrow \infty} \frac{\mathcal{S}_{x_T}(f)}{T}$$

**2.34** Show that if the input to an LTI system is energy-type and the impulse response of the system is also energy-type, then the output is also energy-type. Can you

give an example of an LTI system with an energy-type signal as its input such that the corresponding output signal is not energy-type?

- 2.35** For a lowpass signal with a bandwidth of 6000 Hz, what is the minimum sampling frequency for perfect reconstruction of the signal? What is the minimum required sampling frequency if a guard band of 2000 Hz is required? What is the minimum required sampling frequency and the value of  $K$  for perfect reconstruction if the reconstruction filter has the following frequency response

$$H(f) = \begin{cases} K, & |f| < 7000 \\ K - K \frac{|f| - 7000}{3000}, & 7000 < |f| < 10000 \\ 0, & \text{otherwise} \end{cases}$$

- 2.36** Let the signal  $x(t) = A \operatorname{sinc}(1000t)$  be sampled with a sampling frequency of 2000 samples per second. Determine the most general class of reconstruction filters for perfect reconstruction of this signal.
- 2.37** The lowpass signal  $x(t)$  with a bandwidth of  $W$  is sampled with a sampling interval of  $T_s$  and the signal

$$x_p(t) = \sum_{n=-\infty}^{\infty} x(nT_s) p(t - nT_s)$$

is generated, where  $p(t)$  is an arbitrary shaped pulse (not necessarily time-limited to the interval  $[0, T_s]$ ).

1. Find the Fourier transform of  $x_p(t)$ .
  2. Find the conditions for perfect reconstruction of  $x(t)$  from  $x_p(t)$ .
  3. Determine the required reconstruction filter.
- 2.38** The lowpass signal  $x(t)$  with a bandwidth of  $W$  is sampled at the Nyquist rate and the signal

$$x_1(t) = \sum_{n=-\infty}^{\infty} (-1)^n x(nT_s) \delta(t - nT_s)$$

is generated.

1. Find the Fourier transform of  $x_1(t)$ .
  2. Can  $x(t)$  be reconstructed from  $x_1(t)$  by using an LTI system? Why?
  3. Can  $x(t)$  be reconstructed from  $x_1(t)$  by using a linear time-varying system? How?
- 2.39** A lowpass signal  $x(t)$  with bandwidth  $W$  is sampled with a sampling interval  $T_s$  and the sampled values are denoted by  $x(nT_s)$ . A new signal  $x_1(t)$  is generated by linear interpolation of the sampled values; i.e.,

$$x_1(t) = x(nT_s) + \frac{t - nT_s}{T_s} (x((n+1)T_s) - x(nT_s)) \quad nT_s \leq t < (n+1)T_s$$



1. Find the power spectrum of  $x_1(t)$ .
  2. Under what conditions can the original signal be reconstructed from the sampled signal and what is the required reconstruction filter?
- 2.40** A lowpass signal  $x(t)$  with bandwidth of 50 Hz is sampled at the Nyquist rate and the resulting sampled values are

$$x(nT_s) = \begin{cases} -1, & -4 \leq n < 0 \\ 1, & 0 < n \leq 4 \\ 0, & \text{otherwise} \end{cases}$$

1. Find  $x(.005)$ .
  2. Is this signal power-type or energy-type? Find its power or energy content.
- 2.41** Let  $W$  be arbitrary and  $x(t)$  be a lowpass signal with bandwidth  $W$ .
1. Show that the set of signals  $\{\phi_n(t)\}_{n=-\infty}^{\infty}$  where  $\phi_n = \text{sinc}(2Wt - n)$  represent an orthogonal signal set. How should these signals be weighted to generate an orthonormal set?
  2. Conclude that the reconstruction from the samples relation

$$x(t) = \sum_{n=-\infty}^{\infty} x(nT_s) \text{sinc}(2Wt - n)$$

is an orthogonal expansion relation.

3. From above, show that for all  $n$

$$\int_{-\infty}^{\infty} x(t) \text{sinc}(2Wt - n) dt = Kx(nT_s)$$

and find  $K$ .

- 2.42** In the development of the sampling theorem, we have assumed that samples are taken at multiples of  $T_s$ . What happens if we sample regularly with  $T_s$  as sampling interval but the first sample is taken at some  $0 < t_0 < T_s$ ? Using this result show that

$$x(0) = \sum_{k=-\infty}^{\infty} x(t_0 + kT_s) \text{sinc}(2W(t_0 + kT_s))$$

- 2.43** Prove that

$$x_c(t) = x(t) \cos(2\pi f_0 t) + \hat{x}(t) \sin(2\pi f_0 t)$$

$$x_s(t) = \hat{x}(t) \cos(2\pi f_0 t) - x(t) \sin(2\pi f_0 t)$$

- 2.44** Show that

$$X_c(f) = \frac{1}{2}[X_l(f) + X_l^*(f)]$$

- 2.45** A lowpass signal  $x(t)$  has a Fourier transform shown in Figure P-2.45(a). This signal is applied to the system shown in Figure P-2.45(b). The blocks marked by

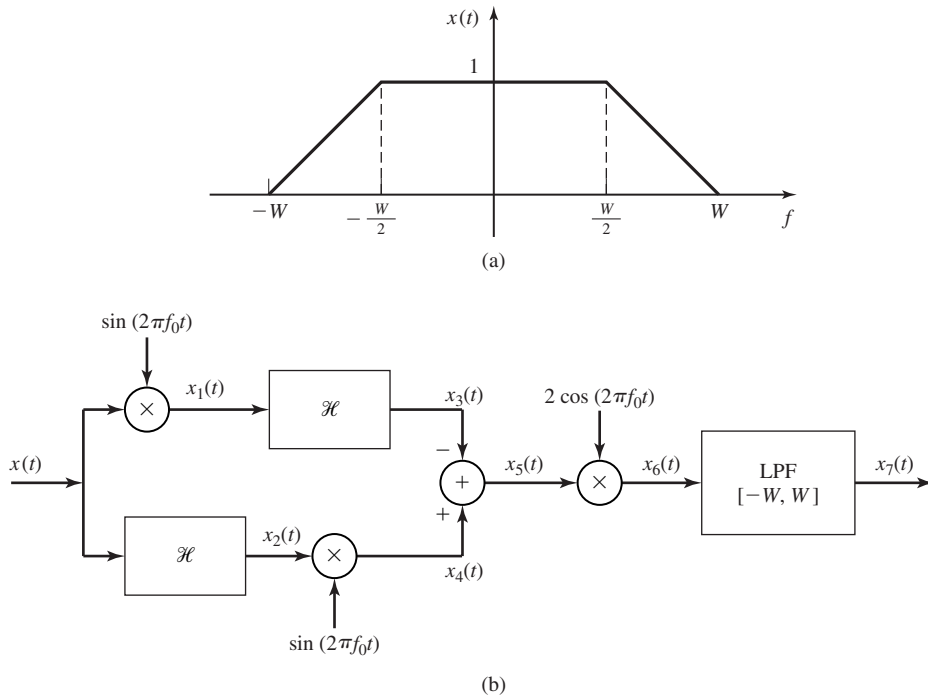


Figure P-2.45

$\mathcal{H}$  represent Hilbert transform blocks and it is assumed that  $W \ll f_0$ . Determine the signals  $x_i(t)$  for  $1 \leq i \leq 7$ , and plot  $X_i(f)$  for  $1 \leq i \leq 7$ .

- 2.46** Show that the Hilbert transform of an even signal is odd and the Hilbert transform of an odd signal is even.
- 2.47** Show that the energy content of a signal is equal to the energy content of its Hilbert transform.
- 2.48** Show that the signal  $x(t)$  and its Hilbert transform are orthogonal; i.e.,

$$\int_{-\infty}^{\infty} x(t)\hat{x}(t) dt = 0$$

- 2.49** Let  $x(t)$  represent a bandpass signal and  $m(t)$  denote a lowpass signal with non-overlapping spectra. Show that the Hilbert transform of  $c(t) = m(t)x(t)$  is equal to  $m(t)\hat{x}(t)$ .
- 2.50** Show that if  $X(f)|_{f=0} = 0$ , then  $\widehat{\hat{x}}(t) = -x(t)$ .
- 2.51** Let  $x(t)$  denote a lowpass signal. Determine the Hilbert transform of  $x(t) \cos(2\pi f_0 t)$ , where  $f_0$  is much larger than the bandwidth of  $x(t)$ .
- 2.52** Show that the Hilbert transform of  $A \sin(2\pi f_0 t + \theta)$  is  $-A \cos(2\pi f_0 t + \theta)$ .
- 2.53** Show that the Hilbert transform of the signal  $e^{j2\pi f_0 t}$  is equal to  $-j \operatorname{sgn}(f_0) e^{j2\pi f_0 t}$ .

**2.54** Show that

$$\mathcal{F}\left[\frac{d}{dt}\widehat{x(t)}\right] = 2\pi|f|\mathcal{F}[x(t)]$$

**2.55** Show that the Hilbert transform of the derivative of a signal is equal to the derivative of its Hilbert transform.

**2.56** The bandpass signal  $x(t) = \text{sinc}t \cos 2\pi f_0 t$  is passed through a bandpass filter with impulse response  $h(t) = \text{sinc}^2(t) \sin 2\pi f_0 t$ . Using the lowpass equivalents of both the input and the impulse response, find the lowpass equivalent of the output and from it find the output  $y(t)$ .

**2.57** The real narrowband signal  $x(t)$ , whose frequency components are in the neighborhood of some  $f_0$  (and  $-f_0$ ), is passed through a filter with transfer function  $H(f)$  and the output is denoted by  $y(t)$ . The magnitude of the transfer function is denoted by  $A(f)$  and its phase is denoted by  $\theta(f)$ . It is assumed that the transfer function of the filter is smooth enough such that in the bandwidth of the input signal the magnitude of the transfer function is essentially constant and its phase can be approximated by its first order Taylor series expansion; i.e.,

$$\begin{aligned} A(f) &\approx A(f_0) \\ \theta(f) &\approx \theta(f_0) + (f - f_0)\theta'(f)|_{f=f_0} \end{aligned}$$

1. Show that  $Y_l(f)$ , the Fourier transform of the lowpass equivalent of the output, can be written as

$$Y_l(f) \approx X_l(f)A(f_0)e^{j(\theta(f_0)+f\theta'(f)|_{f=f_0})}$$

2. Conclude that

$$y(t) \approx A(f_0) + V_x(t - t_g) \cos(2\pi f_0 t - t_p)$$

where  $V_x(t)$  is the envelope of the input  $x(t)$  and

$$\begin{aligned} t_g &= -\frac{1}{2\pi} \frac{d\theta(f)}{df} \Big|_{f=f_0} \\ t_p &= -\frac{1}{2\pi} \frac{\theta(f)}{f} \Big|_{f=f_0} \end{aligned}$$

3. The quantities  $t_g$  and  $t_p$  are called *envelope delay* (or *group delay*) and *phase delay*, respectively. Can you interpret their role and justify this nomenclature?

**2.58** We have seen that the Hilbert transform introduces a  $90^\circ$  phase shift in the components of a signal and the transfer function of a quadrature filter can be written as

$$H(f) = \begin{cases} e^{-j\frac{\pi}{2}}, & f = 0 \\ e^{j\frac{\pi}{2}}, & f < 0 \end{cases}$$

We can generalize this concept to a new transform that introduces a phase shift of  $\theta$  in the frequency components of a signal, by introducing

$$H_\theta(f) = \begin{cases} e^{-j\theta}, & f = 0 \\ e^{j\theta}, & f < 0 \end{cases}$$

and denote the result of this transform by  $x_\theta(t)$ ; i.e.,  $X_\theta(f) = X(f)H_\theta(f)$ , where  $X_\theta(f)$  denotes the Fourier transform of  $x_\theta(t)$ . Throughout this problem assume that the signal  $x(t)$  does not contain any DC components.

1. Find  $h_\theta(t)$ , the impulse response of the filter representing the transform described above.
  2. Show that  $x_\theta(t)$  is a linear combination of  $x(t)$  and its Hilbert transform.
  3. Show that if  $x(t)$  is an energy-type signal,  $x_\theta(t)$  will also be an energy-type signal and its energy content will be equal to the energy content of  $x(t)$ .
- 2.59** Let  $m(t) = \text{sinc}^2(t)$  and let  $x(t) = m(t) \cos 2\pi f_0 t - \hat{m}(t) \sin 2\pi f_0 t$  represent a bandpass signal.
1. Find the pre-envelope,  $z(t)$ , and the lowpass equivalent signal to  $x(t)$ .
  2. Determine and plot the Fourier transform of the signal  $x(t)$ . What is the bandwidth of  $x(t)$ ?
  3. Repeat for  $x(t) = m(t) \cos 2\pi f_0 t + \hat{m}(t) \sin 2\pi f_0 t$ .

# 3

## *Analog Signal Transmission and Reception*

A large number of information sources are analog sources. Analog sources can be modulated and transmitted directly or can be converted to digital data and transmitted using digital modulation techniques. The notion of analog to digital conversion will be examined in detail in Chapter 6.

Speech, image, and video are examples of analog sources of information. Each of these sources is characterized by its bandwidth, dynamic range, and the nature of the signal. For instance, in case of audio, and black and white video, the signal has just one component measuring the pressure or intensity, but in case of color video, the signal has four components measuring red, green, and blue color components, and the intensity.

In spite of the general trend toward digital transmission of analog signals, there is still today a significant amount of analog signal transmission, especially in audio and video broadcast. In this chapter, we treat the transmission of analog signals by carrier modulation. The treatment of the performance of these systems in the presence of noise is being deferred to Chapter 5. We consider the transmission of an analog signal by impressing it on either the amplitude, the phase, or the frequency of a sinusoidal carrier. Methods for demodulation of the carrier-modulated signal to recover the analog information signal are also described.

### **3.1 INTRODUCTION TO MODULATION**

The analog signal to be transmitted is denoted by  $m(t)$ , which is assumed to be a lowpass signal of bandwidth  $W$ , in other words,  $M(f) \equiv 0$ , for  $|f| > W$ . We also assume that the signal is a power-type signal (see Section 2.3) whose power is denoted by  $P_m$ ,

where

$$P_m = \lim_{T \rightarrow \infty} \frac{1}{T} \int_{-T/2}^{T/2} |m(t)|^2 dt$$

The message signal  $m(t)$  is transmitted through the communication channel by impressing it on a carrier signal of the form

$$c(t) = A_c \cos(2\pi f_c t + \phi_c) \quad (3.1.1)$$

where  $A_c$  is the carrier amplitude,  $f_c$  is the carrier frequency, and  $\phi_c$  is the carrier phase. We say that the message signal  $m(t)$  modulates the carrier signal  $c(t)$  in either amplitude, frequency, or phase, if after modulation, the amplitude, frequency, or phase of the signal become functions of the message signal. In effect, modulation converts the message signal  $m(t)$  from lowpass to bandpass, in the neighborhood of the center frequency  $f_c$ .

Modulation of the carrier  $c(t)$  by the message signal  $m(t)$  is performed in order to achieve one or more of the following objectives: (1) The lowpass signal is translated in frequency to the passband of the channel so that the spectrum of the transmitted bandpass signal will match the passband characteristics of the channel; (2) to accommodate for simultaneous transmission of signals from several message sources, by means of frequency-division multiplexing (see Section 3.2.6); and (3) to expand the bandwidth of the transmitted signal in order to increase its noise immunity in transmission over a noisy channel, as we will see in our discussion of angle-modulation noise performance in Chapter 5. We will see that objectives (1) and (2) are met by all of the modulation methods described next. Objective (3) is met by employing angle modulation to spread the signal  $m(t)$  over a larger bandwidth.

In the following sections of this chapter we consider the transmission and reception of analog signals by carrier-amplitude modulation (AM), carrier-frequency modulation (FM) and carrier-phase modulation (PM). Comparisons will be made among these modulation methods on the basis of their bandwidth requirements and their implementation complexity. Their performance in the presence of additive noise disturbances and their power efficiency, will be treated in Chapter 5.

## 3.2 AMPLITUDE MODULATION (AM)

In amplitude modulation, the message signal  $m(t)$  is impressed on the amplitude of the carrier signal  $c(t)$ . There are several different ways of amplitude modulating the carrier signal by  $m(t)$ , each of which results in different spectral characteristics for the transmitted signal. Next, we describe these methods, which are called (1) double-sideband, suppressed carrier AM, (2) conventional double-sideband AM, (3) single-sideband AM, and (4) vestigial-sideband AM.

### 3.2.1 Double-Sideband Suppressed Carrier AM

A double-sideband, suppressed carrier (DSB-SC) AM signal is obtained by multiplying the message signal  $m(t)$  with the carrier signal  $c(t)$ . Thus, we have the amplitude

modulated signal

$$\begin{aligned} u(t) &= m(t)c(t) \\ &= A_c m(t) \cos(2\pi f_c t + \phi_c) \end{aligned}$$

**Bandwidth Requirements.** The spectrum of the modulated signal can be obtained by taking the Fourier transform of  $u(t)$ .

$$\begin{aligned} U(f) &= \mathcal{F}[m(t)] \star \mathcal{F}[A_c \cos(2\pi f_c t + \phi_c)] \\ &= M(f) \star \frac{A_c}{2} [e^{j\phi_c} \delta(f - f_c) + e^{-j\phi_c} \delta(f + f_c)] \\ &= \frac{A_c}{2} [M(f - f_c)e^{j\phi_c} + M(f + f_c)e^{-j\phi_c}] \end{aligned}$$

Figure 3.1 illustrates the magnitude and phase spectra for  $M(f)$  and  $U(f)$ .

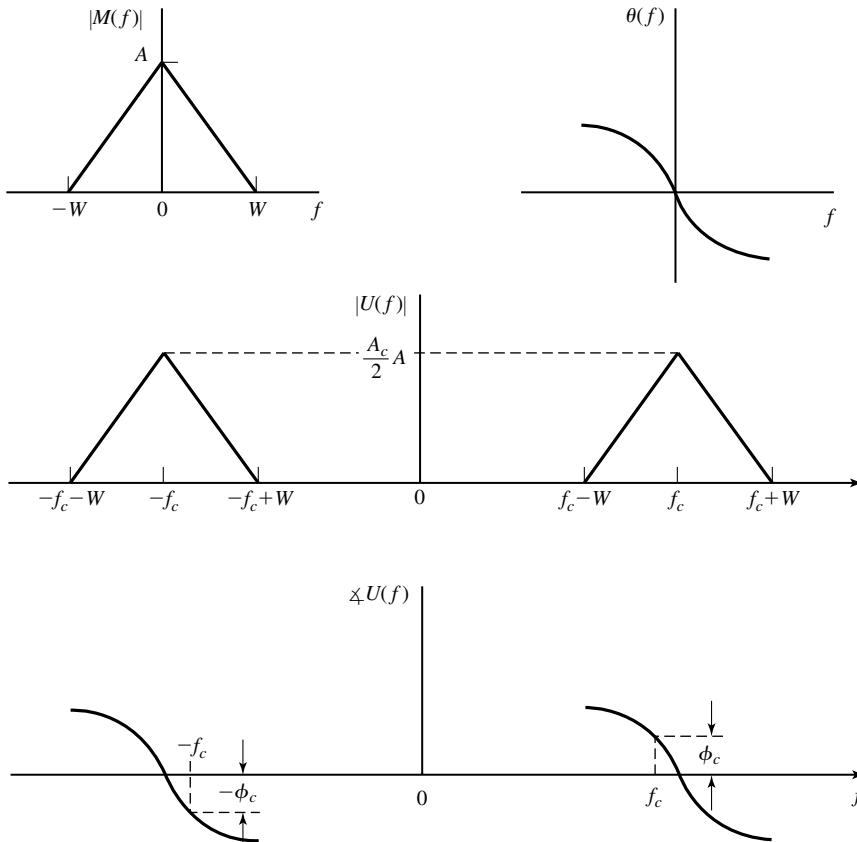


**Figure 3.1** Magnitude and phase spectra of the message signal  $m(t)$  and the DSB AM modulated signal  $u(t)$ .

We observe that the magnitude of the spectrum of the message signal  $m(t)$  has been translated or shifted in frequency by an amount  $f_c$ . The phase of the message signal has been translated in frequency and offset by the carrier phase  $\phi_c$ . Furthermore, the bandwidth occupancy of the amplitude-modulated signal is  $2W$ , whereas the bandwidth of the message signal  $m(t)$  is  $W$ . Therefore, the channel bandwidth required to transmit the modulated signal  $u(t)$  is  $B_c = 2W$ .

The frequency content of the modulated signal  $u(t)$  in the frequency band  $|f| > f_c$  is called the *upper sideband* of  $U(f)$ , and the frequency content in the frequency band  $|f| < f_c$  is called the *lower sideband* of  $U(f)$ . It is important to note that either one of the sidebands of  $U(f)$  contains all the frequencies that are in  $M(f)$ . That is, the frequency content of  $U(f)$  for  $f > f_c$  corresponds to the frequency content of  $M(f)$  for  $f > 0$ , and the frequency content of  $U(f)$  for  $f < -f_c$  corresponds to the frequency content of  $M(f)$  for  $f < 0$ . Hence, the upper sideband of  $U(f)$  contains all the frequencies in  $M(f)$ . A similar statement applies to the lower sideband of  $U(f)$ . Therefore, the lower sideband of  $U(f)$  contains all the frequency content of the message signal  $M(f)$ . Since  $U(f)$  contains both the upper and the lower sidebands, it is called a *double-sideband (DSB) AM signal*.

The other characteristic of the modulated signal  $u(t)$  is that it does not contain a carrier component. That is, all the transmitted power is contained in the modulating (message) signal  $m(t)$ . This is evident from observing the spectrum of  $U(f)$ . We note that, as long as  $m(t)$  does not have any DC component, there is no impulse in  $U(f)$  at  $f = f_c$ , which would be the case if a carrier component was contained in the modulated signal  $u(t)$ . For this reason,  $u(t)$  is called a *suppressed-carrier signal*. Therefore,  $u(t)$  is a DSB-SC AM signal.

### Example 3.2.1

Suppose that the modulating signal  $m(t)$  is a sinusoid of the form

$$m(t) = a \cos 2\pi f_m t \quad f_m \ll f_c$$

Determine the DSB-SC AM signal and its upper and lower sidebands.

**Solution** The DSB-SC AM is expressed in the time domain as

$$\begin{aligned} u(t) &= m(t)c(t) = A_c a \cos 2\pi f_m t \cos(2\pi f_c t + \phi_c) \\ &= \frac{A_c a}{2} \cos[2\pi(f_c - f_m)t + \phi_c] + \frac{A_c a}{2} \cos[2\pi(f_c + f_m)t + \phi_c] \end{aligned}$$

In the frequency domain, the modulated signal has the form

$$\begin{aligned} U(f) &= \frac{A_c a}{4} [e^{j\phi_c} \delta(f - f_c + f_m) + e^{-j\phi_c} \delta(f + f_c - f_m)] \\ &\quad + \frac{A_c a}{4} [e^{j\phi_c} \delta(f - f_c - f_m) + e^{-j\phi_c} \delta(f + f_c + f_m)] \end{aligned}$$

This spectrum is shown in Figure 3.2(a).



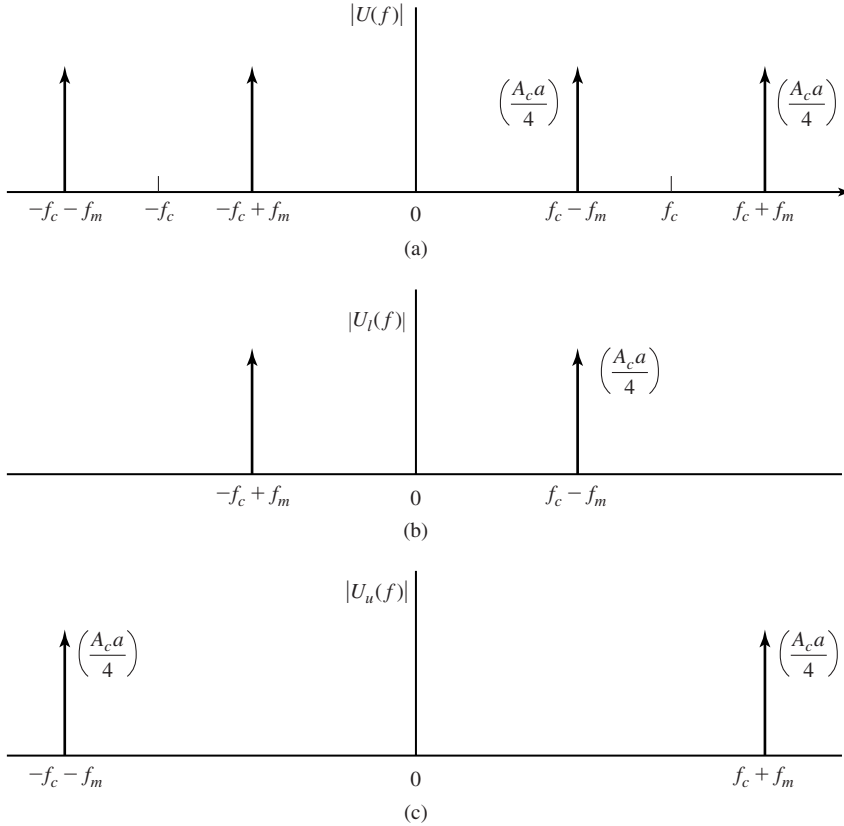


**Figure 3.2** (a) The (magnitude) spectrum of a DSB-SC AM signal for a sinusoidal message signal and (b) its lower and (c) upper sidebands.

The lower sideband of  $u(t)$  is the signal

$$u_l(t) = \frac{A_c a}{2} \cos[2\pi(f_c - f_m)t + \phi_c]$$

and its spectrum is illustrated in Figure 3.2(b). Finally, the upper sideband of  $u(t)$  is the signal

$$u_u(t) = \frac{A_c a}{2} \cos[2\pi(f_c + f_m)t + \phi_c]$$

and its spectrum is illustrated in Figure 3.2(c).

**Power Content of DSB-SC Signals.** In order to compute the power content of the DSB-SC signal, without loss of generality we can assume that the phase of the signal is set to zero. This is because the power in a signal is independent of the phase

of the signal. The time-average autocorrelation function of the signal  $u(t)$  is given by

$$\begin{aligned}
 R_u(\tau) &= \lim_{T \rightarrow \infty} \frac{1}{T} \int_{-T/2}^{T/2} u(t)u(t - \tau) dt \\
 &= \lim_{T \rightarrow \infty} \frac{1}{T} \int_{-T/2}^{T/2} A_c^2 m(t)m(t - \tau) \cos(2\pi f_c t) \cos(2\pi f_c(t - \tau)) dt \\
 &= \frac{A_c^2}{2} \lim_{T \rightarrow \infty} \frac{1}{T} \int_{-T/2}^{T/2} m(t)m(t - \tau) [\cos(4\pi f_c t - 2\pi f_c \tau) + \cos(2\pi f_c \tau)] dt \\
 &= \frac{A_c^2}{2} R_m(\tau) \cos(2\pi f_c \tau) \tag{3.2.1}
 \end{aligned}$$

where we have used the fact that

$$\lim_{T \rightarrow \infty} \int_{-T/2}^{T/2} m(t)m(t - \tau) \cos(4\pi f_c t - 2\pi f_c \tau) dt = 0$$

This is because

$$\begin{aligned}
 &\int_{-\infty}^{\infty} m(t)m(t - \tau) \cos(4\pi f_c t - 2\pi f_c \tau) dt \\
 &\stackrel{(a)}{=} \int_{-\infty}^{\infty} \mathcal{F}[m(t - \tau)] \{\mathcal{F}[m(t) \cos(4\pi f_c t - 2\pi f_c \tau)]\}^* df \\
 &= \int_{-\infty}^{\infty} e^{-j2\pi f \tau} M(f) \left[ \frac{M(f - 2f_c)e^{-j2\pi f_c \tau}}{2} + \frac{M(f + 2f_c)e^{j2\pi f_c \tau}}{2} \right]^* df \\
 &\stackrel{(b)}{=} 0
 \end{aligned}$$

where in (a) we have used Parseval's relation [see Equation (2.2.11)] and in (b) we have used the fact that  $M(f)$  is limited to the frequency band  $[-W, W]$  and  $W \ll f_c$ , hence, there is no frequency overlap between  $M(f)$  and  $M(f \pm 2f_c)$ .

By taking the Fourier transform of both sides of Equation (3.2.1), we can obtain the power-spectral density of the modulated signal as

$$\begin{aligned}
 \mathcal{S}_u(f) &= \mathcal{F} \left[ \frac{A_c^2}{2} R_m(\tau) \cos(2\pi f_c \tau) \right] \\
 &= \frac{A_c^2}{4} [\mathcal{S}_m(f - f_c) + \mathcal{S}_m(f + f_c)] \tag{3.2.2}
 \end{aligned}$$

This shows that the power-spectral density of the DSB-SC signal is the power-spectral density of the message shifted upward and downward by  $f_c$  and scaled by  $A_c^2/4$ . To obtain the total power in the modulated signal, we can either substitute  $\tau = 0$  in the time-average autocorrelation function as given in Equation (3.2.1), or we can integrate the power-spectral density of the modulated signal given in Equation (3.2.2) over all

frequencies. Using the first approach from Equation (3.2.1), we have

$$\begin{aligned}
 P_u &= \frac{A_c^2}{2} R_m(\tau) \cos(2\pi f_c \tau) \Big|_{\tau=0} \\
 &= \frac{A_c^2}{2} R_m(0) \\
 &= \frac{A_c^2}{2} P_m
 \end{aligned} \tag{3.2.3}$$

where  $P_m = R_m(0)$  is the power in the message signal.

### Example 3.2.2

In Example 3.2.1, determine the power-spectral density of the modulated signal, the power in the modulated signal, and the power in each of the sidebands.

**Solution** The message signal is  $m(t) = a \cos 2\pi f_m t$ , its power-spectral density is given by

$$\mathcal{S}_m(f) = \frac{a^2}{4} \delta(f - f_m) + \frac{a^2}{4} \delta(f + f_m) \tag{3.2.4}$$

Substituting in Equation (3.2.2) we obtain the power-spectral density of the modulated signal as

$$\mathcal{S}_u(f) = \frac{A_c^2 a^2}{16} [\delta(f - f_m - f_c) + \delta(f + f_m - f_c) + \delta(f - f_m + f_c) + \delta(f - f_m - f_c)]$$

The total power in the modulated signal is the integral of  $\mathcal{S}_u(f)$  and is given by

$$P_u = \int_{-\infty}^{\infty} \mathcal{S}_u(f) df = \frac{A_c^2 a^2}{4}$$

Because of symmetry of sidebands the powers the upper and lower sidebands,  $P_{us}$  and  $P_{ls}$ , are equal and given by

$$P_{us} = P_{ls} = \frac{A_c^2 a^2}{8}$$

It can also be observed from the power-spectral density of the DSB-SC signal [see Equation (3.2.2)] that the bandwidth of the modulated signal is  $2W$ , twice the bandwidth of the message signal, and that there exists no impulse at the carrier frequency  $\pm f_c$  in the power-spectral density. Therefore, the modulated signal is *suppressed carrier* (SC).

**Demodulation of DSB-SC AM Signals.** In the absence of noise, and with the assumption of an ideal channel, the received signal is equal to the modulated signal; i.e.,

$$\begin{aligned}
 r(t) &= u(t) \\
 &= A_c m(t) \cos(2\pi f_c t + \phi_c)
 \end{aligned} \tag{3.2.5}$$

Suppose we demodulate the received signal by first multiplying  $r(t)$  by a locally generated sinusoid  $\cos(2\pi f_c t + \phi)$ , where  $\phi$  is the phase of the sinusoid, and then passing the product signal through an ideal lowpass filter having a bandwidth  $W$ . The

multiplication of  $r(t)$  with  $\cos(2\pi f_c t + \phi)$  yields

$$\begin{aligned} r(t) \cos(2\pi f_c t + \phi) &= A_c m(t) \cos(2\pi f_c t + \phi_c) \cos(2\pi f_c t + \phi) \\ &= \frac{1}{2} A_c m(t) \cos(\phi_c - \phi) + \frac{1}{2} A_c m(t) \cos(4\pi f_c t + \phi + \phi_c) \end{aligned}$$

The lowpass filter rejects the double frequency components and passes only the lowpass components. Hence, its output is

$$y_\ell(t) = \frac{1}{2} A_c m(t) \cos(\phi_c - \phi) \quad (3.2.6)$$

Note that  $m(t)$  is multiplied by  $\cos(\phi_c - \phi)$ . Thus, the desired signal is scaled in amplitude by a factor that depends on the phase difference between the phase  $\phi_c$  of the carrier in the received signal and the phase  $\phi$  of the locally generated sinusoid. When  $\phi_c \neq \phi$ , the amplitude of the desired signal is reduced by the factor  $\cos(\phi_c - \phi)$ . If  $\phi_c - \phi = 45^\circ$ , the amplitude of the desired signal is reduced by  $\sqrt{2}$  and the signal power is reduced by a factor of two. If  $\phi_c - \phi = 90^\circ$ , the desired signal component vanishes.

The above discussion demonstrates the need for a *phase-coherent or synchronous demodulator* for recovering the message signal  $m(t)$  from the received signal. That is, the phase  $\phi$  of the locally generated sinusoid should ideally be equal to the phase  $\phi_c$  of the received carrier signal.

A sinusoid that is phase-locked to the phase of the received carrier can be generated at the receiver in one of two ways. One method is to add a carrier component into the transmitted signal as illustrated in Figure 3.3.

We call such a carrier component “a pilot tone.” Its amplitude  $A_p$  and, hence, its power  $A_p^2/2$  is selected to be significantly smaller than that of the modulated signal  $u(t)$ . Thus the transmitted signal is double-sideband, but it is no longer a suppressed carrier signal. At the receiver, a narrowband filter tuned to frequency  $f_c$  is used to filter out the pilot signal component and its output is used to multiply the received signal as shown in Figure 3.4.

The reader may show that the presence of the pilot signal results in a *dc* component in the demodulated signal, which must be subtracted out in order to recover  $m(t)$ .

The addition of a pilot tone to the transmitted signal has the disadvantage of requiring that a certain portion of the transmitted signal power must be allocated to the transmission of the pilot. As an alternative, we may generate a phase-locked sinusoidal

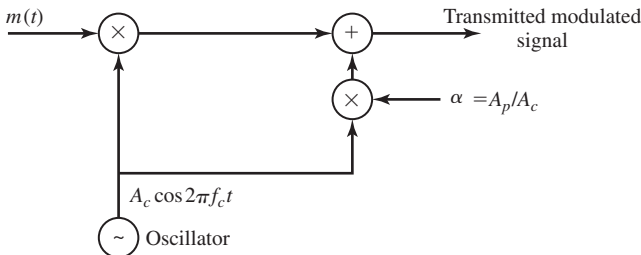


**Figure 3.3** Addition of a pilot tone to a DSB AM signal.

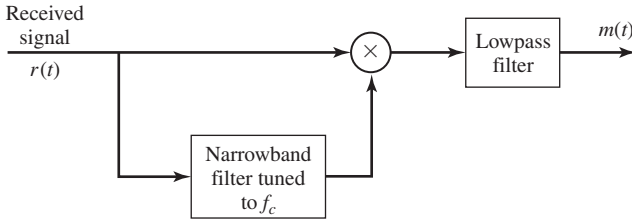


**Figure 3.4** Use of a pilot tone to demodulate a DSB AM signal.

carrier from the received signal  $r(t)$  without the need of a pilot signal. This can be accomplished by use of a *phase-locked loop (PLL)* as described in Section 5.2.

### 3.2.2 Conventional Amplitude Modulation

A conventional AM signal consists of a large carrier component in addition to the double-sideband AM modulated signal. The transmitted signal is expressed mathematically as

$$u(t) = A_c[1 + m(t)] \cos(2\pi f_c t + \phi_c) \quad (3.2.7)$$

where the message waveform is constrained to satisfy the condition that  $|m(t)| \leq 1$ . We observe that  $A_c m(t) \cos(2\pi f_c t + \phi_c)$  is a double-sideband AM signal and  $A_c \cos(2\pi f_c t + \phi_c)$  is the carrier component. Figure 3.5 illustrates an AM signal in the time domain.

As long as  $|m(t)| \leq 1$ , the amplitude  $A_c[1 + m(t)]$  is always positive. This is the desired condition for conventional DSB AM that makes it easy to demodulate, as described next. On the other hand, if  $m(t) < -1$  for some  $t$ , the AM signal is said to be *overmodulated* and its demodulation is rendered more complex. In practice,  $m(t)$  is scaled so that its magnitude is always less than unity.

It is sometimes convenient to express  $m(t)$  as

$$m(t) = am_n(t)$$

where  $m_n(t)$  is normalized such that its minimum value is  $-1$ . This can be done, for

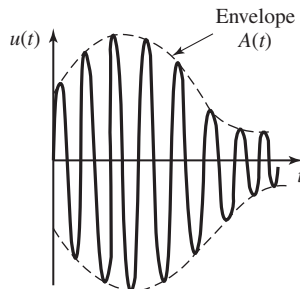


**Figure 3.5** A conventional AM signal in the time domain.

example, by defining

$$m_n(t) = \frac{m(t)}{\max|m(t)|}$$

The scale factor  $a$  is called the *modulation index*. Then the modulated signal can be expressed as

$$u(t) = A_c [1 + am_n(t)] \cos 2\pi f_c t \quad (3.2.8)$$

Let us consider the spectral characteristics of the transmitted signal  $u(t)$ .

**Bandwidth of Conventional AM Signal.** If  $m(t)$  is a deterministic signal with Fourier transform (spectrum)  $M(f)$ , the spectrum of the amplitude-modulated signal  $u(t)$  is

$$\begin{aligned} U(f) &= \mathcal{F}[am_n(t)] \star \mathcal{F}[A_c \cos(2\pi f_c t + \phi_c)] + \mathcal{F}[A_c \cos(2\pi f_c t + \phi_c)] \\ &= aM_n(f) \star \frac{A_c}{2} [e^{j\phi_c} \delta(f - f_c) + e^{-j\phi_c} \delta(f + f_c)] \\ &\quad + \frac{A_c}{2} [e^{j\phi_c} \delta(f - f_c) + e^{-j\phi_c} \delta(f + f_c)] \\ U(f) &= \frac{A_c}{2} [e^{j\phi_c} aM_n(f - f_c) + e^{j\phi_c} \delta(f - f_c) \\ &\quad + e^{-j\phi_c} aM_n(f + f_c) + e^{-j\phi_c} \delta(f + f_c)] \end{aligned}$$

Obviously, the spectrum of a conventional AM signal occupies a bandwidth twice the bandwidth of the message signal.

### Example 3.2.3

Suppose that the modulating signal  $m_n(t)$  is a sinusoid of the form

$$m_n(t) = \cos 2\pi f_m t \quad f_m \ll f_c$$

Determine the DSB AM signal, its upper and lower sidebands, and its spectrum, assuming a modulation index of  $a$ .

**Solution** From Equation (3.2.8), the DSB AM signal is expressed as

$$\begin{aligned} u(t) &= A_c [1 + a \cos 2\pi f_m t] \cos(2\pi f_c t + \phi_c) \\ &= A_c \cos(2\pi f_c t + \phi_c) + \frac{A_c a}{2} \cos[2\pi(f_c - f_m)t + \phi_c] \\ &\quad + \frac{A_c a}{2} \cos[2\pi(f_c + f_m)t + \phi_c] \end{aligned}$$

The lower sideband component is

$$u_\ell(t) = \frac{A_c a}{2} \cos[2\pi(f_c - f_m)t + \phi_c]$$

while the upper sideband component is

$$u_u(t) = \frac{A_c a}{2} \cos[2\pi(f_c + f_m)t + \phi_c]$$

The spectrum of the DSB AM signal  $u(t)$  is

$$\begin{aligned} U(f) &= \frac{A_c}{2} [e^{j\phi_c} \delta(f - f_c) + e^{-j\phi_c} \delta(f + f_c)] \\ &\quad + \frac{A_c a}{4} [e^{j\phi_c} \delta(f - f_c + f_m) + e^{-j\phi_c} \delta(f + f_c - f_m)] \\ &\quad + \frac{A_c a}{4} [e^{j\phi_c} \delta(f - f_c - f_m) + e^{-j\phi_c} \delta(f + f_c + f_m)] \end{aligned}$$

The spectrum  $|U(f)|$  is shown in Figure 3.6. It is interesting to note that the power of the carrier component, which is  $A_c^2/2$ , exceeds the total power ( $A_c^2 a^2/2$ ) of the two sidebands.

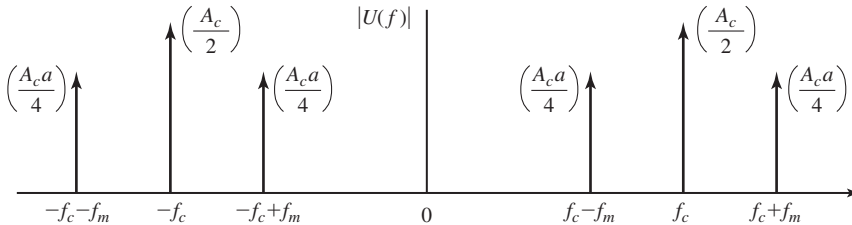


**Figure 3.6** Spectrum of a DSB AM signal in Example 3.2.3.

**Power for Conventional AM Signal.** Conventional AM signal is similar to DSB when  $m(t)$  is substituted with  $1 + am_n(t)$ . As we have already seen in the DSB-SC case, the power in the modulated signal is [see Equation (3.2.3)]

$$P_u = \frac{A_c^2}{2} P_m$$

where  $P_m$  denotes the power in the message signal. For the conventional AM

$$\begin{aligned} P_m &= \lim_{T \rightarrow \infty} \frac{1}{T} \int_{-T/2}^{T/2} (1 + am_n(t))^2 dt \\ &= \lim_{T \rightarrow \infty} \frac{1}{T} \int_{-T/2}^{T/2} (1 + a^2 m_n^2(t)) dt \end{aligned}$$

where we have assumed that the average of  $m_n(t)$  is zero. This is a reasonable assumption for many signals including audio signals. Therefore, for conventional AM

$$P_m = 1 + a^2 P_{m_n}$$

and, hence,

$$P_u = \frac{A_c^2}{2} + \frac{A_c^2}{2} a^2 P_{m_n}$$

The first component in the preceding relation is due to the existence of the carrier and this component does not carry any information. The second component is the information carrying component. Note that the second component is usually much smaller than

the first component ( $|m_n(t)| < 1$ , and for signals with large dynamic range,  $P_{m_n} \ll 1$ ). This shows that the conventional AM systems are far less power efficient compared with DSB-SC systems. The advantage of conventional AM is that it is easily demodulated.

**Demodulation of Conventional DSB AM Signals.** The major advantage of conventional AM signal transmission is the ease with which the signal can be demodulated. There is no need for a synchronous demodulator. Since the message signal  $m(t)$  satisfies the condition  $|m(t)| < 1$ , the envelope (amplitude)  $1 + m(t) > 0$ . If we rectify the received signal, we eliminate the negative values without affecting the message signal as shown in Figure 3.7. The rectified signal is equal to  $u(t)$  when  $u(t) > 0$  and zero when  $u(t) < 0$ . The message signal is recovered by passing the rectified signal through a lowpass filter whose bandwidth matches that of the message signal. The combination of the rectifier and the lowpass filter is called an *envelope detector*.

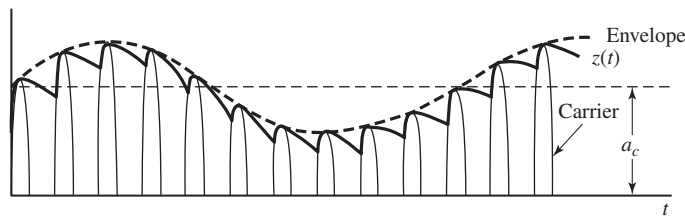


**Figure 3.7** Envelope detection of conventional AM signal.

Ideally, the output of the envelope detector is of the form

$$d(t) = g_1 + g_2m(t) \quad (3.2.9)$$

where  $g_1$  represents a *dc* component and  $g_2$  is a gain factor due to the signal demodulator. The *dc* component can be eliminated by passing  $d(t)$  through a transformer, whose output is  $g_2m(t)$ .

The simplicity of the demodulator has made conventional DSB AM a practical choice for AM radio broadcasting. Since there are literally billions of radio receivers, an inexpensive implementation of the demodulator is extremely important. The power inefficiency of conventional AM is justified by the fact that there are few broadcast transmitters relative to the number of receivers. Consequently, it is cost effective to construct powerful transmitters and sacrifice power efficiency in order to simplify the signal demodulation at the receivers.

### 3.2.3 Single-Sideband AM

In Section 3.2.1 we showed that a DSB-SC AM signal required a channel bandwidth of  $B_c = 2W$  Hz for transmission, where  $W$  is the bandwidth of the baseband signal. However, the two sidebands are redundant. Next, we demonstrate that the transmission of either sideband is sufficient to reconstruct the message signal  $m(t)$  at the receiver. Thus, we reduce the bandwidth of the transmitted to that of the baseband signal.



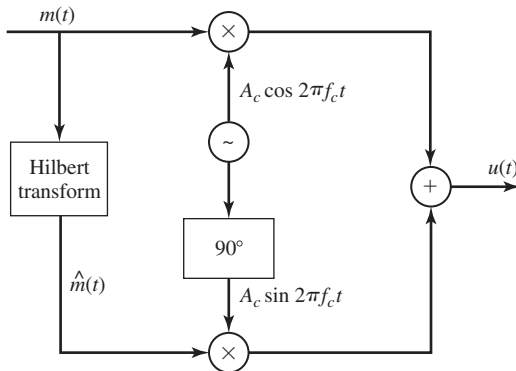


**Figure 3.8** Generation of a single-sideband AM signal.

First, we demonstrate that a single-sideband (SSB) AM signal is represented mathematically as

$$u(t) = A_c m(t) \cos 2\pi f_c t \mp A_c \hat{m}(t) \sin 2\pi f_c t \quad (3.2.10)$$

where  $\hat{m}(t)$  is the Hilbert transform of  $m(t)$  that was introduced in Section 2.5, and the plus-or-minus sign determines which sideband we obtain. We recall that the Hilbert transform may be viewed as a linear filter with impulse response  $h(t) = 1/\pi t$  and frequency response

$$H(f) = \begin{cases} -j, & f > 0 \\ j, & f < 0 \\ 0, & f = 0 \end{cases} \quad (3.2.11)$$

Therefore, the SSB AM signal  $u(t)$  may be generated by using the system configuration shown in Figure 3.8.

The method shown in Figure 3.8 for generating a SSB AM signal is one that employs a Hilbert transform filter. Another method, illustrated in Figure 3.9, generates a DSB-SC AM signal and then employs a filter which selects either the upper sideband or the lower sideband of the double-sideband AM signal.

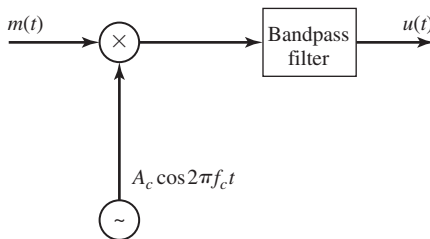


**Figure 3.9** Generation of a single-sideband AM signal by filtering one of the sidebands of a DSB-SC AM signal.

**Spectral Characteristics of the Single Sideband Signal.** Let  $m(t)$  be a signal with Fourier transform (spectrum)  $M(f)$ . An upper single-sideband amplitude-modulated signal (USSB AM) is obtained by eliminating the lower sideband of a DSB

amplitude-modulated signal. Suppose we eliminate the lower sideband of the DSB AM signal,  $u_{\text{DSB}}(t) = 2A_c m(t) \cos 2\pi f_c t$ , by passing it through a highpass filter whose transfer function is given by

$$H(f) = \begin{cases} 1, & |f| > f_c \\ 0, & \text{otherwise} \end{cases}$$

Obviously  $H(f)$  can be written as

$$H(f) = u_{-1}(f - f_c) + u_{-1}(-f - f_c)$$

where  $u_{-1}(\cdot)$  represents the unit step function. Therefore the spectrum of the USSB AM signal is given by

$$U_u(f) = A_c M(f - f_c) u_{-1}(f - f_c) + A_c M(f + f_c) u_{-1}(-f - f_c)$$

or equivalently

$$U_u(f) = A_c M(f) u_{-1}(f) |_{f=f-f_c} + A_c M(f) u_{-1}(-f) |_{f=f+f_c} \quad (3.2.12)$$

Taking inverse Fourier transform of both sides of Equation (3.2.12) and using the modulation property of the Fourier transform, we obtain

$$u_u(t) = A_c m(t) \star \mathcal{F}^{-1} [u_{-1}(f)] e^{j2\pi f_c t} + A_c m(t) \star \mathcal{F}^{-1} [u_{-1}(-f)] e^{-j2\pi f_c t} \quad (3.2.13)$$

By noting that

$$\begin{aligned} \mathcal{F} \left[ \frac{1}{2} \delta(t) + \frac{j}{2\pi t} \right] &= u_{-1}(f) \\ \mathcal{F} \left[ \frac{1}{2} \delta(t) - \frac{j}{2\pi t} \right] &= u_{-1}(-f) \end{aligned} \quad (3.2.14)$$

and substituting Equation (3.2.14) in Equation (3.2.13), we obtain

$$\begin{aligned} u_u(t) &= A_c m(t) \star \left[ \frac{1}{2} \delta(t) + \frac{j}{2\pi t} \right] e^{j2\pi f_c t} + A_c m(t) \star \left[ \frac{1}{2} \delta(t) - \frac{j}{2\pi t} \right] e^{-j2\pi f_c t} \\ &= \frac{A_c}{2} [m(t) + j\hat{m}(t)] e^{j2\pi f_c t} + \frac{A_c}{2} [m(t) - j\hat{m}(t)] e^{-j2\pi f_c t} \end{aligned} \quad (3.2.15)$$

where we have used the identities

$$\begin{aligned} m(t) \star \delta(t) &= m(t) \\ m(t) \star \frac{1}{\pi t} &= \hat{m}(t) \end{aligned}$$

Using Euler's relations in Equation (3.2.15), we obtain

$$u_u(t) = A_c m(t) \cos 2\pi f_c t - A_c \hat{m}(t) \sin 2\pi f_c t \quad (3.2.16)$$

which is the time-domain representation of an USSB AM signal. The expression for the LSSB AM signal can be derived by noting that

$$u_u(t) + u_\ell(t) = u_{\text{DSB}}(t)$$

or

$$A_c m(t) \cos 2\pi f_c t - A_c \hat{m}(t) \sin 2\pi f_c t + u_\ell(t) = 2A_c m(t) \cos 2\pi f_c t$$

and, therefore,

$$u_\ell(t) = A_c m(t) \cos 2\pi f_c t + A_c \hat{m}(t) \sin 2\pi f_c t \quad (3.2.17)$$

Thus, the time domain representation of a SSB AM signal can in general be expressed as

$$u_{\text{SSB}}(t) = A_c m(t) \cos 2\pi f_c t \mp A_c \hat{m}(t) \sin 2\pi f_c t \quad (3.2.18)$$

where the minus sign corresponds to the USSB AM signal and the plus sign corresponds to the LSSB AM signal.

#### Example 3.2.4

Suppose that the modulating signal is a sinusoid of the form

$$m(t) = \cos 2\pi f_m t, \quad f_m \ll f_c$$

Determine the two possible SSB AM signals

**Solution** The Hilbert transform of  $m(t)$  is

$$\hat{m}(t) = \sin 2\pi f_m t \quad (3.2.19)$$

Hence,

$$u(t) = A_c \cos 2\pi f_m t \cos 2\pi f_c t \mp A_c \sin 2\pi f_m t \sin 2\pi f_c t \quad (3.2.20)$$

If we take the upper (−) sign we obtain the upper sideband signal

$$u_u(t) = A_c \cos 2\pi (f_c + f_m)t$$

On the other hand, if we take the lower (+) sign in Equation (3.2.20) we obtain the lower sideband signal

$$u_\ell(t) = A_c \cos 2\pi (f_c - f_m)t$$

The spectra of  $u_u(t)$  and  $u_\ell(t)$  were previously given in Figure 3.2.

**Demodulation of SSB AM Signals.** To recover the message signal  $m(t)$  in the received SSB AM signal, we require a phase coherent or synchronous demodulator, as was the case for DSB-SC AM signals. Thus, for the USSB signal as given in Equation (3.2.18), we have

$$\begin{aligned} r(t) \cos 2\pi f_c t &= u(t) \cos(2\pi f_c t + \phi) \\ &= \frac{1}{2} A_c m(t) \cos \phi + \frac{1}{2} A_c \hat{m}(t) \sin \phi + \text{double frequency terms} \end{aligned} \quad (3.2.21)$$

By passing the product signal in Equation (3.2.21) through an ideal lowpass filter, the double-frequency components are eliminated, leaving us with

$$y_\ell(t) = \frac{1}{2}A_c m(t) \cos \phi + \frac{1}{2}A_c \hat{m}(t) \sin \phi \quad (3.2.22)$$

Note that the effect of the phase offset is not only to reduce the amplitude of the desired signal  $m(t)$  by  $\cos \phi$ , but it also results in an undesirable sideband signal due to the presence of  $\hat{m}(t)$  in  $y_\ell(t)$ . The latter component was not present in a DSB-SC signal and, hence, it was not a factor. However, it is an important element that contributes to the distortion of the demodulated SSB signal.

The transmission of a pilot tone at the carrier frequency is a very effective method for providing a phase-coherent reference signal for performing synchronous demodulation at the receiver. Thus, the undesirable sideband signal component is eliminated. However, this means that a portion of the transmitted power must be allocated to the transmission of the carrier.

The spectral efficiency of SSB AM makes this modulation method very attractive for use in voice communications over telephone channels (wire lines and cables). In this application, a pilot tone is transmitted for synchronous demodulation and shared among several channels.

The filter method shown in Figure 3.9 for selecting one of the two signal sidebands for transmission is particularly difficult to implement when the message signal  $m(t)$  has a large power concentrated in the vicinity of  $f = 0$ . In such a case, the sideband filter must have an extremely sharp cutoff in the vicinity of the carrier in order to reject the second sideband. Such filter characteristics are very difficult to implement in practice.

### 3.2.4 Vestigial-Sideband AM

The stringent frequency-response requirements on the sideband filter in a SSB AM system can be relaxed by allowing a part, called a *vestige*, of the unwanted sideband to appear at the output of the modulator. Thus, we simplify the design of the sideband filter at the cost of a modest increase in the channel bandwidth required to transmit the signal. The resulting signal is called *vestigial-sideband* (VSB) AM.

To generate a VSB AM signal we begin by generating a DSB-SC AM signal and passing it through a sideband filter with frequency response  $H(f)$  as shown in Figure 3.10. In the time domain the VSB signal may be expressed as

$$u(t) = [A_c m(t) \cos 2\pi f_c t] \star h(t) \quad (3.2.23)$$

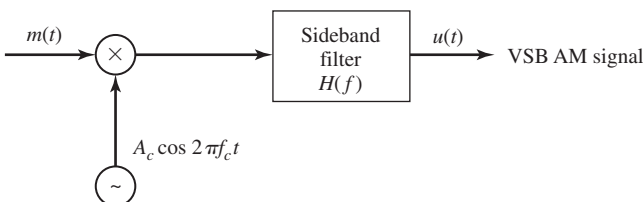


**Figure 3.10** Generation of VSB AM signal.

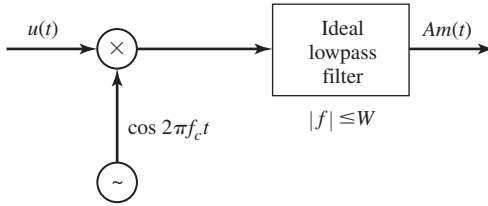


**Figure 3.11** Demodulation of VSB signal.

where  $h(t)$  is the impulse response of the VSB filter. In the frequency domain, the corresponding expression is

$$U(f) = \frac{A_c}{2}[M(f - f_c) + M(f + f_c)]H(f) \quad (3.2.24)$$

To determine the frequency-response characteristics of the filter, let us consider the demodulation of the VSB signal  $u(t)$ . We multiply  $u(t)$  by the carrier component  $\cos 2\pi f_c t$  and pass the result through an ideal lowpass filter, as shown in Figure 3.11. Thus, the product signal is

$$v(t) = u(t) \cos 2\pi f_c t$$

or, equivalently,

$$V(f) = \frac{1}{2}[U(f - f_c) + U(f + f_c)] \quad (3.2.25)$$

If we substitute for  $U(f)$  from Equation (3.2.24) into Equation (3.2.25), we obtain

$$\begin{aligned} V(f) &= \frac{A_c}{4}[M(f - 2f_c) + M(f)]H(f - f_c) \\ &\quad + \frac{A_c}{4}[M(f) + M(f + 2f_c)]H(f + f_c) \end{aligned} \quad (3.2.26)$$

The lowpass filter rejects the double-frequency terms and passes only the components in the frequency range  $|f| \leq W$ . Hence, the signal spectrum at the output of the ideal lowpass filter is

$$V_\ell(f) = \frac{A_c}{4}M(f)[H(f - f_c) + H(f + f_c)] \quad (3.2.27)$$

We require that the message signal at the output of the lowpass filter be undistorted. Hence, the VSB filter characteristic must satisfy the condition

$$H(f - f_c) + H(f + f_c) = \text{constant}, \quad |f| \leq W \quad (3.2.28)$$

This condition is satisfied by a filter that has the frequency-response characteristic shown in Figure 3.12. We note that  $H(f)$  selects the upper sideband and a vestige of the lower sideband. It has odd symmetry about the carrier frequency  $f_c$ , in the frequency range  $f_c - f_a < f < f_c + f_a$ , where  $f_a$  is a conveniently selected frequency that is

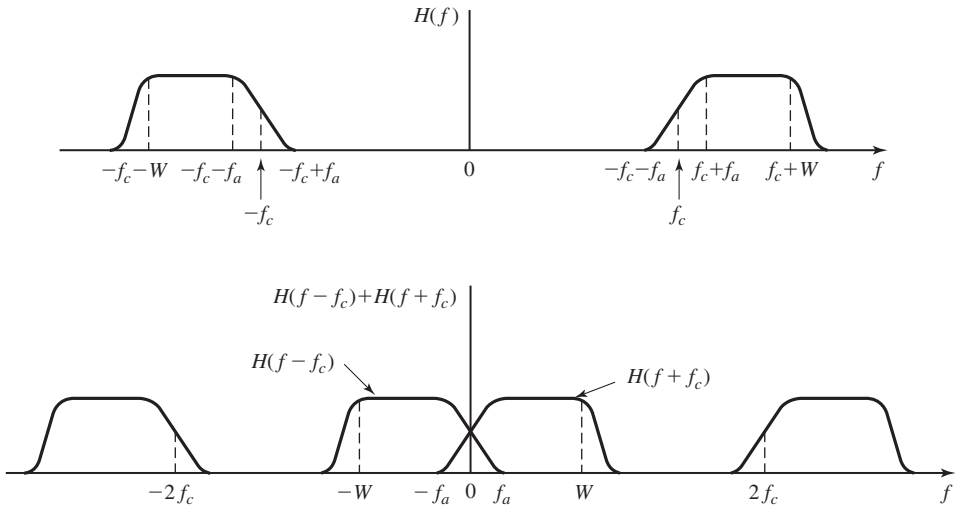


**Figure 3.12** VSB filter characteristics.

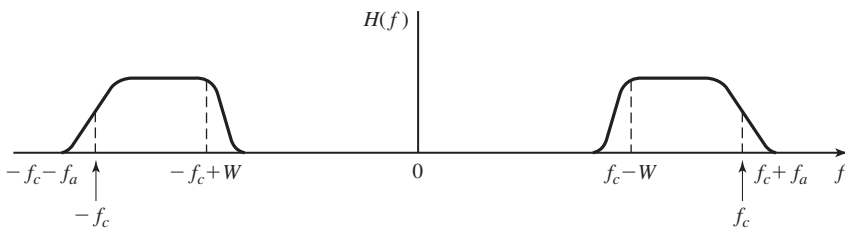


**Figure 3.13** Frequency response of VSB filter for selecting the lower sideband of the message signals.

some small fraction of  $W$ ; i.e.,  $f_a \ll W$ . Thus, we obtain an undistorted version of the transmitted signal. Figure 3.13 illustrates the frequency response of a VSB filter that selects the lower sideband and a vestige of the upper sideband.

In practice, the VSB filter is designed to have some specified phase characteristic. To avoid distortion of the message signal, the VSB filter should be designed to have linear phase over its passband  $f_c - f_a \leq |f| \leq f_c + W$ .

### Example 3.2.5

Suppose that the message signal is given as

$$m(t) = 10 + 4 \cos 2\pi t + 8 \cos 4\pi t + 10 \cos 20\pi t$$

Specify the frequency-response characteristic of a VSB filter that passes the upper sideband and the first frequency component of the lower sideband.

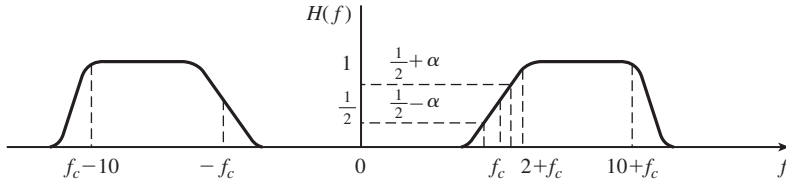


**Figure 3.14** Frequency response characteristics of VSB filter in Example 3.2.5.

**Solution** The spectrum of the DSB-SC AM signal  $u(t) = m(t) \cos 2\pi f_c t$  is

$$U(f) = 5[\delta(f - f_c) + \delta(f + f_c)] + 2[\delta(f - f_c - 1) + \delta(f + f_c + 1)] \\ + 4[\delta(f - f_c - 2) + \delta(f + f_c + 2)] + 5[\delta(f - f_c - 10) + \delta(f + f_c + 10)]$$

The VSB filter can be designed to have unity gain in the range  $2 \leq |f - f_c| \leq 10$ , a gain of  $1/2$  at  $f = f_c$ , a gain of  $1/2 + \alpha$  at  $f = f_c + 1$ , and a gain of  $1/2 - \alpha$  at  $f = f_c - 1$ , where  $\alpha$  is some conveniently selected parameter that satisfies the condition  $0 < \alpha < 1/2$ . Figure 3.14 illustrates the frequency-response characteristic of the VSB filter.

### 3.2.5 Implementation of AM Modulators and Demodulators

There are several different methods for generating AM modulated signals. We shall describe the methods most commonly used in practice. Since the process of modulation involves the generation of new frequency components, modulators are generally characterized as nonlinear and, or, time-variant systems.

**Power-Law Modulation.** Let us consider the use of a nonlinear device such as a P-N diode which has a voltage-current characteristic as shown in Figure 3.15. Suppose that the voltage input to such a device is the sum of the message signal  $m(t)$  and the carrier  $A_c \cos 2\pi f_c t$ , as illustrated in Figure 3.16. The nonlinearity will generate a product of the message  $m(t)$  with the carrier, plus additional terms. The desired modulated signal can be filtered out by passing the output of the nonlinear device through a bandpass filter.

To elaborate on this method, suppose that the nonlinear device has an input-output (square-law) characteristic of the form

$$v_0(t) = a_1 v_i(t) + a_2 v_i^2(t) \quad (3.2.29)$$

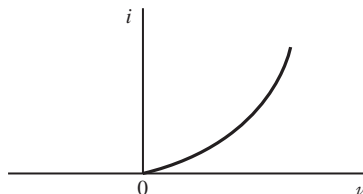


**Figure 3.15** Voltage-current characteristic of P-N diode.

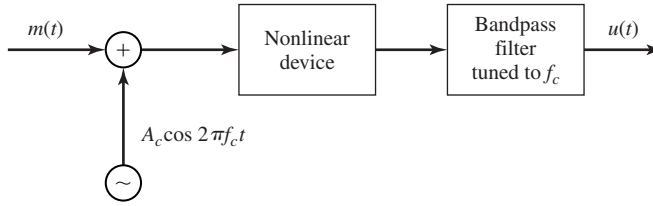


**Figure 3.16** Block diagram of power-law AM modulator.

where  $v_i(t)$  is the input signal,  $v_o(t)$  is the output signal, and the parameters  $(a_1, a_2)$  are constants. Then, if the input to the nonlinear device is

$$v_i(t) = m(t) + A_c \cos 2\pi f_c t, \quad (3.2.30)$$

its output is

$$\begin{aligned} v_o(t) &= a_1[m(t) + A_c \cos 2\pi f_c t] + a_2[m(t) + A_c \cos 2\pi f_c t]^2 \\ &= a_1 m(t) + a_2 m^2(t) + a_2 A_c^2 \cos^2 2\pi f_c t + A_c a_1 \left[ 1 + \frac{2a_2}{a_1} m(t) \right] \cos 2\pi f_c t \end{aligned} \quad (3.2.31)$$

The output of the bandpass filter with bandwidth  $2W$  centered at  $f = f_c$  yields

$$u(t) = A_c a_1 \left[ 1 + \frac{2a_2}{a_1} m(t) \right] \cos 2\pi f_c t \quad (3.2.32)$$

where  $2a_2|m(t)|/a_1 < 1$  by design. Thus, the signal generated by this method is a conventional DSB AM signal.

**Switching Modulator.** Another method for generating an AM modulated signal is by means of a switching modulator. Such a modulator can be implemented by the system illustrated in Figure 3.17(a). The sum of the message signal and the carrier; i.e.,  $v_i(t)$  given by Equation (3.2.30), are applied to a diode that has the input–output voltage characteristic shown in Figure 3.17(b), where  $A_c \gg m(t)$ . The output across the load resistor is simply

$$v_o(t) = \begin{cases} v_i(t), & c(t) > 0 \\ 0, & c(t) < 0 \end{cases} \quad (3.2.33)$$

This switching operation may be viewed mathematically as a multiplication of the input  $v_i(t)$  with the switching function  $s(t)$ ; i.e.,

$$v_o(t) = [m(t) + A_c \cos 2\pi f_c t]s(t) \quad (3.2.34)$$

where  $s(t)$  is shown in Figure 3.17(c).

Since  $s(t)$  is a periodic function, it is represented in the Fourier series as

$$s(t) = \frac{1}{2} + \frac{2}{\pi} \sum_{n=1}^{\infty} \frac{(-1)^{n-1}}{2n-1} \cos[2\pi f_c t(2n-1)] \quad (3.2.35)$$



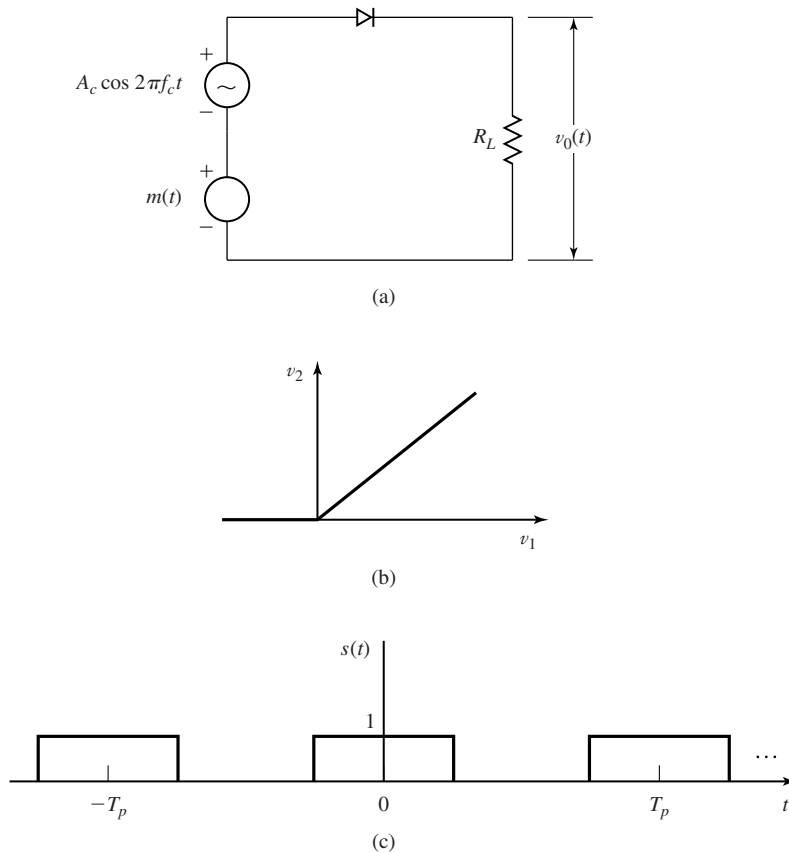


**Figure 3.17** Switching modulator and periodic switching signal.

Hence,

$$\begin{aligned} v_0(t) &= [m(t) + A_c \cos 2\pi f_c t]s(t) \\ &= \frac{A_c}{2} \left[ 1 + \frac{4}{\pi A_c} m(t) \right] \cos 2\pi f_c t + \text{other terms} \end{aligned} \quad (3.2.36)$$

The desired AM modulated signal is obtained by passing  $v_0(t)$  through a bandpass filter with center frequency  $f = f_c$  and bandwidth  $2W$ . At its output, we have the desired conventional DSB AM signal

$$u(t) = \frac{A_c}{2} \left[ 1 + \frac{4}{\pi A_c} m(t) \right] \cos 2\pi f_c t \quad (3.2.37)$$

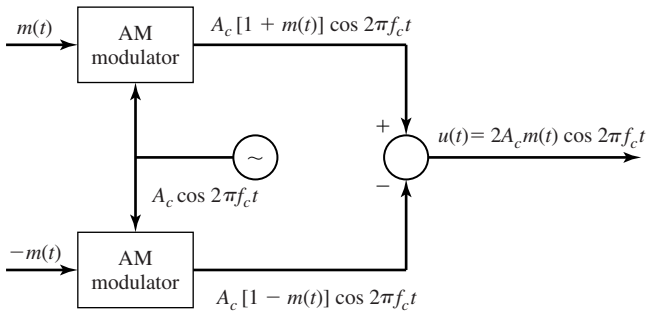


**Figure 3.18** Block diagram of a balanced modulator.

**Balanced Modulator.** A relatively simple method to generate a DSB-SC AM signal is to use two conventional AM modulators arranged in the configuration illustrated in Figure 3.18. For example, we may use two square-law AM modulators as described above. Care must be taken to select modulators with approximately identical characteristics so that the carrier component cancels out at the summing junction.

**Ring Modulator.** Another type of modulator for generating a DSB-SC AM signal is the *ring modulator* illustrated in Figure 3.19. The switching of the diodes is controlled by a square wave of frequency  $f_c$ , denoted as  $c(t)$ , which is applied to the center taps of the two transformers. When  $c(t) > 0$ , the top and bottom diodes conduct, while the two diodes in the crossarms are off. In this case, the message signal  $m(t)$  is multiplied by  $+1$ . When  $c(t) < 0$ , the diodes in the crossarms of the ring conduct, while the other two are switched off. In this case, the message signal  $m(t)$  is multiplied by  $-1$ . Consequently, the operation of the ring modulator may be described mathematically as

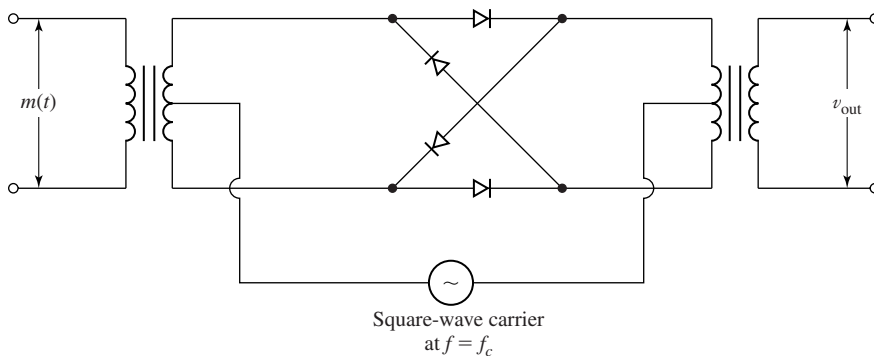


**Figure 3.19** Ring modulator for generating DSB-SC AM signal.

a multiplier of  $m(t)$  by the square-wave carrier  $c(t)$ ; i.e.,

$$v_0(t) = m(t)c(t) \quad (3.2.38)$$

as shown in Figure 3.19.

Since  $c(t)$  is a periodic function, it is represented by the Fourier series

$$c(t) = \frac{4}{\pi} \sum_{n=1}^{\infty} \frac{(-1)^{n-1}}{2n-1} \cos[2\pi f_c(2n-1)t] \quad (3.2.39)$$

Hence, the desired DSB-SC AM signal  $u(t)$  is obtained by passing  $v_0(t)$  through a bandpass filter with center frequency  $f_c$  and bandwidth  $2W$ .

From the discussion above, we observe that the balanced modulator and the ring modulator systems, in effect, multiply the message signal  $m(t)$  with the carrier to produce a DSB-SC AM signal. The multiplication of  $m(t)$  with  $A_c \cos \omega_c t$  is called a mixing operation. Hence, a *mixer* is basically a balanced modulator.

The method shown in Figure 3.8 for generating a SSB signal requires two mixers; i.e., two balanced modulators, in addition to the Hilbert transformer. On the other hand, the filter method illustrated in Figure 3.9 for generating a SSB signal requires a single balanced modulator and a sideband filter.

Let us now consider the demodulation of AM signals. We begin with a description of the envelope detector.

**Envelope Detector.** As previously indicated, conventional DSB AM signals are easily demodulated by means of an envelope detector. A circuit diagram for an envelope detector is shown in Figure 3.20. It consists of a diode and an RC circuit, which is basically a simple lowpass filter.

During the positive half-cycle of the input signal, the diode is conducting and the capacitor charges up to the peak value of the input signal. When the input falls below the voltage on the capacitor, the diode becomes reverse-biased and the input becomes disconnected from the output. During this period, the capacitor discharges slowly through the load resistor  $R$ . On the next cycle of the carrier, the diode conducts again when the input signal exceeds the voltage across the capacitor. The capacitor charges up again to the peak value of the input signal and the process is repeated again.

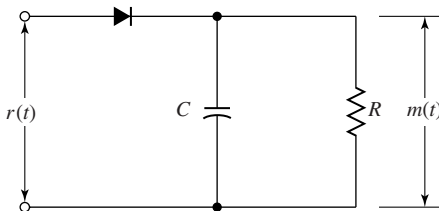


**Figure 3.20** An envelope detector.

The time constant  $RC$  must be selected so as to follow the variations in the envelope of the carrier-modulated signal. In effect,

$$\frac{1}{f_c} \ll RC \ll \frac{1}{W}$$

In such a case, the capacitor discharges slowly through the resistor and, thus, the output of the envelope detector closely follows the message signal.

**Demodulation of DSB-SC AM Signals.** As previously indicated, the demodulation of a DSB-SC AM signal requires a synchronous demodulator. That is, the demodulator must use a coherent phase reference, which is usually generated by means of a phase-locked loop (PLL) (see Section 5.2), to demodulate the received signal.

The general configuration is shown in Figure 3.21. A PLL is used to generate a phase-coherent carrier signal that is mixed with the received signal in a balanced modulator. The output of the balanced modulator is passed through a lowpass filter of bandwidth  $W$  that passes the desired signal and rejects all signal and noise components above  $W$  Hz. The characteristics and operation of the PLL are described in Section 5.2.

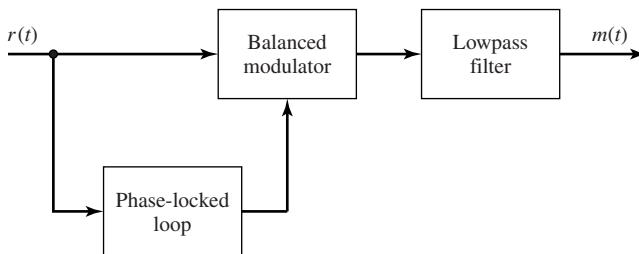


Figure 3.21 Demodulator for DSB-SC AM signal.

**Demodulation of SSB Signals.** The demodulation of SSB AM signals also requires the use of a phase coherent reference. In the case of signals such as speech, that have relatively little or no power content at  $dc$ , it is straightforward to generate the SSB signal, as shown in Figure 3.9, and then to insert a small carrier component that is transmitted along with the message. In such a case we may use the configuration shown in Figure 3.22 to demodulate the SSB signal. We observe that a balanced modulator

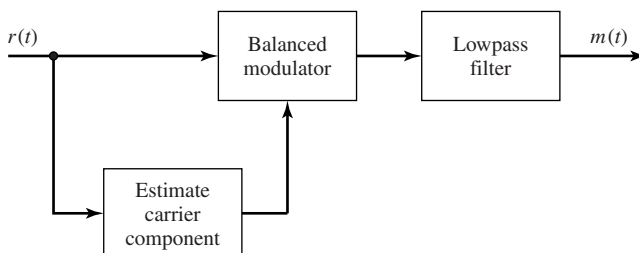


Figure 3.22 Demodulation of SSB AM signal with a carrier component.

is used for the purpose of frequency conversion of the bandpass signal to lowpass or baseband.

**Demodulation of VSB Signals.** In VSB a carrier component is generally transmitted along with the message sidebands. The existence of the carrier component makes it possible to extract a phase-coherent reference for demodulation in a balanced modulator, as shown in Figure 3.22.

In some applications such as TV broadcast, a large carrier component is transmitted along with the message in the VSB signal. In such a case, it is possible to recover the message by passing the received VSB signal through an envelope detector.

### 3.2.6 Signal Multiplexing

We have seen that amplitude modulation of a sinusoidal carrier by a message signal  $m(t)$  translates the message signal in frequency by an amount equal to the carrier frequency  $f_c$ . If we have two or more message signals to transmit simultaneously over the communications channel, it is possible to have each message signal modulate a carrier of a different frequency, where the minimum separation between two adjacent carriers is either  $2W$  (for DSB AM) or  $W$  (for SSB AM), where  $W$  is the bandwidth of each of the message signals. Thus, the various message signals occupy separate frequency bands of the channel and do not interfere with one another in transmission over the channel.

The process of combining a number of separate message signals into a composite signal for transmission over a common channel is called *multiplexing*. There are two commonly used methods for signal multiplexing: (1) time-division multiplexing and (2) frequency-division multiplexing. Time-division multiplexing is usually used in the transmission of digital information and will be described in Chapter 6. Frequency-division multiplexing (FDM) may be used with either analog or digital signal transmission.

In FDM, the message signals are separated in frequency as described above. A typical configuration of an FDM system is shown in Figure 3.23. This figure illustrates the frequency-division multiplexing of  $K$  message signals at the transmitter and their demodulation at the receiver. The lowpass filters at the transmitter are used to ensure that the bandwidth of the message signals is limited to  $W$  Hz. Each signal modulates a separate carrier; hence,  $K$  modulators are required. Then, the signals from the  $K$  modulators are summed and transmitted over the channel. For SSB and VSB modulation, the modulator outputs are filtered prior to summing the modulated signals.

At the receiver of an FDM system, the signals are usually separated by passing through a parallel band of bandpass filters, where each filter is tuned to one of the carrier frequencies and has a bandwidth that is sufficiently wide to pass the desired signal. The output of each bandpass filter is demodulated and each demodulated signal is fed to a lowpass filter that passes the baseband message signal and eliminates the double frequency components.

FDM is widely used in radio and telephone communications. For example, in telephone communications, each voice-message signal occupies a nominal bandwidth of 3 kHz. The message signal is single-sideband modulated for bandwidth efficient

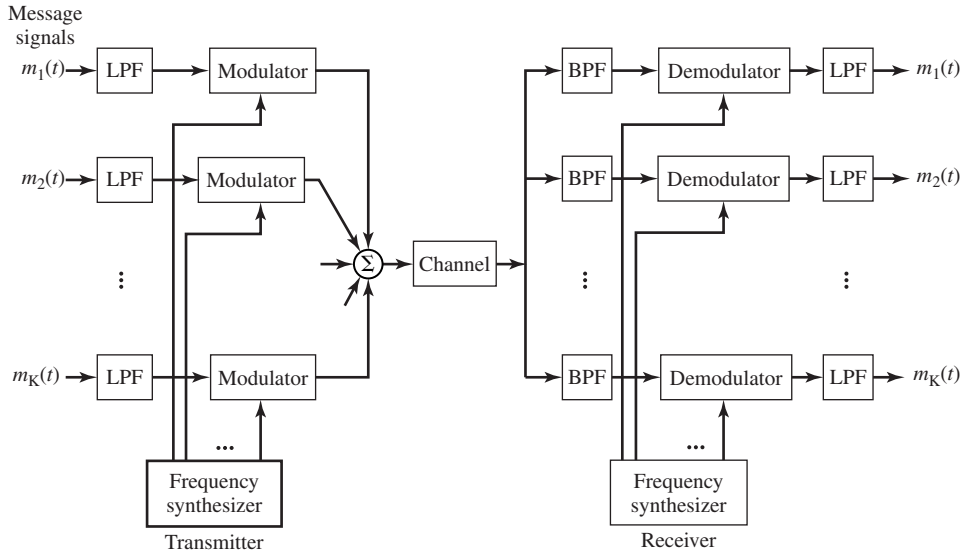


**Figure 3.23** Frequency-division multiplexing of multiple signals.

transmission. In the first level of multiplexing, 12 signals are stacked in frequency, with a frequency separation of 4 kHz between adjacent carriers. Thus, a composite 48-kHz channel, called a *group channel*, is used to transmit the 12 voice-band signals simultaneously. In the next level of FDM, a number of group channels (typically five or six) are stacked together in frequency to form a *supergroup channel*, and the composite signal is transmitted over the channel. Higher-order multiplexing is obtained by combining several supergroup channels. Thus, an FDM hierarchy is employed in telephone communication systems.

**Quadrature-Carrier Multiplexing.** A totally different type of multiplexing allows us to transmit two message signals on the same carrier frequency, using two quadrature carriers  $A_c \cos 2\pi f_c t$  and  $A_c \sin 2\pi f_c t$ . To elaborate, suppose that  $m_1(t)$  and  $m_2(t)$  are two separate message signals to be transmitted over the channel. The signal  $m_1(t)$  amplitude modulates the carrier  $A_c \cos 2\pi f_c t$  and the signal  $m_2(t)$  amplitude modulates the quadrature carrier  $A_c \sin 2\pi f_c t$ . The two signals are added and transmitted over the channel. Hence, the transmitted signal is

$$u(t) = A_c m_1(t) \cos 2\pi f_c t + A_c m_2(t) \sin 2\pi f_c t \quad (3.2.40)$$

Therefore, each message signal is transmitted by DSB-SC AM. This type of signal multiplexing is called *quadrature-carrier multiplexing*.

Figure 3.24 illustrates the modulation and demodulation of the quadrature-carrier multiplexed signals. As shown, a synchronous demodulator is required at the receiver to separate and recover the quadrature-carrier modulated signals.

Quadrature-carrier multiplexing results in a bandwidth-efficient communication system that is comparable in bandwidth efficiency to SSB AM.

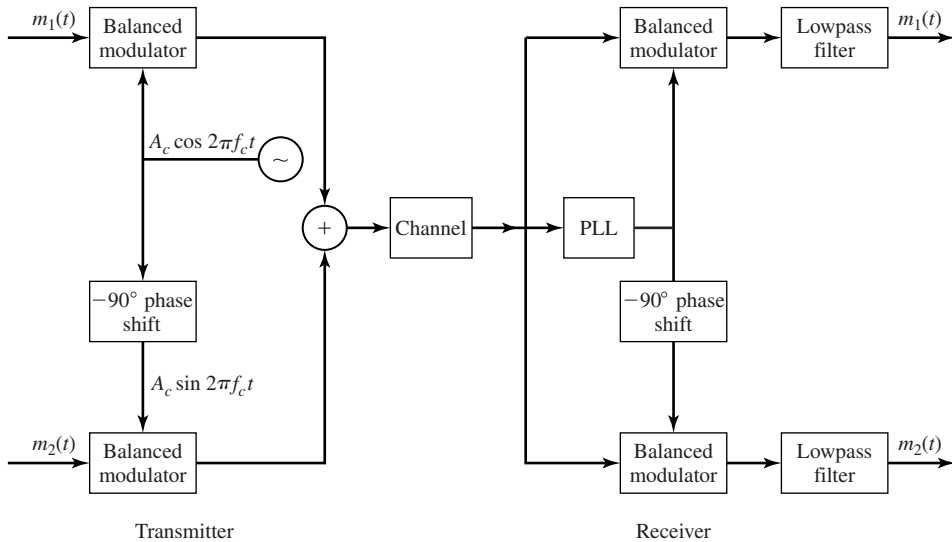


**Figure 3.24** Quadrature-carrier multiplexing.

### 3.3 ANGLE MODULATION

In the previous section we considered amplitude modulation of the carrier as a means for transmitting the message signal. Amplitude-modulation methods are also called *linear-modulation methods*, although conventional AM is not linear in the strict sense.

Another class of modulation methods are frequency and phase modulation which are described in this section. In frequency-modulation (FM) systems, the frequency of the carrier  $f_c$  is changed by the message signal and in phase-modulation (PM) systems the phase of the carrier is changed according to the variations in the message signal. Frequency and phase modulation are obviously quite nonlinear, and very often they are jointly referred to as *angle-modulation methods*. As our analysis in the following sections will show, angle modulation, due to its inherent nonlinearity, is more complex to implement, and much more difficult to analyze. In many cases only an approximate analysis can be done. Another property of angle modulation is its bandwidth-expansion property. Frequency and phase-modulation systems generally expand the bandwidth such that the effective bandwidth of the modulated signal is usually many times the bandwidth of the message signal.<sup>†</sup> With a higher implementation complexity and a higher bandwidth occupancy, one would naturally raise a question as to the usefulness of these systems. As our analysis in Chapter 5 will show, the major benefit of these systems is their high degree of noise immunity. In fact these systems trade-off bandwidth for high noise immunity. That is the reason that FM systems are widely used in high-fidelity music broadcasting and point-to-point communication systems where the transmitter power is quite limited.

<sup>†</sup>Strictly speaking, the bandwidth of the modulated signal, as it will be shown later, is infinite. That is why we talk about the *effective bandwidth*.

### 3.3.1 Representation of FM and PM Signals

An angle-modulated signal in general can be written as

$$u(t) = A_c \cos(\theta(t))$$

$\theta(t)$  is the phase of the signal, and its instantaneous frequency  $f_i(t)$  is given by

$$f_i(t) = \frac{1}{2\pi} \frac{d}{dt} \theta(t) \quad (3.3.1)$$

Since  $u(t)$  is a bandpass signal, it can be represented as

$$u(t) = A_c \cos(2\pi f_c t + \phi(t)) \quad (3.3.2)$$

and, therefore,

$$f_i(t) = f_c + \frac{1}{2\pi} \frac{d}{dt} \phi(t) \quad (3.3.3)$$

If  $m(t)$  is the message signal, then in a PM system we have

$$\phi(t) = k_p m(t) \quad (3.3.4)$$

and in an FM system we have

$$f_i(t) - f_c = k_f m(t) = \frac{1}{2\pi} \frac{d}{dt} \phi(t) \quad (3.3.5)$$

where  $k_p$  and  $k_f$  are phase and frequency *deviation constants*. From the above relationships we have

$$\phi(t) = \begin{cases} k_p m(t), & \text{PM} \\ 2\pi k_f \int_{-\infty}^t m(\tau) d\tau, & \text{FM} \end{cases} \quad (3.3.6)$$

Equation (3.3.6) shows the close and interesting relation between FM and PM systems. This close relationship makes it possible to analyze these systems in parallel and only emphasize their main differences. The first interesting result observed from Equation (3.3.6) is that if we phase modulate the carrier with the integral of a message, it is equivalent to frequency modulation of the carrier with the original message. On the other hand, in Equation (3.3.6) the relation can be expressed as

$$\frac{d}{dt} \phi(t) = \begin{cases} k_p \frac{d}{dt} m(t), & \text{PM} \\ 2\pi m(t), & \text{FM} \end{cases} \quad (3.3.7)$$

which shows that if we frequency modulate the carrier with the derivative of a message, the result is equivalent to phase modulation of the carrier with the message itself. Figure 3.25 shows the above relation between FM and PM. Figure 3.26 illustrates a square-wave signal and its integral, a sawtooth signal, and their corresponding FM and PM signals.



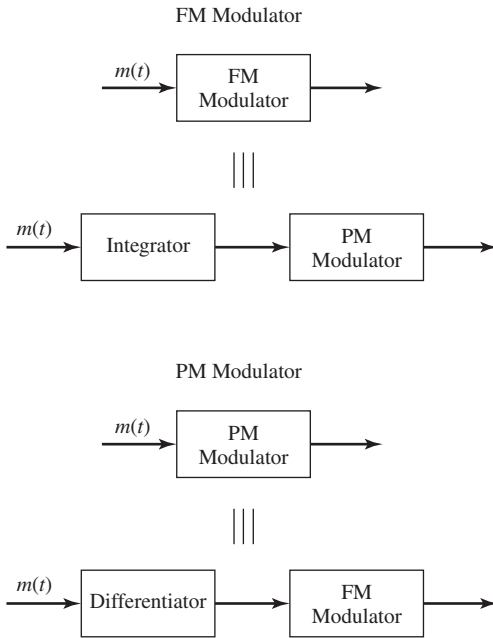


**Figure 3.25** A comparison of FM and PM modulators.

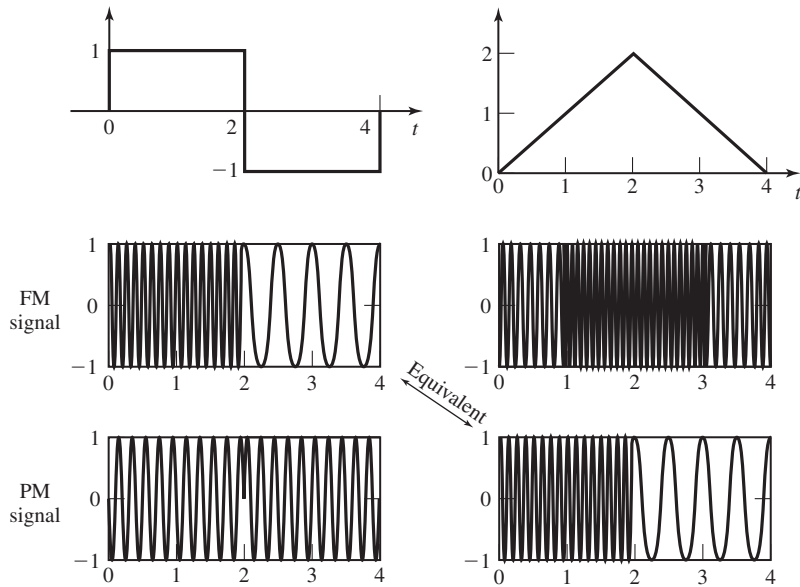


**Figure 3.26** FM and PM of square and sawtooth waves.

The demodulation of an FM signal involves finding the instantaneous frequency of the modulated signal and then subtracting the carrier frequency from it. In the demodulation of PM, the demodulation process is done by finding the phase of the signal and then recovering  $m(t)$ . The maximum phase deviation in a PM system is given by

$$\Delta\phi_{\max} = k_p \max[|m(t)|] \quad (3.3.8)$$

and the maximum frequency-deviation in an FM system is given by

$$\Delta f_{\max} = k_f \max[|m(t)|] \quad (3.3.9)$$

### Example 3.3.1

The message signal

$$m(t) = a \cos(2\pi f_m t)$$

is used to either frequency modulate or phase modulate the carrier  $A_c \cos(2\pi f_c t)$ . Find the modulated signal in each case.

**Solution** In PM we have

$$\phi(t) = k_p m(t) = k_p a \cos(2\pi f_m t) \quad (3.3.10)$$

and in FM we have

$$\phi(t) = 2\pi k_f \int_{-\infty}^t m(\tau) d\tau = \frac{k_f a}{f_m} \sin(2\pi f_m t) \quad (3.3.11)$$

Therefore, the modulated signals will be

$$u(t) = \begin{cases} A_c \cos(2\pi f_c t + k_p a \cos(2\pi f_m t)), & \text{PM} \\ A_c \cos\left(2\pi f_c t + \frac{k_f a}{f_m} \sin(2\pi f_m t)\right), & \text{FM} \end{cases} \quad (3.3.12)$$

By defining

$$\beta_p = k_p a \quad (3.3.13)$$

$$\beta_f = \frac{k_f a}{f_m} \quad (3.3.14)$$

we have

$$u(t) = \begin{cases} A_c \cos(2\pi f_c t + \beta_p \cos(2\pi f_m t)), & \text{PM} \\ A_c \cos(2\pi f_c t + \beta_f \sin(2\pi f_m t)), & \text{FM} \end{cases} \quad (3.3.15)$$

The parameters  $\beta_p$  and  $\beta_f$  are called the *modulation indices* of the PM and FM systems respectively.

We can extend the definition of the modulation index for a general nonsinusoidal signal  $m(t)$  as

$$\beta_p = k_p \max[|m(t)|] \quad (3.3.16)$$

$$\beta_f = \frac{k_f \max[|m(t)|]}{W} \quad (3.3.17)$$

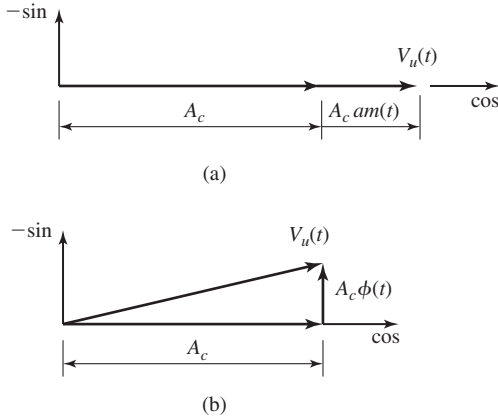


**Figure 3.27** Phasor diagram for the conventional AM (a) and narrowband angle modulation (b).

where  $W$  denotes the bandwidth of the message signal  $m(t)$ . In terms of the maximum phase and frequency deviation  $\Delta\phi_{\max}$  and  $\Delta f_{\max}$ , we have

$$\beta_p = \Delta\phi_{\max} \quad (3.3.18)$$

$$\beta_f = \frac{\Delta f_{\max}}{W} \quad (3.3.19)$$

**Narrowband Angle Modulation.**<sup>†</sup> If in an angle-modulation system the deviation constants  $k_p$  and  $k_f$  and the message signal  $m(t)$  are such that for all  $t$  we have  $\phi(t) \ll 1$ , then we can use a simple approximation to expand  $u(t)$  as

$$\begin{aligned} u(t) &= A_c \cos 2\pi f_c t \cos \phi(t) - A_c \sin 2\pi f_c t \sin \phi(t) \\ &\approx A_c \cos 2\pi f_c t - A_c \phi(t) \sin 2\pi f_c t \end{aligned} \quad (3.3.20)$$

This last equation shows that in this case the modulated signal is very similar to a conventional AM signal. The only difference is that the message signal  $m(t)$  is modulated on a sine carrier rather than a cosine carrier. The bandwidth of this signal is similar to the bandwidth of a conventional AM signal, which is twice the bandwidth of the message signal. Of course this bandwidth is only an approximation to the real bandwidth of the FM signal. A phasor diagram for this signal and the comparable conventional AM signal are given in Figure 3.27. Note that compared to conventional AM, the narrowband angle-modulation scheme has far less amplitude variations. Of course, the angle-modulation system has constant amplitude and, hence, there should be no amplitude variations in the phasor-diagram representation of the system. The slight variations here are due to the first-order approximation that we have used for the expansions of  $\sin(\phi(t))$  and  $\cos(\phi(t))$ . As we will see in Chapter 5, the narrowband angle-modulation method does not provide any better noise immunity compared to a conventional AM system. Therefore, narrowband angle modulation is seldom used in practice for communication purposes. However, these systems can be used as an intermediate stage for generation of wideband angle-modulated signals as we will discuss in Section 3.3.3.

<sup>†</sup>Also known as *low-index angle modulation*.

### 3.3.2 Spectral Characteristics of Angle-Modulated Signals

Due to the inherent nonlinearity of angle-modulation systems the precise characterization of their spectral properties, even for simple message signals, is mathematically intractable. Therefore, the derivation of the spectral characteristics of these signals usually involves the study of very simple modulating signals and certain approximations. Then the results are generalized to the more complicated messages. We will study the spectral characteristics of an angle-modulated signal in three cases: when the modulating signal is a sinusoidal signal, when the modulating signal is a general periodic signal, and when the modulating signal is a general nonperiodic signal.

**Angle Modulation by a Sinusoidal Signal.** Let us begin with the case where the message signal is a sinusoidal signal. As we have seen, in this case for both FM and PM, we have

$$u(t) = A_c \cos(2\pi f_c t + \beta \sin 2\pi f_m t) \quad (3.3.21)$$

where  $\beta$  is the modulation index that can be either  $\beta_p$  or  $\beta_f$ . Therefore, the modulated signal can be written as

$$u(t) = \text{Re}(A_c e^{j2\pi f_c t} e^{j\beta \sin 2\pi f_m t}) \quad (3.3.22)$$

Since  $\sin 2\pi f_m t$  is periodic with period  $T_m = \frac{1}{f_m}$ , the same is true for the complex exponential signal

$$e^{j\beta \sin 2\pi f_m t}$$

Therefore, it can be expanded in a Fourier series representation. The Fourier series coefficients are obtained from the integral

$$\begin{aligned} c_n &= f_m \int_0^{\frac{1}{f_m}} e^{j\beta \sin 2\pi f_m t} e^{-jn2\pi f_m t} dt \\ &\stackrel{u=2\pi f_m t}{=} \frac{1}{2\pi} \int_0^{2\pi} e^{j(\beta \sin u - nu)} du \end{aligned} \quad (3.3.23)$$

This latter integral is a well-known integral known as the *Bessel function of the first kind of order  $n$*  and is denoted by  $J_n(\beta)$ . Therefore, we have the Fourier series for the complex exponential as

$$e^{j\beta \sin 2\pi f_m t} = \sum_{n=-\infty}^{\infty} J_n(\beta) e^{j2\pi n f_m t} \quad (3.3.24)$$

By substituting Equation (3.3.24) in Equation (3.3.22), we obtain

$$\begin{aligned} u(t) &= \text{Re} \left( A_c \sum_{n=-\infty}^{\infty} J_n(\beta) e^{j2\pi n f_m t} e^{j2\pi f_c t} \right) \\ &= \sum_{n=-\infty}^{\infty} A_c J_n(\beta) \cos(2\pi(f_c + n f_m)t) \end{aligned} \quad (3.3.25)$$

Equation (3.3.25) shows that even in this very simple case, where the modulating signal is a sinusoid of frequency  $f_m$ , the angle-modulated signal contains all frequencies of the form  $f_c + n f_m$  for  $n = 0, \pm 1, \pm 2, \dots$ . Therefore, the actual bandwidth of the modulated signal is infinite. However, the amplitude of the sinusoidal components of frequencies  $f_c \pm n f_m$  for large  $n$  is very small. Hence, we can define a finite *effective bandwidth* for the modulated signal. A series expansion for the Bessel function is given by

$$J_n(\beta) = \sum_{k=0}^{\infty} \frac{(-1)^k \left(\frac{\beta}{2}\right)^{n+2k}}{k!(k+n)!} \quad (3.3.26)$$

The above expansion shows that for small  $\beta$ , we can use the approximation

$$J_n(\beta) \approx \frac{\beta^n}{2^n n!} \quad (3.3.27)$$

Thus for a small modulation index  $\beta$ , only the first sideband corresponding to  $n = 1$  is of importance. Also, using the above expansion, it is easy to verify the following symmetry properties of the Bessel function.

$$J_{-n}(\beta) = \begin{cases} J_n(\beta), & n \text{ even} \\ -J_n(\beta), & n \text{ odd} \end{cases} \quad (3.3.28)$$

Plots of  $J_n(\beta)$  for various values of  $n$  are given in Figure 3.28, and a table of the values of the Bessel function is given in Table 3.1.

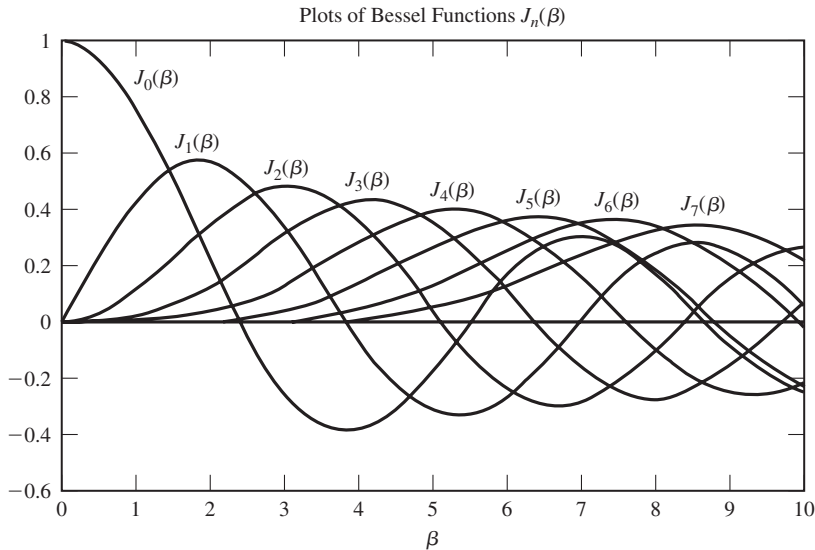


**Figure 3.28** Bessel functions for various values of  $n$ .

**TABLE 3.1** TABLE OF BESSEL FUNCTION VALUES

$n$	$\beta = 0.1$	$\beta = 0.2$	$\beta = 0.5$	$\beta = 1$	$\beta = 2$	$\beta = 5$	$\beta = 8$	$\beta = 10$
0	0.997	0.990	0.938	0.765	0.224	-0.178	0.172	-0.246
1	0.050	0.100	0.242	<u>0.440</u>	<u>0.577</u>	-0.328	0.235	0.043
2	0.001	0.005	0.031	<u>0.115</u>	0.353	0.047	-0.113	0.255
3				<u>0.020</u>	<u>0.129</u>	0.365	-0.291	0.058
4				0.002	<u>0.034</u>	<u>0.391</u>	-0.105	-0.220
5					0.007	<u>0.261</u>	0.186	-0.234
6					0.001	<u>0.131</u>	0.338	-0.014
7						<u>0.053</u>	<u>0.321</u>	0.217
8						0.018	<u>0.223</u>	<u>0.318</u>
9						0.006	<u>0.126</u>	<u>0.292</u>
10						0.001	<u>0.061</u>	0.207
11							0.026	<u>0.123</u>
12							0.010	0.063
13							0.003	0.029
14							0.001	0.012
15								0.004
16								0.001

(From Ziemer and Tranter; © 1990 Houghton Mifflin, reprinted by permission.)

**Example 3.3.2**

Let the carrier be given by  $c(t) = 10 \cos(2\pi f_c t)$  and let the message signal be  $\cos(20\pi t)$ . Further assume that the message is used to frequency modulate the carrier with  $k_f = 50$ . Find the expression for the modulated signal and determine how many harmonics should be selected to contain 99% of the modulated signal power.

**Solution** The power content of the carrier signal is given by

$$P_c = \frac{A_c^2}{2} = \frac{100}{2} = 50 \quad (3.3.29)$$

The modulated signal is represented by

$$\begin{aligned} u(t) &= 10 \cos \left( 2\pi f_c t + 2\pi k_f \int_{-\infty}^t \cos(20\pi \tau) d\tau \right) \\ &= 10 \cos \left( 2\pi f_c t + \frac{50}{10} \sin(20\pi t) \right) \\ &= 10 \cos(2\pi f_c t + 5 \sin(20\pi t)) \end{aligned} \quad (3.3.30)$$

The modulation index is given by

$$\beta = k_f \frac{\max[|m(t)|]}{f_m} = 5 \quad (3.3.31)$$

and, therefore, the FM-modulated signal is

$$\begin{aligned} u(t) &= \sum_{n=-\infty}^{\infty} A_c J_n(\beta) \cos(2\pi(f_c + nf_m)t) \\ &= \sum_{n=-\infty}^{\infty} 10 J_n(5) \cos(2\pi(f_c + 10n)t) \end{aligned} \quad (3.3.32)$$

It is seen that the frequency content of the modulated signal is concentrated at frequencies of the form  $f_c + 10n$  for various  $n$ . To make sure that at least 99% of the total power is within the effective bandwidth, we have to choose  $k$  large enough such that

$$\sum_{n=-k}^{n=k} \frac{100 J_n^2(5)}{2} \geq 0.99 \times 50 \quad (3.3.33)$$

This is a nonlinear equation and its solution (for  $k$ ) can be found by trial and error and by using tables of the Bessel functions. Of course, in finding the solution to this equation we have to employ the symmetry properties of the Bessel function given in Equation (3.3.28). Using these properties we have

$$50 \left[ J_0^2(5) + 2 \sum_{n=1}^k J_n^2(5) \right] \geq 49.5 \quad (3.3.34)$$

Starting with small values of  $k$  and increasing it, we see that the smallest value of  $k$  for which the left-hand side exceeds the right-hand side is  $k = 6$ . Therefore, taking frequencies  $f_c \pm 10k$  for  $0 \leq k \leq 6$  guarantees that 99% of the power of the modulated signal has been included and only one per cent has been left out. This means that, if the modulated signal is passed through an ideal bandpass filter centered at  $f_c$  with a bandwidth of at least 120 Hz, only 1% of the signal power will be eliminated. This gives us a practical way to define the *effective bandwidth* of the angle-modulated signal as being 120 Hz. Figure 3.29 shows the frequencies present in the effective bandwidth of the modulated signal.

In general the effective bandwidth of an angle-modulated signal, which contains at least 98% of the signal power, is given by the relation

$$B_c = 2(\beta + 1) f_m \quad (3.3.35)$$

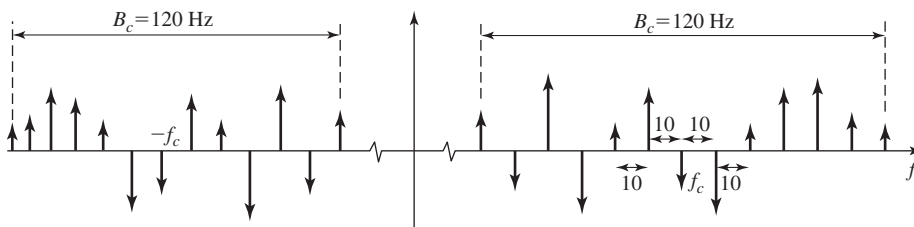


**Figure 3.29** The harmonics present inside the effective bandwidth of Example 3.3.2.

where  $\beta$  is the modulation index and  $f_m$  is the frequency of the sinusoidal message signal. It is instructive to study the effect of the amplitude and frequency of the sinusoidal message signal on the bandwidth and the number of harmonics in the modulated signal. Let the message signal be given by

$$m(t) = a \cos(2\pi f_m t) \quad (3.3.36)$$

The bandwidth<sup>†</sup> of the modulated signal is given by

$$B_c = 2(\beta + 1)f_m = \begin{cases} 2(k_p a + 1)f_m, & \text{PM} \\ 2\left(\frac{k_f a}{f_m} + 1\right)f_m, & \text{FM} \end{cases} \quad (3.3.37)$$

or

$$B_c = \begin{cases} 2(k_p a + 1)f_m, & \text{PM} \\ 2(k_f a + f_m), & \text{FM} \end{cases} \quad (3.3.38)$$

Equation (3.3.38) shows that increasing  $a$ , the amplitude of the modulating signal, in PM and FM has almost the same effect on increasing the bandwidth  $B_c$ . On the other hand, increasing  $f_m$ , the frequency of the message signal, has a more profound effect in increasing the bandwidth of a PM signal as compared to an FM signal. In both PM and FM the bandwidth  $B_c$  increases by increasing  $f_m$ , but in PM this increase is a proportional increase and in FM this is only an additive increase, which in most cases of interest, (for large  $\beta$ ) is not substantial. Now if we look at the number of harmonics in the bandwidth (including the carrier) and denote it with  $M_c$ , we have

$$M_c = 2\lfloor\beta\rfloor + 3 = \begin{cases} 2\lfloor k_p a \rfloor + 3, & \text{PM} \\ 2\left\lfloor \frac{k_f a}{f_m} \right\rfloor + 3, & \text{FM} \end{cases} \quad (3.3.39)$$

Increasing the amplitude  $a$  increases the number of harmonics in the bandwidth of the modulated signal in both cases. However, increasing  $f_m$ , has no effect on the number of harmonics in the bandwidth of the PM signal and decreases the number of harmonics in the FM signal almost linearly. This explains the relative insensitivity of the bandwidth of the FM signal to the message frequency. On the one hand, increasing  $f_m$  decreases the number of harmonics in the bandwidth and, at the same time, it increases the spacing between the harmonics. The net effect is a slight increase in the bandwidth. In PM, however, the number of harmonics remains constant and only the spacing between them increases. Therefore, the net effect is a linear increase in bandwidth. Figure 3.30 shows the effect of increasing the frequency of the message in both FM and PM.

**Angle Modulation by a Periodic Message Signal.** To generalize the preceding results, we now consider angle modulation by an arbitrary periodic message signal  $m(t)$ . Let us consider a PM-modulated signal where

$$u(t) = A_c \cos(2\pi f_c t + \beta m(t)) \quad (3.3.40)$$

<sup>†</sup>From now on, by bandwidth we mean effective bandwidth unless otherwise stated.



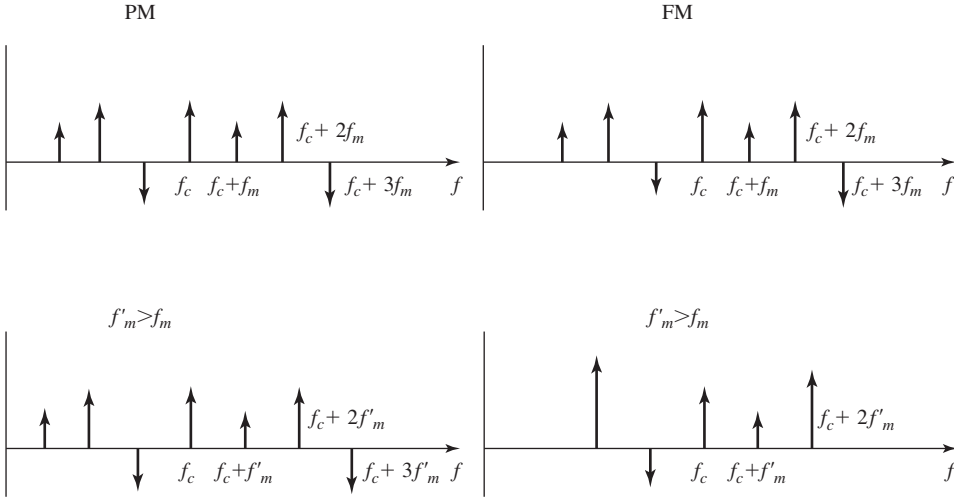


**Figure 3.30** The effect of increasing bandwidth of the message in FM and PM.

We can write this as

$$u(t) = A_c \operatorname{Re} [e^{j2\pi f_c t} e^{j\beta m(t)}] \quad (3.3.41)$$

We are assuming that  $m(t)$  is periodic with period  $T_m = \frac{1}{f_m}$ . Therefore,  $e^{j\beta m(t)}$  will be a periodic signal with the same period, and we can find its Fourier series expansion as

$$e^{j\beta m(t)} = \sum_{n=-\infty}^{\infty} c_n e^{j2\pi n f_m t} \quad (3.3.42)$$

where

$$\begin{aligned} c_n &= \frac{1}{T_m} \int_0^{T_m} e^{j\beta m(t)} e^{-j2\pi n f_m t} dt \\ &\stackrel{u=2\pi f_m t}{=} \frac{1}{2\pi} \int_0^{2\pi} e^{j[\beta m(\frac{u}{2\pi f_m}) - nu]} du \end{aligned} \quad (3.3.43)$$

and

$$\begin{aligned} u(t) &= A_c \operatorname{Re} \left[ \sum_{n=-\infty}^{\infty} c_n e^{j2\pi f_c t} e^{j2\pi n f_m t} \right] \\ &= A_c \sum_{n=-\infty}^{\infty} |c_n| \cos(2\pi(f_c + n f_m)t + \angle c_n) \end{aligned} \quad (3.3.44)$$

It is seen again that the modulated signal contains all frequencies of the form  $f_c + n f_m$ .

The detailed treatment of the spectral characteristics of an angle-modulated signal for a general nonperiodic deterministic message signal  $m(t)$  is quite involved due to the nonlinear nature of the modulation process. However, there exists an approximate relation for the effective bandwidth of the modulated signal, known as the *Carson's rule*, and given by

$$B_c = 2(\beta + 1)W \quad (3.3.45)$$

where  $\beta$  is the modulation index defined as

$$\beta = \begin{cases} k_p \max[|m(t)|], & \text{PM} \\ \frac{k_f \max[|m(t)|]}{W}, & \text{FM} \end{cases} \quad (3.3.46)$$

and  $W$  is the bandwidth of the message signal  $m(t)$ . Since in wideband FM the value of  $\beta$  is usually around 5 or more, it is seen that the bandwidth of an angle-modulated signal is much greater than the bandwidth of various amplitude-modulation schemes, which is either  $W$  (in SSB) or  $2W$  (in DSB or conventional AM).

### 3.3.3 Implementation of Angle Modulators and Demodulators

Any modulation and demodulation process involves the generation of new frequencies that were not present in the input signal. This is true for both amplitude and angle-modulation systems. This means that, if we interpret the modulator as a system with the message signal  $m(t)$  as the input and with the modulated signal  $u(t)$  as the output, this system has frequencies in its output that were not present in the input. Therefore, a modulator (and demodulator) can not be modeled as a linear time-invariant system because a linear time-invariant system can not produce any frequency components in the output that are not present in the input signal.

Angle modulators are, in general, time-varying and nonlinear systems. One method for generating an FM signal directly is to design an oscillator whose frequency changes with the input voltage. When the input voltage is zero, the oscillator generates a sinusoid with frequency  $f_c$ , and when the input voltage changes, this frequency changes accordingly. There are two approaches to designing such an oscillator, usually called a VCO or *voltage-controlled oscillator*. One approach is to use a *varactor diode*. A varactor diode is a capacitor whose capacitance changes with the applied voltage. Therefore, if this capacitor is used in the tuned circuit of the oscillator and the message signal is applied to it, the frequency of the tuned circuit, and the oscillator, will change in accordance with the message signal. Let us assume that the inductance of the inductor in the tuned circuit of Figure 3.31 is  $L_0$  and the capacitance of the varactor diode is given by

$$C(t) = C_0 + k_0m(t) \quad (3.3.47)$$

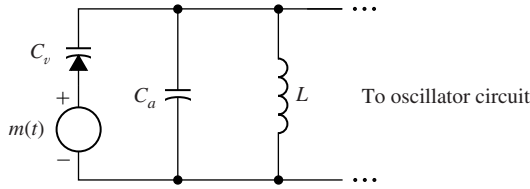


**Figure 3.31** Varactor diode implementation of an angle modulator.

When  $m(t) = 0$ , the frequency of the tuned circuit is given by  $f_c = \frac{1}{2\pi\sqrt{L_0C_0}}$ . In general, for nonzero  $m(t)$ , we have

$$\begin{aligned} f_i(t) &= \frac{1}{2\pi\sqrt{L_0(C_0 + k_0m(t))}} \\ &= \frac{1}{2\pi\sqrt{L_0C_0}} \frac{1}{\sqrt{1 + \frac{k_0}{C_0}m(t)}} \\ &= f_c \frac{1}{\sqrt{1 + \frac{k_0}{C_0}m(t)}} \end{aligned} \quad (3.3.48)$$

Assuming that

$$\epsilon = \frac{k_0}{C_0}m(t) \ll 1$$

and using the approximations

$$\sqrt{1 + \epsilon} \approx 1 + \frac{\epsilon}{2} \quad (3.3.49)$$

$$\frac{1}{1 + \epsilon} \approx 1 - \epsilon, \quad (3.3.50)$$

we obtain

$$f_i(t) \approx f_c \left( 1 - \frac{k_0}{2C_0}m(t) \right) \quad (3.3.51)$$

which is the relation for a frequency-modulated signal.

A second approach for generating an FM signal is by use of a *reactance tube*. In the reactance-tube implementation, an inductor whose inductance varies with the applied voltage is employed and the analysis is very similar to the analysis presented for the varactor diode. It should be noted that although we described these methods for generation of FM signals, due to the close relation between FM and PM signals, basically the same methods can be applied for generation of PM signals (see Figure 3.25).

Another approach for generating an angle-modulated signal is to first generate a narrowband angle-modulated signal, and then change it to a wideband signal. This method is usually known as the *indirect method* for generation of FM and PM signals. Due to the similarity of conventional AM signals, generation of narrowband

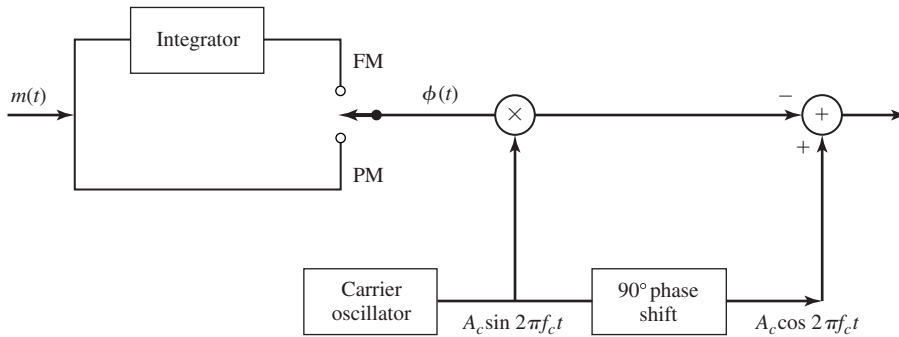


**Figure 3.32** Generation of narrowband angle-modulated signal.

angle-modulated signals is straightforward. In fact any modulator for conventional AM generation can be easily modified to generate a narrowband angle-modulated signal. Figure 3.32 shows the block diagram of a narrowband angle modulator. The next step is to use the narrowband angle-modulated signal to generate a wideband angle-modulated signal. Figure 3.33 shows the block diagram of a system that generates wideband angle-modulated signals from narrowband angle-modulated signals. The first stage of such a system is, of course, a narrowband angle-modulator such as the one shown in Figure 3.32. The narrowband angle-modulated signal enters a frequency multiplier that multiplies the instantaneous frequency of the input by some constant  $n$ . This is usually done by applying the input signal to a nonlinear element and then passing its output through a bandpass filter tuned to the desired central frequency. If the narrowband-modulated signal is represented by

$$u_n(t) = A_c \cos(2\pi f_c t + \phi(t)) \quad (3.3.52)$$

the output of the frequency multiplier (output of the bandpass filter) is given by

$$y(t) = A_c \cos(2\pi n f_c t + n\phi(t)) \quad (3.3.53)$$

In general, this is, of course, a wideband angle-modulated signal. However, there is no guarantee that the carrier frequency of this signal,  $n f_c$ , will be the desired carrier frequency. The last stage of the modulator performs an up or down conversion to shift

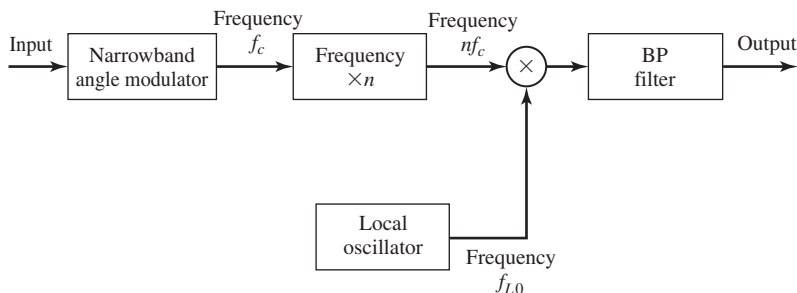


**Figure 3.33** Indirect generation of angle-modulated signals.

the modulated signal to the desired center frequency. This stage consists of a mixer and a bandpass filter. If the frequency of the local oscillator of the mixer is  $f_{L0}$  and we are using a down converter, the final wideband angle-modulated signal is given by

$$u(t) = A_c \cos(2\pi(nf_c - f_{L0})t + n\phi(t)) \quad (3.3.54)$$

Since we can freely choose  $n$  and  $f_{L0}$ , we can generate any modulation index at any desired carrier frequency by this method.

FM demodulators are implemented by generating an AM signal whose amplitude is proportional to the instantaneous frequency of the FM signal, and then using an AM demodulator to recover the message signal. To implement the first step; i.e., transforming the FM signal into an AM signal, it is enough to pass the FM signal through an LTI system whose frequency response is approximately a straight line in the frequency band of the FM signal. If the frequency response of such a system is given by

$$|H(f)| = V_0 + k(f - f_c) \quad \text{for } |f - f_c| < \frac{B_c}{2} \quad (3.3.55)$$

and if the input to the system is

$$u(t) = A_c \cos\left(2\pi f_c t + 2\pi k_f \int_{-\infty}^t m(\tau) d\tau\right), \quad (3.3.56)$$

then, the output will be the signal

$$v_o(t) = A_c(V_0 + k k_f m(t)) \cos\left(2\pi f_c t + 2\pi k_f \int_{-\infty}^t m(\tau) d\tau\right) \quad (3.3.57)$$

The next step is to demodulate this signal to obtain  $A_c(V_0 + k k_f m(t))$ , from which the message  $m(t)$  can be recovered. Figure 3.34 shows a block diagram of these two steps.

There exist many circuits that can be used to implement the first stage of an FM demodulator; i.e., FM to AM conversion. One such candidate is a simple differentiator with

$$|H(f)| = 2\pi f \quad (3.3.58)$$

Another candidate is the rising half of the frequency characteristics of a tuned circuit as shown in Figure 3.35. Such a circuit can be easily implemented, but usually the linear region of the frequency characteristic may not be wide enough. To obtain a linear characteristic over a wider range of frequencies, usually two circuits tuned at two frequencies,  $f_1$  and  $f_2$ , are connected in a configuration which is known as a *balanced discriminator*. A balanced discriminator with the corresponding frequency characteristics is shown in Figure 3.36.

The FM demodulation methods described here that transform the FM signal into an AM signal have a bandwidth equal to the channel bandwidth  $B_c$  occupied by the FM signal. Consequently, the noise that is passed by the demodulator is the noise contained within  $B_c$ .

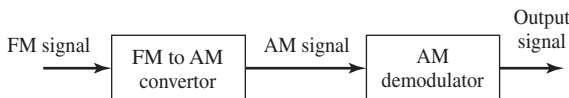


**Figure 3.34** A general FM demodulator.

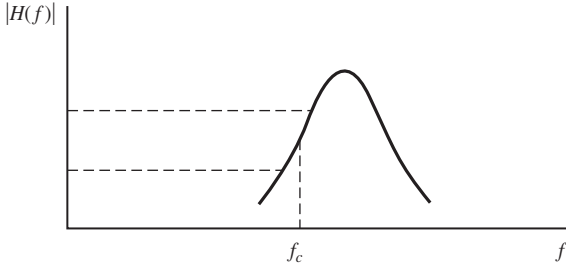


**Figure 3.35** A tuned circuit used in an FM demodulator.

A totally different approach to FM signal demodulation is to use feedback in the FM demodulator to narrow the bandwidth of the FM detector and, as will be seen in Chapter 5, to reduce the noise power at the output of the demodulator. Figure 3.37 illustrates a system in which the FM discrimination is placed in the feedback branch of a feedback system that employs a voltage-controlled oscillator (VCO) path. The bandwidth of the discriminator and the subsequent lowpass filter is designed to match the bandwidth of the message signal  $m(t)$ . The output of the lowpass filter is the desired message signal. This type of FM demodulator is called an *FM demodulator with feedback (FMFB)*. An alternative to FMFB demodulator is the use of a phase-locked loop (PLL), as shown in Figure 3.38. The input to the PLL is the angle-modulated signal (we neglect the presence of noise in this discussion)

$$u(t) = A_c \cos[2\pi f_c t + \phi(t)] \quad (3.3.59)$$

where, for FM,

$$\phi(t) = 2\pi k_f \int_{-\infty}^t m(\tau) d\tau \quad (3.3.60)$$

The VCO generates a sinusoid of a fixed frequency, in this case the carrier frequency  $f_c$ , in the absence of an input control voltage.

Now, suppose that the control voltage to the VCO is the output of the loop filter, denoted as  $v(t)$ . Then, the instantaneous frequency of the VCO is

$$f_v(t) = f_c + k_v v(t) \quad (3.3.61)$$

where  $k_v$  is a deviation constant with units of Hz/volt. Consequently, the VCO output may be expressed as

$$y_v(t) = A_v \sin[2\pi f_c t + \phi_v(t)] \quad (3.3.62)$$

where

$$\phi_v(t) = 2\pi k_v \int_0^t v(\tau) d\tau \quad (3.3.63)$$

The phase comparator is basically a multiplier and filter that rejects the signal component centered at  $2f_c$ . Hence, its output may be expressed as

$$e(t) = \frac{1}{2} A_v A_c \sin[\phi(t) - \phi_v(t)] \quad (3.3.64)$$

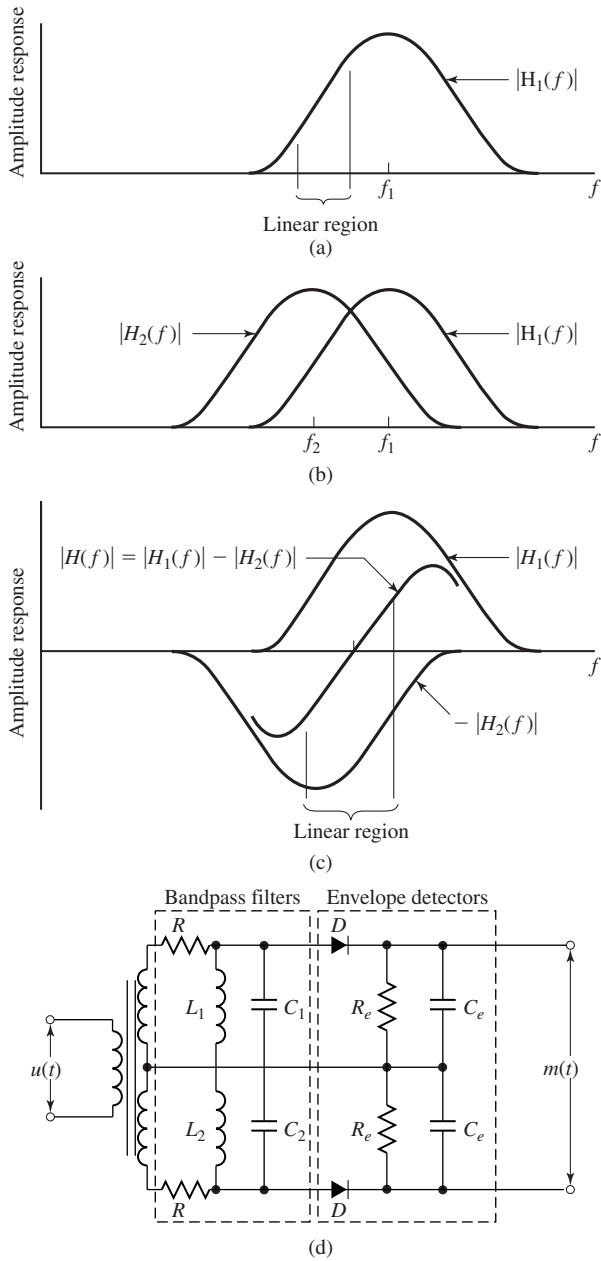


**Figure 3.36** A balanced discriminator and the corresponding frequency response.

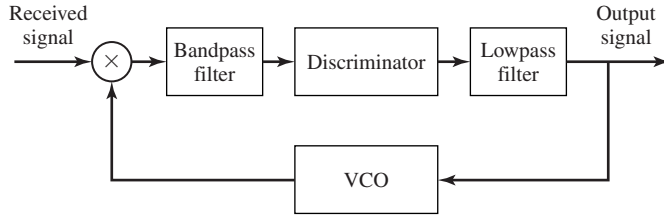


Figure 3.37 Block diagram of FMFB demodulator.

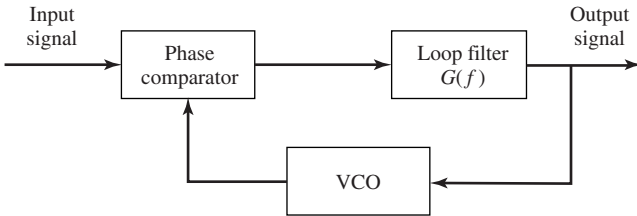


Figure 3.38 Block diagram of PLL-FM demodulator.

where the difference,  $\phi(t) - \phi_v(t) \equiv \phi_e(t)$ , constitutes the phase error. The signal  $e(t)$  is the input to the loop filter.

Let us assume that the PLL is in lock, so that the phase error is small. Then,

$$\sin[\phi(t) - \phi_v(t)] \approx \phi(t) - \phi_v(t) = \phi_e(t) \tag{3.3.65}$$

Under this condition, we may deal with the linearized model of the PLL, shown in Figure 3.39. We may express the phase error as

$$\phi_e(t) = \phi(t) - 2\pi k_v \int_0^t v(\tau) d\tau \tag{3.3.66}$$

or, equivalently, either as

$$\frac{d}{dt} \phi_e(t) + 2\pi k_v v(t) = \frac{d}{dt} \phi(t) \tag{3.3.67}$$

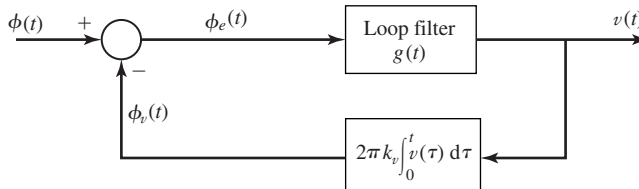


Figure 3.39 Linearized PLL.



or as

$$\frac{d}{dt}\phi_e(t) + 2\pi k_v \int_0^\infty \phi_e(\tau)g(t - \tau) d\tau = \frac{d}{dt}\phi(t) \quad (3.3.68)$$

The Fourier transform of the integro-differential equation in Equation (3.3.68) is

$$(j2\pi f)\Phi_e(f) + 2\pi k_v \Phi_e(f)G(f) = (j2\pi f)\Phi(f) \quad (3.3.69)$$

and, hence,

$$\Phi_e(f) = \frac{1}{1 + \left(\frac{k_v}{jf}\right)G(f)}\Phi(f) \quad (3.3.70)$$

The corresponding equation for the control voltage to the VCO is

$$\begin{aligned} V(f) &= \Phi_e(f)G(f) \\ &= \frac{G(f)}{1 + \left(\frac{k_v}{jf}\right)G(f)}\Phi(f) \end{aligned} \quad (3.3.71)$$

Now, suppose that we design  $G(f)$  such that

$$\left|k_v \frac{G(f)}{jf}\right| \gg 1 \quad (3.3.72)$$

in the frequency band  $|f| < W$  of the message signal. Then from Equation (3.3.71), we have

$$V(f) = \frac{j2\pi f}{2\pi k_v}\Phi(f) \quad (3.3.73)$$

or, equivalently,

$$\begin{aligned} v(t) &= \frac{1}{2\pi k_v} \frac{d}{dt}\phi(t) \\ &= \frac{k_f}{k_v} m(t) \end{aligned} \quad (3.3.74)$$

Since the control voltage of the VCO is proportional to the message signal,  $v(t)$  is the demodulated signal.

We observe that the output of the loop filter with frequency response  $G(f)$  is the desired message signal. Hence, the bandwidth of  $G(f)$  should be the same as the bandwidth  $W$  of the message signal. Consequently, the noise at the output of the loop filter is also limited to the bandwidth  $W$ . On the other hand, the output from the VCO is a wideband FM signal with an instantaneous frequency that follows the instantaneous frequency of the received FM signal.

The major benefit of using feedback in FM signal demodulation is to reduce the threshold effect that occurs when the input signal-to-noise-ratio to the FM demodulator drops below a critical value. The threshold effect is treated in Chapter 5.

### 3.4 RADIO AND TELEVISION BROADCASTING

Radio and television broadcasting is the most familiar form of communication via analog signal transmission. Next, we describe three types of broadcasting, namely, AM radio, FM radio, and television.

#### 3.4.1 AM Radio Broadcasting

Commercial AM radio broadcasting utilizes the frequency band 535–1605 kHz for transmission of voice and music. The carrier frequency allocations range from 540–1600 kHz with 10-kHz spacing.

Radio stations employ conventional AM for signal transmission. The baseband message signal  $m(t)$  is limited to a bandwidth of approximately 5 kHz. Since there are billions of receivers and relatively few radio transmitters, the use of conventional AM for broadcast is justified from an economic standpoint. The major objective is to reduce the cost of implementing the receiver.

The receiver most commonly used in AM radio broadcast is the so called *superheterodyne receiver* shown in Figure 3.40. It consists of a radio frequency (RF) tuned amplifier, a mixer, a local oscillator, an intermediate frequency (IF) amplifier, an envelope detector, an audio frequency amplifier, and a loudspeaker. Tuning for the desired radio frequency is provided by a variable capacitor, which simultaneously tunes the RF amplifier and the frequency of the local oscillator.

In the superheterodyne receiver, every AM radio signal is converted to a common IF frequency of  $f_{IF} = 455$  kHz. This conversion allows the use of a single tuned IF amplifier for signals from any radio station in the frequency band. The IF amplifier is designed to have a bandwidth of 10 kHz, which matches the bandwidth of the transmitted signal.

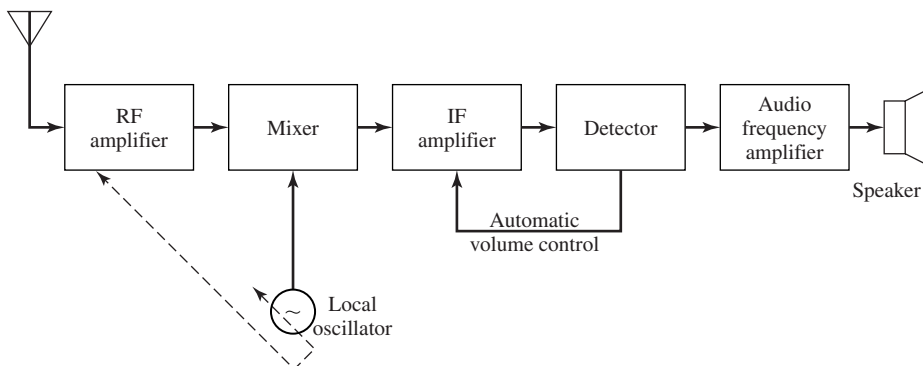


Figure 3.40 Superheterodyne AM receiver.

The frequency conversion to IF is performed by the combination of the RF amplifier and the mixer. The frequency of the local oscillator is

$$f_{LO} = f_c + f_{IF}$$

where  $f_c$  is the carrier frequency of the desired AM radio signal. The tuning range of the local oscillator is 955–2055 kHz. By tuning the RF amplifier to the frequency  $f_c$  and mixing its output with the local oscillator frequency  $f_{LO} = f_c + f_{IF}$ , we obtain two signal components, one centered at the difference frequency  $f_{IF}$  and the second centered at the sum frequency  $2f_c + f_{IF}$ . Only the first component is passed by the IF amplifier.

At the input to the RF amplifier we have signals picked up by the antenna from all radio stations. By limiting the bandwidth of the RF amplifier to the range  $B_c < B_{RF} < 2f_{IF}$  where  $B_c$  is the bandwidth of the AM radio signal (10 kHz), we can reject the radio signal transmitted at the so-called *image frequency*,  $f'_c = f_{LO} + f_{IF}$ . Note that when we mix the local oscillator output,  $\cos 2\pi f_{LO}t$ , with the received signals

$$\begin{aligned} r_1(t) &= A_c[1 + m_1(t)] \cos 2\pi f_c t \\ r_2(t) &= A_c[1 + m_2(t)] \cos 2\pi f'_c t \end{aligned} \quad (3.4.1)$$

where  $f_c = f_{LO} - f_{IF}$  and  $f'_c = f_{LO} + f_{IF}$ , the mixer output consists of the two signals

$$\begin{aligned} y_1(t) &= A_c[1 + m_1(t)] \cos 2\pi f_{IF}t + \text{double frequency term} \\ y_2(t) &= A_c[1 + m_2(t)] \cos 2\pi f_{IF}t + \text{double frequency term} \end{aligned} \quad (3.4.2)$$

where  $m_1(t)$  represents the desired signal and  $m_2(t)$  is the signal transmitted by the radio station transmitting at the carrier frequency  $f'_c = f_{LO} + f_{IF}$ . In order to prevent the signal  $r_2(t)$  from interfering with the demodulation of the desired signal  $r_1(t)$ , the RF amplifier bandwidth is designed to be sufficiently narrow so that the image frequency signal is rejected. Hence,  $B_{RF} < 2f_{IF}$  is the upper limit on the bandwidth of the RF amplifier. In spite of this constraint, the bandwidth of the RF amplifier is still considerably wider than the bandwidth of the IF amplifier. Thus, the IF amplifier, with its narrow bandwidth, provides signal rejection from adjacent channels and the RF amplifier provides signal rejection from image channels. Figure 3.41 illustrates the bandwidths of the RF and IF amplifiers and the requirement for rejecting the image frequency signal.

The output of the IF amplifier is passed through an envelope detector which produces the desired audio-band message signal  $m(t)$ . Finally, the output of the envelope detector is amplified and the amplified signal drives a loudspeaker. Automatic volume control (AVC) is provided by a feedback control loop which adjusts the gain of the IF amplifier based on the power level of the signal at the envelope detector.

### 3.4.2 FM Radio Broadcasting

Commercial FM radio broadcasting utilizes the frequency band 88–108 MHz for transmission of voice and music signals. The carrier frequencies are separated by 200 kHz and the peak-frequency deviation is fixed at 75 kHz. Pre-emphasis is generally used,

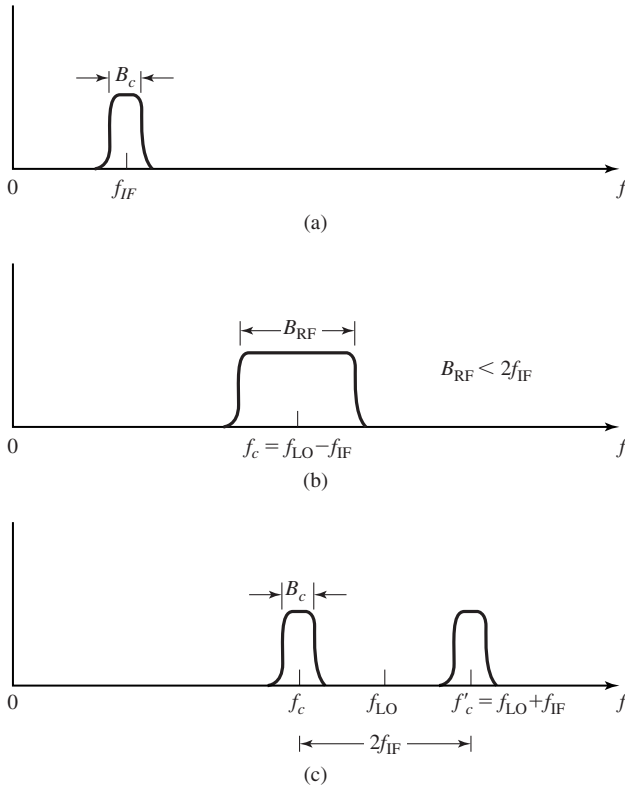


**Figure 3.41** Frequency response characteristics of IF and RF amplifiers.

as described in Chapter 5, to improve the demodulator performance in the presence of noise in the received signal.

The receiver most commonly used in FM radio broadcast is a superheterodyne type. The block diagram of such a receiver is shown in Figure 3.42. As in AM radio reception, common tuning between the RF amplifier and the local oscillator allows the mixer to bring all FM radio signals to a common IF bandwidth of 200 kHz, centered at  $f_{IF} = 10.7$  MHz. Since the message signal  $m(t)$  is embedded in the frequency of the carrier, any amplitude variations in the received signal are a result of additive noise and interference. The amplitude limiter removes any amplitude variations in the received signal at the output of the IF amplifier by band-limiting the signal. A bandpass filter centered at  $f_{IF} = 10.7$  MHz with a bandwidth of 200 kHz is included in the limiter to remove higher order frequency components introduced by the nonlinearity inherent in the hard limiter.

A balanced frequency discriminator is used for frequency demodulation. The resulting message signal is then passed to the audio frequency amplifier which performs the functions of de-emphasis and amplification. The output of the audio amplifier is further filtered by a lowpass filter to remove out-of-band noise and its output is used to drive a loudspeaker.

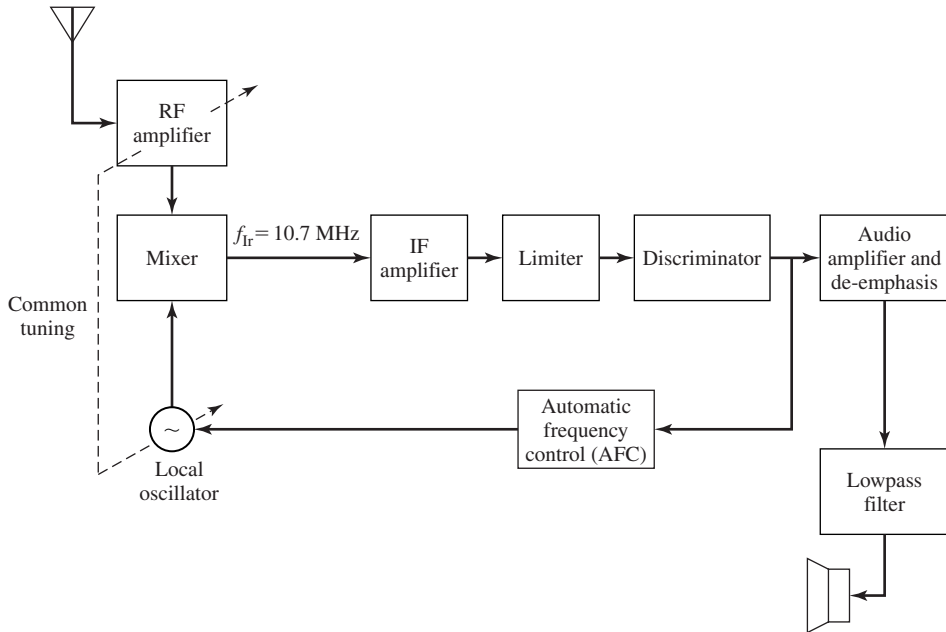


**Figure 3.42** Block diagram of a superheterodyne FM radio receiver.

**FM Stereo Broadcasting.** Many FM radio stations transmit music programs in stereo by using the outputs of two microphones placed in two different parts of the stage. Figure 3.43 shows a block diagram of an FM stereo transmitter. The signals from the left and right microphones,  $m_\ell(t)$  and  $m_r(t)$ , are added and subtracted as shown. The sum signal  $m_\ell(t) + m_r(t)$  is left as is and occupies the frequency band 0–15 kHz. The difference signal  $m_\ell(t) - m_r(t)$  is used to AM modulate (DSB-SC) a 38-kHz carrier that is generated from a 19-kHz oscillator. A pilot tone at the frequency of 19 kHz is added to the signal for the purpose of demodulating the DSB-SC AM signal. The reason for placing the pilot tone at 19 kHz instead of 38 kHz is that the pilot is more easily separated from the composite signal at the receiver. The combined signal is used to frequency modulate a carrier.

By configuring the baseband signal as an FDM signal, a monophonic FM receiver can recover the sum signal  $m_\ell(t) + m_r(t)$  by use of a conventional FM demodulator. Hence, FM stereo broadcasting is compatible with conventional FM. The second requirement is that the resulting FM signal does not exceed the allocated 200-kHz bandwidth.

The FM demodulator for FM stereo is basically the same as a conventional FM demodulator down to the limiter/discriminator. Thus, the received signal is converted to baseband. Following the discriminator, the baseband message signal is separated into the two signals  $m_\ell(t) + m_r(t)$  and  $m_\ell(t) - m_r(t)$  and passed through de-emphasis filters, as shown in Figure 3.44. The difference signal is obtained from the DSB-SC signal by means of a synchronous demodulator using the pilot tone. By taking the sum

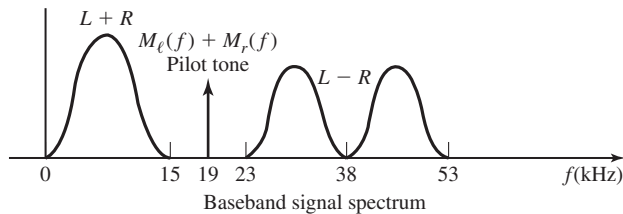
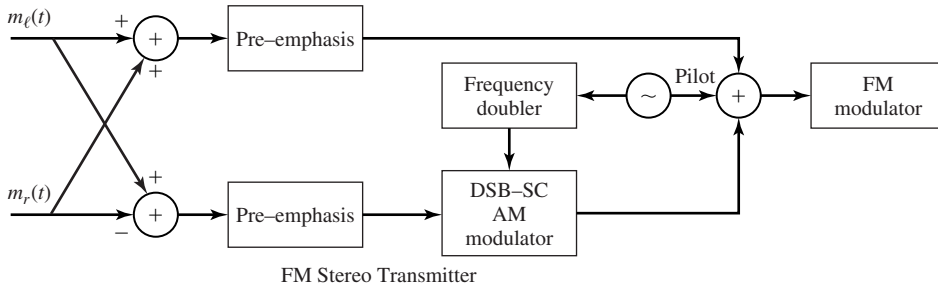


**Figure 3.43** FM stereo transmitter and signal spacing.

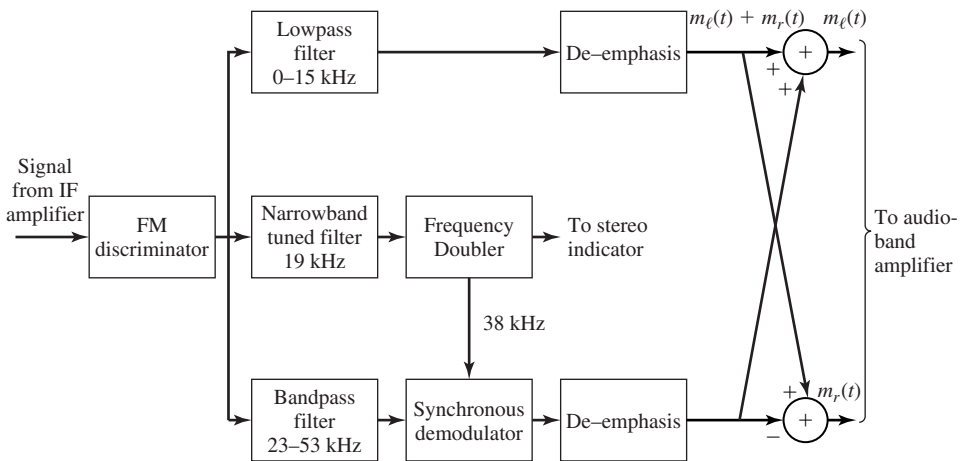


**Figure 3.44** FM stereo receiver.

and difference of the two composite signals, we recover the two signals  $m_\ell(t)$  and  $m_r(t)$ . These audio signals are amplified by audio-band amplifiers and the two outputs drive dual loudspeakers. As indicated above, an FM receiver that is not configured to receive the FM stereo sees only the baseband signal  $m_\ell(t) + m_r(t)$  in the frequency range 0–15 kHz. Thus, it produces a monophonic output signal which consists of the sum of the signals at the two microphones.

### 3.4.3 Television Broadcasting

Commercial TV broadcasting began as black-and-white picture transmission in London in 1936 by the British Broadcasting Corporation (BBC). Color television was demonstrated a few years later, but the move of commercial TV stations to color TV signal transmission was slow in developing. To a large extent, this was due to the high cost of color TV receivers. With the development of the transistor and microelectronics components, the cost of color TV receivers decreased significantly, so that by the middle 1960s color TV broadcasting was widely used by the industry.

The frequencies allocated for TV broadcasting fall in the VHF and UHF frequency bands. Table 5.2 lists the TV channel allocations in the United States. We observe that the channel bandwidth allocated for transmission of TV signals is 6 MHz.

In contrast to radio broadcasting, standards for television signal transmission vary from country to country. The U.S. standard, which we describe below, was set by the National Television Systems Committee (NTSC).

**Black-and-White TV Signals.** The first step in TV signal transmission is to convert a visual image into an electrical signal. The two-dimensional image or picture is converted to a one-dimensional electrical signal by sequentially scanning the image and producing an electrical signal that is proportional to the brightness level of the image. The scanning is performed in a TV camera, which optically focuses the image on a photo cathode tube that consists of a photosensitive surface.

The scanning of the image is performed by an electron beam that produces an output current or voltage which is proportional to the brightness of the image. The resulting electrical signal is called a *video signal*.

The scanning of the electron beam is controlled by two voltages applied across the horizontal and vertical deflection plates. These two voltages are shown in Figure 3.45.

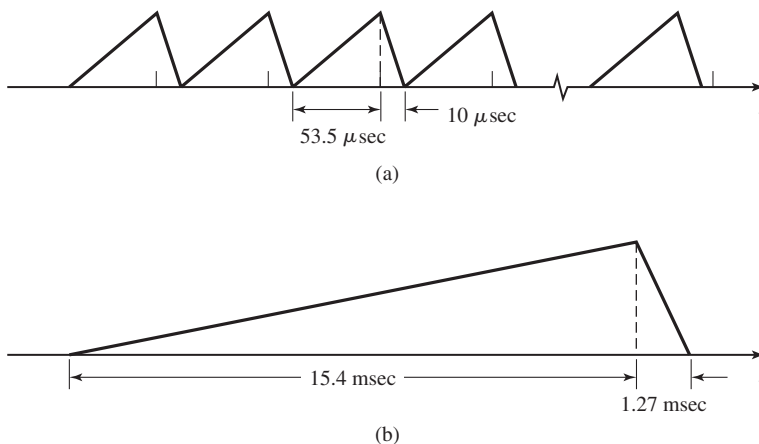


**Figure 3.45** Signal waveforms applied to horizontal (a) and vertical (b) deflection plates.

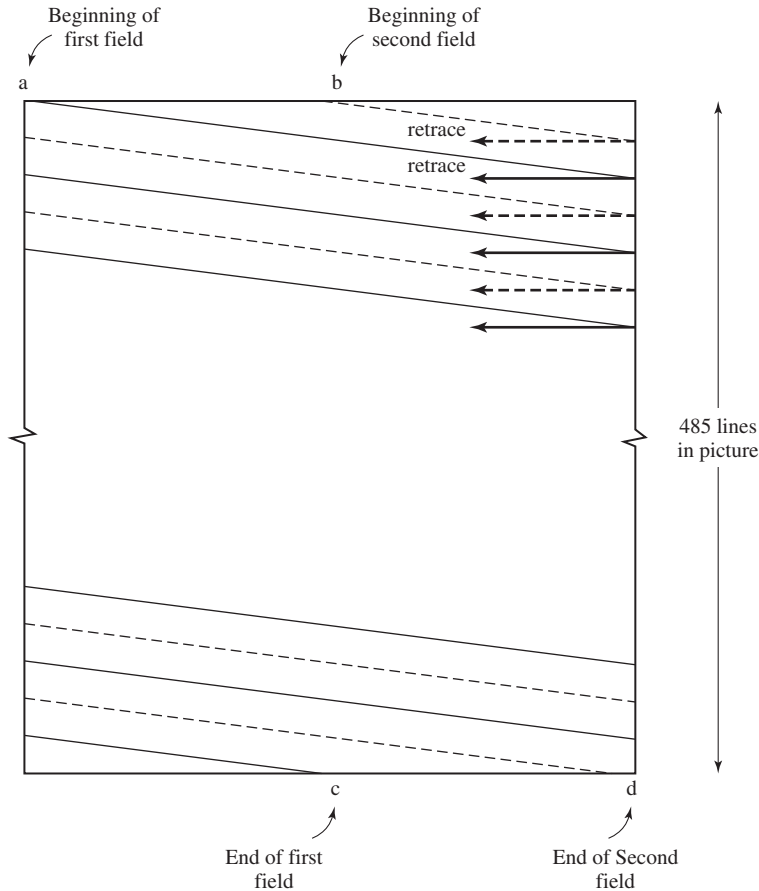


**Figure 3.46** Interlaced scanning pattern.

In this scanning method, the image is divided into 525 lines that define a *frame*, as illustrated in Figure 3.46. The resulting signal is transmitted in  $1/30$  of a second. The number of lines determines the picture resolution and, in combination with the rate of transmission, determine the channel bandwidth required for transmission of the image.

The time interval of  $1/30$  second to transmit a complete image is generally not fast enough to avoid flicker that is annoying to the eyes of the average viewer. To overcome flicker, the scanning of the image is performed in an *interlaced pattern* as shown in Figure 3.46. The interlaced pattern consists of two fields, each consisting of 262.5 lines. Each field is transmitted in  $1/60$  of a second, which exceeds the flicker rate that is observed by the average eye. The first field begins at point “a” and terminates at point “c.” The second field begins at point “b” and terminates at point “d.”

A horizontal line is scanned in  $53.5 \mu\text{sec}$  as indicated by the sawtooth signal waveform applied to the horizontal deflection plates. The beam has  $10 \mu\text{sec}$  to move to



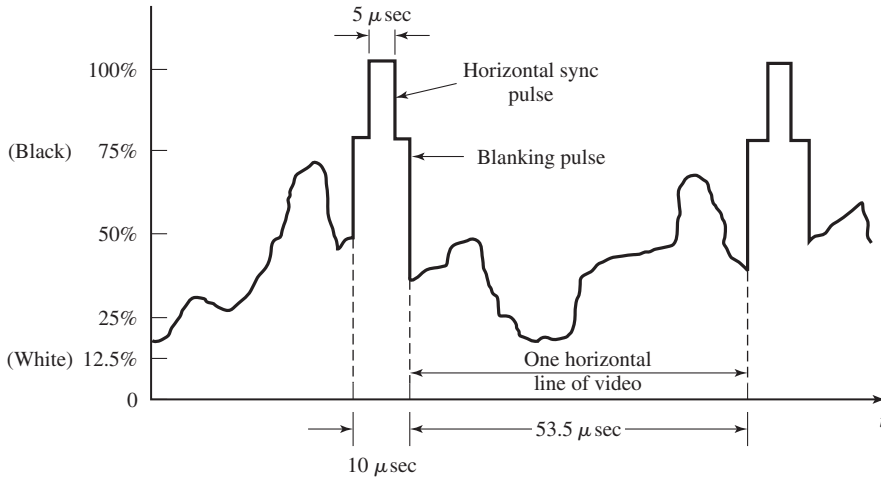


**Figure 3.47** Typical video signal for one horizontal sweep.

the next line. During this interval, a blanking pulse is inserted to avoid the appearance of retrace lines across the TV receiver. A  $5 \mu\text{sec}$  pulse is added to the blanking pulse to provide synchronization for the horizontal sweep circuit at the receiver. A typical video signal is shown in Figure 3.47.

After the transmission of one interlaced field, the vertical sawtooth signal waveform applied to the vertical deflection plates is reset to zero. The retrace interval of 1.27 msec, corresponding to 20 line scans, allows the beam to move from the bottom to the top of the picture. A vertical blanking pulse is inserted during the interval to avoid the appearance of retrace lines at the TV receiver. When we allow for the vertical retrace (twice per frame), the actual number of horizontal lines in the image is 485.

The bandwidth of the video signal can be estimated by viewing the image as a rectangular array of 485 rows by  $(485)(4/3)$  columns, where  $4/3$  is the *aspect ratio* (the ratio of the width to height of the image). Thus, we have 313,633 picture elements (*pixels*) per frame, which are transmitted in  $1/30$  of a second. This is equivalent to a sampling rate of 10.5 MHz, which is sufficient to represent a signal as large as 5.25 MHz. However, the light intensity of adjacent pixels in an image is highly correlated. Hence, the bandwidth of the video signal is less than 5.25 MHz. In commercial TV broadcasting, the bandwidth of the video signal is limited to  $W = 4.2 \text{ MHz}$ .

Since the allocated channel bandwidth for commercial TV is 6 MHz, it is clear that DSB transmission is not possible. The large low-frequency content of the video signal also rules out SSB as a practical modulation method. Hence, VSB is the only viable alternative. By transmitting a large carrier component, the received VSB signal can be simply demodulated by means of an envelope detector. This type of detection significantly simplifies the implementation of the receiver.

The range of frequencies occupied by the transmitted video signal is shown in Figure 3.48. We note that the full upper sideband (4.2 MHz) of the video signal is

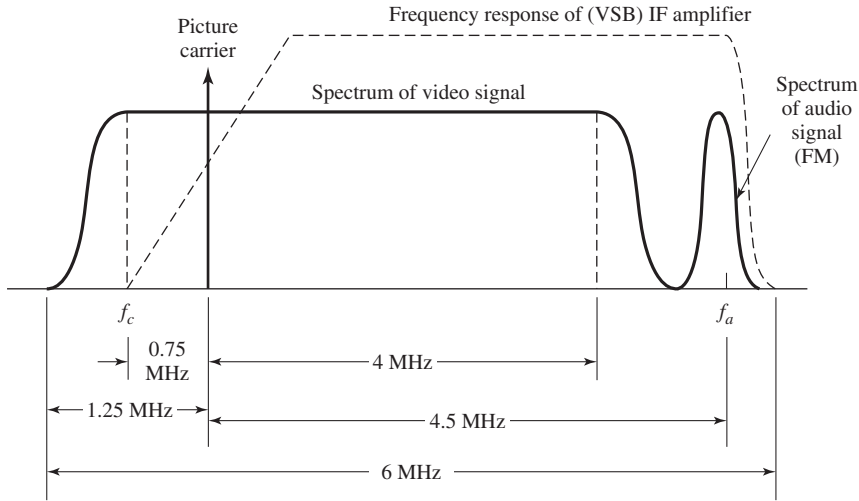


**Figure 3.48** Spectral characteristics of black-and-white television signal.

transmitted along with a portion (1.25 MHz) of the lower sideband. Unlike the conventional VSB spectral shaping described in Section 5.2.4, the lower sideband signal in the frequency range  $f_c$  and  $f_c - 0.75$  MHz is transmitted without attenuation. The frequencies in the range  $f_c - 1.25$  to  $f_c - 0.75$  MHz are attenuated as shown in Figure 3.48 and all frequency components below  $f_c - 1.25$  MHz are blocked. VSB spectral shaping is performed at the IF amplifier of the receiver.

In addition to the video signal, the audio portion of the TV signal is transmitted by frequency modulating a carrier at  $f_c + 4.5$  MHz. The audio-signal bandwidth is limited to  $W = 10$  kHz. The frequency deviation in the FM modulated signal is selected as 25 kHz and the FM signal bandwidth is 70 kHz. Hence, the total channel bandwidth required to transmit the video and audio signals is 5.785 MHz.

Figure 3.49 shows a block diagram of a black-and-white TV transmitter. The corresponding receiver is shown in Figure 3.50. It is a heterodyne receiver. We note that there are two separate tuners, one for the UHF band and one for the VHF band. The TV signals in the UHF band are brought down to the VHF band by a UHF mixer. This frequency conversion makes it possible to use a common RF amplifier for the two frequency bands. Then, the video signal selected by the tuner is translated to a common IF frequency band of 41–47 MHz. The IF amplifier also provides the VSB shaping required prior to signal detection. The output of the IF amplifier is envelope detected to produce the baseband signal.

The audio portion of the signal centered at 4.5 MHz is filtered out by means of an IF filter amplifier and passed to the FM demodulator. The demodulated audio band signal is then amplified by an audio amplifier and its output drives the speaker.

The video component of the baseband signal is passed through a video amplifier which passes frequency components in the range 0–4.2 MHz. Its output is passed to the

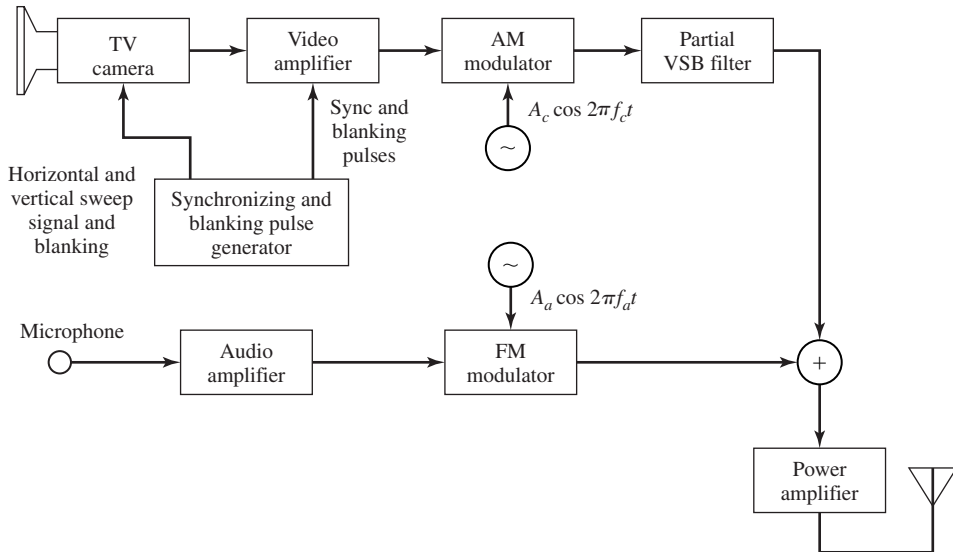


**Figure 3.49** Block diagram of a black-and-white TV transmitter.

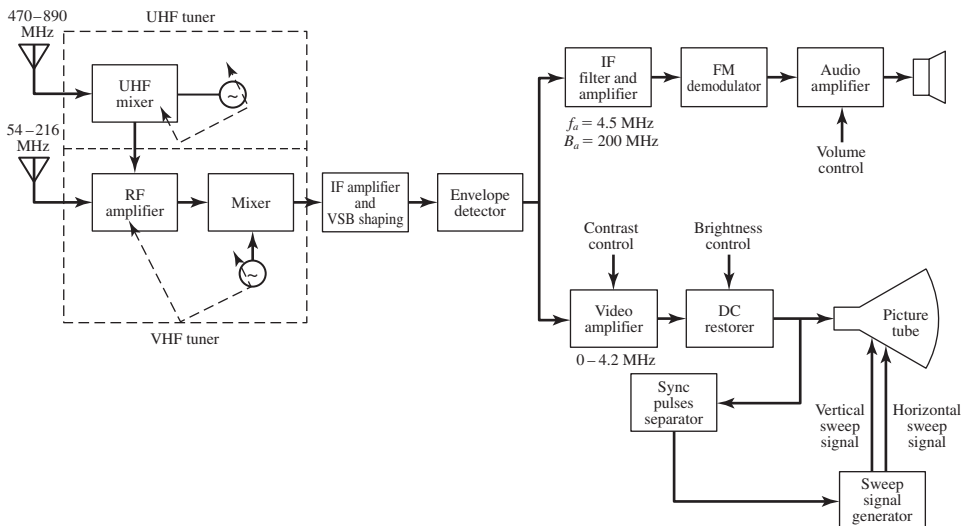


**Figure 3.50** Block diagram of a black-and-white TV receiver.

DC restorer that clamps the blanking pulses and sets the correct dc level. The dc-restored video signal is then fed to the picture tube. The synchronizing pulses contained in the received video signal are separated and applied to the horizontal and vertical sweep generators.

**Compatible Color Television.** The transmission of color information contained in an image can be accomplished by decomposing the colors of pixels into primary colors and transmitting the electrical signals corresponding to these colors. In general, all natural colors are well approximated by appropriate mixing of three primary colors: blue, green, and red. Consequently, if we employ three cameras, one with a blue filter, one with a green filter, and one with a red filter, and transmit the electrical signals  $m_b(t)$ ,  $m_g(t)$ , and  $m_r(t)$ , generated by the three color cameras that view the color image, the received signals can be combined to produce a replica of the original color image.

Such a transmission scheme has two major disadvantages. First, it requires three times the channel bandwidth of black-and-white television. Second, the transmitted color TV signal cannot be received by a black-and-white (monochrome) TV receiver.

The NTSC standard adopted in 1953 in the United States avoids these two problems by transmitting a mixture of the three primary-color signals. Specifically, the three signals transmitted in the standard color TV system are the following three linearly independent combinations:

$$\begin{aligned} m_L(t) &= 0.11m_b(t) + 0.59m_g(t) + 0.30m_r(t) \\ m_I(t) &= -0.32m_b(t) - 0.28m_g(t) + 0.60m_r(t) \\ m_Q(t) &= 0.31m_b(t) - 0.52m_g(t) + 0.21m_r(t) \end{aligned} \quad (3.4.3)$$

The transformation matrix

$$M = \begin{bmatrix} 0.11 & 0.59 & 0.30 \\ -0.32 & -0.28 & 0.60 \\ 0.31 & -0.52 & 0.21 \end{bmatrix} \quad (3.4.4)$$

that is used to construct the new transmitted signals  $m_L(t)$ ,  $m_I(t)$ , and  $m_Q(t)$  is nonsingular and is inverted at the receiver to recover the primary-color signals  $m_b(t)$ ,  $m_g(t)$  and  $m_r(t)$  from  $m_L(t)$ ,  $m_I(t)$  and  $m_Q(t)$ .

The signal  $m_L(t)$  is called the *luminance signal*. It is assigned a bandwidth of 4.2 MHz and transmitted via VSB AM as in monochrome TV transmission. When this signal is received by a monochrome receiver, the result is a conventional black-and-white version of the color image. Thus, compatibility with monochrome TV broadcasting is achieved by transmitting  $m_L(t)$ . There remains the problem of transmitting the additional color information that can be used by a color TV receiver to reconstruct the color image. It is remarkable that the two composite color signals  $m_I(t)$  and  $m_Q(t)$  can be transmitted in the same bandwidth as  $m_L(t)$ , without interfering with  $m_L(t)$ .

The signals  $m_I(t)$  and  $m_Q(t)$  are called *chrominance signals* and are related to hue and saturation of colors. It has been determined experimentally, through subjective tests, that human vision cannot discriminate changes in  $m_I(t)$  and  $m_Q(t)$  over short time intervals and, hence, over small areas of the image. This implies that the high frequency content in the signals  $m_I(t)$  and  $m_Q(t)$  can be eliminated without significantly compromising the quality of the reconstructed image. The end result is that  $m_I(t)$  is limited in bandwidth to 1.6 MHz and  $m_Q(t)$  is limited to 0.6 MHz prior to transmission. These two signals are quadrature-carrier multiplexed on a subcarrier frequency

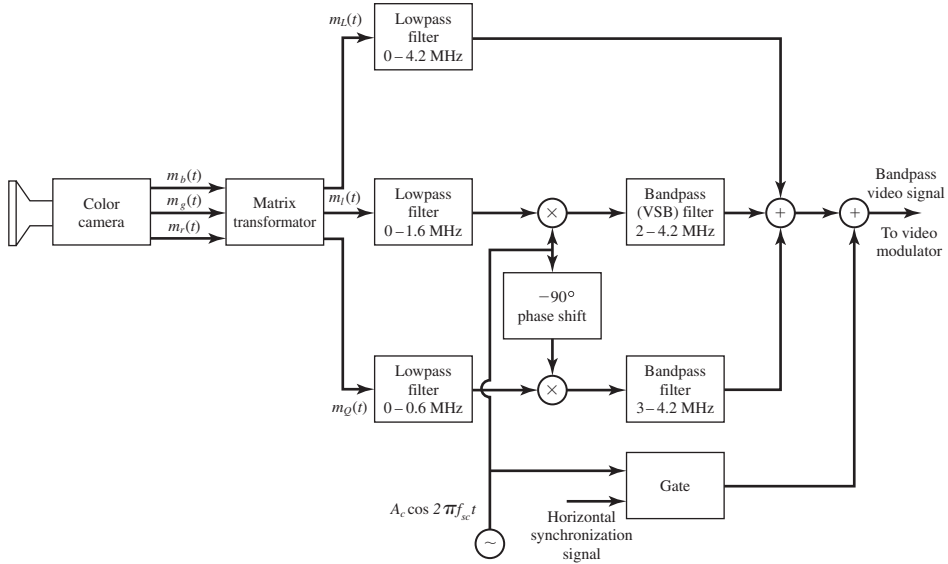


**Figure 3.51** Transmission of primary-color signals and multiplexing of chrominance and luminance signals.

$f_{sc} = f_c + 3.579545$  MHz, as illustrated in Figure 3.51. The signal  $m_I(t)$  is passed through a VSB filter that removes a part of the upper sideband, above 4.2 MHz. The signal  $m_Q(t)$  is transmitted by DSB-SC amplitude modulation. Therefore, the composite video signal may be expressed as

$$m(t) = m_L(t) + m_Q(t) \sin 2\pi f_{sc} t + m_I(t) \cos 2\pi f_{sc} t + \hat{m}'_I(t) \sin 2\pi f_{sc} t \quad (3.4.5)$$

The last two terms in (3.4.5) involving  $m_I(t)$  and  $\hat{m}'_I(t)$ , constitute the VSB AM signal for the chrominance  $m_I(t)$ . The composite signal  $m(t)$  is transmitted by VSB plus carrier in a 6 MHz bandwidth, as shown in Figure 3.52.

The spectrum of the luminance signal  $m_L(t)$  has periodic gaps between harmonics of the horizontal sweep frequency  $f_h$ , which in color TV is  $4.5 \text{ MHz}/286$ . The subcarrier frequency  $f_{sc} = 3.579545$  for transmission of the chrominance signals was chosen because it corresponds to one of these gaps in the spectrum of  $m_L(t)$ . Specifically, it falls between the 227 and 228 harmonics of  $f_h$ . Thus, the chrominance signals are interlaced in the frequency domain with the luminance signal as illustrated in Figure 3.53. As a consequence, the effect of the chrominance signal on the luminance signal  $m_L(t)$  is not perceived by the human eye, due to the persistence of human vision. Therefore, the chrominance signals do not interfere with the demodulation of the luminance signal in both a monochrome TV receiver and a color TV receiver.

Horizontal and vertical synchronization pulses are added to  $m(t)$  at the transmitter. In addition, eight cycles of the color subcarrier  $A_c \cos 2\pi f_{sc} t$ , called a “color burst,” are superimposed on the trailing edge of the blanking pulses, as shown in Figure 3.54, for the purpose of providing a signal for subcarrier phase synchronization at the receiver.

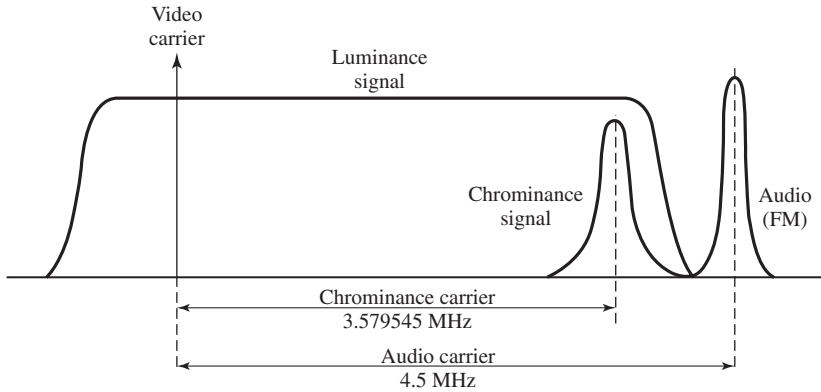


**Figure 3.52** Spectral characteristics of color TV signal.

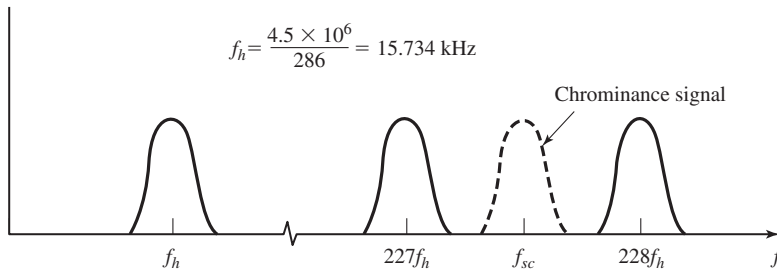


**Figure 3.53** Interlacing of chrominance signals with luminance signals.

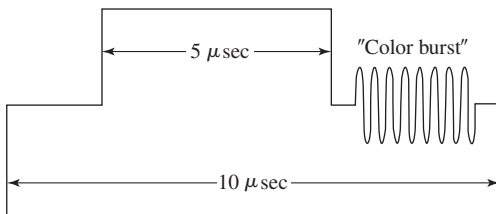


**Figure 3.54** Blanking pulse with color subcarrier.

The front end of the color TV receiver is basically the same as that of a monochrome receiver, down to the envelope detector which converts the 6 MHz VSB signal to baseband. The remaining demultiplexing operations in the color TV receiver are shown in Figure 3.55. We note that a lowpass filter with bandwidth 4.2 MHz is used to recover the luminance signal  $m_L(t)$ . The chrominance signals are stripped off by bandpass filtering and demodulated by the quadrature-carrier demodulator using the output of a VCO that is phase locked to the received color-carrier frequency burst transmitted in each horizontal sweep. The demodulated chrominance signals are lowpass filtered and, along with the luminance signal, are passed to the "inverse matrix" converter that

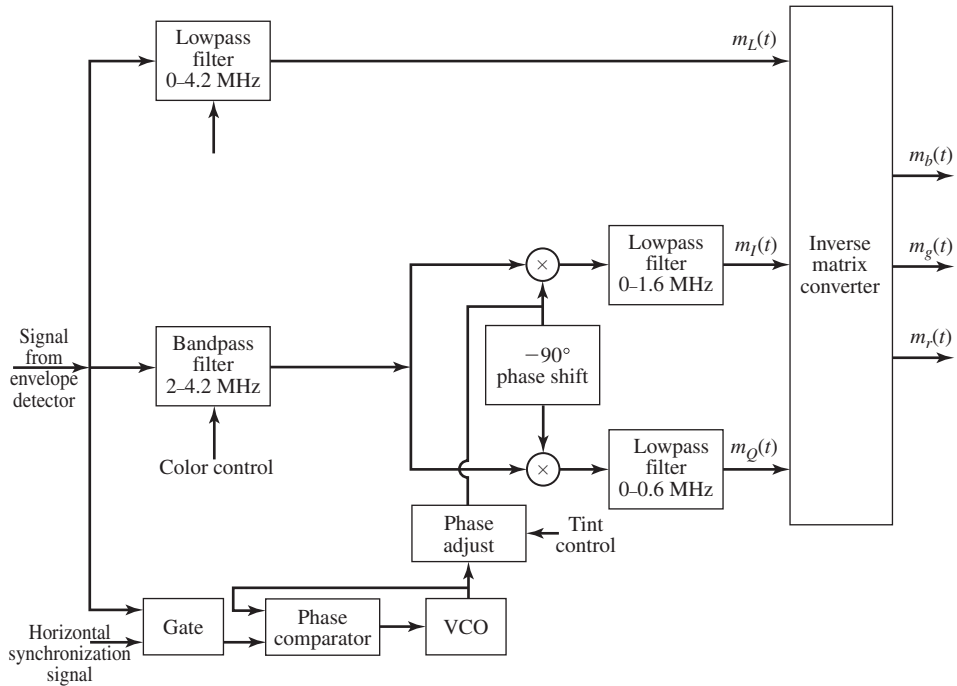


**Figure 3.55** Demultiplexing and demodulation of luminance and chrominance signals in a color TV receiver.

reconstructs the three color signals  $m_b(t)$ ,  $m_g(t)$  and  $m_r(t)$ ; i.e.,

$$\begin{bmatrix} m_b(t) \\ m_g(t) \\ m_r(t) \end{bmatrix} = \begin{bmatrix} 1.00 & -1.10 & 1.70 \\ 1.00 & -0.28 & -0.64 \\ 1.00 & -0.96 & 0.62 \end{bmatrix} \begin{bmatrix} m_L(t) \\ m_I(t) \\ m_Q(t) \end{bmatrix} \quad (3.4.6)$$

The resulting color signals control the three electron guns that strike corresponding blue, green, and red picture elements in a color picture tube. Although color picture tubes are constructed in many different ways, the color mask tube is commonly used in practice. The face of the picture tube contains a matrix of dots of phosphor of the three primary colors with three such dots in each group. Behind each dot color group there is a mask with holes, one hole for each group. The three electron guns are aligned so that each gun can excite one of the three types of color dots. Thus, the three types of color dots are excited simultaneously in different intensities to generate color images.

### 3.5 MOBILE RADIO SYSTEMS

The demand to provide telephone service for people traveling in automobiles, buses, trains, and airplanes has been steadily increasing over the past three to four decades. To meet this demand, radio transmission systems have been developed that link the mobile

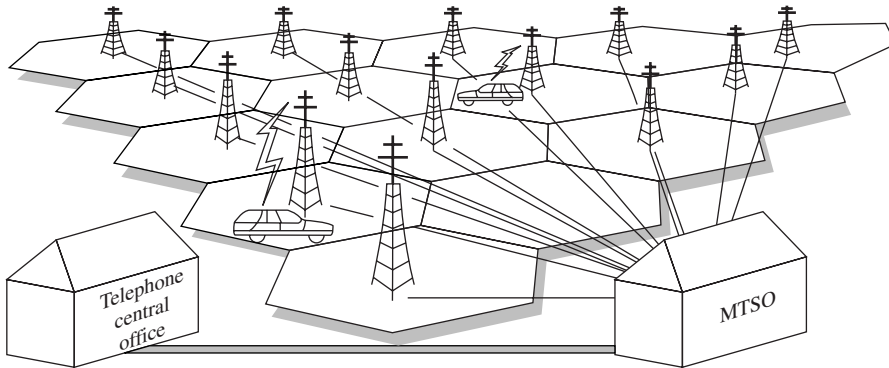


**Figure 3.56** Mobile radio system.

telephone user to the terrestrial telephone network. Today, radio-based systems make it possible for people to communicate via telephone while traveling in airplanes and motor vehicles. In this section, we will briefly describe the analog cellular telephone system that provides telephone service to people with hand-held portable telephones and automobile telephones. Digital cellular systems are studied in Chapter 10.

A major problem with the establishment of any radio communication system is the availability of a portion of the radio spectrum. In the case of radio telephone service, the Federal Communications Commission (FCC) in the United States has assigned parts of the UHF frequency band in the range 806–890 MHz for this use. Similar frequency assignments in the UHF band have been made in Europe and Japan.

The cellular radio concept was adopted as a method for efficient utilization of the available frequency spectrum, especially in highly populated metropolitan areas where the demand for mobile telephone services is the greatest. A geographic area is subdivided into cells, each of which contains a *base station*, as illustrated in Figure 3.56. Each base station is connected via telephone lines to a *mobile telephone switching office* (MTSO), which in turn is connected via telephone lines to a telephone central office (CO) of the terrestrial telephone network.

A mobile user communicates via radio with the base station within the cell. The base station routes the call through the MTSO to another base station if the called party is located in another cell or to the central office of the terrestrial telephone network if the called party is not a mobile. Each mobile telephone is identified by its telephone number and the telephone serial number assigned by the manufacturer. These numbers are automatically transmitted to the MTSO during the initialization of the call for purposes of authentication and billing.

A mobile user initiates a telephone call in the usual manner by keying in the desired telephone number and pressing the “send” button. The MTSO checks the authentication of the mobile user and assigns an available frequency channel for radio transmission of the voice signal from the mobile to the base station. The frequency assignment is sent to the mobile telephone via a supervisory control channel. A second



frequency is assigned for radio transmission from the base station to the mobile user. The simultaneous transmission between the two parties is called *full-duplex operation*. The MTSO interfaces with the central office of the telephone network to complete the connection to the called party. All telephone communications between the MTSO and the telephone network are by means of wideband trunk lines that carry speech signals from many users. Upon completion of the telephone call, when the two parties hang up, the radio channel becomes available for another user.

During the phone call, the MTSO monitors the signal strength of the radio transmission from the mobile user to the base station and, if the signal strength drops below a preset threshold, the MTSO views this as an indication that the mobile user is moving out of the initial cell into a neighboring cell. By communicating with the base stations of neighboring cells, the MTSO finds a neighboring cell that receives a stronger signal and automatically switches, or hands-off, the mobile user to the base station of the adjacent cell. The switching is performed in a fraction of a second and is generally transparent to the two parties. When a mobile user is outside of the assigned service area, the mobile telephone may be placed in a “roam” mode, which allows the mobile user to initiate and receive telephone calls.

In analog transmission of voice-band audio signals via radio, between the base station and the mobile user, the 3-kHz wide audio signal is transmitted via FM using a channel bandwidth of 30 kHz. This represents a bandwidth expansion of approximately a factor of 10. Such a large bandwidth expansion is necessary to obtain a sufficiently large signal-to-noise ratio (SNR) at the output of the FM demodulator. However, the use of FM is highly wasteful of the radio frequency spectrum. The new generation of cellular telephone systems discussed in Chapter 10 use digital transmission of digitized compressed speech (at bit rates of about 10,000 bps) based on LPC encoding and vector quantization of the speech-model parameters as described in Chapter 6. With digital transmission, the cellular telephone system can accommodate a four-fold to tenth-fold increase in the number of simultaneous users with the same available channel bandwidth.

The cellular radio telephone system is designed such that the transmitter powers of the base station and the mobile users are sufficiently small, so that signals do not propagate beyond immediately adjacent cells. This allows for frequencies to be reused in other cells outside of the immediately adjacent cells. Consequently, by making the cells smaller and reducing the radiated power, it is possible to increase frequency reuse and, thus, to increase the bandwidth efficiency and the number of mobile users. Current cellular systems employ cells with a radius in the range of 5–18 km. The base station normally transmits at a power level of 35 W or less and the mobile users transmit at a power level of 3 W or less, approximately. Digital transmission systems are capable of communicating reliably at lower power levels (see Chapter 10).

The cellular radio concept is being extended to different types of personal communication services using low-power, hand-held radio transmitter and receiver. These emerging communication services are made possible by rapid advances in the fabrication of small and powerful integrated circuits that consume very little power and are relatively inexpensive. As a consequence, we will continue to experience exciting new developments in the telecommunications industry, well into the twenty-first century.

### 3.6 FURTHER READING

Analog communication systems are treated in numerous books on basic communication theory, including Sakrison (1968), Shanmugam (1979), Carlson (1986), Stremler (1990), Ziemer and Tranter (1990), Couch (1993), Gibson (1993), and Haykin (2000). Implementation of analog communications systems are dealt with in depth in Clarke and Hess (1971).

### PROBLEMS

- 3.1** The message signal  $m(t) = 2 \cos 400t + 4 \sin(500t + \frac{\pi}{3})$  modulates the carrier signal  $c(t) = A \cos(8000\pi t)$ , using DSB amplitude modulation. Find the time domain and frequency domain representation of the modulated signal and plot the spectrum (Fourier transform) of the modulated signal. What is the power content of the modulated signal?
- 3.2** In a DSB system the carrier is  $c(t) = A \cos 2\pi f_c t$  and the message signal is given by  $m(t) = \text{sinc}(t) + \text{sinc}^2(t)$ . Find the frequency domain representation and the bandwidth of the modulated signal.
- 3.3** The two signals (a) and (b) shown in Figure P-3.3 DSB modulate a carrier signal  $c(t) = A \cos 2\pi f_0 t$ . Precisely plot the resulting modulated signals as a function of time and discuss their differences and similarities.

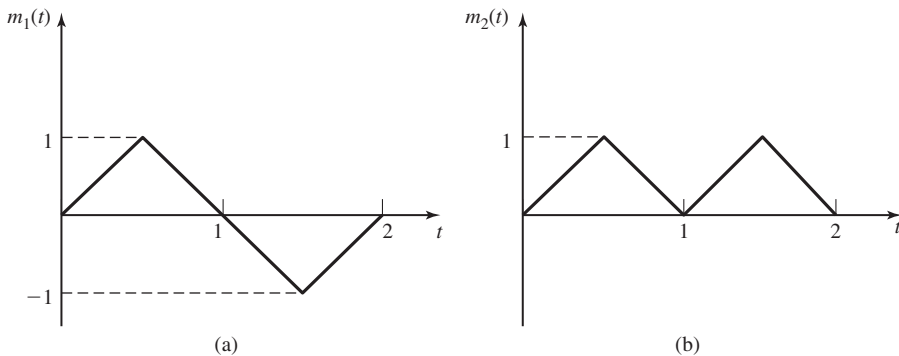


Figure P-3.3

- 3.4** Suppose the signal  $x(t) = m(t) + \cos 2\pi f_c t$  is applied to a nonlinear system whose output is  $y(t) = x(t) + \frac{1}{2}x^2(t)$ . Determine and sketch the spectrum of  $y(t)$  when  $M(f)$  is as shown in Figure P-3.4 and  $W \ll f_c$ .
- 3.5** The modulating signal

$$m(t) = 2 \cos 4000\pi t + 5 \cos 6000\pi t$$

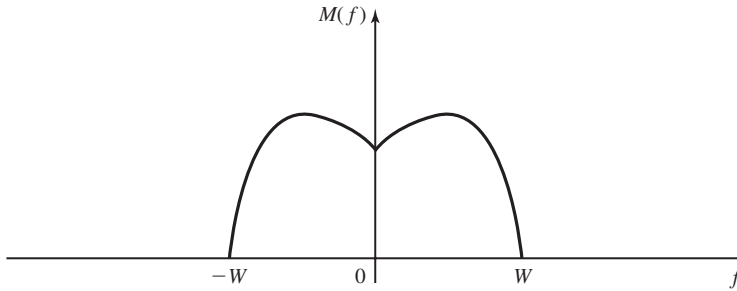


Figure P-3.4

is multiplied by the carrier

$$c(t) = 100 \cos 2\pi f_c t$$

where  $f_c = 50$  kHz. Determine and sketch the power-spectral density of the DSB signal.

- 3.6** A DSB-modulated signal  $u(t) = Am(t) \cos 2\pi f_c t$  is mixed (multiplied) with a local carrier  $x_L(t) = \cos(2\pi f_c t + \theta)$  and the output is passed through a LPF with a bandwidth equal to the bandwidth of the message  $m(t)$ . Denoting the power of the signal at the output of the lowpass filter by  $P_{\text{out}}$  and the power of the modulated signal by  $P_U$ , plot  $\frac{P_{\text{out}}}{P_U}$  as a function of  $\theta$  for  $0 \leq \theta \leq \pi$ .
- 3.7** An AM signal has the form

$$u(t) = [20 + 2 \cos 3000\pi t + 10 \cos 6000\pi t] \cos 2\pi f_c t$$

where  $f_c = 10^5$  Hz.

1. Sketch the (voltage) spectrum of  $u(t)$ .
  2. Determine the power in each of the frequency components.
  3. Determine the modulation index.
  4. Determine the power in the sidebands, the total power, and the ratio of the sidebands power to the total power.
- 3.8** A message signal  $m(t) = \cos 2000\pi t + 2 \cos 4000\pi t$  modulates the carrier  $c(t) = 100 \cos 2\pi f_c t$  where  $f_c = 1$  MHz to produce the DSB signal  $m(t)c(t)$ .
1. Determine the expression for the upper sideband (USB) signal.
  2. Determine and sketch the spectrum of the USB signal.
- 3.9** A DSB-SC signal is generated by multiplying the message signal  $m(t)$  with the periodic rectangular waveform shown in Figure P-3.9 and filtering the product with a bandpass filter tuned to the reciprocal of the period  $T_p$ , with bandwidth  $2W$ , where  $W$  is the bandwidth of the message signal. Demonstrate that the output

$u(t)$  of the BPF is the desired DSB-SC AM signal

$$u(t) = m(t) \sin 2\pi f_c t$$

where  $f_c = 1/T_p$ .

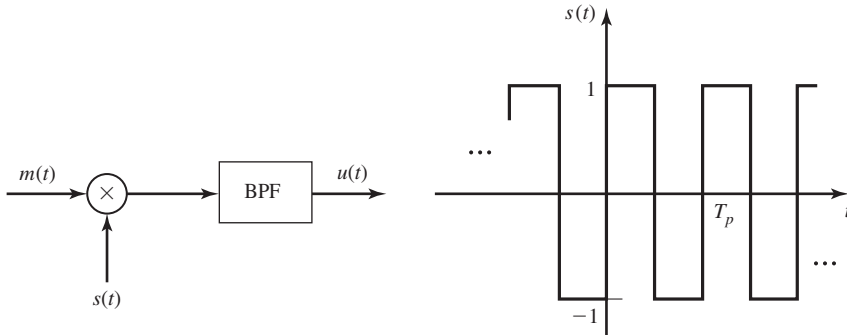


Figure P-3.9

- 3.10** Show that in generating a DSB-SC signal as in Problem P-3.9, it is not necessary that the periodic signal be rectangular. This means that any periodic signal with period  $T_p$  can substitute for the rectangular signal in Figure P-3.9.
- 3.11** The message signal  $m(t)$  has a Fourier transform shown in Figure P-3.11(a). This signal is applied to the system shown in Figure P-3.11(b) to generate the signal  $y(t)$ .
1. Plot  $Y(f)$ , the Fourier transform of  $y(t)$ .
  2. Show that if  $y(t)$  is transmitted, the receiver can pass it through a replica of the system shown in Figure P-3.11(b) to obtain  $m(t)$  back. This means that this system can be used as a simple scrambler to enhance communication privacy.
- 3.12** Show that in a DSB-modulated signal, the envelope of the resulting bandpass signal is proportional to the *absolute value* of the message signal. This means that an envelope detector can be employed as a DSB demodulator if we know that the message signal is always positive.
- 3.13** An AM signal is generated by modulating the carrier  $f_c = 800$  kHz by the signal

$$m(t) = \sin 2000\pi t + 5 \cos 4000\pi t$$

The AM signal

$$u(t) = 100[1 + m(t)] \cos 2\pi f_c t$$

is fed to a  $50 \Omega$  load.

1. Determine and sketch the spectrum of the AM signal.
2. Determine the average power in the carrier and in the sidebands.

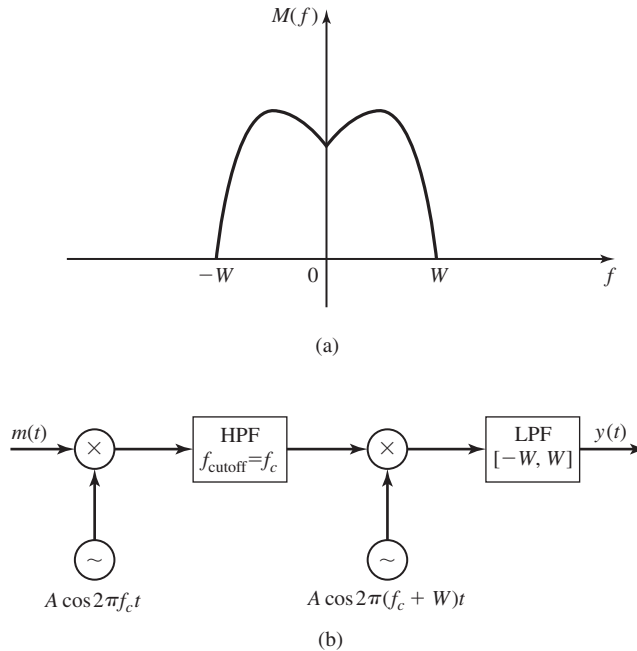


Figure P-3.11

3. What is the modulation index?
4. What is the peak power delivered to the load?

**3.14** The output signal from an AM modulator is

$$u(t) = 5 \cos 1800\pi t + 20 \cos 2000\pi t + 5 \cos 2200\pi t$$

1. Determine the modulating signal  $m(t)$  and the carrier  $c(t)$ .
2. Determine the modulation index.
3. Determine the ratio of the power in the sidebands to the power in the carrier.

**3.15** A DSB-SC AM signal is modulated by the signal

$$m(t) = 2 \cos 2000\pi t + \cos 6000\pi t$$

The modulated signal is

$$u(t) = 100m(t) \cos 2\pi f_c t$$

where  $f_c = 1$  MHz.

1. Determine and sketch the spectrum of the AM signal.
2. Determine the average power in the frequency components.

**3.16** A SSB AM signal is generated by modulating an 800-kHz carrier by the signal  $m(t) = \cos 2000\pi t + 2 \sin 2000\pi t$ . The amplitude of the carrier is  $A_c = 100$ .

1. Determine the signal  $\hat{m}(t)$ .
2. Determine the (time domain) expression for the lower sideband of the SSB AM signal.
3. Determine the magnitude spectrum of the lower sideband SSB signal.

**3.17** Weaver's SSB modulator is illustrated in Figure P-3.17. By taking the input signal as  $m(t) = \cos 2\pi f_m t$ , where  $f_m < W$ , demonstrate that by proper choice of  $f_1$  and  $f_2$  the output is a SSB signal.

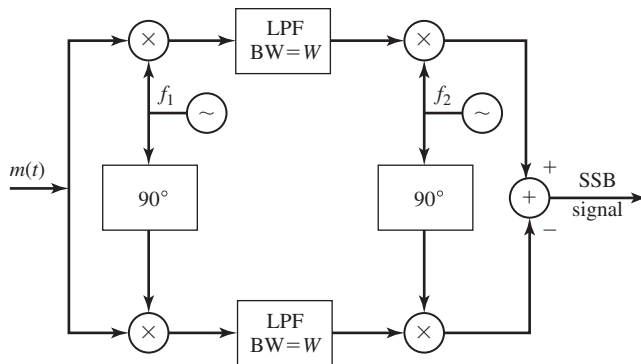


Figure P-3.17

**3.18** The message signal  $m(t)$  whose spectrum is shown in Figure P-3.18 is passed through the system shown in the same figure.

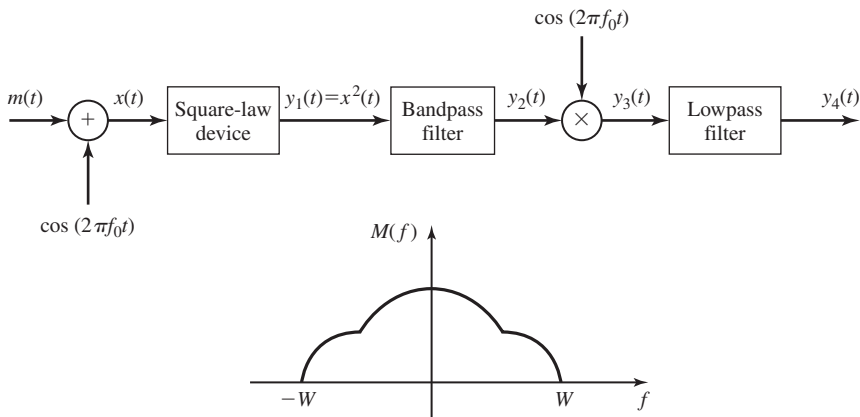


Figure P-3.18

The bandpass filter has a bandwidth of  $2W$  centered at  $f_0$  and the lowpass filter has a bandwidth of  $W$ . Plot the spectra of the signals  $x(t)$ ,  $y_1(t)$ ,  $y_2(t)$ ,  $y_3(t)$ , and  $y_4(t)$ . What are the bandwidths of these signals?

- 3.19** The system shown in Figure P-3.19 is used to generate an AM signal. The modulating signal  $m(t)$  has zero mean and its maximum (absolute) value is  $A_m = \max |m(t)|$ . The nonlinear device has a input–output characteristic

$$y(t) = ax(t) + bx^2(t)$$

- Express  $y(t)$  in terms of the modulating signal  $m(t)$  and the carrier  $c(t) = \cos 2\pi f_c t$ .
- What is the modulation index?
- Specify the filter characteristics that yield an AM signal at its output.

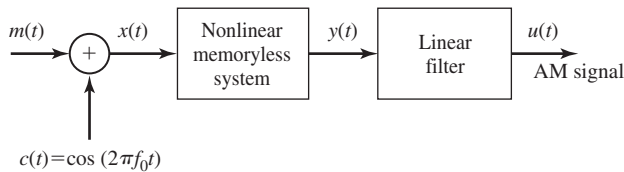


**Figure P-3.19**

- 3.20** The signal  $m(t)$  whose Fourier transform  $M(f)$  is shown in Figure P-3.20 is to be transmitted from point  $A$  to point  $B$ . It is known that the signal is normalized, meaning that  $-1 \leq m(t) \leq 1$ .

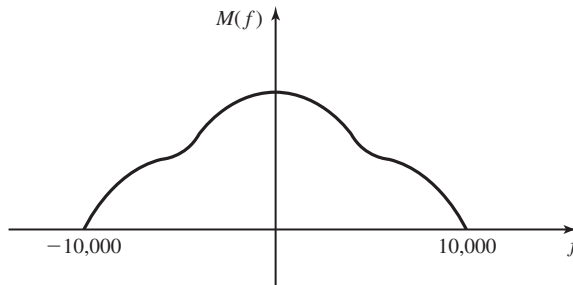


**Figure P-3.20**

- If USSB is employed, what is the bandwidth of the modulated signal?
- If DSB is employed, what is the bandwidth of the modulated signal?
- If an AM modulation scheme with  $a = 0.8$  is used, what is the bandwidth of the modulated signal?

4. If an FM signal with  $k_f = 60$  kHz is used, what is the bandwidth of the modulated signal?
- 3.21 A vestigial sideband modulation system is shown in Figure P-3.21. The bandwidth of the message signal  $m(t)$  is  $W$  and the transfer function of the bandpass filter is shown in the figure.
1. Determine  $h_l(t)$  the lowpass equivalent of  $h(t)$ , where  $h(t)$  represents the impulse response of the bandpass filter.
  2. Derive an expression for the modulated signal  $u(t)$ .

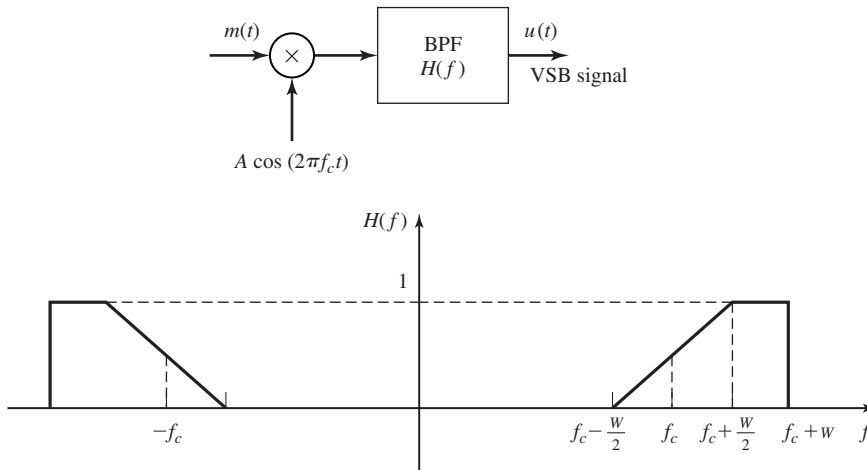
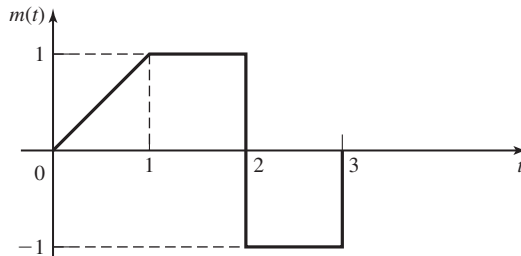


Figure P-3.21

- 3.22 Find expressions for the in-phase and quadrature components,  $x_c(t)$  and  $x_s(t)$ , and envelope and phase,  $V(t)$  and  $\Theta(t)$ , for DSB, SSB, Conventional AM, USSB, LSSB, FM, and PM.
- 3.23 The normalized signal  $m_n(t)$  has a bandwidth of 10,000 Hz and its power content is 0.5 W. The carrier  $A \cos 2\pi f_0 t$  has a power content of 200 W.
1. If  $m_n(t)$  modulates the carrier using SSB amplitude modulation, what will be the bandwidth and the power content of the modulated signal?
  2. If the modulation scheme is DSB-SC, what will be the answer to part 1?
  3. If the modulation scheme is AM with modulation index of 0.6, what will be the answer to part 1?
  4. If modulation is FM with  $k_f = 50,000$ , what will be the answer to part 1?
- 3.24 The message signal  $m(t) = 10 \text{ sinc}(400t)$  frequency modulates the carrier  $c(t) = 100 \cos 2\pi f_c t$ . The modulation index is 6.



1. Write an expression for the modulated signal  $u(t)$ ?
  2. What is the maximum frequency deviation of the modulated signal?
  3. What is the power content of the modulated signal?
  4. Find the bandwidth of the modulated signal.
- 3.25** Signal  $m(t)$  is shown in Figure P-3.25. This signal is used once to frequency modulate a carrier and once to phase modulate the same carrier.



**Figure P-3.25**

1. Find a relation between  $k_p$  and  $k_f$  such that the maximum phase of the modulated signals in both cases are equal.
  2. If  $k_p = k_f = 1$ , what is the maximum instantaneous frequency in each case?
- 3.26** An angle modulated signal has the form

$$u(t) = 100 \cos[2\pi f_c t + 4 \sin 2000\pi t]$$

where  $f_c = 10$  MHz.

1. Determine the average transmitted power.
  2. Determine the peak-phase deviation.
  3. Determine the peak-frequency deviation.
  4. Is this an FM or a PM signal? Explain.
- 3.27** Find the smallest value of the modulation index in an FM system that guarantees that all the modulated signal power is contained in the sidebands and no power is transmitted at the carrier frequency.
- 3.28** Wideband FM can be generated by first generating a narrowband FM signal and then using frequency multiplication to spread the signal bandwidth. Figure P-3.28 illustrates such a scheme, which is called an Armstrong-type FM modulator. The narrowband FM signal has a maximum angular deviation of 0.10 radians in order to keep distortion under control.
1. If the message signal has a bandwidth of 15 kHz and the output frequency from the oscillator is 100 kHz, determine the frequency multiplication that is

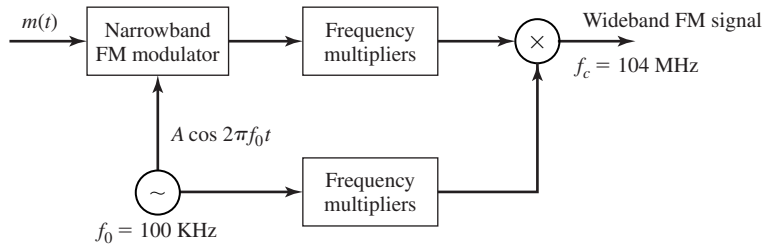


**Figure P-3.28** Armstrong-type FM Modulator.

necessary to generate an FM signal at a carrier frequency of  $f_c = 104$  MHz and a frequency deviation of  $f = 75$  kHz.

2. If the carrier frequency for the wideband FM signal is to be within  $\pm 2$  Hz, determine the maximum allowable drift of the 100 kHz oscillator.

- 3.29** Determine the amplitude and phase of various frequency components of a PM signal with  $k_p = 1$  and  $m(t)$ , a periodic signal given by

$$m(t) = \begin{cases} 1, & 0 \leq t \leq \frac{T_m}{2} \\ -1, & \frac{T_m}{2} \leq t \leq T_m \end{cases} \quad (3.5.1)$$

in one period.

- 3.30** An FM signal is given as

$$u(t) = 100 \cos \left[ 2\pi f_c t + 100 \int_{-\infty}^t m(\tau) d\tau \right]$$

where  $m(t)$  is shown in Figure P-3.30.

1. Sketch the instantaneous frequency as a function of time.
2. Determine the peak-frequency deviation.

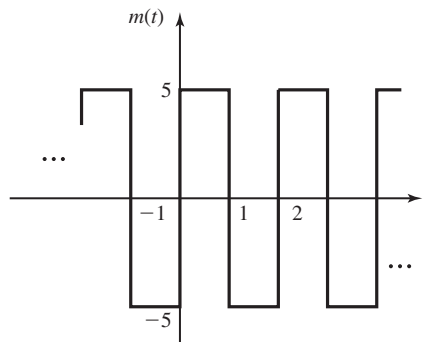


**Figure P-3.30**

**3.31** The carrier  $c(t) = 100 \cos 2\pi f_c t$  is frequency modulated by the signal  $m(t) = 5 \cos 20000\pi t$ , where  $f_c = 10^8$  Hz. The peak frequency deviation is 20 kHz.

1. Determine the amplitude and frequency of all signal components that have a power level of at least 10% of the power of the unmodulated carrier component.
2. From Carson's rule, determine the approximate bandwidth of the FM signal.

**3.32** The carrier  $c(t) = A \cos 2\pi 10^6 t$  is angle modulated (PM or FM) by the sinusoid signal  $m(t) = 2 \cos 2000\pi t$ . The deviation constants are  $k_p = 1.5$  rad/V and  $k_f = 3000$  Hz/V.

1. Determine  $\beta_f$  and  $\beta_p$ .
2. Determine the bandwidth in each case using Carson's rule.
3. Plot the spectrum of the modulated signal in each case (plot only those frequency components that lie within the bandwidth derived in part 2.)
4. If the amplitude of  $m(t)$  is decreased by a factor of two, how would your answers to parts 1–3 change?
5. If the frequency of  $m(t)$  is increased by a factor of two, how would your answers to parts 1–3 change?

**3.33** The carrier  $c(t) = 100 \cos 2\pi f_c t$  is phase modulated by the signal  $m(t) = 5 \cos 2000\pi t$ . The PM signal has a peak-phase deviation of  $\pi/2$ . The carrier frequency is  $f_c = 10^8$  Hz.

1. Determine the magnitude spectrum of the sinusoidal components and sketch the results.
2. Using Carson's rule, determine the approximate bandwidth of the PM signal and compare the results with the analytical result in part 1.

**3.34** An angle-modulated signal has the form

$$u(t) = 100 \cos[2\pi f_c t + 4 \sin 2\pi f_m t]$$

where  $f_c = 10$  MHz and  $f_m = 1000$  Hz.

1. Assuming that this is an FM signal, determine the modulation index and the transmitted signal bandwidth.
2. Repeat part 1 if  $f_m$  is doubled.
3. Assuming that this is a PM signal determine the modulation index and the transmitted signal bandwidth.
4. Repeat part 3 if  $f_m$  is doubled.

**3.35** It is easy to demonstrate that amplitude modulation satisfies the superposition principle, whereas angle modulation does not. To be specific, let  $m_1(t)$  and  $m_2(t)$  be two message signals, and let  $u_1(t)$  and  $u_2(t)$  be the corresponding modulated versions.

1. Show that when the combined message signal  $m_1(t) + m_2(t)$  DSB modulates a carrier  $A_c \cos 2\pi f_c t$ , the result is the sum of the two DSB amplitude-modulated signals  $u_1(t) + u_2(t)$ .
  2. Show that if  $m_1(t) + m_2(t)$  frequency modulates a carrier, the modulated signal is not equal to  $u_1(t) + u_2(t)$ .
- 3.36** An FM discriminator is shown in Figure P-3.36. The envelope detector is assumed to be ideal and has an infinite input impedance. Select the values for  $L$  and  $C$  if the discriminator is to be used to demodulate an FM signal with a carrier  $f_c = 80$  MHz and a peak-frequency deviation of 6 MHz.

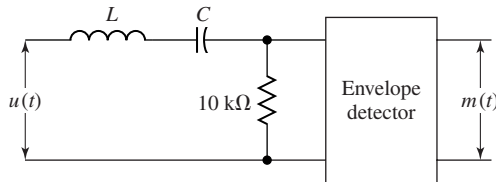


Figure P-3.36

- 3.37** An angle-modulated signal is given as

$$u(t) = 100 \cos [2000\pi t + \phi(t)]$$

where (a)  $\phi(t) = 5 \sin 20\pi t$  and (b)  $\phi(t) = 5 \cos 20\pi t$ . Determine and sketch the amplitude and phase spectra for (a) and (b), and compare the results.

- 3.38** The message signal  $m(t)$  into an FM modulator with peak-frequency deviation  $f_d = 25$  Hz/V is shown in Figure P-3.38. Plot the frequency deviation in Hz and the phase deviation in radians.

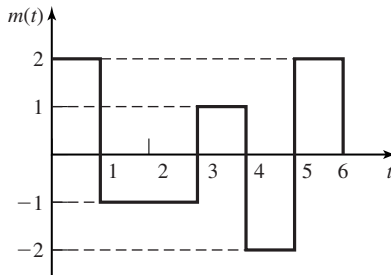


Figure P-3.38

- 3.39** A message signal  $m(t)$  has a bandwidth of 10 kHz and a peak magnitude  $|m(t)|$  of 1 V. Estimate the bandwidth of the signal  $u(t)$  obtained when  $m(t)$  frequency modulates a carrier with a peak frequency deviation of (a)  $f_d = 10$  Hz/V, (b) 100 Hz/V, and (c) 1000 Hz/V.

**3.40** The modulating signal into an FM modulator is

$$m(t) = 10 \cos 16\pi t$$

The output of the FM modulator is

$$u(t) = 10 \cos \left[ 400\pi t + 2\pi k_f \int_{-\infty}^t m(\tau) d\tau \right]$$

where  $k_f = 10$ . If the output of the FM modulator is passed through an ideal BPF centered at  $f_c = 2000$  with a bandwidth of 62 Hz, determine the power of the frequency components at the output of the filter (see Figure P-3.40). What percentage of the transmitter power appears at the output of the BPF?

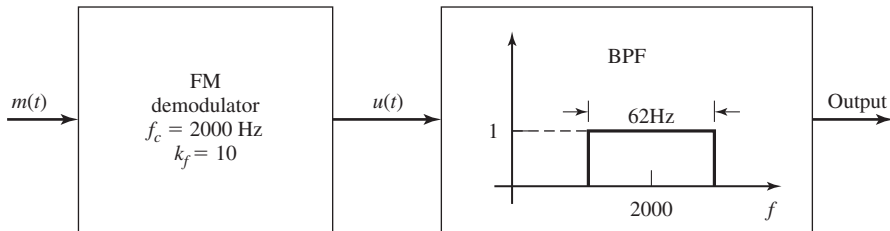


**Figure P-3.40**

**3.41** The message signal  $m_1(t)$  is shown in Figure P-3.41.

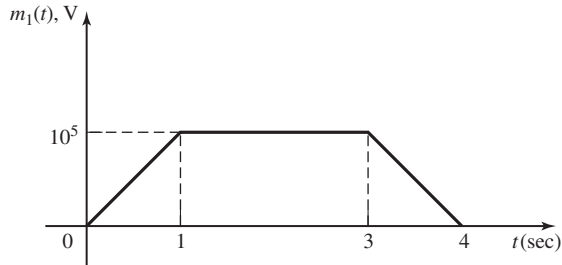


**Figure P-3.41**

and the message signal  $m_2(t) = \text{sinc}(2 \times 10^4 t)$ , in volts again.

1. If  $m_1(t)$  is frequency modulated on a carrier with frequency  $10^6$  Hz with a frequency deviation constant ( $k_f$ ) equal to 5 Hz/V, what is the maximum instantaneous frequency of the modulated signal?
2. If  $m_1(t)$  is phase modulated with phase-deviation constant  $k_p = 3$  radians/V, what is the maximum instantaneous frequency of the modulated signal? What is the minimum instantaneous frequency of the modulated signal?

3. If  $m_2(t)$  is frequency modulated with  $k_f = 10^3$  Hz/V, what is the maximum instantaneous frequency of the modulated signal? What is the bandwidth of the modulated signal?
- 3.42** We wish to transmit 60 voice-band signals by SSB (upper sideband) modulation and frequency-division multiplexing (FDM). Each of the 60 signals has a spectrum as shown in Figure P-3.42. Note that the voice-band signal is band limited to 3 kHz. If each signal is frequency translated separately, we require a frequency synthesizer that produces 60 carrier frequencies to perform the frequency-division multiplexing. On the other hand, if we subdivide the channels into  $L$  groups of  $K$  subchannels each, such that  $LK = 60$ , we may reduce the number of frequencies from the synthesizer to  $L + K$ .
1. Illustrate the spectrum of the SSB signals in a group of  $K$  subchannels. Assume that a 1 kHz guard band separates the signals in adjacent frequency subchannels and that the carrier frequencies are  $f_{c_1} = 10$  kHz,  $f_{c_2} = 14$  kHz,  $\dots$ , etc.
  2. Sketch  $L$  and  $K$  such that  $LK = 60$  and  $L + K$  is a minimum.
  3. Determine the frequencies of the carriers if the 60 FDM signals occupy the frequency band 300 kHz to 540 kHz, and each group of  $K$  signals occupies the band 10 kHz to  $(10 + 4K)$  kHz.

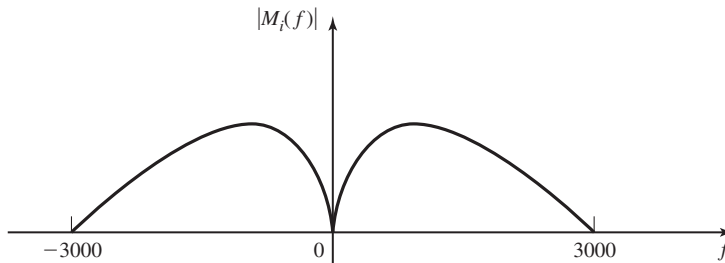


Figure P-3.42

- 3.43** A superheterodyne FM receiver operates in the frequency range of 88–108 MHz. The IF and local oscillator frequencies are chosen such that  $f_{IF} < f_{LO}$ . We require that the image frequency  $f'_c$  fall outside of the 88–108 MHz region. Determine the minimum required  $f_{IF}$  and the range of variations in  $f_{LO}$ ?

# 4

## *Random Processes*

This chapter is devoted to the study of random processes and their properties. Random processes provide good models for both information sources and noise. When a signal is transmitted through a communication channel there are two types of imperfections that cause the received signal to be different from the transmitted signal. One class of imperfections are deterministic in nature, such as linear and nonlinear distortion, intersymbol interference, etc. The second class is nondeterministic (such as addition of noise, multipath fading, etc.). For a quantitative study of these phenomena we model them as random processes.

The information that is to be transmitted is also, by its nature, best modeled as a random process. This is due to the fact that any signal that conveys information must have some uncertainty in it, otherwise its transmission is of no interest. We will explore this aspect later in greater detail in Chapter 6. In this chapter, after a brief review of the basics of probability theory and random variables, we introduce the concept of a random process and the basic tools used in the mathematical analysis of random processes.

### 4.1 PROBABILITY AND RANDOM VARIABLES

In this section we give a brief review of some basics of probability theory that are needed for our treatment of random processes. It is assumed throughout that the reader has already been exposed to probability theory elsewhere and, therefore, our treatment in this section will be brief.

**Probability Space.** The fundamental concept in any probabilistic model is the concept of a *random experiment*, which is any experiment whose outcome, for some

reason, cannot be predicted with certainty. Flipping a coin, throwing a die, and drawing a card from a deck of cards are examples of random experiments. What is common in all these cases is that the result (or outcome) of the experiment is uncertain. A random experiment has certain *outcomes* that are the elementary results of the experiment. In flipping of a coin, “head” and “tail” are the possible outcomes. In throwing a die 1, 2, 3, 4, 5, 6 are the possible outcomes. The set of all possible outcomes is called the *sample space* and denoted by  $\Omega$ . Outcomes are denoted by  $\omega$ 's and certainly each  $\omega$  lies in  $\Omega$ , i.e.,  $\omega \in \Omega$ .

A sample space is *discrete* if the number of its elements are finite or countably infinite, otherwise it is a *nondiscrete* sample space. All the random experiments given above have discrete sample spaces. If one chooses randomly a number between 0 and 1, then the sample space corresponding to this random experiment is nondiscrete.

*Events* are subsets of the sample space for which a probability can be defined (as will be defined in the next paragraph). For discrete sample spaces, any subset of the sample space is an event, that is, a probability can be defined for it. For instance, in throwing a die various events such as “the outcome is even,” “the outcome is greater than 3,” and “the outcome divides 3” can be considered. For a nondiscrete sample space, not every subset of  $\Omega$  can be assigned a probability without sacrificing basic intuitive properties of probability. To overcome this difficulty, we define a  $\sigma$ -field  $\mathcal{B}$  on the sample space  $\Omega$  as a collection of subsets of  $\Omega$  such that the following conditions are satisfied:

1.  $\Omega \in \mathcal{B}$ .
2. If the subset (event)  $E \in \mathcal{B}$  then  $E^c \in \mathcal{B}$  where  $E^c$  denotes the complement of  $E$ .
3. If  $E_i \in \mathcal{B}$  for all  $i$ , then  $\cup_{i=1}^{\infty} E_i \in \mathcal{B}$ .

We define a *probability measure*  $P$  on  $\mathcal{B}$  as a set function assigning nonnegative values to all events  $E$  in  $\mathcal{B}$  such that the following conditions are satisfied:

1.  $0 \leq P(E) \leq 1$  for all  $E \in \mathcal{B}$ .
2.  $P(\Omega) = 1$ .
3. For disjoint events  $E_1, E_2, E_3, \dots$  (i.e., events for which  $E_i \cap E_j = \emptyset$  for all  $i \neq j$ , where  $\emptyset$  is the null set), we have  $P(\cup_{i=1}^{\infty} E_i) = \sum_{i=1}^{\infty} P(E_i)$ .

The triple  $(\Omega, \mathcal{B}, P)$  is called a *probability space*.

Some basic properties of the probability measure follow easily from the set theoretical properties of events together with the basic properties of probability measure. We list some of the most important properties here.

1.  $P(E^c) = 1 - P(E)$ .
2.  $P(\emptyset) = 0$ .
3.  $P(E_1 \cup E_2) = P(E_1) + P(E_2) - P(E_1 \cap E_2)$ .
4. If  $E_1 \subset E_2$  then  $P(E_1) \leq P(E_2)$ .

**Conditional Probability.** Let us assume that the two events  $E_1$  and  $E_2$  are defined on the same probability space with corresponding probabilities  $P(E_1)$  and  $P(E_2)$ . Then, if an observer receives the information that the event  $E_2$  has in fact



occurred, the observer's probability about event  $E_1$  will not be  $P(E_1)$  any more. In fact, the information that the observer received changes the probabilities of various events, and new probabilities, called *conditional probabilities*, are defined. The conditional probability of the event  $E_1$  given the event  $E_2$  is defined by

$$P(E_1|E_2) = \begin{cases} \frac{P(E_1 \cap E_2)}{P(E_2)}, & P(E_2) \neq 0 \\ 0, & \text{otherwise} \end{cases}$$

If it happens that  $P(E_1|E_2) = P(E_1)$  then knowledge of  $E_2$  does not change the probability of occurrence of  $E_1$ . In this case, the events  $E_1$  and  $E_2$  are said to be *statistically independent*. For statistically independent events,  $P(E_1 \cap E_2) = P(E_1)P(E_2)$ .

**Example 4.1.1**

In throwing a fair die, the probability of

$$A = \{\text{The outcome is greater than 3}\}$$

is

$$P(A) = P(4) + P(5) + P(6) = \frac{1}{2} \quad (4.1.1)$$

The probability of

$$B = \{\text{The outcome is even}\} \quad (4.1.2)$$

is

$$P(B) = P(2) + P(4) + P(6) = \frac{1}{2} \quad (4.1.3)$$

In this case,

$$P(A|B) = \frac{P(A \cap B)}{P(B)} = \frac{P(4) + P(6)}{\frac{1}{2}} = \frac{2}{3}$$

If the events  $\{E_i\}_{i=1}^n$  make a partition of the sample space  $\Omega$ ; i.e., if the following two conditions are satisfied

$$\cup_{i=1}^n E_i = \Omega$$

$$E_i \cap E_j = \emptyset \quad \text{for all } 1 \leq i, j \leq n \text{ and } i \neq j$$

then, if for an event  $A$  we have the conditional probabilities  $\{P(A|E_i)\}_{i=1}^n$ ,  $P(A)$  can be obtained by applying the *total probability theorem* stated as

$$P(A) = \sum_{i=1}^n P(E_i)P(A|E_i)$$

*Bayes rule* gives the conditional probabilities  $P(E_i|A)$  by the following relation

$$P(E_i|A) = \frac{P(E_i)P(A|E_i)}{\sum_{j=1}^n P(E_j)P(A|E_j)}$$

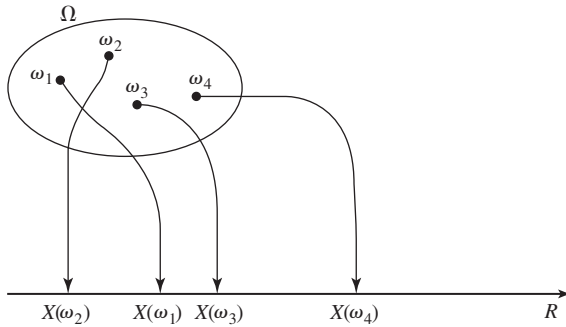


**Figure 4.1** Random variable as a mapping from  $\Omega$  to  $\mathbb{R}$ .

**Random Variables.** A (real) *random variable* is a mapping from the sample space  $\Omega$  to the set of real numbers. A schematic diagram representing a random variable is given in Figure 4.1.

Random variables are denoted by capital letters  $X, Y$ , etc.; individual values of the random variable  $X$  are  $X(\omega)$ . A random variable is *discrete* if the range of its values is either finite or countably infinite. This range is usually denoted by  $\{x_i\}$ .

The *cumulative distribution function (CDF)* of a random variable  $X$  is defined as

$$F_X(x) = P(\omega \in \Omega : X(\omega) \leq x)$$

which can be simply written as

$$F_X(x) = P(X \leq x)$$

and has the following properties:

1.  $0 \leq F_X(x) \leq 1$ .
2.  $F_X(x)$  is nondecreasing.
3.  $\lim_{x \rightarrow -\infty} F_X(x) = 0$  and  $\lim_{x \rightarrow +\infty} F_X(x) = 1$ .
4.  $F_X(x)$  is continuous from the right; i.e.,  $\lim_{\epsilon \downarrow 0} F(x + \epsilon) = F(x)$ .
5.  $P(a < X \leq b) = F_X(b) - F_X(a)$ .
6.  $P(X = a) = F_X(a) - F_X(a^-)$ .

For discrete random variables  $F_X(x)$  is a stair-case function. A random variable is called *continuous* if  $F_X(x)$  is a continuous function. A random variable is called *mixed* if it is neither discrete nor continuous. Examples of CDFs for discrete, continuous, and mixed random variables are shown in Figures 4.2, 4.3, and 4.4, respectively.

The *probability density function (PDF)* of a random variable  $X$  is defined as the derivative of  $F_X(x)$ ; i.e.,

$$f_X(x) = \frac{d}{dx} F_X(x)$$

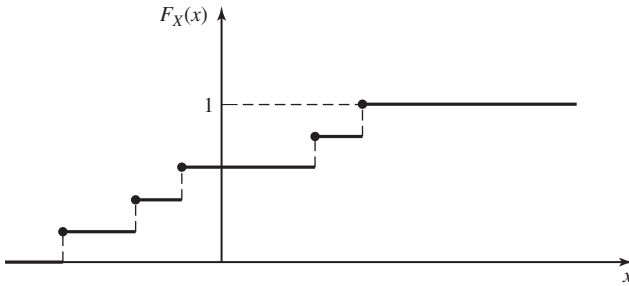


**Figure 4.2** The CDF for a discrete random variable.

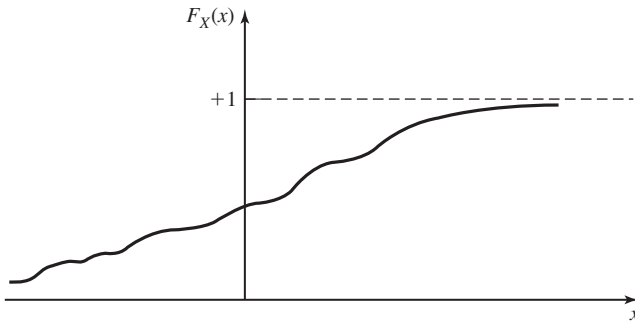


**Figure 4.3** The CDF for a continuous random variable.

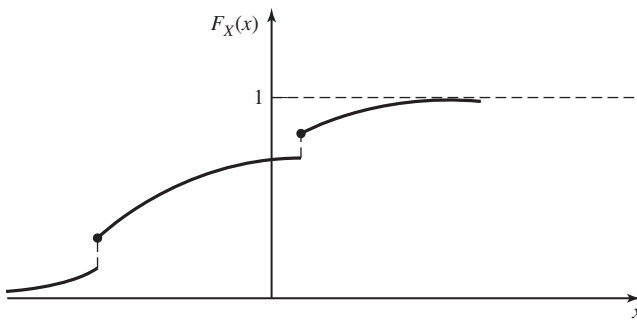


**Figure 4.4** The CDF for a mixed random variable.

In case of discrete or mixed random variables, the PDF involves impulses. The basic properties of PDF are listed here:

1.  $f_X(x) \geq 0$ .
2.  $\int_{-\infty}^{\infty} f_X(x) dx = 1$ .
3.  $\int_{a^+}^{b^+} f_X(x) dx = P(a < X \leq b)$ .
4. In general,  $P(X \in A) = \int_A f_X(x) dx$ .
5.  $F_X(x) = \int_{-\infty}^{x^+} f_X(u) du$ .

For discrete random variables, it is more common to define the *probability mass function (PMF)*, which is defined as  $\{p_i\}$  where  $p_i = P(X = x_i)$ . Obviously for all  $i$  we have  $p_i \geq 0$  and  $\sum_i p_i = 1$ .

**Important Random Variables.** The most commonly used random variables in communications are:

**Bernoulli Random Variable.** This is a discrete random variable taking two values one and zero with probabilities  $p$  and  $1 - p$ . A Bernoulli random variable is a good model for a binary data generator. Also, when binary data is transmitted over a communication channel, some bits are received in error. We can model an error by modulo-2 addition of a 1 to the input bit, thus changing a 0 into a 1 and a 1 into a 0. Therefore, a Bernoulli random variable can be employed to model the channel errors.

**Binomial Random Variable.** This is a discrete random variable giving the number of 1's in a sequence of  $n$  independent Bernoulli trials. The PMF is given by

$$P(X = k) = \begin{cases} \binom{n}{k} p^k (1 - p)^{n-k}, & 0 \leq k \leq n \\ 0, & \text{otherwise} \end{cases}$$

This random variable models, for example, the total number of bits received in error when a sequence of  $n$  bits is transmitted over a channel with bit-error probability of  $p$ .

**Uniform Random Variable.** This is a continuous random variable taking values between  $a$  and  $b$  with equal probabilities over intervals of equal length. The density function is given by

$$f_X(x) = \begin{cases} \frac{1}{b-a}, & a < x < b \\ 0, & \text{otherwise} \end{cases}$$

This is a model for continuous random variables whose range is known, but nothing else is known about the likelihood of various values that the random variable can assume. For example, when the phase of a sinusoid is random it is usually modeled as a uniform random variable between 0 and  $2\pi$ .

**Gaussian or Normal Random Variable.** This is a continuous random variable described by the density function

$$f_X(x) = \frac{1}{\sqrt{2\pi}\sigma} e^{-\frac{(x-m)^2}{2\sigma^2}}$$

The Gaussian random variable is the most important and frequently encountered random variable in communications. The reason is that thermal noise, which is the major source of noise in communication systems, has a Gaussian distribution. The properties of Gaussian noise will be investigated in more detail later in Section 4.4.2. Graphs of the PDFs and PMFs of the above random variables are given in Figures 4.5–4.8.

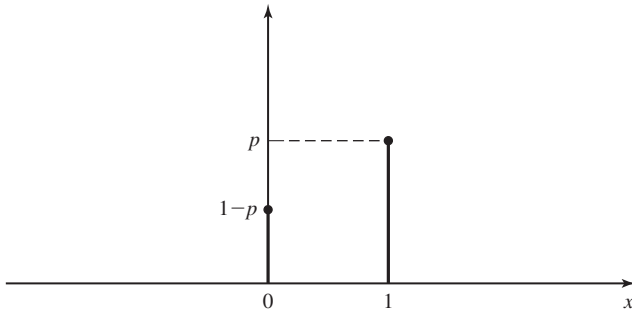


**Figure 4.5** The PMF for the Bernoulli random variable.

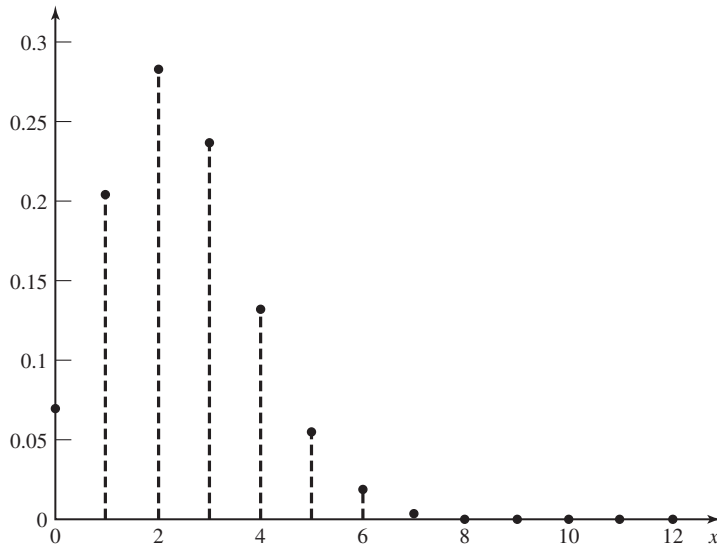


**Figure 4.6** The PMF for the binomial random variable.

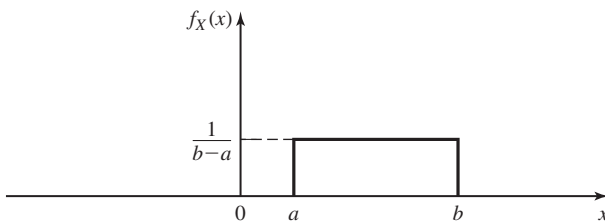


**Figure 4.7** The PDF for the uniform random variable.

The CDF for the Gaussian random variable with  $m = 0$  and  $\sigma = 1$  is denoted by  $\Phi(x)$  and given by

$$\Phi(x) = P(X \leq x) = \int_{-\infty}^x \frac{1}{\sqrt{2\pi}} e^{-\frac{t^2}{2}} dt$$

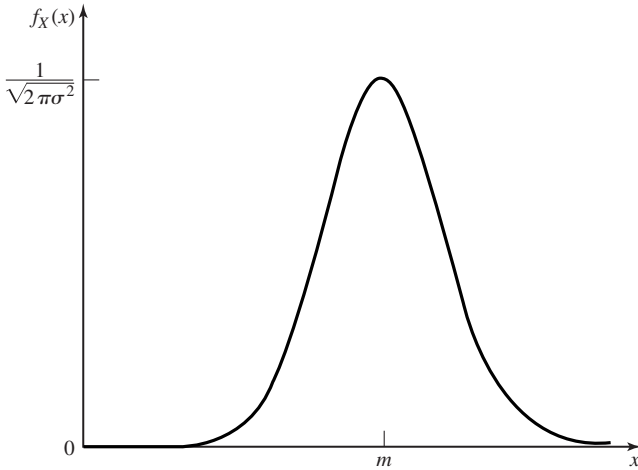


**Figure 4.8** The PDF for the Gaussian random variable.

A closely related function is  $Q(x) = 1 - \Phi(x)$  giving  $P(X > x)$ . This function is well tabulated and frequently used in communications. It is easy to see that  $Q(x)$  satisfies the following relations:

$$Q(-x) = 1 - Q(x) \quad (4.1.4)$$

$$Q(0) = \frac{1}{2} \quad (4.1.5)$$

$$Q(\infty) = 0 \quad (4.1.6)$$

Table 4.1 gives the values of this function for various values of  $x$ .

There exist certain bounds on the  $Q$  function that are widely used to find bounds on error probability of various communication systems. These bounds are investigated in the problems at the end of this chapter. The two mostly used upper bounds are

$$Q(x) \leq \frac{1}{2} e^{-\frac{x^2}{2}} \quad \text{for all } x \geq 0 \quad (4.1.7)$$

and

$$Q(x) < \frac{1}{\sqrt{2\pi}x} e^{-\frac{x^2}{2}} \quad \text{for all } x \geq 0 \quad (4.1.8)$$

The frequently used lower bound is

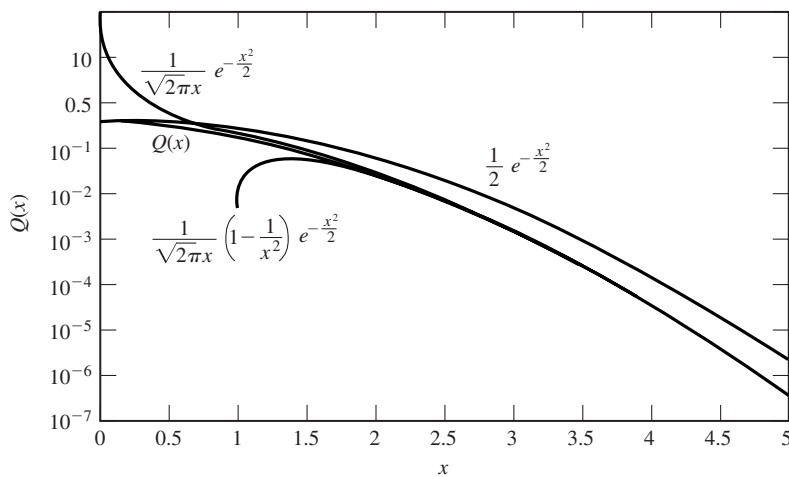
$$Q(x) > \frac{1}{\sqrt{2\pi}x} \left(1 - \frac{1}{x^2}\right) e^{-\frac{x^2}{2}} \quad \text{for all } x \geq 0 \quad (4.1.9)$$

A plot of  $Q(x)$  and these bounds is given in Figure 4.9.

A Gaussian variable can be described in terms of its two parameters  $m$  and  $\sigma$  by  $\mathcal{N}(m, \sigma^2)$ . For this random variable a simple change of variable in the integral that computes  $P(X > x)$  results in  $P(X > x) = Q\left(\frac{x-m}{\sigma}\right)$ . This gives the so-called *tail* probability in a Gaussian random variable.

TABLE 4.1 TABLE OF  $Q(x)$  VALUES

$x$	$Q(x)$	$x$	$Q(x)$	$x$	$Q(x)$
0	5.000000e-01	2.4	8.197534e-03	4.8	7.933274e-07
0.1	4.601722e-01	2.5	6.209665e-03	4.9	4.791830e-07
0.2	4.207403e-01	2.6	4.661189e-03	5.0	2.866516e-07
0.3	3.820886e-01	2.7	3.466973e-03	5.1	1.698268e-07
0.4	3.445783e-01	2.8	2.555131e-03	5.2	9.964437e-08
0.5	3.085375e-01	2.9	1.865812e-03	5.3	5.790128e-08
0.6	2.742531e-01	3.0	1.349898e-03	5.4	3.332043e-08
0.7	2.419637e-01	3.1	9.676035e-04	5.5	1.898956e-08
0.8	2.118554e-01	3.2	6.871378e-04	5.6	1.071760e-08
0.9	1.840601e-01	3.3	4.834242e-04	5.7	5.990378e-09
1.0	1.586553e-01	3.4	3.369291e-04	5.8	3.315742e-09
1.1	1.356661e-01	3.5	2.326291e-04	5.9	1.817507e-09
1.2	1.150697e-01	3.6	1.591086e-04	6.0	9.865876e-10
1.3	9.680049e-02	3.7	1.077997e-04	6.1	5.303426e-10
1.4	8.075666e-02	3.8	7.234806e-05	6.2	2.823161e-10
1.5	6.680720e-02	3.9	4.809633e-05	6.3	1.488226e-10
1.6	5.479929e-02	4.0	3.167124e-05	6.4	7.768843e-11
1.7	4.456546e-02	4.1	2.065752e-05	6.5	4.016001e-11
1.8	3.593032e-02	4.2	1.334576e-05	6.6	2.055790e-11
1.9	2.871656e-02	4.3	8.539898e-06	6.7	1.042099e-11
2.0	2.275013e-02	4.4	5.412542e-06	6.8	5.230951e-12
2.1	1.786442e-02	4.5	3.397673e-06	6.9	2.600125e-12
2.2	1.390345e-02	4.6	2.112456e-06	7.0	1.279813e-12
2.3	1.072411e-02	4.7	1.300809e-06		

Figure 4.9 Bounds on  $Q$ -function.

**Functions of a Random Variable.** A function of a random variable  $Y = g(X)$  is itself a random variable. To find its CDF we can use the definition of the CDF to obtain

$$F_Y(y) = P(\omega \in \Omega : g(X(\omega)) \leq y)$$

In the special case that, for all  $y$ , the equation  $g(x) = y$  has a countable number of solutions  $\{x_i\}$  and, for all these solutions  $g'(x_i)$  exists and is nonzero, we can use the following relation to find the PDF of the random variable  $Y = g(X)$ .

$$f_Y(y) = \sum_i \frac{f_X(x_i)}{|g'(x_i)|} \quad (4.1.10)$$

**Example 4.1.2**

Assuming  $X$  is a Gaussian random variable with  $m = 0$  and  $\sigma = 1$ , find the probability density function of the random variable  $Y$  given by  $Y = aX + b$ .

**Solution** In this case  $g(x) = ax + b$ , therefore  $g'(x) = a$ . The equation  $ax + b = y$  has only one solution given by  $x_1 = \frac{y-b}{a}$ . Using these results, we obtain

$$\begin{aligned} f_Y(y) &= \frac{f_X\left(\frac{y-b}{a}\right)}{|a|} \\ &= \frac{1}{\sqrt{2\pi a^2}} e^{-\frac{(y-b)^2}{2a^2}} \end{aligned} \quad (4.1.11)$$

It is observed that  $Y$  is a Gaussian random variable  $\mathcal{N}(b, a^2)$ .

From the above example, we arrive at the important conclusion that *a linear function of a Gaussian random variable is itself a Gaussian random variable.*

**Statistical Averages.** The *expected value* of the random variable  $X$  is defined as

$$E(X) = \int_{-\infty}^{\infty} x f_X(x) dx$$

and is usually denoted by  $m_X$ . The expected value of a random variable is a measure of the average of the value that the random variable takes in a large number of experiments. In general, the  $n$ th moment of a random variable  $X$  is defined as

$$m_X^{(n)} \stackrel{\text{def}}{=} \int_{-\infty}^{\infty} x^n f_X(x) dx \quad (4.1.12)$$

The expected value of  $Y = g(X)$  is

$$E(g(X)) = \int_{-\infty}^{\infty} g(x) f_X(x) dx$$

For discrete random variables, these equations become

$$E(X) = \sum_i x_i P(X = x_i)$$



and

$$E(g(X)) = \sum_i g(x_i)P(X = x_i)$$

In the special case where  $g(X) = (X - E(X))^2$ ,  $E(Y)$  is called the *variance* of  $X$ , which is a measure of spread of the density function of  $X$ . The variance is denoted by  $\sigma_X^2$  and its square root,  $\sigma_X$ , is called the *standard deviation*. The relation for the variance can be written as  $\sigma_X^2 = E(X^2) - (E(X))^2$ . For any constant  $c$ , the following hold:

1.  $E(cX) = cE(X)$ .
2.  $E(c) = c$ .
3.  $E(X + c) = E(X) + c$ .

It is also easy to verify the following properties of the variance

1.  $\text{VAR}(cX) = c^2\text{VAR}(X)$ .
2.  $\text{VAR}(c) = 0$ .
3.  $\text{VAR}(X + c) = \text{VAR}(X)$ .

**Characteristic Functions.** The characteristic function of a random variable  $X$  is denoted by  $\Psi_X(v)$  and defined as

$$\Psi_X(v) \stackrel{\text{def}}{=} \int_{-\infty}^{\infty} f_X(x)e^{jvx} dx \quad (4.1.13)$$

As it is observed from Equation (4.1.13), the characteristic function of a random variable is closely related to the Fourier transform of its density function. The characteristic function of a random variable provides a simple way to find its various moments. This can be easily shown by using the moments property of the Fourier transform. To obtain the  $n$ th moment of the random variable  $X$ , we can use the relation

$$m_X^{(n)} = \frac{1}{j^n} \frac{d^n}{dv^n} \Psi_X(v) \Big|_{v=0} \quad (4.1.14)$$

The characteristic function of a Gaussian random variable with mean  $m$  and variance  $\sigma^2$  is given by

$$\begin{aligned} \Psi_X(v) &= \int_{-\infty}^{\infty} \left[ \frac{1}{\sqrt{2\pi\sigma^2}} e^{-\frac{(x-m)^2}{2\sigma^2}} \right] e^{jvx} dx \\ &= e^{jvm - \frac{v^2\sigma^2}{2}} \end{aligned} \quad (4.1.15)$$

**Multiple Random Variables.** Let  $X$  and  $Y$  be two random variables defined on the same sample space  $\Omega$ . For these two random variables, we can define the *joint CDF* as

$$F_{X,Y}(x, y) = P(\omega \in \Omega : X(\omega) \leq x, Y(\omega) \leq y)$$

or simply as

$$F_{X,Y}(x, y) = P(X \leq x, Y \leq y)$$

and the *joint PDF* as

$$f_{X,Y}(x, y) = \frac{\partial^2}{\partial x \partial y} F_{X,Y}(x, y)$$

The following relations summarize the basic properties of the joint and *marginal* CDFs and PDFs.

1.  $F_X(x) = F_{X,Y}(x, \infty)$ .
2.  $F_Y(y) = F_{X,Y}(\infty, y)$ .
3.  $f_X(x) = \int_{-\infty}^{\infty} f_{X,Y}(x, y) dy$ .
4.  $f_Y(y) = \int_{-\infty}^{\infty} f_{X,Y}(x, y) dx$ .
5.  $\int_{-\infty}^{\infty} \int_{-\infty}^{\infty} f_{X,Y}(x, y) dx dy = 1$ .
6.  $P((X, Y) \in A) = \iint_{(x,y) \in A} f_{X,Y}(x, y) dx dy$ .
7.  $F_{X,Y}(x, y) = \int_{-\infty}^x \int_{-\infty}^y f_{X,Y}(u, v) du dv$ .

The *conditional PDF* of the random variable  $Y$ , given that the value of the random variable  $X$  is equal to  $x$ , is denoted by  $f_{Y|X}(y|x)$  and defined as

$$f_{Y|X}(y|x) = \begin{cases} \frac{f_{X,Y}(x,y)}{f_X(x)}, & f_X(x) \neq 0 \\ 0, & \text{otherwise} \end{cases}$$

If it happens that the density function after knowledge of  $X$  is the same as the density function before the knowledge of  $X$ , then the random variables are said to be *statistically independent*. For statistically independent random variables,

$$f_{X,Y}(x, y) = f_X(x) f_Y(y)$$

The expected value of  $g(X, Y)$ , where  $g(X, Y)$  is any function of  $X$  and  $Y$ , is obtained from

$$E(g(X, Y)) = \int_{-\infty}^{\infty} \int_{-\infty}^{\infty} g(x, y) f_{X,Y}(x, y) dx dy$$

In the special case where  $g(X, Y) = XY$ , we obtain  $E(XY)$ , which is called the *correlation* of  $X$  and  $Y$ . In the case where  $g(X, Y) = (X - m_X)(Y - m_Y)$ , we obtain  $E(XY) - m_X m_Y$ , which is called the *covariance* of  $X$  and  $Y$ . Note that if  $X = Y$ , then  $\text{COV}(X, Y) = \text{VAR}(X)$ . The normalized version of the covariance, called the *correlation coefficient*, is denoted by  $\rho_{X,Y}$  and is defined as

$$\rho_{X,Y} = \frac{\text{COV}(X, Y)}{\sigma_X \sigma_Y}$$

Using the Cauchy–Schwarz inequality (see Problem 2.9), it can be shown that  $|\rho_{X,Y}| \leq 1$  and  $\rho = \pm 1$  indicates a first order relationship between  $X$  and  $Y$ ; i.e., a relation of the form  $Y = aX + b$ . The case  $\rho = 1$  corresponds to a positive  $a$  and  $\rho = -1$  corresponds

to a negative  $a$ . Also, it is easy to verify that if  $X$  and  $Y$  are independent, then  $\text{COV}(X, Y) = \rho_{X,Y} = 0$ . That is, independence implies lack of correlation ( $\rho = 0$ ). It should be noted that lack of correlation *does not* in general imply independence. That is,  $\rho$  might be zero and the random variables may still be statistically dependent.

Some properties of the expected value and variance applied to multiple random variables are listed below:

1.  $E(\sum_i c_i X_i) = \sum_i c_i E(X_i)$ .
2.  $\text{VAR}(\sum_i c_i X_i) = \sum_i c_i^2 \text{VAR}(X_i) + \sum_i \sum_{j \neq i} c_i c_j \text{COV}(X_i, X_j)$ .

where  $c_i$ 's are constants.

**Multiple Functions of Multiple Random Variables.** If we define two functions of the random variables  $X$  and  $Y$  by

$$\begin{cases} Z = g(X, Y) \\ W = h(X, Y) \end{cases}$$

then the joint CDF and PDF of  $Z$  and  $W$  can be obtained directly by applying the definition of the CDF. However, if it happens that for all  $z$  and  $w$  the set of equations

$$\begin{cases} g(x, y) = z \\ h(x, y) = w \end{cases}$$

has a countable number of solutions  $\{x_i, y_i\}$ , and at these points the determinant of the Jacobian matrix

$$\mathbf{J}(x, y) = \begin{bmatrix} \frac{\partial z}{\partial x} & \frac{\partial z}{\partial y} \\ \frac{\partial w}{\partial x} & \frac{\partial w}{\partial y} \end{bmatrix}$$

is nonzero, then, we have

$$f_{Z,W}(z, w) = \sum_i \frac{f(x_i, y_i)}{|\det \mathbf{J}(x_i, y_i)|} \quad (4.1.16)$$

where  $\det \mathbf{J}$  denotes the determinant of the matrix  $\mathbf{J}$ .

### Example 4.1.3

The two random variables  $X$  and  $Y$  are independent and identically distributed, each with a Gaussian density function with mean equal to zero and variance equal to  $\sigma^2$ . If these two random variables denote the coordinates of a point in the plane, find the probability density function of the magnitude and the phase of that point in polar coordinates.

**Solution** First we have to find the joint PDF of  $X$  and  $Y$ . Since  $X$  and  $Y$  are independent, their joint PDF is the product of their marginal PDFs; i.e.,

$$\begin{aligned} f_{X,Y}(x, y) &= f_X(x) f_Y(y) \\ &= \frac{1}{2\pi\sigma^2} e^{-\frac{x^2+y^2}{2\sigma^2}} \end{aligned} \quad (4.1.17)$$

The magnitude of the point with coordinates  $(X, Y)$  in the polar plane is given by  $V = \sqrt{X^2 + Y^2}$ , and its phase is given by  $\Theta = \arctan \frac{Y}{X}$ . We begin by deriving the joint PDF of  $V$  and  $\Theta$ . In this case,  $g(X, Y) = \sqrt{X^2 + Y^2}$  and  $h(X, Y) = \arctan \frac{Y}{X}$ . The Jacobian

matrix is given by

$$\mathbf{J}(x, y) = \begin{bmatrix} \frac{x}{\sqrt{x^2+y^2}} & \frac{y}{\sqrt{x^2+y^2}} \\ -\frac{y}{x^2+y^2} & \frac{x}{x^2+y^2} \end{bmatrix} \quad (4.1.18)$$

The determinant of the Jacobian matrix can be easily determined to be equal to

$$\begin{aligned} |\det \mathbf{J}(x, y)| &= \frac{1}{\sqrt{x^2 + y^2}} \\ &= \frac{1}{v} \end{aligned} \quad (4.1.19)$$

The set of equations

$$\begin{cases} \sqrt{x^2 + y^2} = v \\ \arctan \frac{y}{x} = \theta \end{cases} \quad (4.1.20)$$

has only one solution given by

$$\begin{cases} x = v \cos \theta \\ y = v \sin \theta \end{cases} \quad (4.1.21)$$

Substituting these results into (4.1.16), we obtain the joint PDF of the magnitude and the phase as

$$\begin{aligned} f_{V,\Theta}(v, \theta) &= v f_{X,Y}(v \cos \theta, v \sin \theta) \\ &= \frac{v}{2\pi\sigma^2} e^{-\frac{v^2}{2\sigma^2}}, \quad v \geq 0, 0 \leq \theta < 2\pi \end{aligned} \quad (4.1.22)$$

To derive the marginal PDFs for the magnitude and the phase, we have to integrate the joint PDF. To obtain the PDF of the phase, we have

$$\begin{aligned} f_{\Theta}(\theta) &= \int_0^{\infty} f_{V,\Theta}(v, \theta) dv \\ &= \frac{1}{2\pi} \int_0^{\infty} \frac{v}{\sigma^2} e^{-\frac{v^2}{2\sigma^2}} dv \\ &= \frac{1}{2\pi} [-e^{-\frac{v^2}{2\sigma^2}}]_0^{\infty} \\ &= \frac{1}{2\pi}, \quad 0 \leq \theta < 2\pi \end{aligned} \quad (4.1.23)$$

Hence, the phase is uniformly distributed on  $[0, 2\pi)$ . To obtain the marginal PDF for the magnitude, we have

$$\begin{aligned} f_V(v) &= \int_0^{2\pi} f_{V,\Theta}(v, \theta) d\theta \\ &= \frac{v}{\sigma^2} e^{-\frac{v^2}{2\sigma^2}}, \quad v \geq 0 \end{aligned} \quad (4.1.24)$$

For negative  $v$ , of course,  $f_V(v) = 0$ . Therefore,

$$f_V(v) = \begin{cases} \frac{v}{\sigma^2} e^{-\frac{v^2}{2\sigma^2}}, & v \geq 0 \\ 0, & v < 0 \end{cases} \quad (4.1.25)$$

This PDF is known as the *Rayleigh probability density function* and has widespread applications in the study of the fading in communication channels. It is also interesting to note that, in Example 4.1.3

$$f_{V,\Theta}(v, \theta) = f_V(v) f_\Theta(\theta) \quad (4.1.26)$$

and, therefore, the magnitude and the phase are independent random variables.

**Jointly Gaussian Random Variables.** *Jointly Gaussian* or *binormal* random variables  $X$  and  $Y$  are defined by the joint density function

$$f_{X,Y}(x, y) = \frac{1}{2\pi\sigma_1\sigma_2\sqrt{1-\rho^2}} \exp\left\{-\frac{1}{2(1-\rho^2)}\right. \\ \left.\times \left[\frac{(x-m_1)^2}{\sigma_1^2} + \frac{(y-m_2)^2}{\sigma_2^2} - \frac{2\rho(x-m_1)(y-m_2)}{\sigma_1\sigma_2}\right]\right\}$$

When the two random variables  $X$  and  $Y$  are distributed according to a binormal distribution, not only  $X$  and  $Y$  are themselves normal random variables, but the conditional densities  $f(x|y)$  and  $f(y|x)$  are also Gaussian. This property is the main difference between jointly Gaussian random variables and two random variables each having a Gaussian distribution. Also, it is straightforward to show that if  $X$  and  $Y$  are jointly Gaussian,  $X$  is Gaussian with mean  $m_1$  and variance  $\sigma_1^2$ ,  $Y$  is Gaussian with mean  $m_2$  and variance  $\sigma_2^2$  and the correlation coefficient between  $X$  and  $Y$  is  $\rho$ .

The definition of two jointly Gaussian random variables can be extended to  $n$  random variables  $X_1, X_2, X_3, \dots, X_n$ . If we define the random vector  $\mathbf{X} = (X_1, X_2, \dots, X_n)$ , and the vector of the means  $\mathbf{m} = (m_1, m_2, \dots, m_n)$ , and the  $n \times n$  covariance matrix  $\mathbf{C}$  such that  $C_{i,j} = \text{COV}(X_i, X_j)$ , then the random variables  $\{X_i\}$  are jointly Gaussian if

$$f(x_1, x_2, \dots, x_n) = \frac{1}{\sqrt{(2\pi)^n \det(\mathbf{C})}} \exp\left\{-\frac{1}{2}(\mathbf{x} - \mathbf{m})\mathbf{C}^{-1}(\mathbf{x} - \mathbf{m})^t\right\}$$

Here are the main properties of jointly Gaussian random variables:

1. If  $n$  random variables are jointly Gaussian, any subset of them is also distributed according to a jointly Gaussian distribution of the appropriate size. In particular, all individual random variables are Gaussian.
2. Jointly Gaussian random variables are completely characterized by their mean vector  $\mathbf{m}$  and covariance matrix  $\mathbf{C}$ . These so-called *second-order* properties completely describe the random variables.
3. Any subset of the jointly Gaussian random variables conditioned on any other subset of the original random variables makes a jointly Gaussian distribution of the appropriate size.
4. Any set of linear combinations of  $(X_1, X_2, \dots, X_n)$  is itself jointly Gaussian. In particular, any linear combination of  $X_i$ 's is a Gaussian random variable.
5. Two uncorrelated jointly Gaussian random variables are independent. Therefore, *for jointly Gaussian random variables, independence and uncorrelatedness are*

*equivalent*. As we have seen before, this is not true in general for non-Gaussian random variables.

**Sums of Random Variables.** If we have a sequence of random variables  $(X_1, X_2, \dots, X_n)$ , with basically the same properties, then the behavior of the average  $Y = \frac{1}{n} \sum_{i=1}^n X_i$  is expected to be “less random” than each  $X_i$ . The *law of large numbers* and the *central limit theorem* are precise statements of this intuitive fact.

The *weak law of large numbers (WLLN)* states that if the random variables  $X_1, X_2, \dots, X_n$  are uncorrelated with the same mean  $m_X$  and variance  $\sigma_X^2 < \infty$ , then for any  $\epsilon > 0$ ,  $\lim_{n \rightarrow \infty} P(|Y - m_X| > \epsilon) = 0$ , where  $Y = \frac{1}{n} \sum_{i=1}^n X_i$ . This means that the average converges (in probability) to the expected value.

The *central limit theorem* not only states the convergence of the average to the mean but also gives some insight into the distribution of the average. This theorem states that if  $(X_1, X_2, \dots, X_n)$  are independent with means  $(m_1, m_2, \dots, m_n)$  and variances  $(\sigma_1^2, \sigma_2^2, \dots, \sigma_n^2)$ , then the CDF of the random variable  $\frac{1}{\sqrt{n}} \sum_{i=1}^n \frac{X_i - m_i}{\sigma_i}$  converges to the CDF of a Gaussian random variable with mean 0 and variance 1. In the special case that the  $X_i$ 's are *independent and identically distributed (i.i.d.)* this theorem says that the CDF of  $Y = \frac{1}{n} \sum_{i=1}^n X_i$  converges to the CDF of a  $\mathcal{N}(m, \frac{\sigma^2}{n})$ . Note that, although from the central limit theorem we can conclude that the average converges to the expected value, we cannot say that the law of large numbers follows from the central limit theorem. This is because the requirements for the central limit theorem to hold are much stronger. For the central limit theorem to hold, we need the random variables to be independent, whereas the law of large numbers holds under the less restrictive condition of uncorrelatedness of the random variables.

This concludes our brief review of the basics of the probability theory. References at the end of this chapter provide sources for further study.

## 4.2 RANDOM PROCESSES: BASIC CONCEPTS

A random process is a natural extension of the concept of random variable when dealing with signals. In analyzing communication systems we are basically dealing with time-varying signals. In our development so far, we have assumed that all the signals are deterministic. In many situations the deterministic assumption on time-varying signals is not a valid assumption, and it is more appropriate to model signals as random rather than deterministic functions. One such example is the case of thermal noise in electronic circuits. This type of noise is due to the random movement of electrons as a result of thermal agitation and, therefore, the resulting current and voltage can only be described statistically. Another example is the reflection of radio waves from different layers of the ionosphere that makes long-range broadcasting of short-wave radio possible. Due to randomness of this reflection, the received signal can again be modeled as a random signal. These two examples show that random signals are suitable for description of certain phenomena in signal transmission.

Another situation where modeling by random processes proves useful is in the characterization of information sources. An information source, such as a speech source,

generates time-varying signals whose contents are not known in advance, otherwise there would be no need to transmit them. Therefore, random processes provide a natural way to model information sources as well.

A *random process*, a *stochastic process*, or a *random signal* can be viewed in two different, although closely related, ways. One way is to view a random process as a collection of time functions, or signals, corresponding to various outcomes of a random experiment. From this viewpoint, corresponding to each outcome  $\omega_i$  in a probability space  $(\Omega, \mathcal{B}, P)$ , there exists a signal  $x(t; \omega_i)$ . This description is very similar to the description of random variables in which a real number is assigned to each outcome  $\omega_i$ . Figure 4.10 depicts this characterization of random processes. Thus, for each  $\omega_i$ , there exists a deterministic time function  $x(t; \omega_i)$ , which is called a *sample function*, or a *realization* of the random process. The collection of all sample functions is called an ensemble.

At each time instant  $t_0$ , and for each  $\omega_i \in \Omega$ , we have the number  $x(t_0; \omega_i)$ . For the different  $\omega_i$ 's at a fixed time  $t_0$ , the numbers  $x(t_0; \omega_i)$ , constitute a random variable denoted by  $X(t_0)$ . After all, a random variable is nothing but an assignment of real numbers to the outcomes of a random experiment. This is a very important observation

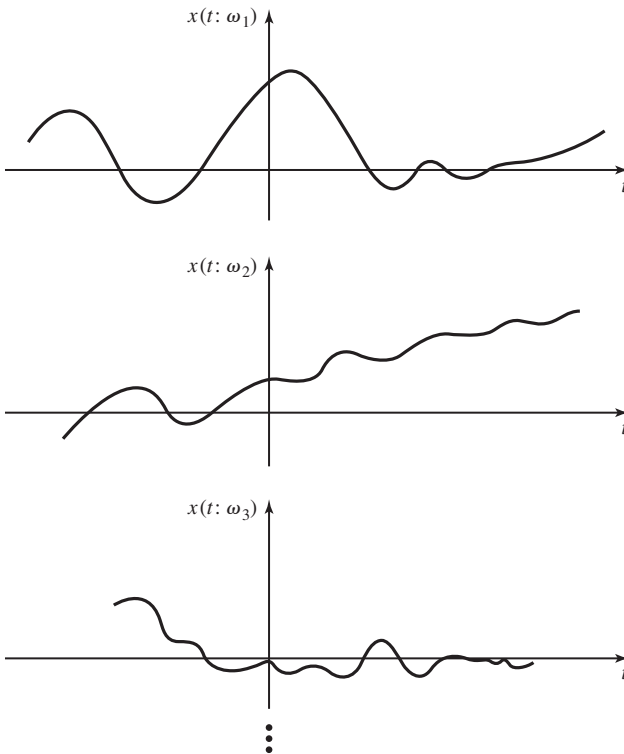


**Figure 4.10** Sample functions of a random process.

and a bridge that connects the concept of a random process to the more familiar concept of a random variable. In other words, *at any time instant the value of a random process constitutes a random variable*.

Alternatively, we may view the random signal at  $t_1, t_2, \dots$ , or in general, all  $t \in \mathbb{R}$  as a collection of random variables  $\{X(t_1), X(t_2), \dots\}$ , or in general,  $\{X(t), t \in \mathbb{R}\}$ . From this viewpoint, a random process is represented as a collection of random variables indexed by some index set (e.g.,  $\mathbb{R}$  in the latter case). If the index set is the set of real numbers, the random process is called a *continuous-time random process*, and if it is the set of all integers, then the random process is a *discrete-time random process*. A discrete-time random process is nothing but a sequence of random variables  $\{X_i\}_{i=-\infty}^{+\infty}$ . This second view of random processes, although less intuitive, is more appropriate for precise mathematical development of the theory of random processes.

### Example 4.2.1

Let  $(\Omega, \mathcal{B}, P)$  denote the probability space corresponding to the random experiment of throwing a die. Obviously, in this case  $\Omega = \{1, 2, 3, 4, 5, 6\}$ . For all  $\omega_i$ , let  $x(t; \omega_i) = \omega_i e^{-t} u_{-1}(t)$  denote a random process. Then  $X(1)$  is a random variable taking values  $e^{-1}, 2e^{-1}, \dots, 6e^{-1}$  each with probability  $\frac{1}{6}$ . Sample functions of this random process are shown in Figure 4.11. For this example, the first viewpoint of random processes is the preferred view.

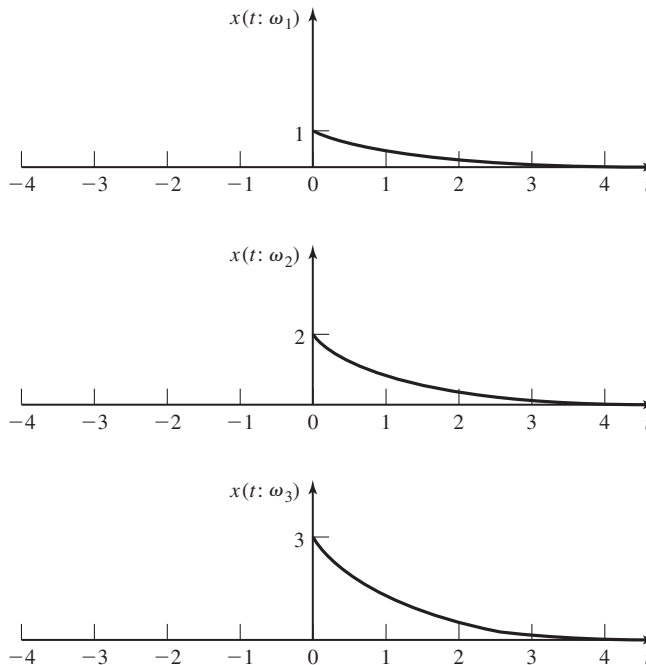


**Figure 4.11** Sample functions of Example 4.2.1.



**Example 4.2.2**

Let  $\omega_i$  denote the outcome of a random experiment consisting of independent drawings from a Gaussian random variable distributed according to  $\mathcal{N}(0, 1)$ . Let the discrete-time random process  $\{X_n\}_{n=0}^{\infty}$  be defined by:  $X_0 = 0$  and  $X_n = X_{n-1} + \omega_n$  for all  $n \geq 1$ . It follows from the basic properties of the Gaussian random variables that for all  $i \geq 1$ ,  $j \geq 1$ , and  $i < j$ ,  $\{X_n\}_i^j$  is a  $j - i + 1$  dimensional Gaussian vector. For this example the second view; i.e., interpreting the random process as a collection of random variables, is more appropriate.

**4.2.1 Description of Random Processes**

Based on the adopted viewpoint, there are two types of descriptions possible for random processes. If the random process is viewed as a collection of signals, the *analytic description* may be appropriate. In this description, analytic expressions are given for each sample in terms of one or more random variables; i.e., the random process is given as  $X(t) = f(t; \boldsymbol{\theta})$  where  $\boldsymbol{\theta} = (\theta_1, \theta_2, \dots, \theta_n)$  is, in general, a random vector with a given joint PDF. This is a very informative description of a random process because it completely describes the analytic form of various realizations of the process. For real-life processes, it is hardly possible to give such a complete description. If an analytic description is not possible, a *statistical description* may be appropriate. Such a description is based on the second viewpoint of random processes, regarding them as a collection of random variables indexed by some index set.

**Definition 4.2.1.** A complete statistical description of a random process  $X(t)$  is known if for any integer  $n$  and any choice of  $(t_1, t_2, \dots, t_n) \in \mathbb{R}^n$  the joint PDF of  $(X(t_1), X(t_2), \dots, X(t_n))$  is given.

If the complete statistical description of the process is given, for any  $n$  the joint density function of  $(X(t_1), X(t_2), \dots, X(t_n))$  is given by  $f_{X(t_1), X(t_2), \dots, X(t_n)}(x_1, x_2, \dots, x_n)$ .

**Definition 4.2.2.** A process  $X(t)$  is described by its *M*th order statistics if for all  $n \leq M$  and all  $(t_1, t_2, \dots, t_n) \in \mathbb{R}^n$  the joint PDF of  $(X(t_1), X(t_2), \dots, X(t_n))$  is given.

A very important special case, in the study of communication systems, is the case of  $M = 2$ , in which second-order statistics are known. This simply means that, at each time instant  $t$ , we have the density function of  $X(t)$ , and for all choices of  $(t_1, t_2)$  the joint density function of  $(X(t_1), X(t_2))$  is given.

**Example 4.2.3**

A random process is defined by  $X(t) = A \cos(2\pi f_0 t + \Theta)$  where  $\Theta$  is a random variable uniformly distributed on  $[0, 2\pi)$ . In this case, we have an analytic description of the random process. Note that by having the analytic description, we can find the complete statistical description. Figure 4.12 shows some samples of this process.

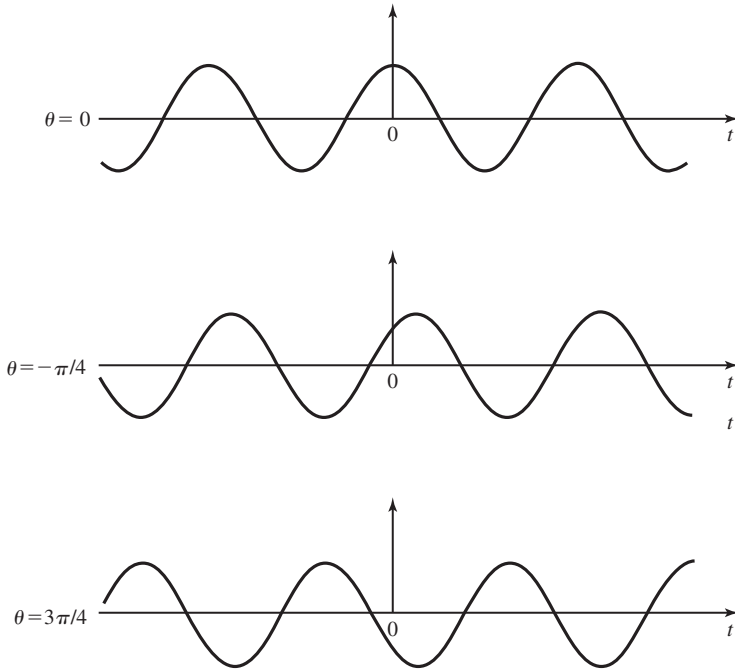


**Figure 4.12** Samples of the random process given in Example 4.2.3.

#### Example 4.2.4

The process  $X(t)$  is defined by  $X(t) = X$ , where  $X$  is a random variable uniformly distributed on  $[-1, 1]$ . In this case again, an analytic description of the random process is given. For this random process, each sample is a constant signal. Samples of this process are shown in Figure 4.13.

#### Example 4.2.5

The process  $X(t)$ ,  $t > 0$ , is defined by the property that for any  $n$  and any  $(t_1, t_2, \dots, t_n) \in \mathbb{R}^+$ , the joint density function of  $\{X(t_i)\}_{i=1}^n$  is a jointly Gaussian vector with mean 0 and covariance matrix described by

$$C_{i,j} = \text{COV}(X(t_i), X(t_j)) = \sigma^2 \min(t_i, t_j)$$

This is a complete statistical description of the random process  $X(t)$ . A sample of this process is shown in Figure 4.14.

Note that in the last example, although a complete statistical description of the process is given, little insight can be obtained in the shape of each realization of the process.

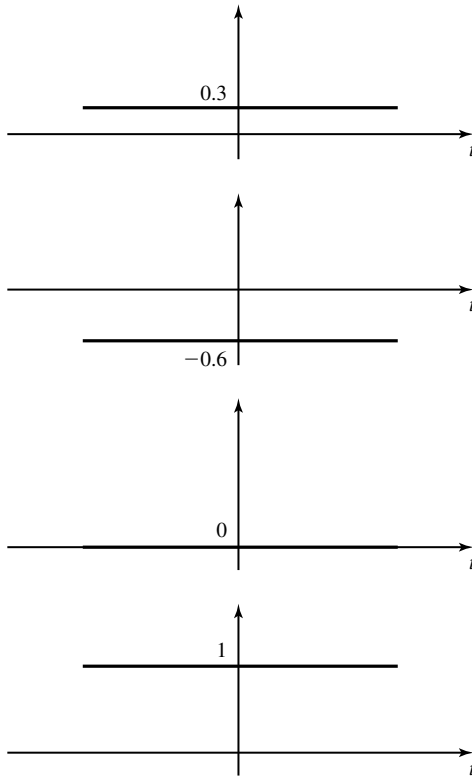


**Figure 4.13** Samples of the random process given in Example 4.2.4.

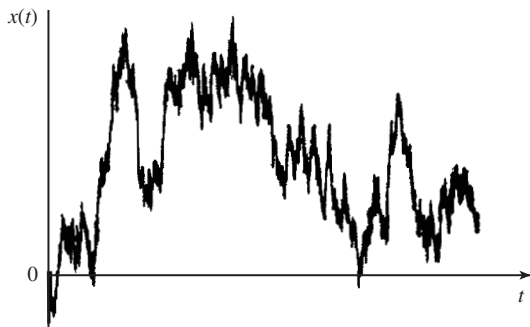


**Figure 4.14** Sample of the process given in Example 4.2.5.

### 4.2.2 Statistical Averages

The facts that at any given time the random process defines a random variable and at any given set of times it defines a random vector, enable us to define various statistical averages for the process via statistical averages of the corresponding random variables.

**Definition 4.2.3.** The *mean*, or *expectation* of the random process  $X(t)$  is a deterministic function of time  $m_X(t)$  that at each time instant  $t_0$  equals the mean of the random variable  $X(t_0)$ . That is,  $m_X(t) = E[X(t)]$  for all  $t$ .

Since at any  $t_0$ , the random variable  $X(t_0)$  is well defined with a PDF  $f_{X(t_0)}(x)$ , we have

$$E[X(t_0)] = m_X(t_0) = \int_{-\infty}^{\infty} x f_{X(t_0)}(x) dx$$

Figure 4.15 gives a pictorial description of this definition.

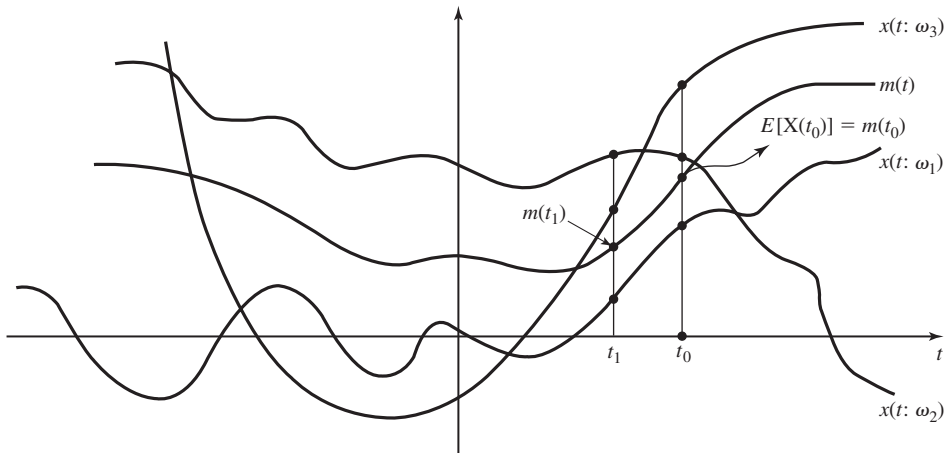


**Figure 4.15** The mean of a random process.

**Example 4.2.6**

The mean of the random process in Example 4.2.3 is obtained by noting that

$$f_{\Theta}(\theta) = \begin{cases} \frac{1}{2\pi} & 0 \leq \theta < 2\pi \\ 0, & \text{otherwise} \end{cases}$$

Hence,

$$E[X(t)] = \int_0^{2\pi} A \cos(2\pi f_0 t + \theta) \frac{1}{2\pi} d\theta = 0$$

We observe that, in this case  $m_X(t)$  is independent of  $t$ .

Another statistical average that plays a very important role in our study of random processes is the *autocorrelation function*. The autocorrelation function is especially important because it completely describes the power-spectral density and the power-content of a large class of random processes.

**Definition 4.2.4.** The *autocorrelation function* of the random process  $X(t)$ , denoted as  $R_{XX}(t_1, t_2)$ , is defined by  $R_{XX}(t_1, t_2) = E[X(t_1)X(t_2)]$ .

From the above definition it is clear that  $R_{XX}(t_1, t_2)$  is a deterministic function of two variables  $t_1$  and  $t_2$ , given by

$$R_{XX}(t_1, t_2) = \int_{-\infty}^{\infty} \int_{-\infty}^{\infty} x_1 x_2 f_{X(t_1), X(t_2)}(x_1, x_2) dx_1 dx_2$$

The autocorrelation function is usually denoted by  $R_X(t_1, t_2)$  for short.

**Example 4.2.7**

The autocorrelation function of the random process in Example 4.2.3 is

$$\begin{aligned} R_X(t_1, t_2) &= E[A \cos(2\pi f_0 t_1 + \Theta) A \cos(2\pi f_0 t_2 + \Theta)] \\ &= A^2 E \left[ \frac{1}{2} \cos 2\pi f_0(t_1 - t_2) + \frac{1}{2} \cos(2\pi f_0(t_1 + t_2) + 2\Theta) \right] \\ &= \frac{A^2}{2} \cos 2\pi f_0(t_1 - t_2) \end{aligned}$$

Note that

$$E[\cos(2\pi f_0(t_1 + t_2) + 2\Theta)] = \int_0^{2\pi} \cos[2\pi f_0(t_1 + t_2) + 2\theta] \frac{1}{2\pi} d\theta = 0$$

**Example 4.2.8**

For the random process given in Example 4.2.4, we have

$$R_X(t_1, t_2) = E(X^2) = \int_{-1}^{+1} \frac{x^2}{2} dx = \frac{1}{3}$$

So far, we have given two methods to describe random processes, an analytic and a statistical description. A statistical description can be a complete description or an  $M$ th order description. Sometimes, even having a second-order statistical description of a random variable is not practical. In these cases, it may be possible to find various statistical averages by averaging over different realizations; in particular, it may be possible to find  $m_X(t)$  and  $R_X(t_1, t_2)$ . Although this information is much less than a complete statistical description of the random process, it may be adequate. In some cases, as we will see later, the mean and autocorrelation function provide a complete statistical description for the important class of Gaussian random processes.

### 4.2.3 Stationary Processes

In a complete statistical description of a random processes, for any  $n$ , and any  $(t_1, t_2, \dots, t_n)$ , the joint PDF  $f_{X(t_1), X(t_2), \dots, X(t_n)}(x_1, x_2, \dots, x_n)$  is given. This joint PDF in general depends on the choice of the time origin. In a very important class of random processes, the joint density function is independent of the choice of the time origin. These processes whose statistical properties are time independent are called *stationary processes*. There are different notions of stationarity. A *strictly stationary process* is a process in which for all  $n$  and all  $(t_1, t_2, \dots, t_n)$ ,  $f_{X(t_1), X(t_2), \dots, X(t_n)}(x_1, x_2, \dots, x_n)$  depends only on the relative position of  $(t_1, t_2, \dots, t_n)$ , and not on their values directly. In other words, a shift in the time origin does not change the statistical properties of the process. A formal definition of a strictly stationary process is the following:

**Definition 4.2.5.** A *strictly stationary process* is a process in which for all  $n$ , all  $(t_1, t_2, \dots, t_n)$ , and all  $\Delta$

$$f_{X(t_1), X(t_2), \dots, X(t_n)}(x_1, x_2, \dots, x_n) = f_{X(t_1+\Delta), X(t_2+\Delta), \dots, X(t_n+\Delta)}(x_1, x_2, \dots, x_n)$$

A process is called  $M$ th order stationary if the above condition holds for all  $n \leq M$ .

It is obvious that for both strictly stationary processes and  $M$ th order stationary processes the density function of  $X(t)$  is time independent.

**Example 4.2.9**

Let  $X(t)$  denote a process such that for all  $n$  and all  $(t_1, t_2, \dots, t_n)$ , the vector  $(X(t_1), X(t_2), \dots, X(t_n))$  is an  $n$ -dimensional Gaussian random variable with mean zero and covariance matrix  $\mathbf{I}_n$  ( $n$ -dimensional unitary matrix). Then clearly  $X(t)$  is a strictly stationary process.

Strict stationarity is a very strong condition that only a few physical processes may satisfy. A less restrictive definition of stationarity is often more useful.

**Definition 4.2.6.** A process  $X(t)$  is *wide-sense stationary* (WSS) if the following conditions are satisfied:

1.  $m_X(t) = E[X(t)]$  is independent of  $t$ .
2.  $R_X(t_1, t_2)$  depends only on the time difference  $\tau = t_1 - t_2$  and not on  $t_1$  and  $t_2$  individually.

Hereafter, the term *stationary* with no adjectives means WSS, and for these processes the mean and autocorrelation are denoted by  $m_X$  and  $R_{XX}(\tau)$ , or simply  $R_X(\tau)$ .

**Example 4.2.10**

For the random process in Exercise 4.2.3, we have already seen that  $m_X = 0$  and  $R_X(t_1, t_2) = \frac{A^2}{2} \cos 2\pi f_0(t_1 - t_2)$ . Therefore, the process is WSS.

A class of processes closely related to stationary processes is the class of *cyclostationary processes*. In cyclostationary processes, the statistical properties are not time independent, but periodic with time. We will give the formal definition of the cyclostationary processes here, but their importance in communication system analysis will become more apparent in Chapters 7 and 8.

**Definition 4.2.7.** A random process  $X(t)$  with mean  $m_X(t)$  and autocorrelation function  $R_X(t + \tau, t)$  is called *cyclostationary*, if both the mean and the autocorrelation are periodic in  $t$  with some period  $T_0$ ; i.e., if

$$m_X(t + T_0) = m_X(t) \tag{4.2.1}$$

and

$$R_X(t + \tau + T_0, t + T_0) = R_X(t + \tau, t) \tag{4.2.2}$$

for all  $t$  and  $\tau$ .

**Example 4.2.11**

Let  $Y(t) = X(t) \cos(2\pi f_0 t)$  where  $X(t)$  is a stationary random process with mean  $m$  and autocorrelation  $R_X(\tau)$ . Then

$$m_Y(t) = E[X(t) \cos(2\pi f_0 t)] = m_X \cos(2\pi f_0 t) \quad (4.2.3)$$

and

$$\begin{aligned} R_Y(t + \tau, t) &= E[X(t + \tau) \cos(2\pi f_0(t + \tau))X(t) \cos(2\pi f_0 t)] \\ &= R_X(\tau) \left[ \frac{1}{2} \cos(2\pi f_0 \tau) + \frac{1}{2} \cos(4\pi f_0 t + 2\pi f_0 \tau) \right] \end{aligned} \quad (4.2.4)$$

It is seen that both  $m_Y(t)$  and  $R_Y(t + \tau, t)$  are periodic with period  $T_0 = \frac{1}{f_0}$ . Therefore the process is cyclostationary.

The following theorem gives the basic properties of the autocorrelation function of a stationary process.

**Theorem 4.2.1.**  $R_X(\tau)$ , the autocorrelation function of the stationary process  $X(t)$ , has the following properties:

1.  $R_X(\tau)$  is an even function; i.e.,  $R_X(-\tau) = R_X(\tau)$ .
2. The maximum absolute value of  $R_X(\tau)$  is achieved at  $\tau = 0$ ; i.e.,  $|R_X(\tau)| \leq R_X(0)$ .
3. If for some  $T_0$  we have  $R_X(T_0) = R_X(0)$ , then for all integers  $k$ ,  $R_X(kT_0) = R_X(0)$ .

*Proof.*

1. By definition

$$R_X(\tau) = E[X(t)X(t - \tau)] = E[X(t - \tau)X(t)] = R_X(-\tau)$$

This proves the first part of the theorem.

2. By noting that

$$E[X(t) \pm X(t - \tau)]^2 \geq 0$$

and expanding the result, we have

$$E[X^2(t)] + E[X^2(t - \tau)] \pm 2E[X(t)X(t - \tau)] \geq 0$$

Hence,

$$\pm R_X(\tau) \leq R_X(0)$$

which means  $|R_X(\tau)| \leq R_X(0)$ .

3. The proof is by mathematical induction. Assume that  $R_X(iT_0) = R_X(0)$ , for  $i = 1, 2, \dots, k-1$ . Expanding

$$\begin{aligned} E[X(t) - X(t - kT_0)]^2 \\ = E[(X(t) - X(t - (k-1)T_0)) + (X(t - (k-1)T_0) - X(t - kT_0))]^2 \end{aligned}$$

we obtain

$$\begin{aligned} 2R_X(0) - 2R_X(kT_0) \\ = E[X(t) - X(t - (k-1)T_0)]^2 + E[X(t - (k-1)T_0) - X(t - kT_0)]^2 \\ + 2E[(X(t) - X(t - (k-1)T_0))(X(t - (k-1)T_0) - X(t - kT_0))] \end{aligned}$$

Now using the relation  $R_X(iT_0) = R_X(0)$  for  $i \leq k-1$ ,

$$E[X(t) - X(t - (k-1)T_0)]^2 = -2R_X((k-1)T_0) + 2R_X(0) = 0$$

and

$$E[X(t - (k-1)T_0) - X(t - kT_0)]^2 = -2R_X(T_0) + 2R_X(0) = 0$$

By applying the Cauchy–Schwarz inequality (Problem 2.9), we obtain

$$\begin{aligned} |E[(X(t) - X(t - (k-1)T_0))(X(t - (k-1)T_0) - X(t - kT_0))]| \\ \leq \sqrt{E[X(t) - X(t - (k-1)T_0)]^2 E[X(t - (k-1)T_0) - X(t - kT_0)]^2} \\ = \sqrt{4(R_X((k-1)T_0) - R_X(0))(R_X(T_0) - R_X(0))} = 0 \end{aligned}$$

from which we conclude  $R_X(kT_0) = R_X(0)$  for all integers  $k$ . ■

**Ergodic Processes.** For a strictly stationary process  $X(t)$  and for any function  $g(x)$ , we can define two types of averages:

1. By looking at a given time  $t_0$  and different realizations of the process, we have a random variable  $X(t_0)$  with density function  $f_{X(t_0)}(x)$ , which is independent of  $t_0$  since the process is strictly stationary. For this random variable, we can find the statistical average (or *ensemble average*) of any function  $g(X)$  as

$$E[g(X(t_0))] = \int_{-\infty}^{\infty} g(x) f_{X(t_0)}(x) dx$$

This value is, of course, independent of  $t_0$ .

2. By looking at an individual realization, we have a deterministic function of time  $x(t; \omega_i)$ . Based on this function, we can find the time average for a function  $g(x)$ , defined as

$$\langle g(x) \rangle_i \stackrel{\text{def}}{=} \lim_{T \rightarrow \infty} \frac{1}{T} \int_{-T/2}^{+T/2} g(x(t; \omega_i)) dt$$



$\langle g(x) \rangle_i$  is, of course, a real number independent of  $t$  but, in general, it is dependent on the particular realization chosen ( $\omega_i$  or  $i$ ). Therefore, for each  $\omega_i$  we have a corresponding real number  $\langle g(x) \rangle_i$ . Hence,  $\langle g(x) \rangle_i$  is the value assumed by a random variable. We denote this random variable by  $\langle g(X) \rangle$ .

If it happens that for all functions  $g(x)$ ,  $\langle g(x) \rangle_i$  is independent of  $i$  and equals  $E[g(X(t_0))]$ , then the process is called *ergodic*.<sup>†</sup>

**Definition 4.2.8.** A stationary process  $X(t)$  is *ergodic* if for all functions  $g(x)$  and all  $\omega_i \in \Omega$

$$\lim_{T \rightarrow \infty} \frac{1}{T} \int_{-T/2}^{+T/2} g(x(t; \omega_i)) dt = E[g(X(t))]$$

In other words, if all time averages are equal to the corresponding statistical averages, then the stationary process is ergodic.

A natural consequence of ergodicity is that in measuring various statistical averages (mean and autocorrelation, for example), it is sufficient to look at *one realization* of the process and find the corresponding time average, rather than considering a large number of realizations and averaging over them.

**Example 4.2.12**

For the process given in Example 4.2.3, for any value of  $0 \leq \theta < 2\pi$  (i.e., for any realization of the process) we have

$$\begin{aligned} \langle g(X(t; \theta)) \rangle &= \lim_{T \rightarrow \infty} \frac{1}{T} \int_{-T/2}^{+T/2} g(A \cos(2\pi f_0 t + \theta)) dt \\ &= \lim_{N \rightarrow \infty} \frac{1}{2NT_0} \int_{-NT_0}^{+NT_0} g(A \cos(2\pi f_0 t + \theta)) dt \\ &= \frac{1}{T_0} \int_0^{T_0} g(A \cos(2\pi f_0 t + \theta)) dt \\ &\stackrel{2\pi f_0 t + \theta = u}{=} \frac{1}{T_0} \int_\theta^{2\pi + \theta} g(A \cos u) \frac{du}{2\pi f_0} \\ &= \frac{1}{2\pi} \int_0^{2\pi} g(A \cos u) du \end{aligned}$$

<sup>†</sup>Our notion of ergodicity and the definition that follows are not precise. A precise definition of ergodicity requires knowledge of measure theory and is not treated here. In fact, our definition of *ergodicity* is one of the properties satisfied by *stationarity and ergodic* processes and sometimes is referred to as *ergodic property*. For most engineering applications, however, this notion is adequate. For a precise definition of ergodicity and some related misconceptions, the reader is referred to Gray and Davisson (1986).

where  $T_0 = \frac{1}{f_0}$ . On the other hand,

$$\begin{aligned} E[X(t)] &= \int_0^{2\pi} g(A \cos(2\pi f_0 t + \theta)) \frac{1}{2\pi} d\theta \\ &\stackrel{2\pi f_0 t + \theta = u}{=} \frac{1}{2\pi} \int_{2\pi f_0 t}^{2\pi f_0 t + 2\pi} g(A \cos(u)) du \\ &= \frac{1}{2\pi} \int_0^{2\pi} g(A \cos u) du \end{aligned}$$

and, therefore, the process is ergodic.

### Example 4.2.13

In the process given in Example 4.2.4, each sample has a different constant value and, therefore, the time average for each  $\omega_i$  depends on  $i$ . This means that the process is not ergodic.

### Example 4.2.14

We have already seen that a sequence of random variables defines a discrete-time random process. Let us assume that the sequence  $\{X_i\}_{i=-\infty}^{\infty}$  is a sequence of independent identically distributed random variables. Then, for any realization, by the law of large numbers, we have  $\lim_{N \rightarrow \infty} \frac{1}{2N} \sum_{i=-N}^N X_i = E[X]$ . This means that i.i.d. processes are ergodic.

Ergodicity is a very strong property. Unfortunately, in general, there exists no simple test for ergodicity. For the important class of Gaussian processes, however, there exists a simple test that we will discuss in Section 4.4.1.

**Power and Energy.** In our discussion of power and energy for deterministic signals we defined two types of signals—energy-type and power-type.

We can extend these notions to random processes. Let  $X(t)$  be a random process with sample functions  $x(t, \omega_i)$ . Then, the energy and power of each sample function are defined as

$$\mathcal{E}_i = \int_{-\infty}^{\infty} x^2(t, \omega_i) dt$$

and

$$P_i = \lim_{T \rightarrow \infty} \frac{1}{T} \int_{-T/2}^{T/2} x^2(t, \omega_i) dt$$

This shows that for each  $\omega_i \in \Omega$  we have real numbers  $\mathcal{E}_i$  and  $P_i$  denoting energy and power respectively and therefore it is clear that both energy and power are random variables which we denote<sup>†</sup> by  $\mathcal{E}_X$  and  $\mathcal{P}_X$ . It makes sense to define the expected values of  $\mathcal{P}_X$  and  $\mathcal{E}_X$  as a measure of the power and energy content of the process. These parameters are defined as follows:

<sup>†</sup>Note that here we are using script letters to denote random variables.

**Definition 4.2.9.** The power content  $P_X$  and the energy content  $E_X$  of the random process  $X(t)$  are defined as

$$P_X = E[\mathcal{P}_X]$$

and

$$\mathcal{E}_X = E[\mathcal{E}_X]$$

where

$$\mathcal{E}_X = \int_{-\infty}^{\infty} X^2(t) dt$$

and

$$\mathcal{P}_X = \lim_{T \rightarrow \infty} \frac{1}{T} \int_{-T/2}^{T/2} X^2(t) dt$$

From this definition,

$$\begin{aligned} \mathcal{E}_X &= E \left[ \int_{-\infty}^{\infty} X^2(t) dt \right] \\ &= \int_{-\infty}^{\infty} E[X^2(t)] dt \\ &= \int_{-\infty}^{\infty} R_X(t, t) dt \end{aligned} \quad (4.2.5)$$

and

$$\begin{aligned} P_X &= E \left[ \lim_{T \rightarrow \infty} \frac{1}{T} \int_{-T/2}^{T/2} X^2(t) dt \right] \\ &= \lim_{T \rightarrow \infty} \frac{1}{T} \int_{-T/2}^{T/2} E[X^2(t)] dt \\ &= \lim_{T \rightarrow \infty} \frac{1}{T} \int_{-T/2}^{T/2} R_X(t, t) dt \end{aligned} \quad (4.2.6)$$

If the process is stationary, then  $R_X(t, t) = R_X(0)$  is independent of  $t$ , and we have

$$P_X = R_X(0)$$

and

$$\mathcal{E}_X = \int_{-\infty}^{\infty} R_X(0) dt$$

It is seen that for stationary processes, if  $\mathcal{E}_X < \infty$ ; i.e., if the process is “energy-type,” then we have  $R_X(0) = E[X^2(t)] = 0$ . This means that for all  $t$ ,  $X(t)$  is zero with probability one. This shows that for the case of stationary processes, only power-type processes are of theoretical and practical interest.

If, in addition to being stationary, the process is also ergodic, then  $\mathcal{P}_X$  is not random anymore, and for *each sample function of the process*, we have

$$P_i = P_X = R_X(0)$$

**Example 4.2.15**

For the process given in Example 4.2.3, which is both stationary and ergodic, we have

$$P_X = R_X(0) = \frac{A^2}{2} \cos(2\pi f_0 \tau) \Big|_{\tau=0} = \frac{A^2}{2}$$

This is, in fact, the power content of each sample function in this process since each realization is a sinusoidal waveform.

**Example 4.2.16**

For the process in Example 4.2.4, which is stationary but not ergodic, we have  $P_X = R_X(0) = \frac{1}{3}$ . In this case, for each sample, which is a constant waveform  $x$  where  $-1 \leq x \leq 1$ , the power is  $x^2$  and the power content of the process is simply  $E[X^2]$ .

**Example 4.2.17**

For the process of Example 4.2.5, which is neither stationary nor ergodic, we have

$$P_X = \lim_{T \rightarrow \infty} \frac{1}{T} \int_0^T R_X(t, t) dt$$

But

$$R_X(t, t) = \sigma^2 \min(t, t) = \sigma^2 t \quad \text{for all } t > 0.$$

Hence,

$$P_X = \lim_{T \rightarrow \infty} \frac{1}{T} \int_0^T \sigma^2 t dt = \infty$$

**Multiple Random Processes.** Multiple random processes arise naturally when dealing with statistical properties of two or more random processes defined on the same probability space. For example, take the case where we are dealing with a random process  $X(t)$  and we pass it through a linear time-invariant system. For each sample function input  $x(t; \omega_i)$ , we have a sample function output defined by  $y(t; \omega_i) = x(t; \omega_i) \star h(t)$ , where  $h(t)$  denotes the impulse response of the system. It is seen that for each  $\omega_i \in \Omega$ , we have two signals  $x(t; \omega_i)$  and  $y(t; \omega_i)$ . Therefore, we are dealing with two random processes  $X(t)$  and  $Y(t)$  defined on the same probability space. Although we can define many random processes on the same probability space, we hardly need anything beyond the case of two random processes in communication systems and, therefore, we will only treat this case. When dealing with two random processes, a natural question is the dependence between the random processes under consideration. To this end, we define independence of two random processes.

**Definition 4.2.10.** Two random processes  $X(t)$  and  $Y(t)$  are *independent* if for all  $t_1, t_2$ , the random variables  $X(t_1)$  and  $Y(t_2)$  are independent. Similarly,  $X(t)$  and  $Y(t)$  are *uncorrelated* if  $X(t_1)$  and  $Y(t_2)$  are uncorrelated for all  $t_1, t_2$ .

From the properties of random variables we know that independence of random processes results in their being uncorrelated, whereas, in general, uncorrelatedness does not imply independence, except for the important class of Gaussian processes for which the two properties are equivalent. We define the correlation function for the case of two random processes as follows.

**Definition 4.2.11.** The *cross-correlation function* between two random processes  $X(t)$  and  $Y(t)$  is defined as

$$R_{XY}(t_1, t_2) = E[X(t_1)Y(t_2)]$$

It is seen from the above definition that, in general,

$$R_{XY}(t_1, t_2) = R_{YX}(t_2, t_1) \quad (4.2.7)$$

The concept of stationarity can also be generalized to joint stationarity for the case of two random processes as follows.

**Definition 4.2.12.** Two random processes  $X(t)$  and  $Y(t)$  are *jointly wide-sense stationary*, or simply *jointly stationary*, if both  $X(t)$  and  $Y(t)$  are individually stationary and the cross correlation function  $R_{XY}(t_1, t_2)$  depends only on  $\tau = t_1 - t_2$ .

**Example 4.2.18**

Assuming that the two random processes  $X(t)$  and  $Y(t)$  are jointly stationary, determine the autocorrelation function of the process  $Z(t) = X(t) + Y(t)$ .

**Solution** By definition

$$\begin{aligned} R_Z(t + \tau, t) &= E[Z(t + \tau)Z(t)] \\ &= E[(X(t + \tau) + Y(t + \tau))(X(t) + Y(t))] \\ &= R_X(\tau) + R_Y(\tau) + R_{XY}(\tau) + R_{XY}(-\tau) \end{aligned}$$

#### 4.2.4 Random Processes and Linear Systems

In the section on multiple random processes, we saw that when a random process passes through a linear time-invariant system the output is also a random process defined on the original probability space. In this section, we will study the properties of the output process based on the knowledge of the input process. We are assuming that a stationary process  $X(t)$  is the input to a linear time-invariant system with impulse response  $h(t)$ , and the output process is denoted by  $Y(t)$  as shown in Figure 4.16.

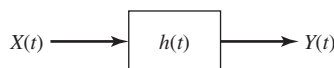


**Figure 4.16** A random process passing through a linear time-invariant system.

The following questions are of interest: Under what conditions will the output process be stationary? Under what conditions will the input and output processes be jointly stationary? How can we obtain the mean and autocorrelation of the output process and the crosscorrelation between the input and output processes. The following theorem answers these questions.

**Theorem 4.2.2.** If a stationary process  $X(t)$  with mean  $m_X$  and autocorrelation function  $R_X(\tau)$  is passed through a linear time-invariant system with impulse response  $h(t)$ , the input and output processes  $X(t)$  and  $Y(t)$  will be jointly stationary with

$$m_Y = m_X \int_{-\infty}^{\infty} h(t) dt \quad (4.2.8)$$

$$R_{XY}(\tau) = R_X(\tau) \star h(-\tau) \quad (4.2.9)$$

$$R_Y(\tau) = R_X(\tau) \star h(\tau) \star h(-\tau) \quad (4.2.10)$$

*Proof.* By noting that  $Y(t) = \int_{-\infty}^{\infty} X(\tau)h(t - \tau) d\tau$ , we see that

$$\begin{aligned} m_Y(t) &= E \left[ \int_{-\infty}^{\infty} X(\tau)h(t - \tau) d\tau \right] \\ &= \int_{-\infty}^{\infty} E[X(\tau)]h(t - \tau) d\tau \\ &= \int_{-\infty}^{\infty} m_X h(t - \tau) d\tau \\ &\stackrel{u=t-\tau}{=} m_X \int_{-\infty}^{\infty} h(u) du \end{aligned}$$

This proves that  $m_Y$  is independent of  $t$  and concludes the first part of the theorem.

For the second part, we have

$$\begin{aligned} R_{XY}(t_1, t_2) &= E[X(t_1)Y(t_2)] \\ &= E \left[ X(t_1) \int_{-\infty}^{\infty} X(s)h(t_2 - s) ds \right] \\ &= \int_{-\infty}^{\infty} E[X(t_1)X(s)]h(t_2 - s) ds \\ &= \int_{-\infty}^{\infty} R_X(t_1 - s)h(t_2 - s) ds \\ &\stackrel{u=s-t_2}{=} \int_{-\infty}^{\infty} R_X(t_1 - t_2 - u)h(-u) du \\ &= \int_{-\infty}^{\infty} R_X(\tau - u)h(-u) du \\ &= R_X(\tau) \star h(-\tau) \end{aligned}$$

The last relation shows that  $R_{XY}(t_1, t_2)$  depends only on  $\tau$ . Therefore, if we prove the third part of the theorem, we have also proved that the input and the output are jointly stationary.

To prove the third part (and hence, finish the proof of the second part) of the theorem, we use the result we obtained above. We observe that

$$\begin{aligned}
 R_Y(t_1, t_2) &= E[Y(t_1)Y(t_2)] \\
 &= E \left[ \left( \int_{-\infty}^{\infty} X(s)h(t_1 - s) ds \right) Y(t_2) \right] \\
 &= \int_{-\infty}^{\infty} R_{XY}(s - t_2)h(t_1 - s) ds \\
 &\stackrel{u=s-t_2}{=} \int_{-\infty}^{\infty} R_{XY}(u)h(t_1 - t_2 - u) du \\
 &= R_{XY}(\tau) \star h(\tau) \\
 &= R_X(\tau) \star h(-\tau) \star h(\tau)
 \end{aligned}$$

where in the last step we have used the result of the preceding step. This shows that  $R_Y$ , the autocorrelation function of the output depends only on  $\tau$  and, hence, the output process is stationary. Therefore, the input and output processes are jointly stationary. ■

#### Example 4.2.19

Assume a stationary process passes through a differentiator. What are the mean and autocorrelation function of the output and what is the cross correlation between the input and output?

**Solution** In a differentiator  $h(t) = \delta'(t)$ . Since  $\delta'(t)$  is odd, it follows that

$$m_Y = m_X \int_{-\infty}^{\infty} \delta'(t) dt = 0$$

and

$$R_{XY} = R_X(\tau) \star \delta'(-\tau) = -R_X(\tau) \star \delta'(\tau) = -\frac{d}{d\tau} R_X(\tau)$$

and

$$R_Y(\tau) = -\frac{d}{d\tau} R_X(\tau) \star \delta'(\tau) = -\frac{d^2}{d\tau^2} R_X(\tau)$$

#### Example 4.2.20

Repeat the previous example for the case where the LTI system is a quadrature filter defined by  $h(t) = \frac{1}{\pi t}$  and, therefore,  $H(f) = -j \operatorname{sgn}(f)$ . The output of the filter is the Hilbert transform of the input in this case (see Section 2.5).

**Solution** We have

$$m_Y = m_X \int_{-\infty}^{\infty} \frac{1}{\pi t} dt = 0$$

because  $\frac{1}{\pi t}$  is an odd function. Also, we have

$$R_{XY}(\tau) = R_X(\tau) \star \frac{1}{-\pi \tau} = -\hat{R}_X(\tau)$$

and

$$R_Y(\tau) = R_{XY}(\tau) \star \frac{1}{\pi \tau} = -\widehat{\hat{R}}_X(\tau) = R_X(\tau)$$

where we have used the fact that  $\widehat{\hat{x}}(t) = -x(t)$ , and assumed that the  $R_X(\tau)$  has no dc component (see Problem 2.50).

## 4.3 RANDOM PROCESSES IN THE FREQUENCY DOMAIN

In the last part of the previous section, we dealt with the passage of random processes through linear systems. We saw that if a stationary process passes through an LTI system, the input and output will be jointly stationary. We also found a relation between the input and output autocorrelation functions and the crosscorrelation function between the input and the output. In Chapter 2, we have seen that using frequency domain techniques greatly simplifies the input–output relation of linear systems. A natural question now is: How can frequency-domain analysis techniques be applied to the case of LTI systems with random inputs? Our main objective in this section is to develop the necessary techniques that can be used in the frequency-domain analysis of LTI systems when driven by random inputs.

A first attempt would be to define Fourier transforms for each sample function of the random process  $x(t; \omega_i)$ , and thus, to define a new process with variable  $f$  on the original probability space. The problem with this approach is that there is no guarantee that all the samples of the random process possess Fourier transforms. In fact, for many processes we can not define a Fourier transform for individual sample functions.

Another approach would be to look at the input–output power spectra. This approach is inspired by the convolution integral relation that exists between input and output autocorrelation functions when a system is driven by a random input signal, and also by the close relationship between the power spectrum of deterministic signals and their time-average autocorrelation functions as seen in Section 2.3. But prior to a formal definition, we have to see what we mean by the power-spectral density of a stochastic process.

### 4.3.1 Power Spectrum of Stochastic Processes

The power spectrum of a stochastic process is a natural extension of the definition of the power spectrum for deterministic signals when the statistical nature of the process is also taken into account.

Let  $X(t)$  denote a random process and let  $x(t; \omega_i)$  denote a sample function of this process. To define the power-spectral density for this sample function, we truncate



it by defining

$$x_T(t; \omega_i) = \begin{cases} x(t; \omega_i), & |t| < T/2 \\ 0, & \text{otherwise} \end{cases}$$

By truncating the signal, we make sure that the result is an energy-type signal, and therefore, possesses a Fourier transform, which we denote by  $X_T(f)$ . From the definition of the energy-spectral density for energy-type signals, we know that the energy-spectral density for this signal is simply  $|X_T(f)|^2$ . Having the energy-spectral density we can *define* the power-spectral density as the average energy-spectral density per unit of time; i.e.,  $\frac{|X_T(f)|^2}{T}$ . Now, by letting  $T$  become arbitrarily large, we define the power-spectral density for the sample function being considered, and we can denote it by  $S_{x_i}(f)$ .

It is obvious that, in general, various sample functions give rise to various  $S_{x_i}(f)$ 's; i.e., for each  $f$  we have a random variable denoting the amount of power at that frequency in each sample function. It makes sense to define the power spectrum as the ensemble average of these values; i.e.,

$$S_X(f) \stackrel{\text{def}}{=} E \left[ \lim_{T \rightarrow \infty} \frac{|X_T(f)|^2}{T} \right] = \lim_{T \rightarrow \infty} \frac{E[|X_T(f)|^2]}{T} \quad (4.3.1)$$

Equation (4.3.1) of the power-spectral density is a straightforward generalization of the corresponding relation for the case of deterministic signals. Although this definition is quite intuitive, using it to find the power-spectral density is not always easy.

#### Example 4.3.1

Find the power-spectral density for the process defined in Example 4.2.4.

**Solution** Let  $X$  denote a random variable uniformly distributed on  $[-1, 1]$ . Then, the truncated random signal is simply

$$X_T(t) = X \Pi\left(\frac{t}{T}\right)$$

Hence,

$$X_T(f) = XT \operatorname{sinc}(Tf)$$

and

$$S_X(f) = \lim_{T \rightarrow \infty} E(X^2)T \operatorname{sinc}^2(Tf)$$

Noting that  $E(X^2) = 1/3$ , we have to find  $\lim_{T \rightarrow \infty} T \operatorname{sinc}^2(Tf)$ . But  $T \operatorname{sinc}^2(Tf)$  is the Fourier transform of  $\Lambda(\frac{t}{T})$ , and as  $T$  goes to infinity, this function goes to 1. Therefore,

$$\lim_{T \rightarrow \infty} T \operatorname{sinc}^2(Tf) = \delta(f)$$

and  $S_X(f) = \frac{1}{3}\delta(f)$ .

There exists a very important theorem known as the *Wiener-Khinchin theorem* that gives the power-spectral density of a random process in terms of its autocorrelation functions.

**Theorem 4.3.1 [Wiener-Khinchin].** If for all finite  $\tau$  and any interval  $\mathcal{A}$  of length  $|\tau|$ , the autocorrelation function of the random process  $X(t)$  satisfies the condition

$$\left| \int_{\mathcal{A}} R_X(t + \tau, t) dt \right| < \infty \quad (4.3.2)$$

then the power-spectral density of  $X(t)$  is the Fourier transform of  $\langle R_X(t + \tau, t) \rangle$  where

$$\langle R_X(t + \tau, t) \rangle \stackrel{\text{def}}{=} \lim_{T \rightarrow \infty} \frac{1}{T} \int_{-T/2}^{T/2} R_X(t + \tau, t) dt \quad (4.3.3)$$

*Proof.* We begin with the definition of the power-spectral density of a random process

$$\mathcal{S}_X(f) = \lim_{T \rightarrow \infty} \frac{1}{T} E |X_T(f)|^2$$

where

$$X_T(f) = \int_{-T/2}^{T/2} X(t) e^{-j2\pi f t} dt$$

Substituting for  $X_T(f)$ , we have

$$\begin{aligned} \mathcal{S}_X(f) &= \lim_{T \rightarrow \infty} \frac{1}{T} E \left[ \int_{-T/2}^{T/2} X(s) e^{-j2\pi f s} ds \int_{-T/2}^{T/2} X(t) e^{+j2\pi f t} dt \right] \\ &= \lim_{T \rightarrow \infty} \frac{1}{T} \int_{-T/2}^{T/2} \int_{-T/2}^{T/2} R_X(s, t) e^{-j2\pi f (s-t)} dt ds \end{aligned}$$

Now we proceed by finding the inverse Fourier transform of the above and showing that it equals  $\langle R_X(t + \tau, t) \rangle$ . We start with

$$\begin{aligned} \mathcal{F}^{-1}[\mathcal{S}_X(f)] &= \lim_{T \rightarrow \infty} \frac{1}{T} \int_{-\infty}^{\infty} e^{+j2\pi f \tau} \int_{-T/2}^{T/2} \int_{-T/2}^{T/2} R_X(s, t) e^{-j2\pi f (s-t)} dt ds df \\ &= \lim_{T \rightarrow \infty} \frac{1}{T} \int_{-T/2}^{T/2} \int_{-T/2}^{T/2} R_X(s, t) dt ds \int_{-\infty}^{\infty} e^{j2\pi f [\tau - (s-t)]} df \end{aligned}$$

Using the fact that  $\mathcal{F}^{-1}[1] = \delta(t)$ , we have

$$\int_{-\infty}^{\infty} e^{j2\pi f [\tau - (s-t)]} df = \delta(\tau - s + t)$$

Substituting this result in the inverse Fourier transform, we obtain

$$\mathcal{F}^{-1}[\mathcal{S}_X(f)] = \lim_{T \rightarrow \infty} \frac{1}{T} \int_{-T/2}^{T/2} dt \int_{-T/2}^{T/2} R_X(s, t) \delta(\tau - s + t) ds$$

But,

$$\int_{-T/2}^{T/2} R_X(s, t) \delta(\tau - s + t) ds = \begin{cases} R_X(t + \tau, t), & -T/2 < t + \tau < T/2 \\ 0, & \text{otherwise} \end{cases}$$

Hence,

$$\mathcal{F}^{-1}[\mathcal{S}_X(f)] = \lim_{T \rightarrow \infty} \frac{1}{T} \int_{-T/2}^{T/2} \left\{ \begin{array}{ll} R_X(t + \tau, t), & -T/2 < t + \tau < T/2 \\ 0, & \text{otherwise} \end{array} \right\} dt$$

This can be written as

$$\mathcal{F}^{-1}[\mathcal{S}_X(f)] = \left\{ \begin{array}{ll} \lim_{T \rightarrow \infty} \frac{1}{T} \int_{-T/2}^{T/2-\tau} R_X(t + \tau, t) dt, & \tau > 0 \\ \lim_{T \rightarrow \infty} \frac{1}{T} \int_{-T/2-\tau}^{T/2} R_X(t + \tau, t) dt, & \tau < 0 \end{array} \right.$$

or

$$\mathcal{F}^{-1}[\mathcal{S}_X(f)] = \left\{ \begin{array}{ll} \lim_{T \rightarrow \infty} \frac{1}{T} \left[ \int_{-T/2}^{T/2} R_X(t + \tau, t) dt - \int_{T/2-\tau}^{T/2} R_X(t + \tau, t) dt \right], & \tau > 0 \\ \lim_{T \rightarrow \infty} \frac{1}{T} \left[ \int_{-T/2}^{T/2} R_X(t + \tau, t) dt - \int_{-T/2}^{-T/2-\tau} R_X(t + \tau, t) dt \right], & \tau < 0 \end{array} \right.$$

Since  $|\int_{\mathcal{A}} R_X(t + \tau, t) dt| < \infty$  for all  $\mathcal{A}$  of length  $\tau$ , as  $T \rightarrow \infty$  the second terms in the above brackets make no contribution. Therefore, by taking the Fourier transform of both sides, we have

$$\mathcal{S}_X(f) = \mathcal{F} \left[ \lim_{T \rightarrow \infty} \frac{1}{T} \int_{-T/2}^{T/2} R_X(t + \tau, t) dt \right] \quad (4.3.4)$$

This concludes the proof of the Wiener-Khinchin theorem.  $\blacksquare$

The following corollaries are immediate results of the Wiener-Khinchin theorem.

**Corollary 4.3.2.** If  $X(t)$  is a stationary process in which  $\tau R_X(\tau)$  remains finite for all finite  $\tau$ , then

$$\mathcal{S}_X(f) = \mathcal{F}[R_X(\tau)] \quad (4.3.5)$$

*Proof.* In this case the condition of the preceding theorem is satisfied and,

$$\langle R_X(t + \tau, t) \rangle = \lim_{T \rightarrow \infty} \frac{1}{T} \int_{-T/2}^{T/2} R_X(\tau) d\tau = R_X(\tau)$$

Applying the Wiener-Khinchin theorem gives the desired result.

**Corollary 4.3.3.** In a cyclostationary process, if

$$\left| \int_0^{T_0} R_X(t + \tau, t) dt \right| < \infty$$

then the condition of the Wiener-Khinchin theorem is satisfied (why?) and the power-spectral density is obtained from by

$$\mathcal{S}_X(f) = \mathcal{F}[\bar{R}_X(\tau)] \quad (4.3.6)$$

where

$$\bar{R}_X(\tau) \stackrel{\text{def}}{=} \frac{1}{T_0} \int_{-T_0/2}^{T_0/2} R_X(t + \tau, t) dt \quad (4.3.7)$$

and  $T_0$  is the period of the cyclostationary process.

*Proof.* The proof is immediate by noting that for a cyclostationary process

$$\lim_{T \rightarrow \infty} \frac{1}{T} \int_{-T/2}^{T/2} R_X(t + \tau, t) dt = \frac{1}{T_0} \int_{-T_0/2}^{T_0/2} R_X(t + \tau, t) dt$$

### Example 4.3.2

It was shown in Example 4.2.11, that if  $X(t)$  is stationary, then  $Y(t) = X(t) \cos(2\pi f_0 t)$  is a cyclostationary process with

$$R_Y(t + \tau, t) = R_X(\tau) \left[ \frac{1}{2} \cos(2\pi f_0 \tau) + \frac{1}{2} \cos(4\pi f_0 t + 2\pi f_0 \tau) \right] \quad (4.3.8)$$

Using the above corollary, we have

$$\begin{aligned} \bar{R}_Y(\tau) &= \frac{1}{T_0} \int_{-T_0/2}^{T_0/2} R_Y(t + \tau, t) dt \\ &= \frac{R_X(\tau)}{2} \cos(2\pi f_0 \tau) \end{aligned} \quad (4.3.9)$$

Therefore,

$$\begin{aligned} S_Y(f) &= \mathcal{F}[\bar{R}_Y(\tau)] \\ &= \frac{1}{4} [\mathcal{S}_X(f + f_0) + \mathcal{S}_X(f - f_0)] \end{aligned} \quad (4.3.10)$$

Based on the Wiener-Khinchin theorem the following observations are in order:

- To find the total power in the process it is enough to integrate the power-spectral density

$$\begin{aligned} P_X &= \int_{-\infty}^{\infty} \mathcal{S}_X(f) df \\ &= \langle R_X(t + \tau, t) \rangle \Big|_{\tau=0} \\ &= \lim_{T \rightarrow \infty} \frac{1}{T} \int_{-T/2}^{T/2} E[X(t + \tau)X(t)] dt \Big|_{\tau=0} \\ &= E \left[ \lim_{T \rightarrow \infty} \frac{1}{T} \int_{-T/2}^{T/2} X^2(t) dt \right] \end{aligned}$$

which is exactly the power content of a random process as defined in Section 2.3.

- For stationary and ergodic processes, each sample function  $x(t; \omega_i)$  is a deterministic function for which we can define the power-spectral density as given in Section 2.3. To this end we define the power-spectral density as the Fourier transform of the (time-average) autocorrelation function of  $x(t; \omega_i)$  defined by

$$R_{x(t; \omega_i)}(\tau) = \lim_{T \rightarrow \infty} \frac{1}{T} \int_{-T/2}^{T/2} x(t; \omega_i) x(t - \tau; \omega_i) dt$$

and

$$S_{x(t; \omega_i)} = \mathcal{F} [R_{x(t; \omega_i)}(\tau)]$$

Now, since the process is ergodic, the time average in the equation defining  $R_{x(t; \omega_i)}(\tau)$  is equal to the corresponding statistical average for all samples  $x(t; \omega_i)$ , namely,

$$\lim_{T \rightarrow \infty} \frac{1}{T} \int_{-T/2}^{T/2} x(t; \omega_i) x(t - \tau; \omega_i) dt = E[X(t)X(t - \tau)] = R_X(\tau)$$

and, therefore,

$$\mathcal{S}_X(f) = \mathcal{F}[R_X(\tau)] = \mathcal{S}_{x(t; \omega_i)}$$

This shows that *for stationary and ergodic processes the power-spectral density of each sample function is equal to the power-spectral density of the process.* In other words, each sample function is a good representative of the spectral characteristics of the entire process. Obviously, the power content of the process is also equal to the power content of each sample function.

- The power-spectral density was originally defined as

$$\lim_{T \rightarrow \infty} \frac{E[|X_T(f)|^2]}{T}$$

From this definition, it is obvious that the power-spectral density is always a real, non-negative and an even function of  $f$ . The fact that the power-spectral density is real and even is a direct consequence of the autocorrelation function being real and even, but non-negativeness of the power-spectral density is not a direct consequence of the properties of the autocorrelation function that we have studied so far.<sup>†</sup> Therefore we can add this property to the already mentioned properties of the autocorrelation function of a stationary process as given in Section 4.2.3.

### Example 4.3.3

For the stationary and ergodic random process in Example 4.2.3 we had

$$R_X(\tau) = \frac{A^2}{2} \cos(2\pi f_0 \tau)$$

Hence,

$$\mathcal{S}_X(f) = \frac{A^2}{4} [\delta(f - f_0) + \delta(f + f_0)]$$

The power-spectral density is shown in Figure 4.17. All the power content of the process is located at  $f_0$  and  $-f_0$  and this is expected because the sample functions of this process are sinusoids with their power at those frequencies.

<sup>†</sup>The fact that  $\mathcal{S}_X(f)$  is non-negative is a consequence of the fact that  $R_X(\tau)$  is *positive semi-definite* in the sense that for any signal  $g(t)$ , we have  $\int_{-\infty}^{\infty} \int_{-\infty}^{\infty} g(t) R_X(t - s) g(s) dt ds \geq 0$ .

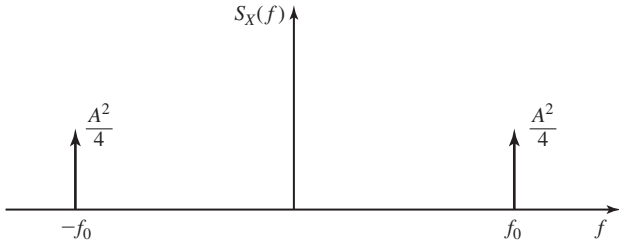


**Figure 4.17** Power-spectral density of the random process of Example 4.2.3.

#### Example 4.3.4

The process of Example 4.2.4 is stationary but not ergodic. In this case,

$$R_X(\tau) = E[X(t + \tau)X(t)] = E[X^2] = \frac{1}{3}$$

Hence,

$$S_X(f) = \mathcal{F}\left[\frac{1}{3}\right] = \frac{1}{3}\delta(f)$$

as was shown before without using the Wiener-Khinchin theorem. It is obvious that, in this case, for each realization of the process, we have a different power spectrum.

#### Example 4.3.5

The process given in Example 4.2.11 with  $x(t)$  as in Example 4.2.4, is cyclostationary with

$$R_X(t + \tau, t) = \frac{1}{6}[\cos(2\pi f_0(2t + \tau)) + \cos(2\pi f_0\tau)]$$

from which we obtain

$$\bar{R}_X(\tau) = \frac{1}{T_0} \int_{-T_0/2}^{T_0/2} R_X(t + \tau, t) dt = \frac{1}{6} \cos(2\pi f_0\tau)$$

Therefore,

$$S_X(f) = \frac{1}{12}[\delta(f - f_0) + \delta(f + f_0)]$$

### 4.3.2 Transmission over LTI Systems

We have already seen that, when a stationary random process with mean  $m_x$  and autocorrelation function  $R_X(\tau)$  passes through a linear time-invariant system with impulse response  $h(t)$ , the output process will be also stationary with mean

$$m_Y = m_X \int_{-\infty}^{\infty} h(t) dt$$

and autocorrelation

$$R_Y(\tau) = R_X(\tau) \star h(\tau) \star h(-\tau)$$

We have also seen that  $X(t)$  and  $Y(t)$  will be jointly stationary with crosscorrelation function

$$R_{XY}(\tau) = R_X(\tau) \star h(-\tau)$$

Translation of these relations into the frequency domain is straightforward. By noting that  $\mathcal{F}[h(-\tau)] = H^*(f)$  and  $\int_{-\infty}^{\infty} h(t) dt = H(0)$ , we have

$$m_Y = m_X H(0) \quad (4.3.11)$$

$$S_Y(f) = S_X(f) |H(f)|^2 \quad (4.3.12)$$

Equation (4.3.11) says that, since the mean of a random process is basically its dc value, the mean value of the response of the system only depends on the value of  $H(f)$  at  $f = 0$  (dc response). The second equation says that, when dealing with the power spectrum, the phase of  $H(f)$  is irrelevant; only the magnitude of  $H(f)$  affects the output power spectrum. This is also intuitive since power depends on the amplitude, and not the phase, of the signal.

We can also define a frequency domain relation for the autocorrelation function. Let us define the *cross-spectral density*  $\mathcal{S}_{XY}(f)$  as

$$\mathcal{S}_{XY}(f) \stackrel{\text{def}}{=} \mathcal{F}[R_{XY}(\tau)] \quad (4.3.13)$$

Then

$$\mathcal{S}_{XY}(f) = \mathcal{S}_X(f) H^*(f) \quad (4.3.14)$$

and since  $R_{YX}(\tau) = R_{XY}(-\tau)$ , we have

$$\mathcal{S}_{YX}(f) = \mathcal{S}_{XY}^*(f) = \mathcal{S}_X(f) H(f) \quad (4.3.15)$$

Note that, although  $\mathcal{S}_X(f)$  and  $\mathcal{S}_Y(f)$  are real non-negative functions,  $\mathcal{S}_{XY}(f)$  and  $\mathcal{S}_{YX}(f)$  can, in general, be complex functions. Figure 4.18 shows how the above quantities are related.

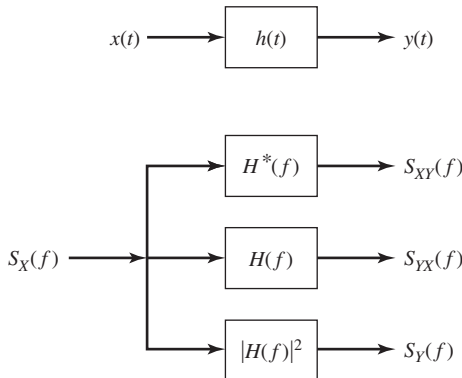


**Figure 4.18** Input–output relations for power-spectral density and cross-spectral density.

**Example 4.3.6**

If the process in Example 4.2.3 passes through a differentiator, we have  $H(f) = j2\pi f$  and, therefore,

$$S_Y(f) = 4\pi^2 f^2 \left[ \frac{A^2}{4} (\delta(f - f_0) + \delta(f + f_0)) \right] = A^2 \pi^2 f_0^2 [\delta(f - f_0) + \delta(f + f_0)]$$

and

$$S_{XY}(f) = (-j2\pi f) S_X(f) = \frac{jA^2 \pi f_0}{2} [\delta(f + f_0) - \delta(f - f_0)]$$

**Example 4.3.7**

Passing the process in Example 4.2.4 through a differentiator results in

$$\begin{aligned} S_Y(f) &= 4\pi^2 f^2 \left( \frac{1}{3} \delta(f) \right) = 0 \\ S_{XY}(f) &= (-j2\pi f) \left( \frac{1}{3} \delta(f) \right) = 0 \end{aligned}$$

These results are intuitive because the sample functions of this process are constant and differentiating them results in zero output.

**Power-Spectral Density of a Sum Process.** In practice, we often encounter the sum of two random processes. For example, in the case of communication over a channel with additive noise, the noise process is added to the signal process. Next, we determine the power-spectral density for the sum of two jointly stationary processes.

Let us assume that  $Z(t) = X(t) + Y(t)$  where  $X(t)$  and  $Y(t)$  are jointly stationary random processes. We already know that  $Z(t)$  is a stationary process with

$$R_Z(\tau) = R_X(\tau) + R_Y(\tau) + R_{XY}(\tau) + R_{YX}(\tau) \quad (4.3.16)$$

Taking the Fourier transform of both sides of this equation and using the result of Problem 4.50, we obtain

$$\begin{aligned} S_Z(f) &= S_X(f) + S_Y(f) + S_{XY}(f) + \underbrace{S_{YX}(f)}_{S_{XY}^*(f)} \\ &= S_X(f) + S_Y(f) + 2 \operatorname{Re} [S_{XY}(f)] \end{aligned} \quad (4.3.17)$$

Equation (4.3.17) shows that the power-spectral density of the sum process is the sum of the power spectra of the individual processes plus a third term which depends on the correlation between the two processes.

If the two processes  $X(t)$  and  $Y(t)$  are uncorrelated, then

$$R_{XY}(\tau) = m_X m_Y$$

Now, if at least one of the processes is zero mean we will have  $R_{XY}(\tau) = 0$  and

$$S_Z(f) = S_X(f) + S_Y(f) \quad (4.3.18)$$



**Example 4.3.8**

Let  $X(t)$  represent the process in Example 4.2.3, and let  $Z(t) = X(t) + \frac{d}{dt}X(t)$ . Then,

$$S_{XY}(f) = \frac{jA^2\pi f_0}{2} [\delta(f + f_0) - \delta(f - f_0)]$$

and, therefore,

$$\text{Re}[S_{XY}(f)] = 0$$

Hence,

$$S_Z(f) = S_X(f) + S_Y(f) = A^2\left(\frac{1}{4} + \pi^2 f_0^2\right)[\delta(f - f_0) + \delta(f + f_0)]$$

## 4.4 GAUSSIAN AND WHITE PROCESSES

Gaussian processes play an important role in communication systems. The fundamental reason for their importance is that thermal noise in electronic devices, which is produced by random movement of electrons due to thermal agitation, can be closely modeled by a Gaussian process. The reason for the Gaussian behavior of thermal noise is that the current introduced by movement of electrons in an electric circuit can be regarded as the sum of small currents of a very large number of sources, namely individual electrons. It can be assumed that at least a majority of these sources behave independently and, therefore, the total current is the sum of a large number of i.i.d. random variables. Now by applying the central limit theorem, this total current has a Gaussian distribution.

Apart from thermal noise, Gaussian processes provide rather good models for some information sources as well. Some interesting properties of the Gaussian processes, which will be discussed in this section, make these processes mathematically tractable and easy to deal with.

### 4.4.1 Gaussian Processes

We start our discussion with a formal definition of Gaussian processes.

**Definition 4.4.1.** A random process  $X(t)$  is a *Gaussian process* if for all  $n$  and all  $(t_1, t_2, \dots, t_n)$ , the random variables  $\{X(t_i)\}_{i=1}^n$  have a jointly Gaussian density function.

From the above definition it is seen that, in particular, at any time instant  $t_0$  the random variable  $X(t_0)$  is Gaussian, and at any two points  $t_1, t_2$  random variables  $(X(t_1), X(t_2))$  are distributed according to a two-dimensional Gaussian random variable. Moreover, since a complete statistical description of  $\{X(t_i)\}_{i=1}^n$  depends only on  $\mathbf{m}$  and  $\mathbf{C}$ , the mean and autocovariance matrices, we have the following theorem.

**Theorem 4.4.1.** For Gaussian processes, knowledge of the mean and autocorrelation; i.e.,  $m_X(t)$  and  $R_X(t_1, t_2)$  gives a complete statistical description of the process. ■

The following theorem is of fundamental importance in dealing with Gaussian processes.

**Theorem 4.4.2.** If the Gaussian process  $X(t)$  is passed through an LTI system, then the output process  $Y(t)$  will also be a Gaussian process.

*Proof.* To prove that  $Y(t)$  is Gaussian we have to prove that for all  $n$  and all  $\{t_i\}_{i=1}^n$ , the vector  $(Y(t_1), Y(t_2), \dots, Y(t_n))$  is a Gaussian vector. In general, we have

$$Y(t_i) = \int_{-\infty}^{\infty} X(\tau)h(t_i - \tau) d\tau = \lim_{N \rightarrow \infty} \lim_{\Delta \rightarrow 0} \sum_{j=-N}^{j=N} X(j\Delta)h(t_i - j\Delta)$$

Hence,

$$\begin{cases} Y(t_1) = \lim_{N \rightarrow \infty} \lim_{\Delta \rightarrow 0} \sum_{j=-N}^{j=N} X(j\Delta)h(t_1 - j\Delta) \\ Y(t_2) = \lim_{N \rightarrow \infty} \lim_{\Delta \rightarrow 0} \sum_{j=-N}^{j=N} X(j\Delta)h(t_2 - j\Delta) \\ \vdots \\ Y(t_n) = \lim_{N \rightarrow \infty} \lim_{\Delta \rightarrow 0} \sum_{j=-N}^{j=N} X(j\Delta)h(t_n - j\Delta) \end{cases}$$

Since  $\{X(j\Delta)\}_{j=-N}^N$  is a Gaussian vector and random variables  $(Y(t_1), Y(t_2), \dots, Y(t_n))$  are linear combinations of random variables  $\{X(j\Delta)\}_{j=-N}^N$ , we conclude that they are also jointly Gaussian. ■

This theorem is a very important result and demonstrates one of the nice properties of Gaussian processes that makes them attractive. For a non-Gaussian process, knowledge of the statistical properties of the input process does not easily lead to the statistical properties of the output process. For Gaussian processes, we know that the output process of an LTI system will also be Gaussian. Hence, a complete statistical description of the output process requires only knowledge of the mean and autocorrelation functions of it. Therefore, it only remains to find the mean and the autocorrelation function of the output process and, as we have already seen in Section 4.2.4, this is an easy task.

Note that the above results hold for all Gaussian processes regardless of stationarity. Since a complete statistical description of Gaussian processes depends only on  $m_X(t)$  and  $R_X(t_1, t_2)$ , we have also the following theorem.

**Theorem 4.4.3.** For Gaussian processes, WSS and strict stationarity are equivalent. ■

We also state the following theorem without proof. This theorem gives sufficient conditions for the ergodicity of zero-mean stationary Gaussian processes. For a proof, see Wong and Hajek (1985).

**Theorem 4.4.4.** A sufficient condition for the ergodicity of the stationary zero-mean Gaussian process  $X(t)$  is that

$$\int_{-\infty}^{\infty} |R_X(\tau)| d\tau < \infty \quad \blacksquare$$

Parallel to the definition of jointly Gaussian random variables we can define *jointly Gaussian random processes*.

**Definition 4.4.2.** The random processes  $X(t)$  and  $Y(t)$  are *jointly Gaussian* if for all  $n, m$  and all  $(t_1, t_2, \dots, t_n)$  and  $(\tau_1, \tau_2, \dots, \tau_m)$ , the random vector  $(X(t_1), X(t_2), \dots, X(t_n), Y(\tau_1), Y(\tau_2), \dots, Y(\tau_m))$  is distributed according to an  $n + m$  dimensional jointly Gaussian distribution.

We have also the following important theorem:

**Theorem 4.4.5.** For jointly Gaussian processes, uncorrelatedness and independence are equivalent.

*Proof.* This is also a straightforward consequence of the basic properties of Gaussian random variables as outlined in our discussion of jointly Gaussian random variables. ■

#### 4.4.2 White Processes

The term *white process* is used to denote the processes in which all frequency components appear with equal power; i.e., the power-spectral density is a constant for all frequencies. This parallels the notion of “white light” in which all colors exist.

**Definition 4.4.3.** A process  $X(t)$  is called a *white process* if it has a flat spectral density; i.e., if  $\mathcal{S}_X(f)$  is a constant for all  $f$ .

The importance of white processes in practice stems from the fact that thermal noise can be closely modeled as a white process over a wide range of frequencies. Also, a wide range of processes used to describe a variety of information sources can be modeled as the output of LTI systems driven by a white process. Figure 4.19 shows the power spectrum of a white process.

If we find the power content of a white process using  $\mathcal{S}_X(f) = C$ , a constant, we will have

$$P_X = \int_{-\infty}^{\infty} \mathcal{S}_X(f) df = \int_{-\infty}^{\infty} C df = \infty$$

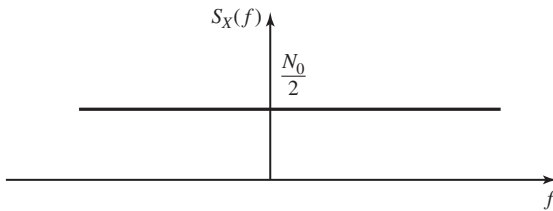


**Figure 4.19** Power-spectral density of a white process.

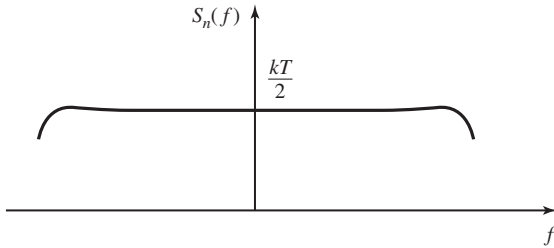


**Figure 4.20** Power spectrum of thermal noise.

Obviously, no real physical process can have infinite power and, therefore, a white process is not a meaningful physical process. However, quantum mechanical analysis of the thermal noise shows that it has a power-spectral density given by

$$\mathcal{S}_n(f) = \frac{\hbar f}{2(e^{\hbar f/kT} - 1)} \quad (4.4.1)$$

in which  $\hbar$  denotes *Planck's constant* (equal to  $6.6 \times 10^{-34}$  Joules  $\times$  second) and  $k$  is *Boltzmann's constant* (equal to  $1.38 \times 10^{-23}$  Joules/Kelvin).  $T$  denotes the temperature in degrees Kelvin. This power spectrum is shown in Figure 4.20.

The above spectrum achieves its maximum at  $f = 0$  and the value of this maximum is  $\frac{kT}{2}$ . The spectrum goes to zero as  $f$  goes to infinity, but the rate of convergence to zero is very slow. For instance, at room temperature ( $T = 300$  K)  $\mathcal{S}_n(f)$  drops to 90% of its maximum at about  $f \approx 2 \times 10^{12}$  Hz, which is beyond the frequencies employed in conventional communication systems. From this we conclude that thermal noise, though not precisely white, for all practical purposes can be modeled as a white process with power spectrum equaling  $\frac{kT}{2}$ . The value  $kT$  is usually denoted by  $N_0$  and, therefore, the power-spectral density of thermal noise is usually given as  $\mathcal{S}_n(f) = \frac{N_0}{2}$ , and sometimes referred to as the *two-sided power-spectral density*, emphasizing that this spectrum extends to both positive and negative frequencies. We will avoid this terminology throughout and simply use *power spectrum* or *power-spectral density*.

Looking at the autocorrelation function for a white process, we see that

$$R_n(\tau) = \mathcal{F}^{-1} \left[ \frac{N_0}{2} \right] = \frac{N_0}{2} \delta(\tau)$$

This shows that for all  $\tau \neq 0$  we have  $R_X(\tau) = 0$ ; i.e., if we sample a white process at two points  $t_1$  and  $t_2$  ( $t_1 \neq t_2$ ), the resulting random variables will be uncorrelated. If in addition to being white, the random process is also Gaussian, the sampled random variables will also be independent.

In short, the thermal noise that we will use in subsequent chapters is assumed to be a stationary, ergodic, zero-mean, white Gaussian process whose power spectrum is  $\frac{N_0}{2} = \frac{kT}{2}$ .

**Noise-Equivalent Bandwidth.** When white Gaussian noise passes through a filter, the output process, although still Gaussian, will not be white anymore. The filter characteristics determine the spectral properties of the output process, and we have

$$S_Y(f) = S_X(f)|H(f)|^2 = \frac{N_0}{2}|H(f)|^2$$

Now, if we want to find the power content of the output process, we have to integrate  $S_Y(f)$ . Thus,

$$P_Y = \int_{-\infty}^{\infty} S_Y(f) df = \frac{N_0}{2} \int_{-\infty}^{\infty} |H(f)|^2 df$$

Therefore, to determine the output power, we have to evaluate the integral  $\int_{-\infty}^{\infty} |H(f)|^2 df$ . To do this calculation, we define  $B_{\text{neq}}$ , the *noise-equivalent bandwidth* of a filter with frequency response  $H(f)$ , as

$$B_{\text{neq}} = \frac{\int_{-\infty}^{\infty} |H(f)|^2 df}{2 H_{\text{max}}^2} \quad (4.4.2)$$

where  $H_{\text{max}}$  denotes the maximum of  $|H(f)|$  in the passband of the filter. Figure 4.21 shows  $H_{\text{max}}$  and  $B_{\text{neq}}$  for a typical filter.

Using the above definition, we have

$$\begin{aligned} P_Y &= \frac{N_0}{2} \int_{-\infty}^{\infty} |H(f)|^2 df \\ &= \frac{N_0}{2} \times 2 B_{\text{neq}} H_{\text{max}}^2 \\ &= N_0 B_{\text{neq}} H_{\text{max}}^2 \end{aligned} \quad (4.4.3)$$

Therefore, by having  $B_{\text{neq}}$ , finding the output noise power becomes a simple task. The noise-equivalent bandwidth of filters and amplifiers is usually provided by the manufacturer.

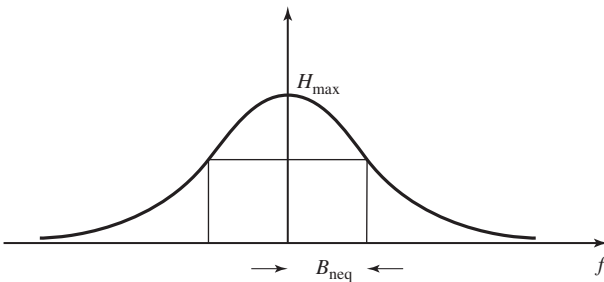


**Figure 4.21** Noise-equivalent bandwidth of a typical filter.

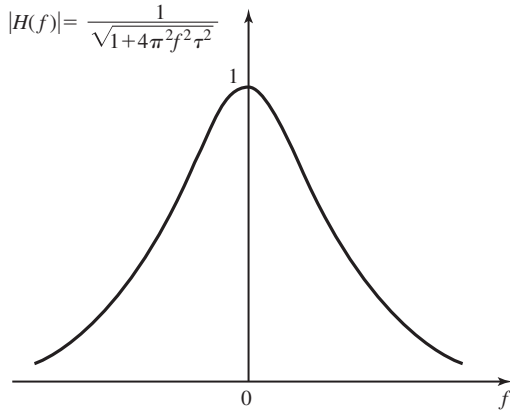


**Figure 4.22** Frequency response of a lowpass  $RC$  filter.

**Example 4.4.1**

Find the noise-equivalent bandwidth of a lowpass  $RC$  filter.

**Solution**  $H(f)$  for this filter is

$$H(f) = \frac{1}{1 + j2\pi f RC}$$

and is shown in Figure 4.22.

Defining  $\tau = RC$ , we have

$$|H(f)| = \frac{1}{\sqrt{1 + 4\pi^2 f^2 \tau^2}}$$

and, therefore,  $H_{\max} = 1$ . We also have

$$\begin{aligned} \int_{-\infty}^{\infty} |H(f)|^2 df &= 2 \int_0^{\infty} \frac{1}{\sqrt{1 + 4\pi^2 f^2 \tau^2}} df \\ &\stackrel{u=2\pi f\tau}{=} 2 \int_0^{\infty} \frac{1}{1 + u^2} \times \frac{du}{2\pi\tau} \\ &= \frac{1}{\pi\tau} \times \frac{\pi}{2} \\ &= \frac{1}{2\tau} \end{aligned}$$

Hence,

$$B_{\text{neq}} = \frac{\frac{1}{2\tau}}{2 \times 1} = \frac{1}{4RC}$$

## 4.5 BANDLIMITED PROCESSES AND SAMPLING

A bandlimited process is a random process whose power-spectral density occupies a finite bandwidth. In other words, a bandlimited process is a process with the property that for all  $|f| \geq W$ , we have  $\mathcal{S}_X(f) \equiv 0$  where  $W$  is the bandwidth of the process.

Almost all of the processes encountered in nature are bandlimited because there is a limit on the bandwidth of all physical systems. Bandlimited processes also arise when passing random processes through bandlimited linear systems. The output, usually called a “filtered process,” is a bandlimited process. The power-spectral density of a typical bandlimited process is shown in Figure 4.23.

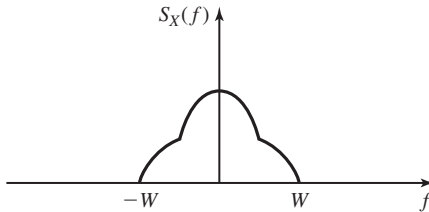


**Figure 4.23** Power spectrum of a bandlimited process.

We have already seen in Section 2.4 that for bandlimited signals there exists the powerful sampling theorem which states that the signal can be perfectly reconstructed from its sampled values as long as the sampling rate is more than twice the highest frequency component in the signal; i.e., the bandlimited signal can be expressed in terms of its samples taken at regular intervals  $T_s$ , where  $T_s \leq \frac{1}{2W}$ , by the relation

$$x(t) = \sum_{k=-\infty}^{\infty} 2WT_s x(kT_s) \operatorname{sinc}(2W(t - kT_s))$$

In the special case where  $T_s = \frac{1}{2W}$ , the above relation simplifies to

$$x(t) = \sum_{k=-\infty}^{\infty} x\left(\frac{k}{2W}\right) \operatorname{sinc}\left(2W\left(t - \frac{k}{2W}\right)\right)$$

One wonders if such a relation exists for bandlimited random processes. In other words, if it is possible to express a bandlimited process in terms of its sampled values. The following theorem, which is the sampling theorem for the bandlimited random processes, shows that this is in fact true.

**Theorem 4.5.1.** Let  $X(t)$  be a stationary bandlimited process; i.e.,  $\mathcal{S}_X(f) \equiv 0$  for  $|f| \geq W$ . Then the following relation holds

$$E \left| X(t) - \sum_{k=-\infty}^{\infty} X(kT_s) \operatorname{sinc}(2W(t - kT_s)) \right|^2 = 0 \quad (4.5.1)$$

where  $T_s = \frac{1}{2W}$  denotes the sampling interval.

*Proof.* Let us start by expanding the above relation. The left-hand side becomes

$$\begin{aligned} E \left| X(t) - \sum_{k=-\infty}^{\infty} X(kT_s) \operatorname{sinc}(2W(t - kT_s)) \right|^2 \\ = R_X(0) - 2 \sum_{k=-\infty}^{\infty} R_X(t - kT_s) \operatorname{sinc}(2W(t - kT_s)) \\ + \sum_{k=-\infty}^{\infty} \sum_{l=-\infty}^{\infty} R_X((k-l)T_s) \operatorname{sinc}(2W(t - kT_s)) \operatorname{sinc}(2W(t - lT_s)) \end{aligned}$$

Introducing the change of variable  $m = l - k$  in the last line of the above relation, we have

$$\begin{aligned} \sum_{k=-\infty}^{\infty} \sum_{l=-\infty}^{\infty} R_X((k-l)T_s) \operatorname{sinc}(2W(t - kT_s)) \operatorname{sinc}(2W(t - lT_s)) \\ = \sum_{k=-\infty}^{\infty} \sum_{m=-\infty}^{\infty} R_X(-mT_s) \operatorname{sinc}(2W(t - kT_s)) \operatorname{sinc}(2W(t - kT_s - mT_s)) \\ = \sum_{k=-\infty}^{\infty} \operatorname{sinc}(2W(t - kT_s)) \sum_{m=-\infty}^{\infty} R_X(mT_s) \operatorname{sinc}(2W(t - kT_s - mT_s)) \end{aligned}$$

where we have used the fact that  $R_X(-mT_s) = R_X(mT_s)$ .

The fact that the process is bandlimited means that the Fourier transform of  $R_X(\tau)$  is bandlimited to  $W$  and, therefore, for  $R_X(\tau)$  we have the expansion

$$R_X(t) = \sum_{k=-\infty}^{\infty} R_X(kT_s) \operatorname{sinc}[2W(t - kT_s)]$$

from which we obtain

$$\sum_{m=-\infty}^{\infty} R_X(mT_s) \operatorname{sinc}[2W(t - kT_s - mT_s)] = R_X(t - kT_s)$$

Therefore,

$$\begin{aligned} E \left| X(t) - \sum_{k=-\infty}^{\infty} X(kT_s) \operatorname{sinc}[2W(t - kT_s)] \right|^2 \\ = R_X(0) - 2 \sum_{k=-\infty}^{\infty} R_X(t - kT_s) \operatorname{sinc}[2W(t - kT_s)] \\ + \sum_{k=-\infty}^{\infty} R_X(t - kT_s) \operatorname{sinc}[2W(t - kT_s)] \\ = R_X(0) - \sum_{k=-\infty}^{\infty} R_X(t - kT_s) \operatorname{sinc}[2W(t - kT_s)] \end{aligned}$$



Now we can apply the result of Problem 2.42 to  $R_X(\tau)$  to obtain

$$R_X(0) = \sum_{k=-\infty}^{\infty} R_X(t - kT_s) \text{sinc}[2W(t - kT_s)]$$

Substituting this result in the expression for  $E[X(t)]$ , we obtain

$$E \left| X(t) - \sum_{k=-\infty}^{\infty} X(kT_s) \text{sinc}[2W(t - kT_s)] \right|^2 = 0$$

This concludes the proof of the theorem. ■

This result is a parallel to the sampling theorem for deterministic signals developed in Section 2.4. Note that, due to the random nature of the entities involved in this case, the equality of  $X(t)$  and  $\sum_{k=-\infty}^{\infty} X(kT_s) \text{sinc}[2W(t - kT_s)]$  is not pointwise, and we can only say that

$$E \left| X(t) - \sum_{k=-\infty}^{\infty} X(kT_s) \text{sinc}[2W(t - kT_s)] \right|^2 = 0$$

This is usually called *equality in quadratic mean* or *equality in the mean-squared sense* and denoted by

$$X(t) \stackrel{\text{q.m.}}{=} \sum_{k=-\infty}^{\infty} X(kT_s) \text{sinc}[2W(t - kT_s)] \quad (4.5.2)$$

Now that we have seen that a bandlimited process can be recovered from its sampled values taken at  $1/2W$  intervals, an interesting question is whether or not these samples are uncorrelated. It can be shown that a necessary and sufficient condition for the uncorrelatedness of these samples is that the power spectrum of the process be flat over the passband; i.e.

$$\mathcal{S}_x(f) = \begin{cases} K & |f| < W \\ 0, & \text{otherwise} \end{cases}$$

Unless this condition is satisfied, the samples of the process will be correlated and this correlation can be exploited to make their transmission easier. This fact will be further explored in Chapter 6.

## 4.6 BANDPASS PROCESSES

Bandpass random processes are the equivalents of bandpass deterministic signals. A bandpass process has all its power located in the neighborhood of some central frequency  $f_0$ .

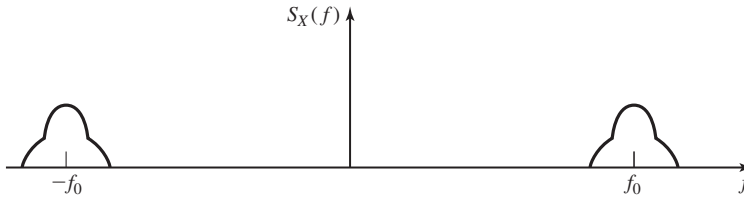


**Figure 4.24** Power spectrum of a bandpass process.

**Definition 4.6.1.**  $X(t)$  is a *bandpass* or *narrowband* process if  $S_X(f) \equiv 0$  for  $|f - f_0| \geq W$ , where  $W < f_0$ .

Although the term *narrowband process* is usually used for the case where  $W \ll f_0$ , we will use both terms *bandpass process* and *narrowband process* interchangeably. Figure 4.24 shows the power spectrum of a bandpass process.

Note that, as in Section 2.5, there is no need for  $f_0$  to be the mid-band frequency, or, in general, there is even no need for  $f_0$  to be in the frequency band of the process.

Bandpass processes are suitable for modeling modulated signals. A random process is usually modulated on a carrier for transmission over a communication channel and the resulting process is a bandpass process. The noise that passes through a bandpass filter at the front end of a receiver is also a bandpass process.

As we have seen in Section 2.5, there are certain ways to express bandpass signals in terms of equivalent lowpass signals. The purpose of this section is to generalize those results to the case of random processes. As we will see, many of the results of Section 2.5 can be generalized in a straightforward manner to bandpass processes.

Let  $X(t)$  be a bandpass process as defined above. Then  $R_X(\tau)$  is a deterministic bandpass signal whose Fourier transform  $S_X(f)$  is nonzero in the neighborhood of  $f_0$ . If  $X(t)$  is passed through a quadrature filter with impulse response  $\frac{1}{\pi t}$ , and transfer function  $H(f) = -j \operatorname{sgn}(f)$ , the output process is the Hilbert transform of the input process, and according to Example 4.2.20, we have

$$R_{X\hat{X}}(\tau) = -\hat{R}_X(\tau)$$

$$R_{\hat{X}}(\tau) = R_X(\tau)$$

Now, parallel to the deterministic case, let us define two new processes  $X_c(t)$  and  $X_s(t)$  by

$$X_c(t) = X(t) \cos(2\pi f_0 t) + \hat{X}(t) \sin(2\pi f_0 t)$$

$$X_s(t) = \hat{X}(t) \cos(2\pi f_0 t) - X(t) \sin(2\pi f_0 t)$$

As in the deterministic case,  $X_c(t)$  and  $X_s(t)$  are called *in-phase* and *quadrature* components of the process  $X(t)$ . Throughout the rest of this chapter, we will assume that the process  $X(t)$  is stationary with zero mean and, based on this assumption, explore the properties of its in-phase and quadrature components.

**Theorem 4.6.1.** If  $X(t)$  is a zero-mean stationary bandpass process, the processes  $X_c(t)$  and  $X_s(t)$  will be zero-mean jointly stationary processes.

*Proof.* The fact that both  $X_c(t)$  and  $X_s(t)$  are zero mean is trivial. It remains to prove that  $R_{X_c}(t + \tau, t)$ ,  $R_{X_s}(t + \tau, t)$ , and  $R_{X_c X_s}(t + \tau, t)$  are functions of  $\tau$  only. We have

$$\begin{aligned}
 R_{X_c}(t + \tau, t) &= E[X_c(t + \tau)X_c(t)] \\
 &= E[(X(t + \tau) \cos(2\pi f_0(t + \tau)) + \hat{X}(t + \tau) \sin(2\pi f_0(t + \tau))) \\
 &\quad \times (X(t) \cos(2\pi f_0 t) + \hat{X}(t) \sin(2\pi f_0 t))] \\
 &= R_X(\tau) \cos(2\pi f_0 t) \cos(2\pi f_0(t + \tau)) - \hat{R}_X(\tau) \sin(2\pi f_0 t) \cos(2\pi f_0(t + \tau)) \\
 &\quad + \hat{R}_X(\tau) \cos(2\pi f_0 t) \sin(2\pi f_0(t + \tau)) + R_X(\tau) \sin(2\pi f_0 t) \sin(2\pi f_0(t + \tau)) \\
 &= R_X(\tau) \cos(2\pi f_0 \tau) + \hat{R}_X(\tau) \sin(2\pi f_0 \tau)
 \end{aligned}$$

where we have used results of Example 4.2.20 and the fact that  $\hat{R}_X(\tau)$  is an odd function, because it is the Hilbert transform of an even function (see Problem 2.46).

It can be proved similarly that

$$R_{X_s}(\tau) = R_X(\tau) \cos(2\pi f_0 \tau) + \hat{R}_X(\tau) \sin(2\pi f_0 \tau)$$

and

$$R_{X_c X_s}(\tau) = R_X(\tau) \sin(2\pi f_0 \tau) - \hat{R}_X(\tau) \cos(2\pi f_0 \tau)$$

In conclusion, we have the following relations to which we will refer frequently

$$\begin{cases} R_{X_c}(\tau) = R_{X_s}(\tau) = R_X(\tau) \cos(2\pi f_0 \tau) + \hat{R}_X(\tau) \sin(2\pi f_0 \tau) \\ R_{X_c X_s}(\tau) = R_X(\tau) \sin(2\pi f_0 \tau) - \hat{R}_X(\tau) \cos(2\pi f_0 \tau) \end{cases} \quad (4.6.1)$$

This concludes the proof of the theorem. ■

**Theorem 4.6.2.**  $X_c(t)$  and  $X_s(t)$  are lowpass processes; i.e., their power spectrum vanishes for  $|f| \geq W$ .

*Proof.* Note that  $R_{X_c}(\tau)$  and  $R_{X_s}(\tau)$  are deterministic signals. Comparing

$$R_{X_c}(\tau) = R_{X_s}(\tau) = R_X(\tau) \cos(2\pi f_0 \tau) + \hat{R}_X(\tau) \sin(2\pi f_0 \tau)$$

with the corresponding relations for deterministic signals as developed in Section 2.5, we observe that the relations describing both  $R_{X_c}(\tau)$  and  $R_{X_s}(\tau)$  are exactly the same relations that describe  $x_c(t)$ , the in-phase component of a deterministic bandpass signal  $x(t)$ . This means that  $R_{X_c}(\tau)$  and  $R_{X_s}(\tau)$  are both lowpass signals. This, in turn, means that the Fourier transform of these signals; i.e.,  $\mathcal{S}_{X_c}(f)$  and  $\mathcal{S}_{X_s}(f)$  are bandlimited to  $|f| < W$  and, therefore, the theorem is proved. ■

From the above theorems it is seen that the processes  $X_c(t)$  and  $X_s(t)$  play the same role as the in-phase and quadrature components for deterministic signals and, therefore, they are called the in-phase and quadrature processes. Furthermore, we have seen that these processes are jointly stationary with *the same power-spectral density*. Parallel to the deterministic case, we can also define the envelope and phase processes by

$$V(t) = \sqrt{X_c^2(t) + X_s^2(t)} \quad (4.6.2)$$

$$\Theta(t) = \arctan \frac{X_s(t)}{X_c(t)} \quad (4.6.3)$$

To find the power spectrum of the in-phase and quadrature components, we have

$$\begin{aligned} \mathcal{S}_{X_c}(f) &= \mathcal{S}_{X_s}(f) \\ &= \mathcal{F}[R_X(\tau) \cos(2\pi f_0 \tau) + \hat{R}_X \sin(2\pi f_0 \tau)] \\ &= \frac{\mathcal{S}_X(f - f_0)}{2} + \frac{\mathcal{S}_X(f + f_0)}{2} \\ &\quad + [-j \operatorname{sgn}(f) \mathcal{S}_X(f)] \star \left[ \frac{\delta(f - f_0) - \delta(f + f_0)}{2j} \right] \\ &= \frac{\mathcal{S}_X(f - f_0)}{2} + \frac{\mathcal{S}_X(f + f_0)}{2} \\ &\quad + \frac{1}{2} \operatorname{sgn}(f + f_0) \mathcal{S}_X(f + f_0) - \frac{1}{2} \operatorname{sgn}(f - f_0) \mathcal{S}_X(f - f_0) \\ &= \frac{\mathcal{S}_X(f - f_0)}{2} [1 - \operatorname{sgn}(f - f_0)] + \frac{\mathcal{S}_X(f + f_0)}{2} [1 + \operatorname{sgn}(f + f_0)] \\ &= \begin{cases} \mathcal{S}_X(f - f_0) & f < -f_0 \\ \mathcal{S}_X(f - f_0) + \frac{1}{2} \mathcal{S}_X(f + f_0) & f = -f_0 \\ \mathcal{S}_X(f - f_0) + \mathcal{S}_X(f + f_0) & |f| < f_0 \\ \mathcal{S}_X(f + f_0) + \frac{1}{2} \mathcal{S}_X(f - f_0) & f = f_0 \\ \mathcal{S}_X(f + f_0) & f > f_0 \end{cases} \end{aligned}$$

From the fact that the original process  $X(t)$  is bandpass, it follows that

$$\mathcal{S}_{X_c}(f) = \mathcal{S}_{X_s}(f) = \begin{cases} \mathcal{S}_X(f - f_0) + \mathcal{S}_X(f + f_0) & |f| < f_0 \\ 0, & \text{otherwise} \end{cases} \quad (4.6.4)$$

This simply means that in order to obtain the power spectrum of both  $X_c(t)$  and  $X_s(t)$ , it is enough to shift the positive-frequency part of  $\mathcal{S}_X(f)$  to the left by  $f_0$  and to shift the negative-frequency part of it to the right by  $f_0$  and add the result. Figure 4.25 shows the relation between  $\mathcal{S}_X(f)$ ,  $\mathcal{S}_{X_c}(f)$  and  $\mathcal{S}_{X_s}(f)$ .

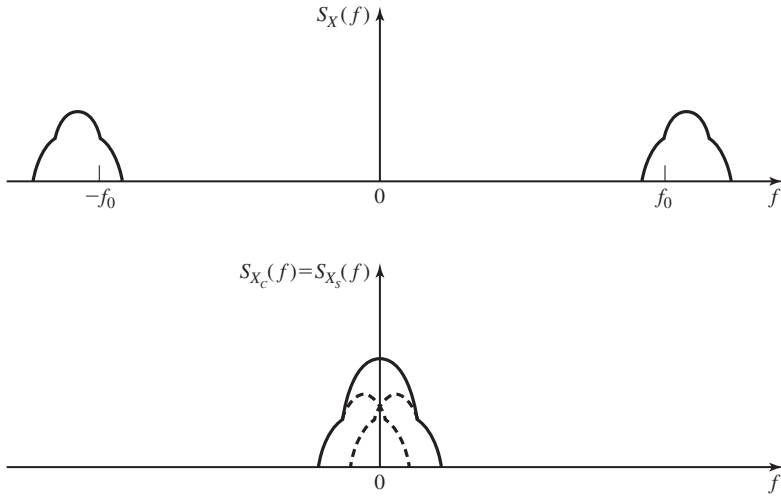


**Figure 4.25** Power spectrum of in-phase and quadrature components.

To obtain the cross-spectral density we have

$$\begin{aligned}
 \mathcal{S}_{X_c X_s}(f) &= \mathcal{F}[R_{X_c X_s}(\tau)] \\
 &= \mathcal{S}_X(f) \star \left[ \frac{\delta(f - f_0) - \delta(f + f_0)}{2j} \right] \\
 &\quad - [-j \operatorname{sgn}(f) \mathcal{S}_X(f)] \star \left[ \frac{\delta(f - f_0) + \delta(f + f_0)}{2} \right] \\
 &= \frac{j}{2} [\mathcal{S}_X(f + f_0) - \mathcal{S}_X(f - f_0)] \\
 &\quad + \frac{j}{2} [\operatorname{sgn}(f + f_0) \mathcal{S}_X(f + f_0) + \operatorname{sgn}(f - f_0) \mathcal{S}_X(f - f_0)] \\
 &= \frac{j}{2} \mathcal{S}_X(f + f_0) [1 + \operatorname{sgn}(f + f_0)] - \frac{j}{2} \mathcal{S}_X(f - f_0) [1 - \operatorname{sgn}(f - f_0)] \\
 &= \begin{cases} -j \mathcal{S}_X(f - f_0) & f < -f_0 \\ \frac{j}{2} \mathcal{S}_X(f + f_0) - j \mathcal{S}_X(f - f_0) & f = -f_0 \\ j [\mathcal{S}_X(f + f_0) - \mathcal{S}_X(f - f_0)] & |f| < f_0 \\ -\frac{j}{2} \mathcal{S}_X(f - f_0) + j \mathcal{S}_X(f + f_0) & f = f_0 \\ j \mathcal{S}_X(f + f_0) & f > f_0 \end{cases}
 \end{aligned}$$

Again, since the process is bandpass, the above relation simplifies to

$$\mathcal{S}_{X_c X_s}(f) = \begin{cases} j [\mathcal{S}_X(f + f_0) - \mathcal{S}_X(f - f_0)] & |f| < f_0 \\ 0, & \text{otherwise} \end{cases}$$

Figure 4.26 shows the relation between  $\mathcal{S}_{X_c X_s}(f)$  and  $\mathcal{S}_X(f)$ .

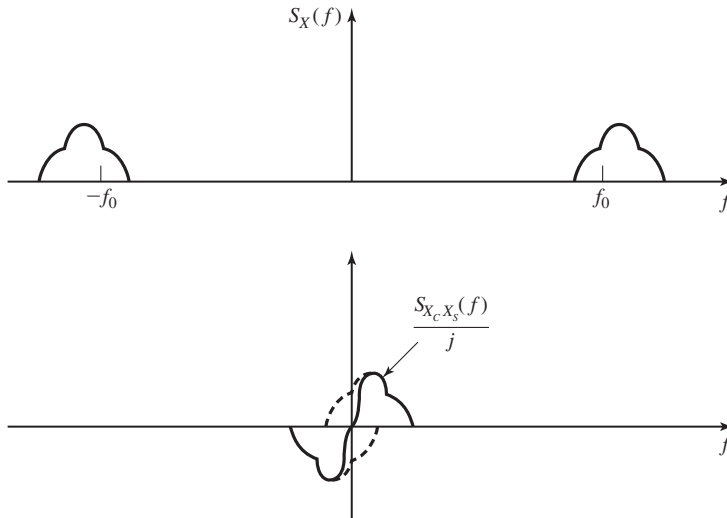


**Figure 4.26** Cross-spectral density of in-phase and quadrature components.

Since the cross correlation function

$$R_{X_c X_s}(\tau) = R_X(\tau) \sin(2\pi f_0 \tau) - \hat{R}_X(\tau) \cos(2\pi f_0 \tau)$$

is an odd function, it follows that  $R_{X_c X_s}(0) = 0$ . This means that at any time instant  $t_0$ , the random variables  $X_c(t_0)$  and  $X_s(t_0)$  are uncorrelated. Of course, from this we cannot conclude that the random processes  $X_c(t)$  and  $X_s(t)$  are uncorrelated since, in general, there is no guarantee that for arbitrary  $t_1$  and  $t_2$  the random variables  $X(t_1)$  and  $X(t_2)$  are uncorrelated. However, if the symmetry condition

$$S_X(f + f_0) = S_X(f - f_0) \quad (4.6.5)$$

is satisfied for all  $|f| < f_0$ , then  $S_{X_c X_s}(f) \equiv 0$  and therefore  $R_{X_c X_s}(\tau) \equiv 0$  for all  $\tau$ . This means that  $X_c(t_1)$  and  $X_s(t_2)$  are uncorrelated for arbitrary  $t_1$  and  $t_2$ , which in turn, means that the random processes  $X_c(t)$  and  $X_s(t)$  are uncorrelated. If  $S_X(f)$  happens to be symmetric around  $f_0$ , then the above condition is satisfied and the processes  $X_c(t)$  and  $X_s(t)$  will be uncorrelated.

If the zero-mean, stationary, and bandpass process  $X(t)$  is Gaussian as well, then  $X_c(t)$  and  $X_s(t)$  will be jointly Gaussian (why?). In this case, uncorrelatedness is equivalent to independence and, therefore, under the above conditions the processes  $X_c(t)$  and  $X_s(t)$  will be independent.

#### Example 4.6.1

The white Gaussian noise process  $N(t)$  with power spectrum  $\frac{N_0}{2}$  passes through an ideal bandpass filter with frequency response

$$H(f) = \begin{cases} 1 & |f - f_c| < W \\ 0, & \text{otherwise} \end{cases}$$

where  $W \ll f_c$ . The output process is denoted by  $X(t)$ . Find the power spectrum and the cross-spectral density of the in-phase and quadrature components in the following two cases:

1.  $f_0$  is chosen to be equal to  $f_c$ .
2.  $f_0$  is chosen to be equal to  $f_c - W$ .

**Solution** The process  $X(t)$  is obviously a bandpass process whose power-spectral density is given by

$$\mathcal{S}_X(f) = \begin{cases} \frac{N_0}{2}, & |f - f_c| < W \\ 0, & \text{otherwise} \end{cases}$$

If we choose  $f_c$  as the central frequency, then to obtain power spectra of  $X_c(t)$  and  $X_s(t)$  we have to shift the positive-frequency part of  $\mathcal{S}_X(f)$  to the left by  $f_0 = f_c$  and the negative-frequency part of it to the right by the same amount and add the results. If we do this, the resulting spectrum will be

$$\mathcal{S}_{X_c}(f) = \mathcal{S}_{X_s}(f) = \begin{cases} N_0, & |f| < W \\ 0, & \text{otherwise} \end{cases}$$

Since we are choosing  $f_0$  to be the axis of symmetry of the spectrum of  $X(t)$ , the process  $X_c(t)$  and  $X_s(t)$  will be independent with this choice and  $\mathcal{S}_{X_c X_s}(f) = 0$ . Figure 4.27 shows the relation between various power spectra in this case.

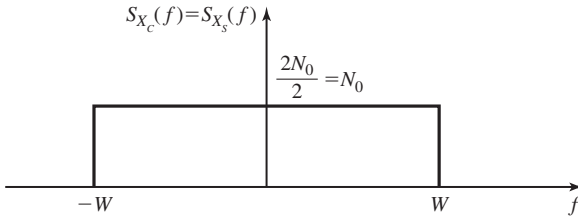


**Figure 4.27** In-phase and quadrature power spectra in first part of Example 4.6.1.

If we choose  $f_0 = f_c - W$  as the central frequency,<sup>†</sup> the results will be quite different. In this case, shifting the positive and negative components of  $X(t)$  by  $f_0$  to the left and right and adding them results in

$$\mathcal{S}_{X_c}(f) = \mathcal{S}_{X_s}(f) = \begin{cases} \frac{N_0}{2}, & |f| < 2W \\ 0, & \text{otherwise} \end{cases}$$

and for the cross-spectral density, we will have

$$\mathcal{S}_{X_c X_s}(f) = \begin{cases} -j\frac{N_0}{2}, & -2W < f < 0 \\ j\frac{N_0}{2}, & 0 < f < 2W \\ 0, & \text{otherwise} \end{cases}$$

<sup>†</sup>Central frequency does not, of course, mean the center of the bandwidth. It means the frequency with respect to which we are expanding the process.

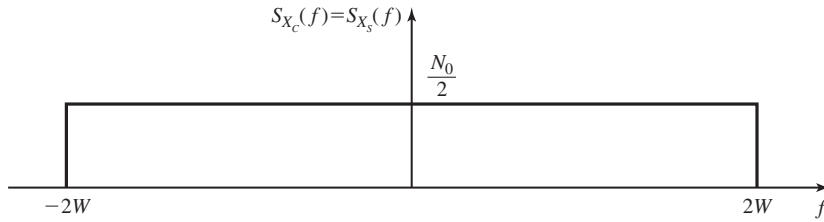


**Figure 4.28** In-phase and quadrature components for second part of Example 4.6.1.

Of course, in this case the processes  $X_c(t)$  and  $X_s(t)$  will not be independent. See Figure 4.28 for this case.

So far, we have defined  $X_c(t)$  and  $X_s(t)$  in terms of  $X(t)$  and  $\hat{X}(t)$  by

$$\begin{cases} X_c(t) = X(t) \cos(2\pi f_0 t) + \hat{X}(t) \sin(2\pi f_0 t) \\ X_s(t) = \hat{X}(t) \cos(2\pi f_0 t) - X(t) \sin(2\pi f_0 t) \end{cases}$$

and have shown that  $X_c(t)$  and  $X_s(t)$  are jointly stationary lowpass processes. Obtaining  $X(t)$  and  $\hat{X}(t)$  in terms of the in-phase and quadrature components is straightforward, and we can summarize the result as

$$\begin{cases} X(t) = X_c(t) \cos(2\pi f_0 t) - X_s(t) \sin(2\pi f_0 t) \\ \hat{X}(t) = X_c(t) \sin(2\pi f_0 t) + X_s(t) \cos(2\pi f_0 t) \end{cases}$$

These relations are frequently used in Chapters 5 and 7 to express bandpass processes in terms of the corresponding lowpass processes.

The power contents of the in-phase and quadrature components of  $X(t)$  can be obtained easily. From

$$R_{X_c}(\tau) = R_{X_s}(\tau) = R_X(\tau) \cos(2\pi f_0 \tau) + \hat{R}_X(\tau) \sin(2\pi f_0 \tau)$$

we have

$$P_{X_c} = P_{X_s} = R_{X_c}(\tau)|_{\tau=0} = R_X(0) = P_X \quad (4.6.6)$$

In other words, the power content of the in-phase and quadrature components is equal to the power content of the original bandpass process.

## 4.7 FURTHER READING

The books by Leon-Garcia (1994), Helstrom (1991), Davenport and Root (1987), Papoulis (1991), Nelson (1995), and Stark and Woods (1994) cover probability and random processes with emphasis on electrical engineering applications. Gray and Davisson (1986) is particularly interesting since it covers random processes for electrical engineers without compromising mathematical vigor. Advanced treatment of the material in this chapter, based on measure theory concepts, can be found in the book by Wong and Hajek (1985).



## PROBLEMS

- 4.1 A random experiment consists of drawing a ball from an urn that contains 4 red balls numbered 1, 2, 3, 4 and three black balls numbered 1, 2, 3. Precisely state what outcomes are contained in the following events.
1.  $E_1 =$  The number on the ball is even.
  2.  $E_2 =$  The color of the ball is red and its number is greater than 1.
  3.  $E_3 =$  The number on the ball is less than 3.
  4.  $E_4 = E_1 \cup E_3$ .
  5.  $E_5 = E_1 \cup (E_2 \cap E_3)$ .
- 4.2 If all balls in the preceding problem are equally likely to be drawn, find the probabilities of  $E_i$ ,  $1 \leq i \leq 5$ .
- 4.3 In a certain city three car brands, A, B, C have 20%, 30%, and 50% of the market share, respectively. The probability that a car needs major repair during its first year of purchase for the three brands is 5%, 10%, and 15%, respectively.
1. What is the probability that a car in this city needs major repair during its first year of purchase?
  2. If a car in this city needs major repair during its first year of purchase, what is the probability that it is made by manufacturer A?
- 4.4 Under what conditions can two disjoint events A and B be independent?
- 4.5 An information source produces 0 and 1 with probabilities 0.3 and 0.7, respectively. The output of the source is transmitted via a channel that has a probability of error (turning a 1 into a 0 or a 0 into a 1) equal to 0.2.
1. What is the probability that at the output a 1 is observed?
  2. What is the probability that a 1 was the output of the source if at the output of the channel a 1 is observed?
- 4.6 A coin is flipped three times and the random variable  $X$  denotes the total number of heads that show up. The probability of a head in one flip of this coin is denoted by  $p$ .
1. What values can the random variable  $X$  take?
  2. What is the PMF of the random variable  $X$ ?
  3. Derive and plot the CDF of  $X$ .
  4. What is the probability that  $X$  exceeds 1?
- 4.7 Coin A has a probability of head equal to  $\frac{1}{4}$  and probability of tail equal to  $\frac{3}{4}$ , and coin B is a fair coin. Each coin is flipped four times. Let the random variable  $X$  denote the number of heads resulting from coin A and  $Y$  denote the resulting number of heads from coin B.

1. What is the probability that  $X = Y = 2$ ?
2. What is the probability that  $X = Y$ ?
3. What is the probability that  $X > Y$ ?
4. What is the probability that  $X + Y \leq 5$ ?

4.8 A random variable  $X$  is defined by the CDF

$$F_X(x) = \begin{cases} 0, & x < 0 \\ \frac{1}{2}x, & 1 \leq x < 1 \\ K, & x \geq 1 \end{cases}$$

1. Find the value of  $K$ .
2. Is this random variable discrete, continuous, or mixed?
3. What is the probability that  $\frac{1}{2} < X \leq 1$ ?
4. What is the probability that  $\frac{1}{2} < X < 1$ ?
5. What is the probability that  $X$  exceeds 2?

4.9 Random variable  $X$  is distributed according to  $f_X(x) = \Lambda(x)$ .

1. Find the CDF of  $X$ .
2. Determine  $P(X > \frac{1}{2})$ .
3. Determine  $P(X > 0 | X < \frac{1}{2})$ .
4. What is  $f_X(x | X > \frac{1}{2})$ ?
5. What is  $E[X | X > \frac{1}{2}]$ ?

4.10 The noise voltage in an electric circuit can be modeled as a Gaussian random variable with mean equal to zero and variance equal to  $10^{-8}$ .

1. What is the probability that the value of the noise exceeds  $10^{-4}$ ? What is the probability that it exceeds  $4 \times 10^{-4}$ ? What is the probability that the noise value is between  $-2 \times 10^{-4}$  and  $10^{-4}$ ?
2. Given that the value of the noise is positive, what is the probability that it exceeds  $10^{-4}$ ?
3. This noise passes through a half-wave rectifier with characteristics

$$g(x) = \begin{cases} x, & x > 0 \\ 0, & x \leq 0 \end{cases}$$

Find the PDF of the rectified noise by first finding its CDF. Why can we not use the general expression in Equation (4.1.10) here?

4. Find the expected value of the rectified noise in the previous part.
5. Now assume that the noise passes through a full-wave rectifier defined by  $g(x) = |x|$ . Find the density function of the rectified noise in this case. What is the expected value of the output noise in this case?

**4.11**  $X$  is a  $\mathcal{N}(0, \sigma^2)$  random variable. This random variable is passed through a system whose input–output relation is given by  $y = g(x)$ . Find the PDF or the PMF of the output random variable  $Y$  in each of the following cases.

1. Square-law device,  $g(x) = ax^2$ .
2. Limiter,

$$g(x) = \begin{cases} -b, & x \leq -b \\ b, & x \geq b \\ x, & |x| < b \end{cases}$$

3. Hard limiter,

$$g(x) = \begin{cases} a, & x > 0 \\ 0, & x = 0 \\ b, & x < 0 \end{cases}$$

4. Quantizer,  $g(x) = x_n$  for  $a_n \leq x < a_{n+1}$ ,  $1 \leq n \leq N$ , where  $x_n$  lies in the interval  $[a_n, a_{n+1}]$  and the sequence  $\{a_1, a_2, \dots, a_{N+1}\}$  satisfies the conditions  $a_1 = -\infty$ ,  $a_{N+1} = \infty$  and for  $i > j$  we have  $a_i > a_j$ .

**4.12** The random variable  $\Phi$  is uniformly distributed on the interval  $[-\frac{\pi}{2}, \frac{\pi}{2}]$ . Find the PDF of  $X = \tan \Phi$ . Find the mean and the variance of  $X$ .

**4.13** Let  $Y$  be a positive valued random variable; i.e.,  $f_Y(y) = 0$  for  $y < 0$ .

1. Let  $\alpha$  be any positive constant. Show that  $P(Y > \alpha) \leq \frac{E[Y]}{\alpha}$  (Markov inequality).
2. Let  $X$  be any random variable with variance  $\sigma^2$  and define  $Y = (X - E[X])^2$  and  $\alpha = \epsilon^2$  for some  $\epsilon$ . Obviously the conditions of the problem are satisfied for  $Y$  and  $\alpha$  as chosen here. Derive the Chebychev inequality

$$P(|X - E[X]| > \epsilon) \leq \frac{\sigma^2}{\epsilon^2}$$

**4.14** Show that for a binomial random variable, the mean is given by  $np$  and the variance is given by  $np(1 - p)$ .

**4.15** Show that for a Poisson random variable defined by the PMF  $P(X = k) = \frac{\lambda^k}{k!} e^{-\lambda}$ ,  $k = 0, 1, 2, \dots$ , the characteristic function is given by  $\psi_X(v) = e^{\lambda(e^{jv} - 1)}$ . Use this result to show that  $E(X) = \lambda$  and  $\text{VAR}(X) = \lambda$ .

**4.16** Let  $X$  denote a Gaussian random variable with mean equal to zero and variance equal to  $\sigma^2$ . Show that

$$E[X^n] = \begin{cases} 0, & n = 2k + 1 \\ 1 \times 3 \times 5 \times \dots \times (n - 1)\sigma^n, & n = 2k \end{cases}$$

**4.17** Two random variables  $X$  and  $Y$  are distributed according to

$$f_{X,Y}(x, y) = \begin{cases} K(x + y), & 0 \leq x, y \leq 1 \\ 0, & \text{otherwise} \end{cases}$$

1. Find  $K$ .
2. What is the probability that  $X + Y > 1$ ?
3. Find  $P(X > Y)$ .
4. What is  $P(X > Y | X + 2Y > 1)$ ?
5. Find  $P(X = Y)$ ?
6. What is  $P(X > 0.5 | X = Y)$ ?
7. Find  $f_X(x)$  and  $f_Y(y)$ .
8. Find  $f_X(x | X + 2Y > 1)$  and  $E(X | X + 2Y > 1)$ .

**4.18** Let  $X_1, X_2, \dots, X_n$  denote i.i.d. random variables, each with PDF  $f_X(x)$ ,

1. If  $Y = \min\{X_1, X_2, \dots, X_n\}$ , find the PDF of  $Y$ .
2. If  $Z = \max\{X_1, X_2, \dots, X_n\}$ , find the PDF of  $Z$ .

**4.19** Show that for a Rayleigh density function

$$f_X(x) = \begin{cases} \frac{x}{\sigma^2} e^{-\frac{x^2}{2\sigma^2}}, & x > 0 \\ 0, & \text{otherwise} \end{cases}$$

we have  $E[X] = \sigma \sqrt{\frac{\pi}{2}}$  and  $\text{VAR}(X) = (2 - \frac{\pi}{2})\sigma^2$ .

**4.20** Let  $X$  and  $Y$  be independent random variables with

$$f_X(x) = \begin{cases} \alpha e^{-\alpha x}, & x > 0 \\ 0, & \text{otherwise} \end{cases}$$

and

$$f_Y(y) = \begin{cases} \beta e^{-\beta y}, & y > 0 \\ 0, & \text{otherwise} \end{cases}$$

where  $\alpha$  and  $\beta$  are assumed to be positive constants. Find the PDF of  $X + Y$ . Treat the special case  $\alpha = \beta$  separately.

**4.21** Two random variables  $X$  and  $Y$  are distributed according to

$$f_{X,Y}(x, y) = \begin{cases} K e^{-x-y}, & x \geq y \geq 0 \\ 0, & \text{otherwise} \end{cases}$$

1. Find the value of the constant  $K$ .
2. Find the marginal density functions of  $X$  and  $Y$ .
3. Are  $X$  and  $Y$  independent?
4. Find  $f_{X|Y}(x | y)$ .
5. Find  $E[X | Y = y]$ .
6. Find  $\text{COV}(X, Y)$  and  $\rho_{X,Y}$ .

- 4.22** Let  $\Theta$  be uniformly distributed on  $[0, \pi]$  and let random variables  $X$  and  $Y$  be defined by  $X = \cos \Theta$  and  $Y = \sin \Theta$ . Show that  $X$  and  $Y$  are uncorrelated but they are not independent.
- 4.23** Let  $X$  and  $Y$  be two independent Gaussian random variables, each with mean zero and variance 1. Define the two events  $E_1(r) = \{X > r \text{ and } Y > r\}$  and  $E_2(r) = \{\sqrt{X^2 + Y^2} > \sqrt{2}r\}$ , where  $r$  is any nonnegative constant.
1. Show that  $E_1(r) \subseteq E_2(r)$ , and therefore,  $P(E_1(r)) \leq P(E_2(r))$ .
  2. Show that  $P(E_1(r)) = Q^2(r)$ .
  3. Use rectangular to polar transformation relations to find  $P(E_2(r))$  and conclude with the bound

$$Q(r) \leq \frac{1}{2}e^{-\frac{r^2}{2}}$$

on the  $Q$  function.

- 4.24** It can be shown that the  $Q$  function can be well approximated by

$$Q(x) \approx \frac{e^{-\frac{x^2}{2}}}{\sqrt{2\pi}}(b_1t + b_2t^2 + b_3t^3 + b_4t^4 + b_5t^5)$$

where  $t = \frac{1}{1+px}$  and

$$p = 0.2316419$$

$$b_1 = 0.31981530$$

$$b_2 = -0.356563782$$

$$b_3 = 1.781477937$$

$$b_4 = -1.821255978$$

$$b_5 = 1.330274429$$

Using this relation write a computer program to compute the  $Q$  function at any given value of its argument. Compute  $Q(x)$  for  $x = 1, 1.5, 2, 2.5, 3, 3.5, 4, 4.5, 5$  and compare the results with those obtained from the table of the  $Q$  function.

- 4.25** Let the random vector  $\mathbf{X} = (X_1, X_2, \dots, X_n)$  be jointly Gaussian distributed with mean  $\mathbf{m}$  and covariance matrix  $\mathbf{C}$ . Define a new random vector  $\mathbf{Y} = \mathbf{A}\mathbf{X}^t + \mathbf{b}$ , where  $\mathbf{Y}$  is an  $n$ -dimensional random vector and  $\mathbf{A}$  and  $\mathbf{b}$  are constant matrices. Using the fact that linear functions of jointly Gaussian random variables are themselves jointly Gaussian, find the mean and covariance matrices of  $\mathbf{Y}$ .
- 4.26** Let  $X$  and  $Y$  be independent Gaussian random variables, each distributed according to  $\mathcal{N}(0, \sigma^2)$ .
1. Find the joint density function of the random variables  $Z = X + Y$  and  $W = 2X - Y$ . What is the correlation coefficient between these two random variables.

2. Find the PDF of the random variable  $R = \frac{X}{Y}$ . What is the mean and the variance of  $R$ ?

**4.27** Random variables  $X$  and  $Y$  are jointly Gaussian with

$$\mathbf{m} = [1 \quad 2]$$

$$\mathbf{C} = \begin{bmatrix} 4 & -4 \\ -4 & 9 \end{bmatrix}$$

1. Find the correlation coefficient between  $X$  and  $Y$ .
  2. If  $Z = 2X + Y$  and  $W = X - 2Y$ , find  $\text{COV}(Z, W)$ .
  3. Find the PDF of  $Z$ .
- 4.28** Let  $X$  and  $Y$  be two jointly Gaussian random variables with means  $m_X$  and  $m_Y$ , variances  $\sigma_X^2$  and  $\sigma_Y^2$  and correlation coefficient  $\rho_{X,Y}$ . Show that  $f_{X|Y}(x|y)$  is a Gaussian distribution with mean  $m_X + \rho \frac{\sigma_X}{\sigma_Y}(y - m_Y)$  and variance  $\sigma_X^2(1 - \rho_{X,Y}^2)$ . What happens if  $\rho = 0$ ? What if  $\rho = \pm 1$ ?
- 4.29**  $X$  and  $Y$  are zero-mean jointly Gaussian random variables, each with variance  $\sigma^2$ . The correlation coefficient between  $X$  and  $Y$  is denoted by  $\rho$ . Random variables  $Z$  and  $W$  are defined by

$$\begin{cases} Z = X \cos \theta + Y \sin \theta \\ W = -X \sin \theta + Y \cos \theta \end{cases}$$

where  $\theta$  is a constant angle.

1. Show that  $Z$  and  $W$  are jointly Gaussian random variables and determine their joint PDF.
  2. For what values of  $\theta$  are the random variables  $Z$  and  $W$  independent?
- 4.30** Two random variables  $X$  and  $Y$  are distributed according to

$$f_{X,Y}(x, y) = \begin{cases} \frac{K}{\pi} e^{-\frac{x^2+y^2}{2}}, & xy \geq 0 \\ 0, & xy < 0 \end{cases}$$

1. Find  $K$ .
  2. Show that  $X$  and  $Y$  are each Gaussian random variables.
  3. Show that  $X$  and  $Y$  are not jointly Gaussian.
  4. Are  $X$  and  $Y$  independent?
  5. Are  $X$  and  $Y$  uncorrelated?
  6. Find  $f_{X|Y}(x|y)$ . Is this a Gaussian distribution?
- 4.31** Let  $X$  and  $Y$  be two independent Gaussian random variables with common variance  $\sigma^2$ . The mean of  $X$  is  $m$  and  $Y$  is a zero-mean random variable. We define

random variable  $V$  as  $V = \sqrt{X^2 + Y^2}$ . Show that

$$f_V(v) = \begin{cases} \frac{v}{\sigma^2} I_0\left(\frac{mv}{\sigma^2}\right) e^{-\frac{v^2+m^2}{2\sigma^2}}, & v > 0 \\ 0, & v \leq 0 \end{cases}$$

where

$$I_0(x) = \frac{1}{2\pi} \int_0^{2\pi} e^{x \cos u} du = \frac{1}{2\pi} \int_{-\pi}^{\pi} e^{x \cos u} du$$

is called the *modified Bessel function of the first kind and zero order*. The distribution of  $V$  is known as the *Ricean distribution*. Show that, in the special case of  $m = 0$ , the Ricean distribution simplifies to the Rayleigh distribution.

- 4.32** A coin whose probability of a head is  $\frac{1}{4}$ , is flipped 2000 times
1. Using the law of large numbers, find a lower bound to the probability that the total number of heads lies between 480 and 520.
  2. Using the central limit theorem, find the probability that the total number of heads lies between 480 and 520.
- 4.33** Find the covariance matrix of the random vector  $X$  in Example 4.2.2.
- 4.34** Find  $m_X(t)$  for the random process  $X(t)$  given in Example 4.2.4. Is it independent of  $t$ ?
- 4.35** Let the random process  $X(t)$  be defined by  $X(t) = A + Bt$ , where  $A$  and  $B$  are independent random variables each uniformly distributed on  $[-1, 1]$ . Find  $m_X(t)$  and  $R_X(t_1, t_2)$ .
- 4.36** What is the autocorrelation function of the random process given in Example 4.2.5?
- 4.37** Show that the process given in Example 4.2.4 is a stationary process.
- 4.38** Is the process given in Example 4.2.5 wide-sense stationary?
- 4.39** Show that any  $M$ th-order stationary process,  $M \geq 2$ , is wide-sense stationary.
- 4.40** Which one of the following functions can be the autocorrelation function of a random process and why?
1.  $f(\tau) = \sin(2\pi f_0 \tau)$ .
  2.  $f(\tau) = \tau^2$ .
  3.  $f(\tau) = \begin{cases} 1 - |\tau| & |\tau| \leq 1 \\ 1 + |\tau| & |\tau| > 1 \end{cases}$
  4.  $f(\tau)$  as shown in Figure P-4.40.
- 4.41** Is the process given in Example 4.2.5 an ergodic process?
- 4.42** Is the process of Example 4.2.1 power-type or energy-type? Is this process stationary?
- 4.43** A random process  $Z(t)$  takes values 0 and 1. A transition from 0 to 1 or from 1 to 0 occurs randomly, and the probability of having  $n$  transitions in a time interval

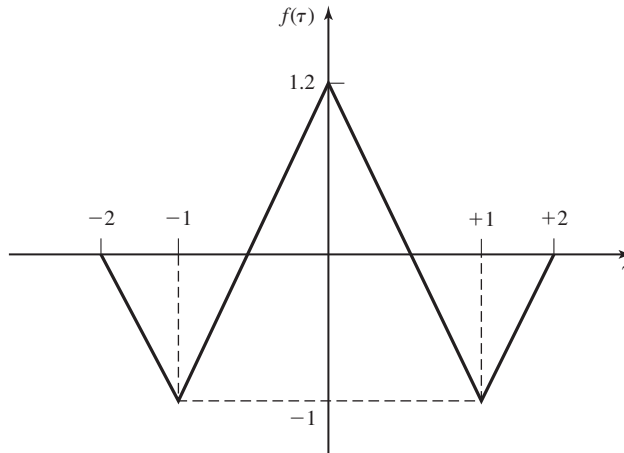


Figure P-4.40

of duration  $\tau$ , ( $\tau > 0$ ), is given by

$$p_N(n) = \frac{1}{1 + \alpha\tau} \left( \frac{\alpha\tau}{1 + \alpha\tau} \right)^n, \quad n = 0, 1, 2, \dots$$

where  $\alpha > 0$  is a constant. We further assume that at  $t = 0$ ,  $X(0)$  is equally likely to be 0 or 1.

1. Find  $m_Z(t)$ .
2. Find  $R_Z(t + \tau, t)$ . Is  $Z(t)$  stationary? Is it cyclostationary?
3. Determine the power of  $Z(t)$ .

**4.44** The random process  $X(t)$  is defined by

$$X(t) = X \cos 2\pi f_0 t + Y \sin 2\pi f_0 t$$

where  $X$  and  $Y$  are two zero-mean independent Gaussian random variables each with variance  $\sigma^2$ .

1. Find  $m_X(t)$ .
2. Find  $R_X(t + \tau, t)$ . Is  $X(t)$  stationary? Is it cyclostationary?
3. Find the power-spectral density of  $X(t)$ .
4. Answer the above questions for the case where  $\sigma_X^2 = \sigma_Y^2$

**4.45** Let  $\{A_k\}_{k=-\infty}^{\infty}$  be a sequence of random variables with  $E[A_k] = m$  and  $E[A_k A_j] = R_A(k - j)$ . We further assume that  $R_A(k - j) = R_A(j - k)$ . Let  $p(t)$  be any deterministic signal whose Fourier transform is  $P(f)$ , and define the



random process

$$X(t) = \sum_{k=-\infty}^{+\infty} A_k p(t - kT)$$

where  $T$  is a constant.

1. Find  $m_X(t)$ .
2. Find  $R_X(t + \tau, t)$ .
3. Show that this process is cyclostationary with period  $T$ .
4. Show that

$$\bar{R}_X(\tau) = \frac{1}{T} \int_0^T R_X(t + \tau, t) dt = \frac{1}{T} \sum_{n=-\infty}^{\infty} R_A(n) R_p(\tau - nT)$$

where  $R_p(\tau) = p(\tau) \star p(-\tau)$  is the (deterministic) autocorrelation function of  $p(t)$ .

5. Show that the power-spectral density of  $X(t)$  is given by

$$S_X(f) = \frac{|P(f)|^2}{T} \left[ R_A(0) + 2 \sum_{k=1}^{\infty} R_A(k) \cos 2\pi k f T \right]$$

- 4.46** Using the result of Problem 4.45 find the power-spectral density of the random process

$$X(t) = \sum_{n=-\infty}^{\infty} A_n p(t - nT)$$

in the following cases

1.  $A_n$ 's are independent random variables each taking values  $\pm 1$  with equal probability and

$$p(t) = \begin{cases} 1, & 0 \leq t \leq T \\ 0, & \text{otherwise} \end{cases}$$

2.  $A_n$ 's take values 0 and 1 with equal probability, all the other conditions as in part 1.
3. Solve parts 1 and 2 for the case where

$$p(t) = \begin{cases} 1, & 0 \leq t \leq 3T \\ 0, & \text{otherwise} \end{cases}$$

4. In each of the above cases find the bandwidth that contains 95% of the total power of the process.

- 4.47** Let  $A_n$ 's denote a sequence of independent binary valued random variables, each taking values  $\pm 1$  with equal probability. Random variables  $B_n$  are defined

according to  $B_n = A_n + A_{n-1}$ , and the random process  $X(t)$  is defined as  $X(t) = \sum_{n=-\infty}^{\infty} B_n p(t - nT)$ .

1. Using the results of Problem 4.45 determine the power-spectral density of  $X(t)$ .
2. Assuming that

$$p(t) = \begin{cases} 1, & 0 \leq t \leq T \\ 0, & \text{otherwise} \end{cases}$$

plot a sample function of  $X(t)$ . Find the power-spectral density of  $X(t)$  and plot it.

3. Let  $B_n = A_n + \alpha A_{n-1}$  and find the power-spectral density of  $X(t)$ . How does the value of  $\alpha$  change the power-spectral density of  $X(t)$ . What is the effect of the value of  $\alpha$  on the 95%-power bandwidth of the process?
- 4.48** Let  $X(t)$  be a cyclostationary process with period  $T$ . From Corollary 4.3.3, we have seen that, in order to find the power-spectral density of  $X(t)$ , we first determine  $\bar{R}(\tau) = \frac{1}{T} \int_0^T R_X(t + \tau, t) dt$  and then find  $\mathcal{F}[\bar{R}(\tau)]$ . We now obtain this result by another approach.
1. Let  $\Theta$  be a random variable, independent of  $X(t)$  and uniformly distributed on  $[0, T]$ . Show that  $Y(t) = X(t + \Theta)$  is stationary and its autocorrelation function is given as

$$R_Y(\tau) = \frac{1}{T} \int_0^T R_X(t + \tau, t) dt$$

2. Show that  $Y(t)$  and  $X(t)$  have equal power-spectral densities.
3. Conclude that

$$\mathcal{S}_X(f) = \mathcal{F} \left[ \frac{1}{T} \int_0^T R_X(t + \tau, t) dt \right]$$

- 4.49** The RMS bandwidth of a process is defined as

$$W_{\text{RMS}} = \frac{\int_0^{\infty} f^2 \mathcal{S}_X(f) df}{\int_0^{\infty} \mathcal{S}_X(f) df}$$

Show that for a stationary process, we have

$$W_{\text{RMS}} = - \frac{1}{4\pi^2 R_X(0)} \left. \frac{d^2}{d\tau^2} R_X(\tau) \right|_{\tau=0}$$

- 4.50** Show that for jointly stationary processes  $X(t)$  and  $Y(t)$ , we have  $R_{XY}(\tau) = R_{YX}(-\tau)$ . From this, conclude that  $\mathcal{S}_{XY}(f) = \mathcal{S}_{YX}^*(f)$ .
- 4.51** A zero-mean white Gaussian noise with power-spectral density of  $\frac{N_0}{2}$  passes through an ideal lowpass filter with bandwidth  $B$ .

1. Find the autocorrelation of the output process  $Y(t)$ .
  2. Assuming  $\tau = \frac{1}{2B}$ , find the joint PDF of the random variables  $Y(t)$  and  $Y(t + \tau)$ . Are these random variables independent?
- 4.52** Find the output autocorrelation function for a delay line with delay  $\Delta$  when the input is a stationary process with autocorrelation  $R_X(\tau)$ . Interpret the result.
- 4.53** We have proved that when the input to an LTI system is stationary, the output is also stationary. Is the converse of this theorem also true? That is, if we know that the output process is stationary, can we conclude that the input process is necessarily stationary?
- 4.54** It was shown in this chapter that if a stationary random process  $X(t)$  with autocorrelation function  $R_X(\tau)$  is applied to an LTI system with impulse response  $h(t)$ , the output  $Y(t)$  is also stationary with autocorrelation function  $R_Y(\tau) = R_X(\tau) \star h(\tau) \star h(-\tau)$ . In this problem, we show that a similar relation holds for cyclostationary processes.

1. Let  $X(t)$  be a cyclostationary process applied to an LTI system with impulse response  $h(t)$ . Show that the output process is also cyclostationary.
2. Show that

$$\bar{R}_Y(t, t + \tau) = \bar{R}_X(t, t + \tau) \star h(\tau) \star h(-\tau)$$

3. Conclude that the relation

$$\mathcal{S}_Y(f) = \mathcal{S}_X(f) |H(f)|^2$$

is true for both stationary and cyclostationary processes.

- 4.55** Generalize the result of the Example 4.3.8 to show that if  $X(t)$  is stationary,
1.  $X(t)$  and  $\frac{d}{dt}X(t)$  are uncorrelated processes.
  2. The power spectrum of  $Z(t) = X(t) + \frac{d}{dt}X(t)$  is the sum of the power spectra of  $X(f)$  and  $\frac{d}{dt}X(f)$ .

Express the power spectrum of the sum in terms of the power spectrum of  $X(t)$ .

- 4.56**  $X(t)$  is a stationary process with power-spectral density  $\mathcal{S}_X(f)$ . This process passes through the system shown in Figure P-4.56.

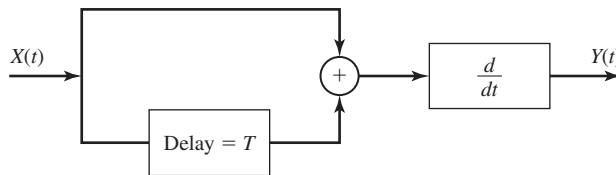


**Figure P-4.56**

1. Is  $Y(t)$  stationary? Why?
2. What is the power-spectral density of  $Y(t)$ ?

3. What frequency components *cannot* be present in the output process and why?

4.57 The stationary random process  $X(t)$  has a power-spectral density denoted by  $S_X(f)$ .

1. What is the power-spectral density of  $Y(t) = X(t) - X(t - T)$ ?
2. What is the power-spectral density of  $Z(t) = X'(t) - X(t)$ ?
3. What is the power-spectral density of  $W(t) = Y(t) + Z(t)$ ?

4.58 Show that for two jointly stationary processes  $X(t)$  and  $Y(t)$ , we have

$$|R_{XY}(\tau)| \leq R_X(0)R_Y(0) \leq \frac{1}{2}[R_X(0) + R_Y(0)]$$

4.59 The stationary process  $X(t)$  is passed through an LTI system and the output process is denoted by  $Y(t)$ . Find the output autocorrelation function and the crosscorrelation function between the input and the output processes in each of the following cases.

1. A delay system with delay  $\Delta$ .
2. A system with  $h(t) = \frac{1}{t}$ .
3. A system with  $h(t) = e^{-\alpha t}u(t)$  where  $\alpha > 0$ .
4. A system described by the differential equation

$$\frac{d}{dt}Y(t) + Y(t) = \frac{d}{dt}X(t) - X(t)$$

5. A finite time averager defined by the input–output relation

$$y(t) = \frac{1}{2T} \int_{t-T}^{t+T} x(\tau) d\tau$$

where  $T$  is a constant.

4.60 Give an example of two processes  $X(t)$  and  $Y(t)$  for which  $R_{XY}(t + \tau, t)$  is a function of  $\tau$  but  $X(t)$  and  $Y(t)$  are not stationary.

4.61 For each of the following processes, find the power-spectral density

1.  $X(t) = A \cos(2\pi f_0 t + \Theta)$ , where  $A$  is a constant and  $\Theta$  is a random variable uniformly distributed on  $[0, \frac{\pi}{4}]$ .
2.  $X(t) = X + Y$ , where  $X$  and  $Y$  are independent,  $X$  is uniform on  $[-1, 1]$  and  $Y$  is uniform on  $[0, 1]$ .

4.62  $X(t)$  is a stationary random process with autocorrelation function  $R_X(\tau) = e^{-\alpha|\tau|}$ ,  $\alpha > 0$ . This process is applied to an LTI system with  $h(t) = e^{-\beta t}u(t)$ , where  $\beta > 0$ . Find the power-spectral density of the output process  $Y(t)$ . Treat the cases  $\alpha \neq \beta$  and  $\alpha = \beta$  separately.

**4.63** Let  $Y(t) = X(t) + N(t)$ , where  $X(t)$  and  $N(t)$  are signal and noise processes. It is assumed that  $X(t)$  and  $N(t)$  are jointly stationary with autocorrelation functions  $R_X(\tau)$  and  $R_N(\tau)$  and crosscorrelation function  $R_{XN}(\tau)$ . It is desired to separate the signal from the noise by passing  $Y(t)$  through an LTI system with impulse response  $h(t)$  and transfer function  $H(f)$ . The output process is denoted by  $\hat{X}(t)$ , which is desired to be as close to  $X(t)$  as possible.

1. Find the crosscorrelation between  $\hat{X}(t)$  and  $X(t)$  in terms of  $h(\tau)$ ,  $R_X(\tau)$ ,  $R_N(\tau)$ , and  $R_{XN}(\tau)$ .
2. Show that the LTI system that minimizes  $E[X(t) - \hat{X}(t)]^2$  has a transfer function

$$H(f) = \frac{S_X(f) + S_{XN}(f)}{S_X(f) + S_N(f) + 2\text{Re}[S_{XN}(f)]}$$

3. Now assume that  $X(t)$  and  $N(t)$  are independent and  $N(t)$  is a zero-mean white Gaussian process with power-spectral density  $\frac{N_0}{2}$ . Find the optimal  $H(f)$  under these conditions. What is the corresponding value of  $E[X(t) - \hat{X}(t)]^2$  in this case?
4. In the special case of  $S_N(f) = 1$ ,  $S_X(f) = \frac{1}{1+f^2}$ , and  $S_{XN}(f) = 0$ , find the optimal  $H(f)$ .

**4.64** In this problem, we examine the estimation of a random process from observation of another random process. Let  $X(t)$  and  $Z(t)$  be two jointly stationary random processes. We are interested in designing an LTI system with impulse response  $h(t)$  such that when  $Z(t)$  is passed through it the output process  $\hat{X}(t)$  is as close to  $X(t)$  as possible. In other words, we are interested in the best *linear* estimate of  $X(t)$  based on the observation of  $Y(t)$  in order to minimize  $E[X(t) - \hat{X}(t)]^2$ .

1. Let us assume we have two LTI systems with impulse responses  $h(t)$  and  $g(t)$ .  $Z(t)$  is applied to both systems and the outputs are denoted by  $\hat{X}(t)$  and  $\tilde{X}(t)$ , respectively. The first filter is designed such that its output satisfies the condition

$$E[(X(t) - \hat{X}(t))Z(t - \tau)] = 0$$

for all values of  $\tau$  and  $t$ , where the second filter does not satisfy this property. Show that

$$E[X(t) - \tilde{X}(t)]^2 \geq E[X(t) - \hat{X}(t)]^2$$

i.e., the necessary and sufficient condition for an optimal filter is that its output should satisfy the *orthogonality condition* as given by

$$E[(X(t) - \hat{X}(t))Z(t - \tau)] = 0$$

which simply means that the estimation error  $\epsilon(t) = X(t) - \hat{X}(t)$  must be orthogonal to the observable process  $Z(t)$  at all times.

2. Show that the optimal  $h(t)$  must satisfy

$$R_{XZ}(\tau) = R_Z(\tau) \star h(\tau)$$

3. Show that the optimal filter satisfies

$$H(f) = \frac{S_{XZ}(f)}{S_Z(f)}$$

4. Derive an expression for  $E[\epsilon^2(t)]$  when the optimal filter is employed.

- 4.65** The random process  $X(t)$  is defined by

$$X(t) = \sum_{n=-\infty}^{\infty} A_n \operatorname{sinc} 2W(t - nT)$$

where  $A_n$ 's are independent random variables with mean zero and common variance  $\sigma^2$ .

1. Use the result of Problem 4.45 to obtain the power-spectral density of  $X(t)$ .
  2. In the special case of  $T = \frac{1}{2W}$  what is the power content of  $X(t)$ ?
  3. Now let  $X_1(t)$  be a zero-mean stationary process with power-spectral density  $S_{X_1}(f) = \frac{N_0}{2} \Pi(\frac{f}{2W})$  and let  $A_n = X_1(nT)$ , where  $T = \frac{1}{2W}$ . Determine the power-spectral density of  $X(t)$  and its power content. What is the relation between  $X_1(t)$  and  $X(t)$ ?
- 4.66** What is the noise-equivalent bandwidth of an ideal bandpass filter with bandwidth  $W$ ?
- 4.67** Work out Example 4.6.1 with  $f_0 = f_c - \frac{W}{2}$ .
- 4.68** Verify the Equation (4.6.6) for both parts of Example 4.6.1.
- 4.69** A zero-mean white Gaussian noise,  $n_w(t)$ , with power-spectral density  $\frac{N_0}{2}$ , is passed through an ideal filter whose passband is from 3–11 KHz. The output process is denoted by  $n(t)$ .
1. If  $f_0 = 7$  KHz, find  $S_{n_c}(f)$ ,  $S_{n_s}(f)$ , and  $R_{n_c n_s}(\tau)$ , where  $n_c(t)$  and  $n_s(t)$  are the in-phase and quadrature components of  $n(t)$ .
  2. Repeat part 1 with  $f_0 = 6$  KHz.
- 4.70** Let  $p(t)$  be a bandpass signal with in-phase and quadrature components  $p_c(t)$  and  $p_s(t)$  and let  $X(t) = \sum_{n=-\infty}^{\infty} A_n p(t - nT)$ , where  $A_n$ 's are independent random variables. Express  $X_c(t)$  and  $X_s(t)$  in terms of  $p_c(t)$  and  $p_s(t)$ .
- 4.71** Let  $X(t)$  be a bandpass process and let  $V(t)$  denote its envelope. Show that for all choices of the center frequency  $f_0$ ,  $V(t)$  remains unchanged.
- 4.72** Let  $n_w(t)$  be a zero-mean white Gaussian noise with power-spectral density  $\frac{N_0}{2}$ , and let this noise be passed through an ideal bandpass filter with bandwidth  $2W$  centered at frequency  $f_c$ . Denote the output process by  $n(t)$ .

1. Assuming  $f_0 = f_c$ , find the power content of the in-phase and quadrature components of  $n(t)$ .
2. Find the density function of  $V(t)$ , the envelope of  $n(t)$ .
3. Now assume  $X(t) = A \cos 2\pi f_0 t + n(t)$  where  $A$  is a constant. What is the density function of the envelope of  $X(t)$ ?

**4.73** A noise process has a power-spectral density given by

$$\mathcal{S}_n(f) = \begin{cases} 10^{-8} \left(1 - \frac{|f|}{10^8}\right), & |f| < 10^8 \\ 0, & |f| > 10^8 \end{cases}$$

This noise is passed through an ideal bandpass filter with a bandwidth of 2 MHz centered at 50 MHz.

1. Find the power content of the output process.
2. Write the output process in terms of the in-phase and quadrature components and find the power in each component. Assume  $f_0 = 50$  MHz.
3. Find the power-spectral density of the in-phase and quadrature components.
4. Now assume that the filter is not an ideal filter and is described by

$$|H(f)|^2 = \begin{cases} |f| - 49 \times 10^6, & 49 \text{ MHz} < |f| < 51 \text{ MHz}, \\ 0, & \text{otherwise} \end{cases}$$

Repeat parts 1, 2, and 3 with this assumption.

# 5

## *Effect of Noise on Analog Communication Systems*

In Chapter 3, we studied the important characteristics of analog communication systems. These characteristics included time-domain and frequency-domain representations of the modulated signal, bandwidth requirements, and power content of the modulated signal and, finally, modulator and demodulator implementation of various analog communication systems.

In this chapter the effect of noise on various analog communication systems will be analyzed. As we will see, angle-modulation systems and particularly FM, can provide a high degree of noise immunity, and therefore are desirable in cases of severe noise and/or low signal power. This noise immunity is obtained at the price of sacrificing channel bandwidth because, as we have seen in Chapter 3, the bandwidth requirements of angle-modulation systems is considerably higher than amplitude-modulation systems.

This chapter starts with an analysis of the performance of linear-modulation systems in the presence of noise. Then, the performance of phase-locked loops (PLL) that are used for carrier synchronization is studied. The effect of noise on angle-modulation systems is treated next and, finally, the effects of transmission loss and noise on analog communication systems in general are analyzed.

### **5.1 EFFECT OF NOISE ON LINEAR-MODULATION SYSTEMS**

In this section we determine the *signal-to-noise ratio (SNR)* of the output of the receiver that demodulates the amplitude-modulated signals. In evaluating the effect of noise on the various types of analog-modulated signals, it is also interesting to compare the result with the effect of noise on an equivalent baseband communication system. We begin the evaluation of the effect of noise on a baseband system.



### 5.1.1 Effect of Noise on a Baseband System

Since baseband systems serve as a basis for comparison of various modulation systems, we begin with a noise analysis of a baseband system. In this case, there exists no demodulator, and the receiver consists only of a lowpass filter with bandwidth  $W$ . The noise power at the output of the receiver is, therefore,

$$\begin{aligned} P_{n_o} &= \int_{-W}^{+W} \frac{N_0}{2} df \\ &= N_0 W \end{aligned} \quad (5.1.1)$$

If we denote the received power by  $P_R$ , the baseband SNR is given by

$$\left( \frac{S}{N} \right)_b = \frac{P_R}{N_0 W} \quad (5.1.2)$$

### 5.1.2 Effect of Noise on DSB-SC AM

In DSB, we have

$$u(t) = A_c \cos(2\pi f_c t + \phi_c) \quad (5.1.3)$$

and, therefore, the received signal at the output of the receiver noise-limiting filter is

$$\begin{aligned} r(t) &= u(t) + n(t) \\ &= A_c m(t) \cos(2\pi f_c t + \phi_c) + n_c(t) \cos 2\pi f_c t - n_s(t) \sin 2\pi f_c t \end{aligned} \quad (5.1.4)$$

where we have used the in-phase and quadrature components of the noise as discussed in Section 4.6.

Suppose we demodulate the received signal by first multiplying  $r(t)$  by a locally generated sinusoid  $\cos(2\pi f_c t + \phi)$ , where  $\phi$  is the phase of the sinusoid, and then passing the product signal through an ideal lowpass filter having a bandwidth  $W$ . The multiplication of  $r(t)$  with  $\cos(2\pi f_c t + \phi)$  yields

$$\begin{aligned} r(t) \cos(2\pi f_c t + \phi) &= A_c m(t) \cos(2\pi f_c t + \phi_c) \cos(2\pi f_c t + \phi) + n(t) \cos(2\pi f_c t + \phi) \\ &= \frac{1}{2} A_c m(t) \cos(\phi_c - \phi) + \frac{1}{2} A_c m(t) \cos(4\pi f_c t + \phi + \phi_c) \\ &\quad + \frac{1}{2} [n_c(t) \cos \phi + n_s(t) \sin \phi] \\ &\quad + \frac{1}{2} [n_c(t) \cos(4\pi f_c t + \phi) - n_s(t) \sin(4\pi f_c t + \phi)] \end{aligned} \quad (5.1.5)$$

The lowpass filter rejects the double-frequency components and passes only the lowpass components. Hence, its output is

$$y(t) = \frac{1}{2} A_c m(t) \cos(\phi_c - \phi) + \frac{1}{2} [n_c(t) \cos \phi + n_s(t) \sin \phi] \quad (5.1.6)$$

As it was discussed in Chapter 3, the effect of a phase difference between the transmitter and the receiver is a reduction equal to  $\cos^2(\phi_c - \phi)$  in the received signal

power. This can be avoided by employing a PLL as described in Section 5.2. The effect of a PLL is to generate a sinusoid at the receiver with the same frequency and phase of the carrier. If a PLL is employed, then  $\phi = \phi_c$ , and the demodulator is called a *coherent* or *synchronous demodulator*. In our analysis in this section, we assume that we are employing a coherent demodulator. With this assumption and without loss of generality, we can assume  $\phi = \phi_c = 0$ , and Equation (5.1.6) reduces to

$$y(t) = \frac{1}{2} [A_c m(t) + n_c(t)] \quad (5.1.7)$$

Therefore, at the receiver output the message signal and the noise components are additive and we are able to define a meaningful SNR. The message signal power is given by

$$P_o = \frac{A_c^2}{4} P_m \quad (5.1.8)$$

and the noise power is given by

$$\begin{aligned} P_{n_o} &= \frac{1}{4} P_{n_c} \\ &= \frac{1}{4} P_n \end{aligned} \quad (5.1.9)$$

where we have used the fact that the power contents of  $n_c(t)$  and  $n(t)$  are equal. This was shown in Section 4.6 as seen in Equation (4.6.6). The power content of  $n(t)$  can be found by noting that it is the result of passing  $n_w(t)$  through a filter with bandwidth  $B_c$ . Therefore, the power-spectral density of  $n(t)$  is given by

$$\mathcal{S}_n(f) = \begin{cases} \frac{N_0}{2}, & |f - f_c| < W \\ 0, & \text{otherwise} \end{cases} \quad (5.1.10)$$

The noise power is

$$\begin{aligned} P_n &= \int_{-\infty}^{\infty} \mathcal{S}_n(f) df \\ &= \frac{N_0}{2} \times 4W \\ &= 2WN_0 \end{aligned} \quad (5.1.11)$$

Now we can find the output SNR as

$$\begin{aligned} \left( \frac{S}{N} \right)_o &= \frac{P_o}{P_{n_o}} \\ &= \frac{\frac{A_c^2}{4} P_m}{\frac{1}{4} 2WN_0} \\ &= \frac{A_c^2 P_m}{2WN_0} \end{aligned} \quad (5.1.12)$$

In this case, the received signal power is  $P_R = \frac{A_c^2 P_m}{2}$ . Therefore, by using Equation (5.1.2), we obtain

$$\begin{aligned} \left(\frac{S}{N}\right)_{\text{DSB}} &= \frac{P_R}{N_0 W} \\ &= \left(\frac{S}{N}\right)_b \end{aligned} \quad (5.1.13)$$

It is seen that in DSB-SC AM, the output SNR is the same as the SNR for a baseband system. Therefore, DSB-SC AM does not provide any SNR improvement over a simple baseband communication system.

### 5.1.3 Effect of Noise on SSB AM

In this case

$$u(t) = A_c m(t) \cos 2\pi f_c t \pm A_c \hat{m}(t) \sin 2\pi f_c t \quad (5.1.14)$$

Therefore, the input to the demodulator is

$$\begin{aligned} r(t) &= A_c m(t) \cos 2\pi f_c t \pm A_c \hat{m}(t) \sin 2\pi f_c t + n(t) \\ &= (A_c m(t) + n_c(t)) \cos 2\pi f_0 t + (\pm A_c \hat{m}(t) - n_s(t)) \sin 2\pi f_c t \end{aligned} \quad (5.1.15)$$

Here again we assume that demodulation occurs with an ideal-phase reference. Hence, the output of the lowpass filter is the in-phase component (with a coefficient of  $\frac{1}{2}$ ) of the above signal; i.e.

$$y(t) = \frac{A_c}{2} m(t) + \frac{1}{2} n_c(t) \quad (5.1.16)$$

It is observed that, in this case, again the signal and the noise components are additive and a meaningful SNR at the receiver output can be defined. Parallel to our discussion of DSB we have

$$P_o = \frac{A_c^2}{4} P_m \quad (5.1.17)$$

and

$$P_{n_o} = \frac{1}{4} P_{n_c} = \frac{1}{4} P_n \quad (5.1.18)$$

The noise power-spectral density in this case is  $N_0/2$  over the bandwidth of the front-end filter at the receiver, which here has a bandwidth of  $W$ . For instance, in the USSB case, we have

$$\mathcal{S}_n(f) = \begin{cases} \frac{N_0}{2}, & f_c \leq |f| \leq f + f_c \\ 0, & \text{otherwise} \end{cases}$$

Therefore,

$$P_n = \int_{-\infty}^{\infty} \mathcal{S}_n(f) df = \frac{N_0}{2} \times 2W = WN_0 \quad (5.1.19)$$

Therefore,

$$\left(\frac{S}{N}\right)_{oSSB} = \frac{P_o}{P_{n_o}} = \frac{A_c^2 P_m}{WN_0} \quad (5.1.20)$$

But, in this case,

$$P_R = P_U = A_c^2 P_m \quad (5.1.21)$$

and, therefore,

$$\left(\frac{S}{N}\right)_{oSSB} = \frac{P_R}{WN_0} = \left(\frac{S}{N}\right)_b \quad (5.1.22)$$

Therefore, the SNR in a SSB system is equivalent to that of a DSB system.

#### 5.1.4 Effect of Noise on Conventional AM

In conventional DSB AM, the modulated signal is

$$u(t) = A_c[1 + am_n(t)] \cos 2\pi f_c t \quad (5.1.23)$$

Therefore, the received signal at the input to the demodulator is

$$r(t) = [A_c[1 + am_n(t)] + n_c(t)] \cos 2\pi f_c t - n_s(t) \sin 2\pi f_c t \quad (5.1.24)$$

where  $a$  is the modulation index and  $m_n(t)$  is normalized so that its minimum value is  $-1$ . If a synchronous demodulator is employed, the situation is basically similar to the DSB case, except that we have  $1 + am_n(t)$  instead of  $m(t)$ . Therefore, in this case, after mixing and lowpass filtering, we have

$$y_1(t) = \frac{1}{2}\{A_c[1 + am_n(t)] + n_c(t)\} \quad (5.1.25)$$

However, in this case, the desired signal is  $m(t)$ , not  $1 + am_n(t)$ . The dc component in the demodulated waveform is removed by a dc blocking device and, hence, the lowpass filter output is

$$y(t) = \frac{1}{2}A_c am_n(t) + \frac{n_c(t)}{2} \quad (5.1.26)$$

In this case, from Equation (5.1.24), we obtain the received signal power  $P_R$  as

$$P_R = \frac{A_c^2}{2} [1 + a^2 P_{m_n}] \quad (5.1.27)$$

where we have assumed that the message signal is zero mean. Now we can derive the

output SNR for the coherent demodulator. From Equation (5.1.26)

$$\begin{aligned}
 \left(\frac{S}{N}\right)_{oAM} &= \frac{\frac{1}{4}A_c^2 a^2 P_{m_n}}{\frac{1}{4}P_{n_c}} \\
 &= \frac{A_c^2 a^2 P_{m_n}}{2N_0 W} \\
 &= \frac{a^2 P_{m_n}}{1 + a^2 P_{m_n}} \frac{\frac{A_c^2}{2} [1 + a^2 P_{m_n}]}{N_0 W} \\
 &= \frac{a^2 P_{m_n}}{1 + a^2 P_{m_n}} \frac{P_R}{N_0 W} \\
 &= \frac{a^2 P_{m_n}}{1 + a^2 P_{m_n}} \left(\frac{S}{N}\right)_b \\
 &= \eta \left(\frac{S}{N}\right)_b
 \end{aligned} \tag{5.1.28}$$

where we have used Equation (5.1.2) and

$$\eta = \frac{a^2 P_{m_n}}{1 + a^2 P_{m_n}} \tag{5.1.29}$$

denotes the modulation efficiency.

From above it is seen that, since  $a^2 P_{m_n} < 1 + a^2 P_{m_n}$ , the SNR in conventional AM is always smaller than the SNR in a baseband system. In practical applications, the modulation index  $a$  is in the range of 0.8–0.9. The power content of the normalized message process depends on the message source. For speech signals that usually have a large dynamic range,  $P_{m_n}$  is in the neighborhood of 0.1. This means that the overall loss in SNR compared to a baseband system is a factor of 0.075 or equivalent to a loss of 11 dB. The reason for this loss is that a large part of the transmitter power is used to send the carrier component of the modulated signal and not the desired signal.

To analyze the envelope detector performance in the presence of noise, we have to use certain approximations. This is mainly due to the nonlinear structure of the envelope detector that makes an exact analysis difficult. In this case the demodulator detects the envelope of the received signal and the noise process. The input to the envelope detector is

$$r(t) = [A_c\{1 + am_n(t)\} + n_c(t)] \cos 2\pi f_c t - n_s(t) \sin 2\pi f_c t \tag{5.1.30}$$

and, therefore, the envelope of  $r(t)$  is given by (see Equation (4.6.2))

$$V_r(t) = \sqrt{[A_c[1 + am_n(t)] + n_c(t)]^2 + n_s^2(t)} \tag{5.1.31}$$

Now, we assume that the signal component in  $r(t)$  is much stronger than the noise

component. With this assumption, we have

$$P(n_s(t) \ll [A_c[1 + am_n(t)]]) \approx 1 \quad (5.1.32)$$

Therefore, with high probability

$$V_r(t) \approx [A_c[1 + am_n(t)] + n_c(t)] \quad (5.1.33)$$

After removing the dc component, we obtain

$$y(t) = A_c am_n(t) + n_c(t) \quad (5.1.34)$$

which is basically the same as  $y(t)$  for the synchronous demodulation without the  $\frac{1}{2}$  coefficient. This coefficient, of course, has no effect on the final SNR, and therefore we conclude that, under the assumption of high SNR at the receiver input, the performance of synchronous and envelope demodulators is the same. However, if the above assumption is not true, with synchronous demodulation we still have additive signal and noise at the receiver output, but with envelope demodulation, the signal and noise become intermingled. To see this, let us assume that at the receiver input the noise power<sup>†</sup> is much stronger than the signal power. This means that

$$\begin{aligned} V_r(t) &= \sqrt{[A_c[1 + am_n(t)] + n_c(t)]^2 + n_s^2(t)} \\ &= \sqrt{A_c^2(1 + am_n(t))^2 + n_c^2(t) + n_s^2(t) + 2A_cn_c(t)(1 + am_n(t))} \\ &\stackrel{a}{\approx} \sqrt{(n_c^2(t) + n_s^2(t)) \left[ 1 + \frac{2A_cn_c(t)}{n_c^2(t) + n_s^2(t)}(1 + am_n(t)) \right]} \\ &\stackrel{b}{\approx} V_n(t) \left[ 1 + \frac{A_cn_c(t)}{V_n^2(t)}(1 + am_n(t)) \right] \\ &= V_n(t) + \frac{A_cn_c(t)}{V_n(t)}(1 + am_n(t)) \end{aligned} \quad (5.1.35)$$

where in (a) we have used the fact that  $(1 + am_n(t))^2$  is small compared to the other components and in (b) we have denoted  $\sqrt{n_c^2(t) + n_s^2(t)}$  by  $V_n(t)$ , the envelope of the noise process, and have used the approximation  $\sqrt{1 + \epsilon} \approx 1 + \frac{\epsilon}{2}$ , for small  $\epsilon$ , where

$$\epsilon = \frac{2A_cn_c(t)}{n_c^2(t) + n_s^2(t)}(1 + am_n(t)) \quad (5.1.36)$$

From Equation (5.1.35), it is observed that at the demodulator output, the signal and the noise components are no longer additive and, in fact, the signal component is multiplied by noise and is no longer distinguishable. In this case, no meaningful SNR can be defined. It is said that this system *is operating below the threshold*. The

<sup>†</sup>By noise power at the receiver input we mean the power of the noise within the bandwidth of the modulated signal, or equivalently, the noise power at the output of the noise-limiting filter.

subject of threshold and its effect on the performance of a communication system will be covered in Section 5.3.1 when we discuss the noise performance in angle modulation.

### Example 5.1.1

The message signal  $m(t)$  has a bandwidth of 10 KHz, a power of 16 W and a maximum amplitude of 6. It is desirable to transmit this message to a destination via a channel with 80-dB attenuation and additive white noise with power-spectral density  $S_n(f) = \frac{N_0}{2} = 10^{-12}$  W/Hz, and achieve a SNR at the modulator output of at least 50 dB. What is the required transmitter power and channel bandwidth if the following modulation schemes are employed?

1. DSB AM
2. SSB AM
3. Conventional AM with modulation index equal to 0.8

**Solution** We first determine  $\left(\frac{S}{N}\right)_b$  as a basis of comparison.

$$\left(\frac{S}{N}\right)_b = \frac{P_R}{N_0 W} = \frac{P_R}{2 \times 10^{-12} \times 10^4} = \frac{10^8 P_R}{2}$$

Since the channel attenuation is 80 dB, the ratio of transmitted power  $P_T$  to received power  $P_R$  is

$$10 \log \frac{P_T}{P_R} = 80$$

and, therefore,

$$P_R = 10^{-8} P_T$$

Hence,

$$\left(\frac{S}{N}\right)_b = \frac{10^8 \times 10^{-8} P_T}{2} = \frac{P_T}{2}$$

1. For DSB AM, we have

$$\left(\frac{S}{N}\right)_o = \left(\frac{S}{N}\right)_b = \frac{P_T}{2} \sim 50 \text{ dB} = 10^5$$

therefore,

$$\frac{P_T}{2} = 10^5 \implies P_T = 2 \times 10^5 \text{ W} \sim 200 \text{ KW}$$

and

$$\text{BW} = 2W = 2 \times 10000 = 20000 \text{ Hz} \sim 20 \text{ KHz}$$

2. For SSB AM,

$$\left(\frac{S}{N}\right)_o = \left(\frac{S}{N}\right)_b = \frac{P_T}{2} = 10^5 \implies P_T = 200 \text{ KW}$$

and

$$BW = W = 10000 \text{ Hz} = 10 \text{ KHz}$$

3. For conventional AM, with  $a = 0.8$ ,

$$\left(\frac{S}{N}\right)_o = \eta \left(\frac{S}{N}\right)_b = \eta \frac{P_T}{2}$$

where  $\eta$  is the modulation efficiency given by

$$\eta = \frac{a^2 P_{m_n}}{1 + a^2 P_{m_n}}$$

First we find  $P_{m_n}$ , the power content of the normalized message signal. Since  $\max|m(t)| = 6$ , we have

$$P_{m_n} = \frac{P_m}{(\max|m(t)|)^2} = \frac{P_m}{36} = \frac{16}{36} = \frac{4}{9}$$

Hence,

$$\eta = \frac{0.8^2 \times \frac{4}{9}}{1 + 0.8^2 \times \frac{4}{9}} \approx 0.22$$

Therefore,

$$\left(\frac{S}{N}\right)_o \approx 0.22 \frac{P_T}{2} = 0.11 P_T = 10^5$$

or

$$P_T \approx 909 \text{ KW}$$

The bandwidth of conventional AM is equal to the bandwidth of DSB AM; i.e.,

$$BW = 2W = 20 \text{ KHz}$$

## 5.2 CARRIER-PHASE ESTIMATION WITH A PHASE-LOCKED LOOP (PLL)

In this section, we describe a method for generating a phase reference for synchronous demodulation of a DSB-SC AM signal. The received noise-corrupted signal at the input to the demodulator is given by (compare with Equation (3.2.5)).

$$\begin{aligned} r(t) &= u(t) + n(t) \\ &= A_c m(t) \cos(2\pi f_c t + \phi_c) + n(t) \end{aligned} \quad (5.2.1)$$

First, we note that the received signal  $r(t)$  has a zero mean, since the message signal  $m(t)$  is zero mean; i.e.,  $m(t)$  contains no *dc* component. Consequently, the average power at the output of a narrowband filter tuned to the carrier frequency  $f_c$  is zero. This fact implies that we cannot extract a carrier-signal component directly from  $r(t)$ .



If we square  $r(t)$ , the squared signal contains a spectral component at twice the carrier frequency; i.e.,

$$\begin{aligned} r^2(t) &= A_c^2 m^2(t) \cos^2(2\pi f_c t + \phi_c) + \text{noise terms} \\ &= \frac{1}{2} A_c^2 m^2(t) + \frac{1}{2} A_c^2 m^2(t) \cos(4\pi f_c t + 2\phi_c) + \text{noise terms} \end{aligned} \quad (5.2.2)$$

Since  $m^2(t) > 0$ , there is signal power at the frequency  $2f_c$ , which can be used to drive a phase-locked loop (PLL).

In order to isolate the desired double-frequency component from the rest of the frequency components, the squared-input signal is passed through a narrowband filter that is tuned to the frequency  $2f_c$ . The mean value of the output of such a filter is a sinusoid with frequency  $2f_c$ , phase  $2\phi_c$ , and amplitude  $A_c^2 m^2(t) H(2f_c)/2$ , where  $|H(2f_c)|$  is the gain (attenuation) of the filter at  $f = 2f_c$ . Thus, squaring the input signal produces a sinusoidal component at twice the carrier frequency which can be used as the input to a PLL. The general configuration for the carrier-phase estimation system is illustrated in Figure 5.1.

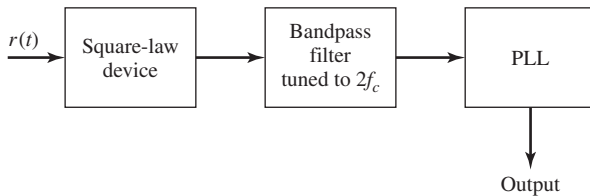


**Figure 5.1** System for carrier-phase estimation.

### 5.2.1 The Phase-Locked Loop (PLL)

The PLL consists of a multiplier, a loop filter, and a voltage-controlled oscillator (VCO), as shown in Figure 5.2. Suppose that the input to the PLL is the sinusoid  $\cos(4\pi f_c t + 2\phi)$  and the output of the VCO is  $\sin(4\pi f_c t + 2\hat{\phi})$ , where  $\hat{\phi}$  represents the estimate of  $\phi$ . The product of these two signals produces the signal

$$\begin{aligned} e(t) &= \cos(4\pi f_c t + 2\phi) \sin(4\pi f_c t + 2\hat{\phi}) \\ &= \frac{1}{2} \sin 2(\hat{\phi} - \phi) + \frac{1}{2} \sin(8\pi f_c t + 2\hat{\phi} + 2\phi) \end{aligned} \quad (5.2.3)$$

Note that  $e(t)$  contains a low-frequency term ( $dc$ ) and a term at four times the carrier.

The loop filter is a lowpass filter that responds only to the low-frequency component  $\sin 2(\hat{\phi} - \phi)$  and removes the component at  $4f_c$ . This filter is usually selected to

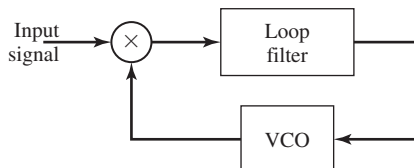


**Figure 5.2** Basic elements of a PLL.

have the relatively simple transfer function

$$G(s) = \frac{1 + \tau_2 s}{1 + \tau_1 s} \quad (5.2.4)$$

where the time constants  $\tau_1$  and  $\tau_2$  are design parameters ( $\tau_1 \gg \tau_2$ ) that control the bandwidth of the loop. A higher-order filter that contains additional poles may be used, if necessary, to obtain a better loop response.

The output of the loop,  $v(t)$ , provides the control voltage for the VCO whose implementation is described in Section 3.3.3, in the context of FM modulation. The VCO is basically a sinusoidal signal generator with an instantaneous phase given by

$$4\pi f_c t + 2\hat{\phi} = 4\pi f_c t + K_v \int_{-\infty}^t v(\tau) d\tau \quad (5.2.5)$$

where  $K_v$  is a gain constant in radians/volt-sec. Hence, the carrier-phase estimate at the output of the VCO is

$$2\hat{\phi} = K_v \int_{-\infty}^t v(\tau) d\tau \quad (5.2.6)$$

and its transfer function is  $K_v/s$ .

Because the double-frequency term resulting from the multiplication of the input signal to the loop with the output of the VCO is removed by the loop filter, the PLL may be represented by the closed-loop system model shown in Figure 5.3. The sine function of the phase difference  $2(\hat{\phi} - \phi)$  makes the system nonlinear and, as a consequence, the analysis of the PLL performance in the presence of noise is somewhat involved, although it is mathematically tractable for simple-loop filters.

In steady-state operation when the loop is tracking the phase of the received carrier, the phase error  $\hat{\phi} - \phi$  is small and, hence,

$$\frac{1}{2} \sin 2(\hat{\phi} - \phi) \approx \hat{\phi} - \phi \quad (5.2.7)$$

With this approximation, the PLL is represented by the *linear model* shown in Figure 5.4. This linear model has a closed-loop transfer function.

$$H(s) = \frac{K G(s)/s}{1 + K G(s)/s} \quad (5.2.8)$$

where the factor of 1/2 has been absorbed into the gain parameter  $K$ . By substituting

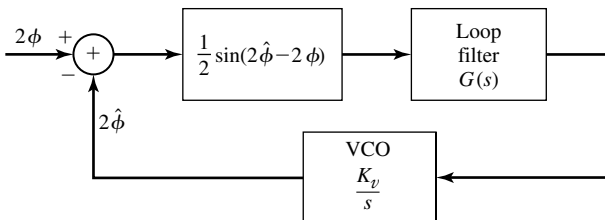
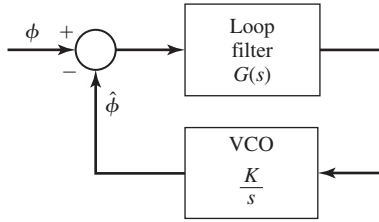


Figure 5.3 Model of a PLL.



**Figure 5.4** Linear model of a PLL.

from Equation (5.2.4) for  $G(s)$  into Equation (5.2.8), we obtain

$$H(s) = \frac{1 + \tau_2 s}{1 + (\tau_2 + \frac{1}{K})s + \frac{\tau_1}{K}s^2} \quad (5.2.9)$$

Hence, the closed-loop system function for the linearized PLL is second order when the loop filter has a single pole and a single zero. The parameter  $\tau_2$  determines the position of the zero in  $H(s)$ , while  $K$ ,  $\tau_1$ , and  $\tau_2$  control the position of the closed-loop system poles.

The denominator of  $H(s)$  may be expressed in the standard form

$$D(s) = s^2 + 2\zeta\omega_n s + \omega_n^2 \quad (5.2.10)$$

where  $\zeta$  is called the *loop-damping factor* and  $\omega_n$  is the *natural frequency* of the loop. In terms of the loop parameters,  $\omega_n = \sqrt{K/\tau_1}$  and  $\zeta = \omega_n(\tau_2 + 1/K)/2$ , the closed-loop transfer function becomes

$$H(s) = \frac{(2\zeta\omega_n - \omega_n^2/K)s + \omega_n^2}{s^2 + 2\zeta\omega_n s + \omega_n^2} \quad (5.2.11)$$

The magnitude response  $20 \log |H(j\omega)|$  as a function of the normalized frequency  $\omega/\omega_n$  is illustrated in Figure 5.5, with the damping factor as a parameter and  $\tau_1 \gg 1$ . Note that,  $\zeta = 1$  results in a critically damped loop response,  $\zeta < 1$  produces an underdamped loop response, and  $\zeta > 1$  yields an overdamped loop response.

The (one-sided) noise equivalent bandwidth of the loop is (see Problem 5.6)

$$B_{eq} = \frac{\tau_2^2(1/\tau_2^2 + K/\tau_1)}{4(\tau_2 + \frac{1}{K})} = \frac{1 + (\tau_2\omega_n)^2}{8\zeta/\omega_n} \quad (5.2.12)$$

In practice, the selection of the bandwidth of the PLL involves a trade-off between speed of response and noise in the phase estimate. On the one hand, it is desirable to select the bandwidth of the loop to be sufficiently wide in order to track any time variations in the phase of the received carrier. On the other hand, a wideband PLL allows more noise to pass into the loop, which corrupts the phase estimate. Next, we assess the effects of noise in the quality of the phase estimate.

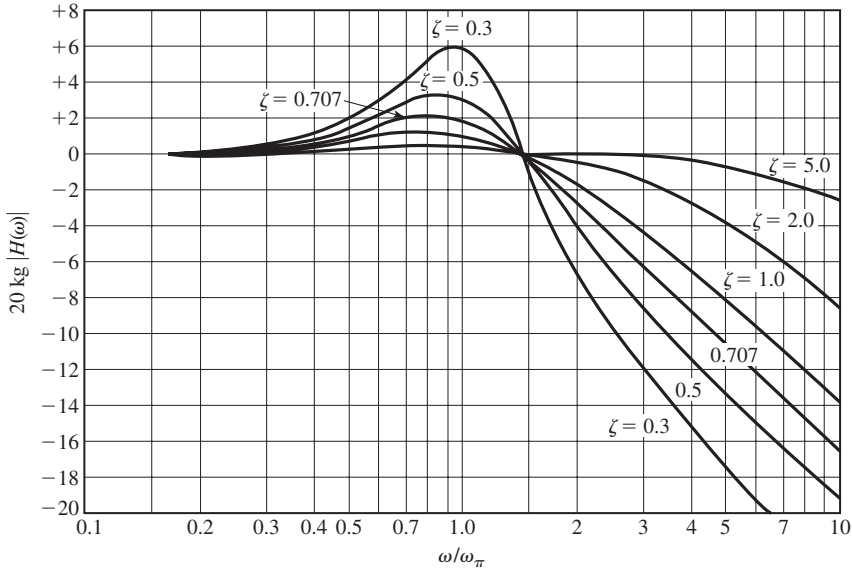


**Figure 5.5** Frequency response of a second-order loop. (From *Phaselock Techniques*, 2nd Ed., by F. M. Gardner; © 1979 by John Wiley & Sons. Reprinted with permission of the publisher.)

### 5.2.2 Effect of Additive Noise on Phase Estimation

In order to evaluate the effects of noise on the estimate of the carrier phase, let us assume that the PLL is tracking a sinusoidal signal of the form

$$s(t) = A_c \cos[2\pi f_c t + \phi(t)] \quad (5.2.13)$$

which is corrupted by the additive narrowband noise

$$n(t) = n_c(t) \cos 2\pi f_c t - n_s(t) \sin 2\pi f_c t \quad (5.2.14)$$

The in-phase and quadrature components of the noise are assumed to be statistically independent, stationary Gaussian noise processes with (two-sided) power-spectral density  $N_0/2$  W/Hz. By using simple trigonometric identities, the noise term in Equation (5.2.14) can be expressed as

$$n(t) = x_c(t) \cos[2\pi f_c t + \phi(t)] - x_s(t) \sin[2\pi f_c t + \phi(t)] \quad (5.2.15)$$

where

$$\begin{aligned} x_c(t) &= n_c(t) \cos \phi(t) + n_s(t) \sin \phi(t) \\ x_s(t) &= -n_c(t) \sin \phi(t) + n_s(t) \cos \phi(t) \end{aligned} \quad (5.2.16)$$

We note that

$$x_c(t) + jx_s(t) = [n_c(t) + jn_s(t)]e^{-j\phi(t)} \quad (5.2.17)$$

It is easy to verify that a phase shift does not change the first two moments of  $n_c(t)$  and  $n_s(t)$ , so that the quadrature components  $x_c(t)$  and  $x_s(t)$  have exactly the same statistical characteristics as  $n_c(t)$  and  $n_s(t)$  (see also Problem 4.29).

Now, if  $s(t) + n(t)$  is multiplied by the output of the VCO and the double-frequency terms are neglected, the input to the loop filter is the noise-corrupted signal

$$e(t) = A_c \sin \Delta\phi + x_c(t) \sin \Delta\phi - x_s(t) \cos \Delta\phi \quad (5.2.18)$$

where, by definition,  $\Delta\phi = \hat{\phi} - \phi$  is the phase error. Thus, we have the equivalent model for the PLL with additive noise as shown in Figure 5.6.

When the power  $P_c = A_c^2/2$  of the incoming signal is much larger than the noise power, the phase estimate  $\hat{\phi} \approx \phi$ . Then, we may linearize the PLL and, thus, easily determine the effect of the additive noise on the quality of the estimate  $\hat{\phi}$ . Under these conditions, the model for the linearized PLL with additive noise is illustrated in Figure 5.7. Note that the gain parameter  $A_c$  may be normalized to unity, provided that the noise term is scaled by  $1/A_c$ . Thus, the noise term becomes

$$n_1(t) = \frac{x_c(t)}{A_c} \sin \Delta\phi - \frac{x_s(t)}{A_c} \cos \Delta\phi \quad (5.2.19)$$

Since the noise  $n_1(t)$  is additive at the input to the loop, the variance of the phase error  $\Delta\phi$ , which is also the variance of the VCO output phase, is

$$\sigma_{\hat{\phi}}^2 = \frac{N_0 B_{\text{neq}}}{A_c^2} \quad (5.2.20)$$

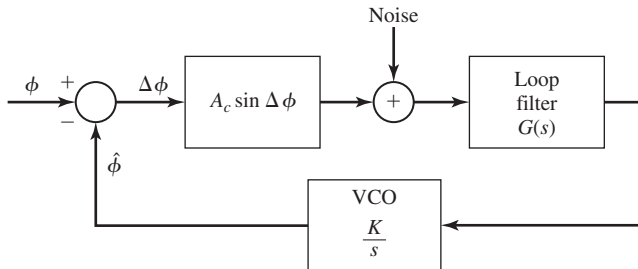


**Figure 5.6** Equivalent model of PLL with additive noise.

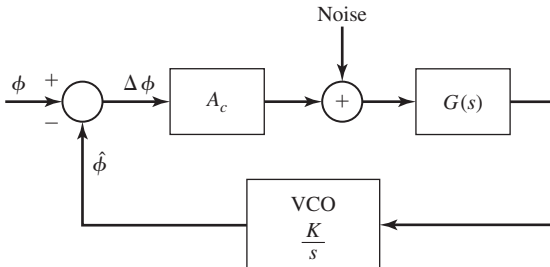


**Figure 5.7** Linearized model of PLL with additive noise.

where  $B_{\text{neq}}$  is the (one-sided) noise-equivalent bandwidth of the loop, given by Equation (5.2.12). Note that  $A_c^2/2$  is the power of the input sinusoid and  $\sigma_{\hat{\phi}}^2$  is simply the ratio of the total noise power within the bandwidth of the PLL divided by the input signal power. Hence,

$$\sigma_{\hat{\phi}}^2 = \frac{1}{\rho_L} \quad (5.2.21)$$

where  $\rho_L$  is defined as the SNR

$$\rho_L = \frac{A_c^2/2}{B_{\text{neq}}N_0/2} \quad (5.2.22)$$

Thus, the variance of  $\hat{\phi}$  is inversely proportional to the SNR.

The expression for the variance  $\sigma_{\hat{\phi}}^2$  of the VCO-phase error applies to the case where the SNR is sufficiently high so that the linear model for the PLL applies. An exact analysis based on the nonlinear PLL is mathematically tractable when  $G(s) = 1$ , which results in a first-order loop. In this case, the PDF for the phase error can be derived [see Viterbi (1966)], and has the form

$$f(\Delta\phi) = \frac{\exp(\rho_L \cos \Delta\phi)}{2\pi I_0(\rho_L)} \quad (5.2.23)$$

where  $\rho_L$  is the SNR defined in Equation (5.2.22),  $B_{\text{neq}}$  is the appropriate noise-equivalent bandwidth of the first-order loop, and  $I_0(\cdot)$  is the modified Bessel function of order zero.

From the expression for  $f(\Delta\phi)$  we may obtain the exact value of the variance  $\sigma_{\hat{\phi}}^2$  for the phase error of a first-order PLL. This is plotted in Figure 5.8 as a function of  $1/\rho_L$ . Also shown for comparison is the result obtained with the linearized PLL model. Note that the variance for the linear model is close to the exact variance for  $\rho_L > 3$ . Hence, the linear model is adequate for practical purposes.

Approximate analysis of the statistical characteristics of the phase error for the nonlinear PLL have also been performed. Of particular importance is the transient behavior of the nonlinear PLL during initial acquisition. Another important problem is the behavior of the PLL at low SNR. It is known, for example, that when the SNR at the input to the PLL drops below a certain value, there is a rapid deterioration in the performance of the PLL. The loop begins to lose lock and an impulsive-type of noise, characterized as clicks, is generated, which degrades the performance of the loop. Results on these topics can be found in the texts by Viterbi (1966), Lindsey (1972), Lindsey and Simon (1973), and Gardner (1979), and in the survey papers by Gupta (1975) and Lindsey and Chie (1981).

**Squaring Loop.** Now that we have established the effect of noise on the performance of the PLL, let us return to the problem of carrier synchronization based on the system shown in Figure 5.9. The squaring of the received signal that produces the frequency component at  $2f_c$  also enhances the noise power level at the input to the PLL and, thus, it increases the variance of the phase error.

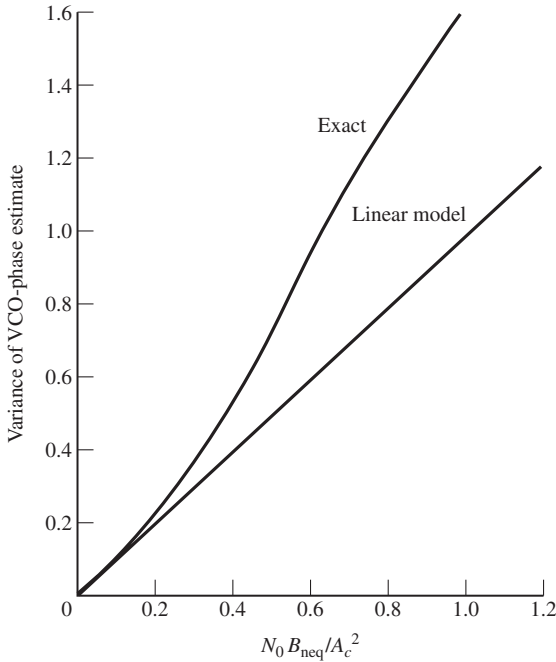


**Figure 5.8** Comparison of VCO-phase variance for exact and approximate (linear order) first-order PLL. (From *Principles of Coherent Communication*, by A. J. Viterbi; © 1966 by McGraw-Hill. Reprinted with permission of the publisher.)

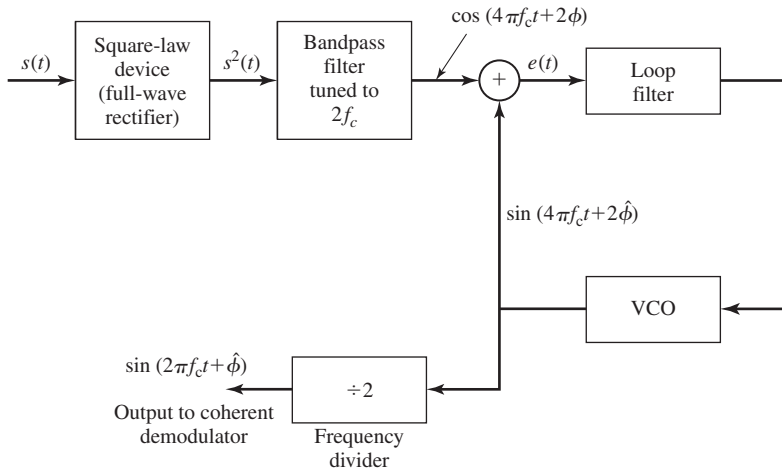


**Figure 5.9** Carrier recovery using a square-law device.

To elaborate on this point, let the input to the squarer be  $u(t) + n(t)$ . The output is

$$y(t) = u^2(t) + 2u(t)n(t) + n^2(t) \tag{5.2.24}$$

The noise terms are  $2u(t)n(t)$  and  $n^2(t)$ . By computing the autocorrelation and power-spectral density of these two noise components, one can show that both components

have spectral power in the frequency band centered at  $2f_c$ . Consequently, the bandpass filter with bandwidth  $B_{\text{neq}}$  centered at  $2f_c$ , which produces the desired sinusoidal signal component that drives the PLL, also passes noise due to these two noise terms.

Let us select the bandwidth of the loop to be significantly smaller than the bandwidth  $B_{bp}$  of the bandpass filter, so that the total noise spectrum at the input to the PLL may be approximated by a constant within the loop bandwidth. This approximation allows us to obtain a simple expression for the variance of the phase error as

$$\sigma_{\hat{\phi}}^2 = \frac{1}{\rho_L S_L} \quad (5.2.25)$$

where  $S_L$  is called the squaring loss and is given as

$$S_L = \frac{1}{1 + \frac{B_{bp}/2B_{\text{neq}}}{\rho_L}} \quad (5.2.26)$$

Since  $S_L < 1$ , we have an increase in the variance of the phase error caused by the added noise power that results from the squaring operation. For example, when  $\rho_L = B_{bp}/2B_{\text{neq}}$ , the loss is 3 dB or, equivalently, the variance in the estimate increases by a factor of two.

Finally, we observe that the output of the VCO from the squaring loop must be frequency divided by a factor of two and phase shifted by  $90^\circ$  to generate the carrier signal for demodulating the received signal.

**Costas Loop.** A second method for generating a properly phased carrier for a DSB-SC AM signal is illustrated by the block diagram in Figure 5.10. The received signal

$$r(t) = A_c m(t) \cos(2\pi f_c t + \phi) + n(t)$$

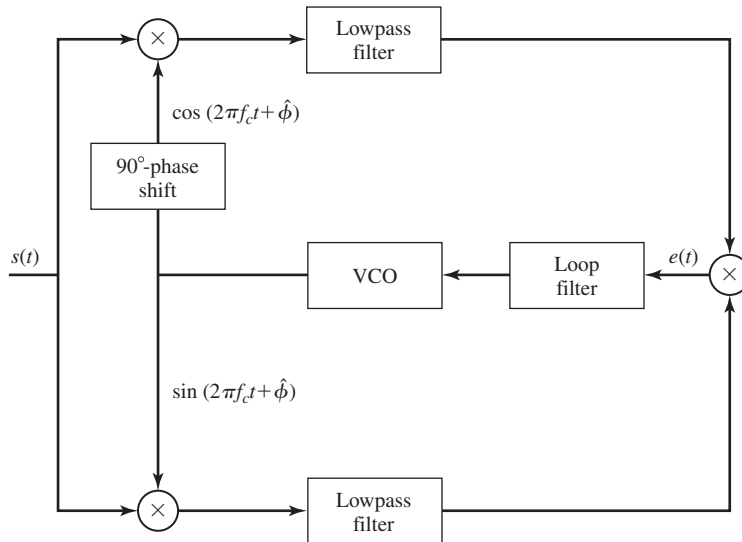


**Figure 5.10** Block diagram of Costas loop.



is multiplied by  $\cos(2\pi f_c t + \hat{\phi})$  and  $\sin(2\pi f_c t + \hat{\phi})$ , which are outputs from the VCO. The two products are

$$\begin{aligned} y_c(t) &= [A_c m(t) \cos(2\pi f_c t + \phi) \\ &\quad + n_c(t) \cos 2\pi f_c t - n_s(t) \sin 2\pi f_c t] \cos(2\pi f_c t + \hat{\phi}) \\ &= \frac{A_c}{2} m(t) \cos \Delta\phi + \frac{1}{2} [n_c(t) \cos \hat{\phi} + n_s(t) \sin \hat{\phi}] \\ &\quad + \text{double-frequency terms} \end{aligned} \quad (5.2.27)$$

$$\begin{aligned} y_s(t) &= [A_c m(t) \cos(2\pi f_c t + \phi) \\ &\quad + n_c(t) \cos 2\pi f_c t - n_s(t) \sin 2\pi f_c t] \sin(2\pi f_c t + \hat{\phi}) \\ &= \frac{A_c}{2} m(t) \sin \Delta\phi + \frac{1}{2} [n_c(t) \sin \hat{\phi} - n_s(t) \cos \hat{\phi}] \\ &\quad + \text{double-frequency terms} \end{aligned} \quad (5.2.28)$$

where  $\Delta\phi = \hat{\phi} - \phi$ . The double-frequency terms are eliminated by the lowpass filters following the multiplications.

An error signal is generated by multiplying the two outputs  $y'_c(t)$  and  $y'_s(t)$  of the lowpass filters. Thus,

$$\begin{aligned} e(t) &= y'_c(t) y'_s(t) \\ &= \frac{A_c^2}{8} m^2(t) \sin 2\Delta\phi + \frac{A_c}{4} m(t) [n_c(t) \cos \hat{\phi} + n_s(t) \sin \hat{\phi}] \sin \Delta\phi \\ &\quad + \frac{A_c}{4} m(t) [n_c(t) \sin \hat{\phi} - n_s(t) \cos \hat{\phi}] \cos \Delta\phi \\ &\quad + \frac{1}{4} [n_c(t) \cos \hat{\phi} + n_s(t) \sin \hat{\phi}] [n_c(t) \sin \hat{\phi} - n_s(t) \cos \hat{\phi}] \end{aligned}$$

This error signal is filtered by the loop filter whose output is the control voltage that drives the VCO.

We note that the error signal into the loop filter consists of the desired term  $(A_c^2 m^2(t)/8) \sin 2\Delta\phi$ , plus terms that involve signal  $\times$  noise and noise  $\times$  noise. These terms are similar to the two noise terms at the input of the PLL for the squaring method. In fact, if the loop filter in the Costas loop is identical to that used in the squaring loop, the two loops are equivalent. Under this condition, the PDF of the phase error and the performance of the two loops are identical.

In conclusion, the squaring PLL and the Costas PLL are two practical methods for deriving a carrier-phase estimate for synchronous demodulation of a DSB-SC AM signal.

### 5.3 EFFECT OF NOISE ON ANGLE MODULATION

In this section, we will study the performance of angle-modulated signals when contaminated by additive white Gaussian signals and compare this performance with the performance of amplitude-modulated signals. Recall that in amplitude modulation, the

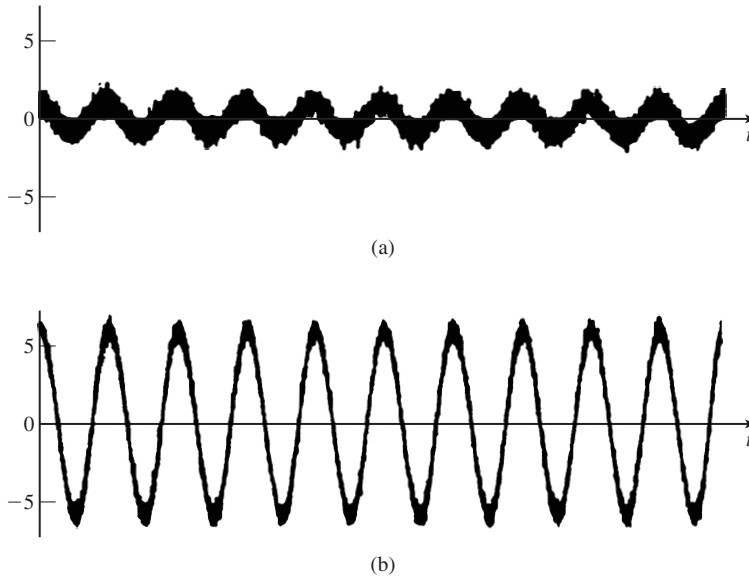


**Figure 5.11** Effect of noise on the zero crossings of (a) low-power and (b) high-power modulated signals.

message information is contained in the amplitude of the modulated signal, and since noise is additive, the noise is directly added to the signal. However, in a frequency-modulated signal, the noise is added to the amplitude and the message information is contained in the frequency of the modulated signal. Therefore, the message is contaminated by the noise to the extent that the added noise changes the frequency of the modulated signal. The frequency of a signal can be described by its zero crossings. Therefore, the effect of additive noise on the demodulated FM signal can be described by the changes that it produces in the zero crossings of the modulated FM signal. Figure 5.11 shows the effect of additive noise on the zero crossings of two frequency-modulated signals, one with high power and the other with low power. From the above discussion and also from Figure 5.11, it should be clear that the effect of noise in an FM system is less than that for an AM system. It is also observed that the effect of noise in a low-power FM system is more than in a high-power FM system. The analysis that we present in this chapter verifies our intuition based on these observations.

The block diagram of the receiver for a general angle-modulated signal is shown in Figure 5.12. The angle-modulated signal is represented as<sup>†</sup>

$$\begin{aligned}
 u(t) &= A_c \cos(2\pi f_c t + \phi(t)) \\
 &= \begin{cases} A_c \cos(2\pi f_c t + 2\pi k_f \int_{-\infty}^t m(\tau) d\tau), & \text{FM} \\ A_c \cos(2\pi f_c t + k_p m(t)), & \text{PM} \end{cases} \quad (5.3.1)
 \end{aligned}$$

<sup>†</sup>When we refer to the modulated signal, we mean the signal as received by the receiver. Therefore, the signal power is the power in the received signal not the transmitted power.

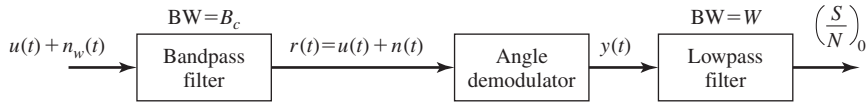


**Figure 5.12** Block diagram of receiver for a general angle-demodulated signal.

The additive white Gaussian noise  $n_w(t)$  is added to  $u(t)$  and the result is passed through a noise-limiting filter whose role is to remove the out-of-band noise. The bandwidth of this filter is equal to the bandwidth of the modulated signal, and therefore, it passes the modulated signal without distortion. However, it eliminates the out-of-band noise and, hence, the noise output of the filter is a bandpass Gaussian noise denoted by  $n(t)$ . The output of this filter is

$$\begin{aligned} r(t) &= u(t) + n(t) \\ &= u(t) + n_c(t) \cos 2\pi f_c t - n_s(t) \sin 2\pi f_c t \end{aligned} \quad (5.3.2)$$

As with conventional AM noise-performance analysis, a precise analysis is quite involved due to the nonlinearity of the demodulation process. Let us make the assumption that the signal power is much higher than the noise power. Then, if the bandpass noise is represented as

$$\begin{aligned} n(t) &= \sqrt{n_c^2(t) + n_s^2(t)} \cos\left(2\pi f_c t + \arctan \frac{n_s(t)}{n_c(t)}\right) \\ &= V_n(t) \cos(2\pi f_c t + \Phi_n(t)) \end{aligned} \quad (5.3.3)$$

where  $V_n(t)$  and  $\Phi_n(t)$  represent the envelope and the phase of the bandpass noise process, respectively, the assumption that the signal is much larger than the noise means that

$$p(V_n(t) \ll A_c) \approx 1 \quad (5.3.4)$$

Therefore, the phasor diagram of the signal and the noise are as shown in Figure 5.13. From this figure it is obvious that we can write

$$\begin{aligned} r(t) &\approx \left( A_c + V_n(t) \cos(\Phi_n(t) - \phi(t)) \right) \cos\left( 2\pi f_c t + \phi(t) \right. \\ &\quad \left. + \arctan \frac{V_n(t) \sin(\Phi_n(t) - \phi(t))}{A_c + V_n(t) \cos(\Phi_n(t) - \phi(t))} \right) \\ &\approx \left( A_c + V_n(t) \cos(\Phi_n(t) - \phi(t)) \right) \\ &\quad \times \cos\left( 2\pi f_c t + \phi(t) + \frac{V_n(t)}{A_c} \sin(\Phi_n(t) - \phi(t)) \right) \end{aligned}$$

The demodulator processes this signal and, depending whether it is a phase or a frequency demodulator, its output will be the phase or the instantaneous frequency of this

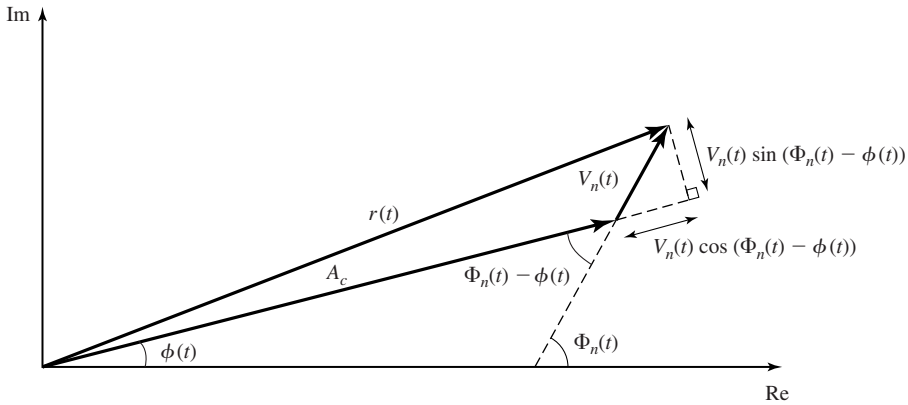


**Figure 5.13** Phasor diagram of signal and noise in an angle-modulated system.

signal.<sup>†</sup> Therefore, noting that

$$\phi(t) = \begin{cases} k_p m(t), & \text{PM} \\ 2\pi k_f \int_{-\infty}^t m(\tau) d\tau, & \text{FM} \end{cases} \quad (5.3.5)$$

the output of the demodulator is given by

$$\begin{aligned} y(t) &= \begin{cases} k_p m(t) + Y_n(t), & \text{PM} \\ k_f m(t) + \frac{1}{2\pi} \frac{d}{dt} Y_n(t), & \text{FM} \end{cases} \\ &= \begin{cases} k_p m(t) + \frac{V_n(t)}{A_c} \sin(\Phi_n(t) - \phi(t)), & \text{PM} \\ k_f m(t) + \frac{1}{2\pi} \frac{d}{dt} \frac{V_n(t)}{A_c} \sin(\Phi_n(t) - \phi(t)), & \text{FM} \end{cases} \end{aligned} \quad (5.3.6)$$

where, we have defined

$$Y_n(t) \stackrel{\text{def}}{=} \frac{V_n(t)}{A_c} \sin(\Phi_n(t) - \phi(t)). \quad (5.3.7)$$

The first term in Equations (5.3.5–5.3.7) is the desired signal component and the second term is the noise component. From this expression, we observe that the noise component is inversely proportional to the signal amplitude  $A_c$ . Hence, the higher the signal level, the lower will be the noise level. This is in agreement with the intuitive reasoning presented at the beginning of this section based on Figure 5.11. Note also that this is not the case with amplitude modulation. In AM systems, the noise component is independent of the signal component and a scaling of the signal power does not affect the received noise power.

<sup>†</sup>Of course, in the FM case the demodulator output is the instantaneous frequency deviation of  $v(t)$  from the carrier frequency  $f_c$ .

Let us study the properties of the noise component given by

$$\begin{aligned}
 Y_n(t) &= \frac{V_n(t)}{A_c} \sin(\Phi_n(t) - \phi(t)) \\
 &= \frac{1}{A_c} [V_n(t) \sin \Phi_n(t) \cos \phi(t) - V_n(t) \cos \Phi_n(t) \sin \phi(t)] \\
 &= \frac{1}{A_c} [n_s(t) \cos \phi(t) - n_c(t) \sin \phi(t)] \tag{5.3.8}
 \end{aligned}$$

The autocorrelation function of this process is given by

$$\begin{aligned}
 E[Y_n(t + \tau)Y_n(t)] &= \frac{1}{A_c^2} E[R_{n_s}(\tau) \cos(\phi(t)) \cos(\phi(t + \tau)) \\
 &\quad + R_{n_c}(\tau) \sin(\phi(t + \tau)) \sin(\phi(t))] \\
 &= \frac{1}{A_c^2} R_{n_c}(\tau) E[\cos(\phi(t + \tau) - \phi(t))] \tag{5.3.9}
 \end{aligned}$$

where we have used the fact that the noise process is stationary and  $R_{n_c}(\tau) = R_{n_s}(\tau)$  and  $R_{n_c n_s}(\tau) = 0$  [see Equation (4.6.1) and Example (4.6.1)]. Now we assume that the message  $m(t)$  is a sample function of a zero-mean, stationary Gaussian process  $M(t)$  with the autocorrelation function  $R_M(\tau)$ . Then, in both PM and FM modulation,  $\phi(t)$  will also be a sample function of a zero-mean stationary, Gaussian process  $\Phi(t)$ . For PM this is obvious because

$$\Phi(t) = k_p M(t) \tag{5.3.10}$$

and in the FM case, we have

$$\Phi(t) = 2\pi k_f \int_{-\infty}^t M(\tau) d\tau \tag{5.3.11}$$

Noting that  $\int_{-\infty}^t$  represents a linear time-invariant operation it is seen that, in this case,  $\Phi(t)$  is the output of an LTI system whose input is a zero-mean, stationary Gaussian process. Consequently  $\Phi(t)$  will also be a zero-mean, stationary Gaussian process.

At any fixed time  $t$ , the random variable  $Z(t, \tau) = \Phi(t + \tau) - \Phi(t)$  is the difference between two jointly Gaussian random variables. Therefore, it is itself a Gaussian random variable with mean equal to zero and variance

$$\begin{aligned}
 \sigma_Z^2 &= E[\Phi^2(t + \tau)] + E[\Phi^2(t)] - 2R_\Phi(\tau) \\
 &= 2[R_\Phi(0) - R_\Phi(\tau)] \tag{5.3.12}
 \end{aligned}$$

Now, using this result in Equation (5.3.9) we obtain

$$\begin{aligned}
 E[Y_n(t + \tau)Y_n(t)] &= \frac{1}{A_c^2} R_{n_c}(\tau) E[\cos(\Phi(t + \tau) - \Phi(t))] \\
 &= \frac{1}{A_c^2} R_{n_c}(\tau) \operatorname{Re} [E e^{j(\Phi(t + \tau) - \Phi(t))}] \\
 &= \frac{1}{A_c^2} R_{n_c}(\tau) \operatorname{Re} [E e^{jZ(t, \tau)}] \\
 &= \frac{1}{A_c^2} R_{n_c}(\tau) \operatorname{Re} [e^{-\frac{1}{2}\sigma_Z^2}] \\
 &= \frac{1}{A_c^2} R_{n_c}(\tau) \operatorname{Re} [e^{-(R_\Phi(0) - R_\Phi(\tau))}] \\
 &= \frac{1}{A_c^2} R_{n_c}(\tau) e^{-(R_\Phi(0) - R_\Phi(\tau))} \tag{5.3.13}
 \end{aligned}$$

where we have used Equation (4.1.15). This result shows that under the assumption of a stationary Gaussian message, the noise process at the output of the demodulator is also a stationary process whose autocorrelation function is given above and whose power-spectral density is

$$\begin{aligned}
 \mathcal{S}_Y(f) &= \mathcal{F}[R_Y(\tau)] \\
 &= \mathcal{F}\left[\frac{1}{A_c^2} R_{n_c}(\tau) e^{-(R_\Phi(0) - R_\Phi(\tau))}\right] \\
 &= \frac{e^{-R_\Phi(0)}}{A_c^2} \mathcal{F}[R_{n_c}(\tau) e^{R_\Phi(\tau)}] \\
 &= \frac{e^{-R_\Phi(0)}}{A_c^2} \mathcal{F}[R_{n_c}(\tau) g(\tau)] \\
 &= \frac{e^{-R_\Phi(0)}}{A_c^2} \mathcal{S}_{n_c}(f) \star G(f) \tag{5.3.14}
 \end{aligned}$$

where  $g(\tau) = e^{R_\Phi(\tau)}$  and  $G(f)$  is its Fourier transform.

It can be shown (see Problem 5.12) that bandwidth of  $g(\tau)$  is half the bandwidth  $B_c$  of the angle-modulated signal, which for high modulation indices is much larger than  $W$ , the message bandwidth. Since the bandwidth of the angle-modulated signal is defined as the frequencies that contain 98%–99% of the signal power,  $G(f)$  is very small in the neighborhood of  $|f| = \frac{B_c}{2}$  and, of course,

$$\mathcal{S}_{n_c}(f) = \begin{cases} N_0, & |f| < \frac{B_c}{2} \\ 0, & \text{otherwise} \end{cases} \tag{5.3.15}$$

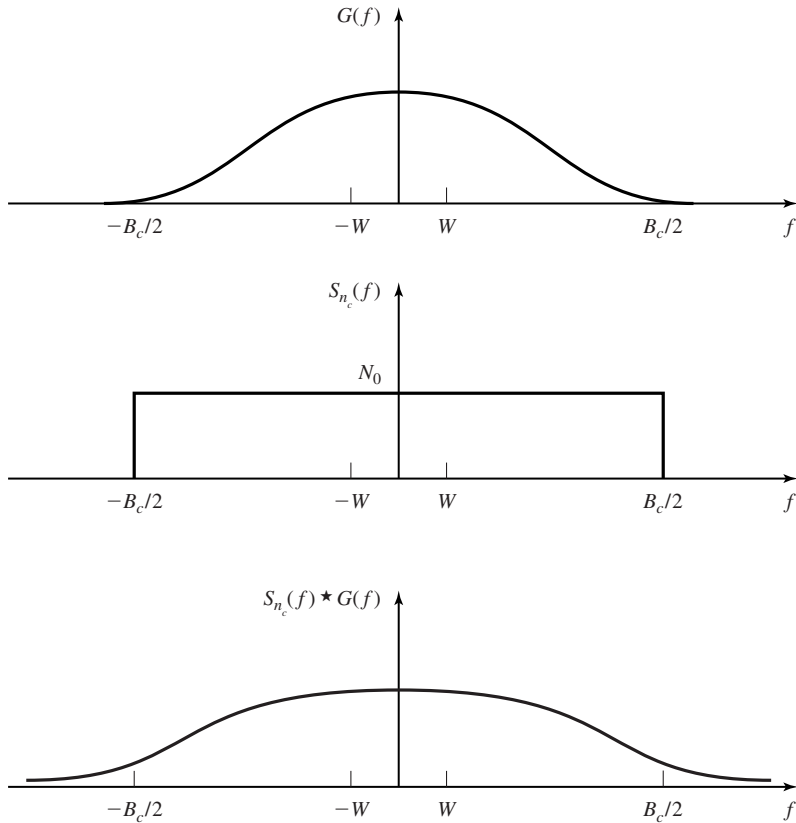


**Figure 5.14** Typical plots of  $G(f)$ ,  $S_{n_c}(f)$ , and the result of their convolution.

A typical example of  $G(f)$ ,  $S_{n_c}(f)$  and the result of their convolution is shown in Figure 5.14. Because  $G(f)$  is very small in the neighborhood of  $|f| = \frac{B_c}{2}$ , the resulting  $S_Y(f)$  has almost a flat spectrum for  $|f| < W$ , the bandwidth of the message. From Figure 5.14 it is obvious that for all  $|f| < W$ , we have

$$\begin{aligned}
 S_Y(f) &= \frac{e^{-R_\Phi(0)}}{A_c^2} S_{n_c}(f) \star G(f) \\
 &= \frac{e^{-R_\Phi(0)}}{A_c^2} N_0 \int_{-\frac{B_c}{2}}^{\frac{B_c}{2}} G(f) df \\
 &\approx \frac{e^{-R_\Phi(0)}}{A_c^2} N_0 \int_{-\infty}^{\infty} G(f) df \\
 &= \frac{e^{-R_\Phi(0)}}{A_c^2} N_0 g(\tau) \Big|_{\tau=0}
 \end{aligned}$$

$$\begin{aligned}
 &= \frac{e^{-R_{\Phi}(0)}}{A_c^2} N_0 e^{R_{\Phi}(0)} \\
 &= \frac{N_0}{A_c^2}
 \end{aligned} \tag{5.3.16}$$

It should be noted that Equation (5.3.16) is a good approximation only for  $|f| < W$ . This means that for  $|f| < W$ , the spectrum of the noise components in the PM and FM case are given by

$$S_{n_o}(f) = \begin{cases} \frac{N_0}{A_c^2}, & \text{PM} \\ \frac{N_0}{A_c^2} f^2, & \text{FM} \end{cases} \tag{5.3.17}$$

where we have used the fact that in FM the noise component is given by  $\frac{1}{2\pi} \frac{d}{dt} Y_n(t)$  as previously indicated in Equation (5.3.6). The power spectrum of the noise component at the output of the demodulator in the frequency interval  $|f| < W$  for PM and FM is shown in Figure 5.15. It is interesting to note that PM has a flat noise spectrum and FM has a parabolic noise spectrum. Therefore, the effect of noise in FM for higher-frequency components is much higher than the effect of noise on lower-frequency components. The noise power at the output of the lowpass filter is the noise power in the frequency

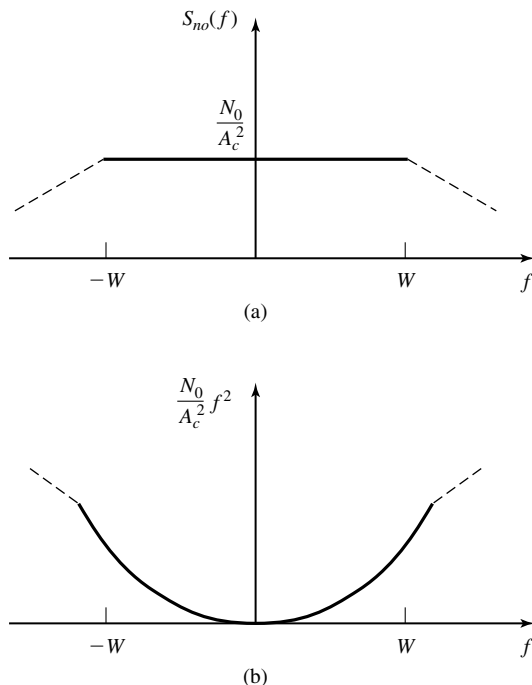


**Figure 5.15** Noise power spectrum at demodulator output in (a) PM and (b) FM.



range  $[W, +W]$ . Therefore, it is given by

$$\begin{aligned}
 P_{n_o} &= \int_{-W}^{+W} \mathcal{S}_{n_o}(f) df \\
 &= \begin{cases} \int_{-W}^{+W} \frac{N_0}{A_c^2} df, & \text{PM} \\ \int_{-W}^{+W} f^2 \frac{N_0}{A_c^2} df, & \text{FM} \end{cases} \\
 &= \begin{cases} \frac{2WN_0}{A_c^2}, & \text{PM} \\ \frac{2N_0W^3}{3A_c^2}, & \text{FM} \end{cases} \quad (5.3.18)
 \end{aligned}$$

Now we can use Equation (5.3.6) to determine the output SNR in angle modulation. First, we have the output signal power

$$P_{s_o} = \begin{cases} k_p^2 P_M, & \text{PM} \\ k_f^2 P_M, & \text{FM} \end{cases} \quad (5.3.19)$$

Then, the SNR, defined as

$$\left( \frac{S}{N} \right)_o = \frac{P_{s_o}}{P_{n_o}}$$

becomes

$$\left( \frac{S}{N} \right)_o = \begin{cases} \frac{k_p^2 A_c^2}{2} \frac{P_M}{N_0 W}, & \text{PM} \\ \frac{3k_f^2 A_c^2}{2W^2} \frac{P_M}{N_0 W}, & \text{FM} \end{cases} \quad (5.3.20)$$

Noting that  $\frac{A_c^2}{2}$  is the received signal power, denoted by  $P_R$ , and

$$\begin{cases} \beta_p = k_p \max|m(t)|, & \text{PM} \\ \beta_f = \frac{k_f \max|m(t)|}{W}, & \text{FM} \end{cases} \quad (5.3.21)$$

we may express the output SNR as

$$\left( \frac{S}{N} \right)_o = \begin{cases} P_R \left( \frac{\beta_p}{\max|m(t)|} \right)^2 \frac{P_M}{N_0 W}, & \text{PM} \\ 3P_R \left( \frac{\beta_f}{\max|m(t)|} \right)^2 \frac{P_M}{N_0 W}, & \text{FM} \end{cases} \quad (5.3.22)$$

If we denote  $\frac{P_R}{N_0 W}$  by  $\left( \frac{S}{N} \right)_b$ , the SNR of a baseband system with the same received power, we obtain

$$\left( \frac{S}{N} \right)_o = \begin{cases} \frac{P_M \beta_p^2}{(\max|m(t)|)^2} \left( \frac{S}{N} \right)_b, & \text{PM} \\ 3 \frac{P_M \beta_f^2}{(\max|m(t)|)^2} \left( \frac{S}{N} \right)_b, & \text{FM} \end{cases} \quad (5.3.23)$$

Note that in the above expression  $\frac{P_M}{(\max|m(t)|)^2}$  is the average-to-peak-power ratio of the message signal (or, equivalently, the power content of the normalized message,  $P_{M_n}$ ).

Therefore,

$$\left(\frac{S}{N}\right)_o = \begin{cases} \beta_p^2 P_{M_n} \left(\frac{S}{N}\right)_b, & \text{PM} \\ 3\beta_f^2 P_{M_n} \left(\frac{S}{N}\right)_b, & \text{FM} \end{cases} \quad (5.3.24)$$

Now using Carson's rule  $B_c = 2(\beta + 1)W$ , we can express the output SNR in terms of the bandwidth expansion factor, which is defined to be the ratio of the channel bandwidth to the message bandwidth and denoted by  $\Omega$

$$\Omega = \frac{B_c}{W} = 2(\beta + 1) \quad (5.3.25)$$

From this relationship we have  $\beta = \frac{\Omega}{2} - 1$ . Therefore,

$$\left(\frac{S}{N}\right)_o = \begin{cases} P_M \left(\frac{\frac{\Omega}{2}-1}{\max|m(t)|}\right)^2 \left(\frac{S}{N}\right)_b, & \text{PM} \\ 3P_M \left(\frac{\frac{\Omega}{2}-1}{\max|m(t)|}\right)^2 \left(\frac{S}{N}\right)_b, & \text{FM} \end{cases} \quad (5.3.26)$$

From Equations (5.3.22) and (5.3.26), we observe that:

1. In both PM and FM, the output SNR is proportional to the square of the modulation index  $\beta$ . Therefore, increasing  $\beta$  increases the output SNR even with low received power. This is in contrast to amplitude modulation where such an increase in the received SNR is not possible.
2. The increase in the received SNR is obtained by increasing the bandwidth. Therefore, angle modulation provides a way to trade-off bandwidth for transmitted power.
3. The relation between the output SNR and the bandwidth expansion factor,  $\Omega$ , is a quadratic relation. This is far from optimal.<sup>†</sup> We will see in Chapter 9 that the optimal relation between the output SNR and the bandwidth expansion factor is an exponential relation.
4. Although we can increase the output SNR by increasing  $\beta$ , having a large  $\beta$  means having a large  $B_c$  (by Carson's rule). Having a large  $B_c$  means having a large noise power at the input of the demodulator. This means that the approximation  $p(V_n(t) \ll A_c) \approx 1$  will no longer apply and that the above analysis will not hold. In fact, if we increase  $\beta$  such that the above approximation does not hold, a phenomenon known as the *threshold effect* will occur, and the signal will be lost in the noise.
5. A comparison of the above result with the SNR in amplitude modulation shows that, in both cases, increasing the transmitter power will increase the output SNR,

<sup>†</sup>By optimal relation we mean the maximum saving in transmitter power for a given expansion in bandwidth. An optimal system achieves the fundamental limits on communication predicted by information theory.

but the mechanisms are totally different. In AM, any increase in the received power directly increases the signal power at the output of the receiver. This is due basically to the fact that the message is in the amplitude of the transmitted signal and an increase in the transmitted power directly affects the demodulated signal power. However, in angle modulation, the message is in the phase of the modulated signal and, consequently, increasing the transmitter power does not increase the demodulated message power. In angle modulation what increases the output SNR is a *decrease in the received noise power* as seen from Equation (5.3.18) and Figure 5.11.

6. In FM, the effect of noise is higher at higher frequencies. This means that signal components at higher frequencies will suffer more from noise than the lower-frequency components. In some applications, where FM is used to transmit SSB-FDM signals, those channels which are modulated on higher-frequency carriers suffer from more noise. To compensate for this effect, such channels must have a higher-signal level. The quadratic characteristics of the demodulated noise spectrum in FM is the basis of pre-emphasis and de-emphasis filtering that will be discussed in Section 5.3.2.

### 5.3.1 Threshold Effect in Angle Modulation

The noise analysis of angle demodulation schemes is based on the assumption that the SNR at the demodulator input is high. With this crucial assumption, we observed that the signal and noise components at the demodulator output are additive, and we were able to carry out the analysis. This assumption of high SNR is a simplifying assumption that is usually made in analysis of nonlinear-modulation systems. Due to the nonlinear nature of the demodulation process, there is no reason that the additive signal and noise components at the input of the modulator result in additive signal and noise components at the output of the demodulator. In fact, this assumption is not at all correct in general, and the signal and noise processes at the output of the demodulator are completely mixed in a single process by a complicated nonlinear functional. Only under the high SNR assumption is this highly nonlinear functional approximated as an additive form. Particularly at low SNRs, signal and noise components are so intermingled that one can not recognize the signal from the noise and, therefore, no meaningful SNR as a measure of performance can be defined. In such cases, the signal is not distinguishable from the noise and a *mutilation* or *threshold effect* is present. There exists a specific signal to noise ratio at the input of the demodulator known as the *threshold SNR*, beyond which signal mutilation occurs. The existence of the threshold effect places an upper limit on the trade-off between bandwidth and power in an FM system. This limit is a practical limit in the value of the modulation index  $\beta_f$ . The analysis of the threshold effect and derivation of the threshold index  $\beta_f$  is quite involved and beyond the scope of our analysis. The interested reader is referred to the references cited at the end of this chapter for an analytic treatment of the subject. Here we only mention some results on the threshold effect in FM.

It can be shown that at threshold the following approximate relation between  $\frac{P_R}{N_0 W} = \left(\frac{S}{N}\right)_b$  and  $\beta_f$  holds in an FM system:

$$\left(\frac{S}{N}\right)_{b,\text{th}} = 20(\beta + 1) \quad (5.3.27)$$

From the above relation, given a received power  $P_R$ , we can calculate the maximum allowed  $\beta$  to make sure that the system works above threshold. Also, given a bandwidth allocation of  $B_c$ , we can find an appropriate  $\beta$  using Carson's rule  $B_c = 2(\beta + 1)W$ . Then, using the threshold relation given above, we determine the required minimum received power to make the whole allocated bandwidth usable.

In general, there are two factors that limit the value of the modulation index  $\beta$ . The first is the limitation on channel bandwidth which affects  $\beta$  through Carson's rule. The second is the limitation on the received power that limits the value of  $\beta$  to less than what is derived from Equation (5.3.27). Figure 5.16 shows plots of the SNR in an FM system as a function of the baseband SNR. The SNR values in these curves are in dB and different curves correspond to different values of  $\beta$  as marked. The effect of threshold is apparent from the sudden drops in the output SNR. These plots are drawn

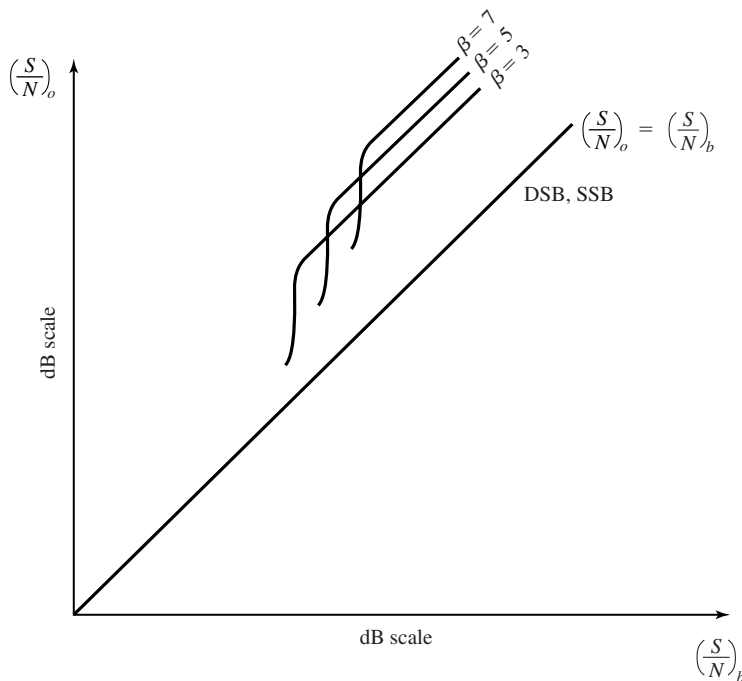


**Figure 5.16** Output SNR vs. baseband SNR in an FM system for various values of  $\beta$ .

for a sinusoidal message for which

$$\frac{P_M}{(\max|m(t)|)^2} = \frac{1}{2} \quad (5.3.28)$$

In such a case,

$$\left(\frac{S}{N}\right)_o = \frac{3}{2}\beta^2\left(\frac{S}{N}\right)_b \quad (5.3.29)$$

As an example, for  $\beta = 5$ , the above relation yields

$$\left(\frac{S}{N}\right)_o \Big|_{\text{dB}} = 15.7 + \left(\frac{S}{N}\right)_b \Big|_{\text{dB}} \quad (5.3.30)$$

$$\left(\frac{S}{N}\right)_{b,\text{th}} = 120 \sim 20.8 \text{ dB} \quad (5.3.31)$$

On the other hand, if  $\beta = 2$ , we have

$$\left(\frac{S}{N}\right)_o \Big|_{\text{dB}} = 7.8 + \left(\frac{S}{N}\right)_b \Big|_{\text{dB}} \quad (5.3.32)$$

$$\left(\frac{S}{N}\right)_{b,\text{th}} = 60 \sim 17.8 \text{ dB} \quad (5.3.33)$$

From this discussion it is apparent that, if for example  $\left(\frac{S}{N}\right)_b = 20 \text{ dB}$ , then, regardless of the available bandwidth, we can not use  $\beta = 5$  for such a system because the demodulator will not demodulate below the threshold of 20.8 dB. However,  $\beta = 2$  can be used which yields an SNR equal to 27.8 dB at the output of the receiver. This is an improvement of 7.8 dB compared to a baseband system.

In general, if we want to employ the maximum available bandwidth, we must choose the largest possible  $\beta$  that guarantees the system operates above threshold. This is the value of  $\beta$  that satisfies

$$\left(\frac{S}{N}\right)_{b,\text{th}} = 20(\beta + 1) \quad (5.3.34)$$

By substituting this value in Equation (5.3.24), we obtain

$$\left(\frac{S}{N}\right)_o = 60\beta^2(\beta + 1)P_{M_n} \quad (5.3.35)$$

which relates a desired output SNR to the highest possible  $\beta$  that achieves that SNR.

### Example 5.3.1

Design an FM system that achieves an SNR at the receiver equal to 40 dB and requires the minimum amount of transmitter power. The bandwidth of the channel is 120 KHz, the message bandwidth is 10 KHz, the average-to-peak-power ratio for the message,  $P_{M_n} = \frac{P_M}{(\max|m(t)|)^2}$  is  $\frac{1}{2}$ , and the (one-sided) noise power-spectral density is  $N_0 = 10^{-8} \text{ W/Hz}$ . What is the required transmitter power if the signal is attenuated by 40 dB in transmission through the channel?

**Solution** First we have to see whether the threshold or the bandwidth impose a more restrictive bound on the modulation index. By Carson's rule

$$B_c = 2(\beta + 1)W$$

$$120,000 = 2(\beta + 1) \times 10,000$$

from which we obtain  $\beta = 5$ . Using the relation

$$\left(\frac{S}{N}\right)_o = 60\beta^2(\beta + 1)P_{M_n} \quad (5.3.36)$$

with  $\left(\frac{S}{N}\right)_o = 10^4$ , we obtain  $\beta \approx 6.6$ . Since the value of  $\beta$  given by the bandwidth constraint is less than the value of  $\beta$  given by the power constraint, we are limited in bandwidth as opposed to being limited in power. Therefore, we choose  $\beta = 5$  which, when substituted in the expression for the output SNR

$$\left(\frac{S}{N}\right)_o = \frac{3}{2}\beta^2\left(\frac{S}{N}\right)_b \quad (5.3.37)$$

yields

$$\left(\frac{S}{N}\right)_b = \frac{800}{3} = 266.6 \sim 24.26 \text{ dB} \quad (5.3.38)$$

Since  $\left(\frac{S}{N}\right)_b = \frac{P_R}{N_0W}$  with  $W = 10,000$  and  $N_0 = 10^{-8}$ , we obtain

$$P_R = \frac{8}{300} = 0.0266 \sim -15.74 \text{ dB} \quad (5.3.39)$$

and

$$P_T = -15.74 + 40 = 24.26 \text{ dB} \sim 266.66 \text{ W} \quad (5.3.40)$$

Had there been no bandwidth constraint we could have chosen  $\beta = 6.6$ , which results in  $\left(\frac{S}{N}\right)_b \approx 153$ . In turn, we have  $P_R \approx 0, 0153$ , and  $P_T \approx 153 \text{ W}$ .

**Threshold Extension in Frequency Modulation.** We have already seen that the nonlinear demodulation effect in angle modulation in general results in nonadditive signal and noise at the output of the demodulator. In high received signal-to-noise ratios, the nonlinear-demodulation process can be well approximated by a linear equivalent and, therefore, signal and noise at the demodulator output will be additive. At high noise levels, however, this approximation is not valid anymore and the threshold effect results in signal mutilation. We have also seen that, in general, the modulated signal bandwidth increases with the modulation index and since the power of the noise entering the receiver is proportional to the system bandwidth, higher-modulation indices cause the threshold effect to appear at higher-received powers.

In order to reduce the threshold, in other words, in order to delay the threshold effect to appear at lower-received signal power, it is sufficient to decrease the input-noise power at the receiver. This can be done by decreasing the effective system bandwidth at the receiver.

Two approaches to FM threshold extension are to employ FMFB or PLL-FM (see Figures 3.38 and 3.39) at the receiver. We have already seen in Section 3.3.3 in the discussion following FMFB and PLL-FM systems, that these systems are capable

of reducing the effective bandwidth of the receiver. This is exactly what is needed for extending the threshold in FM demodulation. Therefore, in applications where power is very limited and bandwidth is abundant, these systems can be employed to make it possible to use the available bandwidth more efficiently. Using FMFB, the threshold can be extended approximately by 5–7 dB.

### 5.3.2 Pre-emphasis and De-emphasis Filtering

As observed in Figure 5.15, the noise power-spectral density at the output of the demodulator in PM is flat within the message bandwidth whereas for FM the noise power spectrum has a parabolic shape. This means that for low-frequency components of the message signal FM performs better and for high-frequency components PM is a better choice. Therefore, if we can design a system that for low-frequency components of the message signal performs frequency modulation and for high frequency components works as a phase modulator, we have a better overall performance compared to each system alone. This is the idea behind pre-emphasis and de-emphasis filtering techniques.

The objective in pre-emphasis and de-emphasis filtering is to design a system which behaves like an ordinary frequency modulator–demodulator pair in the low frequency band of the message signal and like a phase modulator–demodulator pair in the high-frequency band of the message signal. Since a phase modulator is nothing but the cascade connection of a differentiator and a frequency modulator, we need a filter in cascade with the modulator that at low frequencies does not affect the signal and at high frequencies acts as a differentiator. A simple highpass filter is a very good approximation to such a system. Such a filter has a constant gain for low frequencies and at higher frequencies it has a frequency characteristic approximated by  $K|f|$ , which is the frequency characteristic of a differentiator. At the demodulator side, for low frequencies we have a simple FM demodulator and for high-frequency components we have a phase demodulator, which is the cascade of a simple FM demodulator and an integrator. Therefore, at the demodulator, we need a filter that at low frequencies has a constant gain and at high frequencies behaves as an integrator. A good approximation to such a filter is a simple lowpass filter. The modulator filter which emphasizes high frequencies is called the *pre-emphasis* filter and the demodulator filter which is the inverse of the modulator filter is called the *de-emphasis* filter. Frequency responses of a sample pre-emphasis and de-emphasis filter are given in Figure 5.17.

Another way to look at pre-emphasis and de-emphasis filtering is to note that, due to the high level of noise in the high-frequency components of the message in FM, it is desirable to attenuate the high-frequency components of the demodulated signal. This results in a reduction in the noise level, but it causes the higher-frequency components of the message signal to be also attenuated. To compensate for the attenuation of the higher components of the message signal, we can amplify these components at the transmitter before modulation. Therefore, at the transmitter we need a highpass filter and at the receiver we must use a lowpass filter. The net effect of these filters should be a flat-frequency response. Therefore, the receiver filter should be the inverse of the

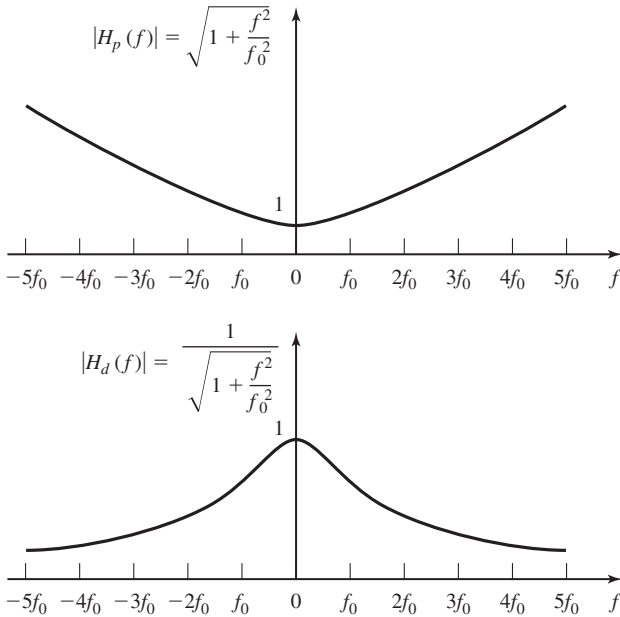


**Figure 5.17** Pre-emphasis (a) and de-emphasis (b) filter characteristics.

transmitter filter.

The characteristics of the pre-emphasis and de-emphasis filters depend largely on the power-spectral density of the message process. In commercial FM broadcasting of music and voice, first-order lowpass and highpass RC filters with a time constant of 75 microseconds ( $\mu\text{s}$ ) are employed. In this case, the frequency response of the receiver (de-emphasis) filter is given by

$$H_d(f) = \frac{1}{1 + j\frac{f}{f_0}} \quad (5.3.41)$$

where  $f_0 = \frac{1}{2\pi \times 75 \times 10^{-6}} \approx 2100$  Hz is the 3-dB frequency of the filter.

To analyze the effect of pre-emphasis and de-emphasis filtering on the overall SNR in FM broadcasting, we note that, because the transmitter and the receiver filters cancel the effect of each other, the received power in the message signal remains unchanged and we only have to consider the effect of filtering on the received noise. Of course, the only filter that has an effect on the received noise is the receiver filter that shapes the power-spectral density of the noise within the message bandwidth. The noise component before filtering has a parabolic power spectrum. Therefore, the noise component after the de-emphasis filter has a power-spectral density given by

$$\begin{aligned} \mathcal{S}_{n_{\text{PD}}}(f) &= \mathcal{S}_{n_o}(f) |H_d(f)|^2 \\ &= \frac{N_0}{A_c^2} f^2 \frac{1}{1 + \frac{f^2}{f_0^2}} \end{aligned} \quad (5.3.42)$$



where we have used Equation (5.3.17). The noise power at the output of the demodulator now can be obtained as

$$\begin{aligned}
 P_{n_{PD}} &= \int_{-W}^{+W} \mathcal{S}_{n_{PD}}(f) df \\
 &= \frac{N_0}{A_c^2} \int_{-W}^{+W} \frac{f^2}{1 + \frac{f^2}{f_0^2}} df \\
 &= \frac{2N_0 f_0^3}{A_c^2} \left[ \frac{W}{f_0} - \arctan \frac{W}{f_0} \right] \tag{5.3.43}
 \end{aligned}$$

Because the demodulated message signal power in this case is equal to that of a simple FM system with no pre-emphasis and de-emphasis filtering, the ratio of the output SNRs in these two cases is inversely proportional to the noise power ratios; i.e.,

$$\begin{aligned}
 \frac{\left(\frac{S}{N}\right)_{o_{PD}}}{\left(\frac{S}{N}\right)_o} &= \frac{P_{n_o}}{P_{n_{PD}}} \\
 &= \frac{\frac{2N_0 W^3}{3A_c^2}}{\frac{2N_0 f_0^3}{A_c^2} \left[ \frac{W}{f_0} - \arctan \frac{W}{f_0} \right]} \\
 &= \frac{1}{3} \frac{\left(\frac{W}{f_0}\right)^3}{\frac{W}{f_0} - \arctan \frac{W}{f_0}} \tag{5.3.44}
 \end{aligned}$$

where we have used Equation (5.3.18). Equation (5.3.44) gives the improvement obtained by employing pre-emphasis and de-emphasis filtering.

### Example 5.3.2

In commercial FM broadcasting  $W = 15$  KHz,  $f_0 = 2100$  Hz, and  $\beta = 5$ . Assuming that the average-to-peak-power ratio of the message signal is 0.5, find the improvement in output SNR of FM with pre-emphasis and de-emphasis filtering compared to a baseband system.

**Solution** From Equation (5.3.26) we have

$$\begin{aligned}
 \left(\frac{S}{N}\right)_o &= 3 \times 5^2 \times 0.5 \times \left(\frac{S}{N}\right)_b \\
 &= 37.5 \left(\frac{S}{N}\right)_b \\
 &\sim 15.7 + \left(\frac{S}{N}\right)_b \Big|_{\text{dB}} \tag{5.3.45}
 \end{aligned}$$

Therefore, FM with no pre-emphasis and de-emphasis filtering performs 15.7-dB better than a baseband system. For FM with pre-emphasis and de-emphasis filtering, we have

$$\begin{aligned}
 \left(\frac{S}{N}\right)_{\text{opD}} &= \frac{1}{3} \frac{\left(\frac{W}{f_o}\right)^3}{\frac{W}{f_o} - \arctan \frac{W}{f_o}} \left(\frac{S}{N}\right)_o \\
 &= \frac{1}{3} \frac{\left(\frac{15000}{2100}\right)^3}{\frac{15000}{2100} - \arctan \frac{15000}{2100}} \left(\frac{S}{N}\right)_o \\
 &= 21.3 \left(\frac{S}{N}\right)_o \\
 &\sim 13.3 + \left(\frac{S}{N}\right)_o \Big|_{\text{dB}} \\
 &\sim 13.3 + 15.7 + \left(\frac{S}{N}\right)_b \Big|_{\text{dB}} \\
 &\sim 29 + \left(\frac{S}{N}\right)_b \Big|_{\text{dB}} \tag{5.3.46}
 \end{aligned}$$

The overall improvement compared to a baseband system is, therefore, 29 dB.

## 5.4 COMPARISON OF ANALOG-MODULATION SYSTEMS

Now we are at a point that we can present an overall comparison of different analog communication systems. The systems that we have studied include linear-modulation systems (DSB-SC, Conventional AM, SSB-SC, VSB) and nonlinear systems (FM and PM).

The comparison of these systems can be done from various points of view. Here we present a comparison based on three important practical criteria:

1. The bandwidth efficiency of the system.
2. The power efficiency of the system as reflected in its performance in the presence of noise.
3. The ease of implementation of the system (transmitter and receiver).

**Bandwidth Efficiency.** The most bandwidth-efficient analog communication system is the SSB-SC system with a transmission bandwidth equal to the signal bandwidth. This system is widely used in bandwidth-critical applications such as voice transmission over microwave and satellite links, and some point-to-point communication systems in congested areas. Since SSB-SC cannot effectively transmit dc, it cannot be used for transmission of signals that have a significant dc component such as image signals. A good compromise is the VSB system, which has a bandwidth slightly larger than SSB and is capable of transmitting dc values. VSB is widely used in TV broadcasting, and also in some data communication systems. PM and particularly FM are least-favorable systems when bandwidth is the major concern, and their use is only justified by their high level of noise immunity.

**Power Efficiency.** A criterion for comparing power efficiency of various systems is the comparison of their output SNR at a given received signal power. We have already seen that angle-modulation schemes and particularly FM provide a high level of noise immunity and, therefore, power efficiency. FM is widely used on power-critical communication links such as point-to-point communication systems and high fidelity radio broadcasting. It is also used for transmission of voice (which has been already SSB/FDM multiplexed) on microwave LOS and satellite links. Conventional AM and VSB+C are the least power-efficient systems and are not used when the transmitter power is a major concern. However, their use is justified by the simplicity of the receiver structure.

**Ease of Implementation.** The simplest receiver structure is the receiver for conventional AM, and the structure of the receiver for VSB+C system is only slightly more complicated. FM receivers are also easy to implement. These three systems are widely used for AM, TV, and high-fidelity FM broadcasting (including FM stereo). The power inefficiency of the AM transmitter is compensated by the extremely simple structure of literally hundreds of millions of receivers. DSB-SC and SSB-SC require synchronous demodulation and, therefore, their receiver structure is much more complicated. These systems are, therefore, never used for broadcasting purposes. Since the receiver structure of SSB-SC and DSB-SC have almost the same complexity and the transmitter of SSB-SC is slightly more complicated compared to DSB-SC, DSB-SC is hardly used in practice, due to its relative bandwidth inefficiency.

## 5.5 EFFECTS OF TRANSMISSION LOSSES AND NOISE IN ANALOG COMMUNICATION SYSTEMS

In any communication system there are usually two dominant factors that limit the performance of the system. One important factor is additive noise generated by electronic devices that are used to filter and amplify the communication signal. A second factor that affects the performance of a communication system is signal attenuation. Basically all physical channels, including wireline and radio channels, are lossy. Hence, the signal is attenuated (reduced in amplitude) as it travels through the channel. A simple mathematical model of the attenuation may be constructed, as shown in Figure 5.18, by

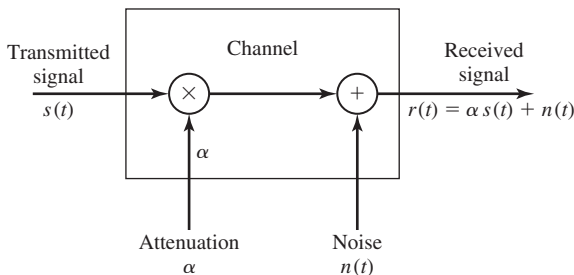


**Figure 5.18** Mathematical model of channel with attenuation and additive noise.

multiplying the transmitted signal by a factor  $\alpha < 1$ . Consequently, if the transmitted signal is  $s(t)$ , the received signal is

$$r(t) = \alpha s(t) + n(t) \quad (5.5.1)$$

Clearly, the effect of signal attenuation is to reduce the amplitude of the desired signal  $s(t)$  and, thus, to render the communication signal more vulnerable to additive noise.

In many channels, such as wirelines and microwave LOS channels, signal attenuation can be offset by using amplifiers to boost the level of the signal during transmission. However, an amplifier also introduces additive noise in the process of amplification and, thus, corrupts the signal. This additional noise must be taken into consideration in the design of the communication system.

In this section, we consider the effects of attenuation encountered in signal transmission through a channel and additive thermal noise generated in electronic amplifiers. We also demonstrate how these two factors influence the design of a communication system.

### 5.5.1 Characterization of Thermal Noise Sources

Any conductive two-terminal device is generally characterized as lossy and has some resistance, say  $R$  ohms. A resistor which is at a temperature  $T$  above absolute zero contains free electrons that exhibit random motion and, thus, result in a noise voltage across the terminals of the resistor. Such a noise voltage is called *thermal noise*.

In general, any physical resistor (or lossy device) may be modeled by a noise source in series with a noiseless resistor, as shown in Figure 5.19. The output  $n(t)$  of the noise source is characterized as a sample function of a random process. Based on quantum mechanics, the power-spectral density of thermal noise (see Section 4.4) is given as

$$\mathcal{S}_R(f) = \frac{2R\hbar|f|}{(e^{\frac{\hbar|f|}{kT}} - 1)} \text{ V}^2/\text{Hz} \quad (5.5.2)$$

where  $\hbar$  is Planck's constant,  $k$  is Boltzmann's constant, and  $T$  is the temperature of the resistor in degree Kelvin; i.e.,  $T = 273 + C$ , where  $C$  is in degrees Centigrade. As indicated in Section 4.4, at frequencies below  $10^{12}$  Hz (which includes all conventional

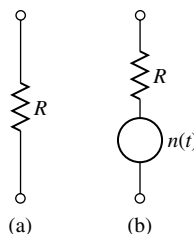


**Figure 5.19** A physical resistor (a) is modeled as a noiseless resistor in series with a noise source (b).

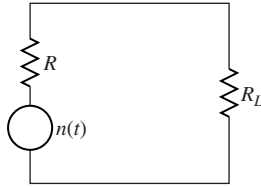


**Figure 5.20** Noisy resistor connected to a load resistance  $R_L$ .

communication systems) and at room temperature,

$$e^{\frac{\hbar|f|}{kT}} \approx 1 + \frac{\hbar|f|}{kT} \quad (5.5.3)$$

Consequently, the power-spectral density is well approximated as

$$S_R(f) = 2RkT \text{ V}^2/\text{Hz} \quad (5.5.4)$$

When connected to a load resistance with value  $R_L$ , the noise voltage shown in Figure 5.20 delivers the maximum power when  $R = R_L$ . In such a case, the load is matched to the source and the maximum power delivered to the load is  $E[N^2(t)]/4R_L$ . Therefore, the power-spectral density of the noise voltage across the load resistor is

$$S_n(f) = \frac{kT}{2} \text{ W/Hz} \quad (5.5.5)$$

As previously indicated in Section 3.4.2,  $kT$  is usually denoted by  $N_0$ . Hence, the power-spectral density of thermal noise is generally expressed as

$$S_n(f) = \frac{N_0}{2} \text{ W/Hz} \quad (5.5.6)$$

For example, at room temperature ( $T_0 = 290 \text{ K}$ ),  $N_0 = 4 \times 10^{-21} \text{ W/Hz}$ .

### 5.5.2 Effective Noise Temperature and Noise Figure

When we employ amplifiers in communication systems to boost the level of a signal, we are also amplifying the noise corrupting the signal. Since any amplifier has some finite passband, we may model an amplifier as a filter with frequency-response characteristic  $H(f)$ . Let us evaluate the effect of the amplifier on an input thermal noise source.

Figure 5.21 illustrates a thermal noise source connected to a matched two-port network having frequency response  $H(f)$ . The output of this network is connected to a matched load. First, we recall that the noise power at the output of the network is

$$P_{no} = \int_{-\infty}^{\infty} S_n(f) |H(f)|^2 df = \frac{N_0}{2} \int_{-\infty}^{\infty} |H(f)|^2 df \quad (5.5.7)$$

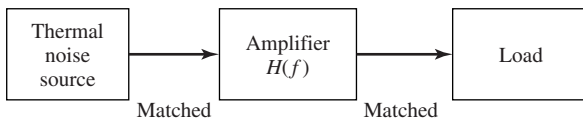


**Figure 5.21** Thermal noise converted to amplifier and load.

From Section 3.4.2, we recall that the noise-equivalent bandwidth of the filter is defined as

$$B_{\text{neq}} = \frac{1}{2\mathcal{G}} \int_{-\infty}^{\infty} |H(f)|^2 df \quad (5.5.8)$$

where, by definition,  $\mathcal{G} = |H(f)|_{\text{max}}^2$  is the *maximum available power gain* of the amplifier. Consequently, the output noise power from an ideal amplifier that introduces no additional noise may be expressed as

$$P_{no} = \mathcal{G}N_0B_{\text{neq}} \quad (5.5.9)$$

Any practical amplifier introduces additional noise at its output due to internally generated noise. Hence, the noise power at its output may be expressed as

$$\begin{aligned} P_{no} &= \mathcal{G}N_0B_{\text{neq}} + P_{ni} \\ &= \mathcal{G}kTB_{\text{neq}} + P_{ni} \end{aligned} \quad (5.5.10)$$

where  $P_{ni}$  is the power of the amplifier output due to internally generated noise. Therefore,

$$P_{no} = \mathcal{G}kB_{\text{neq}} \left( T + \frac{P_{ni}}{\mathcal{G}kB_{\text{neq}}} \right) \quad (5.5.11)$$

This leads us to define a quantity

$$T_e = \frac{P_{ni}}{\mathcal{G}kB_{\text{neq}}} \quad (5.5.12)$$

which we call the *effective noise temperature* of the two-port network (amplifier). Then,

$$P_{no} = \mathcal{G}kB_{\text{neq}}(T + T_e) \quad (5.5.13)$$

Thus, we interpret the output noise as originating from a thermal noise source at temperature  $T + T_e$ .

A signal source at the input to the amplifier with power  $P_{si}$  will produce an output with power

$$P_{so} = \mathcal{G}P_{si} \quad (5.5.14)$$

Hence, the output SNR from the two-port network is

$$\begin{aligned} \left( \frac{S}{N} \right)_0 &= \frac{P_{so}}{P_{no}} = \frac{\mathcal{G}P_{si}}{\mathcal{G}kTB_{\text{neq}}(1 + T_e/T)} \\ &= \frac{P_{si}}{N_0B_{\text{neq}}(1 + T_e/T)} \\ &= \frac{1}{1 + T_e/T} \left( \frac{S}{N} \right)_i \end{aligned} \quad (5.5.15)$$

where, by definition,  $(S/N)_i$  is the input SNR to the two-port network. We observe that the SNR at the output of the amplifier is degraded (reduced) by the factor  $(1 + T_e/T)$ .

Thus,  $T_e$  is a measure of the noisiness of the amplifier. An ideal amplifier is one for which  $T_e = 0$ .

When  $T$  is taken as room temperature  $T_0$  (290 K) the factor  $(1 + T_e/T_0)$  is called the *noise figure* of the amplifier. Specifically, the noise figure of a two-port network is defined as the ratio of the output noise power  $P_{no}$  to the output noise power of an ideal (noiseless) two-port network for which the thermal noise source is at room temperature ( $T_0 = 290$  K). Clearly, the ratio

$$F = \left(1 + \frac{T_e}{T_0}\right) \quad (5.5.16)$$

is the noise figure of the amplifier. Consequently, Equation (5.5.15) may be expressed as

$$\left(\frac{S}{N}\right)_0 = \frac{1}{F} \left(\frac{S}{N}\right)_i \quad (5.5.17)$$

By taking the logarithm of both sides of Equation (5.5.17), we obtain

$$10 \log \left(\frac{S}{N}\right)_0 = -10 \log F + 10 \log \left(\frac{S}{N}\right)_i \quad (5.5.18)$$

Hence,  $10 \log F$  represents the loss in SNR due to the additional noise introduced by the amplifier. The noise figure for many low-noise amplifiers such as traveling wave tubes is below 3 dB. Conventional integrated circuit amplifiers have noise figures of 6 dB–7 dB.

It is easy to show (see Problem 5.18) that the overall noise figure of a cascade of  $K$  amplifiers with gains  $\mathcal{G}_k$  and corresponding noise figures  $F_k$ ,  $1 \leq k \leq K$  is

$$F = F_1 + \frac{F_2 - 1}{\mathcal{G}_1} + \frac{F_3 - 1}{\mathcal{G}_1 \mathcal{G}_2} + \cdots + \frac{F_K - 1}{\mathcal{G}_1 \mathcal{G}_2 \cdots \mathcal{G}_{K-1}} \quad (5.5.19)$$

This expression is known as *Fries' formula*. We observe that the dominant term is  $F_1$ , which is the noise figure of the first amplifier stage. Therefore, the front end of a receiver should have a low-noise figure and a high gain. In that case, the remaining terms in the sum will be negligible.

### Example 5.5.1

Suppose an amplifier is designed of three identical stages, each of which has a gain of  $\mathcal{G}_i = 5$  and a noise figure  $F_i = 6$ ,  $i = 1, 2, 3$ . Determine the overall noise figure of the cascade of the three stages.

**Solution** From Equation (5.5.19), we obtain

$$F = F_1 + \frac{F_2 - 1}{\mathcal{G}_1} + \frac{F_3 - 1}{\mathcal{G}_1 \mathcal{G}_2}$$

where  $F_1 = F_2 = F_3 = 6$  and  $\mathcal{G}_1 = \mathcal{G}_2 = 5$ . Hence,

$$F = 6 + 1 + 0.2 = 7.2$$

or, equivalently,  $F_{\text{dB}} = 8.57$  dB.

### 5.5.3 Transmission Losses

As we indicated previously, any physical channel attenuates the signal transmitted through it. The amount of signal attenuation generally depends on the physical medium, the frequency of operation, and the distance between the transmitter and the receiver. We define the loss  $\mathcal{L}$  in signal transmission as the ratio of the input (transmitted) power to the output (received) power of the channel; i.e.,

$$\mathcal{L} = \frac{P_T}{P_R} \quad (5.5.20)$$

or, in decibels, as

$$\mathcal{L}_{\text{dB}} \equiv 10 \log \mathcal{L} = 10 \log P_T - 10 \log P_R \quad (5.5.21)$$

In wireline channels, the transmission loss is usually given in terms of dB per unit length; e.g., dB/Km. For example, the transmission loss in coaxial cable of 1 cm diameter is about 2 dB/Km at a frequency of 1 MHz. This loss generally increases with an increase in frequency.

#### Example 5.5.2

Determine the transmission loss for a 10-Km and a 20-Km coaxial cable if the loss/Km is 2 dB at the frequency operation.

**Solution** The loss for the 10-Km channel is  $\mathcal{L}_{\text{dB}} = 20$  dB. Hence, the output (received) power is  $P_R = P_T/\mathcal{L} = 10^{-2}P_T$ . For the 20-Km channel, the loss is  $\mathcal{L}_{\text{dB}} = 40$  dB. Hence,  $P_R = 10^{-4}P_T$ . Note that doubling the cable length increased the attenuation by two orders of magnitude.

In LOS radio systems the transmission loss is given as

$$\mathcal{L} = \left( \frac{4\pi d}{\lambda} \right)^2 \quad (5.5.22)$$

where  $\lambda = c/f$  is the wavelength of the transmitted signal,  $c$  is the speed of light ( $3 \times 10^8$  m/sec),  $f$  is the frequency of the transmitted signal, and  $d$  is the distance between the transmitter and the receiver in meters. In radio transmission,  $\mathcal{L}$  is called the *free-space path loss*.

#### Example 5.5.3

Determine the free-space path loss for a signal transmitted at  $f = 1$  MHz over distances of 10 Km and 20 Km.

**Solution** The loss given in Equation (5.5.22) for a signal at a wavelength  $\lambda = 300$  m is

$$\begin{aligned} \mathcal{L}_{\text{dB}} &= 20 \log_{10}(4\pi \times 10^4/300) \\ &= 52.44 \text{ dB} \end{aligned} \quad (5.5.23)$$

for the 10-Km path and

$$\begin{aligned} \mathcal{L}_{\text{dB}} &= 20 \log_{10}(8\pi \times 10^4/300) \\ &= 58.44 \text{ dB} \end{aligned} \quad (5.5.24)$$

for the 20-Km path. It is interesting to note that doubling the distance in radio transmission increases the free-space path loss by 6 dB.



**Example 5.5.4**

A signal is transmitted through a 10-Km coaxial line channel which exhibits a loss of 2 dB/Km. The transmitted signal power is  $P_{T\text{dB}} = -30$  dBW ( $-30$  dBW means 30 dB below 1 W or, simply, 1 mW). Determine the received signal power and the power at the output of an amplifier which has a gain of  $\mathcal{G}_{\text{dB}} = 15$  dB.

**Solution** The transmission loss for the 10-Km channel is  $\mathcal{L}_{\text{dB}} = 20$  dB. Hence, the received signal power is

$$P_{R\text{dB}} = P_{T\text{dB}} - \mathcal{L}_{\text{dB}} = -30 - 20 = -50 \text{ dBW} \quad (5.5.25)$$

The amplifier boosts the received signal power by 15 dB. Hence, the power at the output of the amplifier is

$$\begin{aligned} P_{o\text{dB}} &= P_{R\text{dB}} + G_{\text{dB}} \\ &= -50 + 15 = -35 \text{ dBW} \end{aligned} \quad (5.5.26)$$

**5.5.4 Repeaters for Signal Transmission**

*Analog repeaters* are basically amplifiers that are generally used in telephone wireline channels and microwave LOS radio channels to boost the signal level and, thus, to offset the effect of signal attenuation in transmission through the channel.

Figure 5.22 illustrates a system in which a repeater is used to amplify the signal that has been attenuated by the lossy transmission medium. Hence, the input signal power at the input to the repeater is

$$P_R = P_T / \mathcal{L} \quad (5.5.27)$$

The output power from the repeater is

$$P_0 = \mathcal{G}P_R = \mathcal{G}P_T / \mathcal{L} \quad (5.5.28)$$

We may select the amplifier gain  $\mathcal{G}$  to offset the transmission loss. Hence,  $\mathcal{G} = \mathcal{L}$  and  $P_0 = P_T$ .

Now, the SNR at the output of the repeater is

$$\begin{aligned} \left(\frac{S}{N}\right)_1 &= \frac{1}{F_a} \left(\frac{S}{N}\right)_i \\ &= \frac{1}{F_a} \left(\frac{P_R}{N_0 B_{\text{neq}}}\right) = \frac{1}{F_a} \left(\frac{P_T}{\mathcal{L} N_0 B_{\text{neq}}}\right) \\ &= \frac{1}{F_a \mathcal{L}} \left(\frac{P_T}{N_0 B_{\text{neq}}}\right) \end{aligned} \quad (5.5.29)$$

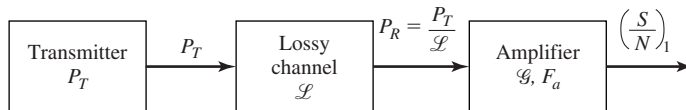


**Figure 5.22** A communication system employing a repeater to compensate for channel loss.

Based on this result, we may view the lossy transmission medium followed by the amplifier as a cascade of two networks, one with a noise figure  $\mathcal{L}$  and the other with a noise figure  $F_a$ . Then, for the cascade connection, the overall noise figure is

$$F = \mathcal{L} + \frac{F_a - 1}{\mathcal{G}_a} \quad (5.5.30)$$

If we select  $\mathcal{G}_a = 1/\mathcal{L}$ , then,

$$F = \mathcal{L} + \frac{F_a - 1}{1/\mathcal{L}} = \mathcal{L}F_a \quad (5.5.31)$$

Hence, the cascade of the lossy transmission medium and the amplifier is equivalent to a single network with noise figure  $\mathcal{L}F_a$ .

Now, suppose that we transmit the signal over  $K$  segments of the channel where each segment has its own repeater, as shown in Figure 5.23. Then, if  $F_i = \mathcal{L}_i F_{ai}$  is the noise figure of the  $i$ th section, the overall noise figure for the  $K$  sections is

$$F = \mathcal{L}_1 F_{a1} + \frac{\mathcal{L}_2 F_{a2} - 1}{\mathcal{L}_1/\mathcal{G}_{a1}} + \frac{\mathcal{L}_3 F_{a3} - 1}{(\mathcal{L}_1/\mathcal{G}_{a1})(\mathcal{L}_2/\mathcal{G}_{a2})} \cdots \\ + \frac{\mathcal{L}_K F_{aK} - 1}{(\mathcal{L}_1/\mathcal{G}_{a1})(\mathcal{L}_2/\mathcal{G}_{a2}) \cdots (\mathcal{L}_K/\mathcal{G}_{aK})} \quad (5.5.32)$$

Therefore, the SNR at the output of the repeater (amplifier) at the receiver is

$$\left(\frac{S}{N}\right)_0 = \frac{1}{F} \left(\frac{S}{N}\right)_i \\ = \frac{1}{F} \left(\frac{P_T}{N_0 B_{\text{neq}}}\right) \quad (5.5.33)$$

In the important special case where the  $K$  segments are identical; i.e.,  $\mathcal{L}_i = \mathcal{L}$  for all  $i$  and  $F_{ai} = F_a$  for all  $i$ , and where the amplifier gains are designed to offset the losses in each segment; i.e.,  $\mathcal{G}_{ai} = \mathcal{L}_i$  for all  $i$ , then the overall noise figure becomes

$$F = K\mathcal{L}F_a - (K - 1) \approx K\mathcal{L}F_a \quad (5.5.34)$$

Hence,

$$\left(\frac{S}{N}\right)_0 \approx \frac{1}{K\mathcal{L}F_a} \left(\frac{P_T}{N_0 B_{\text{neq}}}\right) \quad (5.5.35)$$

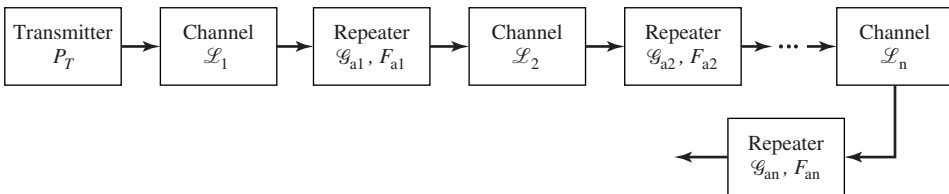


**Figure 5.23** A communication system employing repeaters.

Therefore, the overall noise figure for the cascade of the  $K$  identical segments is simply  $K$  times the noise figure of one segment.

**Example 5.5.5**

A signal with bandwidth 4 kHz is to be transmitted a distance of 200 Km over a wireline channel that has an attenuation of 2 dB/Km. (1) Determine the transmitter power  $P_T$  required to achieve an SNR of  $(S/N)_0 = 30$  dB at the output of the receiver amplifier which has a noise figure  $F_{a\text{dB}} = 5$  dB. (2) Repeat the calculation when a repeater is inserted every 10 Km in the wireline channel, where the repeater has a gain of 20 dB and a noise figure of  $F_a = 5$  dB. Assume that the noise-equivalent bandwidth of each repeater is  $B_{\text{neq}} = 4$  KHz and that  $N_0 = 4 \times 10^{-21}$  W/Hz.

**Solution** (1) The total loss in the 200-Km wireline is 400 dB. From Equation (5.5.35), with  $K = 1$ , we have

$$10 \log(S/N) = -10 \log \mathcal{L} - 10 \log F_a - 10 \log(N_0 B_{\text{neq}}) + 10 \log P_T$$

Hence,

$$\begin{aligned} P_{T\text{dB}} &= (S/N)_{\text{dB}} + F_{a\text{dB}} + (N_0 B_{\text{neq}})_{\text{dB}} + 10 \log \mathcal{L} \\ &= 30 + 5 + 400 + (N_0 B_{\text{neq}})_{\text{dB}} \end{aligned}$$

But,

$$(N_0 B_{\text{neq}})_{\text{dB}} = 10 \log(1.6 \times 10^{-17}) = -168 \text{ dBW.}$$

where dBW denotes the power level relative to 1 W. Therefore,

$$\begin{aligned} P_{T\text{dB}} &= 435 - 168 = 267 \text{ dB} \\ P_T &= 5 \times 10^{26} \text{ W} \end{aligned}$$

which is an astronomical figure.

(2) The use of a repeater every 10 Km reduces the per segment loss to  $\mathcal{L}_{\text{dB}} = 20$  dB. There are 20 repeaters, and each repeater has a noise figure of 5 dB. Hence, Equation (5.5.35) yields

$$\begin{aligned} (S/N)_{\text{dB}} &= -10 \log K - 10 \log \mathcal{L} - 10 \log F_a - 10 \log(N_0 B_{\text{neq}}) + 10 \log P_T \\ 30 &= -13 - 20 - 5 + 168 + P_{T\text{dB}} \end{aligned}$$

Therefore,

$$P_{T\text{dB}} = -100 \text{ dBW}$$

or, equivalently,

$$P_T = 10^{-10} \text{ W (0.1 pW)}$$

The above example clearly illustrates the advantage of using analog repeaters in communication channels that span large distances. However, we also observed that analog repeaters add noise to the signal and, consequently, degrade the output SNR. It is clear from Equation (5.5.35) that the transmitted power  $P_T$  must be increased linearly with the number  $K$  of repeaters in order to maintain the same  $(S/N)_0$  as  $K$  increases. Hence, for every factor of two increase in  $K$ , the transmitted power  $P_T$  must be increased by 3 dB.

## 5.6 FURTHER READING

Analysis of the effect of noise on analog communication systems can be found in Carlson (1986), Ziemer and Tranter (1990), Couch (1993), and Gibson (1993). The book by Sakrison (1968) provides a detailed analysis of FM in the presence of noise. Phase-locked loops are treated in detail in Viterbi (1966), Lindsey (1972), Lindsey and Simon (1973), and Gardner (1979), and in the survey papers by Gupta (1975) and Lindsey and Chie (1981). Taub and Schilling (1986) provides in-depth treatment of the effect of threshold and various methods for threshold extension in FM.

## PROBLEMS

- 5.1** The received signal  $r(t) = s(t) + n(t)$  in a communication system is passed through an ideal LPF with bandwidth  $W$  and unity gain. The signal component  $s(t)$  has a power-spectral density

$$\mathcal{S}_s(f) = \frac{P_0}{1 + (f/B)^2}$$

where  $B$  is the 3-dB bandwidth. The noise component  $n(t)$  has a power-spectral density  $N_0/2$  for all frequencies. Determine and plot the SNR as a function of the ratio  $W/B$ . What is the filter bandwidth  $W$  that yields a maximum SNR?

- 5.2** The input to the system shown in Figure P-5.2 is the signal plus noise waveform

$$r(t) = A_c \cos 2\pi f_c t + n(t)$$

where  $n(t)$  is a sample function of a white-noise process with spectral density  $N_0/2$ .

1. Determine and sketch the frequency response of the RC filter.
2. Sketch the frequency response of the overall system.
3. Determine the SNR at the output of the ideal LPF assuming that  $W > f_c$ . Sketch the SNR as a function of  $W$  for fixed values of  $R$  and  $C$ .

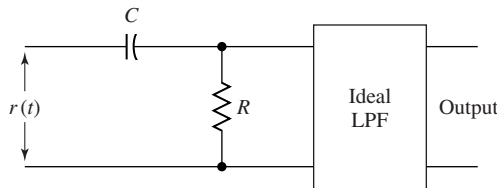


**Figure P-5.2**

- 5.3** A DSB amplitude-modulated signal with power-spectral density as shown in Figure P-5.3(a) is corrupted with additive noise that has a power-spectral density  $N_0/2$  within the passband of the signal. The received signal-plus-noise is demodulated and low pass filtered as shown in Figure P-5.3(b). Determine the SNR at the output of the LPF.

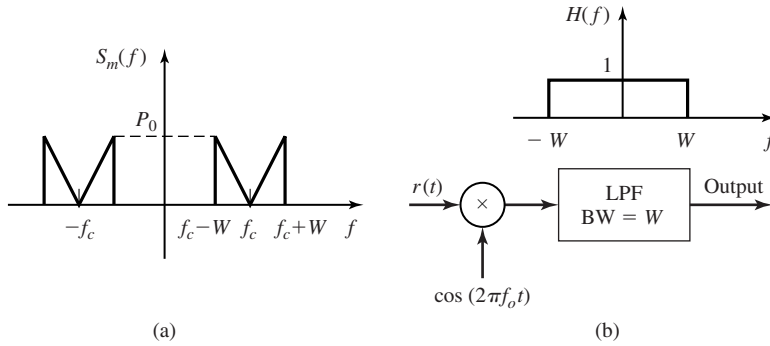


Figure P-5.3

5.4 A certain communication channel is characterized by 90-dB attenuation and additive white noise with power-spectral density of  $\frac{N_0}{2} = 0.5 \times 10^{-14}$  W/Hz. The bandwidth of the message signal is 1.5 MHz and its amplitude is uniformly distributed in the interval  $[-1, 1]$ . If we require that the SNR after demodulation be 30 dB, in each of the following cases find the necessary transmitter power.

1. USSB modulation.
2. Conventional AM with a modulation index of 0.5.
3. DSB-SC modulation.

5.5 A sinusoidal message signal whose frequency is less than 1000 Hz, modulates the carrier  $c(t) = 10^{-3} \cos 2\pi f_c t$ . The modulation scheme is conventional AM and the modulation index is 0.5. The channel noise is additive white with power-spectral density of  $\frac{N_0}{2} = 10^{-12}$  W/Hz. At the receiver, the signal is processed as shown in Figure P-5.5(a). The frequency response of the bandpass noise-limiting filter is shown in Figure P-5.5(b).

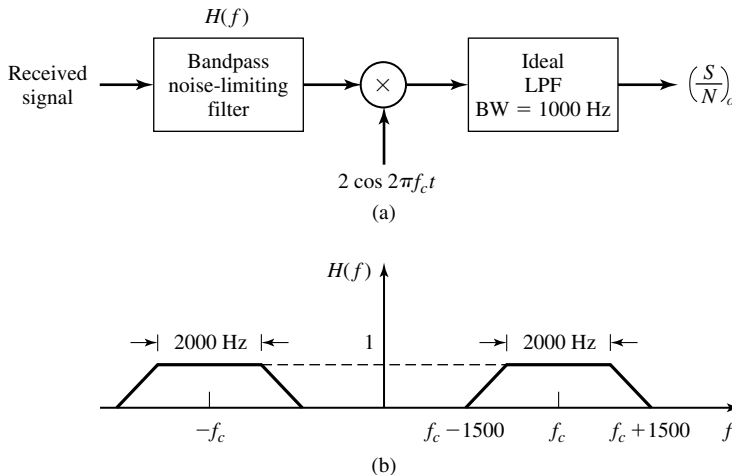


Figure P-5.5

1. Find the signal power and the noise power at the output of the noise-limiting filter.
  2. Find the output SNR.
- 5.6 Derive the expression for the (one-sided) noise-equivalent bandwidth of the PLL given by Equation (5.2.12).
- 5.7 In an analog communication system, *demodulation gain* is defined as the ratio of the SNR at the output of the demodulator to the SNR at the output of the noise-limiting filter at the receiver front end. Find expressions for the demodulation gain in each of the following cases:
1. DSB.
  2. SSB.
  3. Conventional AM with a modulation index of  $a$ . What is the largest possible demodulation gain in this case?
  4. FM with modulation index  $\beta_f$ .
  5. PM with modulation index  $\beta_p$ .
- 5.8 In a broadcasting communication system the transmitter power is 40 KW, the channel attenuation is 80 dB, and the noise power-spectral density is  $10^{-10}$  W/Hz. The message signal has a bandwidth of  $10^4$  Hz.
1. Find the predetection SNR (SNR in  $r(t) = ku(t) + n(t)$ )
  2. Find the output SNR if the modulation is DSB.
  3. Find the output SNR if the modulation is SSB.
  4. Find the output SNR if the modulation is conventional AM with a modulation index of 0.85 and normalized message power of 0.2.
- 5.9 A communication channel has a bandwidth of 100 KHz. This channel is to be used for transmission of an analog source  $m(t)$ , where  $|m(t)| < 1$ , whose bandwidth is  $W = 4$  KHz. The power content of the message signal is 0.1 W.
1. Find the ratio of the output SNR of an FM system that utilizes the whole bandwidth, to the output SNR of a conventional AM system with a modulation index of  $a = 0.85$ ? What is this ratio in dB?
  2. Show that if an FM system and a PM system are employed and these systems have the same output signal to noise ratio, we have
 
$$\frac{BW_{PM}}{BW_{FM}} = \frac{\sqrt{3}\beta_f + 1}{\beta_f + 1}$$
- 5.10 The normalized message signal  $m_n(t)$  has a bandwidth of 5000 Hz and power of 0.1 W, and the channel has a bandwidth of 100 KHz and attenuation of 80 dB. The noise is white with power-spectral density  $0.5 \times 10^{-12}$  W/Hz and the transmitter power is 10 KW.
1. If AM with  $a = 0.8$  is employed what is  $(\frac{S}{N})_o$ ?
  2. If FM is employed what is the highest possible  $(\frac{S}{N})_o$ ?

**5.11** A normalized message signal has a bandwidth of  $W = 8$  KHz and a power of  $P_{M_n} = \frac{1}{2}$ . It is required to transmit this signal via a channel with an available bandwidth of 60 KHz and attenuation of 40 dB. The channel noise is additive and white with a power-spectral density of  $\frac{N_0}{2} = 10^{-12}$  W/Hz. A frequency-modulation scheme, with no pre-emphasis/de-emphasis filtering, has been proposed for this purpose.

1. If it is desirable to have an SNR of at least 40 dB at the receiver output, what is the minimum required transmitter power and the corresponding modulation index?
2. If the minimum required SNR is increased to 60 dB, how would your answer change?
3. If in part 2, we are allowed to employ pre-emphasis/de-emphasis filters with a time constant of  $\tau = 75 \mu\text{sec}$ , how would the answer to part 2 change?

**5.12** Let  $\Phi(t)$  denote a zero-mean, stationary Gaussian process with autocorrelation function  $R_\Phi(\tau)$ . This process modulates a sinusoid to generate the angle-modulated process  $U(t) = A_c \cos(2\pi f_c t + \Phi(t))$ .

1. Show that, in general,  $U(t)$  is not a stationary process.
2. Show that  $\bar{R}_U(\tau)$ , the average autocorrelation function of  $U(t)$  is given by

$$\bar{R}_U(\tau) = \lim_{T \rightarrow \infty} \frac{1}{T} \int_{-T/2}^{T/2} R_U(t, t + \tau) dt = \frac{A_c^2}{2} \cos(2\pi f_c \tau) g(\tau)$$

where

$$g(\tau) = e^{-(R_\Phi(0) - R_\Phi(\tau))}$$

3. Determine the power-spectral density of  $U(t)$ , and show that

$$S_U(f) = \frac{A_c^2}{4} [G(f - f_c) + G(f + f_c)]$$

where

$$G(f) = e^{-R_\Phi(0)} \mathcal{F}[e^{R_\Phi(\tau)}]$$

This shows that the bandwidth of the angle-modulated process  $U(t)$  is twice the bandwidth of  $\mathcal{F}[e^{R_\Phi(\tau)}]$ .

**5.13** In the transmission of telephone signals over LOS microwave links, a combination of FDM-SSB and FM is often employed. A block diagram of such a system is shown in Figure P-5.13. Each of the signals  $m_i(t)$  is bandlimited to  $W$  Hz and these signals are USSB modulated on carriers  $c_i(t) = A_i \cos 2\pi f_{c_i} t$  where  $f_{c_i} = (i - 1)W$ ,  $1 \leq i \leq K$  and  $m(t)$  is the sum of all USSB modulated signals. This signal is FM modulated on a carrier with frequency  $f_c$  with a modulation index of  $\beta$ .

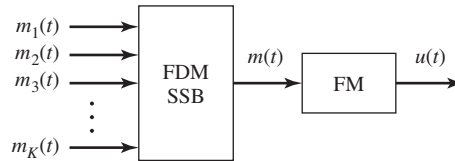


Figure P-5.13

1. Plot a typical spectrum of the USSB modulated signal  $m(t)$ .
  2. Determine the bandwidth of  $m(t)$ .
  3. At the receiver side, the received signal  $r(t) = u(t) + n_w(t)$  is first FM demodulated and then passed through a bank of USSB demodulators. Show that the noise power entering these demodulators depends on  $i$ .
  4. Determine an expression for the ratio of the noise power entering the demodulator whose carrier frequency is  $f_i$  to the noise power entering the demodulator with carrier frequency  $f_j$ ,  $1 \leq i, j \leq K$ .
  5. How should the carrier amplitudes  $A_i$  be chosen to guarantee that, after USSB demodulation, the SNR for all channels is the same?
- 5.14** A power meter that measures average power is connected to the output of a transmitter as shown in Figure P-5.14. The meter reading is 20 W when it is connected to a  $50 \Omega$  load. Determine:
1. The voltage across the load resistance.
  2. The current through the load resistance.
  3. The power level in dBm units.

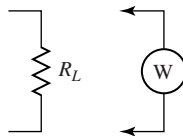


Figure P-5.14

- 5.15** A twisted-pair telephone wireline channel with characteristic impedance  $Z_c = 300 \Omega$  is terminated with a load of  $Z_L = 300 \Omega$ . The telephone line is 200 Km long and has a loss of 2 dB/Km.
1. If the average transmitted power  $P_T = 10$  dBm, determine the received power  $P_R$  if the line contains no repeaters.
  2. If repeaters with a gain of 20 dB are used to boost the signal on the channel and if each repeater requires an input signal level of 10 dBm, determine the number of repeaters and their spacing. The noise figure of each repeater is 6 dB.



- 5.16** A radio antenna pointed in a direction of the sky has a noise temperatures of 50 K. The antenna feeds the received signal to the preamplifier which has a gain of 35 dB over a bandwidth of 10 MHz and a noise figure of 2 dB.
1. Determine the effective noise temperature at the input to the preamplifier.
  2. Determine the noise power at the output of the preamplifier.
- 5.17** An amplifier has a noise-equivalent bandwidth  $B_{\text{neq}} = 25$  KHz and a maximum available power gain of  $\mathcal{G} = 30$  dB. Its output noise power is  $10^8 kT_0$ . Determine the effective noise temperature and the noise figure.
- 5.18** Prove that the effective noise temperature of  $k$  two-port networks in cascade is

$$T_e = T_{e1} + \frac{T_{e2}}{\mathcal{G}_1} + \frac{T_{e3}}{\mathcal{G}_1 \mathcal{G}_2} + \cdots + \frac{T_{ek}}{\mathcal{G}_1 \mathcal{G}_2 \cdots \mathcal{G}_k}$$

# 6

## *Information Sources and Source Coding*

Communication systems are designed to transmit information. In any communication system there exists an information source that produces the information, and the purpose of the communication system is to transmit the output of the source to the destination. In radio broadcasting, for instance, the information source is either a speech source or a music source. In TV broadcasting, the information source is a video source whose output is a moving image. In FAX transmission, the information source produces a still image. In communication between computers, either binary data or ASCII characters are transmitted and, therefore, the source can be modeled as a binary or ASCII source. In storage of binary data on a computer disk, the source is again a binary source.

In Chapters 3 and 5 we studied transmission of analog information using different types of analog modulation and, in particular, we studied the trade-off between bandwidth and power in FM modulation. The rest of this book deals with transmission of digital data. Digital data transmission provides higher level of noise immunity, more flexibility in bandwidth-power trade-off, the possibility of applying cryptographic and antijamming techniques, and ease of implementation using large-scale integration. In order to be able to employ the benefits of digital data transmission, we have to first convert analog information into digital form. Conversion of analog signals into digital data should be carried out in a way that the least amount of information is lost. Therefore, it is necessary to have a precise notion of information.

Everyone has an intuitive notion of the meaning of information. However, performance analysis of communication systems can hardly be conceived without a quantitative measure of information and mathematical modeling of information sources. Hartley, Nyquist, and Shannon were the pioneers in defining quantitative measures for information. In this chapter, we investigate mathematical modeling of information

sources and provide a measure of information. Then we will see how the output of an information source can be made more compact and, therefore, easier to transmit or store.

## 6.1 MODELING OF INFORMATION SOURCES

The intuitive and common notion of information refers to any new knowledge about something. One can obtain information via hearing, seeing, or other means of perception. The information source, therefore, produces outputs which are of interest to the receiver of information, who does not know these outputs in advance. The role of the communication-system designer is to make sure that this information is transmitted to the receiver correctly. Since the output of the information source is a time-varying unpredictable function (if predictable, there is no need to transmit it) it can be modeled as a random process. We have already seen in Chapter 4 that in communication channels the existence of noise causes stochastic dependence between the input and output of the channel. Therefore, the communication-system designer designs a system that transmits the output of a random process (information source) to a destination via a random medium (channel) and ensures low distortion.

Information sources can be modeled by random processes, and the properties of the random process depend on the nature of the information source. For example, when modeling speech signals, the resulting random process has all its power in a frequency band of approximately 300–4000 Hz. Therefore, the power-spectral density of the speech signal also occupies this band of frequencies. A typical power-spectral density for the speech signal is shown in Figure 6.1. Video signals are restored from a still or moving image and, therefore, the bandwidth depends on the required resolution. For TV transmission, depending on the system employed (NTSC, PAL or SECAM), this band is typically between 0–4.5 MHz and 0–6.5 MHz. For telemetry data the bandwidth, of course, depends on the rate of change of data.

What is common in all these processes is that they are bandlimited processes and, therefore, can be sampled at the Nyquist rate or larger and reconstructed from the sampled values. Therefore, it makes sense to confine ourselves to discrete-time random processes in this chapter because all information sources of interest can be modeled by such a process. The mathematical model for an information source is shown in Figure 6.2. Here the source is modeled by a discrete-time random process  $\{X_i\}_{i=-\infty}^{\infty}$ . The alphabet over which the random variables  $X_i$  are defined can be either discrete (in

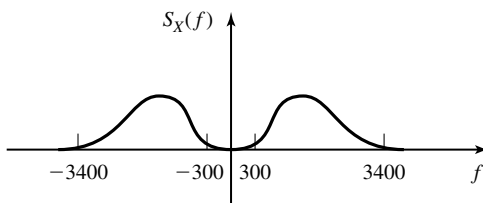


**Figure 6.1** Typical power spectrum of speech signal.

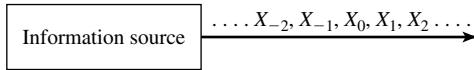


**Figure 6.2** Mathematical model for a discrete-time information source.

transmission of binary data, for instance) or continuous (e.g., sampled speech). The statistical properties of the discrete-time random process depend on the nature of the information source.

In this chapter, we will only study rather simple models for information sources. Study of more complicated models is mathematically demanding and beyond the scope of our treatment. However, even simple models enable us to define precisely a measure of information and bounds on compression of information.

The simplest model for the information source that we study is the *discrete memoryless source* (DMS). A DMS is a discrete-time, discrete-amplitude random process in which all  $X_i$ 's are generated independently and with the same distribution. Therefore a DMS generates a sequence of i.i.d. random variables taking values in a discrete set.

Let set  $\mathcal{A} = \{a_1, a_2, \dots, a_N\}$  denote the set in which the random variable  $X$  takes its values, and let the probability mass function for the discrete random variable  $X$  be denoted by  $p_i = p(X = a_i)$  for all  $i = 1, 2, \dots, N$ . A full description of the DMS is given by the set  $\mathcal{A}$ , called the alphabet, and the probabilities  $\{p_i\}_{i=1}^N$ .

#### Example 6.1.1

An information source is described by the alphabet  $\mathcal{A} = \{0, 1\}$  and  $p(X_i = 1) = 1 - p(X_i = 0) = p$ . This is an example of a discrete memoryless source. In the special case where  $p = 0.5$  the source is called a *binary symmetric source*, or BSS for short.

### 6.1.1 Measure of Information

In order to give a quantitative measure of information, we will start with the basic model of an information source and try to define the information content of the source in such a way that certain intuitive properties are satisfied. Let us assume that the source that we are considering is a discrete source. Let the outputs of this source be revealed to an interested party. Let  $a_1$  be the most-likely and  $a_N$  be the least-likely output. For example, one could imagine the source to represent both the weather condition and air pollution in a certain city (in the northern hemisphere) during July. In this case,  $\mathcal{A}$  represents various combinations of various weather conditions and pollution such as hot and polluted, hot and lightly polluted, cold and highly polluted, cold and mildly polluted, very cold and lightly polluted, etc. The question is: which output conveys more information,  $a_1$  or  $a_N$  (the most probable or the least probable one)? Intuitively, revealing  $a_N$  (or, equivalently, very cold and lightly polluted in the previous example) reveals the most information. From this it follows that a rational measure of information for an output of an information source should be a decreasing function of the probability of that output. A second intuitive property of a measure of information is that a small change in the probability of a certain output should not change the information delivered by that output by a large amount. In other words, the information measure should be a decreasing and continuous function of the probability of the source output.

Now let us assume that the information about output  $a_j$  can be broken into two independent parts, say  $a_{j1}$  and  $a_{j2}$ ; i.e.,  $X_j = (X^{(j1)}, X^{(j2)})$ ,  $a_j = \{a^{j1}, a^{j2}\}$ , and  $p(X = a_j) = p(X^{(j1)} = a^{j1})p(X^{(j2)} = a^{j2})$ . This can happen, for example, if we assume that the temperature and pollution were almost independent and, therefore, each source output can be broken into two independent components. Since the components are independent, revealing the information about one component (temperature) does not provide any information about the other component (pollution) and, therefore, intuitively the amount of information provided by revealing  $a_j$  is the sum of the informations obtained by revealing  $a^{j1}$  and  $a^{j2}$ . From the above discussion, we can conclude that the amount of information revealed about an output  $a_j$  with probability  $p_j$  must satisfy the following three conditions:

1. The information content of output  $a_j$  depends only on the probability of  $a_j$  and not on the value of  $a_j$ . We denote this function by  $I(p_j)$  and call it *self-information*.
2. Self-information is a continuous function of  $p_j$ ; i.e.,  $I(\cdot)$  is a continuous function.
3. Self-information is a decreasing function of its argument i.e., least probable outcomes convey most information.
4. If  $p_j = p^{(j1)}p^{(j2)}$ , then  $I(p_j) = I(p^{(j1)}) + I(p^{(j2)})$ .

It can be proved that the only function that satisfies all the above properties is the logarithmic function; i.e.,  $I(x) = -\log(x)$ . The base of logarithm is not important and defines the unit by which the information is measured. If the base is 2, the information is expressed in *bits*, and if the natural logarithm is employed, the unit is *nats*. From this point on we assume all logarithms are in base 2 and all information is given in bits.

Now that the information revealed about each source output  $a_i$  is defined as the self-information of that output, given by  $-\log(p_i)$ , we can define the information content of the source as the weighted average of the self-information of all source outputs. This is justified by the fact that various source outputs appear with their corresponding probabilities. Therefore, the information revealed by an unidentified source output is the weighted average of the self-information of the various source outputs; i.e.,  $\sum_{i=1}^N p_i I(p_i) = \sum_{i=1}^N -p_i \log p_i$ . The information content of the information source is known as the *entropy* of the source and is denoted by  $H(X)$ .

**Definition 6.1.1.** The entropy of a discrete random variable  $X$  is a function of its PMF and is defined by

$$H(X) = - \sum_{i=1}^N p_i \log p_i = \sum_{i=1}^N p_i \log \left( \frac{1}{p_i} \right) \quad (6.1.1)$$

where  $0 \log 0 = 0$ . Note that there exists a slight abuse of notation here. One would expect  $H(X)$  to denote a function of the random variable  $X$  and, hence, be a random variable itself. However,  $H(X)$  is a function of the PMF of the random variable  $X$  and is, therefore, a number.

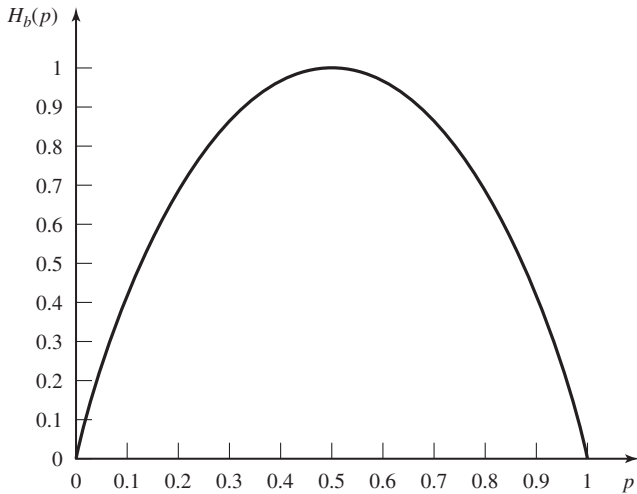


**Figure 6.3** The binary entropy function.

### Example 6.1.2

In the binary memoryless source with probabilities  $p$  and  $1 - p$ , respectively, we have

$$H(X) = -p \log p - (1 - p) \log(1 - p) \quad (6.1.2)$$

This function, denoted by  $H_b(p)$ , is known as the *binary entropy function* and a plot of it is given in Figure 6.3.

### Example 6.1.3

A source with bandwidth 4000 Hz is sampled at the Nyquist rate. Assuming that the resulting sequence can be approximately modeled by a DMS with alphabet  $\mathcal{A} = \{-2, -1, 0, 1, 2\}$  and with corresponding probabilities  $\{\frac{1}{2}, \frac{1}{4}, \frac{1}{8}, \frac{1}{16}, \frac{1}{16}\}$ , determine the rate of the source in bits/sec.

**Solution** We have

$$H(X) = \frac{1}{2} \log 2 + \frac{1}{4} \log 4 + \frac{1}{8} \log 8 + 2 \times \frac{1}{16} \log 16 = \frac{15}{8} \text{ bits/sample}$$

and since we have 8000 samples/sec the source produces information at a rate of 15,000 bits/sec.

## 6.1.2 Joint and Conditional Entropy

When dealing with two or more random variables, exactly in the same way that joint and conditional probabilities are introduced, one can introduce joint and conditional entropies. These concepts are especially important when dealing with sources with memory.

**Definition 6.1.2.** The *joint entropy* of two discrete random variables  $(X, Y)$  is defined by

$$H(X, Y) = - \sum_{x,y} p(x, y) \log p(x, y) \quad (6.1.3)$$

For the case of  $n$  random variables  $\mathbf{X} = (X_1, X_2, \dots, X_n)$ , we have

$$H(\mathbf{X}) = - \sum_{x_1, x_2, \dots, x_n} p(x_1, x_2, \dots, x_n) \log p(x_1, x_2, \dots, x_n) \quad (6.1.4)$$

As seen, the joint entropy is simply the entropy of a vector-valued random variable.

The conditional entropy of the random variable  $X$ , given the random variable  $Y$ , can be defined by noting that if  $Y = y$ , then the PMF of the random variable  $X$  will be  $p(x | y)$ , and the corresponding entropy is  $H(X | Y = y) = - \sum_x p(x | y) \log p(x | y)$ , which is intuitively the amount of uncertainty in  $X$  when one knows  $Y = y$ . The weighted average of the above quantities over all  $y$  is the uncertainty in  $X$  when  $Y$  is known. This quantity is known as the conditional entropy and defined as follows:

**Definition 6.1.3.** The *conditional entropy* of the random variable  $X$  given the random variable  $Y$  is defined by

$$H(X | Y) = - \sum_{x, y} p(x, y) \log p(x | y) \quad (6.1.5)$$

In general, we have

$$H(X_n | X_1, \dots, X_{n-1}) = - \sum_{x_1, \dots, x_n} p(x_1, \dots, x_n) \log p(x_n | x_1, \dots, x_{n-1}) \quad (6.1.6)$$

**Example 6.1.4**

Using chain rule for PMFs,  $p(x, y) = p(y)p(x | y)$ , show that  $H(X, Y) = H(Y) + H(X | Y)$ . Generalize this result to the case of  $n$  random variables to show the following chain rule for entropies

$$H(\mathbf{X}) = H(X_1) + H(X_2 | X_1) + \dots + H(X_n | X_1, X_2, \dots, X_{n-1}) \quad (6.1.7)$$

**Solution** From the definition of the joint entropy of two random variables, we have

$$\begin{aligned} H(X, Y) &= - \sum_{x, y} p(x, y) \log p(x, y) \\ &= - \sum_{x, y} p(x, y) \log [p(y)p(x | y)] \\ &= - \sum_{x, y} p(x, y) \log p(y) - \sum_{x, y} p(x, y) \log p(x | y) \\ &= - \sum_y p(y) \log p(y) - \sum_{x, y} p(x, y) \log p(x | y) \\ &= H(Y) + H(X | Y) \end{aligned} \quad (6.1.8)$$

where in the last step we have used

$$\sum_x p(x, y) = p(y) \quad (6.1.9)$$

This relation says that the information content of the pair  $(X, Y)$  is equal to the information content of  $Y$  plus the information content of  $X$  after  $Y$  is known. Equivalently, it says that

the same information is transferred by either revealing the pair  $(X, Y)$ , or by first revealing  $Y$  and then revealing the remaining information in  $X$ . The proof for general  $n$  is similar and is left as an exercise. In the case where the random variables  $(X_1, X_2, \dots, X_n)$  are independent, Equation (6.1.6) reduces to

$$H(\mathbf{X}) = \sum_{i=1}^n H(X_i) \quad (6.1.10)$$

If the random variable  $X_n$  denotes the output of a discrete (not necessarily memoryless) source at time  $n$ , then  $H(X_2 | X_1)$  denotes the fresh information provided by source output  $X_2$  to someone who already knows the source output  $X_1$ . In the same way,  $H(X_n | X_1, X_2, \dots, X_{n-1})$  denotes the fresh information in  $X_n$  for an observer who has observed the sequence  $(X_1, X_2, \dots, X_{n-1})$ . The limit of the above conditional entropy as  $n$  tends to infinity is known as the *entropy rate* of the random process.

**Definition 6.1.4.** The *entropy rate* of a stationary discrete-time random process is defined by

$$H = \lim_{n \rightarrow \infty} H(X_n | X_1, X_2, \dots, X_{n-1})$$

Stationarity ensures the existence of the limit, and it can be proved that an alternative definition of the entropy rate for sources with memory is given by

$$H = \lim_{n \rightarrow \infty} \frac{1}{n} H(X_1, X_2, \dots, X_n).$$

Entropy rate plays the role of entropy for sources with memory. It is basically a measure of the uncertainty per output symbol of the source.

## 6.2 SOURCE-CODING THEOREM

The source-coding theorem is one of the three fundamental theorems of information theory introduced by Shannon (1948a, 1948b). The source-coding theorem establishes a fundamental limit on the rate at which the output of an information source can be compressed without causing a large error probability. We have seen already that the entropy of an information source is a measure of the uncertainty or, equivalently, the information content of the source. Therefore, it is natural that in the statement of the source-coding theorem, the entropy of the source plays a major role.

The entropy of an information source has a very intuitive meaning. Let us assume that we are observing outputs of length  $n$  of a DMS where  $n$  is very large. Then, according to the law of large numbers (see Chapter 4), in this sequence, with high probability (that goes to 1 as  $n \rightarrow \infty$ ) letter  $a_1$  is repeated approximately  $np_1$  times, letter  $a_2$  is repeated approximately  $np_2$  times,  $\dots$ , and letter  $a_N$  is repeated approximately  $np_N$  times. This means that for  $n$  large enough, with probability approaching one, every sequence from the source has the same composition and, therefore, the same probability. To put it in another way, asymptotically “almost everything is almost equally



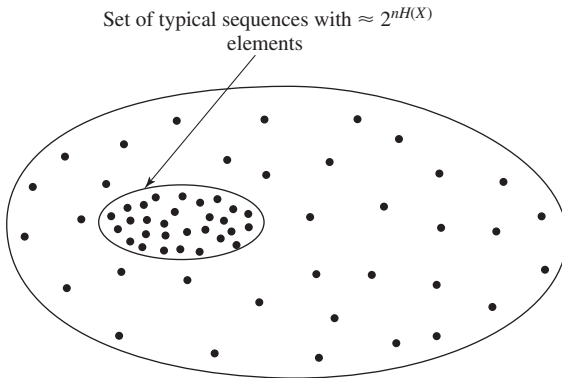


**Figure 6.4** The set of typical and nontypical sequences.

probable.”<sup>†</sup> The sequences  $\mathbf{x}$  that have the above structure are called *typical sequences*. The probability of a typical sequence is given by

$$\begin{aligned}
 P(\mathbf{X} = \mathbf{x}) &\approx \prod_{i=1}^N p_i^{np_i} \\
 &= \prod_{i=1}^N 2^{np_i \log p_i} \\
 &= 2^{n \sum_{i=1}^N p_i \log p_i} \\
 &= 2^{-nH(X)}
 \end{aligned}$$

(In this chapter, all the logarithms are in base 2, and all entropies are in bits unless otherwise specified.) This means that for large  $n$  almost all the output sequences of length  $n$  of the source are equally probable with probability  $\approx 2^{-nH(X)}$ . These are called typical sequences. On the other hand, the probability of the set of nontypical sequences is negligible.

Since the probability of the typical sequences is almost one and each typical sequence has a probability of almost  $2^{-nH(X)}$ , the total number of typical sequences is almost  $2^{nH(X)}$ . Therefore, although a source of alphabet size  $N$  can produce  $N^n$  sequences of length  $n$ , the “effective” number of outputs is  $2^{nH(X)}$ . By effective number of outputs we mean that almost nothing is lost by neglecting the other outputs, and the probability of having lost anything goes to zero as  $n$  goes to infinity. Figure 6.4 gives a schematic diagram of the property mentioned above. This is a very important result, which tells us that for all practical purposes, it is enough to consider the set of typical sequences rather than the set of all possible outputs of the source. The error introduced in ignoring nontypical sequences can be made smaller than any given  $\epsilon > 0$  by choosing  $n$  to be large enough. This is the essence of *data compression*, the practice of representing the output of the source with a smaller number of sequences compared to the number of the outputs that the source really produces.

<sup>†</sup>Borrowed from Cover and Thomas (1991).

From the above result and since  $\epsilon$  is an arbitrary positive number, it is seen that we can only represent the typical source outputs without introducing considerable error. Since the total number of typical sequences is roughly  $2^{nH(X)}$ , we need  $nH(X)$  bits to represent them. However, these bits are used to represent source outputs of length  $n$ . Therefore, on the average, any source output requires  $H(X)$  bits for an essentially error-free representation. This, once again, justifies the notion of entropy as the amount of information per source output.

So far we have assumed that the source is discrete and memoryless and therefore it can be represented by an i.i.d. random variable. Such a source can only be compressed if its PMF is not uniform. For  $X$  uniformly distributed, we have  $H(X) = \log N$  and, therefore,  $2^{nH(X)} = 2^{n \log N} = N^n$ . This means that the “effective” number of source outputs of length  $n$  is equal to the total number of source outputs, and no compression is possible.

We have not considered the case where the source has memory. For a source with memory, the outputs of the source are not independent and, therefore, previous outputs reveal some information about the future ones. This means that the rate at which fresh information is produced decreases as more and more source outputs are revealed. A classic example of such a case is the English alphabet, which shows a lot of dependency between letters and words (a “q” is almost always followed by a “u,” a single letter between two spaces is either “T” or “a,” etc.). The entropy per letter for a large text of English is roughly the limit of  $H(X_n | X_1, X_2, \dots, X_{n-1})$  as  $n$  becomes large (the entropy rate defined in Section 6.1.2). In general stationary sources, the entropy rate has the same significance as the entropy for the case of memoryless sources and defines the number of “effective” source outputs for  $n$  large enough; i.e.,  $2^{nH}$  where  $H$  is the entropy rate.

Studies with statistical models of printed English show that the entropy rate converges rather quickly, and for  $n = 10$  we are very close to the limit. These studies show that for  $n = 1$ ; i.e., a memoryless source model, we have  $H(X) = 4.03$  bits/letter. As the memory increases, the size of the space over which conditional probabilities are computed increases rapidly and it is not easy to find the conditional probabilities required to compute the entropy rate. Some methods for estimating these conditional probabilities have been proposed in the literature and, based on these methods, the entropy of printed English is estimated to be around 1.3 bits/letter. It is worth mentioning here that in these studies only the 26 letters of the English alphabet and the space mark (a total of 27) have been considered.

So far, we have given an informal description of the source-coding theorem and justified it. A formal statement of the theorem, without proof, is given next. The interested reader is referred to the references at the end of this chapter for a proof.

**Theorem 6.2.1 [Source-Coding Theorem].** A source with entropy (or entropy rate)  $H$  can be encoded with arbitrarily small error probability at any rate  $R$  (bits/source output) as long as  $R > H$ . Conversely If  $R < H$ , the error probability will be bounded away from zero, independent of the complexity of the encoder and the decoder employed. ■

This theorem, first proved by Shannon (1948a), only gives necessary and sufficient conditions for the existence of source codes. It does not provide any algorithm for the design of codes that achieve the performance predicted by this theorem. In the next section, we present two algorithms for compression of information sources. One is due to Huffman (1952), and the second is due to Ziv and Lempel (1977, 1978).

## 6.3 SOURCE-CODING ALGORITHMS

In the preceding section, we observed that  $H$ , the entropy of a source, gives a sharp bound on the rate at which a source can be compressed for reliable reconstruction. This means that at rates above entropy it is possible to design a code with an error probability as small as desired, whereas at rates below entropy such a code does not exist. This important result however does not provide specific algorithms to design codes approaching this bound. In this section, we will introduce two algorithms to design codes that perform very close to the entropy bound. These coding methods are the Huffman coding algorithm and the Lempel-Ziv source-coding algorithm.

### 6.3.1 The Huffman Source-Coding Algorithm

In Huffman coding, fixed-length blocks of the source output are mapped to variable-length binary blocks. This is called *fixed- to variable-length* coding. The idea is to map the more frequently occurring fixed-length sequences to shorter binary sequences and the less frequently occurring ones to longer binary sequences. In variable-length coding, synchronization is a problem. This means that there should be one and only one way to break the binary-received sequence into code words. The following example clarifies this point.

#### Example 6.3.1

Let us assume that the possible outputs of an information source are  $\{a_1, a_2, a_3, a_4, a_5\}$ , and consider the following three codes for this source

Letter	Probability	Codewords			
		Code 1	Code 2	Code 3	Code 4
$a_1$	$p_1 = \frac{1}{2}$	1	1	0	00
$a_2$	$p_2 = \frac{1}{4}$	01	10	10	01
$a_3$	$p_3 = \frac{1}{8}$	001	100	110	10
$a_4$	$p_4 = \frac{1}{16}$	0001	1000	1110	11
$a_5$	$p_5 = \frac{1}{16}$	00001	10000	1111	110

In the first code, each code word ends with a 1. Therefore, as soon as the decoder observes a 1, it knows that the code word has ended and a new code word will start. This means that the code is a *self-synchronizing code*. In the second code each code word starts with a 1. Therefore, upon observing a 1, the decoder knows that a new code word has started

and, hence, the previous bit was the last bit of the previous code word. This code is again self-synchronizing but not as desirable as the first code. The reason is that in this code we have to wait to receive the first bit of the next code word to recognize that a new code word has started, whereas in code 1 we recognize the last bit without having to receive the first bit of the next code word. Both codes 1 and 2 therefore are *uniquely decodable*. However, only code 1 is *instantaneous*. Codes 1 and 3 have the nice property that no code word is the prefix of another code word. It is said that they satisfy the *prefix condition*. It can be proved that a necessary and sufficient condition for a code to be uniquely decodable and instantaneous is that it satisfy the prefix condition. This means that both codes 1 and 3 are uniquely decodable and instantaneous. However, code 3 has the advantage of having a smaller average code word length. In fact, for code 1 the average code word length is

$$E[L] = 1 \times \frac{1}{2} + 2 \times \frac{1}{4} + 3 \times \frac{1}{8} + 4 \times \frac{1}{16} + 5 \times \frac{1}{16} = \frac{31}{16}$$

and for code 3

$$E[L] = 1 \times \frac{1}{2} + 2 \times \frac{1}{4} + 3 \times \frac{1}{8} + 4 \times \frac{1}{16} + 4 \times \frac{1}{16} = \frac{30}{16}$$

Code 4 has a major disadvantage. This code is not uniquely decodable. For example, the sequence 110110 can be decoded in two ways, as  $a_5a_5$  or as  $a_4a_2a_3$ . Codes that are not uniquely decodable, are not desirable and should be avoided in practice. From the discussion above it is seen that the most desirable of the above four codes is code 3, which is uniquely decodable, instantaneous, and has the least-average code word length. This code is an example of a *Huffman code* to be discussed shortly.

As already mentioned, the idea in Huffman coding is to choose code word lengths such that more probable sequences have shorter code words. If we can map each source output of probability  $p_i$  to a code word of length approximately  $\log \frac{1}{p_i}$  and at the same time ensure unique decodability, we can achieve an average code word length of approximately  $H(X)$ . Huffman codes are uniquely decodable instantaneous codes with minimum-average code word length. In this sense they are optimal. By optimality we mean that, among all codes that satisfy the prefix condition (and therefore are uniquely decodable and instantaneous), Huffman codes have the minimum-average code word length. Next, we present the algorithm for the design of the Huffman code. From the algorithm, it is obvious that the resulting code satisfies the prefix condition. The proof of the optimality is omitted and the interested reader is referred to the references at the end of this chapter.

### Huffman Encoding Algorithm.

1. Sort source outputs in decreasing order of their probabilities.
2. Merge the two least-probable outputs into a single output whose probability is the sum of the corresponding probabilities.
3. If the number of remaining outputs is 2, then go to the next step, otherwise go to step 1.

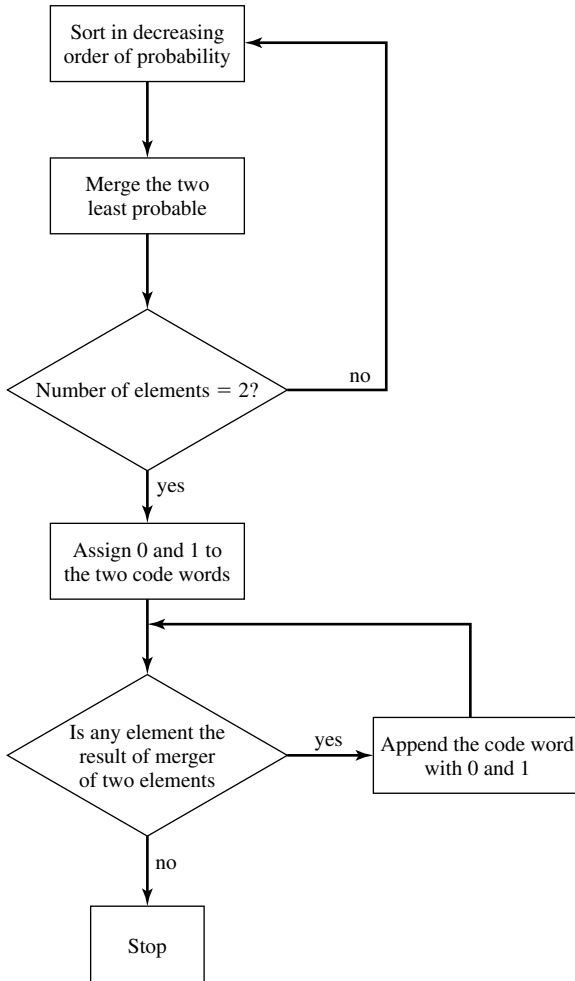


**Figure 6.5** Huffman coding algorithm.

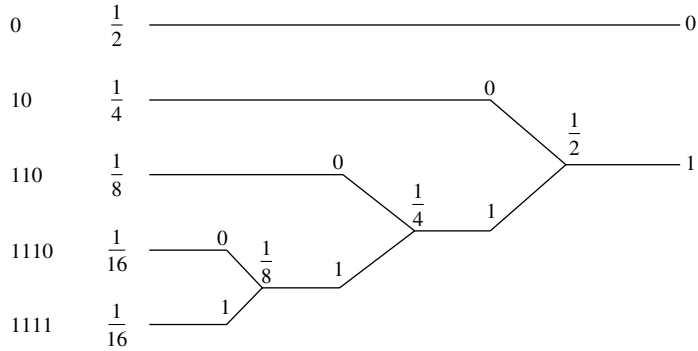
4. Arbitrarily assign 0 and 1 as code words for the two remaining outputs.
5. If an output is the result of the merger of two outputs in a preceding step, append the current code word with a 0 and a 1 to obtain the code word for the preceding outputs and then repeat 5. If no output is preceded by another output in a preceding step, then stop.

Figure 6.5 shows a flow chart of this algorithm.

### Example 6.3.2

Design a Huffman code for the source given in the preceding example.

**Solution** The tree diagram shown below summarizes the design steps for code construction and the resulting code words.



It can be shown that the average length of a Huffman code, defined by

$$\bar{R} = \sum_{x \in \mathcal{X}} p(x)l(x) \tag{6.3.1}$$

where  $l(x)$  is the length of the code word corresponding to the source output  $x$ , satisfies the following inequality

$$H(X) \leq \bar{R} < H(X) + 1 \tag{6.3.2}$$

Now, if instead of single-source letters, the Huffman code is designed for sequences of source letters of length  $n$  ( $n$ th extension of the source), we would have

$$H(\mathbf{X}^n) \leq \bar{R}_n < H(\mathbf{X}^n) + 1$$

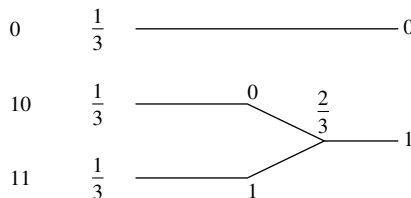
where  $\bar{R}_n$  denotes the average code word length for the extended source sequence and, therefore,  $\bar{R} = \frac{1}{n}\bar{R}_n$ . In case the source we are dealing with is memoryless, we also have  $H(\mathbf{X}^n) = nH(X)$ . Substituting these in the above equation and dividing by  $n$  we have

$$H(X) \leq \bar{R} < H(X) + \frac{1}{n} \tag{6.3.3}$$

Therefore, for  $n$  large enough  $\bar{R}$  can be made as close to  $H(X)$  as desired. It is also obvious that for discrete sources with memory,  $\bar{R}$  approaches the entropy rate of the source.

**Example 6.3.3**

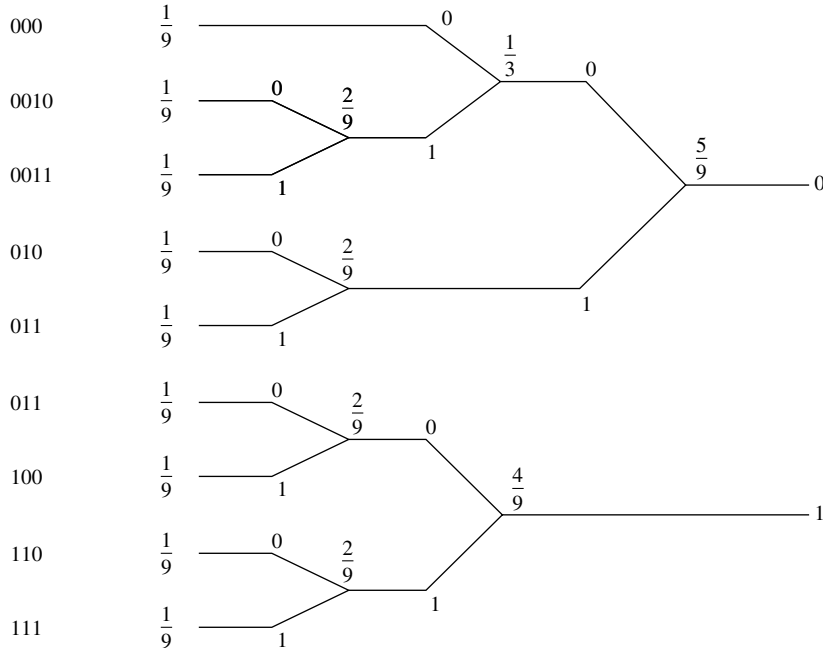
A DMS with equiprobable outputs and alphabet  $\mathcal{A} = \{a_1, a_2, a_3\}$  has the Huffman code designed here.



The entropy of the source is  $H(X) = \log 3 = 1.585$  and  $\bar{R} = \frac{5}{3} = 1.667$ . If we use sequences of two letters, we will have the source

$$\mathcal{A}^2 = \{(a_1, a_1), (a_1, a_2), (a_1, a_3), \dots, (a_3, a_2), (a_3, a_3)\}$$

with the probability vector  $\mathbf{p}^{(2)} = \{\frac{1}{9}, \frac{1}{9}, \frac{1}{9}, \frac{1}{9}, \frac{1}{9}, \frac{1}{9}, \frac{1}{9}, \frac{1}{9}, \frac{1}{9}\}$ . A Huffman code for this source is designed in the following tree diagram.



Here the average code word length is  $\bar{R}_2 = 3.222$  bits/pair of source outputs or 1.611 bits/each source output. Comparing this with the previous example we see that the average length in this case is closer to the entropy of the source.

In our treatment only binary Huffman codes were treated. The algorithm for design of binary Huffman codes can be easily generalized to an algorithm for the design of general  $M$ -ary Huffman codes. We will examine the general algorithm in a problem at the end of this chapter.

### 6.3.2 The Lempel-Ziv Source-Coding Algorithm

We have already seen that Huffman codes are optimal in the sense that for a given source they provide a prefix code with minimum-average block length. Nevertheless, there exist major problems implementing Huffman codes. One problem is that Huffman codes depend strongly on the source probabilities (statistics). The source statistics have to be known in advance to design a Huffman code. If we can only observe the source outputs, then we have to do the coding in two passes. In the first pass, we estimate the statistics of the source (which, in the case of sources with memory and in cases

where we want to apply Huffman coding to the extension of the source, becomes quite time consuming) and in the second pass coding is done. The other problem with Huffman codes is that if the code is designed for source blocks of length 1, it only employs variations in the frequency of the source outputs and not the source memory. If one wants to employ the source memory as well, one has to design the code for blocks of length 2 or more and this exponentially increases the complexity of the algorithm. For instance, encoding of ASCII characters with a block length of 1 requires a tree with 256 terminal nodes, but if a block length of 2 is desired the size of the tree and, therefore, the complexity of coding becomes much higher. In certain applications, such as storage in magnetic or optical media where high transfer rates are desirable, the complexity and speed of Huffman coding becomes a bottleneck.

The Lempel-Ziv algorithm belongs to the class of *universal source-coding algorithms*; i.e., algorithms that are independent of the source statistics. This algorithm is a *variable- to fixed-length* coding scheme. This means that any sequence of source outputs is uniquely parsed into phrases of varying length and these phrases are encoded using code words of equal length. Parsing is done by identifying phrases of the smallest length that have not appeared so far. To this end, the parser observes the source output, and as long as the new source output sequence after the last phrase coincides with one of the existing phrases, no new phrase is introduced and another letter from the source is considered. As soon as the new output sequence is different from the previous phrases, it is recognized as a new phrase and encoded. The encoding scheme is simple. The new phrase is the concatenation of a previous phrase and a new source output. To encode it, *the binary expansion of the lexicographic ordering of the previous phrase and the new bit are concatenated*. For example, let us assume that we want to parse and encode the following sequence:

0100001100001010000010100000110000010100001001001

Parsing the sequence by the rules explained before results in the following phrases:

0, 1, 00, 001, 10, 000, 101, 0000, 01, 010, 00001, 100, 0001, 0100, 0010, 01001, . . . . It is seen that all the phrases are different and each phrase is a previous phrase concatenated with a new source output. The number of phrases is 16. This means that for each phrase we need 4 bits, plus an extra bit to represent the new source output. The above sequence is encoded by 0000 0, 0000 1, 0001 0, 0011 1, 0010 0, 0011 0, 0101 1, 0110 0, 0001 1, 1001 0, 1000 1, 0101 0, 0110 1, 1010 0, 0100 0, 1110 1, . . . . Table 6.1 summarizes this procedure.

This representation can hardly be called a data compression scheme because a sequence of length 49 has been mapped into a sequence of length 80, but as the length of the original sequence is increased, the compression role of this algorithm becomes more apparent. It can be proved that for a stationary and ergodic source, as the length of the sequence increases, the number of bits in the compressed sequence approaches  $nH(X)$ , where  $H(X)$  is the entropy rate of the source. The decompression of the encoded sequence is straightforward and can be done very easily.

One problem with the Lempel-Ziv algorithm is how the number of phrases should be chosen. Here we have chosen 16 phrases and, therefore, 4 bits to represent each phrase. In general, any fixed number of phrases will sooner or later become too small



**TABLE 6.1** SUMMARY OF LEMPEL-ZIV EXAMPLE

	Dictionary Location	Dictionary Contents	Codeword	
1	0001	0	0000	0
2	0010	1	0000	1
3	0011	00	0001	0
4	0100	001	0011	1
5	0101	10	0010	0
6	0110	000	0011	0
7	0111	101	0101	1
8	1000	0000	0110	0
9	1001	01	0001	1
10	1010	010	1001	0
11	1011	00001	1000	1
12	1100	100	0101	0
13	1101	0001	0110	1
14	1110	0100	1010	0
15	1111	0010	0100	0
16			1110	1

and overflow would occur. For example, if we were to continue coding of the above source for additional input letters, we could not add the new phrases to our dictionary because we have assigned four bits for representation of the elements of the dictionary and we have already 16 phrases in the dictionary. To solve this problem, the encoder and decoder must purge those elements from their dictionaries that are not useful anymore and substitute new elements for them. The purging method should, of course, be a method on which the encoder and the decoder have agreed.

The Lempel-Ziv algorithm is widely used in practice to compress computer files. The “compress” and “uncompress” utilities under the UNIX<sup>®</sup> operating system and numerous other algorithms (ZIP, ZOO, LZH, ARJ, etc.) are implementations of various versions of this algorithm.

## 6.4 RATE-DISTORTION THEORY

In Section 6.2, we saw that it is possible to encode the output of a discrete-memoryless information source at a rate arbitrarily close to its entropy and still be able to recover the output reliably. Reliable reconstruction of the source means that the error probability can be made to approach zero as the block length approaches infinity. In many cases, however, transmitting at rates close to entropy is not possible. For example, if one has limited storage space and the entropy of the information source is greater than the storage capacity, error-free retrieval of the source output from the stored data is impossible. In cases such as this, some *lossy* compression technique has to be employed and some *distortion* will be introduced.

An example of such a case is the encoding of the output of an analog source. The samples of an analog source are real numbers, and in order to represent a real

number an infinite number of bits are required. Therefore, in a practical digital system there exists no way to transmit or store analog data without any loss in precision. To encode analog samples, the samples must be quantized and the quantized values are then encoded using one of the source-encoding algorithms.

In this section, we will study the case of data compression subject to a fidelity criterion. We first introduce some quantities that are needed for quantitative analysis of this case and then define the rate-distortion function.

### 6.4.1 Mutual Information

For discrete random variables,  $H(X|Y)$  denotes the entropy (or uncertainty) of the random variable  $X$  after random variable  $Y$  is known. Therefore, if the starting entropy of the random variable  $X$  is  $H(X)$ , then  $H(X) - H(X|Y)$  denotes the amount of uncertainty of  $X$  that has been removed by revealing random variable  $Y$ . In other words,  $H(X) - H(X|Y)$  is the amount of information provided by the random variable  $Y$  about random variable  $X$ . This quantity plays an important role in both source and channel coding and is called the *mutual information* between two random variables.

**Definition 6.4.1.** The *mutual information* between two discrete random variables  $X$  and  $Y$  is denoted by  $I(X; Y)$  and defined by

$$I(X; Y) = H(X) - H(X|Y). \quad (6.4.1)$$

#### Example 6.4.1

Let  $X$  and  $Y$  be binary random variables with  $P(X=0, Y=0) = \frac{1}{3}$ ,  $P(X=1, Y=0) = \frac{1}{3}$  and  $P(X=0, Y=1) = \frac{1}{3}$ . Find  $I(X; Y)$  in this case.

**Solution** From above  $P(X=0) = P(Y=0) = \frac{2}{3}$  and, therefore,  $H(X) = H(Y) = H_b(\frac{2}{3}) = 0.919$ . On the other hand, the  $(X, Y)$  pair is a random vector uniformly distributed on three values  $(0, 0)$ ,  $(1, 0)$ , and  $(0, 1)$ . Therefore,  $H(X, Y) = \log 3 = 1.585$ . From this, we have  $H(X|Y) = H(X, Y) - H(Y) = 1.585 - 0.919 = 0.666$  and  $I(X; Y) = H(X) - H(X|Y) = 0.919 - 0.666 = 0.253$ .

Mutual information has certain properties that are explored in problems and summarized here.

1.  $I(X; Y) \geq 0$  with equality if and only if  $X$  and  $Y$  are independent.
2.  $I(X; Y) \leq \min(H(X), H(Y))$ .
3.  $I(X; Y) = \sum_{x,y} p(x, y) \log \frac{p(x,y)}{p(x)p(y)}$ .
4.  $I(X; Y) = H(X) + H(Y) - H(X, Y)$ .
5.  $I(X; Y|Z)$  is the conditional mutual information and defined by  $I(X; Y|Z) = H(X|Z) - H(X|Y, Z)$ .
6.  $I(X; Y|Z) = \sum_z p(z) I(X; Y|Z=z)$ .
7.  $I(XY; Z) = I(X; Z) + I(Y; Z|X)$ . This is the chain rule for mutual information.
8. In general,  $I(X_1, \dots, X_n; Y) = I(X_1; Y) + I(X_2; Y|X_1) + \dots + I(X_n; Y|X_1, \dots, X_{n-1})$ .

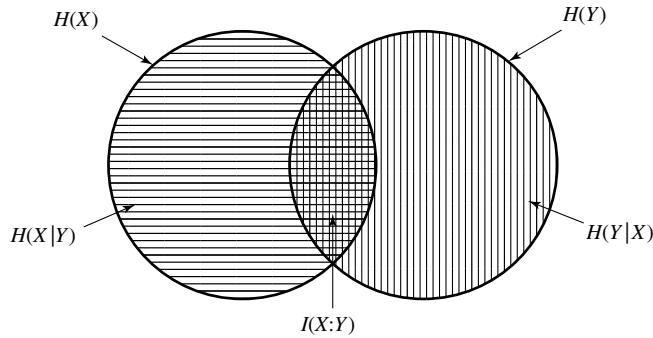


**Figure 6.6** Entropy, conditional entropy, and mutual information.

Figure 6.6 represents the relation among entropy, conditional entropy and mutual information quantities.

### 6.4.2 Differential Entropy

So far we have defined entropy and mutual information for discrete sources. If we are dealing with a discrete-time, continuous-alphabet source whose outputs are real numbers, nothing exists that has the intuitive meaning of entropy. In the continuous case, another quantity that resembles entropy, called *differential entropy*, is defined. However, it does not have the intuitive meaning of entropy. In fact, to reconstruct the output of a continuous source reliably, an infinite number of bits/source output are required because any output of the source is a real number and the binary expansion of a real number has infinitely many bits.

**Definition 6.4.2.** The *differential entropy* of a continuous random variable  $X$  with PDF  $f_X(x)$  is denoted by  $h(X)$  and defined by

$$h(X) = - \int_{-\infty}^{\infty} f_X(x) \log f_X(x) dx \quad (6.4.2)$$

where  $0 \log 0 = 0$ .

#### Example 6.4.2

Determine the differential entropy of a random variable  $X$  uniformly distributed on  $[0, a]$ .

**Solution** Using the definition of differential entropy

$$h(X) = - \int_0^a \frac{1}{a} \log \frac{1}{a} dx = \log a$$

It is seen that for  $a < 1$ , we have  $h(X) < 0$ , which is in contrast to the nonnegativity of the discrete entropy. Also, for  $a = 1$ ,  $h(X) = 0$  without  $X$  being deterministic. This is again in contrast to the properties of discrete entropy.

**Example 6.4.3**

Determine the differential entropy of a Gaussian random variable with mean zero and variance  $\sigma^2$ .

**Solution** The PDF is  $f(x) = \frac{1}{\sqrt{2\pi\sigma^2}} e^{-\frac{x^2}{2\sigma^2}}$ . Therefore, using natural logarithms we find the differential entropy in nats

$$\begin{aligned} h(X) &= - \int_{-\infty}^{\infty} \ln \left( \frac{1}{\sqrt{2\pi\sigma^2}} \right) f(x) dx - \int_{-\infty}^{\infty} \ln \left( e^{-\frac{x^2}{2\sigma^2}} \right) f(x) dx \\ &= \ln(\sqrt{2\pi\sigma^2}) + \frac{\sigma^2}{2\sigma^2} \\ &= \frac{1}{2} \ln(2\pi e\sigma^2) \text{ nats} \end{aligned} \quad (6.4.3)$$

where we have used  $\int_{-\infty}^{\infty} f(x) dx = 1$  and  $\int_{-\infty}^{\infty} x^2 f(x) dx = \sigma^2$ . Changing the base of logarithms to 2, we have

$$h(X) = \frac{1}{2} \log_2(2\pi e\sigma^2) \text{ bits} \quad (6.4.4)$$

Extensions of the definition of differential entropy to joint random variables and conditional differential entropy are straightforward. For two random variables, we have

$$h(X, Y) = - \int_{-\infty}^{\infty} \int_{-\infty}^{\infty} f(x, y) \log f(x, y) dx dy \quad (6.4.5)$$

and

$$h(X | Y) = h(X, Y) - h(Y) \quad (6.4.6)$$

The mutual information between two continuous random variables  $X$  and  $Y$  is defined similarly to the discrete case as

$$I(X; Y) = h(Y) - h(Y | X) = h(X) - h(X | Y) \quad (6.4.7)$$

Although differential entropy does not have the intuitive interpretation of discrete entropy, it can be shown that the mutual information of continuous random variables has basically the same interpretation as the mutual information of discrete random variables; i.e., the information provided by one random variable about the other random variable.

**6.4.3 Rate-Distortion Function**

Returning to our original problem of representing a continuous source with finite number of bits/symbol, the question is: if the source output is to be compressed and represented by a certain number of bits/symbol, how close can the compressed version and the original version be? This question is not applicable only to continuous sources. A similar question can be asked for discrete sources. Let there be a discrete source with entropy  $H(X)$ . This means that we can transmit the output of this source using  $H(X)$  bits/source output and with arbitrarily small-error probability. Now let us assume that using  $H(X)$  bits/source symbol is too high and that we can not tolerate it (for example

in magnetic disk storage, the disk space required becomes huge). Now that the number of available bits/source output is less than  $H(X)$ , error-free restoration of the source is not possible and some errors will be inevitable. The question is: at a given number of bits/source symbol, what is the minimum achievable error rate and, of course, how can this minimum be achieved? The question can also be asked in the opposite direction; i.e., what is the minimum number of bits/source output required to reproduce the source at a certain level of distortion?

To formally present the above discussion, we have to define the notion of distortion. Distortion in reproduction of a source is a measure of fidelity or closeness of the reproduction to the original source output. In a high-fidelity reproduction, the reproduced signal is very close to the original signal and distortion is low, whereas in a low-fidelity reproduction there exists more “distance” between the original signal and the reproduction and, therefore, a higher distortion. A “distortion measure” is a measure of how far apart the signal and its reproduction are. One could think of many distortion measures between a signal  $x(t)$  and its reproduction  $\hat{x}(t)$ , for instance,  $\max_t |x(t) - \hat{x}(t)|$ ,  $\lim_{T \rightarrow \infty} \frac{1}{T} \int_{-T/2}^{T/2} |x(t) - \hat{x}(t)| dt$ , and  $\lim_{T \rightarrow \infty} \frac{1}{T} \int_{-T/2}^{T/2} (x(t) - \hat{x}(t))^2 dt$  are three distortion measures.

A good distortion measure must satisfy two properties. First, it has to be a good approximation to the perception process, and second, it has to be simple enough to be mathematically tractable. The first property simply says that, for example, if we are dealing with speech transmission and in perception of speech the phase of the waveform is not a very crucial factor, the distortion measure should not be heavily dependent on exact phase reproduction. On the other hand, if we are dealing with image perception, phase plays an important role and, therefore, this must be reflected in our choice of the distortion measure. Finding a distortion measure that meets both of these requirements is usually not an easy task.

In general, a distortion measure is a distance between  $x$  and its reproduction  $\hat{x}$  denoted by  $d(x, \hat{x})$ . In the discrete case a commonly used distortion measure is the *Hamming distortion* defined by

$$d_H(x, \hat{x}) = \begin{cases} 1 & x \neq \hat{x} \\ 0, & \text{otherwise} \end{cases}$$

In the continuous case the *squared-error distortion* defined by

$$d(x, \hat{x}) = (x - \hat{x})^2$$

is frequently used. It is also assumed that we are dealing with a *per-letter distortion measure*, meaning that the distortion between sequences is the average of the distortion between their components; i.e.,

$$d(\mathbf{x}^n, \hat{\mathbf{x}}^n) = \frac{1}{n} \sum_{i=1}^n d(x_i, \hat{x}_i)$$

This assumption simply means that the position of the “error” in reproduction is not important and the distortion is not context dependent.

Now, since the source output is a random process,  $d(\mathbf{X}^n, \hat{\mathbf{X}}^n)$  is a random variable. We define the distortion for the source as the expected value of this random variable,

$$D = E[d(\mathbf{X}^n, \hat{\mathbf{X}}^n)] = \frac{1}{n} \sum_{i=1}^n E[d(X_i, \hat{X}_i)] = E[d(X, \hat{X})]$$

where in the last step we have used the stationarity assumption on the source (independence of the distributions from the index  $i$ ).

#### Example 6.4.4

Show that with Hamming distortion,  $D$  represents the error probability.

#### Solution

$$\begin{aligned} D &= E[d_H(X, \hat{X})] = 1 \times P[X \neq \hat{X}] + 0 \times P[X = \hat{X}] \\ &= P[X \neq \hat{X}] = P[\text{error}] \end{aligned}$$

With all these definitions, our original question can be restated as follows: given a memoryless information source with alphabet  $\mathcal{X}$  and probability distribution  $p(x)$ , a reproduction alphabet  $\hat{\mathcal{X}}$  and a distortion measure  $d(x, \hat{x})$  defined for all  $x \in \mathcal{X}$  and  $\hat{x} \in \hat{\mathcal{X}}$ , what is  $R$ , the minimum number of bits/source output required to guarantee that the average distortion between the source-output sequence and the corresponding reproduction-output sequence does not exceed some given  $D$ ? It is obvious that  $R$  is a decreasing function of  $D$ ; i.e., if we need high-fidelity reproduction (low  $D$ ) we require a high  $R$ . The relation between  $R$  and  $D$  is expressed via the *rate-distortion function*. The following theorem gives the general form of the rate-distortion function. For a proof, the reader is referred to the references at the end of this chapter.

**Theorem 6.4.1 [Rate-Distortion].** The minimum number of bits/source output required to reproduce a memoryless source with distortion less than or equal to  $D$  is called the *rate-distortion function*, denoted by  $R(D)$  and given by

$$R(D) = \min_{p(\hat{x}|x): E[d(X, \hat{X})] \leq D} I(X; \hat{X}) \quad (6.4.8)$$

Figure 6.7 is a schematic representation of this theorem. The space of source outputs of length  $n$ ; i.e.,  $\mathcal{X}^n$  is divided into  $2^{nR}$  regions. If the output of the source,  $\mathbf{x}^n$  falls in region  $i$ , the binary representation of  $i$  is transmitted to the decoder. Since  $1 \leq i \leq 2^{nR}$ , the binary representation is of length  $nR$  and, therefore, coding is done at a rate of  $R$  bits/source output. The decoder, after receiving the binary representation of  $i$ , generates a predetermined sequence  $\hat{\mathbf{x}}^n$  such that its average distance (distortion) from the  $\mathbf{x}$  sequences in region  $i$  is minimum. This is the best representation of the region  $i$  sequences. Note that, for large values of  $R$ , we have a large number of regions and, therefore, our representation is very precise (fine quantization), whereas for small  $R$ , the number of regions is small and the distortion is large (coarse quantization). There exist two extreme cases. The first happens when there is only one region ( $R = 0$ ). In this case, the representation point is in some sense (which will be clarified later) the centroid of the whole input space. The second extreme case is when each region consists of a single

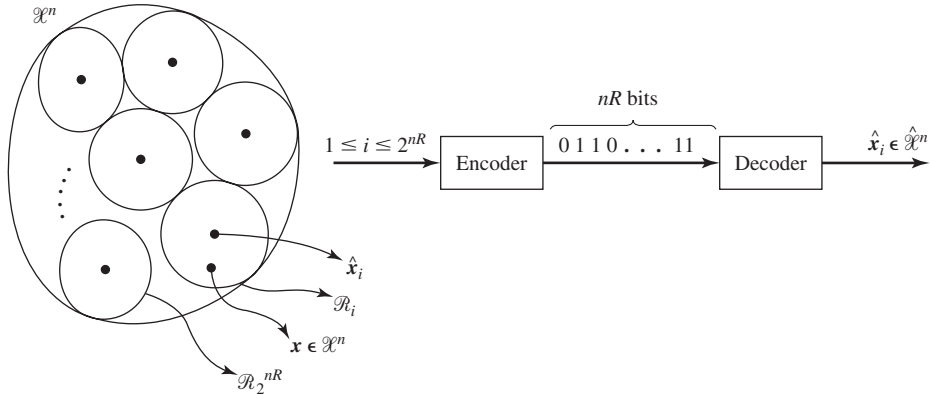


**Figure 6.7** Schematic representation of the rate-distortion theorem.

source output. In this case  $R$  is taking its maximum value and the distortion is zero.<sup>†</sup> From the rate-distortion theorem it is seen that if the rate-distortion function is given for a source and a distortion measure, we know the minimum number of bits/source symbol required to reconstruct the source with any given distortion measure. Given any rate, we can determine the minimum achievable distortion if a code of that rate is used. It should be emphasized that, as was the case with the source-coding theorem, the results indicated by the rate-distortion function are “fundamental limits” in the sense that they can only be achieved asymptotically and with increasing complexity of the encoding–decoding schemes.

#### Example 6.4.5

For a binary memoryless source with  $P(X_i = 1) = 1 - P(X_i = 0) = p$ , and with Hamming distortion, it can be shown that the rate-distortion function is given by

$$R(D) = \begin{cases} H_b(p) - H_b(D) & 0 \leq D \leq \min\{p, 1 - p\} \\ 0, & \text{otherwise} \end{cases} \quad (6.4.9)$$

1. Assuming  $p = 0.5$ , how many bits/source output are required to transmit this information source with a probability of error at most equal to 0.25?
2. With  $p = 0.5$ , and a channel that can transmit 0.75 bits/each source output, what is the minimum achievable error probability?

#### Solution

1. Recall that for Hamming distortion, the error probability and the average distortion coincide (see Example 6.4.4). Therefore,  $P_e = D = 0.25$  and since  $p = 0.5$ , we are dealing with the case where  $0 \leq D \leq \min\{p, 1 - p\}$ . This means that  $R(0.25) = H_b(0.5) - H_b(0.25)$ , which results in  $R \approx 0.189$ .
2. For  $R = 0.75$ , we must solve the equation  $H_b(p) - H_b(D) = 0.75$ , where  $H_b(p) = H_b(0.5) = 1$  and, therefore,  $H_b(D) = 0.25$ , which gives  $P_e = D = 0.042$ .

<sup>†</sup>The distortion is zero when the source alphabet and the representation alphabet are the same. In general, the distortion is given by  $D_{\min} = E[\min_{\hat{x}} d(X, \hat{x})] = \sum_x p(x) \min_{\hat{x}} d(x, \hat{x})$ .

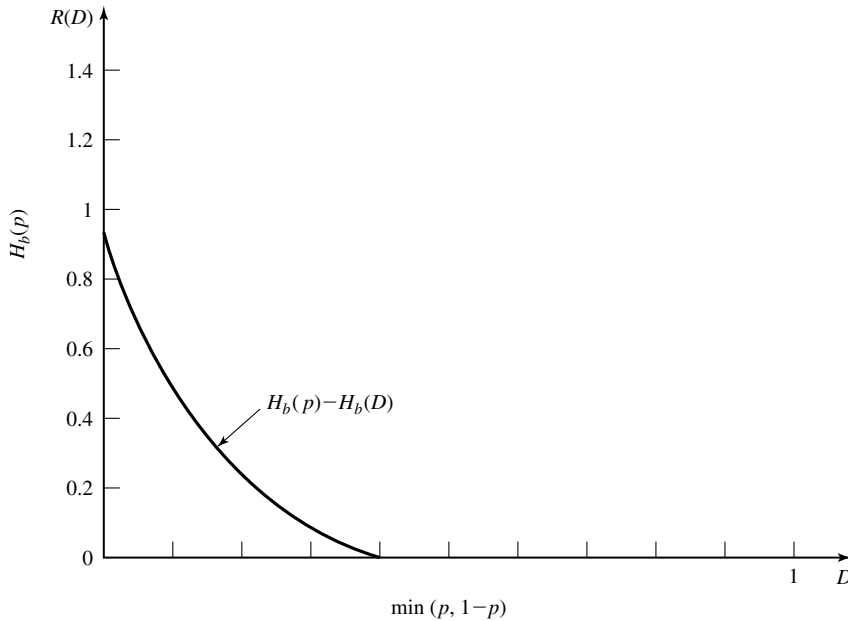


**Figure 6.8** Rate-distortion function for a binary source with Hamming distortion.

A plot of the rate-distortion function for a binary source and with a Hamming distortion measure is given in Figure 6.8. Note that for zero distortion (zero-error probability), we have  $R(D) = H_b(p)$ , which is in agreement with the source-coding theorem. Assuming  $p < 0.5$ , for  $D = p$  we have  $R(D) = 0$ ; i.e., we can reproduce the source at a distortion of  $p$  with no transmission at all, by setting the reproduction vector to be the all-zero vector. This means that  $D = p_e = P[X \neq \hat{X}] = P[X \neq 0] = P[X = 1] = p$ .

It can also be shown that for a zero-mean Gaussian source with variance  $\sigma^2$  and with squared-error distortion measure, the rate-distortion function is given by

$$R(D) = \begin{cases} \frac{1}{2} \log \frac{\sigma^2}{D} & 0 \leq D \leq \sigma^2 \\ 0, & \text{otherwise} \end{cases} \quad (6.4.10)$$

A plot of this rate-distortion function is given in Figure 6.9. An interesting question now is: by what factor is the distortion decreased if the rate of the coding of the source is increased by one bit? The answer, of course, depends on the rate-distortion function of the source (which, in turn, depends on the source statistics and the distortion measure). Let us consider the case of a zero-mean Gaussian discrete memoryless source with squared-error distortion. Since for  $0 \leq D \leq \sigma^2$ ,  $R(D) = \frac{1}{2} \log \frac{\sigma^2}{D}$ , we can express the *distortion-rate function* as  $D(R) = \sigma^2 2^{-2R}$ . Obviously, increasing  $R$  by 1 will decrease  $D$  by a factor of 4, or equivalently by 6 dB. This means that every 1 bit of transmission capability/source output reduces the distortion by 6 dB.



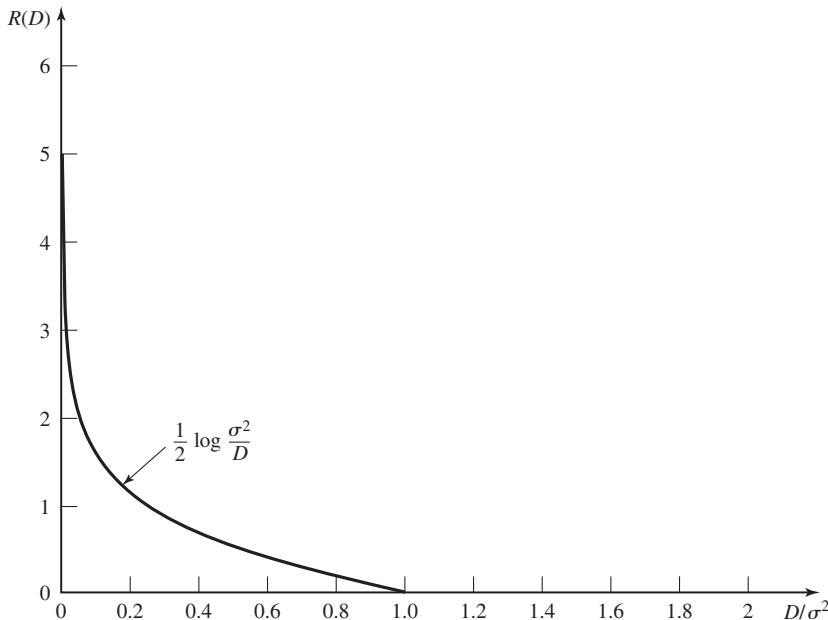


**Figure 6.9** Rate-distortion function for a Gaussian source with squared-error distortion.

#### Example 6.4.6

In the representation of a zero-mean unit-variance Gaussian source, what is the minimum attainable distortion if 8 bits/source output are employed? By what factor is the distortion decreased if we use 16 bits/source output?

**Solution** Using the relation  $D(R) = \sigma^2 2^{-2R}$  with  $R = 8$  and  $\sigma = 1$ , we have  $D = \frac{1}{2^{16}} \approx 1.52 \times 10^{-5}$ . If instead of 8, 16 bits are employed, the distortion is reduced by 48 dB, or a factor of  $4^8$ .

## 6.5 QUANTIZATION

In Section 6.4, we saw that when dealing with analog sources, a precise description of the source requires an infinite number of bits/source output, which is not an achievable goal. Therefore, in transmission of analog sources some distortion is always present, and the goal is to minimize this distortion. We also introduced the rate-distortion function which gives a fundamental limit on the tradeoff between the code rate and the distortion. In this section, we will investigate practical schemes to represent the output of an analog source at low rates and, at the same time, without introducing excessive distortion. As we have already seen, the fundamental limit promised by the rate-distortion function can only be approached asymptotically, that is, by using very complex encoders and decoders. The encoder observes source outputs of length  $n$ ,  $\mathbf{x} \in \mathcal{X}^n$ , and maps them into representation sequences of length  $n$ ,  $\hat{\mathbf{x}}^n \in \hat{\mathcal{X}}^n$ . The number of the latter sequences

is  $2^{nR}$  and therefore  $R$  bits/source output are required for their transmission. The larger the value of  $n$ , the closer to the rate-distortion limit the system operates. This means that an effective quantization scheme should work on blocks of source outputs rather than single-source outputs. Quantizers that operate on blocks of source output are called “*vector quantizers*,” as opposed to “*scalar quantizers*,” which quantize single-source outputs. In this section, we will study both scalar and vector quantizers.

Other than the classification of quantizers into scalar and vector quantizers, one can classify quantizers (or, in general, source coders), on the basis of their general method for compressing data, as either *waveform coders* or *analysis-synthesis coders*. In waveform coding for data compression, the output of the source, which is a waveform, is compressed using one of several compression schemes. In this approach the mechanism by which the waveform is generated is not important and the only important factors are the characteristics of the source output as a waveform; i.e., its bandwidth, power-spectral density, statistical properties, etc. Since in this approach, the mechanism by which the waveform is generated is not important, the results are very robust and can be applied to all sources regardless of their nature. In analysis-synthesis coders, the waveform is not directly compressed and transmitted. Instead, a model for production of the waveform is adopted and the main parameters of that model are compressed and transmitted. For example, in speech coding the mechanism by which speech is produced can be modeled as a time-varying filter excited by either white noise or a sequence of impulses. In the analysis-synthesis approach to speech coding, parameters of the time-varying filter and its inputs are quantized (by scalar or vector quantization) and transmitted. At the receiving end, a filter that simulates the behavior of the vocal tract is generated and then excited by the appropriate input and, thus, a close replica of the waveform is generated. This approach is certainly a model-based approach and does not have the generality of the waveform-coding approach. On the positive side, model-based quantization schemes achieve better compression ratios compared to waveform coders.

### 6.5.1 Scalar Quantization

In scalar quantization each single-source output is quantized into a number of levels and these levels are encoded into a binary sequence. In general, each source output is a real number, but transmission of real numbers requires an infinite number of bits. Therefore, it is required to map the set of real numbers into a finite set and, at the same time, minimize the distortion introduced. In scalar quantization, the set of real numbers  $\mathbb{R}$  is partitioned into  $N$  disjoint subsets denoted by  $\mathcal{R}_k$ ,  $1 \leq k \leq N$ . Corresponding to each subset  $\mathcal{R}_k$ , a representation point  $\hat{x}_k$ , which usually belongs to  $\mathcal{R}_k$ , is chosen. If the source output at time  $i$ ,  $x_i$ , belongs to  $\mathcal{R}_k$ , then it is represented by  $\hat{x}_k$ , which is the *quantized version* of  $x$ .  $\hat{x}_k$  is then represented by a binary sequence and transmitted. Since there are  $N$  possibilities for the quantized levels,  $\log N$  bits are enough to encode these levels into binary sequences ( $N$  is generally chosen to be a power of 2). Therefore, the number of bits required to transmit each source output is  $R = \log N$  bits. The price that we have paid for a decrease in rate from infinity to  $\log N$  is, of course, the introduction of distortion.

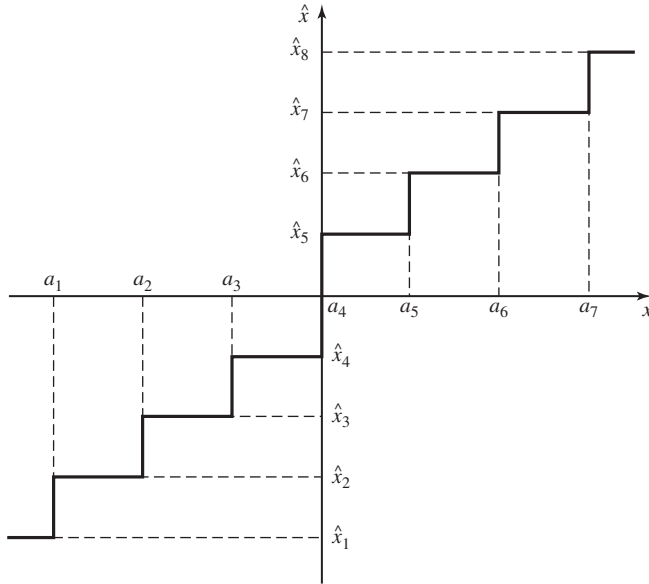


**Figure 6.10** Example of an 8-level quantization scheme.

Figure 6.10 shows an example of an eight-level quantization scheme. In this scheme, the eight regions are defined as  $\mathcal{R}_1 = (-\infty, a_1]$ ,  $\mathcal{R}_2 = (a_1, a_2]$ ,  $\dots$ ,  $\mathcal{R}_8 = (a_7, +\infty)$ . The representation point (or quantized value) in each region is denoted by  $\hat{x}_i$  and shown in the figure. The quantization function  $Q$  is defined by

$$Q(x) = \hat{x}_i \quad \text{for all } x \in \mathcal{R}_i \quad (6.5.1)$$

This function is also shown in the figure. As seen, the quantization function is a nonlinear function that is noninvertible. This is because all points in  $\mathcal{R}_i$  are mapped into a single point  $\hat{x}_i$ . Because the quantization function is noninvertible, some information is lost in the process of quantization and this lost information is not recoverable.

If we are using the squared-error distortion measure, then

$$d(x, \hat{x}) = (x - Q(x))^2 = \tilde{x}^2$$

where  $\tilde{x} = x - \hat{x} = x - Q(x)$ . Since  $X$  is a random variable, so are  $\hat{X}$  and  $\tilde{X}$ , and therefore

$$D = E[d(X, \hat{X})] = E(X - Q(X))^2$$

### Example 6.5.1

The source  $X(t)$  is a stationary Gaussian source with mean zero and power-spectral density

$$\mathcal{S}_x(f) = \begin{cases} 2 & |f| < 100 \text{ Hz} \\ 0, & \text{otherwise} \end{cases}$$

The source is sampled at the Nyquist rate, and each sample is quantized using the 8-level quantizer shown in Figure 6.10 with  $a_1 = -60$ ,  $a_2 = -40$ ,  $a_3 = -20$ ,  $a_4 = 0$ ,  $a_5 = 20$ ,  $a_6 = 40$ ,  $a_7 = 60$ , and  $\hat{x}_1 = -70$ ,  $\hat{x}_2 = -50$ ,  $\hat{x}_3 = -30$ ,  $\hat{x}_4 = -10$ ,  $\hat{x}_5 = 10$ ,  $\hat{x}_6 = 30$ ,  $\hat{x}_7 = 50$ ,  $\hat{x}_8 = 70$ . What is the resulting distortion and rate?

**Solution** The sampling frequency is  $f_s = 200$  Hz. Each sample is a zero-mean Gaussian random variable with variance

$$\sigma^2 = E(X_i^2) = R_X(\tau)|_{\tau=0} = \int_{-\infty}^{\infty} \mathcal{S}_X(f) df = \int_{-100}^{100} 2 df = 400$$

Since each sample is quantized into 8 levels, then  $\log 8 = 3$  bits are required per sample and, therefore, the required rate is

$$R = 3f_s = 600 \text{ bits/sec.}$$

To find the distortion, we have to evaluate  $E(X - \hat{X})^2$  for each sample. We will prove in a problem at the end of this chapter (see Problem 6.45) that, as long as the process is stationary this is equal to  $P_{\tilde{X}(t)}$ , the power content of the process  $\tilde{X}(t)$ , or equivalently, the time-average distortion introduced by quantization. But

$$D = E(X - \hat{X})^2 = \int_{-\infty}^{\infty} (x - Q(x))^2 f_X(x) dx$$

where  $f_X(x)$  denotes the PDF of the random variable  $X$ . From here, we have

$$D = \sum_{i=1}^8 \int_{\mathcal{B}_i} (x - Q(x))^2 f_X(x) dx$$

or, equivalently,

$$D = \int_{-\infty}^{a_1} (x - \hat{x}_1)^2 f_X(x) dx + \sum_{i=2}^7 \int_{a_{i-1}}^{a_i} (x - \hat{x}_i)^2 f_X(x) dx + \int_{a_7}^{\infty} (x - \hat{x}_8)^2 f_X(x) dx \quad (6.5.2)$$

where  $f_X(x)$  in the above is  $\frac{1}{\sqrt{2\pi 400}} e^{-\frac{x^2}{800}}$ . Substituting  $\{a_i\}_{i=1}^7$  and  $\{\hat{x}_i\}_{i=1}^8$  in the above integral and evaluating the result with the  $Q$ -function table, we obtain  $D \approx 33.38$ . Note that, if we were to use zero bits/source output, then the best strategy would be to set the reconstructed signal equal to zero. In this case, we would have a distortion of  $D = E(X - 0)^2 = \sigma^2 = 400$ . The above quantization scheme and transmission of three bits/source output has enabled us to reduce the distortion to 33.38. It is also interesting to compare the above result with the result predicted by the rate-distortion bound. Substituting  $R = 3$  and  $\sigma = 20$ , in

$$R = \frac{1}{2} \log \frac{\sigma^2}{D}$$

we obtain  $D = 6.25$ . Obviously, the simple quantization scheme shown in Figure 6.10 is far from optimal. The reason for this poor performance is threefold. First and foremost, the rate-distortion bound is an asymptotic bound and holds for optimal mapping of *blocks* of source outputs when the length of the block tends to infinity, whereas, in this example, we have employed a scalar quantizer operating on single-source outputs. The second reason

is that even as a scalar quantizer with 8 levels (3 bits/source output), no attempt has been made to design an optimal quantizer by choosing the  $\{a_i\}$  and  $\hat{x}_i$ 's appropriately. The third reason is that after quantization the 8 outputs  $\{\hat{x}_i\}_{i=1}^8$  are not equiprobable and can be further compressed. In this example

$$P(\hat{x}_i) = \int_{a_{i-1}}^{a_i} \frac{1}{\sqrt{2\pi}400} e^{-\frac{x^2}{800}} dx \quad \text{for } 2 \leq i \leq 7$$

and

$$P(\hat{x}_1) = P(\hat{x}_8) = \int_{a_7}^{\infty} \frac{1}{\sqrt{2\pi}400} e^{-\frac{x^2}{800}} dx$$

which results in  $P(\hat{x}_1) = P(\hat{x}_8) = .0014$ ,  $P(\hat{x}_2) = P(\hat{x}_7) = 0.0214$ ,  $P(\hat{x}_3) = P(\hat{x}_6) = 0.1359$ ,  $P(\hat{x}_4) = P(\hat{x}_5) = 0.3414$ . Using the source-coding theorem, we see that the output of the quantizer can be compressed further to  $H(\hat{X}) = 2.105$  bits/source output. This means that a more fair comparison is to compare 33.38 with the value of the rate-distortion function at  $R = 2.105$ , which results in  $D = 21.61$  as opposed to 6.25.

In the above example we have chosen  $E(X - Q(X))^2$ , which is called *mean-squared distortion*, or *quantization noise*, as the measure of performance. A more meaningful measure of performance is a normalized version of the quantization noise, normalized with respect to the power of the original signal.

**Definition 6.5.1.** If the random variable  $X$  is quantized to  $Q(X)$ , the *signal-to-quantization-noise ratio (SQNR)* is defined by

$$\text{SQNR} = \frac{E(X^2)}{E(X - Q(X))^2} \quad (6.5.3)$$

When dealing with signals, the quantization-noise power is

$$P_{\hat{X}} = \lim_{T \rightarrow \infty} \frac{1}{T} \int_{-\frac{T}{2}}^{\frac{T}{2}} E(X(t) - Q(X(t)))^2 dt \quad (6.5.4)$$

and the signal power is

$$P_X = \lim_{T \rightarrow \infty} \frac{1}{T} \int_{-\frac{T}{2}}^{\frac{T}{2}} E(X^2(t)) dt \quad (6.5.5)$$

Hence, the SQNR is

$$\text{SQNR} = \frac{P_X}{P_{\hat{X}}} \quad (6.5.6)$$

It can be shown (see Problem 6.45 at the end of this chapter) that if  $X(t)$  is stationary, then the above relation simplifies to Equation (6.5.3) where  $X$  is the random variable representing  $X(t)$  at any point.

**Uniform Quantization.** Uniform quantizers are the simplest examples of scalar quantizers. In a uniform quantizer the entire real line is partitioned into  $N$  regions. All regions except  $\mathcal{R}_1$  and  $\mathcal{R}_N$  are of equal length, which is denoted by  $\Delta$ . This means that for all  $1 \leq i \leq N - 1$ , we have  $a_{i+1} - a_i = \Delta$ . Figure 6.10 is an example

of an 8-level uniform quantizer. In a uniform quantizer, the distortion is given by

$$\begin{aligned}
 D = & \int_{-\infty}^{a_1} (x - \hat{x}_1)^2 f_X(x) dx + \sum_{i=1}^{N-2} \int_{a_1+(i-1)\Delta}^{a_1+i\Delta} (x - \hat{x}_{i+1})^2 f_X(x) dx \\
 & + \int_{a_1+(N-2)\Delta}^{\infty} (x - \hat{x}_N)^2 f_X(x) dx
 \end{aligned} \quad (6.5.7)$$

It is seen from Equation (6.5.7) that  $D$  is a function of  $N + 2$  design parameters, namely  $a_1$ ,  $\Delta$ , and  $\{\hat{x}_i\}_{i=1}^N$ . In order to design the optimal uniform quantizer, one has to differentiate  $D$  with respect to the above variables and find the values that minimize  $D$ .

Further assumptions simplify the above relation to some extent. If we assume that  $f_X(x)$  is an even function of  $x$  (symmetric density function), then the best quantizer will also have symmetry properties. This means that for even  $N$ , we will have  $a_i = -a_{N-i} = -(\frac{N}{2} - i)\Delta$  for all  $1 \leq i \leq \frac{N}{2}$  (which means  $a_{\frac{N}{2}} = 0$ ), and  $\hat{x}_i = -\hat{x}_{N+1-i}$  for  $1 \leq i \leq \frac{N}{2}$ . In this case, we have

$$D = 2 \int_{-\infty}^{(-\frac{N}{2}-1)\Delta} (x - \hat{x}_1)^2 f_X(x) dx + 2 \sum_{i=1}^{\frac{N}{2}-1} \int_{(-\frac{N}{2}+i)\Delta}^{(-\frac{N}{2}+i+1)\Delta} (x - \hat{x}_{i+1})^2 f_X(x) dx \quad (6.5.8)$$

When  $N$  is odd, we have a situation such as the one shown in Figure 6.11. In this case,  $a_i = -a_{N-i} = (-\frac{N}{2} + i)\Delta$ , for  $1 \leq i \leq \frac{N-1}{2}$  and  $\hat{x}_i = -\hat{x}_{N+1-i}$  for  $1 \leq i \leq \frac{N+1}{2}$ , which means  $\hat{x}_{\frac{N+1}{2}} = 0$ . The distortion is given by

$$\begin{aligned}
 D = & 2 \int_{-\infty}^{(-\frac{N}{2}+1)\Delta} (x - \hat{x}_1)^2 f_X(x) dx \\
 & + 2 \sum_{i=1}^{\frac{N-3}{2}} \int_{(-\frac{N}{2}+i)\Delta}^{(-\frac{N}{2}+i+1)\Delta} (x - \hat{x}_{i+1})^2 f_X(x) dx + \int_{-\frac{\Delta}{2}}^{\frac{\Delta}{2}} x^2 f_X(x) dx
 \end{aligned} \quad (6.5.9)$$

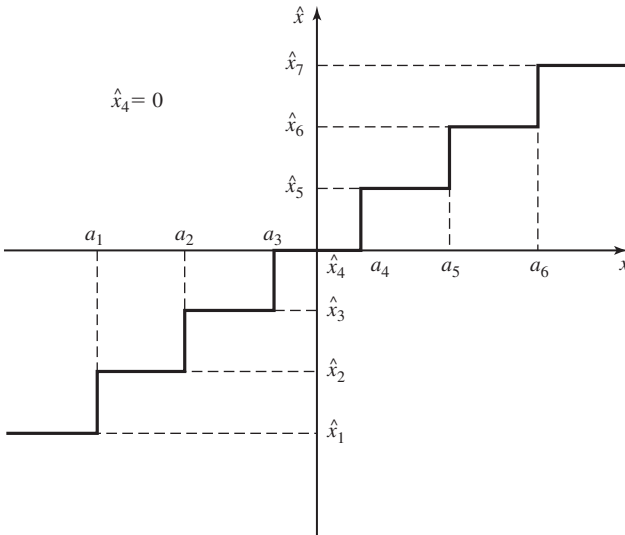


Figure 6.11 7-level uniform quantizer.

Minimization of distortion in these cases, although much simpler compared to the general case, is still a tedious task and is done mainly by numerical techniques. Table 6.2 gives the optimal quantization level spacing for a zero-mean unit variance Gaussian random variable when  $\hat{x}$ 's are chosen to be the mid-points of the quantization regions.

**TABLE 6.2** OPTIMAL UNIFORM QUANTIZER FOR A GAUSSIAN SOURCE

No. output levels $N$	Output-level spacing $\Delta$	Mean-squared error $D$	Informational entropy $H(\hat{x})$
1	—	1.000	0.0
2	1.596	0.3634	1.000
3	1.224	0.1902	1.536
4	0.9957	0.1188	1.904
5	0.8430	0.08218	2.183
6	0.7334	0.06065	2.409
7	0.6508	0.04686	2.598
8	0.5860	0.03744	2.761
9	0.5338	0.03069	2.904
10	0.4908	0.02568	3.032
11	0.4546	0.02185	3.148
12	0.4238	0.01885	3.253
13	0.3972	0.01645	3.350
14	0.3739	0.01450	3.440
15	0.3534	0.01289	3.524
16	0.3352	0.01154	3.602
17	0.3189	0.01040	3.676
18	0.3042	0.009430	3.746
19	0.2909	0.008594	3.811
20	0.2788	0.007869	3.874
21	0.2678	0.007235	3.933
22	0.2576	0.006678	3.990
23	0.2482	0.006185	4.045
24	0.2396	0.005747	4.097
25	0.2315	0.005355	4.146
26	0.2240	0.005004	4.194
27	0.2171	0.004687	4.241
28	0.2105	0.004401	4.285
29	0.2044	0.004141	4.328
30	0.1987	0.003905	4.370
31	0.1932	0.003688	4.410
32	0.1881	0.003490	4.449
33	0.1833	0.003308	4.487
34	0.1787	0.003141	4.524
35	0.1744	0.002986	4.560
36	0.1703	0.002843	4.594

(From Max; © 1960 IEEE.)

**Nonuniform Quantization.** If we relax the condition that the quantization regions (except for the first and the last one) be of equal length, then we are minimizing the distortion with less constraints and, therefore, the resulting quantizer will perform better compared to a uniform quantizer with the same number of levels. Let us assume that we are interested in designing the optimal quantizer with  $N$  levels of quantization with no other constraint on the regions. The distortion will be given by

$$D = \int_{-\infty}^{a_1} (x - \hat{x}_1)^2 f_X(x) dx + \sum_{i=1}^{N-2} \int_{a_i}^{a_{i+1}} (x - \hat{x}_{i+1})^2 f_X(x) dx + \int_{a_{N-1}}^{\infty} (x - \hat{x}_N)^2 f_X(x) dx \quad (6.5.10)$$

There exist a total of  $2N - 1$  variables in Equation (6.5.10) and the minimization of  $D$  is to be done with respect to these variables. Differentiating with respect to  $a_i$  yields

$$\frac{\partial}{\partial a_i} D = f_X(a_i)[(a_i - \hat{x}_i)^2 - (a_i - \hat{x}_{i+1})^2] = 0 \quad (6.5.11)$$

which results in

$$a_i = \frac{1}{2}(\hat{x}_i + \hat{x}_{i+1}) \quad (6.5.12)$$

This result simply means that, in an optimal quantizer, *the boundaries of the quantization regions are the midpoints of the quantized values*. Because quantization is done on a minimum distance basis, each  $x$  value is quantized to the nearest  $\{\hat{x}_i\}_{i=1}^N$ .

To determine the quantized values  $\hat{x}_i$ , we differentiate  $D$  with respect to  $\hat{x}_i$  and define  $a_0 = -\infty$  and  $a_N = +\infty$ . Thus, we obtain

$$\frac{\partial}{\partial \hat{x}_i} D = \int_{a_{i-1}}^{a_i} 2(x - \hat{x}_i) f_X(x) dx = 0 \quad (6.5.13)$$

which results in

$$\begin{aligned} \hat{x}_i &= \frac{\int_{a_{i-1}}^{a_i} x f_X(x) dx}{\int_{a_{i-1}}^{a_i} f_X(x) dx} \\ &= \frac{\int_{a_{i-1}}^{a_i} x f_X(x) dx}{P(a_{i-1} < X \leq a_i)} \\ &= \int_{a_{i-1}}^{a_i} x \frac{f_X(x)}{P(a_{i-1} < X \leq a_i)} dx \\ &= \int_{-\infty}^{+\infty} x f_X(x | a_{i-1} < X \leq a_i) dx \\ &= E[X | a_{i-1} < X \leq a_i] \end{aligned} \quad (6.5.14)$$



where we have used the definition of the conditional density function

$$f_X(x | a_{i-1} < X \leq a_i) = \begin{cases} \frac{f_X(x)}{P(a_{i-1} < X \leq a_i)} & a_{i-1} < x \leq a_{i-1} \\ 0, & \text{otherwise} \end{cases}$$

Equation (6.5.14) shows that in an optimal quantizer *the quantized value (or representation point) for a region should be chosen to be the centroid (conditional expected value) of that region*. Equations (6.5.12) and (6.5.14) give the necessary conditions for a scalar quantizer to be optimal and are known as the Lloyd-Max conditions. The criteria for optimal quantization can then be summarized as

1. The boundaries of the quantization regions are the midpoints of the corresponding quantized values (nearest neighbor law).
2. The quantized values are the centroids of the quantization regions.

Although the above rules are very simple, they do not result in analytical solutions to the optimal quantizer design. The usual method of designing the optimal quantizer is to start with a set of quantization regions and then using the second criterion, to find the quantized values. Then, we design new quantization regions for the new quantized values, and alternating between the two steps until the distortion does not change much from one step to the next. Based on this method, one can design the optimal quantizer for various source statistics. Table 6.3 shows the optimal nonuniform quantizers for various values of  $N$  for a zero-mean unit variance Gaussian source.

### Example 6.5.2

How would the results of the previous example change if instead of the uniform quantizer shown in Figure 6.10, we used an optimal nonuniform quantizer with the same number of levels?

**Solution** We can find the quantization regions and the quantized values from Table 6.3 with  $N = 8$ . It should be noted that this table is designed for a unit variance Gaussian source, and to obtain the values for the source under study, all the  $\hat{x}$  and  $a$  values read from the table should be multiplied by the  $\sigma$  of the source, which is 20 in this case. This gives us the values  $a_1 = -a_7 = -34.96$ ,  $a_2 = -a_6 = -21$ ,  $a_3 = -a_5 = -10.012$ ,  $a_4 = 0$  and  $\hat{x}_1 = -\hat{x}_8 = -43.04$ ,  $\hat{x}_2 = -\hat{x}_7 = -26.88$ ,  $\hat{x}_3 = -\hat{x}_6 = -15.12$ ,  $\hat{x}_4 = -\hat{x}_5 = -4.902$ . Based on these values, the distortion is evaluated to be  $D = 13.816$ . The SQNR is

$$\text{SQNR} = \frac{400}{13.816} = 28.95 \sim 14.62 \text{ dB}$$

If one computes the probability of each quantized value using the relation

$$P(\hat{x}_i) = \int_{a_{i-1}}^{a_i} f_X(x) dx$$

and finds the entropy of the random variable  $\hat{X}$ , one would obtain  $H(\hat{X}) = 2.825$  bit/source output. The distortion obtained from the rate-distortion function with  $R = 2.825$  and with  $\sigma = 20$  is  $D = 7.966$ . The difference between 13.816 and 7.966 is purely the difference between a quantization scheme based on individual-source outputs (scalar quantization) and blocks of source outputs (vector quantization).

**TABLE 6.3** OPTIMAL NONUNIFORM QUANTIZER FOR A GAUSSIAN SOURCE

$N$	$\pm a_i$	$\pm \hat{x}_i$	$D$	$H(\hat{X})$
1	—	0	1	0
2	0	0.7980	0.3634	1
3	0.6120	0, 1.224	0.1902	1.536
4	0, 0.9816	0.4528, 1.510	0.1175	1.911
5	0.3823, 1.244	0, 0.7646, 1.724	0.07994	2.203
6	0, 0.6589, 1.447	0.3177, 1.000, 1.894	0.05798	2.443
7	0.2803, 0.8744, 1.611	0, 0.5606, 1.188, 2.033	0.04400	2.647
8	0, 0.5006, 1.050, 1.748	0.2451, 0.7560, 1.344, 2.152	0.03454	2.825
9	0.2218, 0.6812, 1.198, 1.866	0, 0.4436, 0.9188, 1.476, 2.255	0.02785	2.983
10	0, 0.4047, 0.8339, 1.325, 1.968	0.1996, 0.6099, 1.058, 1.591, 2.345	0.02293	3.125
11	0.1837, 0.5599, 0.9656, 1.436, 2.059	0, 0.3675, 0.7524, 1.179, 1.693, 2.426	0.01922	3.253
12	0, 0.3401, 0.6943, 1.081, 1.534, 2.141	0.1684, 0.5119, 0.8768, 1.286, 1.783, 2.499	0.01634	3.372
13	0.1569, 0.4760, 0.8126, 1.184, 1.623, 2.215	0, 0.3138, 0.6383, 0.9870, 1.381, 1.865, 2.565	0.01406	3.481
14	0, 0.2935, 0.5959, 0.9181, 1.277, 1.703, 2.282	0.1457, 0.4413, 0.7505, 1.086, 1.468, 1.939, 2.625	0.01223	3.582
15	0.1369, 0.4143, 0.7030, 1.013, 1.361, 1.776, 2.344	0, 0.2739, 0.5548, 0.8512, 1.175, 1.546, 2.007, 2.681	0.01073	3.677
16	0, 0.2582, 0.5224, 0.7996, 1.099, 1.437, 1.844, 2.401	0.1284, 0.3881, 0.6568, 0.9424, 1.256, 1.618, 2.069, 2.733	0.009497	3.765
17	0.1215, 0.3670, 0.6201, 0.8875, 1.178, 1.508, 1.906, 2.454	0, 0.2430, 0.4909, 0.7493, 1.026, 1.331, 1.685, 2.127, 2.781	0.008463	3.849
18	0, 0.2306, 0.4653, 0.7091, 0.9680, 1.251, 1.573, 1.964, 2.504	0.1148, 0.3464, 0.5843, 0.8339, 1.102, 1.400, 1.746, 2.181, 2.826	0.007589	3.928
19	0.1092, 0.3294, 0.5551, 0.7908, 1.042, 1.318, 1.634, 2.018, 2.55	0, 0.2184, 0.4404, 0.6698, 0.9117, 1.173, 1.464, 1.803, 2.232, 2.869	0.006844	4.002
20	0, 0.2083, 0.4197, 0.6375, 0.8661, 1.111, 1.381, 1.690, 2.068, 2.594	0.1038, 0.3128, 0.5265, 0.7486, 0.9837, 1.239, 1.524, 1.857, 2.279, 2.908	0.006203	4.074
21	0.09918, 0.2989, 0.5027, 0.7137, 0.9361, 1.175, 1.440, 1.743, 2.116, 2.635	0, 0.1984, 0.3994, 0.6059, 0.8215, 1.051, 1.300, 1.579, 1.908, 2.324, 2.946	0.005648	4.141
22	0, 0.1900, 0.3822, 0.5794, 0.7844, 1.001, 1.235, 1.495, 1.793, 2.160, 2.674	0.09469, 0.2852, 0.4793, 0.6795, 0.8893, 1.113, 1.357, 1.632, 1.955, 2.366, 2.982	0.005165	4.206
23	0.09085, 0.2736, 0.4594, 0.6507, 0.8504, 1.062, 1.291, 1.546, 1.841, 2.203, 2.711	0, 0.1817, 0.3654, 0.5534, 0.7481, 0.9527, 1.172, 1.411, 1.682, 2.000, 2.406, 3.016	0.004741	4.268
24	0, 0.1746, 0.3510, 0.5312, 0.7173, 0.9122, 1.119, 1.344, 1.595, 1.885, 2.243, 2.746	0.08708, 0.2621, 0.4399, 0.6224, 0.8122, 1.012, 1.227, 1.462, 1.728, 2.042, 2.444, 3.048	0.004367	4.327
25	0.08381, 0.2522, 0.4231, 0.5982, 0.7797, 0.9702, 1.173, 1.394, 1.641, 1.927, 2.281, 2.779	0, 0.1676, 0.3368, 0.5093, 0.6870, 0.8723, 1.068, 1.279, 1.510, 1.772, 2.083, 2.480, 3.079	0.004036	4.384
26	0, 0.1616, 0.3245, 0.4905, 0.6610, 0.8383, 1.025, 1.224, 1.442, 1.685, 1.968, 2.318, 2.811	0.08060, 0.2425, 0.4066, 0.5743, 0.7477, 0.9289, 1.121, 1.328, 1.556, 1.814, 2.121, 2.514, 3.109	0.003741	4.439
27	0.07779, 0.2340, 0.3921, 0.5587, 0.7202, 0.8936, 1.077, 1.273, 1.487, 1.727, 2.006, 2.352, 2.842	0, 0.1556, 0.3124, 0.4719, 0.6354, 0.8049, 0.9824, 1.171, 1.374, 1.599, 1.854, 2.158, 2.547, 3.137	0.003477	4.491
28	0, 0.1503, 0.3018, 0.04556, 0.6132, 0.7760, 0.9460, 1.126, 1.319, 1.529, 1.766, 2.042, 2.385, 2.871	0.07502, 0.2256, 0.3780, 0.5333, 0.6930, 0.8589, 1.033, 1.118, 1.419, 1.640, 1.892, 2.193, 2.578, 3.164	0.003240	4.542

(From Max; © 1960 IEEE.)

### 6.5.2 Vector Quantization

In scalar quantization, each output of the discrete-time source (which is usually the result of sampling of a continuous-time source) is quantized separately and then encoded. For example, if we are using a 4-level scalar quantizer and encoding each level into 2 bits, we are using 2 bits/each source output. This quantization scheme is shown in Figure 6.12.

Now if we consider two samples of the source at each time, and interpret these two samples as a point  $a$  in plane, the scalar quantizer partitions the entire plane into 16 quantization regions, as shown in Figure 6.13. It is seen that the regions in the two-dimensional space are all of rectangular shape. If we allow 16 regions of any shape in the two-dimensional space, we are capable of obtaining better results. This means that we are quantizing 2 source outputs at a time using 16 regions, which is equivalent to 4 bits/two source outputs, or 2 bits/each source output. Therefore, the number of bits/source output for quantizing two samples at a time is equal to the number of bits/source output obtained in the scalar case. Because we are relaxing the requirement of having rectangular regions, the performance will be improved. Now if we take three samples at a time and quantize the entire three-dimensional space into 64 regions, we will have even less distortion with the same number of bits/source output. The idea of vector quantization is to take blocks of source outputs of length  $n$ , and design the quantizer in the  $n$ -dimensional Euclidean space rather than doing the quantization based on single samples in one-dimensional space.

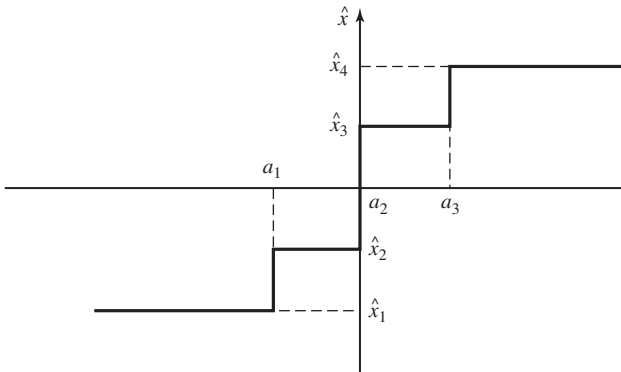


Figure 6.12 4-level scalar quantizer.

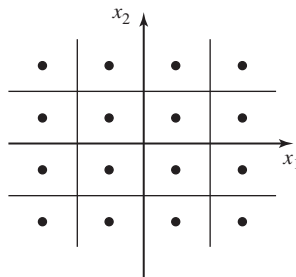
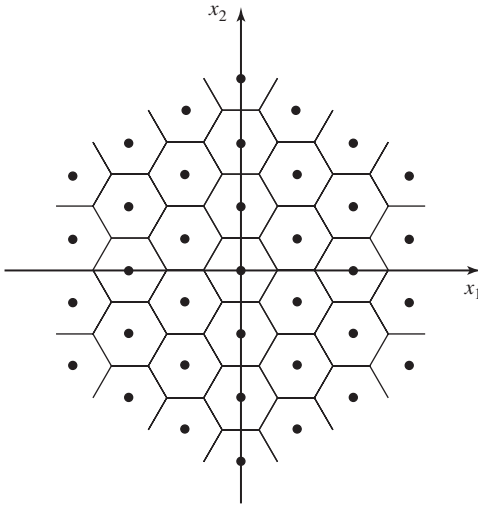


Figure 6.13 Scalar 4-level quantization applied to two samples.



**Figure 6.14** Vector quantization in two dimensions.

Let us assume that the quantization regions in the  $n$ -dimensional space are denoted by  $\mathcal{R}_i$ ,  $1 \leq i \leq K$ . These  $K$  regions partition the  $n$ -dimensional space. Each block of source output of length  $n$  is denoted by  $\mathbf{x} \in \mathbb{R}^n$ , and if  $\mathbf{x} \in \mathcal{R}_i$ , it is quantized to  $Q(\mathbf{x}) = \hat{\mathbf{x}}_i$ . Figure 6.14 shows this quantization scheme for  $n = 2$ . Now since there are a total of  $K$  quantized values,  $\log K$  bits are enough to represent these values. This means that we require  $\log K$  bits/ $n$  source outputs or, the rate of the source code is

$$R = \frac{\log K}{n} \text{ bits/source output} \quad (6.5.15)$$

The optimal vector quantizer of dimension  $n$  and number of levels  $K$  is the one that chooses the region  $\mathcal{R}_i$ 's and the quantized values  $\hat{\mathbf{x}}_i$ 's such that the resulting distortion is minimized. Applying the same procedure that we used for the case of scalar quantization, we obtain the following criteria for an optimal vector quantizer design:

1. Region  $\mathcal{R}_i$  is the set of all points in the  $n$ -dimensional space that are closer to  $\hat{\mathbf{x}}_i$  than any other  $\hat{\mathbf{x}}_j$ , for all  $j \neq i$ .

$$\mathcal{R}_i = \{\mathbf{x} \in \mathbb{R}^n : \|\mathbf{x} - \hat{\mathbf{x}}_i\| < \|\mathbf{x} - \hat{\mathbf{x}}_j\|, \forall j \neq i\}$$

2.  $\hat{\mathbf{x}}_i$  is the centroid of the region  $\mathcal{R}_i$ .

$$\hat{\mathbf{x}}_i = \frac{1}{P(\mathbf{X} \in \mathcal{R}_i)} \iint \dots \int_{\mathcal{R}_i} \mathbf{x} f_{\mathbf{X}}(\mathbf{x}) d\mathbf{x}$$

A practical approach to designing optimal vector quantizers is based on the same approach employed in designing optimal scalar quantizers. Starting from a given set of quantization regions, we derive the optimal quantized vectors for these regions using criterion 2, then repartition the space using the first criterion, and going back and forth until changes in distortion are negligible.

Vector quantization has found widespread applications in speech and image coding, and numerous algorithms for reducing its computational complexity have been proposed. It can be also proved that for stationary and ergodic sources, the performance of the vector quantizer approaches the optimal performance given by the rate-distortion function as  $n$  becomes large.

## 6.6 WAVEFORM CODING

Waveform-coding schemes are designed to reproduce the waveform output of the source at the destination with as small a distortion as possible. In these techniques, no attention is paid to the mechanism that produces the waveform, and all attempts are directed at reproduction of the source output at the destination with high fidelity. Because the structure of the source plays no role in the design of waveform coders and only properties of the waveform affect the design, waveform coders are robust and can be used with a variety of sources as long as the waveforms produced by the sources have certain similarities. In this section, we study some basic waveform-coding methods that are widely applied to a variety of sources.

### 6.6.1 Pulse-Code Modulation (PCM)

Pulse-code modulation is the simplest and oldest waveform-coding scheme. A pulse-code modulator consists of three basic sections, a sampler, a quantizer, and an encoder. A functional block diagram of a PCM system is shown in Figure 6.15.

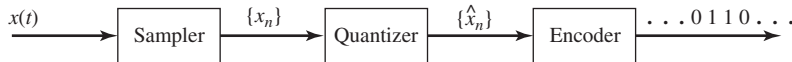


**Figure 6.15** Block diagram of a PCM system.

The waveform entering the sampler is a bandlimited waveform with bandwidth  $W$ . Usually there exists a filter with bandwidth  $W$  prior to the sampler to prevent any components beyond  $W$  from entering the sampler. This filter is called the *presampling filter*. The sampling is done at a rate higher than the Nyquist rate to allow for some guard-band. The sampled values then enter a scalar quantizer. The quantizer is either a uniform quantizer, which results in a uniform PCM system, or a nonuniform quantizer. The choice of the quantizer is based on the characteristics of the source output. The output of the quantizer is then encoded into a binary sequence of length  $\nu$  where  $N = 2^\nu$  is the number of quantization levels.

**Uniform PCM.** In uniform PCM, it is assumed that the range of the input samples is  $[-x_{\max}, +x_{\max}]$  and the number of quantization levels  $N$  is a power of 2,  $N = 2^\nu$ . From this, the length of each quantization region is given by

$$\Delta = \frac{2x_{\max}}{N} = \frac{x_{\max}}{2^{\nu-1}} \quad (6.6.1)$$

The quantized values in uniform PCM are chosen to be the midpoints of the quantization regions and, therefore, the error  $\tilde{x} = x - Q(x)$  is a random variable taking values in the interval  $(-\frac{\Delta}{2}, +\frac{\Delta}{2}]$ . In ordinary PCM applications, the number of levels ( $N$ ) is usually high and the range of variations of the input signal (amplitude variations  $x_{\max}$ ) is small. This means that the length of each quantization region ( $\Delta$ ) is small and, under these assumptions, in each quantization region the error  $\tilde{X} = X - Q(X)$  can be well approximated by a uniformly distributed random variable on  $(-\frac{\Delta}{2}, +\frac{\Delta}{2}]$ . The distortion introduced by quantization (quantization noise) is, therefore,

$$E[\tilde{X}^2] = \int_{-\frac{\Delta}{2}}^{+\frac{\Delta}{2}} \frac{1}{\Delta} \tilde{x}^2 d\tilde{x} = \frac{\Delta^2}{12} = \frac{x_{\max}^2}{3N^2} = \frac{x_{\max}^2}{3 \times 4^v} \quad (6.6.2)$$

where  $v$  is the number of bits/source sample. The SQNR ratio then becomes

$$\text{SQNR} = \frac{\overline{X^2}}{\overline{\tilde{X}^2}} = \frac{3 \times N^2 \overline{X^2}}{x_{\max}^2} = \frac{3 \times 4^v \overline{X^2}}{x_{\max}^2} \quad (6.6.3)$$

If we denote the normalized  $X$  by  $\check{X}$ , that is  $\check{X} = \frac{X}{x_{\max}}$ , then

$$\text{SQNR} = 3 \times N^2 \overline{\check{X}^2} = 3 \times 4^v \overline{\check{X}^2} \quad (6.6.4)$$

Note that by definition  $|\check{X}| \leq 1$  and, therefore,  $\overline{\check{X}^2} \leq 1$ . This means that  $3N^2 = 3 \times 4^v$  is an upperbound to the SQNR in uniform PCM. This also means that SQNR in uniform PCM deteriorates as the dynamic range of the source increases because an increase in the dynamic range of the source results in a decrease in  $\overline{\check{X}^2}$ . In a problem at the end of this chapter (see Problem 6.57), we will see that this sensitivity to the source dynamic range can be improved by employing nonuniform PCM.

Expressing SQNR in dB, one obtains

$$\text{SQNR}|_{\text{dB}} \approx P_{\check{X}}|_{\text{dB}} + 6v + 4.8 \quad (6.6.5)$$

It is seen that each extra bit (increase in  $v$  by one) increases the SQNR by 6 decibels. This increase is comparable to that of an optimal system, as was shown in Section 6.4.

### Example 6.6.1

What is the resulting SQNR for a signal uniformly distributed on  $[-1, 1]$  when uniform PCM with 256 levels is employed.

**Solution** Since  $x_{\max} = 1$ , then  $\check{X} = X$  and  $P_{\check{X}} = \int_{-1}^1 \frac{1}{2} x^2 dx = \frac{1}{3}$ . Therefore, using  $v = \log 256 = 8$ , we have

$$\text{SQNR} = 3 \times 4^v \overline{\check{X}^2} = 4^v = 65536 \sim 48.16 \text{ dB}$$

The issue of bandwidth requirements of pulse transmission systems, of which PCM is an example, is dealt with in detail in Chapter 8. Here we briefly discuss some results concerning the bandwidth requirements of a PCM system. If a signal has a bandwidth of  $W$ , then the minimum number of samples for perfect reconstruction of the signal is given by the sampling theorem and is equal to  $2W$  samples/sec. If some guard-band is required, then the number of samples/sec is  $f_s$ , which is more than

$2W$ . For each sample  $\nu$  bits are used, therefore a total of  $\nu f_s$  bits/sec are required for transmission of the PCM signal. In case of sampling at the Nyquist rate, this is equal to  $2\nu W$  bits/sec. The minimum bandwidth requirement for transmission of  $R$  bits/sec (or, more precisely,  $R$  pulses/sec) is  $\frac{R}{2}$  (see Chapter 8).<sup>†</sup> Therefore the minimum bandwidth requirement of a PCM system is

$$\text{BW} = \frac{\nu f_s}{2} \quad (6.6.6)$$

which, in the case of sampling at the Nyquist rate, gives the absolute minimum bandwidth requirement as

$$\text{BW} = \nu W \quad (6.6.7)$$

This means that a PCM system expands the bandwidth of the original signal by a factor of at least  $\nu$ .

**Nonuniform PCM.** As long as the statistics of the input signal are close to the uniform distribution, uniform PCM works fine. However, in coding of certain signals such as speech, the input distribution is far from being uniformly distributed. For a speech waveform, in particular, there exists a higher probability for smaller amplitudes and lower probability for larger amplitudes. Therefore, it makes sense to design a quantizer with more quantization regions at lower amplitudes and less quantization regions at larger amplitudes. The resulting quantizer will be a nonuniform quantizer having quantization regions of various sizes.

The usual method for performing nonuniform quantization<sup>‡</sup> is to first pass the samples through a nonlinear element that compresses the large amplitudes (reduces dynamic range of the signal) and then perform a uniform quantization on the output. At the receiving end, the inverse (expansion) of this nonlinear operation is applied to obtain the sampled value. This technique is called *companding* (*compressing-expanding*). A block diagram of this system is shown in Figure 6.16.



**Figure 6.16** Block diagram of a nonuniform PCM system.

There are two types of companders that are widely used for speech coding. The  $\mu$ -law compander used in the U.S. and Canada employs the logarithmic function at the transmitting side, where  $|x| \leq 1$ ,

$$g(x) = \frac{\log(1 + \mu|x|)}{\log(1 + \mu)} \text{sgn}(x) \quad (6.6.8)$$

<sup>†</sup>A more practical bandwidth requirement is  $\frac{R}{\alpha}$ , where  $1 < \alpha < 2$ .

<sup>‡</sup>Sometimes the term *nonlinear quantization* is used, which is misleading because all quantization schemes, uniform or nonuniform, are nonlinear.

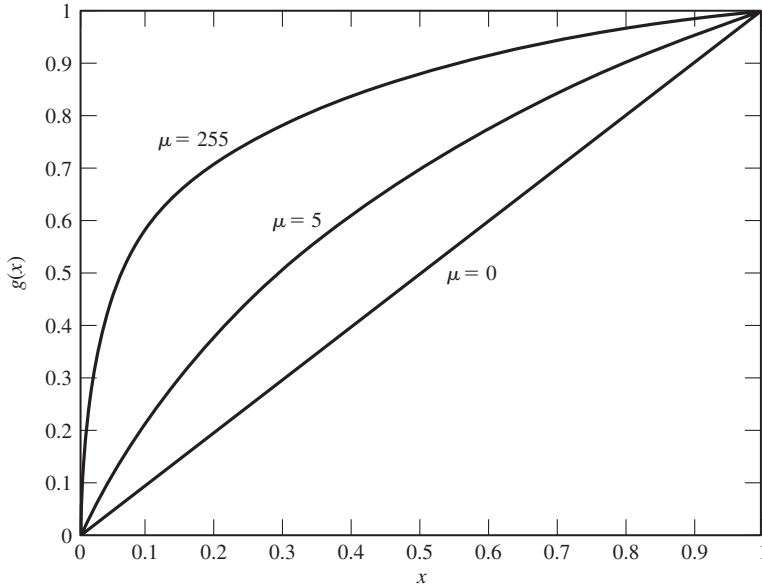


Figure 6.17  $\mu$ -law compander characteristics.

The parameter  $\mu$  controls the amount of compression and expansion. The standard PCM system in the U.S. and Canada employs a compressor with  $\mu = 255$ , followed by a uniform quantizer with 128 levels (7 bits/sample). Use of a compander in this system improves the performance of the system by about 24 decibels. A plot of the  $\mu$ -law compander characteristics is shown in Figure 6.17.

The second widely used logarithmic compressor is the  $A$ -law compander. The characteristic of this compander is given by

$$g(x) = \frac{1 + \log A|x|}{1 + \log A} \operatorname{sgn}(x) \quad (6.6.9)$$

where  $A$  is chosen to be 87.56. The performance of this compander is comparable to the performance of the  $\mu$ -law compander. The characteristics of this compander are shown in Figure 6.18.

**Optimal Compander Design.** In Section 6.5.1, we studied the criteria for optimal quantizer design. We approach the problem of optimum compander design in the same manner. This approach gives us an approximation to the characteristics of the optimal compressor that, when followed by a uniform quantizer, gives close to optimal performance. By defining  $a_0 = -x_{\max}$  and  $a_N = +x_{\max}$ , we have

$$D = \sum_{i=1}^N \int_{a_{i-1}}^{a_i} (x - \hat{x}_i)^2 f_X(x) dx \quad (6.6.10)$$



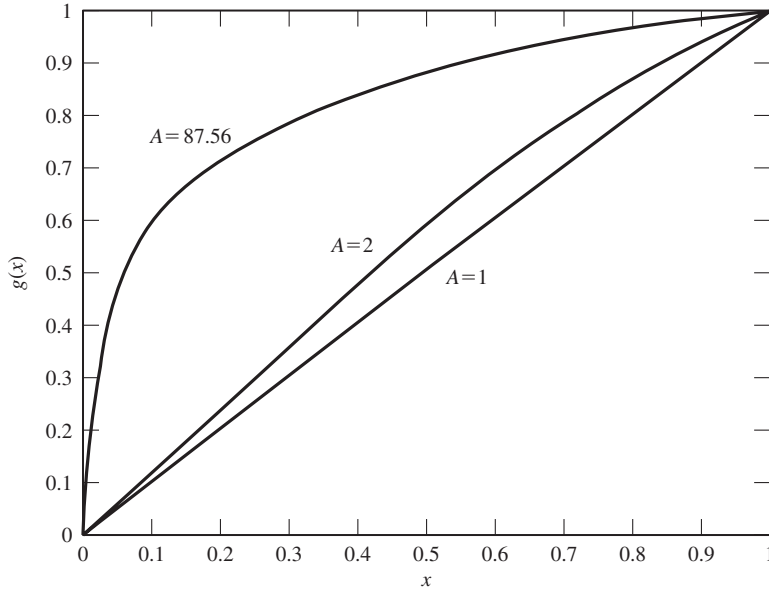


**Figure 6.18** A-law compander characteristics.

If the number of quantization regions is large and the density function is smooth enough, one can assume a uniform distribution in each region and, therefore,  $\hat{x}_i = \frac{a_{i-1} + a_i}{2}$ . After substituting for  $\hat{x}_i$  in the above relation, we have

$$D \approx \sum_{i=1}^N f_X(a_{i-1}) \frac{\Delta_i^3}{12} \quad (6.6.11)$$

where  $\Delta_i = a_i - a_{i-1}$ . Noting that the input to the compressor is a nonuniformly quantized sample with quantization regions of size  $\Delta_i$  and the output is a uniformly quantized sample with quantization regions of equal size  $\Delta$ , from Figure 6.19 we see

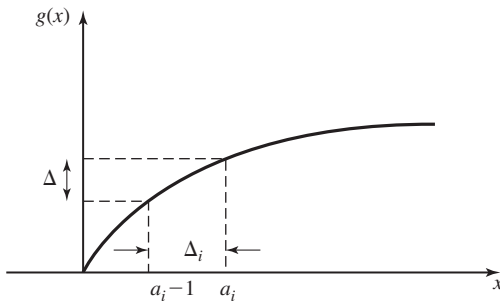


**Figure 6.19** Compander input-output relation.

that

$$g'(a_{i-1}) \approx \frac{\Delta}{\Delta_i} \quad (6.6.12)$$

We are assuming that the function  $g(x)$  maps the interval  $[-x_{\max}, x_{\max}]$  into  $[-y_{\max}, y_{\max}]$  and, therefore, the boundary conditions are

$$\begin{cases} g(-x_{\max}) = -y_{\max} \\ g(x_{\max}) = y_{\max} \end{cases} \quad (6.6.13)$$

Substituting from Equation (6.6.12) into Equation (6.6.11), we have

$$D \approx \frac{1}{12} \sum_{i=1}^N f_X(a_{i-1}) \left[ \frac{\Delta}{g'(a_{i-1})} \right]^2 \Delta_i \quad (6.6.14)$$

Using the relation  $\Delta = \frac{y_{\max}}{2^{v-1}}$ , and assuming that  $N$  is very large, one obtains

$$D \approx \frac{y_{\max}^2}{3 \times 4^v} \int_{-\infty}^{\infty} \frac{f_X(x)}{[g'(x)]^2} dx \quad (6.6.15)$$

where  $g(x)$  denotes the characteristics of the compressor. The above relation gives the distortion when a compressor with characteristics  $g(x)$  is employed. One can minimize  $D$  to obtain the optimal compressor. The resulting optimal compressor has the form

$$g(x) = y_{\max} \left[ \frac{2 \int_{-\infty}^x [f_X(\eta)]^{\frac{1}{3}} d\eta}{\int_{-\infty}^{\infty} [f_X(\eta)]^{\frac{1}{3}} d\eta} - 1 \right] \quad (6.6.16)$$

and the resulting distortion is

$$D = \frac{1}{12 \times 4^v} \left[ \int_{-\infty}^{\infty} [f_X(\eta)]^{\frac{1}{3}} d\eta \right]^3 \quad (6.6.17)$$

### 6.6.2 Differential Pulse-Code Modulation (DPCM)

In a PCM system, after sampling the information signal, each sample is quantized independently using a scalar quantizer. This means that previous sample values have no effect on the quantization of the new samples. However, as was mentioned in Section 4.5, when a bandlimited random process is sampled at the Nyquist rate or faster, the sampled values are usually correlated random variables. The exception is the case when the spectrum of the process is flat within its bandwidth. This means that the previous samples give some information about the next sample, and this information can be employed to improve the performance of the PCM system. For instance, if the previous sample values were small, with high probability the next sample value will be small as well and, hence, it is not necessary to quantize a wide range of values to achieve a good performance.

In the simplest form of differential pulse-code modulation (DPCM), the difference between two adjacent samples is quantized. Because two adjacent samples are highly correlated, their difference has small variations and, therefore, to achieve a certain

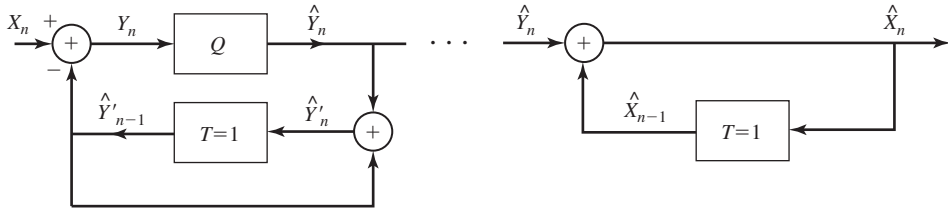


**Figure 6.20** A simple DPCM system.

level of performance fewer bits are required to quantize it. This means that DPCM can achieve performance levels compared to PCM at lower bit rates.

Figure 6.20 shows a block diagram of this simple DPCM scheme. As seen in the figure, the input to the quantizer is not simply  $X_n - X_{n-1}$ , but rather  $X_n - \hat{Y}'_{n-1}$ . We will see that  $\hat{Y}'_{n-1}$  is closely related to  $X_{n-1}$ , and the above choice has the advantage that accumulation of quantization noise is prevented. The input to the quantizer,  $Y_n$ , is quantized by a scalar quantizer (uniform or nonuniform) to produce  $\hat{Y}'_n$ . Using the relations

$$Y_n = X_n - \hat{Y}'_{n-1} \quad (6.6.18)$$

and

$$\hat{Y}'_n = \hat{Y}'_n + \hat{Y}'_{n-1} \quad (6.6.19)$$

we obtain the quantization error between the input and the output of the quantizer as

$$\begin{aligned} \hat{Y}'_n - Y_n &= \hat{Y}'_n - (X_n - \hat{Y}'_{n-1}) \\ &= \hat{Y}'_n - X_n + \hat{Y}'_{n-1} \\ &= \hat{Y}'_n - X_n \end{aligned} \quad (6.6.20)$$

At the receiving end, we have

$$\hat{X}_n = \hat{Y}'_n + \hat{X}_{n-1} \quad (6.6.21)$$

By comparing Equations (6.6.19) and (6.6.21), it is seen that  $\hat{Y}'_n$  and  $\hat{X}_n$  satisfy the same difference equation with the same excitation function (i.e.,  $\hat{Y}'_n$ ). Therefore, if the initial conditions of  $\hat{Y}'_n$  and  $\hat{X}_n$  are chosen to be the same, they will be equal. For instance, if we let  $\hat{Y}'_{-1} = \hat{X}_{-1} = 0$ , then for all  $n$  we will have  $\hat{Y}'_n = \hat{X}_n$ . Substituting this in Equation (6.6.20), one obtains

$$\hat{Y}'_n - Y_n = \hat{X}_n - X_n \quad (6.6.22)$$

This shows that the quantization error between  $X_n$  and its reproduction  $\hat{X}_n$  is the same as the quantization error between the input and the output of the quantizer. However, the range of variations of  $Y_n$  is usually much smaller compared to that of  $X_n$  and, therefore,  $Y_n$  can be quantized with fewer bits.

In a more complex version of DPCM, instead of using only the previous sample, the last  $p$  samples are used to predict the value of the next sample. Then the difference between the sample  $X_n$  and its predicted value is quantized. Usually a linear predictor of the form  $\sum_{i=1}^p a_i X_{n-i}$  is employed, and the coefficients of the predictor  $a_i$  are chosen to minimize the mean-squared error between the sample  $X_n$  and its predicted value

$$D = E \left( X_n - \sum_{i=1}^p a_i X_{n-i} \right)^2 \quad (6.6.23)$$

Expanding and assuming the process  $X_n$  to be stationary, one obtains

$$D = R_X(0) - 2 \sum_{i=1}^p a_i R_X(i) + \sum_{i=1}^p \sum_{j=1}^p a_i a_j R_X(i-j) \quad (6.6.24)$$

To minimize  $D$ , we differentiate with respect to the  $a_i$ 's and find the roots. After differentiating, we have

$$\sum_{i=1}^p a_i R_X(i-j) = R_X(j) \quad 1 \leq j \leq p \quad (6.6.25)$$

where  $R_X$  denotes the autocorrelation function of the process  $X_n$ . Solving the above set of equations (usually referred to as *Yule-Walker equations*), one can find the optimal set of predictor coefficients  $\{a_i\}_{i=1}^p$ .

Figure 6.21 shows the block diagram of a general DPCM system. This block diagram is quite similar to the block diagram shown in Figure 6.20. The only difference is that the delay  $T = 1$  has been substituted with the prediction filter  $\sum_{i=1}^p a_i X_{n-i}$ . Exactly the same analysis shows that

$$\hat{Y}_n - Y_n = \hat{X}_n - X_n \quad (6.6.26)$$

Because we are using a  $p$ -step predictor, we are using more information in predicting  $X_n$  and, therefore, the range of variations of  $Y_n$  will be less. This in turn means that even lower bit rates are possible here. Differential PCM systems find wide applications in speech and image compression.

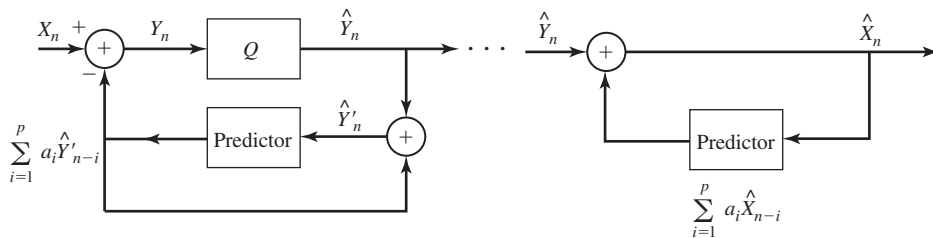


Figure 6.21 A general DPCM system.

### 6.6.3 Delta Modulation ( $\Delta M$ )

Delta modulation ( $\Delta M$ ) is a simplified version of the simple DPCM scheme shown in Figure 6.20. In delta modulation, the quantizer is a 1-bit (two-level) quantizer with magnitudes  $\pm\Delta$ . A block diagram of a  $\Delta M$  system is shown in Figure 6.22. The same analysis that was applied to the simple DPCM system is valid here.

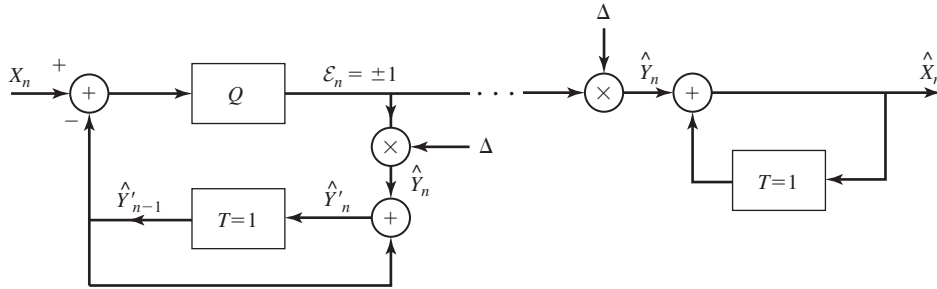


Figure 6.22  $\Delta M$  system.

Because in delta modulation only 1 bit/sample is employed, the quantization noise will be high unless the dynamic range of  $Y_n$  is very low. This in turn means that  $X_n$  and  $X_{n-1}$  must have a very high correlation coefficient. To have high correlation between  $X_n$  and  $X_{n-1}$ , one has to sample at rates much higher than the Nyquist rate. Therefore, in  $\Delta M$  the sampling rate is usually much higher than the Nyquist rate but, since the number of bits/sample is only 1, the total number of bits/second required to transmit a waveform is lower than that of a PCM system.

A major advantage of  $\Delta M$  is the very simple structure of the system. At the receiving end we have the following relation for the reconstruction of  $\hat{X}_n$

$$\hat{X}_n - \hat{X}_{n-1} = \hat{Y}_n \quad (6.6.27)$$

By solving this equation for  $\hat{X}_n$ , and assuming zero initial conditions, one obtains

$$\hat{X}_n = \sum_{i=0}^n \hat{Y}_i \quad (6.6.28)$$

This means that to obtain  $\hat{X}_n$ , one only has to accumulate the values of  $\hat{Y}_n$ . If the sampled values are represented by impulses, the accumulator will be a simple integrator. This simplifies the block diagram of a  $\Delta M$  system to Figure 6.23.

The step-size  $\Delta$  is a very important parameter in designing a delta modulator system. Large values of  $\Delta$  cause the modulator to follow rapid changes in the input signal but at the same time cause excessive quantization noise when input changes slowly. This case is shown in Figure 6.24. As seen in this figure, for large  $\Delta$ , when the inputs varies slowly, a large quantization noise occurs, which is known as *granular noise*. The case of a too small  $\Delta$  is shown in Figure 6.25. In this case we have problem with rapid changes in the input. When the input changes rapidly (high input slope), it

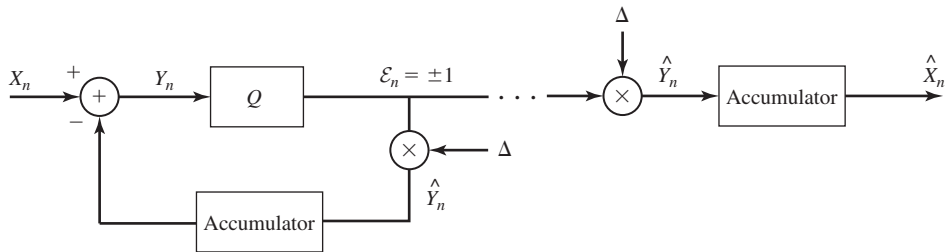


Figure 6.23  $\Delta$ M with integrators.

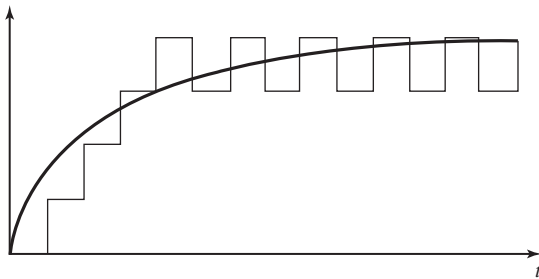


Figure 6.24 Large  $\Delta$  and granular noise.

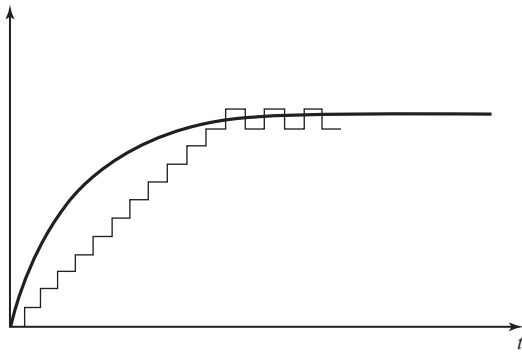
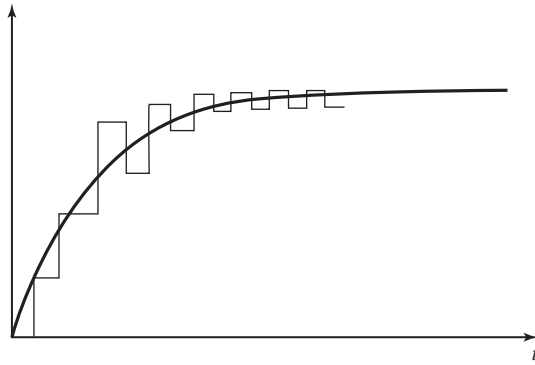


Figure 6.25 Small  $\Delta$  and slope-overload distortion.

takes a rather long time for the output to follow the input and an excessive quantization noise is caused in this period. This type of distortion, which is caused by high slope of the input waveform, is called *slope-overload distortion*.

**Adaptive  $\Delta$ M.** We have seen that too large a step size causes granular noise and too small step size results in slope-overload distortion. This means that a good choice for  $\Delta$  is a “medium” value, but in some cases the performance of the best medium value (i.e., the one minimizing the mean-squared distortion) is not satisfactory. An approach that works well in these cases is to change the step size according to changes in the input. If the input tends to change rapidly, the step size is chosen to be large such that the output can follow the input quickly and no slope-overload distortion results. When



**Figure 6.26** Performance of adaptive  $\Delta M$ .

the input is more or less flat (slowly varying) the step size is changed to a small value to prevent granular noise. Such changes in the step size are shown in Figure 6.26.

To adaptively change the step size one has to design a mechanism for recognizing large and small input slopes. If the slope of the input is small, the output of the quantizer  $\hat{Y}$  alternates between  $\Delta$  and  $-\Delta$  as shown in Figure 6.26. This is the case where granular noise is the main source of noise and one has to decrease the step size. However, in the case of slope overload, the output cannot follow the input rapidly and the output of the quantizer will be a succession of  $+\Delta$ 's or  $-\Delta$ 's. From the above it is seen that the sign of two successive  $\hat{Y}_n$ 's is a good criterion for changing the step size. If the two successive outputs have the same sign, the step size should be increased, and if they are of opposite signs, it should be decreased.

A particularly simple rule to change the step size is given by

$$\Delta_n = \Delta_{n-1} K^{\epsilon_n \times \epsilon_{n-1}} \quad (6.6.29)$$

where  $\epsilon_n$  is the output of the quantizer before being scaled by the step size and  $K$  is some constant larger than one. It has been verified that in the 20–60 kbits/sec range, with a choice of  $K = 1.5$ , the performance of adaptive  $\Delta M$  systems is 5–10 dB better than the performance of  $\Delta M$  when applied to speech sources.

## 6.7 ANALYSIS-SYNTHESIS TECHNIQUES

In contrast to waveform coding, analysis-synthesis techniques are methods that are based on a model for the mechanism that produces the waveform. The parameters of the model that are extracted from the source waveform are quantized, encoded, and transmitted to the receiving end. At the receiving end, based on the received information, the same model is synthesized and used to generate an output similar to the original waveform. These systems are mainly used for speech coding, and in this section we will briefly treat one such system known as *linear predictive coding* or LPC.

Speech is produced as a result of excitation of the vocal tract by the vocal cords. This mechanism can be modeled as a time-varying filter (the vocal tract) excited by a

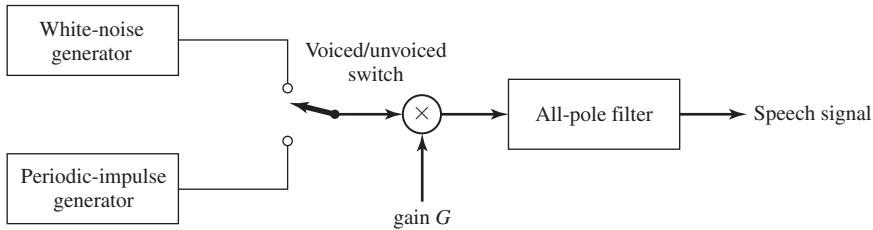


**Figure 6.27** Model for speech generation mechanism.

signal generator. The vocal tract is a combination of the throat, mouth, tongue, lips, and the nose, that change shape during generation of speech and, therefore, it is modeled as a time-varying system. The properties of the excitation signal highly depend on the type of speech sounds, either *voiced* or *unvoiced*. For voiced speech, the excitation can be modeled as a periodic sequence of impulses at a frequency  $f_0$ , the value of which depends on the speaker. The reciprocal  $\frac{1}{f_0}$  is called the *pitch period*. For unvoiced speech, the excitation is well modeled as a white noise. This model is shown in Figure 6.27. The vocal tract filter is usually modeled as an all-pole filter described by the difference equation

$$X_n = \sum_{i=1}^p a_i X_{n-i} + G w_n \quad (6.7.1)$$

where  $w_n$  denotes the input sequence (white noise or impulses),  $G$  is a gain parameter,  $\{a_i\}$  are the filter coefficients, and  $p$  is the number of poles of the filter. The process  $w_n$ , which represents that part of  $X_n$  which is not contained in the previous  $p$  samples, is called the *innovation process*.

Speech signals are known to be stationary for short periods of time, of the order of 20–30 msec. This characteristic behavior follows from the observation that the vocal tract can not change instantaneously. Hence, over 20–30 msec intervals, the all-pole filter coefficients may be assumed to be fixed. At the encoder, we observe a 20–30 msec record of speech from which we estimated the model parameters  $\{a_i\}$ , the type of excitation signal (white noise or impulse), the pitch period  $\frac{1}{f_0}$  if the speech is voiced, and the gain parameter  $G$ .

To elaborate on this process, suppose that the speech signal is filtered to 3 KHz and sampled at a rate of 8000 samples/sec. The signal samples are subdivided into blocks of 160 samples, corresponding to 20-msec intervals. Let  $\{x_n, 1 \leq n \leq 160\}$  be the sequence of samples for a block. The encoder must measure the model parameters to be transmitted to the receiver.

Linear prediction is used to determine the filter coefficients at the encoder. A linear predictor of order  $p$  is an all-zero digital filter with input  $\{x_n\}$  and output

$$\hat{x}_n = \sum_{k=1}^p a_k x_{n-k} \quad \text{for } 1 \leq n \leq N \quad (6.7.2)$$



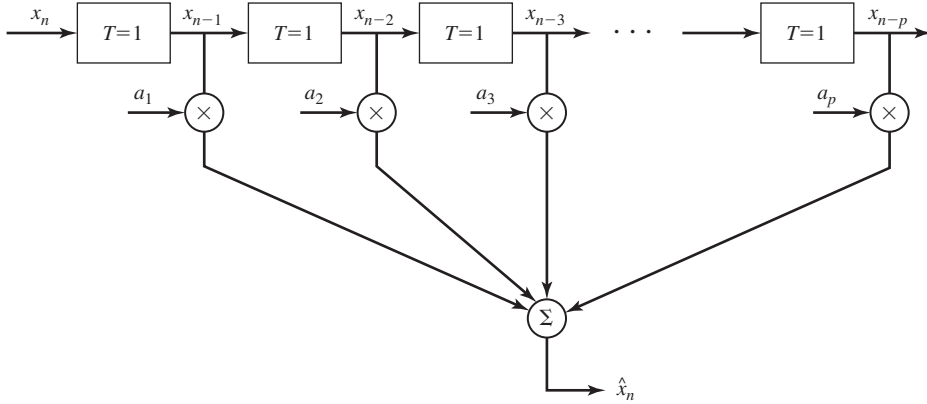


**Figure 6.28** Functional block diagram of linear prediction.

where we have assumed that outside the interval of interest  $x_n = 0$ . Figure 6.28 illustrates the functional block diagram for the prediction process. The difference between the actual speech sample  $x_n$  and the predicted value  $\hat{x}_n$  constitutes the prediction error  $e_n$ ; i.e.,

$$\begin{aligned} e_n &= x_n - \hat{x}_n \\ &= x_n - \sum_{k=1}^p a_k x_{n-k} \end{aligned} \quad (6.7.3)$$

In order to extract as much information as possible from the previous values of  $X_n$ , we choose the coefficients  $\{a_i\}$  so that the average of the squared-error terms; i.e.,

$$\begin{aligned} \mathcal{E}_p &= \frac{1}{N} \sum_{n=1}^N e_n^2 \\ &= \frac{1}{N} \sum_{n=1}^N \left( x_n - \sum_{k=1}^p a_k x_{n-k} \right)^2 \end{aligned} \quad (6.7.4)$$

is minimized. By differentiating  $\mathcal{E}_p$  with respect to each of the prediction filter coefficients  $\{a_i\}$  and setting the derivative to zero, we obtain a set of linear equations for the filter coefficients; i.e.,

$$\frac{1}{N} \sum_{n=1}^N x_n x_{n-i} = \frac{1}{N} \sum_{n=1}^N \sum_{k=1}^p a_k x_{n-i} x_{n-k} \quad \text{for } 1 \leq i \leq p \quad (6.7.5)$$

Since we have assumed that outside the stationary interval,  $1 \leq n \leq N$ , we have  $x_n = 0$ ,

we can write the Equation (6.7.5) as

$$\begin{aligned} \frac{1}{N} \sum_{n=-\infty}^{\infty} x_n x_{n-i} &= \frac{1}{N} \sum_{n=-\infty}^{\infty} \sum_{k=1}^p a_k x_{n-i} x_{n-k} \\ &= \sum_{k=1}^p a_k \left[ \frac{1}{N} \sum_{n=-\infty}^{\infty} x_{n-i} x_{n-k} \right] \end{aligned} \quad (6.7.6)$$

Now if we define

$$\hat{R}_i = \frac{1}{N} \sum_{n=-\infty}^{\infty} x_n x_{n-i} \quad (6.7.7)$$

we can write Equation (6.7.6) as

$$\hat{R}_i = \sum_{k=1}^p a_k \hat{R}_{i-k} \quad \text{for } 1 \leq i \leq p \quad (6.7.8)$$

which is the same as the Yule-Walker Equation (6.6.25) derived in Section 6.6. We can further simplify the above equation to the matrix equation

$$\mathbf{r} = \hat{\mathbf{R}}\mathbf{a} \quad (6.7.9)$$

where  $\mathbf{a}$  is the vector of the linear predictor coefficients,  $\hat{\mathbf{R}}$  is a  $p \times p$  matrix whose  $(i, j)$ th element is  $\hat{R}_{i-j}$ , and  $\mathbf{r}$  is a vector whose components are  $\hat{R}_i$ 's. It can be easily verified from the definition of  $\hat{R}_i$  that

$$\hat{R}_i = \hat{R}_{-i} \quad (6.7.10)$$

and, therefore, the matrix  $\hat{\mathbf{R}}$  is a symmetric matrix. Also it is obvious that all elements of  $\hat{\mathbf{R}}$  that are on a line parallel to the diagonal elements are equal. Such a matrix is called a *Toeplitz matrix* and there exist efficient recursive algorithms for finding its inverse. One such algorithm is the well known Levinson-Durbin algorithm. The interested reader is referred to the references at the end of this chapter for the details of this algorithm.

For the optimal choice of the predictor coefficients, the squared-error term can be shown to be

$$\mathcal{E}_p^{\min} = \hat{R}_0 - \sum_{k=1}^p \hat{R}_k \quad (6.7.11)$$

According to the speech-production model

$$\begin{aligned} \mathcal{E}_p^{\min} &= \frac{1}{N} \sum_{n=1}^N \left[ x_n - \sum_{k=1}^p a_k x_{n-k} \right]^2 \\ &= G^2 \frac{1}{N} \sum_{n=1}^N w_n^2 \end{aligned} \quad (6.7.12)$$

If we normalize the excitation sequence  $\{w_n\}$  such that  $\frac{1}{N} \sum_{n=1}^N w_n^2 = 1$ , we obtain the

value of the gain predictor as

$$G = \sqrt{\epsilon_p^{\min}} \quad (6.7.13)$$

The estimation of the type of excitation (impulsive or noise), and the estimate of the pitch period  $\frac{1}{f_0}$  when the excitation consists of impulses, may be accomplished by various algorithms. One simple approach is to transform the speech data into the frequency domain and look for sharp peaks in the signal spectrum. If the spectrum exhibits peaks at some fundamental frequency  $\frac{1}{f_0}$ , the excitation is taken to be a periodic impulse train with period  $\frac{1}{f_0}$ . If the spectrum of the speech samples exhibits no sharp peaks, the excitation is taken as white noise.

The prediction filter coefficients, gain, voiced–unvoiced information, and pitch  $\frac{1}{f_0}$  are quantized and transmitted to the receiver for each block of sampled speech. The speech signal is synthesized from these parameters using the system model shown in Figure 6.27. Typically the voiced–unvoiced information requires 1 bit, the pitch frequency is represented by 6 bits, the gain parameter can be represented by 5 bits using logarithmic companding, and the prediction coefficients require 8–10 bits/coefficient. Based on linear-predictive coding, speech can be compressed to bit rates as low as 2400 bits/sec. One could alternatively use vector quantization when quantizing the LPC parameters. This would further reduce the bit rate. In contrast, PCM applied to speech has a bit rate of 56,000 bits/sec.

LPC is widely used in speech coding to reduce the bandwidth. By vector quantizing the LPC parameters, good quality speech can be achieved at bit rates of about 4800 bits/sec. One version of LPC with vector quantization has been adopted as a standard for speech compression in mobile (cellular) telephone systems. Efficient speech coding is a very active area for research, and we expect to see further reduction in the bit rate of commercial speech encoders over the coming years.

## 6.8 DIGITAL AUDIO TRANSMISSION AND DIGITAL AUDIO RECORDING

Audio signals constitute a large part of our daily communications. Today, thousands of radio stations broadcast audio signals in analog form. The quality of voice-signal broadcasting is generally acceptable as long as the voice signal is intelligible. On the other hand, the quality of music signals that are broadcast via AM radio is relatively low fidelity because the bandwidth of the transmitted signal is restricted through regulation (by the Federal Communication Commission). FM radio broadcast of analog signals provides higher fidelity by using a significantly larger channel bandwidth for signal transmission. In the near future, commercial radio broadcasting of audio signals will convert to digital form.

In the transmission of audio signals on telephone channels, the conversion from analog to digital transmission, which has been taking place over the past three decades is now nearly complete. We will describe some of the current developments in the digital encoding of audio signals for telephone transmission.

The entertainment industry has experienced the most dramatic changes and benefits in the conversion of analog audio signals to digital form. The development of the compact disc (CD) player and the digital audio tape recorder has rendered the previous analog recording systems technically obsolete. We shall use the CD player as a case study of the sophisticated source encoding/decoding and channel encoding/decoding methods that have been developed over the past few years for digital audio systems.

### 6.8.1 Digital Audio in Telephone Transmission Systems

Nearly all of the transmission of speech signals over telephone channels is currently digital. The encoding of speech signals for transmission over telephone channels has been a topic of intense research for over 50 years and continues to be today. A wide variety of methods for speech-source encoding have been developed over the years, many of which are in use today.

The general configuration for a speech signal encoder is shown in Figure 6.29. Because the frequency content of speech signals is limited to below 3200 Hz, the speech signal is first passed through an anti-aliasing lowpass filter and then sampled. To ensure that aliasing is negligible, a sampling rate of 8000 Hz or higher is typically selected. The analog samples are then quantized and represented in digital form for transmission over telephone channels.

PCM and DPCM are widely used waveform-encoding methods for digital speech transmission. Logarithmic  $\mu = 255$  compression, given by Equation (6.6.8) is generally used for achieving nonuniform quantization. The typical bit rate for PCM is 64,000 bits/sec, while for DPCM the bit rate is 32,000 bits/sec.

PCM and DPCM encoding and decoding are generally performed in a telephone central office where telephone lines from subscribers in a common geographical area are connected to the telephone transmission system. The PCM or DPCM encoded speech signals are transmitted from one telephone central office to another in digital form over so-called *trunk lines* that are capable of carrying the digitized speech signals of many subscribers. The method for simultaneous transmission of several signals over a common communication channel is called *multiplexing*. In the case of PCM and DPCM transmission, the signals from different subscribers are multiplexed in time, hence, the

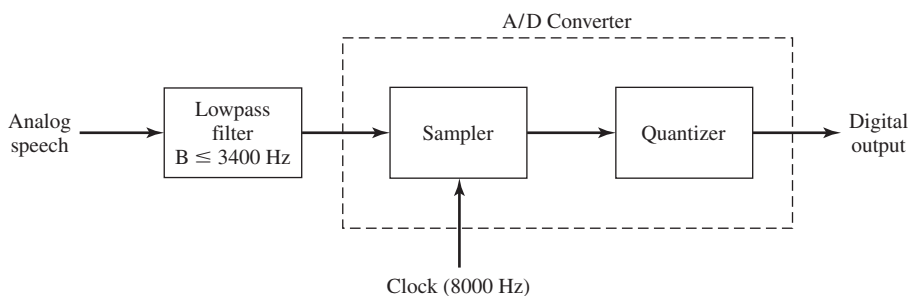


**Figure 6.29** Analog-to-digital conversion of speech signals.

name *time-division multiplexing* (TDM). In TDM, a given time interval  $T_f$  is selected as a frame. Each frame is subdivided into  $N$  subintervals of duration  $T_f/N$ , where  $N$  corresponds to the number of users that will use the common communication channel. Then, each subscriber who wishes to use the channel for transmission is assigned a subinterval within each frame. In PCM, each user transmits one 8-bit sample in each subinterval.

In digital speech transmission over telephone lines via PCM there is a standard TDM hierarchy that has been established for accommodating multiple subscribers. In the first level of the TDM hierarchy, 24 digital subscriber signals are time-division multiplexed into a single high-speed data stream of 1.544 Mbits/sec ( $24 \times 64$  kbs plus a few additional bits for control purposes). The resulting combined TDM signal is usually called a DS-1 channel. In the second level of TDM, four DS-1 channels are multiplexed into a DS-2 channel, having the bit rate of 6.312 Mbits/sec. In a third level of hierarchy, seven DS-2 channels are combined via TDM producing a DS-3 channel, which has a bit rate of 44.736 Mbits/sec. Beyond DS-3, there are two more levels of TDM hierarchy. Figure 6.30 illustrates the TDM hierarchy for the North American telephone system.

In mobile cellular radio systems (see Section 3.5 for a description) for transmission of speech signals, the available channel bandwidth per user is small and cannot support the high bit rates required by waveform-encoding methods such as PCM and DPCM. For this application, the analysis-synthesis method based on linear predictive coding (LPC) as described in Section 6.7, is used to estimate the set of model parameters from short segments of the speech signal. The speech model parameters are then transmitted over the channel using vector quantization. Thus, a bit rate in the range of 4800–9600 bits/sec is achieved with LPC.

In mobile cellular communication systems the base station in each cell serves as the interface to the terrestrial telephone system. LPC speech compression is only required for the radio transmission between the mobile subscriber and the base station in any cell. At the base station interface, the LPC-encoded speech is converted to PCM or DPCM for transmission over the terrestrial telephone system at a bit rate of 64,000 bits/sec or 32,000 bits/sec, respectively. Hence, we note that a speech signal

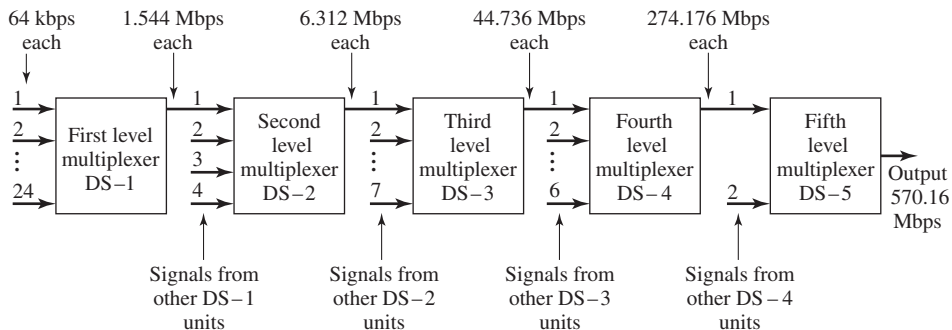


**Figure 6.30** Digital TDM hierarchy for North American telephone communication system.

transmitted from a mobile subscriber to a fixed subscriber will undergo two different types of encoding, whereas speech-signal communication between two mobiles serviced by different base stations connected via the terrestrial telephone system, will undergo four encoding and decoding operations.

### 6.8.2 Digital Audio Recording

Historically, audio recording became a reality with the invention of the phonograph during the second half of the nineteenth century. The phonograph had a lifetime of approximately 100 years before it was supplanted by the compact disc, which was introduced in 1982. During the 100-year period, we witnessed the introduction of a wide variety of records, the most popular of which proved to be the long-playing (LP) record which was introduced in 1948. LP records provide relatively high-quality analog audio recording.

In spite of their wide acceptance and popularity, analog audio recordings have a number of limitations, including a limited dynamic range (typically about 70 dB) and a relatively low SNR (typically about 60 dB). By comparison, the dynamic range of orchestral music is in the range of 100–120 dB. This means that, to record the music in analog form, the dynamic range has to be decreased to fit the range that can be accommodated by the recording system. Otherwise, at low music levels, noise will be audible and, if one wishes to prevent this, saturation will occur at high music levels. The compression of the dynamic range of music during recording is usually done by controlling the volume of the input signal.

Digital audio recording and playback allow us to improve the fidelity of recorded music by increasing the dynamic range and the SNR. Furthermore, digital recordings are generally more durable and do not deteriorate with playing time, as do analog recordings. Below, we describe a compact disc (CD) system as an example of a commercially successful digital audio system that was introduced in 1982. Table 6.4 provides a comparison of some important specifications of an LP record and a CD system. The advantages of the latter are clearly evident.

From a systems point of view, the CD system embodies most of the elements of a modern digital communications system. These include analog-to-digital (A/D) and

**TABLE 6.4** COMPARISON OF LP RECORDS WITH CD SYSTEM

Specification/Feature	LP record	CD system
Frequency response	30 Hz–20 KHZ $\pm 3$ dB	20 Hz–20 KHz +0.5/ -1 dB
Dynamic range	70 dB @ 1 KHz	>90 dB
Signal-to-noise ratio	60 dB	>90 dB
Harmonic distortion	1–2%	0.005%
Durability	High-frequency response degrades with playing	Permanent
Stylus life	500–600 hours	5000 hours

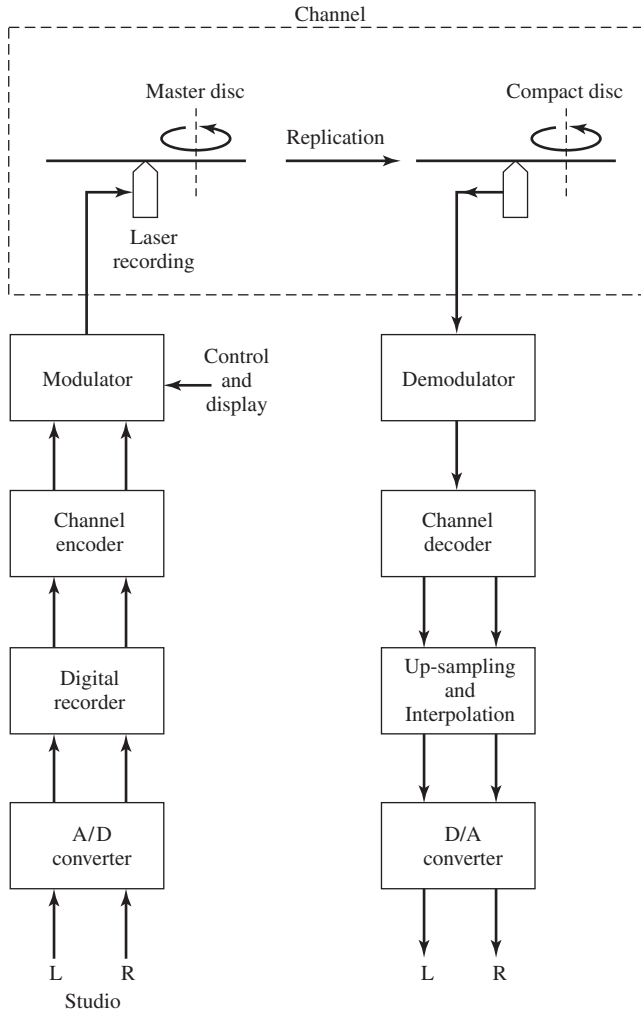


**Figure 6.31** CD digital audio system.

digital-to-analog (D/A) conversion, interpolation, modulation/demodulation and channel coding/decoding. A general block diagram of the elements of a CD digital audio system are illustrated in Figure 6.31. Next, we describe the main features of the source encoder and decoder.

The two audio signals from the left (L) and right (R) microphones in a recording studio or a concert hall are sampled and digitized by passing them through an A/D converter. Recall that the frequency band of audible sound is limited to approximately 20 KHz. Therefore, the corresponding Nyquist sampling rate is 40 KHz. To allow for some frequency guard-band and to prevent aliasing, the sampling rate in a CD system

has been selected to be 44.1 KHz. This frequency is compatible with video recording equipment that is commonly used for digital recording of audio signals on magnetic tape.

The samples of both the L and R signals are quantized using uniform PCM with 16 bits/sample. According to the formula for SQNR given by Equation (6.6.5), 16-bit uniform quantization results in an SQNR of over 90 dB. In addition, the total harmonic distortion achieved is 0.005%. The PCM bytes from the digital recorder are encoded to provide protection against channel errors in the readback process and passed to the modulator.

At the modulator, digital control and display information is added, including a table of contents of the disc. This information allows for programmability of the CD player. The type of modulation and demodulation and the channel coding and decoding operation will be described in Chapters 8 and 9.

Using a laser, the digital signal from the modulator is optically recorded in the surface of a glass disc that is coated with photoresist. This results in a master disc which is used to produce CDs by a series of processes that ultimately convert the information into tiny pits on the plastic disc. The disc is coated with a reflective aluminum coating and then with a protective lacquer.

In the CD player, a laser is used to optically scan a track on the disc at a constant velocity of 1.25 m/sec and, thus, reads the digitally recorded signal. After the L and R signals are demodulated and passed through the channel decoder, the digital audio signal is converted back to an analog audio signal by means of a D/A converter.

The L and R digital audio signals into the D/A converter have a precision of 16 bits. In principle, the digital-to-analog conversion of the two 16-bit signals at the 44.1 KHz sampling rate is relatively simple. However, the practical implementation of a 16-bit D/A converter is very expensive. On the other hand, inexpensive D/A converters with 12-bit (or less) precision are readily available. The problem is to devise a method for D/A conversion that employs a low-precision and, hence, low-cost D/A converter, while maintaining the 16-bit precision of the digital audio signal.

The practical solution to this problem is to expand the bandwidth of the digital audio signal by oversampling through interpolation and digital filtering prior to analog conversion. The basic approach is shown in the block diagram given in Figure 6.32. The 16-bit L and R digital audio signals are up-sampled by some multiple  $U$  by inserting  $U - 1$  zeros between successive 16-bit signal samples. This process effectively increases the sampling rate to  $U \times 44.1$  KHz. The high-rate L and R signals are then filtered by a finite-duration impulse response (FIR) digital filter which produces a high-rate, high-precision output. The combination of up-sampling and filtering is a practical method for realizing a *digital interpolator*. The FIR filter is designed to have linear phase and a bandwidth of approximately 20 KHz. It serves the purpose of eliminating the spectral images created by the up-sampling process and is sometimes called an *anti-imaging filter*.

If we observe the high sample rate, high-precision L and R digital audio signals of the output of the FIR digital filter, we will find that successive samples are nearly the same, differing only in the low-order bits. Consequently, it is possible to represent successive samples of the digital audio signals by their differences and, thus, to reduce



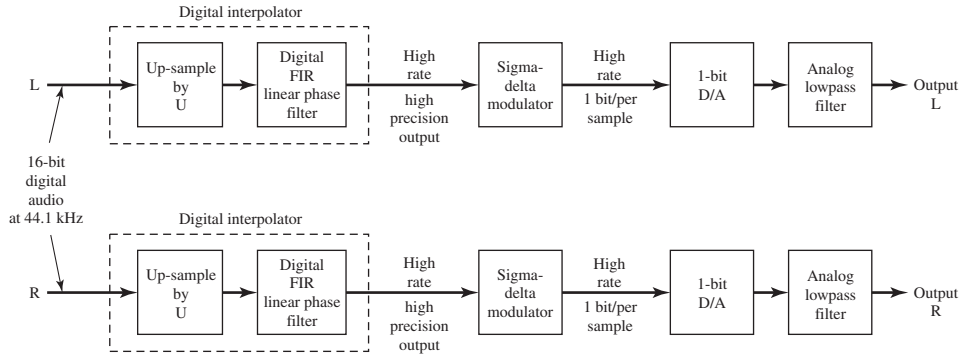


Figure 6.32 D/A conversion by oversampling/interpolation.

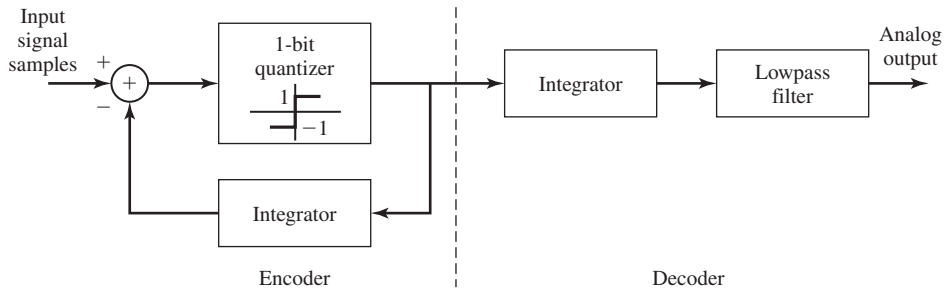


Figure 6.33 Conventional  $\Delta M$  system.

the dynamic range of the signals. If the oversampling factor  $U$  is sufficiently large,  $\Delta M$  may be employed to reduce the quantized output to a precision of 1 bit/sample. Thus, the D/A converter is considerably simplified. An oversampling factor  $U = 256$  is normally chosen in practice. This raises the sampling rate to 11.2896 MHz.

Recall that the general configuration for the conventional  $\Delta M$  system is as shown in Figure 6.33. Suppose we move the integrator from the decoder to the input of the delta modulator (DM). This has two effects. First, it preemphasizes the low frequencies in the input signal and, thus, it increases the correlation of the signal into the DM. Second, it simplifies the DM decoder because the differentiator (the inverse system) required at the decoder is canceled by the integrator. Hence, the decoder is reduced to a simple lowpass filter. Furthermore, the two integrators at the encoder can be replaced by a single integrator placed before the quantizer. The resulting system, shown in Figure 6.34, is called a *sigma-delta modulator* (SDM). Figure 6.35 illustrates a SDM that employs a single-digital integrator (first-order SDM) with a system function

$$H(z) = \frac{z^{-1}}{1 - z^{-1}}$$

Thus, the SDM simplifies the D/A conversion process by requiring only a 1-bit D/A

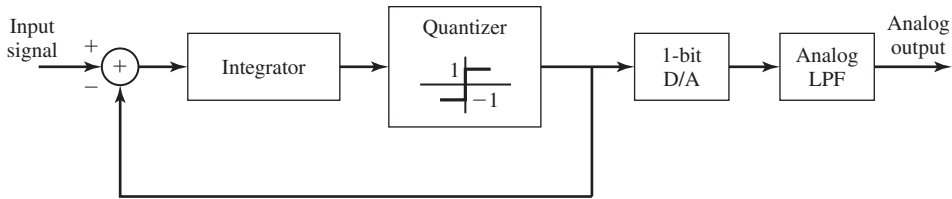


**Figure 6.34** Basic configuration of a SDM followed by a 1-bit D/A converter and lowpass smoothing filter.

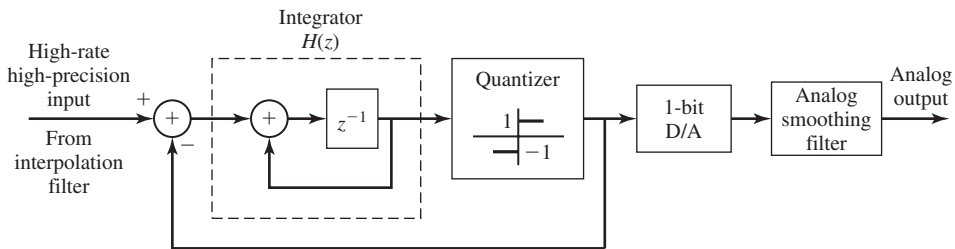


**Figure 6.35** SDM D/A converter with first-order integrator.

followed by a conventional analog filter (a Butterworth filter, for example) for providing anti-aliasing protection and signal smoothing. The output analog filters have a passband of approximately 20 KHz and, thus, eliminate any noise above the desired signal band. In modern CD players, the interpolator, the SDM, the 1-bit D/A converter, and the lowpass smoothing filter are generally implemented on a single integrated chip.

## 6.9 THE JPEG IMAGE-CODING STANDARD

The JPEG standard, adopted by the Joint Photographic Experts Group, is a widely used standard for lossy compression of still images. Although several standards for image compression exist, JPEG is by far the most widely accepted. The JPEG standard achieves very good to excellent image quality and is applicable to both color and gray-scale images. The standard is also rather easy to implement and can be implemented in software with acceptable computational complexity.

JPEG belongs to the class of transform coding techniques; i.e., coding techniques that do not compress the signal (in this case image) directly but compress the transform of it. The most widely used transform technique in image coding is the Discrete Cosine Transform (DCT). The major benefits of DCT are its high degree of energy compaction properties and the availability of a fast algorithm for computation of the transform. The energy compaction property of the DCT results in transform coefficients with only a few of them having significant values, so that nearly all of the energy is contained in those particular components.

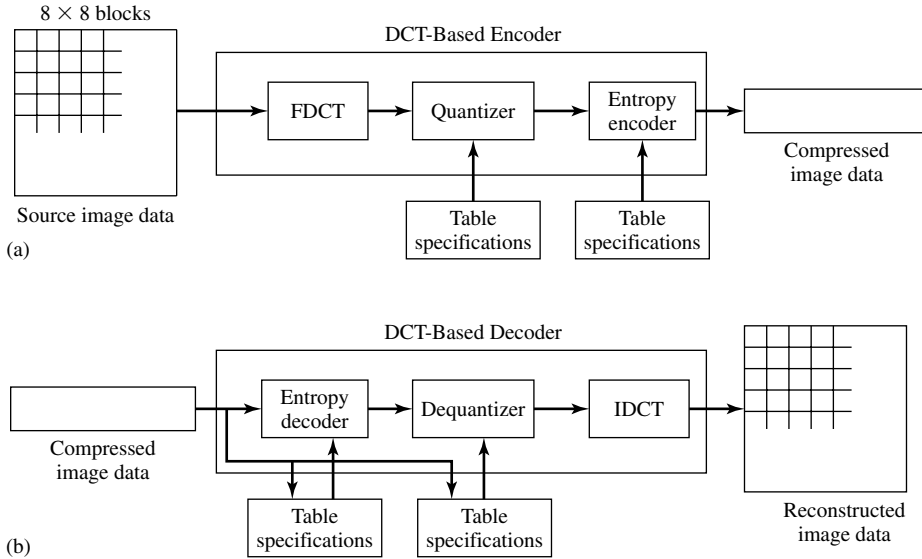


**Figure 6.36** The block diagram of a JPEG encoder.

The DCT of an  $N \times N$  picture with luminance function  $x(m, n)$ ,  $0 \leq m, n \leq N-1$  can be obtained using the following equations:

$$X(0, 0) = \frac{1}{N} \sum_{k=0}^{N-1} \sum_{l=0}^{N-1} x(k, l) \quad (6.9.1)$$

$$X(u, v) = \frac{2}{N} \sum_{k=0}^{N-1} \sum_{l=0}^{N-1} x(k, l) \cos \left[ \frac{(2k+1)u\pi}{2N} \right] \cos \left[ \frac{(2l+1)v\pi}{2N} \right] \quad u, v \neq 0 \quad (6.9.2)$$

The  $X(0, 0)$  coefficient is usually called the DC component and the other coefficients are called the AC components.

The JPEG encoder consists of three blocks, the DCT component, the quantizer, and the encoder as shown in Figure 6.36.

**The DCT Component.** A picture consists of many pixels arranged in an  $m \times n$  array. The first step in DCT transformation of the image is to divide the picture array into  $8 \times 8$  subarrays. This size of subarrays has been chosen as a compromise of complexity and quality. In some other standards,  $4 \times 4$  or  $16 \times 16$  subarrays are chosen. If the number of rows or columns ( $m$  or  $n$ ) is not a multiple of 8, then the last row (or column) is replicated to make it a multiple of 8. The replications are removed at the decoder.

After generating the subarrays, the DCT of each subarray is computed. This process generates 64 DCT coefficients, for each subarray starting from the DC component  $X(0, 0)$  and going up to  $X(7, 7)$ . The process is shown in Figure 6.37.

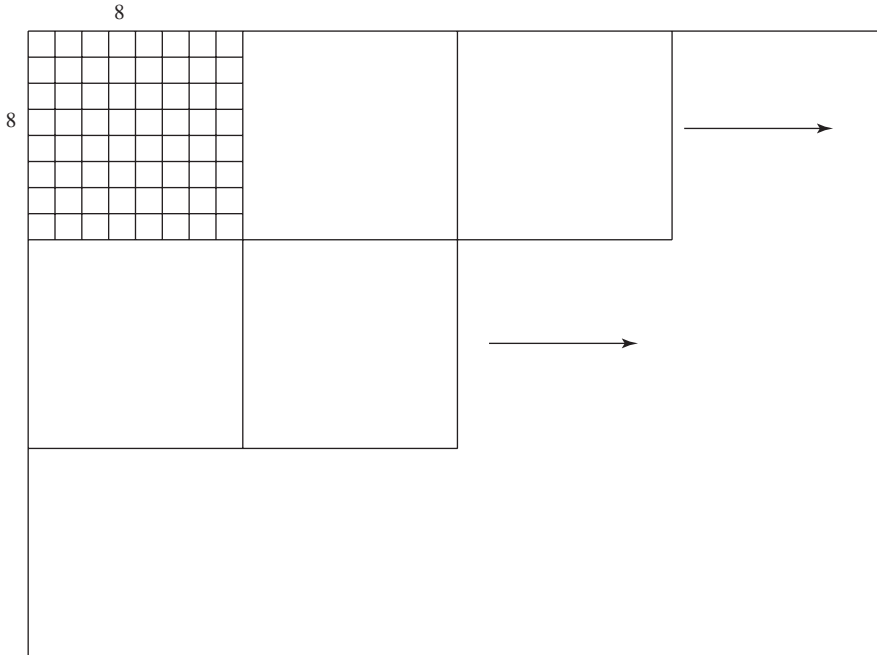


**Figure 6.37** The DCT transformation in JPEG.

**The Quantizer.** Due to the energy-compaction property of the DCT, only low-frequency components of the DCT coefficients have significant values.

Since the DC component carries most of the energy, and also since there exists a strong correlation between the DC component of a subarray and the DC component of the preceding subarray, for quantization of DC components a uniform differential-quantization scheme is employed. The AC components are quantized using uniform-quantization schemes. Although all components are quantized using a uniform scheme, different uniform-quantization schemes use different step-sizes. All quantizers, however, have the same number of quantization regions, namely 256.

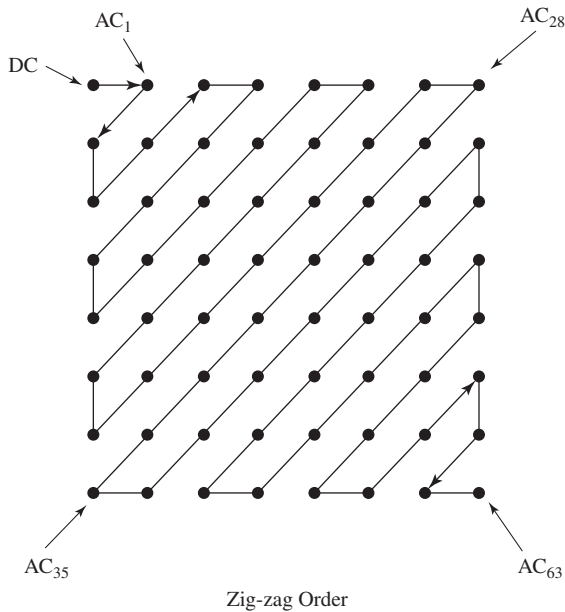
A 64-element quantization table determines the step size for uniform quantization of each DCT component. These step-sizes are obtained using psychovisual experiments. The output of the quantization step is an  $8 \times 8$  array with nonzero elements only at the top left corner and many zero elements in other locations. A sample quantization table illustrating the quantization steps for different coefficients is shown in Table 6.5.

After the quantization process, the quantized DCT coefficients are arranged in a vector by zig-zag sampling as shown in Figure 6.38.

Using this type of sampling, we obtain a vector  $\mathbf{X}$  of length 64 with nonzero values only in the first few components.

**TABLE 6.5** QUANTIZATION TABLE FOR JPEG

16	11	10	16	24	40	51	61
12	12	14	19	26	58	60	55
14	13	16	24	40	57	69	56
14	17	22	29	51	87	80	62
18	22	37	56	68	109	103	77
24	35	55	64	81	104	113	92
49	64	78	87	103	121	120	101
72	92	95	98	112	100	103	99

**Figure 6.38** Zig-zag sampling of the DCT coefficients.

**The Encoding.** The quantization step provides lossy compression of the image using the method described above. After this step, entropy coding is employed to provide lossless compression of the quantized values. One of the entropy-coding methods specified in the JPEG standard is Huffman coding, as discussed in Section 6.3.1. Huffman codes, in this case, are based on tables specifying codewords for different amplitudes. Since the quantized subarrays contain a large number of zeros, some form of runlength coding is used to compress these zeros. The interested reader can refer to the references at the end of this chapter for further details.

**Compression and Picture Quality in JPEG.** Depending on the rate, JPEG can achieve high compression ratios with moderate to excellent image quality for both gray-scale and color images. At rates of 0.2–0.5 bits/pixel, moderate to good quality pictures can be obtained that are sufficient for some applications. Increasing the rate

to 0.5–0.75 bits/pixel results in good to very-good quality images that are sufficient for many applications. At 0.75–1.5 bits/pixel, excellent quality images are obtained sufficient for most applications. Finally, at rates of 1.5–2 bits/pixel, the resulting image is practically indistinguishable from the original. These rates are sufficient for the most demanding applications.

## 6.10 FURTHER READING

Any standard text on information theory covers source-coding theorems and algorithms in detail. Gallager (1968), Blahut (1987), and particularly Cover and Thomas (1991) provide nice and readable treatments of the subject. Our treatment of the Lempel-Ziv algorithm follows that of Cover and Thomas (1991). Berger (1971) is devoted entirely to rate-distortion theory. Jayant and Noll (1984) and Gersho and Gray (1992) examine various quantization and waveform-coding techniques in detail. Gersho and Gray (1992) includes detailed treatment of vector quantization. Analysis-synthesis techniques and linear-predictive coding are treated in books on speech coding such as Markel and Gray (1976), Rabiner and Schafer (1978), and Deller, Proakis, and Hansen (2000). The JPEG standard is described in detail in the book by Gibson, et al. (1998).

Among the original works contributing to the material covered in this chapter, we mention Shannon (1948a, 1959), Huffman (1952), Lloyd (1957), Max (1960), Ziv and Lempel (1978), and Linde, Buzo, and Gray (1980).

## PROBLEMS

- 6.1 A source has an alphabet  $\{a_1, a_2, a_3, a_4, a_5, a_6\}$  with corresponding probabilities  $\{0.1, 0.2, 0.3, 0.05, 0.15, 0.2\}$ . Find the entropy of this source. Compare this entropy with the entropy of a uniformly distributed source with the same alphabet.
- 6.2 Let the random variable  $X$  be the output of the source that is uniformly distributed with size  $N$ . Find its entropy.
- 6.3 Show that  $H(X) \geq 0$  with equality holding if and only if  $X$  is deterministic.
- 6.4 Let  $X$  be a geometrically distributed random variable; i.e.,

$$P(X = k) = p(1 - p)^{k-1} \quad k = 1, 2, 3, \dots$$

1. Find the entropy of  $X$ .
  2. Knowing that  $X > K$ , where  $K$  is a positive integer, what is the entropy of  $X$ ?
- 6.5 Let  $Y = g(X)$ , where  $g$  denotes a deterministic function. Show that, in general,  $H(Y) \leq H(X)$ . When does equality hold?
  - 6.6 An information source can be modeled as a bandlimited process with a bandwidth of 6000 Hz. This process is sampled at a rate higher than the Nyquist rate to provide a guard band of 2000 Hz. It is observed that the resulting samples take values in the set  $\mathcal{A} = \{-4, -3, -1, 2, 4, 7\}$  with probabilities 0.2, 0.1, 0.15, 0.05, 0.3, 0.2.

What is the entropy of the discrete-time source in bits/output (sample)? What is the entropy in bits/sec?

- 6.7** Let  $X$  denote a random variable distributed on the set  $\mathcal{A} = \{a_1, a_2, \dots, a_N\}$  with corresponding probabilities  $\{p_1, p_2, \dots, p_N\}$ . Let  $Y$  be another random variable defined on the same set but distributed uniformly. Show that

$$H(X) \leq H(Y)$$

with equality if and only if  $X$  is also uniformly distributed. (Hint: First prove the inequality  $\ln x \leq x - 1$  with equality for  $x = 1$ , then apply this inequality to  $\sum_{n=1}^N p_n \ln(\frac{1}{p_n})$ ).

- 6.8** A random variable  $X$  is distributed on the set of all positive integers  $1, 2, 3, \dots$  with corresponding probabilities  $p_1, p_2, p_3, \dots$ . We further know that the expected value of this random variable is given to be  $m$ ; i.e.,

$$\sum_{i=1}^{\infty} i p_i = m$$

Show that among all random variables that satisfy the above condition, the geometric random variable which is defined by

$$p_i = \frac{1}{m} \left(1 - \frac{1}{m}\right)^{i-1} \quad i = 1, 2, 3, \dots$$

has the highest entropy. (Hint: Define two distributions on the source, the first one being the geometric distribution given above and the second one an arbitrary distribution denoted by  $q_i$ , and then apply the approach of Problem 6.7.)

- 6.9** Two binary random variables  $X$  and  $Y$  are distributed according to the joint distribution  $p(X = Y = 0) = p(X = 0, Y = 1) = p(X = Y = 1) = \frac{1}{3}$ . Compute  $H(X)$ ,  $H(Y)$ ,  $H(X | Y)$ ,  $H(Y | X)$ , and  $H(X, Y)$ .
- 6.10** Show that if  $Y = g(X)$  where  $g$  denotes a deterministic function, then  $H(Y | X) = 0$ .
- 6.11** A memoryless source has the alphabet  $\mathcal{A} = \{-5, -3, -1, 0, 1, 3, 5\}$  with corresponding probabilities  $\{0.05, 0.1, 0.1, 0.15, 0.05, 0.25, 0.3\}$ .

1. Find the entropy of the source.
2. Assume that the source is quantized according to the quantization rule

$$\begin{cases} q(-5) = g(-3) = -4, \\ q(-1) = q(0) = q(1) = 0 \\ q(3) = q(5) = 4 \end{cases}$$

Find the entropy of the quantized source.

- 6.12** Using both definitions of the entropy rate of a process, prove that for a DMS the entropy rate and the entropy are equal.

**6.13** A Markov process is a process with one-step memory; i.e., a process such that

$$p(x_n | x_{n-1}, x_{n-2}, x_{n-3}, \dots) = p(x_n | x_{n-1})$$

for all  $n$ . Show that for a stationary Markov process the entropy rate is given by  $H(X_n | X_{n-1})$ .

**6.14** Show that

$$H(X | Y) = \sum_y p(y) H(X | Y = y)$$

**6.15** Let  $X$  and  $Y$  denote two jointly distributed discrete valued random variables

1. Show that

$$H(X) = - \sum_{x,y} p(x, y) \log p(x)$$

and

$$H(Y) = - \sum_{x,y} p(x, y) \log p(y)$$

2. Use the above result to show that

$$H(X, Y) \leq H(X) + H(Y)$$

When does the equality hold? (Hint: Consider the two distributions  $p(x, y)$  and  $p(x)p(y)$  on the product set  $\mathcal{X} \times \mathcal{Y}$ , and apply the inequality proved in Problem 6.7 to  $\sum_{x,y} p(x, y) \log \frac{p(x)p(y)}{p(x,y)}$ .)

**6.16** Use the result of Problem 6.15 to show that

$$H(X | Y) \leq H(X)$$

with equality if and only if  $X$  and  $Y$  are independent.

**6.17** Show that  $H(X)$  is a concave function of the probability distribution on  $\mathcal{X}$ ; i.e., for any two probability distribution vectors  $\mathbf{p}_1$  and  $\mathbf{p}_2$  on  $\mathcal{X}$ , and any  $0 \leq \lambda \leq 1$  we have

$$\lambda H(\mathbf{p}_1) + \bar{\lambda} H(\mathbf{p}_2) \leq H(\lambda \mathbf{p}_1 + \bar{\lambda} \mathbf{p}_2)$$

where  $\bar{\lambda} \stackrel{\text{def}}{=} 1 - \lambda$ . (Note: You have to first show that  $\lambda \mathbf{p}_1 + \bar{\lambda} \mathbf{p}_2$  is a legitimate probability vector.)

**6.18** Show that in general

$$H(X_1, X_2, \dots, X_n) \leq \sum_{i=1}^n H(X_i)$$

When does the equality hold?

**6.19** Assume that a BSS generates a sequence of  $n$  outputs.

1. What is the probability that this sequence consists of all zeros?
2. What is the probability that this sequence consists of all ones?



3. What is the probability that in this sequence the first  $k$  symbols are ones and the next  $n - k$  symbols are zeros?
  4. What is the probability that this sequence has  $k$  ones and  $n - k$  zeros?
  5. How would your answers change if instead of a BSS we were dealing with a general binary DMS with  $p(X_i = 1) = p$ .
- 6.20** Give an estimate of the number of binary sequences of length 10,000 with 3000 zeros and 7000 ones.
- 6.21** A memoryless ternary source with output alphabet  $a_1, a_2,$  and  $a_3$  and corresponding probabilities 0.2, 0.3, 0.5 produces sequences of length 1000.
1. Approximately what is the number of typical sequences in the source output?
  2. What is the ratio of typical sequences to nontypical sequences?
  3. What is the probability of a typical sequence?
  4. What is the number of bits required to represent all output sequences?
  5. What is the number of bits required to represent only the typical output sequences?
  6. What is the most probable sequence and what is its probability?
  7. Is the most probable sequence a typical sequence?
- 6.22** A source has an alphabet  $\{a_1, a_2, a_3, a_4\}$  with corresponding probabilities  $\{0.1, 0.2, 0.3, 0.4\}$ .
1. Find the entropy of the source.
  2. What is the minimum required average code word length to represent this source for error-free reconstruction?
  3. Design a Huffman code for the source and compare the average length of the Huffman code with the entropy of the source.
  4. Design a Huffman code for the second extension of the source (take two letters at a time). What is the average code word length? What is the average required binary letters per each source output letter?
  5. Which one is a more efficient coding scheme, Huffman coding of the original source or Huffman coding of the second extension of the source?
- 6.23** Design a Huffman code for a source with  $n$  output letters and corresponding probabilities  $\{\frac{1}{2}, \frac{1}{4}, \frac{1}{8}, \dots, \frac{1}{2^{n-1}}, \frac{1}{2^{n-1}}\}$ . Show that the average code word length for such a source is equal to the source entropy.
- 6.24** Show that  $\{01, 100, 101, 1110, 1111, 0011, 0001\}$  cannot be a Huffman code for any source probability distribution.
- 6.25** Design a *ternary* Huffman code, using 0, 1, 2 as letters, for a source with output alphabet probabilities given by  $\{0.05, 0.1, 0.15, 0.17, 0.18, 0.22, 0.13\}$ . What is the resulting average code word length? Compare the average code word length

with the entropy of the source. (In what base would you compute the logarithms in the expression for the entropy for a meaningful comparison?)

- 6.26** Design a ternary Huffman code for a source with output alphabet probabilities given by  $\{0.05, 0.1, 0.15, 0.17, 0.13, 0.4\}$ . (Hint: You can add a dummy source output with zero probability.)
- 6.27** Find the Lempel-Ziv source code for the binary source sequence

00010010000001100001000000010000001010000100000011010000000110

Recover the original sequence back from the Lempel-Ziv source code. (Hint: You require two passes of the binary sequence to decide on the size of the dictionary.)

- 6.28** Using the definition of  $H(X)$  and  $H(X|Y)$  show that

$$I(X; Y) = \sum_{x,y} p(x, y) \log \frac{p(x, y)}{p(x)p(y)}$$

Now by using the approach of Problem 6.7 show that  $I(X; Y) \geq 0$  with equality if and only if  $X$  and  $Y$  are independent.

- 6.29** Show that

1.  $I(X; Y) \leq \min\{H(X), H(Y)\}$ .
2. If  $|\mathcal{X}|$  and  $|\mathcal{Y}|$  represent the size of sets  $\mathcal{X}$  and  $\mathcal{Y}$ , respectively, then  $I(X; Y) \leq \min\{\log|\mathcal{X}|, \log|\mathcal{Y}|\}$ .

- 6.30** Show that  $I(X; Y) = H(X) + H(Y) - H(X, Y) = H(Y) - H(Y|X) = I(Y; X)$ .

- 6.31** Let  $X$  denote a binary random variable with  $p(X=0) = 1 - p(X=1) = p$  and let  $Y$  be a binary random variable that depends on  $X$  through  $p(Y=1|X=0) = p(Y=0|X=1) = \epsilon$ .

1. Find  $H(X)$ ,  $H(Y)$ ,  $H(Y|X)$ ,  $H(X, Y)$ ,  $H(X|Y)$ , and  $I(X; Y)$ .
2. For a fixed  $\epsilon$ , which  $p$  maximizes  $I(X; Y)$ ?
3. For a fixed  $p$ , which  $\epsilon$  minimizes  $I(X; Y)$ ?

- 6.32** Show that

$$I(X; YZW) = I(X; Y) + I(X; Z|Y) + I(X; W|ZY)$$

Can you interpret this relation?

- 6.33** Let  $X$ ,  $Y$ , and  $Z$  be three discrete random variables.

1. Show that if  $p(x, y, z) = p(z)p(x|z)p(y|x)$ , we have

$$I(X; Y|Z) \leq I(X; Y)$$

2. Show that if  $p(x, y, z) = p(x)p(y)p(z|x, y)$ , then

$$I(X; Y) \leq I(X; Y|Z)$$

3. In each case give an example where strict inequality holds.

**6.34** Let  $\mathcal{X}$  and  $\mathcal{Y}$  denote finite sets. We denote the probability vectors on  $\mathcal{X}$  by  $\mathbf{p}$  and the conditional probability matrices on  $\mathcal{Y}$  given  $\mathcal{X}$  by  $\mathbf{Q}$ . Then  $I(X; Y)$  can be represented as a function of the probability distribution on  $\mathcal{X}$  and the conditional probability distribution on  $\mathcal{Y}$  given  $\mathcal{X}$  as  $I(\mathbf{p}; \mathbf{Q})$ .

1. Show that  $I(\mathbf{p}; \mathbf{Q})$  is a concave function in  $\mathbf{p}$ ; i.e., for any  $\mathbf{Q}$ , any  $0 \leq \lambda \leq 1$ , and any two probability vectors  $\mathbf{p}_1$  and  $\mathbf{p}_2$  on  $\mathcal{X}$ , we have

$$\lambda I(\mathbf{p}_1; \mathbf{Q}) + \bar{\lambda} I(\mathbf{p}_2; \mathbf{Q}) \leq I(\lambda \mathbf{p}_1 + \bar{\lambda} \mathbf{p}_2; \mathbf{Q})$$

where  $\bar{\lambda} \stackrel{\text{def}}{=} 1 - \lambda$ .

2. Show that  $I(\mathbf{p}; \mathbf{Q})$  is a convex function in  $\mathbf{Q}$ ; i.e., for any  $\mathbf{p}$ , any  $0 \leq \lambda \leq 1$ , and any two conditional probabilities  $\mathbf{Q}_1$  and  $\mathbf{Q}_2$ , we have

$$I(\mathbf{p}; \lambda \mathbf{Q}_1 + \bar{\lambda} \mathbf{Q}_2) \leq \lambda I(\mathbf{p}; \mathbf{Q}_1) + \bar{\lambda} I(\mathbf{p}; \mathbf{Q}_2)$$

(Note: You have to first show that  $\lambda \mathbf{p}_1 + \bar{\lambda} \mathbf{p}_2$  and  $\lambda \mathbf{Q}_1 + \bar{\lambda} \mathbf{Q}_2$  are a legitimate probability vector and conditional probability matrix, respectively.)

**6.35** Let the random variable  $X$  be continuous with PDF  $f_X(x)$  and let  $Y = aX$  where  $a$  is a nonzero constant.

1. Show that  $h(Y) = \log|a| + h(X)$ .
2. Does a similar relation hold if  $X$  is a discrete random variable?

**6.36** Find the differential entropy of the continuous random variable  $X$  in the following cases

1.  $X$  is an exponential random variable with parameter  $\lambda > 0$ ; i.e.,

$$f_X(x) = \begin{cases} \frac{1}{\lambda} e^{-\frac{x}{\lambda}}, & x > 0 \\ 0, & \text{otherwise} \end{cases}$$

2.  $X$  is a Laplacian random variable with parameter  $\lambda > 0$ ; i.e.,

$$f_X(x) = \frac{1}{2\lambda} e^{-\frac{|x|}{\lambda}}$$

3.  $X$  is a triangular random variable with parameter  $\lambda > 0$ ; i.e.,

$$f_X(x) = \begin{cases} \frac{x+\lambda}{\lambda^2}, & -\lambda \leq x \leq 0 \\ \frac{-x+\lambda}{\lambda^2}, & 0 < x \leq \lambda \\ 0, & \text{otherwise} \end{cases}$$

**6.37** Generalize the technique developed in Problem 6.7 to continuous random variables and show that for continuous  $X$  and  $Y$

1.  $h(X|Y) \leq h(X)$  with equality if and only if  $X$  and  $Y$  are independent.
2.  $I(X; Y) \geq 0$  with equality if and only if  $X$  and  $Y$  are independent.

- 6.38** Using an approach similar to Problem 6.8, show that among all continuous random variables distributed on the positive real line and having a given mean  $m$ , the exponential random variable has the highest differential entropy.
- 6.39** Using the method of Problem 6.8, show that among all continuous random variables with a given variance  $\sigma^2$ , the Gaussian random variable has the highest differential entropy.
- 6.40** A memoryless source emits 2000 binary symbols/sec and each symbol has a probability of 0.25 to be equal to 1 and 0.75 to be equal to 0.
1. What is the minimum number of bits/sec required for error-free transmission of this source?
  2. What is the minimum number of bits/sec required for reproduction of this source with an error probability not exceeding 0.1?
  3. What is the minimum number of bits/sec required for reproduction of this source with an error not exceeding 0.25? What is the best decoding strategy in this case?
- 6.41** A Gaussian source with mean zero and variance 1 is to be transmitted via a channel that can provide a transmission capacity of 1 bit/each source output (see Figure P-6.41).
1. What is the minimum mean-squared-error achievable?
  2. If the maximum tolerable distortion is 0.01, what is the required transmission capacity/source output?



Figure P-6.41

- 6.42** It can be shown that the rate distortion function for a Laplacian source,  $f_X(x) = \frac{1}{2\lambda} e^{-\frac{|x|}{\lambda}}$  with an absolute value of error distortion measure  $d(x, \hat{x}) = |x - \hat{x}|$  is given by

$$R(D) = \begin{cases} \log \frac{\lambda}{D}, & 0 \leq D \leq \lambda \\ 0, & D > \lambda \end{cases}$$

(see Berger [1971]).

1. How many bits/sample are required to represent the outputs of this source with an average distortion not exceeding  $\frac{\lambda}{2}$ ?
2. Plot  $R(D)$  for three different values of  $\lambda$  and discuss the effect of changes in  $\lambda$  on these plots.

- 6.43** It can be shown that if  $X$  is a zero-mean continuous random variable with variance  $\sigma^2$ , its rate distortion function, subject to squared-error distortion measure, satisfies the lower and upper bounds given by the inequalities

$$h(X) - \frac{1}{2} \log(2\pi e D) \leq R(D) \leq \frac{1}{2} \log \frac{\sigma^2}{2}$$

where  $h(X)$  denotes the differential entropy of the random variable  $X$  (see Cover and Thomas [1991]).

1. Show that for a Gaussian random variable, the lower and upper bounds coincide.
2. Plot the lower and upper bounds for a Laplacian source with  $\sigma = 1$ .
3. Plot the lower and upper bounds for a triangular source with  $\sigma = 1$ .

(Hint: Use the results of Problem 6.36.)

- 6.44** With the assumptions of Example 6.4.6, if we want to reduce the distortion by a factor of 1000, how many extra bits/source symbol have to be introduced?
- 6.45** Let  $X(t)$  be a strictly stationary random process.

1. Show that  $Q(X(t))$  is also strictly stationary for any function  $Q$ .
2. From above conclude that  $X(t) - Q(X(t))$  is also strictly stationary and, therefore, in any quantizer

$$\text{SQNR} = \frac{E(X^2)}{E(X - Q(X))^2} = \frac{P_X}{P_{\tilde{X}}} = \frac{R_X(0)}{R_{\tilde{X}}(0)}$$

where  $\tilde{X}(t) = X(t) - Q(X(t))$

- 6.46** Let  $X(t)$  denote a wide-sense stationary Gaussian process with  $P_X = 10$ .
1. Using Table 6.2 design a 16-level optimal uniform quantizer for this source.
  2. What is the resulting distortion if the quantizer in part 1 is employed?
  3. What is the minimum number of bits/source symbol required to represent the quantized source?
  4. Compare this result with the result obtained from the rate-distortion bound that achieves the same amount of distortion.
  5. What is the amount of improvement in SQNR (in dB) that results from doubling the number of quantization levels from 8 to 16?
- 6.47** Using Table 6.2 design an optimal quantizer for the source given in Example 6.5.1. Compare the distortion of this quantizer to the distortion obtained there. What is the entropy of the quantized source in this case?
- 6.48** Solve Problem 6.46 using Table 6.3 instead of 6.2 to design an optimal nonuniform quantizer for the Gaussian source.
- 6.49** Consider the encoding of the two random variables  $X$  and  $Y$ , which are uniformly distributed on the region between the two-squares as shown in Figure P-6.49.

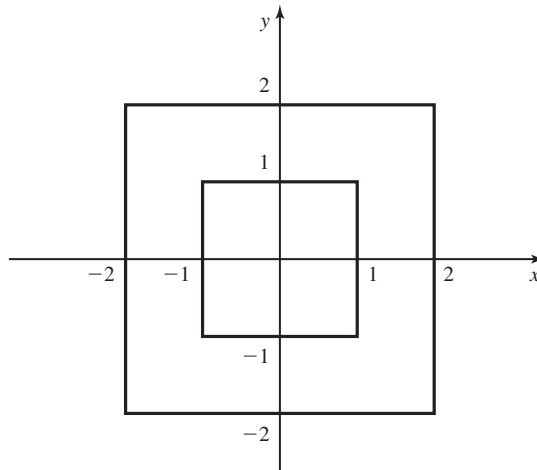


Figure P-6.49

1. Find  $f_X(x)$  and  $f_Y(y)$ .
  2. Assume each of the random variables  $X$  and  $Y$  are quantized using 4-level uniform quantizers. What is the resulting distortion? What is the resulting number of bits/pair  $(X, Y)$ ?
  3. Now assume instead of scalar quantizers for  $X$  and  $Y$ , we employ a vector quantizer to achieve the same level of distortion as in part 2. What is the resulting number of bits/source output pair  $(X, Y)$ ?
- 6.50** Two random variables  $X$  and  $Y$  are uniformly distributed on the square shown in Figure P-6.50.

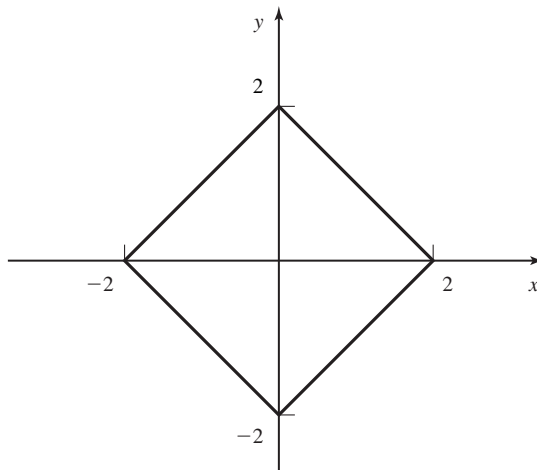
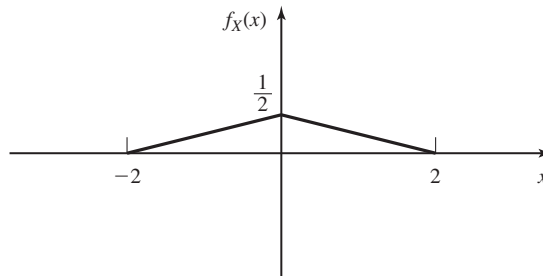


Figure P-6.50

1. Find  $f_X(x)$  and  $f_Y(y)$ .
  2. Assume that each of the random variables  $X$  and  $Y$  are quantized using 4-level uniform quantizers. What is the resulting distortion? What is the resulting number of bits/pair  $(X, Y)$ ?
  3. Now assume that instead of scalar quantizers for  $X$  and  $Y$ , we employ a vector quantizer with the same number of bits/source output pair  $(X, Y)$  as in part 2. What is the resulting distortion for this vector quantizer?
- 6.51** Solve Example 6.6.1 for the case when the samples are uniformly distributed on  $[-2, 2]$ .
- 6.52** A stationary random process has an autocorrelation function given by  $R_X = \frac{A^2}{2} e^{-|\tau|} \cos 2\pi f_0 \tau$  and it is known that the random process never exceeds 6 in magnitude. Assuming  $A = 6$ ,
1. How many quantization levels are required to guarantee a SQNR of at least 60 dB?
  2. Assuming that the signal is quantized to satisfy the condition of part 1 and assuming the approximate bandwidth of the signal is  $W$ , what is the minimum required bandwidth for transmission of a binary PCM signal based on this quantization scheme?
- 6.53** A signal can be modeled as a lowpass stationary process  $X(t)$  whose PDF at any time  $t_0$  is given in Figure P-6.53.



**Figure P-6.53**

The bandwidth of this process is 5 KHz, and it is desired to transmit it using a PCM system.

1. If sampling is done at the Nyquist rate and a uniform quantizer with 32 levels is employed, what is the resulting SQNR? What is the resulting bit rate?
2. If the available bandwidth of the channel is 40 KHz, what is the highest achievable SQNR?

3. If instead of sampling at the Nyquist rate we require a guard-band of at least 2 KHz, and the bandwidth of the channel is 40 KHz again, what is the highest achievable SQNR?

**6.54** A stationary source is distributed according a triangular PDF,  $f_X(x) = \frac{1}{2}\Lambda(\frac{x}{2})$ . This source is quantized using a 4-level uniform quantizer described below

$$Q(x) = \begin{cases} 1.5, & 1 < x \leq 2 \\ 0.5, & 0 < x \leq 1 \\ -0.5, & -1 < x \leq 0 \\ -1.5, & -2 \leq x \leq -1 \end{cases}$$

1. Find the entropy of the quantized source.
  2. Determine the PDF of the random variable representing the quantization error; i.e.,  $\tilde{X} = X - Q(X)$ .
- 6.55** The random process  $X(t)$  is defined by  $X(t) = Y \cos(2\pi f_0 t + \Theta)$  where  $Y$  and  $\Theta$  are two independent random variables,  $Y$  uniform on  $[-3, 3]$  and  $\Theta$  uniform on  $[0, 2\pi]$ .
1. Find the autocorrelation function of  $X(t)$  and its power-spectral density.
  2. If  $X(t)$  is to be transmitted to maintain a SQNR of at least 40 dB using a uniform PCM system, what is the required number of bits/sample and the least bandwidth requirement (in terms of  $f_0$ )?
  3. If the SQNR is to be increased by 24 dB, how many more bits/sample have to be introduced and what is the new minimum bandwidth requirement in this case?
- 6.56** In our analysis of PCM systems, it was always assumed that the transmitted bits are received with no errors. However, practical channels cause errors. Let us assume that the output of a PCM system is transmitted via a channel whose error probability is denoted by  $p_b$ . It is further assumed that  $p_b$  is small enough such that, in transmission of the  $\nu$  bits resulting from encoding of each quantized sample, either no error occurs or at most one error occurs. This means that the probability of each transmitted bit being in error is  $p_b$  and the probability of no error in transmission of  $\nu$  bits is roughly  $1 - \nu p_b$ . We also assume that, for the binary representation of each quantized value, natural binary coding (NBC) is employed; i.e., the lowest quantized level is mapped into a sequence of zeros and the largest level is mapped into a sequence of all ones and all the other levels are mapped according to their relative value.
1. Show that if an error occurs in the least significant bit, its effect on the quantized value is equivalent to  $\Delta$ , the spacing between the levels; if an error occurs in the next bit its effect on the quantized value is  $2\Delta, \dots$ , if an error occurs in the most significant bit, its effect on the quantized value is  $2^{\nu-1}\Delta$ .



2. From above, show that the mean-squared-error resulting from channel errors is given by

$$D_{\text{channel}} = p_b \Delta^2 \frac{4^v - 1}{3}$$

where  $\Delta = \frac{2x_{\max}}{N} = \frac{x_{\max}}{2^{v-1}}$  is the spacing between adjacent levels.

3. From the above conclude that the total distortion which is the sum of the quantization distortion and the transmission distortion due to channel errors, can be expressed by

$$D_{\text{total}} = \frac{x_{\max}^2}{3 \times N^2} (1 + 4p_b(N^2 - 1)) = \frac{x_{\max}^2}{3 \times 4^v} (1 + 4p_b(4^v - 1))$$

4. Finally, show that the SNR defined as the ratio of the signal power to the total noise power is given by

$$\text{SNR} = \frac{3N^2 \overline{\check{X}^2}}{1 + 4p_b(N^2 - 1)} = \frac{3 \times 4^v \overline{\check{X}^2}}{1 + 4p_b(4^v - 1)}$$

where  $\check{X} = \frac{X}{x_{\max}}$ .

**6.57** In this problem we study the performance of nonuniform PCM systems. Let the signal samples be distributed according to the PDF  $f_X(x)$ .

1. Use Equation 6.6.15 to show that for a  $\mu$ -law compander

$$\begin{aligned} D &\approx \frac{[\ln(1 + \mu)]^2 x_{\max}^2}{3\mu^2 N^2} (\mu^2 E(\check{X}^2) + 2\mu E(|\check{X}|) + 1) \\ &= \frac{[\ln(1 + \mu)]^2 x_{\max}^2}{3\mu^2 4^v} (\mu^2 E(\check{X}^2) + 2\mu E(|\check{X}|) + 1) \end{aligned}$$

where  $\check{X}$  represents the normalized random variable  $\frac{X}{x_{\max}}$ .

2. Show that

$$\begin{aligned} \text{SQNR} &= \frac{3\mu^2 N^2}{(\ln(1 + \mu))^2} \frac{E(\check{X}^2)}{\mu^2 E(\check{X}^2) + 2\mu E(|\check{X}|) + 1} \\ &= \frac{3\mu^2 4^v}{(\ln(1 + \mu))^2} \frac{E(\check{X}^2)}{\mu^2 E(\check{X}^2) + 2\mu E(|\check{X}|) + 1} \end{aligned}$$

3. Compare the above result with the SQNR for a uniform quantizer and conclude that

$$\text{SQNR}_{\mu\text{-law}} = \text{SQNR}_{\text{uniform}} G(\mu, \check{X})$$

and determine  $G(\mu, \check{X})$ .

4. Now assume that  $X$  is a truncated zero-mean Gaussian random variable truncated to  $[-4\sigma_x, 4\sigma_x]$ . Plot both the  $\text{SQNR}_{\mu\text{-law}}$  and the  $\text{SQNR}_{\text{uniform}}$

in dB as a function of  $E(\check{X}^2)$  (in dB) for  $\mu = 255$  and  $\nu = 8$ . Compare the results and note the relative insensitivity of the  $\mu$ -law scheme to the dynamic range of the input signal.

**6.58** Design an optimal compander for a source with a triangular PDF given by

$$f_X(x) = \begin{cases} x + 1, & -1 \leq x \leq 0 \\ -x + 1, & 0 \leq x \leq 1 \\ 0, & \text{otherwise} \end{cases}$$

Plot the resulting  $g(x)$  and determine the SQNR.

**6.59** In a CD player, the sampling rate is 44.1 KHz and the samples are quantized using a 16-bit/sample quantizer. Determine the resulting number of bits for a piece of music with a duration of 50 minutes.

## *Digital Transmission through the Additive White Gaussian Noise Channel*

In Chapter 6, we described methods for converting the output of a signal source into a sequence of binary digits. In this chapter, we consider the transmission of the digital information sequence over communication channels that are characterized as *additive white Gaussian noise (AWGN)* channels. The AWGN channel is one of the simplest mathematical models for various physical communication channels, including wirelines and some radio channels. Such channels are basically analog channels, which means that the digital information sequence to be transmitted must be mapped into analog signal waveforms.

Our treatment focuses on the characterization and the design of analog signal waveforms that carry digital information and their performance on an AWGN channel. We consider both *baseband channels*; i.e., channels having frequency passbands that usually include zero frequency ( $f = 0$ ), and *bandpass channels*; i.e., channels having frequency passbands far removed from  $f = 0$ . When the digital information is transmitted through a baseband channel, there is no need to use a carrier frequency for transmission of the digitally modulated signals. On the other hand, there are many communication channels, including telephone channels, radio channels, and satellite channels, that are bandpass channels. In such channels, the information-bearing signal is impressed on a sinusoidal carrier, which shifts the frequency content of the information-bearing signal to the appropriate frequency band that is passed by the channel. Thus, the signal is transmitted by carrier modulation.

We begin by developing a geometric representation of these types of signals, which is useful in assessing their performance characteristics. Then, we describe several different types of analog signal waveforms for transmitting digital information and give their geometric representation. The optimum demodulation and detection of these

signals is then described and their performance on the AWGN channel is evaluated in terms of the probability of error. The various modulation methods are compared on the basis of their performance characteristics, their bandwidth requirements and their implementation complexity.

## 7.1 GEOMETRIC REPRESENTATION OF SIGNAL WAVEFORMS

The Gram-Schmidt orthogonalization procedure may be used to construct an orthonormal basis for a set of signals. In this section, we develop a geometric representation of signal waveforms as points in a signal space. Such a representation provides a compact characterization of signal sets for transmitting information over a channel and simplifies the analysis of their performance. Using vector representation, waveform communication channels are represented by vector channels. This reduces the complexity of analysis considerably.

Suppose we have a set of  $M$  signal waveforms  $s_m(t)$ ,  $1 \leq m \leq M$  which are to be used for transmitting information over a communication channel. From the set of  $M$  waveforms, we first construct a set of  $N \leq M$  orthonormal waveforms, where  $N$  is the dimension of the signal space. For this purpose, we use the Gram-Schmidt orthogonalization procedure.

**Gram-Schmidt Orthogonalization Procedure.** We begin with the first waveform  $s_1(t)$ , which is assumed to have energy  $\mathcal{E}_1$ . The first waveform of the orthonormal set is constructed simply as

$$\psi_1(t) = \frac{s_1(t)}{\sqrt{\mathcal{E}_1}} \quad (7.1.1)$$

Thus,  $\psi_1(t)$  is simply  $s_1(t)$  normalized to unit energy.

The second waveform is constructed from  $s_2(t)$  by first computing the projection of  $s_2(t)$  onto  $\psi_1(t)$ , which is

$$c_{21} = \int_{-\infty}^{\infty} s_2(t)\psi_1(t) dt \quad (7.1.2)$$

Then,  $c_{21}\psi_1(t)$  is subtracted from  $s_2(t)$  to yield

$$d_2(t) = s_2(t) - c_{21}\psi_1(t) \quad (7.1.3)$$

Now,  $d_2(t)$  is orthogonal to  $\psi_1(t)$ , but it does not possess unit energy. If  $\mathcal{E}_2$  denotes the energy in  $d_2(t)$ , then the energy normalized waveform that is orthogonal to  $\psi_1(t)$  is

$$\psi_2(t) = \frac{d_2(t)}{\sqrt{\mathcal{E}_2}} \quad (7.1.4)$$

$$\mathcal{E}_2 = \int_{-\infty}^{\infty} d_2^2(t) dt \quad (7.1.5)$$

In general, the orthogonalization of the  $k$ th function leads to

$$\psi_k(t) = \frac{d_k(t)}{\sqrt{\mathcal{E}_k}} \quad (7.1.6)$$

where

$$d_k(t) = s_k(t) - \sum_{i=1}^{k-1} c_{ki} \psi_i(t) \quad (7.1.7)$$

$$\mathcal{E}_k = \int_{-\infty}^{\infty} d_k^2(t) dt \quad (7.1.8)$$

and

$$c_{ki} = \int_{-\infty}^{\infty} s_k(t) \psi_i(t) dt, \quad i = 1, 2, \dots, k-1 \quad (7.1.9)$$

Thus, the orthogonalization process is continued until all the  $M$  signal waveforms  $\{s_m(t)\}$  have been exhausted and  $N \leq M$  orthonormal waveforms have been constructed. The  $N$  orthonormal waveforms  $\{\psi_n(t)\}$  form a *basis* in the  $N$ -dimensional signal space. The dimensionality  $N$  of the signal space will be equal to  $M$  if all the  $M$  signal waveforms are linearly independent; i.e., if none of the signal waveforms is a linear combination of the other signal waveforms.

#### Example 7.1.1

Let us apply the Gram-Schmidt procedure to the set of four waveforms illustrated in Figure 7.1(a). The waveform  $s_1(t)$  has energy  $\mathcal{E}_1 = 2$ , so that  $\psi_1(t) = s_1(t)/\sqrt{2}$ . Next we observe that  $c_{21} = 0$ , so that  $\psi_1(t)$  and  $s_2(t)$  are orthogonal. Therefore,  $\psi_2(t) = s_2(t)/\sqrt{\mathcal{E}_2} = s_2(t)/\sqrt{2}$ . To obtain  $\psi_3(t)$ , we compute  $c_{31}$  and  $c_{32}$ , which are  $c_{31} = 0$  and  $c_{32} = -\sqrt{2}$ . Hence,

$$d_3(t) = s_3(t) + \sqrt{2}\psi_2(t)$$

Since  $d_3(t)$  has unit energy, it follows that  $\psi_3(t) = d_3(t)$ . Finally, we find that  $c_{41} = \sqrt{2}$ ,  $c_{42} = 0$ ,  $c_{43} = 1$ . Hence,

$$d_4(t) = s_4(t) - \sqrt{2}\psi_1(t) - \psi_3(t) = 0$$

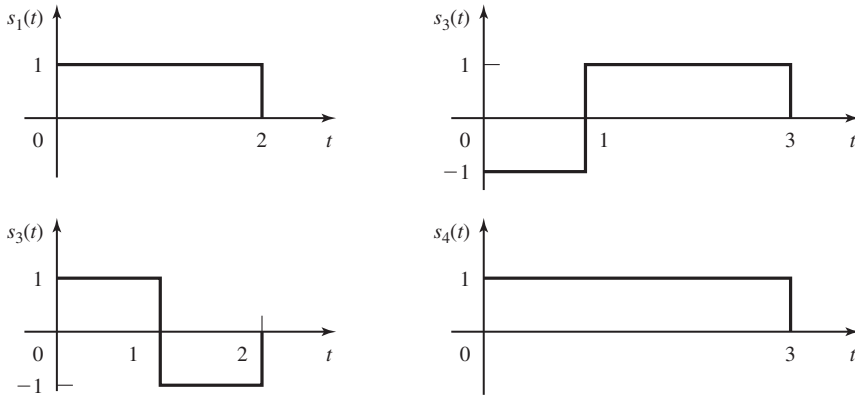
Thus,  $s_4(t)$  is a linear combination of  $\psi_1(t)$  and  $\psi_3(t)$  and, consequently, the dimensionality of the signal set is  $N = 3$ . The functions  $\psi_1(t)$ ,  $\psi_2(t)$ , and  $\psi_3(t)$  are shown in Figure 7.1(b)

Once we have constructed the set of orthogonal waveforms  $\{\psi_n(t)\}$ , we can express the  $M$  signals  $\{s_m(t)\}$  as exact linear combinations of the  $\{\psi_n(t)\}$ . Hence, we may write

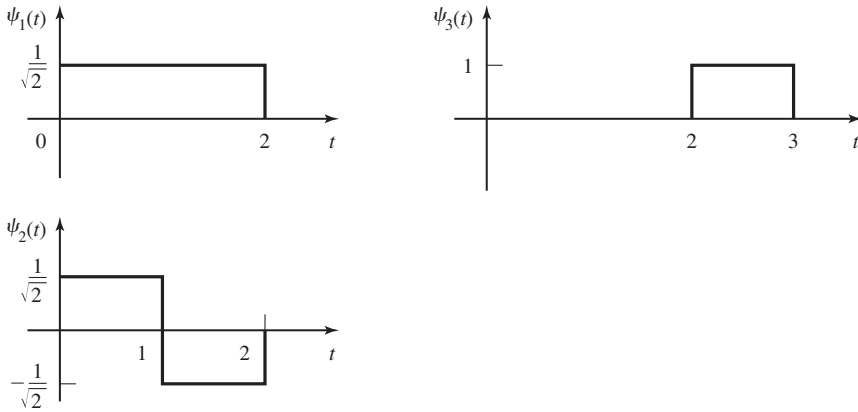
$$s_m(t) = \sum_{n=1}^N s_{mn} \psi_n(t), \quad m = 1, 2, \dots, M \quad (7.1.10)$$

where

$$s_{mn} = \int_{-\infty}^{\infty} s_m(t) \psi_n(t) dt$$



(a) Original signal set



(b) Orthonormal waveforms

**Figure 7.1** Application of Gram-Schmidt orthogonalization procedure to signals  $\{s_i(t)\}$ .

and

$$\mathcal{E}_m = \int_{-\infty}^{\infty} s_m^2(t) dt = \sum_{n=1}^N s_{mn}^2 \quad (7.1.11)$$

Based on the expression in Equation (7.1.7), each signal waveform may be represented by the vector

$$\mathbf{s}_m = (s_{m1}, s_{m2}, \dots, s_{mN}) \quad (7.1.12)$$

or equivalently, as a point in  $N$ -dimensional signal space with coordinates  $\{s_{mi}, i = 1, 2, \dots, N\}$ . The energy of the  $m$ th signal waveform is simply the square of the length of the vector or, equivalently, the square of the Euclidean distance from the origin to the point in the  $N$ -dimensional space. We can also show that the inner product of two

signals is equal to the inner product of their vector representations; i.e.,

$$\int_{-\infty}^{\infty} s_m(t)s_n(t) dt = \mathbf{s}_m \cdot \mathbf{s}_n \quad (7.1.13)$$

Thus, any  $N$ -dimensional signal can be represented geometrically as a point in the signal space spanned by the  $N$  orthonormal functions  $\{\psi_n(t)\}$ .

### Example 7.1.2

Let us determine the vector representation of the four signals shown in Figure 7.1(a) by using the orthonormal set of functions in Figure 7.1(b). Since the dimensionality of the signal space is  $N = 3$ , each signal is described by three components, which are obtained by projecting each of the four signal waveforms on the three orthonormal basis functions  $\psi_1(t)$ ,  $\psi_2(t)$ ,  $\psi_3(t)$ . Thus, we obtain  $\mathbf{s}_1 = (\sqrt{2}, 0, 0)$ ,  $\mathbf{s}_2 = (0, \sqrt{2}, 0)$ ,  $\mathbf{s}_3 = (0, -\sqrt{2}, 1)$ ,  $\mathbf{s}_4 = (\sqrt{2}, 0, 1)$ . These signal vectors are shown in Figure 7.2.

Finally, we should observe that the set of basis functions  $\{\psi_n(t)\}$  obtained by the Gram-Schmidt procedure is not unique. For example, another set of basis functions that span the three-dimensional space is shown in Figure 7.3. For this basis, the signal

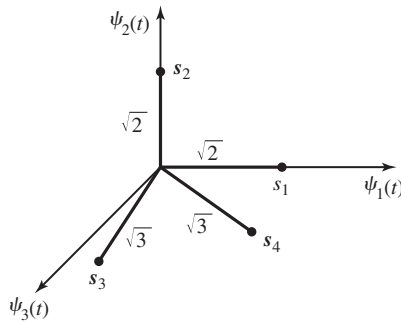


**Figure 7.2** Signal vectors corresponding to the signals  $s_i(t)$ ,  $i = 1, 2, 3, 4$ .

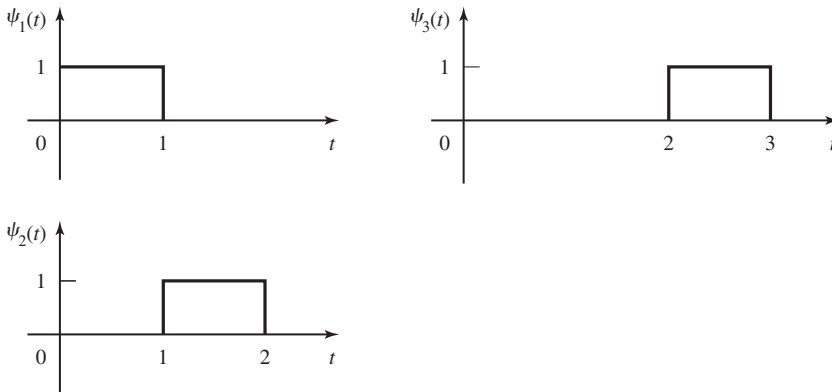


**Figure 7.3** Alternate set of basis functions.

vectors are  $\mathbf{s}_1 = (1, 1, 0)$ ,  $\mathbf{s}_2 = (1, -1, 0)$ ,  $\mathbf{s}_3 = (-1, 1, 1)$ , and  $\mathbf{s}_4 = (1, 1, 1)$ . The reader should note that the change in the basis functions does not change the dimensionality of the space  $N$ , the lengths (energies) of the signal vectors, or the inner product of any two vectors.

Although the Gram-Schmidt orthogonalization procedure is guaranteed to generate an orthonormal basis for representation of the signal set, in many cases it is simpler to use a method based on inspection to generate the orthonormal basis. We explore this method in the problems at the end of this chapter.

## 7.2 PULSE AMPLITUDE MODULATION

In *pulse amplitude modulation (PAM)*, the information is conveyed by the amplitude of the transmitted signal. Let us first consider PAM signals that are appropriate for baseband channels.

**Baseband Signals.** Binary PAM is the simplest digital modulation method. In binary PAM, the information bit 1 may be represented by a pulse of amplitude  $A$  and the information bit 0 is represented by a pulse of amplitude  $-A$ , as shown in Figure 7.4. This type of signaling is also called *binary antipodal signaling*. Pulses are transmitted at a bit rate  $R_b = 1/T_b$  bits/sec, where  $T_b$  is called the bit interval. Although the pulses are shown as rectangular, in practical systems, the rise time and decay time are nonzero and the pulses are generally smoother. The pulse shape determines the spectral characteristics of the transmitted signal as described in Chapter 8.

The generalization of PAM to nonbinary ( $M$ -ary) pulse transmission is relatively straightforward. Instead of transmitting one bit at a time, the binary information sequence is subdivided into blocks of  $k$  bits, called *symbols*, and each block, or symbol, is represented by one of  $M = 2^k$  pulse amplitude values. Thus with  $k = 2$ , we have  $M = 4$  pulse amplitude values. Figure 7.5 illustrates the PAM signals for  $k = 2$ ,  $M = 4$ . Note that when the bit rate  $R_b$  is fixed, the symbol interval is

$$T = \frac{k}{R_b} = kT_b \quad (7.2.1)$$

as shown in Figure 7.6.

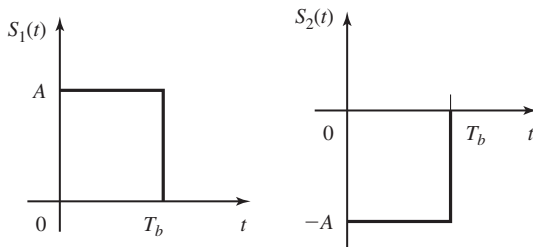


**Figure 7.4** Binary PAM signals.



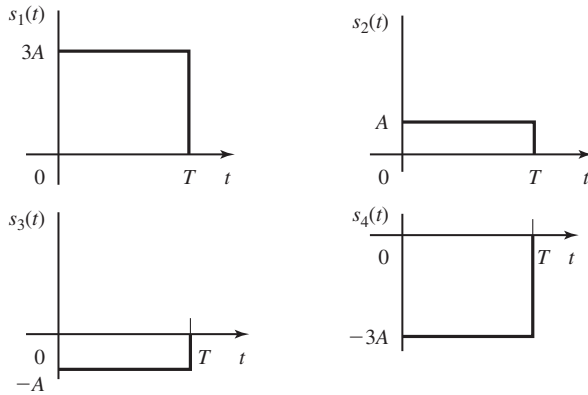


**Figure 7.5**  $M = 4$  PAM signal waveforms.

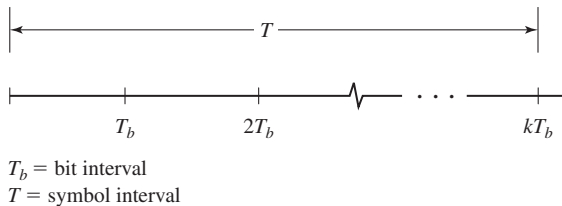
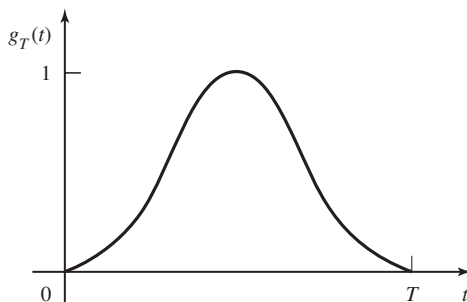


**Figure 7.6** Relationship between the symbol interval and the bit interval.

We may characterize the PAM signals in terms of their basic properties. In general, the  $M$ -ary PAM signal waveforms may be expressed as

$$s_m(t) = A_m g_T(t), \quad m = 1, 2, \dots, M, \quad 0 \leq t \leq T \quad (7.2.2)$$

where  $g_T(t)$  is a pulse of some arbitrary shape as shown for example in Figure 7.7. We observe that the distinguishing feature among the  $M$  signals is the signal amplitude. All the  $M$  signals have the same pulse shape. Another important feature of these signals is



(a)

**Figure 7.7** Signal pulse for PAM.

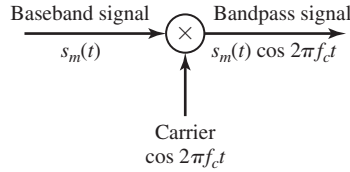


**Figure 7.8** Amplitude modulates sinusoidal carrier by the baseband signal.

their energies. We note the signals have different energies; i.e.,

$$\mathcal{E}_m = \int_0^T s_m^2(t) dt = A_m^2 \int_0^T g_T^2(t) dt = A_m^2 \mathcal{E}_g, \quad m = 1, 2, \dots, M \quad (7.2.3)$$

where  $\mathcal{E}_g$  is the energy of the signal pulse  $g_T(t)$ .

**Bandpass Signals.** To transmit the digital signal waveforms through a bandpass channel by amplitude modulation, the baseband signal waveforms  $s_m(t)$ ,  $m = 1, 2, \dots, M$  are multiplied by a sinusoidal carrier of the form  $\cos 2\pi f_c t$ , as shown in Figure 7.8, where  $f_c$  is the carrier frequency and corresponds to the center frequency in the passband of the channel. Thus, the transmitted signal waveforms may be expressed as

$$u_m(t) = A_m g_T(t) \cos 2\pi f_c t, \quad m = 1, 2, \dots, M \quad (7.2.4)$$

As previously described in Section 3.2, amplitude modulation of the carrier  $\cos 2\pi f_c t$  by the baseband signal waveforms  $s_m(t) = A_m g_T(t)$ , shifts the spectrum of the baseband signal by an amount  $f_c$  and, thus places the signal into the passband of the channel. Recall that the Fourier transform of the carrier is  $[\delta(f - f_c) + \delta(f + f_c)]/2$ . Because multiplication of two signals in the time domain corresponds to the convolution of their spectra in the frequency domain, the spectrum of the amplitude-modulated signal given by Equation (7.2.4) is

$$U_m(f) = \frac{A_m}{2} [G_T(f - f_c) + G_T(f + f_c)] \quad (7.2.5)$$

Thus, the spectrum of the baseband signal  $s_m(t) = A_m g_T(t)$ , is shifted in frequency by an amount equal to the carrier frequency  $f_c$ . The result is a DSB-SC AM signal, as illustrated in Figure 7.9. The upper sideband of the carrier modulated signal is comprised of the frequency content of  $u_m(t)$  for  $|f| > f_c$ ; i.e., for  $f_c < |f| \leq f_c + W$ . The lower sideband of  $u_m(t)$  comprises the frequency content for  $|f| < f_c$ ; i.e., for  $f_c - W \leq |f| < f_c$ . Hence, the DSB-SC amplitude-modulated signal occupies a channel bandwidth of  $2W$ , which is twice the bandwidth required to transmit the baseband signal.

The energy of the bandpass signal waveforms  $u_m(t)$ ,  $m = 1, 2, \dots, M$ , given by Equation (7.2.4) is defined as

$$\begin{aligned} \mathcal{E}_m &= \int_{-\infty}^{\infty} u_m^2(t) dt = \int_{-\infty}^{\infty} A_m^2 g_T^2(t) \cos^2 2\pi f_c t dt \\ &= \frac{A_m^2}{2} \int_{-\infty}^{\infty} g_T^2(t) dt + \frac{A_m^2}{2} \int_{-\infty}^{\infty} g_T^2(t) \cos 4\pi f_c t dt \end{aligned} \quad (7.2.6)$$

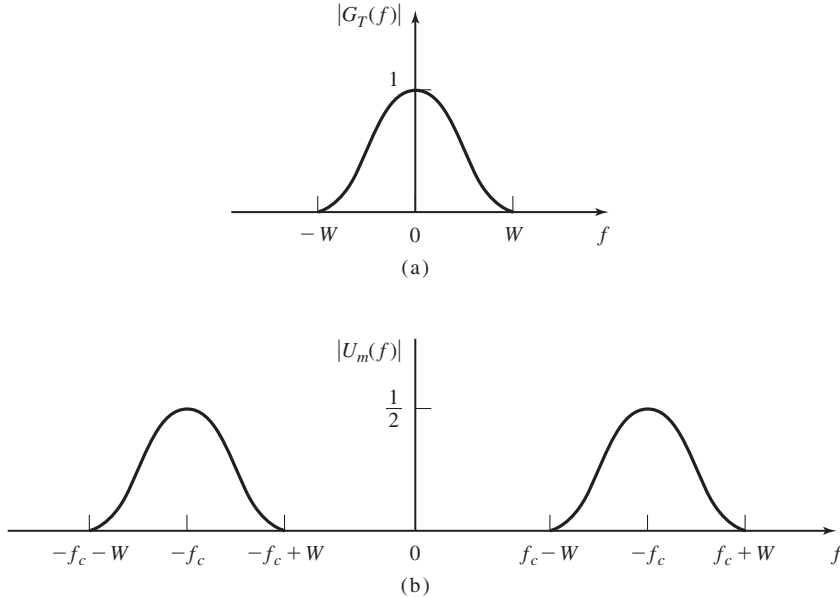


**Figure 7.9** Spectra of (a) baseband and (b) amplitude-modulated signals.

We note that when  $f_c \gg W$ , the term

$$\int_{-\infty}^{\infty} g_T^2(t) \cos 4\pi f_c t \, dt \quad (7.2.7)$$

involves the integration of the product of a slowly varying function, namely  $g_T^2(t)$ , with a rapidly varying sinusoidal term, namely  $\cos 4\pi f_c t$  as shown in Figure 7.10. Because  $g_T(t)$  is slowly varying relative to  $\cos 4\pi f_c t$ , the integral in Equation (7.2.7) over a single cycle of  $\cos 4\pi f_c t$  is zero and, hence, the integral over an arbitrary number of cycles is also zero. Consequently,

$$\mathcal{E}_m = \frac{A_m^2}{2} \int_{-\infty}^{\infty} g_T^2(t) \, dt = \frac{A_m^2}{2} \mathcal{E}_g \quad (7.2.8)$$

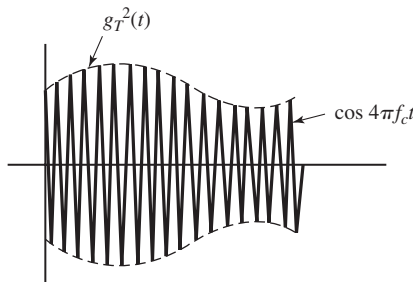


**Figure 7.10** The signal  $g_T^2(t) \cos 4\pi f_c t$ .

where  $\mathcal{E}_g$  is the energy in the signal pulse  $g_T(t)$ . Thus, we have shown that the energy in the bandpass signal is one-half of the energy in the baseband signal. The scale factor of  $\frac{1}{2}$  is due to the carrier component  $\cos 2\pi f_c t$ , which has an average power of  $\frac{1}{2}$ .

When the transmitted pulse shape  $g_T(t)$  is rectangular; i.e.,

$$g_T(t) = \begin{cases} \sqrt{\frac{\mathcal{E}_g}{T}} & 0 \leq t \leq T \\ 0, & \text{otherwise} \end{cases} \quad (7.2.9)$$

the amplitude-modulated carrier signal is usually called *amplitude-shift keying (ASK)*.

**Geometric Representation of PAM Signals.** The baseband signal waveforms for  $M$ -ary PAM are given in Equation (7.2.2), where  $M = 2^k$ , and  $g_T(t)$  is a pulse with peak amplitude normalized to unity as previously illustrated in Figure 7.7.

The  $M$ -ary PAM waveforms are one-dimensional signals, which may be expressed as

$$s_m(t) = s_m \psi(t), \quad m = 1, 2, \dots, M \quad (7.2.10)$$

where the basis function  $\psi(t)$  is defined as

$$\psi(t) = \frac{1}{\sqrt{\mathcal{E}_g}} g_T(t), \quad 0 \leq t \leq T \quad (7.2.11)$$

$\mathcal{E}_g$  is the energy of the signal pulse  $g_T(t)$ , and the signal coefficients (one-dimensional vectors) are simply

$$s_m = \sqrt{\mathcal{E}_g} A_m, \quad m = 1, 2, \dots, M \quad (7.2.12)$$

An important parameter is the Euclidean distance between two signal points, which is defined as

$$d_{mn} = \sqrt{|s_m - s_n|^2} = \sqrt{\mathcal{E}_g (A_m - A_n)^2} \quad (7.2.13)$$

If we select the signal amplitudes  $\{A_m\}$  to be symmetrically spaced about zero and equally distant between adjacent signal amplitudes, we obtain the signal points for symmetric PAM, as shown in Figure 7.11.

We observe that the PAM signals have different energies. In particular, the energy of the  $m$ th signal is

$$\mathcal{E}_m = s_m^2 = \mathcal{E}_g A_m^2, \quad m = 1, 2, \dots, M \quad (7.2.14)$$

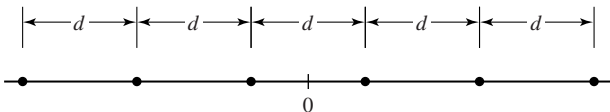


**Figure 7.11** Signal points (constellation) for symmetric PAM.

For equally probable signals, the average energy is

$$\mathcal{E}_{av} = \frac{1}{M} \sum_{m=1}^M \mathcal{E}_m = \frac{\mathcal{E}_g}{M} \sum_{m=1}^M A_m^2 \quad (7.2.15)$$

If the signal amplitudes are symmetric about the origin, then

$$A_m = (2m - 1 - M), \quad m = 1, 2, \dots, M \quad (7.2.16)$$

and, hence, the average energy is

$$\mathcal{E}_{av} = \frac{\mathcal{E}_g}{M} \sum_{m=1}^M (2m - 1 - M)^2 = \mathcal{E}_g(M^2 - 1)/3 \quad (7.2.17)$$

When the baseband PAM signals are impressed on a carrier, the basic geometric representation of the digital PAM signal waveforms remains the same. The bandpass signal waveforms  $u_m(t)$  may be expressed as

$$u_m(t) = s_m \psi(t) \quad (7.2.18)$$

where the basic signal waveform  $\psi(t)$  is defined as

$$\psi(t) = \sqrt{\frac{2}{\mathcal{E}_g}} g_T(t) \cos 2\pi f_c t \quad (7.2.19)$$

and

$$s_m = \sqrt{\frac{\mathcal{E}_g}{2}} A_m, \quad m = 1, 2, \dots, M \quad (7.2.20)$$

Note that the only change in the geometric representation of bandpass PAM signals, compared to baseband signals, is the scale factor  $\sqrt{2}$ , which appears in Equations (7.2.19) and (7.2.20).

## 7.3 TWO-DIMENSIONAL SIGNAL WAVEFORMS

As we observed, PAM signal waveforms are basically one-dimensional signals. In this section, we consider the construction of two-dimensional signals.

### 7.3.1 Baseband Signals

Let us begin with the construction of two orthogonal signals. Two signal waveforms  $s_1(t)$  and  $s_2(t)$  are said to be orthogonal over the interval  $(0, T)$  if

$$\int_0^T s_1(t)s_2(t) dt = 0 \quad (7.3.1)$$

Two examples of orthogonal signals are illustrated in Figure 7.12. Note that the two signals  $s_1(t)$  and  $s_2(t)$  completely overlap over the interval  $(0, T)$ , while the signals  $s'_1(t)$  and  $s'_2(t)$  are nonoverlapping in time. Both signal pairs satisfy the orthogonality

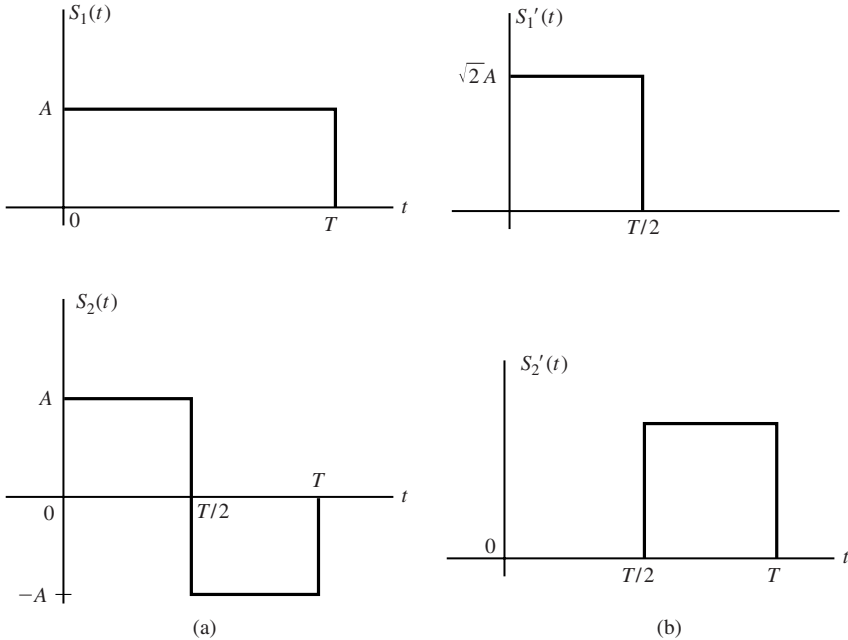


**Figure 7.12** Two sets of orthogonal signals.

property in Equation (7.3.1) and both signal pairs have identical energy; i.e.,

$$\mathcal{E} = \int_0^T s_1^2(t) dt = \int_0^T s_2^2(t) dt = \int_0^T [s_1'(t)]^2 dt = \int_0^T [s_2'(t)]^2 dt = A^2T \quad (7.3.2)$$

Either pair of these signals may be used to transmit binary information, with one signal waveform corresponding to a 1 and the other signal waveform conveying the information bit 0.

Geometrically, these signal waveforms can be represented as signal vectors in two-dimensional space. As basis functions, we may select the unit energy, rectangular functions

$$\psi_1(t) = \begin{cases} \sqrt{2/T}, & 0 \leq t \leq T/2 \\ 0, & \text{otherwise} \end{cases} \quad (7.3.3)$$

$$\psi_2(t) = \begin{cases} \sqrt{2/T}, & T/2 < t \leq T \\ 0, & \text{otherwise} \end{cases}$$

Then, the signal waveforms  $s_1(t)$  and  $s_2(t)$  shown in Figure 7.12(a) can be expressed as

$$\begin{aligned} s_1(t) &= s_{11}\psi_1(t) + s_{12}\psi_2(t) \\ s_2(t) &= s_{21}\psi_1(t) + s_{22}\psi_2(t) \end{aligned} \quad (7.3.4)$$

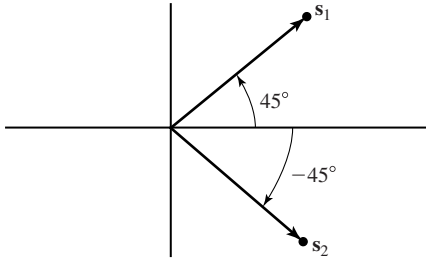


**Figure 7.13** The two signal vectors corresponding to the signals waveforms  $s_1(t)$  and  $s_2(t)$ .

where

$$\mathbf{s}_1 = (s_{11}, s_{12}) = (A\sqrt{T/2}, A\sqrt{T/2}) \quad (7.3.5)$$

$$\mathbf{s}_2 = (s_{21}, s_{22}) = (A\sqrt{T/2}, -A\sqrt{T/2})$$

The signal vectors  $\mathbf{s}_1$  and  $\mathbf{s}_2$  are illustrated in Figure 7.13. Note that the signal vectors are separated by  $90^\circ$ , so that they are orthogonal. Furthermore, the square of the length of each vector gives the energy in each signal; i.e.,

$$\mathcal{E}_1 = \|\mathbf{s}_1\|^2 = A^2T \quad (7.3.6)$$

$$\mathcal{E}_2 = \|\mathbf{s}_2\|^2 = A^2T$$

The Euclidean distance between the two signals is

$$d_{12} = \sqrt{\|\mathbf{s}_1 - \mathbf{s}_2\|^2} = A\sqrt{2T} = \sqrt{2A^2T} = \sqrt{2\mathcal{E}} \quad (7.3.7)$$

where  $\mathcal{E} = \mathcal{E}_1 = \mathcal{E}_2$  is the signal energy.

Similarly, the pair of orthogonal signals shown in Figure 7.12(b) can be expressed as in Equation (7.3.4), where

$$\mathbf{s}'_1 = (A\sqrt{T}, 0) = (\sqrt{\mathcal{E}}, 0) \quad (7.3.8)$$

$$\mathbf{s}'_2 = (0, A\sqrt{T}) = (0, \sqrt{\mathcal{E}})$$

These two signal vectors are illustrated in Figure 7.14. Note that  $\mathbf{s}'_1$  and  $\mathbf{s}'_2$  are related to the signal vectors shown in Figure 7.13 by a simple  $45^\circ$  rotation. Hence, the Euclidean

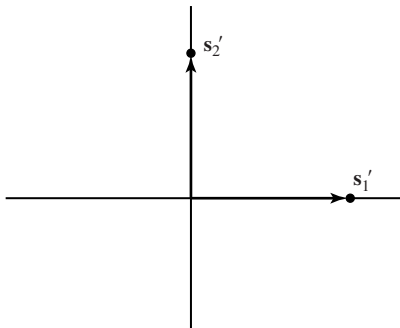


**Figure 7.14** The two signal vectors corresponding to the signal waveforms  $s'_1(t)$  and  $s'_2(t)$ .

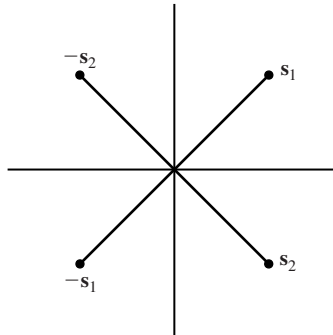


**Figure 7.15** Signal constellation for  $M = 4$  biorthogonal signals.

distance between the signal points  $s'_1$  and  $s'_2$  is identical to that for signal points  $s_1$  and  $s_2$ .

Suppose that we wish to construct four signal waveforms in two dimensions. With four signal waveforms, we can transmit two information bits in a signaling interval of length  $T$ . If we begin with the two orthogonal signals  $s_1(t)$  and  $s_2(t)$ , shown in Figure 7.12(a), and their corresponding vector representation in Figure 7.13, it is easy to see that a simple construction is one that adds two additional signal vectors, namely,  $-s_1$  and  $-s_2$ . Thus, we obtain the 4-point signal-point constellation shown in Figure 7.15, which corresponds to the analog signal waveforms  $s_1(t)$ ,  $s_2(t)$ ,  $-s_1(t)$ , and  $-s_2(t)$ . Since the pair  $s_1(t)$  and  $s_2(t)$  are orthogonal and the pair  $-s_1(t)$  and  $-s_2(t)$  are orthogonal, the signal set consisting of the four signal waveforms is called a set of *biorthogonal signals*.

The procedure for constructing a larger set of signal waveforms is relatively straightforward. Specifically, we can add additional signal points (signal vectors) in the two-dimensional plane, and construct the corresponding signal waveforms by using the two orthonormal basis functions  $\psi_1(t)$  and  $\psi_2(t)$  given by Equation (7.3.3). For example, suppose we wish to construct  $M = 8$  two-dimensional signal waveforms, all of equal energy  $\mathcal{E}$ . These eight signal points are illustrated in Figure 7.16, and allow us to transmit three bits at a time. The corresponding eight signal waveforms are the two sets of biorthogonal signal waveforms constructed from the two pairs of orthogonal signals shown in Figure 7.12.

Alternatively, suppose that we remove the condition that all eight waveforms have equal energy. For example, suppose that we select four biorthogonal waveforms

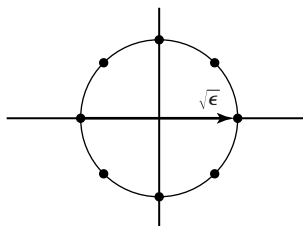


**Figure 7.16**  $M = 8$  signal-point constellation corresponding to the two points of orthogonal signal waveforms in Figure 7.12 and their negatives, i.e.,  $s_1(t)$ ,  $s_2(t)$ ,  $s'_1(t)$ ,  $s'_2(t)$ ,  $-s_1(t)$ ,  $-s_2(t)$ ,  $-s'_1(t)$  and  $-s'_2(t)$ .



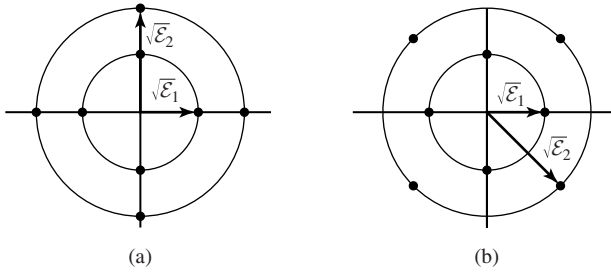


**Figure 7.17** Two  $M = 8$  signal-point constellations in two dimensions, corresponding to a superposition of two sets of biorthogonal signal waveforms with different energies.

that have energy  $\mathcal{E}_1$  and another four biorthogonal waveforms that have energy  $\mathcal{E}_2$ , where  $\mathcal{E}_2 > \mathcal{E}_1$ . Two possible eight signal-point constellations are shown in Figure 7.17, where the signal points are located on two concentric circles of radii  $\sqrt{\mathcal{E}_1}$  and  $\sqrt{\mathcal{E}_2}$ . In Section 7.6.5 we show that the signal set in Figure 7.17(b) is preferable in an AWGN channel to that shown in Figure 7.17(a).

### 7.3.2 Two-dimensional Bandpass Signals—Carrier-Phase Modulation

In the case of PAM, we recall that bandpass signal waveforms, appropriate for transmission on bandpass channels, were generated by taking a set of baseband signals and impressing them on a carrier. In a similar manner, if we have a set of  $M$  two-dimensional signal waveforms, say  $s_m(t)$ ,  $m = 1, 2, \dots, M$ , we can generate a set of  $M$  bandpass signal waveforms as

$$u_m(t) = s_m(t) \cos 2\pi f_c t, \quad m = 1, 2, \dots, M, \quad 0 \leq t \leq T \quad (7.3.9)$$

In this section, we consider the special case in which the  $M$  two-dimensional bandpass signals waveforms are constrained to have the same energy; i.e.,

$$\begin{aligned} \mathcal{E}_m &= \int_0^T u_m^2(t) dt = \int_0^T s_m^2(t) \cos^2 2\pi f_c t dt \\ &= \frac{1}{2} \int_0^T s_m^2(t) dt + \frac{1}{2} \int_0^T s_m^2(t) \cos 4\pi f_c t dt \end{aligned} \quad (7.3.10)$$

As indicated previously, the integral of the double-frequency component in Equation (7.3.10) averages to zero when  $f_c \gg W$ , where  $W$  is the bandwidth of the baseband signal  $s_m(t)$ . Hence,

$$\mathcal{E}_m = \frac{1}{2} \int_0^T s_m^2(t) dt = \mathcal{E}_s \quad \text{for all } m \quad (7.3.11)$$

where  $\mathcal{E}_s$  denotes the energy/signal or/symbol.

As we indicated in the discussion following Equation (7.1.12), when all the signal waveforms have the same energy, the corresponding signal points in the geometric representation of the signal waveforms fall on a circle of radius  $\sqrt{\mathcal{E}_s}$ . For example, in the case of the four biorthogonal waveforms, the signal points are as shown in Figure 7.15 or, equivalently, any phase-rotated version of these signal points.

From this geometric representation for  $M = 4$ , we observe that the signal points are equivalent to a single signal whose phase is shifted by multiples of  $\pi/2$ . That is, a bandpass signal of the form  $s(t) \cos(2\pi f_c t + \pi m/2)$ ,  $m = 0, 1, 2, 3$ , has the same geometric representation as an  $M = 4$  general biorthogonal signal set. Therefore, a simple way to generate a set of  $M$  bandpass signals having equal energy is to impress the information on the phase of the carrier. Thus, we have a carrier-phase modulated signal.

The general representation of a set of  $M$  carrier-phase modulated signal waveforms is

$$u_m(t) = g_T(t) \cos\left(2\pi f_c t + \frac{2\pi m}{M}\right), \quad m = 0, 1, \dots, M-1, \quad 0 \leq t \leq T \quad (7.3.12)$$

where  $g_T(t)$  is a baseband pulse shape, which determines the spectral characteristics of the transmitted signal, as will be demonstrated in Chapter 8. When  $g_T(t)$  is a rectangular pulse, defined as

$$g_T(t) = \sqrt{\frac{2\mathcal{E}_s}{T}}, \quad 0 \leq t \leq T \quad (7.3.13)$$

the corresponding transmitted signal waveforms

$$u_m(t) = \sqrt{\frac{2\mathcal{E}_s}{T}} \cos\left(2\pi f_c t + \frac{2\pi m}{M}\right), \quad m = 0, 1, \dots, M-1, \quad 0 \leq t \leq T \quad (7.3.14)$$

have a constant envelope (the pulse shape  $g_T(t)$  is a rectangular pulse) and the carrier phase changes abruptly at the beginning of each signal interval. This type of digital-phase modulation is called *phase-shift keying* (PSK). Figure 7.18 illustrates a four-phase ( $M = 4$ ) PSK signal waveform, usually called a quadrature PSK (QPSK) signal.

By viewing the angle of the cosine function in Equation (7.3.14) as the sum of two angles, we may express the waveforms in Equation (7.3.14) as

$$u_m(t) = g_T(t) A_{mc} \cos 2\pi f_c t - g_T(t) A_{ms} \sin 2\pi f_c t \quad (7.3.15)$$

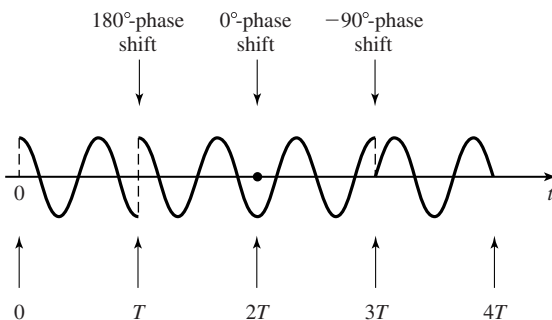


**Figure 7.18** Example of a four PSK signal.

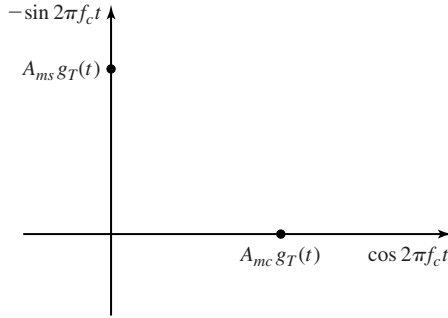


**Figure 7.19** Digital-phase modulation viewed as two amplitude-modulated quadrature carriers.

where

$$A_{mc} = \cos 2\pi m/M, \quad m = 0, 1, \dots, M - 1 \tag{7.3.16}$$

$$A_{ms} = \sin 2\pi m/M, \quad m = 0, 1, \dots, M - 1$$

Thus, a phase-modulated signal may be viewed as two quadrature carriers with amplitudes  $g_T(t)A_{mc}$  and  $g_T(t)A_{ms}$  as shown in Figure 7.19, which depend on the transmitted phase in each signal interval.

It follows from Equation (7.3.15) that digital phase-modulated signals can be represented geometrically as two-dimensional vectors with components  $\sqrt{\mathcal{E}_s} \cos 2\pi m/M$ , and  $\sqrt{\mathcal{E}_s} \sin 2\pi m/M$ , i.e.,

$$\mathbf{s}_m = (\sqrt{\mathcal{E}_s} \cos 2\pi m/M, \quad \sqrt{\mathcal{E}_s} \sin 2\pi m/M) \tag{7.3.17}$$

Note that the orthogonal basis functions are  $\psi_1(t) = \sqrt{\frac{2}{\mathcal{E}_g}} g_T(t) \cos 2\pi f_c t$ , and  $\psi_2(t) = -\sqrt{\frac{2}{\mathcal{E}_g}} g_T(t) \sin 2\pi f_c t$ . Signal-point constellations for  $M = 2, 4, 8$  are illustrated in Figure 7.20. We observe that binary-phase modulation is identical to binary PAM.

The mapping or assignment of  $k$  information bits into the  $M = 2^k$  possible phases may be done in a number of ways. The preferred assignment is to use *Gray encoding*, in which adjacent phases differ by one binary digit as illustrated in Figure 7.20. Because

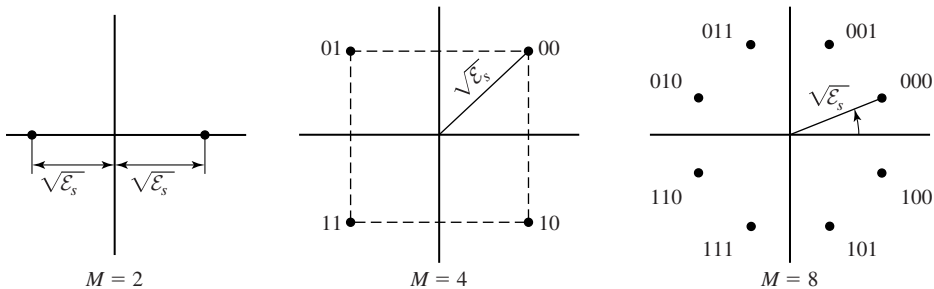


**Figure 7.20** PSK signal constellations.

the most likely errors caused by noise involve the erroneous selection of an adjacent phase to the transmitted phase, only a single bit error occurs in the  $k$ -bit sequence with Gray encoding.

The Euclidean distance between any two signal points in the constellation is

$$\begin{aligned} d_{mn} &= \sqrt{\|\mathbf{s}_m - \mathbf{s}_n\|^2} \\ &= \sqrt{2\mathcal{E}_s \left(1 - \cos \frac{2\pi(m-n)}{M}\right)} \end{aligned} \quad (7.3.18)$$

and the minimum Euclidean distance (distance between two adjacent signal points) is simply

$$d_{\min} = \sqrt{2\mathcal{E}_s \left(1 - \cos \frac{2\pi}{M}\right)} \quad (7.3.19)$$

As we shall demonstrate in Equation (7.6.10), the minimum Euclidean distance  $d_{\min}$  plays an important role in determining the error-rate performance of the receiver that demodulates and detects the information in the presence of additive Gaussian noise.

### 7.3.3 Two-dimensional Bandpass Signals—Quadrature Amplitude Modulation

In our discussion of carrier-phase modulation, we observed that the bandpass signal waveforms may be represented as given by Equation (7.3.15), in which the signal waveforms are viewed as two orthogonal carrier signals,  $\cos 2\pi f_c t$  and  $\sin 2\pi f_c t$ , modulated by the information bits. However, the carrier-phase modulation signal waveforms are constrained to have equal energy  $\mathcal{E}_s$ , which implies that the signal points in the geometric representation of the signal waveforms lie on a circle of radius  $\sqrt{\mathcal{E}_s}$ . If we remove the constant energy restriction, we can construct signal waveforms that are not constrained to fall on a circle.

The simplest way to construct such signals is to impress separate information bits on each of the quadrature carriers,  $\cos 2\pi f_c t$  and  $\sin 2\pi f_c t$ . This type of digital modulation is called *quadrature amplitude modulation (QAM)*. We may view this method of information transmission as a form of quadrature-carrier multiplexing, previously described in Section 3.2.6.

The transmitted signal waveforms have the form

$$u_m(t) = A_{mc}g_T(t) \cos 2\pi f_c t + A_{ms}g_T(t) \sin 2\pi f_c t, \quad m = 1, 2, \dots, M \quad (7.3.20)$$

where  $\{A_{mc}\}$  and  $\{A_{ms}\}$  are the sets of amplitude levels that are obtained by mapping  $k$ -bit sequences into signal amplitudes. For example, Figure 7.21 illustrates a 16-QAM signal constellation that is obtained by amplitude modulating each quadrature carrier by  $M = 4$  PAM. In general, rectangular signal constellations result when two quadrature carriers are each modulated by PAM.

More generally, QAM may be viewed as a form of combined digital amplitude and digital-phase modulation. Thus, the transmitted QAM signal waveforms may be

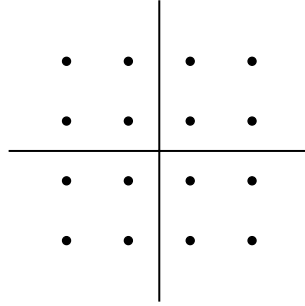


**Figure 7.21**  $M = 16$ -QAM signal constellation.

expressed as

$$u_{mn}(t) = A_m g_T(t) \cos(2\pi f_c t + \theta_n), \quad m = 1, 2, \dots, M_1 \quad (7.3.21)$$

$$n = 1, 2, \dots, M_2$$

If  $M_1 = 2^{k_1}$  and  $M_2 = 2^{k_2}$ , the combined amplitude- and phase-modulation method results in the simultaneous transmission of  $k_1 + k_2 = \log_2 M_1 M_2$  binary digits occurring at a symbol rate  $R_b/(k_1 + k_2)$ . Figure 7.22 illustrates the functional block diagram of a QAM modulator.

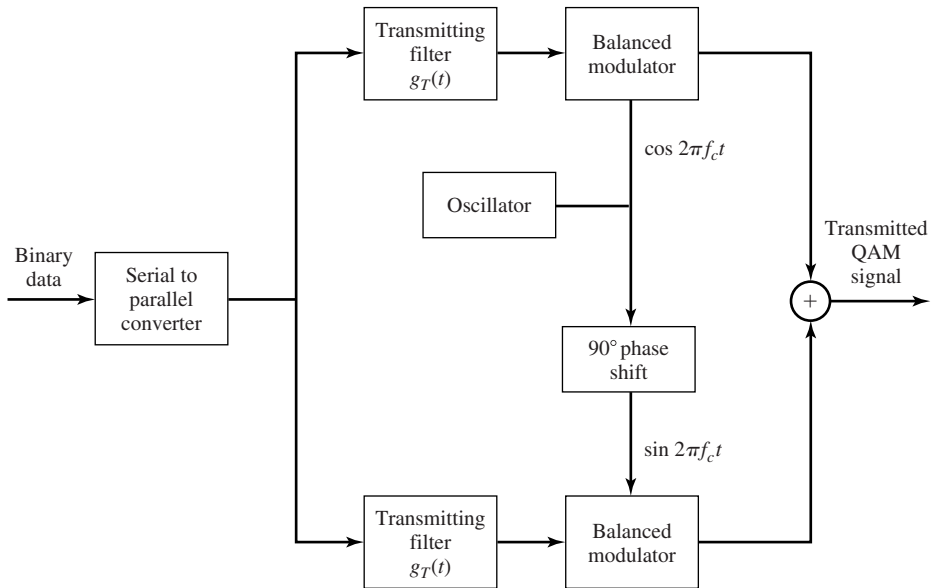


**Figure 7.22** Functional block diagram of modulator for QAM.

It is clear that the geometric signal representation of the signals given by Equations (7.3.20) and (7.3.21) is in terms of two-dimensional signal vectors of the form

$$s_m = (\sqrt{\mathcal{E}_s} A_{mc}, \sqrt{\mathcal{E}_s} A_{ms}), \quad m = 1, 2, \dots, M \quad (7.3.22)$$

Examples of signal space constellations for QAM are shown in Figure 7.23.

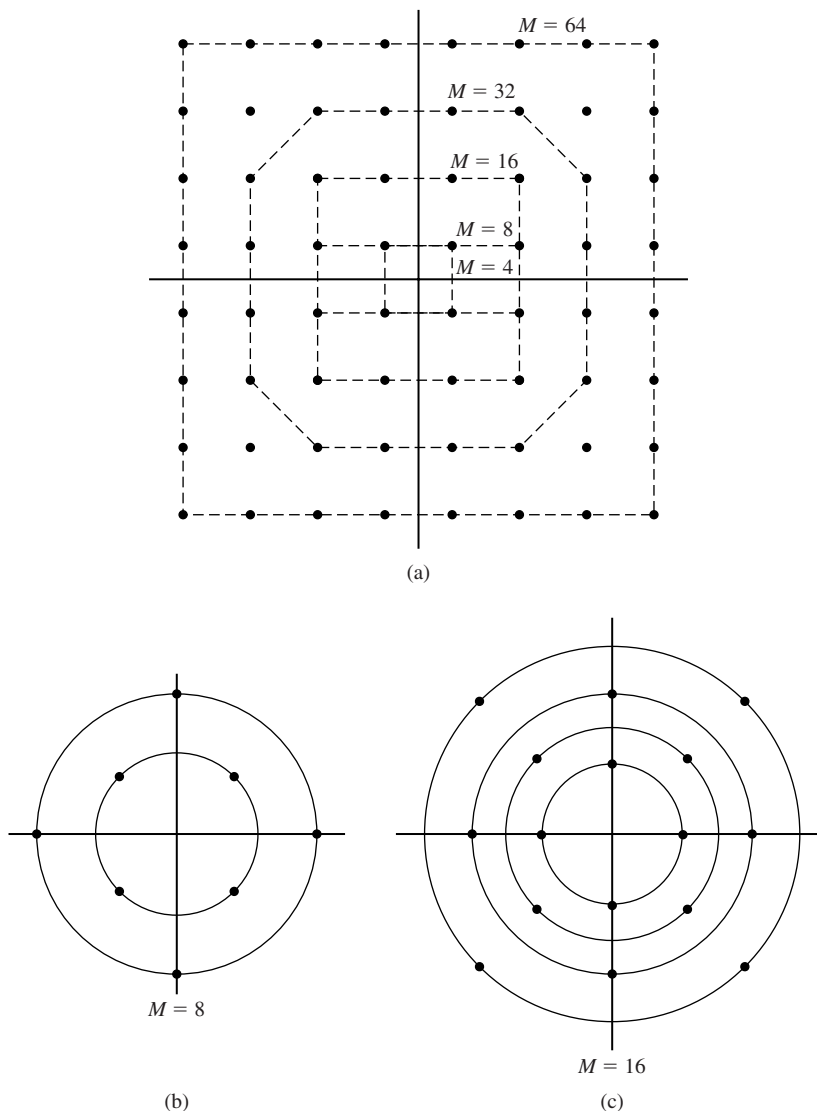


**Figure 7.23** (a) Rectangular signal-space constellations for QAM. (b, c) Examples of combined PAM-PSK signal-space constellations.

The average transmitted energy for these signal constellations is simply the sum of the average energies on each of the quadrature carriers. For rectangular signal constellations, as shown in Figure 7.23(a), the average energy/symbol is given by  $\mathcal{E}_{av} = \frac{1}{M} \sum_{i=1}^M \|\mathbf{s}_i\|^2$ . The Euclidean distance between any pair of signal points is

$$d_{mn} = \sqrt{\|\mathbf{s}_m - \mathbf{s}_n\|^2} \quad (7.3.23)$$

## 7.4 MULTIDIMENSIONAL SIGNAL WAVEFORMS

In the previous section, we observed that a number of signal waveforms, say  $M = 2^k$ , can be constructed in two dimensions. By transmitting any one of these  $M$  signal waveforms in a given interval of time, we convey  $k$  bits of information. In this section, we consider the design of a set of  $M = 2^k$  signal waveforms having more than two dimensions. We will show in Section 7.6.6 the advantages of using such multidimensional signal waveforms to transmit information.

We begin by constructing  $M$  signal waveforms that are mutually orthogonal, where each waveform has dimension  $N = M$ .

### 7.4.1 Orthogonal Signal Waveforms

First, we consider the construction of baseband orthogonal signals and, then, discuss the design of bandpass signals.

**Baseband Signals.** Orthogonal signal waveforms at baseband can be constructed in a variety of ways. Figure 7.24 illustrates two sets of  $M = 4$  orthogonal signal waveforms. We observe that the signal waveforms  $s_i(t)$ ,  $i = 1, 2, 3, 4$  completely overlap over the interval  $(0, T)$ , while the signal waveforms  $s'_i(t)$ ,  $i = 1, 2, 3, 4$  are nonoverlapping in time. These are just two examples of a set of  $M = 4$  orthogonal signal waveforms. In general, if we begin with a set of  $K$  baseband signal waveforms, we can use the Gram-Schmidt procedure to construct  $M \leq K$  mutually orthogonal signal waveforms. The  $M$  signal waveforms are simply the orthonormal signal waveforms  $\psi_i(t)$ ,  $i = 1, 2, \dots, M$ , obtained from the Gram-Schmidt procedure. For example, a set of  $M = 2^k$  overlapping orthogonal signal waveforms can be constructed from Hadamard sequences, also called Walsh-Hadamard sequences (see Problem 7.31).

When the  $M$  orthogonal signal waveforms are nonoverlapping in time, the digital information that is transmitted is conveyed by the time interval in which the signal pulse occupies. This type of signaling is usually called pulse position modulation (PPM). In this case, the  $M$  baseband signal waveforms may be expressed as

$$s_m(t) = A g_T(t - (m-1)T/M), \quad m = 1, 2, \dots, M \quad (7.4.1)$$

$$(m-1)T/M \leq t \leq mT/M$$

where  $g_T(t)$  is a signal pulse of duration  $T/M$  and of arbitrary shape.

Although each signal waveform in a set of  $M$  orthogonal signal waveforms may be designed to have different energy, it is desirable for practical reasons that all  $M$  signal waveforms have the same energy. For example, in the case of  $M$  PPM signals

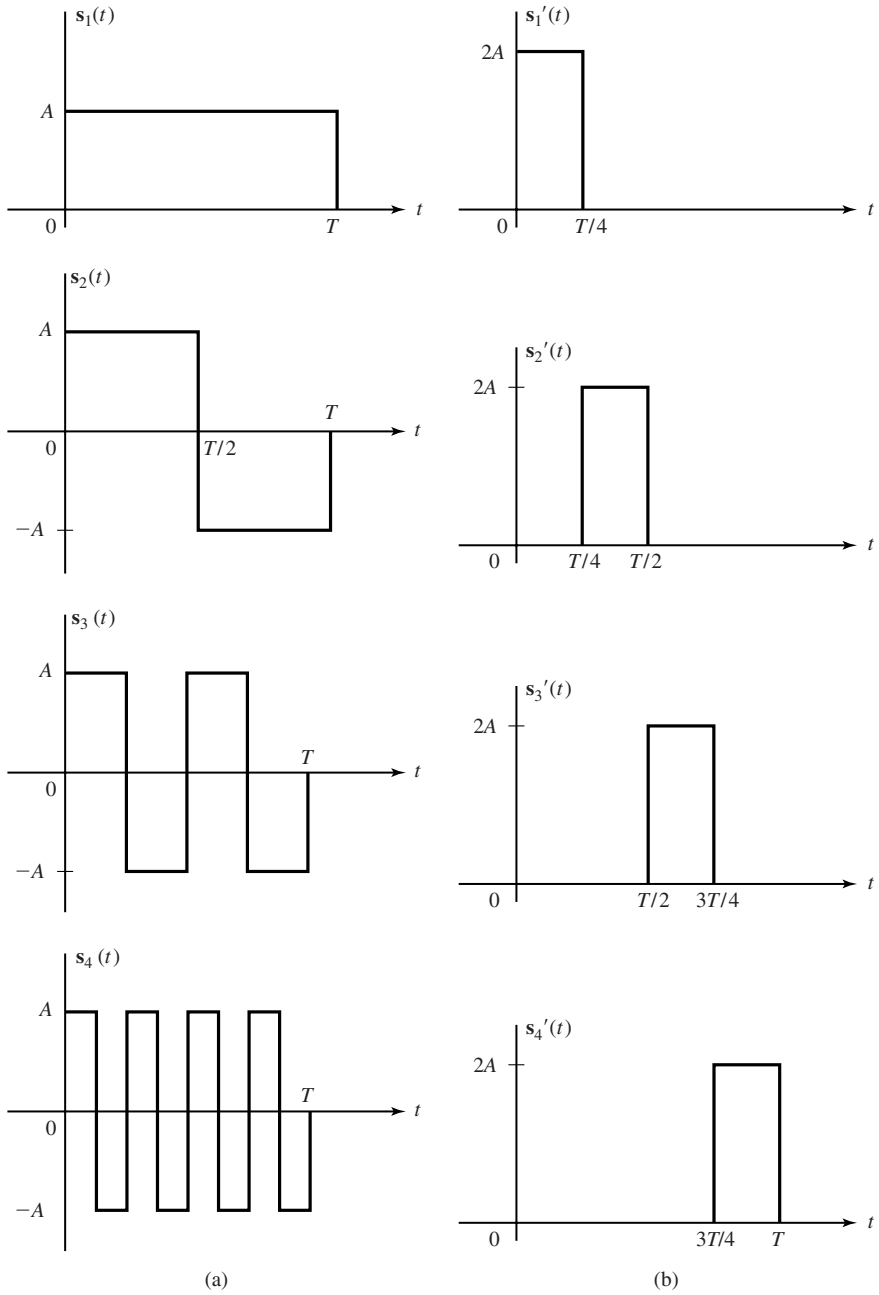


**Figure 7.24** Two sets of  $M = 4$  orthogonal signal waveforms.



(nonoverlapping signal pulses of duration  $T/M$ ), all signal waveforms have the same amplitude  $A$  and, hence,

$$\begin{aligned} \int_0^T s_m^2(t) dt &= A^2 \int_{(m-1)T/M}^{mT/M} g_T^2(t - (m-1)T/M) dt \\ &= A^2 \int_0^{T/M} g_T^2(t) dt = \mathcal{E}_s, \quad \text{all } m \end{aligned} \quad (7.4.2)$$

The geometric representation of PPM signal waveforms is relatively simple. We define the  $M$  basis functions as

$$\psi_m(t) = \begin{cases} \frac{1}{\sqrt{\mathcal{E}_s}} g(t - (m-1)T/M), & (m-1)T/M \leq t \leq mT/M \\ 0, & \text{otherwise} \end{cases} \quad (7.4.3)$$

for  $m = 1, 2, \dots, M$ . Hence,  $M$ -ary PPM signal waveforms are represented geometrically by the  $M$ -dimensional vectors.

$$\begin{aligned} \mathbf{s}_1 &= (\sqrt{\mathcal{E}_s}, 0, 0, \dots, 0) \\ \mathbf{s}_2 &= (0, \sqrt{\mathcal{E}_s}, 0, \dots, 0) \\ &\vdots \\ \mathbf{s}_M &= (0, 0, 0, \dots, \sqrt{\mathcal{E}_s}) \end{aligned} \quad (7.4.4)$$

Clearly, these vectors are orthogonal; i.e.,  $\mathbf{s}_i \cdot \mathbf{s}_j = 0$  when  $i \neq j$ . It is also interesting to note that the  $M$  signal vectors are mutually equidistant; i.e.,

$$d_{mn} = \sqrt{\|\mathbf{s}_m - \mathbf{s}_n\|^2} = \sqrt{2\mathcal{E}_s}, \quad \text{for all } m \neq n \quad (7.4.5)$$

Hence, the minimum distance between signal points is  $\sqrt{2\mathcal{E}_s}$ . Figure 7.25 shows an example of  $M = 3$  orthogonal signals.

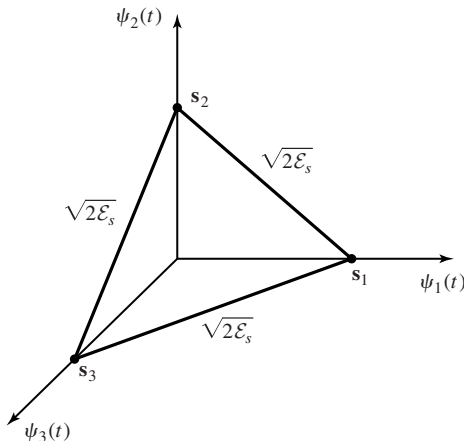


**Figure 7.25** Orthogonal signals for  $M = N = 3$ .

**Bandpass Signals.** Bandpass orthogonal signals can be constructed from a set of baseband orthogonal signals waveforms  $s_m(t)$ ,  $m = 1, 2, \dots, M$ , by simply multiplying the baseband orthogonal signal waveforms by the carrier  $\cos 2\pi f_c t$ . Hence, the  $M$  bandpass signals constructed in this manner are

$$u_m(t) = s_m(t) \cos 2\pi f_c t, \quad m = 1, 2, \dots, M \quad (7.4.6)$$

$$0 \leq t \leq T$$

The energy in each of the bandpass signal waveforms is one-half of the energy of the corresponding baseband signal waveforms. To demonstrate the orthogonality of the bandpass signal waveforms, we have

$$\begin{aligned} \int_0^T u_m(t)u_n(t) dt &= \int_0^T s_m(t)s_n(t) \cos^2 2\pi f_c t dt \\ &= \frac{1}{2} \int_0^T s_m(t)s_n(t) dt + \frac{1}{2} \int_0^T s_m(t)s_n(t) \cos 4\pi f_c t dt \\ &= 0 \end{aligned}$$

where the double frequency term is zero on a cycle-by-cycle when the carrier frequency  $f_c$  is large compared to the bandwidth of the baseband signals.

$M$ -ary PPM signals achieve orthogonality in the time domain by means of non-overlapping pulses. As an alternative, we can construct a set of  $M$  carrier-modulated signals which achieve orthogonality in the frequency domain. This type of modulation is generally called carrier-frequency modulation. The simplest form is frequency-shift keying, which is described next. Other types of carrier-frequency modulation are described in Chapter 10.

**Frequency-Shift Keying (FSK).** The simplest form of frequency modulation is binary frequency-shift keying. In binary FSK we employ two different frequencies, say  $f_1$  and  $f_2 = f_1 + \Delta f$ , to transmit a binary information sequence. The choice of frequency separation  $\Delta f = f_2 - f_1$  is considered below. Thus, the two signal waveforms may be expressed as

$$u_1(t) = \sqrt{\frac{2\mathcal{E}_b}{T_b}} \cos 2\pi f_1 t, \quad 0 \leq t \leq T_b$$

$$u_2(t) = \sqrt{\frac{2\mathcal{E}_b}{T_b}} \cos 2\pi f_2 t, \quad 0 \leq t \leq T_b \quad (7.4.7)$$

where  $\mathcal{E}_b$  is the signal energy/bit and  $T_b$  is the duration of the bit interval.

More generally,  $M$ -ary FSK may be used to transmit a block of  $k = \log_2 M$  bits/signal waveform. In this case, the  $M$  signal waveforms may be expressed as

$$u_m(t) = \sqrt{\frac{2\mathcal{E}_s}{T}} \cos(2\pi f_c t + 2\pi m \Delta f t), \quad m = 0, 1, \dots, M-1, \quad 0 \leq t \leq T \quad (7.4.8)$$

where  $\mathcal{E}_s = k\mathcal{E}_b$  is the energy/symbol,  $T = kT_b$  is the symbol interval and  $\Delta f$  is the frequency separation between successive frequencies; i.e.,  $\Delta f = f_m - f_{m-1}$ , where  $f_m = f_c + m\Delta f$ .

Note that the  $M$  FSK waveforms have equal energy  $\mathcal{E}_s$ . The frequency separation  $\Delta f$  determines the degree to which we can discriminate among the  $M$  possible transmitted signals. As a measure of the similarity (or dissimilarity) between a pair of signal waveforms, we define the correlation coefficients  $\gamma_{mn}$  as

$$\gamma_{mn} = \frac{1}{\mathcal{E}_s} \int_0^T u_m(t)u_n(t) dt \quad (7.4.9)$$

By substituting for  $u_m(t)$  and  $u_n(t)$  in Equation (7.4.9), we obtain

$$\begin{aligned} \gamma_{mn} &= \frac{1}{\mathcal{E}_s} \int_0^T \frac{2\mathcal{E}_s}{T} \cos(2\pi f_c t + 2\pi m \Delta f t) \cos(2\pi f_c t + 2\pi n \Delta f t) dt \\ &= \frac{1}{T} \int_0^T \cos 2\pi(m-n)\Delta f t dt + \frac{1}{T} \int_0^T \cos[4\pi f_c t + 2\pi(m+n)\Delta f t] dt \\ &= \frac{\sin 2\pi(m-n)\Delta f T}{2\pi(m-n)\Delta f T} \end{aligned} \quad (7.4.10)$$

where the second integral vanishes when  $f_c \gg 1/T$ . A plot of  $\gamma_{mn}$  as a function of the frequency separation  $\Delta f$  is given in Figure 7.26. We observe that the signal waveforms are orthogonal when  $\Delta f$  is a multiple of  $1/2T$ . Hence, the minimum frequency separation between successive frequencies for orthogonality is  $1/2T$ . We also note that the minimum value of the correlation coefficient is  $\gamma_{mn} = -0.217$ , which occurs at the frequency separations  $\Delta f = 0.715/T$ .

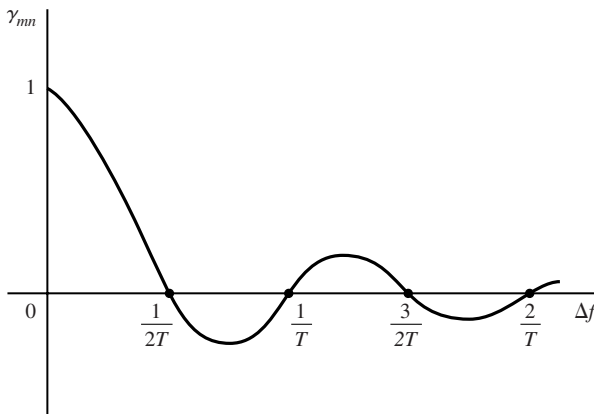


**Figure 7.26** Crosscorrelation coefficient as a function of frequency separation for FSK signals.

$M$ -ary orthogonal FSK waveforms have a geometric representation as  $M$ ,  $M$ -dimensional orthogonal vectors, given as

$$\begin{aligned} \mathbf{s}_1 &= (\sqrt{\mathcal{E}_s}, 0, 0, \dots, 0) \\ \mathbf{s}_2 &= (0, \sqrt{\mathcal{E}_s}, 0, \dots, 0) \\ &\vdots \\ \mathbf{s}_M &= (0, 0, \dots, 0, \sqrt{\mathcal{E}_s}) \end{aligned} \quad (7.4.11)$$

where the basis functions are  $\psi_m(t) = \sqrt{2/T} \cos 2\pi(f_c + m\Delta f)t$ . The distance between pairs of signal vectors is  $d = \sqrt{2\mathcal{E}_s}$  for all  $m, n$ , which is also minimum distance among the  $M$  signals.

### 7.4.2 Biorthogonal Signal Waveforms

As in the case of orthogonal signals, biorthogonal signals can be constructed for transmission through baseband channels and passband channels.

**Baseband Signals.** We have already described the construction of  $M = 4$  biorthogonal signals in two dimensions using the signal waveforms in Figure 7.12. In general, a set of  $M$  biorthogonal signals can be constructed from a set of  $M/2$  orthogonal signals  $s_i(t)$ ,  $i = 1, 2, \dots, M/2$  and their negatives  $-s_i(t)$ ,  $i = 1, 2, \dots, M/2$ . As we shall observe in Section 7.6.10, the channel bandwidth required to transmit the information sequence by use of biorthogonal signals is just one-half of that required to transmit  $M$  orthogonal signals. For this reason, biorthogonal signals are preferred in some applications over orthogonal signals.

The geometric representation of  $M$ -ary biorthogonal signals  $\{s_m(t), 1 \leq m \leq M/2, -s_m(t), M/2 + 1 \leq m \leq M\}$  is straightforward. We begin with  $M/2$  orthogonal vectors in  $N = M/2$  dimensions and then append their negatives. For example, if the  $M/2$  orthogonal waveforms are PPM signals, the  $M$  orthogonal vectors are given as

$$\begin{aligned} \mathbf{s}_1 &= (\sqrt{\mathcal{E}_s}, 0, 0, \dots, 0) \\ \mathbf{s}_2 &= (0, \sqrt{\mathcal{E}_s}, 0, \dots, 0) \\ &\vdots \quad \quad \quad \vdots \\ \mathbf{s}_{M/2} &= (0, 0, 0, \dots, \sqrt{\mathcal{E}_s}) \\ \mathbf{s}_{\frac{M}{2}+1} &= (-\sqrt{\mathcal{E}_s}, 0, 0, \dots, 0) \\ &\vdots \quad \quad \quad \vdots \\ \mathbf{s}_M &= (0, 0, 0, \dots, -\sqrt{\mathcal{E}_s}) \end{aligned} \quad (7.4.12)$$

Figure 7.15 illustrates the signal constellation for  $M = 4$  biorthogonal signals. We observe that this signal constellation is identical to the signal constellation for quadrature (four phase) phase-shift keying.

**Bandpass Signals.** Given a set of  $M$  baseband biorthogonal signals waveforms  $\{s_m(t)\}$ , a corresponding set of  $M$  bandpass signals  $\{u_m(t)\}$  is obtained by

modulating the carrier  $\cos 2\pi f_c t$  with the baseband signal waveforms; i.e.,

$$u_m(t) = s_m(t) \cos 2\pi f_c t, \quad m = 1, 2, \dots, M \\ 0 \leq t \leq T \quad (7.4.13)$$

The geometric representation of the bandpass signals is identical to that of the corresponding baseband signals, where the energy of the bandpass signal waveforms is one-half of that of the corresponding baseband signals.

### 7.4.3 Simplex Signal Waveforms

Another set of  $M$  signal waveforms that can be constructed from  $M$  orthogonal signals is obtained by subtracting the average of the  $M$  orthogonal signals from each of the orthogonal signal waveforms. The  $M$  signal waveforms that result are called *simplex signal waveforms*. Thus, if we have  $M$  orthogonal baseband signal waveforms  $\{s_m(t)\}$ , the simplex signal waveforms, denoted as  $\{s'_m(t)\}$ , are constructed as

$$s'_m(t) = s_m(t) - \frac{1}{M} \sum_{k=1}^M s_k(t) \quad (7.4.14)$$

Then, it follows that (see Problem 7.7) the energy of these signals  $s'_m(t)$  is

$$\mathcal{E}'_s = \int_0^T [s'_m(t)]^2 dt = \left(1 - \frac{1}{M}\right) \mathcal{E}_s \quad (7.4.15)$$

and

$$\int_0^T s'_m(t) s'_n(t) dt = -\frac{1}{M-1} \mathcal{E}_s, \quad m \neq n \quad (7.4.16)$$

where  $\mathcal{E}_s$  is the energy of each of the orthogonal signals and  $\mathcal{E}'_s$  is the energy of each of the signals in the simplex signal set. Note that the waveforms in the simplex set have smaller energy than the waveforms in the orthogonal signal set. Second, we note that simplex signal waveforms are not orthogonal. Instead, they have a negative correlation, which is equal for all pairs of signal waveforms. It is conjectured that among all the possible  $M$ -ary signal waveforms of equal energy  $\mathcal{E}_s$ , the simplex signal set results in the smallest probability of error when used to transmit information on an additive white Gaussian noise channel.

The geometric representation of a set of  $M$  simplex signals is obtained by subtracting the mean-signal vector from a set of  $M$  orthogonal vectors. Thus, we have

$$\mathbf{s}'_m = \mathbf{s}_m - \frac{1}{M} \sum_{k=1}^M \mathbf{s}_k, \quad n = 1, 2, \dots, M \quad (7.4.17)$$

The effect of subtracting the mean signal

$$\bar{\mathbf{s}} = \frac{1}{M} \sum_{k=1}^M \mathbf{s}_k \quad (7.4.18)$$

from each orthogonal vector is to translate the origin of the  $M$  orthogonal signals to the point  $\bar{\mathbf{s}}$  and to minimize the energy in the signal set  $\{\mathbf{s}'_m\}$ .

If the energy per signal for the orthogonal signals is  $\mathcal{E}_s = \|\mathbf{s}_m\|^2$ , then the energy for the simplex signals is

$$\begin{aligned}\mathcal{E}'_s &= \|\mathbf{s}'_m\|^2 = \|\mathbf{s}_m - \bar{\mathbf{s}}\|^2 \\ &= \left(1 - \frac{1}{M}\right) \mathcal{E}_s\end{aligned}\quad (7.4.19)$$

The distance between any two signal points is not changed by the translation of the origin; i.e., the distance between signal points remains at  $d = \sqrt{2\mathcal{E}'_s}$ . Finally, as indicated above, the  $M$  simplex signals are correlated. The crosscorrelation coefficient (normalized crosscorrelation) between the  $m$ th and  $n$ th signals is

$$\begin{aligned}\gamma_{mn} &= \frac{\mathbf{s}'_m \cdot \mathbf{s}'_n}{\|\mathbf{s}'_m\| \|\mathbf{s}'_n\|} \\ &= \frac{-1/M}{(1 - 1/M)} = -\frac{1}{M - 1}\end{aligned}\quad (7.4.20)$$

Hence, all the signals have the same pair-wise correlation. Figure 7.27 illustrates a set of  $M = 4$  simplex signals.

Finally, we mention that by modulating the carrier signal  $\cos 2\pi f_c t$  by a set of  $M$  baseband simplex signal waveforms we obtain a set of  $M$  bandpass signal waveforms that satisfy the properties of the baseband simplex signals.

#### 7.4.4 Binary-Coded Signal Waveforms

Signal waveforms for transmitting digital information may also be constructed from a set of  $M$  binary code words of the form

$$\mathbf{c}_m = (c_{m1}, c_{m2}, \dots, c_{mN}), \quad m = 1, 2, \dots, M \quad (7.4.21)$$

where  $c_{mj} = 0$  or 1 for all  $m$  and  $j$ .  $N$  is called the block length, or dimension, of the

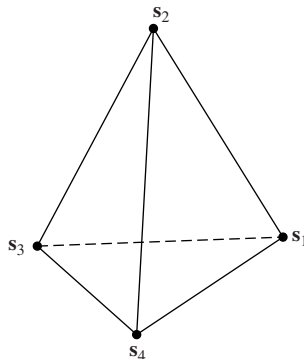


**Figure 7.27** Signal constellation for  $M = 4$  simplex signals.

code words. Given  $M$  code words, we can construct  $M$  signal waveforms by mapping a code bit  $c_{mj} = 1$  into a pulse  $g_T(t)$  of duration  $T/N$  and a code bit  $c_{mj} = 0$  into the negative pulse  $-g_T(t)$ .

**Example 7.4.1**

Given the code words

$$\mathbf{c}_1 = [1 \ 1 \ 1 \ 1 \ 0]$$

$$\mathbf{c}_2 = [1 \ 1 \ 0 \ 0 \ 1]$$

$$\mathbf{c}_3 = [1 \ 0 \ 1 \ 0 \ 1]$$

$$\mathbf{c}_4 = [0 \ 1 \ 0 \ 1 \ 0]$$

construct a set of  $M = 4$  signal waveforms, as described above, using a rectangular pulse  $g_T(t)$ .

**Solution** As indicated above, a code bit 1 is mapped into the rectangular pulse  $g_T(t)$  of duration  $T/4$ , and a code bit 0 is mapped into the rectangular pulse  $-g_T(t)$ . Thus, we construct the four waveforms shown in Figure 7.28 that correspond to the four code words.

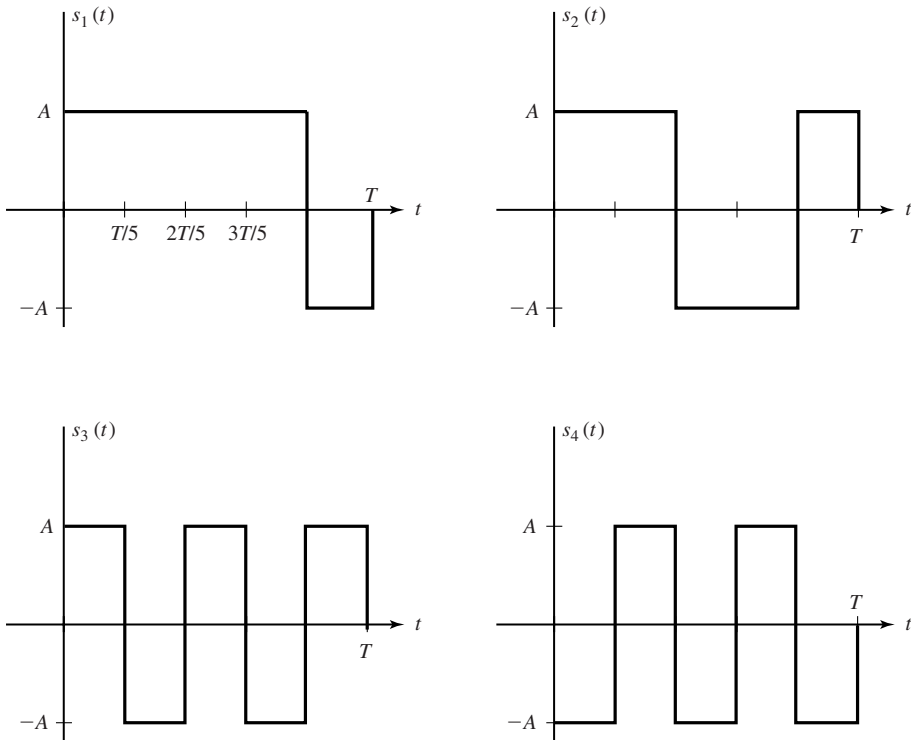


**Figure 7.28** A set of  $M = 4$  signal waveforms of dimension  $N = 5$  constructed from the four code words in Example 7.4.1.

Let us consider the geometric representation of a set of  $M$  signal waveforms generated from a set of  $M$  binary words of the form

$$\mathbf{c}_m = (c_{m1}, c_{m2}, \dots, c_{mN}), \quad m = 1, 2, \dots, M \quad (7.4.22)$$

where  $c_{mj} = 0$  or  $1$  for all  $m$  and  $j$ . The  $M$  signal waveforms are of dimension  $N$  and are represented geometrically in vector form as

$$\mathbf{s}_m = (s_{m1}, s_{m2}, \dots, s_{mN}), \quad m = 1, 2, \dots, M \quad (7.4.23)$$

where  $s_{mj} = \pm\sqrt{\mathcal{E}_s/N}$  for all  $m$  and  $j$ .

In general, there are  $2^N$  possible signals that can be constructed from the  $2^N$  possible binary code words. The  $M$  code words are a subset of the  $2^N$  possible binary code words. We also observe that the  $2^N$  possible signal points correspond to the vertices of an  $N$ -dimensional hypercube with its center at the origin. Figure 7.29 illustrates the signal points in  $N = 2$  and  $N = 3$  dimensions.

The  $M$  signals constructed in this manner have equal energy  $\mathcal{E}_s$ . The crosscorrelation coefficient between any pair of signals depends on how we select the  $M$  signals from the  $2^N$  possible signals. This topic is treated in Chapter 9. It is apparent that any adjacent signal points have a crosscorrelation coefficient of (see Problem 7.2)

$$\gamma = \frac{N - 2}{N} \quad (7.4.24)$$

and a corresponding Euclidean distance

$$d = 2\sqrt{\mathcal{E}_s/N} \quad (7.4.25)$$

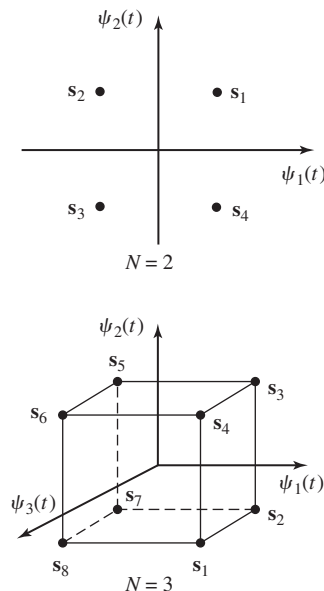


**Figure 7.29** Signal-space diagrams for signals generated from binary codes.



## 7.5 OPTIMUM RECEIVER FOR DIGITALLY MODULATED SIGNALS IN ADDITIVE WHITE GAUSSIAN NOISE

Let us consider a digital communication system that transmits digital information by use of any one of the  $M$ -ary signal waveforms described in the preceding sections. Thus, the input sequence to the modulator is subdivided into  $k$ -bit blocks or symbols and each of the  $M = 2^k$  symbols is associated with a corresponding baseband signal waveform from the set  $\{s_m(t), m = 1, 2, \dots, M\}$ . Each signal waveform is transmitted within the symbol (signaling) interval or time slot of duration  $T$ . To be specific, we consider the transmission of information over the interval  $0 \leq t \leq T$ .

The channel is assumed to corrupt the signal by the addition of white Gaussian noise as shown in Figure 7.30. Thus, the received signal in the interval  $0 \leq t \leq T$  may be expressed as

$$r(t) = s_m(t) + n(t), \quad 0 \leq t \leq T \quad (7.5.1)$$

where  $n(t)$  denotes the sample function of the additive white Gaussian noise (AWGN) process with power-spectral density  $S_n(f) = \frac{N_0}{2}$  W/Hz. Based on the observation of  $r(t)$  over the signal interval, we wish to design a receiver that is optimum in the sense that it minimizes the probability of making an error.

It is convenient to subdivide the receiver into two parts, the signal demodulator and the detector. The function of the signal demodulator is to convert the received waveform  $r(t)$  into an  $N$ -dimensional vector  $\mathbf{r} = (r_1, r_2, \dots, r_N)$ , where  $N$  is the dimension of the transmitted signal waveforms. The function of the detector is to decide which of the  $M$  possible signal waveforms was transmitted based on observation of the vector  $\mathbf{r}$ .

Two realizations of the signal demodulator are described in Sections 7.5.1 and 7.5.2. One is based on the use of signal correlators. The second is based on the use of matched filters. The optimum detector that follows the signal demodulator is designed to minimize the probability of error.

### 7.5.1 Correlation-Type Demodulator

In this section, we describe a correlation-type demodulator that decomposes the received signal and the noise into  $N$ -dimensional vectors. In other words, the signal and the noise

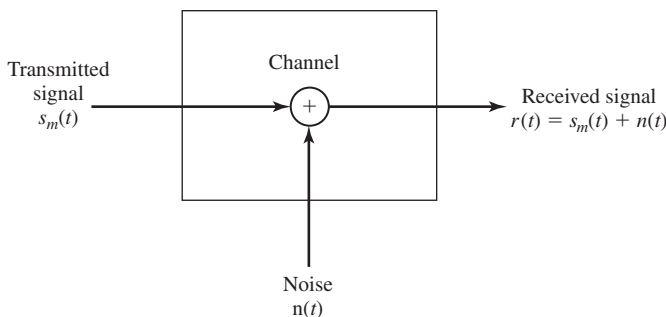


**Figure 7.30** Model for received signal passed through an AWGN channel.

are expanded into a series of linearly weighted orthonormal basis functions  $\{\psi_n(t)\}$ . It is assumed that the  $N$  basis functions  $\{\psi_n(t)\}$  span the signal space, so that every one of the possible transmitted signals of the set  $\{s_m(t), 1 \leq m \leq M\}$  can be represented as a weighted linear combination of  $\{\psi_n(t)\}$ . In the case of the noise, the functions  $\{\psi_n(t)\}$  do not span the noise space. However, we show below that the noise terms that fall outside the signal space are irrelevant to the detection of the signal.

Suppose the received signal  $r(t)$  is passed through a parallel bank of  $N$  cross correlators which basically compute the projection of  $r(t)$  onto the  $N$  basis functions  $\{\psi_n(t)\}$ , as illustrated in Figure 7.31. Thus, we have

$$\int_0^T r(t) \psi_k(t) dt = \int_0^T [s_m(t) + n(t)] \psi_k(t) dt$$

$$r_k = s_{mk} + n_k, \quad k = 1, 2, \dots, N \quad (7.5.2)$$

where

$$s_{mk} = \int_0^T s_m(t) \psi_k(t) dt, \quad k = 1, 2, \dots, N$$

$$n_k = \int_0^T n(t) \psi_k(t) dt, \quad k = 1, 2, \dots, N \quad (7.5.3)$$

Equation (7.5.2) is equivalent to

$$\mathbf{r} = \mathbf{s}_m + \mathbf{n} \quad (7.5.4)$$

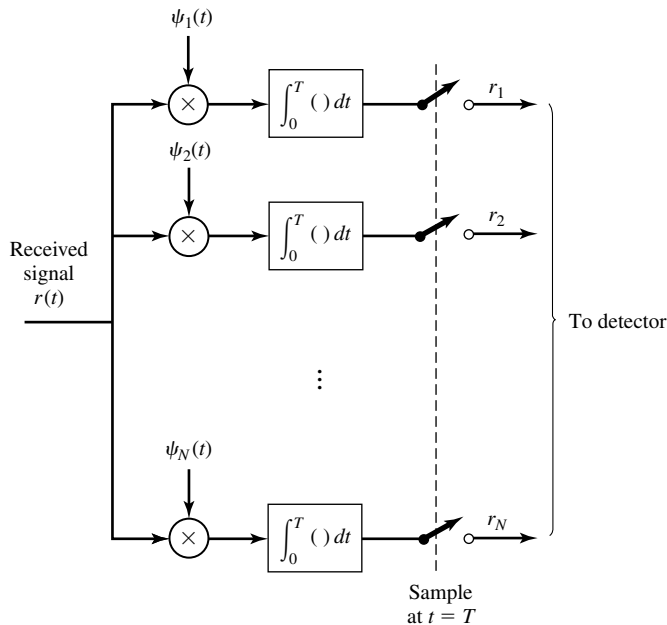


Figure 7.31 Correlation-type demodulator.

where the signal is now represented by the vector  $\mathbf{s}_m$  with components  $s_{mk}$ ,  $k = 1, 2, \dots, N$ . Their values depend on which of the  $M$  signals was transmitted. The components of  $\mathbf{n}$ , i.e.,  $\{n_k\}$ , are random variables that arise from the presence of the additive noise.

In fact, we can express the received signal  $r(t)$  in the interval  $0 \leq t \leq T$  as

$$\begin{aligned} r(t) &= \sum_{k=1}^N s_{mk} \psi_k(t) + \sum_{k=1}^N n_k \psi_k(t) + n'(t) \\ &= \sum_{k=1}^N r_k \psi_k(t) + n'(t) \end{aligned} \quad (7.5.5)$$

The term  $n'(t)$ , defined as

$$n'(t) = n(t) - \sum_{k=1}^N n_k \psi_k(t) \quad (7.5.6)$$

is a zero-mean, Gaussian noise process that represents the difference between the original noise process  $n(t)$  and that part which corresponds to the projection of  $n(t)$  onto the basis functions  $\{\psi_k(t)\}$ . We will show below that  $n'(t)$  is irrelevant to the decision as to which signal was transmitted. Consequently, the decision may be based entirely on the correlator output signal and noise components  $r_k = s_{mk} + n_k$ ,  $k = 1, 2, \dots, N$ .

Since the signals  $\{s_m(t)\}$  are deterministic, the signal components are deterministic. The noise components  $\{n_k\}$  are Gaussian. Their mean values are

$$E[n_k] = \int_0^T E[n(t)] \psi_k(t) dt = 0 \quad (7.5.7)$$

for all  $n$ . Their covariances are

$$\begin{aligned} E[n_k n_m] &= \int_0^T E[n(t)n(\tau)] \psi_k(t) \psi_m(\tau) dt d\tau \\ &= \int_0^T \int_0^T \frac{N_0}{2} \delta(t - \tau) \psi_k(t) \psi_m(\tau) dt d\tau \\ &= \frac{N_0}{2} \int_0^T \psi_k(t) \psi_m(t) dt \\ &= \frac{N_0}{2} \delta_{mk} \end{aligned} \quad (7.5.8)$$

where  $\delta_{mk} = 1$  when  $m = k$  and zero otherwise. Therefore, the  $N$  noise components  $\{n_k\}$  are zero-mean, uncorrelated Gaussian random variables with a common variance  $\sigma_n^2 = N_0/2$ , and

$$f(\mathbf{n}) = \prod_{i=1}^N f(n_i) = \frac{1}{(\pi N_0)^{N/2}} e^{-\sum_{i=1}^N \frac{n_i^2}{N_0}}$$

From the previous development, it follows that the correlator outputs  $\{r_k\}$  conditioned on the  $m$ th signal being transmitted are Gaussian random variables with mean

$$E[r_k] = E[s_{mk} + n_k] = s_{mk} \quad (7.5.9)$$

and equal variance

$$\sigma_r^2 = \sigma_n^2 = N_0/2 \quad (7.5.10)$$

Since the noise components  $\{n_k\}$  are uncorrelated Gaussian random variables, they are also statistically independent. As a consequence, the correlator outputs  $\{r_k\}$  conditioned on the  $m$ th signal being transmitted are statistically independent Gaussian variables. Hence, the conditional probability density functions (PDFs) of the random variables  $(r_1, r_2, \dots, r_N) = \mathbf{r}$  are simply

$$f(\mathbf{r} | \mathbf{s}_m) = \prod_{k=1}^N f(r_k | s_{mk}), \quad m = 1, 2, \dots, M \quad (7.5.11)$$

where

$$f(r_k | s_{mk}) = \frac{1}{\sqrt{\pi N_0}} e^{-(r_k - s_{mk})^2 / N_0}, \quad k = 1, 2, \dots, N \quad (7.5.12)$$

By substituting Equation (7.5.12) into Equation (7.5.11), we obtain the joint conditional PDFs as

$$f(\mathbf{r} | \mathbf{s}_m) = \frac{1}{(\pi N_0)^{N/2}} \exp \left[ - \sum_{k=1}^N (r_k - s_{mk})^2 / N_0 \right] \quad (7.5.13)$$

$$= \frac{1}{(\pi N_0)^{N/2}} \exp[-\|\mathbf{r} - \mathbf{s}_m\|^2 / N_0], \quad m = 1, 2, \dots, M \quad (7.5.14)$$

As a final point, we wish to show that the correlator outputs  $(r_1, r_2, \dots, r_N)$  are *sufficient statistics* for reaching a decision on which of the  $M$  signals was transmitted; i.e., that no additional relevant information can be extracted from the remaining noise process  $n'(t)$ . Indeed,  $n'(t)$  is uncorrelated with the  $N$  correlator outputs  $\{r_k\}$ ; i.e.,

$$\begin{aligned} E[n'(t)r_k] &= E[n'(t)]s_{mk} + E[n'(t)n_k] \\ &= E[n'(t)n_k] \\ &= E \left\{ \left[ n(t) - \sum_{j=1}^N n_j \psi_j(t) \right] n_k \right\} \\ &= \int_0^T E[n(t)n(\tau)] \psi_k(\tau) d\tau - \sum_{j=1}^N E(n_j n_k) \psi_j(t) \\ &= \frac{N_0}{2} \psi_k(t) - \frac{N_0}{2} \psi_k(t) = 0 \end{aligned} \quad (7.5.15)$$

Since  $n'(t)$  and  $\{r_k\}$  are Gaussian and uncorrelated, they are also statistically

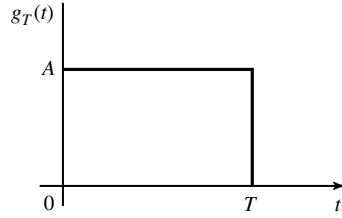


**Figure 7.32** Signal pulse for Example 7.5.1.

independent. Consequently,  $n'(t)$  does not contain any information that is relevant to the decision as to which signal waveform was transmitted. All the relevant information is contained in the correlator outputs  $\{r_k\}$ . Hence,  $n'(t)$  may be ignored.

### Example 7.5.1

Consider an  $M$ -ary PAM signal set in which the basic pulse shape  $g_T(t)$  is rectangular as shown in Figure 7.32. The additive noise is a zero-mean white Gaussian noise process. Determine the basis function  $\psi(t)$  and the output of the correlation-type demodulator.

**Solution** The energy in the rectangular pulse is

$$\mathcal{E}_g = \int_0^T g_T^2(t) dt = \int_0^T A^2 dt = A^2 T$$

Since the PAM signal set has a dimension  $N = 1$ , there is only one basis function  $\psi(t)$ . This is obtained from Equation (7.2.11), and given as

$$\begin{aligned} \psi(t) &= \frac{1}{\sqrt{A^2 T}} g_T(t) \\ &= \begin{cases} \frac{1}{\sqrt{T}}, & 0 \leq t \leq T \\ 0, & \text{otherwise} \end{cases} \end{aligned}$$

The output of the correlation-type demodulator is

$$r = \int_0^T r(t) \psi(t) dt = \frac{1}{\sqrt{T}} \int_0^T r(t) dt$$

It is interesting to note that the correlator becomes a simple integrator when  $\psi(t)$  is rectangular. If we substitute for  $r(t)$ , we obtain

$$\begin{aligned} r &= \frac{1}{\sqrt{T}} \int_0^T [s_m(t) + n(t)] dt \\ &= \frac{1}{\sqrt{T}} \left[ \int_0^T s_m \psi(t) dt + \int_0^T n(t) dt \right] \\ r &= s_m + n \end{aligned}$$

where the noise term  $E[n] = 0$ , and

$$\begin{aligned}\sigma_n^2 &= E \left\{ \frac{1}{T} \int_0^T \int_0^T n(t)n(\tau) dt d\tau \right\} \\ &= \frac{1}{T} \int_0^T \int_0^T E[n(t)n(\tau)] dt d\tau \\ &= \frac{N_0}{2T} \int_0^T \int_0^T \delta(t - \tau) dt d\tau = \frac{N_0}{2}\end{aligned}$$

The probability density function for the sampled output is

$$f(r | s_m) = \frac{1}{\sqrt{\pi N_0}} e^{-(r-s_m)^2/N_0}$$

## 7.5.2 Matched-Filter-Type Demodulator

Instead of using a bank of  $N$  correlators to generate the variables  $\{r_k\}$ , we may use a bank of  $N$  linear filters. To be specific, let us suppose that the impulse responses of the  $N$  filters are

$$h_k(t) = \psi_k(T - t), \quad 0 \leq t \leq T \quad (7.5.16)$$

where  $\{\psi_k(t)\}$  are the  $N$  basis functions and  $h_k(t) = 0$  outside of the interval  $0 \leq t \leq T$ . The outputs of these filters are

$$\begin{aligned}y_k(t) &= \int_0^t r(\tau) h_k(t - \tau) d\tau \\ &= \int_0^t r(\tau) \psi_k(T - t + \tau) d\tau, \quad k = 1, 2, \dots, N\end{aligned} \quad (7.5.17)$$

Now, if we sample the outputs of the filters at  $t = T$ , we obtain

$$y_k(T) = \int_0^T r(\tau) \psi_k(\tau) d\tau = r_k, \quad k = 1, 2, \dots, N \quad (7.5.18)$$

Hence, the sampled outputs of the filters at time  $t = T$  are exactly the same as the set of values  $\{r_k\}$  obtained from the  $N$  linear correlators.

A filter whose impulse response  $h(t) = s(T - t)$ , where  $s(t)$  is assumed to be confined to the time interval  $0 \leq t \leq T$ , is called the *matched filter* to the signal  $s(t)$ . An example of a signal and its matched filter are shown in Figure 7.33. The response of  $h(t) = s(T - t)$  to the signal  $s(t)$  is

$$y(t) = \int_0^t s(\tau) s(T - t + \tau) d\tau$$

which is basically the time-autocorrelation function of the signal  $s(t)$ . Figure 7.34 illustrates  $y(t)$  for the triangular signal pulse shown in Figure 7.33. We note that the autocorrelation function  $y(t)$  is an even function of  $t$  which attains a peak at  $t = T$ .

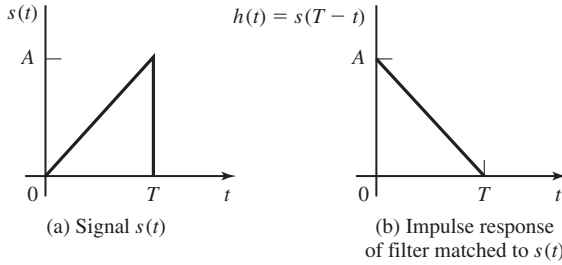


**Figure 7.33** Signal  $s(t)$  and filter matched to  $s(t)$ .

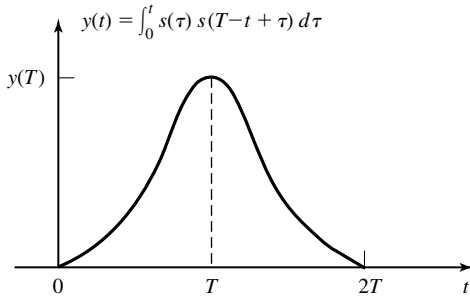


**Figure 7.34** Matched filter output is the autocorrelation function of  $s(t)$ .

In the case of the demodulator described above, the  $N$  matched filters are matched to the basis functions  $\{\psi_k(t)\}$ . Figure 7.35 illustrates the matched filter-type demodulator that generates the observed variables  $\{r_k\}$ .

**Properties of the Matched Filter.** A matched filter has some interesting properties. Let us prove the most important property, which may be stated as follows: If a signal  $s(t)$  is corrupted by AWGN, the filter with impulse response matched to  $s(t)$  maximizes the output SNR.

To prove this property, let us assume that the received signal  $r(t)$  consists of the signal  $s(t)$  and AWGN  $n(t)$  which has zero-mean and power-spectral density  $S_n(f) = N_0/2$  W/Hz. Suppose the signal  $r(t)$  is passed through a filter with impulse response  $h(t)$ ,  $0 \leq t \leq T$ , and its output is sampled at time  $t = T$ . The filter response to the signal and noise components is

$$\begin{aligned} y(t) &= \int_0^t r(\tau) h(t-\tau) d\tau \\ &= \int_0^t s(\tau) h(t-\tau) d\tau + \int_0^t n(\tau) h(t-\tau) d\tau \end{aligned} \quad (7.5.19)$$

At the sampling instant  $t = T$ , the signal and noise components are

$$\begin{aligned} y(T) &= \int_0^T s(\tau) h(T-\tau) d\tau + \int_0^T n(\tau) h(T-\tau) d\tau \\ &= y_s(T) + y_n(T) \end{aligned} \quad (7.5.20)$$

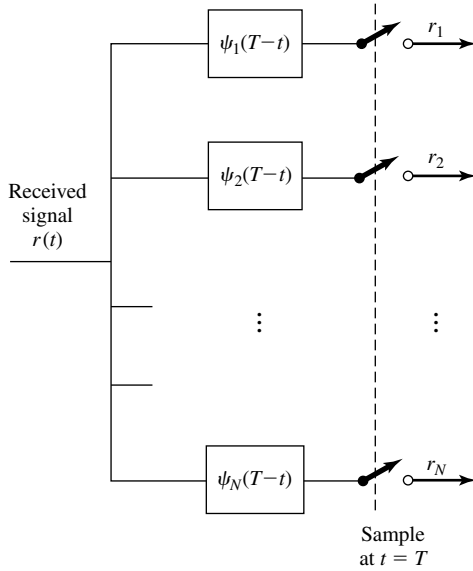


**Figure 7.35** Matched filter-type demodulator.

where  $y_s(T)$  represents the signal component and  $y_n(T)$  represents the noise component. The problem is to select the filter impulse response that maximizes the output SNR defined as

$$\left(\frac{S}{N}\right)_0 = \frac{y_s^2(T)}{E[y_n^2(T)]} \quad (7.5.21)$$

The denominator in Equation (7.5.21) is simply the variance of the noise term at the output of the filter. Let us evaluate  $E[y_n^2(T)]$ . We have

$$\begin{aligned} E[y_n^2(T)] &= \int_0^T \int_0^T E[n(\tau)n(t)]h(T-\tau)h(T-t) dt d\tau \\ &= \frac{N_0}{2} \int_0^T \int_0^T \delta(t-\tau)h(T-\tau)h(T-t) dt d\tau \\ &= \frac{N_0}{2} \int_0^T h^2(T-t) dt \end{aligned} \quad (7.5.22)$$

Note that the variance depends on the power-spectral density of the noise and the energy in the impulse response  $h(t)$ .

By substituting for  $y_s(T)$  and  $E[y_n^2(T)]$  into Equation (7.5.21), we obtain the expression for the output SNR as

$$\left(\frac{S}{N}\right)_0 = \frac{[\int_0^T s(\tau)h(T-\tau) d\tau]^2}{\frac{N_0}{2} \int_0^T h^2(T-t) dt} = \frac{[\int_0^T h(\tau)s(T-\tau) d\tau]^2}{\frac{N_0}{2} \int_0^T h^2(T-t) dt} \quad (7.5.23)$$



Since the denominator of the SNR depends on the energy in  $h(t)$ , the maximum output SNR over  $h(t)$  is obtained by maximizing the numerator of  $(S/N)_0$  subject to the constraint that the denominator is held constant. The maximization of the numerator is most easily performed by use of the Cauchy–Schwarz (see Problem 2.9) inequality, which states, in general, that if  $g_1(t)$  and  $g_2(t)$  are finite energy signals, then

$$\left[ \int_{-\infty}^{\infty} g_1(t)g_2(t) dt \right]^2 \leq \int_{-\infty}^{\infty} g_1^2(t) dt \int_{-\infty}^{\infty} g_2^2(t) dt \quad (7.5.24)$$

where equality holds when  $g_1(t) = Cg_2(t)$  for any arbitrary constant  $C$ . If we set  $g_1(t) = h(t)$  and  $g_2(t) = s(T - t)$ , it is clear that the  $(S/N)_0$  is maximized when  $h(t) = Cs(T - t)$ ; i.e.,  $h(t)$  is matched to the signal  $s(t)$ . The scale factor  $C^2$  drops out of the expression for  $(S/N)_0$  since it appears in both the numerator and the denominator.

The output (maximum) SNR obtained with the matched filter is

$$\begin{aligned} \left( \frac{S}{N} \right)_o &= \frac{2}{N_0} \int_0^T s^2(t) dt \\ &= \frac{2\mathcal{E}_s}{N_0} \end{aligned} \quad (7.5.25)$$

Note that the output SNR from the matched filter depends on the energy of the waveform  $s(t)$  but not on the detailed characteristics of  $s(t)$ . This is another interesting property of the matched filter.

**Frequency Domain Interpretation of the Matched Filter.** The matched filter has an interesting frequency domain interpretation. Since  $h(t) = s(T - t)$ , the Fourier transform of this relationship is

$$\begin{aligned} H(f) &= \int_0^T s(T - t)e^{-j2\pi ft} dt \\ &= \left[ \int_0^T s(\tau)e^{j2\pi f\tau} d\tau \right] e^{-j2\pi fT} \\ &= S^*(f)e^{-j2\pi fT} \end{aligned} \quad (7.5.26)$$

We observe that the matched filter has a frequency response which is the complex conjugate of the transmitted signal spectrum multiplied by the phase factor  $e^{-j2\pi fT}$ , which represents the sampling delay of  $T$ . In other words,  $|H(f)| = |S(f)|$ , so that the magnitude response of the matched filter is identical to the transmitted signal spectrum. On the other hand, the phase of  $H(f)$  is the negative of the phase of  $S(f)$ .

Now, if the signal  $s(t)$ , with spectrum  $S(f)$ , is passed through the matched filter, the filter output has a spectrum  $Y(f) = |S(f)|^2 e^{-j2\pi fT}$ . Hence, the output waveform is

$$\begin{aligned} y_s(t) &= \int_{-\infty}^{\infty} Y(f)e^{j2\pi ft} df \\ &= \int_{-\infty}^{\infty} |S(f)|^2 e^{-j2\pi fT} e^{j2\pi ft} df \end{aligned} \quad (7.5.27)$$

By sampling the output of the matched filter at  $t = T$ , we obtain

$$y_s(T) = \int_{-\infty}^{\infty} |S(f)|^2 df = \int_0^T s^2(t) dt = \mathcal{E}_s \quad (7.5.28)$$

where the last step follows from Parseval's relation.

The noise of the output of the matched filter has a power-spectral density

$$\mathcal{S}_o(f) = |H(f)|^2 N_0/2 \quad (7.5.29)$$

Hence, the total noise power at the output of the matched filter is

$$\begin{aligned} P_n &= \int_{-\infty}^{\infty} \mathcal{S}_o(f) df \\ &= \int_{-\infty}^{\infty} \frac{N_0}{2} |H(f)|^2 df = \frac{N_0}{2} \int_{-\infty}^{\infty} |S(f)|^2 df = \frac{\mathcal{E}_s N_0}{2} \end{aligned} \quad (7.5.30)$$

The output SNR is simply the ratio of the signal power  $P_s$ , given by

$$P_s = y_s^2(T) \quad (7.5.31)$$

to the noise power  $P_n$ . Hence,

$$\left( \frac{S}{N} \right)_o = \frac{P_s}{P_n} = \frac{\mathcal{E}_s^2}{\mathcal{E}_s N_0/2} = \frac{2\mathcal{E}_s}{N_0} \quad (7.5.32)$$

which agrees with the result given by Equation (7.5.25).

### Example 7.5.2

Consider the  $M = 4$  biorthogonal signals constructed from the binary PPM signals and their negatives in Figure 7.12(b), for transmitting information over an AWGN channel. The noise is assumed to have zero mean and power-spectral density  $N_0/2$ . Determine the basis functions for this signal set, the impulse response of the matched-filter demodulators, and the output waveforms of the matched filter demodulators when the transmitted signal is  $s_1(t)$ .

**Solution** The  $M = 4$  biorthogonal signals have dimension  $N = 2$ . Hence, two basis functions are needed to represent the signals. From Figure 7.12(b), we choose  $\psi_1(t)$  and  $\psi_2(t)$  as

$$\begin{aligned} \psi_1(t) &= \begin{cases} \sqrt{\frac{2}{T}}, & 0 \leq t \leq \frac{T}{2} \\ 0, & \text{otherwise} \end{cases} \\ \psi_2(t) &= \begin{cases} \sqrt{\frac{2}{T}}, & \frac{T}{2} \leq t \leq T \\ 0, & \text{otherwise} \end{cases} \end{aligned} \quad (7.5.33)$$

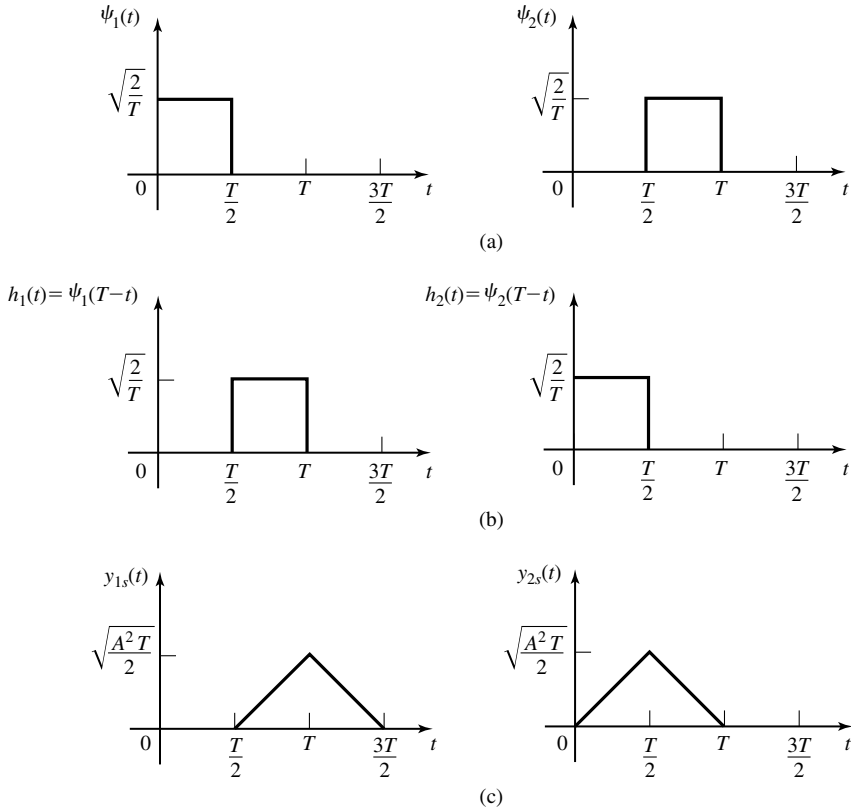


**Figure 7.36** Basis functions and matched filter responses for Example 7.2.2.

These waveforms are illustrated in Figure 7.36(a). The impulse responses of the two matched filters are

$$\begin{aligned}
 h_1(t) = \psi_1(T-t) &= \begin{cases} \sqrt{\frac{2}{T}}, & \frac{T}{2} \leq t \leq T \\ 0, & \text{otherwise} \end{cases} \\
 h_2(t) = \psi_2(T-t) &= \begin{cases} \sqrt{\frac{2}{T}}, & 0 \leq t \leq T/2 \\ 0, & \text{otherwise} \end{cases}
 \end{aligned} \tag{7.5.34}$$

and are illustrated in Figure 7.36(b).

If  $s_1(t)$  is transmitted, the (noise-free) responses of the two matched filters are shown in Figure 7.36(c). Since  $y_1(t)$  and  $y_2(t)$  are sampled at  $t = T$ , we observe that  $y_{1s}(T) = \sqrt{\frac{A^2T}{2}}$  and  $y_{2s}(T) = 0$ . Note that  $A^2T/2 = \mathcal{E}_s$ , the signal energy. Hence, the received vector formed from the two matched filter outputs at the sampling instant

$t = T$  is

$$\mathbf{r} = (r_1, r_2) = (\sqrt{\mathcal{E}_s} + n_1, n_2) \quad (7.5.35)$$

where  $n_1 = y_{1n}(T)$  and  $n_2 = y_{2n}(T)$  are the noise components at the outputs of the matched filters, given by

$$y_{kn}(T) = \int_0^T n(t) \psi_k(t) dt, \quad k = 1, 2 \quad (7.5.36)$$

Clearly,  $E[n_k] = E[y_{kn}(T)] = 0$ . Their variance is

$$\begin{aligned} \sigma_n^2 &= E[y_{kn}^2(T)] = \int_0^T \int_0^T E[n(t)n(\tau)] \psi_k(t) \psi_k(\tau) dt d\tau \\ &= \frac{N_0}{2} \int_0^T \int_0^T \delta(t - \tau) \psi_k(\tau) \psi_k(t) dt d\tau \\ &= \frac{N_0}{2} \int_0^T \psi_k^2(t) dt = \frac{N_0}{2} \end{aligned} \quad (7.5.37)$$

Observe that the  $(S/N)_o$  for the first matched filter is

$$\left(\frac{S}{N}\right)_o = \frac{(\sqrt{\mathcal{E}_s})^2}{N_0/2} = \frac{2\mathcal{E}_s}{N_0}$$

which agrees with our previous result. Also note that the four possible outputs of the two matched filters, corresponding to the four possible transmitted signals are  $(r_1, r_2) = (\sqrt{\mathcal{E}_s} + n_1, n_2)$ ,  $(n_1, \sqrt{\mathcal{E}_s} + n_2)$ ,  $(-\sqrt{\mathcal{E}_s} + n_1, n_2)$ , and  $(n_1, -\sqrt{\mathcal{E}_s} + n_2)$ .

### 7.5.3 The Optimum Detector

In Sections 7.5.1 and 7.5.2, we demonstrated that, for a signal transmitted over an AWGN channel, either a correlation-type demodulator or a matched-filter-type demodulator produces the vector  $\mathbf{r} = (r_1, r_2, \dots, r_N)$  which contains all the relevant information in the received signal waveform. In this section, we describe the optimum decision rule based on the observation vector  $\mathbf{r}$ . For this development, we assume that there is no memory in signals transmitted in successive signal intervals.

As it is seen from Equation (7.5.4), the received vector  $\mathbf{r}$  is the sum of two vectors,  $\mathbf{s}_m$ , the vector equivalent of the transmitted signal, and  $\mathbf{n}$ , the noise vector. The vector  $\mathbf{s}_m$  is a point in the signal constellation and the vector  $\mathbf{n}$  is an  $N$ -dimensional random vector with i.i.d. components each being a Gaussian random variable with mean 0 and variance  $N_0/2$ . Since components of the noise are independent and have the same mean and variance, the distribution of the noise vector  $\mathbf{n}$  in the  $N$ -dimensional space has spherical symmetry. When  $\mathbf{s}_m$  is transmitted, the received vector  $\mathbf{r}$ , which represents the transmitted signal  $\mathbf{s}_m$  plus the spherically symmetric noise  $\mathbf{n}$ , can be represented by a spherical cloud centered at  $\mathbf{s}_m$ . The density of this cloud is higher at the center and becomes less as we depart from  $\mathbf{s}_m$ ; i.e., these points become less likely to be received. The variance of the noise  $N_0/2$  determines the density of the noise

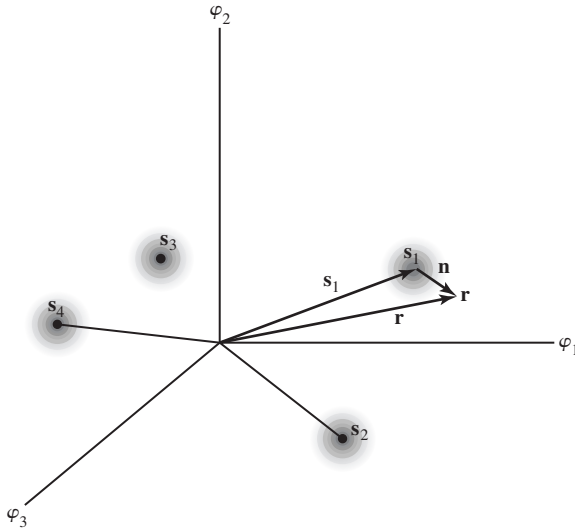


**Figure 7.37** Signal constellation, noise cloud and received vector for  $N = 3$  and  $M = 4$ . It is assumed that  $\mathbf{s}_1$  is transmitted.

cloud around the center signal  $\mathbf{s}_m$ . For low  $N_0/2$ , the cloud is quite centered around  $\mathbf{s}_m$  and its density (representing the probability) reduces sharply as the distance from the center is increased. For high  $N_0/2$ , the cloud is spread and larger distances have a higher probability compared with the low  $N_0/2$  case. The signal constellation, the noise cloud, and the received vector are shown in Figure 7.37 for the case of  $N = 3$  and  $M = 4$ .

We wish to design a signal detector that makes a decision on the transmitted signal in each signal interval based on the observation of the vector  $\mathbf{r}$  in each interval, such that the probability of a correct decision is maximized. With this goal in mind, we consider a decision rule based on the computation of the *posterior probabilities* defined as

$$P(\text{signal } \mathbf{s}_m \text{ was transmitted} \mid \mathbf{r}) \quad m = 1, 2, \dots, M$$

which we abbreviate as  $P(\mathbf{s}_m \mid \mathbf{r})$ . The decision criterion is based on selecting the signal corresponding to the maximum of the set of posterior probabilities  $\{P(\mathbf{s}_m \mid \mathbf{r})\}$ . At the end of this section we show that this criterion maximizes the probability of a correct decision and, hence, minimizes the probability of error. Intuitively this decision is the best possible decision that minimizes the error probability. It is clear that in the absence of any received information  $\mathbf{r}$ , the best decision is to choose the signal  $\mathbf{s}_m$  that has the highest *prior* probability  $P(\mathbf{s}_m)$ . After receiving the information  $\mathbf{r}$ , the prior probabilities  $P(\mathbf{s}_m)$  are substituted with the *posterior* (conditional) probabilities  $P(\mathbf{s}_m \mid \mathbf{r})$  and the receiver chooses  $\mathbf{s}_m$  that maximizes  $P(\mathbf{s}_m \mid \mathbf{r})$ . This decision criterion is called the *maximum a posteriori probability* (MAP) criterion.

Using Bayes rule, the posterior probabilities may be expressed as

$$P(\mathbf{s}_m | \mathbf{r}) = \frac{f(\mathbf{r} | \mathbf{s}_m)P(\mathbf{s}_m)}{f(\mathbf{r})} \quad (7.5.38)$$

where  $f(\mathbf{r} | \mathbf{s}_m)$  is the conditional PDF of the observed vector given  $\mathbf{s}_m$ , and  $P(\mathbf{s}_m)$  is the *a priori probability* of the  $m$ th signal being transmitted. The denominator of Equation (7.5.38) may be expressed as

$$f(\mathbf{r}) = \sum_{m=1}^M f(\mathbf{r} | \mathbf{s}_m)P(\mathbf{s}_m) \quad (7.5.39)$$

From Equations (7.5.38) and (7.5.39) we observe that the computation of the posterior probabilities  $P(\mathbf{s}_m | \mathbf{r})$  requires knowledge of the *a priori probabilities*  $P(\mathbf{s}_m)$  and the conditional PDFs  $f(\mathbf{r} | \mathbf{s}_m)$  for  $m = 1, 2, \dots, M$ .

Some simplification occurs in the MAP criterion when the  $M$  signals are equally probable a priori; i.e.,  $P(\mathbf{s}_m) = 1/M$  for all  $M$ . Furthermore, we note that the denominator in Equation (7.5.38) is independent of which signal is transmitted. Consequently, the decision rule based on finding the signal that maximizes  $P(\mathbf{s}_m | \mathbf{r})$  is equivalent to finding the signal that maximizes  $f(\mathbf{r} | \mathbf{s}_m)$ .

The conditional PDF  $f(\mathbf{r} | \mathbf{s}_m)$  or any monotonic function of it is usually called the *likelihood function*. The decision criterion based on the maximum of  $f(\mathbf{r} | \mathbf{s}_m)$  over the  $M$  signals is called the *maximum-likelihood (ML) criterion*. We observe that a detector based on the MAP criterion and one that is based on the ML criterion make the same decisions as long as the a priori probabilities  $P(\mathbf{s}_m)$  are all equal; i.e., the signals  $\{\mathbf{s}_m\}$  are equiprobable.

In the case of an AWGN channel, the likelihood function  $f(\mathbf{r} | \mathbf{s}_m)$  is given by Equation (7.5.11). To simplify the computations, we may work with the natural logarithm of  $f(\mathbf{r} | \mathbf{s}_m)$ , which is a monotonic function. Thus,

$$\ln f(\mathbf{r} | \mathbf{s}_m) = \frac{-N}{2} \ln(\pi N_0) - \frac{1}{N_0} \sum_{k=1}^N (r_k - s_{mk})^2 \quad (7.5.40)$$

The maximum of  $\ln f(\mathbf{r} | \mathbf{s}_m)$  over  $\mathbf{s}_m$  is equivalent to finding the signal  $\mathbf{s}_m$  that minimizes the Euclidean distance

$$D(\mathbf{r}, \mathbf{s}_m) = \sum_{k=1}^N (r_k - s_{mk})^2 \quad (7.5.41)$$

We call  $D(\mathbf{r}, \mathbf{s}_m)$   $m = 1, 2, \dots, M$ , the *distance metrics*. Hence, for the AWGN channel, the decision rule based on the ML criterion reduces to finding the signal  $\mathbf{s}_m$  that is closest in distance to the received signal vector  $\mathbf{r}$ . We will refer to this decision rule as *minimum distance detection*.

Another interpretation of the optimum decision rule based on the ML criterion is obtained by expanding the distance metrics in Equation (7.5.41) as

$$\begin{aligned} D(\mathbf{r}, \mathbf{s}_m) &= \sum_{n=1}^N r_n^2 - 2 \sum_{n=1}^N r_n s_{mn} + \sum_{n=1}^N s_{mn}^2 \\ &= \|\mathbf{r}\|^2 - 2\mathbf{r} \cdot \mathbf{s}_m + \|\mathbf{s}_m\|^2, \quad m = 1, 2, \dots, M \end{aligned} \quad (7.5.42)$$

The term  $\|\mathbf{r}\|^2$  is common to all decision metrics and, hence, it may be ignored in the computations of the metrics. The result is a set of modified distance metrics

$$D'(\mathbf{r}, \mathbf{s}_m) = -2\mathbf{r} \cdot \mathbf{s}_m + \|\mathbf{s}_m\|^2 \quad (7.5.43)$$

Note that selecting the signal  $\mathbf{s}_m$  that minimizes  $D'(\mathbf{r}, \mathbf{s}_m)$  is equivalent to selecting the signal that maximizes the metric  $C(\mathbf{r}, \mathbf{s}_m) = -D'(\mathbf{r}, \mathbf{s}_m)$ ; i.e.,

$$C(\mathbf{r}, \mathbf{s}_m) = 2\mathbf{r} \cdot \mathbf{s}_m - \|\mathbf{s}_m\|^2 \quad (7.5.44)$$

The term  $\mathbf{r} \cdot \mathbf{s}_m$  represents the projection of the received signal vector onto each of the  $M$  possible transmitted signal vectors. The value of each of these projections is a measure of the correlation between the received vector and the  $m$ th signal. For this reason, we call  $C(\mathbf{r}, \mathbf{s}_m)$ ,  $m = 1, 2, \dots, M$ , the *correlation metrics* for deciding which of the  $M$  signals was transmitted. Finally, the terms  $\|\mathbf{s}_m\|^2 = \mathcal{E}_m$ ,  $m = 1, 2, \dots, M$ , may be viewed as bias terms that serve as compensation for signal sets that have unequal energies, such as PAM. If all signals have the same energy,  $\|\mathbf{s}_m\|^2$  may also be ignored in the computation of the correlation metrics  $C(\mathbf{r}, \mathbf{s}_m)$  and the distance metrics  $D(\mathbf{r}, \mathbf{s}_m)$  or  $D'(\mathbf{r}, \mathbf{s}_m)$ .

In summary, we have demonstrated that the optimum ML detector computes a set of  $M$  distances  $D(\mathbf{r}, \mathbf{s}_m)$  or  $D'(\mathbf{r}, \mathbf{s}_m)$  and selects the signal corresponding to the smallest (distance) metric. Equivalently, the optimum ML detector computes a set of  $M$  correlation metrics  $C(\mathbf{r}, \mathbf{s}_m)$  and selects the signal corresponding to the largest correlation metric.

The above development for the optimum detector treated the important case in which all signals are equally probable. In this case, the MAP criterion is equivalent to the ML criterion. However, when the signals are not equally probable, the optimum MAP detector bases its decision on the probabilities  $P(\mathbf{s}_m | \mathbf{r})$ ,  $m = 1, 2, \dots, M$ , given by Equation (7.5.38) or, equivalently, on the posterior probability *metrics*,

$$PM(\mathbf{r}, \mathbf{s}_m) = f(\mathbf{r} | \mathbf{s}_m)P(\mathbf{s}_m) \quad (7.5.45)$$

The following example illustrates this computation for binary PAM signals.

### Example 7.5.3

Consider the case of binary PAM signals in which the two possible signal points are  $s_1 = -s_2 = \sqrt{\mathcal{E}_b}$ , where  $\mathcal{E}_b$  is the energy per bit. The prior probabilities are  $P(s_1) = p$  and  $P(s_2) = 1 - p$ . Determine the metrics for the optimum MAP detector when the transmitted signal is corrupted with AWGN.

**Solution** The received signal vector (one dimensional) for binary PAM is

$$r = \pm \sqrt{\mathcal{E}_b} + y_n(T) \quad (7.5.46)$$

where  $y_n(T)$  is a zero-mean Gaussian random variable with variance  $\sigma_n^2 = N_0/2$ . Consequently, the conditional PDFs  $f(r | s_m)$  for the two signals are

$$f(r | s_1) = \frac{1}{\sqrt{2\pi}\sigma_n} e^{-(r - \sqrt{\mathcal{E}_b})^2 / 2\sigma_n^2} \quad (7.5.47)$$

$$f(r | s_2) = \frac{1}{\sqrt{2\pi}\sigma_n} e^{-(r + \sqrt{\mathcal{E}_b})^2 / 2\sigma_n^2} \quad (7.5.48)$$

Then the metrics  $\text{PM}(\mathbf{r}, \mathbf{s}_1)$  and  $\text{PM}(\mathbf{r}, \mathbf{s}_2)$  defined by Equation (7.5.45) are

$$\begin{aligned} \text{PM}(\mathbf{r}, \mathbf{s}_1) &= pf(r | s_1) \\ &= \frac{p}{\sqrt{2\pi}\sigma_n} e^{-(r - \sqrt{\mathcal{E}_b})^2 / 2\sigma_n^2} \end{aligned} \quad (7.5.49)$$

$$\text{PM}(\mathbf{r}, \mathbf{s}_2) = \frac{1-p}{\sqrt{2\pi}\sigma_n} e^{-(r + \sqrt{\mathcal{E}_b})^2 / 2\sigma_n^2} \quad (7.5.50)$$

If  $\text{PM}(\mathbf{r}, \mathbf{s}_1) > \text{PM}(\mathbf{r}, \mathbf{s}_2)$ , we select  $s_1$  as the transmitted signal; otherwise, we select  $s_2$ . This decision rule may be expressed as

$$\frac{\text{PM}(\mathbf{r}, \mathbf{s}_1)}{\text{PM}(\mathbf{r}, \mathbf{s}_2)} \underset{s_2}{\overset{s_1}{>}} 1 \quad (7.5.51)$$

But

$$\frac{\text{PM}(\mathbf{r}, \mathbf{s}_1)}{\text{PM}(\mathbf{r}, \mathbf{s}_2)} = \frac{p}{1-p} e^{[(r + \sqrt{\mathcal{E}_b})^2 - (r - \sqrt{\mathcal{E}_b})^2] / 2\sigma_n^2} \quad (7.5.52)$$

so that Equation (7.5.51) may be expressed as

$$\frac{(r + \sqrt{\mathcal{E}_b})^2 - (r - \sqrt{\mathcal{E}_b})^2}{2\sigma_n^2} \underset{s_2}{\overset{s_1}{>}} \ln \frac{1-p}{p} \quad (7.5.53)$$

or, equivalently,

$$\sqrt{\mathcal{E}_b} r \underset{s_2}{\overset{s_1}{>}} \frac{\sigma_n^2}{2} \ln \frac{1-p}{p} = \frac{N_0}{4} \ln \frac{1-p}{p} \quad (7.5.54)$$

This is the final form for the optimum detector. It computes the correlation metric  $C(\mathbf{r}, \mathbf{s}_1) = r\sqrt{\mathcal{E}_b}$  and compares it with the threshold  $(N_0/4) \ln(1-p)/p$ .

It is interesting to note that in the case of unequal prior probabilities, it is necessary to know not only the values of the prior probabilities but also the value of the power-spectral density  $N_0$ , in order to compute the threshold. When  $p = 1/2$ , the threshold is zero, and knowledge of  $N_0$  is not required by the detector.

We conclude this section with the proof that the decision rule based on the maximum-likelihood criterion minimizes the probability of error when the  $M$  signals are equally probable a priori. Let us denote by  $R_m$  the region in the  $N$ -dimensional space for



which we decide that signal  $s_m(t)$  was transmitted when the vector  $\mathbf{r} = (r_1, r_2, \dots, r_N)$  is received. The probability of a decision error given that  $s_m(t)$  was transmitted is

$$P(e | \mathbf{s}_m) = \int_{R_m^c} f(\mathbf{r} | \mathbf{s}_m) d\mathbf{r} \quad (7.5.55)$$

where  $R_m^c$  is the complement of  $R_m$ . The average probability of error is

$$\begin{aligned} P(e) &= \sum_{m=1}^M \frac{1}{M} P(e | \mathbf{s}_m) \\ &= \sum_{m=1}^M \frac{1}{M} \int_{R_m^c} f(\mathbf{r} | \mathbf{s}_m) d\mathbf{r} \\ &= \sum_{m=1}^M \frac{1}{M} \left[ 1 - \int_{R_m} f(\mathbf{r} | \mathbf{s}_m) d\mathbf{r} \right] \end{aligned} \quad (7.5.56)$$

We note that  $P(e)$  is minimized by selecting the signal  $\mathbf{s}_m$  if  $f(\mathbf{r} | \mathbf{s}_m)$  is larger than  $f(\mathbf{r} | \mathbf{s}_k)$  for all  $m \neq k$ .

Similarly for the MAP criterion, when the  $M$  signals are not equally probable, the average probability of error is

$$P(e) = 1 - \sum_{m=1}^M \int_{R_m} P(\mathbf{s}_m | \mathbf{r}) f(\mathbf{r}) d\mathbf{r}$$

$P(e)$  is a minimum when the points that are to be included in each particular region  $R_m$  are those for which  $P(\mathbf{s}_m | \mathbf{r})$  exceeds all other posterior probabilities.

### 7.5.4 Demodulation and Detection of Carrier-Amplitude Modulated Signals

The demodulation of a bandpass digital PAM signal may be accomplished by means of correlation or matched filtering. However, as we will observe from the following development, the presence of the carrier introduces an additional complication in the demodulation.

The transmitted PAM signal in a signaling interval has the form

$$u_m(t) = A_m g_T(t) \cos 2\pi f_c t, \quad 0 \leq t \leq T \quad (7.5.57)$$

The received signal may be expressed as

$$r(t) = A_m g_T(t) \cos 2\pi f_c t + n(t), \quad 0 \leq t \leq T \quad (7.5.58)$$

where  $n(t)$  is a bandpass noise process, which is represented as

$$n(t) = n_c(t) \cos 2\pi f_c t - n_s(t) \sin 2\pi f_c t \quad (7.5.59)$$

By crosscorrelating the received signal  $r(t)$  with the basis function  $\psi(t)$ , we have

$$\begin{aligned} \int_0^T r(t)\psi(t) dt &= A_m \sqrt{\frac{2}{\mathcal{E}_g}} \int_0^T g_T^2(t) \cos^2 2\pi f_c t dt + \int_0^T n(t)\psi(t) dt \\ &= A_m \sqrt{\mathcal{E}_g/2} + n \end{aligned} \quad (7.5.60)$$

where  $n$  represents the additive noise component at the output of the correlator.

An identical result is obtained if a matched filter is used in place of the correlator to demodulate the received signal.

**Carrier-Phase Recovery.** In the above development, we assumed that the function  $\psi(t)$  is perfectly synchronized with the signal component of  $r(t)$  in both time and carrier phase, as shown in Figure 7.38 for PAM. In practice, however, these ideal conditions do not hold. First of all, the propagation delay encountered in transmitting a signal through the channel results in a carrier-phase offset in the received signal. Second, the oscillator that generates the carrier signal  $\cos 2\pi f_c t$  at the receiver, is not generally phase locked to the oscillator used at the transmitter. Practical oscillators usually drift in frequency and phase. Consequently, the demodulation of the bandpass PAM signal, as illustrated in Figure 7.38, is ideal, but it is not practical. In a practical system, it is necessary to generate a phase-coherent carrier at the receiver to perform the demodulation of the received signal.

In general, the received signal has a carrier phase offset  $\phi$ . To estimate  $\phi$  from the received signal requires that we observe  $r(t)$  over many signal intervals. Because the message signal, when observed over many signal intervals, is zero mean due to the randomness in the signal amplitude values  $\{A_m\}$ , the transmitted DSB-SC amplitude-modulated signal has zero-average power at the carrier frequency  $f_c$ . Consequently, it is not possible to estimate the carrier phase directly from  $r(t)$ . However, if we square  $r(t)$ , we generate a frequency component at  $f = 2f_c$  that has nonzero-average power. This component can be filtered out by a narrowband filter tuned to  $2f_c$ , which can be

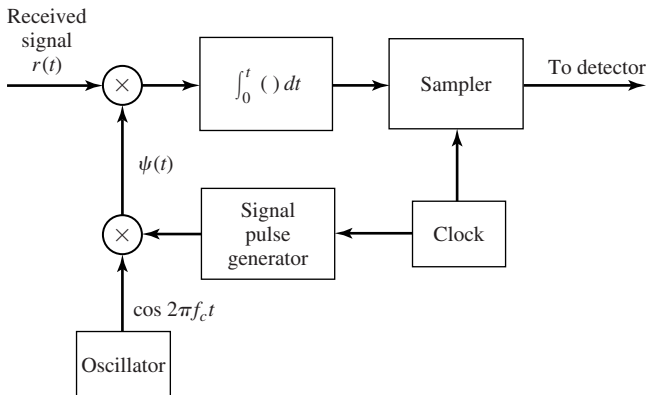


**Figure 7.38** Demodulation of bandpass digital PAM signal.

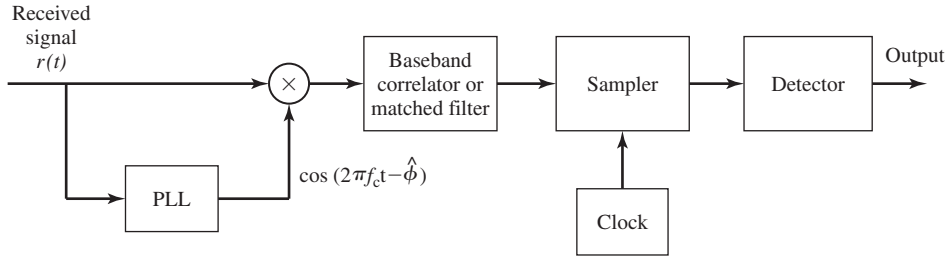


Figure 7.39 Demodulation of carrier-amplitude modulated signal.

used to drive a PLL, as described in Section 5.2. A functional block diagram of the receiver that employs a PLL for estimating the carrier phase is shown in Figure 7.39.

The Costas loop, also described in Section 5.2, is an alternative method for estimating the carrier phase from the received signal  $r(t)$ . Recall from our discussion in Section 5.2 that the PLL and the Costas loop yield phase estimates that are comparable in quality in the presence of additive channel noise.

As an alternative to performing the correlation or matched filtering at baseband as shown in Figure 7.39, we may perform crosscorrelation or matched filtering either at bandpass or at some convenient intermediate frequency. In particular, a bandpass correlator may be used to multiply the received signal  $r(t)$  by the amplitude-modulated carrier  $g_T(t) \cos(2\pi f_c t + \hat{\phi})$ , where  $\cos(2\pi f_c t + \hat{\phi})$  is the output of the PLL. The product signal is integrated over the signaling interval  $T$ , the output of the integrator is sampled at  $t = T$ , and the sample is passed to the detector. If a matched filter instead of a correlator is used, the filter impulse response is  $g_T(T - t) \cos[2\pi f_c(T - t) - \hat{\phi}]$ . The functional block diagrams for these demodulators are shown in Figure 7.40.

**Optimum Detector.** In the case of a perfect (noise-free) carrier-phase estimate,  $\phi = \hat{\phi}$ , and the input to the detector is the signal plus noise term given by Equation (7.5.60). As in the case of baseband PAM, for equiprobable messages, the optimum detector bases its decision on the distance metrics

$$D(r, s_m) = (r - s_m)^2, \quad m = 1, 2, \dots, M \quad (7.5.61)$$

or, equivalently, on the correlation metrics

$$C(r, s_m) = 2rs_m - s_m^2 \quad (7.5.62)$$

### 7.5.5 Demodulation and Detection of Carrier-Phase Modulated Signals

The received bandpass signal from an AWGN channel in a signaling interval  $0 \leq t \leq T$ , may be expressed as

$$\begin{aligned} r(t) &= u_m(t) + n(t) \\ &= [A_{mc}g_T(t) + n_c(t)] \cos 2\pi f_c t - [A_{ms}g_T(t) + n_s(t)] \sin 2\pi f_c t \\ & \quad m = 0, 2, \dots, M - 1 \end{aligned} \quad (7.5.63)$$

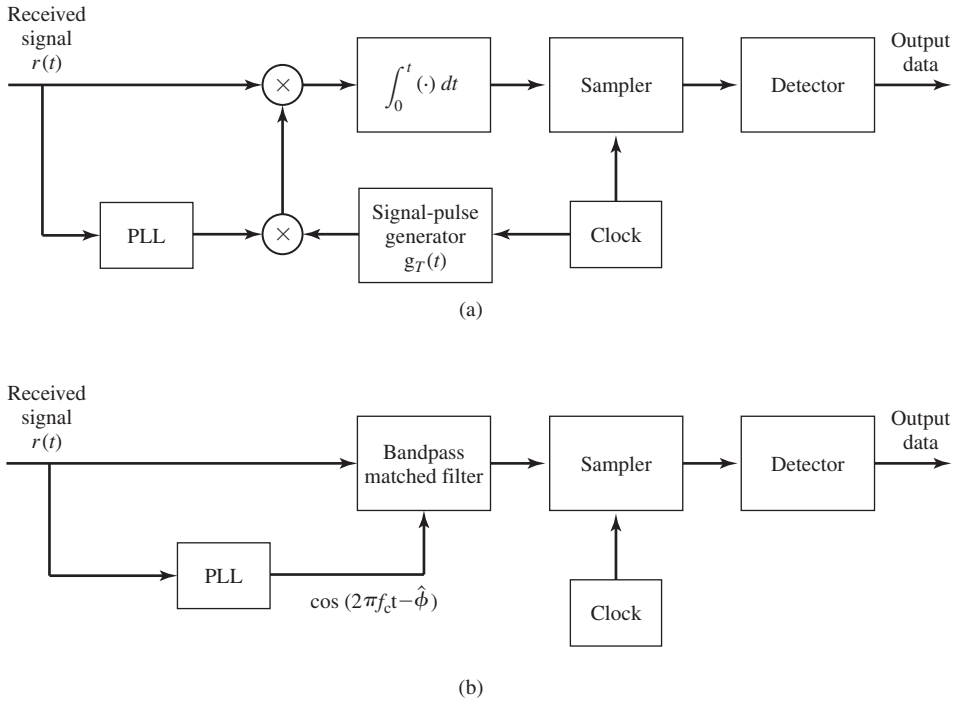


**Figure 7.40** Bandpass demodulation of digital PAM signal via (a) bandpass correlation and (b) bandpass matched filtering.

where  $n(t)$  is the additive bandpass Gaussian noise and  $A_{mc}$  and  $A_{ms}$  are the information-bearing signal components that are related to the transmitted carrier phase by Equation (7.3.16).

The received signal may be correlated with  $\psi_1(t) = \sqrt{\frac{2}{\mathcal{E}_g}} g_T(t) \cos 2\pi f_c t$  and  $\psi_2(t) = -\sqrt{\frac{2}{\mathcal{E}_g}} g_T(t) \sin 2\pi f_c t$ . The outputs of the two correlators yield the two noise-corrupted signal components, which may be expressed as

$$\begin{aligned} \mathbf{r} &= \mathbf{s}_m + \mathbf{n} \\ &= (\sqrt{\mathcal{E}_s} \cos 2\pi m/M + n_c, \quad \sqrt{\mathcal{E}_s} \sin 2\pi m/M + n_s) \end{aligned} \quad (7.5.64)$$

where, by definition

$$\begin{aligned} n_c &= \frac{1}{\sqrt{2\mathcal{E}_g}} \int_0^T g_T(t) n_c(t) dt \\ n_s &= \frac{1}{\sqrt{2\mathcal{E}_g}} \int_0^T n_s(t) g_T(t) dt \end{aligned} \quad (7.5.65)$$

Because the quadrature noise components  $n_c(t)$  and  $n_s(t)$  are zero mean and uncorrelated [see the argument following Equation (4.6.10)]; it follows that  $E[n_c] = E[n_s] = 0$  and  $E[n_c n_s] = 0$ .

The variance of the noise components is

$$\begin{aligned} E[n_c^2] &= E[n_s^2] = \frac{1}{2\mathcal{E}_g} \int_0^T \int_0^T g_T(t)g_T(\tau)E[n_c(t)n_c(\tau)] dt d\tau \\ &= \frac{N_0}{2\mathcal{E}_g} \int_0^T g_T^2(t) dt \\ &= N_0/2 \end{aligned} \quad (7.5.66)$$

The optimum detector projects the received signal vector onto each of the  $M$  possible transmitted signal vectors  $\{\mathbf{s}_m\}$  and selects the vector corresponding to the largest projection; i.e., we compute the correlation metrics

$$C(\mathbf{r}, \mathbf{s}_m) = \mathbf{r} \cdot \mathbf{s}_m, \quad m = 0, 1, \dots, M - 1 \quad (7.5.67)$$

and select the signal vector that results in the largest correlation.

Because all signals have equal energy, an equivalent detector metric for digital-phase modulation is to compute the phase of the received signal vector  $\mathbf{r} = (r_1, r_2)$

$$\Theta_r = \tan^{-1} \frac{r_2}{r_1} \quad (7.5.68)$$

and select the signal from the set  $\{\mathbf{s}_m\}$  whose phase is closest to  $\Theta_r$ . In the following section, we evaluate the probability of error based on the phase metric given by Equation (7.5.68).

**Carrier-Phase Estimation.** As previously indicated, in any carrier-modulation system, the oscillators employed at the transmitter and the receiver are not phase-locked, in general. As a consequence, the received signal will be of the form

$$r(t) = A_{mc}g_T(t) \cos(2\pi f_c t + \phi) - A_{ms}g_T(t) \sin(2\pi f_c t + \phi) + n(t) \quad (7.5.69)$$

where  $\phi$  is the carrier-phase offset. This phase offset must be estimated at the receiver, and the phase estimate must be used in the demodulation of the received signal. Hence, the received signal must be correlated with the two orthogonal basis functions.

$$\begin{aligned} \psi_1(t) &= \sqrt{\frac{2}{\mathcal{E}_g}} g_T(t) \cos(2\pi f_c t + \hat{\phi}) \\ \psi_2(t) &= -\sqrt{\frac{2}{\mathcal{E}_g}} g_T(t) \sin(2\pi f_c t + \hat{\phi}) \end{aligned} \quad (7.5.70)$$

where  $\hat{\phi}$  is the estimate of the carrier phase, as shown in Figure 7.41 for the case in which  $g_T(t)$  is a rectangular pulse.

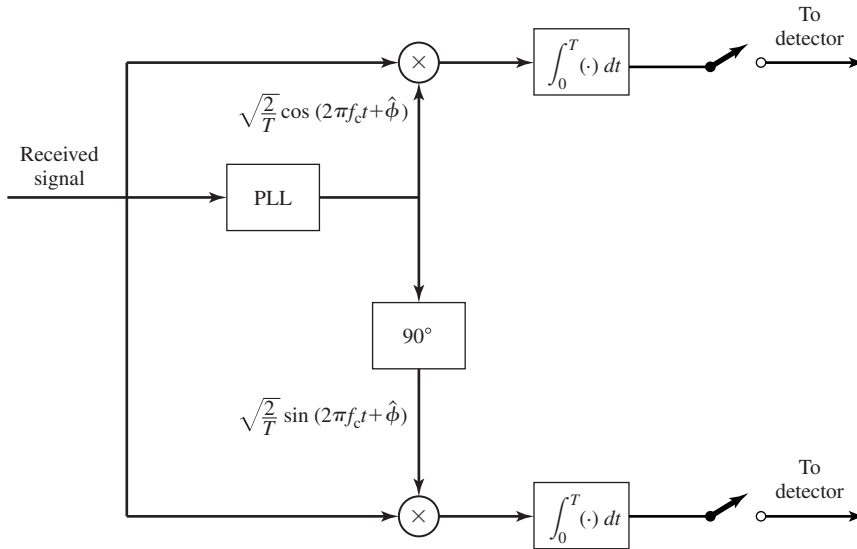


**Figure 7.41** Demodulator for PSK signals.

When the digital information is transmitted via  $M$ -phase modulation of a carrier, a PLL may be used to estimate the carrier-phase offset. For  $M = 2$ , the squaring PLL and the Costas loop described in Section 5.2 are directly applicable.

For  $M > 2$ , the received signal may first be raised to the  $M$ th power as shown in Figure 7.42. Thus, if the received signal  $r(t)$  has the form

$$\begin{aligned} r(t) &= s_m(t) + n(t) \\ &= g_T(t) \cos\left(2\pi f_c t + \phi + \frac{2\pi m}{M}\right) + n(t) \end{aligned} \quad (7.5.71)$$

and we pass  $r(t)$  through an  $M$ th power device, the output signal will contain harmonics of the carrier  $f_c$ . The harmonic that we wish to select is  $\cos(2\pi M f_c t + M\phi)$  for driving the PLL. We note that

$$M\left(\frac{2\pi m}{M}\right) = 2\pi m = 0 \pmod{2\pi}, \quad m = 1, 2, \dots, M \quad (7.5.72)$$

Thus, the information is removed from the  $M$ th harmonic. The bandpass filter tuned to the frequency  $M f_c$  produces the desired frequency component  $\cos(2\pi M f_c t + M\phi)$  driving the PLL. The VCO output is  $\sin(2\pi M f_c t + M\hat{\phi})$ , so this output is divided in frequency by  $M$  to yield  $\sin(2\pi f_c t + \hat{\phi})$  and phase-shifted by  $\pi/2$  to yield  $\cos(2\pi f_c t + \hat{\phi})$ . The two quadrature-carrier components are then passed to the demodulator.

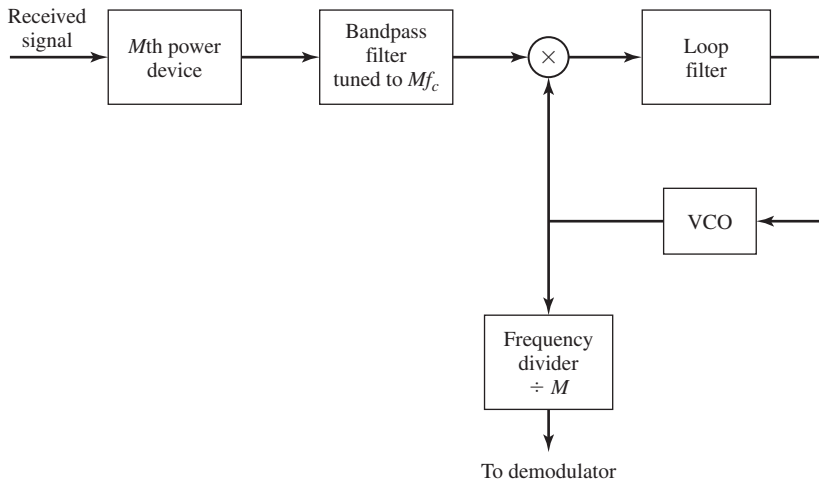


**Figure 7.42** Carrier-phase estimation for  $M$ -ary PSK signals.

We should note that the quadrature-phase carrier components generated as described above contain phase ambiguities of multiples of  $2\pi/M$  that result from multiplying the carrier phase  $\phi$  by  $M$ . Because  $M\phi \pmod{2\pi}$  is less than  $2\pi$ , dividing the resulting angle by  $M$  yields a phase estimate of  $|\hat{\phi}| < 2\pi/M$ , when, in fact, the true carrier phase may exceed this estimate by multiples of  $2\pi/M$ , i.e., by  $2\pi k/M$ , for  $k = 1, 2, \dots, M-1$ . Such phase ambiguities can be overcome by differentially encoding the data at the transmitter and differentially decoding at the detector, as described below.

Just as in the case of the squaring PLL, the  $M$ th power PLL operates in the presence of noise that has been enhanced by the  $M$ th power-law device. The variance of the phase error in the PLL resulting from the additive noise may be expressed in the simple form

$$\sigma_{\hat{\phi}}^2 = \frac{1}{S_{ML}\rho_L} \quad (7.5.73)$$

where  $\rho_L$  is the loop SNR and  $S_{ML}$  is the  $M$ -phase power loss.  $S_{ML}$  has been evaluated by Lindsey and Simon (1973) for  $M = 4$  and  $M = 8$ .

Another method for extracting a carrier-phase estimate  $\hat{\phi}$  from the received signal for  $M$ -ary-phase modulation is the decision-feedback PLL (DFPLL), which is shown in Figure 7.43. The received signal is demodulated by using two quadrature phase-locked carriers to yield  $\mathbf{r} = (r_1, r_2)$  at the sampling instants. The phase estimate  $\hat{\Theta}_r = \tan^{-1} r_2/r_1$  is computed at the detector and quantized to the nearest of the  $M$  possible transmitted phases, which we denote as  $\hat{\theta}_m$ . The two outputs of the quadrature multipliers are delayed by one symbol interval  $T$  and multiplied by  $\cos \theta_m$  and  $-\sin \theta_m$ . Thus, we

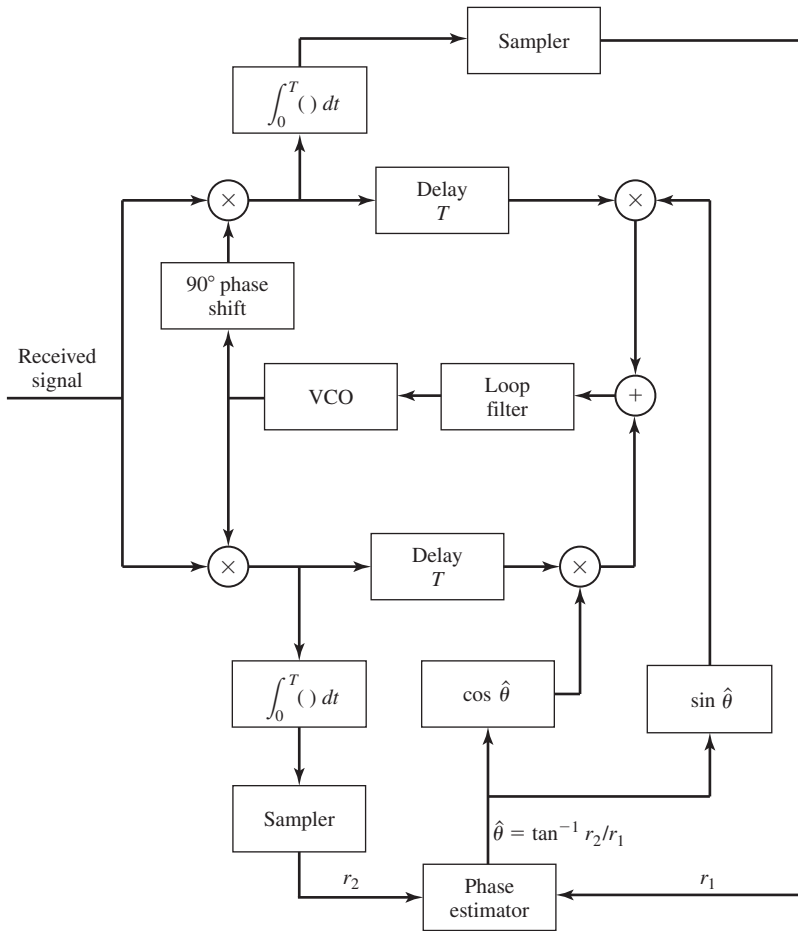


**Figure 7.43** Carrier recovery for  $M$ -ary PSK using a DFPLL.

obtain

$$\begin{aligned}
 -r(t) \cos(2\pi f_c t + \hat{\phi}) \sin \theta_m &= -\frac{1}{2}[g_T(t) \cos \theta_m + n_c(t)] \sin \theta_m \cos(\phi - \hat{\phi}) \\
 &\quad + \frac{1}{2}[g_T(t) \sin \theta_m + n_s(t)] \sin \theta_m \sin(\phi - \hat{\phi}) \\
 &\quad + \text{double-frequency terms}
 \end{aligned}$$

$$\begin{aligned}
 -r(t) \sin(2\pi f_c t + \hat{\phi}) \cos \theta_m &= \frac{1}{2}[g_T(t) \cos \theta_m + n_c(t)] \cos \theta_m \sin(\phi - \hat{\phi}) \\
 &\quad + \frac{1}{2}[g_T(t) \sin \theta_m + n_s(t)] \cos \theta_m \cos(\phi - \hat{\phi}) \\
 &\quad + \text{double-frequency terms}
 \end{aligned}$$



These two signals are added together to generate the error signal

$$\begin{aligned}
 e(t) = & g_T(t) \sin(\phi - \hat{\phi}) + \frac{1}{2}n_c(t) \sin(\phi - \hat{\phi} - \theta_m) \\
 & + \frac{1}{2}n_s(t) \cos(\phi - \hat{\phi} - \theta_m) \\
 & + \text{double-frequency terms} \qquad (7.5.74)
 \end{aligned}$$

This error signal is the input to the loop filter that provides the control signal for the VCO.

We observe that the two quadrature noise components in Equation (7.5.74) appear as additive terms and no term involves a product of two noise components as in the output of the  $M$ th power-law device. Consequently, there is no power loss resulting from nonlinear operations on the received signal in the DFPLL. The  $M$ -phase decision-feedback tracking loop also has a phase ambiguities of  $2\pi k/M$ , necessitating the need for differentially encoding the information sequence prior to transmission and differentially decoding the received sequence at the detector to recover the information.

**Differential-Phase Modulation and Demodulation.** The performance of ideal, coherent phase modulation/demodulation is closely attained in communication systems that transmit a carrier signal along with the information signal. The carrier-signal component, usually referred to as a pilot signal, may be filtered from the received signal and used to perform phase-coherent demodulation. However, when no separate carrier signal is transmitted, the receiver must estimate the carrier phase from the received signal. As indicated in the Section 7.5.5, the phase at the output of a PLL has ambiguities of multiples of  $2\pi/M$ , necessitating the need to differentially encode the data prior to modulation. This differential encoding allows us to decode the received data at the detector in the presence of the phase ambiguities.

In differential encoding, the information is conveyed by phase shifts between any two successive signal intervals. For example, in binary-phase modulation the information bit 1 may be transmitted by shifting the phase of the carrier by  $180^\circ$  relative to the previous carrier phase, while the information bit 0 is transmitted by a zero-phase shift relative to the phase in the preceding signaling interval. In four-phase modulation, the relative phase shifts between successive intervals are  $0^\circ$ ,  $90^\circ$ ,  $180^\circ$ , and  $270^\circ$ , corresponding to the information bits 00, 01, 11, 10, respectively. The generalization of differential encoding for  $M > 4$  is straightforward. The phase-modulated signals resulting from this encoding process are called *differentially encoded*. The encoding is performed by a relatively simple logic circuit preceding the modulator.

Demodulation and detection of the differentially encoded phase-modulated signal may be performed as described in the preceding section using the output of a PLL to perform the demodulation. The received signal phase  $\Theta_r = \tan^{-1} r_2/r_1$  at the detector is mapped into one of the  $M$  possible transmitted signal phases  $\{\theta_m\}$  that is closest to  $\Theta_r$ . Following the detector is a relatively simple phase comparator that compares the

phases of the detected signal over two consecutive intervals to extract the transmitted information. Thus, phase ambiguities of  $2\pi/M$  are rendered irrelevant.

A differentially encoded phase-modulated signal also allows another type of demodulation that does not require the estimation of the carrier phase. Instead, the phase of the received signal in any given signaling interval is compared to the phase of the received signal from the preceding signaling interval. To elaborate, suppose that we demodulate the differentially encoded signal by multiplying  $r(t)$  with  $\cos 2\pi f_c t$  and  $\sin 2\pi f_c t$  and integrating the two products over the interval  $T$ . At the  $k$ th signaling interval, the demodulator output is

$$r_k = \sqrt{\mathcal{E}_s} e^{j(\theta_k - \phi)} + n_k \quad (7.5.75)$$

where  $\theta_k$  is the phase angle of the transmitted signal at the  $k$ th signaling interval,  $\phi$  is the carrier phase, and  $n_k = n_{kc} + jn_{ks}$  is the noise vector. Similarly, the received signal vector at the output of the demodulator in the preceding signaling interval is

$$r_{k-1} = \sqrt{\mathcal{E}_s} e^{j(\theta_{k-1} - \phi)} + n_{k-1} \quad (7.5.76)$$

The decision variable for the phase detector is the phase difference between these two complex numbers. Equivalently, we can project  $r_k$  onto  $r_{k-1}$  and use the phase of the resulting complex number; i.e.,

$$r_k r_{k-1}^* = \mathcal{E}_s e^{j(\theta_k - \theta_{k-1})} + \sqrt{\mathcal{E}_s} e^{j(\theta_k - \phi)} n_{k-1} + \sqrt{\mathcal{E}_s} e^{-j(\theta_{k-1} - \phi)} n_k + n_k n_{k-1}^* \quad (7.5.77)$$

which, in the absence of noise, yields the phase difference  $\theta_k - \theta_{k-1}$ . Thus, the mean value of  $r_k r_{k-1}^*$  is independent of the carrier phase. Differentially encoded PSK signaling that is demodulated and detected as described above is called *differential PSK (DPSK)*.

The demodulation and detection of DPSK using matched filters is illustrated in Figure 7.44. If the pulse  $g_T(t)$  is rectangular, the matched filters may be replaced by integrators, which are also called *integrate-and-dump filters*.

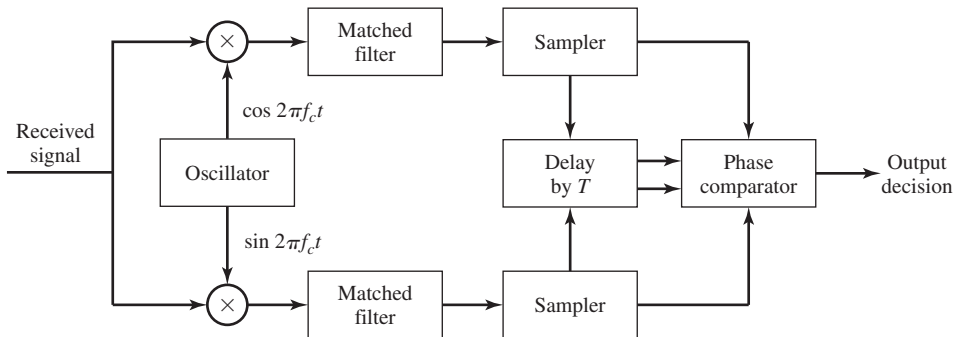


**Figure 7.44** Block diagram of DPSK demodulator.

### 7.5.6 Demodulation and Detection of Quadrature Amplitude Modulated Signals

Let us assume that a carrier-phase offset is introduced in the transmission of the signal through the channel. In addition, the received signal is corrupted by additive Gaussian noise. Hence,  $r(t)$  may be expressed as

$$r(t) = A_{mc}g_T(t) \cos(2\pi f_c t + \phi) + A_{ms}g_T(t) \sin(2\pi f_c t + \phi) + n(t) \quad (7.5.78)$$

Suppose that an estimate  $\hat{\phi}$  of the carrier phase is available at the demodulator. Then, the received signal may be correlated with the two basis functions

$$\begin{aligned} \psi_1(t) &= \sqrt{\frac{2}{\mathcal{E}_g}} g_T(t) \cos(2\pi f_c t + \hat{\phi}) \\ \psi_2(t) &= \sqrt{\frac{2}{\mathcal{E}_g}} g_T(t) \sin(2\pi f_c t + \hat{\phi}) \end{aligned} \quad (7.5.79)$$

as illustrated in Figure 7.45, and the outputs of the correlators are sampled and passed

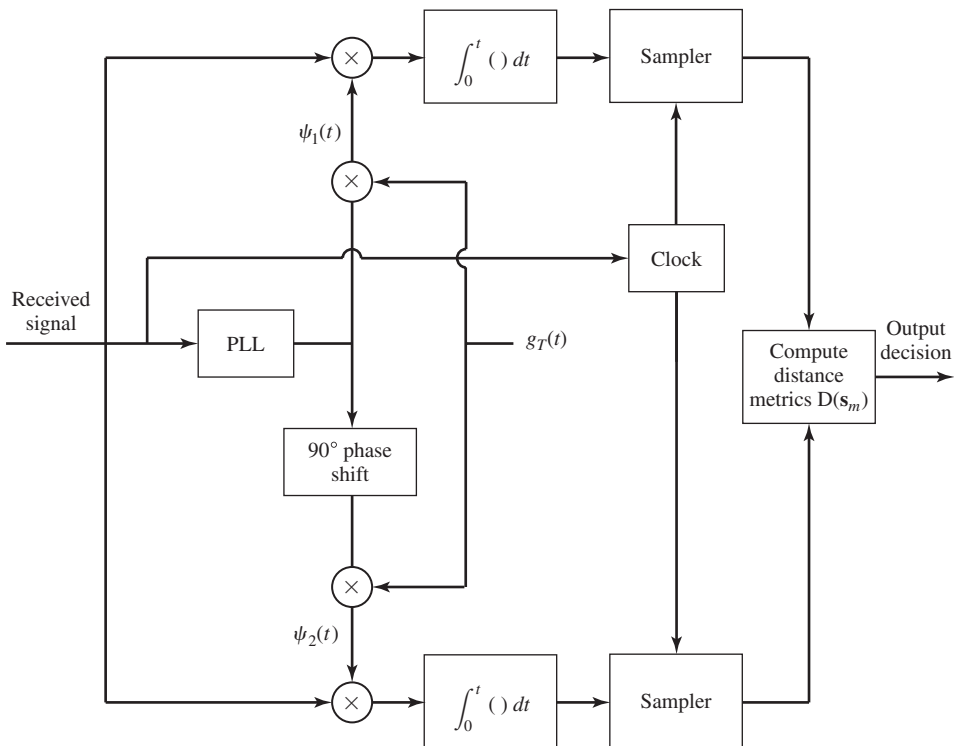


Figure 7.45 Demodulation and detection of QAM signals.

to the detector.

The input to the detector consists of the two sampled components  $r_1, r_2$ , where ( $\mathcal{E}_s \equiv \mathcal{E}_g/2$ )

$$\begin{aligned} r_1 &= A_{mc}\sqrt{\mathcal{E}_s}\cos(\phi - \hat{\phi}) + A_{ms}\sqrt{\mathcal{E}_s}\sin(\phi - \hat{\phi}) + n_c\sin\hat{\phi} - n_s\cos\hat{\phi} \\ r_2 &= A_{mc}\sqrt{\mathcal{E}_s}\sin(\phi - \hat{\phi}) + A_{ms}\sqrt{\mathcal{E}_s}\cos(\phi - \hat{\phi}) + n_c\sin\hat{\phi} - n_s\cos\hat{\phi} \end{aligned} \quad (7.5.80)$$

We observe that the effect of an imperfect phase estimate is twofold. First, the desired signal components in  $r_1$  and  $r_2$  are reduced in amplitude by the factor  $\cos(\phi - \hat{\phi})$ . In turn, this reduces the SNR by the factor  $\cos^2(\phi - \hat{\phi})$ . Second, there is a leakage of the quadrature signal components into the desired signal. This signal leakage, which is scaled by  $\sin(\phi - \hat{\phi})$ , causes a significant performance degradation unless  $\phi - \hat{\phi}$  is very small. This point serves to emphasize the importance of having an accurate carrier-phase estimate in order to demodulate the QAM signal.

The optimum detector computes the distance metrics

$$D(\mathbf{r}, \mathbf{s}_m) = \|\mathbf{r} - \mathbf{s}_m\|^2, \quad m = 1, 2, \dots, M \quad (7.5.81)$$

and selects the signal corresponding to the smallest value of  $D(\mathbf{r}, \mathbf{s}_m)$ . If a correlation metric is used in place of a distance metric, it is important to recognize that correlation metrics must employ bias correction because the QAM signals are not equal energy signals.

**Carrier-Phase Estimation.** As we have indicated above, the demodulation of a QAM signal requires a carrier that is phase-locked to the phase of the received carrier signal. Carrier-phase estimation for QAM can be accomplished in a number of different ways depending on the signal-point constellation and the phase relationships of the various signal points.

For example, let us consider the 8-point QAM signal constellation shown in Figure 7.17(b). The signal points in this constellation have one of two possible amplitude values and eight possible phases. The phases are spaced  $45^\circ$  apart. This phase symmetry allows us to use a PLL driven by the output of an 8th power-law device that generates a carrier component at  $8f_c$ , where  $f_c$  is the carrier frequency. Thus, the method illustrated in Figure 7.42 may be used in general for any QAM signal constellation that contains signal points with phases that are multiples of some phase angle  $\theta$ , where  $L\theta = 360^\circ$  for some integer  $L$ .

Another method for extracting a carrier-phase estimate  $\hat{\phi}$  from the received  $M$ -ary QAM signal is the DFPLL previously described in Section 7.5.5. The basic idea in the DFPLL is to estimate the phase of the QAM signal in each signal interval and remove the phase modulation from the carrier. The DFPLL may be used with any QAM signal, irrespective of the phase relationships among the signal points. To be specific, let us express the received QAM signal in the form

$$r(t) = A_m g_T(t) \cos(2\pi f_c t + \theta_n + \phi) + n(t), \quad (7.5.82)$$

where  $\theta_n$  is the phase of the signal point and  $\phi$  is the carrier phase. This signal is demodulated by crosscorrelating  $r(t)$  with  $\psi_1(t)$  and  $\psi_2(t)$ , which are given by Equation

(7.5.79). The sampled values at the output of the correlators are

$$\begin{aligned} r_1 &= A_m \sqrt{\mathcal{E}_s} \cos(\theta_n + \phi - \hat{\phi}) + n_c \cos(\theta_n + \phi - \hat{\phi}) - n_s \sin(\theta_n + \phi - \hat{\phi}) \\ r_2 &= A_m \sqrt{\mathcal{E}_s} \sin(\theta_n + \phi - \hat{\phi}) + n_c \sin(\theta_n + \phi - \hat{\phi}) - n_s \sin(\theta_n + \phi - \hat{\phi}) \end{aligned} \quad (7.5.83)$$

Now suppose that the detector, based on  $r_1$  and  $r_2$ , has made the correct decision on the transmitted signal point. Then we multiply  $r_1$  by  $-\sin \theta_n$  and  $r_2$  by  $\cos \theta_n$ . Thus, we obtain

$$\begin{aligned} -r_1 \sin \theta_n &= A_m \sqrt{\mathcal{E}_s} \cos(\theta_n + \phi - \hat{\phi}) \sin \theta_n + \text{noise component} \\ &= A_m \sqrt{\mathcal{E}_s} [-\sin \theta_n \cos \theta_n \cos(\phi - \hat{\phi}) + \sin^2 \theta_n \sin(\phi - \hat{\phi})] \\ &\quad + \text{noise component} \\ r_2 \cos \theta_n &= A_m \sqrt{\mathcal{E}_s} \sin(\theta_n + \phi - \hat{\phi}) \cos \theta_n + \text{noise component} \\ &= A_m \sqrt{\mathcal{E}_s} [\sin \theta_n \cos \theta_n \cos(\phi - \hat{\phi}) + \cos^2 \theta_n \sin(\phi - \hat{\phi})] \\ &\quad + \text{noise component} \end{aligned} \quad (7.5.84)$$

By adding these two terms we obtain an error signal  $e(t)$ , given as

$$\begin{aligned} e(t) &= r_2 \cos \theta_n - r_1 \sin \theta_n \\ &= A_m \mathcal{E}_s \sin(\phi - \hat{\phi}) + \text{noise components} \end{aligned} \quad (7.5.85)$$

This error signal is now passed to the loop filter that drives the VCO. Thus, only the phase of the QAM signal is used in obtaining an estimate of the carrier phase. Consequently, the general block diagram for the DFPLL, given in Figure 7.43, also applies to carrier-phase estimation for an  $M$ -ary QAM signal.

As in the case of digitally phase-modulated signals, the method described above for carrier-phase recovery results in phase ambiguities. This problem is solved generally by differential encoding of the data sequence at the input to the modulator.

### 7.5.7 Demodulation and Detection of Frequency-Modulated Signals

Let us assume that the FSK signals are transmitted through an additive white Gaussian noise channel. Furthermore, we assume that each signal is delayed in the transmission through the channel. Consequently, the filtered received signal at the input to the demodulator may be expressed as

$$r(t) = \sqrt{\frac{2\mathcal{E}_s}{T}} \cos(2\pi f_c t + 2\pi m \Delta f t + \phi_m) + n(t) \quad (7.5.86)$$

where  $\phi_m$  denotes the phase shift of the  $m$ th signal (due to the transmission delay) and  $n(t)$  represents the additive bandpass noise, which may be expressed as

$$n(t) = n_c(t) \cos 2\pi f_c t - n_s(t) \sin 2\pi f_c t \quad (7.5.87)$$

The demodulation and detection of the  $M$  FSK signals may be accomplished by one of two methods. One approach is to estimate the  $M$  carrier-phase shifts  $\{\phi_m\}$  and

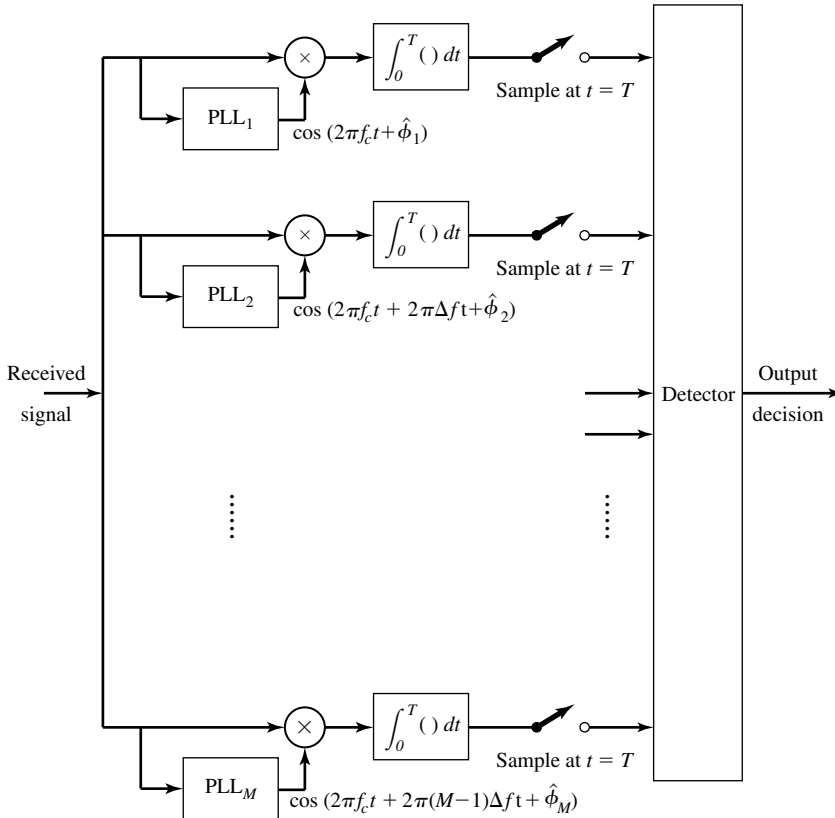


**Figure 7.46** Phase-coherent demodulation of  $M$ -ary FSK signals.

perform *phase-coherent demodulation and detection*. As an alternative method, the carrier phases may be ignored in the demodulation and detection of the FSK signals. The latter is called *noncoherent demodulation and detection*.

In phase-coherent demodulation, the received signal  $r(t)$  is correlated with each of the  $M$  possible received signals  $\cos(2\pi f_c t + 2\pi m \Delta f t + \hat{\phi}_m)$ ,  $m = 0, 1, \dots, M-1$ , where  $\{\hat{\phi}_m\}$  are the carrier phase estimates. A block diagram illustrating this type of demodulation is shown in Figure 7.46. It is interesting to note that when  $\hat{\phi}_m \neq \phi_m$ ,  $m = 0, 1, \dots, M-1$  (imperfect phase estimates), the frequency separation required for signal orthogonality at the demodulator is  $\Delta f = 1/T$  (see Problem 7.51), which is twice the minimum separation for orthogonality when  $\phi = \hat{\phi}$ .

The requirement for estimating  $M$  carrier phases makes coherent demodulation of FSK signals extremely complex and impractical, especially when the number of signals is large. Therefore, we shall not consider coherent detection of FSK signals.

Instead, we now consider a method for demodulation and detection that does not require knowledge of the carrier phases. The demodulation may be accomplished as

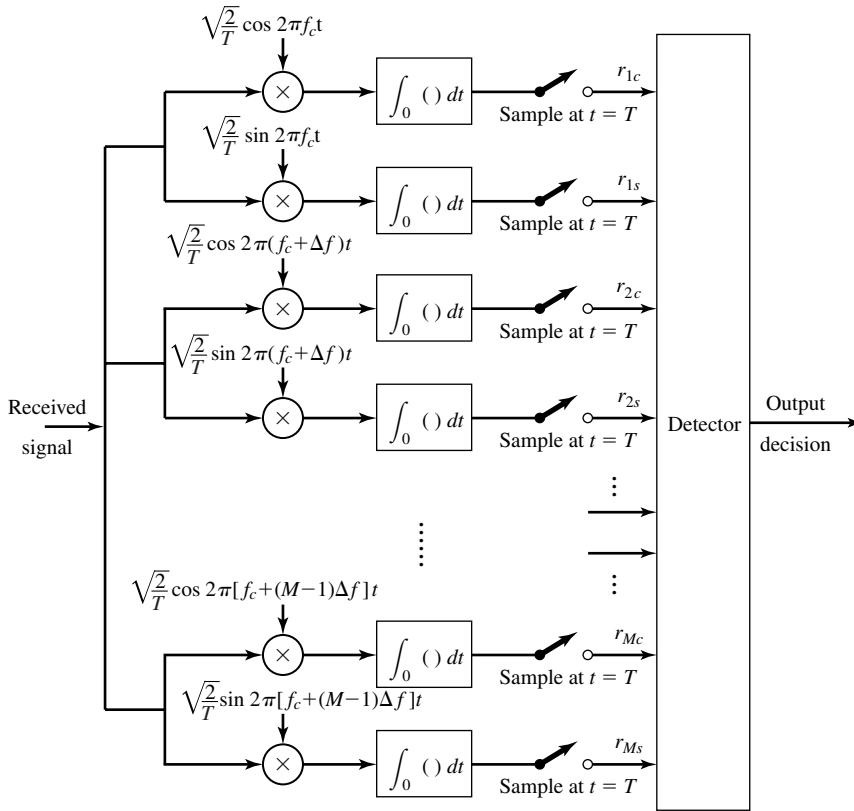


**Figure 7.47** Demodulation of  $M$ -ary FSK signals for noncoherent detection.

shown in Figure 7.47. In this case there are two correlators per signal waveform, or a total of  $2M$  correlators, in general. The received signal is correlated with the basis functions (quadrature carriers)  $\sqrt{\frac{2}{T}} \cos(2\pi f_c t + 2\pi m \Delta f t)$  and  $\sqrt{\frac{2}{T}} \sin(2\pi f_c t + 2\pi m \Delta f t)$  for  $m = 0, 1, \dots, M - 1$ . The  $2M$  outputs of the correlators are sampled at the end of the signal interval and the  $2M$  samples are passed to the detector. Thus, if the  $m$ th signal is transmitted, the  $2M$  samples at the detector may be expressed as

$$\begin{aligned}
 r_{kc} &= \sqrt{\mathcal{E}_s} \left[ \frac{\sin 2\pi(k-m)\Delta f T}{2\pi(k-m)\Delta f T} \cos \phi_m - \frac{\cos 2\pi(k-m)\Delta f T - 1}{2\pi(k-m)\Delta f T} \sin \phi_m \right] + n_{kc} \\
 r_{ks} &= \sqrt{\mathcal{E}_s} \left[ \frac{\cos 2\pi(k-m)\Delta f T - 1}{2\pi(k-m)\Delta f T} \cos \phi_m + \frac{\sin 2\pi(k-m)\Delta f T}{2\pi(k-m)\Delta f T} \sin \phi_m \right] + n_{ks}
 \end{aligned} \tag{7.5.88}$$

where  $n_{kc}$  and  $n_{ks}$  denote the Gaussian noise components in the sampled outputs.

We observe that when  $k = m$ , the sampled values to the detector are

$$\begin{aligned} r_{mc} &= \sqrt{\mathcal{E}_s} \cos \phi_m + n_{mc} \\ r_{ms} &= \sqrt{\mathcal{E}_s} \sin \phi_m + n_{ms} \end{aligned} \quad (7.5.89)$$

Furthermore, we observe that when  $k \neq m$ , the signal components in the samples  $r_{kc}$  and  $r_{ks}$  will vanish, independent of the values of the phase shift  $\phi_k$ , provided that the frequency separation between successive frequencies is  $\Delta f = 1/T$ . In such a case, the other  $2(M - 1)$  correlator outputs consist of noise only; i.e.,

$$r_{kc} = n_{kc}, \quad r_{ks} = n_{ks}, \quad k \neq m \quad (7.5.90)$$

In the following development, we assume that  $\Delta f = 1/T$ , so that the signals are orthogonal.

It is easily shown (see Problem 7.52) that the  $2M$  noise samples  $\{n_{kc}\}$  and  $\{n_{ks}\}$  are zero-mean, mutually uncorrelated Gaussian random variables with equal variance  $\sigma^2 = N_0/2$ . Consequently, the joint PDF for  $r_{mc}$  and  $r_{ms}$  conditioned on  $\phi_m$  is

$$f_{\mathbf{r}_m}(r_{mc}, r_{ms} | \phi_m) = \frac{1}{2\pi\sigma^2} e^{-[(r_{mc} - \sqrt{\mathcal{E}_s} \cos \phi_m)^2 + (r_{ms} - \sqrt{\mathcal{E}_s} \sin \phi_m)^2]/2\sigma^2} \quad (7.5.91)$$

and for  $m \neq k$ , we have

$$f_{\mathbf{r}_k}(r_{kc}, r_{ks}) = \frac{1}{2\pi\sigma^2} e^{-(r_{kc}^2 + r_{ks}^2)/2\sigma^2} \quad (7.5.92)$$

Given the  $2M$  observed random variables  $\{r_{kc}, r_{ks}, k = 1, 2, \dots, M\}$ , the optimum detector selects the signal that corresponds to the maximum of the posterior probabilities

$$P[\mathbf{s}_m \text{ was transmitted} | \mathbf{r}] \equiv P(\mathbf{s}_m | \mathbf{r}), \quad m = 1, 2, \dots, M \quad (7.5.93)$$

where  $\mathbf{r}$  is the  $2M$  dimensional vector with elements  $\{r_{kc}, r_{ks}, k = 1, 2, \dots, M\}$ . Let us derive the form for the optimum noncoherent detector for the case of binary FSK. The generalization to  $M$ -ary FSK is straightforward.

**Optimum Detector for Binary FSK.** In binary orthogonal FSK, the two posterior probabilities are

$$\begin{aligned} P(\mathbf{s}_1 | \mathbf{r}) &= \frac{f_{\mathbf{r}}(\mathbf{r} | \mathbf{s}_1) P(\mathbf{s}_1)}{f_{\mathbf{r}}(\mathbf{r})} \\ P(\mathbf{s}_2 | \mathbf{r}) &= \frac{f_{\mathbf{r}}(\mathbf{r} | \mathbf{s}_2) P(\mathbf{s}_2)}{f_{\mathbf{r}}(\mathbf{r})} \end{aligned} \quad (7.5.94)$$

and, hence, the optimum detection rule may be expressed as

$$P(\mathbf{s}_1 | \mathbf{r}) \underset{s_2}{\overset{s_1}{\gtrless}} P(\mathbf{s}_2 | \mathbf{r}) \quad (7.5.95)$$

or, equivalently,

$$\frac{f_{\mathbf{r}}(\mathbf{r} | \mathbf{s}_1) P(\mathbf{s}_1)}{f_{\mathbf{r}}(\mathbf{r})} \underset{s_2}{\overset{s_1}{\gtrless}} \frac{f_{\mathbf{r}}(\mathbf{r} | \mathbf{s}_2) P(\mathbf{s}_2)}{f_{\mathbf{r}}(\mathbf{r})} \quad (7.5.96)$$



where  $\mathbf{r}$  is the four-dimensional vector  $\mathbf{r} = (r_{1c}, r_{1s}, r_{2c}, r_{2s})$ . The relation in Equation (7.5.96) simplifies to the detection rule

$$\frac{f_{\mathbf{r}}(\mathbf{r} | \mathbf{s}_1)}{f_{\mathbf{r}}(\mathbf{r} | \mathbf{s}_2)} \underset{s_2}{\overset{s_1}{\geq}} \frac{P(\mathbf{s}_2)}{P(\mathbf{s}_1)} \quad (7.5.97)$$

The ratio of PDFs in the left-hand side of Equation (7.5.97) is the likelihood ratio, which we denote as

$$\Lambda(\mathbf{r}) = \frac{f_{\mathbf{r}}(\mathbf{r} | \mathbf{s}_1)}{f_{\mathbf{r}}(\mathbf{r} | \mathbf{s}_2)} \quad (7.5.98)$$

The right-hand side of Equation (7.5.97) is the ratio of the two prior probabilities, which takes the value of unity when the two signals are equally probable.

The PDFs  $f_{\mathbf{r}}(\mathbf{r} | \mathbf{s}_1)$  and  $f_{\mathbf{r}}(\mathbf{r} | \mathbf{s}_2)$  in the likelihood ratio may be expressed as

$$\begin{aligned} f_{\mathbf{r}}(\mathbf{r} | \mathbf{s}_1) &= f_{\mathbf{r}_2}(r_{2c}, r_{2s}) \int_0^{2\pi} f_{\mathbf{r}_1}(r_{1c}, r_{1s} | \phi_1) f_{\phi_1}(\phi_1) d\phi_1 \\ f_{\mathbf{r}}(\mathbf{r} | \mathbf{s}_2) &= f_{\mathbf{r}_1}(r_{1c}, r_{1s}) \int_0^{2\pi} f_{\mathbf{r}_2}(r_{2c}, r_{2s} | \phi_2) f_{\phi_2}(\phi_2) d\phi_2 \end{aligned} \quad (7.5.99)$$

where  $f_{\mathbf{r}_m}(r_{mc}, r_{ms} | \phi_m)$  and  $f_{\mathbf{r}_k}(r_{kc}, r_{ks})$ ,  $m \neq k$ , are given by Equations (7.5.91) and (7.5.92), respectively. Thus, the carrier phases  $\phi_1$  and  $\phi_2$  are eliminated by simply averaging  $f_{\mathbf{r}_m}(r_{mc}, r_{ms} | \phi_m)$ .

The uniform PDF for  $\phi_m$  represents the most ignorance regarding the phases of the carriers. This is called the *least favorable* PDF for  $\phi_m$ . With  $f_{\phi_m}(\phi_m) = 1/2\pi$ ,  $0 \leq \phi_m < 2\pi$ , substituted into the integrals given in Equation (7.5.99), we obtain

$$\begin{aligned} &\frac{1}{2\pi} \int_0^{2\pi} f_{\mathbf{r}_m}(\mathbf{r}_{mc}, \mathbf{r}_{ms} | \phi_m) d\phi_m \\ &= \frac{1}{2\pi \sigma^2} e^{-(r_{mc}^2 + r_{ms}^2 + \mathcal{E}_s)/2\sigma^2} \frac{1}{2\pi} \int_0^{2\pi} e^{\sqrt{\mathcal{E}_s}(r_{mc} \cos \phi_m + r_{ms} \sin \phi_m)/\sigma^2} d\phi_m \end{aligned} \quad (7.5.100)$$

But

$$\frac{1}{2\pi} \int_0^{2\pi} e^{\sqrt{\mathcal{E}_s}(r_{mc} \cos \phi_m + r_{ms} \sin \phi_m)/\sigma^2} d\phi_m = I_0 \left( \frac{\sqrt{\mathcal{E}_s(r_{mc}^2 + r_{ms}^2)}}{\sigma^2} \right) \quad (7.5.101)$$

where  $I_0(x)$  is the modified Bessel function of order zero. This function is a monotonically increasing function of its argument as illustrated in Figure 7.48.  $I_0(x)$  has the power series expansion

$$I_0(x) = \sum_{k=0}^{\infty} \frac{x^{2k}}{2^{2k} (k!)^2} \quad (7.5.102)$$

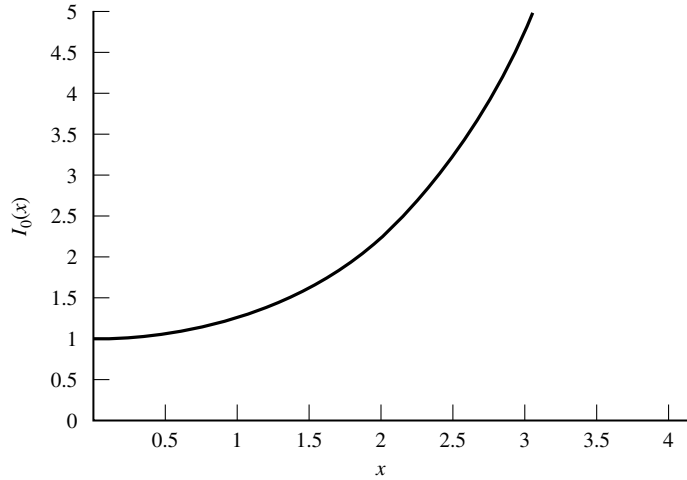


Figure 7.48 Graph of  $I_0(x)$ .

From (7.5.97)–(7.5.99), we obtain the likelihood ratio  $\Lambda(\mathbf{r})$  in the form

$$\Lambda(\mathbf{r}) = \frac{I_0\left(\sqrt{\mathcal{E}_s(r_{1c}^2 + r_{1s}^2)}/\sigma^2\right)}{I_0\left(\sqrt{\mathcal{E}_s(r_{2c}^2 + r_{2s}^2)}/\sigma^2\right)} \underset{s_2}{\overset{s_1}{>}} \frac{P(\mathbf{s}_2)}{P(\mathbf{s}_1)} \quad (7.5.103)$$

Thus, the optimum detector computes the two envelopes  $r_1 = \sqrt{r_{1c}^2 + r_{1s}^2}$  and  $r_2 = \sqrt{r_{2c}^2 + r_{2s}^2}$  and the corresponding values of the Bessel function  $I_0(\sqrt{\mathcal{E}_s r_1^2}/\sigma^2)$  and  $I_0(\sqrt{\mathcal{E}_s r_2^2}/\sigma^2)$  to form the likelihood ratio. We observe that this computation requires knowledge of the noise variance  $\sigma^2$  and the signal energy  $\mathcal{E}_s$ . The likelihood ratio is then compared with the threshold  $P(\mathbf{s}_2)/P(\mathbf{s}_1)$  to determine which signal was transmitted.

A significant simplification in the implementation of the optimum detector occurs when the two signals are equally probable. In such a case, the threshold becomes unity and, due to the monotonicity of the Bessel function, the optimum detector rule simplifies to

$$\sqrt{r_{1c}^2 + r_{1s}^2} \underset{s_2}{\overset{s_1}{>}} \sqrt{r_{2c}^2 + r_{2s}^2} \quad (7.5.104)$$

Thus, the optimum detector bases its decision on the two envelopes  $r_1 = \sqrt{r_{1c}^2 + r_{1s}^2}$  and  $r_2 = \sqrt{r_{2c}^2 + r_{2s}^2}$  and, hence, it is called an *envelope detector*.

We observe that the computation of the envelopes of the received signal samples at the output of the demodulator renders the carrier signal phases  $\{\phi_m\}$  irrelevant in the

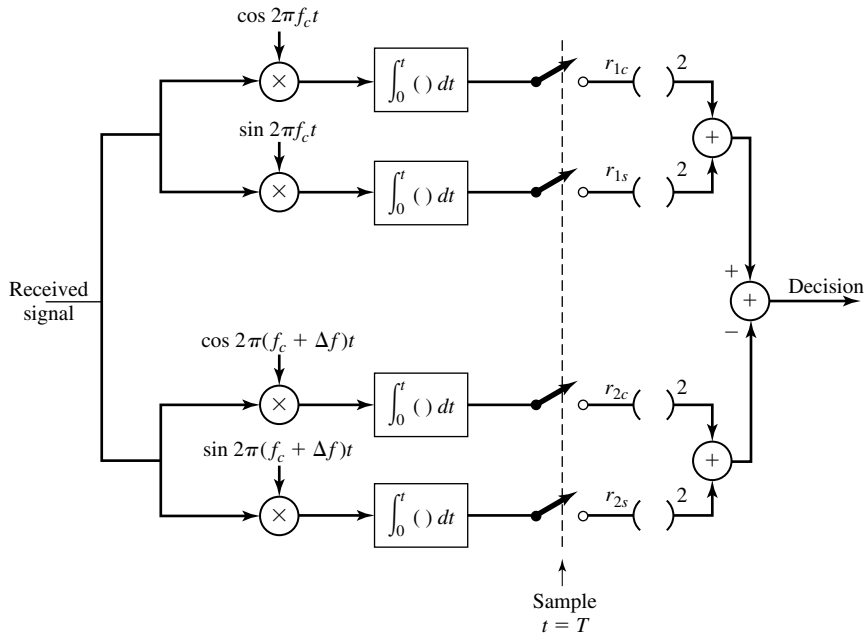


**Figure 7.49** Demodulation and square-law detection of binary FSK signals.

decision as to which signal was transmitted. Equivalently, the decision may be based on the computation of the squared envelopes  $r_1^2$  and  $r_2^2$ , in which case the detector is called a *square-law detector*. Figure 7.49 shows the block diagram of the demodulator and the square-law detector.

The generalization of the optimum demodulator and detector to  $M$ -ary orthogonal FSK signals is straightforward. As illustrated in Figure 7.47, the output of the optimum demodulator at the sampling instant consists of the  $2M$  vector components  $(r_{1c}, r_{1s}, r_{2c}, r_{2s}, \dots, r_{Mc}, r_{Ms})$ . Then, the optimum noncoherent detector computes the  $M$  envelopes as

$$r_m = \sqrt{r_{mc}^2 + r_{ms}^2}, \quad m = 1, 2, \dots, M \quad (7.5.105)$$

Thus, the unknown carrier phases of the received signals are rendered irrelevant to the decision as to which signal was transmitted. When all the  $M$  signals are equally likely to be transmitted, the optimum detector selects the signal corresponding to the largest envelope (or squared envelope). In the case of nonequally probable transmitted signals, the optimum detector must compute the  $M$  posterior probabilities in Equation (7.5.93) and then select the signal corresponding to the largest posterior probability.

## 7.6 PROBABILITY OF ERROR FOR SIGNAL DETECTION IN ADDITIVE WHITE GAUSSIAN NOISE

In this section, we evaluate the performance of the detector in terms of the probability of error when the additive noise is white and Gaussian. First, we consider binary modulation and, then,  $M$ -ary types of modulation.

### 7.6.1 Probability of Error for Binary Modulation

Let us consider binary PAM baseband signals, where the two signal waveforms are  $s_1(t) = g_T(t)$  and  $s_2(t) = -g_T(t)$ , where  $g_T(t)$  is an arbitrary pulse which is nonzero in the interval  $0 \leq t \leq T_b$  and zero elsewhere.

Since  $s_1(t) = -s_2(t)$ , these signals are said to be *antipodal*. The energy in the pulse  $g_T(t)$  is equal to the energy per bit  $\mathcal{E}_b$ . As in Section 7.2, PAM signals are represented geometrically as one-dimensional vectors. Hence, for binary PAM, the signal points are  $s_1 = \sqrt{\mathcal{E}_b}$  and  $s_2 = -\sqrt{\mathcal{E}_b}$ . Figure 7.50 illustrates the two signal points.

Let us assume that the two signals are equally likely and that signal  $s_1(t)$  was transmitted. Then, the received signal from the (matched filter or correlation-type) demodulator is

$$r = s_1 + n = \sqrt{\mathcal{E}_b} + n \quad (7.6.1)$$

where  $n$  represents the additive Gaussian noise component which has zero mean and variance  $\sigma_n^2 = N_0/2$ . In this case, the decision rule based on the correlation metric given by Equation (7.5.44) compares  $r$  with the threshold zero. If  $r > 0$ , the decision is made in favor of  $s_1(t)$  and if  $r < 0$ , the decision is made that  $s_2(t)$  was transmitted. Clearly, the two conditional PDFs of  $r$  are

$$f(r | s_1) = \frac{1}{\sqrt{\pi N_0}} e^{-(r - \sqrt{\mathcal{E}_b})^2 / N_0} \quad (7.6.2)$$

$$f(r | s_2) = \frac{1}{\sqrt{\pi N_0}} e^{-(r + \sqrt{\mathcal{E}_b})^2 / N_0} \quad (7.6.3)$$

These two conditional PDFs are shown in Figure 7.51.

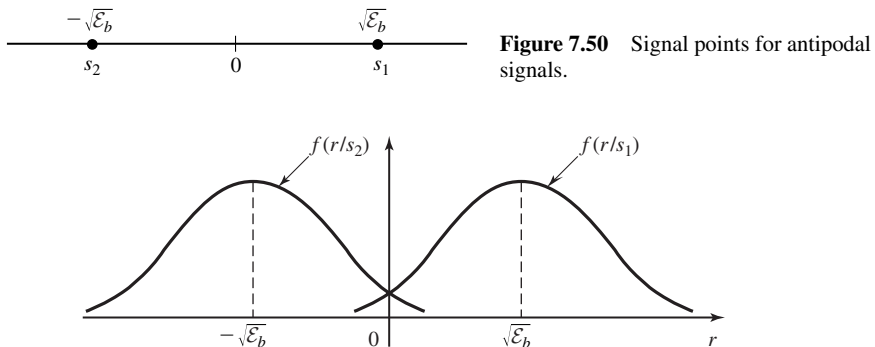


Figure 7.51 Conditional PDF's of two signals.

Given that  $s_1(t)$  was transmitted, the probability of error is simply the probability that  $r < 0$ ; i.e.,

$$P(e | s_1) = \int_{-\infty}^0 p(r | s_1) dr \quad (7.6.4)$$

$$= \frac{1}{\sqrt{\pi N_0}} \int_{-\infty}^0 e^{-(r - \sqrt{\mathcal{E}_b})^2 / N_0} dr \quad (7.6.5)$$

$$= \frac{1}{\sqrt{2\pi}} \int_{-\infty}^{-\sqrt{2\mathcal{E}_b/N_0}} e^{-x^2/2} dx \quad (7.6.6)$$

$$= \frac{1}{\sqrt{2\pi}} \int_{\sqrt{2\mathcal{E}_b/N_0}}^{\infty} e^{-x^2/2} dx \quad (7.6.7)$$

$$= Q\left(\sqrt{\frac{2\mathcal{E}_b}{N_0}}\right) \quad (7.6.8)$$

where  $Q(x)$  is the  $Q$ -function defined previously in Section 5.1. Similarly, if we assume that  $s_2(t)$  was transmitted,  $r = -\sqrt{\mathcal{E}_b} + n$  and the probability that  $r > 0$  is also  $P(e | s_2) = Q(\sqrt{\frac{2\mathcal{E}_b}{N_0}})$ . Since the signals  $s_1(t)$  and  $s_2(t)$  are equally likely to be transmitted, the average probability of error is

$$\begin{aligned} P_b &= \frac{1}{2}P(e | s_1) + \frac{1}{2}P(e | s_2) \\ &= Q\left(\sqrt{\frac{2\mathcal{E}_b}{N_0}}\right) \end{aligned} \quad (7.6.9)$$

We should observe two important characteristics of this performance measure. First, we note that the probability of error depends only on the ratio  $\mathcal{E}_b/N_0$  and not on any other detailed characteristics of the signals and the noise. Second, we note that  $2\mathcal{E}_b/N_0$  is also the output SNR from the matched filter (and correlation-type) demodulator. The ratio  $\mathcal{E}_b/N_0$  is usually called the *signal-to-noise ratio* (SNR), or SNR/bit.

We also observe that the probability of error may be expressed in terms of the distance between the two signals  $s_1$  and  $s_2$ . From Figure 7.50, we observe that the two signals are separated by the distance  $d_{12} = 2\sqrt{\mathcal{E}_b}$ . By substituting  $\mathcal{E}_b = d_{12}^2/4$  in (7.6.9) we obtain

$$P_b = Q\left(\sqrt{\frac{d_{12}^2}{2N_0}}\right) \quad (7.6.10)$$

This expression illustrates the dependence of the error probability on the distance between the two signal points. It can be shown that Equation (7.6.10) can be used for computing the error probability of *any* binary communication system with two equiprobable messages.

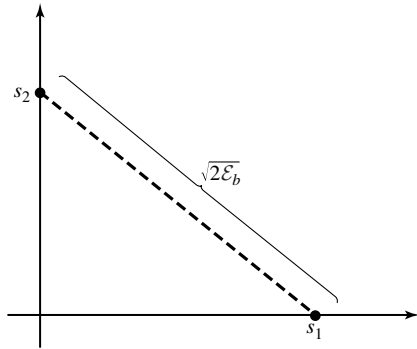


**Figure 7.52** Signal points for orthogonal signals.

Next, let us evaluate the error probability for binary orthogonal signals. Recall the binary PPM is an example of binary orthogonal signaling. In this case, the signal vectors  $\mathbf{s}_1$  and  $\mathbf{s}_2$  are two-dimensional, as shown in Figure 7.52, and may be expressed, according to Equation (7.3.8), as

$$\mathbf{s}_1 = (\sqrt{\mathcal{E}_b}, 0) \quad (7.6.11)$$

$$\mathbf{s}_2 = (0, \sqrt{\mathcal{E}_b}) \quad (7.6.12)$$

where  $\mathcal{E}_b$  denotes the energy for each of the waveforms. Note that the distance between these signal points is  $d_{12} = \sqrt{2\mathcal{E}_b}$ .

To evaluate the probability of error, let us assume that  $\mathbf{s}_1$  was transmitted. Then, the received vector at the output of the demodulator is

$$\mathbf{r} = [\sqrt{\mathcal{E}_b} + n_1, n_2] \quad (7.6.13)$$

We can now substitute for  $\mathbf{r}$  into the correlation metrics given by Equation (7.5.44) to obtain  $C(\mathbf{r}, \mathbf{s}_1)$  and  $C(\mathbf{r}, \mathbf{s}_2)$ . Then the probability of error is the probability that  $C(\mathbf{r}, \mathbf{s}_2) > C(\mathbf{r}, \mathbf{s}_1)$ . Thus,

$$P(e | \mathbf{s}_1) = P[C(\mathbf{r}, \mathbf{s}_2) > C(\mathbf{r}, \mathbf{s}_1)] = P[n_2 - n_1 > \sqrt{\mathcal{E}_b}] \quad (7.6.14)$$

Since  $n_1$  and  $n_2$  are zero-mean, statistically independent Gaussian random variables, each with variance  $N_0/2$ , the random variable  $x = n_2 - n_1$  is zero mean Gaussian with variance  $N_0$ . Hence,

$$P(n_2 - n_1 > \sqrt{\mathcal{E}_b}) = \frac{1}{\sqrt{2\pi N_0}} \int_{\sqrt{\mathcal{E}_b}}^{\infty} e^{-x^2/2N_0} dx \quad (7.6.15)$$

$$= \frac{1}{\sqrt{2\pi}} \int_{\sqrt{\mathcal{E}_b/N_0}}^{\infty} e^{-x^2/2} dx \quad (7.6.16)$$

$$= Q \left[ \sqrt{\frac{\mathcal{E}_b}{N_0}} \right] \quad (7.6.17)$$

Due to symmetry, the same error probability is obtained when we assume that  $\mathbf{s}_2$  is transmitted. Consequently, the average error probability for binary orthogonal signals is

$$P_b = Q \left[ \sqrt{\frac{\mathcal{E}_b}{N_0}} \right] \quad (7.6.18)$$

If we compare the probability of error for binary antipodal signals with that for binary orthogonal signals, we find that orthogonal signals require a factor of two more energy to achieve the same error probability as antipodal signals. Since  $10 \log_{10} 2 = 3$  dB, we say that orthogonal signals are 3-dB poorer than antipodal signals. The difference of 3 dB is simply due to the distance between the two signal points, which is  $d_{12}^2 = 2\mathcal{E}_b$  for orthogonal signals, whereas  $d_{12}^2 = 4\mathcal{E}_b$  for antipodal signals.

The error probability versus  $20 \log_{10} \mathcal{E}_b/N_0$  for these two types of signals is shown in Figure 7.53. As observed from this figure, at any given error probability, the  $\mathcal{E}_b/N_0$  required for orthogonal signals is 3-dB more than that for antipodal signals.

### 7.6.2 Probability of Error for $M$ -ary PAM

In this section, we derive the probability of error for  $M$ -ary PAM transmitted over an AWGN channel. Recall that baseband  $M$ -ary PAM signals are represented geometrically as  $M$  one-dimensional signal points with values

$$s_m = \sqrt{\mathcal{E}_g} A_m, \quad m = 1, 2, \dots, M \quad (7.6.19)$$

where  $\mathcal{E}_g$  is the energy of the basic signal pulse  $g_T(t)$ . The amplitude values may be expressed as

$$A_m = (2m - 1 - M), \quad m = 1, 2, \dots, M \quad (7.6.20)$$

where the distance between adjacent signal points is  $2\sqrt{\mathcal{E}_g}$ .

As previously indicated in Section 7.2, the PAM signals have different energies, denoted as  $\{\mathcal{E}_m\}$ . The average energy is

$$\mathcal{E}_{av} = \frac{1}{M} \sum_{m=1}^M \mathcal{E}_m \quad (7.6.21)$$

$$= \frac{\mathcal{E}_g}{M} \sum_{m=1}^M (2m - 1 - M)^2 \quad (7.6.22)$$

$$= \frac{\mathcal{E}_g}{M} \frac{M(M^2 - 1)}{3} \quad (7.6.23)$$

$$= \left( \frac{M^2 - 1}{3} \right) \mathcal{E}_g \quad (7.6.24)$$

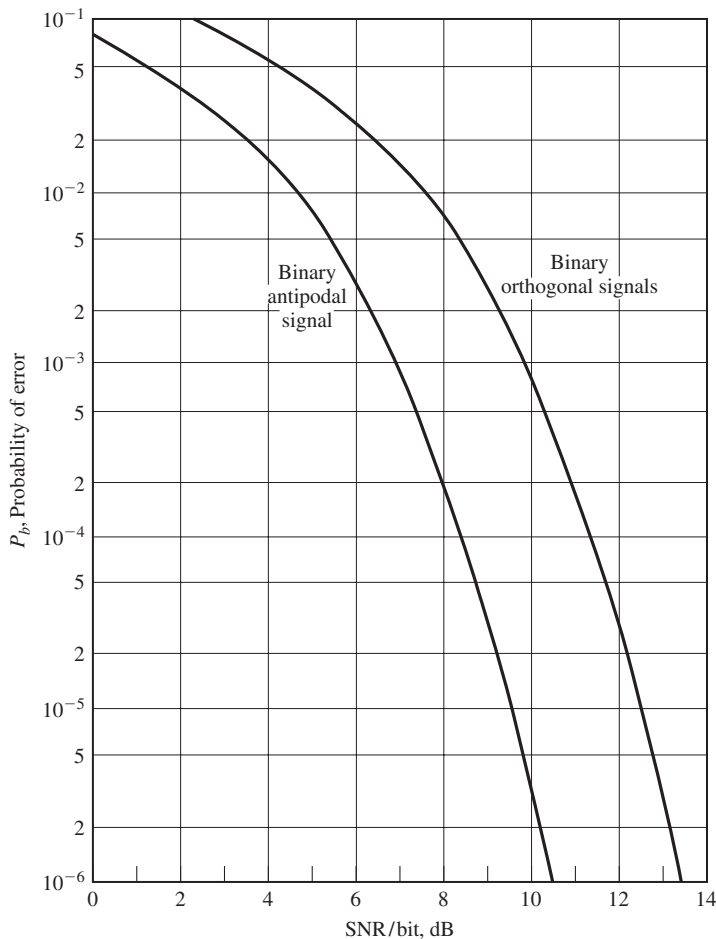


**Figure 7.53** Probability of error for binary signals.

Equivalently, we may characterize these signals in terms of their average power, which is

$$P_{av} = \frac{\mathcal{E}_{av}}{T} = \left( \frac{M^2 - 1}{3} \right) \frac{\mathcal{E}_g}{T} \quad (7.6.25)$$

The average probability of error for  $M$ -ary PAM can be determined from the decision rule that maximizes the correlation metrics given by Equation (7.5.44). Equivalently, the detector compares the demodulator output  $r$  with a set of  $M - 1$  thresholds, which are placed at the midpoints of successive amplitude levels, as shown in Figure 7.54. Thus, a decision is made in favor of the amplitude level that is closest to  $r$ .



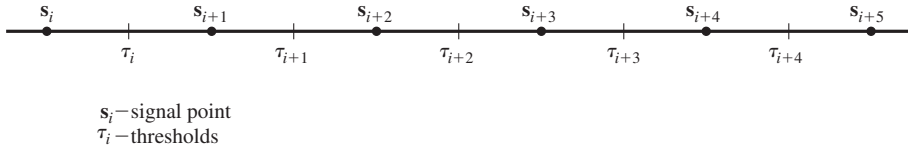


**Figure 7.54** Placement of thresholds at midpoints of successive amplitude levels.

The placing of the thresholds as shown in Figure 7.54, helps in evaluating the probability of error. We note that if the  $m$ th amplitude level is transmitted, the demodulator output is

$$r = s_m + n = \sqrt{\mathcal{E}_g} A_m + n \quad (7.6.26)$$

where the noise variable  $n$  has zero mean and variance  $\sigma_n^2 = N_0/2$ . On the basis that all amplitude levels are equally likely a priori, the average probability of a symbol error is simply the probability that the noise variable  $n$  exceeds in magnitude one-half of the distance between levels. However, when either one of the two outside levels  $\pm(M-1)$  is transmitted, an error can occur in one direction only. Thus, we have

$$P_M = \frac{M-1}{M} P(|r - s_m| > \sqrt{\mathcal{E}_g}) \quad (7.6.27)$$

$$= \frac{M-1}{M} \frac{2}{\sqrt{\pi N_0}} \int_{\sqrt{\mathcal{E}_g}}^{\infty} e^{-x^2/N_0} dx \quad (7.6.28)$$

$$= \frac{M-1}{M} \frac{2}{\sqrt{2\pi}} \int_{\sqrt{2\mathcal{E}_g/N_0}}^{\infty} e^{-x^2/2} dx \quad (7.6.29)$$

$$= \frac{2(M-1)}{M} Q\left(\sqrt{\frac{2\mathcal{E}_g}{N_0}}\right) \quad (7.6.30)$$

The error probability in Equation (7.6.30) can also be expressed in terms of the average transmitted power. From Equation (7.6.25), we note that

$$\mathcal{E}_g = \frac{3}{M^2 - 1} P_{av} T \quad (7.6.31)$$

By substituting for  $\mathcal{E}_g$  in Equation (7.6.30), we obtain the average probability of a symbol error for PAM in terms of the average power as

$$P_M = \frac{2(M-1)}{M} Q\left(\sqrt{\frac{6P_{av} T}{(M^2 - 1)N_0}}\right) \quad (7.6.32)$$

or, equivalently,

$$P_M = \frac{2(M-1)}{M} Q \left( \sqrt{\frac{6\mathcal{E}_{av}}{(M^2-1)N_0}} \right) \quad (7.6.33)$$

where  $\mathcal{E}_{av} = P_{av}T$  is the average energy.

In plotting the probability of a symbol error for  $M$ -ary signals such as  $M$ -ary PAM, it is customary to use the average SNR/bit as the basic parameter. Since  $T = kT_b$  and  $k = \log_2 M$ , Equation (7.6.33) may be expressed as

$$P_M = \frac{2(M-1)}{M} Q \left( \sqrt{\frac{6(\log_2 M)\mathcal{E}_{bav}}{(M^2-1)N_0}} \right) \quad (7.6.34)$$

where  $\mathcal{E}_{bav} = P_{av}T_b$  is the average bit energy and  $\mathcal{E}_{bav}/N_0$  is the average SNR/bit. Figure 7.55 illustrates the probability of a symbol error as a function of  $10 \log_{10} \mathcal{E}_{bav}/N_0$  with  $M$  as a parameter. Note that the case  $M = 2$  corresponds to the error probability for binary antipodal signals. We also observe that the SNR/bit increases by over 4 dB for every factor of two increase in  $M$ . For large  $M$ , the additional SNR/bit required to increase  $M$  by a factor of two approaches 6 dB.

**Bandpass PAM Signals.** In this case, the input to the detector, as shown in Equation (7.5.60), is

$$\begin{aligned} r &= A_m \sqrt{\mathcal{E}_g/2} + n \\ &= s_m + n \end{aligned}$$

where the Gaussian random variable  $n$  has mean  $E(n) = 0$  and variance

$$\begin{aligned} \sigma_n^2 &= E(n^2) \\ &= \int_0^T \int_0^T E[n(t)n(\tau)] \psi(t)\psi(\tau) dt d\tau \\ &= \frac{N_0}{2} \int_0^T \psi^2(t) dt = \frac{N_0}{2} \end{aligned}$$

Following the development for baseband PAM signals, the probability of a symbol error is

$$P_M = \frac{M-1}{M} P(|r - s_m| > \sqrt{\mathcal{E}_g/2}) \quad (7.6.35)$$

$$= \frac{2(M-1)}{M} Q \left( \sqrt{\frac{\mathcal{E}_g}{N_0}} \right) \quad (7.6.36)$$

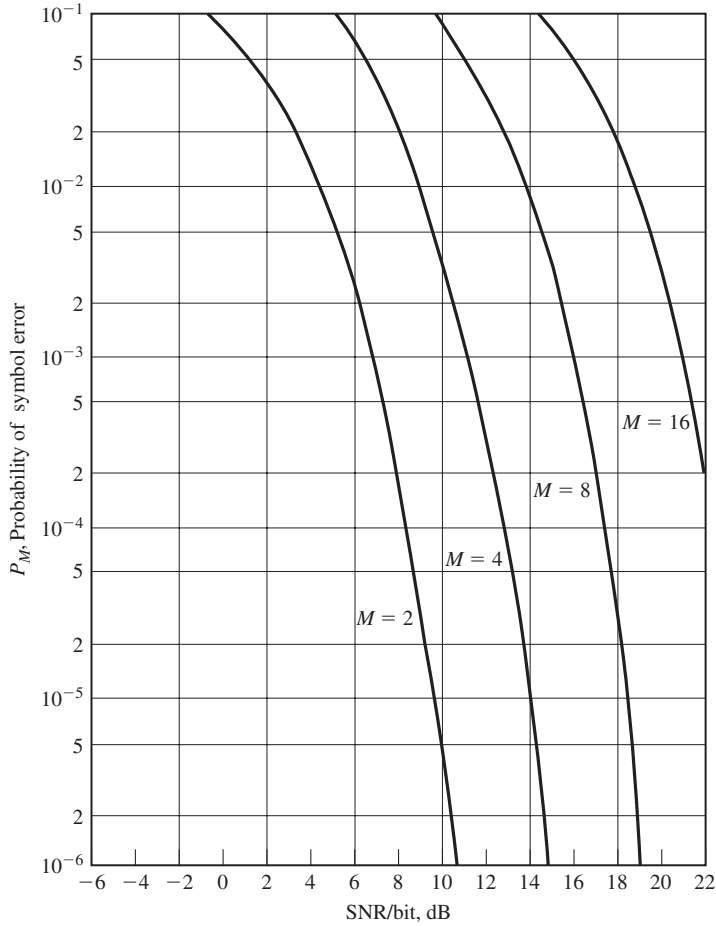


**Figure 7.55** Probability of a symbol error for PAM.

Then, we relate the average transmitted energy to  $\mathcal{E}_g$ . We have

$$\mathcal{E}_{av} = P_{av}T \quad (7.6.37)$$

$$= \sum_{m=1}^M \mathcal{E}_m \quad (7.6.38)$$

$$= \frac{\mathcal{E}_g}{2} \sum_{m=1}^M (2m - 1 - M)^2 \quad (7.6.39)$$

$$= \frac{M^2 - 1}{6} \mathcal{E}_g \quad (7.6.40)$$

Hence,

$$\mathcal{E}_g = \frac{6P_{av}T}{M^2 - 1} \quad (7.6.41)$$

Substitution of Equation (7.6.41) into Equation (7.6.36) yields the desired form for the probability of error for  $M$ -ary PAM; i.e.,

$$P_M = \frac{2(M-1)}{M} Q \left( \sqrt{\frac{6P_{av}T}{(M^2-1)N_0}} \right) \quad (7.6.42)$$

This is exactly the same result as the probability of a symbol error for  $M$ -ary PAM transmission over a baseband AWGN channel.

### 7.6.3 Probability of Error for Phase-Coherent PSK Modulation

In this section, we shall evaluate the probability of error for  $M$ -ary phase modulation in AWGN with the optimum demodulator and detector. The optimum detector based on the phase metric given by Equation (7.5.68) will be used in this computation. It is assumed that a perfect estimate of the received carrier phase is available. Consequently, the performance that we derive below is for ideal phase-coherent modulation.

Let us consider the case in which the transmitted signal phase is  $\theta = 0$ , corresponding to the signal  $u_0(t)$ . Hence, the transmitted signal vector is

$$\mathbf{s}_0 = (\sqrt{\mathcal{E}_s}, 0) \quad (7.6.43)$$

and the received signal vector has components

$$r_1 = \sqrt{\mathcal{E}_s} + n_c \quad (7.6.44)$$

$$r_2 = n_s$$

Because  $n_c$  and  $n_s$  are jointly Gaussian random variables, it follows that  $r_1$  and  $r_2$  are jointly Gaussian random variables with  $E[r_1] = \sqrt{\mathcal{E}_s}$ ,  $E[r_2] = 0$  and  $\sigma_{r_1}^2 = \sigma_{r_2}^2 = N_0/2 = \sigma_r^2$ . Consequently,

$$f_r(r_1, r_2) = \frac{1}{2\pi\sigma_r^2} e^{-[(r_1 - \sqrt{\mathcal{E}_s})^2 + r_2^2]/2\sigma_r^2} \quad (7.6.45)$$

The detector metric is the phase  $\Theta_r = \tan^{-1} r_2/r_1$ . The PDF of  $\Theta_r$  is obtained by a change in variables from  $(r_1, r_2)$  to

$$\begin{aligned} V &= \sqrt{r_1^2 + r_2^2} \\ \Theta_r &= \tan^{-1} \frac{r_2}{r_1} \end{aligned} \quad (7.6.46)$$

This change in variables yields the joint PDF

$$f_{V, \Theta_r}(v, \theta_r) = \frac{v}{2\pi\sigma_r^2} e^{- (v^2 + \mathcal{E}_s - 2\sqrt{\mathcal{E}_s}v \cos \theta_r)/2\sigma_r^2} \quad (7.6.47)$$

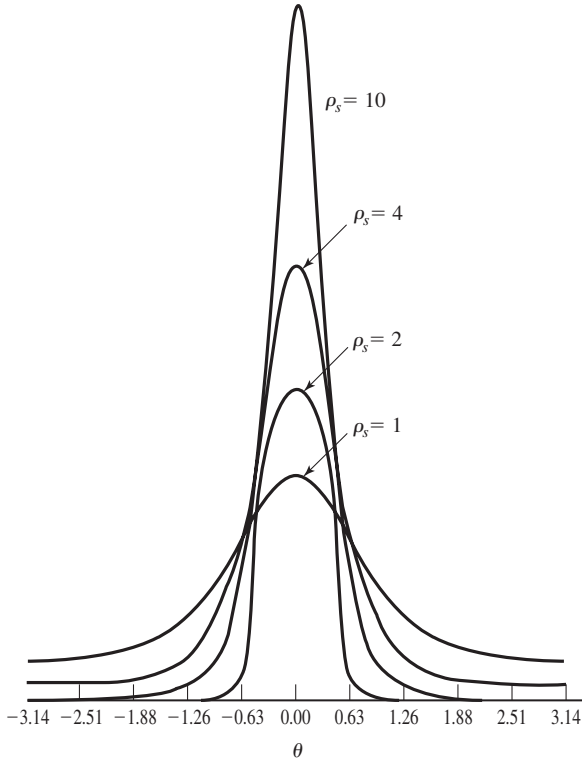


**Figure 7.56** Probability density function  $p(\theta)$  for  $\rho_s = 1, 2, 4, 10$ .

Integration of  $f_{V, \Theta_r}(v, \theta_r)$  over the range of  $v$  yields  $f_{\Theta_r}(\theta_r)$ , i.e.,

$$f_{\Theta_r}(\theta_r) = \int_0^{\infty} f_{V, \Theta_r}(v, \theta_r) dv \quad (7.6.48)$$

$$= \frac{1}{2\pi} e^{-2\rho_s \sin^2 \theta_r} \int_0^{\infty} v e^{-(v - \sqrt{4\rho_s} \cos \theta_r)^2 / 2} dv \quad (7.6.49)$$

where for convenience, we have defined the symbol SNR as  $\rho_s = \mathcal{E}_s/N_0$ . Figure 7.56 illustrates  $f_{\Theta_r}(\theta_r)$  for several values of the SNR parameter  $\rho_s$  when the transmitted phase is zero. Note that  $f_{\Theta_r}(\theta_r)$  becomes narrower and more peaked about  $\theta_r = 0$  as the SNR  $\rho_s$  increases.

When  $u_0(t)$  is transmitted, a decision error is made if the noise causes the phase to fall outside the range  $-\pi/M \leq \Theta_r \leq \pi/M$ . Hence, the probability of a symbol error is

$$P_M = 1 - \int_{-\pi/M}^{\pi/M} f_{\Theta_r}(\theta) d\Theta \quad (7.6.50)$$

In general, the integral of  $f_{\Theta_r}(\theta)$  does not reduce to a simple form and must be evaluated numerically, except for  $M = 2$  and  $M = 4$ .

For binary-phase modulation, the two signals  $u_0(t)$  and  $u_1(t)$  are antipodal and, hence, the error probability is

$$P_2 = Q\left(\sqrt{\frac{2\mathcal{E}_b}{N_0}}\right) \quad (7.6.51)$$

When  $M = 4$ , we have in effect two binary-phase modulation signals in phase quadrature. With a perfect estimate of the carrier phase, there is no crosstalk or interference between the signals on the two quadrature carriers and, hence, the bit error probability is identical to that in Equation (7.6.51). On the other hand, the symbol error probability for  $M = 4$  is determined by noting that

$$P_c = (1 - P_2)^2 = \left[1 - Q\left(\sqrt{\frac{2\mathcal{E}_b}{N_0}}\right)\right]^2 \quad (7.6.52)$$

where  $P_c$  is the probability of a correct decision for the 2-bit symbol. The result in Equation (7.6.52) follows from the statistical independence of the noise on the quadrature carriers. Therefore, the symbol error probability for  $M = 4$  is

$$P_4 = 1 - P_c \quad (7.6.53)$$

$$= 2Q\left(\sqrt{\frac{2\mathcal{E}_b}{N_0}}\right) \left[1 - \frac{1}{2}Q\left(\sqrt{\frac{2\mathcal{E}_b}{N_0}}\right)\right] \quad (7.6.54)$$

For  $M > 4$ , the symbol error probability  $P_M$  is obtained by numerically integrating Equation (7.6.50). Figure 7.57 illustrates this error probability as a function of the SNR/bit for  $M = 2, 4, 8, 16,$  and  $32$ . The graphs clearly illustrate the penalty in SNR/bit as  $M$  increases beyond  $M = 4$ . For example, at  $P_M = 10^{-5}$ , the difference between  $M = 4$  and  $M = 8$  is approximately 4 dB, and the difference between  $M = 8$  and  $M = 16$  is approximately 5 dB. For large values of  $M$ , doubling the number of phases requires an additional 6 dB/bit to achieve the same performance.

An approximation to the error probability for large values of  $M$  and for large SNR may be obtained by first approximating  $f_{\Theta_r}(\theta)$ . For  $\mathcal{E}_s/N_0 \gg 1$  and  $|\Theta_r| \leq \pi/2$ ,  $f_{\Theta_r}(\theta_r)$  is well approximated as

$$f_{\Theta_r}(\theta_r) \approx \sqrt{\frac{2\rho_s}{\pi}} \cos \theta_r e^{-2\rho_s \sin^2 \theta_r} \quad (7.6.55)$$

By substituting for  $f_{\Theta_r}(\theta_r)$  in Equation (7.6.50) and performing the change in variable

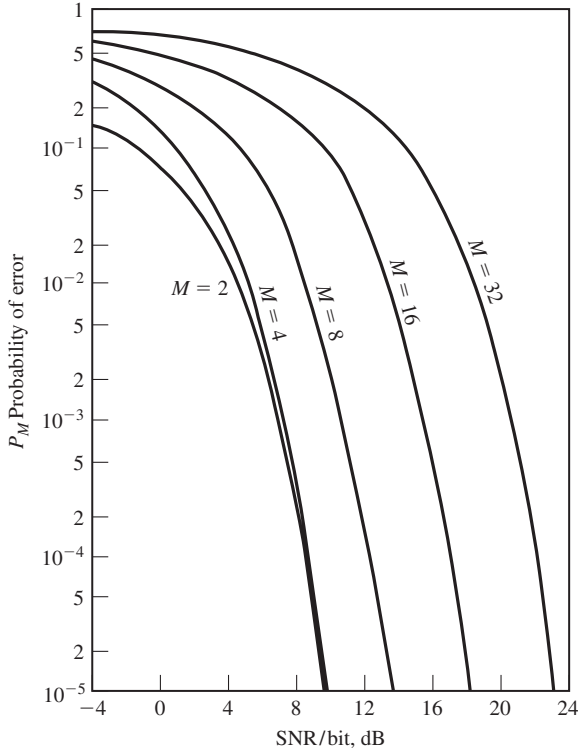


**Figure 7.57** Probability of a symbol error for PSK signals.

from  $\theta_r$  to  $u = 2\sqrt{\rho_s} \sin \theta_r$ , we find that

$$P_M \approx 1 - \int_{-\pi/M}^{\pi/M} \sqrt{\frac{2\rho_s}{\pi}} \cos \theta_r e^{-2\rho_s \sin^2 \theta_r} d\theta_r \quad (7.6.56)$$

$$\approx \frac{2}{\sqrt{2\pi}} \int_{\sqrt{2\rho_s} \sin \pi/M}^{\infty} e^{-u^2/2} du \quad (7.6.57)$$

$$= 2Q \left( \sqrt{2\rho_s} \sin \frac{\pi}{M} \right) \quad (7.6.58)$$

$$= 2Q \left( \sqrt{2k\rho_b} \sin \frac{\pi}{M} \right) \quad (7.6.59)$$

where  $k = \log_2 M$  and  $\rho_s = k\rho_b$ . We note that this approximation to the error probability is good for all values of  $M$ . For example, when  $M = 2$  and  $M = 4$ , we have  $P_2 = P_4 = 2Q(\sqrt{2\rho_b})$ , which compares favorably (a factor of 2 difference) with the exact error probability given by Equation (7.6.51).

The equivalent bit error probability for  $M$ -ary-phase modulation is rather tedious to derive due to its dependence on the mapping of  $k$ -bit symbols into the corresponding

signal phases. When a Gray code is used in the mapping, two  $k$ -bit symbols corresponding to adjacent signal phases differ in only a single bit. Because the most probable errors due to noise result in the erroneous selection of an adjacent phase to the true phase, most  $k$ -bit symbol errors contain only a single bit error. Hence, the equivalent bit-error probability for  $M$ -ary-phase modulation is well approximated as

$$P_b \approx \frac{1}{k} P_M \quad (7.6.60)$$

The performance analysis given above applies to phase-coherent demodulation with conventional (absolute) phase mapping of the information into signal phases. As previously indicated in Section 7.5.5, when phase ambiguities result in the estimation of the carrier phase, the information symbols are differentially encoded at the transmitter and differentially decoded at the receiver. Coherent demodulation of differentially encoded phase-modulated signals results in a higher probability of error than the error probability derived for absolute-phase encoding. With differentially encoded signals, an error in the detected phase due to noise will frequently result in decoding errors over two consecutive signaling intervals. This is especially the case for error probabilities below  $10^{-1}$ . Therefore, the probability of error for differentially encoded  $M$ -ary phase-modulated signals is approximately twice the probability of error for  $M$ -ary phase modulation with absolute-phase encoding. However, a factor-of-2 increase in the error probability translates into a relatively small loss in SNR, as can be seen from Figure 7.57.

#### 7.6.4 Probability of Error for DPSK

Let us now consider the evaluation of the error probability performance of a DPSK demodulator and detector. The derivation of the exact value of the probability of error for  $M$ -ary DPSK is extremely difficult, except for  $M = 2$ . The major difficulty is encountered in the determination of the PDF for the phase of the random variable  $r_k r_{k-1}^*$  given by Equation (7.5.77). However, an approximation to the performance of DPSK is easily obtained, as we now demonstrate.

Without loss of generality, suppose the phase difference  $\theta_k - \theta_{k-1} = 0$ . Furthermore, the exponential factors  $e^{-j(\theta_{k-1}-\phi)}$  and  $e^{j(\theta_k-\phi)}$  in Equation (7.5.77) can be absorbed into the Gaussian noise components  $n_{k-1}$  and  $n_k$ , (see Problem 4.29), without changing their statistical properties. Therefore,  $r_n r_{n-1}^*$  in Equation (7.5.77) can be expressed as

$$r_k r_{k-1}^* = \mathcal{E}_s + \sqrt{\mathcal{E}_s}(n_k + n_{k-1}^*) + n_k n_{k-1}^* \quad (7.6.61)$$

The complication in determining the PDF of the phase is the term  $n_k n_{k-1}^*$ . However, at SNRs of practical interest, the term  $n_k n_{k-1}^*$  is small relative to the dominant noise term  $\sqrt{\mathcal{E}_s}(n_k + n_{k-1}^*)$ . If we neglect the term  $n_k n_{k-1}^*$  and we also normalize  $r_k r_{k-1}^*$  by dividing through by  $\sqrt{\mathcal{E}_s}$ , the new set of decision metrics become

$$\begin{aligned} x &= \sqrt{\mathcal{E}_s} + \text{Re}(n_k + n_{k-1}^*) \\ y &= \text{Im}(n_k + n_{k-1}^*) \end{aligned} \quad (7.6.62)$$



The variables  $x$  and  $y$  are uncorrelated Gaussian random variables with identical variances  $\sigma_n^2 = N_0$ . The phase is

$$\Theta_r = \tan^{-1} \frac{y}{x} \quad (7.6.63)$$

At this stage we have a problem that is identical to the one we solved previously for phase-coherent demodulation and detection. The only difference is that the noise variance is now twice as large as in the case of PSK. Thus, we conclude that the performance of DPSK is 3-dB poorer than that for PSK. This result is relatively good for  $M \geq 4$ , but it is pessimistic for  $M = 2$  in the sense that the loss in binary DPSK relative to binary PSK is less than 3 dB at large SNR. This is demonstrated next.

In binary DPSK, the two possible transmitted phase differences are zero and  $\pi$  radians. As a consequence, only the real part of  $r_k r_{k-1}^*$  is needed for recovering the information. We express the real part as

$$\text{Re}(r_k r_{k-1}^*) = \frac{1}{2}(r_k r_{k-1}^* + r_k^* r_{k-1})$$

Because the phase difference between the two successive signaling intervals is zero, an error is made if  $\text{Re}(r_k r_{k-1}^*)$  is less than zero. The probability that  $r_k r_{k-1}^* + r_k^* r_{k-1} < 0$  is a special case of a derivation, given in Appendix A, concerned with the probability that a general quadratic form in complex-valued Gaussian random variables is less than zero. The result for the error probability of binary DPSK is

$$P_2 = \frac{1}{2} e^{-\rho_b} \quad (7.6.64)$$

where  $\rho_b = \mathcal{E}_b/N_0$  is the SNR/bit.

The graph of Equation (7.6.64) is shown in Figure 7.58. Also shown in this figure is the probability of error for binary PSK. We observe that at error probabilities below  $10^{-4}$ , the difference in SNR between binary PSK and binary DPSK is less than 1 dB.

### 7.6.5 Probability of Error for QAM

To determine the probability of error for QAM, we must specify the signal-point constellation. We begin with QAM signal sets that have  $M = 4$  points. Figure 7.59 illustrates two 4-point signal sets. The first is a four-phase-modulated signal and the second is a QAM signal with two amplitude levels, labeled  $A_1$  and  $A_2$ , and four phases. Because the probability of error is dominated by the minimum distance between pairs of signal points, let us impose the condition that  $d_{\min} = 2A$  for both signal constellations and let us evaluate the average transmitter power, based on the premise that all signal points are equally probable. For the four-phase signal we have

$$P_{av} = \frac{1}{4}(4)A^2 = A^2 \quad (7.6.65)$$

For the two-amplitude, four-phase QAM, we place the points on circles of radii  $A$  and

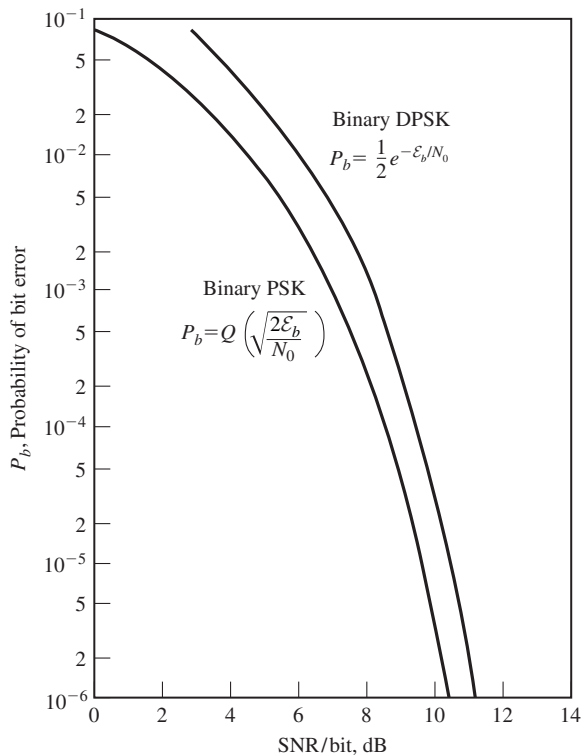


Figure 7.58 Probability of error for binary PSK and DPSK.

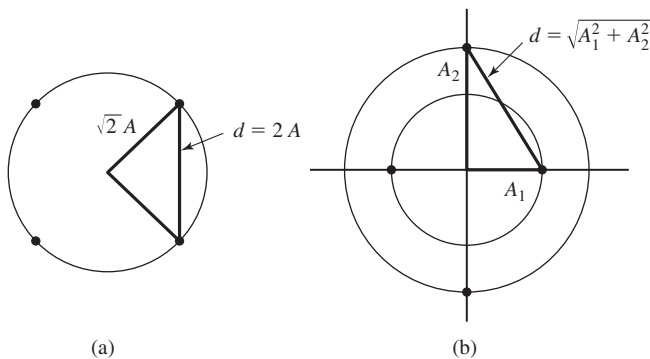


Figure 7.59 Two 4-point signal constellations.

$\sqrt{3}A$ . Thus,  $d_{\min} = 2A$ , and

$$P_{av} = \frac{1}{4} \left[ 2 \left( \frac{3}{2} \right) A^2 + 2 \frac{A^2}{2} \right] = A^2 \tag{7.6.66}$$

which is the same average power as the  $M = 4$ -phase signal constellation. Hence, for all

practical purposes, the error-rate performance of the two signal sets is the same. In other words, there is no advantage of the two-amplitude QAM signal set over  $M = 4$ -phase modulation.

Next, let us consider  $M = 8$  QAM. In this case, there are many possible signal constellations. We shall consider the four signal constellations shown in Figure 7.60, all of which consist of two amplitudes and have a minimum distance between signal points of  $2A$ . The coordinates  $(A_{mc}, A_{ms})$  for each signal point, normalized by  $A$ , are given in the figure. Assuming that the signal points are equally probable, the average transmitted signal power is

$$\begin{aligned} P_{av} &= \frac{1}{M} \sum_{m=1}^M \frac{1}{2} (A_{mc}^2 + A_{ms}^2) \\ &= \frac{A^2}{2M} \sum_{m=1}^M (a_{mc}^2 + a_{ms}^2) \end{aligned} \quad (7.6.67)$$

where  $(a_{mc}, a_{ms})$  are the coordinates of the signal points, normalized by  $A$ .

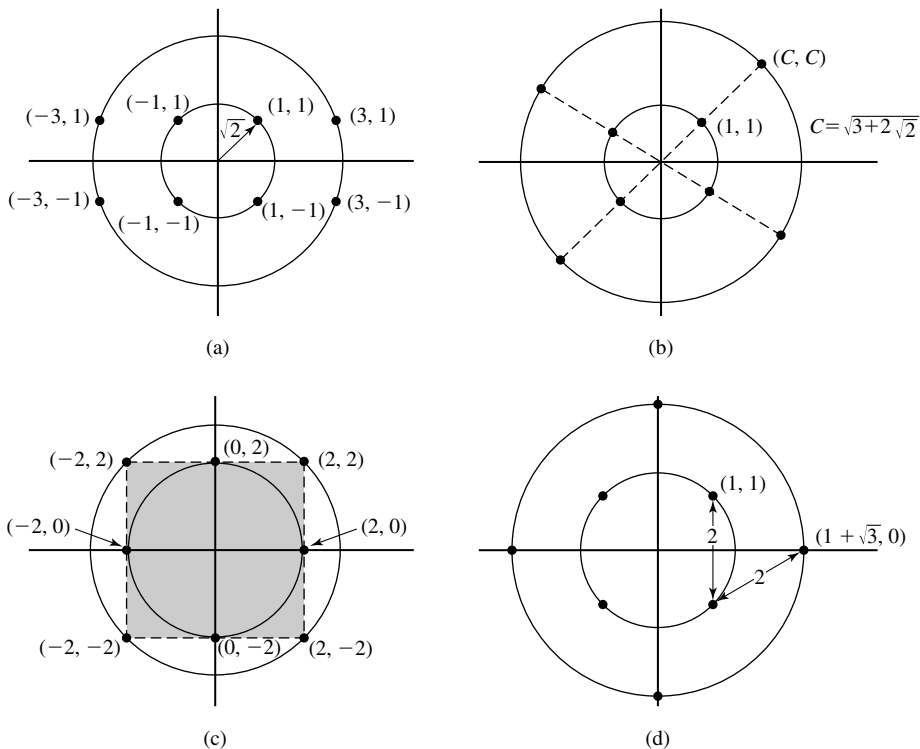


**Figure 7.60** Four 8-point QAM signal constellations.

The first two signal sets in Figure 7.60 contain signal points that fall on a rectangular grid and have  $P_{av} = 3A^2$ . The third signal set requires an average transmitted power  $P_{av} = 3.41A^2$ , and the fourth requires  $P_{av} = 2.36A^2$ . Therefore, the fourth signal set requires approximately 1-dB less power than the first two and 1.6-dB less power than the third to achieve the same probability of error. This signal constellation is known to be the best 8-point QAM constellation because it requires the least power for a given minimum distance between signal points.

For  $M \geq 16$ , there are many more possibilities for selecting the QAM signal points in the two-dimensional space. For example, we may choose a circular multi-amplitude constellation for  $M = 16$ , as shown in Figure 7.61. In this case, the signal points at a given amplitude level are phase rotated by  $\pi/4$  relative to the signal points at adjacent amplitude levels. This 16-QAM constellation is a generalization of the optimum 8-QAM constellation. However, the circular 16-QAM constellation is not the best 16-point QAM signal constellation for the AWGN channel.

Rectangular QAM signal constellations have the distinct advantage of being easily generated as two PAM signals impressed on phase-quadrature carriers. In addition, they are easily demodulated as previously described. Although they are not the best  $M$ -ary QAM signal constellations for  $M \geq 16$ , the average transmitted power required to achieve a given minimum distance is only slightly greater than the average power required for the best  $M$ -ary QAM signal constellation. For these reasons, rectangular  $M$ -ary QAM signals are most frequently used in practice.

For rectangular signal constellations in which  $M = 2^k$  where  $k$  is even, the QAM signal constellation is equivalent to two PAM signals on quadrature carriers, each having  $\sqrt{M} = 2^{k/2}$  signal points. Because the signals in the phase-quadrature components are perfectly separated by coherent detection when  $\phi = \hat{\phi}$ , the probability of error for QAM is easily determined from the probability of error for PAM. Specifically, the probability

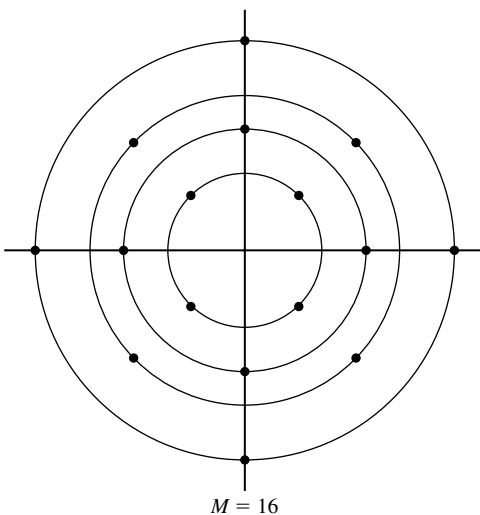


**Figure 7.61** Circular 16-point QAM signal constellation.

of a correct decision for the  $M$ -ary QAM system is

$$P_c = (1 - P_{\sqrt{M}})^2 \quad (7.6.68)$$

where  $P_{\sqrt{M}}$  is the probability of error of a  $\sqrt{M}$ -ary PAM with one-half the average power in each quadrature signal of the equivalent QAM system. By appropriately modifying the probability of error for  $M$ -ary PAM, we obtain

$$P_{\sqrt{M}} = 2 \left(1 - \frac{1}{\sqrt{M}}\right) Q \left( \sqrt{\frac{3}{M-1} \frac{\mathcal{E}_{av}}{N_0}} \right) \quad (7.6.69)$$

where  $\mathcal{E}_{av}/N_0$  is the average SNR/symbol. Therefore, the probability of a symbol error for the  $M$ -ary QAM is

$$P_M = 1 - (1 - P_{\sqrt{M}})^2 \quad (7.6.70)$$

We note that this result is exact for  $M = 2^k$  when  $k$  is even. On the other hand, when  $k$  is odd, there is no equivalent  $\sqrt{M}$ -ary PAM system. This is no problem, however, because it is rather easy to determine the error rate for a rectangular signal set. If we employ the optimum detector that bases its decisions on the optimum distance metrics given by Equation (7.5.41), it is relatively straightforward to show that the symbol error probability is tightly upper-bounded as

$$\begin{aligned} P_M &\leq 1 - \left[ 1 - 2Q \left( \sqrt{\frac{3\mathcal{E}_{av}}{(M-1)N_0}} \right) \right]^2 \\ &\leq 4Q \left( \sqrt{\frac{3k\mathcal{E}_{bav}}{(M-1)N_0}} \right) \end{aligned} \quad (7.6.71)$$

for any  $k \geq 1$ , where  $\mathcal{E}_{bav}/N_0$  is the average SNR/bit. The probability of a symbol error is plotted in Figure 7.62 as a function of the average SNR/bit.

It is interesting to compare the performance of QAM with that of phase modulation for any given signal size  $M$ , because both types of signals are two-dimensional. Recall that for  $M$ -ary phase modulation, the probability of a symbol error is approximated as

$$P_M \approx 2Q \left( \sqrt{2\rho_s} \sin \frac{\pi}{M} \right) \quad (7.6.72)$$

where  $\rho_s$  is the SNR/symbol. For  $M$ -ary QAM, we may use the expression in Equation (7.6.69). Because the error probability is dominated by the argument of the  $Q$ -function, we may simply compare the arguments of  $Q$  for the two signal formats. Thus, the ratio of these two arguments is

$$\mathcal{R}_M = \frac{3/(M-1)}{2 \sin^2 \pi/M} \quad (7.6.73)$$

For example, when  $M = 4$ , we have  $\mathcal{R}_M = 1$ . Hence, 4-PSK and 4-QAM yield comparable performance for the same SNR/symbol. On the other hand, when  $M > 4$  we find that  $\mathcal{R}_M > 1$ , so that  $M$ -ary QAM yields better performance than  $M$ -ary PSK.

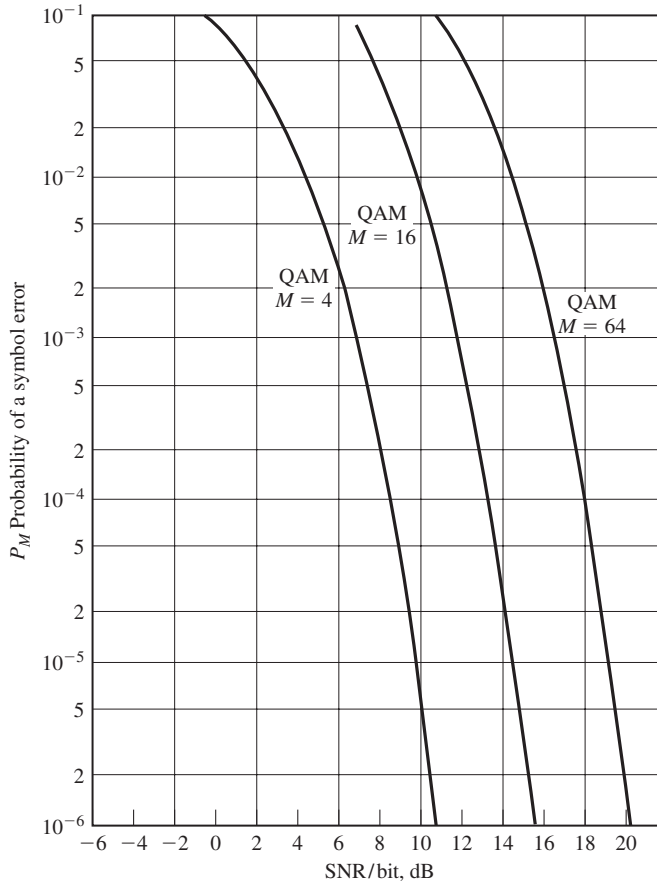


**Figure 7.62** Probability of a symbol error for QAM.

Table 7.1 illustrates the SNR advantage of QAM over PSK for several values of  $M$ . For example, we observe that 32-QAM has a 7-dB SNR advantage over 32-PSK.

### 7.6.6 Probability of Error for $M$ -ary Orthogonal Signals

We recall that PPM is a modulation method that results in orthogonal signals whose vector space representation is given by Equation (7.4.11). Note that all signals have equally energy, denoted as  $\mathcal{E}_s$ .

For equal energy orthogonal signals, the optimum detector selects the signal resulting in the largest crosscorrelation between the received vector  $\mathbf{r}$  and each of the  $M$  possible transmitted signal vectors  $\{\mathbf{s}_m\}$ , i.e.,

$$C(\mathbf{r}, \mathbf{s}_m) = \mathbf{r} \cdot \mathbf{s}_m = \sum_{k=1}^M r_k s_{mk}, \quad m = 1, 2, \dots, M \quad (7.6.74)$$

**TABLE 7.1** SNR ADVANTAGE OF *M*-ARY QAM OVER *M*-ARY PSK

<i>M</i>	$10 \log_{10} \mathcal{R}_M$
8	1.65
16	4.20
32	7.02
64	9.95

To evaluate the probability of error, let us suppose that the signal  $\mathbf{s}_1$  is transmitted. Then the received signal vector is

$$\mathbf{r} = (\sqrt{\mathcal{E}_s} + n_1, n_2, n_3, \dots, n_M) \quad (7.6.75)$$

where  $n_1, n_2, \dots, n_M$  are zero-mean, mutually statistically independent Gaussian random variables with equal variance  $\sigma_n^2 = N_0/2$ . In this case, the outputs from the bank of *M* correlators are

$$\begin{aligned} C(\mathbf{r}, \mathbf{s}_1) &= \sqrt{\mathcal{E}_s}(\sqrt{\mathcal{E}_s} + n_1) \\ C(\mathbf{r}, \mathbf{s}_2) &= \sqrt{\mathcal{E}_s}n_2 \\ &\vdots \\ C(\mathbf{r}, \mathbf{s}_M) &= \sqrt{\mathcal{E}_s}n_M \end{aligned} \quad (7.6.76)$$

Note that the scale factor  $\sqrt{\mathcal{E}_s}$  may be eliminated from the correlator outputs by dividing each output by  $\sqrt{\mathcal{E}_s}$ . Then, with this normalization, the PDF of the first correlator output ( $r_1 = \sqrt{\mathcal{E}_s} + n_1$ ) is

$$f_{r_1}(x_1) = \frac{1}{\sqrt{\pi N_0}} e^{-(x_1 - \sqrt{\mathcal{E}_s})^2/N_0} \quad (7.6.77)$$

and the PDFs of the other  $M - 1$  correlator outputs are

$$f_{r_m}(x_m) = \frac{1}{\sqrt{\pi N_0}} e^{-x_m^2/N_0}, \quad m = 2, 3, \dots, M \quad (7.6.78)$$

It is mathematically convenient to first derive the probability that the detector makes a correct decision. This is the probability that  $r_1$  is larger than each of the other  $M - 1$  correlator outputs  $n_2, n_3, \dots, n_M$ . This probability may be expressed as

$$P_c = \int_{-\infty}^{\infty} P(n_2 < r_1, n_3 < r_1, \dots, n_M < r_1 | r_1) f_{r_1}(r_1) dr_1 \quad (7.6.79)$$

where  $P(n_2 < r_1, n_3 < r_1, \dots, n_M < r_1 | r_1)$  denotes the joint probability that  $n_2, n_3, \dots, n_M$  are all less than  $r_1$ , conditioned on any given  $r_1$ . Then this joint probability is averaged over all  $r_1$ . Since the  $\{r_m\}$  are statistically independent, the joint

probability factors into a product of  $M - 1$  marginal probabilities of the form

$$\begin{aligned}
 P(n_m < r_1 | r_1) &= \int_{-\infty}^{r_1} f_{r_m}(x_m) dx_m, \quad m = 2, 3, \dots, M \\
 &= \frac{1}{\sqrt{2\pi}} \int_{-\infty}^{\sqrt{2r_1^2/N_0}} e^{-x^2/2} dx \\
 &= 1 - Q\left(\sqrt{\frac{2r_1^2}{N_0}}\right)
 \end{aligned} \tag{7.6.80}$$

These probabilities are identical for  $m = 2, 3, \dots, M$  and, hence, the joint probability under consideration is simply the result in Equation (7.6.80) raised to the  $(M - 1)$  power. Thus, the probability of a correct decision is

$$P_c = \int_{-\infty}^{\infty} \left[1 - Q\left(\sqrt{\frac{2r_1^2}{N_0}}\right)\right]^{M-1} f(r_1) dr_1 \tag{7.6.81}$$

and the probability of a  $k$ -bit symbol error is

$$P_M = 1 - P_c \tag{7.6.82}$$

Therefore,

$$P_M = \frac{1}{\sqrt{2\pi}} \int_{-\infty}^{\infty} \{1 - [1 - Q(x)]^{M-1}\} e^{-(x - \sqrt{2\mathcal{E}_s/N_0})^2/2} dx \tag{7.6.83}$$

The same expression for the probability of error is obtained when any one of the other  $M - 1$  signals is transmitted. Since all the  $M$  signals are equally likely, the expression for  $P_M$  given in Equation (7.6.83) is the average probability of a symbol error. This expression can be evaluated numerically.

In comparing the performance of various digital modulation methods, it is desirable to have the probability of error expressed in terms of the SNR/bit,  $\mathcal{E}_b/N_0$ , instead of the SNR/symbol  $\mathcal{E}_s/N_0$ . With  $M = 2^k$ , each symbol conveys  $k$  bits of information and, hence,  $\mathcal{E}_s = k\mathcal{E}_b$ . Thus, Equation (7.6.83) may be expressed in terms of  $\mathcal{E}_b/N_0$  by substituting for  $\mathcal{E}_s$ .

Sometimes, it is also desirable to convert the probability of a symbol error into an equivalent probability of a binary digit error. For equiprobable orthogonal signals, all symbol errors are equiprobable and occur with probability

$$\frac{P_M}{M-1} = \frac{P_M}{2^k-1} \tag{7.6.84}$$

Furthermore, there are  $\binom{n}{k}$  ways in which  $n$  bits out of  $k$  may be in error. Hence, the average number of bit errors per  $k$ -bit symbol is

$$\sum_{n=1}^k n \binom{n}{k} \frac{P_M}{2^k-1} = k \frac{2^{k-1}}{2^k-1} P_M \tag{7.6.85}$$



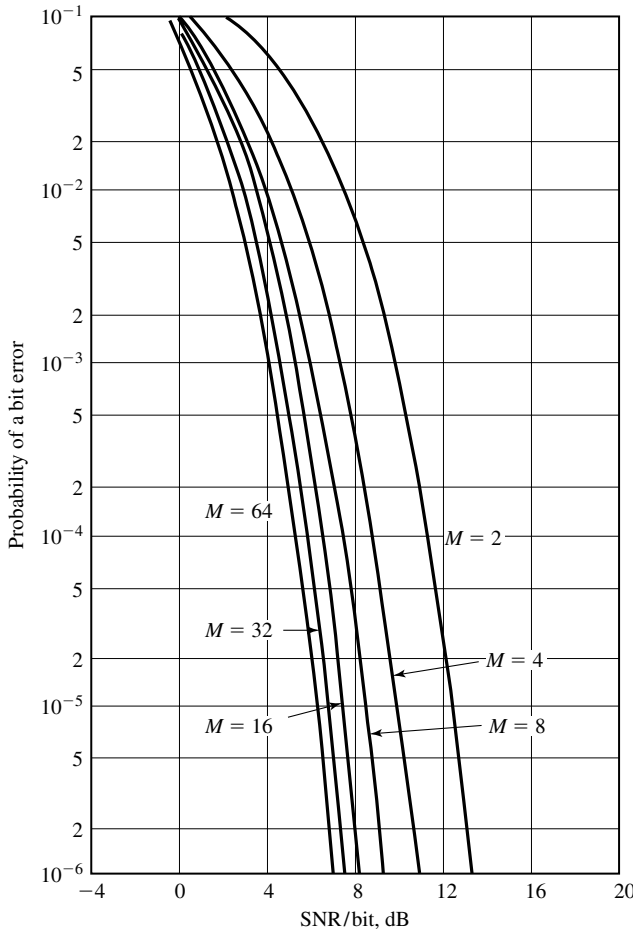


**Figure 7.63** Probability of bit error for coherent detection of orthogonal signals.

and the average bit-error probability is just the result in Equation (7.6.85) divided by  $k$ , the number of bits/symbol. Thus,

$$P_b = \frac{2^{k-1}}{2^k - 1} P_M \approx \frac{P_M}{2}, \quad k \gg 1 \quad (7.6.86)$$

The graphs of the probability of a binary digit error as a function of the SNR/bit,  $\mathcal{E}_b/N_0$ , are shown in Figure 7.63 for  $M = 2, 4, 8, 16, 32, 64$ . This figure illustrates that by increasing the number  $M$  of waveforms, one can reduce the SNR/bit required to achieve a given probability of a bit error. For example, to achieve a  $P_b = 10^{-5}$ , the required SNR/bit is a little more than 12 dB for  $M = 2$ , but if  $M$  is increased to 64 signal waveforms ( $k = 6$  bits/symbol), the required SNR/bit is approximately 6 dB. Thus, a savings of over 6 dB (a factor of four reduction) is realized in transmitter power (or energy) required to achieve a  $P_b = 10^{-5}$  by increasing  $M$  from  $M = 2$  to  $M = 64$ .

What is the minimum required  $\mathcal{E}_b/N_0$  to achieve an arbitrarily small probability of error as  $M \rightarrow \infty$ ? This question is answered next.

**A Union Bound on the Probability of Error.** Let us investigate the effect of increasing  $M$  on the probability of error for orthogonal signals. To simplify the mathematical development, we first derive an upper-bound on the probability of a symbol error which is much simpler than the exact form given in Equation (7.6.83).

Recall that the probability of error for binary orthogonal signals is given by Equation (7.6.17). Now, if we view the detector for  $M$  orthogonal signals as one that makes  $M - 1$  binary decisions between the correlator output  $C(\mathbf{r}, \mathbf{s}_1)$  that contains the signal and the other  $M - 1$  correlator outputs  $C(\mathbf{r}, \mathbf{s}_m)$ ,  $m = 2, 3, \dots, M$ , the probability of error is upper-bounded by the *union bound* of the  $M - 1$  events. That is, if  $E_i$  represents the event that  $C(\mathbf{r}, \mathbf{s}_m) > C(\mathbf{r}, \mathbf{s}_1)$  for  $m \neq 1$ , then we have  $P_M = P(U_{i=1}^n E_i) \leq \sum_{i=1}^n P(E_i)$ . Hence,

$$P_M \leq (M - 1)P_2 = (M - 1)Q(\sqrt{\mathcal{E}_s/N_0}) < MQ(\sqrt{\mathcal{E}_s/N_0}) \quad (7.6.87)$$

This bound can be simplified further by upper-bounding  $Q(\sqrt{\mathcal{E}_s/N_0})$  [see Equation (4.1.7)]. We have

$$Q(\sqrt{\mathcal{E}_s/N_0}) < e^{-\mathcal{E}_s/2N_0} \quad (7.6.88)$$

Thus,

$$\begin{aligned} P_M &< M e^{-\mathcal{E}_s/2N_0} = 2^k e^{-k\mathcal{E}_b/2N_0} \\ P_M &< e^{-k(\mathcal{E}_b/N_0 - 2 \ln 2)/2} \end{aligned} \quad (7.6.89)$$

As  $k \rightarrow \infty$ , or equivalently, as  $M \rightarrow \infty$ , the probability of error approaches zero exponentially, provided that  $\mathcal{E}_b/N_0$  is greater than  $2 \ln 2$ ; i.e.,

$$\frac{\mathcal{E}_b}{N_0} > 2 \ln 2 = 1.39 \text{ (1.42 dB)} \quad (7.6.90)$$

The simple upper-bound on the probability of error given by Equation (7.6.89) implies that as long as  $\text{SNR} > 1.42$  dB, we can achieve an arbitrarily low  $P_M$ . However, this union-bound is not a very tight upper-bound at a sufficiently low SNR due to the fact that the upper-bound for the  $Q$ -function in Equation (7.6.88) is loose. In fact, by more elaborate bounding techniques, it is shown in Section 9.4 that the upper-bound in Equation (7.6.89) is sufficiently tight for  $\mathcal{E}_b/N_0 < 4 \ln 2$ . For  $\mathcal{E}_b/N_0 > 4 \ln 2$ , a tighter upper-bound on  $P_M$  is

$$P_M < 2e^{-k(\sqrt{\mathcal{E}_b/N_0} - \sqrt{\ln 2})^2} \quad (7.6.91)$$

Consequently,  $P_M \rightarrow 0$  as  $k \rightarrow \infty$ , provided that

$$\frac{\mathcal{E}_b}{N_0} > \ln 2 = 0.693 \text{ (-1.6 dB)} \quad (7.6.92)$$

Hence  $-1.6$  dB is the minimum required SNR/bit to achieve an arbitrarily small probability of error in the limit as  $k \rightarrow \infty$  ( $M \rightarrow \infty$ ). This minimum SNR/bit ( $-1.6$  dB) is called the *Shannon limit* for an additive white Gaussian noise channel.

### 7.6.7 Probability of Error for $M$ -ary Biorthogonal Signals

As previously indicated in Section 7.4.2, a set of  $M = 2^k$  biorthogonal signals are constructed from  $M/2$  orthogonal signals by including the negatives of the orthogonal signals. Thus, we achieve a reduction in the complexity of the demodulator for the biorthogonal signals relative to that for the orthogonal signals, since the former is implemented with  $M/2$  crosscorrelators or matched filters, whereas the latter requires  $M$  matched filters or crosscorrelators.

To evaluate the probability of error for the optimum detector, let us assume that the signal  $s_1(t)$  corresponding to the vector  $\mathbf{s}_1 = (\sqrt{\mathcal{E}_s}, 0, 0, \dots, 0)$  was transmitted. Then, the received signal vector is

$$\mathbf{r} = (\sqrt{\mathcal{E}_s} + n_1, n_2, \dots, n_{M/2}) \quad (7.6.93)$$

where the  $\{n_m\}$  are zero-mean, mutually statistically independent and identically distributed Gaussian random variables with variance  $\sigma_n^2 = N_0/2$ . The optimum detector decides in favor of the signal corresponding to the largest in magnitude of the crosscorrelators

$$C(\mathbf{r}, \mathbf{s}_m) = \mathbf{r} \cdot \mathbf{s}_m = \sum_{k=1}^{M/2} r_k s_{mk}, \quad m = 1, 2, \dots, M/2 \quad (7.6.94)$$

while the sign of this largest term is used to decide whether  $s_m(t)$  or  $-s_m(t)$  was transmitted. According to this decision rule, the probability of a correct decision is equal to the probability that  $r_1 = \sqrt{\mathcal{E}_s} + n_1 > 0$  and  $r_1$  exceeds  $|r_m| = |n_m|$  for  $m = 2, 3, \dots, M/2$ . But,

$$P(|n_m| < r_1 | r_1 > 0) = \frac{1}{\sqrt{\pi N_0}} \int_{-r_1}^{r_1} e^{-x^2/N_0} dx = \frac{1}{\sqrt{2\pi}} \int_{-r_1/\sqrt{N_0/2}}^{r_1/\sqrt{N_0/2}} e^{-x^2/2} dx \quad (7.6.95)$$

Then, the probability of a correct decision is

$$P_c = \int_0^\infty \left[ \frac{1}{\sqrt{2\pi}} \int_{-r_1/\sqrt{N_0/2}}^{r_1/\sqrt{N_0/2}} e^{-x^2/2} dx \right]^{\frac{M}{2}-1} f(r_1) dr_1$$

Upon substitution for  $f(r_1)$ , we obtain

$$P_c = \int_{-\sqrt{2\mathcal{E}_s/N_0}}^\infty \left[ \frac{1}{\sqrt{2\pi}} \int_{-(v+\sqrt{2\mathcal{E}_s/N_0})}^{v+\sqrt{2\mathcal{E}_s/N_0}} e^{-x^2/2} dx \right]^{\frac{M}{2}-1} e^{-v^2/2} dv \quad (7.6.96)$$

where we have used the PDF of  $r_1$  given in Equation (7.6.77). Finally, the probability of a symbol error  $P_M = 1 - P_c$ .

$P_c$  and, hence,  $P_M$  may be evaluated numerically for different values of  $M$  from (7.6.74). The graph shown in Figure 7.64 illustrates  $P_M$  as a function of  $\mathcal{E}_b/N_0$ , where  $\mathcal{E}_s = k\mathcal{E}_b$ , for  $M = 2, 4, 8, 16$ , and  $32$ . We observe that this graph is similar to that for orthogonal signals (see Figure 7.63). However, in this case, the probability of error

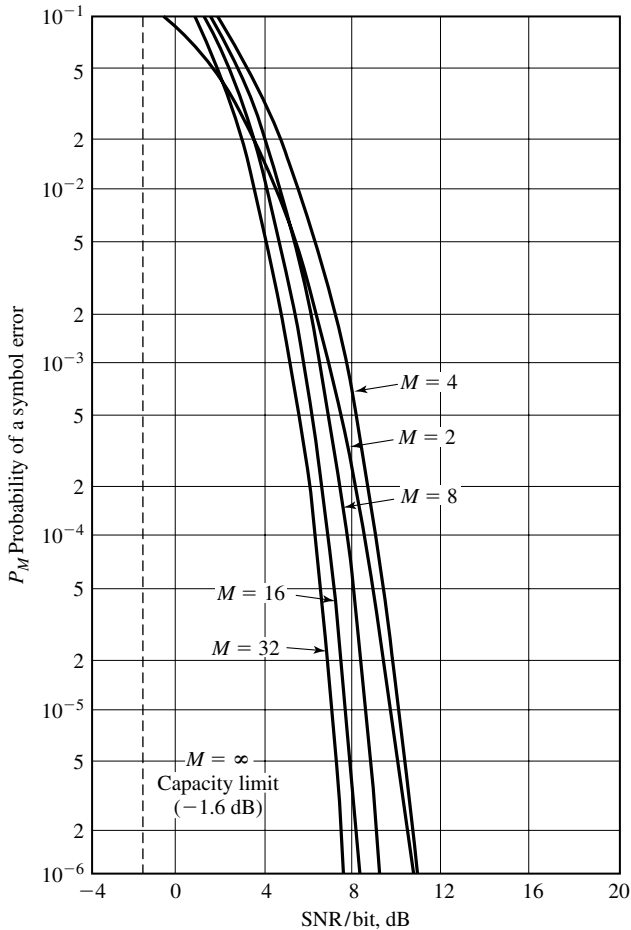


**Figure 7.64** Probability of symbol error for biorthogonal signals.

for  $M = 4$  is greater than that for  $M = 2$ . This is due to the fact that we have plotted the symbol error probability  $P_M$  in Figure 7.64. If we plot the equivalent bit error probability we would find that the graphs for  $M = 2$  and  $M = 4$  coincide. As in the case of orthogonal signals, as  $M \rightarrow \infty$  (or  $k \rightarrow \infty$ ), the minimum required  $\mathcal{E}_b/N_0$  to achieve an arbitrarily small probability of error is  $-1.6$  dB, the Shannon limit.

### 7.6.8 Probability of Error for $M$ -ary Simplex Signals

Next we consider the probability of error for  $M$  simplex signals. Recall from Section 7.4.3 that simplex signals are a set of  $M$  equally correlated signals with mutual crosscorrelation coefficient  $\gamma_{mn} = -1/(M - 1)$ . These signals have the same minimum separation of  $\sqrt{2\mathcal{E}_s}$  between adjacent signal points in  $M$ -dimensional space as orthogonal signals. They achieve this mutual separation with a transmitted energy of

$\mathcal{E}_s(M-1)/M$ , which is less than that required for orthogonal signals by a factor of  $(M-1)/M$ . Consequently, the probability of error for simplex signals is identical to the probability of error for orthogonal signals, but this performance is achieved with a savings of

$$10 \log(1 - \gamma_{mn}) = 10 \log \frac{M}{M-1} \text{ dB} \quad (7.6.97)$$

in SNR.

### 7.6.9 Probability of Error for Noncoherent Detection of FSK

Let us consider  $M$ -ary orthogonal FSK signals that are detected noncoherently. We assume that the  $M$  signals are equally probable a priori and that  $s_1(t)$  was transmitted in the interval  $0 \leq t \leq T$ .

The  $M$ -decision metrics at the detector are the  $M$  envelopes

$$r_m = \sqrt{r_{mc}^2 + r_{ms}^2} \quad m = 1, 2, \dots, M \quad (7.6.98)$$

where

$$\begin{aligned} r_{1c} &= \sqrt{\mathcal{E}_s} \cos \phi_1 + n_{1c} \\ r_{1s} &= \sqrt{\mathcal{E}_s} \sin \phi_1 + n_{1s} \end{aligned} \quad (7.6.99)$$

and

$$\begin{aligned} r_{mc} &= n_{mc}, \quad m = 2, 3, \dots, M \\ r_{ms} &= n_{ms}, \quad m = 2, 3, \dots, M \end{aligned} \quad (7.6.100)$$

The additive noise components  $\{n_{mc}\}$  and  $\{n_{ms}\}$  are mutually statistically independent zero-mean Gaussian variables with equal variance  $\sigma^2 = N_0/2$ . Thus, the PDFs of the random variables at the input to the detector are

$$f_{r_1}(r_{1c}, r_{1s}) = \frac{1}{2\pi\sigma^2} e^{-(r_{1c}^2 + r_{1s}^2 + \mathcal{E}_s)/2\sigma^2} I_0 \left( \sqrt{\frac{\mathcal{E}_s(r_{1c}^2 + r_{1s}^2)}{\sigma^2}} \right) \quad (7.6.101)$$

$$f_{r_m}(r_{mc}, r_{ms}) = \frac{1}{2\pi\sigma^2} e^{-(r_{mc}^2 + r_{ms}^2)/2\sigma^2}, \quad m = 2, 3, \dots, M \quad (7.6.102)$$

Let us make a change in variables in the joint PDFs given by Equations (7.6.101) and (7.6.102). We define the normalized variables

$$\begin{aligned} R_m &= \frac{\sqrt{r_{mc}^2 + r_{ms}^2}}{\sigma} \\ \Theta_m &= \tan^{-1} \frac{r_{ms}}{r_{mc}} \end{aligned} \quad (7.6.103)$$

Clearly,  $r_{mc} = \sigma R_m \cos \Theta_m$  and  $r_{ms} = \sigma R_m \sin \Theta_m$ . The Jacobian of this transformation is

$$|\mathbf{J}| = \begin{vmatrix} \sigma \cos \Theta_m & \sigma \sin \Theta_m \\ -\sigma R_m \sin \Theta_m & \sigma R_m \cos \Theta_m \end{vmatrix} = \sigma^2 R_m \quad (7.6.104)$$

Consequently,

$$f_{R_1 \Theta_1}(R_1, \Theta_1) = \frac{R_1}{2\pi} e^{-(R_1^2 + 2\mathcal{E}_s/N_0)/2} I_0 \left( \sqrt{\frac{2\mathcal{E}_s}{N_0}} R_1 \right) \quad (7.6.105)$$

$$f_{R_m \Theta_m}(R_m, \Theta_m) = \frac{R_m}{2\pi} e^{-R_m^2/2}, \quad m = 2, 3, \dots, M \quad (7.6.106)$$

Finally, by averaging  $f_{R_m \Theta_m}(R_m, \Theta_m)$  over  $\Theta_m$ , the factor of  $2\pi$  is (see Problem 4.31) eliminated from Equations (7.6.105) and (7.6.106). Thus, we find that  $R_1$  has a Rice probability distribution and  $R_m$ ,  $m = 2, 3, \dots, M$  are each Rayleigh distributed.

The probability of a correct decision is simply the probability that  $R_1 > R_2$  and  $R_1 > R_3, \dots$  and  $R_1 > R_M$ . Hence,

$$\begin{aligned} P_c &= P(R_2 < R_1, R_3 < R_1, \dots, R_M < R_1) \\ &= \int_0^\infty P(R_2 < R_1, R_3 < R_1, \dots, R_M < R_1 | R_1 = x) f_{R_1}(x) dx \quad (7.6.107) \end{aligned}$$

Because the random variables  $R_m$ ,  $m = 2, 3, \dots, M$  are statistically i.i.d., the joint probability in Equation (7.6.107) conditioned on  $R_1$  factors into a product of  $M - 1$  identical terms. Thus,

$$P_c = \int_0^\infty [P(R_2 < R_1 | R_1 = x)]^{M-1} f_{R_1}(x) dx \quad (7.6.108)$$

where

$$\begin{aligned} P(R_2 < R_1 | R_1 = x) &= \int_0^x f_{R_2}(r_2) dr_2 \\ &= 1 - e^{-x^2/2} \quad (7.6.109) \end{aligned}$$

The  $(M - 1)$ st power of Equation (7.6.109) may be expressed as

$$[1 - e^{-x^2/2}]^{M-1} = \sum_{n=0}^{M-1} (-1)^n \binom{M-1}{n} n e^{-nx^2/2} \quad (7.6.110)$$

Substitution of this result in Equation (7.6.108) and integration over  $x$  yields the probability of a correct decision as

$$P_c = \sum_{n=0}^{M-1} (-1)^n \binom{M-1}{n} \frac{1}{n+1} e^{-n\rho_s/(n+1)} \quad (7.6.111)$$

where  $\rho_s = \mathcal{E}_s/N_0$  is the SNR/symbol. Then, the probability of a symbol error which

is  $P_M = 1 - P_c$ , becomes

$$P_M = \sum_{n=1}^{M-1} (-1)^{n+1} \binom{M-1}{n} \frac{1}{n+1} e^{-nk\rho_b/(n+1)} \quad (7.6.112)$$

where  $\rho_b = \mathcal{E}_b/N_0$  is the SNR/bit.

For binary FSK ( $M = 2$ ), Equation (7.6.112) reduces to the simple form

$$P_2 = \frac{1}{2} e^{-\rho_b/2} \quad (7.6.113)$$

We observe that the performance of noncoherent FSK is 3-dB worse than binary DPSK.

For  $M > 2$ , we may compute the probability of a bit error by making use of the relationship

$$P_b = \frac{2^{k-1}}{2^k - 1} P_M \quad (7.6.114)$$

which was established in Section 7.6.6. Figure 7.65 shows the bit-error probability as function of the SNR/bit  $\rho_b$  for  $M = 2, 4, 8, 16, 32$ . Just as in the case of coherent detection of  $M$ -ary orthogonal signals (see Section 7.6.6), we observe that for any given bit-error probability, the SNR/bit decreases as  $M$  increases. It will be shown in Chapter 9 that, in the limit as  $M \rightarrow \infty$  (or  $k = \log_2 M \rightarrow \infty$ ), the probability of a bit-error  $P_b$  can be made arbitrarily small provided that the SNR/bit is greater than the Shannon limit of  $-1.6$  dB.

### 7.6.10 Comparison of Modulation Methods

The digital modulation methods described in this chapter can be compared in a number of ways. For example, one can compare them on the basis of the SNR required to achieve a specified probability of error. However, such a comparison would not be very meaningful unless it were made on the basis of some constraint, such as a fixed data rate of transmission.

Suppose that the bit rate  $R_b$  is fixed, and let us consider the channel bandwidth required to transmit the various signals. If we employ  $M$ -ary PAM, where  $M = 2^k$ , the channel bandwidth required to transmit the signal is simply the bandwidth of the signal pulse  $g_T(t)$ , which depends on its detailed characteristics. For our purposes, we assume that  $g_T(t)$  is a pulse of duration  $T$  and that its bandwidth  $W$  is approximately  $1/2T$ , where  $T$  is the symbol interval. In one symbol interval we can transmit  $k$  information bits, so  $T = k/R_b$  seconds. Hence, the channel bandwidth required to transmit the  $M$ -ary PAM signal is

$$W = R_b/2k = R_b/2 \log_2 M \text{ Hz} \quad (7.6.115)$$

If the PAM signal is transmitted at bandpass as a double-sideband suppressed carrier signal, the required channel bandwidth is twice that for the baseband channel. However, the bandwidth of the bandpass PAM signal can be reduced by a factor of two by transmitting only one of the sidebands, either the upper or the lower sideband

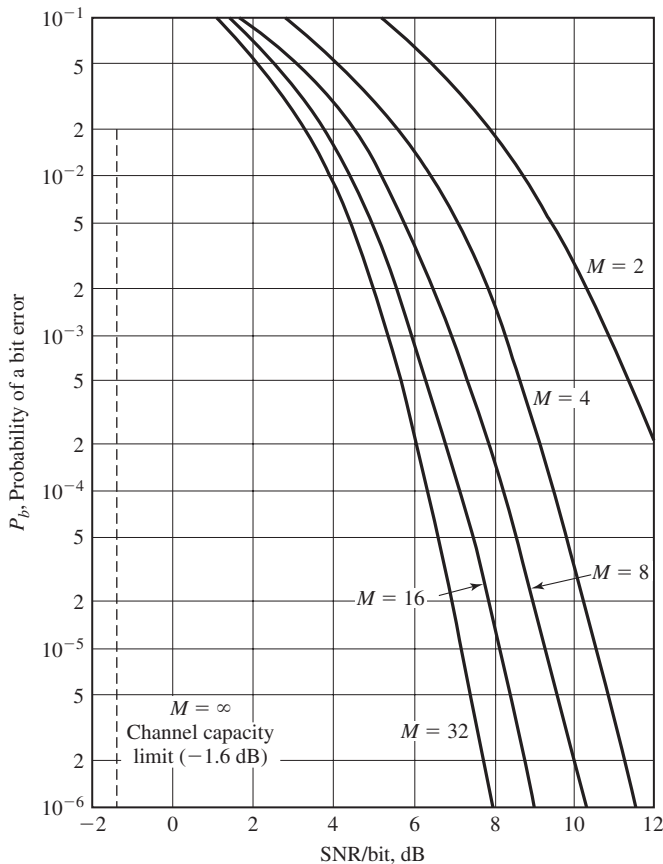


**Figure 7.65** Probability of a bit error for noncoherent detection of orthogonal FSK signals.

of the bandpass signal. Thus, the required channel bandwidth of the single-sideband bandpass PAM signal is exactly the same as the bandwidth of the baseband signal.

In the case of QAM, the channel bandwidth is (approximately)  $W = 1/T$ , but since the information is carried on two quadrature carriers,  $T = 2k/R_b$ , where  $k$  is the number of information bits/carrier. Hence,

$$\begin{aligned} W &= R_b/2k = R_b/2 \log_2 M_{\text{PAM}} \\ &= R_b/\log_2 M_{\text{QAM}} \end{aligned} \quad (7.6.116)$$

where the number of signals for  $M$ -ary QAM, denoted as  $M_{\text{QAM}}$ , is equal to the square of the number  $M_{\text{PAM}}$  of PAM signals.



For  $M$ -ary-phase modulation, the channel bandwidth required to transmit the multiphase signals is  $W = 1/T$ , where  $T = k/R_b$ . Hence,

$$W = R_b/k = R_b/\log_2 M \quad (7.6.117)$$

Note that PAM, QAM, and PSK signals have the characteristic that, for a fixed bit rate  $R_b$ , the channel bandwidth decreases as the number of signals  $M$  increases. This means that with increasing  $M$  the system becomes more bandwidth efficient. On the other hand examination of Figures 7.55, 7.57, and 7.62 shows that in all these systems, at a given  $\mathcal{E}_b/N_0$ , increasing  $M$  increases the error probability and thus deteriorates the performance. In other words, in these systems increasing  $M$  increases the bandwidth efficiency and decreases the power efficiency. This is a direct consequence of the fact that in these systems the dimensionality of the signal space  $N$  is one (for PAM) or two (for PSK and QAM) and is independent of  $M$ .

Orthogonal signals have totally different bandwidth requirements. For example, if we employ PPM signals, the symbol interval  $T$  is subdivided into  $M$  subintervals of duration  $T/M$  and pulses of width  $T/M$  are transmitted in the corresponding subintervals. Consequently, the channel bandwidth required to transmit the PPM signals is

$$W = M/2T = M/2(k/R_b) = MR_b/2 \log_2 M \text{ Hz}$$

An identical result is obtained if the  $M$  orthogonal signals are constructed as  $M$ -ary-FSK with minimum frequency separation of  $1/2T$  for orthogonality. Biorthogonal and simplex signals result in similar relationships as PPM (orthogonal). In the case of biorthogonal signals, the required bandwidth is one-half of that for orthogonal signals. From the bandwidth relation for orthogonal signals, it is seen that for a fixed  $R_b$ , increasing  $M$  increases the bandwidth proportional to  $M/(2 \log_2 M)$ . This shows that in this case increasing  $M$  decreases the bandwidth efficiency of the system. On the other hand, examination of Figures 7.63 and 7.64 shows that in these systems, for a fixed  $\mathcal{E}_b/N_0$ , increasing  $M$  improves the performance of the system and, thus, improves the power efficiency of the system. It is also interesting to note that in orthogonal, biorthogonal, and simplex signaling schemes, the dimensionality of the space is not fixed and increases with increasing  $M$ .

From the above discussion, it is clear that the characteristics of PAM, PSK, and QAM on one hand and orthogonal, biorthogonal, and simplex schemes on the other hand are completely different and, therefore, their applications are also quite different.

A compact and meaningful comparison of these modulation methods is one that is based on the normalized data rate  $R_b/W$  (bits per second per hertz of bandwidth) versus the SNR/bit ( $\mathcal{E}_b/N_0$ ) required to achieve a given error probability. For PAM and orthogonal signals, we have

$$\text{PAM: } \frac{R_b}{W} = 2 \log_2 M_{\text{PAM}} \quad (7.6.118)$$

$$\text{QAM: } \frac{R_b}{W} = \log_2 M_{\text{QAM}} \quad (7.6.119)$$

$$\text{PSK: } \frac{R_b}{W} = \log_2 M_{\text{PSK}} \tag{7.6.120}$$

$$\text{orthogonal: } \frac{R_b}{W} = \frac{2 \log_2 M}{M} \tag{7.6.121}$$

Figure 7.66 illustrates the graph of  $R_b/W$  (measure of bandwidth efficiency) versus  $(\mathcal{E}_b/N_0)$  (measure of power efficiency) for PAM, QAM, PSK, and orthogonal signals for the case in which the symbol error probability is  $P_M = 10^{-5}$ . We observe that, as discussed before, in the case of PAM, QAM, and PSK, increasing the number of signal points  $M$  results in a higher bit rate to bandwidth ratio  $R_b/W$ . However, the cost of achieving the higher data rate is an increase in the SNR/bit. Consequently,  $M$ -ary

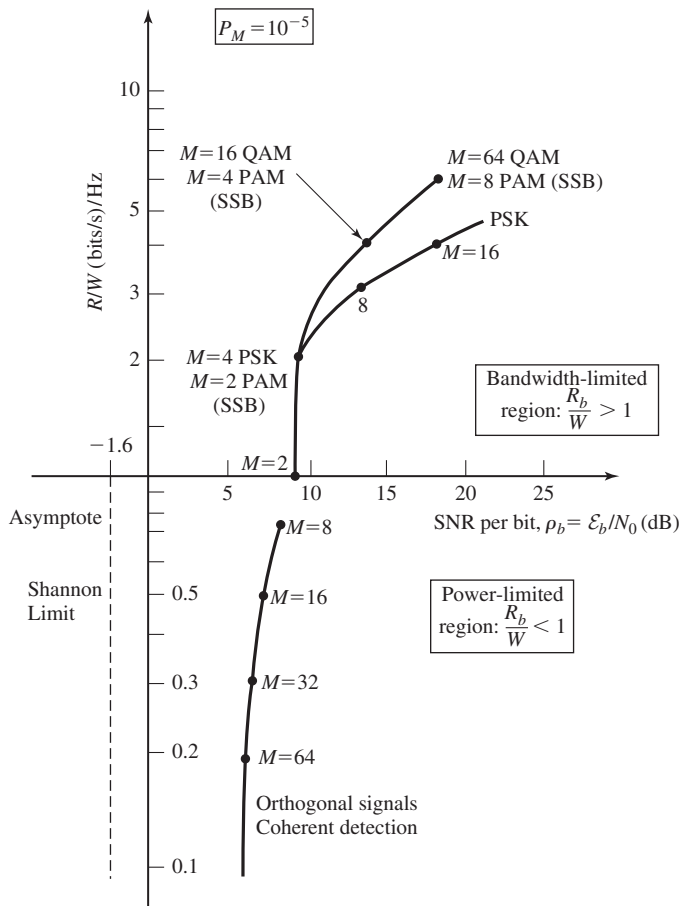


**Figure 7.66** Comparison of several modulation methods at  $10^{-5}$  symbol error probability.

**TABLE 7.2** QAM SIGNAL CONSTELLATIONS

Number of signal points $M$	Increase in average power (dB) relative to $M = 2$
4	3
8	6.7
16	10.0
32	13.2
64	16.2
128	19.2

PAM, QAM, and PSK are appropriate for communication channels that are bandwidth limited, where we desire a bit rate-to-bandwidth ratio  $R_b/W > 1$ , and where there is sufficiently high SNR to support multiple signal amplitudes and phases. Telephone channels are examples of such bandlimited channels.

We have already observed that the cost of doubling the number of phases (increasing the number of bits/symbol by one bit) in PSK approaches 6 dB (a factor of 4) in additional transmitted power for large  $M$ . A similar comparison for QAM indicates that the increase in transmitted power is approximately 3 dB/additional bit/symbol. Table 7.2 gives the factor  $10 \log_2(M - 1)/3$ , which represents the increase in average power required to maintain a given level of performance for QAM as the number of signal points in the rectangular constellation increases. Thus, we observe that QAM (and PAM) is preferable to PSK for large signal constellation sizes.

In contrast to PAM, QAM, and PSK,  $M$ -ary orthogonal signals yield a bit rate-to-bandwidth ratio of  $R_b/W \leq 1$ . As  $M$  increases,  $R_b/W$  decreases due to an increase in the required channel bandwidth. However, the SNR/bit required to achieve a given error probability (in this case,  $P_M = 10^{-5}$ ) decreases as  $M$  increases. Consequently,  $M$ -ary orthogonal signals, as well as biorthogonal and simplex signals, are appropriate for power-limited channels that have sufficiently large bandwidth to accommodate a large number of signals. In this case, as  $M \rightarrow \infty$ , the error probability can be made as small as desired, provided that  $\mathcal{E}_b/N_0 > 0.693$  (-1.6 dB). This is the minimum SNR/bit required to achieve reliable transmission in the limit as the channel bandwidth  $W \rightarrow \infty$  and the corresponding bit rate-to-bandwidth ratio  $R_b/W \rightarrow 0$ .

## 7.7 PERFORMANCE ANALYSIS FOR WIRELINE AND RADIO COMMUNICATION CHANNELS

In the transmission of digital signals through an AWGN channel, we have observed that the performance of the communication system, measured in terms of the probability of error, depends on the received SNR,  $\mathcal{E}_b/N_0$ , where  $\mathcal{E}_b$  is the transmitted energy/bit and  $N_0/2$  is the power-spectral density of the additive noise. Hence, the additive noise ultimately limits the performance of the communication system.

In addition to the additive noise, another factor that affects the performance of a communication system is channel attenuation. As indicated in Chapter 5, all physical

channels, including wirelines and radio channels, are lossy. Hence, the signal is attenuated as it travels through the channel. The simple mathematical model for the attenuation shown previously in Figure 5.18 may also be used for the purpose of digital communication. Consequently, if the transmitted signal is  $s(t)$ , the received signal is

$$r(t) = \alpha s(t) + n(t) \quad (7.7.1)$$

Then, if the energy in the transmitted signal is  $\mathcal{E}_b$ , the energy in the received signal is  $\alpha^2 \mathcal{E}_b$ . Consequently, the received signal has an SNR  $\alpha^2 \mathcal{E}_b / N_0$ . As in the case of analog communication systems, the effect of signal attenuation in digital communication systems is to reduce the energy in the received signal and, thus, to render the communication system more vulnerable to additive noise.

Recall that in analog communication systems, amplifiers called repeaters are used to periodically boost the signal strength in transmission through the channel. However, each amplifier also boosts the noise in the system. In contrast, digital communication systems allow us to detect and regenerate a clean (noise-free) signal in a transmission channel. Such devices, called *regenerative repeaters*, are frequently used in wireline and fiber optic communication channels.

### 7.7.1 Regenerative Repeaters

The front end of each regenerative repeater consists of a demodulator/detector that demodulates and detects the transmitted digital information sequence sent by the preceding repeater. Once detected, the sequence is passed to the transmitter side of the repeater which maps the sequence into signal waveforms that are transmitted to the next repeater. This type of repeater is called a regenerative repeater.

Since a noise-free signal is regenerated at each repeater, the additive noise does not accumulate. However, when errors occur in the detector of a repeater, the errors are propagated forward to the following repeaters in the channel. To evaluate the effect of errors on the performance of the overall system, suppose that the modulation is binary PAM, so that the probability of a bit error for one hop (signal transmission from one repeater to the next repeater in the chain) is

$$P_2 = Q \left( \sqrt{\frac{2\mathcal{E}_b}{N_0}} \right)$$

Since errors occur with low probability, we may ignore the probability that any one bit will be detected incorrectly more than once in transmission through a channel with  $K$  repeaters. Consequently, the number of errors will increase linearly with the number of regenerative repeaters in the channel and, therefore, the overall probability of error may be approximated as

$$P_b \approx K Q \left( \sqrt{\frac{2\mathcal{E}_b}{N_0}} \right) \quad (7.7.2)$$

In contrast, the use of  $K$  analog repeaters in the channel reduces the received SNR

by  $K$  and, hence, the bit-error probability is

$$P_b \approx Q \left( \sqrt{\frac{2\mathcal{E}_b}{KN_0}} \right) \quad (7.7.3)$$

Clearly, for the same probability of error performance, the use of regenerative repeaters results in a significant savings in transmitter power compared with analog repeaters. Hence, in digital communication systems, regenerative repeaters are preferable. However, in wireline telephone channels that are used to transmit both analog and digital signals, analog repeaters are generally employed.

### Example 7.7.1

A binary digital communication system transmits data over a wireline channel of length 1000 Km. Repeaters are used every 10 Km to offset the effect of channel attenuation. Determine the  $\mathcal{E}_b/N_0$  that is required to achieve a probability of a bit error of  $10^{-5}$  if (1) analog repeaters are employed, and (2) regenerative repeaters are employed.

**Solution** The number of repeaters used in the system is  $K = 100$ . If regenerative repeaters are used, the  $\mathcal{E}_b/N_0$  obtained from Equation (7.7.2) is

$$10^{-5} = 100Q \left( \sqrt{\frac{2\mathcal{E}_b}{N_0}} \right)$$

$$10^{-7} = Q \left( \sqrt{\frac{2\mathcal{E}_b}{N_0}} \right)$$

which yields approximately 11.3 dB. If analog repeaters are used, the  $\mathcal{E}_b/N_0$  obtained from Equation (7.7.3) is

$$10^{-5} = Q \left( \sqrt{\frac{2\mathcal{E}_b}{100N_0}} \right)$$

which yields an  $\mathcal{E}_b/N_0$  of 29.6 dB. Hence, the difference on the required SNR is about 18.3 dB, or approximately, 70 times the transmitter power of the digital communication system.

## 7.7.2 Link Budget Analysis for Radio Channels

In the design of radio communication systems that transmit over LOS microwave satellite channels, we must also consider the effect of the antenna characteristics in determining the SNR at the receiver that is required to achieve a given level of performance. The system design procedure is described next.

Suppose that a transmitting antenna radiates isotropically in free space at a power level  $P_T$  watts, as shown in Figure 7.67. The power density at a distance  $d$  from the antenna is  $P_T/4\pi d^2$  W/m<sup>2</sup>. If the transmitting antenna has directivity in a particular direction, the power density in that direction is increased by a factor called the *antenna gain*  $G_T$ . Then, the power density at a distance  $d$  is  $P_T G_T/4\pi d^2$  W/m<sup>2</sup>. The product

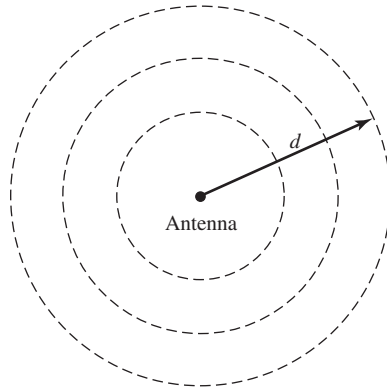


**Figure 7.67** Antenna that radiates isotropically in free space.

$P_T G_T$  is usually called the *effective isotropically radiated power* (EIRP), which is basically the radiated power relative to an isotropic antenna for which  $G_T = 1$ .

A receiving antenna pointed in the direction of the radiated power gathers a portion of the power that is proportional to its cross-sectional area. Hence, the received power extracted by the antenna is expressed as

$$P_R = \frac{P_T G_T A_R}{4\pi d^2} \quad (7.7.4)$$

where  $A_R$  is the *effective area of the antenna*. The basic relationship between the antenna gain and its effective area, obtained from basic electromagnetic theory, is

$$A_R = \frac{G_R \lambda^2}{4\pi} m^2 \quad (7.7.5)$$

where  $\lambda$  is the wavelength of the transmitted signal.

If we substitute for  $A_R$  from Equation (7.7.5) into Equation (7.7.4), we obtain the expression for the received power as

$$P_R = \frac{P_T G_T G_R}{(4\pi d/\lambda)^2} \quad (7.7.6)$$

The factor  $(4\pi d/\lambda)^2 = \mathcal{L}_s$  is the free-space path loss. Other losses, such as atmospheric losses, that may be encountered in the transmission of the signal are accounted for by introducing an additional loss factor  $\mathcal{L}_a$ . Therefore, the received power may be expressed as

$$P_R = \frac{P_T G_T G_R}{\mathcal{L}_s \mathcal{L}_a} \quad (7.7.7)$$

or, equivalently,

$$P_R|_{\text{dB}} = P_T|_{\text{dB}} + G_T|_{\text{dB}} + G_R|_{\text{dB}} - \mathcal{L}_s|_{\text{dB}} - \mathcal{L}_a|_{\text{dB}} \quad (7.7.8)$$

The effective area for an antenna generally depends on the wavelength  $\lambda$  of the radiated power and the physical dimension of the antenna. For example, a parabolic

(dish) antenna of diameter  $D$  has an effective area

$$A_R = \frac{\pi D^2}{4} \eta \quad (7.7.9)$$

where  $\pi D^2/4$  is the physical area and  $\eta$  is the *illumination efficiency factor*, which is typically in the range  $0.5 \leq \eta \leq 0.6$ . Hence, the antenna gain for a parabolic antenna of diameter  $D$  is

$$G_R = \eta \left( \frac{\pi D}{\lambda} \right)^2, \quad \text{parabolic antenna} \quad (7.7.10)$$

As a second example, a horn antenna of physical area  $A$  has an efficiency factor of 0.8, an effective area of  $A_R = 0.8A$ , and a gain of

$$G_R = \frac{10A}{\lambda^2}, \quad \text{horn antenna} \quad (7.7.11)$$

Another parameter that is related to the gain (directivity) of an antenna is its beamwidth, denoted as  $\Theta_B$  and illustrated in Figure 7.68. Usually, the beamwidth is measured as the  $-3$ -dB width of the antenna pattern. For example, the  $-3$ -dB beamwidth of a parabolic antenna is approximately

$$\Theta_b \approx 70\lambda/D \text{ deg}$$

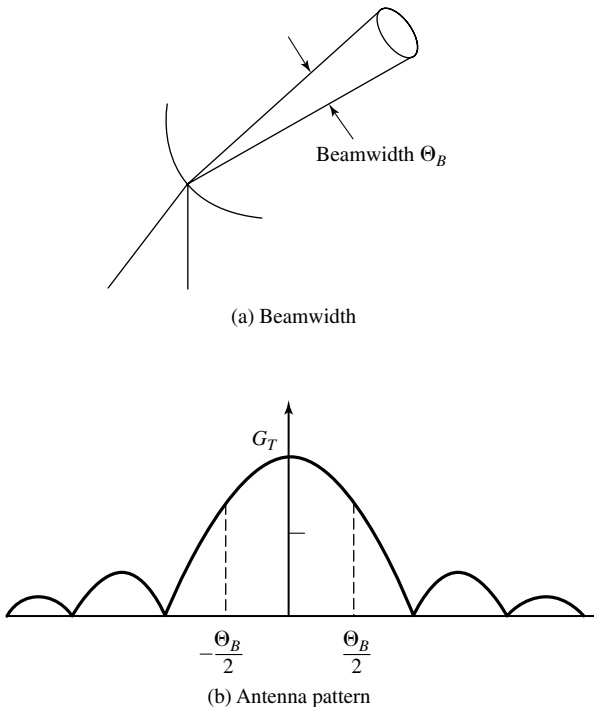


**Figure 7.68** A narrow beam antenna and its radiation pattern.

so that  $G_T$  is inversely proportional to  $\Theta_B^2$ . Hence, a decrease of the beamwidth by a factor of two, which is obtained by doubling the diameter, increases the antenna gain by a factor of four (6 dB).

### Example 7.7.2

A satellite in geosynchronous orbit (36,000 km above the earth's surface) radiates 100 W of power (20 dBW). The transmitting antenna has a gain of 18 dB, so that the EIRP = 38 dBW. The earth station employs a 3-meter parabolic antenna and the downlink is transmitting at a frequency of 4 GHz. Determine the received power.

**Solution** The wavelength  $\lambda = 0.075$  m. Hence, the free-space path loss is

$$\mathcal{L}_s|_{\text{dB}} = 20 \log \left( \frac{4\pi d}{\lambda} \right) = 195.6 \text{ dB}$$

Assuming  $\eta = 0.5$ , the antenna gain is 39 dB. Since no other losses are assumed,

$$\begin{aligned} P_R|_{\text{dB}} &= 20 + 18 + 39 - 195.6 \\ &= -118.6 \text{ dBW} \end{aligned}$$

or, equivalently,

$$P_R = 2.5 \times 10^{-11} \text{ W}$$

We may carry the computation one step further by relating the  $\mathcal{E}_b/N_0$  required to achieve a specified level of performance to  $P_R$ . Since,

$$\frac{\mathcal{E}_b}{N_0} = \frac{T_b P_R}{N_0} = \frac{1}{R_b} \frac{P_R}{N_0} \quad (7.7.12)$$

it follows that

$$\frac{P_R}{N_0} = R_b \left( \frac{\mathcal{E}_b}{N_0} \right)_{\text{req}} \quad (7.7.13)$$

where  $(\mathcal{E}_b/N_0)_{\text{req}}$  is the required SNR/bit to achieve the desired performance. The relation in Equation (7.7.13) allows us to determine the bit rate  $R_b$ . We have

$$10 \log_{10} R_b = \left( \frac{P_R}{N_0} \right)_{\text{dB}} - 10 \log_{10} \left( \frac{\mathcal{E}_b}{N_0} \right)_{\text{req}} \quad (7.7.14)$$

### Example 7.7.3

If  $(\mathcal{E}_b/N_0)_{\text{req}} = 10$  dB, determine the bit rate for the satellite communication system in Example 7.7.2. Assume that the receiver front-end has a noise temperature of 300 K, which is typical for a receiver in the 4 GHz range.

**Solution** Since  $T_0 = 290$  K and  $T_e = 10$  K, it follows that

$$N_0 = kT = 4.1 \times 10^{-21} \text{ W/Hz}$$

or, equivalently,  $-203.9$  dBW/Hz. Then,

$$\begin{aligned} \left( \frac{P_R}{N_0} \right)_{\text{dB}} &= -118.6 + 203.9 \\ &= 85.3 \text{ dB/Hz} \end{aligned}$$



Therefore, from Equation (7.7.14) we obtain

$$\begin{aligned} 10 \log_{10} R_b &= 85.3 - 10 \\ &= 75.3 \end{aligned}$$

or, equivalently,

$$R_b = 33.9 \times 10^6 \text{ bps}$$

We conclude that this satellite channel can support a bit rate of 33.9 Mbps.

## 7.8 SYMBOL SYNCHRONIZATION

In a digital communication system, the output of the receiving filter  $y(t)$  must be sampled periodically at the symbol rate, at the precise sampling time instants  $t_m = mT + \tau_0$ , where  $T$  is the symbol interval and  $\tau_0$  is a nominal time delay that accounts for the propagation time of the signal from the transmitter to the receiver. To perform this periodic sampling, we require a clock signal at the receiver. The process of extracting such a clock signal at the receiver is usually called *symbol synchronization* or *timing recovery*.

Timing recovery is one of the most critical functions that is performed at the receiver of a synchronous digital communication system. We should note that the receiver must know not only the frequency ( $1/T$ ) at which the outputs of the matched filters or correlators are sampled, but also where to take the samples within each symbol interval. The choice of sampling instant within the symbol interval of duration  $T$  is called the *timing phase*.

The best timing phase corresponds to the time instant within the symbol interval where the output of the receiver filter is a maximum. In a practical communication system, the receiver clock must be continuously adjusted in frequency ( $1/T$ ) and in timing phase  $\tau_0$  to compensate for frequency drifts between the oscillators used in the transmitter and receiver clocks and, thus, to optimize the sampling time instants of the matched filter or correlator outputs.

Symbol synchronization can be accomplished in one of several ways. In some communication systems the transmitter and receiver clocks are synchronized to a master clock, which provides a very precise timing signal. In this case, the receiver must estimate and compensate for the relative time delay between the transmitted and received signals. Such may be the case for radio communication systems that operate in the very low frequency (VLF) band (below 30 kHz), where precise clock signals are transmitted from a master radio station.

Another method for achieving symbol synchronization is for the transmitter to simultaneously transmit the clock frequency  $1/T$  or a multiple of  $1/T$  along with the information signal. The receiver may simply employ a narrowband filter tuned to the transmitted clock frequency and, thus, extract the clock signal for sampling. This approach has the advantage of being simple to implement. There are several disadvantages, however. One is that the transmitter must allocate some of its available

power to the transmission of the clock signal. Another is that some small fraction of the available channel bandwidth must be allocated for the transmission of the clock signal. In spite of these disadvantages, this method is frequently used in telephone transmission systems that employ large bandwidths to transmit the signals of many users. In such a case, the transmission of a clock signal is shared in the demodulation of the signals among the many users. Through this shared use of the clock signal, the penalty in transmitter power and in bandwidth allocation is reduced proportionally by the number of users.

A clock signal can also be extracted from the received data signal. There are a number of different methods that can be used at the receiver to achieve self-synchronization. Below we consider four approaches to the problem of achieving symbol synchronization from the received signal.

### 7.8.1 Early-Late Gate Synchronizers

One method for generating a symbol timing signal at the receiver exploits the symmetry properties of the signal at the output of the matched filter or correlator. To describe this method, let us consider the rectangular pulse  $s(t)$ ,  $0 \leq t \leq T$ , shown in Figure 7.69(a). The output of the filter matched to  $s(t)$  attains its maximum value at time  $t = T$ , as shown in Figure 7.69(b). Thus, the output of the matched filter is the time autocorrelation function of the pulse  $s(t)$ . Of course, this statement holds for any arbitrary pulse shape, so the approach that we describe applies in general to any signal pulse. Clearly, the proper time to sample the output of the matched filter for a maximum output is at  $t = T$ ; i.e., at the peak of the correlation function.

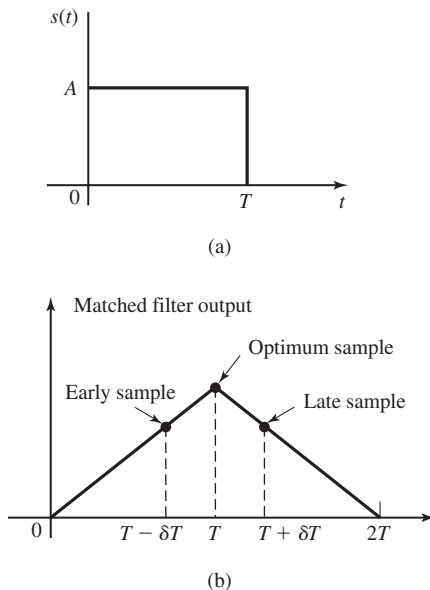


**Figure 7.69** (a) Rectangular signal pulse and (b) its matched filter output.

In the presence of noise, the identification of the peak value of the signal is generally difficult. Instead of sampling the signal at the peak, suppose we sample early, at  $t = T - \delta T$  and late at  $t = T + \delta T$ . The absolute values of the early samples  $|y[m(t - \delta T)]|$  and the late samples  $|y[m(t + \delta T)]|$  will be smaller (on the average in the presence of noise) than the samples of the peak value  $|y(mT)|$ . Since the autocorrelation function is even with respect to the optimum sampling time  $t = T$ , the absolute values of the correlation function at  $t = T - \delta T$  and  $t = T + \delta T$  are equal. Under this condition, the proper sampling time is the midpoint between  $t = T - \delta T$  and  $t = T + \delta T$ . This condition forms the basis for the early-late gate symbol synchronizer.

Figure 7.70 illustrates the block diagram of an early-late gate synchronizer. In this figure, correlators are used in place of the equivalent matched filters. The two correlators integrate over the symbol interval  $T$ , but one correlator starts integrating  $\delta T$  early relative to the estimated optimum sampling time and the other integrator starts integrating  $\delta T$  late relative to the estimated optimum sampling time. An error signal is formed by taking the difference between the absolute values of the two correlator outputs. To smooth the noise corrupting the signal samples, the error signal is passed through a lowpass filter. If the timing is off relative to the optimum sampling time, the average error signal at the output of the lowpass filter is nonzero, and the clock

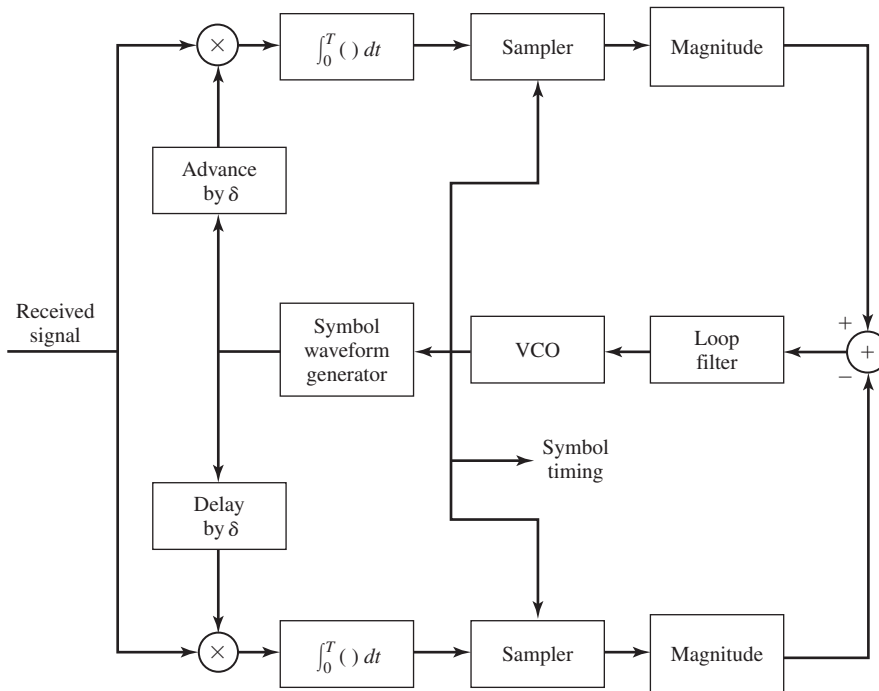


**Figure 7.70** Block diagram of early-late gate synchronizer.

signal is either retarded or advanced, depending on the sign of the error. Thus, the smoothed error signal is used to drive a voltage-controlled oscillator (VCO), whose output is the desired clock signal that is used for sampling. The output of the VCO is also used as a clock signal for a symbol waveform generator that puts out the same basic pulse waveform as that of the transmitting filter. This pulse waveform is advanced and delayed and then fed to the two correlators, as shown in Figure 7.70. Note that if the signal pulses are rectangular, there is no need for a signal pulse generator within the tracking loop.

We observe that the early–late gate synchronizer is basically a closed-loop control system whose bandwidth is relatively narrow compared to the symbol rate  $1/T$ . The bandwidth of the loop determines the quality of the timing estimate. A narrowband loop provides more averaging over the additive noise and, thus, improves the quality of the estimated sampling instants, provided that the channel propagation delay is constant and the clock oscillator at the transmitter is not drifting with time (drifting very slowly with time). On the other hand, if the channel propagation delay is changing with time and, or, the transmitter clock is also drifting with time, then the bandwidth of the loop must be increased to provide for faster tracking of time variations in symbol timing. This increases the noise in the loop and degrades the quality of the timing estimate.

In the tracking mode, the two correlators are affected by adjacent symbols. However, if the sequence of information symbols has zero mean, as is the case for PAM and some other signal modulations, the contribution to the output of the correlators from adjacent symbols averages out to zero in the lowpass filter.

An equivalent realization of the early–late gate synchronizer that is somewhat easier to implement is shown in Figure 7.71. In this case, the clock from the VCO is advanced and delayed by  $\delta T$ , and these clock signals are used to sample the outputs of the two correlators.

### 7.8.2 Minimum Mean-Square-Error Method

Another approach to the problem of timing recovery from the received signal is based on the minimization of the mean-square-error (MSE) between the samples at the output of the receiver filter and the desired symbols. We assume that the baseband signal at the transmitter is of the form

$$v(t) = \sum_{n=-\infty}^{\infty} a_n g_T(t - nT) \quad (7.8.1)$$

where  $\{a_n\}$  is the data sequence and  $T$  is the symbol interval. To be specific, we assume that  $v(t)$  is a PAM baseband signal and the data sequence  $\{a_n\}$  is a zero-mean, stationary sequence with statistically i.i.d. elements. Therefore, the signal  $v(t)$  has zero mean; i.e.,  $E[v(t)] = 0$ . Furthermore, as illustrated in the next chapter, the autocorrelation function of  $v(t)$  is periodic in  $T$  and, hence,  $v(t)$  is a cyclostationary process.

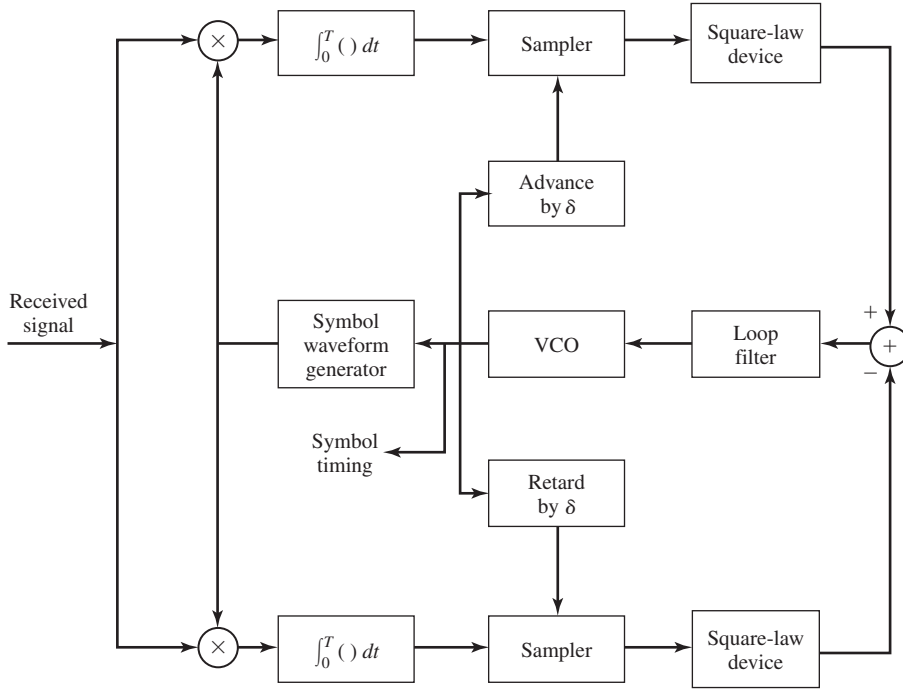


**Figure 7.71** Block diagram of early-late gate synchronizer—an alternative form.

The received signal at the output of the matched filter at the receiver may be expressed as

$$y(t) = \sum_{n=-\infty}^{\infty} a_n x(t - nT - \tau_0) + v(t) \quad (7.8.2)$$

where  $x(t) = g_T(t) \star g_R(t)$ ,  $g_R(t)$  is the impulse response of the receiver filter,  $v(t)$  represents the noise at the output of the receiver filter and  $\tau_0$  ( $\tau_0 < T$ ) represents the timing phase.

The MSE between the output of the receiver filter and the desired symbol at the  $m$ th symbol interval is defined as

$$\text{MSE} = E\{[y_m(\tau_0) - a_m]^2\} \quad (7.8.3)$$

where

$$y_m(\tau_0) = \sum_{n=-\infty}^{\infty} a_m x(mT - nT - \tau_0) + v(mT) \quad (7.8.4)$$

Since the desired symbol  $a_m$  is not known a priori at the receiver, we may use the output of the detector, denoted as  $\hat{a}_m$ , for the  $m$ th symbol; i.e., we substitute  $\hat{a}_m$  for  $a_m$  in the

MSE expression. Hence, the MSE is redefined as

$$\text{MSE} = E\{[y_m(\tau_0) - \hat{a}_m]^2\} \quad (7.8.5)$$

The minimum of (MSE) with respect to the timing phase  $\tau_0$  is found by differentiating Equation (7.8.5) with respect to  $\tau_0$ . Thus, we obtain the necessary condition

$$\sum_m [y_m(\tau_0) - \hat{a}_m] \frac{dy_m(\tau_0)}{d\tau_0} = 0 \quad (7.8.6)$$

An interpretation of the necessary condition in Equation (7.8.6) is that the optimum sampling time corresponds to the condition that the error signal  $[y_m(\tau_0) - \hat{a}_m]$  is uncorrelated with the derivative  $dy_m(\tau_0)/d\tau_0$ . Since the detector output is used in the formation of the error signal  $[y_m(\tau_0) - \hat{a}_m]$ , this timing phase-estimation method is said to be *decision-directed*.

Figure 7.72 illustrates an implementation of the system that is based on the condition given in Equation (7.8.6). Note that the summation operation is implemented as a lowpass filter, which averages a number of symbols. The averaging time is roughly equal to the reciprocal of the bandwidth of the filter. The filter output drives the voltage-controlled oscillator (VCO), which provides the best MSE estimate of the timing phase  $\tau_0$ .

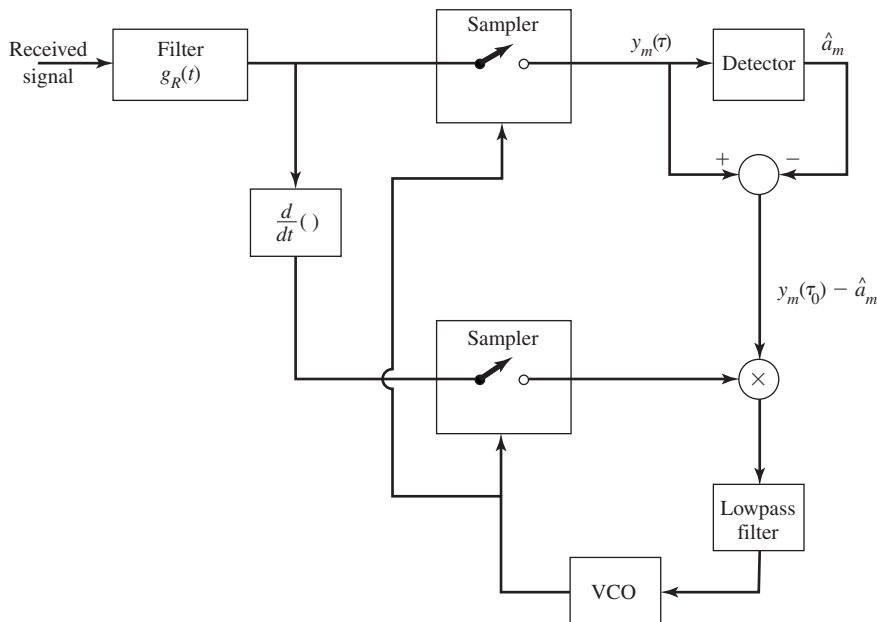


**Figure 7.72** Timing recovery based on minimization of MSE.

### 7.8.3 Maximum-Likelihood Methods

In the ML criterion, the optimum symbol timing is obtained by maximizing the *likelihood function*.

$$\Lambda(\tau_0) = \sum_m a_m y_m(\tau_0) \quad (7.8.7)$$

where  $y_m(\tau_0)$  is the sampled output of the receiving filter given by Equation (7.8.4). From a mathematical viewpoint, the likelihood function can be shown to be proportional to the probability of the received signal (vector) conditioned on a known transmitted signal. Physically,  $\Lambda(\tau_0)$  is simply the output of the matched filter or correlator at the receiver averaged over a number of symbols.

A necessary condition for  $\tau_0$  to be the ML estimate is that

$$\frac{d\Lambda(\tau_0)}{d\tau_0} = \sum_m a_m \frac{dy_m(\tau_0)}{d\tau_0} = 0 \quad (7.8.8)$$

This result suggests the implementation of the tracking loop shown in Figure 7.73. We observe that the product of the detector output  $\hat{a}_m$  with  $dy_m(\tau_0)/d\tau_0$  is averaged by a lowpass filter that drives the VCO. Since the detector output is used in the estimation method, the estimate  $\hat{\tau}$  is decision-directed.

As an alternative to the use of the output symbols from the detector, we may use a *nondecision-directed method* that does not require knowledge of the information symbols. This method is based on averaging over the statistics of the symbols. For example, we may square the output of the receiving filter and maximize the function

$$\Lambda_2(\tau_0) = \sum_m y_m^2(\tau_0) \quad (7.8.9)$$

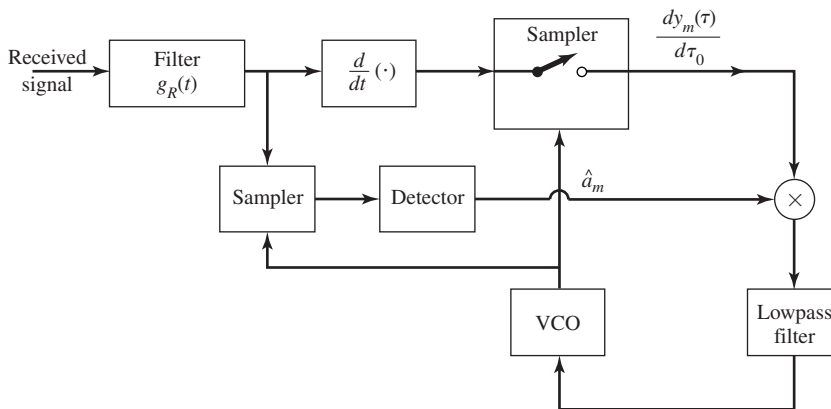


**Figure 7.73** Decision-directed ML timing recovery method for baseband PAM.

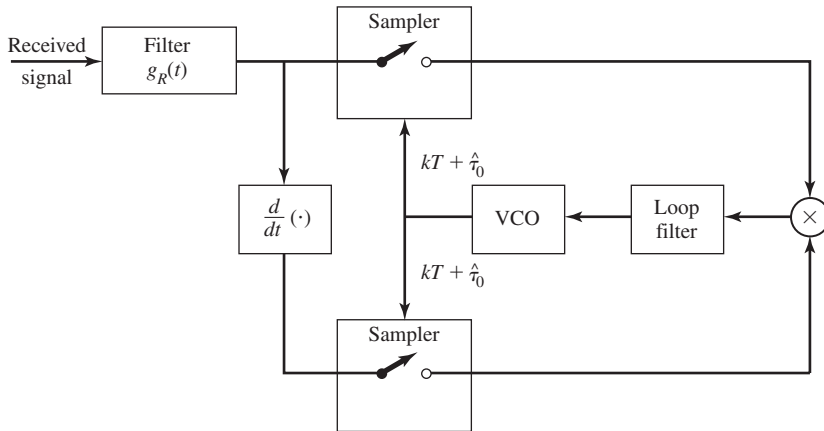


**Figure 7.74** Nondecision-directed estimation of timing for baseband PAM.

with respect to  $\tau_0$ . Thus, we obtain

$$\frac{d\Lambda_2(\tau_0)}{d\tau_0} = 2 \sum_m y_m(\tau_0) \frac{dy_m(\tau_0)}{d\tau_0} = 0 \quad (7.8.10)$$

The condition for the optimum  $\tau_0$  given by Equation (7.8.10) may be satisfied by the implementation shown in Figure 7.74. In this case, there is no need to know the data sequence  $\{a_m\}$ . Hence, the method is nondecision-directed.

### 7.8.4 Spectral-Line Methods

Since the signal component at the output of the receiver filter is periodic with period  $T$ , we can recover a clock signal with frequency  $1/T$  by filtering out a signal component at  $f = 1/T$ . We observe, however, that  $E[y(t)] = 0$  because  $E[a_n] = 0$ . Therefore,  $y(t)$  cannot be used directly to generate a frequency component at  $f = 1/T$ . On the other hand, we may perform a nonlinear operation on  $y(t)$  to generate power at  $f = 1/T$  and its harmonics.

Let us consider a square-law nonlinearity. If we square the signal  $y(t)$  given by Equation (7.8.2) and take the expected value with respect to the data sequence  $\{a_n\}$ , we obtain

$$\begin{aligned} E[y^2(t)] &= E \left[ \sum_n \sum_m a_n a_m x(t - nT - \tau_0) x(t - mT - \tau_0) \right] + \text{noise component} \\ &= \sigma_a^2 \sum_{n=-\infty}^{\infty} x^2(t - nT - \tau_0) + \text{noise component} \end{aligned} \quad (7.8.11)$$

where  $\sigma_a^2 = E[a_n^2]$ . Since  $E[y^2(t)] > 0$ , we may use  $y^2(t)$  to generate the desired frequency component.



Let us use the Poisson Sum Formula on the signal component (see Problem 2.23) to express Equation (7.8.11) in the form of a Fourier series. Hence,

$$\sigma_a^2 \sum_n x^2(t - nT - \tau_0) = \frac{\sigma_a^2}{T} \sum_m c_m e^{j2\pi m(t-\tau_0)/T} \quad (7.8.12)$$

where

$$c_m = \int_{-\infty}^{\infty} X(f) X\left(\frac{m}{T} - f\right) df \quad (7.8.13)$$

By design, we assume that the transmitted signal spectrum is confined to frequencies below  $1/T$ . Hence,  $X(f) = 0$  for  $|f| > 1/T$  and, consequently, there are only three nonzero terms ( $m = 0, \pm 1$ ) in (7.8.12). Therefore, the square of the signal component contains a dc component and a component at the frequency  $1/T$ .

The above development suggests that we square the signal  $y(t)$  at the output of the receiving filter and filter  $y^2(t)$  with a narrowband filter  $B(f)$  tuned to the symbol rate  $1/T$ . If we set the filter response  $B(1/T) = 1$ , then

$$\frac{\sigma_a^2}{T} \text{Re} [c_1 e^{j2\pi(t-\tau_0)/T}] = \frac{\sigma_a^2}{T} c_1 \cos \frac{2\pi}{T}(t - \tau_0) \quad (7.8.14)$$

so that the timing signal is a sinusoid with a phase of  $-2\pi\tau_0/T$ , assuming that  $X(f)$  is real. We may use alternate zero crossings of the timing signal as an indication of the correct sampling times. However, the alternate zero crossings of the signal given by Equation (7.8.14) occur at

$$\frac{2\pi}{T}(t - \tau_0) = (4k + 1)\frac{\pi}{2} \quad (7.8.15)$$

or, equivalently, at

$$t = kT + \tau_0 + \frac{T}{4} \quad (7.8.16)$$

which is offset in time by  $T/4$  relative to the desired zero crossings. In a practical system the timing offset can be easily compensated either by relatively simple clock circuitry or by designing the bandpass filter  $B(f)$  to have a  $\pi/2$  phase shift at  $f = 1/T$ . Figure 7.75 illustrates this method for generating a timing signal at the receiver.

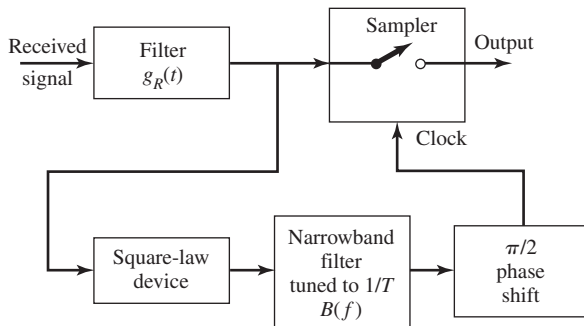


**Figure 7.75** Symbol timing based on spectral-line method.

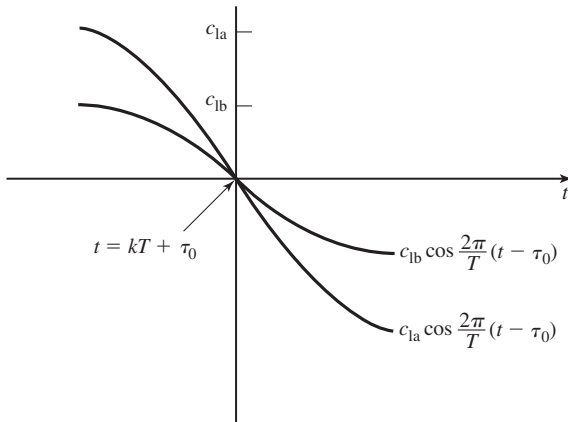


**Figure 7.76** Illustration of the slope of the sinusoid at the zero crossing as a function of the amplitude.

The additive noise that corrupts the signal will generally cause fluctuations in the zero crossings of the desired signal. The effect of the fluctuations will depend on the amplitude  $c_1$  of the mean timing sinusoidal signal given by Equation (7.8.14). We note that the signal amplitude  $c_1$  is proportional to the slope of the timing signal in the vicinity of the zero crossing as shown in Figure 7.76. Therefore, the larger the amplitude  $c_1$ , the larger will be the slope and, consequently, the timing errors due to the noise will be smaller. From Equation (7.8.13) we observe that  $c_1$  depends on the amount of spectral overlap of  $X(f)$  and  $X(1/T - f)$ . Thus,  $c_1$  depends on the amount by which the bandwidth of  $X(f)$  exceeds the Nyquist bandwidth  $1/2T$ ; i.e.,  $c_1$  depends on the excess bandwidth of the signal, which is defined as the band of frequencies of the signal  $X(f)$  beyond  $f = 1/2T$ . If the excess bandwidth is zero, i.e.,  $X(f) = 0$ , for  $|f| > 1/2T$ , then  $c_1 = 0$ , and this method fails to provide a timing signal. If the excess bandwidth is large, say  $\alpha/2T$  where  $\alpha = 1/2$  or  $1$ , the timing signal amplitude will be sufficiently large to yield relatively accurate symbol timing estimates.

### 7.8.5 Symbol Synchronization for Carrier-Modulated Signals

The symbol-timing synchronization methods described in Section 7.8.4 for baseband signals apply as well to bandpass signals. Because any carrier-modulated signal can be converted to a baseband signal by a simple frequency translation, symbol timing can be recovered from the received signal after frequency conversion to baseband.

For QAM signals the spectral-line methods described in Section 7.8.4 have proved to be particularly suitable for timing recovery. Figure 7.77 illustrates a spectral-line method which is based on filtering out a signal component at the frequency  $1/2T$  and squaring the filter output to generate a sinusoidal signal at the desired symbol rate  $1/T$ . Because the demodulation of the QAM signal is accomplished as described above, by multiplication of the input signal with the two quadrature-carrier signals  $\psi_1(t)$  and  $\psi_2(t)$ , the in-phase and quadrature signal components at the outputs of the two correlators are used as the inputs to the two bandpass filters tuned to  $1/2T$ . The

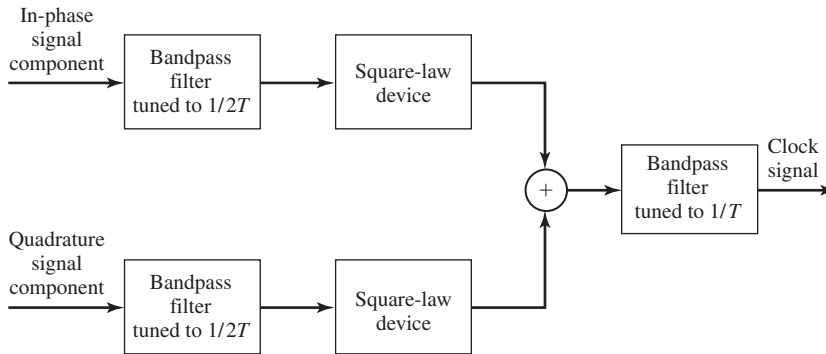


**Figure 7.77** Block diagram of timing recovery method for QAM.

two filter outputs are squared (rectified), summed, and then filtered by a narrowband filter tuned to the clock frequency  $1/T$ . Thus, we generate a sinusoidal signal that is the appropriate clock signal for sampling the outputs of the correlators to recover the information.

In many modern communication systems, the received signal is processed (demodulated) digitally after it has been sampled at the Nyquist rate or faster. In such a case, symbol timing and carrier phase are recovered by signal-processing operations performed on the signal samples. Thus, a PLL for carrier recovery is implemented as a digital PLL and the clock recovery loop of a type described in this section is also implemented as a digital loop. Timing recovery methods based on sampled signals have been described and analyzed by Mueller and Muller (1976).

## 7.9 FURTHER READING

The geometrical representation of digital signals as vectors was first used by Kotelnikov (1947), and by Shannon (1948) in his classic papers. This approach was popularized by Wozencraft and Jacobs (1965). Today this approach to signal analysis and design is widely used. Similar treatments to that given in the text may be found in most books on digital communications.

The matched filter was introduced by North (1943), who showed that it maximized the SNR. Analysis of various binary and  $M$ -ary modulation signals in AWGN were performed in the two decades following Shannon's work. Treatments similar to that given in this chapter may be found in most books on digital communications.

A number of books and tutorial papers have been published on the topic of time synchronization. Books that cover both carrier-phase recovery and time synchronization have been written by Stiffler (1971), Lindsey (1972), and Lindsey and Simon (1973), Meyr and Ascheid (1992), and Mengali and D'Andrea (1997). The tutorial paper by Franks (1980) presents a very readable introduction to this topic.

Symbol synchronization for carrier-modulated signals is a topic that has been treated thoroughly and analyzed in many journal articles. Of particular importance are the journal papers by Lyon (1975a,b) that treat timing recovery for QAM signals and the paper by Mueller and Muller (1976) that describes symbol timing methods based on digital processing of signal samples.

## PROBLEMS

**7.1** Determine the average energy of a set of  $M$  PAM signals of the form

$$s_m(t) = s_m \psi(t), \quad m = 1, 2, \dots, M \\ 0 \leq t \leq T$$

where

$$s_m = \sqrt{\mathcal{E}_g} A_m, \quad m = 1, 2, \dots, M$$

The signals are equally probable with amplitudes that are symmetric about zero and are uniformly spaced with distance  $d$  between adjacent amplitudes as shown in Figure 7.11.

**7.2** Show that the correlation coefficient of two adjacent signal points corresponding to the vertices of an  $N$ -dimensional hypercube with its center at the origin is given by

$$\gamma = \frac{N-2}{N}$$

and their Euclidean distance is

$$d = 2\sqrt{\mathcal{E}_s/N}$$

**7.3** Consider the three waveforms  $\psi_n(t)$  shown in Figure P-7.3.

1. Show that these waveforms are orthonormal.
2. Express the waveform  $x(t)$  as a weighted linear combination of  $\psi_n(t)$ ,  $n = 1, 2, 3$ , if

$$x(t) = \begin{cases} -1, & 0 \leq t \leq 1 \\ 1, & 1 \leq t \leq 3 \\ -1, & 3 \leq t \leq 4 \end{cases}$$

and determine the weighting coefficients.

**7.4** Use the orthonormal waveforms in Problem P-7.3 to approximate the function

$$x(t) = \sin(\pi t/4)$$

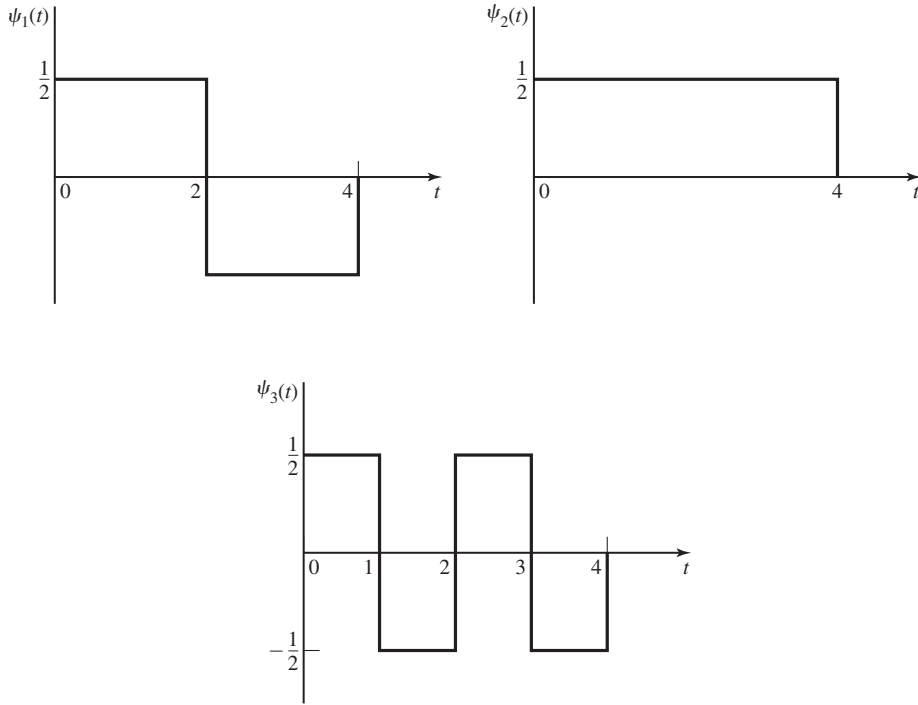


Figure P-7.3

over the interval  $0 \leq t \leq 4$  by the linear combination

$$\hat{x}(t) = \sum_{n=1}^3 c_n \psi_n(t)$$

1. Determine the expansion coefficients  $\{c_n\}$  that minimize the mean-square approximation error

$$E = \int_0^4 [x(t) - \hat{x}(t)]^2 dt$$

2. Determine the residual mean square error  $E_{\min}$ .

**7.5** Consider the four waveforms shown in Figure P-7.5.

1. Determine the dimensionality of the waveforms and a set of basis functions.
2. Use the basis functions to represent the four waveforms by vectors  $\mathbf{s}_1, \mathbf{s}_2, \mathbf{s}_3, \mathbf{s}_4$ .
3. Determine the minimum distance between any pair of vectors.

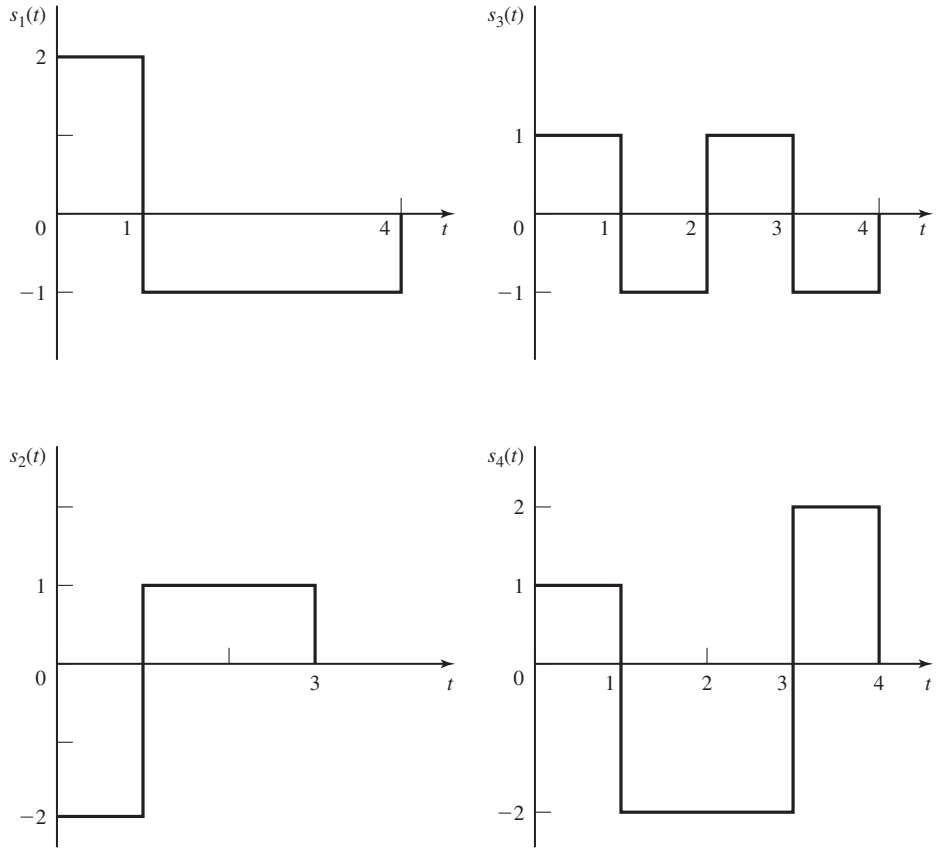


Figure P-7.5

- 7.6 Determine a set of orthonormal functions for the four signals shown in Figure P-7.6.
- 7.7 Consider a set of  $M$  orthogonal signal waveforms  $s_m(t)$ ,  $1 \leq m \leq M$ ,  $0 \leq t \leq T$ , all of which have the same energy  $\mathcal{E}$ . Define a new set of  $M$  waveforms as

$$s'_m(t) = s_m(t) - \frac{1}{M} \sum_{k=1}^M s_k(t), \quad \begin{matrix} 1 \leq m \leq M \\ 0 \leq t \leq T \end{matrix}$$

Show that the  $M$  signal waveform  $\{s'_m(t)\}$  have equal energy, given by

$$\mathcal{E}' = (M - 1)\mathcal{E}/M$$

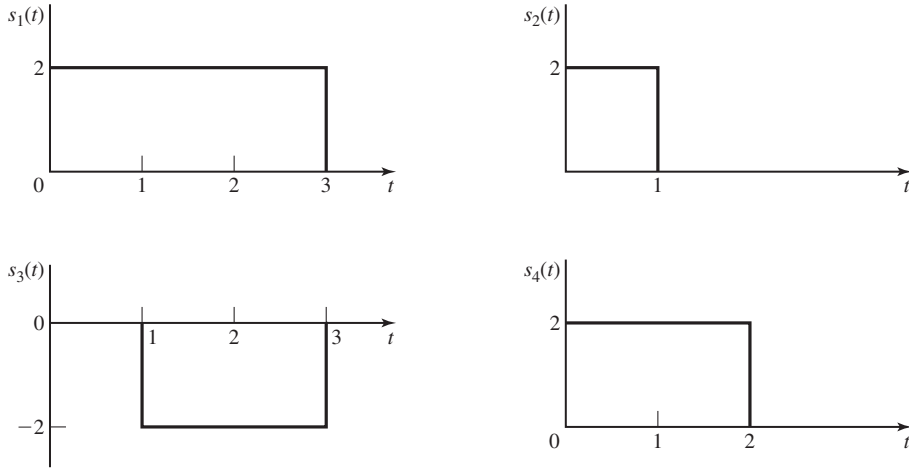


Figure P-7.6

and are equally correlated, with correlation coefficient

$$\gamma_{mn} = \frac{1}{\mathcal{E}'} \int_0^T s'_m(t)s'_n(t) dt = -\frac{1}{M-1}$$

- 7.8** Suppose that two signal waveforms  $s_1(t)$  and  $s_2(t)$  are orthogonal over the interval  $(0, T)$ . A sample function  $n(t)$  of a zero-mean, white noise process is crosscorrelated with  $s_1(t)$ , and  $s_2(t)$ , to yield

$$n_1 = \int_0^T s_1(t)n(t) dt$$

$$n_2 = \int_0^T s_2(t)n(t) dt$$

Prove that  $E(n_1 n_2) = 0$ .

- 7.9** A binary digital communication system employs the signals

$$s_0(t) = 0, \quad 0 \leq t \leq T$$

$$s_1(t) = A, \quad 0 \leq t \leq T$$

for transmitting the information. This is called *on-off signaling*. The demodulator crosscorrelates the received signal  $r(t)$  with  $s_1(t)$  and samples the output of the correlator at  $t = T$ .

1. Determine the optimum detector for an AWGN channel and the optimum threshold, assuming that the signals are equally probable.
2. Determine the probability of error as a function of the SNR. How does on-off signaling compare with antipodal signaling?

- 7.10** A binary PAM communication system employs rectangular pulses of duration  $T_b$  and amplitudes  $\pm A$  to transmit digital information at a rate  $R_b = 10^5$  bps. If the power-spectral density of the additive Gaussian noise is  $N_0/2$ , where  $N_0 = 10^{-2}$  W/Hz, determine the value of  $A$  that is required to achieve a probability of error  $P_b = 10^{-6}$ .
- 7.11** In a binary PAM system for which the two signals occur with unequal probabilities ( $p$  and  $1 - p$ ), the optimum detector is specified by Equation (7.5.54).
1. Determine the average probability of error as a function of  $(\mathcal{E}_b/N_0)$  and  $p$ .
  2. Evaluate the probability of error for  $p = 0.3$  and  $p = 0.5$ , with  $\mathcal{E}_b/N_0 = 10$ .
- 7.12** A binary PAM communication system is used to transmit data over an AWGN channel. The prior probabilities for the bits are  $P(a_m = 1) = 1/3$  and  $P(a_m = -1) = 2/3$ .
1. Determine the optimum threshold at the detector.
  2. Determine the average probability of error.
- 7.13** Binary antipodal signals are used to transmit information over an AWGN channel. The prior probabilities for the two input symbols (bits) are  $1/3$  and  $2/3$ .
1. Determine the optimum maximum-likelihood decision rule for the detector.
  2. Determine the average probability of error as a function of  $\mathcal{E}_b/N_0$ .
- 7.14** The received signal in a binary communication system that employs antipodal signals is

$$r(t) = s(t) + n(t)$$

where  $s(t)$  is shown in Figure P-7.14 and  $n(t)$  is AWGN with power-spectral density  $N_0/2$  W/Hz.

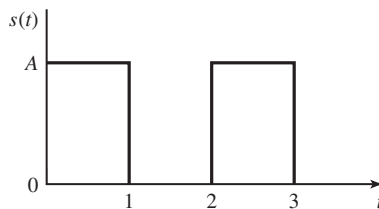


**Figure P-7.14**

1. Sketch the impulse response of the filter matched to  $s(t)$ .
2. Sketch the output of the matched filter to the input  $s(t)$ .



3. Determine the variance the noise of the output of the matched filter at  $t = 3$ .
4. Determine the probability of error as a function of  $A$  and  $N_0$ .

**7.15** A matched filter has the frequency response

$$H(f) = \frac{1 - e^{-j2\pi fT}}{j2\pi f}$$

1. Determine the impulse response  $h(t)$  corresponding to  $H(f)$ .
2. Determine the signal waveform to which the filter characteristic is matched.

**7.16** Prove that when a sinc pulse  $g_T(t)$  is passed through its matched filter, the output is the same sinc pulse.

**7.17** The demodulation of the binary antipodal signals

$$s_1(t) = -s_2(t) = \begin{cases} \sqrt{\frac{E_b}{T}}, & 0 \leq t \leq T \\ 0, & \text{otherwise} \end{cases}$$

can be accomplished by use of a single integrator, as shown in Figure P-7.17, which is sampled periodically at  $t = kT$ ,  $k = 0, \pm 1, \pm 2, \dots$ . The additive noise is zero-mean Gaussian with power-spectral density of  $\frac{N_0}{2}$  W/Hz.

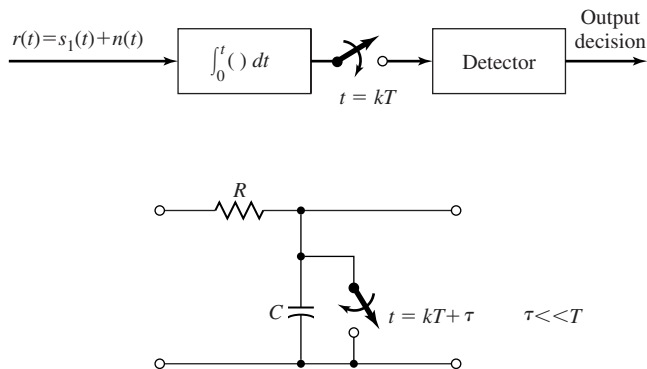


**Figure P-7.17**

1. Determine the output SNR of the demodulator at  $t = T$ .
  2. If the ideal integrator is replaced by the RC filter shown in Figure P-7.17, determine the output SNR as a function of the time constant  $RC$ .
  3. Determine the value of  $RC$  that maximizes the output SNR.
- 7.18** Sketch the impulse response of the filter matched to the pulses shown in Figure P-7.18. Also determine and sketch the outputs of each of the matched filters.

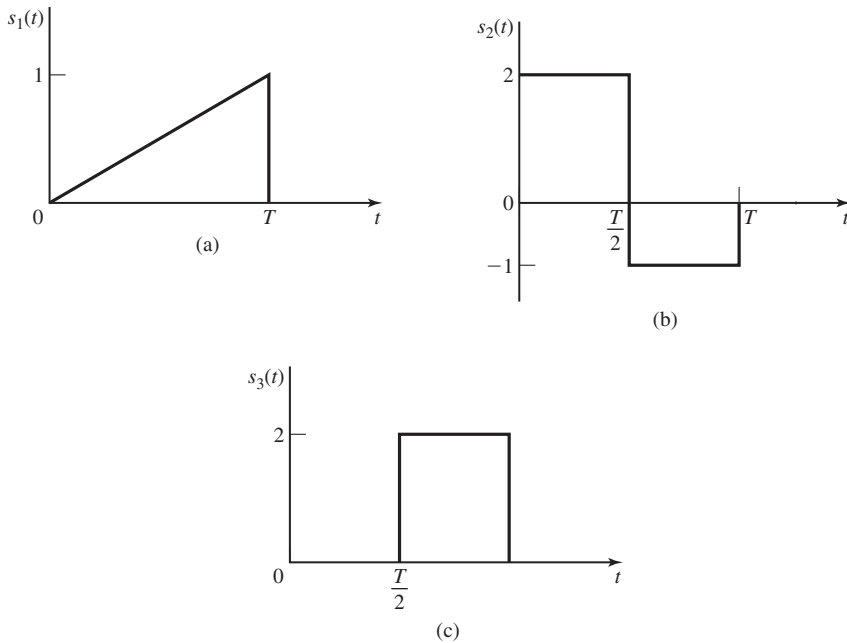


Figure P-7.18

**7.19** Three messages  $m_1$ ,  $m_2$ , and  $m_3$  are to be transmitted over an AWGN channel with noise power-spectral density  $\frac{N_0}{2}$ . The messages are

$$s_1(t) = \begin{cases} 1 & 0 \leq t \leq T \\ 0, & \text{otherwise} \end{cases}$$

$$s_2(t) = -s_3(t) = \begin{cases} 1 & 0 \leq t \leq \frac{T}{2} \\ -1 & \frac{T}{2} \leq t \leq T \\ 0, & \text{otherwise} \end{cases}$$

1. What is the dimensionality of the signal space?
2. Find an appropriate basis for the signal space (Hint: You can find the basis without using the Gram-Schmidt procedure).
3. Draw the signal constellation for this problem.
4. Derive and sketch the optimal decision regions  $R_1$ ,  $R_2$ , and  $R_3$ .
5. Which of the three messages is more vulnerable to errors and why? In other words which of  $P(\text{Error} | m_i \text{ transmitted})$ ,  $i = 1, 2, 3$  is larger?

**7.20** In this chapter we showed that an optimal demodulator can be realized as:

- A correlation-type demodulator
- A matched-filter type demodulator

where in both cases  $\psi_j(t)$ ,  $1 \leq j \leq N$ , were used for correlating  $r(t)$ , or designing the matched filters. Show that an optimal demodulator for a general  $M$ -ary communication system can also be designed based on correlating  $r(t)$  with  $s_i(t)$ ,  $1 \leq i \leq M$ , or designing filters that are matched to  $s_i(t)$ 's,  $1 \leq i \leq M$ . Precisely describe the structure of such demodulators by giving their block diagram and all relevant design parameters, and compare their complexity with the complexity of the demodulators obtained in the text.

**7.21** In a binary antipodal signalling scheme the signals are given by

$$s_1(t) = -s_2(t) = \begin{cases} \frac{2At}{T} & 0 \leq t \leq \frac{T}{2} \\ 2A \left(1 - \frac{t}{T}\right) & \frac{T}{2} \leq t \leq T \\ 0, & \text{otherwise} \end{cases}$$

The channel is AWGN and  $\mathcal{S}_n(f) = \frac{N_0}{2}$ . The two signals have prior probabilities  $p_1$  and  $p_2 = 1 - p_1$ .

1. Determine the structure of the optimal receiver.
2. Determine an expression for the error probability.
3. Plot error probability as a function of  $p_1$  for  $0 \leq p_1 \leq 1$ .

**7.22** In an additive white Gaussian noise channel with noise power-spectral density of  $\frac{N_0}{2}$ , two equiprobable messages are transmitted by

$$s_1(t) = \begin{cases} \frac{At}{T}, & 0 \leq t \leq T \\ 0, & \text{otherwise} \end{cases}$$

$$s_2(t) = \begin{cases} A \left(1 - \frac{t}{T}\right) & 0 \leq t \leq T \\ 0, & \text{otherwise} \end{cases}$$

1. Determine the structure of the optimal receiver.
2. Determine the probability of error.

**7.23** Consider a signal detector with an input

$$r = \pm A + n$$

where  $+A$  and  $-A$  occur with equal probability and the noise variable  $n$  is characterized by the (Laplacian) pdf shown in Figure P-7.23.

1. Determine the probability of error as a function of the parameters  $A$  and  $\sigma$ .
2. Determine the "SNR" required to achieve an error probability of  $10^{-5}$ . How does the SNR compare with the result for a Gaussian PDF?

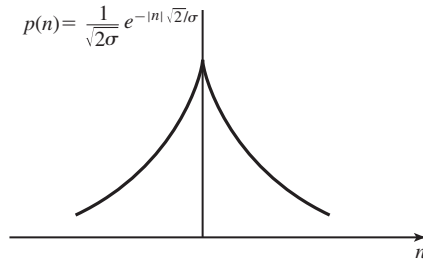


Figure P-7.23

**7.24** A Manchester encoder maps an information 1 into 10 and a 0 into 01. The signal waveforms corresponding to the Manchester code are shown in Figure P-7.24. Determine the probability of error if the two signals are equally probable.

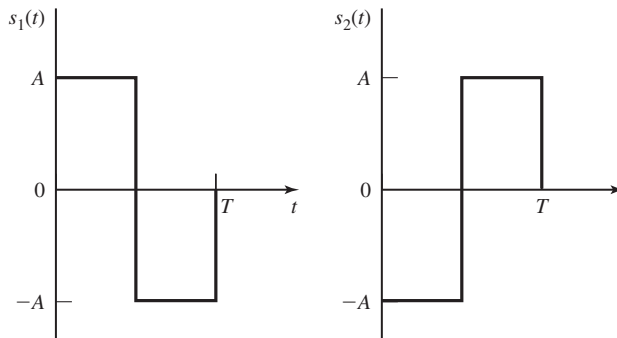


Figure P-7.24

**7.25** A three-level PAM system is used to transmit the output of a memoryless ternary source whose rate is 2000 symbols/sec. The signal constellation is shown in Figure P-7.25. Determine the input to the detector, the optimum threshold that minimizes the average probability of error, and the average probability of error.

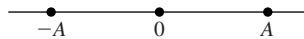


Figure P-7.25

**7.26** Consider a biorthogonal signal set with  $M = 8$  signal points. Determine a union bound for the probability of a symbol error as a function of  $\mathcal{E}_b/N_0$ . The signal points are equally likely a priori.

- 7.27** Consider an  $M$ -ary digital communication system where  $M = 2^N$ , and  $N$  is the dimension of the signal space. Suppose that the  $M$  signal vectors lie on the vertices of a hypercube that is centered at the origin, as illustrated in Figure 7.29. Determine the average probability of a symbol error as a function of  $\mathcal{E}_s/N_0$  where  $\mathcal{E}_s$  is the energy/symbol,  $N_0/2$  is the power-spectral density of the AWGN, and all signal points are equally probable.
- 7.28** Consider the signal waveform

$$s(t) = \sum_{k=1}^n c_k p(t - nT_c)$$

where  $p(t)$  is a rectangular pulse of unit amplitude and duration  $T_c$ . The  $\{c_i\}$  may be viewed as a code vector  $\mathbf{c} = [c_1, c_2, \dots, c_n]$ , where the elements  $c_i = \pm 1$ . Show that the filter matched to the waveform  $s(t)$  may be realized as a cascade of a filter matched to  $p(t)$  followed by a discrete-time filter matched to the vector  $\mathbf{c}$ . Determine the value of the output of the matched filter at the sampling instant  $t = nT_c$ .

- 7.29** A speech signal is sampled at a rate of 8 kHz, logarithmically compressed and encoded into a PCM format using 8 bits/sample. The PCM data is transmitted through an AWGN baseband channel via  $M$ -level PAM. Determine the bandwidth required for transmission when (a)  $M = 4$ , (b)  $M = 8$ , and (c)  $M = 16$ .
- 7.30** Two equiprobable messages are transmitted via an additive white Gaussian noise channel with noise power-spectral density of  $\frac{N_0}{2} = 1$ . The messages are transmitted by the following two signals

$$s_1(t) = \begin{cases} 1 & 0 \leq t \leq 1 \\ 0 & \text{otherwise} \end{cases}$$

and  $s_2(t) = s_1(t - 1)$ . It is intended to implement the receiver using a correlation type structure, but due to imperfections in the design of the correlators, the structure shown in Figure P-7.30 has been implemented. The imperfection appears in the integrator in the upper branch where instead of  $\int_0^1$  we have  $\int_0^{1.5}$ . The decision

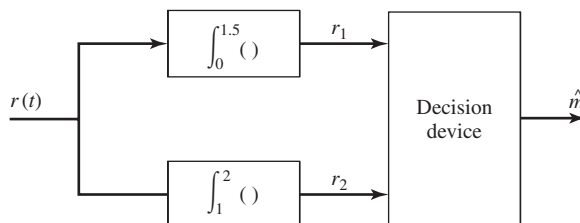


Figure P-7.30

device, therefore, observes  $r_1$  and  $r_2$  and based on this observation has to decide which message was transmitted. What decision rule should be adopted by the decision device for an optimal decision?

- 7.31** A Hadamard matrix is defined as a matrix whose elements are  $\pm 1$  and its row vectors are pairwise orthogonal. In the case when  $n$  is a power of 2, an  $n \times n$  Hadamard matrix is constructed by means of the recursion

$$\mathbf{H}_2 = \begin{bmatrix} 1 & 1 \\ 1 & -1 \end{bmatrix} \quad \mathbf{H}_{2n} = \begin{bmatrix} \mathbf{H}_n & \mathbf{H}_n \\ \mathbf{H}_n & -\mathbf{H}_n \end{bmatrix}$$

1. Let  $\mathbf{c}_i$  denote the  $i$ th row of an  $n \times n$  Hadamard matrix as defined above. Show that the waveforms constructed as

$$s_i(t) = \sum_{k=1}^n c_{ik} p(t - kT_c), \quad i = 1, 2, \dots, n$$

are orthogonal, where  $p(t)$  is an arbitrary pulse confined to the time interval  $0 \leq t \leq T_c$ .

2. Show that the matched filters (or crosscorrelators) for the  $n$  waveforms  $\{s_i(t)\}$  can be realized by a single filter (or correlator) matched to the pulse  $p(t)$  followed by a set of  $n$  crosscorrelators using the code words  $\{\mathbf{c}_i\}$ .

- 7.32** The discrete sequence

$$r_k = \sqrt{\mathcal{E}_c} c_k + n_k, \quad k = 1, 2, \dots, n$$

represents the output sequence of samples from a demodulator, where  $c_k = \pm 1$  are elements of one of two possible codewords,  $\mathbf{c}_1 = [1, 1, \dots, 1]$  and  $\mathbf{c}_2 = [1, 1, \dots, 1, -1, \dots, -1]$ . The codeword  $\mathbf{c}_2$  has  $w$  elements which are  $+1$  and  $n - w$  elements which are  $-1$ , where  $w$  is some positive integer. The noise sequence  $\{n_k\}$  is white Gaussian with variance  $\sigma^2$ .

1. What is the optimum maximum-likelihood detector for the two possible transmitted signals?
  2. Determine the probability error as a function of the parameter  $(\sigma^2, \mathcal{E}_b, w)$ .
  3. What is the value of  $w$  that minimizes the error probability?
- 7.33** A baseband digital communication system employs the signals shown in Figure P-7.33(a) for transmission of two equiprobable messages. It is assumed the communication problem studied here is a “one shot” communication problem, that is, the above messages are transmitted just once and no transmission takes place afterwards. The channel has no attenuation ( $\alpha = 1$ ) and the noise is AWG

with power-spectral density  $\frac{N_0}{2}$ .

1. Find an appropriate orthonormal basis for the representation of the signals.
2. In a block diagram, give the precise specifications of the optimal receiver using matched filters. Label the block diagram carefully.
3. Find the error probability of the optimal receiver.
4. Show that the optimal receiver can be implemented by using just *one* filter [see block diagram shown in Figure P-7.33(b)]. What are the characteristics of the matched filter and the sampler and decision device?
5. Now assume the channel is not ideal, but has an impulse response of  $c(t) = \delta(t) + \frac{1}{2}\delta(t - \frac{T}{2})$ . Using the same matched filter you used in the previous part, design an optimal receiver.
6. Assuming that the channel impulse response is  $c(t) = \delta(t) + a\delta(t - \frac{T}{2})$ , where  $a$  is a random variable uniformly distributed on  $[0, 1]$ , and using the same matched filter, design the optimal receiver.

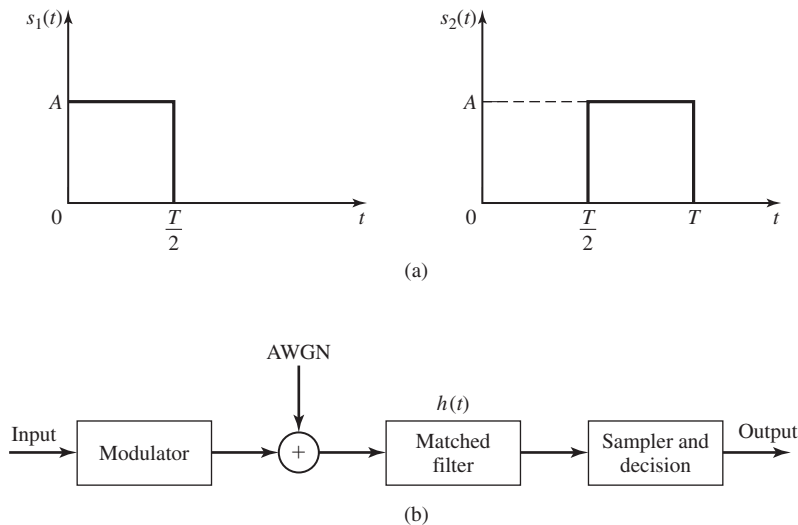


Figure P-7.33

- 7.34** Suppose that binary PSK is used for transmitting information over an AWGN with power-spectral density of  $N_0/2 = 10^{-10}$  W/Hz. The transmitted signal energy is  $\mathcal{E}_b = A^2T/2$ , where  $T$  is the bit interval and  $A$  is the signal amplitude. Determine the signal amplitude required to achieve an error probability of  $10^{-6}$ , if the data rate is (a) 10 kbps, (b) 100 kbs, (c) 1 Mbps.

**7.35** Consider the signal

$$u(t) = \begin{cases} \frac{A}{T}t \cos 2\pi f_c t, & 0 \leq t \leq T \\ 0, & \text{otherwise} \end{cases}$$

1. Determine the impulse response of the matched filter for the signal.
2. Determine the output of the matched filter at  $t = T$ .
3. Suppose the signal  $u(t)$  is passed through a correlator which correlates the input  $u(t)$  with  $u(t)$ . Determine the value of the correlator output at  $t = T$ . Compare your result with that in part (b).

**7.36** A carrier component is transmitted on the quadrature carrier in a communication system that transmits information via binary PSK. Hence, the received signal has the form

$$v(t) = \pm\sqrt{2P_s} \cos(2\pi f_c t + \phi) + \sqrt{2P_c} \sin(2\pi f_c t + \phi) + n(t)$$

where  $\phi$  is the carrier phase and  $n(t)$  is AWGN. The unmodulated carrier component is used as a pilot signal at the receiver to estimate the carrier phase.

1. Sketch a block diagram of the receiver, including the carrier-phase estimator.
2. Illustrate mathematically the operations involved in the estimation of the carrier-phase  $\phi$ .
3. Express the probability of error for the detection of the binary PSK signal as a function of the total transmitted power  $P_T = P_s + P_c$ . What is the loss in performance due to the allocation of a portion of the transmitted power to the pilot signal? Evaluate the loss for  $P_c/P_T = 0.1$ .

**7.37** In the demodulation of a binary PSK signal received in white Gaussian noise, a phase-locked loop is used to estimate the carrier-phase  $\phi$ .

1. Determine the effect of a phase error  $\phi - \hat{\phi}$  on the probability of error.
2. What is the loss in SNR if the phase error  $\phi - \hat{\phi} = 45^\circ$ ?

**7.38** Suppose that the loop filter [see Equation (5.2.4)] for a PLL has the transfer function

$$G(s) = \frac{1}{s + \sqrt{2}}$$

1. Determine the closed-loop transfer function  $H(s)$  and indicate if the loop is stable.
2. Determine the damping factor and the natural frequency of the loop.

**7.39** Consider the PLL for estimating the carrier phase of a signal in which the loop filter is specified as

$$G(s) = \frac{K}{1 + \tau_1 s}$$



1. Determine the closed-loop transfer function  $H(s)$  and its gain at  $f = 0$ .
  2. For what range of value of  $\tau_1$  and  $K$  is the loop stable?
- 7.40 The loop filter  $G(s)$  in a PLL is implemented by the circuit shown in Figure P-7.40. Determine the system function  $G(s)$  and express the time constants  $\tau_1$  and  $\tau_2$  [see Equation (5.2.4)] in terms of the circuit parameters.

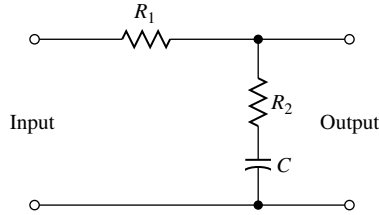


Figure P-7.40

- 7.41 The loop filter  $G(s)$  in a PLL is implemented with the active filter shown in Figure P-7.41. Determine the system function  $G(s)$  and express the time constants  $\tau_1$  and  $\tau_2$  [see Equation (5.2.4)] in terms of the circuit parameters.

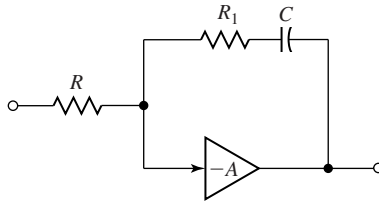


Figure P-7.41

- 7.42 Consider the four-phase and eight-phase signal constellations shown in Figure P-7.42. Determine the radii  $r_1$  and  $r_2$  of the circles, such that the distance

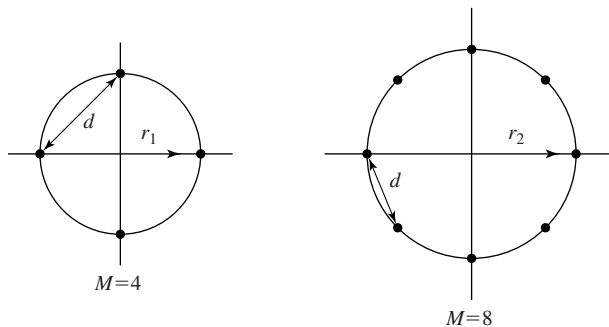
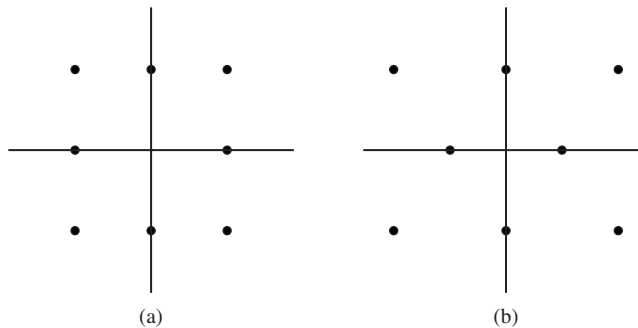


Figure P-7.42

between two adjacent points in the two constellations is  $d$ . From this result, determine the additional transmitted energy required in the 8-PSK signal to achieve the same error probability as the four-phase signal at high SNR, where the probability of error is determined by errors in selecting adjacent points.

- 7.43** Consider the two 8-point QAM signal constellation shown in Figure P-7.43. The minimum distance between adjacent points is  $2A$ . Determine the average transmitted power for each constellation assuming that the signal points are equally probable. Which constellation is more power efficient?



**Figure P-7.43**

- 7.44** The 16-QAM signal constellation shown in Figure P-7.44 is an international standard for telephone-line modems (called V.29). Determine the optimum decision boundaries for the detector, assuming that the SNR is sufficiently high so that errors only occur between adjacent points.
- 7.45** Specify a Gray code for the 16-QAM V.29 signal constellation shown in Problem 7.44.
- 7.46** Consider the octal signal-point constellations in Figure P-7.46.
1. The nearest neighbor signal points in the 8-QAM signal constellation are separated in distance by  $A$  units. Determine the radii  $a$  and  $b$  of the inner and outer circles.
  2. The adjacent signal points in the 8-PSK are separated by a distance of  $A$  units. Determine the radius  $r$  of the circle.
  3. Determine the average transmitter powers for the two signal constellations and compare the two powers. What is the relative power advantage of one constellation over the other? (Assume that all signal points are equally probable).
- 7.47** Consider a digital communication system that transmits information via QAM over a voice-band telephone channel at a rate 2400 symbols/second. The additive noise is assumed to be white and Gaussian.

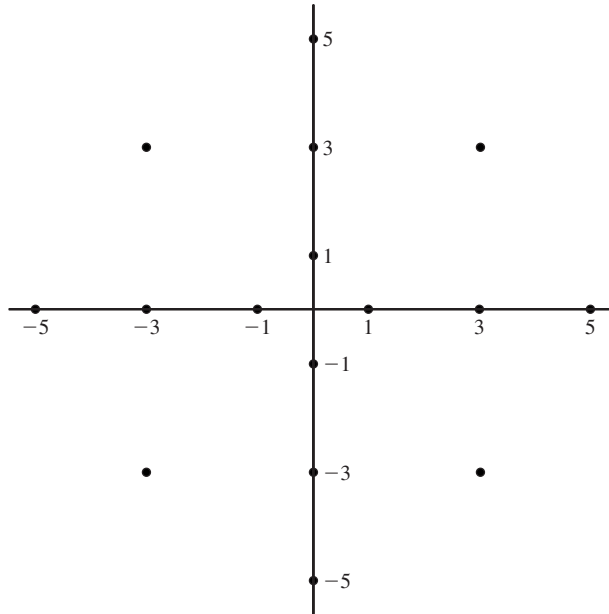


Figure P-7.44

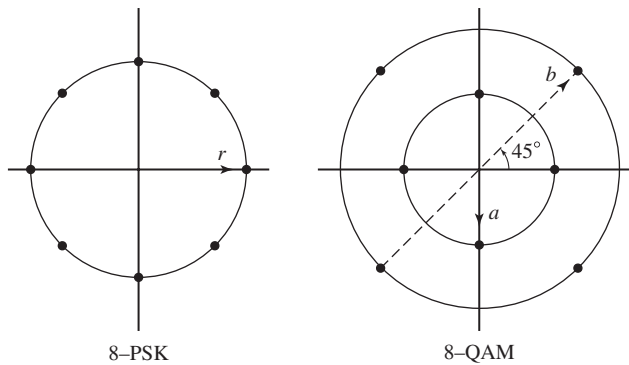


Figure P-7.46

1. Determine the  $\mathcal{E}_b/N_0$  required to achieve an error probability of  $10^{-5}$  at 4800 bps.
2. Repeat (1) for a bit rate of 9600 bps.
3. Repeat (1) for a bit rate of 19,200 bps.
4. What conclusions do you reach from these results.

- 7.48** Consider the 8-point QAM signal constellation shown in Figure P-7.46.
1. Assign three data bits to each point of the signal constellation such that nearest (adjacent) points differ in only one bit position.
  2. Determine the symbol rate if the desired bit rate is 90 Mbps.
  3. Compare the SNR required for the 8-point QAM modulation with that of an 8-point PSK modulation having the same error probability.
  4. Which signal constellation, 8-point QAM or 8-point PSK, is more immune to phase errors? Explain the reason for your answer.
- 7.49** In Section 7.4.1 it was shown that the minimum frequency separation for orthogonality of binary FSK signals with coherent detection is  $\Delta f = \frac{1}{2T}$ . However a lower error probability is possible with coherent detection of FSK if  $\Delta f$  is increased beyond  $\frac{1}{2T}$ . Show that the minimum value of  $\Delta f$  is  $\frac{0.715}{T}$  and determine the probability of error for this choice of  $\Delta f$ .
- 7.50** The lowpass equivalent signal waveforms for three signal sets are shown in Figure P-7.50. Each set may be used to transmit one of four equally probable messages over an additive white Gaussian noise channel with noise power-spectral density  $\frac{N_0}{2}$ .
1. Classify the signal waveforms in set I, set II, and set III. In other words, state the category or class to which each signal set belongs.
  2. What is the *average* transmitted energy for each signal set?
  3. For signal set I, specify the average probability of error if the signals are detected coherently.
  4. For signal set II, give a union bound on the probability of a symbol error if the detection is performed (a) coherently and (b) noncoherently.
  5. Is it possible to use noncoherent detection on signal set III? Explain.
  6. Which signal set or signal sets would you select if you wished to achieve a bit rate to bandwidth ( $\frac{R}{W}$ ) ratio of at least 2. Explain your answer.
- 7.51** Consider the phase-coherent demodulator for  $M$ -ary FSK signals as shown in Figure 7.45.
1. Assume that the signal

$$u_0(t) = \sqrt{\frac{2\mathcal{E}_s}{T}} \cos 2\pi f_c t, \quad 0 \leq t \leq T$$

was transmitted and determine the output of the  $M - 1$  correlators at  $t = T$ , corresponding to the signals  $u_m(t)$ ,  $m = 1, 2, \dots, M - 1$ , when  $\hat{\phi}_m \neq \phi_m$ .

2. Show that the minimum frequency separation required for the signal orthogonality at the demodulator when  $\hat{\phi}_m \neq \phi_m$  is  $\Delta f = \frac{1}{T}$ .

- 7.52** In the demodulation and noncoherent detection of  $M$ -ary FSK signals, as

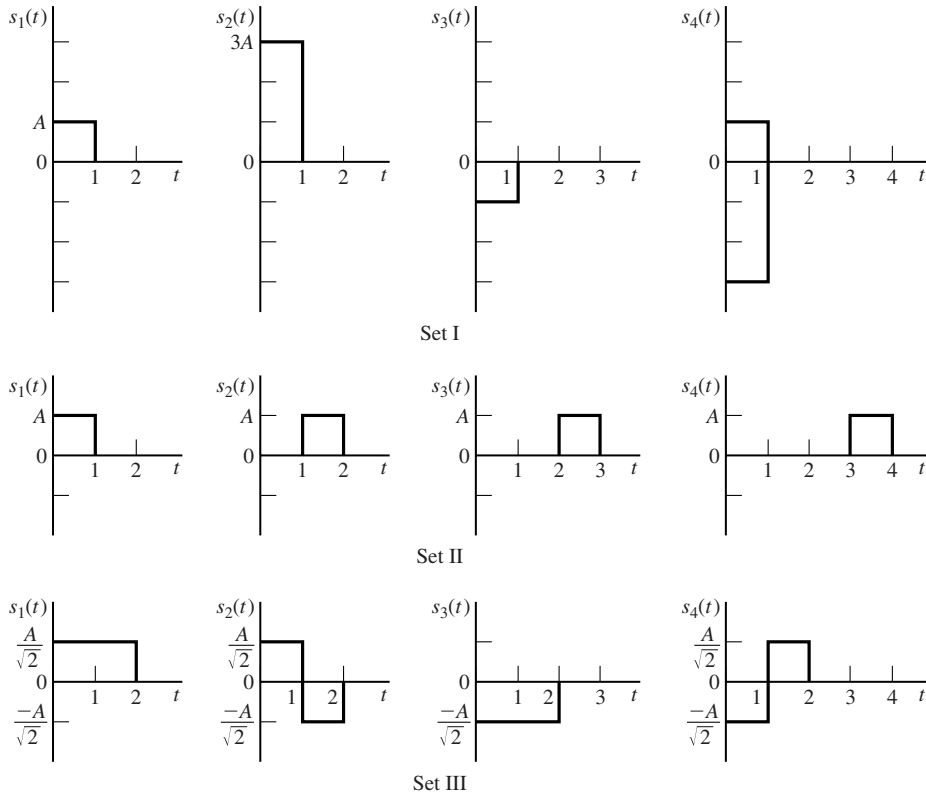


Figure P-7.50

illustrated in Figure 7.47, show that the  $2M$  noise samples given in Equations (7.5.88) and (7.5.89) are zero-mean, mutually independent Gaussian random variables with equal variance  $\sigma^2 = \frac{N_0}{2}$ .

**7.53** In on-off keying of a carrier-modulated signal, the two possible signals are

$$s_0(t) = 0, \quad 0 \leq t \leq T_b$$

$$s_1(t) = \sqrt{\frac{2\mathcal{E}_b}{T_b}} \cos 2\pi f_c t, \quad 0 \leq t \leq T_b$$

The corresponding received signals are

$$r(t) = n(t), \quad 0 \leq t \leq T_b$$

$$r(t) = \sqrt{\frac{2\mathcal{E}_b}{T_b}} \cos(2\pi f_c t + \phi) + n(t), \quad 0 \leq t \leq T_b$$

where  $\phi$  is the carrier phase and  $n(t)$  is AWGN.

1. Sketch a block diagram of the receiver (demodulator and detector) that employs noncoherent (envelope) detection.
  2. Determine the probability density functions for the two possible decision variables at the detector corresponding to the two possible received signals.
  3. Derive the probability of error for the detector.
- 7.54** Digital information is to be transmitted by carrier modulation through an additive Gaussian noise channel with a bandwidth of 100 kHz and  $N_0 = 10^{-10}$  W/Hz. Determine the maximum rate that can be transmitted through the channel for four-phase PSK, binary FSK, and four-frequency orthogonal FSK which is detected noncoherently.
- 7.55** Consider a transmission line channel that employs  $n - 1$  regenerative repeaters plus the terminal receiver in the transmission of binary information. We assume that the probability of error at the detector of each receiver is  $p$  and that errors among repeaters are statistically independent.

1. Show that the binary error probability at the terminal receiver is

$$P_n = \frac{1}{2}[1 - (1 - 2p)^n]$$

2. If  $p = 10^{-6}$  and  $n = 100$ , determine an approximate value of  $P_n$ .
- 7.56** A digital communication system consists of a transmission line with 100 digital (regenerative) repeaters. Binary antipodal signals are used for transmitting the information. If the overall end-to-end error probability is  $10^{-6}$ , determine the probability of error for each repeater and the required  $\mathcal{E}_b/N_0$  to achieve this performance in AWGN.
- 7.57** A radio transmitter has a power output of  $P_T = 1$  watt at a frequency of  $10^9$  Hz (1 GHz). The transmitting and receiving antennas are parabolic dishes with diameter  $D = 3$  meters.
1. Determine the antenna gains.
  2. Determine the EIRP for transmitter.
  3. The distance (free space) between the transmitting and receiving antennas is 20 km. Determine the signal power at the output of the receiving antenna in dBm.
- 7.58** A radio communication system transmits at a power level of 0.1 watt at 1 GHz. The transmitting and receiving antennas are parabolic, each having a diameter of one meter. The receiver is located 30 km from the transmitter.
1. Determine the gains of the transmitting and receiving antennas.
  2. Determine the EIRP of the transmitted signal.
  3. Determine the signal power from the receiving antenna.

- 7.59** A satellite in synchronous orbit is used to communicate with an earth station at a distance of  $4 \times 10^7$  m. The satellite has an antenna with a gain of 15 dB and a transmitter power of 3 W. The earth station uses a 10 m parabolic antenna with an efficiency of 0.6. The frequency band is at  $f = 10$  GHz. Determine the received power level at the output of the receiver antenna.
- 7.60** A spacecraft in space located  $10^8$  meters from the earth is sending data at a rate of  $R$  bps. The frequency band is centered at 2 GHz and the transmitted power is 10 W. The earth station uses a parabolic antenna, 50 m in diameter, and the spacecraft has an antenna with a gain of 10 dB. The noise temperature of the receiver front end is  $T = 300$  K.
1. Determine the received power level.
  2. If the desired  $\mathcal{E}_b/N_0 = 10$  dB, determine the maximum bit rate that the spacecraft can transmit.
- 7.61** Consider the front-end of the receiver shown in the block diagram in Figure P-7.61. The received signal power at the input to the first amplifier is  $-113$  dBm, and the received noise power-spectral density is  $-175$  dBm/Hz. The bandpass filter has a bandwidth of 10 MHz, and gains and noise figures are as shown. Determine the SNR  $P_s/P_n$  at the input to the demodulator.

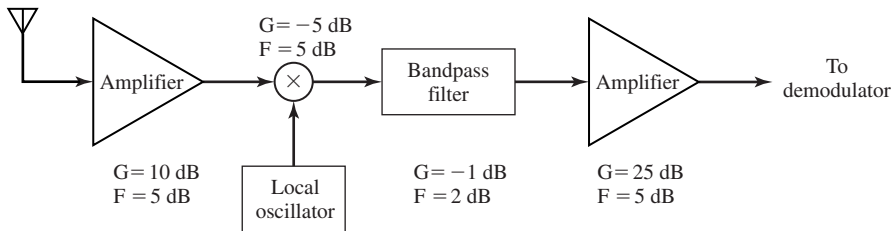
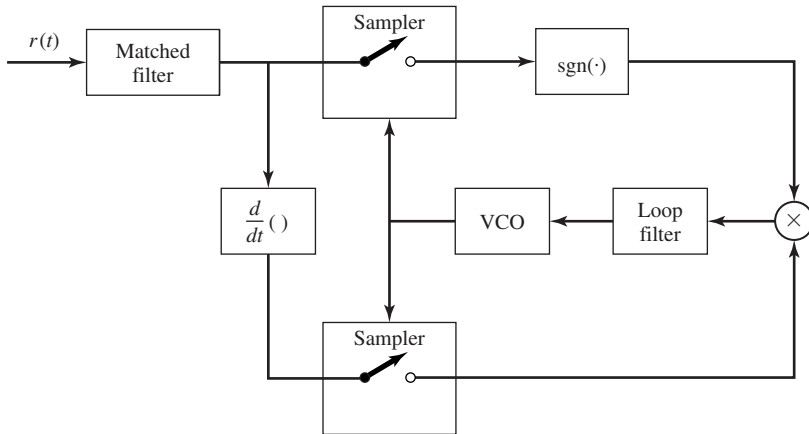


Figure P-7.61

- 7.62** A satellite in geosynchronous orbit is used as a regenerative repeater in a digital communication system. Let us consider the satellite-to-earth link in which the satellite antenna has a gain of 6 dB and the earth-station antenna has a gain of 50 dB. The downlink is operated at a center frequency of 4 GHz, and the signal bandwidth is 1 MHz. If the required  $(\mathcal{E}_b/N_0)$  for reliable communication is 15 dB, determine the transmitted power for the satellite downlink. It is assumed that  $N_0 = 4.1 \times 10^{-21}$  W/Hz.
- 7.63** One of the Mariner spacecrafts that traveled to the planet Mercury sent its data to earth through a distance of  $1.6 \times 10^{11}$  m. The transmitting antenna had a gain of 27 dB and operated at a frequency  $f = 2.3$  GHz. The transmitter power was 17 W. The earth station employed parabolic antenna with a 64-m diameter and an efficiency of 0.55. The receiver had an effective noise temperature of  $T_e = 15$  K.

If the desired SNR/bit ( $\mathcal{E}_b/N_0$ ) was 6 dB, determine the data rate that could have been supported by the communication link.

**7.64** Show that the early-late gate synchronizer illustrated in Figure 7.70 is a close approximation to the timing recovery system illustrated in Figure P-7.64.



**Figure P-7.64**

**7.65** Based on a ML criterion, determine a carrier-phase estimation method for binary on-off keying modulation.



## *Digital Transmission through Bandlimited AWGN Channels*

In the preceding chapter, we considered digital communication over an AWGN channel and evaluated the probability of error performance of the optimum receiver for several different types of baseband and carrier-modulation methods. In this chapter, we treat digital communication over a channel that is modeled as a linear filter with a bandwidth limitation. Bandlimited channels most frequently encountered in practice are telephone channels, microwave LOS radio channels, satellite channels, and underwater acoustic channels.

In general, a linear filter channel imposes more stringent requirements on the design of modulation signals. Specifically, the transmitted signals must be designed to satisfy the bandwidth constraint imposed by the channel. The bandwidth constraint generally precludes the use of rectangular pulses at the output of the modulator. Instead, the transmitted signals must be shaped to restrict their bandwidth to that available on the channel. The design of bandlimited signals is one of the topics treated in this chapter.

We will see that a linear filter channel distorts the transmitted signal. The channel distortion results in intersymbol interference at the output of the demodulator and leads to an increase in the probability of error at the detector. Devices or methods for correcting or undoing the channel distortion, called *channel equalizers*, are then described.

### 8.1 DIGITAL TRANSMISSION THROUGH BANDLIMITED CHANNELS

A bandlimited channel such as a telephone wireline is characterized as a linear filter with impulse response  $c(t)$  and frequency response  $C(f)$ , where

$$C(f) = \int_{-\infty}^{\infty} c(t)e^{-j2\pi ft} dt \quad (8.1.1)$$

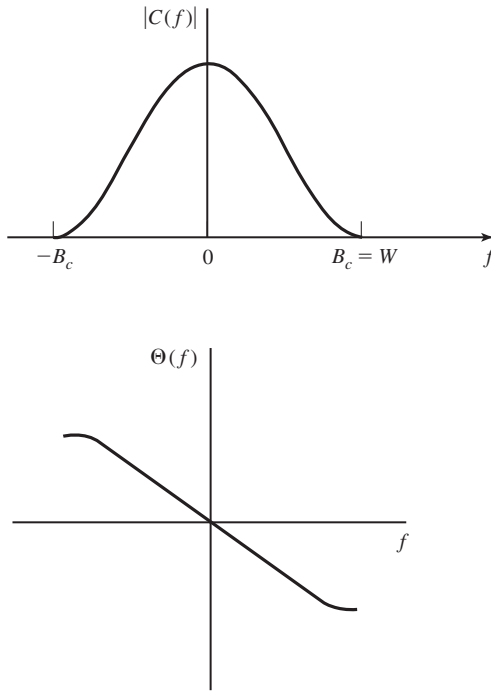


**Figure 8.1** Magnitude and phase responses of bandlimited channel.

If the channel is a baseband channel that is bandlimited to  $B_c$  Hz, then  $C(f) = 0$  for  $|f| > B_c$ . Any frequency components at the input to the channel that are higher than  $B_c$  Hz will not be passed by the channel. For this reason, we consider the design of signals for transmission through the channel that are bandlimited to  $W = B_c$  Hz, as shown in Figure 8.1. Henceforth,  $W$  will denote the bandwidth limitation of the signal and the channel.

Now, suppose that the input to a bandlimited channel is a signal waveform  $g_T(t)$ . Then, the response of the channel is the convolution of  $g_T(t)$  with  $c(t)$ ; i.e.,

$$h(t) = \int_{-\infty}^{\infty} c(\tau)g_T(t - \tau) d\tau = c(t) \star g_T(t) \quad (8.1.2)$$

or, when expressed in the frequency domain, we have

$$H(f) = C(f)G_T(f) \quad (8.1.3)$$

where  $G_T(f)$  is the spectrum (Fourier transform) of the signal  $g_T(t)$  and  $H(f)$  is the spectrum of  $h(t)$ . Thus, the channel alters or distorts the transmitted signal  $g_T(t)$ .

Let us assume that the signal at the output of the channel is corrupted by AWGN. Then, the signal at the input to the demodulator is of the form  $h(t) + n(t)$ , where  $n(t)$  denotes the AWGN. Recall from the preceding chapter that in the presence of AWGN,

a demodulator that employs a filter which is matched to the signal  $h(t)$  maximizes the SNR at its output. Therefore, let us pass the received signal  $h(t) + n(t)$  through a filter that has a frequency response

$$G_R(f) = H^*(f) e^{-j2\pi f t_0} \quad (8.1.4)$$

where  $t_0$  is some nominal time delay at which we sample the filter output.

The signal component at the output of the matched filter at the sampling instant  $t = t_0$  is

$$y_s(t_0) = \int_{-\infty}^{\infty} |H(f)|^2 df = \mathcal{E}_h, \quad (8.1.5)$$

which is the energy in the channel output  $h(t)$ . The noise component at the output of the matched filter has a zero mean and a power-spectral density

$$\mathcal{S}_n(f) = \frac{N_0}{2} |H(f)|^2 \quad (8.1.6)$$

Hence, the noise power at the output of the matched filter has a variance

$$\sigma_n^2 = \int_{-\infty}^{\infty} \mathcal{S}_n(f) df = \frac{N_0}{2} \int_{-\infty}^{\infty} |H(f)|^2 df = \frac{N_0 \mathcal{E}_h}{2} \quad (8.1.7)$$

The SNR at the output of the matched filter is

$$\left( \frac{S}{N} \right)_0 = \frac{\mathcal{E}_h^2}{N_0 \mathcal{E}_h / 2} = \frac{2\mathcal{E}_h}{N_0} \quad (8.1.8)$$

This is the result for the SNR at the output of the matched filter that was obtained in the Chapter 7 except that the received signal energy  $\mathcal{E}_h$  has replaced the transmitted signal energy  $\mathcal{E}_s$ . Compared to the previous result, the major difference in this development is that the filter impulse response is matched to the received signal  $h(t)$  instead of the transmitted signal. Note that the implementation of the matched filter at the receiver requires that  $h(t)$  or, equivalently, the channel impulse response  $c(t)$  must be known to the receiver.

### Example 8.1.1

The signal pulse  $g_T(t)$ , defined as

$$g_T(t) = \frac{1}{2} \left[ 1 + \cos \frac{2\pi}{T} \left( t - \frac{T}{2} \right) \right], \quad 0 \leq t \leq T$$

is transmitted through a baseband channel with frequency-response characteristic as shown in Figure 8.2(a). The signal pulse is illustrated in Figure 8.2(b). The channel output is corrupted by AWGN with power-spectral density  $N_0/2$ . Determine the matched filter to the received signal and the output SNR.

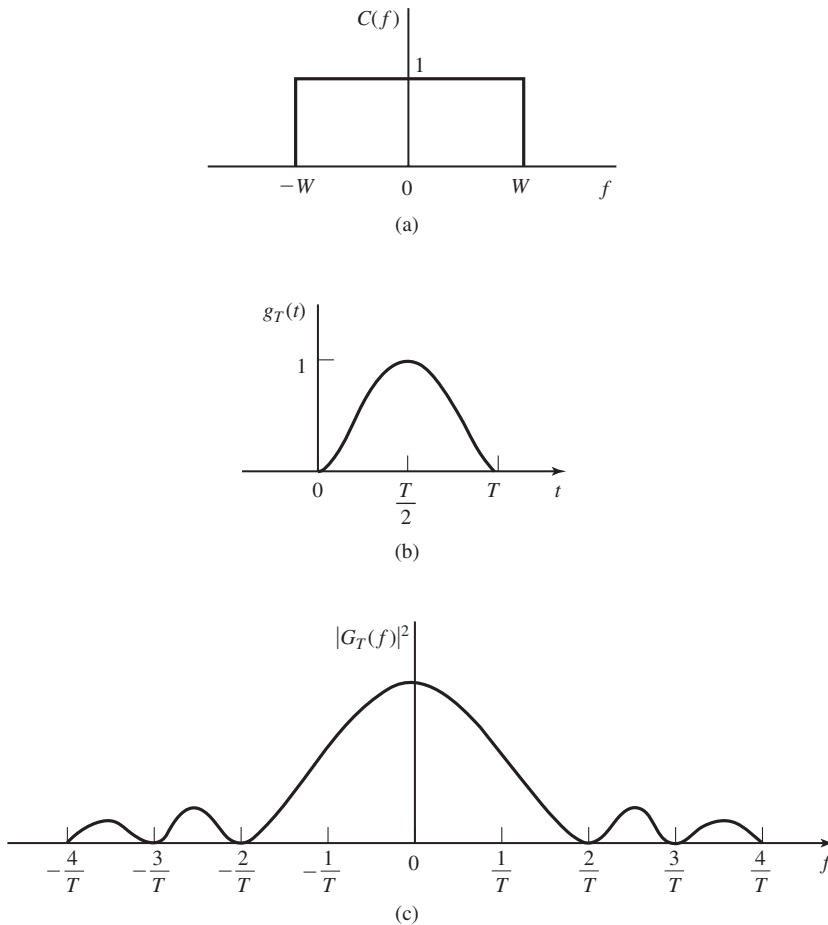


**Figure 8.2** The signal pulse in (b) is transmitted through the ideal bandlimited channel shown in (a). The spectrum of  $g_T(t)$  is shown in (c).

**Solution** This problem is most easily solved in the frequency domain. First, the spectrum of the signal pulse is

$$\begin{aligned} G_T(f) &= \frac{T}{2} \frac{\sin \pi f T}{\pi f T (1 - f^2 T^2)} e^{-j\pi f T} \\ &= \frac{T}{2} \frac{\text{sinc } \pi f T}{(1 - f^2 T^2)} e^{-j\pi f T} \end{aligned}$$

The spectrum  $|G_T(f)|^2$  is shown in Figure 8.2(c). Hence,

$$\begin{aligned} H(f) &= C(f)G_T(f) \\ &= \begin{cases} G_T(f), & |f| \leq W \\ 0, & \text{otherwise} \end{cases} \end{aligned}$$

Then, the signal component at the output of the filter matched to  $H(f)$  is

$$\begin{aligned}\mathcal{E}_h &= \int_{-W}^W |G_T(f)|^2 df \\ &= \frac{1}{(2\pi)^2} \int_{-W}^W \frac{(\sin \pi f T)^2}{f^2(1-f^2 T^2)^2} df \\ &= \frac{T}{(2\pi)^2} \int_{-WT}^{WT} \frac{\sin^2 \pi \alpha}{\alpha^2(1-\alpha^2)^2} d\alpha\end{aligned}$$

The variance of the noise component is

$$\sigma_n^2 = \frac{N_0}{2} \int_{-W}^W |G_T(f)|^2 df = \frac{N_0 \mathcal{E}_h}{2}$$

Hence, the output SNR is

$$\left(\frac{S}{N}\right)_0 = \frac{2\mathcal{E}_h}{N_0}$$

In this example, we observe that the signal at the input to the channel is not bandlimited. Hence, only a part of the transmitted signal energy is received. The amount of signal energy at the output of the matched filter depends on the value of the channel bandwidth  $W$  when the signal pulse duration is fixed (see Problem 8.1). The maximum value of  $\mathcal{E}_h$ , obtained as  $W \rightarrow \infty$ , is

$$\max \mathcal{E}_h = \int_{-\infty}^{\infty} |G_T(f)|^2 df = \int_0^T g_T^2(t) dt$$

In the above development, we considered the transmission and reception of only a single signal waveform  $g_T(t)$  through a bandlimited channel with impulse response  $c(t)$ . We observed that the performance of the system is determined by  $\mathcal{E}_h$ , the energy in the received signal  $h(t)$ . To maximize the received SNR, we have to make sure that the power-spectral density of the transmitted signal matches the frequency band of the channel. To this end we must study the power-spectral density of the input signal. This will be done in Section 8.2. The impact of the channel bandwidth limitation is felt when we consider the transmission of a sequence of signal waveforms. This problem is treated in the following section.

### 8.1.1 Digital PAM Transmission through Bandlimited Baseband Channels

Let us consider the baseband PAM communication system illustrated by the functional block diagram in Figure 8.3. The system consists of a transmitting filter having an impulse response  $g_T(t)$ , the linear filter channel with AWGN, a receiving filter with impulse response  $g_R(t)$ , a sampler that periodically samples the output of the receiving filter, and a symbol detector. The sampler requires the extraction of a timing signal from the received signal as described in Section 7.8. This timing signal serves as a clock that specifies the appropriate time instants for sampling the output of the receiving filter.

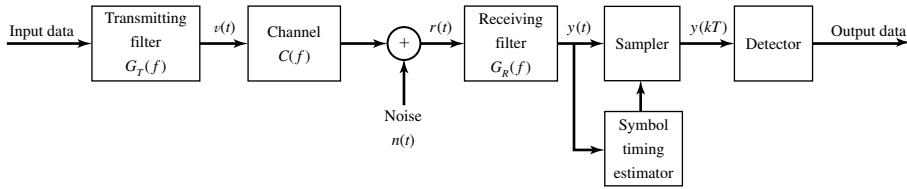


**Figure 8.3** Block diagram of digital PAM system.

First we consider digital communications by means of  $M$ -ary PAM. Hence, the input binary data sequence is subdivided into  $k$ -bit symbols and each symbol is mapped into a corresponding amplitude level that amplitude modulates the output of the transmitting filter. The baseband signal at the output of the transmitting filter (the input to the channel) may be expressed as

$$v(t) = \sum_{n=-\infty}^{\infty} a_n g_T(t - nT) \quad (8.1.9)$$

where  $T = k/R_b$  is the symbol interval ( $1/T = R_b/k$  is the symbol rate),  $R_b$  is the bit rate, and  $\{a_n\}$  is a sequence of amplitude levels corresponding to the sequence of  $k$ -bit blocks of information bits.

The channel output, which is the received signal at the demodulator, may be expressed as

$$r(t) = \sum_{n=-\infty}^{\infty} a_n h(t - nT) + n(t) \quad (8.1.10)$$

where  $h(t)$  is the impulse response of the cascade of the transmitting filter and the channel; i.e.,  $h(t) = c(t) \star g_T(t)$ ,  $c(t)$  is the impulse response of the channel, and  $n(t)$  represents the AWGN.

The received signal is passed through a linear receiving filter with impulse response  $g_R(t)$  and frequency response  $G_R(f)$ . If  $g_R(t)$  is matched to  $h(t)$ , then its output SNR is a maximum at the proper sampling instant. The output of the receiving filter may be expressed as

$$y(t) = \sum_{n=-\infty}^{\infty} a_n x(t - nT) + v(t) \quad (8.1.11)$$

where  $x(t) = h(t) \star g_R(t) = g_T(t) \star c(t) \star g_R(t)$  and  $v(t) = n(t) \star g_R(t)$  denotes the additive noise at the output of the receiving filter.

To recover the information symbols  $\{a_n\}$ , the output of the receiving filter is sampled periodically, every  $T$  seconds. Thus, the sampler produces

$$y(mT) = \sum_{n=-\infty}^{\infty} a_n x(mT - nT) + v(mT) \quad (8.1.12)$$

or, equivalently,

$$\begin{aligned} y_m &= \sum_{n=-\infty}^{\infty} a_n x_{m-n} + v_m \\ &= x_0 a_m + \sum_{n \neq m} a_n x_{m-n} + v_m \end{aligned} \quad (8.1.13)$$

where  $x_m = x(mT)$ ,  $v_m = v(mT)$ , and  $m = 0, \pm 1, \pm 2, \dots$ . A timing signal extracted from the received signal as described in Section 7.8 is used as a clock for sampling the received signal.

The first term on the right-hand side (RHS) of Equation (8.1.13) is the desired symbol  $a_m$ , scaled by the gain parameter  $x_0$ . When the receiving filter is matched to the received signal  $h(t)$ , the scale factor is

$$\begin{aligned} x_0 &= \int_{-\infty}^{\infty} h^2(t) dt = \int_{-\infty}^{\infty} |H(f)|^2 df \\ &= \int_{-W}^W |G_T(f)|^2 |C(f)|^2 df \equiv \mathcal{E}_h \end{aligned} \quad (8.1.14)$$

as indicated by the development of Equations (8.1.4) and (8.1.5). The second term on the RHS of Equation (8.1.13) represents the effect of the other symbols at the sampling instant  $t = mT$ , called the *intersymbol interference* (ISI). In general, ISI causes a degradation in the performance of the digital communication system. Finally, the third term,  $v_m$ , that represents the additive noise, is a zero-mean Gaussian random variable with variance  $\sigma_v^2 = N_0 \mathcal{E}_h / 2$ , previously given by Equation (8.1.7).

By appropriate design of the transmitting and receiving filters, it is possible to satisfy the condition  $x_n = 0$  for  $n \neq 0$ , so that the ISI term vanishes. In this case, the only term that can cause errors in the received digital sequence is the additive noise. The design of transmitting and receiving filters is considered in Section 8.3.

### 8.1.2 Digital Transmission through Bandlimited Bandpass Channels

The development given in Section 8.1.1 for baseband PAM is easily extended to carrier modulation via PAM, QAM, and PSK. In a carrier-amplitude modulated signal, the baseband PAM given by  $v(t)$  in Equation (8.1.9) modulates the carrier, so that the transmitted signal  $u(t)$  is simply

$$u(t) = v(t) \cos 2\pi f_c t \quad (8.1.15)$$

Thus, the baseband signal  $v(t)$  is shifted in frequency by  $f_c$ .

A QAM signal is a bandpass signal which, in its simplest form, may be viewed as two amplitude-modulated carrier signals in phase quadrature. That is, the QAM signal may be expressed as

$$u(t) = v_c(t) \cos 2\pi f_c t + v_s(t) \sin 2\pi f_c t \quad (8.1.16)$$

where

$$\begin{aligned} v_c(t) &= \sum_{n=-\infty}^{\infty} a_{nc} g_T(t - nT) \\ v_s(t) &= \sum_{n=-\infty}^{\infty} a_{ns} g_T(t - nT) \end{aligned} \quad (8.1.17)$$

and  $\{a_{nc}\}$  and  $\{a_{ns}\}$  are the two sequences of amplitudes carried on the two quadrature carriers. A more compact mathematical representation of the baseband signal is the equivalent complex-valued baseband signal

$$\begin{aligned} v(t) &= v_c(t) - jv_s(t) \\ &= \sum_{n=-\infty}^{\infty} (a_{nc} - ja_{ns}) g_T(t - nT) \\ &= \sum_{n=-\infty}^{\infty} a_n g_T(t - nT) \end{aligned} \quad (8.1.18)$$

where the sequence  $\{a_n = a_{nc} - ja_{ns}\}$  is now a complex-valued sequence representing the signal points from the QAM signal constellation. The corresponding bandpass QAM signal  $u(t)$  may also be represented as

$$u(t) = \text{Re}[v(t)e^{j2\pi f_c t}] \quad (8.1.19)$$

In a similar manner, we can represent a digital carrier-phase modulated signal as in Equation (8.1.19), where the equivalent baseband signal is

$$v(t) = \sum_{n=-\infty}^{\infty} a_n g_T(t - nT) \quad (8.1.20)$$

and the sequence  $\{a_n\}$  takes the value from the set of possible (phase) values  $\{e^{-j2\pi m/M}, m = 0, 1, \dots, M-1\}$ . Thus, all three carrier-modulated signals, PAM, QAM, and PSK can be represented as in Equations (8.1.19) and (8.1.20), where the only difference is in the values taken by the transmitted sequence  $\{a_n\}$ .

The signal  $v(t)$  given by Equation (8.1.20) is called the *equivalent lowpass signal*. In the case of QAM and PSK, this equivalent lowpass signal is a baseband signal which is complex-valued because the information-bearing sequence  $\{a_n\}$  is complex-valued. In the case of PAM,  $v(t)$  is a real-valued baseband signal.

When transmitted through the bandpass channel, the received bandpass signal may be represented as

$$w(t) = \text{Re}[r(t)e^{j2\pi f_c t}] \quad (8.1.21)$$

where  $r(t)$  is the equivalent lowpass (baseband) signal, which may be expressed as

$$r(t) = \sum_{n=-\infty}^{\infty} a_n h(t - nT) + n(t) \quad (8.1.22)$$



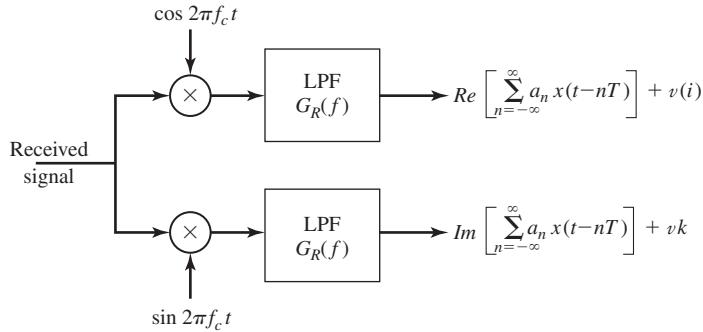


**Figure 8.4** Conversion of the bandpass received signal to baseband.

and where, as in the case of baseband transmission,  $h(t)$  is the impulse response of the cascade of the transmitting filter and the channel; i.e.,  $h(t) = c(t) \star g_T(t)$ , where  $c(t)$  is the impulse response of the equivalent lowpass channel and  $n(t)$  represents the additive Gaussian noise expressed as an equivalent lowpass (baseband) noise.

The received bandpass signal can be converted to a baseband signal by multiplying  $w(t)$  with the quadrature carrier signals  $\cos 2\pi f_c t$  and  $\sin 2\pi f_c t$  and eliminating the double frequency terms by passing the two quadrature components through separate lowpass filters, as shown in Figure 8.4. Each one of the lowpass filters is assumed to have an impulse response  $g_R(t)$ . Hence, we can represent the two quadrature components at the outputs of these lowpass filters as an equivalent complex-valued signal of the form

$$y(t) = \sum_{m=-\infty}^{\infty} a_m x(t - nT) + v(t) \quad (8.1.23)$$

which is identical to the form given by Equation (8.1.11) for the real baseband signal. Consequently, the signal design problem for bandpass signals is basically the same as that described in Section 8.1.1 for baseband signals.

In Section 8.3, we consider the design of bandlimited transmitting and receiving filters that either eliminate ISI or control ISI. However, first we will determine the power-spectral density of the transmitted digital signal. Thus, we will establish the relationship between the spectral characteristics of the transmitted signal and the channel bandwidth requirements.

## 8.2 THE POWER SPECTRUM OF DIGITALLY MODULATED SIGNALS

First, we will derive the power spectrum of a baseband signal and, then, we consider the power spectrum of the bandpass signal.

### 8.2.1 The Power Spectrum of the Baseband Signal

As shown above, the equivalent baseband transmitted signal for a digital PAM, PSK, or QAM signal is represented in the general form as

$$v(t) = \sum_{n=-\infty}^{\infty} a_n g_T(t - nT) \quad (8.2.1)$$

where  $\{a_n\}$  is the sequence of values selected from either a PAM, QAM, or PSK signal constellation corresponding to the information symbols from the source, and  $g_T(t)$  is the impulse response of the transmitting filter. Since the information sequence  $\{a_n\}$  is random,  $v(t)$  is a sample function of a random process  $V(t)$ . In this section we evaluate the power-density spectrum of  $V(t)$ . Our approach is to derive the autocorrelation function of  $V(t)$  and then to determine its Fourier transform.

First, the mean value of  $v(t)$  is

$$\begin{aligned} E[V(t)] &= \sum_{n=-\infty}^{\infty} E(a_n) g_T(t - nT) \\ &= m_a \sum_{n=-\infty}^{\infty} g_T(t - nT) \end{aligned} \quad (8.2.2)$$

where  $m_a$  is the mean value of the random sequence  $\{a_n\}$ . Note that although  $m_a$  is a constant, the term  $\sum_n g_T(t - nT)$  is a periodic function with period  $T$ . Hence, the mean value of  $V(t)$  is periodic with period  $T$ .

The autocorrelation function of  $V(t)$  is

$$R_V(t + \tau, t) = E[V^*(t) V(t + \tau)] = \sum_{n=-\infty}^{\infty} \sum_{m=-\infty}^{\infty} E(a_n^* a_m) g_T(t - nT) g_T(t + \tau - mT) \quad (8.2.3)$$

In general, we assume that the information sequence  $\{a_n\}$  is wide-sense stationary with autocorrelation sequence

$$R_a(n) = E(a_m^* a_{n+m}) \quad (8.2.4)$$

Hence, Equation (8.2.3) may be expressed as

$$\begin{aligned} R_V(t + \tau, t) &= \sum_{n=-\infty}^{\infty} \sum_{m=-\infty}^{\infty} R_a(m - n) g_T(t - nT) g_T(t + \tau - mT) \\ &= \sum_{m=-\infty}^{\infty} R_a(m) \sum_{n=-\infty}^{\infty} g_T(t - nT) g_T(t + \tau - nT - mT) \end{aligned} \quad (8.2.5)$$

We observe that the second summation in Equation (8.2.5), namely

$$\sum_{n=-\infty}^{\infty} g_T(t - nT) g_T(t + \tau - nT - mT) \quad (8.2.6)$$

is periodic with period  $T$ . Consequently, the autocorrelation function  $R_V(t + \tau, t)$  is periodic in the variable  $t$ ; i.e.,

$$R_V(t + T + \tau, t + T) = R_V(t + \tau, t) \quad (8.2.7)$$

Therefore, the random process  $V(t)$  has a periodic mean and a periodic autocorrelation. Such a random process is *cyclostationary* (see Definition 4.2.7).

The power-spectral density of a cyclostationary process can be determined by first averaging the autocorrelation function  $R_V(t + \tau, t)$  over a single period  $T$  and then computing the Fourier transform of the average autocorrelation function (see Corollary to Theorem 4.3.1). Thus, we have

$$\begin{aligned} \bar{R}_V(\tau) &= \frac{1}{T} \int_{-T/2}^{T/2} R_V(t + \tau, t) dt \\ &= \sum_{m=-\infty}^{\infty} R_a(m) \sum_{n=-\infty}^{\infty} \frac{1}{T} \int_{-T/2}^{T/2} g_T(t - nT) g_T(t + \tau - nT - mT) dt \\ &= \sum_{m=-\infty}^{\infty} R_a(m) \sum_{n=-\infty}^{\infty} \frac{1}{T} \int_{nT-T/2}^{nT+T/2} g_T(t) g_T(t + \tau - mT) dt \\ &= \frac{1}{T} \sum_{m=-\infty}^{\infty} R_a(m) \int_{-\infty}^{\infty} g_T(t) g_T(t + \tau - mT) dt \end{aligned} \quad (8.2.8)$$

We interpret the integral in Equation (8.2.8) as the time-autocorrelation function of  $g_T(t)$  and define it as [see Equation (2.3.1)]

$$R_g(\tau) = \int_{-\infty}^{\infty} g_T(t) g_T(t + \tau) dt \quad (8.2.9)$$

With this definition, the average autocorrelation function of  $V(t)$  becomes

$$\bar{R}_V(\tau) = \frac{1}{T} \sum_{m=-\infty}^{\infty} R_a(m) R_g(\tau - mT) \quad (8.2.10)$$

We observe that the expression for  $\bar{R}_V(\tau)$  in Equation (8.2.10) has the form of a convolution sum. Hence the Fourier transform of Equation (8.2.10) becomes

$$\begin{aligned} S_V(f) &= \int_{-\infty}^{\infty} \bar{R}_V(\tau) e^{-j2\pi f\tau} d\tau \\ &= \frac{1}{T} \sum_{m=-\infty}^{\infty} R_a(m) \int_{-\infty}^{\infty} R_g(\tau - mT) e^{-j2\pi f\tau} d\tau \\ &= \frac{1}{T} S_a(f) |G_T(f)|^2 \end{aligned} \quad (8.2.11)$$

where  $\mathcal{S}_a(f)$  is the power spectrum of the information sequence  $\{a_n\}$ , defined as

$$\mathcal{S}_a(f) = \sum_{m=-\infty}^{\infty} R_a(m) e^{-j2\pi f m T} \quad (8.2.12)$$

and  $G_T(f)$  is the spectrum of the transmitting filter.  $|G_T(f)|^2$  is the Fourier transform of  $R_g(\tau)$ .

The result in Equation (8.2.11) illustrates the dependence of the power-spectral density  $\mathcal{S}_V(f)$  of the transmitted signal on (1) the spectral characteristics  $G_T(f)$  of the transmitting filter and (2) the spectral characteristics  $\mathcal{S}_a(f)$  of the information sequence  $\{a_n\}$ . Both  $G_T(f)$  and  $\mathcal{S}_a(f)$  can be designed to control the shape and form of the power spectral density of the transmitted signal.

Whereas the dependence of  $\mathcal{S}_V(f)$  on  $G_T(f)$  is easily understood, the effect of the autocorrelation properties of the information sequence  $\{a_n\}$  is more subtle. First, we observe that for an arbitrary autocorrelation  $R_a(m)$ , the corresponding power-spectral density  $\mathcal{S}_a(f)$  is periodic in frequency with period  $1/T$ . In fact, we note that  $\mathcal{S}_a(f)$ , given by Equation (8.2.12), has the form of an exponential Fourier series with  $\{R_a(m)\}$  as the Fourier coefficients. Consequently, the autocorrelation sequence  $\{R_a(m)\}$  is simply

$$R_a(m) = T \int_{-1/2T}^{1/2T} \mathcal{S}_a(f) e^{j2\pi f m T} df \quad (8.2.13)$$

Second, let us consider the case in which the information symbols in the sequence  $\{a_n\}$  are mutually uncorrelated. Then,

$$R_a(m) = \begin{cases} \sigma_a^2 + m^2, & m = 0 \\ m^2, & m \neq 0 \end{cases} \quad (8.2.14)$$

where  $\sigma_a^2 = E(a_n^2) - m_a^2$  is the variance of an information symbol. By substituting for  $R_a(m)$  into (8.2.12), we obtain the power-spectral density

$$\mathcal{S}_a(f) = \sigma_a^2 + m_a^2 \sum_{m=-\infty}^{\infty} e^{-j2\pi f m T} \quad (8.2.15)$$

The term involving the summation on the RHS of Equation (8.2.15) is periodic with period  $1/T$ . It may be viewed as the exponential Fourier series of a periodic train of impulses where each impulse has an area  $1/T$  (see Table 2.1). Therefore, Equation (8.2.15) can be expressed as

$$\mathcal{S}_a(f) = \sigma_a^2 + \frac{m_a^2}{T} \sum_{m=-\infty}^{\infty} \delta\left(f - \frac{m}{T}\right) \quad (8.2.16)$$

Substitution of this expression into  $\mathcal{S}_V(f)$  given by Equation (8.2.11) yields the desired result for the power-spectral density of the transmitted signal  $V(t)$  when the sequence

of information symbols is uncorrelated; i.e.,

$$S_V(f) = \frac{\sigma_a^2}{T} |G_T(f)|^2 + \frac{m_a^2}{T^2} \sum_{m=-\infty}^{\infty} \left| G_T \left( \frac{m}{T} \right) \right|^2 \delta \left( f - \frac{m}{T} \right) \quad (8.2.17)$$

The expression for the power-spectral density of the transmitted signal given by Equation (8.2.17) is purposely separated into two terms to emphasize the two different types of spectral components. The first term  $\sigma_a^2 |G_T(f)|^2 / T$  is the continuous spectrum and its shape depends of  $G_T(f)$ . The second term in Equation (8.2.17) consists of discrete frequency components spaced  $1/T$  apart in frequency. Each spectral line has a power that is proportional to  $|G_T(f)|^2$  evaluated at  $f = m/T$ . We note that the discrete frequency components can be eliminated by selecting the information symbol sequence  $\{a_n\}$  to have zero mean. This condition is usually imposed in digital-modulation methods because discrete spectral lines are considered to be undesirable. To be specific, the mean  $m_a$  in digital PAM, PSK, or QAM signals is easily forced to be zero by selecting the signal constellation points to be symmetrically positioned in the complex plane relative to the origin. Under the condition that  $m_a = 0$ , we have

$$S_V(f) = \frac{\sigma_a^2}{T} |G_T(f)|^2 \quad (8.2.18)$$

Thus, the system designer can control the spectral characteristics of the transmitted digital PAM signal. The following example illustrates the spectral shaping resulting from  $g_T(t)$ .

### Example 8.2.1

Determine the power-spectral density in Equation (8.2.17), when  $g_T(t)$  is the rectangular pulse shown in Figure 8.5(a).

**Solution** The Fourier transform of  $g_T(t)$  is

$$G_T(f) = AT \frac{\sin \pi f T}{\pi f T} e^{-j\pi f T}$$

Hence,

$$\begin{aligned} |G_T(f)|^2 &= (AT)^2 \left( \frac{\sin \pi f T}{\pi f T} \right)^2 \\ &= (AT)^2 \text{sinc}^2(fT) \end{aligned}$$

This spectrum is illustrated in Figure 8.5(b). We note that it contains nulls at multiples of  $1/T$  in frequency and that it decays inversely as the square of the frequency variable. As a consequence of the spectral nulls in  $G_T(f)$ , all but one of the discrete spectral components in Equation (8.2.17) vanish. Thus, upon substitution for  $|G_T(f)|^2$  into Equation (8.12.17), we obtain the result

$$\begin{aligned} S_V(f) &= \sigma_a^2 A^2 T \left( \frac{\sin \pi f T}{\pi f T} \right)^2 + A^2 m_a^2 \delta(f) \\ &= \sigma_a^2 A^2 T \text{sinc}^2(fT) + A^2 m_a^2 \delta(f) \end{aligned}$$

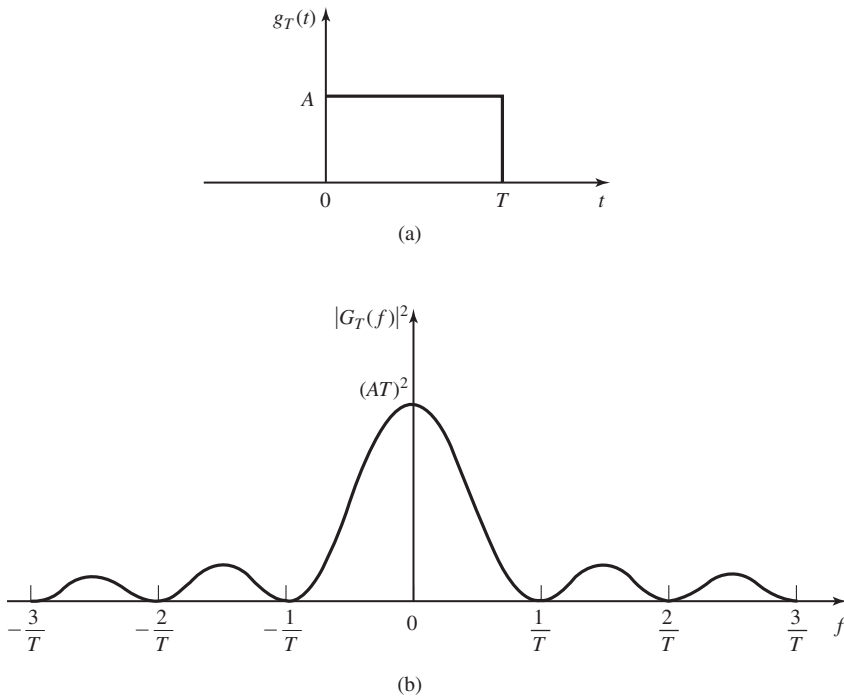


**Figure 8.5** A rectangular pulse  $g_T(t)$  and its energy density spectrum  $|G_T(f)|^2$ .

Example 8.2.2 illustrates the spectral shaping that can be achieved by operations performed on the input information sequence.

**Example 8.2.2**

Consider a binary sequence  $\{b_n\}$ , from which we form the symbols

$$a_n = b_n + b_{n-1}$$

The  $\{b_n\}$  are assumed to be uncorrelated binary valued ( $\pm 1$ ) random variables, each having a zero mean and a unit variance. Determine the power-spectral density of the transmitted signal.

**Solution** The autocorrelation function of the sequence  $\{a_n\}$  is

$$\begin{aligned} R_a(m) &= E[a_n a_{n+m}] \\ &= E[(b_n + b_{n-1})(b_{n+m} + b_{n+m-1})] \\ &= \begin{cases} 2 & m = 0 \\ 1 & m = \pm 1 \\ 0, & \text{otherwise} \end{cases} \end{aligned}$$

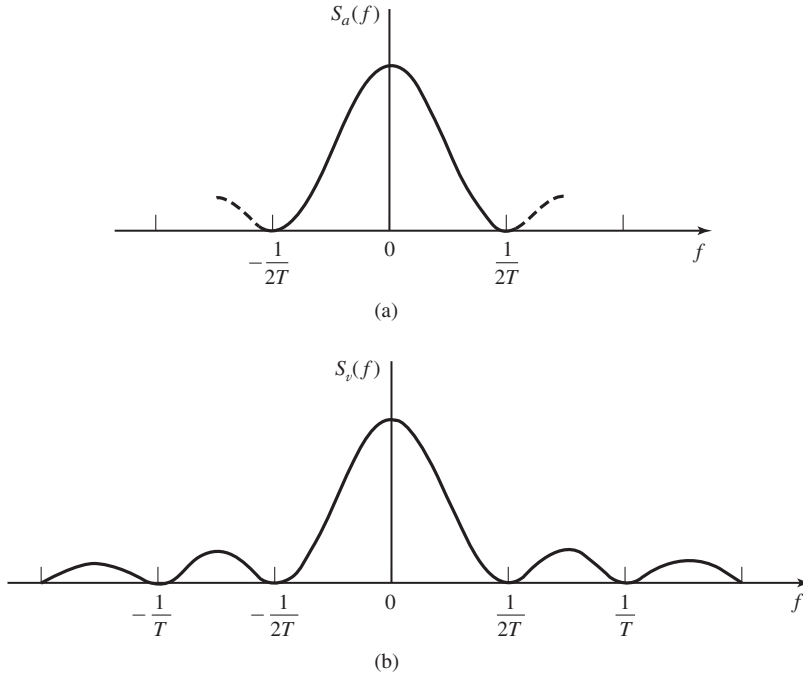


**Figure 8.6** Power-density spectra for (a) information sequence and (b) PAM modulated signal.

Hence, the power-spectral density of the input sequence is

$$\begin{aligned} S_a(f) &= 2(1 + \cos 2\pi fT) \\ &= 4 \cos^2 \pi fT \end{aligned}$$

and the corresponding power spectrum for the modulated signal is, from Equation (8.2.17),

$$S_V(f) = \frac{4}{T} |G_T(f)|^2 \cos^2 \pi fT$$

Figure 8.6 illustrates the power-density spectrum  $S_a(f)$  of the input sequence, and the corresponding  $S_V(f)$  when  $G_T(f)$  is the spectrum of the rectangular pulse.

As demonstrated in the example, the transmitted signal spectrum can be shaped by having a correlated sequence  $\{a_n\}$  as the input to the modulator.

### 8.2.2 The Power Spectrum of a Carrier-Modulated Signal

In Section 8.2.1, we showed that the power spectrum of the equivalent baseband signal  $v(t)$  given by Equation (8.2.1) for PAM, QAM, and PSK is

$$S_V(f) = \frac{1}{2} S_a(f) |G_T(f)|^2 \quad (8.2.19)$$

where  $\mathcal{S}_a(f)$  is the power spectrum of the information sequence  $\{a_n\}$ , defined as

$$\mathcal{S}_a(f) = \sum_{m=-\infty}^{\infty} R_a(m) e^{-j2\pi f m T} \quad (8.2.20)$$

and  $R_a(m)$  is the autocorrelation of the information sequence  $\{a_n\}$ ; i.e.

$$R_a(m) = E[a_n^* a_{n+m}] \quad (8.2.21)$$

The relationship between the power spectrum of the baseband signal to the power spectrum of the bandpass signal is relatively simple. Let us consider the bandpass PAM signal as an example. The autocorrelation function of the bandpass signal

$$u(t) = v(t) \cos 2\pi f_c t$$

is

$$\begin{aligned} R_U(t + \tau, t) &= E[U(t)U(t + \tau)] \\ &= E[V(t)V(t + \tau)] \cos 2\pi f_c t \cos 2\pi f_c (t + \tau) \\ &= R_V(t + \tau, t) \cos 2\pi f_c t \cos 2\pi f_c (t + \tau) \end{aligned}$$

By expressing the product of the two cosine functions in terms of the cosine of the difference plus the sum of the two angles, we obtain

$$R_U(t + \tau, t) = \frac{1}{2} R_V(t + \tau, t) [\cos 2\pi f_c \tau + \cos 2\pi f_c (2t + \tau)]$$

Then, the average of  $R_U(t + \tau, t)$  over a single period  $T$  yields

$$\bar{R}_U(\tau) = \frac{1}{2} \bar{R}_V(\tau) \cos 2\pi f_c \tau \quad (8.2.22)$$

where the second term involving the double frequency term averages to zero for each period of  $\cos 4\pi f_c t$ .

The Fourier transform of  $\bar{R}_U(t)$  yields the power spectrum of the bandpass signal as

$$\mathcal{S}_U(f) = \frac{1}{4} [\mathcal{S}_V(f - f_c) + \mathcal{S}_V(f + f_c)] \quad (8.2.23)$$

Although the derivation that resulted in Equation (8.2.23) was carried out for a bandpass PAM signal, the same expression applies to QAM and PSK. The three bandpass signals differ only in the autocorrelation  $R_a(m)$  of the sequence  $\{a_n\}$  and, hence, in the power spectrum  $\mathcal{S}_a(f)$  of  $\{a_n\}$ .



### 8.3 SIGNAL DESIGN FOR BANDLIMITED CHANNELS

Recall from Section 8.1.1 that the output of the transmitting filter in a digital PAM or PSK or QAM communication system may be expressed as

$$v(t) = \sum_{n=-\infty}^{\infty} a_n g_T(t - nT) \quad (8.3.1)$$

and the output of the channel, which is the received signal at the demodulator, may be expressed as

$$r(t) = \sum_{n=-\infty}^{\infty} a_n h(t - nT) + n(t) \quad (8.3.2)$$

where  $h(t) = c(t) \star g_T(t)$ ,  $c(t)$  is the impulse response of the channel,  $g_T(t)$  is the impulse response of the transmitting filter, and  $n(t)$  is a sample function of an additive, white Gaussian noise process.

In this section, we consider the problem of designing a bandlimited transmitting filter. The design will be done first under the condition that there is no channel distortion. Later, we consider the problem of filter design when the channel distorts the transmitted signal. Since  $H(f) = C(f)G_T(f)$ , the condition for distortion-free transmission is that the frequency response characteristic  $C(f)$  of the channel have a constant magnitude and a linear phase over the bandwidth of the transmitted signal; i.e.,

$$C(f) = \begin{cases} C_0 e^{-j2\pi f t_0}, & |f| \leq W \\ 0, & |f| > W \end{cases} \quad (8.3.3)$$

where  $W$  is the available channel bandwidth,  $t_0$  represents an arbitrary finite delay, which we set to zero for convenience, and  $C_0$  is a constant gain factor which we set to unity for convenience. Thus, under the condition that the channel is distortion-free,  $H(f) = G_T(f)$  for  $|f| \leq W$  and zero for  $|f| > W$ . Consequently, the matched filter has a frequency response  $H^*(f) = G_T^*(f)$  and its output at the periodic sampling times  $t = mT$  has the form

$$y(mT) = x(0)a_m + \sum_{n \neq m} a_n x(mT - nT) + v(mT) \quad (8.3.4)$$

or, more simply,

$$y_m = x_0 a_m + \sum_{n \neq m} a_n x_{m-n} + v_m \quad (8.3.5)$$

where  $x(t) = g_T(t) \star g_R(t)$  and  $v(t)$  is the output response of the matched filter to the input AWGN process  $n(t)$ .

The middle term on the RHS of Equation (8.3.5) represents the ISI. The amount of ISI and noise that is present in the received signal can be viewed on an oscilloscope. Specifically, we may display the received signal on the vertical input with the horizontal sweep rate set at  $1/T$ . The resulting oscilloscope display is called an *eye pattern* because

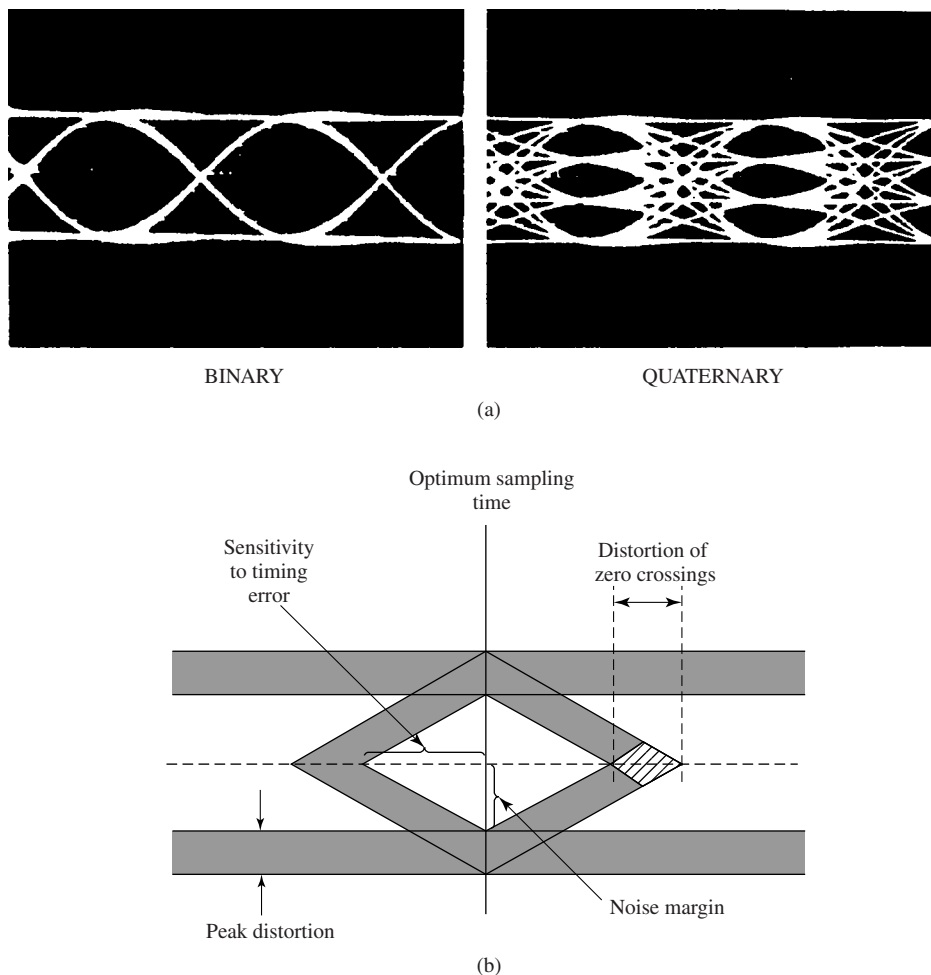


**Figure 8.7** Eye patterns. (a) Examples of eye patterns for binary and quaternary amplitude-shift keying (or PAM) and (b) Effect of ISI on eye opening.

of its resemblance to the human eye. Examples of two eye patterns, one for binary PAM and the other for quaternary ( $M = 4$ ) PAM, are illustrated in Figure 8.7(a).

The effect of ISI is to cause the eye to close, thereby reducing the margin for additive noise to cause errors. Figure 8.7(b) illustrates the effect of ISI in reducing the opening of the eye. Note that ISI distorts the position of the zero crossings and causes a reduction in the eye opening. As a consequence, the system is more sensitive to a synchronization error and exhibits a smaller margin against additive noise.

Below we consider the problem of signal design under two conditions, namely, (1) that there is no ISI at the sampling instants and (2) that a controlled amount of ISI is allowed.

### 8.3.1 Design of Bandlimited Signals for Zero ISI—The Nyquist Criterion

As indicated above, in a general digital communication system that transmits through a bandlimited channel, the Fourier transform of the signal at the output of the receiving filter is given by  $X(f) = G_T(f)C(f)G_R(f)$  where  $G_T(f)$  and  $G_R(f)$  denote the transmitter and receiver filters frequency responses and  $C(f)$  denotes the frequency response of the channel. We have also seen that the output of the receiving filter, sampled at  $t = mT$  is given by

$$y_m = x(0)a_m + \sum_{\substack{n=-\infty \\ n \neq m}}^{\infty} x(mT - nT)a_n + v(mT) \quad (8.3.6)$$

To remove the effect of ISI, it is necessary and sufficient that  $x(mT - nT) = 0$  for  $n \neq m$  and  $x(0) \neq 0$ , where without loss of generality we can assume  $x(0) = 1$ .<sup>†</sup> This means that the overall communication system has to be designed such that

$$x(nT) = \begin{cases} 1, & n = 0 \\ 0, & n \neq 0 \end{cases} \quad (8.3.7)$$

In this section, we derive the necessary and sufficient condition for  $X(f)$  in order for  $x(t)$  to satisfy the above relation. This condition is known as the *Nyquist pulse-shaping criterion* or *Nyquist condition for zero ISI* and is stated in the following theorem.

**Theorem 8.3.1 [Nyquist].** A necessary and sufficient condition for  $x(t)$  to satisfy

$$x(nT) = \begin{cases} 1, & n = 0 \\ 0, & n \neq 0 \end{cases} \quad (8.3.8)$$

is that its Fourier transform  $X(f)$  satisfy

$$\sum_{m=-\infty}^{\infty} X\left(f + \frac{m}{T}\right) = T \quad (8.3.9)$$

*Proof.* In general,  $x(t)$  is the inverse Fourier transform of  $X(f)$ . Hence,

$$x(t) = \int_{-\infty}^{\infty} X(f)e^{j2\pi ft} df \quad (8.3.10)$$

At the sampling instants  $t = nT$ , this relation becomes

$$x(nT) = \int_{-\infty}^{\infty} X(f)e^{j2\pi fnT} df \quad (8.3.11)$$

Let us break up the integral in Equation (8.3.11) into integrals covering the finite range

<sup>†</sup>The choice of  $x(0)$  is equivalent to the choice of a constant gain factor in the receiving filter. This constant gain factor has no effect on the overall system performance since it scales both the signal and the noise.

of  $1/T$ . Thus, we obtain

$$\begin{aligned}
 x(nT) &= \sum_{m=-\infty}^{\infty} \int_{(2m-1)/2T}^{(2m+1)/2T} X(f) e^{j2\pi f n T} df \\
 &= \sum_{m=-\infty}^{\infty} \int_{-1/2T}^{1/2T} X\left(f + \frac{m}{T}\right) e^{j2\pi f n T} dt \\
 &= \int_{-1/2T}^{1/2T} \left[ \sum_{m=-\infty}^{\infty} X\left(f + \frac{m}{T}\right) \right] e^{j2\pi f n T} dt \\
 &= \int_{-1/2T}^{1/2T} Z(f) e^{j2\pi f n T} dt \tag{8.3.12}
 \end{aligned}$$

where we have defined  $Z(f)$  by

$$Z(f) = \sum_{m=-\infty}^{\infty} X\left(f + \frac{m}{T}\right) \tag{8.3.13}$$

Obviously,  $Z(f)$  is a periodic function with period  $\frac{1}{T}$ , and therefore it can be expanded in terms of its Fourier series coefficients  $\{z_n\}$  as

$$Z(f) = \sum_{m=-\infty}^{\infty} z_n e^{j2\pi n f T} \tag{8.3.14}$$

where

$$z_n = T \int_{-\frac{1}{2T}}^{\frac{1}{2T}} Z(f) e^{-j2\pi n f T} df \tag{8.3.15}$$

Comparing Equations (8.3.15) and (8.3.12) we obtain

$$z_n = T x(-nT) \tag{8.3.16}$$

Therefore, the necessary and sufficient conditions for Equation (8.3.8) to be satisfied is that

$$z_n = \begin{cases} T & n = 0 \\ 0, & n \neq 0 \end{cases} \tag{8.3.17}$$

which, when substituted into Equation (8.3.14), yields

$$Z(f) = T \tag{8.3.18}$$

or, equivalently,

$$\sum_{m=-\infty}^{\infty} X\left(f + \frac{m}{T}\right) = T \tag{8.3.19}$$

This concludes the proof of the theorem. ■

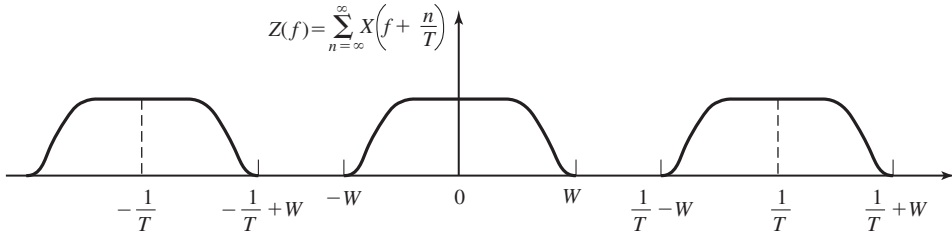


**Figure 8.8** Plot of  $Z(f)$  for the case  $T < \frac{1}{2W}$ .

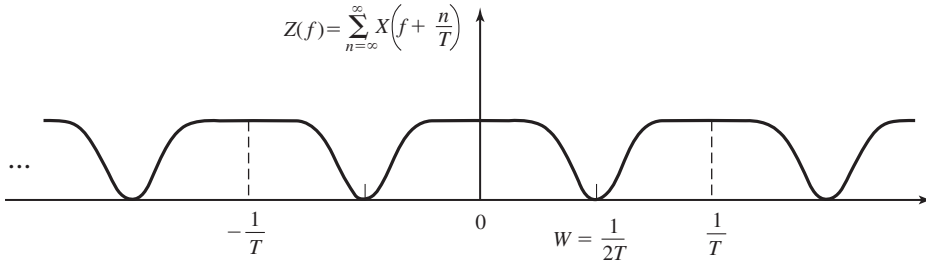


**Figure 8.9** Plot of  $Z(f)$  for the case  $T = \frac{1}{2W}$ .

Now, suppose that the channel has a bandwidth of  $W$ . Then  $C(f) \equiv 0$  for  $|f| > W$  and consequently,  $X(f) = 0$  for  $|f| > W$ . We distinguish three cases:

1.  $T < \frac{1}{2W}$ , or equivalently,  $\frac{1}{T} > 2W$ . Since  $Z(f) = \sum_{n=-\infty}^{+\infty} X(f + \frac{n}{T})$  consists of nonoverlapping replicas of  $X(f)$ , separated by  $\frac{1}{T}$  as shown in Figure 8.8, there is no choice for  $X(f)$  to ensure  $Z(f) \equiv T$  in this case, and there is no way that we can design a system with no ISI.
2.  $T = \frac{1}{2W}$ , or equivalently,  $\frac{1}{T} = 2W$  (the Nyquist rate). In this case, the replicas of  $X(f)$ , separated by  $\frac{1}{T}$ , are about to overlap as shown in Figure 8.9. It is clear that in this case there exists only one  $X(f)$  that results in  $Z(f) = T$ , namely,

$$X(f) = \begin{cases} T & |f| < W \\ 0, & \text{otherwise} \end{cases} \quad (8.3.20)$$

or,  $X(f) = T \Pi(\frac{f}{2W})$ , which results in

$$x(t) = \text{sinc}\left(\frac{t}{T}\right) \quad (8.3.21)$$

This means that the smallest value of  $T$  for which transmission with zero ISI is possible is  $T = \frac{1}{2W}$  and for this value,  $x(t)$  has to be a sinc function. The difficulty with this choice of  $x(t)$  is that it is noncausal and therefore nonrealizable. To make it realizable, usually a delayed version of it; i.e.,  $\text{sinc}(\frac{t-t_0}{T})$  is used and  $t_0$  is chosen such that for  $t < 0$ , we have  $\text{sinc}(\frac{t-t_0}{T}) \approx 0$ . Of course with this choice of

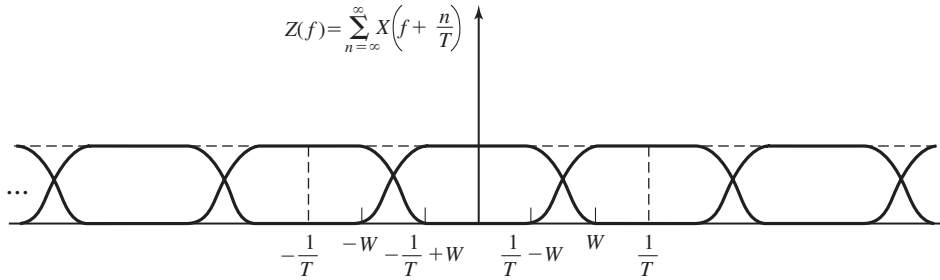


**Figure 8.10** Plot of  $Z(f)$  for the case  $T > 1/2W$ .

$x(t)$ , the sampling time must also be shifted to  $mT + t_0$ . A second difficulty with this pulse shape is that its rate of convergence to zero is slow. The tails of  $x(t)$  decay as  $1/t$ , consequently, a small mistiming error in sampling the output of the matched filter at the demodulator results in an infinite series of ISI components. Such a series is not absolutely summable because of the  $1/t$  rate of decay of the pulse and, hence, the sum of the resulting ISI does not converge.

3. For  $T > \frac{1}{2W}$ ,  $Z(f)$  consists of overlapping replications of  $X(f)$  separated by  $\frac{1}{T}$ , as shown in Figure 8.10. In this case, there exist numerous choices for  $X(f)$ , such that  $Z(f) \equiv T$ .

A particular pulse spectrum, for the  $T > \frac{1}{2W}$  case, that has desirable spectral properties and has been widely used in practice is the raised cosine spectrum. The raised cosine frequency characteristic is given as (see Problem 8.11)

$$X_{rc}(f) = \begin{cases} T, & 0 \leq |f| \leq (1 - \alpha)/2T \\ \frac{T}{2} [1 + \cos \frac{\pi T}{\alpha} (|f| - \frac{1-\alpha}{2T})], & \frac{1-\alpha}{2T} \leq |f| \leq \frac{1+\alpha}{2T} \\ 0, & |f| > \frac{1+\alpha}{2T} \end{cases} \quad (8.3.22)$$

where  $\alpha$  is called the *rolloff factor*, which takes values in the range  $0 \leq \alpha \leq 1$ . The bandwidth occupied by the signal beyond the Nyquist frequency  $\frac{1}{2T}$  is called the *excess bandwidth* and is usually expressed as a percentage of the Nyquist frequency. For example, when  $\alpha = \frac{1}{2}$ , the excess bandwidth is 50%, and when  $\alpha = 1$  the excess bandwidth is 100%. The pulse  $x(t)$  having the raised cosine spectrum is

$$\begin{aligned} x(t) &= \frac{\sin \pi t/T}{\pi t/T} \frac{\cos(\pi \alpha t/T)}{1 - 4\alpha^2 t^2/T^2} \\ &= \text{sinc}(t/T) \frac{\cos(\pi \alpha t/T)}{1 - 4\alpha^2 t^2/T^2} \end{aligned} \quad (8.3.23)$$

Note that  $x(t)$  is normalized so that  $x(0) = 1$ . Figure 8.11 illustrates the raised cosine spectral characteristics and the corresponding pulses for  $\alpha = 0, 1/2, 1$ . We note that

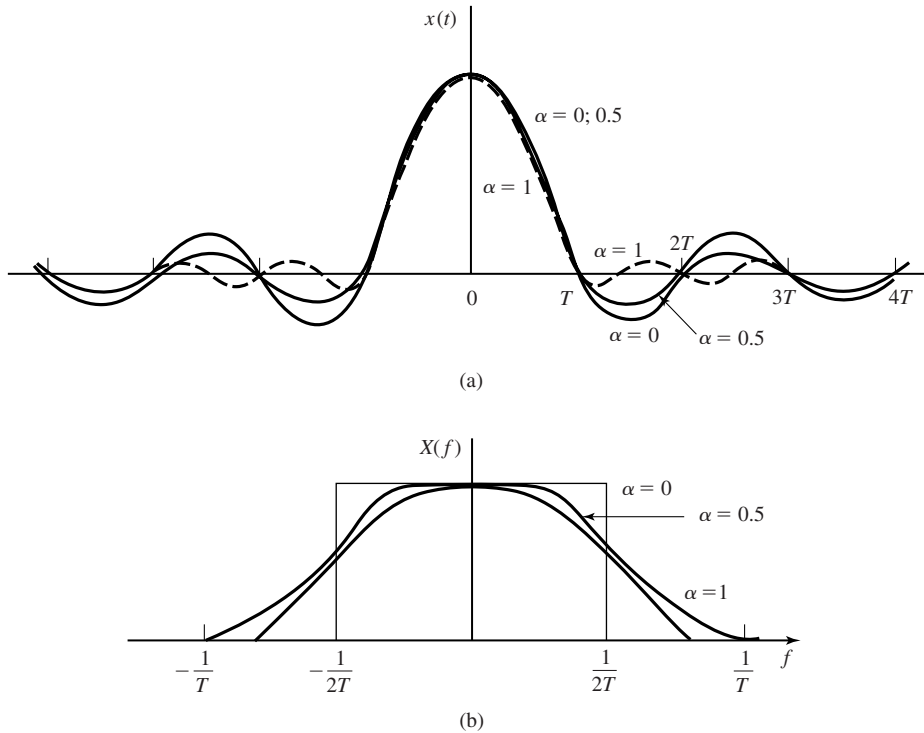


**Figure 8.11** Pulses having a raised cosine spectrum.

for  $\alpha = 0$ , the pulse reduces to  $x(t) = \text{sinc}(t/T)$ , and the symbol rate  $1/T = 2W$ . When  $\alpha = 1$ , the symbol rate is  $1/T = W$ . In general, the tails of  $x(t)$  decay as  $1/t^3$  for  $\alpha > 0$ . Consequently, a mistiming error in sampling leads to a series of intersymbol interference components that converges to a finite value.

Due to the smooth characteristics of the raised cosine spectrum, it is possible to design practical filters for the transmitter and the receiver that approximate the overall desired frequency response. In the special case where the channel is ideal with  $C(f) = \Pi(\frac{f}{2W})$ , we have

$$X_{\text{rc}}(f) = G_T(f)G_R(f) \quad (8.3.24)$$

In this case, if the receiver filter is matched to the transmitter filter we have  $X_{\text{rc}}(f) = G_T(f)G_R(f) = |G_T(f)|^2$ . Ideally,

$$G_T(f) = \sqrt{|X_{\text{rc}}(f)|} e^{-j2\pi f t_0} \quad (8.3.25)$$

and  $G_R(f) = G_T^*(f)$ , where  $t_0$  is some nominal delay that is required to assure physical realizability of the filter. Thus, the overall raised cosine spectral characteristic is split evenly between the transmitting filter and the receiving filter. We should also note that an additional delay is necessary to ensure the physical realizability of the receiving filter.

### 8.3.2 Design of Bandlimited Signals with Controlled ISI—Partial Response Signals

As we have observed from our discussion of signal design for zero ISI, it is necessary to reduce the symbol rate  $1/T$  below the Nyquist rate of  $2W$  symbols/sec in order to realize practical transmitting and receiving filters. On the other hand, suppose we choose to relax the condition of zero ISI and, thus, achieve a symbol transmission rate of  $2W$  symbols/sec. By allowing for a controlled amount of ISI, we can achieve this symbol rate.

We have already seen in that the condition of zero ISI is  $x(nT) = 0$  for  $n \neq 0$ . However, suppose that we design the bandlimited signal to have controlled ISI at one time instant. This means that we allow one additional nonzero value in the samples  $\{x(nT)\}$ . The ISI that we introduce is deterministic or “controlled” and, hence, it can be taken into account at the receiver, as discussed next.

One special case that leads to (approximately) physically realizable transmitting and receiving filters is specified by the samples<sup>†</sup>

$$x(nT) = \begin{cases} 1, & n = 0, 1 \\ 0, & \text{otherwise} \end{cases} \quad (8.3.26)$$

Now, using Equation (8.3.16), we obtain

$$z_n = \begin{cases} T & n = 0, -1 \\ 0, & \text{otherwise} \end{cases} \quad (8.3.27)$$

which when substituted into Equation (8.3.14) yields

$$Z(f) = T + T e^{-j2\pi fT} \quad (8.3.28)$$

As in the preceding section, it is impossible to satisfy the above equation for  $T < \frac{1}{2W}$ . However, for  $T = \frac{1}{2W}$ , we obtain

$$\begin{aligned} X(f) &= \begin{cases} \frac{1}{2W} [1 + e^{-j\frac{\pi f}{W}}], & |f| < W \\ 0, & \text{otherwise} \end{cases} \\ &= \begin{cases} \frac{1}{W} e^{-j\frac{\pi f}{2W}} \cos\left(\frac{\pi f}{2W}\right), & |f| < W \\ 0, & \text{otherwise} \end{cases} \end{aligned} \quad (8.3.29)$$

Therefore,  $x(t)$  is given by

$$x(t) = \text{sinc}(2Wt) + \text{sinc}(2Wt - 1) \quad (8.3.30)$$

This pulse is called a duobinary signal pulse. It is illustrated, along with its magnitude spectrum in Figure 8.12. We note that the spectrum decays to zero smoothly, which means that physically realizable filters can be designed that approximate this spectrum very closely. Thus, a symbol rate of  $2W$  is achieved.

<sup>†</sup>It is convenient to deal with samples of  $x(t)$  that are normalized to unity for  $n = 0, 1$ .



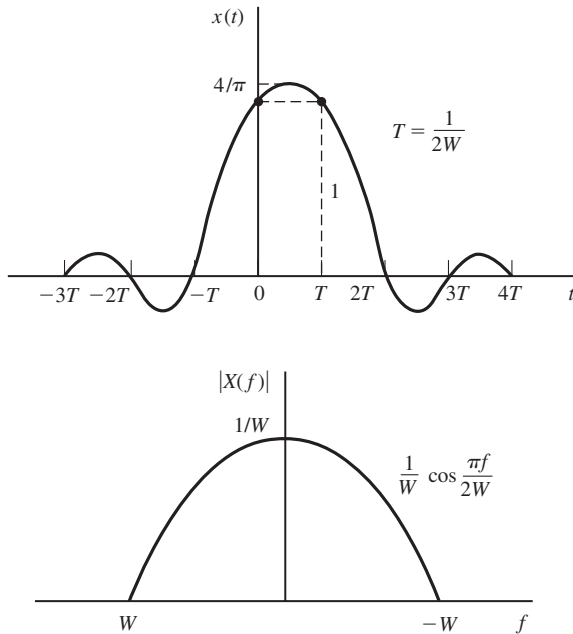


**Figure 8.12** Time domain and frequency-domain characteristics of a duobinary signal.

Another special case that leads to (approximately) physically realizable transmitting and receiving filters is specified by the samples

$$x\left(\frac{n}{2W}\right) = x(nT) = \begin{cases} 1, & n = -1 \\ -1, & n = 1 \\ 0, & \text{otherwise} \end{cases} \quad (8.3.31)$$

The corresponding pulse  $x(t)$  is given as

$$x(t) = \text{sinc}(t + T)/T - \text{sinc}(t - T)/T \quad (8.3.32)$$

and its spectrum is

$$X(f) = \begin{cases} \frac{1}{2W} e^{j\pi f/W} - e^{-j\pi f/W} = \frac{j}{W} \sin \frac{\pi f}{W}, & |f| \leq W \\ 0, & |f| > W \end{cases} \quad (8.3.33)$$

This pulse and its magnitude spectrum are illustrated in Figure 8.13. It is called a *modified duobinary signal pulse*. It is interesting to note that the spectrum of this signal has a zero at  $f = 0$ , making it suitable for transmission over a channel that does not pass dc.

One can obtain other interesting and physically realizable filter characteristics, as shown by Kretzmer (1966) and Lucky et al. (1968), by selecting different values for the samples  $\{x(n/2W)\}$  and more than two nonzero samples. However, as we select more nonzero samples, the problem of unraveling the controlled ISI becomes more cumbersome and impractical.

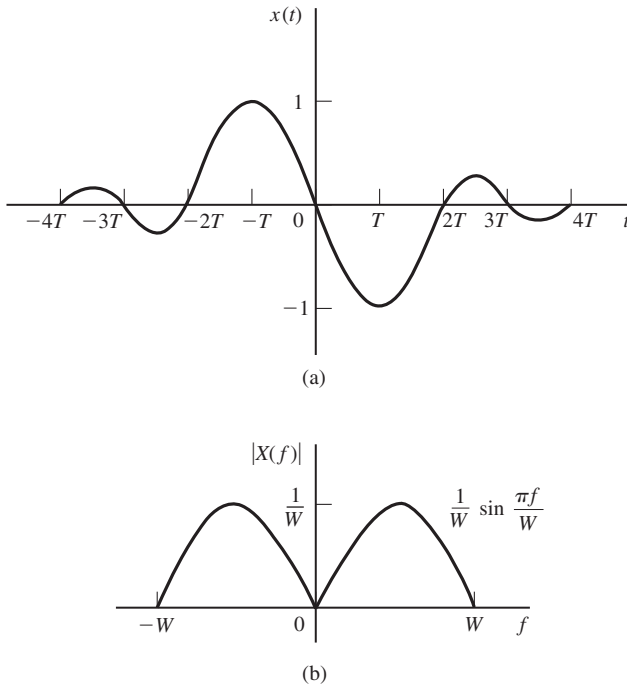


**Figure 8.13** Time domain and frequency domain characteristics of a modified duobinary signal.

In general, the class of bandlimited signals pulses that have the form

$$x(t) = \sum_{n=-\infty}^{\infty} x\left(\frac{n}{2W}\right) \frac{\sin 2\pi W(t - n/2W)}{2\pi W(t - n/2W)} \quad (8.3.34)$$

and their corresponding spectra

$$X(f) = \begin{cases} \frac{1}{2W} \sum_{n=-\infty}^{\infty} x\left(\frac{n}{2W}\right) e^{-jn\pi f/W}, & |f| \leq W \\ 0, & |f| > W \end{cases} \quad (8.3.35)$$

are called *partial response signals* when controlled ISI is purposely introduced by selecting two or more nonzero samples from the set  $\{x(n/2W)\}$ . The resulting signal pulses allow us to transmit information symbols at the Nyquist rate of  $2W$  symbols per second. The detection of the received symbols in the presence of controlled ISI is described in Sections 8.4 and 8.5.

## 8.4 PROBABILITY OF ERROR IN DETECTION OF DIGITAL PAM

In this section we evaluate the performance of the receiver for demodulating and detecting an  $M$ -ary PAM signal in the presence of additive, white Gaussian noise at its input. First, we consider the case in which the transmitter and receiver filters  $G_T(f)$  and  $G_R(f)$  are designed for zero ISI. Then, we consider the case in which  $G_T(f)$  and  $G_R(f)$  are designed such that  $x(t) = g_T(t) \star g_R(t)$  is either a duobinary signal

or a modified duobinary signal. Although our focus in this section is the performance evaluation of PAM, our treatment can be generalized to two-dimensional modulations, such as PSK and QAM, and multidimensional signals.

#### 8.4.1 Probability of Error for Detection of Digital PAM with Zero ISI

In the absence of ISI, the received signal sample at the output of the receiving matched filter has the form

$$y_m = x_0 a_m + v_m \quad (8.4.1)$$

where

$$x_0 = \int_{-W}^W |G_T(f)|^2 df = \mathcal{E}_g \quad (8.4.2)$$

and  $v_m$  is the additive Gaussian noise which has zero mean and variance

$$\sigma_v^2 = \mathcal{E}_g N_0 / 2 \quad (8.4.3)$$

In general,  $a_m$  takes one of  $M$  possible equally spaced amplitude values with equal probability. Given a particular amplitude level, the problem is to determine the probability of error.

The problem of evaluating the probability of error for digital PAM in a bandlimited, additive white Gaussian noise channel, in the absence of ISI, is identical to the evaluation of the error probability for  $M$ -ary PAM as given in Section 7.6.2. The final result that is obtained from the derivation is

$$P_M = \frac{2(M-1)}{M} Q \left[ \sqrt{\frac{2\mathcal{E}_g}{N_0}} \right] \quad (8.4.4)$$

But  $\mathcal{E}_g = 3\mathcal{E}_{av}/(M^2 - 1)$ ,  $\mathcal{E}_{av} = k \mathcal{E}_{bav}$  is the average energy per symbol and  $\mathcal{E}_{bav}$  is the average energy/bit. Hence,

$$P_M = \frac{2(M-1)}{M} Q \left[ \sqrt{\frac{6(\log_2 M)\mathcal{E}_{bav}}{(M^2 - 1)N_0}} \right] \quad (8.4.5)$$

This is exactly the form for the probability of error of  $M$ -ary PAM derived previously in Section 7.6.2. In the treatment of PAM given in this chapter we imposed the additional constraint that the transmitted signal is bandlimited to the bandwidth allocated for the channel. Consequently, the transmitted signal pulses were designed to be bandlimited and to have zero ISI.

In contrast, no bandwidth constraint was imposed on the PAM signals considered in Section 7.6.2. Nevertheless, the receivers (demodulators and detectors) in both cases are optimum (matched filters) for the corresponding transmitted signals. Consequently, no loss in error-rate performance results from the bandwidth constraint when the signal pulse is designed for zero ISI and the channel does not distort the transmitted signal.

### 8.4.2 Symbol-by-Symbol Detection of Data with Controlled ISI

In this section we describe a symbol-by-symbol method for detecting the information symbols at the demodulator when the received signal contains controlled ISI. This symbol detection method is relatively easy to implement. A second method, based on the maximum-likelihood criterion for detecting a sequence of symbols, is described in Section 8.5.2. This second method minimizes the probability of error but is a little more complex to implement. In particular, we consider the detection of the duobinary and the modified duobinary partial response signals. In both cases, we assume that the desired spectral characteristic  $X(f)$  for the partial response signal is split evenly between the transmitting and receiving filters; i.e.,  $|G_T(f)| = |G_R(f)| = |X(f)|^{1/2}$ .

For the duobinary signal pulse,  $x(nT) = 1$ , for  $n = 0, 1$  and zero otherwise. Hence, the samples at the output of the receiving filter have the form

$$y_m = b_m + v_m = a_m + a_{m-1} + v_m \quad (8.4.6)$$

where  $\{a_m\}$  is the transmitted sequence of amplitudes and  $\{v_m\}$  is a sequence of additive Gaussian noise samples. Let us ignore the noise for the moment and consider the binary case where  $a_m = \pm 1$  with equal probability. Then,  $b_m$  takes on one of three possible values, namely,  $b_m = -2, 0, 2$  with corresponding probabilities  $1/4, 1/2, 1/4$ . If  $a_{m-1}$  is the detected symbol from the  $(m-1)$ st signaling interval, its effect on  $b_m$ , the received signal in the  $m$ th signaling interval, can be eliminated by subtraction, thus allowing  $a_m$  to be detected. This process can be repeated sequentially for every received symbol.

The major problem with this procedure is that errors arising from the additive noise tend to propagate. For example, if  $a_{m-1}$  is in error, its effect on  $b_m$  is not eliminated but, in fact, it is reinforced by the incorrect subtraction. Consequently, the detection of  $a_m$  is also likely to be in error.

Error propagation can be avoided by *precoding* the data at the transmitter instead of eliminating the controlled ISI by subtraction at the receiver. The precoding is performed on the binary data sequence prior to modulation. From the data sequence  $\{d_n\}$  of 1's and 0's that is to be transmitted, a new sequence  $\{p_n\}$ , called the *precoded sequence* is generated. For the duobinary signal, the precoded sequence is defined as

$$p_m = d_m \ominus p_{m-1}, \quad m = 1, 2, \dots \quad (8.4.7)$$

where the symbol  $\ominus$  denotes modulo-2 subtraction.<sup>†</sup> Then, we set  $a_m = -1$  if  $p_m = 0$  and  $a_m = 1$  if  $p_m = 1$ ; i.e.,  $a_m = 2p_m - 1$ .

The noise-free samples at the output of the receiving filter are given as

$$\begin{aligned} b_m &= a_m + a_{m-1} \\ &= (2p_m - 1) + (2p_{m-1} - 1) \\ &= 2(p_m + p_{m-1} - 1) \end{aligned} \quad (8.4.8)$$

<sup>†</sup>Although this is identical to modulo-2 addition, it is convenient to view the precoding operation for duobinary in terms of modulo-2 subtraction.

**TABLE 8.1** BINARY SIGNALING WITH DUOBINARY PULSES

Data sequence $d_n$	1	1	1	0	1	0	0	1	0	0	0	1	1	0	1	
Precoded sequence $p_n$	0	1	0	1	1	0	0	0	1	1	1	1	0	1	1	0
Transmitted sequence $a_n$	-1	1	-1	1	1	-1	-1	-1	1	1	1	1	-1	1	1	-1
Received sequence $b_n$	0	0	0	2	0	-2	-2	0	2	2	2	0	0	2	0	
Decoded sequence $d_n$	1	1	1	0	1	0	0	1	0	0	0	1	1	0	1	

Consequently,

$$p_m + p_{m-1} = \frac{b_m}{2} + 1 \quad (8.4.9)$$

Since  $d_m = p_m \oplus p_{m-1}$ , it follows that the data sequence  $d_m$  is obtained from  $b_m$  by using the relation

$$d_m = \frac{b_m}{2} - 1 \pmod{2} \quad (8.4.10)$$

Consequently, if  $b_m = \pm 2$ ,  $d_m = 0$  and if  $b_m = 0$ ,  $d_m = 1$ . An example that illustrates the precoding and decoding operations is given in Table 8.1. In the presence of additive noise the sampled outputs from the receiving filter are given by Equation (8.4.6). In this case  $y_m = b_m + v_m$  is compared with the two thresholds set at +1 and -1. The data sequence  $\{d_n\}$  is obtained according to the detection rule

$$d_m = \begin{cases} 1, & \text{if } -1 < y_m < 1 \\ 0, & \text{if } |y_m| \geq 1 \end{cases} \quad (8.4.11)$$

The extension from binary PAM to multilevel PAM signaling using the duobinary pulses is straightforward. In this case the  $M$ -level amplitude sequence  $\{a_m\}$  results in a (noise-free) sequence

$$b_m = a_m + a_{m-1}, \quad m = 1, 2, \dots \quad (8.4.12)$$

which has  $2M - 1$  possible equally spaced levels. The amplitude levels are determined from the relation

$$a_m = 2p_m - (M - 1) \quad (8.4.13)$$

where  $\{p_m\}$  is the precoded sequence that is obtained from an  $M$ -level data sequence  $\{d_m\}$  according to the relation

$$p_m = d_m \ominus p_{m-1} \pmod{M} \quad (8.4.14)$$

where the possible values of the sequence  $\{d_m\}$  are  $0, 1, 2, \dots, M - 1$ .

**TABLE 8.2** FOUR-LEVEL TRANSMISSION WITH DUOBINARY PULSES

Data sequence $d_n$	0	0	1	3	1	2	0	3	3	2	0	1	0	
Precoded sequence $p_n$	0	0	0	1	2	3	3	1	2	1	1	3	2	2
Transmitted sequence $a_n$	-3	-3	-3	-1	1	3	3	-1	1	-1	-1	3	1	1
Received sequence $b_n$	-6	-6	-4	0	4	6	2	0	0	-2	2	4	2	
Decoded sequence $d_n$	0	0	1	3	1	2	0	3	3	2	0	1	0	

In the absence of noise, the samples at the output of the receiving filter may be expressed as

$$\begin{aligned} b_m &= a_m + a_{m-1} \\ &= 2[p_m + p_{m-1} - (M - 1)] \end{aligned} \quad (8.4.15)$$

Hence,

$$p_m + p_{m-1} = \frac{b_m}{2} + (M - 1) \quad (8.4.16)$$

Since  $d_m = p_m + p_{m-1} \pmod{M}$ , it follows that

$$d_m = \frac{b_m}{2} + (M - 1) \pmod{M} \quad (8.4.17)$$

An example illustrating multilevel precoding and decoding is given in Table 8.2.

In the presence of noise, the received signal-plus-noise is quantized to the nearest of the possible signal levels and the rule given above is used on the quantized values to recover the data sequence.

In the case of the modified duobinary pulse, the controlled ISI is specified by the values  $x(n/2W) = -1$ , for  $n = 1$ ,  $x(n/2W) = 1$  for  $n = -1$ , and zero otherwise. Consequently, the noise-free sampled output from the receiving filter is given as

$$b_m = a_m - a_{m-2} \quad (8.4.18)$$

where the  $M$ -level sequence  $\{a_n\}$  is obtained by mapping a precoded sequence according to the relation Equation (8.2.43) and

$$p_m = d_m \oplus p_{m-2} \pmod{M} \quad (8.4.19)$$

From these relations, it is easy to show that the detection rule for recovering the data sequence  $\{d_m\}$  from  $\{b_m\}$  in the absence of noise is

$$d_m = \frac{b_m}{2} \pmod{M} \quad (8.4.20)$$

As demonstrated above, the precoding of the data at the transmitter makes it possible to detect the received data on a symbol-by-symbol basis without having to look back at previously detected symbols. Thus, error propagation is avoided.

The symbol-by-symbol detection rule described above is not the optimum detection scheme for partial response signals. Nevertheless, symbol-by-symbol detection is relatively simple to implement and is used in many practical applications involving duobinary and modified duobinary pulse signals. Its performance is evaluated in Section 8.4.3.

### 8.4.3 Probability of Error for Detection of Partial Response Signals

In this section we determine the probability of error for detection of digital  $M$ -ary PAM signaling using duobinary and modified duobinary pulses. The channel is assumed to be an ideal bandlimited channel with additive white Gaussian noise. The model for the communications system is shown in Figure 8.14.

We consider the symbol-by-symbol detector. The performance of the optimum ML sequence detector is described in Section 8.5.3.

**Symbol-by-Symbol Detector.** At the transmitter, the  $M$ -level data sequence  $\{d_n\}$  is precoded as described previously. The precoder output is mapped into one of  $M$  possible amplitude levels. Then the transmitting filter with frequency response  $G_T(f)$  has an output

$$v(t) = \sum_{n=-\infty}^{\infty} a_n g_T(t - nT) \quad (8.4.21)$$

The partial-response function  $X(f)$  is divided equally between the transmitting and receiving filters. Hence, the receiving filter is matched to the transmitted pulse, and the cascade of the two filters results in the frequency characteristic

$$|G_T(f)G_R(f)| = |X(f)| \quad (8.4.22)$$

The matched filter output is sampled at  $t = nT = n/2W$  and the samples are fed to the decoder. For the duobinary signal, the output of the matched filter at the sampling instant may be expressed as

$$\begin{aligned} y_m &= a_m + a_{m-1} + v_m \\ &= b_m + v_m \end{aligned} \quad (8.4.23)$$

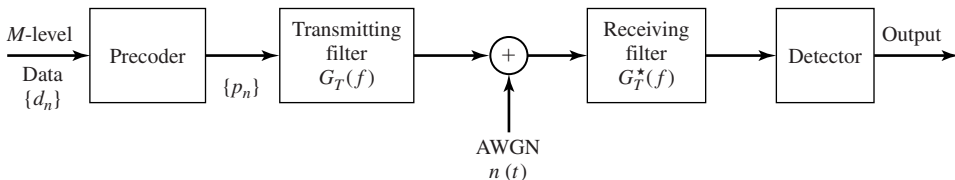


**Figure 8.14** Block diagram of modulator and demodulator for partial response signals.

where  $v_m$  is the additive noise component. Similarly, the output of the matched filter for the modified duobinary signal is

$$\begin{aligned} y_m &= a_m - a_{m-2} + v_m \\ &= b_m + v_m \end{aligned} \quad (8.4.24)$$

For binary transmission, let  $a_m = \pm d$ , where  $2d$  is the distance between signal levels. Then, the corresponding values of  $b_m$  are  $(2d, 0, -2d)$ . For  $M$ -ary PAM signal transmission, where  $a_m = \pm d, \pm 3d, \dots, \pm(M-1)d$ , the received signal levels are  $b_m = 0, \pm 2d, \pm 4d, \dots, \pm 2(M-1)d$ . Hence, the number of received levels is  $2M-1$ .

The input transmitted symbols  $\{a_m\}$  are assumed to be equally probable. Then, for duobinary and modified duobinary signals, it is easily demonstrated that, in the absence of noise, the received output levels have a (triangular) probability mass function of the form

$$P(b = 2md) = \frac{M - |m|}{M^2}, \quad m = 0, \pm 1, \pm 2, \dots, \pm(M-1) \quad (8.4.25)$$

where  $b$  denotes the noise-free received level and  $2d$  is the distance between any two adjacent received signal levels.

The channel corrupts the signal transmitted through it by the addition of white Gaussian noise with zero-mean and power-spectral density  $N_0/2$ .

We assume that a symbol error is committed whenever the magnitude of the additive noise exceeds the distance  $d$ . This assumption neglects the rare event that a large noise component with magnitude exceeding  $d$  may result in a received signal level that yields a correct symbol decision. The noise component  $v_m$  is zero-mean, Gaussian with variance

$$\begin{aligned} \sigma_v^2 &= \frac{N_0}{2} \int_{-W}^W |G_R(f)|^2 df \\ &= \frac{N_0}{2} \int_{-W}^W |X(f)| df = 2N_0/\pi \end{aligned} \quad (8.4.26)$$

for both the duobinary and the modified duobinary signals. Hence, an upper bound on the symbol probability of error is

$$\begin{aligned} P_M &< \sum_{m=-(M-2)}^{M-2} P(|y - 2md| > d | b = 2md) P(b = 2md) \\ &\quad + 2P(y + 2(M-1)d > d | b = -2(M-1)d) P(b = -2(M-1)d) \\ &= P(|y| > d | b = 0) \left[ 2 \sum_{m=0}^{M-1} P(b = 2md) - P(b = 0) - P(b = -2(M-1)d) \right] \\ &= \left( 1 - \frac{1}{M^2} \right) P(|y| > d | b = 0) \end{aligned} \quad (8.4.27)$$



But

$$\begin{aligned} P(|y| > d | b = 0) &= \frac{2}{\sqrt{2\pi}\sigma_v} \int_d^\infty e^{-x^2/2\sigma_v^2} dx \\ &= 2Q\left(\sqrt{\frac{\pi d^2}{2N_0}}\right) \end{aligned} \quad (8.4.28)$$

Therefore, the average probability of a symbol error is upper-bounded as

$$P_M < 2\left(1 - \frac{1}{M^2}\right) Q\left(\sqrt{\frac{\pi d^2}{2N_0}}\right) \quad (8.4.29)$$

The scale factor  $d$  in Equation (8.4.29) can be eliminated by expressing  $d$  in terms of the average power transmitted into the channel. For the  $M$ -ary PAM signal in which the transmitted levels are equally probable, the average power at the output of the transmitting filter is

$$\begin{aligned} P_{av} &= \frac{E(a_m^2)}{T} \int_{-W}^W |G_T(f)|^2 df \\ &= \frac{E(a_m^2)}{T} \int_{-W}^W |X(f)| df = \frac{4}{\pi T} E(a_m^2) \end{aligned} \quad (8.4.30)$$

where  $E(a_m^2)$  is the mean square value of the  $M$  signal levels, which is

$$E(a_m^2) = \frac{d^2(M^2 - 1)}{3} \quad (8.4.31)$$

Therefore,

$$d^2 = \frac{3\pi P_{av}T}{4(M^2 - 1)} \quad (8.4.32)$$

By substituting the value of  $d^2$  from Equation (8.4.32) into Equation (8.4.29), we obtain the upper-bound for the symbol error probability as

$$P_M < 2\left(1 - \frac{1}{M^2}\right) Q\left(\sqrt{\left(\frac{\pi}{4}\right)^2 \frac{6}{M^2 - 1} \frac{\mathcal{E}_{av}}{N_0}}\right) \quad (8.4.33)$$

where  $\mathcal{E}_{av}$  is the average energy/transmitted symbol, which can be also expressed in terms of the average bit energy as  $\mathcal{E}_{av} = k\mathcal{E}_{bav} = (\log_2 M)\mathcal{E}_{bav}$ .

The expression in Equation (8.4.33) for the probability of error of  $M$ -ary PAM holds for both a duobinary and a modified duobinary partial response signal. If we compare this result with the error probability of  $M$ -ary PAM with zero ISI, which can be obtained by using a signal pulse with a raised cosine spectrum, we note that the performance of partial response duobinary or modified duobinary has a loss of

$(\pi/4)^2$  or 2.1 dB. This loss in SNR is due to the fact that the detector for the partial response signals makes decisions on a symbol-by-symbol basis, thus, ignoring the inherent memory contained in the received signal at the input to the detector.

To observe the memory in the received sequence, let us look at the noise-free received sequence for binary transmission given in Table 8.1. The sequence  $\{b_m\}$  is 0, -2, 0, 2, 0, -2, 0, 2, 2, . . . . We note that it is not possible to have a transition from -2 to +2 or from +2 to -2 in one symbol interval. For example, if the signal level at the input to the detector is -2, the next signal level can be either -2 or 0. Similarly, if the signal level at a given sampling instant is 2, the signal level in the following time instant can be either 2 or 0. In other words, it is not possible to encounter a transition from -2 to 2 or vice versa between two successive received samples from the matched filter. However, a symbol-by-symbol detector does not exploit this constraint or inherent memory in the received sequence. In Section 8.5.3, we derive the performance of the ML sequence detector that exploits the inherent memory in the modulation and, consequently, regains a large part of the 2.1-dB loss suffered by the symbol-by-symbol detector.

## 8.5 DIGITALLY MODULATED SIGNALS WITH MEMORY

In our treatment of signal design for bandlimited channels in Section 8.3, we observed that we can shape the spectrum of the transmitted signal by introducing memory in the modulation. The two examples cited in that section are the duobinary and modified duobinary partial response signals. In essence, the spectrum shaping obtained with these partial response signals may be viewed as resulting from the memory introduced in the transmitted sequence of symbols; i.e., the sequence of symbols are correlated and, as a consequence, the power spectrum of the transmitted symbol sequence is colored (nonwhite).

Signal dependence among signals transmitted in different signal intervals is generally accomplished by encoding the data at the input to the modulator by means of a *modulation code*. Such a code generally places restrictions on the sequence of symbols into the modulator and, thus, introduces memory in the transmitted signal. In this section, we consider modulation signals with memory and characterize them in terms of their spectral characteristics and their performance in an additive white Gaussian noise channel. We confine our treatment to baseband signals. The generalization to bandpass signals is relatively straightforward, as we have already observed in our treatment of the spectral characteristics of digitally modulated signals.

Signal dependence among signals transmitted in different signal intervals can also result from intersymbol interference introduced by channel distortion. The memory imposed by the channel on the received signals requires that the detector at the receiver must be designed to estimate the received information symbols by observing and processing the received signal over a time duration that encompasses the channel memory. Signal detectors that function in this manner are generally called equalizers and are treated in Section 8.6.

### 8.5.1 Modulation Codes and Modulation Signals with Memory

Modulation codes are usually employed in magnetic recording, in optical recording, and in digital communications over cable systems to achieve spectral shaping of the modulated signal that matches the passband characteristics of the channel. Let us consider magnetic recording as an example.

In magnetic recording, we encounter two basic problems. One problem is concerned with the packing density that is used to write the data on the magnetic medium (disk or tape). Of course, we would like to write as many bits as possible on a single track. However, there is a limit as to how close successive bits in a sequence are stored, and this limit is imposed by the medium. Let us explore this problem further.

Figure 8.15 illustrates a block diagram of the magnetic recording system. The binary data sequence to be stored is used to generate a write current. This current may be viewed as the output of the “modulator.” The two most commonly used methods to map the data sequence into the write current waveform are the so-called NRZ (non-return-to-zero) and NRZI (non-return-to-zero-inverse) methods. These two waveforms are illustrated in Figure 8.16. We note that NRZ is identical to binary PAM in which the information bit 1 is represented by a rectangular pulse of amplitude  $A$  and the information bit 0 is represented by a rectangular pulse of amplitude  $-A$ . In contrast, the NRZI signal waveform is different from NRZ in that transitions from one amplitude level to another ( $A$  to  $-A$  or  $-A$  to  $A$ ), occur only when the information bit is a 1. No transition occurs when the information bit is a 0; i.e., the amplitude level remains the same as the previous signal level. The positive amplitude pulse results in magnetizing the medium on one (direction) polarity and the negative pulse magnetizes the medium in the opposite (direction) polarity.

Since the input data sequence is basically random with equally probable 1's and 0's, whether we use NRZ or NRZI, we will encounter level transitions for  $A$  to  $-A$  or  $-A$  to  $A$  with probability  $1/2$  for every data bit. The readback signal for a positive transition ( $-A$  to  $A$ ) is a pulse that is well modeled mathematically as

$$p(t) = \frac{1}{1 + (2t/T_{50})^2} \quad (8.5.1)$$

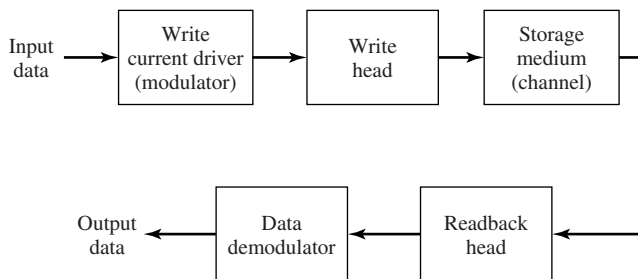


**Figure 8.15** Block diagram of magnetic storage read/write system.

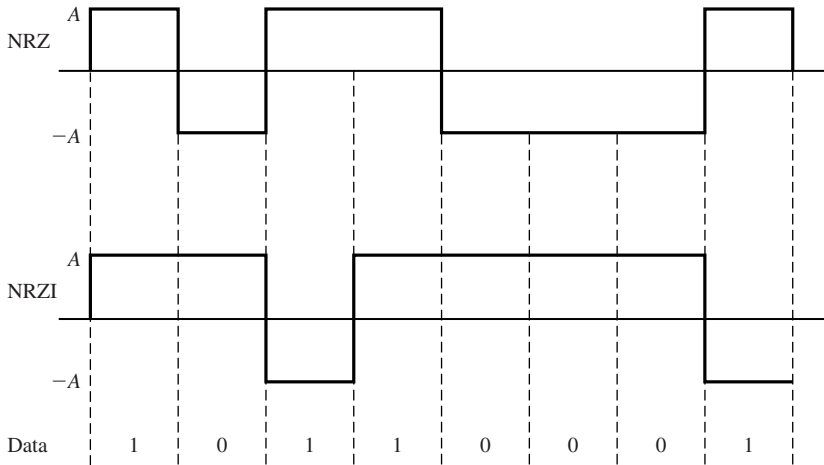


Figure 8.16 NRZ and NRZI signals.

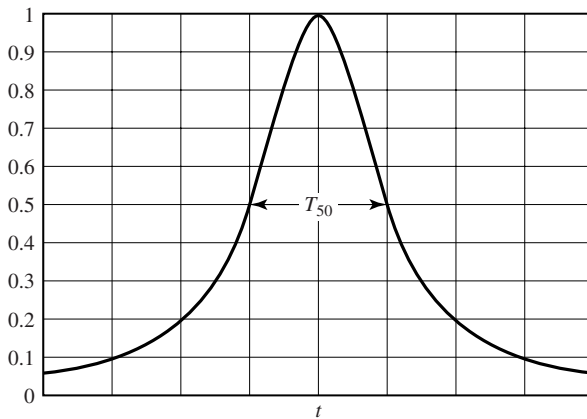
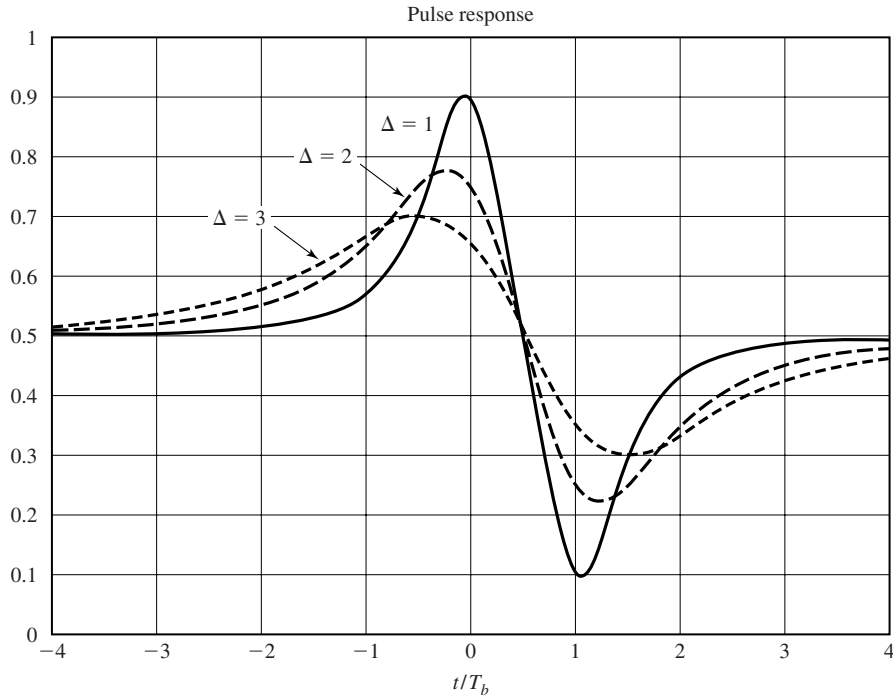


Figure 8.17 Readback pulse in magnetic recording system.

where  $T_{50}$  is defined as the width of the pulse at its 50% amplitude level, as shown in Figure 8.17. Similarly, the readback signal for a negative transition ( $A$  to  $-A$ ) is the pulse  $-p(t)$ . The value of  $T_{50}$  is determined by the characteristics of the medium and the read/write heads.

Now, suppose we write a positive transition followed by a negative transition, and let us vary the time interval between the two transitions, which we denote as  $T_b$  (the bit time interval). Figure 8.18 illustrates the readback signal pulses, which are obtained by a superposition of  $p(t)$  with  $-p(t - T_b)$ . The parameter,  $\Delta = T_{50}/T_b$ , is defined as the *normalized density*. The closer the bit transitions ( $T_b$  small), the larger will be the value of the normalized density and, hence, the larger will be the packing density. We notice that as  $\Delta$  is increased, the peak amplitudes of the readback signal



**Figure 8.18** Readback signal response to a pulse.

are reduced and are also shifted in time from the desired time instants. In other words, the pulses interfere with one another, thus, limiting the density with which we can write. This problem serves as a motivation to design modulation codes that take the original data sequence and transform (encode) it into another sequence that results in a write waveform in which amplitude transitions are spaced further apart. For example, if we use NRZI, the encoded sequence into the modulator must contain one or more 0's between 1's.

The second problem encountered in magnetic recording is the need to avoid (or minimize) having a dc content in the modulated signal (the write current), due to the frequency-response characteristics of the readback system and associated electronics. This requirement also arises in digital communication over cable channels. This problem can also be overcome by altering (encoding) the data sequence into the modulator. A class of codes that satisfy these objectives are the modulation codes described below.

**Runlength-Limited Codes.** Codes that have a restriction on the number of consecutive 1's or 0's in a sequence are generally called *runlength-limited codes*. These codes are generally described by two parameters, say  $d$  and  $\kappa$ , where  $d$  denotes the minimum number of 0's between 1's in a sequence, and  $\kappa$  denotes the maximum number of 0's between two 1's in a sequence. When used with NRZI modulation, the effect of

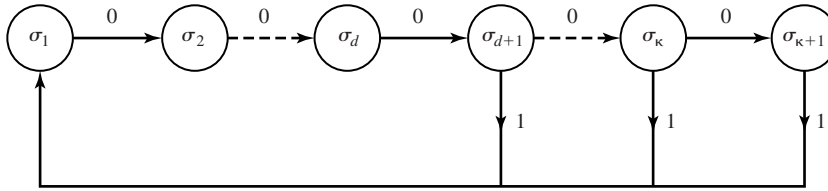


**Figure 8.19** Finite-state sequential machine for a  $(d, \kappa)$ -coded sequence.

placing  $d$  zeros between successive 1's is to spread the transitions farther apart, thus, reducing the overlap in the channel response due to successive transitions. By setting an upper limit  $\kappa$  on the runlength of 0's ensures that transitions occur frequently enough so that symbol timing information can be recovered from the received modulated signal. Runlength-limited codes are usually called  $(d, \kappa)$  codes.<sup>†</sup>

The  $(d, \kappa)$ -code sequence constraints may be represented by a finite-state sequential machine with  $\kappa + 1$  states, denoted as  $\sigma_i$ ,  $1 \leq i \leq \kappa + 1$ , as shown in Figure 8.19. We observe that an output data bit 0 takes the sequence from state  $\sigma_i$  to  $\sigma_{i+1}$ ,  $i \leq \kappa$ . The output data bit 1 takes the sequence to state  $\sigma_1$ . The output bit from the encoder may be a 1 only when the sequence is in state  $\sigma_i$ ,  $d + 1 \leq i \leq \kappa + 1$ . When the sequence is in state  $\sigma_{\kappa+1}$ , the output bit is always 1.

The finite-state sequential machine may also be represented by a *state transition matrix*, denoted as  $\mathbf{D}$ , which is a square  $(\kappa + 1) \times (\kappa + 1)$  matrix with elements  $d_{ij}$ , where

$$\begin{aligned} d_{i1} &= 1, & i &\geq d + 1 \\ d_{ij} &= 1, & j &= i + 1 \\ d_{ij} &= 0, & &\text{otherwise} \end{aligned} \quad (8.5.2)$$

### Example 8.5.1

Determine the state transition matrix for a  $(d, \kappa) = (1, 3)$  code.

**Solution** The  $(1, 3)$  code has four states. From Figure 8.19 we obtain its state transition matrix which is

$$\mathbf{D} = \begin{bmatrix} 0 & 1 & 0 & 0 \\ 1 & 0 & 1 & 0 \\ 1 & 0 & 0 & 1 \\ 1 & 0 & 0 & 0 \end{bmatrix} \quad (8.5.3)$$

An important parameter of any  $(d, \kappa)$  code is the number of sequences of a certain length, say  $n$ , which satisfy the  $(d, \kappa)$  constraints. As  $n$  is allowed to increase, the number of sequences  $N(n)$  which satisfy the  $(d, \kappa)$  constraint also increases. The number of information bits that can be uniquely represented with  $N(n)$  code sequences is

$$k = \lceil \log_2 N(n) \rceil$$

<sup>†</sup>Runlength-limited codes are usually called  $(d, k)$  codes, where  $k$  is the maximum runlength of zeros. We have substituted the Greek letter  $\kappa$  for  $k$ , to avoid confusion with our previous use of  $k$ .

where  $\lfloor x \rfloor$  denotes the largest integer contained in  $x$ . The maximum code rate is then  $R_c = k/n$ .

The capacity of a  $(d, \kappa)$  code is defined as

$$C(d, \kappa) = \lim_{n \rightarrow \infty} \frac{1}{n} \log_2 N(n) \quad (8.5.4)$$

Clearly,  $C(d, \kappa)$  is the maximum possible rate that can be achieved with the  $(d, \kappa)$  constraints. Shannon (1948) showed that the capacity is given as

$$C(d, \kappa) = \log_2 \lambda_{\max} \quad (8.5.5)$$

where  $\lambda_{\max}$  is the largest real eigenvalue of the state transition matrix  $\mathbf{D}$ .

### Example 8.5.2

Determine the capacity of a  $(d, \kappa) = (1, 3)$  code.

**Solution** Using the state-transition matrix given in Example 8.5.1 for the  $(1, 3)$  code, we have

$$\begin{aligned} \det(\mathbf{D} - \lambda \mathbf{I}) &= \det \begin{bmatrix} -\lambda & 1 & 0 & 0 \\ 1 & -\lambda & 1 & 0 \\ 1 & 0 & -\lambda & 1 \\ 1 & 0 & 0 & -\lambda \end{bmatrix} \\ &= \lambda^4 - \lambda^2 - \lambda - 1 = 0 \end{aligned} \quad (8.5.6)$$

The maximum real root of this polynomial is found to be  $\lambda_{\max} = 1.4656$ . Therefore, the capacity  $C(1, 3) = \log_2 \lambda_{\max} = 0.5515$ .

The capacities of  $(d, \kappa)$  codes for  $0 \leq d \leq 6$  and  $2 \leq \kappa \leq 15$ , are given in Table 8.3. We observe that  $C(d, \kappa) < 1/2$  for  $d \geq 3$ , and any value of  $\kappa$ . The most commonly used codes for magnetic recording employ a  $d \leq 2$ , hence, their rate  $R_c$  is at least  $1/2$ .

**TABLE 8.3** CAPACITY  $C(d, \kappa)$  VERSUS RUNLENGTH PARAMETERS  $d$  AND  $\kappa$

$k$	$d = 0$	$d = 1$	$d = 2$	$d = 3$	$d = 4$	$d = 5$	$d = 6$
2	.8791	.4057					
3	.9468	.5515	.2878				
4	.9752	.6174	.4057	.2232			
5	.9881	.6509	.4650	.3218	.1823		
6	.9942	.6690	.4979	.3746	.2269	.1542	
7	.9971	.6793	.5174	.4057	.3142	.2281	.1335
8	.9986	.6853	.5293	.4251	.3432	.2709	.1993
9	.9993	.6888	.5369	.4376	.3620	.2979	.2382
10	.9996	.6909	.5418	.4460	.3746	.3158	.2633
11	.9998	.6922	.5450	.4516	.3833	.3285	.2804
12	.9999	.6930	.5471	.4555	.3894	.3369	.2924
12	.9999	.6935	.5485	.4583	.3937	.3432	.3011
14	.9999	.6938	.5495	.4602	.3968	.3478	.3074
15	.9999	.6939	.5501	.4615	.3991	.3513	.3122
$\infty$	1.000	.6942	.5515	.4650	.4057	.3620	.3282

Now, let us turn our attention to the construction of some runlength-limited codes. In general,  $(d, \kappa)$  codes can be constructed either as fixed-length codes or variable-length codes. In a fixed-length code, each bit or block of  $k$  bits, is encoded into a block of  $n > k$  bits.

In principle, the construction of a fixed-length code is straightforward. For a given block length  $n$ , we may select the subset of the  $2^n$  codewords that satisfy the specified runlength constraints. From this subset, we eliminate codewords that do not satisfy the runlength constraints when concatenated. Thus, we obtain a set of codewords that satisfies the constraints and can be used in the mapping of the input data bits to the encoder. The encoding and decoding operations can be performed by use of a look-up table.

**Example 8.5.3**

Construct a  $d = 0, \kappa = 2$  code of length  $n = 3$ , and determine its efficiency.

**Solution** By listing all the codewords, we find that the following five codewords satisfy the  $(0, 2)$  constraint:  $(0\ 1\ 0)$ ,  $(0\ 1\ 1)$ ,  $(1\ 0\ 1)$ ,  $(1\ 1\ 0)$ ,  $(1\ 1\ 1)$ . We may select any four of these codewords and use them to encode the pairs of data bits  $(00, 01, 10, 11)$ . Thus, we have a rate  $k/n = 2/3$  code that satisfies the  $(0, 2)$  constraint.

The fixed-length code in this example is not very efficient. The capacity of a  $(0, 2)$  code is  $C(0, 2) = 0.8791$ , so that this code has an *efficiency* of

$$\text{efficiency} = \frac{R_c}{C(d, \kappa)} = \frac{2/3}{0.8791} = 0.76$$

Surely, better  $(0, 2)$  codes can be constructed by increasing the block length  $n$ .

In the following example, we place no restriction on the maximum runlength zeros.

**Example 8.5.4**

Construct a  $d = 1, \kappa = \infty$  code of length  $n = 5$ .

**Solution** In this case, we are placing no constraint on the number of consecutive zeros. To construct the code we select from the set of 32 possible codewords, the ones that satisfy the  $d = 1$  constraint. There are eight such codewords, which implies that we can encode three information bits with each codeword. The code is given in Table 8.4. Note that the first bit of each codeword is a 0, whereas the last bit may be either 0 or 1. Consequently, the  $d = 1$  constraint is satisfied when these codewords are concatenated. This code has

**TABLE 8.4** FIXED LENGTH  $d = 1, \kappa = \infty$  CODE

Input data bits	Output coded sequence
000	00000
001	00001
010	00010
011	00100
100	00101
101	01000
110	01001
111	01010



a rate  $R_c = 3/5$ . When compared with the capacity  $C(1, \infty) = 0.6942$ , obtained from Table 8.3, the code efficiency is 0.864, which is quite acceptable.

The code construction method described in the two examples above produces fixed-length  $(d, \kappa)$  codes that are *state independent*. By “state independent,” we mean that fixed-length codewords can be concatenated without violating the  $(d, \kappa)$  constraints. In general, fixed-length, state-independent  $(d, \kappa)$  codes require large block lengths, except in cases such as those in the examples above, where  $d$  is small. Simpler (shorter-length) codes are generally possible by allowing for state-dependence and for variable-length codewords. Next, we consider codes for which both input blocks to the encoder and the output blocks may have variable length. In order for the codewords to be uniquely decodable at the receiver, the variable-length code should satisfy the prefix condition, previously described in Chapter 6.

#### Example 8.5.5

Construct a simple variable-length  $d = 0, \kappa = 2$  code.

**Solution** A very simple uniquely decodable  $(0, 2)$  code is the following:

$$\begin{aligned} 0 &\rightarrow 01 \\ 10 &\rightarrow 10 \\ 11 &\rightarrow 11 \end{aligned}$$

The code in the above example has a fixed output block size but a variable input block size. In general, both the input and output blocks may be variable. The following example illustrates the latter case.

#### Example 8.5.6

Construct a  $(2, 7)$  variable block size code.

**Solution** The solution to this code construction is certainly not unique nor is it trivial. We picked this example because the  $(2, 7)$  code has been widely used by IBM in many of its disk storage systems. The code is listed in Table 8.5. We observe that the input data blocks of 2, 3, and 4 bits are mapped into output data blocks of 4, 6, and 8 bits, respectively. Hence, the code rate is  $R_c = 1/2$ . Since this is the code rate for all codewords, the code is called a *fixed-rate* code. This code has an efficiency of  $0.5/0.5174 = 0.966$ . Note that this code satisfies the prefix condition.

**TABLE 8.5** CODE BOOK FOR VARIABLE-LENGTH (2,7) CODE

Input data bits	Output coded sequence
10	1000
11	0100
011	000100
010	001000
000	100100
0011	00100100
0010	00001000

**TABLE 8.6** ENCODER FOR (1, 3) MILLER CODE

Input data bits	Output coded sequence
0	$x0$
1	01

Another code that has been widely used in magnetic recording is the rate  $1/2$ ,  $(d, \kappa) = (1, 3)$  code given in Table 8.6. We observe that when the information bit is a 0, the first output bit is either 1, if the previous input bit was 0, or a 0, if the previous input bit was a 1. When the information bit is a 1, the encoder output is 01. Decoding of this code is simple. The first bit of the two-bit block is redundant and may be discarded. The second bit is the information bit. This code is usually called the *Miller code*. We observe that this is a state-dependent code which is described by the state diagram shown in Figure 8.20. There are two states labeled  $S_1$  and  $S_2$  with transitions as shown in the figure. When the encoder is a state  $S_1$ , an input bit 1 results in the encoder staying in state  $S_1$  and outputs 01. This is denoted as 1/01. If the input bit is a 0 the encoder enters state  $S_2$  and outputs 00. This is denoted as 0/00. Similarly, if the encoder is in state  $S_2$ , an input bit 0 causes no transition and the encoder output is 10. On the other hand, if the input bit is a 1, the encoder enters state  $S_1$  and outputs 01.

**Trellis Representation of State-Dependent  $(d, \kappa)$  Codes.** The state diagram provides a relatively compact representation of a state-dependent code. Another way to describe such codes that have memory is by means of a graph called a *trellis*. A trellis is a graph that illustrates the state transitions as a function of time. It consists of a set of nodes representing the states that characterize the memory in the code at different instants in time and interconnections between pairs of nodes that indicate the transitions between successive instants of time. For example, Figure 8.21 shows the trellis for the  $d = 1, \kappa = 3$  Miller code whose state diagram is shown in Figure 8.20.

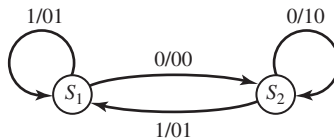


**Figure 8.20** State diagrams for  $d = 1, \kappa = 3$  (Miller) code.

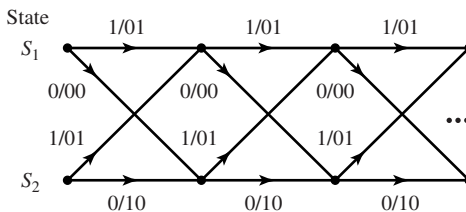


**Figure 8.21** Trellis for  $d = 1, \kappa = 3$  (Miller) code.

**The Mapping of Coded Bits Into Signal Waveforms.** The output sequence from a  $(d, \kappa)$  encoder is mapped by the modulator into signal waveforms for transmission over the channel. If the binary digit 1 is mapped into a rectangular pulse of amplitude  $A$  and the binary digit 0 is mapped into a rectangular pulse of amplitude  $-A$ , the result is a  $(d, \kappa)$ -coded NRZ modulated signal. We note that the duration of the rectangular pulses is  $T_c = R_c/R_b = R_c T_b$ , where  $R_b$  is the information (bit) rate into the encoder,  $T_b$  is the corresponding (uncoded) bit interval, and  $R_c$  is the code rate for the  $(d, \kappa)$  code.

When the  $(d, \kappa)$  code is a state-independent fixed-length code with code rate  $R_c = k/n$ , we may consider each  $n$ -bit block as generating one signal waveform of duration  $nT_c$ . Thus, we have  $M = 2^k$  signal waveforms, one for each of the  $2^k$  possible  $k$ -bit data blocks. These coded waveforms have the general form given by Equations (7.4.22) and (7.4.23). In this case, there is no dependence between the transmission of successive waveforms.

In contrast to the situation considered above, where the  $(d, \kappa)$  code is state independent and NRZ modulation is used for transmission of the coded bits, the modulation signal is no longer memoryless when NRZI is used and, or, the  $(d, \kappa)$  code is state dependent. Let us first consider the effect of mapping the coded bits into an NRZI signal waveform.

An NRZI modulated signal is itself state dependent. The signal-amplitude level is changed from its current value ( $\pm A$ ) only when the bit to be transmitted is a 1. It is interesting to note that the NRZI signal may be viewed as an NRZ signal preceded by another encoding operation, called *precoding*, of the binary sequence, as shown in Figure 8.22. The precoding operation is described mathematically by the relation

$$p_k = d_k \oplus p_{k-1}$$

where  $\{d_k\}$  is the binary sequence into the precoder,  $\{p_k\}$  is the output binary sequence from the precoder, and  $\oplus$  denotes modulo-2 addition. This type of encoding is called *differential encoding*, and is characterized by the state diagram shown in Figure 8.23(a). Then, the sequence  $\{p_k\}$  is transmitted by NRZ. Thus, when  $p_k = 1$ , the modulator output is a rectangular pulse of amplitude  $A$  and when  $p_k = 0$ , the modulator output is a rectangular pulse of amplitude  $-A$ . When the signal waveforms are superimposed on the state diagram of Figure 8.23(a), we obtain the corresponding state diagram shown in Figure 8.23(b).

It is apparent from the state diagram that differential encoding or precoding as described above introduces memory in the modulated signal. As in the case of state-dependent  $(d, \kappa)$  codes, a trellis diagram may be used to illustrate the time dependence of the modulated signal. The trellis diagram for the NRZI signal is shown in Figure 8.24. When the output of a state-dependent  $(d, \kappa)$  encoder is followed by an NRZI modulator, we may simply combine the two state diagrams into a single state diagram for the  $(d, \kappa)$

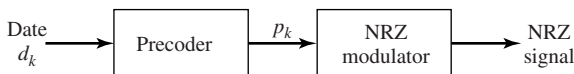


**Figure 8.22** Method for generating an NRZI signal using precoding.

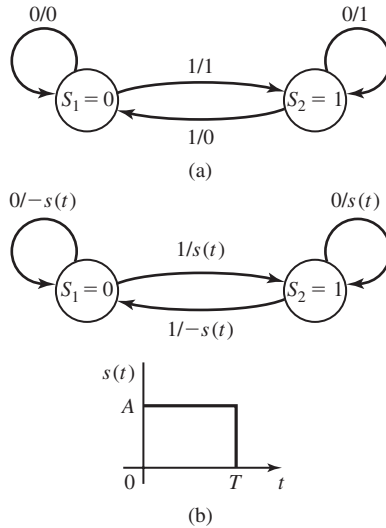


**Figure 8.23** State diagram for NRZI signal.

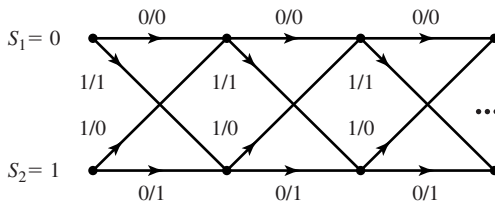


**Figure 8.24** The trellis for an NRZI signal.

code with precoding. A similar combination can be performed with the corresponding trellises. The following example illustrates the approach for the (1, 3) Miller code followed by NRZI modulation.

**Example 8.5.7**

Determine the state diagram of the combined (1, 3) Miller code followed by the precoding inherent in NRZI modulation.

**Solution** Since the (1, 3) Miller code has two states and the precoder has two states, the state diagram for the combined encoder has four states, which we denote as  $(S_M, S_N) = (\sigma_1, s_1), (\sigma_1, s_2), (\sigma_2, s_1), (\sigma_2, s_2)$ , where  $S_M = \{\sigma_1, \sigma_2\}$  represents the two states of the Miller code and  $S_N = \{s_1, s_2\}$  represents the two states of the precoder for NRZI. For each data input bit into the Miller encoder we obtain two output bits which are then precoded to yield two precoded output bits. The resulting state diagram is shown in Figure 8.25, where the first bit denotes the information bit into the Miller encoder and the next two bits represent the corresponding output of the precoder.

The trellis diagram for the Miller precoded sequence may be obtained directly from the combined state diagram or from a combination of the trellises of the two codes. The result of this combination is the four-state trellis, one stage of which is shown in Figure 8.26.

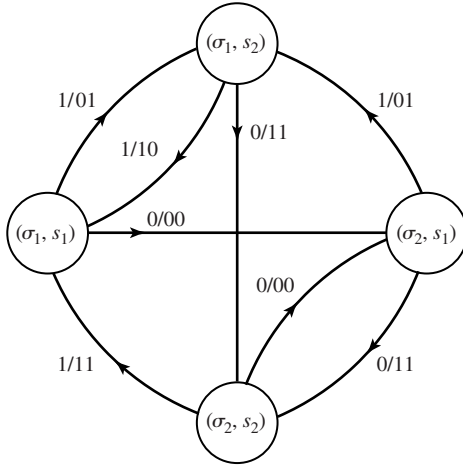


**Figure 8.25** State diagram of the Miller code followed by the precoder.

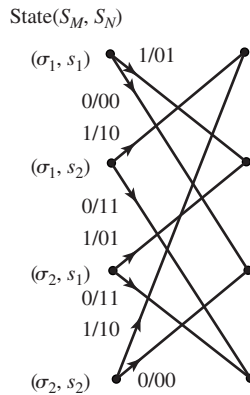


**Figure 8.26** One stage of trellis diagram for the Miller code followed by the precoder.

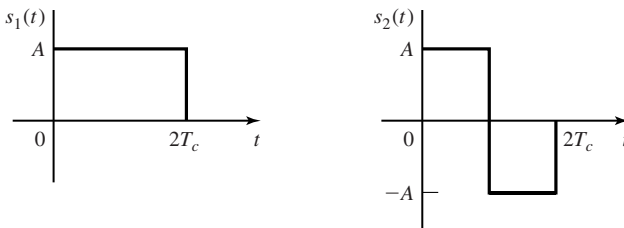


**Figure 8.27** Signal waveforms for Miller-precoded pairs of bits.

It is interesting to note that the four signal waveforms obtained by mapping each pair of bits of the Miller-precoded sequence into an NRZ signal are biorthogonal. In particular, the pair of bits 11 map into the waveform  $s_1(t)$  and the bits 01 map into the waveform  $s_2(t)$ , shown in Figure 8.27. Then, the encoded bits 00 map into  $-s_1(t)$  and the bits 10 map into  $-s_2(t)$ . Since  $s_1(t)$  and  $s_2(t)$  are orthogonal, the set of four waveforms constitute a biorthogonal set of  $M = 4$  waveforms. Hence, in the state

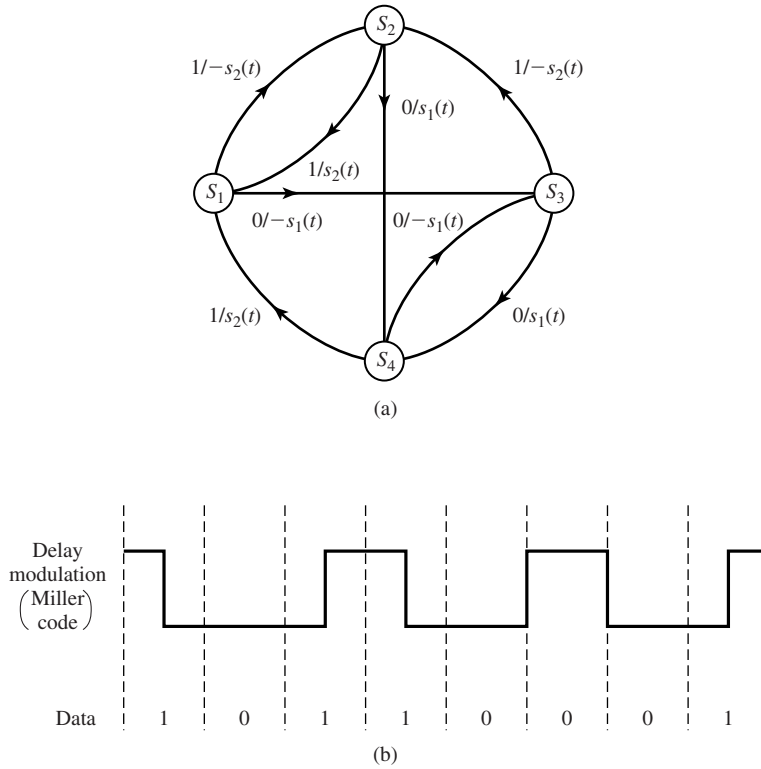


**Figure 8.28** State diagram for the Miller-precoded signal and sample waveform.

diagram for the Miller-precoded sequence we may substitute the signal waveforms from the modulator in place of the encoder output bits. This state diagram is illustrated in Figure 8.28, where the four states are simply designated as  $S_i$ ,  $1 \leq i \leq 4$ . The resulting modulated signal has also been called *delay modulation*.

Modulated signals with memory such as NRZI and Miller coded/NRZI (delay modulation) are generally characterized by a  $K$ -state Markov chain with *stationary state probabilities*  $\{p_i, i = 1, 2, \dots, K\}$ . Associated with each transition is a signal waveform  $s_j(t)$ ,  $j = 1, 2, \dots, K$ . Thus, the transition probability  $p_{ij}$  denotes the probability that signal waveform  $s_j(t)$  is transmitted in a given signaling interval after the transmission of the signal waveform  $s_i(t)$  in the previous signaling interval. The transition probabilities may be arranged in matrix form as

$$\mathbf{P} = \begin{bmatrix} p_{11} & p_{12} & \dots & p_{1K} \\ p_{21} & p_{22} & \dots & p_{2K} \\ \vdots & \vdots & \ddots & \vdots \\ p_{K1} & p_{K2} & \dots & p_{KK} \end{bmatrix} \quad (8.5.7)$$

where  $\mathbf{P}$  is the *transition probability matrix*. The transition probability matrix is easily obtained from the state diagram and the corresponding probabilities of occurrence of the input bits (or, equivalently, the stationary state probabilities  $\{p_i\}$ ).

For the NRZI signal with equal state probabilities  $p_1 = p_2 = 1/2$  and state diagram shown in Figure 8.23, the transition probability matrix is

$$\mathbf{P} = \begin{bmatrix} \frac{1}{2} & \frac{1}{2} \\ \frac{1}{2} & \frac{1}{2} \end{bmatrix} \quad (8.5.8)$$

Similarly, the transition probability matrix for the Miller-coded NRZI modulated signal with equally likely symbols ( $p_1 = p_2 = p_3 = p_4 = 1/4$ ) is

$$\mathbf{P} = \begin{bmatrix} 0 & \frac{1}{2} & 0 & \frac{1}{2} \\ 0 & 0 & \frac{1}{2} & \frac{1}{2} \\ \frac{1}{2} & \frac{1}{2} & 0 & 0 \\ \frac{1}{2} & 0 & \frac{1}{2} & 0 \end{bmatrix} \quad (8.5.9)$$

As we shall see later, in Section 8.5.4, the transition probability matrix is useful in determining the power-spectral density of a modulated signal with memory.

**Modulation Code for the Compact Disc System.** In the design of a modulation code for the compact disc system, several factors had to be considered. One constraint is that the maximum runlength of zeros must be sufficiently small to allow the system to synchronize from the readback signal. To satisfy this constraint,  $\kappa = 10$  was chosen. A second factor is the frequency content of the modulated signal below 20 kHz. In a CD system, the servo-control systems that keep the laser beam on a specified track and the focusing circuits are controlled by signals in the frequency range 0–20 kHz. To avoid interference with these control signals, the modulated information signal must fall above this frequency range. The runlength-limited code that was implemented for this purpose is a  $(d, \kappa) = (2, 10)$  code that results in a coded information-bearing signal that occupies the frequency range 20 kHz to 1.5 MHz.

The  $d = 2, \kappa = 10$  code selected is a fixed-length code that encodes eight information bits into 14 coded bits and is called EFM (eight-to-fourteen modulation). Since each audio signal sample is quantized to 16 bits, a 16-bit sample is divided into two 8-bit bytes and encoded. By enumerating all the 14-bit codewords, one can show that there are 267 distinct codewords that satisfy the  $(d, \kappa)$  constraints. Of these, 256 codewords are selected to form the code. However, the  $(d, \kappa)$  constraints are not satisfied when the codewords are concatenated (merged in a sequence). To remedy this problem, three additional bits are added to the 14, called “merging” bits. The three merging bits serve two purposes. First of all, if the  $d$ -constraint is not satisfied in concatenation, we choose 0’s for the merging bits. On the other hand, if the  $\kappa$ -constraint is being violated due to concatenation, we select one of the bits as 1. Since two bits are sufficient to accomplish these goals, the third merging bit may be viewed as an added

degree of freedom. This added degree of freedom allows us to use the merging bits to minimize the low-frequency content of the modulated signal. Since the merging bits carry no audio signal information, they are discarded in the readback process prior to decoding.

A measure of the low-frequency content of a digital modulated signal is the *running digital sum* (RDS), which is the difference between the total zeros and the total ones in the coded sequence accumulated from the beginning of the disc. In addition to satisfying the  $(d, \kappa)$  constraints, the three merging bits are selected so as to bring the RDS as close to zero as possible. Thus, the three merging bits are instrumental in reducing the low-frequency content below 20 kHz by an additional factor of 10 (in power).

In addition to the coded information bits and merging bits, additional bits are added for control and display (C & D), synchronization bits, and parity bits. The data bits, control bits, parity bits, and synchronization bits are arranged in a frame structure, consisting of 588 bits/frame. The frame structure is illustrated in Figure 8.29.

### 8.5.2 The Maximum-Likelihood Sequence Detector

When the signal has no memory, the symbol-by-symbol detector described in Section 7.5 is optimum in the sense of minimizing the probability of a symbol error. On the other hand, when the transmitted signal has memory; i.e., the signals transmitted in successive symbol intervals are interdependent, the optimum detector bases its decisions on observation of a sequence of received signals over successive signal intervals.

Consider as an example the NRZI signal described in Section 8.5.1. Its memory is characterized by the trellis shown in Figure 8.24. The signal transmitted in each signal interval is binary PAM. Hence, there are two possible transmitted signals corresponding to the signal points  $s_1 = -s_2 = \sqrt{\mathcal{E}_b}$ , where  $\mathcal{E}_b$  is the energy/bit. As shown in Section 7.5, the output of the matched-filter or correlation-type demodulator for binary PAM in the  $k$ th signal interval may be expressed as

$$r_k = \pm\sqrt{\mathcal{E}_b} + n_k \quad (8.5.10)$$

where  $n_k$  is a zero-mean Gaussian random variable with variance  $\sigma_n^2 = N_0/2$ . Consequently, the conditional PDFs for the two possible transmitted signals are

$$\begin{aligned} f(r_k | s_1) &= \frac{1}{\sqrt{2\pi}\sigma_n} e^{-(r_k - \sqrt{\mathcal{E}_b})^2/2\sigma_n^2} \\ f(r_k | s_2) &= \frac{1}{\sqrt{2\pi}\sigma_n} e^{-(r_k + \sqrt{\mathcal{E}_b})^2/2\sigma_n^2} \end{aligned} \quad (8.5.11)$$

Now, suppose we observe the sequence of matched-filter outputs  $r_1, r_2, \dots, r_K$ . Since the channel noise is assumed to be white and Gaussian, and  $\psi(t - iT), \psi(t - jT)$  for  $i \neq j$  are orthogonal, it follows that  $E(n_k n_j) = 0, k \neq j$ . Hence, the noise sequence  $n_1, n_2, \dots, n_k$  is also white. Consequently, for any given transmitted sequence  $\mathbf{s}^{(m)}$ , the



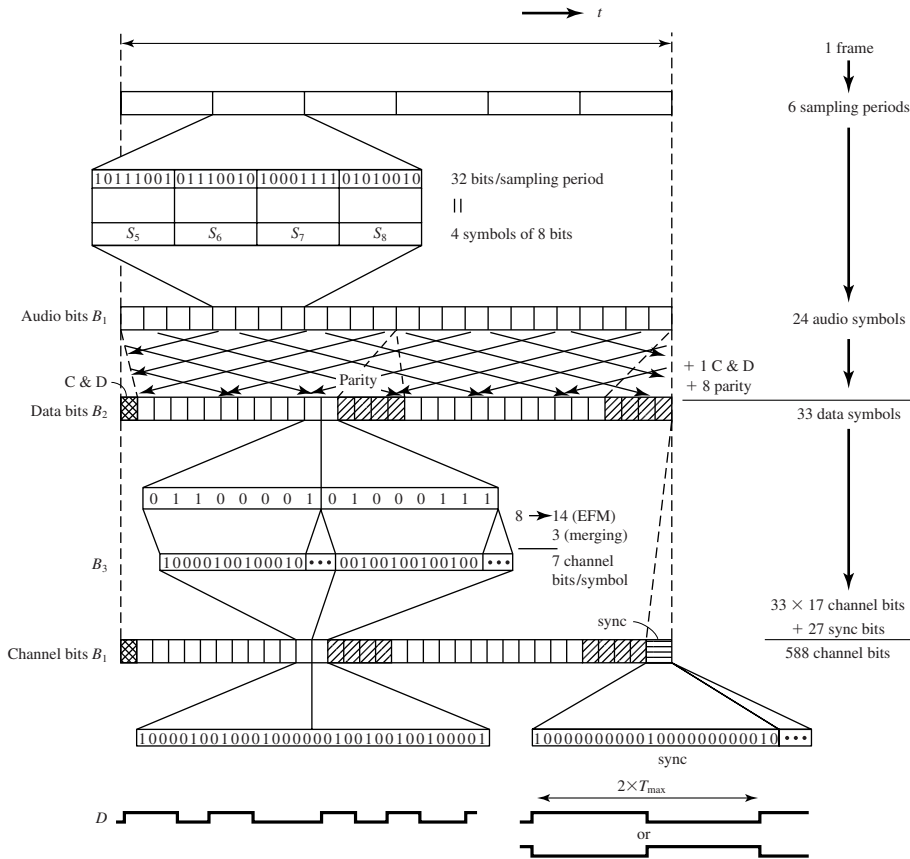


**Figure 8.29** Frame structure of data in a compact disc. The information is divided into frames; the figure gives one frame of the successive bit streams. There are six sampling periods for one frame, each sampling period giving 32 bits (16 for each of the two audio channels). These 32 bits are divided to make four symbols in the “audio bit stream”  $B_1$ . In the “data bit stream,”  $B_2$  eight parity symbols and one C & D symbol have been added to the 24 audio symbols. To scatter possible errors, the symbols of different frames in  $B_1$  are interleaved, so that the audio signals in one frame of  $B_2$  originate from different frames in  $B_1$ . The modulation translated the eight data bits of a symbol of  $B_2$  into fourteen channel bits, to which three ‘merging bits’ are added ( $B_3$ ). The frames are marked with a synchronization signal of the form illustrated (bottom right); the final result is the “channel bit stream” ( $B_1$ ) used for writing on the master disc, in such a way that each 1 indicates a pit edge ( $D$ ). (From paper by Heemskerk and Schouhamer Immink, 1982.)

joint PDF of  $r_1, r_2, \dots, r_K$  may be expressed as a product of  $k$  marginal PDFs; i.e.,

$$\begin{aligned} p(r_1, r_2, \dots, r_K | \mathbf{s}^{(m)}) &= \prod_{k=1}^K p(r_k | s_k^{(m)}) \\ &= \prod_{k=1}^K \frac{1}{\sqrt{2\pi}\sigma_n} e^{(r_k - s_k^{(m)})^2 / 2\sigma_n^2} \\ &= \left( \frac{1}{\sqrt{2\pi}\sigma_n} \right)^K \exp \left[ - \sum_{k=1}^K (r_k - s_k^{(m)})^2 / 2\sigma_n^2 \right] \end{aligned} \quad (8.5.12)$$

where either  $s_k = \sqrt{\mathcal{E}_b}$  or  $s_k = -\sqrt{\mathcal{E}_b}$ . Then, given the received sequence  $r_1, r_2, \dots, r_K$  at the output of the matched-filter or correlation-type demodulator, the detector determines the sequence  $\mathbf{s}^{(m)} = \{s_1^{(m)}, s_2^{(m)}, \dots, s_K^{(m)}\}$  that maximizes the conditional PDF  $p(r_1, r_2, \dots, r_K | \mathbf{s}^{(m)})$ . Such a detector is called the *maximum-likelihood (ML) sequence detector*.

By taking the logarithm of Equation (8.5.12) and neglecting the terms that are independent of  $(r_1, r_2, \dots, r_K)$  we find that an equivalent ML sequence detector selects the sequence  $\mathbf{s}^{(m)}$  that minimizes the *Euclidean distance metric*

$$D(\mathbf{r}, \mathbf{s}^{(m)}) = \sum_{k=1}^K (r_k - s_k^{(m)})^2 \quad (8.5.13)$$

In searching through the trellis for the sequence that minimizes the Euclidean distance  $D(\mathbf{r}, \mathbf{s}^{(m)})$ , it may appear that we must compute the distance  $D(\mathbf{r}, \mathbf{s}^{(m)})$  for every possible path (sequence). For the NRZI example given above, which employs binary modulation, the total number of paths is  $2^K$ , where  $K$  is the number of outputs obtained from the demodulator. However, this is not the case. We may reduce the number of sequences in the trellis search by using the *Viterbi algorithm* to eliminate sequences as new data is received from the demodulator.

The Viterbi algorithm is a sequential trellis search algorithm for performing ML sequence detection. It is described in more detail in Chapter 9 as a decoding algorithm for channel-coded systems. We describe it below in the context of the NRZI signal. We assume that the search process begins initially at state  $S_1$ . The corresponding trellis is shown in Figure 8.30. At time  $t = T$ , we receive  $r_1 = s_1^{(m)} + n$ , from the demodulator

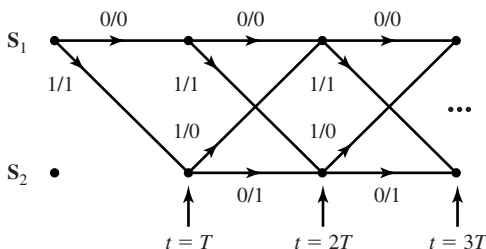


**Figure 8.30** Trellis for NRZI signal with initial state  $S_1$ .

and at  $t = 2T$  we receive  $r_2 = s_2^{(m)} + n_2$ . Since the signal memory is one bit, which we denote as  $L = 1$ , we observe that the trellis reaches its regular (steady-state) form after the first transition. Thus, upon receipt of  $r_2$  at  $t = 2T$  (and thereafter), we observe that there are two signal paths entering each of the two nodes and two signal paths leaving each node. The two paths entering node  $S_1$  at  $t = 2T$  correspond to the information bits  $(0, 0)$  and  $(1, 1)$  or, equivalently, to the signal points  $(-\sqrt{\mathcal{E}_b}, -\sqrt{\mathcal{E}_b})$  and  $(\sqrt{\mathcal{E}_b}, -\sqrt{\mathcal{E}_b})$ , respectively. The two paths entering node  $S_2$  at  $t = 2T$  correspond to the information bits  $(0, 1)$  and  $(1, 0)$  or, equivalently, to the signal points  $(-\sqrt{\mathcal{E}_b}, \sqrt{\mathcal{E}_b})$  and  $(\sqrt{\mathcal{E}_b}, \sqrt{\mathcal{E}_b})$ , respectively.

For the two paths entering node  $S_1$ , we compute the two Euclidean distance metrics

$$\begin{aligned}\mu_2(0, 0) &= (r_1 + \sqrt{\mathcal{E}_b})^2 + (r_2 + \sqrt{\mathcal{E}_b})^2 \\ \mu_2(1, 1) &= (r_1 - \sqrt{\mathcal{E}_b})^2 + (r_2 + \sqrt{\mathcal{E}_b})^2\end{aligned}\tag{8.5.14}$$

by using the outputs  $r_1$  and  $r_2$  from the demodulator. The Viterbi algorithm compares these two metrics and discards the path having the larger (greater distance) metric. The other path with the lower metric is saved and is called the *survivor* at  $t = 2T$ . The elimination of one of the two paths may be done without compromising the optimality of the trellis search, because any extension of the path with the larger distance beyond  $t = 2T$  will always have a larger metric than the survivor that is extended along the same path beyond  $t = 2T$ .

Similarly, for the two paths entering node  $S_2$  at  $t = 2T$ , we compute the two Euclidean distance metrics

$$\begin{aligned}\mu_2(0, 1) &= (r_1 + \sqrt{\mathcal{E}_b})^2 + (r_2 - \sqrt{\mathcal{E}_b})^2 \\ \mu_2(1, 0) &= (r_1 - \sqrt{\mathcal{E}_b})^2 + (r_2 - \sqrt{\mathcal{E}_b})^2\end{aligned}\tag{8.5.15}$$

by using the outputs  $r_1$  and  $r_2$  from the demodulator. The two metrics are compared and the signal path with the larger metric is eliminated. Thus, at  $t = 2T$ , we are left with two survivor paths, one at node  $S_1$  and the other at node  $S_2$ , and their corresponding metrics. The signal paths at nodes  $S_1$  and  $S_2$  are then extended along the two survivor paths.

Upon receipt of  $r_3$  at  $t = 3T$ , we compute the metrics of the two paths entering state  $S_1$ . Suppose the survivors at  $t = 2T$  are the paths  $(0, 0)$  at  $S_1$  and  $(0, 1)$  at  $S_2$ . Then, the two metrics for the paths entering  $S_1$  at  $t = 3T$  are

$$\begin{aligned}\mu_3(0, 0, 0) &= \mu_2(0, 0) + (r_3 + \sqrt{\mathcal{E}_b})^2 \\ \mu_3(0, 1, 1) &= \mu_2(0, 1) + (r_3 + \sqrt{\mathcal{E}_b})^2\end{aligned}\tag{8.5.16}$$

These two metrics are compared and the path with the larger (distance) metric is eliminated. Similarly, the metrics for the two paths entering  $S_2$  at  $t = 3T$  are

$$\begin{aligned}\mu_3(0, 0, 1) &= \mu_2(0, 0) + (r_3 - \sqrt{\mathcal{E}_b})^2 \\ \mu_3(0, 1, 0) &= \mu_2(0, 1) + (r_3 - \sqrt{\mathcal{E}_b})^2\end{aligned}\tag{8.5.17}$$

These two metrics are compared and the path with the larger (distance) metric is eliminated.

This process is continued as each new signal sample is received from the demodulator. Thus, the Viterbi algorithm computes two metrics for the two signal paths entering a node at each stage of the trellis search and eliminates one of the two paths at each node. The two survivor paths are then extended forward to the next stage. Therefore, the number of paths searched in the trellis is reduced by a factor of two at each stage.

It is relatively easy to generalize the trellis search performed by the Viterbi algorithm for  $M$ -ary modulation. For example, delay modulation employs  $M = 4$  signals and is characterized by the four-state trellis shown in Figure 8.26. We observe that each state has two signal paths entering and two signal paths leaving each node. The memory of the signal is  $L = 1$ . Hence, the Viterbi algorithm will have four survivors at each stage and their corresponding metrics. Two metrics corresponding to the two entering paths are computed at each node and one of the two signal paths entering the node is eliminated at each state of the trellis. Thus, the Viterbi algorithm minimizes the number of trellis paths searched in performing ML sequence detection.

From the description of the Viterbi algorithm given above, it is unclear as to how decisions are made on the individual detected information symbols given the surviving sequences. If we have advanced to some stage, say  $K$ , where  $K \gg L$ , in the trellis and we compare the surviving sequences, we will find that, with probability approaching one, all surviving sequences will be identical in bit (or symbol) positions  $K - 5L$  and less. In a practical implementation of the Viterbi algorithm, decisions on each information bit (or symbol) are forced after a delay of  $5L$  bits (or symbols) and, hence, the surviving sequences are truncated to the  $5L$  most recent bits (or symbols). Thus, a variable delay in bit or symbol detection is avoided. The loss in performance resulting from the suboptimum detection procedure is negligible if the delay is at least  $5L$ .

#### Example 8.5.8

Describe the decision rule for detecting the data sequence in an NRZI signal with a Viterbi algorithm having a delay of  $5L$  bits.

**Solution** The trellis for the NRZI signal is shown in Figure 8.30. In this case  $L = 1$ , hence the delay in bit detection is set to 5 bits. Hence, at  $t = 6T$ , we will have two surviving sequences, one for each of the two states, and the corresponding metrics  $\mu_6(b_1, b_2, b_3, b_4, b_5, b_6)$  and  $\mu_6(b'_1, b'_2, b'_3, b'_4, b'_5, b'_6)$ . At this stage, with probability nearly equal to one the bit  $b_1$  will be the same as  $b'_1$ ; i.e., both surviving sequences will have a common first branch. If  $b_1 \neq b'_1$ , we may select the bit ( $b_1$  or  $b'_1$ ) corresponding to the smaller of the two metrics. Then the first bit is dropped from the two surviving sequences. At  $t = 7T$ , the two metrics  $\mu_7(b_2, b_3, b_4, b_5, b_6, b_7)$  and  $\mu_7(b'_2, b'_3, b'_4, b'_5, b'_6, b'_7)$  will be used to determine the decision on bit  $b_2$ . This process continues at each stage of the search through the trellis for the minimum distance sequence. Thus the detection delay is fixed at 5 bits.

### 8.5.3 Maximum-Likelihood Sequence Detection of Partial Response Signals

It is clear from our previous discussion that partial response waveforms are signal waveforms with memory. This memory is conveniently represented by a trellis. For example, the trellis for the duobinary partial response signal for binary data transmission is illustrated in Figure 8.31. For binary modulation, this trellis contains two states,

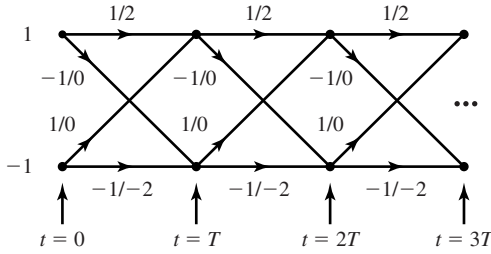


**Figure 8.31** Trellis for duobinary partial response signal.

corresponding to the two possible input values of  $a_m$ ; i.e.,  $a_m = \pm 1$ . Each branch in the trellis is labeled by two numbers. The first number on the left is the new data bit; i.e.,  $a_{m+1} = \pm 1$ . This number determines the transition to the new state. The number on the right is the received signal level.

The duobinary signal has a memory of length  $L = 1$ . Hence, for binary modulation the trellis has  $S_t = 2^L$  states. In general, for  $M$ -ary modulation, the number of trellis states is  $M^L$ .

The optimum ML sequence detector selects the most probable path through the trellis upon observing the received data sequence  $\{y_m\}$  at the sampling instants  $t = mT$ ,  $m = 1, 2, \dots$ . In general, each node in the trellis will have  $M$  incoming paths and  $M$  corresponding metrics. One out of the  $M$  incoming paths is selected as the most probable, based on the values of the metrics and the other  $M - 1$  paths and their metrics, are discarded. The surviving path at each node is then extended to  $M$  new paths, one for each of the  $M$  possible input symbols, and the search process continues. This is basically the Viterbi algorithm for performing the trellis search.

For the class of partial response signals, the received sequence  $\{y_m, 1 \leq m \leq N\}$  is generally described statistically by the joint PDF  $f(\mathbf{y}_N | \mathbf{a}_N)$ , where  $\mathbf{y}_N = (y_1, y_2, \dots, y_N)^t$  and  $\mathbf{a}_N = (a_1, a_2, \dots, a_N)^t$  and  $N > L$ . When the additive noise is zero-mean Gaussian,  $f(\mathbf{y}_N | \mathbf{a}_N)$  is a multivariate Gaussian PDF; i.e.,

$$f(\mathbf{y}_N | \mathbf{a}_N) = \frac{1}{(2\pi^{N/2})|\det(\mathbf{C})|^{1/2}} e^{-\frac{1}{2}(\mathbf{y}_N - \mathbf{b}_N)^t \mathbf{C}^{-1}(\mathbf{y}_N - \mathbf{b}_N)} \quad (8.5.18)$$

where  $\mathbf{b}_N = (b_1, b_2, \dots, b_N)^t$  is the mean of the vector  $\mathbf{y}_N$  and  $\mathbf{C}$  is the  $N \times N$  covariance matrix of  $\mathbf{y}_N$ . Then, the maximum-likelihood sequence detector selects the sequence through the trellis that maximizes the PDF  $f(\mathbf{y}_N | \mathbf{a}_N)$ .

The computations for finding the most probable sequence through the trellis is simplified by taking the natural logarithms of  $f(\mathbf{y}_N | \mathbf{a}_N)$ . Thus,

$$\ln f(\mathbf{y}_N | \mathbf{a}_N) = -\frac{N}{2} \ln(2\pi) - \frac{1}{2} \ln |\det(\mathbf{C})| - (\mathbf{y}_N - \mathbf{b}_N)^t \mathbf{C}^{-1}(\mathbf{y}_N - \mathbf{b}_N)/2 \quad (8.5.19)$$

Given the received sequence  $\{y_m\}$ , the data sequence  $\{a_m\}$  that maximizes  $\ln f(\mathbf{y}_N | \mathbf{a}_N)$  is identical to the sequence  $\{a_m\}$  that minimizes  $(\mathbf{y}_N - \mathbf{b}_N)^t \mathbf{C}^{-1}(\mathbf{y}_N - \mathbf{b}_N)$ ; i.e.,

$$\hat{\mathbf{a}}_N = \arg \min_{\mathbf{a}_N} (\mathbf{y}_N - \mathbf{b}_N)^t \mathbf{C}^{-1}(\mathbf{y}_N - \mathbf{b}_N) \quad (8.5.20)$$

The search through the trellis for the minimum distance path may be performed sequentially by use of the Viterbi algorithm. Let us consider the duobinary signal waveform with binary modulation and suppose that we begin at the initial state with  $a_0 = 1$ . Then upon receiving  $y_1 = a_1 + a_0 + v_1$  at time  $t = T$  and  $y_2 = a_2 + a_1 + v_2$  at time  $t = 2T$ , we have four candidate paths, corresponding to  $(a_1, a_2) = (1, 1), (-1, 1), (1, -1)$  and  $(-1, -1)$ . The first two candidate paths merge at state 1 at  $t = 2T$ . For the two paths merging at state 1, we compute the metrics  $\mu_2(1, 1)$  and  $\mu_2(-1, 1)$  and select the more probable path. A similar computation is performed at state  $-1$  for the two sequences  $(1, -1)$  and  $(-1, -1)$ . Thus, one of the two sequences at each node is saved and the other is discarded. The trellis search continues upon receipt of the signal sample  $y_3$  at time  $t = 3T$ , by extending the two surviving paths from time  $t = 2T$ .

The metric computations are complicated by the correlation of the noise samples at the output of the matched filter for the partial response signal. For example, in the case of the duobinary signal waveform, the correlation of the noise sequence  $\{v_m\}$  is over two successive signal samples. Hence,  $v_m$  and  $v_{m+k}$  are correlated for  $k = 1$  and uncorrelated for  $k > 1$ . In general, a partial response signal waveform with memory  $L$  will result in a correlated noise sequence at the output of the matched filter, which satisfies the condition  $E(v_m v_{m+k}) = 0$  for  $k > L$ . Ungerboeck (1974) described a sequential trellis search (Viterbi) algorithm for correlated noise (see Problem 8.26).

Some simplification in the metric computations results if we ignore the noise correlation by assuming that  $E(v_m v_{m+k}) = 0$  for  $k > 0$ . Then, by assumption the covariance matrix  $\mathbf{C} = \sigma_v^2 \mathbf{I}$  where  $\sigma_v^2 = E(v_m^2)$  and  $\mathbf{I}$  is the  $N \times N$  identity matrix. In this case, Equation (8.5.20) simplifies to

$$\begin{aligned} \hat{\mathbf{a}}_N &= \arg \min_{\mathbf{a}_N} [(\mathbf{y}_N - \mathbf{b}_N)^t (\mathbf{y}_N - \mathbf{b}_N)] \\ &= \arg \min_{\mathbf{a}_N} \left[ \sum_{m=1}^N \left( y_m - \sum_{k=0}^L x_k a_{m-k} \right)^2 \right] \end{aligned} \quad (8.5.21)$$

where

$$b_m = \sum_{k=0}^L x_k a_{m-k} \quad (8.5.22)$$

and  $x_k = x(kT)$  are the sampled values of the partial response signal waveform. In this case, the metric computations at each node of the trellis have the form

$$\mu_m(\mathbf{a}_m) = \mu_{m-1}(\mathbf{a}_{m-1}) + \left( y_m - \sum_{k=0}^L x_k a_{m-k} \right)^2 \quad (8.5.23)$$

where  $\mu_m(\mathbf{a}_m)$  are the metrics at time  $t = mT$ ,  $\mu_{m-1}(\mathbf{a}_{m-1})$  are the metrics at time  $t = (m-1)T$  and the second term on the right-hand side of Equation (8.5.23) are the new increments to the metrics based on the new received samples  $y_m$ .

As previously indicated in Section 8.5.2, ML sequence detection introduces a variable delay in detecting each transmitted information symbol. In practice, the variable

delay is avoided by truncating the surviving sequences to  $N_t$  most recent symbols, where  $N_t \gg 5L$ , thus achieving a fixed delay. In case the  $M^L$  surviving sequences at time  $t = mT$  disagree on the symbol  $a_{m-N_t}$ , the symbol in the most probable surviving sequence may be chosen. The loss in performance resulting from this truncation is negligible if  $N_t > 5L$ .

**Example 8.5.9**

For the duobinary partial response signal, express the metric computations performed at  $t = 2T$  and  $t = 3T$ , based on the received signal samples  $y_m = b_m + v_m$  for  $m = 1, 2, 3$ , where the noise correlation is ignored.

**Solution** The metrics are generally given by Equation (8.5.23). Upon receipt of  $y_1$  and  $y_2$  and with  $a_0 = 1$ , the metrics for the two paths merging at state 1 are

$$\begin{aligned}\mu_2(1, 1) &= (y_1 - 2)^2 + (y_2 - 2)^2 \\ \mu_2(-1, 1) &= y_1^2 + y_2^2\end{aligned}$$

If  $\mu_2(1, 1) < \mu_2(-1, 1)$  we select the path  $(1, 1)$  as the more probable and discard  $(-1, 1)$ . Otherwise, we select the path  $(-1, 1)$  and discard the path  $(1, 1)$ . The path with the smaller metric is called the survivor and the sequence  $(a_1, a_2)$  and the corresponding metric are saved.

A similar computation is performed at state  $-1$  for the sequences  $(1, -1)$  and  $(-1, -1)$ . Then, we have

$$\begin{aligned}\mu_2(1, -1) &= (y_1 - 2)^2 + y_2^2 \\ \mu_2(-1, -1) &= y_1^2 + (y_2 + 2)^2\end{aligned}$$

We compare the metrics  $\mu_2(1, -1)$  and  $\mu_2(-1, -1)$  and select the sequence with the smaller metric.

Upon receipt of  $y_3$  at  $t = 3T$ , we consider the extensions of the survivor paths. Suppose that the two survivor paths are  $(a_1, a_2) = (1, 1)$  and  $(a_1, a_2) = (1, -1)$ . Then, at state 1 (at  $t = 3T$ ) we have the two merging paths  $(a_1, a_2, a_3) = (1, 1, 1)$  and  $(1, -1, 1)$ . Their corresponding metrics are

$$\begin{aligned}\mu_3(1, 1, 1) &= \mu_2(1, 1) + (y_3 - 2)^2 \\ \mu_3(1, -1, 1) &= \mu_2(1, -1) + y_3^2\end{aligned}$$

We compare the metrics for these two merging paths and select the path with the smaller metric as the survivor.

Similarly, at state  $-1$  (at  $t = 3T$ ), we have the two merging paths  $(1, 1, -1)$  and  $(1, -1, -1)$ , and their corresponding metrics

$$\begin{aligned}\mu_3(1, 1, -1) &= \mu_2(1, 1) + y_3^2 \\ \mu_3(1, -1, -1) &= \mu_2(1, -1) + (y_3 + 2)^2\end{aligned}$$

We select the path with the smaller metric as the survivor at state  $-1$ . This process continues upon receipt of additional data at  $t = kT$ ,  $k = 4, 5, \dots$

**Error Probability of the Maximum-Likelihood Sequence Detector.** In general, the computation of the exact probability of error is extremely difficult. Instead,

we shall determine an approximation to the probability of error, which is based on comparing the metrics of two paths which merge at a node and which are separated by the smallest Euclidean distance of all other paths. Our derivation is performed for the duobinary partial response signal waveform.

Let us consider the trellis for the duobinary partial response signal shown in Figure 8.31. We assume that we start in state 1 at  $t = 0$  and that the first two transmitted symbols are  $a_1 = 1$  and  $a_2 = 1$ . Then, at  $t = T$  we receive  $y_1 = 2d + v_1$  and at  $t = 2T$  we receive  $y_2 = 2d + v_2$ . An error is made at state 1 if the path  $(a_1, a_2) = (-1, 1)$  is more probable than the path  $(a_1, a_2) = (1, 1)$ , given the received values of  $y_1$  and  $y_2$ . This path error event is the dominant path error event and, hence, it serves as a good approximation to the probability of error for the ML sequence detector.

We recall that the metric for the path  $(a_1, a_2) = (1, 1)$  is

$$\mu_2(1, 1) = [y_1 - 2d \quad y_2 - 2d] \mathbf{C}^{-1} \begin{bmatrix} y_1 - 2d \\ y_2 - 2d \end{bmatrix} \quad (8.5.24)$$

where the covariance matrix  $\mathbf{C}$  is given by (see Problem 8.30)

$$\mathbf{C} = \frac{2N_0}{\pi} \begin{bmatrix} 1 & \frac{1}{3} \\ \frac{1}{3} & 1 \end{bmatrix} \quad (8.5.25)$$

For the path  $(a_1, a_2) = (-1, 1)$ , the corresponding metric is

$$\mu_2(-1, 1) = [y_1 \quad y_2] \mathbf{C}^{-1} \begin{bmatrix} y_1 \\ y_2 \end{bmatrix} \quad (8.5.26)$$

The probability of a path error event is simply the probability that the metric  $\mu_2(-1, 1)$  is smaller than the metric  $\mu_2(1, 1)$ ; i.e.,

$$P_2 = P[\mu_2(-1, 1) < \mu_2(1, 1)] \quad (8.5.27)$$

By substituting  $y_1 = 2d + v_1$  and  $y_2 = 2d + v_2$  into Equations (8.5.24) and (8.5.26) we find that

$$P_2 = P(v_1 + v_2 < -2d) \quad (8.5.28)$$

Since  $v_1$  and  $v_2$  are zero-mean (correlated) Gaussian variables, their sum is also zero-mean Gaussian. The variance of the sum  $z = v_1 + v_2$  is simply  $\sigma_z^2 = 16N_0/3\pi$ . Therefore,

$$P_2 = P(z < -2d) = Q\left(\frac{2d}{\sigma_z}\right) = Q\left(\sqrt{\frac{4d^2}{\sigma_z^2}}\right) \quad (8.5.29)$$

From Equation (8.4.32) we have (with  $M = 2$ ) the expression for  $d^2$  as

$$d^2 = \frac{\pi P_{av} T}{4} = \frac{\pi \mathcal{E}_b}{4} \quad (8.5.30)$$



Hence, the probability of the path error event is

$$P_2 = Q\left(\sqrt{\frac{1.5\pi^2}{16} \left(\frac{2\mathcal{E}_b}{N_0}\right)}\right) \quad (8.5.31)$$

First, we note that this path error event results in one bit-error in the sequence of two bits. Hence, the bit-error probability is  $P_2/2$ . Second, there is a reduction in SNR of  $10\log(1.5\pi^2/16) = -0.34$  dB relative to the case of no intersymbol interference. This small SNR degradation is apparently the penalty incurred in exchange for the bandwidth efficiency of the partial response signal. Finally, we observe that the ML sequence detector has gained back 1.76 dB of the 2.1 dB degradation inherent in the symbol-by-symbol detector.

### 8.5.4 The Power Spectrum of Digital Signals with Memory

In Section 8.5.1, we demonstrated that state-dependent modulation codes resulted in modulated signals with memory. Such signals were described by Markov chains which are basically graphs that include the possible “states” of the modulator with corresponding state probabilities  $\{p_i\}$ , and state transitions with corresponding state transition probabilities  $\{p_{ij}\}$ .

The power-spectral density of digitally modulated signals that are characterized by Markov chains may be derived by following the basic procedure given in Section 8.2. Thus, we may determine the autocorrelation function and then evaluate its Fourier transform to obtain the power-spectral density. For signals that are generated by a Markov chain with transition probability matrix  $\mathbf{P}$ , as generally given by Equation (8.5.7), the power-spectral density of the modulated signal may be expressed in the general form

$$\begin{aligned} \mathcal{S}(f) = & \frac{1}{T^2} \sum_{n=-\infty}^{\infty} \left| \sum_{i=1}^K p_i S_i\left(\frac{n}{T}\right) \right|^2 \delta\left(f - \frac{n}{T}\right) + \frac{1}{T} \sum_{i=1}^K p_i |S'_i(f)|^2 \\ & + \frac{2}{T} \operatorname{Re} \left[ \sum_{i=1}^K \sum_{j=1}^K p_i S_i^*(f) S'_j(f) P_{ij}(f) \right] \end{aligned} \quad (8.5.32)$$

where  $K$  is the number of states of the modulator,  $S_i(f)$  is the Fourier transform of the signal waveform  $s_i(t)$ ,  $S'_i(f)$  is the Fourier transform of  $s'_i(t)$ , where  $s'_i(t) = s_i(t) - \sum_{k=1}^K p_k s_k(t)$ , and  $P_{ij}(f)$  is the Fourier transform of the discrete-time sequence  $p_{ij}(n)$ , defined as

$$P_{ij}(f) = \sum_{n=1}^{\infty} p_{ij}(n) e^{-j2\pi n f T} \quad (8.5.33)$$

The term  $p_{ij}(n)$  denotes the probability that a signal  $s_j(t)$  is transmitted  $n$  signaling intervals after the transmission of  $s_i(t)$ . Hence,  $\{p_{ij}(n)\}$  are the transition probabilities in the transition probability matrix  $\mathbf{P}^n$ . Note that when  $n = 1$ ,  $\mathbf{P}^n \equiv \mathbf{P}$ , which is the matrix given by Equation (8.5.7).

**Example 8.5.10**

Determine the power-spectral density of the NRZI signal.

**Solution** The NRZI signal is characterized by the transition probability matrix

$$\mathbf{P} = \begin{bmatrix} \frac{1}{2} & \frac{1}{2} \\ \frac{1}{2} & \frac{1}{2} \end{bmatrix}$$

We note that  $\mathbf{P}^n = \mathbf{P}$  for all  $n > 1$ . Hence, with  $K = 2$  states and  $g_T(t) = s_1(t) = -s_2(t)$ , we obtain

$$\begin{aligned} \mathcal{S}(f) &= \frac{(2p-1)^2}{T^2} \sum_{n=-\infty}^{\infty} \left| G_T\left(\frac{n}{T}\right) \right|^2 \delta\left(f - \frac{n}{T}\right) \\ &\quad + \frac{4p(1-p)}{T} |G_T(f)|^2 \end{aligned} \quad (8.5.34)$$

where for a rectangular pulse of amplitude  $A$ ,

$$\begin{aligned} |G_T(f)|^2 &= (AT)^2 \left( \frac{\sin \pi f T}{\pi f T} \right)^2 \\ &= (AT)^2 \operatorname{sinc}^2(fT) \end{aligned}$$

We observe that when  $p = 1/2$  (equally probable signals) the impulse spectrum vanishes and  $\mathcal{S}(f)$  reduces to

$$\mathcal{S}(f) = \frac{1}{T} |G_T(f)|^2$$

We observe that the power spectrum of the NRZI signal for equally probable signals is identical to the expression in (8.2.18), which applies to an uncorrelated sequence  $\{a_n\}$  into the modulator. Hence, we conclude that the simple precoding operation in NRZI does not result in a correlated sequence.

**Example 8.5.11**

Determine the power spectral density of the delay modulated (Miller encoded) signal described in Section 8.5.1.

**Solution** The transition probability matrix of a delay modulated signal is [see Equation (8.5.9)]

$$\mathbf{P} = \begin{bmatrix} 0 & \frac{1}{2} & 0 & \frac{1}{2} \\ 0 & 0 & \frac{1}{2} & \frac{1}{2} \\ \frac{1}{2} & \frac{1}{2} & 0 & 0 \\ \frac{1}{2} & 0 & \frac{1}{2} & 0 \end{bmatrix}$$

The state probabilities are  $p_i = 1/4$ , for  $i = 1, 2, 3, 4$ . Powers of  $\mathbf{P}$  are easily obtained by use of the relation (see Problem 8.8)

$$\mathbf{P}^4 \boldsymbol{\gamma} = -\frac{1}{4} \boldsymbol{\gamma} \quad (8.5.35)$$

where  $\gamma$  is the signal correlation matrix with elements

$$\gamma_{ij} = \frac{1}{T} \int_0^T s_i(t)s_j(t) dt$$

and the four signals  $\{s_i(t), i = 1, 2, 3, 4\}$  are shown in Figure 8.27, where  $s_3(t) = -s_2(t)$  and  $s_4(t) = -s_1(t)$ . It is easily seen that

$$\gamma = \begin{bmatrix} 1 & 0 & 0 & -1 \\ 0 & 1 & -1 & 0 \\ 0 & -1 & 1 & 0 \\ -1 & 0 & 0 & 1 \end{bmatrix} \quad (8.5.36)$$

Consequently, powers of  $\mathbf{P}$  can be generated from the relation

$$\mathbf{P}^{k+4}\gamma = -\frac{1}{4}\mathbf{P}^k\gamma, \quad k \geq 1 \quad (8.5.37)$$

With the aid of these relations, the power spectral density of the delay modulated signal is obtained from Equation (8.5.32). It may be expressed in the form

$$\begin{aligned} \mathcal{S}(f) = & \frac{1}{2(\pi fT)^2(17 + 8 \cos 8\pi fT)} [23 - 2 \cos \pi fT - 22 \cos 2\pi fT \\ & - 12 \cos 3\pi fT + 5 \cos 4\pi fT + 12 \cos 5\pi fT + 2 \cos 6\pi fT \\ & - 8 \cos 7\pi fT + 2 \cos 8\pi fT] \end{aligned} \quad (8.5.38)$$

The power-spectral densities of the NRZI and the delay modulated signal are shown in Figure 8.32. We observe that the NRZI signal has a lowpass power spectrum with a peak of  $f = 0$ . On the other hand, the delay modulated signal has very little power in the vicinity of  $f = 0$ . It also has a relatively narrow power-spectral density. These two characteristics make it particularly suitable for use in magnetic recording storage

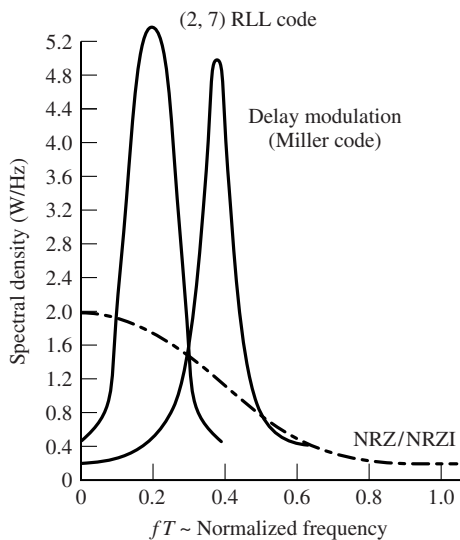


**Figure 8.32** Power-spectral density (one-sided) of Miller code (delay modulation), and NRZ/NRZI baseband signals.

channels which use flux-sensing heads for writing on and reading off a disk. Also shown for comparison in Figure 8.32 is the power-spectral density of the modulated signal generated by a  $(d, \kappa) = (2, 7)$  code followed by NRZI. The  $(2, 7)$  runlength-limited code, previously given in Table 8.5, is also widely used in magnetic recording channels.

When there is no memory in the modulation method, the signal waveform transmitted in each signaling interval is independent of the waveforms transmitted in previous signaling intervals. The power-spectral density of the resulting signal may still be expressed in the form of Equation (8.5.32) if the transition probability matrix is replaced by

$$\mathbf{P} = \begin{bmatrix} p_1 & p_2 & \cdots & p_K \\ p_1 & p_2 & \cdots & p_K \\ \vdots & \vdots & & \vdots \\ p_1 & p_2 & \cdots & p_K \end{bmatrix} \quad (8.5.39)$$

and we impose the condition that  $\mathbf{P}^n = \mathbf{P}$  for all  $n > 1$ , as a consequence of the memoryless modulation. Under these conditions, the expression for  $\mathcal{S}(f)$  given Equation (8.5.32) reduces to the simpler form

$$\begin{aligned} \mathcal{S}(f) &= \frac{1}{T^2} \sum_{n=-\infty}^{\infty} \left| \sum_{i=1}^K p_i S_i \left( \frac{n}{T} \right) \right|^2 \delta \left( f - \frac{n}{T} \right) + \frac{1}{T} \sum_{i=1}^K p_i (1 - p_i) |S_i(f)|^2 \\ &\quad - \frac{2}{T} \sum_{i=1}^K \sum_{\substack{j=1 \\ i < j}}^K p_i p_j \operatorname{Re}[S_i(f) S_j^*(f)] \end{aligned} \quad (8.5.40)$$

We observe that our previous result for the power-spectral density of memoryless PAM modulation given by Equation (8.2.17) is a special case of the expression in Equation (8.5.40). Specifically, if we have  $K = M$  signals which are amplitude-scaled versions of a basic pulse  $g_T(t)$ ; i.e.,  $s_m(t) = a_m g_T(t)$ , where  $a_m$  is the signal amplitude, then  $S_m(f) = a_m G_T(f)$  and Equation (8.5.40) becomes

$$\begin{aligned} \mathcal{S}(f) &= \frac{1}{T^2} \left( \sum_{i=1}^M a_i p_i \right)^2 \sum_{n=-\infty}^{\infty} \left| G_T \left( \frac{n}{T} \right) \right|^2 \delta \left( f - \frac{n}{T} \right) \\ &\quad + \frac{1}{T} \left[ \sum_{i=1}^M p_i (1 - p_i) a_i^2 - 2 \sum_{i=1}^M \sum_{\substack{j=1 \\ i < j}}^M p_i p_j a_i a_j \right] |G_T(f)|^2 \end{aligned} \quad (8.5.41)$$

If we compare Equation (8.2.17) with Equation (8.5.41), we find that these expressions are identical, where the mean and variance of the information sequence is

$$\begin{aligned} m_a &= \sum_{i=1}^M a_i p_i \\ \sigma_a^2 &= \sum_{i=1}^M p_i (1 - p_i) a_i^2 - 2 \sum_{i=1}^M \sum_{\substack{j=1 \\ i < j}}^M p_i p_j a_i a_j \end{aligned} \quad (8.5.42)$$

Therefore Equation (8.5.40) is the more general form for the power-spectral density of memoryless modulated signals, since it applies to signals that may have different pulse shapes.

## 8.6 SYSTEM DESIGN IN THE PRESENCE OF CHANNEL DISTORTION

In Section 8.3.1 we described a signal design criterion that results in zero ISI at the output of the receiving filter. Recall that a signal pulse  $x(t)$  will satisfy the condition of zero ISI at the sampling instants  $t = nT$ ,  $n = \pm 1, \pm 2, \dots$ , if its spectrum  $X(f)$  satisfies the condition given by Equation (8.3.9). From this condition we concluded that for ISI free transmission over a channel, the transmitter-receiver filters and the channel transfer function must satisfy

$$G_T(f)C(f)G_R(f) = X_{rc}(f) \quad (8.6.1)$$

where  $X_{rc}(f)$  denotes the Fourier transform of an appropriate raised cosine pulse whose parameters depend on the channel bandwidth  $W$  and the transmission interval  $T$ . Obviously, there are an infinite number of transmitter-receiver filter pairs that satisfy the above condition. In this section, we are concerned with the design of a digital communication system that suppresses ISI in a channel with distortion. We first present a brief coverage of various types of channel distortion and then we consider the design of transmitter and receiver filters.

We distinguish two types of distortion. *Amplitude distortion* results when the amplitude characteristic  $|C(f)|$  is not constant for  $|f| \leq W$ . The second type of distortion, called *phase distortion*, results when the phase characteristic  $\Theta_c(f)$  is nonlinear in frequency.

Another view of phase distortion is obtained by considering the derivative of  $\Theta_c(f)$ . Thus, we define the *envelope delay* characteristic as (see Problems 2.57 and 8.40)

$$\tau(f) = -\frac{1}{2\pi} \frac{d\Theta_c(f)}{df} \quad (8.6.2)$$

When  $\Theta_c(f)$  is linear in  $f$ , the envelope delay is constant for all frequencies. In this case, all frequencies in the transmitted signal pass through the channel with the same fixed-time delay. In such a case, there is no phase distortion. However, when  $\Theta_c(f)$  is nonlinear, the envelope delay  $\tau(f)$  varies with frequency and the various frequency components in the input signal undergo different delays in passing through the channel. In such a case we say that the transmitted signal has suffered from *delay distortion*.

Both amplitude and delay distortion cause intersymbol interference in the received signal. For example, let us assume that we have designed a pulse with a raised cosine spectrum that has zero ISI at the sampling instants. An example of such a pulse is illustrated in Figure 8.33(a). When the pulse is passed through a channel filter with constant amplitude  $|C(f)| = 1$  for  $|f| < W$  and a quadratic phase characteristic (linear envelope delay), the received pulse at the output of the channel is shown in Figure 8.33(b). Note that the periodic zero crossings have been shifted by the delay distortion, so that the

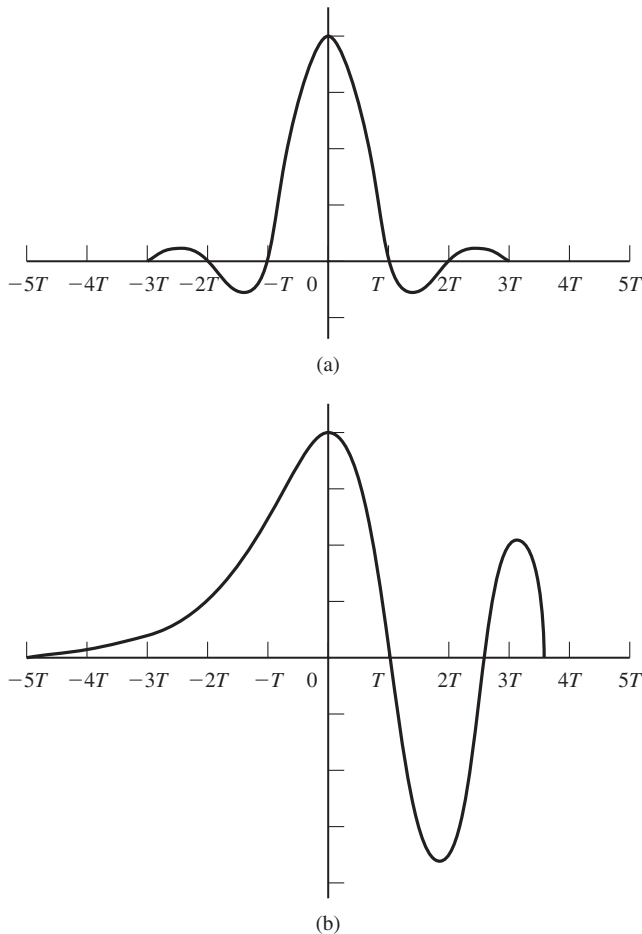


**Figure 8.33** Effect of channel distortion in (a) channel input and (b) channel output.

resulting pulse suffers from ISI. Consequently, a sequence of successive pulses would be smeared into one another and the peaks of the pulses would no longer be distinguishable due to the ISI.

Next, we consider two problems. First, we consider the design of transmitting and receiving filters in the presence of channel distortion when the channel characteristics are known. Second, we consider the design of special filters, called channel equalizers, that automatically and adaptively correct for the channel distortion when the channel characteristics; i.e.,  $|C(f)|$  and  $\angle\Theta_c(f)$ , are unknown.

### 8.6.1 Design of Transmitting and Receiving Filters for a Known Channel

In this section, we assume that the channel frequency response characteristic  $C(f)$  is known and consider the problem of designing a transmitting filter and a receiving

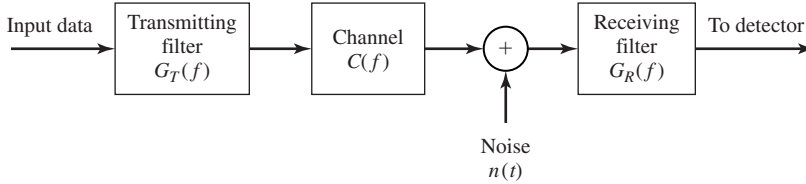


**Figure 8.34** System configuration for design of  $G_T(f)$  and  $G_R(f)$ .

filter that maximize the SNR at the output of the receiving filter and results in zero ISI. Figure 8.34 illustrates the overall system under consideration.

For the signal component, we must satisfy the condition

$$G_T(f)C(f)G_R(f) = X_{rc}(f)e^{-j\pi f t_0}, \quad |f| \leq W \quad (8.6.3)$$

where  $X_{rc}(f)$  is the desired raised cosine spectrum that yields zero ISI at the sampling instants, and  $t_0$  is a time delay which is necessary to ensure the physical realizability of the transmitter and receiver filters.

The noise at the output of the receiving filter may be expressed as

$$v(t) = \int_{-\infty}^{\infty} n(t - \tau)g_R(\tau) d\tau \quad (8.6.4)$$

where  $n(t)$  is the input to the filter. The noise  $n(t)$  is assumed to be zero-mean Gaussian. Hence,  $v(t)$  is zero-mean Gaussian, with a power-spectral density

$$\mathcal{S}_v(f) = \mathcal{S}_n(f)|G_R(f)|^2 \quad (8.6.5)$$

where  $\mathcal{S}_n(f)$  is the spectral density of the noise process  $n(t)$ .

For simplicity, we consider binary PAM transmission. Then, the sampled output of the matched filter is

$$y_m = x_0 a_m + v_m = a_m + v_m \quad (8.6.6)$$

where  $x_0$  is normalized to unity,  $a_m = \pm d$ , and  $v_m$  represents the noise term which is zero-mean Gaussian with variance

$$\sigma_v^2 = \int_{-\infty}^{\infty} \mathcal{S}_n(f)|G_R(f)|^2 df \quad (8.6.7)$$

Consequently, the probability of error is

$$P_2 = \frac{1}{\sqrt{2\pi}} \int_{d/\sigma_v}^{\infty} e^{-y^2/2} dy = Q\left(\sqrt{\frac{d^2}{\sigma_v^2}}\right) \quad (8.6.8)$$

Now, suppose that we select the filter at the transmitter to have the frequency response

$$G_T(f) = \frac{\sqrt{X_{rc}(f)}}{C(f)} e^{-j2\pi f t_0} \quad (8.6.9)$$

where  $t_0$  is a suitable delay to ensure causality. Then, the cascade of the transmit filter and the channel results in the frequency response

$$G_T(f)C(f) = \sqrt{X_{rc}(f)} e^{-j2\pi f t_0} \quad (8.6.10)$$

In the presence of additive white Gaussian noise, the filter at the receiver is designed to be matched to the received signal pulse. Hence, its frequency response

$$G_R(f) = \sqrt{X_{rc}(f)} e^{-j2\pi f t_r} \quad (8.6.11)$$

where  $t_r$  is an appropriate delay.

Let us compute the SNR  $d^2/\sigma_v^2$  for these filter characteristics. The noise variance is

$$\sigma_v^2 = \frac{N_0}{2} \int_{-\infty}^{\infty} |G_R(f)|^2 df = \frac{N_0}{2} \int_{-W}^W X_{rc}(f) df = \frac{N_0}{2} \quad (8.6.12)$$

The average transmitted power is

$$P_{av} = \frac{E(a_m^2)}{T} \int_{-\infty}^{\infty} g_T^2(t) dt = \frac{d^2}{T} \int_{-W}^W \frac{X_{rc}(f)}{|C(f)|^2} df \quad (8.6.13)$$

and, hence,

$$d^2 = P_{av} T \left[ \int_{-W}^W \frac{X_{rc}(f)}{|C(f)|^2} df \right]^{-1} \quad (8.6.14)$$

Therefore, the SNR  $d^2/\sigma_v^2$  is given as

$$\frac{d^2}{\sigma_v^2} = \frac{2P_{av}T}{N_0} \left[ \int_{-W}^W \frac{X_{rc}(f)}{|C(f)|^2} df \right]^{-1} \quad (8.6.15)$$

We note that the term,

$$10 \log_{10} \int_{-W}^W \frac{X_{rc}(f)}{|C(f)|^2} df \quad (8.6.16)$$

with  $|C(f)| \leq 1$  for  $|f| \leq W$ , represents the loss in performance in dB of the communication system due to channel distortion. When the channel is ideal,  $|C(f)| = 1$  for  $|f| \leq W$  and, hence, there is no performance loss. We also note that this loss is entirely due to amplitude distortion in the channel, because the phase distortion has been totally compensated by the transmit filter.

### Example 8.6.1

Determine the magnitude of the transmitting and receiving filter characteristics for a binary communication system that transmits data at a rate of 4800 bits/sec over a channel with frequency (magnitude) response

$$|C(f)| = \frac{1}{\sqrt{1 + \left(\frac{f}{W}\right)^2}}, \quad |f| \leq W$$

where  $W = 4800$  Hz. The additive noise is zero-mean, white, Gaussian with spectral density  $N_0/2 = 10^{-15}$  W/Hz.



**Solution** Since  $W = 1/T = 4800$  we use a signal pulse with a raised cosine spectrum and  $\alpha = 1$ . Thus,

$$\begin{aligned} X_{\text{rc}}(f) &= \frac{T}{2}[1 + \cos(\pi T|f|)] \\ &= T \cos^2\left(\frac{\pi|f|}{9600}\right) \end{aligned}$$

Then,

$$|G_T(f)| = \sqrt{T \left[1 + \left(\frac{f}{W}\right)^2\right]} \cos \frac{\pi|f|}{9600}, \quad |f| \leq 4800 \text{ Hz}$$

$$|G_R(f)| = \sqrt{T} \cos \frac{\pi|f|}{9600}, \quad |f| \leq 4800 \text{ Hz}$$

and  $|G_T(f)| = |G_R(f)| = 0$  for  $|f| > 4800$  Hz

### 8.6.2 Channel Equalization

In the preceding section, we described the design of transmitting and receiving filters for digital PAM transmission when the frequency response characteristics of the channel are known. Our objective was to design these filters for zero ISI at the sampling instants. This design methodology is appropriate when the channel is precisely known and its characteristics do not change with time.

In practice we often encounter channels whose frequency response characteristics are either unknown or change with time. For example, in data transmission over the dial-up telephone network, the communication channel will be different every time we dial a number, because the channel route will be different. Once a connection is made, however, the channel will be time-invariant for a relatively long period of time. This is an example of a channel whose characteristics are unknown a priori. Examples of time-varying channels are radio channels, such as ionospheric propagation channels. These channels are characterized by time-varying frequency response characteristics. These types of channels are examples where the optimization of the transmitting and receiving filters, as described in Section 8.6.1, is not possible.

Under these circumstances, we may design the transmitting filter to have a square-root raised cosine frequency response; i.e.,

$$G_T(f) = \begin{cases} \sqrt{X_{\text{rc}}(f)} e^{-j2\pi f t_0}, & |f| \leq W \\ 0, & |f| > W \end{cases}$$

and the receiving filter, with frequency response  $G_R(f)$ , to be matched to  $G_T(f)$ . Therefore,

$$|G_T(f)||G_R(f)| = X_{\text{rc}}(f) \quad (8.6.17)$$

Then, due to channel distortion, the output of the receiving filter is

$$y(t) = \sum_{n=-\infty}^{\infty} a_n \bar{x}(t - nT) + v(t) \quad (8.6.18)$$

where  $x(t) = g_T(t) \star c(t) \star g_R(t)$ . The filter output may be sampled periodically to produce the sequence

$$\begin{aligned} y_m &= \sum_{n=-\infty}^{\infty} a_n x_{m-n} + v_m \\ &= x_0 a_m + \sum_{\substack{n=-\infty \\ n \neq m}}^{+\infty} a_n x_{m-n} + v_m \end{aligned} \quad (8.6.19)$$

where  $x_n = x(nT)$ ,  $n = 0, \pm 1, \pm 2, \dots$ . The middle term on the right-hand side of Equation (8.6.19) represents the ISI.

In any practical system, it is reasonable to assume that the ISI affects a finite number of symbols. Hence, we may assume that  $x_n = 0$  for  $n < -L_1$  and  $n > L_2$ , where  $L_1$  and  $L_2$  are finite, positive integers. Consequently, the ISI observed at the output of the receiving filter may be viewed as being generated by passing the data sequence  $\{a_m\}$  through an FIR filter with coefficients  $\{x_n, -L_1 \leq n \leq L_2\}$ , as shown in Figure 8.35. This filter is called the *equivalent discrete-time channel filter*. Since its input is the discrete information sequence (binary or  $M$ -ary), the output of the discrete-time channel filter may be characterized as the output of a finite-state machine corrupted by additive Gaussian noise. Hence, the noise-free output of the filter is described by a trellis having  $M^L$  states where  $L = L_1 + L_2$ .

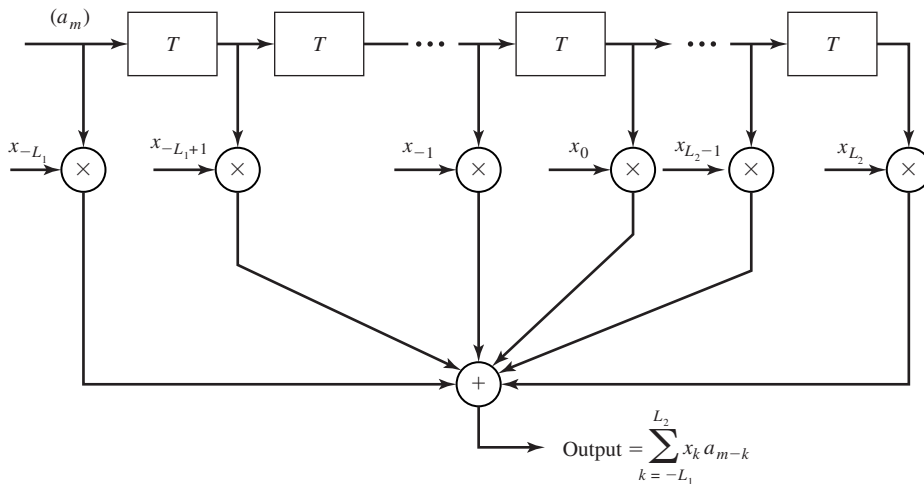


**Figure 8.35** Equivalent discrete-time channel filter.

**Maximum-Likelihood Sequence Detection.** The optimum detector for the information sequence  $\{a_m\}$  based on the observation of the received sequence  $\{y_m\}$ , given by Equation (8.6.19), is a ML sequence detector. The detector is akin to the ML sequence detector described in the context of detecting partial response signals which have controlled ISI. The Viterbi algorithm provides a method for searching through the trellis for the ML signal path. To accomplish this search, the equivalent channel filter coefficients  $\{x_n\}$  must be known or measured by some method. At each stage of the trellis search, there are  $M^L$  surviving sequences with  $M^L$  corresponding Euclidean distance path metrics.

Due to the exponential increase in the computational complexity of the Viterbi algorithm with the span (length  $L$ ) of the ISI, this type of detection is practical only when  $M$  and  $L$  are small. For example in mobile cellular telephone systems which employ digital transmission of speech signals,  $M$  is usually selected to be small; e.g.,  $M = 2$  or 4, and  $2 \leq L \leq 5$ . In this case, the ML sequence detector may be implemented with reasonable complexity. However, when  $M$  and  $L$  are large, the ML sequence detector becomes impractical. In such a case other more practical but suboptimum methods are used to detect the information sequence  $\{a_m\}$  in the presence of ISI. Nevertheless, the performance of the ML sequence detector for a channel with ISI serves as a benchmark for comparing its performance with that of suboptimum methods. Two suboptimum methods are described below.

**Linear Equalizers.** To compensate for the channel distortion, we may employ a linear filter with adjustable parameters. The filter parameters are adjusted on the basis of measurements of the channel characteristics. These adjustable filters are called *channel equalizers* or, simply, *equalizers*.

On channels whose frequency-response characteristics are unknown, but time-invariant, we may measure the channel characteristics, adjust the parameters of the equalizer, and once adjusted, the parameters remain fixed during the transmission of data. Such equalizers are called *preset equalizers*. On the other hand, *adaptive equalizers* update their parameters on a periodic basis during the transmission of data.

First, we consider the design characteristics for a linear equalizer from a frequency domain viewpoint. Figure 8.36 shows a block diagram of a system that employs a linear filter as a channel equalizer.

The demodulator consists of a receiving filter with frequency response  $G_R(f)$  in cascade with a channel equalizing filter that has a frequency response  $G_E(f)$ . Since

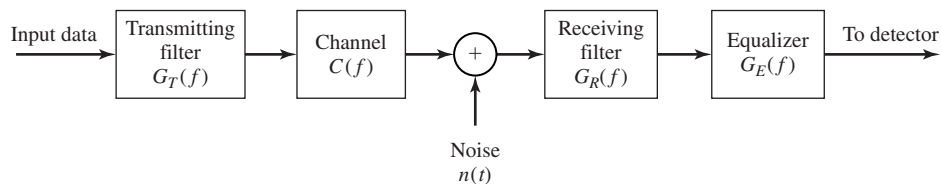


**Figure 8.36** Block diagram of a system with an equalizer.

$G_R(f)$  is matched to  $G_T(f)$  and they are designed so that their product satisfies Equation (8.6.17),  $|G_E(f)|$  must compensate for the channel distortion. Hence, the equalizer frequency response must equal the inverse of the channel response; i.e.,

$$G_E(f) = \frac{1}{C(f)} = \frac{1}{|C(f)|} e^{-j\Theta_c(f)} |f| \leq W \quad (8.6.20)$$

where  $|G_E(f)| = 1/|C(f)|$  and the equalizer phase characteristic  $\Theta_E(f) = -\Theta_c(f)$ . In this case, the equalizer is said to be the *inverse channel filter* to the channel response.

We note that the inverse channel filter completely eliminates ISI caused by the channel. Since it forces the ISI to be zero at the sampling times  $t = nT$ , the equalizer is called a *zero-forcing equalizer*. Hence, the input to the detector is of the form

$$y_m = a_m + v_m$$

where  $v_m$  is the noise component, which is zero-mean Gaussian with a variance

$$\begin{aligned} \sigma_v^2 &= \int_{-\infty}^{\infty} \mathcal{S}_n(f) |G_R(f)|^2 |G_E(f)|^2 df \\ &= \int_{-W}^W \frac{\mathcal{S}_n(f) |X_{rc}(f)|}{|C(f)|^2} df \end{aligned} \quad (8.6.21)$$

where  $\mathcal{S}_n(f)$  is the power-spectral density of the noise. When the noise is white,  $\mathcal{S}_n(f) = N_0/2$  and the variance becomes

$$\sigma_v^2 = \frac{N_0}{2} \int_{-W}^W \frac{|X_{rc}(f)|}{|C(f)|^2} df \quad (8.6.22)$$

In general, the noise variance at the output of the zero-forcing equalizer is higher than the noise variance at the output of the optimum receiving filter  $|G_R(f)|$  given by Equation (8.6.12) for the case in which the channel is known.

### Example 8.6.2

The channel given in Example 8.6.1 is equalized by a zero-forcing equalizer. Assuming that the transmitting and receiving filters satisfy Equation (8.6.17), determine the value of the noise variance at the sampling instants and the probability of error.

**Solution** When the noise is white, the variance of the noise at the output of the zero-forcing equalizer (input to the detector) is given by Equation (8.6.22). Hence,

$$\begin{aligned} \sigma_v^2 &= \frac{N_0}{2} \int_{-W}^W \frac{|X_{rc}(f)|}{|C(f)|^2} df \\ &= \frac{TN_0}{2} \int_{-W}^W \left[ 1 + \left( \frac{f}{W} \right)^2 \right] \cos^2 \frac{\pi|f|}{2W} df \\ &= N_0 \int_0^1 (1 + x^2) \cos^2 \frac{\pi x}{2} dx \\ &= \left( \frac{2}{3} - \frac{1}{\pi^2} \right) N_0 \end{aligned}$$

The average transmitted power is

$$\begin{aligned} P_{av} &= \frac{(M^2 - 1)d^2}{3T} \int_{-W}^W |G_T(f)|^2 df \\ &= \frac{(M^2 - 1)d^2}{3T} \int_{-W}^W |X_{rc}(f)| df \\ &= \frac{(M^2 - 1)d^2}{3T} \end{aligned}$$

The general expression for the probability of error is given as

$$P_M = \frac{2(M - 1)}{M} Q \left( \sqrt{\frac{3P_{av}T}{(M^2 - 1)(2/3 - 1/\pi^2)N_0}} \right)$$

If the channel were ideal, the argument of the Q-function would be  $6P_{av}T/(M^2 - 1)N_0$ . Hence, the loss in performance due to the nonideal channel is given by the factor  $2(2/3 - \frac{1}{\pi^2}) = 1.133$  or 0.54 dB.

Let us now consider the design of a linear equalizer from a time-domain viewpoint. We noted previously that in real channels, the ISI is limited to a finite number of samples, say  $L$  samples. As a consequence, in practice the channel equalizer is approximated by a finite duration impulse response (FIR) filter, or transversal filter, with adjustable tap coefficients  $\{c_n\}$ , as illustrated in Figure 8.37. The time delay  $\tau$  between adjacent taps may be selected as large as  $T$ , the symbol interval, in which case the FIR equalizer is called a *symbol-spaced equalizer*. In this case the input to the equalizer is the sampled sequence given by Equation (8.6.19). However, we note that when  $1/T < 2W$ , frequencies in the received signal above the folding frequency  $1/T$

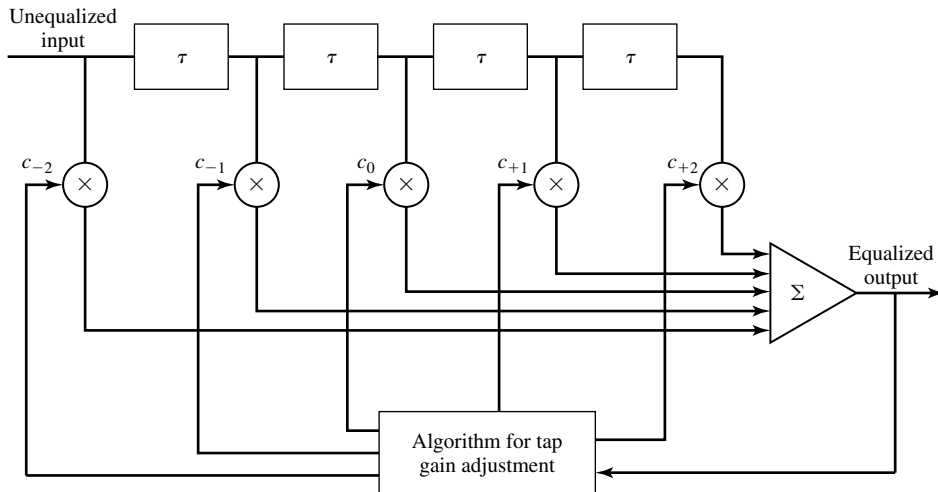


**Figure 8.37** Linear transversal filter.

are aliased into frequencies below  $1/T$ . In this case, the equalizer compensates for the aliased channel-distorted signal.

On the other hand, when the time delay  $\tau$  between adjacent taps is selected such that  $1/\tau \geq 2W > 1/T$ , no aliasing occurs and, hence, the inverse channel equalizer compensates for the true channel distortion. Since  $\tau < T$ , the channel equalizer is said to have *fractionally spaced taps* and it is called a *fractionally spaced equalizer*. In practice,  $\tau$  is often selected as  $\tau = T/2$ . Notice that, in this case, the sampling rate at the output of the filter  $G_R(f)$  is  $\frac{2}{T}$ .

The impulse response of the FIR equalizer is

$$g_E(t) = \sum_{n=-N}^N c_n \delta(t - n\tau) \quad (8.6.23)$$

and the corresponding frequency response is

$$G_E(f) = \sum_{n=-N}^N c_n e^{-j2\pi f n\tau} \quad (8.6.24)$$

where  $\{c_n\}$  are the  $(2N + 1)$  equalizer coefficients, and  $N$  is chosen sufficiently large so that the equalizer spans the length of the ISI; i.e.,  $2N + 1 \geq L$ . Since  $X(f) = G_T(f)C(f)G_R(f)$  and  $x(t)$  is the signal pulse corresponding to  $X(f)$ , then the equalized output signal pulse is

$$q(t) = \sum_{n=-N}^N c_n x(t - n\tau) \quad (8.6.25)$$

The zero-forcing condition can now be applied to the samples of  $q(t)$  taken at times  $t = mT$ . These samples are

$$q(mT) = \sum_{n=-N}^N c_n x(mT - n\tau), \quad m = 0, \pm 1, \dots, \pm N \quad (8.6.26)$$

Since there are  $2N + 1$  equalizer coefficients, we can control only  $2N + 1$  sampled values of  $q(t)$ . Specifically, we may force the conditions

$$q(mT) = \sum_{n=-N}^N c_n x(mT - n\tau) = \begin{cases} 1, & m = 0 \\ 0, & m = \pm 1, \pm 2, \dots, \pm N \end{cases} \quad (8.6.27)$$

which may be expressed in matrix form as  $\mathbf{X}\mathbf{c} = \mathbf{q}$ , where  $\mathbf{X}$  is a  $(2N + 1) \times (2N + 1)$  matrix with elements  $\{x(mT - n\tau)\}$ ,  $\mathbf{c}$  is the  $(2N + 1)$  coefficient vector and  $\mathbf{q}$  is the  $(2N + 1)$  column vector with one nonzero element. Thus, we obtain a set of  $2N + 1$  linear equations for the coefficients of the zero-forcing equalizer.

We should emphasize that the FIR zero-forcing equalizer does not completely eliminate ISI because it has a finite length. However, as  $N$  is increased the residual ISI can be reduced and in the limit as  $N \rightarrow \infty$ , the ISI is completely eliminated.

**Example 8.6.3**

Consider a channel distorted pulse  $x(t)$ , at the input to the equalizer, given by the expression

$$x(t) = \frac{1}{1 + \left(\frac{2t}{T}\right)^2}$$

where  $1/T$  is the symbol rate. The pulse is sampled at the rate  $2/T$  and equalized by a zero-forcing equalizer. Determine the coefficients of a five-tap zero-forcing equalizer.

**Solution** According to Equation (8.6.27), the zero-forcing equalizer must satisfy the equations

$$q(mT) = \sum_{n=-2}^2 c_n x(mT - nT/2) = \begin{cases} 1, & m = 0 \\ 0, & m = \pm 1, \pm 2 \end{cases}$$

The matrix  $\mathbf{X}$  with elements  $x(mT - nT/2)$  is given as

$$\mathbf{X} = \begin{bmatrix} \frac{1}{5} & \frac{1}{10} & \frac{1}{17} & \frac{1}{26} & \frac{1}{37} \\ 1 & \frac{1}{2} & \frac{1}{5} & \frac{1}{10} & \frac{1}{17} \\ \frac{1}{5} & \frac{1}{2} & 1 & \frac{1}{2} & \frac{1}{5} \\ \frac{1}{17} & \frac{1}{10} & \frac{1}{5} & \frac{1}{2} & 1 \\ \frac{1}{37} & \frac{1}{26} & \frac{1}{17} & \frac{1}{10} & \frac{1}{5} \end{bmatrix} \quad (8.6.28)$$

The coefficient vector  $\mathbf{C}$  and the vector  $\mathbf{q}$  are given as

$$\mathbf{c} = \begin{bmatrix} c_{-2} \\ c_{-1} \\ c_0 \\ c_1 \\ c_2 \end{bmatrix} \quad \mathbf{q} = \begin{bmatrix} 0 \\ 0 \\ 1 \\ 0 \\ 0 \end{bmatrix} \quad (8.6.29)$$

Then, the linear equations  $\mathbf{X}\mathbf{c} = \mathbf{q}$  can be solved by inverting the matrix  $\mathbf{X}$ . Thus, we obtain

$$\mathbf{c}_{\text{opt}} = \mathbf{X}^{-1}\mathbf{q} = \begin{bmatrix} -2.2 \\ 4.9 \\ -3 \\ 4.9 \\ -2.2 \end{bmatrix} \quad (8.6.30)$$

One drawback to the zero-forcing equalizer is that it ignores the presence of additive noise. As a consequence, its use may result in significant noise enhancement. This is easily seen by noting that in a frequency range where  $C(f)$  is small, the channel equalizer  $G_E(f) = 1/C(f)$  compensates by placing a large gain in that frequency range. Consequently, the noise in that frequency range is greatly enhanced. An alternative is to relax the zero ISI condition and select the channel equalizer characteristic such that the combined power in the residual ISI and the additive noise at the output of the equalizer is minimized. A channel equalizer that is optimized based on the minimum mean-square-error (MMSE) criterion accomplishes the desired goal.

To elaborate, let us consider the noise-corrupted output of the FIR equalizer which is

$$z(t) = \sum_{n=-N}^N c_n y(t - n\tau) \quad (8.6.31)$$

where  $y(t)$  is the input to the equalizer, given by Equation (8.6.18). The output is sampled at times  $t = mT$ . Thus, we obtain

$$z(mT) = \sum_{n=-N}^N c_n y(mT - n\tau) \quad (8.6.32)$$

The desired response sample at the output of the equalizer at  $t = mT$  is the transmitted symbol  $a_m$ . The error is defined as the difference between  $a_m$  and  $z(mT)$ . Then, the mean-square-error (MSE) between the actual output sample  $z(mT)$  and the desired values  $a_m$  is

$$\begin{aligned} \text{MSE} &= E[z(mT) - a_m]^2 \\ &= E \left[ \sum_{n=-N}^N c_n y(mT - n\tau) - a_m \right]^2 \\ &= \sum_{n=-N}^N \sum_{k=-N}^N c_n c_k R_Y(n - k) - 2 \sum_{k=-N}^N c_k R_{AY}(k) + E(a_m^2) \end{aligned} \quad (8.6.33)$$

where the correlations are defined as

$$\begin{aligned} R_Y(n - k) &= E[y(mT - n\tau)y(mT - k\tau)] \\ R_{AY}(k) &= E[y(mT - k\tau)a_m] \end{aligned} \quad (8.6.34)$$

and the expectation is taken with respect to the random information sequence  $\{a_m\}$  and the additive noise.

The MMSE solution is obtained by differentiating Equation (8.6.33) with respect to the equalizer coefficients  $\{c_n\}$ . Thus, we obtain the necessary conditions for the MMSE as

$$\sum_{n=-N}^N c_n R_Y(n - k) = R_{YA}(k), \quad k = 0, \pm 1, 2, \dots, \pm N \quad (8.6.35)$$

These are  $(2N + 1)$  linear equations for the equalizer coefficients. In contrast to the zero-forcing solution described previously, these equations depend on the statistical properties (the autocorrelation) of the noise as well as the ISI through the autocorrelation  $R_Y(n)$ .

In practice, we would not normally know the autocorrelation  $R_Y(n)$  and the crosscorrelation  $R_{AY}(n)$ . However, these correlation sequences can be estimated by



transmitting a test signal over the channel and using the time average estimates

$$\begin{aligned}\hat{R}_Y(n) &= \frac{1}{K} \sum_{k=1}^K y(kT - n\tau)y(kT) \\ \hat{R}_{AY}(n) &= \frac{1}{K} \sum_{k=1}^K y(kT - n\tau) a_k\end{aligned}\tag{8.6.36}$$

in place of the ensemble averages to solve for the equalizer coefficients given by Equation (8.6.35).

**Adaptive Equalizers.** We have shown that the tap coefficients of a linear equalizer can be determined by solving a set of linear equations. In the zero-forcing optimization criterion, the linear equations are given by Equation (8.6.27). On the other hand, if the optimization criterion is based on minimizing the MSE, the optimum equalizer coefficients are determined by solving the set of linear equations given by Equation (8.6.35).

In both cases, we may express the set of linear equations in the general matrix form

$$\mathbf{B}\mathbf{c} = \mathbf{d}\tag{8.6.37}$$

where  $\mathbf{B}$  is a  $(2N + 1) \times (2N + 1)$  matrix,  $\mathbf{c}$  is a column vector representing the  $2N + 1$  equalizer coefficients, and  $\mathbf{d}$  is a  $(2N + 1)$ -dimensional column vector. The solution of Equation (8.6.37) yields

$$\mathbf{c}_{\text{opt}} = \mathbf{B}^{-1}\mathbf{d}\tag{8.6.38}$$

In practical implementations of equalizers, the solution of Equation (8.6.37) for the optimum coefficient vector is usually obtained by an iterative procedure that avoids the explicit computation of the inverse of the matrix  $\mathbf{B}$ . The simplest iterative procedure is the method of steepest descent, in which one begins by choosing arbitrarily the coefficient vector  $\mathbf{c}$ , say  $\mathbf{c}_0$ . This initial choice of coefficients corresponds to a point on the criterion function that is begin optimized. For example, in the case of the MSE criterion, the initial guess  $\mathbf{c}_0$  corresponds to a point on the quadratic MSE surface in the  $(2N + 1)$ -dimensional space of coefficients. The gradient vector, defined as  $\mathbf{g}_0$ , which is the derivative of the MSE with respect to the  $2N + 1$  filter coefficients, is then computed at this point on the criterion surface and each tap coefficient is changed in the direction opposite to its corresponding gradient component. The change in the  $j$ th tap coefficient is proportional to the size of the  $j$ th gradient component.

For example, the gradient vector, denoted as  $\mathbf{g}_k$ , for the MSE criterion, found by taking the derivatives of the MSE with respect to each of the  $2N + 1$  coefficients, is

$$\mathbf{g}_k = \mathbf{B}\mathbf{c}_k - \mathbf{d}, \quad k = 0, 1, 2, \dots\tag{8.6.39}$$

Then the coefficient vector  $\mathbf{c}_k$  is updated according to the relation

$$\mathbf{c}_{k+1} = \mathbf{c}_k - \Delta\mathbf{g}_k\tag{8.6.40}$$

where  $\Delta$  is the *step-size parameter* for the iterative procedure. To ensure convergence of the iterative procedure,  $\Delta$  is chosen to be a small positive number. In such a case, the

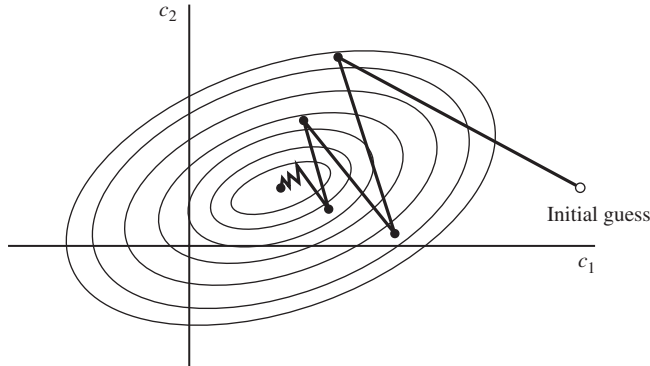


**Figure 8.38** Example of convergence characteristics of a gradient algorithm. (From *Introduction to Adaptive Arrays*, by R.A. Monzigo and T.W. Miller; ©1980 by John Wiley & Sons. Reprinted with permission of the publisher.)

gradient vector  $\mathbf{g}_k$  converges toward zero; i.e.,  $\mathbf{g}_k \rightarrow \mathbf{0}$  as  $k \rightarrow \infty$ , and the coefficient vector  $\mathbf{c}_k \rightarrow \mathbf{c}_{\text{opt}}$  as illustrated in Figure 8.38 based on two-dimensional optimization. In general, convergence of the equalizer tap coefficients to  $\mathbf{c}_{\text{opt}}$  cannot be attained in a finite number of iterations with the steepest-descent method. However, the optimum solution  $\mathbf{c}_{\text{opt}}$  can be approached as closely as desired in a few hundred iterations. In digital communication systems that employ channel equalizers, each iteration corresponds to a time interval for sending one symbol and, hence, a few hundred iterations to achieve convergence to  $\mathbf{c}_{\text{opt}}$  corresponds to a fraction of a second.

Adaptive channel equalization is required for channels whose characteristics change with time. In such a case, the ISI varies with time. The channel equalizer must track such time variations in the channel response and adapt its coefficients to reduce the ISI. In the context of the above discussion, the optimum coefficient vector  $\mathbf{c}_{\text{opt}}$  varies with time due to time variations in the matrix  $\mathbf{B}$  and, for the case of the MSE criterion, time variations in the vector  $\mathbf{d}$ . Under these conditions, the iterative method described above can be modified to use estimates of the gradient components. Thus, the algorithm for adjusting the equalizer tap coefficients may be expressed as

$$\hat{\mathbf{c}}_{k+1} = \hat{\mathbf{c}}_k - \Delta \hat{\mathbf{g}}_k \quad (8.6.41)$$

where  $\hat{\mathbf{g}}_k$  denotes an estimate of the gradient vector  $\mathbf{g}_k$  and  $\hat{\mathbf{c}}_k$  denotes the estimate of the tap coefficient vector.

In the case of the MSE criterion, the gradient vector  $\mathbf{g}_k$  given by Equation (8.6.39) may also be expressed as (see Problem 8.46).

$$\mathbf{g}_k = -E(e_k \mathbf{y}_k)$$

An estimate  $\hat{\mathbf{g}}_k$  of the gradient vector at the  $k$ th iteration is computed as

$$\hat{\mathbf{g}}_k = -e_k \mathbf{y}_k \quad (8.6.42)$$

where  $e_k$  denotes the difference between the desired output from the equalizer at the  $k$ th time instant and the actual output  $z(kT)$ , and  $\mathbf{y}_k$  denotes the column vector of  $2N + 1$

received signal values contained in the equalizer at time instant  $k$ . The *error signal*  $e_k$  is expressed as

$$e_k = a_k - z_k \quad (8.6.43)$$

where  $z_k = z(kT)$  is the equalizer output given by Equation (8.6.32) and  $a_k$  is the desired symbol. Hence, by substituting Equation (8.6.42) into Equation (8.6.41), we obtain the adaptive algorithm for optimizing the tap coefficients (based on the MSE criterion) as

$$\hat{\mathbf{c}}_{k+1} = \hat{\mathbf{c}}_k + \Delta e_k \mathbf{y}_k \quad (8.6.44)$$

Since an estimate of the gradient vector is used in Equation (8.6.44) the algorithm is called a *stochastic gradient algorithm*. It is also known as the *LMS algorithm*.

A block diagram of an adaptive equalizer that adapts its tap coefficients according to Equation (8.6.44) is illustrated in Figure 8.39. Note that the difference between the desired output  $a_k$  and the actual output  $z_k$  from the equalizer is used to form the error signal  $e_k$ . This error is scaled by the step-size parameter  $\Delta$ , and the scaled error signal  $\Delta e_k$  multiplies the received signal values  $\{y(kT - n\tau)\}$  at the  $2N + 1$  taps. The products  $\Delta e_k y(kT - n\tau)$  at the  $(2N + 1)$  taps are then added to the previous values of the tap coefficients to obtain the updated tap coefficients, according to Equation (8.6.44). This computation is repeated for each received symbol. Thus, the equalizer coefficients are updated at the symbol rate.

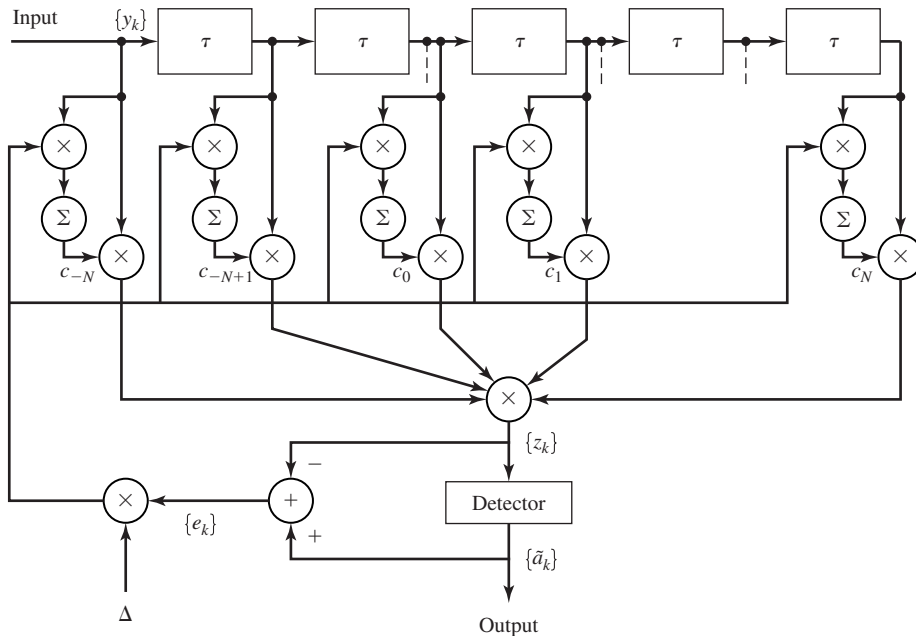


**Figure 8.39** Linear adaptive equalizer based on the MSE criterion.

Initially, the adaptive equalizer is trained by the transmission of a known pseudo-random sequence  $\{a_m\}$  over the channel. At the demodulator, the equalizer employs the known sequence to adjust its coefficients. Upon initial adjustment, the adaptive equalizer switches from a *training mode* to a *decision-directed mode*, in which case the decisions at the output of the detector are sufficiently reliable so that the error signal is formed by computing the difference between the detector output and the equalizer output; i.e.,

$$e_k = \tilde{a}_k - z_k \quad (8.6.45)$$

where  $\tilde{a}_k$  is the output of the detector. In general, decision errors at the output of the detector occur infrequently and, consequently, such errors have little effect on the performance of the tracking algorithm given by Equation (8.6.44).

A rule of thumb for selecting the step-size parameter so as to ensure convergence and good tracking capabilities in slowly varying channels is

$$\Delta = \frac{1}{5(2N + 1)P_R} \quad (8.6.46)$$

where  $P_R$  denotes the received signal-plus-noise power, which can be estimated from the received signal.

The convergence characteristics of the stochastic gradient algorithm in Equation (8.6.44) is illustrated in Figure 8.40. These graphs were obtained from a computer simulation of an 11-tap adaptive equalizer operating a channel with a rather modest amount of ISI. The input signal-plus-noise power  $P_R$  was normalized to unity. The rule of thumb given in Equation (8.6.46) for selecting the step size gives  $\Delta = 0.018$ . The effect of making  $\Delta$  too large is illustrated by the large jumps in MSE as shown for  $\Delta = 0.115$ . As  $\Delta$  is decreased, the convergence is slowed somewhat, but a lower MSE is achieved, indicating that the estimated coefficients are closer to  $\mathbf{c}_{\text{opt}}$ .

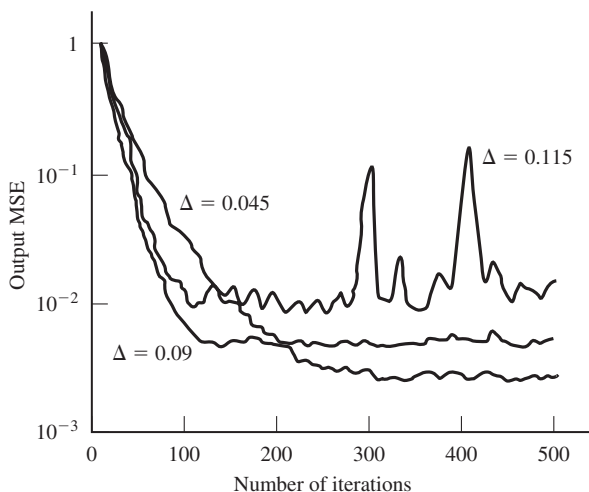


**Figure 8.40** Initial convergence characteristics of the LMS algorithm with different step sizes. (From *Digital Signal Processing* by J. G. Proakis and D. G. Manolakis; ©1988, Macmillan. Reprinted with permission of the publisher.)

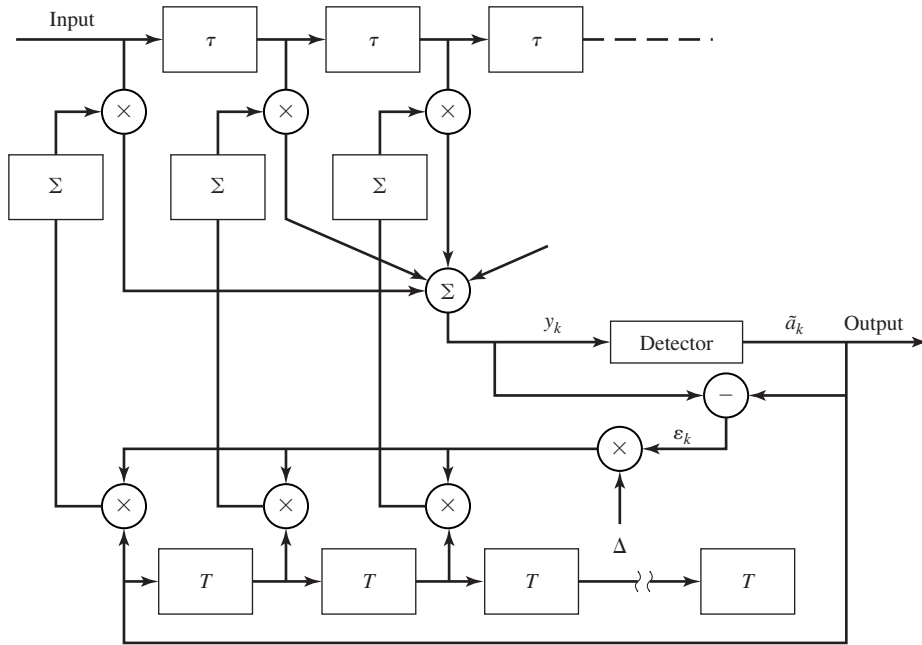


**Figure 8.41** An adaptive zero-forcing equalizer.

Although we have described in some detail the operation of an adaptive equalizer which is optimized on the basis of the MSE criterion, the operation of an adaptive equalizer based on the zero-forcing method is very similar. The major difference lies in the method for estimating the gradient vectors  $\mathbf{g}_k$  at each iteration. A block diagram of an adaptive zero-forcing equalizer is shown in Figure 8.41. For more details on the tap coefficient update method for a zero-forcing equalizer, the reader is referred to the papers by Lucky (1965, 1966); and the texts by Lucky, Salz, and Weldon (1968); and Proakis (2001).

**Decision-Feedback Equalizer.** The linear filter equalizers described above are very effective on channels, such as wireline telephone channels, where the ISI is not severe. The severity of the ISI is directly related to the spectral characteristics and not necessarily to the time span of the ISI. For example, consider the ISI resulting from two channels which are illustrated in Figure 8.42. The time span for the ISI in Channel A is 5 symbol intervals on each side of the desired signal component, which has a value of 0.72. On the other hand, the time span for the ISI in Channel B is one symbol interval on each side of the desired signal component, which has a value of 0.815. The energy of the total response is normalized to unity for both channels.

In spite of the shorter ISI span, Channel B results in more severe ISI. This is evidenced in the frequency response characteristics of these channels, which are shown in Figure 8.43. We observe that Channel B has a spectral null (the frequency response  $C(f) = 0$  for some frequencies in the band  $|f| \leq W$ ) at  $f = 1/2T$ , whereas this does

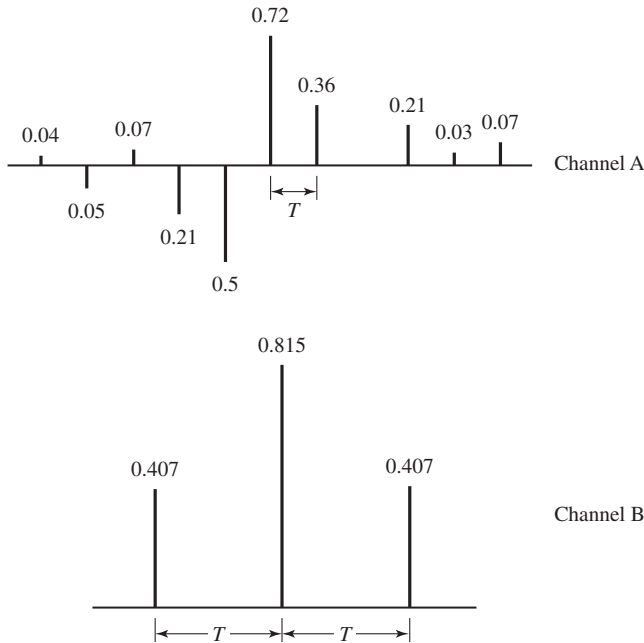
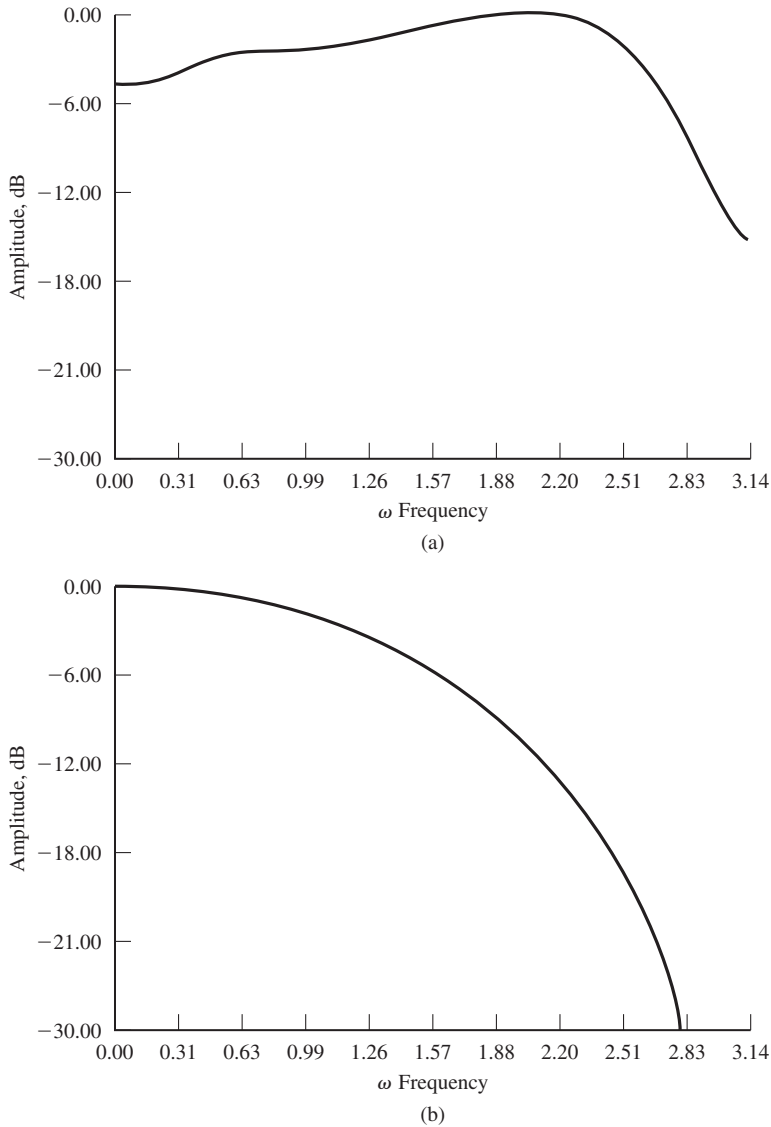


Figure 8.42 Two channels with ISI.

not occur in the case of Channel A. Consequently, a linear equalizer will introduce a large gain in its frequency response to compensate for the channel null. Thus, the noise in Channel B will be enhanced much more than in Channel A. This implies that the performance of the linear equalizer for Channel B will be significantly poorer than that for Channel A. This fact is borne out by the computer simulation results for the performance of the linear equalizer for the two channels, as shown in Figure 8.44. Hence, the basic limitation of a linear equalizer is that it performs poorly on channels having spectral nulls. Such channels are often encountered in radio communications, such as ionospheric transmission at frequencies below 30 MHz and mobile radio channels, such as those used for cellular radio communications.

A *decision-feedback equalizer* (DFE) is a nonlinear equalizer that employs previous decisions to eliminate the ISI caused by previously detected symbols on the current symbol to be detected. A simple block diagram for a DFE is shown in Figure 8.45. The DFE consists of two filters. The first filter is called a *feedforward filter* and it is generally a fractionally spaced FIR filter with adjustable tap coefficients. This filter is identical in form to the linear equalizer described above. Its input is the received filtered signal  $y(t)$ . The second filter is a *feedback filter*. It is implemented as an FIR filter with symbol-spaced taps having adjustable coefficients. Its input is the set of previously detected symbols. The output of the feedback filter is subtracted from the output of the feedforward filter to form the input to the detector. Thus, we have

$$z_m = \sum_{n=1}^{N_1} c_n y(mT - n\tau) - \sum_{n=1}^{N_2} b_n \tilde{a}_{m-n} \quad (8.6.47)$$



**Figure 8.43** Amplitude spectra for (a) channel A shown in Figure 8.42(a) and (b) channel B shown in Figure 8.42(b).

where  $\{c_n\}$  and  $\{b_n\}$  are the adjustable coefficients of the feedforward and feedback filters, respectively,  $\tilde{a}_{m-n}$ ,  $n = 1, 2, \dots, N_2$  are the previously detected symbols,  $N_1$  is the length of the feedforward filter and  $N_2$  is the length of the feedback filter. Based on the input  $z_m$ , the detector determines which of the possible transmitted symbols is closest in distance to the input signal  $z_m$ . Thus, it makes its decision and outputs  $\tilde{a}_m$ .

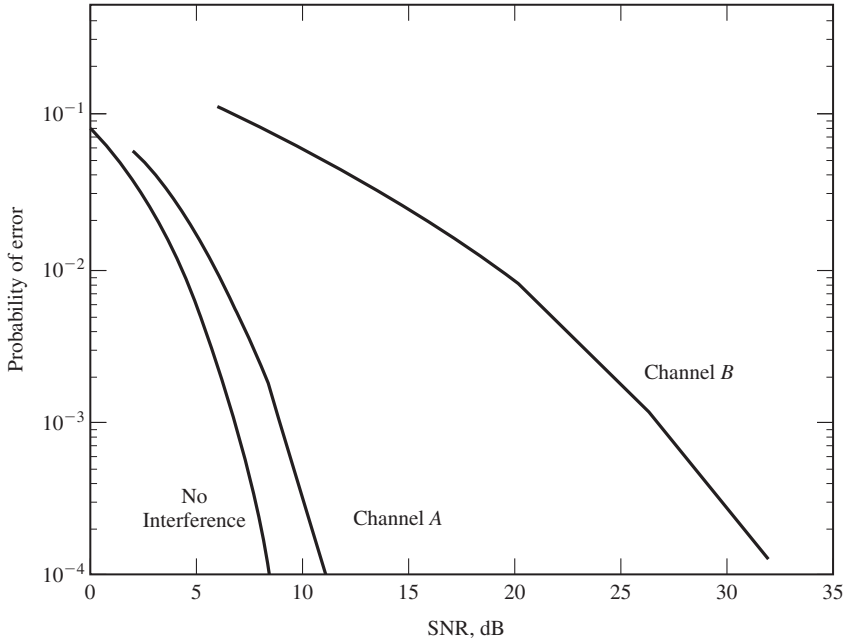


**Figure 8.44** Error-rate performance of linear MSE equalizer.

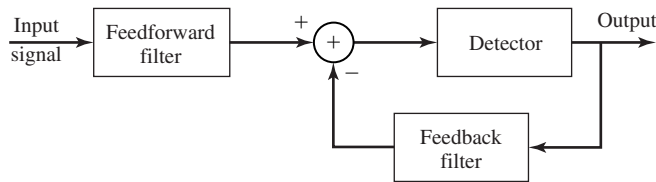


**Figure 8.45** Block diagram of DFE.

What makes the DFE nonlinear is the nonlinear characteristic of the detector which provides the input to the feedback filter.

The tap coefficients of the feedforward and feedback filters are selected to optimize some desired performance measure. For mathematical simplicity, the MSE criterion is usually applied and a stochastic gradient algorithm is commonly used to implement an adaptive DFE. Figure 8.46 illustrates the block diagram of an adaptive DFE whose tap coefficients are adjusted by means of the LMS stochastic gradient algorithm. Figure 8.47 illustrates the probability of error performance of the DFE, obtained by computer simulation, for binary PAM transmission over Channel B. The gain in performance relative to that of a linear equalizer is clearly evident.

We should mention that decision errors from the detector that are fed to the feedback filter have a small effect on the performance of the DFE. In general, a small



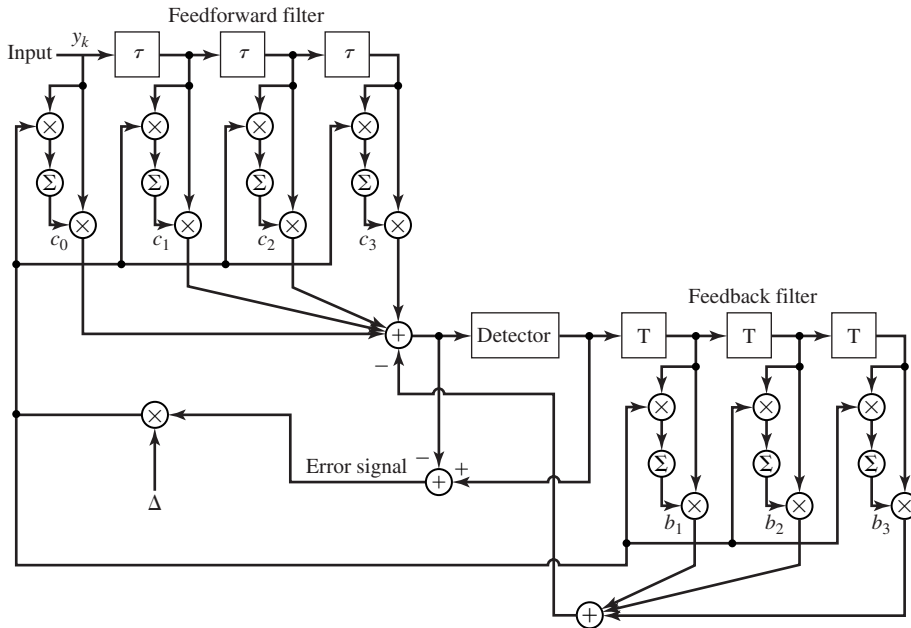
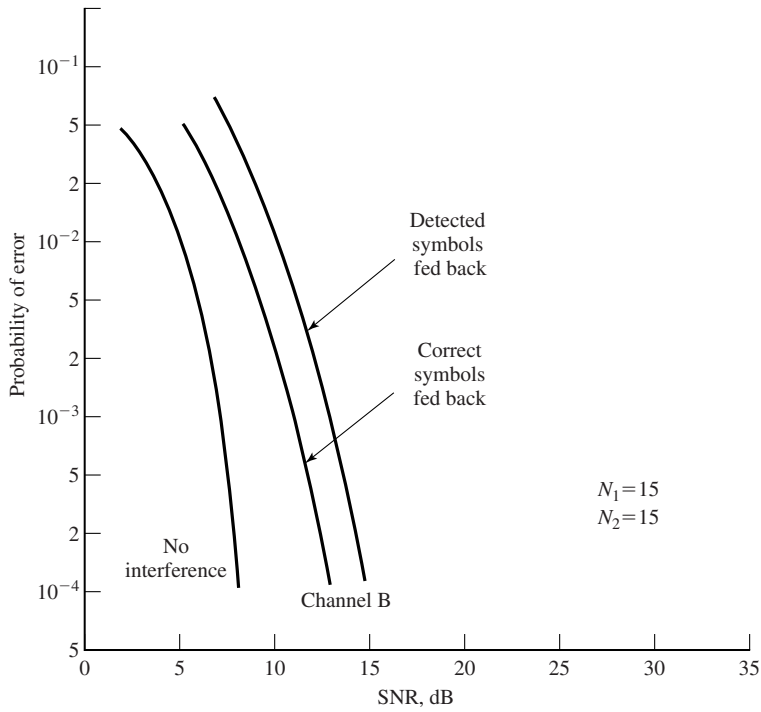


Figure 8.46 Adaptive DFE.

loss in performance of one to two dB is possible at error rates below  $10^{-2}$ , but the decision errors in the feedback filters are not catastrophic.

Although the DFE outperforms a linear equalizer, it is not the optimum equalizer from the viewpoint of minimizing the probability of error. As indicated previously, the optimum detector in a digital communication system in the presence of ISI is a ML symbol sequence detector. It is particularly appropriate for channels with severe ISI, when the ISI spans only a few signals. For example Figure 8.48 illustrates the error probability performance of the Viterbi algorithm for a binary PAM signal transmitted through channel B (see Figure 8.42). For purposes of comparison, we also illustrate the probability of error for a decision feedback equalizer. Both results were obtained by computer simulation. We observe that the performance of the ML sequence detector is about 4.5-dB better than that of the DFE at an error probability of  $10^{-4}$ . Hence, this is one example where the ML sequence detector provides a significant performance gain on a channel which has a relatively short ISI span.

In conclusion, we mention that adaptive equalizers are widely used in high-speed digital communication systems for telephone channels. High-speed telephone line modems (bit rate above 2400 bps) generally include an adaptive equalizer that is implemented as an FIR filter with coefficients that are adjusted based on the MMSE criterion. Depending on the data speed, the equalizer typically spans between 20 and 70 symbols. The LMS algorithm given by Equation (8.6.44) is usually employed for the adjustment of the equalizer coefficients adaptively.



**Figure 8.47** Performance of DFE with and without error propagation.

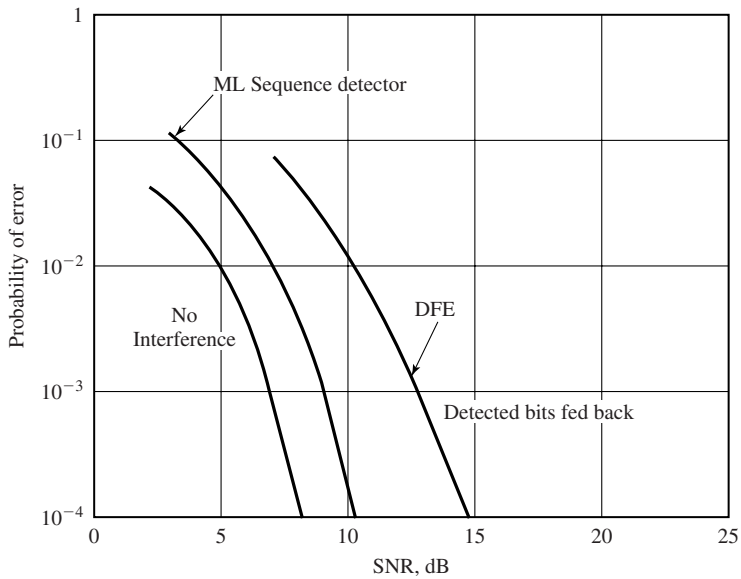


**Figure 8.48** Performance of Viterbi detector and DFE for channel B.

## 8.7 MULTICARRIER MODULATION AND OFDM

In the preceding sections, we considered digital transmission through nonideal channels and observed that such channels cause intersymbol interference when the reciprocal of the system rate is significantly smaller than the time dispersion (duration of the impulse response) of the nonideal channel. In such a case, a channel equalizer is employed at the receiver to compensate for the channel distortion. If the channel is a bandpass channel with a specified bandwidth, the information-bearing signal may be generated at the baseband and then translated in frequency to the passband of the channel. Thus, the information-bearing signal is transmitted on a single carrier. We also observed that intersymbol interference usually results in some performance degradation, even in the case where the optimum detector is used to recover the information symbols at the receiver.

An alternative approach to the design of a bandwidth-efficient communication system in the presence of channel distortion is to subdivide the available channel bandwidth into a number of equal-bandwidth subchannels, where the bandwidth of each subchannel is sufficiently narrow so that the frequency response characteristics of the subchannels are nearly ideal. Such a subdivision of the overall bandwidth into smaller subchannels is illustrated in Figure 8.49. Thus, we create  $K = W/\Delta f$  subchannels, where different information symbols can be transmitted simultaneously in the  $K$  subchannels. Consequently, the data is transmitted by frequency-division multiplexing (FDM).

With each subchannel, we associate a carrier

$$x_k(t) = \sin 2\pi f_k t, \quad k = 0, 1, \dots, K - 1 \quad (8.7.1)$$

where  $f_k$  is the mid-frequency in the  $k$ th subchannel. By selecting the symbol rate  $1/T$  on each of the subchannels to be equal to the separation  $\Delta f$  of adjacent subcarriers, the subcarriers are orthogonal over the symbol interval  $T$ , independent of the relative phase relationship between subcarriers; i.e.,

$$\int_0^T \sin(2\pi f_k t + \phi_k) \sin(2\pi f_j t + \phi_j) dt = 0 \quad (8.7.2)$$

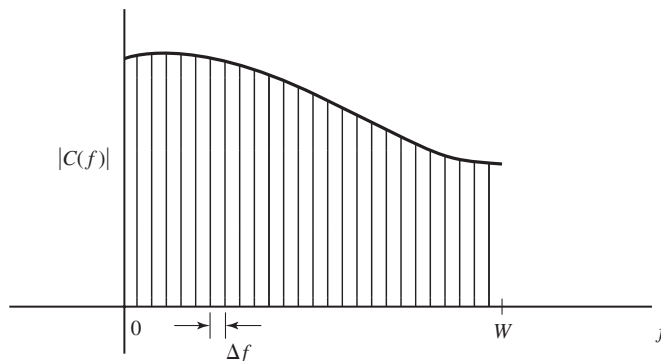


**Figure 8.49** Subdivision of the channel bandwidth  $W$  into narrowband subchannels of equal width  $\Delta f$ .

where  $f_k - f_j = n/T$ ,  $n = 1, 2, \dots$ , independent of the values of the phases  $\phi_k$  and  $\phi_j$ . In this case, we have orthogonal frequency-division multiplexing (OFDM).

With an OFDM system having  $K$  subchannels, the symbol rate on each subcarrier is reduced by a factor of  $N$  relative to the symbol rate on a single carrier system that employs the entire bandwidth  $W$  and transmits data at the same rate as OFDM. Hence, the symbol interval in the OFDM system is  $T = K T_s$ , where  $T_s$  is the symbol interval in the single-carrier system. By selecting  $K$  to be sufficiently large, the symbol interval  $T$  can be made significantly larger than the time duration of the channel-time dispersion. Thus, intersymbol interference can be made arbitrarily small by selection of  $K$ . In other words, each subchannel appears to have a fixed frequency response  $C(f_k)$ ,  $k = 0, 1, \dots, K - 1$ .

As long as we maintain time synchronization among the subcarriers, OFDM allows us to transmit a different number of bits/symbol on each subcarrier. Hence, subcarriers that yield a higher SNR due to a lower attenuation can be modulated to carry more bits/symbol than subchannels that yield a lower SNR (high attenuation). For example, QAM with different constellation sizes may be used in an OFDM system.

The modulator and demodulator in an OFDM system can be implemented by use of a parallel bank of filters based on the discrete Fourier transform (DFT). When the number of subchannels is large, say  $K > 25$ , the modulator and demodulator in an OFDM system are efficiently implemented by use of the fast Fourier transform algorithm (FFT) to compute the DFT. Next, we describe an OFDM system in which the modulator and demodulator are implemented based on the DFT.

A major problem with the multicarrier modulation in general and OFDM system in particular is the high peak-to-average power ratio (PAR) that is inherent in the transmitted signal. Large signal peaks occur in the transmitted signal when the signals in the  $K$  subchannels add constructively in phase. Such large signal peaks may saturate the power amplifier at the transmitter and, thus, cause intermodulation distortion in the transmitted signal. Intermodulation distortion can be reduced and, generally, avoided by reducing the power in the transmitted signal and, thus, operating the power amplifier at the transmitter in the linear range. Such a power reduction results in inefficient operation of the OFDM system.

A variety of methods have been devised to reduce PAR in multicarrier systems. A relatively simple method is to insert different phase shifts in each of the subcarriers, where the phase shifts are selected pseudorandomly, or by means of some algorithm, to reduce the PAR. Additional methods are cited in the references cited in Section 8.8.

### 8.7.1 An OFDM System Implemented via the FFT Algorithm

In this section, we describe an OFDM system in which QAM is used for data transmission on each of the subcarriers and the FFT algorithm is used in the implementation of the modulator and demodulator.

The basic block diagram of the OFDM is illustrated in Figure 8.50. A serial-to-parallel buffer subdivides the information sequence into frames of  $B_f$  bits. The  $B_f$  bits in each frame are parsed into  $K$  groups, where the  $i$ th group is assigned  $b_i$  bits.

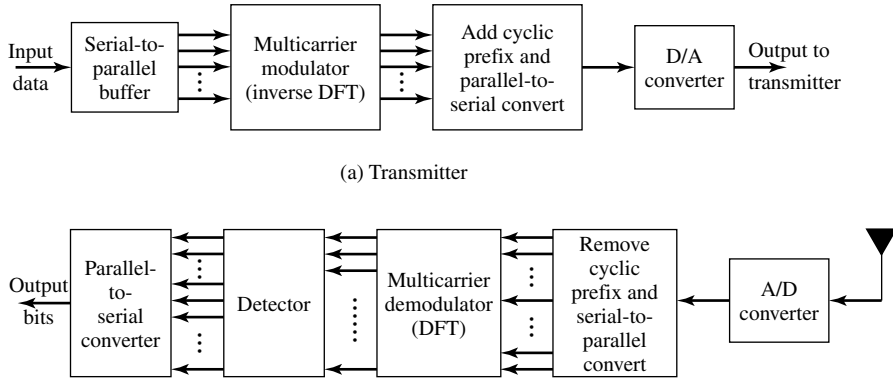


**Figure 8.50** Block diagram of a multicarrier OFDM digital communication system.

Hence,

$$\sum_{i=1}^K b_i = B_f \quad (8.7.3)$$

We may view the multicarrier modulator as generating  $K$  independent QAM subchannels, where the symbol rate for each subchannel is  $1/T$  and the signal in each subchannel has a distinct QAM constellation. Hence, the number of signal points for the  $i$ th subchannel is  $M_i = 2^{b_i}$ . Let us denote the complex-valued signal points corresponding to the information signals on the  $K$  subchannels by  $X_k$ ,  $k = 0, 1, \dots, K - 1$ . These information symbols  $\{X_k\}$  represent the values of the discrete Fourier transform (DFT) of a multicarrier OFDM signal  $x(t)$ , where the modulation on each subcarrier is QAM. Since  $x(t)$  must be a real-valued signal, its  $N$ -point DFT  $\{X_k\}$  must satisfy the symmetry property  $X_{N-k} = X_k^*$ . Therefore, we create  $N = 2K$  symbols from  $K$  information symbols by defining

$$X_{N-k} = X_k^*, \quad k = 1, 2, \dots, K - 1 \quad (8.7.4)$$

$$X'_0 = \text{Re}(X_0) \quad (8.7.5)$$

$$X_N = \text{Im}(X_0) \quad (8.7.6)$$

Note that the information symbol  $X_0$  is split into two parts, both of which are real. If we denote the new sequence of symbols as  $\{X'_k, k = 0, 1, \dots, N - 1\}$ , the  $N$ -point inverse DFT (IDFT) yields the real-valued sequence

$$x_n = \frac{1}{\sqrt{N}} \sum_{k=0}^{N-1} X'_k e^{j2\pi nk/N} \quad n = 0, 1, \dots, N - 1 \quad (8.7.7)$$

where  $1/\sqrt{N}$  is simply a scale factor. This sequence  $\{x_n, 0 \leq n \leq N - 1\}$  corresponds to samples of the multicarrier OFDM signal  $x(t)$ , consisting of  $K$  subcarriers, which

may be expressed as

$$x(t) = \frac{1}{\sqrt{N}} \sum_{k=0}^{N-1} X'_k e^{j2\pi kt/T}, \quad 0 \leq t \leq T \quad (8.7.8)$$

where  $T$  is the signal duration and  $x_n = x(nT/N)$ ,  $n = 0, 1, \dots, N-1$ . The subcarrier frequencies are  $f_k = k/T$ ,  $k = 0, 1, \dots, K-1$ . The signal samples  $\{x_n\}$  generated by computing the IDFT are passed through a digital-to-analog (D/A) converter, where output, ideally, is the OFDM signal waveform  $x(t)$ .

With  $x(t)$  as the input to the channel, the channel output at the receiver may be expressed as

$$r(t) = x(t) \star c(t) + n(t) \quad (8.7.9)$$

where  $c(t)$  is the impulse response of the channel and  $\star$  denotes convolution. Since the bandwidth  $\Delta f$  of each subchannel is selected to be very small relative to the overall channel bandwidth  $W = K\Delta f$ , the symbol duration  $T = 1/\Delta f$  is large compared to the duration of the channel impulse response. To be specific, suppose that the channel impulse response spans  $m+1$  signal samples, where  $m \ll N$ . A simple way to completely avoid intersymbol interference (ISI) is to insert a time guard of duration  $mT/N$  between transmission of successive data blocks. This allows the response of the channel to die out before the next block of  $K$  symbols are transmitted.

An alternative method to avoid ISI is to append a so-called cyclic prefix to each block of  $N$  signal samples  $\{x_n, 0 \leq n \leq N-1\}$ . The cyclic prefix for the block of samples consists of the samples  $x_{N-m}, x_{N-m+1}, \dots, x_{N-1}$ . These samples are appended to the beginning of the block, thus, creating a signal sequence of length  $N+m$  samples, which may be indexed from  $n = -m$  to  $n = N-1$ , where the first  $m$  samples constitute the cyclic prefix. Then, if the sample values of the channel response are  $\{c_n, 0 \leq n \leq m\}$ , the convolution of  $\{c_n\}$  with  $\{x_n, -m \leq n \leq N-1\}$  produce the received signal  $\{r_n\}$ . Since the ISI in any pair of successive signal transmission blocks affects the first  $m$  signal samples, we discard the first  $m$  samples of  $\{r_n\}$  and demodulate the signal based on the received signal samples  $\{r_n, 0 \leq n \leq N-1\}$ .

If we view the channel characteristics in the frequency domain, the channel frequency response at the subcarrier frequencies  $f_k = k/T$  is

$$C_k = C \left( \frac{2\pi k}{N} \right) = \sum_{n=0}^m c_n e^{-j2\pi nk/N}, \quad k = 0, 1, \dots, N-1 \quad (8.7.10)$$

Since the ISI is eliminated by the use of either the cyclic prefix or the time guard band, the demodulated sequence of symbols may be expressed as

$$\hat{X}_k = C_k X'_k + \eta_k, \quad k = 0, 1, \dots, N-1 \quad (8.7.11)$$

where  $\{\hat{X}_k\}$  is the output of the  $N$ -point DFT computed by the demodulator and  $\{\eta_k\}$  is the additive noise corrupting the signal.

As illustrated in Figure 8.50, the received signal is demodulated by computing the DFT of the received signal after it has been passed through an analog-to-digital

(A/D) converter. As in the case of the OFDM modulator, the DFT computation at the demodulator is performed efficiently by use of the FFT algorithm.

In order to recover the information symbols from the values of the computed DFT, it is necessary to estimate and compensate for the channel factors  $\{C_k\}$ . The channel measurement can be accomplished by initially transmitting either a known modulated sequence on each of the subcarriers or, simply, transmitting the unmodulated subcarriers. If the channel characteristics vary slowly with time, the time variations can be tracked by using the decisions at the output of the detector in a decision-directed manner. Thus, the multicarrier OFDM system can be made to operate adaptively. The transmission rate on each of the subcarriers can be optimized by properly allocating the average transmitted power and the number of bits that are transmitted by each subcarrier. The SNR per subchannel may be defined as

$$\text{SNR}_k = \frac{T P_k |C_k|^2}{\sigma_{nk}^2} \quad (8.7.12)$$

where  $T$  is the symbol duration,  $P_k$  is the average transmitted power allocated to the  $k$ th subchannel,  $|C_k|^2$  is the squared magnitude of the frequency response of the  $k$ th subchannel, and  $\sigma_{nk}^2$  is the corresponding noise variance. In subchannels with high SNR, we transmit more bits/symbol by using a larger QAM constellation compared to subchannels with low SNR. Thus, the bit rate on each subchannel can be optimized in such a way that the error-rate performance among the subchannels is equalized to satisfy the desired specifications.

Multicarrier OFDM using QAM modulation on each of the subcarriers as described above has been implemented for a variety of applications, including high-speed transmission over telephone lines, such as digital subcarrier lines. This type of multicarrier OFDM modulation has also been called *discrete-multitone (DMT) modulation*. Multicarrier OFDM is also used in digital audio broadcasting in Europe and other parts of the world and in digital cellular communication systems.

## 8.8 FURTHER READING

The pioneering work on signal design for bandwidth-constrained channels was done by Nyquist (1928). The use of binary partial response signals was originally proposed in the paper by Lender (1963) and was later generalized by Kretzmer (1966). The problem of optimum transmitter and receiver filter design was investigated by Gerst and Diamond (1961), Tufts (1965), Smith (1965), and Berger and Tufts (1967).

Adaptive equalization for digital communication was introduced by Lucky (1965, 1966). Widrow (1966) devised the LMS algorithm for adaptively adjusting the equalizer coefficients.

The Viterbi algorithm was devised by Viterbi (1967) for the purpose of decoding convolutional codes, which are described in Chapter 9. Its use as the ML sequence detector for partial response signals and, more generally, for symbols corrupted by

intersymbol interference, was proposed and analyzed by Forney (1972) and Omura (1971). A comprehensive treatment of adaptive equalization algorithms is given in the book by Proakis (2001).

There is a large amount of literature on multicarrier digital communication systems. One of the earliest systems, described by Doeltz et al. (1957) and called Kineplex, was used for digital transmission in the high-frequency radio band. Other early work on the multicarrier system design is described in the papers by Chang (1966) and Saltzberg (1967). The use of DFT for modulation and demodulation of multicarrier OFDM systems was proposed by Weinstein and Ebert (1971). More recent references on applications of OFDM in practical systems are the papers by Chow et al. (1995) and Bingham (1990). The recent book by Bahai and Saltzberg (1999) provides a comprehensive treatment of OFDM.

The problem of PAR reduction in multicarrier systems has been investigated by many people. The interested reader may refer to the papers by Boyd (1986), Popovic (1991), Jones et al. (1994), Wilkinson and Jones (1995), Wulich (1996), Tellado and Cioffi (1998), and Tarokh and Jafarkhani (2000).

## PROBLEMS

- 8.1** In Example 8.1.1, the ideal channel of bandwidth  $W$  limits the transmitted signal energy that passes through the channel. The received signal energy as a function of the channel bandwidth is

$$\mathcal{E}_h(W) = \frac{T}{(2\pi)^2} \int_{-WT}^{WT} \frac{\sin^2 \pi \alpha}{\alpha^2 (1 - \alpha^2)^2} d\alpha$$

where  $\alpha = fT$ .

1. Evaluate (numerically)  $\mathcal{E}_h(W)$  for  $W = \frac{1}{2T}, \frac{1}{T}, \frac{1.5}{T}, \frac{2}{T}, \frac{2.5}{T}, \frac{3}{T}$ , and plot  $\frac{\mathcal{E}_h(W)}{T}$  as a function of  $W$ .
2. Determine the value of  $\mathcal{E}_h(W)$  in the limit as  $W \rightarrow \infty$ . For the computation you may use the time-domain relation

$$\lim_{W \rightarrow \infty} \mathcal{E}_h(W) = \int_{-\infty}^{+\infty} g_T^2(t) dt$$

- 8.2** In a binary PAM system, the input to the detector is

$$y_m = a_m + n_m + i_m$$

where  $a_m = \pm 1$  is the desired signal,  $n_m$  is a zero-mean Gaussian random variable with variance  $\sigma_n^2$ , and  $i_m$  represents the ISI due to channel distortion. The ISI term is a random variable which takes the values,  $-\frac{1}{2}, 0, \frac{1}{2}$  with probabilities  $\frac{1}{4}, \frac{1}{2}, \frac{1}{4}$ , respectively. Determine the average probability of error as a function of  $\sigma_n^2$ .

- 8.3** In a binary PAM system, the clock that specifies the sampling of the correlator output is offset from the optimum sampling time by 10%.



1. If the signal pulse used is rectangular, determine the loss in SNR due to the mistiming.
  2. Determine the amount of intersymbol interference introduced by the mistiming and determine its effect on performance.
- 8.4** The elements of the sequence  $\{a_n\}_{n=-\infty}^{+\infty}$  are independent binary random variables taking values of  $\pm 1$  with equal probability. This data sequence is used to modulate the basic pulse  $g(t)$  shown in Figure P-8.4(a). The modulated signal is

$$X(t) = \sum_{n=-\infty}^{+\infty} a_n g(t - nT)$$

1. Find the power-spectral density of  $X(t)$ .
2. If  $g_1(t)$  [shown in Figure P-8.4(b)] is used instead of  $g(t)$ , how would the power spectrum in part 1 change?
3. In part 2, assume we want to have a null in the spectrum at  $f = \frac{1}{4T}$ . This is done by a precoding of the form  $b_n = a_n + \alpha a_{n-1}$ . Find  $\alpha$  that provides the desired null.
4. Is it possible to employ a precoding of the form  $b_n = a_n + \sum_{i=1}^N \alpha_i a_{n-i}$  for some finite  $N$  such that the final power spectrum will be identical to zero for  $\frac{1}{3T} \leq |f| \leq \frac{1}{2T}$ ? If yes, how? If no, why? (Hint: use properties of analytic functions.)

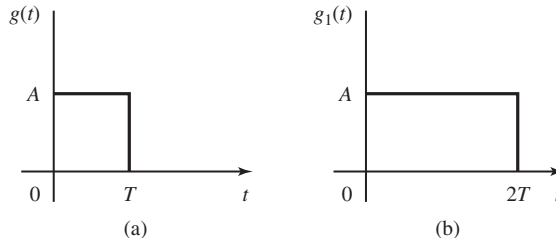


**Figure P-8.4**

- 8.5** The information sequence  $\{a_n\}_{n=-\infty}^{\infty}$  is a sequence of i.i.d. random variables each taking values  $+1$  and  $-1$  with equal probability. This sequence is to be transmitted at baseband by a biphase coding scheme described by

$$s(t) = \sum_{n=-\infty}^{\infty} a_n g(t - nT)$$

where  $g(t)$  is shown in Figure P-8.5.

1. Find the power-spectral density of  $s(t)$ .
2. Assume that it is desirable to have a null in the power spectrum at  $f = \frac{1}{T}$ . To this end we use a precoding scheme by introducing  $b_n = a_n + ka_{n-1}$ , where  $k$  is some constant, and then transmit the  $\{b_n\}$  sequence using the same  $g(t)$ . Is it possible to choose  $k$  to produce a frequency null at  $f = \frac{1}{T}$ ? If yes what is the appropriate value and what is the resulting power spectrum?
3. Now assume we want to have nulls at all multiples of  $f_0 = \frac{1}{2T}$ . Is it possible to have these nulls with an appropriate choice of  $k$  in the previous part? If not what kind of precoding do you suggest to result in the desired nulls?

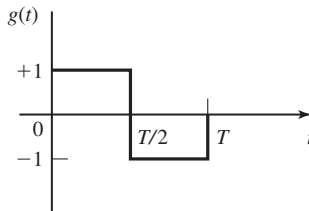


Figure P-8.5

- 8.6** The two signal waveforms for binary PSK signal transmission with discontinuous phase are

$$s_0(t) = \sqrt{\frac{2\mathcal{E}_b}{T_b}} \cos \left[ 2\pi \left( f - \frac{\Delta f}{2} \right) t + \theta_0 \right], \quad 0 \leq t \leq T$$

$$s_1(t) = \sqrt{\frac{2\mathcal{E}_b}{T_b}} \cos \left[ 2\pi \left( f + \frac{\Delta f}{2} \right) t + \theta_1 \right], \quad 0 \leq t \leq T$$

where  $\Delta f = 1/T \ll f_c$ , and  $\theta_0$  and  $\theta_1$  are uniformly distributed random variables on the interval  $(0, 2\pi)$ . The signals  $s_0(t)$  and  $s_1(t)$  are equally probable.

1. Determine the power-spectral density of the FSK signal.
  2. Show that the power-spectral density decays as  $1/f^2$  for  $f \gg f_c$ .
- 8.7** Consider a four-phase PSK signal that is represented by the equivalent lowpass signal.

$$v(t) = \sum_n a_n g(t - nT)$$

where  $a_n$  takes on one of the four possible values  $\frac{\pm 1 \pm j}{\sqrt{2}}$  with equal probability. The sequence of information symbols  $\{a_n\}$  is statistically independent.

1. Determine and sketch the power-spectral density of  $v(t)$  when

$$g(t) = \begin{cases} A, & 0 \leq t \leq T \\ 0, & \text{otherwise} \end{cases}$$

2. Repeat part 1 when

$$g(t) = \begin{cases} A \sin \frac{\pi t}{2}, & 0 \leq t \leq T \\ 0, & \text{otherwise} \end{cases}$$

3. Compare the spectra obtained in parts 1 and 2 in terms of the 3-dB bandwidth and the bandwidth to the first spectral null.

- 8.8** Starting with the definition of the transition probability matrix for delay modulation given in Example 8.5.11, demonstrate that the relation

$$\mathbf{P}^4 \boldsymbol{\gamma} = -\frac{1}{4} \boldsymbol{\gamma}$$

holds and, hence,

$$\mathbf{P}^{k+4} \boldsymbol{\gamma} = -\frac{1}{4} \mathbf{P}^k \boldsymbol{\gamma}, \quad k \geq 1$$

- 8.9** The frequency-response characteristic of a lowpass channel can be approximated by

$$H(f) = \begin{cases} 1 + \alpha \cos 2\pi f t_0, & |\alpha| < 1, \quad |f| \leq W \\ 0, & \text{otherwise} \end{cases}$$

where  $W$  is channel bandwidth. An input signal  $s(t)$  whose spectrum is bandlimited to  $W$  Hz is passed through the channel.

1. Show that

$$y(t) = s(t) + \frac{\alpha}{2} [s(t - t_0) + s(t + t_0)]$$

Thus, the channel produces a pair of echoes.

2. Suppose the received signal  $y(t)$  is passed through a filter matched to  $s(t)$ . Determine the output of the matched filter at  $t = kT$ ,  $k = 0, \pm 1, \pm 2, \dots$ , where  $T$  is the symbol duration.
3. What is the ISI pattern resulting from the channel if  $t_0 = T$ ?

- 8.10** A wireline channel of length 1000 km is used to transmit data by means of binary PAM. Regenerative repeaters are spaced at 50-km apart along the system. Each segment of the channel has an ideal (constant) frequency response over the frequency band  $0 \leq f \leq 1200$ , and an attenuation of 1 dB/km. The channel noise is AWGN.

1. What is the highest bit rate that can be transmitted without ISI?
2. Determine the required  $\mathcal{E}_b/N_0$  to achieve a bit error of  $P_2 = 10^{-7}$  for each repeater.

3. Determine the transmitted power at each repeater to achieve the desired  $\mathcal{E}_b/N_0$ , where  $N_0 = 4.1 \times 10^{-21}$  W/Hz.
- 8.11 Show that a pulse having the raised cosine spectrum given by Equation (8.3.22) satisfies the Nyquist criterion given by Equation (8.3.9) for any value of the roll-off factor  $\alpha$ .
- 8.12 Show that for any value of  $\alpha$  the raised cosine spectrum given by Equation (8.3.22) satisfies

$$\int_{-\infty}^{+\infty} X_{\text{rc}}(f) df = 1$$

(Hint: Use the fact that  $X_{\text{rc}}(f)$  satisfies the Nyquist criterion given by Equation (8.3.9).

- 8.13 Theorem 8.3.1 gives the necessary and sufficient condition for the spectrum  $X(f)$  of the pulse  $x(t)$  that yields zero ISI. Prove that for any pulse that is bandlimited to  $|f| < 1/T$ , the zero ISI condition is satisfied if  $\text{Re}[X(f)]$ , for  $f > 0$ , consists of a rectangular function plus an arbitrary odd function about  $f = 1/2T$  and  $\text{Im}[X(f)]$  is any arbitrary even function about  $f = 1/2T$ .
- 8.14 A voice-band telephone channel has a passband characteristic in the frequency range  $300 < f < 3000$  Hz.
1. Select a symbol rate and a power efficient constellation size to achieve 9600 bits/sec signal transmission.
  2. If a square-root raised cosine pulse is used for the transmitter pulse  $g_T(t)$ , select the roll-off factor. Assume that the channel has an ideal frequency response characteristic.

- 8.15 Design an  $M$ -ary PAM system that transmits digital information over an ideal channel with bandwidth  $W = 2400$  Hz. The bit rate is 14,400 bits/sec. Specify the number of transmitted points, the number of received signal points using a duobinary signal pulse, and the required  $\mathcal{E}_b$  to achieve an error probability of  $10^{-6}$ . The additive noise is zero-mean Gaussian with a power-spectral density  $10^{-4}$  W/Hz.
- 8.16 A binary PAM signal is generated by exciting a raised cosine roll-off filter with a 50% roll-off factor and is then DSB-SC amplitude modulated on a sinusoidal carrier as illustrated in Figure P-8.16. The bit rate is 2400 bits/sec.

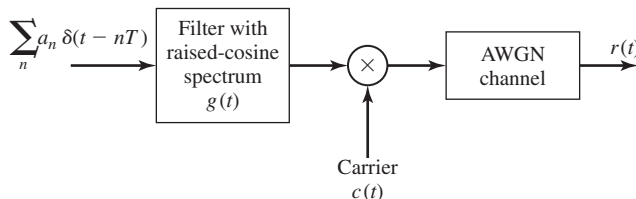


Figure P-8.16

1. Determine the spectrum of the modulated binary PAM signal and sketch it.
  2. Draw the block diagram illustrating the optimum demodulator/detector for the received signal which is equal to the transmitted signal plus additive, white Gaussian noise.
- 8.17** When the additive noise at the input to the modulator is colored, the filter matched to the signal no longer maximizes the output SNR. In such a case we may consider the use of a prefilter that “whitens” the colored noise. The prefilter is followed by a filter matched to the prefiltered signal. Towards this end, consider the configuration shown in Figure P-8.17.
1. Determine the frequency-response characteristic of the prefilter that whitens the noise.
  2. Determine the frequency-response characteristic of the filter matched to  $\bar{s}(t)$ .
  3. Consider the prefilter and the matched filter as a single “generalized matched filter.” What is the frequency-response characteristic of this filter?
  4. Determine the SNR at the input to the detector.

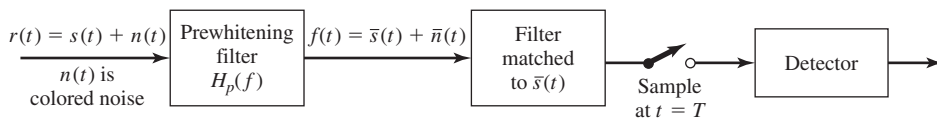


Figure P-8.17

- 8.18** A voice-band telephone channel passes the frequencies in the band from 300 to 3300 Hz. It is desired to design a modem that transmits at a symbol rate of 2400 symbols/sec, with the objective of achieving 9600 bits/sec. Select an appropriate QAM signal constellation, carrier frequency, and the roll-off factor of a pulse with a raised cosine spectrum that utilizes the entire frequency band. Sketch the spectrum of the transmitted signal pulse and indicate the important frequencies.
- 8.19** Determine the bit rate that can be transmitted through a 4 KHz voice-band telephone (bandpass) channel if the following modulation methods are used: (1) binary PSK, (2) four-phase PSK, (3) 8-point QAM, (4) binary orthogonal FSK, with noncoherent detection, (5) orthogonal four-FSK with noncoherent detection, and (6) orthogonal 8-FSK with noncoherent detection. For parts 1–3, assume that the transmitter pulse shape has a raised cosine spectrum with a 50% roll-off.
- 8.20** An ideal voice-band telephone line channel has a bandpass frequency-response characteristic spanning the frequency range 600–3000 Hz.
1. Design an  $M = 4$  PSK (quadrature PSK or QPSK) system for transmitting data at a rate of 2400 bits/sec and a carrier frequency  $f_c = 1800$ . For spectral

shaping, use a raised cosine frequency-response characteristic. Sketch a block diagram of the system and describe their functional operation.

2. Repeat part 1 if the bit rate  $R = 4800$  bits/sec.

- 8.21** A 4 KHz bandpass channel is to be used for transmission of data at a rate of 9600 bits/sec. If  $N_0/2 = 10^{-10}$  W/Hz is the spectral density of the additive, zero-mean Gaussian noise in the channel, design a QAM modulation and determine the average power that achieves a bit-error probability of  $10^{-6}$ . Use a signal pulse with a raised cosine spectrum having a roll-off factor of at least 50%.
- 8.22** Consider the transmission of data via PAM over a voice-band telephone channel that has a bandwidth of 3000 Hz. Show how the symbol rate varies as a function of the excess bandwidth. In particular, determine the symbol rate for excess bandwidths of 25%, 33%, 50%, 67%, 75%, and 100%.
- 8.23** The binary sequence 10010110010 is the input to the precoder whose output is used to modulate a duobinary transmitting filter. Construct a table as in Table 8.2 showing the precoded sequence, the transmitted amplitude levels, the received signal levels and the decoded sequence.
- 8.24** Repeat the Problem 8.23 for a modified duobinary signal pulse.
- 8.25** A precoder for a partial response signal fails to work if the desired partial response at  $n = 0$  is zero modulo  $M$ . For example, consider the desired response for  $M = 2$ :

$$x(nT) = \begin{cases} 2, & n = 0 \\ 1, & n = 1 \\ -1, & n = 2 \\ 0, & \text{otherwise} \end{cases}$$

Show why this response cannot be precoded.

- 8.26** In the case of correlated noise, the relation in the Viterbi algorithm may be expressed in general as [Ungerboeck, (1974)]

$$\mu(\mathbf{a}) = 2 \sum_n a_n r_n - \sum_n \sum_m a_n a_m x_{n-m}$$

where  $x_n = x(nT)$  is the sampled signal output of the matched filter,  $\{a_n\}$  is the data sequence, and  $\{r_n\}$  is the received signal sequence at the output of the matched filter. Determine the metric for the duobinary signal.

- 8.27** Sketch and label the trellis for a duobinary signal waveform used in conjunction with the precoding given by Equation (8.4.7). Repeat this for the modified duobinary signal waveform with the precoder given by Equation (8.4.19). Comment on any similarities and differences.
- 8.28** Consider the use of a (square-root) raised cosine signal pulse with a roll-off factor of unity for transmission of binary PAM over an ideal bandlimited channel that

passes the pulse without distortion. Thus, the transmitted signal is

$$v(t) = \sum_{k=-\infty}^{\infty} a_k g_T(t - kT_b)$$

where the signal interval  $T_b = T/2$ . Thus, the symbol rate is double of that for no ISI.

1. Determine the ISI values at the output of a matched-filter demodulator.
  2. Sketch the trellis for the ML sequence detector and label the states.
- 8.29** A binary antipodal signal is transmitted over a nonideal bandlimited channel, which introduces ISI over two adjacent symbols. For an isolated transmitted signal pulse  $s(t)$ , the (noise-free) output of the demodulator is  $\sqrt{\mathcal{E}_b}$  at  $t = T$ ,  $\sqrt{\mathcal{E}_b}/4$  at  $t = 2T$ , at zero for  $t = kT$ ,  $k > 2$ , where  $\mathcal{E}_b$  is the signal energy and  $T$  is the signaling interval.
1. Determine the average probability of error assuming that the two signals are equally probable and the additive noise is white and Gaussian.
  2. By plotting the error probability obtained in part 1 and that for the case of no ISI, determine the relative difference in SNR of the error probability of  $10^{-6}$ .
- 8.30** Show that the covariance matrix  $\mathbf{C}$  for the noise at the output of the matched filter for the duobinary pulse is given by Equation (8.5.25).
- 8.31** As indicated in Section 8.5.1, the running digital sum (RDS) is defined as the difference between the total number of accumulated zeros and the total number of accumulated ones in a sequence. If the RDS is limited to the range

$$-2 \leq \text{RDS} \leq 2$$

determine the state transition matrix and the capacity of the corresponding code.

- 8.32** Determine the capacity of a  $(0, 1)$  runlength-limited code. Compare its capacity with that of a  $(1, \infty)$  code and explain the relationship.
- 8.33** A ternary signal format is designed for a channel that does not pass dc. The binary input information sequence is transmitted by mapping a 1 into either a positive pulse or a negative pulse, and a zero is transmitted by the absence of a pulse. Hence, for the transmission of 1's, the polarity of the pulses alternate. This is called an AMI (alternate mark inversion) code. Determine the capacity of the code.
- 8.34** Give an alternative description of the AMI code described in Problem 8.33 using the RDS with the constraint that the RDS can take only the values 0 and +1.
- 8.35** ( $kBnT$  codes) From Problem 8.33 we note that the AMI code is a "pseudoternary" code in that it transmits one bit/symbol using a ternary alphabet, which has the capacity of  $\log_2 3 = 1.58$  bits. Such a code does not provide sufficient spectral shaping. Better spectral shaping is achieved by the class of block codes designated as  $kBnT$ , where  $k$  denotes the number of information bits and  $n$  denotes the number of ternary symbols/block. By selecting the largest  $k$  possible for each  $n$ ,

we obtain the table shown below.

$k$	$n$	Code
1	1	1B1T
3	2	3B2T
4	3	4B3T
6	4	6B4T

Determine the efficiency of these codes by computing the ratio of the rate of the code in bits/symbol divided by  $\log_2 3$ . Note that 1B1T is the AMI code.

**8.36** This problem deals with the capacity of two  $(d, \kappa)$  codes.

1. Determine the capacity of a  $(d, \kappa)$  code that has the following state transition matrix:

$$D = \begin{bmatrix} 1 & 1 \\ 1 & 0 \end{bmatrix}$$

2. Repeat (step 1) when  $D$  is given as

$$D = \begin{bmatrix} 1 & 1 \\ 0 & 1 \end{bmatrix}$$

3. Comment on the differences between parts 1 and 2.

**8.37** A simplified model of the telegraph code consists of two symbols (Blahut, 1990). A dot consists of one time unit of line closure followed by one time unit of line open. A dash consists of three units of line closure followed by one time unit of line open.

1. If we view this code as a constrained code with symbols of equal duration, give the constraints.
2. Determine the state transition matrix.
3. Determine the capacity.

**8.38** Determine the state transition matrix for the runlength-constrained code described by the state diagram shown in Figure P-8.38. Sketch the corresponding trellis.

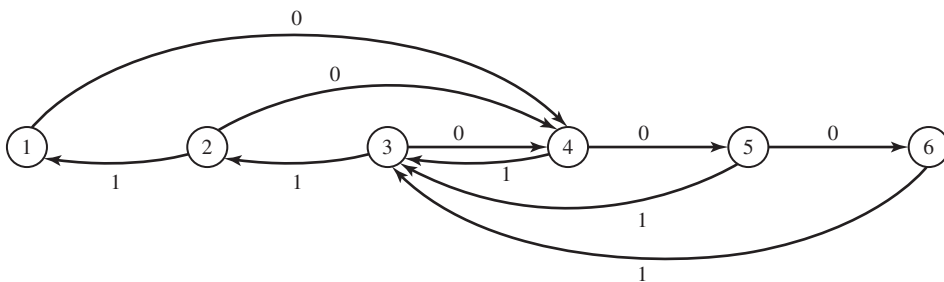


Figure P-8.38



- 8.39** Determine the transition matrix for the  $(2, 7)$  runlength-limited code specified by the state diagram shown in Figure P-8.39.

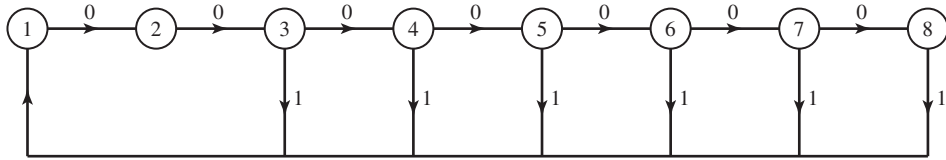


Figure P-8.39

- 8.40** Determine the frequency response characteristics for the RC circuit shown in Figure P-8.40. Also determine the expression for the envelope delay.

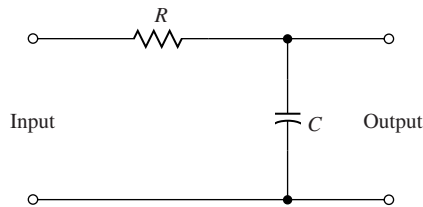


Figure P-8.40

- 8.41** Consider the RC lowpass filter shown in Figure P-8.40 where  $\tau = RC = 10^{-6}$ .
- Determine and sketch the envelope (group) delay of the filter as a function of frequency (see Problem 2.57).
  - Suppose that the input to the filter is a lowpass signal of bandwidth  $\Delta f = 1$  kHz. Determine the effect of the RC filter on this signal.
- 8.42** A microwave radio channel has a frequency response

$$C(f) = 1 + 0.3 \cos 2\pi fT$$

Determine the frequency-response characteristic for the optimum transmitting and receiving filters that yield zero ISI at a rate of  $1/T$  symbols/sec and have a 50%-excess bandwidth. Assume that the additive noise spectrum is flat.

- 8.43**  $M = 4$  PAM modulation is used for transmitting at a bit rate of 9600 bits/sec on a channel having a frequency response

$$C(f) = \frac{1}{1 + j \frac{f}{2400}}$$

$|f| \leq 2400$ , and  $C(f) = 0$ , otherwise. The additive noise is zero-mean, white Gaussian with power-spectral density  $\frac{N_0}{2}$  W/Hz. Determine the (magnitude) frequency response characteristic of the optimum transmitting and receiving filters.

**8.44** Binary PAM is used to transmit information over an unequalized linear filter channel. When  $a = 1$  is transmitted the noise-free output of the demodulator is

$$x_m = \begin{cases} 0.3, & m = 1 \\ 0.9, & m = 0 \\ 0.3, & m = -1 \\ 0, & \text{otherwise} \end{cases}$$

1. Design a three-tap zero-forcing linear equalizer so that the output is

$$q_m = \begin{cases} 1, & m = 0 \\ 0, & m = \pm 1 \end{cases}$$

2. Determine  $q_m$  for  $m = \pm 2, \pm 3$ , by convolving the impulse response of the equalizer with the channel response.

**8.45** The transmission of a signal pulse with a raised cosine spectrum through a channel results in the following (noise-free) sampled output from the demodulator:

$$x_k = \begin{cases} -0.5, & k = -2 \\ 0.1, & k = -1 \\ 1, & k = 0 \\ -0.2, & k = 1 \\ 0.05, & k = 2 \\ 0, & \text{otherwise} \end{cases}$$

1. Determine the tap coefficients of a three-tap linear equalizer based on the zero-forcing criterion.

2. For the coefficients determined in part 1, determine the output of the equalizer for the case of the isolated pulse. Thus, determine the residual ISI and its span in time.

**8.46** Show that the gradient vector in the minimization of the MSE may be expressed as

$$\mathbf{g}_k = -E[e_k \mathbf{y}_k]$$

where the error  $e_k = a_k - z_k$ , and the estimate of  $\mathbf{g}_k$ ; i.e.,

$$\hat{\mathbf{g}}_k = -e_k \mathbf{y}_k$$

satisfies the condition that  $E[\hat{\mathbf{g}}_k] = \mathbf{g}_k$ .

**8.47** A nonideal bandlimited channel introduces ISI over three successive symbols. The (noise-free) response of the matched filter demodulator sampled at the sampling time  $t = kT$  is

$$\int_{-\infty}^{\infty} s(t)s(t - kT) dt = \begin{cases} \mathcal{E}_b, & k = 0 \\ 0.9\mathcal{E}_b, & k = \pm 1 \\ 0.1\mathcal{E}_b, & k = \pm 2 \\ 0, & \text{otherwise} \end{cases}$$

1. Determine the tap coefficients of a three-tap linear equalizer that equalizes the channel (received signal) response to an equivalent partial response (duobinary) signal

$$y_k = \begin{cases} \mathcal{E}_b, & k = 0, 1 \\ 0, & \text{otherwise} \end{cases}$$

2. Suppose that the linear equalizer in part 1 is followed by a Viterbi sequence detector for the partial response signal. Give an estimate of the error probability if the additive noise is white and Gaussian, with power-spectral density  $N_0/2$  W/Hz.
- 8.48** Determine the tap weight coefficients of a three-tap zero-forcing equalizer if the ISI spans three symbols and is characterized by the values  $x(0) = 1$ ,  $x(-1) = 0.3$ ,  $x(1) = 0.2$ . Also determine the residual ISI at the output of the equalizer for the optimum tap coefficients.
- 8.49** In LOS microwave radio transmission, the signal arrives at the receiver via two propagation paths, the direct path and a delayed path that occurs due to signal reflection from surrounding terrain. Suppose that the received signal has the form

$$r(t) = s(t) + \alpha s(t - T) + n(t)$$

where  $s(t)$  is the transmitted signal,  $\alpha$  is the attenuation ( $\alpha < 1$ ) of the secondary path and  $n(t)$  is AWGN.

1. Determine the output of the demodulator at  $t = T$  and  $t = 2T$  that employs a filter matched to  $s(t)$ .
  2. Determine the probability of error for a symbol-by-symbol detector if the transmitted signal is binary antipodal and the detector ignores the ISI.
  3. What is the error-rate performance of a simple (one-tap) (DFE) that estimates  $\alpha$  and removes the ISI? Sketch the detector structure that employs a DFE.
- 8.50** Repeat Problem 8.48 using the MMSE as the criterion for optimizing the tap coefficients. Assume that the noise power spectrum is 0.1 W/Hz.
- 8.51** In a magnetic recording channel, where the readback pulse resulting from a positive transition in the write current has the form (see Figure 8.17).

$$p(t) = \frac{1}{1 + \left(\frac{2t}{T_{50}}\right)^2}$$

a linear equalizer is used to equalize the pulse to a partial response. The parameter  $T_{50}$  is defined as the width of the pulse at the 50%-amplitude level. The bit rate

is  $1/T_b$  and the ratio of  $T_{50}/T_b = \Delta$  is the normalized density of the recording. Suppose the pulse is equalized to the partial-response values

$$x(nT) = \begin{cases} 1, & n = -1, 1 \\ 2, & n = 0 \\ 0, & \text{otherwise} \end{cases}$$

where  $x(t)$  represents the equalized pulse shape.

1. Determine the spectrum  $X(f)$  of the bandlimited equalized pulse.
  2. Determine the possible output levels at the detector, assuming that successive transitions can occur at the rate  $1/T_b$ .
  3. Determine the error-rate performance of the symbol-by-symbol detector for this signal assuming that the additive noise is zero-mean Gaussian with variance  $\sigma^2$ .
- 8.52** Sketch the trellis for the Viterbi detector of the equalized signal in Problem 8.51 and label all the states. Also, determine the minimum Euclidean distance between merging paths.
- 8.53** (Carrierless QAM or PSK Modem) Consider the transmission of a QAM or  $M$ -ary PSK ( $M \geq 4$ ) signal at a carrier frequency  $f_c$ , where the carrier is comparable to the bandwidth of the baseband signal. The bandpass signal may be represented as

$$s(t) = \text{Re} \left[ \sum_n a_n g(t - nT) e^{j2\pi f_c t} \right]$$

1. Show that  $s(t)$  can be expressed as

$$s(t) = \text{Re} \left[ \sum_n a'_n Q(t - nT) \right]$$

where  $Q(t)$  is defined as

$$Q(t) = q(t) + j\hat{q}(t)$$

$$q(t) = g(t) \cos 2\pi f_c t$$

$$\hat{q}(t) = g(t) \sin 2\pi f_c t$$

and  $a'_n$  is a phase rotated symbol; i.e.,  $a'_n = a_n e^{j2\pi f_c nT}$ .

2. Using filters with responses  $q(t)$  and  $\hat{q}(t)$ , sketch the block diagram of the modulator and demodulator implementation that does not require the mixer to translate the signal to bandpass at the modulator and to baseband at the demodulator.

**8.54** (Carrierless amplitude or phase (CAP) modulation) In some practical applications in wireline data transmission, the bandwidth of the signal to be transmitted is comparable to the carrier frequency. In such systems, it is possible to eliminate the step of mixing the baseband signal with the carrier component. Instead, the bandpass signal can be synthesized directly, by embedding the carrier component in the realization of the shaping filter. Thus, the modem is realized as shown in the block diagram in Figure P-8.54, where the shaping filters have the impulse responses

$$q(t) = g(t) \cos 2\pi f_c t$$

$$\hat{q}(t) = g(t) \sin 2\pi f_c t$$

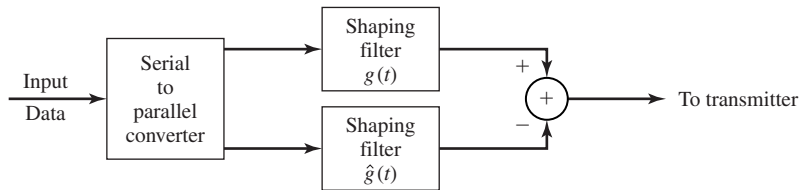
and  $g(t)$  is a pulse that has a square-root raised cosine spectral characteristic.

1. Show that

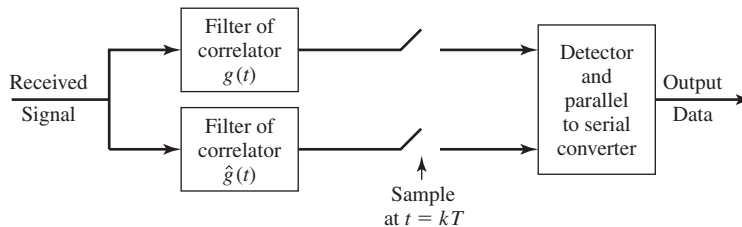
$$\int_{-\infty}^{\infty} q(t)\hat{q}(t) dt = 0$$

and that the system can be used to transmit two dimensional signals, e.g., PSK and QAM.

2. Under what conditions is this CAP modem identical to the carrierless QAM/PSK modem treated in Problem 8-53?



(a) Modulator



(b) Demodulator

**Figure P-8.54** CAP modem.

- 8.55** Show that the sequence  $\{x_n, 0 \leq n \leq N - 1\}$  given by Equation (8.7.7) corresponds to the samples of  $x(t)$  given by Equation (8.7.8). Also, prove that  $x(t)$  given by Equation (8.7.6) is a real-valued signal.
- 8.56** Show that the IDFT of a sequence  $\{X_k, 0 \leq k \leq N - 1\}$ , can be computed by passing the sequence  $\{X_k\}$  through a parallel bank of  $N$  linear discrete-time filters with system functions

$$H_n(z) = \frac{1}{1 - e^{j2\pi n/N} z^{-1}}, \quad n = 0, 1, \dots, N - 1$$

and sampling the filter outputs at  $n = N$ .

# *Channel Capacity and Coding*

The goal of any communication system is to transmit information from an *information source* to a *destination* via a *communication channel*. A communications engineer usually has very little control over these three components. The engineer's role is to design transmitters and receivers that send the source output over the channel to the destination with high fidelity (low distortion, that can be error probability or any other distortion measure, as discussed in Chapter 6). The mathematical model for information sources together with a quantitative measure of information were presented in Chapter 6. In this chapter, we study the other important component of a communication system; i.e., the communication channel. We also introduce the concept of coding for protection of messages against channel errors.

## **9.1 MODELING OF COMMUNICATION CHANNELS**

As defined in Chapter 1, a communication channel is any medium over which information can be transmitted or in which information can be stored. Coaxial cable, ionospheric propagation, free space, fiber optic cables, and magnetic and optical disks are examples of communication channels. What is common among all these is that they accept signals at their inputs and deliver signals at their outputs at a later time (storage case) or at another location (transmission case). Therefore, each communication channel is characterized by a relation between its input and output. In this sense a communication channel is a *system*.

There are many factors that cause the output of a communication channel to be different from its input. Among these factors are attenuation, nonlinearities, bandwidth limitations, multipath propagation, and noise. All these factors contribute to a usually

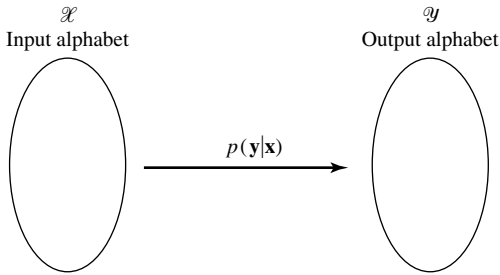


**Figure 9.1** A discrete channel.

complex input–output relation in a communication channel. Due to the presence of fading and noise, the input–output relation in a communication channel is, generally, a stochastic relation.

Channels encountered in practice are generally waveform channels that accept (continuous-time) waveforms as their inputs and produce waveforms as their outputs. Because the bandwidth of any practical channel is limited, by using the sampling theorem, a waveform channel becomes equivalent to a discrete-time channel. In a discrete-time channel both input and output are discrete-time signals.

In a discrete-time channel, if the values that the input and output variables can take are finite, or countably infinite, the channel is called a *discrete channel*. An example of a discrete channel is a binary-input binary-output channel. In general, a discrete channel is defined by  $\mathcal{X}$ , the input alphabet,  $\mathcal{Y}$ , the output alphabet, and  $p(\mathbf{y} | \mathbf{x})$  the conditional PMF of the output sequence given the input sequence. A schematic representation of a discrete channel is given in Figure 9.1. In general, the output  $y_i$  does not only depend on the input at the same time  $x_i$  but also on the previous inputs (channels with ISI, see Chapter 8), or even previous and future inputs (in storage channels). Therefore, a channel can have *memory*. However, if a discrete channel does not have memory, it is called a *discrete-memoryless channel*, and for such a channel, for any  $\mathbf{y} \in \mathcal{Y}^n$  and  $\mathbf{x} \in \mathcal{X}^n$ , we have

$$p(\mathbf{y} | \mathbf{x}) = \prod_{i=1}^n p(y_i | x_i) \quad (9.1.1)$$

All channel models that we will discuss in this chapter are memoryless.

A special case of a discrete-memoryless channel is the *binary-symmetric channel*. Figure 9.2 shows a binary-symmetric channel. In a binary-symmetric channel,  $\epsilon = P(0 | 1) = P(1 | 0)$  is called the *crossover probability*.

### Example 9.1.1

Let us assume that we are dealing with an additive white Gaussian noise channel with binary antipodal signaling. We have already seen in chapter 7 that, in such a channel, the error probability of a 1 being detected as 0 or a 0 being detected as 1 is given by

$$\epsilon = P(1 | 0) = P(0 | 1) = Q\left(\sqrt{\frac{2\mathcal{E}_b}{N_0}}\right) \quad (9.1.2)$$



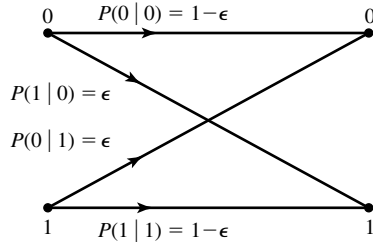


**Figure 9.2** The binary-symmetric channel.

where  $N_0$  is the noise power-spectral density and  $E_b$  denotes the energy content of each of the antipodal signals representing 0 and 1. This discrete channel is an example of a binary symmetric channel.

### Example 9.1.2

In an AWGN channel with binary antipodal signaling, the input is either  $\sqrt{\mathcal{E}_b}$  or  $-\sqrt{\mathcal{E}_b}$ . The output is the sum of the input and the Gaussian noise. Therefore, for this binary-input, continuous-output channel we have  $\mathcal{X} = \{\pm\sqrt{\mathcal{E}_b}\}$  and  $\mathcal{Y} = \mathbb{R}$  and

$$f(y|x) = \frac{1}{\sqrt{2\pi\sigma^2}} e^{-\frac{(y-x)^2}{2\sigma^2}}$$

where  $\sigma^2$  denotes the variance of the noise.

The most important continuous alphabet channel is the discrete-time additive white Gaussian noise channel with an input power constraint. In this channel both  $\mathcal{X}$  and  $\mathcal{Y}$  are the set of real numbers, and the input–output relation is given by

$$Y = X + Z \quad (9.1.3)$$

where  $Z$  denotes the channel noise, which is assumed to be Gaussian with mean equal to 0 and variance equal to  $P_N$ . It is further assumed that inputs to this channel satisfy some power constraint. For example, for large  $n$ , input blocks of length  $n$  satisfy

$$\frac{1}{n} \sum_{i=1}^n x_i^2 \leq P \quad (9.1.4)$$

where  $P$  is some fixed power constraint. This channel model is shown in Figure 9.3.

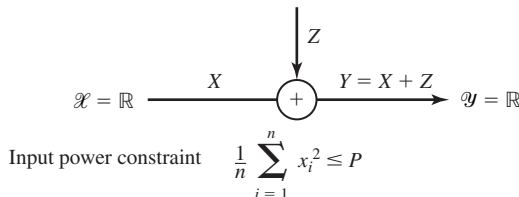


**Figure 9.3** Additive white Gaussian noise channel with power constraint.

## 9.2 CHANNEL CAPACITY

We have already seen in Chapter 6, that  $H(X)$  defines a fundamental limit on the rate at which a discrete source can be encoded without errors in its reconstruction, and  $R(D)$  gives a fundamental rate for reproduction of the source output with distortion less than or equal to  $D$ . A similar “fundamental limit” exists also for information transmission over communication channels.

Of course, the main objective when transmitting information over any communication channel is *reliability*, which is measured by the probability of correct reception at the receiver. Due to the presence of noise, at first glance it seems that the error probability is always bounded away from zero by some positive number. However, a fundamental result of information theory is that reliable transmission (that is transmission with error probability less any given value) is possible even over noisy channels as long as the transmission rate is less than some number called the *channel capacity*. This remarkable result, first shown by Shannon (1948), is known as the *noisy channel-coding theorem*. What the noisy channel coding theorem says is that *the basic limitation that noise causes in a communication channel is not on the reliability of communication, but on the speed of communication*.

Figure 9.4 shows a discrete-memoryless channel with four inputs and outputs. If the receiver receives  $a$  it does not know whether an  $a$  or a  $d$  was transmitted; if it receives a  $b$  it does not know whether an  $a$  or a  $b$  was transmitted, etc.; therefore, there always exists a possibility of error. But if the transmitter and the receiver agree that the transmitter only uses letters  $a$  and  $c$ , then there exists no ambiguity. In this case, if the receiver receives  $a$  or  $b$  it knows that an  $a$  was transmitted; and if it receives a  $c$  or  $d$  it knows that a  $c$  was transmitted. This means that the two symbols  $a$  and  $c$  can be transmitted over this channel with no error; i.e., we are able to avoid errors by using only a subset of the possible inputs to the channel. Admittedly, using a smaller subset of possible inputs reduces the number of possible inputs, but this is the price that must be paid for reliable communication. This is the essence of the noisy channel-coding theorem; i.e., using only those inputs whose corresponding possible outputs are disjoint.

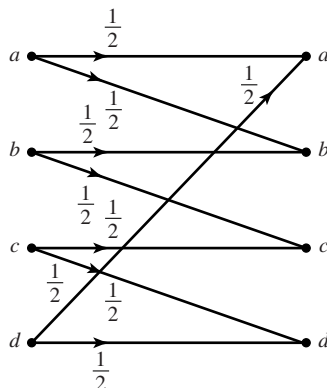


**Figure 9.4** An example of a discrete channel.

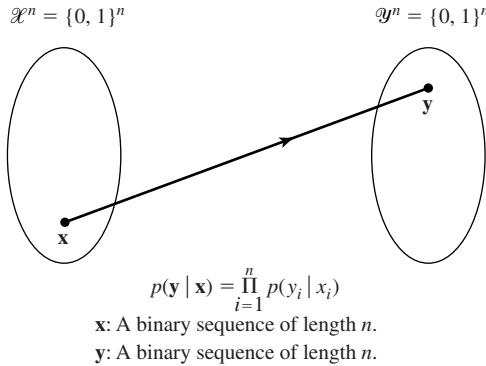


**Figure 9.5**  $n$ th extension of a binary symmetric channel.

The chosen inputs should be in some sense “far apart” such that their “images” under the channel operation are nonoverlapping (or have negligible overlaps).

Looking at the binary symmetric channel and trying to apply the same approach as above, we observe that there is no way that one can have nonoverlapping outputs. In fact, this is the case with most channels. In order to be able to use the results of the above argument for the binary symmetric channel, one has to apply it not to the channel itself, but to the *extension channel*. The  $n$ th extension of a channel with input and output alphabets  $\mathcal{X}$  and  $\mathcal{Y}$  and conditional probabilities  $p(y | x)$  is a channel with input and output alphabets  $\mathcal{X}^n$  and  $\mathcal{Y}^n$  and conditional probability  $p(\mathbf{y} | \mathbf{x}) = \prod_{i=1}^n p(y_i | x_i)$ . The  $n$ th extension of a binary symmetric channel takes binary blocks of length  $n$  as its input and its output. This channel is shown in Figure 9.5. By the law of large numbers as discussed in Chapter 4, for  $n$  large enough, if a binary sequence of length  $n$  is transmitted over the channel, the output will disagree with the input with high probability at  $n\epsilon$  positions. The number of possible sequences that disagree with a sequence of length  $n$  at  $n\epsilon$  positions is given by

$$\binom{n}{n\epsilon}$$

Using Stirling’s approximation  $n! \approx n^n e^{-n} \sqrt{2\pi n}$ , we obtain

$$\binom{n}{n\epsilon} \approx 2^{nH_b(\epsilon)} \tag{9.2.1}$$

where  $H_b(\epsilon) = -\epsilon \log_2 \epsilon - (1 - \epsilon) \log_2 (1 - \epsilon)$  is the binary entropy function as defined in Chapter 6. This means that, for any input block, there exist roughly  $2^{nH_b(\epsilon)}$  highly probable corresponding outputs. On the other hand, the total number of highly probable output sequences is roughly  $2^{nH(Y)}$ . The maximum number of input sequences that produce almost nonoverlapping output sequences, therefore, is at most equal to

$$M = \frac{2^{nH(Y)}}{2^{nH_b(\epsilon)}} = 2^{n(H(Y) - H_b(\epsilon))} \tag{9.2.2}$$

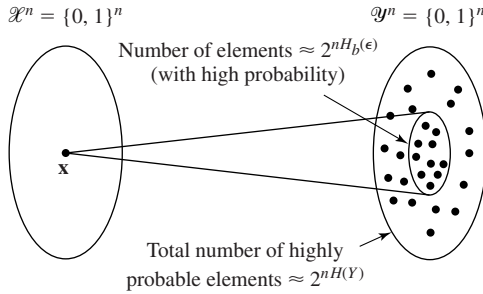


**Figure 9.6** Schematic representation of a BSC.

and the transmission rate/channel use is

$$R = \frac{\log M}{n} = H(Y) - H_b(\epsilon) \quad (9.2.3)$$

Figure 9.6 gives a schematic representation of this case.

In the relation  $R = H(Y) - H_b(\epsilon)$ ,  $\epsilon$  depends on the channel and we cannot control it. However, the probability distribution of the random variable  $Y$  depends both on the input distribution  $p(x)$  and the channel properties characterized by  $\epsilon$ . To maximize the transmission rate over the channel, one has to choose  $p(x)$  that maximizes  $H(Y)$ . If  $X$  is chosen to be a uniformly distributed random variable; i.e.,  $P(X=0) = P(X=1) = 0.5$ , so will be  $Y$  and  $H(Y)$  will be maximized. The maximum value of  $H(Y)$  is 1 and, therefore, we obtain

$$R = 1 - H_b(\epsilon) \quad (9.2.4)$$

It can be proved that the above rate is the maximum rate at which reliable transmission over the BSC is possible. By *reliable transmission* we mean that the error probability can be made to tend to 0 as the block length  $n$  tends to infinity. A plot of the channel capacity in this case is given in Figure 9.7. It is interesting to note that the cases  $\epsilon = 0$  and  $\epsilon = 1$  both result in  $C = 1$ . This means that a channel that always flips the input is as good as the channel that transmits the input with no errors. The worst case, of course, happens when the channel flips the input with probability  $1/2$ .

The maximum rate at which one can communicate over a discrete-memoryless channel and still make the error probability approach 0 as the code block length increases, is called the *channel capacity* and is denoted by  $C$ . The noisy channel-coding theorem stated next gives the capacity of a general discrete-memoryless channel.

**Theorem 9.2.1 [Noisy Channel-Coding Theorem].** The capacity of a discrete-memoryless channel is given by

$$C = \max_{p(x)} I(X; Y) \quad (9.2.5)$$

where  $I(X; Y)$  is the mutual information between the channel input  $X$  and the output  $Y$ , previously defined in Chapter 6. If the transmission rate  $R$  is less than  $C$ , then for any  $\delta > 0$  there exists a code with block length  $n$  large enough whose error probability is less than  $\delta$ . If  $R > C$ , the error probability of any code with any block length is bounded away from 0. ■

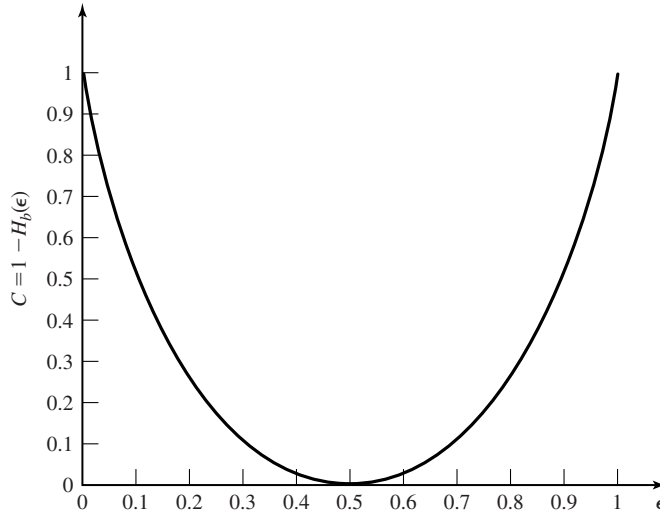


**Figure 9.7** The capacity of a BSC.

This theorem is one of the fundamental results in information theory and gives a fundamental limit on the possibility of reliable communication over a noisy channel. According to this theorem, regardless of all other properties, any communication channel is characterized by a number called capacity that determines how much information can be transmitted over it. Therefore, to compare two channels from an information transmission point of view, it is enough to compare their capacities.

**Example 9.2.1**

Find the capacity of the channel shown in Figure 9.8.

**Solution** We have to find the input distribution that maximizes  $I(X; Y)$ . We have

$$I(X; Y) = H(Y) - H(Y | X)$$

But

$$H(Y | X) = P(X = a)H(Y | X = a) + P(X = b)H(Y | X = b) + P(X = c)H(Y | X = c)$$

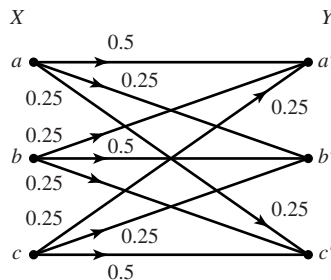


**Figure 9.8** The DMC of Example 9.2.1.

From the channel input–output relation it is seen that for all the three case  $X = a$ ,  $X = b$ , and  $X = c$ ,  $Y$  is a ternary random variable with probabilities 0.25, 0.25, and 0.5. Therefore,

$$H(Y | X = a) = H(Y | X = b) = H(Y | X = c) = 1.5$$

Then, because  $P(X = a) + P(X = b) + P(X = c) = 1$ ,

$$H(Y | X) = 1.5$$

and

$$I(X; Y) = H(Y) - 1.5$$

To maximize  $I(X; Y)$ , it remains to maximize  $H(Y)$ , which is maximized when  $Y$  is an equiprobable random variable. But it is not clear if there exists an input distribution that results in a uniform distribution on the output. However, in this special case (due to the symmetry of the channel) a uniform input distribution results in a uniform output distribution and for this distribution

$$H(Y) = \log 3 = 1.585$$

This means that the capacity of this channel is given by

$$C = 1.585 - 1.5 = .085 \text{ bits/transmission}$$

### 9.2.1 Gaussian Channel Capacity

A discrete-time Gaussian channel with input power constraint is characterized by the input–output relation

$$Y = X + Z \tag{9.2.6}$$

where  $Z$  is a zero-mean Gaussian random variable with variance  $P_N$ , and for  $n$  large enough, an input power constraint of the form

$$\frac{1}{n} \sum_{i=1}^n x_i^2 \leq P \tag{9.2.7}$$

applies to any input sequence of length  $n$ . For blocks of length  $n$  at the input, the output, and the noise, we have

$$\mathbf{y} = \mathbf{x} + \mathbf{z} \tag{9.2.8}$$

If  $n$  is large, by the law of large numbers, we have

$$\frac{1}{n} \sum_{i=1}^n z_i^2 = \frac{1}{n} \sum_{i=1}^n (y_i - x_i)^2 \leq P_N \tag{9.2.9}$$

or

$$\|\mathbf{y} - \mathbf{x}\|^2 \leq nP_N \tag{9.2.10}$$

This means that, with probability approaching one (as  $n$  increases),  $\mathbf{y}$  will be located in an  $n$ -dimensional sphere (hypersphere) of radius  $\sqrt{nP_N}$  and centered at  $\mathbf{x}$ . On the other

hand, due to the power constraint of  $P$  on the input and the independence of the input and noise, the output power is the sum of the input power and the noise power, i.e.,

$$\frac{1}{n} \sum_{i=1}^n y_i^2 \leq P + P_N \quad (9.2.11)$$

or

$$\|\mathbf{y}\|^2 \leq n(P + P_N) \quad (9.2.12)$$

This implies that the output sequences (again, asymptotically and with high probability) will be inside an  $n$ -dimensional hypersphere of radius  $\sqrt{n(P + P_N)}$  and centered at the origin. Figure 9.9 shows the sequences in the output space. The question now is: How many  $\mathbf{x}$  sequences can we transmit over this channel such that the hyperspheres corresponding to these sequences do not overlap in the output space? Obviously if this condition is satisfied, then the input sequences can be decoded reliably. An equivalent question is: how many hyperspheres of radius  $\sqrt{nP_N}$  can we pack in a hypersphere of radius  $\sqrt{n(P_N + P)}$ ? The answer is roughly the ratio of the volumes of the two hyperspheres. If we denote the volume of an  $n$ -dimensional hypersphere by

$$V_n = K_n R^n \quad (9.2.13)$$

where  $R$  denotes the radius and  $K_n$  is independent of  $R$ , we see that the number of

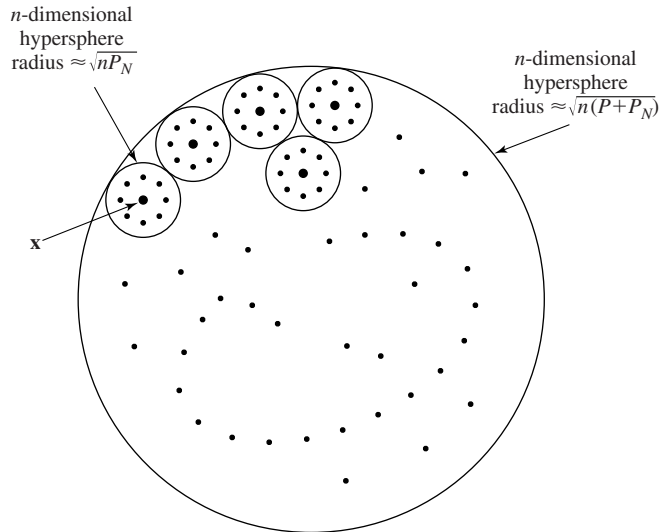


**Figure 9.9** The output sequences of a Gaussian channel with power constraint.

messages that can be reliably transmitted over this channel is equal to

$$\begin{aligned}
 M &= \frac{K_n(n(P_N + P))^{\frac{n}{2}}}{K_n(nP_N)^{\frac{n}{2}}} \\
 &= \left( \frac{P_N + P}{P_N} \right)^{\frac{n}{2}} \\
 &= \left( 1 + \frac{P}{P_N} \right)^{\frac{n}{2}} \tag{9.2.14}
 \end{aligned}$$

Therefore, the capacity of a discrete-time additive white Gaussian noise channel with input power constraint  $P$  is given by

$$\begin{aligned}
 C &= \frac{1}{n} \log M \\
 &= \frac{1}{n} \cdot \frac{n}{2} \log \left( 1 + \frac{P}{P_N} \right) \\
 &= \frac{1}{2} \log \left( 1 + \frac{P}{P_N} \right) \tag{9.2.15}
 \end{aligned}$$

When dealing with a continuous-time, bandlimited, additive white Gaussian noise channel with noise power-spectral density  $\frac{N_0}{2}$ , input power constraint  $P$ , and bandwidth  $W$ , one can sample at the Nyquist rate and obtain a discrete-time channel. The power/sample will be  $P$  and the noise power/sample will be

$$P_N = \int_{-W}^{+W} \frac{N_0}{2} df = WN_0$$

Substituting these results in Equation (9.2.15), we obtain

$$C = \frac{1}{2} \log \left( 1 + \frac{P}{N_0 W} \right) \quad \text{bits/transmission} \tag{9.2.16}$$

If we multiply this result by the number of transmissions/sec, which is  $2W$ , we obtain the channel capacity in bits/sec

$$C = W \log \left( 1 + \frac{P}{N_0 W} \right) \quad \text{bits/sec} \tag{9.2.17}$$

This is the celebrated Shannon's formula for the capacity of an additive white Gaussian noise channel.

### Example 9.2.2

Find the capacity of a telephone channel with bandwidth  $W = 3000$  Hz, and SNR of 39 dB.

**Solution** The SNR of 39 dB is equivalent to 7943. Using Shannon's relation we have

$$C = 3000 \log(1 + 7943) \approx 38,867 \quad \text{bits/sec}$$



### 9.3 BOUNDS ON COMMUNICATION

From the previous section, the capacity of an additive white Gaussian noise channel is given by

$$C = W \log \left( 1 + \frac{P}{N_0 W} \right)$$

From this result, the basic factors that determine the channel capacity are the channel bandwidth  $W$ , the noise power spectrum  $N_0$  and the signal power  $P$ . There exists a trade-off between  $P$  and  $W$  in the sense that one can compensate for the other. Increasing the input signal power obviously increases the channel capacity, because when one has more power to spend, one can choose a larger number of input levels that are far apart and, therefore, more information bits/transmission are possible. However, the increase in capacity as a function of power is logarithmic and slow. This is because if one is transmitting with a certain number of input levels that are  $\Delta$  apart to allow a certain level of immunity against noise, and wants to increase the number of input levels, one has to introduce new levels with amplitudes higher than the existing levels, and this requires a lot of power. This fact notwithstanding, the capacity of the channel can be increased to any value by increasing the input power.

The effect of the channel bandwidth, however, is quite different. Increasing  $W$  has two contrasting effects. On one hand, on a higher bandwidth channel one can transmit more samples/sec and, therefore, increase the transmission rate. On the other hand, a higher bandwidth means higher input noise to the receiver and this reduces its performance. This is seen from the two  $W$ 's that appear in the relation that describes the channel capacity. To see the effect of increasing the bandwidth, we let the bandwidth  $W$  tend to infinity and using L'Hospital's rule we obtain

$$\lim_{W \rightarrow \infty} C = \frac{P}{N_0} \log e = 1.44 \frac{P}{N_0} \quad (9.3.1)$$

This means that, contrary to the power case, by increasing the bandwidth alone one can not increase the capacity to any desired value. Figure 9.10 shows  $C$  plotted versus  $W$ .

In any practical communication system, we must have  $R < C$ . If an AWGN channel is employed we have

$$R < W \log \left( 1 + \frac{P}{N_0 W} \right) \quad (9.3.2)$$

By dividing both sides by  $W$  and defining  $r = \frac{R}{W}$ , the spectral bit rate, we obtain

$$r < \log \left( 1 + \frac{P}{N_0 W} \right) \quad (9.3.3)$$

If  $\mathcal{E}_b$  is the energy per bit, then  $\mathcal{E}_b = \frac{P}{R}$ . By substituting in the previous relation, we obtain

$$r < \log \left( 1 + r \frac{\mathcal{E}_b}{N_0} \right) \quad (9.3.4)$$

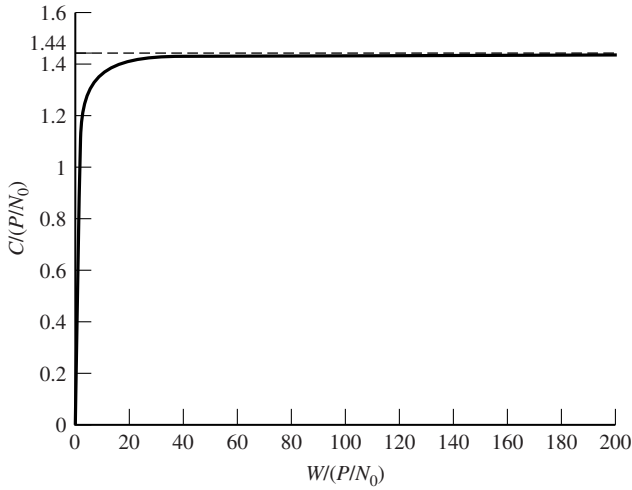


**Figure 9.10** Plot of channel capacity versus bandwidth.

or, equivalently,

$$\frac{\mathcal{E}_b}{N_0} > \frac{2^r - 1}{r} \tag{9.3.5}$$

This relation is plotted in Figure 9.11.

The curve defined by

$$r = \log \left( 1 + r \frac{\mathcal{E}_b}{N_0} \right) \tag{9.3.6}$$

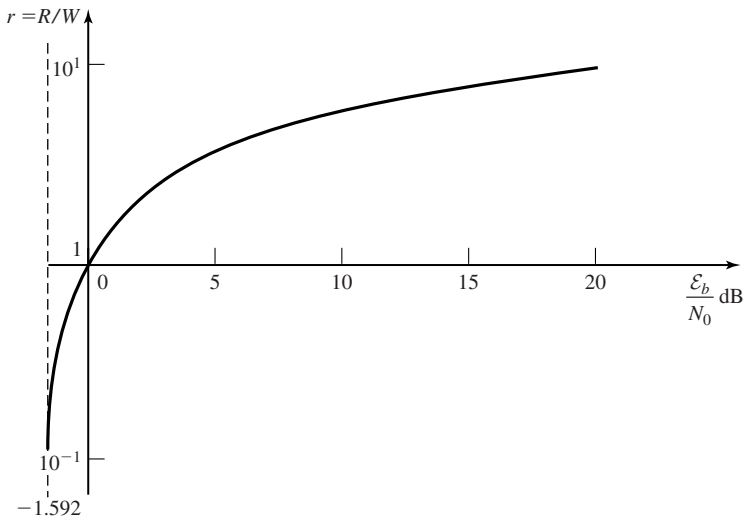


**Figure 9.11** Spectral bit rate versus SNR/bit in an optimal system.

divides the plane into two regions. In one region (below the curve), reliable communication is possible and in another region (above the curve), reliable communication is not possible. The performance of any communication system can be denoted by a point in this plane and the closer the point is to this curve, the closer is the performance of the system to an optimal system. From this curve, it is seen that (as  $r$  tends to 0),

$$\frac{\mathcal{E}_b}{N_0} = \ln 2 = 0.693 \sim -1.6 \text{ dB} \quad (9.3.7)$$

is an absolute minimum for reliable communication. In other words, for reliable communication, we must have

$$\frac{\mathcal{E}_b}{N_0} > 0.693 \quad (9.3.8)$$

In Figure 9.11, when  $r \ll 1$ , we are dealing with a case where bandwidth is large and the main concern is limitation on power. This case is usually referred to as the *power-limited case*. Signaling schemes, with high dimensionality, such as orthogonal, biorthogonal, and simplex are frequently used in these cases. The case where  $r \gg 1$ , happens when the bandwidth of the channel is small, and therefore is referred to as the *bandwidth-limited case*. Low dimensional signaling schemes with crowded constellations, e.g., 256-QAM, are implemented in these cases.

In Chapter 6, we introduced the fundamental limits that exist in coding of information sources. These fundamental limits are expressed in terms of the entropy of the source, the rate-distortion function associated with the source, and the corresponding distortion measure. Entropy gives a lower bound on the rate of the codes that are capable of reproducing the source with no error, and the rate-distortion function gives a lower bound on the rate of the codes capable of reproducing the source with distortion  $D$ . If we want to transmit a source  $U$  reliably via a channel with capacity  $C$ , we require that

$$H(U) < C \quad (9.3.9)$$

If transmission with a maximum distortion equal to  $D$  is desired, then the condition is

$$R(D) < C \quad (9.3.10)$$

These two relations define fundamental limits on the transmission of information. In both cases, we have assumed that for each source output one transmission over the channel is possible.

### Example 9.3.1

A zero-mean Gaussian source with power-spectral density

$$S_X(f) = \Pi\left(\frac{f}{20,000}\right)$$

is to be transmitted via a telephone channel described in Example 9.2.2. What is the minimum distortion achievable if mean-squared distortion is used?

**Solution** The bandwidth of the source is 10,000 Hz, and it therefore can be sampled at a rate of 20,000 samples/sec. The power of the source is

$$P_X = \int_{-\infty}^{\infty} \mathcal{S}_X(f) df = 20,000$$

The variance of each sample is given by

$$\sigma^2 = 20,000$$

and the rate distortion function for  $D < 20,000$  is given by

$$R(D) = \frac{1}{2} \log \frac{\sigma^2}{D} = \frac{1}{2} \log \frac{20,000}{D} \quad \text{bits/sample}$$

which is equivalent to

$$R(D) = 10,000 \log \frac{20,000}{D} \quad \text{bits/sec}$$

Since the capacity of the channel in question, derived in Example 9.2.2, is 38,867 bits/sec, we can derive the least possible distortion by solving

$$38,867 = 10,000 \log \frac{20,000}{D}$$

for  $D$ , which results in  $D = 1352$ .

In general, it can be shown that the rate-distortion function for a waveform Gaussian source with power-spectral density

$$\mathcal{S}_X(f) = \begin{cases} A, & |f| < W_s \\ 0, & \text{otherwise} \end{cases} \quad (9.3.11)$$

and with distortion measure

$$d(u(t), v(t)) = \lim_{T \rightarrow \infty} \frac{1}{T} \int_{-T/2}^{T/2} [u(t) - v(t)]^2 dt \quad (9.3.12)$$

is given by

$$R(D) = \begin{cases} W_s \log \left( \frac{2AW_s}{D} \right) & D < 2AW_s \\ 0, & D \geq 2AW_s \end{cases} \quad (9.3.13)$$

If this source is to be transmitted via an additive white Gaussian noise channel with bandwidth  $W_c$ , power  $P$ , and noise-spectral density  $N_0$ , the minimum achievable distortion is obtained by solving the equation

$$W_c \log \left( 1 + \frac{P}{N_0 W_c} \right) = W_s \log \left( \frac{2AW_s}{D} \right) \quad (9.3.14)$$

From this equation, we obtain

$$D = 2AW_s \left( 1 + \frac{P}{N_0 W_c} \right)^{-\frac{W_c}{W_s}} \quad (9.3.15)$$

It is seen that, in an optimal system, distortion decreases exponentially as  $\frac{W_c}{W_s}$  increases. The ratio  $\frac{W_c}{W_s}$  is called the *bandwidth-expansion factor*. We can also find the SQNR as

$$\text{SQNR} = \frac{2AW_s}{D} = \left(1 + \frac{P}{N_0 W_c}\right)^{\frac{W_c}{W_s}} \quad (9.3.16)$$

The important conclusion is that in an optimal system, the final signal-to-noise (distortion) ratio increases exponentially with the bandwidth expansion factor. This is a criteria by which we can compare the performance of various waveform transmission systems.

### 9.3.1 Transmission of Analog Sources by PCM

We have seen in Chapter 6 that PCM is one of the most commonly used schemes for transmission of analog data. Here, we find the performance characteristics of a PCM system when transmitting data over a noisy channel, and compare the results with that of an optimal system.

We have already seen in Section 6.6, that in a PCM system the quantization noise (distortion) is given by

$$E[\tilde{X}^2] = \frac{x_{\max}^2}{3 \times 4^v}$$

where  $x_{\max}$  denotes the maximum input amplitude and  $v$  is the number of bits/sample. If the source bandwidth is  $W_s$ , then the sampling frequency in an optimal system is  $f_s = 2W_s$ , and the bit rate is  $R = 2vW_s$ . Assuming that the binary data is directly transmitted over the channel, the minimum channel bandwidth that can accommodate this bit rate (Nyquist criterion, see Chapter 8) is

$$W_c = \frac{R}{2} = vW_s \quad (9.3.17)$$

Therefore, the quantization noise can be expressed as

$$E[\tilde{X}^2] = \frac{x_{\max}^2}{3 \times 4^{\frac{W_c}{W_s}}} \quad (9.3.18)$$

Now if the output of a PCM system is transmitted over a noisy channel with error probability  $P_b$ , some bits will be received in error and another type of distortion, due to transmission, will also be introduced. This distortion will be independent from the quantization distortion and since the quantization error is zero mean, the total distortion will be the sum of these distortions (see Section 4.3.2). To simplify the calculation of the transmission distortion, we assume that  $P_b$  is small enough such that in a block of length  $v$ , either no error or one error can occur. This one error can occur at any of the  $v$  locations and, therefore, its contribution to the total distortion varies accordingly. If an error occurs in the least significant bit, it results in a change of  $\Delta$  in the output level; if it happens in the next bit, it results in  $2\Delta$  change in the output; and if it occurs at the most significant bit, it causes a level change equal to  $2^{v-1}\Delta$  at the output. Assuming these

are the only possible errors, one obtains the following expression for the transmission distortion

$$E[D_T^2] = \sum_{i=1}^{\nu} P_b (2^{i-1} \Delta)^2 = P_b \Delta^2 \frac{4^{\nu} - 1}{3} \quad (9.3.19)$$

and the total distortion will be

$$D_{\text{total}} = \frac{x_{\text{max}}^2}{3 \times 4^{\frac{w_c}{w_s}}} + P_b \Delta^2 \frac{4^{\frac{w_c}{w_s}} - 1}{3} \quad (9.3.20)$$

We note that

$$\Delta = \frac{2x_{\text{max}}}{2^{\nu}} = \frac{x_{\text{max}}}{2^{\nu-1}} \quad (9.3.21)$$

Substituting for  $\Delta$ , and assuming  $4^{\nu} \gg 1$ , the expression for  $D_{\text{total}}$  simplifies to

$$D_{\text{total}} \approx \frac{x_{\text{max}}^2}{3} \left( 4^{-\frac{w_c}{w_s}} + 4P_b \right) \quad (9.3.22)$$

The signal-to-noise (distortion) ratio at the receiving end is, therefore,

$$\text{SNR} = \frac{3\bar{X}^2}{x_{\text{max}}^2 \left( 4^{-\frac{w_c}{w_s}} + 4P_b \right)} \quad (9.3.23)$$

The value of  $P_b$ , of course, depends on the modulation scheme employed to transmit the outputs of the PCM system. If binary antipodal signaling is employed, then

$$P_b = Q \left( \sqrt{\frac{2\mathcal{E}_b}{N_0}} \right) \quad (9.3.24)$$

and if binary orthogonal signaling with coherent detection is used, then

$$P_b = Q \left( \sqrt{\frac{\mathcal{E}_b}{N_0}} \right) \quad (9.3.25)$$

From the expression for the SNR, it is seen that for small  $P_b$ , the SNR grows almost exponentially with  $\frac{w_c}{w_s}$ , the bandwidth-expansion factor, and in this sense, a PCM system uses the available bandwidth efficiently. Recall from Section 5.3, that another frequently used system that trades bandwidth for noise immunity is an FM system. However, the SNR of an FM system is a quadratic function of the bandwidth-expansion factor [see Equation (5.3.26)] and, therefore, an FM system is not as bandwidth efficient as a PCM system.

## 9.4 CODING FOR RELIABLE COMMUNICATION

In Chapter 7, it was shown that both in baseband and carrier-modulation schemes, the error probability is a function of the distance between the points in the signal constellation. In fact, for binary equiprobable signals the error probability can be expressed as

[see Equation (7.6.10)]

$$P_e = Q\left(\frac{d_{12}}{\sqrt{2N_0}}\right) \quad (9.4.1)$$

where  $d_{12}$  is the Euclidean distance between  $s_1(t)$  and  $s_2(t)$ , given by

$$d_{12}^2 = \int_{-\infty}^{\infty} [s_1(t) - s_2(t)]^2 dt \quad (9.4.2)$$

On the other hand, we have seen that in the binary case, with coherent demodulation, antipodal signaling performs best and has a Euclidean distance  $d_{12} = 2\sqrt{\mathcal{E}}$ . Therefore,

$$P_e = Q\left(\sqrt{\frac{2\mathcal{E}_b}{N_0}}\right) \quad (9.4.3)$$

From the above, it is seen that to decrease the error probability, one has to increase the signal energy. Increasing the signal energy can be done in two ways, either increasing the transmitter power, or increasing the transmission duration. Increasing the transmitter power is not always feasible because each transmitter has a limitation on its average power. Increasing the transmission duration, in turn, decreases the transmission rate and, therefore, it seems that the only way to make the error probability vanish is to let the transmission rate vanish. In fact, this was the communication engineers' viewpoint in the pre-Shannon era.

We have also seen in Chapter 7 that, by employing orthogonal signals, one can achieve reliable transmission at nonzero rate, as long as  $\frac{\mathcal{E}_b}{N_0} > 2 \ln 2$ . Here, we show that  $\frac{\mathcal{E}_b}{N_0} > \ln 2$  is sufficient to achieve reliable transmission. Note that this is the same condition which guarantees reliable transmission over an additive white Gaussian noise channel when the bandwidth goes to infinity (see Figure 9.11 and Equation (9.3.7)).

#### 9.4.1 A Tight Bound on Error Probability of Orthogonal Signals

To find a tighter bound on the error probability of orthogonal signals compared to the one obtained in Chapter 7, we use another bounding technique. The problem with the union bound employed in Chapter 7 is that it is not tight for small SNRs. To compensate for this we use two bounds, one for large SNRs, which is essentially the union bound, and another bound for small SNRs.

In Chapter 7, it was shown that the message-error probability for orthogonal signals is given by

$$P_M = \frac{1}{\sqrt{2\pi}} \int_{-\infty}^{\infty} [1 - (1 - Q(u))^{M-1}] \exp\left[-\frac{\left(u - \sqrt{\frac{2\mathcal{E}_s}{N_0}}\right)^2}{2}\right] du \quad (9.4.4)$$

Defining

$$a = \sqrt{\frac{2\mathcal{E}_s}{N_0}} \quad (9.4.5)$$

and

$$f(u) = \frac{1}{\sqrt{2\pi}} e^{-\frac{u^2}{2}} \quad (9.4.6)$$

we have

$$P_M = \int_{-\infty}^{\infty} [1 - (1 - Q(u))^{M-1}] f(u - a) du \quad (9.4.7)$$

Using the inequality  $nx + (1 - x)^n \geq 1$ , which holds for all  $0 \leq x \leq 1$  and  $n \geq 1$ ,<sup>†</sup> we obtain

$$(1 - Q(u))^{M-1} \geq 1 - (M - 1)Q(u) \quad (9.4.8)$$

and, therefore,

$$1 - (1 - Q(u))^{M-1} \leq (M - 1)Q(u) < MQ(u) < Me^{-u^2/2} \quad (9.4.9)$$

where in the last step we have used the well-known bound on  $Q(x)$  introduced in Section 4.1. This bound is basically the union bound, which we will use for large SNRs (large  $u$ ). For small SNRs, we use the obvious bound

$$1 - (1 - Q(u))^{M-1} \leq 1 \quad (9.4.10)$$

Substituting these bounds into Equation (9.4.7), we obtain

$$P_M < \int_{-\infty}^{y_0} f(u - a) du + M \int_{y_0}^{\infty} e^{-u^2/2} f(u - a) du = P_1 + MP_2 \quad (9.4.11)$$

where  $y_0$  can be any arbitrary number. To obtain the tightest bound, we differentiate the right-hand side of Equation (9.4.11) with respect to  $y_0$  and set the derivative equal to 0. Thus, we obtain

$$f(y_0 - a) - Me^{-y_0^2/2} f(y_0 - a) = 0 \quad (9.4.12)$$

or

$$e^{y_0^2/2} = M \quad (9.4.13)$$

from which we have

$$y_0 = \sqrt{2 \ln M} = \sqrt{2 \ln M \log_2 M} = \sqrt{2k \ln 2} \quad (9.4.14)$$

<sup>†</sup>To see this, define  $g(x) = nx + (1 - x)^n$ , then  $g(0) = 1$  and  $g'(x) = n - n(1 - x)^{n-1}$ . But for  $0 \leq x \leq 1$ , we have  $0 \leq 1 - x \leq 1$  and, therefore,  $(1 - x)^{n-1} \leq 1$ , for all  $n \geq 1$ . This means that, for  $0 \leq x \leq 1$ ,  $g'(x) \geq 0$  and, therefore,  $g(x)$  is an increasing function in this interval. This, in turn means  $g(x) \geq 1$  for  $0 \leq x \leq 1$  and  $n \geq 1$ .



The next step is to find bounds on  $P_1$  and  $P_2$ , and, therefore, on  $P_M$ . For  $P_1$ , we have

$$P_1 = \int_{-\infty}^{y_0} f(u-a) du = \int_{-\infty}^{y_0-a} f(x) dx = \int_{a-y_0}^{\infty} f(x) dx = Q(a-y_0) \quad (9.4.15)$$

By using bounds on  $Q$ , we obtain

$$P_1 \leq \frac{1}{2} e^{-(a-y_0)^2/2} < e^{-(a-y_0)^2/2} \quad \text{for } y_0 \leq a \quad (9.4.16)$$

To bound  $P_2$  we have

$$\begin{aligned} P_2 &= \int_{y_0}^{\infty} e^{-u^2/2} f(u-a) du \\ &= \int_{y_0}^{\infty} e^{-\frac{u^2}{2}} \times \frac{1}{\sqrt{2\pi}} e^{-(u-a)^2/2} du \\ &= e^{-a^2/4} \int_{y_0}^{\infty} \frac{1}{\sqrt{2\pi}} e^{-(u-\frac{a}{2})^2} du \\ &= e^{-a^2/4} \frac{1}{\sqrt{2}} \int_{\sqrt{2}(y_0-\frac{a}{2})}^{\infty} \frac{1}{\sqrt{2\pi}} e^{-x^2/2} dx \\ &= \frac{1}{\sqrt{2}} e^{-a^2/4} Q \left[ \sqrt{2} \left( y_0 - \frac{a}{2} \right) \right] \end{aligned} \quad (9.4.17)$$

Using the fact that for all  $x$ ,  $Q(x) \leq 1$ , and that for  $x \geq 0$ , we have  $Q(x) \leq \frac{1}{2} e^{-x^2/2}$ , we obtain

$$P_2 \leq \begin{cases} e^{-a^2/4} e^{-(y_0-\frac{a}{2})^2}, & y_0 \geq \frac{a}{2} \\ e^{-a^2/4}, & y_0 \leq \frac{a}{2} \end{cases} \quad (9.4.18)$$

Substituting the derived bounds on  $P_1$  and  $P_2$  in Equation (9.4.11) and using  $M = e^{y_0^2/2}$ , we obtain

$$P_M < \begin{cases} e^{-(a-y_0)^2/2} + e^{y_0^2/2} e^{-a^2/4}, & 0 \leq y_0 \leq \frac{a}{2} \\ e^{-(a-y_0)^2/2} + e^{y_0^2/2} e^{-a^2/4 - (y_0-a/2)^2}, & \frac{a}{2} \leq y_0 \leq a \end{cases} \quad (9.4.19)$$

For  $0 \leq y_0 \leq \frac{a}{2}$ , we have

$$e^{-(a-y_0)^2/2} + e^{y_0^2/2} e^{-a^2/4} = e^{y_0^2/2 - a^2/4} [1 + e^{-(y_0-\frac{a}{2})^2}] \leq 2e^{y_0^2/2 - a^2/4} \quad (9.4.20)$$

and for  $\frac{a}{2} \leq y_0 \leq a$ , the two exponents in Equation (9.4.19) are the same. Using these, the bound simplifies to

$$P_M < \begin{cases} 2e^{y_0^2/2 - a^2/4} & 0 \leq y_0 \leq \frac{a}{2} \\ 2e^{-(a-y_0)^2/2}, & \frac{a}{2} \leq y_0 \leq a \end{cases} \quad (9.4.21)$$

Now, using the relations

$$y_0 = \sqrt{2k \ln 2} \quad (9.4.22)$$

and

$$a = \sqrt{\frac{2\mathcal{E}_s}{N_0}} = \sqrt{\frac{2k\mathcal{E}_b}{N_0}} \quad (9.4.23)$$

we obtain the final result

$$P_M < \begin{cases} 2e^{-\frac{k}{2}(\mathcal{E}_b/N_0 - 2\ln 2)}, & 0 \leq \ln M \leq \frac{\mathcal{E}_s}{4N_0} \\ 2e^{-k(\sqrt{\mathcal{E}_b/N_0} - \sqrt{\ln 2})^2}, & \frac{\mathcal{E}_s}{4N_0} \leq \ln M \leq \frac{\mathcal{E}_s}{N_0} \end{cases} \quad (9.4.24)$$

The first bound coincides with the union bound derived in Chapter 7. The second bound is better than the union bound for large values of  $M$  (smaller  $\frac{\mathcal{E}_b}{N_0}$ ). This bound shows that the condition for reliable communications is  $\frac{\mathcal{E}_b}{N_0} > \ln 2$  rather than  $\frac{\mathcal{E}_b}{N_0} > 2 \ln 2$  derived in Chapter 7. We can also express these bounds in terms of the transmission rate and the channel capacity. By using the relations

$$k = RT \quad (9.4.25)$$

$$\mathcal{E}_b = \frac{P}{R} \quad (9.4.26)$$

$$R = \frac{1}{T} \log M \quad (9.4.27)$$

$$C_\infty = \frac{P}{N_0} \ln 2 \quad (9.4.28)$$

we obtain

$$P_M < \begin{cases} 2 \times 2^{-T(\frac{1}{2}C_\infty - R)}, & 0 \leq R \leq \frac{1}{4}C_\infty \\ 2 \times 2^{-T(\sqrt{C_\infty} - \sqrt{R})^2}, & \frac{1}{4}C_\infty \leq R \leq C_\infty \end{cases} \quad (9.4.29)$$

or, equivalently,

$$P_M < 2 \times 2^{-TE^*(R)} \quad (9.4.30)$$

where

$$E^*(R) = \begin{cases} \frac{1}{2}C_\infty - R, & 0 \leq R \leq \frac{1}{4}C_\infty \\ (\sqrt{C_\infty} - \sqrt{R})^2, & \frac{1}{4}C_\infty \leq R \leq C_\infty \end{cases} \quad (9.4.31)$$

The function  $E^*(R)$  is called the *channel reliability function* and is plotted in Figure 9.12.

### 9.4.2 The Promise of Coding

From the above discussion, it is seen that orthogonal signals are capable of achieving the capacity at nonvanishing rates. However, the price paid for this is quite high. To achieve this performance, we have to let  $k \rightarrow \infty$ , or  $T \rightarrow \infty$ . On the other hand, the number of orthogonal signals is given by  $M = 2^k = 2^{RT}$ . If one wants, for instance, to employ PPM signaling, this means that the time duration  $T$  has to be divided into  $2^{RT}$

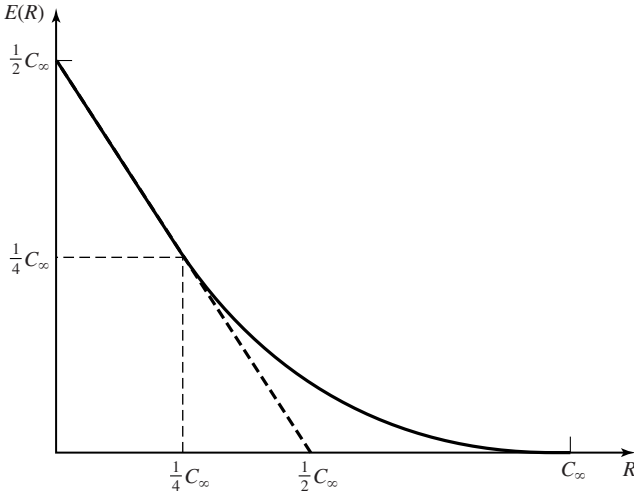


**Figure 9.12** The reliability function for AWGN channel with infinite bandwidth.

slots each of duration  $\frac{T}{2^{RT}}$ . This, in turn, means that the width of the pulses approaches zero exponentially and, therefore, the bandwidth required to transmit them increases exponentially as well.<sup>†</sup> Now the question is: does there exist a way to transmit messages reliably over a noisy channel at a positive rate without an exponential increase in the bandwidth? The answer is positive and the tool to achieve this goal is coding. The following example clarifies the point.

#### Example 9.4.1

In a digital communication system, the transmitter power is  $P$  and the rate of the source is  $R$ . The system employs a  $M = 4$ -PSK signaling where a pair of information bits are mapped into any of the four signals shown in the constellation depicted in Figure 9.13. It is readily seen that  $\mathcal{E}_b = \frac{P}{R}$ , and the minimum Euclidean distance between any two

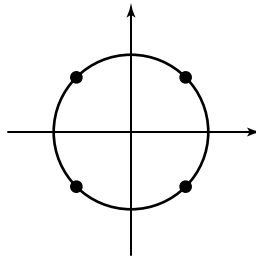


**Figure 9.13** Signal constellation for 4-PSK.

<sup>†</sup>This exponential increase in bandwidth requirement is a characteristic of all orthogonal signaling schemes and not a peculiar property of the PPM signaling employed here. It can be shown that the number of the orthogonal signals that are “almost” bandlimited to a bandwidth of  $W$  and “almost” time-limited to a duration  $T$  is  $2WT$ . Therefore, an exponential increase in  $M$  of the form  $M = 2^{RT}$  requires an exponential increase in  $W$ .

signals is given by

$$d_{\min}^2 = 4\mathcal{E}_b = 4\frac{P}{R} \quad (9.4.32)$$

Now let us assume that, instead of transmitting an  $M = 4$ -PSK signal (which is two dimensional), *three* orthonormal signals are employed to transmit the same *two* bits. For example, we can assume that the orthonormal signals are given by  $\psi(t)$ ,  $\psi(t - T)$ , and  $\psi(t - 2T)$  where  $\psi(t)$  is equal to zero outside the interval  $[0, T]$  and

$$\int_0^T \psi^2(t) dt = 1 \quad (9.4.33)$$

Let us assume that instead of the 4-PSK signals we transmit the following four signals

$$s_1(t) = \sqrt{\mathcal{E}} (+\psi(t) + \psi(t - T) + \psi(t - 2T)) \quad (9.4.34)$$

$$s_2(t) = \sqrt{\mathcal{E}} (+\psi(t) - \psi(t - T) - \psi(t - 2T)) \quad (9.4.35)$$

$$s_3(t) = \sqrt{\mathcal{E}} (-\psi(t) - \psi(t - T) + \psi(t - 2T)) \quad (9.4.36)$$

$$s_4(t) = \sqrt{\mathcal{E}} (-\psi(t) + \psi(t - T) - \psi(t - 2T)) \quad (9.4.37)$$

or, equivalently, in vector notation

$$\mathbf{s}_1 = \sqrt{\mathcal{E}} (+1, +1, +1) \quad (9.4.38)$$

$$\mathbf{s}_2 = \sqrt{\mathcal{E}} (+1, -1, -1) \quad (9.4.39)$$

$$\mathbf{s}_3 = \sqrt{\mathcal{E}} (-1, -1, +1) \quad (9.4.40)$$

$$\mathbf{s}_4 = \sqrt{\mathcal{E}} (-1, +1, -1) \quad (9.4.41)$$

The corresponding constellation is shown in the three-dimensional space in Figure 9.14. It is seen that with this choice of code words, each code word differs from any other code word at two components. Therefore, the Euclidean distance between any two signals is given by

$$d_{ij}^2 = \|\mathbf{s}_i - \mathbf{s}_j\|^2 = 8\mathcal{E} \quad \text{for } i \neq j \quad (9.4.42)$$

To find  $\mathcal{E}$  in terms of  $P$ , we note that in a time interval of  $T$ , two bits are transmitted.

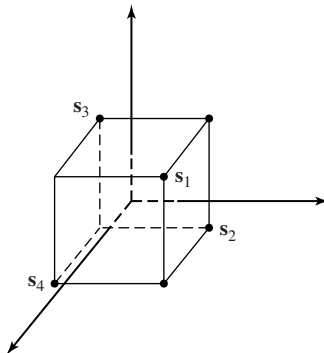


**Figure 9.14** Code words on the vertices of a cube.

Therefore,

$$2\mathcal{E}_b = 3\mathcal{E} \quad (9.4.43)$$

and

$$\mathcal{E} = \frac{2}{3}\mathcal{E}_b = \frac{2}{3}\frac{P}{R} \quad (9.4.44)$$

Thus,

$$d_{ij}^2 = \frac{16}{3}\frac{P}{R} \quad \text{for } i \neq j \quad (9.4.45)$$

Comparing this with the minimum distance in the 4-PSK signal, we observe that the minimum-distance squared has increased by a factor of

$$\frac{d_{ij}^2}{d_{4\text{PSK}}^2} = \frac{\frac{16}{3}\frac{P}{R}}{4\frac{P}{R}} = \frac{4}{3} \quad (9.4.46)$$

Because the error probability is a decreasing function of the minimum Euclidean distance, we have reduced the error probability by employing this new scheme. In fact, it can be said that the resulting reduction in error probability is equivalent to the reduction in error probability due to an increase in power by a factor of  $\frac{4}{3}$ . This, in turn is equivalent to a 1.25-dB power gain. This power gain, of course, has not been obtained for free. It is seen that with this signaling scheme in a time duration of  $\frac{2}{R}$ , which is the time duration to transmit two bits, we have to transmit three signals. Therefore the width of these signals is reduced by a factor of  $\frac{2}{3}$ , and the bandwidth required to transmit them is increased by a factor of  $\frac{3}{2}$ . A second problem with this scheme is that, obviously, it is more elaborate and requires a more complex decoding scheme.

The above exercise basically describes what a coding scheme does. Coding results in a lower error probability (which is equivalent to a higher effective SNR) at the price of increasing the bandwidth and the complexity of the system. It should be mentioned here that, although employing coding increases the bandwidth,<sup>†</sup> this increase is not exponential, as was the case with orthogonal signaling.

In a general signaling scheme with coded waveforms, sequences of length  $k = RT$  of the source outputs are mapped into sequences of length  $n$  of the form

$$\mathbf{s}_i = \sqrt{\mathcal{E}} \underbrace{(\pm 1, \pm 1, \dots, \pm 1)}_n \quad (9.4.47)$$

These points are located on the vertices of a hypercube of edge length  $2\sqrt{\mathcal{E}}$ . The ratio

$$R_c = \frac{k}{n} \quad (9.4.48)$$

is defined to be the *code rate*. There exist a total of  $2^n$  vertices of an  $n$ -dimensional hypercube of which we have to choose  $M = 2^k$  as code words. Obviously, one has to select these  $2^k$  vertices in such a way that they are as far apart from each other as

<sup>†</sup>There exist coding-modulation schemes that increase the Euclidean distance between code words but do not increase the bandwidth. These schemes will be treated in Section 9.9.

possible. This makes the Euclidean distance between them large and, thus, reduces the error probability.

Let us assume that we have chosen  $2^k$  vertices of the hypercube as the code words and each code word differs from another code word in at least  $d_{\min}^H$  components. This parameter is called the *minimum Hamming distance of the code* and will be defined more precisely in Section 9.5. The relation between Euclidean distance and Hamming distance is very simple. If the sequences  $\mathbf{s}_i$  and  $\mathbf{s}_j$  differ in  $d_{ij}^H$  locations, then their Euclidean distance  $d_{ij}^E$  is related to  $d_{ij}^H$  by

$$(d_{ij}^E)^2 = \sum_{\substack{1 \leq l \leq n \\ l: s_l^i \neq s_l^j}} (\pm 2\sqrt{\mathcal{E}})^2 = 4d_{ij}^H \mathcal{E} \quad (9.4.49)$$

This means that the minimum Euclidean distance can be expressed in terms of the minimum Hamming distance as

$$(d_{\min}^E)^2 = 4d_{\min}^H \mathcal{E} \quad (9.4.50)$$

Now if we assume  $\mathbf{s}_i$  is transmitted, and use the union bound (see Chapter 7), we have

$$\begin{aligned} P_{ei} &\leq MQ \left( \sqrt{\frac{4d_{\min}^H \mathcal{E}}{2N_0}} \right) \\ &\leq \frac{M}{2} e^{-d_{\min}^H \mathcal{E}/N_0} \end{aligned} \quad (9.4.51)$$

where in the last step, we have used the bound on the  $Q$  function introduced in Section 4.1. Now noting that the energy content of each code word is  $n\mathcal{E}$ , and this has to be equal to  $PT$ , we have

$$\mathcal{E} = \frac{PT}{n} = \frac{RT}{n} \mathcal{E}_b = \frac{k}{n} \mathcal{E}_b = R_c \mathcal{E}_b \quad (9.4.52)$$

where we have used the relation  $\mathcal{E}_b = \frac{P}{R}$ . Hence,

$$P_e \leq \frac{M}{2} e^{-d_{\min}^H R_c \mathcal{E}_b / N_0} \quad (9.4.53)$$

(the index  $i$  has been deleted because the bound is independent of  $i$ ). If no coding were employed, that is if we used all the vertices of a  $k$ -dimensional hypercube rather than  $2^k$  vertices of an  $n$ -dimensional hypercube, we would have the following union bound on the error probability

$$\begin{aligned} P_e &\leq MQ \left( \sqrt{\frac{2\mathcal{E}_b}{N_0}} \right) \\ &\leq \frac{M}{2} e^{-\mathcal{E}_b/N_0} \end{aligned} \quad (9.4.54)$$

Comparing the two bounds, one concludes that coding has resulted in a power gain equivalent to

$$G_{\text{coding}} = d_{\min}^{\text{H}} R_c \quad (9.4.55)$$

which is called the *asymptotic-coding gain*, or simply, the *coding gain*. As seen here, the coding gain is a function of two main code parameters, the minimum Hamming distance and the code rate. Note that in general,  $R_c < 1$  and  $d_{\min}^{\text{H}} \geq 1$  and, therefore, the coding gain can be greater or less than one.<sup>†</sup> It turns out that there exist many codes that can provide good coding gains. The relation defining the coding gain once again emphasizes that for a given  $n$  and  $k$  the best code is the code that can provide the highest minimum Hamming distance.

To study the bandwidth requirements of coding, we observe that when no coding is used, the width of the pulses employed to transmit one bit is given by

$$T_b = \frac{1}{R} \quad (9.4.56)$$

After using coding, in the same time duration that  $k$  pulses were transmitted, we must now transmit  $n$  pulses, which means that the duration of each pulse is reduced by a factor of  $\frac{k}{n} = R_c$ . Therefore, the *bandwidth-expansion ratio* is given by

$$B = \frac{W_{\text{coding}}}{W_{\text{no coding}}} = \frac{1}{R_c} = \frac{n}{k} \quad (9.4.57)$$

Thus, the bandwidth has increased linearly. It can be proved that in an AWGN channel, there exists a sequence of codes with parameters  $(n_i, k_i)$  with fixed rate  $(\frac{k_i}{n_i} = R_c$  independent of  $i$ ) satisfying

$$R_c = \frac{k}{n} < \frac{1}{2} \log \left( 1 + \frac{P}{N_0 W} \right) \quad (9.4.58)$$

where  $\frac{1}{2} \log(1 + \frac{P}{N_0 W})$  is the capacity of the channel in bits/transmission,<sup>‡</sup> for which the error probability goes to zero as  $n_i$  becomes larger and larger. Obviously, for such a scheme, the bandwidth expands by a modest factor and does not, as in orthogonal signaling, grow exponentially.

In this chapter, we study two major types of codes, *block codes*, and *convolutional codes*. Block codes are codes that have already been described. In a block code, the information sequence is broken into blocks of length  $k$  and each block is mapped into channel inputs of length  $n$ . This mapping is independent from the previous blocks; i.e., there exists no memory from one block to another block. In convolutional codes, there exists a shift register of length  $k_0 L$  as shown in Figure 9.15. The information bits enter the shift register  $k_0$  bits at a time and then  $n_0$  bits which are linear combinations of various shift register bits are transmitted over the channel. These  $n_0$  bits depend not only on the recent  $k_0$  bits that just entered the shift register, but also on the  $(L - 1)k_0$

<sup>†</sup>Although in a very bad code design we can even have  $d_{\min}^{\text{H}} = 0$ , we will ignore such cases.

<sup>‡</sup>Recall that the capacity of this channel in bits/sec is  $W \log(1 + \frac{P}{N_0 W})$ .

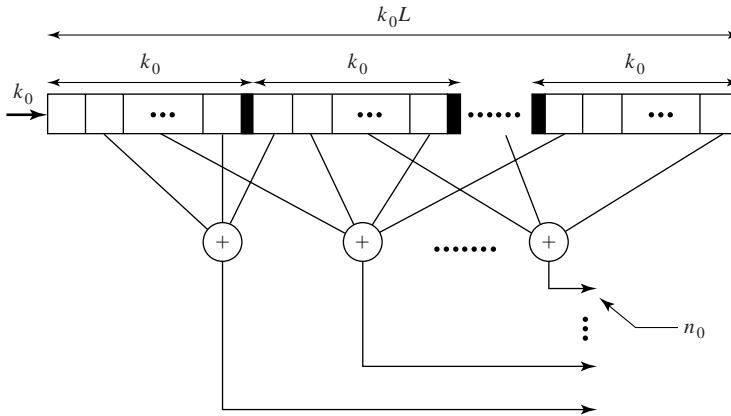


Figure 9.15 A convolutional encoder.

previous contents of the shift register that constitute its *state*. The quantity

$$m_c = L \tag{9.4.59}$$

is defined as the *constraint length* of the convolutional code and the number of states of the convolutional code are equal to  $2^{(L-1)k_0}$ . The rate of a convolutional code is defined as

$$R_c = \frac{k_0}{n_0} \tag{9.4.60}$$

The main difference between block codes and convolutional codes is the existence of memory in convolutional codes.

### 9.5 LINEAR BLOCK CODES

An  $(n, k)$  block code<sup>†</sup> is completely defined by  $M = 2^k$  binary sequences of length  $n$  called *code words*. A code  $C$  consists of  $M$  code words  $\mathbf{c}_i$  for  $1 \leq i \leq 2^k$ .

$$C = \{\mathbf{c}_1, \mathbf{c}_2, \dots, \mathbf{c}_M\}$$

where each  $\mathbf{c}_i$  is a sequence of length  $n$  with components equal to 0 or 1.

**Definition 9.5.1.** A block code is *linear* if any linear combination of two code words is also a code word. In the binary case this requires that if  $\mathbf{c}_i$  and  $\mathbf{c}_j$  are code words then  $\mathbf{c}_i \oplus \mathbf{c}_j$  is also a code word, where  $\oplus$  denotes component-wise modulo-2 addition.

With this definition, it is readily seen that a linear block code is a  $k$ -dimensional subspace of an  $n$ -dimensional space. It is also obvious that the all zero sequence  $\mathbf{0}$  is a code word of any linear block code since it can be written as  $\mathbf{c}_i \oplus \mathbf{c}_i$  for any code word  $\mathbf{c}_i$ . Note that according to the above definition linearity of a code only depends on the code

<sup>†</sup>From now on we will deal with binary codes unless otherwise specified.



words and not on the way that the information sequences (messages) are mapped to the code words. However, it is natural to assume that if the information sequence  $\mathbf{x}_1$  (of length  $k$ ) is mapped into the code word  $\mathbf{c}_1$  (of length  $n$ ) and the information sequence  $\mathbf{x}_2$  is mapped into  $\mathbf{c}_2$ , then  $\mathbf{x}_1 \oplus \mathbf{x}_2$  is mapped into  $\mathbf{c}_1 \oplus \mathbf{c}_2$ . From now on we will assume that the linear codes that we study possess this special property.

**Example 9.5.1**

A (5, 2) code is defined by

$$C = \{00000, 10100, 01111, 11011\}$$

It is very easy to verify that this code is linear. If the mapping between the information sequences and code words is given by

$$00 \rightarrow 00000$$

$$01 \rightarrow 01111$$

$$10 \rightarrow 10100$$

$$11 \rightarrow 11011$$

the special property mentioned above is satisfied as well. If the mapping is given by

$$00 \rightarrow 10100$$

$$01 \rightarrow 01111$$

$$10 \rightarrow 00000$$

$$11 \rightarrow 11011$$

the special property is not satisfied. However, in both cases the code is linear.

Now we define some of the basic parameters that characterize a code.

**Definition 9.5.2.** The *Hamming distance* between two code words  $\mathbf{c}_i$  and  $\mathbf{c}_j$  is the number of components at which the two code words differ, and is denoted by  $d(\mathbf{c}_i, \mathbf{c}_j)$ .<sup>†</sup>

**Definition 9.5.3.** The *Hamming weight*, or simply the *weight* of a code word  $\mathbf{c}_i$  is the number of nonzero components of the code word and is denoted by  $w(\mathbf{c}_i)$ .

**Definition 9.5.4.** The minimum distance of a code is the minimum Hamming distance between any two different code words; i.e.,

$$d_{\min} = \min_{\substack{\mathbf{c}_i, \mathbf{c}_j \\ i \neq j}} d(\mathbf{c}_i, \mathbf{c}_j) \quad (9.5.1)$$

**Definition 9.5.5.** The minimum weight of a code is the minimum of the weights of the code words except the all-zero code word.

$$w_{\min} = \min_{\mathbf{c}_i \neq \mathbf{0}} w(\mathbf{c}_i) \quad (9.5.2)$$

<sup>†</sup>From now on Hamming distance is denoted by  $d$  and Euclidean distance is denoted by  $d^E$ .

**Theorem 9.5.1.** In any linear code,  $d_{\min} = w_{\min}$ .

*Proof.* If  $\mathbf{c}$  is a code word, then  $w(\mathbf{c}) = d(\mathbf{c}, \mathbf{0})$ . Also if  $\mathbf{c}_i$  and  $\mathbf{c}_j$  are code words so is  $\mathbf{c} = \mathbf{c}_i \oplus \mathbf{c}_j$  and, moreover,  $d(\mathbf{c}_i, \mathbf{c}_j) = w(\mathbf{c})$ . This implies that, in a linear code corresponding to any weight of a code word, there exists a Hamming distance between two code words, and corresponding to any Hamming distance there exists a weight of a code word. In particular, it shows that  $d_{\min} = w_{\min}$ . ■

**Generator and Parity Check Matrices.** In an  $(n, k)$  linear block code let the code word corresponding to the information sequences  $\mathbf{e}_1 = (1000 \dots 0)$ ,  $\mathbf{e}_2 = (0100 \dots 0)$ ,  $\mathbf{e}_3 = (0010 \dots 0)$ ,  $\dots$ ,  $\mathbf{e}_k = (0000 \dots 1)$  be denoted by  $\mathbf{g}_1, \mathbf{g}_2, \mathbf{g}_3, \dots, \mathbf{g}_k$ , respectively, where each of the  $\mathbf{g}_i$  sequences is a binary sequence of length  $n$ . Now, any information sequence  $\mathbf{x} = (x_1, x_2, x_3, \dots, x_k)$  can be written as

$$\mathbf{x} = \sum_{i=1}^k x_i \mathbf{e}_i \quad (9.5.3)$$

and, therefore, the corresponding code word will be

$$\mathbf{c} = \sum_{i=1}^k x_i \mathbf{g}_i \quad (9.5.4)$$

If we define the *generator matrix* for this code as

$$\mathbf{G} \stackrel{\text{def}}{=} \begin{bmatrix} \mathbf{g}_1 \\ \mathbf{g}_2 \\ \vdots \\ \mathbf{g}_k \end{bmatrix} = \begin{bmatrix} g_{11} & g_{12} & \dots & g_{1n} \\ g_{21} & g_{22} & \dots & g_{2n} \\ \vdots & \vdots & \ddots & \vdots \\ g_{k1} & g_{k2} & \dots & g_{kn} \end{bmatrix} \quad (9.5.5)$$

then, we can write

$$\mathbf{c} = \mathbf{xG} \quad (9.5.6)$$

This shows that any linear combination of the rows of the generator matrix is a code word. The generator matrix for any linear block code is a  $k \times n$  matrix of rank  $k$  (because by definition the dimension of the subspace is  $k$ ). The generator matrix of a code completely describes the code. When the generator matrix is given, the structure of an encoder is quite simple.

### Example 9.5.2

Find the generator matrix for the first code given in Example 9.5.1.

**Solution** We have to find the code words corresponding to information sequences (10) and (01). These are (10100) and (01111), respectively. Therefore,

$$\mathbf{G} = \begin{bmatrix} 10100 \\ 01111 \end{bmatrix} \quad (9.5.7)$$

It is seen that for the information sequence  $(x_1, x_2)$ , the code word is given by

$$(c_1, c_2, c_3, c_4, c_5) = (x_1, x_2)\mathbf{G} \quad (9.5.8)$$

or

$$\begin{aligned}c_1 &= x_1 \\c_2 &= x_2 \\c_3 &= x_1 \oplus x_2 \\c_4 &= x_2 \\c_5 &= x_2\end{aligned}$$

The above code has the property that the code word corresponding to each information sequence starts with a replica of the information sequence itself followed by some extra bits. Such a code is called a *systematic code* and the extra bits following the information sequence in the code word are called the *parity check bits*. A necessary and sufficient condition for a code to be systematic is that the generator matrix be in the form

$$\mathbf{G} = [\mathbf{I}_k \mid \mathbf{P}] \quad (9.5.9)$$

where  $\mathbf{I}_k$  denotes a  $k \times k$  identity matrix and  $\mathbf{P}$  is a  $k \times (n - k)$  binary matrix. In a systematic code, we have

$$c_i = \begin{cases} x_i, & 1 \leq i \leq k \\ \sum_{j=1}^k p_{ji} x_j, & k + 1 \leq i \leq n \end{cases} \quad (9.5.10)$$

where all summations are modulo-2.

By definition a linear block code  $C$  is a  $k$ -dimensional linear subspace of the  $n$ -dimensional space. From linear algebra, we know that if we take all sequences of length  $n$  that are orthogonal to all vectors of this  $k$ -dimensional linear subspace, the result will be an  $(n - k)$ -dimensional linear subspace called the *orthogonal complement* of the  $k$ -dimensional subspace. This  $(n - k)$ -dimensional subspace naturally defines an  $(n, n - k)$  linear code which is known as the *dual* of the original  $(n, k)$  code  $C$ . The dual code is denoted by  $C^\top$ . Obviously the code words of the original code  $C$  and the dual code  $C^\top$  are orthogonal to each other. In particular, if we denote the generator matrix of the dual code by  $\mathbf{H}$ , which is an  $(n - k) \times n$  matrix, then any code word of the original code is orthogonal to all rows of  $\mathbf{H}$ ; i.e.,

$$\mathbf{c}\mathbf{H}^\top = \mathbf{0} \quad \text{for all } \mathbf{c} \in C \quad (9.5.11)$$

The matrix  $\mathbf{H}$ , which is the generator matrix of the dual code  $C^\top$ , is called the *parity check matrix* of the original code  $C$ . Since all rows of the generator matrix are code words, we conclude that

$$\mathbf{G}\mathbf{H}^\top = \mathbf{0} \quad (9.5.12)$$

In the special case of a systematic code, where

$$\mathbf{G} = [\mathbf{I}_k \mid \mathbf{P}] \quad (9.5.13)$$

the parity check matrix has the following form

$$\mathbf{H} = [ -\mathbf{P}^t \mid \mathbf{I}_k ] \quad (9.5.14)$$

Note that in the binary case  $-\mathbf{P}^t = \mathbf{P}^t$ .

**Example 9.5.3**

Find the parity check matrix for the code given in Example 9.5.1.

**Solution** Here

$$\mathbf{G} = \begin{bmatrix} 10100 \\ 01111 \end{bmatrix}$$

$$\mathbf{I} = \begin{bmatrix} 10 \\ 01 \end{bmatrix}$$

$$\mathbf{P} = \begin{bmatrix} 100 \\ 111 \end{bmatrix}$$

Noting that in the binary case  $-\mathbf{P}^t = \mathbf{P}^t$ , we conclude that

$$\mathbf{P}^t = \begin{bmatrix} 11 \\ 01 \\ 01 \end{bmatrix}$$

and, therefore,

$$\mathbf{H} = \left[ \begin{array}{cc|ccc} 11 & & 100 & & \\ 01 & & 010 & & \\ 01 & & 001 & & \end{array} \right]$$

**Hamming Codes.** Hamming codes are a class of linear block codes with  $n = 2^m - 1$ ,  $k = 2^m - m - 1$  and  $d_{\min} = 3$ , for some integer  $m \geq 2$ . As we will see in Section 9.5.1, with this minimum distance, these codes are capable of providing error-correction capabilities for single errors. The parity check matrix for these codes has a very simple structure. It consists of all binary sequences of length  $m$  except the all zero sequence. The rate of these codes is given by

$$R_c = \frac{2^m - m - 1}{2^m - 1} \quad (9.5.15)$$

which is close to 1 for large values of  $m$ . Therefore, Hamming codes are high-rate codes with relatively small minimum distance ( $d_{\min} = 3$ ). We will see later that the minimum distance of a code is closely related to its error-correcting capabilities. Therefore, Hamming codes have limited error-correcting capability.

**Example 9.5.4**

Find the parity check matrix and the generator matrix of a (7, 4) Hamming code in the systematic form.

**Solution** In this case  $m = 3$  and, therefore,  $\mathbf{H}$  consists of all binary sequences of length 3 except the all zero sequence. We generate the parity check matrix in the systematic

form as

$$\mathbf{H} = \left[ \begin{array}{cccc|ccc} 1 & 0 & 1 & 1 & 1 & 0 & 0 \\ 1 & 1 & 0 & 1 & 0 & 1 & 0 \\ 0 & 1 & 1 & 1 & 0 & 0 & 1 \end{array} \right]$$

and the generator matrix is obtained to be

$$\mathbf{G} = \left[ \begin{array}{cccc|ccc} 1 & 0 & 0 & 0 & 1 & 1 & 0 \\ 0 & 1 & 0 & 0 & 0 & 1 & 1 \\ 0 & 0 & 1 & 0 & 1 & 0 & 1 \\ 0 & 0 & 0 & 1 & 1 & 1 & 1 \end{array} \right]$$

### 9.5.1 Decoding and Performance of Linear Block Codes

The main purpose of using coding in communication systems is to increase the Euclidean distance between the transmitted signals and, hence, to reduce the error probability at a given transmitted power. This was shown by an example in the previous section. Referring to Figure 9.14, we see that this goal is achieved by choosing the code words to be as far apart on the vertices of the cube as possible. This means that a good measure for comparing the performance of two codes is the Hamming distance between code words. Keeping track of all distances between any two code words is difficult, and in many cases impossible. Therefore, the comparison between various codes is usually done based on the minimum distance of the code, which for linear codes is equal to the minimum weight. From this, it follows that for a given  $n$  and  $k$ , a code with a larger  $d_{\min}$  (or  $w_{\min}$ ), usually performs better compared with a code with a smaller minimum distance.

**Soft-Decision Decoding.** In Chapters 7 and 8 we have seen that the optimum signal-detection scheme on an additive white Gaussian noise channel is detection based on minimizing the Euclidean distance between the received signal and the transmitted signal. This means that, after receiving the output of the channel and passing it through the matched filters, we choose one of the message signals that is closest to the received signal in the Euclidean distance sense. In using coded waveforms the situation is the same. Assuming we are employing binary PSK for transmission of the coded message, a code word  $\mathbf{c}_i = (c_{i1}, c_{i2}, \dots, c_{in})$  is mapped into the sequence  $s_i(t) = \sum_{k=1}^n \psi_{ik}(t - (k-1)T)$ , where

$$\psi_{ik}(t) = \begin{cases} \psi(t), & c_{ik} = 1 \\ -\psi(t), & c_{ik} = 0 \end{cases} \quad (9.5.16)$$

and  $\psi(t)$  is a signal of duration  $T$  and energy  $\mathcal{E}$ , which is equal to zero outside the interval  $[0, T]$ . Now, the Euclidean distance between two arbitrary signal waveforms is

$$(d_{ij}^E)^2 = \sum_{\substack{1 \leq k \leq n \\ k: c_{ik} \neq c_{jk}}} (\pm 2\sqrt{\mathcal{E}})^2 = 4d_{ij}^H \mathcal{E} \quad (9.5.17)$$

This gives a simple relation between the Euclidean and the Hamming distance when a binary PSK signaling scheme (or any antipodal signaling scheme) is employed. For

orthogonal signaling, where  $\psi_1(t)$  and  $\psi_2(t)$  are orthogonal, the equivalent relation is

$$(d_{ij}^E)^2 = \sum_{\substack{1 \leq k \leq n \\ k: c_{ik} \neq c_{jk}}} \int_0^T [\psi_1(t) - \psi_2(t)]^2 dt = 2d_{ij}^H \mathcal{E} \quad (9.5.18)$$

Now, using the general relation

$$P_e = Q\left(\frac{d^E}{\sqrt{2N_0}}\right) \quad (9.5.19)$$

we obtain

$$P(j \text{ received} | i \text{ sent}) = \begin{cases} Q\left(\sqrt{\frac{d_{ij}\mathcal{E}}{N_0}}\right), & \text{for orthogonal signaling} \\ Q\left(\sqrt{\frac{d_{ij}2\mathcal{E}}{N_0}}\right), & \text{for antipodal signaling} \end{cases} \quad (9.5.20)$$

Since  $d_{ij} \geq d_{\min}$ , and since  $Q(x)$  is a decreasing function of  $x$ , we conclude that

$$P(j \text{ received} | i \text{ sent}) = \begin{cases} Q\left(\sqrt{\frac{d_{\min}\mathcal{E}}{N_0}}\right), & \text{for orthogonal signaling} \\ Q\left(\sqrt{\frac{d_{\min}2\mathcal{E}}{N_0}}\right), & \text{for antipodal signaling} \end{cases} \quad (9.5.21)$$

Now using the union bound (see Chapter 7), we obtain

$$P(\text{error} | i \text{ sent}) \leq \begin{cases} (M-1)Q\left(\sqrt{\frac{d_{\min}\mathcal{E}}{N_0}}\right), & \text{for orthogonal signaling} \\ (M-1)Q\left(\sqrt{\frac{2d_{\min}\mathcal{E}}{N_0}}\right), & \text{for antipodal signaling} \end{cases} \quad (9.5.22)$$

and assuming equiprobable messages, we finally conclude that

$$P_e \leq \begin{cases} (M-1)Q\left(\sqrt{\frac{d_{\min}\mathcal{E}}{N_0}}\right), & \text{for orthogonal signaling} \\ (M-1)Q\left(\sqrt{\frac{2d_{\min}\mathcal{E}}{N_0}}\right), & \text{for antipodal signaling} \end{cases} \quad (9.5.23)$$

These are bounds on the error probability of a coded communication system when optimal demodulation is employed. By optimal demodulation, we mean passing the received signal  $r(t)$  through a bank of matched filters to obtain the received vector  $\mathbf{r}$ , and then finding the closest point in the constellation to  $\mathbf{r}$  in the Euclidean distance sense. This type of decoding that involves finding the minimum Euclidean distance is called *soft-decision decoding*, and requires real number computation.

### Example 9.5.5

Compare the performance of an uncoded data transmission system with the performance of a coded system using the (7, 4) Hamming code given in Example 9.5.4 when applied to the transmission of a binary source with rate  $R = 10^4$  bits/sec. The channel is assumed to be an additive white Gaussian noise channel, the received power is  $1 \mu\text{W}$  and the noise power-spectral density is  $\frac{N_0}{2} = 10^{-11}$ . The modulation scheme is binary PSK.

**Solution**

1. If no coding is employed, we have

$$P_b = Q\left(\sqrt{\frac{2\mathcal{E}_b}{N_0}}\right) = Q\left(\sqrt{\frac{2P}{RN_0}}\right) \quad (9.5.24)$$

But  $\frac{2P}{RN_0} = \frac{10^{-6}}{10^4 \times 10^{-11}} = 10$  and, therefore,

$$P_b = Q(\sqrt{10}) = Q(3.16) \approx 7.86 \times 10^{-4} \quad (9.5.25)$$

The error probability for four bits will be

$$P_{\text{error in 4 bits}} = 1 - (1 - P_b)^4 \approx 3.1 \times 10^{-3} \quad (9.5.26)$$

2. If coding is employed, we have  $d_{\min} = 3$ , and

$$\frac{\mathcal{E}}{N_0} = R_c \frac{\mathcal{E}_b}{N_0} = R_c \frac{P}{RN_0} = \frac{4}{7} \times 5 = \frac{20}{7}$$

Therefore, the *message* error probability is given by

$$P_e \leq (M - 1)Q\left(\sqrt{\frac{2d_{\min}\mathcal{E}}{N_0}}\right) = 15Q\left(\sqrt{3\frac{40}{7}}\right) = 15Q(4.14) \approx 2.6 \times 10^{-4}$$

It is seen that, using this simple code decreases the error probability by a factor of 12. Of course, the price that has been paid is an increase in the bandwidth required for transmission of the messages. This bandwidth expansion ratio is given by

$$\frac{W_{\text{coded}}}{W_{\text{uncoded}}} = \frac{1}{R_c} = \frac{7}{4} = 1.75$$

**Hard-Decision Decoding.** A simpler and more frequently used decoding scheme is to make hard binary decisions on the components of the received vector  $\mathbf{r}$ , and then to find the code word that is closest to it in the Hamming distance sense. The following example clarifies the distinction between soft and hard decisions.

**Example 9.5.6**

A (3,1) code consists of the two code words 000 and 111. The code words are transmitted using binary PSK modulation with  $\mathcal{E} = 1$ . The received vector (the sampled outputs of the matched filters) is  $\mathbf{r} = (.5, .5, -3)$ . If soft decision is employed, we have to compare the Euclidean distance between  $\mathbf{r}$  and the two constellation points (1, 1, 1) and (-1, -1, -1) and choose the smaller one. We have  $(d^E(\mathbf{r}, (1, 1, 1)))^2 = .5^2 + .5^2 + 4^2 = 16.5$  and  $(d^E(\mathbf{r}, (-1, -1, -1)))^2 = 1.5^2 + 1.5^2 + (-2)^2 = 8.5$  and, therefore, a soft-decision decoder would decode  $\mathbf{r}$  as (-1, -1, -1) or, equivalently, (0, 0, 0). However, if hard-decision decoding is employed,  $\mathbf{r}$  is first component-wise detected as 1 or 0. This requires a comparison of the components of  $\mathbf{r}$  with the zero threshold. The resulting vector  $\mathbf{y}$  is therefore  $\mathbf{y} = (1, 1, 0)$ . Now, we have to compare  $\mathbf{y}$  with the (1, 1, 1) and (0, 0, 0) and find the closer one in the Hamming distance sense. The result is, of course, (1, 1, 1). As seen in this example, the results of soft-decision decoding and hard-decision decoding can be quite different. Of course, soft-decision decoding is the optimal detection method and achieves a lower probability of error.

$$\begin{array}{cccc}
 \mathbf{c}_1 & & \mathbf{c}_2 & & \mathbf{c}_3 & & \mathbf{c}_M \\
 \mathbf{e}_1 & & \mathbf{e}_1 \oplus \mathbf{c}_2 & & \mathbf{e}_1 \oplus \mathbf{c}_3 & & \mathbf{e}_1 \oplus \mathbf{c}_M \\
 \mathbf{e}_2 & & \mathbf{e}_2 \oplus \mathbf{c}_2 & & \mathbf{e}_2 \oplus \mathbf{c}_3 & & \mathbf{e}_2 \oplus \mathbf{c}_M \\
 \vdots & & \vdots & & \vdots & & \vdots \\
 \mathbf{e}_2^{(n-k)-1} & & \mathbf{e}_2^{(n-k)-1} \oplus \mathbf{c}_2 & & \mathbf{e}_2^{(n-k)-1} \oplus \mathbf{c}_3 & & \mathbf{e}_2^{(n-k)-1} \oplus \mathbf{c}_M
 \end{array}$$

Figure 9.16 The standard array.

There are three basic steps involved in hard-decision decoding. First, we perform demodulation by passing the received  $r(t)$  through the matched filters and sampling the output to obtain the  $\mathbf{r}$  vector. Second, we compare the components of  $\mathbf{r}$  with the thresholds and quantize each component to one of the two levels to obtain the  $\mathbf{y}$  vector. Finally, we perform decoding by finding the code word that is closest to  $\mathbf{y}$  in the Hamming distance sense. In this section, we present a systematic approach to perform hard-decision decoding.

First we will define the notion of a *standard array*. Let the code words of the code in question be denoted by  $\mathbf{c}_1, \mathbf{c}_2, \dots, \mathbf{c}_M$ , where each of the code words is of length  $n$  and  $M = 2^k$ , and let  $\mathbf{c}_1$  denote the all-zero code word. A standard array is a  $2^{n-k} \times 2^k$  array whose elements are binary sequences of length  $n$  and is generated by writing all the code words in a row starting with the all zero code word. This constitutes the first row of the standard array. To write the second row, we look among all the binary sequences of length  $n$  that are not in the first row of the array. Choose one of these code words that has the minimum weight and call it  $\mathbf{e}_1$ . Write it under<sup>†</sup>  $\mathbf{c}_1$  and write  $\mathbf{e}_1 \oplus \mathbf{c}_i$  under  $\mathbf{c}_i$  for  $2 \leq i \leq M$ . The third row of the array is completed in a similar way. From the binary  $n$ -tuples that *have not been used in the first two rows*, we choose one with minimum weight and call it  $\mathbf{e}_2$ . Then, the elements of the third row become  $\mathbf{c}_i \oplus \mathbf{e}_2$ . This process is continued until no binary  $n$ -tuples remain to start a new row. Figure 9.16 shows the standard array generated as explained above. Each row of the standard array is called a *coset* and the first element of each coset ( $\mathbf{e}_l$ , in general) is called the *coset leader*.

The standard array has the following important properties.

**Theorem 9.5.2.** All elements of the standard array are distinct.

*Proof.* Let us assume two elements of the standard array are equal. This can happen in two ways.

1. The two equal elements belong to the same coset. In this case we have  $\mathbf{c}_l \oplus \mathbf{c}_i = \mathbf{e}_j \oplus \mathbf{c}_j$ , from which we conclude  $\mathbf{c}_i = \mathbf{c}_j$  which is impossible.
2. The two equal elements belong to two different cosets. Here we have  $\mathbf{e}_l \oplus \mathbf{c}_i = \mathbf{e}_k \oplus \mathbf{c}_j$  for  $l \neq k$ , which means  $\mathbf{e}_l = \mathbf{e}_k \oplus (\mathbf{c}_i \oplus \mathbf{c}_j)$ . By linearity of the code  $\mathbf{c}_i \oplus \mathbf{c}_j$  is also a code word; let us call it  $\mathbf{c}_m$ . Therefore,  $\mathbf{e}_l = \mathbf{e}_k \oplus \mathbf{c}_m$  and, hence,  $\mathbf{e}_l$  and  $\mathbf{e}_k$  belong to the same coset, which is impossible since by assumption  $k \neq l$ . ■

<sup>†</sup>Note that  $\mathbf{c}_1 \oplus \mathbf{e}_1 = \mathbf{e}_1$ , since  $\mathbf{c}_1 = (0, 0, \dots, 0)$ .



From this theorem, we conclude that the standard array contains exactly  $2^{n-k}$  rows.

**Theorem 9.5.3.** If  $\mathbf{y}_1$  and  $\mathbf{y}_2$  are elements of the same coset, we have  $\mathbf{y}_1\mathbf{H}^t = \mathbf{y}_2\mathbf{H}^t$ .

*Proof.* It is enough to note that since  $\mathbf{y}_1$  and  $\mathbf{y}_2$  are in the same coset,  $\mathbf{y}_1 = \mathbf{e}_l \oplus \mathbf{c}_i$  and  $\mathbf{y}_2 = \mathbf{e}_l \oplus \mathbf{c}_j$ , therefore

$$\mathbf{y}_1\mathbf{H}^t = (\mathbf{e}_l \oplus \mathbf{c}_i)\mathbf{H}^t = \mathbf{e}_l\mathbf{H}^t + \mathbf{0} = (\mathbf{e}_l \oplus \mathbf{c}_j)\mathbf{H}^t = \mathbf{y}_2\mathbf{H}^t \quad \blacksquare$$

From this theorem, we conclude that each coset of the standard array can be uniquely identified by the product  $\mathbf{e}_l\mathbf{H}^t$ . In general, for any binary sequence  $\mathbf{y}$  of length  $n$ , we define the *syndrome*  $\mathbf{s}$  as

$$\mathbf{s} = \mathbf{y}\mathbf{H}^t \quad (9.5.27)$$

If  $\mathbf{y} = \mathbf{e}_l \oplus \mathbf{c}_i$ ; i.e.,  $\mathbf{y}$  belongs to the  $(l + 1)$ st coset, then obviously  $\mathbf{s} = \mathbf{e}_l\mathbf{H}^t$ . The syndrome is a binary sequence of length  $2^{n-k}$  and corresponding to each coset there exists a unique syndrome. Obviously, the syndrome corresponding to the first coset, which consists of the code words, is  $\mathbf{s} = \mathbf{0}$ .

**Example 9.5.7**

Find the standard array for the (5, 2) code with code words 00000, 10100, 01111, 11011. Also find the syndromes corresponding to each coset.

**Solution** The generator polynomial of the code is

$$\mathbf{G} = \begin{bmatrix} 1 & 0 & 1 & 0 & 0 \\ 0 & 1 & 1 & 1 & 1 \end{bmatrix}$$

and the parity check matrix corresponding to  $\mathbf{G}$  is

$$\mathbf{H} = \begin{bmatrix} 1 & 1 & 1 & 0 & 0 \\ 0 & 1 & 0 & 1 & 0 \\ 0 & 1 & 0 & 0 & 1 \end{bmatrix}$$

Using the construction explained above, we obtain the standard array

00000	01111	10100	11011	syndrome = 000
10000	11111	00100	01011	syndrome = 100
01000	00111	11100	10011	syndrome = 111
00010	01101	10110	11001	syndrome = 010
00001	01110	10101	11010	syndrome = 001
11000	10111	01100	00011	syndrome = 011
10010	11101	00110	01001	syndrome = 110
10001	11110	00101	01010	syndrome = 101

Assuming that the received vector  $\mathbf{r}$  has been component-wise compared with a threshold and the resulting binary vector is  $\mathbf{y}$ , we have to find the code word which is at minimum Hamming distance from  $\mathbf{y}$ . First, we find in which coset  $\mathbf{y}$  is located. To do this, we find the syndrome of  $\mathbf{y}$  by calculating  $\mathbf{s} = \mathbf{y}\mathbf{H}^t$ . After finding  $\mathbf{s}$ , we refer to

the standard array and find the coset corresponding to  $\mathbf{s}$ . Let us assume that the coset leader corresponding to this coset is  $\mathbf{e}_l$ . Because  $\mathbf{y}$  belongs to this coset, it is of the form  $\mathbf{e}_l \oplus \mathbf{c}_i$  for some  $i$ . The Hamming distance of  $\mathbf{y}$  from any code word  $\mathbf{c}_j$  is, therefore,

$$d(\mathbf{y}, \mathbf{c}_j) = w(\mathbf{y} \oplus \mathbf{c}_j) = w(\mathbf{e}_l \oplus \mathbf{c}_i \oplus \mathbf{c}_j) \quad (9.5.28)$$

Because the code is linear,  $\mathbf{c}_i \oplus \mathbf{c}_j = \mathbf{c}_k$  for some  $1 \leq k \leq M$ . This means that,

$$d(\mathbf{y}, \mathbf{c}_j) = w(\mathbf{c}_k \oplus \mathbf{e}_l) \quad (9.5.29)$$

but  $\mathbf{c}_k \oplus \mathbf{e}_l$  belongs to the same coset that  $\mathbf{y}$  belongs to. Therefore, to minimize  $d(\mathbf{y}, \mathbf{c}_j)$ , we have to find the minimum weight element in the coset to which  $\mathbf{y}$  belongs. By construction of the standard array, this element is the coset leader; i.e., we choose  $\mathbf{c}_k = \mathbf{0}$  and therefore  $\mathbf{c}_j = \mathbf{c}_i$ . This means that  $\mathbf{y}$  is decoded into  $\mathbf{c}_i$  by finding

$$\mathbf{c}_i = \mathbf{y} \oplus \mathbf{e}_l \quad (9.5.30)$$

Therefore, the procedure for hard-decision decoding can be summarized as follows

1. Find  $\mathbf{r}$ , the vector representation of the received signal.
2. Compare each component of  $\mathbf{r}$  to the optimal threshold (usually 0) and make a binary decision on it to obtain the binary vector  $\mathbf{y}$ .
3. Find  $\mathbf{s} = \mathbf{y}\mathbf{H}^t$  the syndrome of  $\mathbf{y}$ .
4. Find the coset corresponding to  $\mathbf{s}$  by using the standard array.
5. Find the coset leader  $\mathbf{e}$  and decode  $\mathbf{y}$  as  $\mathbf{c} = \mathbf{y} \oplus \mathbf{e}$ .

Because in this decoding scheme the difference between the vector  $\mathbf{y}$  and the decoded vector  $\mathbf{c}$  is  $\mathbf{e}$ , the binary  $n$ -tuple  $\mathbf{e}$  is frequently referred to as the *error pattern*. This means that *the coset leaders constitute the set of all correctable error patterns*.

To obtain error bounds in hard-decision decoding we note that, since a decision is made on each individual bit, the error probability for each bit for antipodal signaling is

$$P_b = Q\left(\sqrt{\frac{2\mathcal{E}_b}{N_0}}\right) \quad (9.5.31)$$

and for orthogonal signaling, is to

$$P_b = Q\left(\sqrt{\frac{\mathcal{E}_b}{N_0}}\right) \quad (9.5.32)$$

The channel between the input code word  $\mathbf{c}$  and the output of the hard limiter  $\mathbf{y}$  is a binary-input binary-output channel that can be modeled by a binary-symmetric channel with crossover probability  $P_b$ . Because the code is linear the distance between any two code words  $\mathbf{c}_i$  and  $\mathbf{c}_j$  is equal to the distance between the all zero code word  $\mathbf{0}$  and the code word  $\mathbf{c}_i \oplus \mathbf{c}_j = \mathbf{c}_k$ . Thus, without loss of generality, we can assume that the all-zero code word is transmitted. If  $\mathbf{0}$  is transmitted, the error probability, by the union bound, cannot exceed  $(M - 1)$  times the probability of decoding the code word that is closest to  $\mathbf{0}$  in the Hamming distance sense. For this code word, denoted by  $\mathbf{c}$ , which is

at distance  $d_{\min}$  from  $\mathbf{0}$  we have

$$P(\mathbf{c} | \mathbf{0} \text{ sent}) \leq \begin{cases} \sum_{i=\frac{d_{\min}+1}{2}}^{d_{\min}} \binom{d_{\min}}{i} P_b^i (1 - P_b)^{d_{\min}-i}, & d_{\min} \text{ odd} \\ \sum_{i=\frac{d_{\min}}{2}+1}^{d_{\min}} \binom{d_{\min}}{i} P_b^i (1 - P_b)^{d_{\min}-i} \\ \quad + \frac{1}{2} \binom{d_{\min}}{\frac{d_{\min}}{2}} P_b^{\frac{d_{\min}}{2}} (1 - P_b)^{\frac{d_{\min}}{2}}, & d_{\min} \text{ even} \end{cases}$$

or, in general,

$$P(\mathbf{c} | \mathbf{0} \text{ sent}) \leq \sum_{i=\lceil \frac{d_{\min}+1}{2} \rceil}^{d_{\min}} \binom{d_{\min}}{i} P_b^i (1 - P_b)^{d_{\min}-i} \quad (9.5.33)$$

Therefore,

$$P_e \leq (M - 1) \sum_{i=\lceil \frac{d_{\min}+1}{2} \rceil}^{d_{\min}} \binom{d_{\min}}{i} P_b^i (1 - P_b)^{d_{\min}-i} \quad (9.5.34)$$

This gives an upper bound on the error probability of a linear block code using hard-decision decoding. As seen here both in soft-decision and hard-decision decoding,  $d_{\min}$  plays a major role in bounding the error probability. This means that, for a given  $(n, k)$ , it is desirable to have codes with large  $d_{\min}$ .

It can be shown that the difference between the performance of soft- and hard-decision decoding is roughly 2 dB for an additive white Gaussian noise channel. That is, the error probability of a soft-decision decoding scheme is comparable to the error probability of a hard-decision scheme whose power is 2-dB higher than the soft-decision scheme. It can also be shown that if instead of quantization of each component of  $\mathbf{r}$  to two levels, an 8-level quantizer (three bits/component) is employed, the performance difference with soft decision (infinite precision) reduces to 0.1 dB. This multilevel quantization scheme, which is a compromise between soft (infinite precision) and hard decision, is also referred to as soft decision in the literature.

### Example 9.5.8

If hard-decision decoding is employed in Example 9.5.5, how will the results change?

**Solution** Here  $P_b = Q(\sqrt{\frac{40}{7}}) = Q(2.39) = 0.0084$  and  $d_{\min} = 3$ . Therefore,

$$\begin{aligned} P_e &\leq \binom{7}{2} P_b^2 (1 - P_b)^5 + \binom{7}{3} P_b^3 (1 - P_b)^4 + \dots + P_b^7 \\ &\approx 21 P_b^2 \approx 1.5 \times 10^{-3} \end{aligned}$$

In this case, coding has decreased the error probability by a factor of 2, compared to 12 in the soft-decision case.

**Error Detection versus Error Correction.** Let  $C$  be a linear block code with minimum distance  $d_{\min}$ . Then, if  $\mathbf{c}$  is transmitted and hard-decision decoding is employed, any code word will be decoded correctly if the received  $\mathbf{y}$  is closer to  $\mathbf{c}$  than any

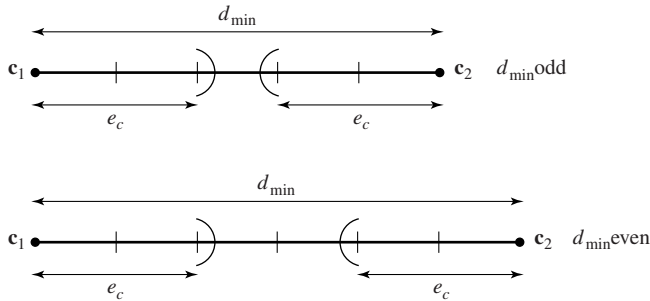


Figure 9.17 Relation between  $e_c$  and  $d_{\min}$ .

other code word. This situation is shown in Figure 9.17. As shown, around each code word there is a “Hamming sphere” of radius  $e_c$ , where  $e_c$  denotes the number of correctable errors. As long as these spheres are disjoint, the code is capable of correcting  $e_c$  errors. A little thinking shows that the condition for nonoverlapping spheres is

$$\begin{cases} 2e_c + 1 = d_{\min} & d_{\min} \text{ odd} \\ 2e_c + 2 = d_{\min} & d_{\min} \text{ even} \end{cases}$$

or

$$e_c = \begin{cases} \frac{d_{\min}-1}{2} & d_{\min} \text{ odd} \\ \frac{d_{\min}-2}{2} & d_{\min} \text{ even} \end{cases} \quad (9.5.35)$$

which can be summarized as

$$e_c = \left\lfloor \frac{d_{\min} - 1}{2} \right\rfloor \quad (9.5.36)$$

In some cases, we are interested in decoding procedures that can *detect* errors rather than correcting them. For example, in a communication system where a feedback link is available from the receiver to the transmitter, it might be desirable to detect if an error has occurred and if so, to ask the transmitter via the feedback channel to retransmit the message. If we denote the error-detection capability of a code by  $e_d$ , then obviously, in the absence of error correction,  $e_d = d_{\min} - 1$ , because if  $d_{\min} - 1$  or fewer errors occur, the transmitted code word will be converted to a noncode word sequence and, therefore, an error is detected. If both error correction and error detection are desirable, then there is naturally a trade-off between these. Figure 9.18 demonstrates this. From

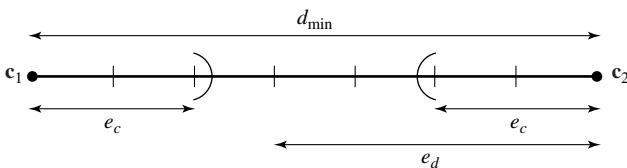


Figure 9.18 Relation between  $e_c$ ,  $e_d$  and  $d_{\min}$ .

this picture, we see that

$$e_c + e_d = d_{\min} - 1 \quad (9.5.37)$$

with the extra condition  $e_c \leq e_d$ .

### 9.5.2 Burst-Error-Correcting-Codes

Most of the linear block codes are designed for correcting *random errors*; i.e., errors that occur independently from the location of other channel errors. Certain channel models including the additive white Gaussian noise channel, can be well modeled as channels with random errors. In some other physical channels, however, the assumption of independently generated errors is not a valid assumption. One such example is a fading channel, as will be discussed in Section 10.1. In such a channel, if the channel is in deep fade, a large number of errors occur in sequence; i.e., the errors have a *bursty nature*. Obviously, in this channel, the probability of error at a certain location or time, depends on whether or not its adjacent bits are received correctly. Another example of a channel with bursty errors is a compact disc (see Section 9.10). Any physical damage to a compact disc, such as a scratch, damages a sequence of bits and, therefore, the errors tend to occur in *bursts*. Of course, any random error-correcting code can be used to correct bursts of errors as long as the number of errors is less than half of the minimum distance of the code. But the knowledge of the bursty nature of errors makes it possible to design more efficient coding schemes. Two particular codes that are designed to be used for burst-error-correction are Fire codes and Burton codes. The interested reader is referred to Lin and Costello (1983) for a discussion of these codes.

An effective method for correction of error bursts is to *interleave* the coded data such that the location of errors looks random and is distributed over many code words rather than a few code words. In this way, the number of errors that occur in each block is low and can be corrected by using a random error-correcting code. At the receiver, a *deinterleaver* is employed to undo the effect of the interleaver. A block diagram of a coding system employing interleaving/deinterleaving is shown in Figure 9.19.

An *interleaver of depth  $m$*  reads  $m$  code words of length  $n$  each and arranges them in a block with  $m$  rows and  $n$  columns. Then, this block is read by column and the output is sent to the digital modulator. At the receiver, the output of the detector is supplied to the deinterleaver, which generates the same  $m \times n$  block structure and then reads by row and sends the output to the channel decoder. This is shown in Figure 9.20.

Let us assume that  $m = 8$  and the code in use is a (15, 11) Hamming code capable of correcting one error/code word. Then, the block generated by the interleaver is a  $8 \times 15$  block containing 120 binary symbols. Obviously, any burst of errors of length 8 or less will result in at most one error/code word and, therefore, can be corrected. If

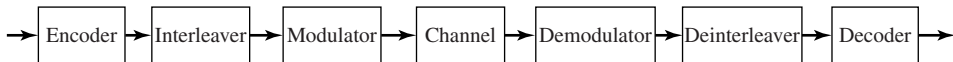


**Figure 9.19** Block diagram of a system that employs interleaving/deinterleaving for burst-error-correction.

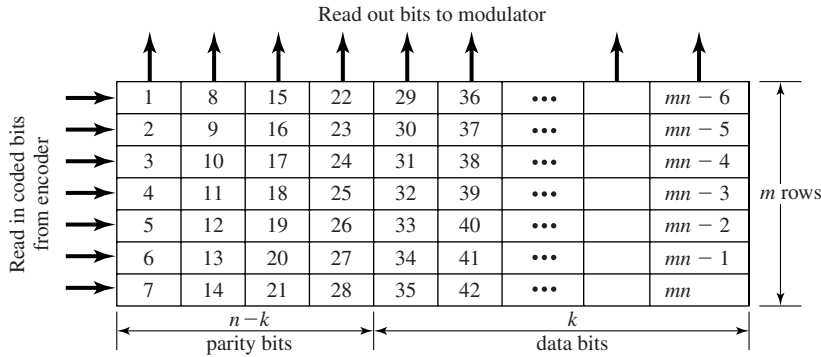


Figure 9.20 A block interleaver for coded data.

interleaving/deinterleaving was not employed, an error burst of length 8 could possibly result in erroneous detection in 2 code words (up to 22 information bits).

## 9.6 CYCLIC CODES

Cyclic codes are a subset of linear block codes for which easily implementable encoders and decoders exist. In this section, we will study the structure of cyclic codes.

**Definition 9.6.1.** A *cyclic code* is a linear block code with the extra condition that if  $\mathbf{c}$  is a code word, a cyclic shift<sup>†</sup> of it is also a code word.

### Example 9.6.1

The code {000, 110, 101, 011} is a cyclic code because it is easily verified to be linear and a cyclic shift of any code word is also a code word. The code {000, 010, 101, 111} is not cyclic because, although it is linear, a cyclic shift of 101 is not a code word.

### 9.6.1 The Structure of Cyclic Codes

To study the properties of cyclic codes, it is easier to represent each code word as a polynomial, called the code word polynomial. The code word polynomial corresponding to  $\mathbf{c} = (c_1, c_2, \dots, c_{n-1}, c_n)$  is simply defined to be

$$c(p) = \sum_{i=1}^n c_i p^{n-i} = c_1 p^{n-1} + c_2 p^{n-2} + \dots + c_{n-1} p + c_n \tag{9.6.1}$$

The code word polynomial of  $\mathbf{c}^{(1)} = (c_2, c_3, \dots, c_{n-2}, c_{n-1}, c_n, c_1)$ , the cyclic shift of  $\mathbf{c}$ , is

$$c^{(1)}(p) = c_2 p^{n-1} + c_3 p^{n-2} + \dots + c_{n-1} p^2 + c_n p + c_1 \tag{9.6.2}$$

<sup>†</sup>A cyclic shift of the code word  $\mathbf{c} = (c_1, c_2, \dots, c_{n-1}, c_n)$  is defined to be  $\mathbf{c}^{(1)} = (c_2, c_3, \dots, c_{n-1}, c_n, c_1)$ .

which can be written as

$$c^{(1)}(p) = pc(p) + c_1(p^n + 1) \quad (9.6.3)$$

Noting that in the binary field addition and subtraction are equivalent, this reduces to

$$pc(p) = c^{(1)}(p) + c_1(p^n + 1) \quad (9.6.4)$$

or

$$c^{(1)}(p) = pc(p) \pmod{(p^n + 1)} \quad (9.6.5)$$

If we shift  $c^{(1)}$  once more the result will also be a code word and its code word polynomial will be

$$c^{(2)}(p) = pc^{(1)}(p) \pmod{(p^n + 1)} \quad (9.6.6)$$

$$= p^2c(p) \pmod{(p^n + 1)} \quad (9.6.7)$$

where

$$a(p) = b(p) \pmod{d(p)}$$

means that  $a(p)$  and  $b(p)$  have the same remainder when divided by  $d(p)$ . In general, for  $i$  shifts we have the code word polynomial

$$c^{(i)}(p) = p^i c(p) \pmod{(p^n + 1)} \quad (9.6.8)$$

For  $i = n$ , we have

$$c^{(n)}(p) = p^n c(p) \pmod{(p^n + 1)} \quad (9.6.9)$$

$$= (p^n + 1)c(p) + c(p) \pmod{(p^n + 1)} \quad (9.6.10)$$

$$= c(p) \quad (9.6.11)$$

The above result is obvious because shifting any code word  $n$  times leaves it unchanged.

The following theorem, which we will state without proof,<sup>†</sup> is fundamental in further study of cyclic codes.

**Theorem 9.6.1.** In any  $(n, k)$  cyclic code all code word polynomials are multiples of a polynomial of degree  $n - k$  of the form

$$g(p) = p^{n-k} + g_2 p^{n-k-1} + g_3 p^{n-k-2} + \cdots + g_{n-k} p + 1$$

called the *generator polynomial*, where  $g(p)$  divides  $p^n + 1$ . Furthermore, for any information sequence  $\mathbf{x} = (x_1, x_2, \dots, x_{k-1}, x_k)$ , we have the *information sequence polynomial*  $X(p)$  defined by

$$X(p) = x_1 p^{k-1} + x_2 p^{k-2} + \cdots + x_{k-1} p + x_k$$

and the code word polynomial corresponding to  $\mathbf{x}$  is given by  $c(p) = X(p)g(p)$ . ■

<sup>†</sup>See Lin and Costello (1983) for a proof.

The fact that any code word polynomial is the product of the generator polynomial and the information sequence polynomial, implies that  $\mathbf{c} = (c_1, c_2, \dots, c_{n-1}, c_n)$  is the discrete convolution of the two sequences  $\mathbf{x} = (x_1, x_2, \dots, x_k)$  and  $\mathbf{g} = (1, g_2, \dots, g_{n-k}, 1)$ . This fact is very important in designing cyclic encoders.

**Example 9.6.2**

To generate a (7, 4) cyclic code we need a generator polynomial of degree  $n - k = 3$ . This polynomial has to divide  $p^7 + 1$ . Since

$$p^7 + 1 = (p + 1)(p^3 + p^2 + 1)(p^3 + p + 1)$$

the only third degree polynomials that divide  $p^7 + 1$  are  $p^3 + p^2 + 1$  and  $p^3 + p + 1$ . We can choose either of these polynomials to generate a cyclic code. If we choose

$$g(p) = p^3 + p^2 + 1$$

and multiply it by all  $X(p)$  polynomials of the form

$$X(p) = x_1p^3 + x_2p^2 + x_3p + x_4$$

where  $x_i$  is either one or zero, we generate 16 code word polynomials from which we can obtain the code words. The  $X(p)$  polynomial is the *message polynomial* or the *information sequence polynomial* corresponding to the binary sequence to be encoded and, in general,

$$c(p) = X(p)g(p)$$

The following table shows the input binary sequences and the corresponding code words:

Input	$X(p)$	$c(p) = X(p)g(p)$	Code word
0000	0	0	0000000
0001	1	$p^3 + p^2 + 1$	0001101
0010	$p$	$p^4 + p^3 + p$	0011010
0100	$p^2$	$p^5 + p^4 + p^2$	0110100
1000	$p^3$	$p^6 + p^5 + p^3$	1101000
0011	$p + 1$	$p^4 + p^2 + p + 1$	0010110
0110	$p^2 + p$	$p^5 + p^3 + p^2 + p$	0101110
1100	$p^3 + p^2$	$p^6 + p^4 + p^3 + p^2$	1011100
1001	$p^3 + 1$	$p^6 + p^5 + p^2 + 1$	1100101
0101	$p^2 + 1$	$p^5 + p^4 + p^3 + 1$	0111001
1010	$p^3 + p$	$p^6 + p^5 + p^4 + p$	1110010
0111	$p^2 + p + 1$	$p^5 + p + 1$	0100011
1110	$p^3 + p^2 + p$	$p^6 + p^2 + p$	1000110
1101	$p^3 + p^2 + 1$	$p^6 + p^4 + 1$	1010001
1011	$p^3 + p + 1$	$p^6 + p^5 + p^4 + p^3 + p^2 + p + 1$	1111111
1111	$p^3 + p^2 + p + 1$	$p^6 + p^3 + p + 1$	1001011

As seen from the above table all cyclic shifts of a given code word are code words themselves.



**The Generator Matrix.** Since the generator matrix  $\mathbf{G}$  for a linear block code is not unique, for any cyclic code, with a given generator polynomial, there exist many generator matrices. Here, we describe a method to obtain a generator matrix in the systematic form. A generator matrix is in the systematic form if it can be written in the form

$$\mathbf{G} = [\mathbf{I}_k \mid \mathbf{P}] \quad (9.6.12)$$

On the other hand, all rows of the generator matrix are code words. This means that the polynomials corresponding to different rows of the generator matrix are all multiples of the generator polynomial  $g(p)$ . On the other hand the  $i$ th row of the matrix  $\mathbf{G}$  is

$$\mathbf{g}_i = (0, 0, \dots, 0, 1, 0, \dots, 0, p_{i,1}, p_{i,2}, \dots, p_{i,n-k}) \quad 1 \leq i \leq k \quad (9.6.13)$$

where the first  $k$  components of  $\mathbf{g}_i$  are all zeros except the  $i$ th component which is 1 and  $p_{i,j}$  denotes the  $(i, j)$ th element of the matrix  $\mathbf{P}$ . From above, the polynomial corresponding to  $\mathbf{g}_i$  is

$$g_i(p) = p^{n-i} + p_{i,1}p^{n-k-1} + p_{i,2}p^{n-k-2} + \dots + p_{i,n-k} \quad (9.6.14)$$

Because  $g_i(p)$  is the code word polynomial corresponding to the code word  $\mathbf{g}_i$ , it has to be a multiple of  $g(p)$ , the generator polynomial of the cyclic code under study. Therefore, we have

$$g_i(p) = p^{n-i} + p_{i,1}p^{n-k-1} + p_{i,2}p^{n-k-2} + \dots + p_{i,n-k} = X(p)g(p) \quad (9.6.15)$$

Now, since  $g(p)$  is of degree  $n - k$  we conclude that

$$p^{n-i} + p_{i,1}p^{n-k-1} + p_{i,2}p^{n-k-2} + \dots + p_{i,n-k} = p^{n-i} \pmod{g(p)} \quad 1 \leq i \leq k \quad (9.6.16)$$

This relation shows that having  $g(p)$  we can find all  $p_{i,j}$ 's for all  $1 \leq i \leq k$  and  $1 \leq j \leq n - k$ . Therefore,  $\mathbf{P}$  can be obtained from  $g(p)$  and, thus, we obtain  $\mathbf{G}$ , the generator matrix.

### Example 9.6.3

Find the generator matrix in the systematic form for the  $(7, 4)$  cyclic code generated by  $g(p) = p^3 + p^2 + 1$ .

**Solution** We observe that

$$p^6 \pmod{p^3 + p^2 + 1} = p^2 + p$$

$$p^5 \pmod{p^3 + p^2 + 1} = p + 1$$

$$p^4 \pmod{p^3 + p^2 + 1} = p^2 + p + 1$$

$$p^3 \pmod{p^3 + p^2 + 1} = p^2 + 1$$

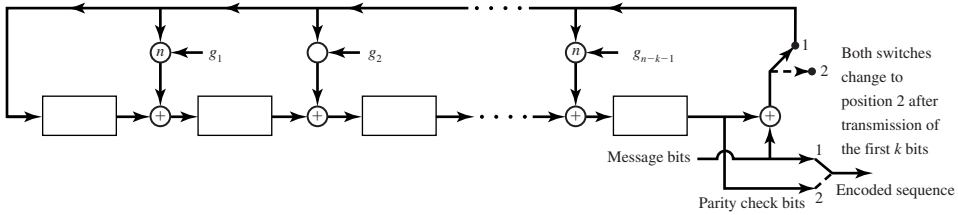


Figure 9.21 Implementation of a cyclic encoder.

Now having the  $p_{i,j}$ 's, we can find  $\mathbf{G}$  as follows

$$\mathbf{G} = \begin{bmatrix} 1 & 0 & 0 & 0 & 1 & 1 & 0 \\ 0 & 1 & 0 & 0 & 0 & 1 & 1 \\ 0 & 0 & 1 & 0 & 1 & 1 & 1 \\ 0 & 0 & 0 & 1 & 1 & 0 & 1 \end{bmatrix}$$

**Encoding of Cyclic Codes.** Compared to the general class of linear block codes, cyclic codes have more built in structure and this extra structure makes the implementation of their encoders easier. The cyclic encoders can be implemented by shift registers. In this section, we examine some basic structures for encoding of cyclic codes. An easily implementable cyclic encoder is based on the observation that any code word polynomial can be obtained by multiplying the generator polynomial  $g(p)$  by the input sequence polynomial  $X(p)$ , or equivalently by convolving sequences  $\mathbf{x}$  and  $\mathbf{p}$ . This can easily be done by a digital filter-like structure as shown in Figure 9.21. The main advantage of cyclic codes is the existence of an easily implementable decoder for them. The interested reader is referred to the book by Lin and Costello (1983) for details on decoding of cyclic codes.

**Example 9.6.4**

The encoder for the (7, 4) cyclic code this structure is shown in Figure 9.22.

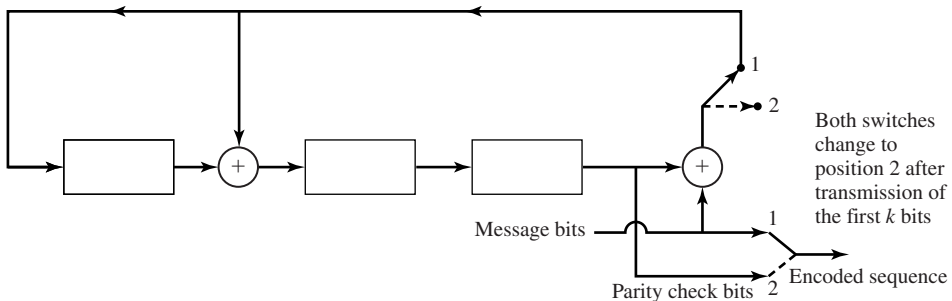


Figure 9.22 A cyclic (7, 4) encoder.

**BCH Codes.** *Bose, Chaudhuri, and Hocquenghem (BCH) codes* are a subclass of cyclic codes that, in general, can be designed for correction of  $t$  errors. This versatility in design and the existence of an efficient decoding algorithm for these codes (the Berlekamp-Massey algorithm) makes these codes particularly attractive.

To be more specific, for any  $m$  and  $t$ , there exists a BCH code with parameters

$$n = 2^m - 1 \quad (9.6.17)$$

$$n - k \leq mt \quad (9.6.18)$$

$$d_{\min} = 2t + 1 \quad (9.6.19)$$

Since  $m$  and  $t$  are arbitrary, the designer of the communication system has a large number of selections in this family of codes. BCH codes are well tabulated. Table 9.1 shows a table of the coefficients of the generator polynomials for BCH codes of length  $7 \leq n \leq 255$ . The coefficients of  $g(p)$  are given in octal form. Thus, the coefficients of the generator polynomial of the (15, 5) code are 2467, which in binary form is 10,100,110,111. Consequently, the generator polynomial for this code is  $g(p) = p^{10} + p^8 + p^5 + p^4 + p^2 + p + 1$ .

More information on the properties of BCH codes and their decoding algorithms can be found in Lin and Costello (1983) and Blahut (1983).

**Reed-Solomon Codes.** *Reed-Solomon codes* are a subset of BCH codes and, therefore, belong to the family of cyclic codes. Reed-Solomon codes are nonbinary codes; i.e., in a code word  $\mathbf{c} = (c_1, c_2, \dots, c_n)$ , the elements  $c_i$ ,  $1 \leq i \leq n$ , are members of a  $q$ -ary alphabet. In most practical cases  $q$  is chosen to be a power of 2, say  $q = 2^k$ . In such a case,  $k$ -information bits are mapped into a single element from the  $q$ -ary alphabet and, then, using an  $(N, K)$  Reed-Solomon code,  $K$ ,  $q$ -ary symbols are mapped into  $N$   $q$ -ary symbols and transmitted over the channel. Figure 9.23 shows this procedure.

A Reed-Solomon code is a BCH code defined by the following parameters.

$$N = q - 1 = 2^k - 1 \quad (9.6.20)$$

$$K = 1, 3, \dots, N - 2 \quad (9.6.21)$$

$$D_{\min} = N - K + 1 \quad (9.6.22)$$

$$R_c = \frac{K}{N} \quad (9.6.23)$$

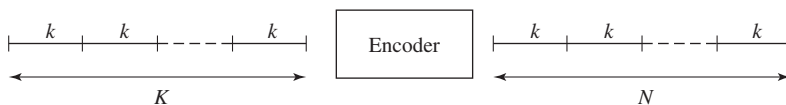


**Figure 9.23** A Reed-Solomon encoder.

**TABLE 9.1** COEFFICIENTS OF THE GENERATOR POLYNOMIALS OF BCH CODES

$n$	$k$	$t$	$g(p)$
7	4	1	13
15	11	1	23
	7	2	721
	5	3	2467
31	26	1	45
	21	2	3551
	16	3	107657
	11	5	5423325
	6	7	313365047
63	57	1	103
	51	2	12471
	45	3	1701317
	39	4	166623567
	36	5	1033500423
	30	6	157464165547
	24	7	17323260404441
	18	10	1363026512351725
	16	11	6331141367235453
	10	13	472622305527250155
	7	15	5231045543503271737
127	120	1	211
	113	2	41567
	106	3	11554743
	99	4	3447023271
	92	5	624730022327
	85	6	130704476322273
	78	7	26230002166130115
	71	9	6255010713253127753
	64	10	1206534025570773100045
	57	11	335265252505705053517721
	50	13	54446512523314012421501421
	43	14	17721772213651227521220574343
	36	15	3146074666522075044764575721735
	29	21	403114461367670603667530141176155
	22	23	123376070404722522435445626637647043
	15	27	22057042445604554770523013762217604353
	8	31	7047264052751030651476224271567733130217
255	247	1	435
	239	2	267543
	231	3	156720665
	223	4	75626641375
	215	5	23157564726421
	207	6	16176560567636227
	199	7	7633031270420722341
	191	8	2663470176115333714567
	187	9	52755313540001322236351

(continued)

**TABLE 9.1** COEFFICIENTS OF THE GENERATOR POLYNOMIALS OF BCH CODES (*continued*)

$n$	$k$	$t$	$g(p)$
179	10		22624710717340432416300455
171	11		15416214212342356077061630637
163	12		7500415510075602551574724514601
155	13		3757513005407665015722506464677633
147	14		1642130173537165525304165305441011711
139	15		461401732060175561570722730247453567445
131	18		215713331471510151261250277442142024165471
123	19		120614052242066003717210326516141226272506267
115	21		60526665572100247263636404600276352556313472737
107	22		22205772322066256312417300235347420176574750154441
99	23		10656667253473174222741416201574332252411076432303431
91	25		6750265030327444172723631724732511075550762720724344561
87	26		110136763414743236435231634307172046206722545273311721317
79	27		66700035637657500020270344207366174621015326711766541342355
71	29		24024710520644321515554172112331163205444250362557643221706035
63	30		10754475055163544325315217357707003666111726455267613656702543301
55	31		73154252035011001330152753060320543254143267550105570444260354 73617
47	42		25335420170626465630330413774062331751233341454460450050660245 52543173
45	43		152020560552341611311013463764237401563670024470762373033202157 025051541
37	45		51363302550670074141774472454375304207357061743234323476443547 37403044003
29	47		30257155366730714655270640123613771153422423242011741140602547 57410403565037
21	55		12562152570603326560017731536076121032273414056530745425211531 21614466513473725
13	59		46417320050525645444265737142500660043306774454765614031746772 1357026134460500547
9	63		15726025217472463201031043255355134614162367212044074545112766 115547705561677516057

†(From paper by Stenbit; © 1964 IEEE. Reprinted with permission.)

This code is capable of correcting up to

$$t = \frac{D_{\min} - 1}{2} \quad (9.6.24)$$

symbol errors.

Reed-Solomon codes have particularly good distance properties, are quite suitable for use in conjunction with  $q$ -ary modulation, and are useful in situations where errors tend to happen in “bursts” rather than randomly. This latter property is a consequence of the fact that bursts of errors cause only a few *symbol* errors in a Reed-Solomon code, which can easily be corrected. In binary codes, the same burst results in many bits in error which may not be easily corrected.

Reed-Solomon codes can also be concatenated with a binary code to provide higher levels of error protection. The binary code used in concatenation with the Reed-Solomon codes could be either a block code or a convolutional code. The binary encoder and decoder are located right before the modulator and after the demodulator, respectively, and are called the *inner* encoder-decoder pair. We will discuss these codes in Section 9.8.

## 9.7 CONVOLUTIONAL CODES

Convolutional codes are different from the block codes by the existence of memory in the encoding scheme. In block codes, each block of  $k$  input bits is mapped into a block of length  $n$  of output bits by a rule defined by the code (for example by  $\mathbf{G}$  or  $g(p)$ ) and regardless of the previous inputs to the encoder. The rate of such a code is given by

$$R_c = \frac{k}{n} \quad (9.7.1)$$

In convolutional codes, each block of  $k$  bits is again mapped into a block of  $n$  bits to be transmitted over the channel, but these  $n$  bits are not only determined by the present  $k$ -information bits but also by the previous information bits. This dependence on the previous information bits causes the encoder to be a finite state machine.

To be more specific, the block diagram of a convolutional encoder is given in Figure 9.24. The convolutional encoder consists of a shift register with  $kL$  stages where  $L$  is called the *constraint length* of the code. At each instant of time,  $k$ -information bits enter the shift register and the contents of the last  $k$  stages of the shift register are dropped. After the  $k$  bits have entered the shift register,  $n$ -linear combinations of the contents of the shift register, as shown in the figure, are computed and used to generate the encoded waveform. From the above coding procedure, it is obvious that the  $n$ -encoder outputs not only depend on the most recent  $k$  bits that have entered the

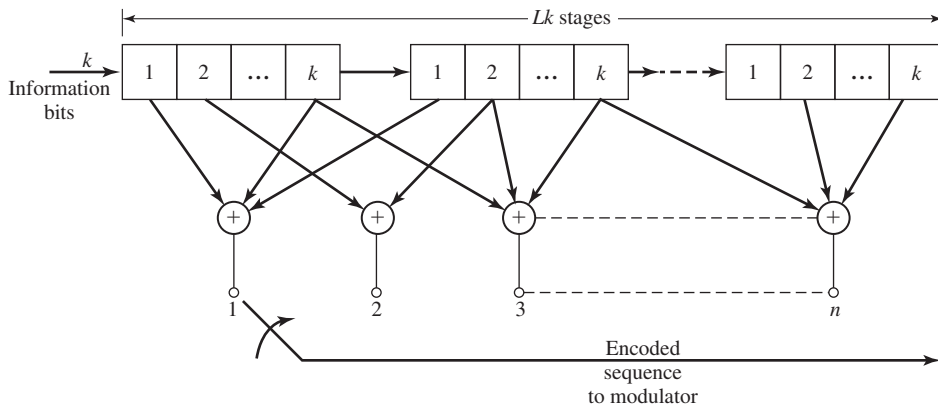


**Figure 9.24** The block diagram of a convolutional encoder.

encoder but also on the  $(L - 1)k$  contents of the first  $(L - 1)k$  stages of the shift register before the  $k$  bits arrived. Therefore, the shift register is a finite state machine with  $2^{(L-1)k}$  states. Because for each  $k$ -input bits, we have  $n$ -output bits, the rate of this code is simply

$$R_c = \frac{k}{n} \quad (9.7.2)$$

### Example 9.7.1

A convolutional encoder is shown in Figure 9.25. In this encoder  $k = 1$ ,  $n = 2$ , and  $L = 3$ . Therefore, the rate of the code is  $\frac{1}{2}$  and the number of states is  $2^{(L-1)k} = 4$ . One way to describe such a code (other than drawing the encoder) is to specify how the two output bits of the encoder depend on the contents of the shift register. This is usually done by specifying  $n$  vectors  $\mathbf{g}_1, \mathbf{g}_2, \dots, \mathbf{g}_n$ , known as *generator sequences* of the convolutional code. The  $i$ th  $1 \leq i \leq 2^{kL}$  component of  $\mathbf{g}_j$ ,  $1 \leq j \leq n$ , is 1 if the  $i$ th stage of the shift register is connected to the combiner corresponding to the  $j$ th bit in the output and 0 otherwise. In the above example, the generator sequences are given by

$$\mathbf{g}_1 = [1 \quad 0 \quad 1]$$

$$\mathbf{g}_2 = [1 \quad 1 \quad 1]$$

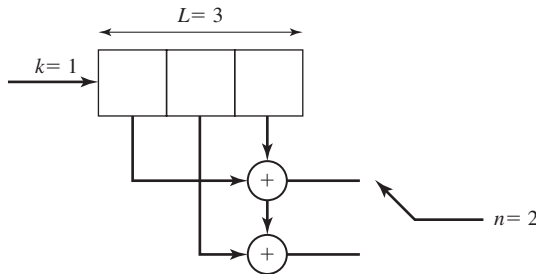


**Figure 9.25** A rate  $\frac{1}{2}$  convolutional encoder.

### 9.7.1 Basic Properties of Convolutional Codes

Because a convolutional encoder has finite memory, it can easily be represented by a *state-transition diagram*. In the state-transition diagram, each state of the convolutional encoder is represented by a box and transitions between states are denoted by lines connecting these boxes. On each line both the input(s) causing that transition and the corresponding output are specified. The number of lines emerging from each state is, therefore, equal to the number of possible inputs to the encoder at that state, which is equal to  $2^k$ . The number of lines merging at each state is equal to the number of states from which a transition is possible to this state. This is equal to the number of possible combinations of bits that leave the encoder as the  $k$  bits enter the encoder. This, again, is equal to  $2^k$ . Figure 9.26 shows the state transition matrix for the convolutional code of Figure 9.25.

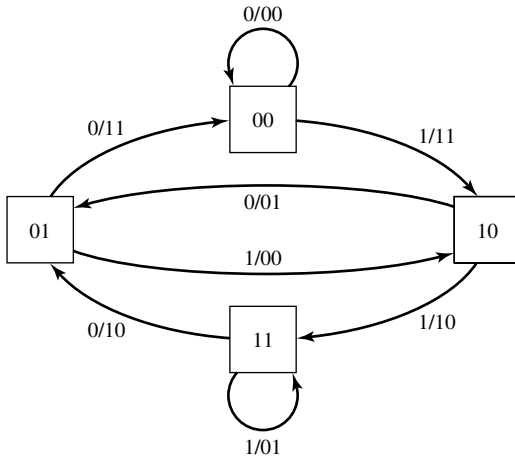


**Figure 9.26** State transition diagram for the encoder of Figure 9.25.

A second, and more popular method, to describe convolutional codes is to specify their *trellis diagram*. The trellis diagram is a way to show the transition between various states as the time evolves. The trellis diagram is obtained by specifying all states on a vertical axis and repeating this vertical axis along the time axis. Then, each transition from a state to another state is denoted by a line connecting the two states on two adjacent vertical axes. In a sense, the trellis diagram is nothing but a repetition of the state-transition diagram along the time axes. As was the case with the state transition diagram, here again we have  $2^k$  branches of the trellis leaving each state and  $2^k$  branches merging at each. In the case where  $k = 1$ , it is common to denote the branch corresponding to a 0 input by a bold line and the branch corresponding to a 1 input to the encoder by a dashed line. Figure 9.27 shows the trellis diagram for the code described by the encoder of Figure 9.25.

**Encoding.** The encoding procedure in a convolutional code is very simple. We assume that the encoder, before the first information bit enters it, is loaded with zeros (the all-zero state). The information bits enter the encoder  $k$  bits at a time and

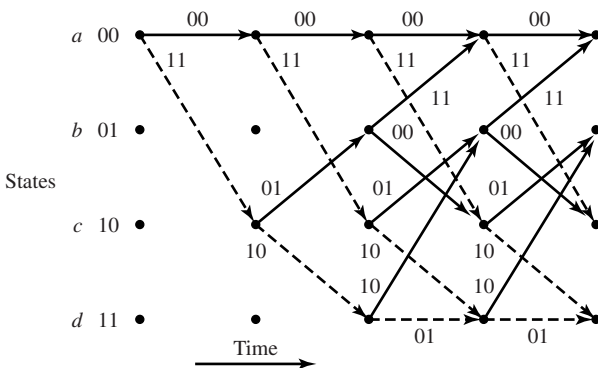


**Figure 9.27** Trellis diagram for the encoder of Figure 9.25.



the corresponding  $n$ -output bits are transmitted over the channel. This procedure is continued until the last group of  $k$  bits are loaded into the encoder and the corresponding  $n$ -output bits are sent over the channel. We will assume, for simplicity, that after the last set of  $k$  bits, another set of  $k(L - 1)$  zeros enter the encoder and the corresponding  $n$  outputs are transmitted over the channel. This returns the encoder to the all-zero state and makes it ready for next transmission.

### Example 9.7.2

In the convolutional code shown in Figure 9.25, what is the encoded sequence corresponding to the information sequence  $\mathbf{x} = (1101011)$ ?

**Solution** It is enough to note that the encoder is in state 0 before transmission, and after transmission of the last information bit two 0 bits are transmitted. This means that the transmitted sequence is  $\mathbf{x}_1 = (110101100)$ . Using this transmission sequence we have the following code word  $\mathbf{c} = (111010000100101011)$ .

**The Transfer Function.** For every convolutional code, the transfer function gives information about the various paths through the trellis that start from the all-zero state and return to this state for the first time. According to the coding convention described before, any code word of a convolutional encoder corresponds to a path through the trellis that starts from the all-zero state and returns to the all-zero state. As we will see in Section 9.7.4, the transfer function of a convolutional code plays a major role in bounding the error probability of the code. To obtain the transfer function of a convolutional code, we split the all-zero state into two states, one denoting the starting state and one denoting the first return to the all-zero state. All the other states are denoted as in-between states. Corresponding to each branch connecting two states, a function of the form  $D^\alpha N^\beta J$  is defined where  $\alpha$  denotes the number of ones in the output bit sequence for that branch and  $\beta$  is the number of ones in the corresponding input sequence for that branch. The *transfer function* of the convolutional code is, then, the transfer function of the flow graph between the starting all-zero state and the final all-zero state, and will be a function of the tree parameters  $D, N, J$  and denoted by  $T(D, N, J)$ . Each element of  $T(D, N, J)$  corresponds to a path through the trellis starting from the all-zero state and ending at the all-zero state. The exponent of  $J$  indicates the number of branches spanned by that path, the exponent of  $D$  shows the number of ones in the code word corresponding to that path (or equivalently the Hamming weight of the code word), and finally, the exponent of  $N$  indicates the number of ones in the input information sequence. Since  $T(D, N, J)$  indicates the properties of all paths through the trellis starting from the all-zero path and returning to it *for the first time*, then, in deriving it, any self loop at the all-zero state is ignored. To obtain the transfer function of the convolutional code, one can use all rules that can be used to obtain the transfer function of a flow graph.

### Example 9.7.3

Find the transfer function of the convolutional code of Figure 9.25.

**Solution** Figure 9.28 shows the diagram used to find the transfer function of this code. The code has a total of four states denoted by the contents of the first two stages of the

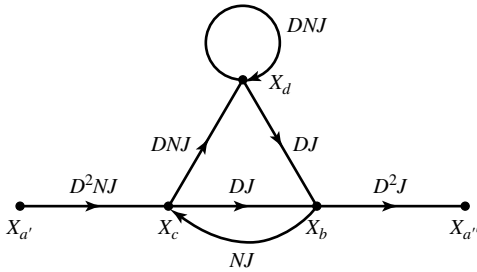


**Figure 9.28** Flow graph for finding the transfer function.

shift register. We denote these states by the following letters

$$00 \rightarrow a$$

$$01 \rightarrow b$$

$$10 \rightarrow c$$

$$11 \rightarrow d$$

As seen in the figure, state  $a$  is split into states  $a'$  and  $a''$  denoting the starting and returning state. Using the flow graph relations, we can write

$$X_c = X_{a'} D^2 N J + N J X_b$$

$$X_b = D J X_d + D J X_c$$

$$X_d = D N J X_c + D N J X_d$$

$$X_{a''} = D^2 J X_b$$

Eliminating  $X_b$ ,  $X_c$ , and  $X_d$  results in

$$T(D, N, J) = \frac{X_{a''}}{X_{a'}} = \frac{D^5 N J^3}{1 - D N J - D N J^2} \quad (9.7.3)$$

Now, expanding  $T(D, N, J)$  in a polynomial form, we obtain

$$T(D, N, J) = D^5 N J^3 + D^6 N^2 J^4 + D^6 N^2 J^5 + D^7 N^3 J^5 + \dots \quad (9.7.4)$$

The term  $D^5 N J^3$  indicates that there exists a path through the trellis starting from the all-zero state and returning to the all-zero state for the first time, which spans three branches, corresponding to an input-information sequence containing one 1 (and, therefore, two 0's), and the code word for this path has Hamming weight equal to 5. This path is indicated with bold lines in the Figure 9.29. This path is somewhat similar to the minimum-weight code word in block codes. In fact, this path corresponds to the code word that is at "minimum distance" from the all zero code word. This minimum distance which is equal to the minimum power of  $D$  in the expansion of  $T(D, N, J)$  is called the *free distance of the code* and denoted by  $d_{\text{free}}$ . The free distance of the above code is equal to 5. The general form of the transfer function is, therefore,

$$T(D, N, J) = \sum_{d=d_{\text{free}}}^{\infty} a_d D^d N^{f(d)} J^{g(d)} \quad (9.7.5)$$

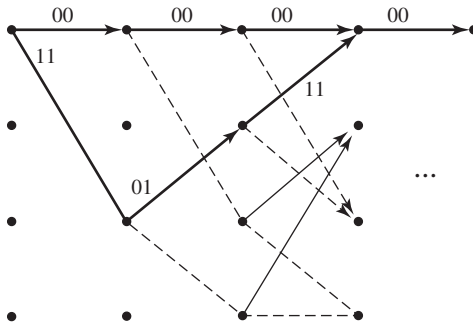


**Figure 9.29** The path corresponding to  $D^5NJ^3$  in code represented in Figure 9.25.

A shorter form of transfer function, which only provides information about the weight of the code words, can be obtained from  $T(D, N, J)$  by setting  $N = J = 1$ . This shorter form will be denoted by

$$T_1(D) = \sum_{d=d_{\text{free}}}^{\infty} a_d D^d \quad (9.7.6)$$

and will later be used in deriving bounds on the error probabilities of the convolutional codes.

#### Example 9.7.4

For the code of Figure 9.25 we have

$$\begin{aligned} T_1(D) &= \frac{D^5 NJ^3}{1 - DNJ - DNJ^2} \Big|_{N=J=1} \\ &= \frac{D^5}{1 - 2D} \\ &= D^5 + 2D^6 + 4D^7 + \dots \\ &= \sum_{i=0}^{\infty} 2^i D^{5+i} \end{aligned}$$

**Catastrophic Codes.** A convolutional code maps a (usually long) sequence of input-information bits into a code word to be transmitted over the channel. The purpose of coding is to provide higher levels of protection against channel noise. Obviously, a code that maps information sequences that are far apart into code words that are not far apart is not a good code since these two code words can be mistaken rather easily and the result would be a large number of bit errors in the information stream. A limiting case of this undesirable property happens when two information sequences that are different in infinitely many positions are mapped into code words that differ only in a finite number of positions. In such a case, since the code words differ in a finite number of bits, there always exists the probability that they will be erroneously decoded and this, in turn, results in an infinite number of errors in detecting the input information sequence. Codes that exhibit this property are called *catastrophic codes* and should be avoided in practice.

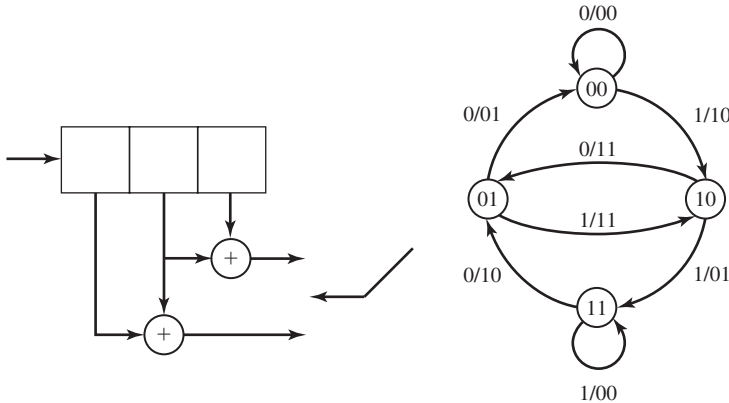


**Figure 9.30** Encoder and the state-transition diagram for a catastrophic code.

As an example of a catastrophic code, let us consider the  $(2, 1)$  code described by

$$\mathbf{g}_1 = [1 \quad 1 \quad 0]$$

$$\mathbf{g}_2 = [0 \quad 1 \quad 1]$$

The encoder and the state-transition diagram for this code are given in Figure 9.30. As seen in this diagram, there exists a self loop in state “11” that corresponds to a “1” input to the encoder and the corresponding output consists of all zeros. Therefore, if an input-information stream consists of all ones, the corresponding output will be

$$\mathbf{c} = (10010000 \dots 0001001)$$

If we compare this code word to the code word corresponding to the all-zero information sequence

$$\mathbf{c}_0 = (0000 \dots 000)$$

we observe that, although the information sequences are different in a large number of positions, the corresponding output sequences are quite close (the Hamming distance being only 4) and therefore they can be mistaken very easily. The existence of such a self loop corresponding to  $k$  inputs which are not all zeros and for which the  $n$  output bits are all zeros, shows that a code is catastrophic and should, therefore, be avoided.

### 9.7.2 Optimum Decoding of Convolutional Codes—The Viterbi Algorithm

In our discussion of various decoding schemes for block codes, we saw that there exists the possibility of soft- and hard-decision decoding. In soft-decision decoding,  $\mathbf{r}$ , the vector denoting the outputs of the matched filters is compared to the various signal points in the constellation of the coded-modulation system, and the one closest to it in Euclidean distance is chosen. In hard-decision decoding,  $\mathbf{r}$ , is first turned into a

binary sequence  $\mathbf{y}$  by making decisions on individual components of  $\mathbf{r}$ , and then the code word, which is closest to  $\mathbf{y}$  in the Hamming distance, is chosen. It is seen that in both approaches, a fundamental task is *to find a path through the trellis that is at minimum distance from a given sequence*. This fundamental problem arises in many areas of communications, and other disciplines of electrical engineering. Particularly, the same problem is encountered in ML sequence estimation when transmitting over bandlimited channels with intersymbol interference (see Chapter 8), demodulation of CPM schemes (see Chapter 10), speech recognition, some pattern-classification schemes, etc. All these problems are essentially the same and can be titled as *optimal trellis searching algorithms*. The well known Viterbi algorithm, described previously in Sections 8.5 and 8.6, provides a satisfactory solution to all these problems.

In hard-decision decoding of convolutional codes, we want to choose a path through the trellis whose code word, denoted by  $\mathbf{c}$ , is at minimum Hamming distance from the quantized received sequence  $\mathbf{y}$ . In hard-decision decoding, the channel is binary memoryless (the fact that the channel is memoryless follows from the fact that the channel noise is assumed to be white). Because the desired path starts from the all-zero state and returns back to the all-zero state, we assume that this path spans a total of  $m$  branches, and since each branch corresponds to  $n$  bits of the encoder output, the total number of bits in  $\mathbf{c}$ , and also in  $\mathbf{y}$ , is  $mn$ . We denote the sequence of bits corresponding to the  $i$ th branch by  $\mathbf{c}_i$  and  $\mathbf{y}_i$ , respectively, where  $1 \leq i \leq m$ , and each  $\mathbf{c}_i$  and  $\mathbf{y}_i$  is of length  $n$ . The Hamming distance between  $\mathbf{c}$  and  $\mathbf{y}$  is, therefore,

$$d(\mathbf{c}, \mathbf{y}) = \sum_{i=1}^m d(\mathbf{c}_i, \mathbf{y}_i) \quad (9.7.7)$$

In soft-decision decoding, we have a similar situation with three differences.

1. Instead of  $\mathbf{y}$ , we are dealing directly with the vector  $\mathbf{r}$ , the vector output of the optimal (matched-filter type or correlators-type) digital demodulator.
2. Instead of the binary 0, 1 sequence  $\mathbf{c}$ , we are dealing with the corresponding sequence  $\mathbf{c}'$  with

$$c'_{ij} = \begin{cases} \sqrt{\mathcal{E}}, & c_{ij} = 1 \\ -\sqrt{\mathcal{E}}, & c_{ij} = 0 \end{cases} \quad \text{for } 1 \leq i \leq m \quad \text{and} \quad 1 \leq j \leq n$$

3. Instead of Hamming distance, we are using Euclidean distance. This is a consequence of the fact that the channel under study is an additive white Gaussian noise channel.

From the above, we have

$$d_E^2(\mathbf{c}', \mathbf{r}) = \sum_{i=1}^m d_E^2(\mathbf{c}'_i, \mathbf{r}_i) \quad (9.7.8)$$

From Equations (9.7.7) and (9.7.8), it is seen that the generic form of the problem we have to solve is: given a vector  $\mathbf{a}$  to find a path through the trellis, starting at the all-zero state  $S_1 = 0$  and ending at the all-zero state  $S_m = 0$ , such that some distance

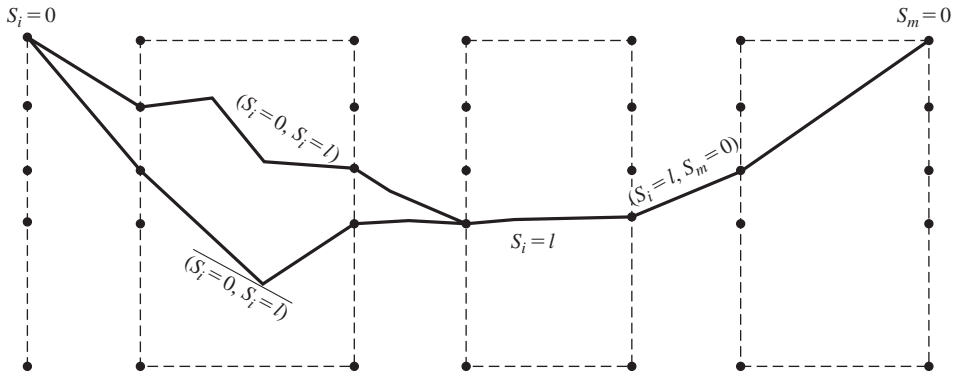


**Figure 9.31** Comparison of the optimal path,  $(S_1 = 0, S_i = l, S_m = 0)$ , with a suboptimal path consisting of the concatenation of  $(S_1 = 0, S_i = l)$  and  $(S_i = l, S_m = 0)$ .

measure between  $\mathbf{a}$  and a sequence  $\mathbf{b}$  corresponding to that path is minimized.<sup>†</sup> The important fact that makes this problem easy to solve is that the distance between  $\mathbf{a}$  and  $\mathbf{b}$  in both cases of interest can be written as the sum of distances corresponding to individual branches of the path. This is easily observed from Equations (9.7.7) and (9.7.8).

Let us assume that the general problem is formulated as minimizing a metric  $\mu$  in the form

$$\mu(\mathbf{a}, \mathbf{b}) = \sum_{i=1}^m \mu(\mathbf{a}_i, \mathbf{b}_i)$$

First, observe that if the path  $(S_1 = 0, S_i = l, S_m = 0)$ ,  $1 \leq i \leq m$ , is the optimal path, where  $0 \leq l \leq M - 1$  ( $M = 2^{(L-1)k}$  is the number of states), then the metric contribution of the path  $(S_1 = 0, S_i = l)$  is lower than the metric contribution of any other path  $(S_1 = 0, S_i = l')$  connecting  $S_1 = 0$  to  $S_i = l$ . Otherwise, the path consisting of  $(S_1 = 0, S_i = l')$  and  $(S_i = l, S_m = 0)$  would be the optimal path. This is shown in Figure 9.31.

In Problem 9.42, it is shown that the number of branches entering each state in the trellis is  $2^k$ . Let  $\Lambda_{i-1}$  denote the set of  $2^k$  states that are connected with a branch to  $S_i = l$ . If the path from  $S_1 = 0$  to  $S_i = l$  is the optimal path between these two states, then this path must be the concatenation of an optimal path connecting  $S_1 = 0$  to a state  $S_{i-1} = \lambda$  for some  $\lambda \in \Lambda_{i-1}$ , and the branch connecting  $S_{i-1} = \lambda$  to  $S_i = l$ . The optimal path connecting  $S_1 = 0$  to  $S_{i-1} = \lambda$  is called a *survivor path* at state  $S_{i-1} = \lambda$ , or simply a survivor. Therefore, in order to find the survivor path at state  $S_i = l$ , it is sufficient to have the survivors (and their metrics) for all  $S_{i-1} = \lambda$ ,  $\lambda \in \Lambda_{i-1}$ , append them with the

<sup>†</sup>The problem can also be formulated as a maximization problem. For example, instead of minimizing the Euclidean distance, one could maximize the correlation.

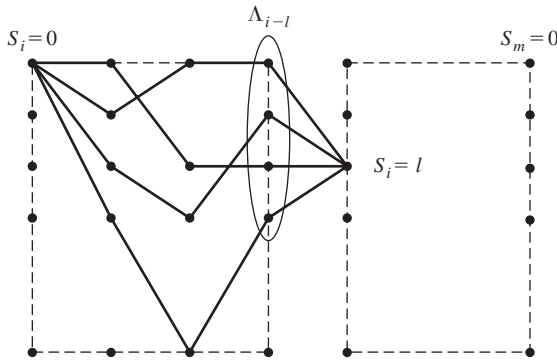


**Figure 9.32** Finding a new survivor from old survivors.

branches connecting elements of  $\Lambda_{i-1}$  to  $S_i = l$ , find the metric of the resulting paths from  $S_1 = 0$  to  $S_i = l$ , and pick the one with minimum metric; this will be the new survivor path at  $S_i = l$ . This process is started at  $S_1 = 0$  and is finished at  $S_m = 0$ ; the final survivor at  $S_m = 0$  is the optimal path and the best (maximum-likelihood) match to the received sequence. This process is shown in Figure 9.32.

At each step, the new survivor metric is

$$\mu(S_1 = 0, S_i = l) = \min_{\lambda \in \Lambda_{i-1}} \{ \mu(S_1 = 0, S_{i-1} = \lambda) + \mu(S_{i-1} = \lambda, S_i = l) \} \quad (9.7.9)$$

Having found the survivor metric, the new survivor at  $S_i = l$  is the path  $(S_1 = 0, S_{i-1} = \lambda, S_i = l)$  for the  $\lambda$  that minimizes the survivor metric in Equation 9.7.9.

The above procedure can be summarized with the Viterbi algorithm.

1. Parse the received sequence into  $m$  subsequences each of length  $n$ .
2. Draw a trellis of depth  $m$  for the code under study. For the last  $L - 1$  stages of the trellis, draw only paths corresponding to the all-zero input sequences (this is done because we know that the input sequence has been padded with  $k(L - 1)$  zeros).
3. Set  $i = 1$ , and set the metric of the initial all-zero state equal to zero.
4. Find the distance of the  $i$ th subsequence of the received sequence to all branches connecting  $i$ th stage states to the  $(i + 1)$ st-stage states of the trellis.
5. Add these distances to the metrics of the  $i$ th stage states to obtain the metric candidates for the  $(i + 1)$ st-stage states. For each state of the  $(i + 1)$ st stage, there are  $2^k$  metrics candidate, each corresponding to one branch ending at that state.
6. For each state at the  $(i + 1)$ st stage, choose the minimum of the metric candidates, label the branch corresponding to this minimum value as the *survivor*, and assign the minimum of the metric candidates as the metrics of the  $(i + 1)$ st-stage states.
7. If  $i = m$ , go to step 8, otherwise increase  $i$  by 1 and go to step 4.
8. Starting with the all-zero state at the final stage, go back through the trellis along the survivors to reach the initial all-zero state. This path is the optimal path and the input-bit sequence corresponding to it is the ML decoded information sequence.

To obtain the best guess about the input bit sequence, remove the last  $k(L - 1)$  zeros from this sequence.

As seen from the above algorithm, the decoding delay and the amount of memory required for decoding a long information sequence is unacceptable. The decoding cannot be started until the whole sequence (which, in the case of convolutional codes, can be very long) is received, and all surviving paths have to be stored. In practice, a suboptimal solution that does not cause these problems is desirable. One such approach, referred to as *path-memory truncation*, is that the decoder at each stage only searches  $\delta$  stages back in the trellis instead of searching back to the start of the trellis. With this approach at the  $(\delta + 1)$ th stage, the decoder makes a decision on the input bits corresponding to the first stage of the trellis (the first  $k$  bits) and future received bits do not change this decision. This means that the decoding delay will be  $k\delta$  bits and it is only required to keep the surviving paths corresponding to the last  $\delta$  stages. Computer simulations have shown that if  $\delta \approx 5L$ , the degradation in performance due to path-memory truncation is negligible.

**Example 9.7.5**

Let us assume that in hard-decision decoding, the quantized received sequence is

$$\mathbf{y} = (01101111010001)$$

The convolutional code is the one given in Figure 9.25. Find the ML information sequence and the number of errors.

**Solution** The code is a  $(2, 1)$  code with  $L = 3$ . The length of the received sequence  $\mathbf{y}$  is 14. This means that  $m = 7$  and we have to draw a trellis of depth 7. Also note that, because the input-information sequence is padded with  $k(L - 1) = 2$  zeros, for the final two stages of the trellis we will only draw the branches corresponding to all zero inputs. This also means that the actual length of the input sequence is 5, which, after padding with 2 zeros, has increased to 7. The trellis diagram for this case is shown in

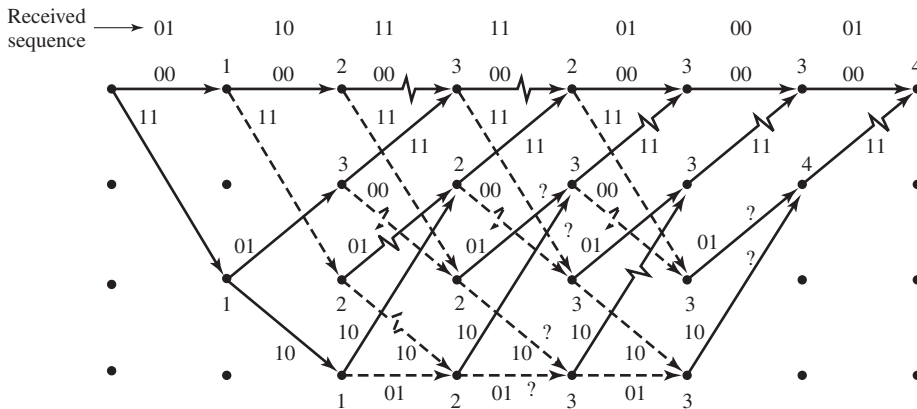


**Figure 9.33** The trellis diagram for Viterbi decoding of the sequence (01101111010001).



Figure 9.33. The parsed received sequence  $\mathbf{y}$  is also shown in this figure. Note that, in drawing the trellis in the last two stages, we have only considered the zero inputs to the encoder (notice that, in the final two stages, there exist no dashed lines corresponding to 1 inputs). Now, the metric of the initial all-zero state is set to zero and the metrics of the next stage are computed. In this step, there is only one branch entering each state, therefore there is no comparison, and the metrics (which are the Hamming distances between that part of the received sequence and the branches of the trellis) are added to the metric of the previous state. In the next stage, there exists no comparison either. In the third stage, for the first time we have two branches entering each state. This means that a comparison has to be made here and survivors are to be chosen. From the two branches that enter each state, one which corresponds to the least total accumulated metric remains as a survivor and the other branches are deleted. If at any stage, two paths result in the same metric, each one of them can be a survivor. Such cases have been marked by a “?” in the trellis diagram. The procedure is continued to the final all-zero state of the trellis and then starting from that state, we move along the surviving paths to the initial all-zero state. This path, which is denoted by a heavy path through the trellis is the optimal path. The input bit sequence corresponding to this path is 1100000 where the last two zeros are not information bits but were added to return the encoder to the all-zero state. Therefore, the information sequence is 11000. The corresponding code word for the selected path is 11101011000000, which is at Hamming distance 4 from the received sequence. No other path through the trellis is at a Hamming distance less than 4 from the received  $\mathbf{y}$ .

For soft-decision decoding a similar procedure is followed with squared Euclidean distance substituted for Hamming distance.

### 9.7.3 Other Decoding Algorithms for Convolutional Codes

The Viterbi algorithm provides maximum-likelihood decoding for convolutional codes. However, as we have already seen, the complexity of the algorithm is proportional to the number of states in the trellis diagram. This means that the complexity of the algorithm increases exponentially with the constraint length of the convolutional codes. Therefore, the Viterbi algorithm can be applied only to codes with low-constraint lengths. For higher constraint-length codes other suboptimal decoding schemes have been proposed. These include the sequential decoding of Wozencraft (1957); the Fano algorithm (1963), the stack algorithm (Zigangirov (1966) and Jelinek (1969)); the feedback-decoding algorithm (Heller (1975)); and majority logic decoding (Massey (1963)).

### 9.7.4 Bounds on Error Probability of Convolutional Codes

Finding bounds on the error performance of convolutional codes is different from the method used to find error bounds for block codes, because, here we are dealing with sequences of very large length and, since the free distance of these codes is usually small, some errors will eventually occur. The number of errors is a random variable that depends both on the channel characteristics (SNR in soft-decision decoding and crossover probability in hard-decision decoding) and the length of the input sequence.

The longer the input sequence, the higher the probability of making errors. Therefore, it makes sense to normalize the number of bit errors to the length of the input sequence. A measure that is usually adopted for comparing the performance of convolutional codes, is the expected number of bits received in error/input bit.

To find a bound on the average number of bits in error for each input bit, we first derive a bound on the average number of bits in error for each input sequence of length  $k$ . To determine this, let us assume that the all-zeros sequence is transmitted<sup>†</sup> and, up to stage  $l$  in the decoding, there has been no error. Now  $k$ -information bits enter the encoder and result in moving to the next stage in the trellis. We are interested in finding a bound on the expected number of errors that can occur due to this input block of length  $k$ . Because we are assuming that up to stage  $l$  there has been no error, then up to this stage the all-zero path through the trellis has the minimum metric. Now, moving to the next stage (stage  $(l + 1)$ th), it is possible that another path through the trellis will have a metric less than the all-zero path and, therefore, cause errors. If this happens, we must have a path through the trellis that merges with the all-zero path, for the first time, at the  $(l + 1)$ st stage and has a metric less than the all-zero path. Such an event is called the *first-error-event* and the corresponding probability is called the *first-error-event probability*. This situation is depicted in Figure 9.34.

Our first step would be bounding the first-error-event probability. Let  $P_2(d)$  denote the probability that a path through the trellis which is at Hamming distance  $d$  from the all-zero path, is the survivor at the  $(l + 1)$ st stage. Denoting the number of paths of weight  $d$  by  $a_d$ , we can bound the first-error-event probability by

$$P_e \leq \sum_{d=d_{\text{free}}}^{\infty} a_d P_2(d) \quad (9.7.10)$$

where on the right-hand side, we have included all paths through the trellis that merge with the all-zero path at the  $(l + 1)$ st stage. The value of  $P_2(d)$  depends on whether soft- or hard-decision decoding is employed.

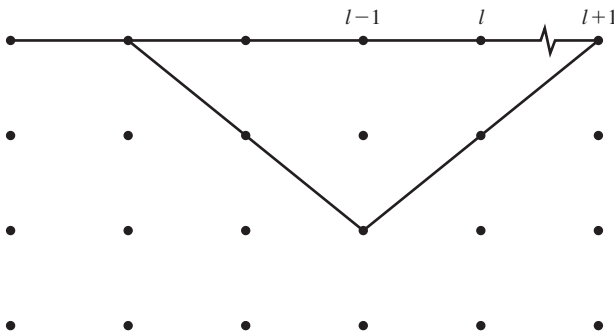


**Figure 9.34** The path corresponding to the first-error-event.

<sup>†</sup>Because of the linearity of convolutional codes we can, without loss of generality, make this assumption.

For soft-decision decoding, if antipodal signaling (binary PSK) is used, we have

$$\begin{aligned}
 P_2(d) &= Q\left(\frac{d^E}{\sqrt{2N_0}}\right) \\
 &= Q\left(\sqrt{\frac{2\mathcal{E}d}{N_0}}\right) \\
 &= Q\left(\sqrt{2R_c d \frac{\mathcal{E}_b}{N_0}}\right)
 \end{aligned} \tag{9.7.11}$$

and, therefore,

$$P_e \leq \sum_{d=d_{\text{free}}}^{\infty} a_d Q\left(\sqrt{2R_c d \frac{\mathcal{E}_b}{N_0}}\right) \tag{9.7.12}$$

Using the upper bound on the  $Q$  function, we have

$$Q\left(\sqrt{2R_c d \frac{\mathcal{E}_b}{N_0}}\right) \leq \frac{1}{2} e^{-R_c d \mathcal{E}_b / N_0}. \tag{9.7.13}$$

Now, noting that

$$e^{-R_c d \mathcal{E}_b / N_0} = D^d \Big|_{D=e^{-R_c \mathcal{E}_b / N_0}} \tag{9.7.14}$$

we finally obtain

$$P_e \leq \frac{1}{2} \sum_{d=d_{\text{free}}}^{\infty} a_d D^d \Big|_{D=e^{-R_c \mathcal{E}_b / N_0}} = \frac{1}{2} T_1(D) \Big|_{D=e^{-R_c \mathcal{E}_b / N_0}} \tag{9.7.15}$$

This is a bound on the first-error-event probability. To find a bound on the average number of bits in error for  $k$ -input bits,  $\bar{P}_b(k)$ , we note that each path through the trellis causes a certain number of input bits to be decoded erroneously. For a general  $D^d N^{f(d)} J^{g(d)}$  in the expansion of  $T(D, N, J)$ , there are a total of  $f(d)$  nonzero-input bits. This means that the average number of input bits in error can be obtained by multiplying the probability of choosing each path by the total number of input errors that would result if that path were chosen. Hence, the average number of bits in error, in the soft-decision case, can be bounded by

$$\begin{aligned}
 \bar{P}_b(k) &\leq \sum_{d=d_{\text{free}}}^{\infty} a_d f(d) Q\left(\sqrt{2R_c d \frac{\mathcal{E}_b}{N_0}}\right) \\
 &\leq \frac{1}{2} \sum_{d=d_{\text{free}}}^{\infty} a_d f(d) e^{-R_c d \mathcal{E}_b / N_0}
 \end{aligned} \tag{9.7.16}$$

If we define

$$\begin{aligned} T_2(D, N) &= T(D, N, J)|_{J=1} \\ &= \sum_{d=d_{\text{free}}}^{\infty} a_d D^d N^{f(d)} \end{aligned} \quad (9.7.17)$$

we have

$$\frac{\partial T_2(D, N)}{\partial N} = \sum_{d=d_{\text{free}}}^{\infty} a_d f(d) D^d N^{f(d)-1} \quad (9.7.18)$$

Therefore, using Equations (9.7.16) and (9.7.18), one obtains

$$\bar{P}_b(k) \leq \frac{1}{2} \left. \frac{\partial T_2(D, N)}{\partial N} \right|_{N=1, D=e^{-R_c \frac{\mathcal{E}_b}{N_0}}} \quad (9.7.19)$$

To obtain the average number of bits in error for each input bit, we have to divide this bound by  $k$ . Thus, the final result is

$$\bar{P}_b = \frac{1}{2k} \left. \frac{\partial T_2(D, N)}{\partial N} \right|_{N=1, D=e^{-R_c \frac{\mathcal{E}_b}{N_0}}} \quad (9.7.20)$$

For high SNRs, the first term corresponding to the minimum distance, is the dominant term, and we have the approximation

$$\bar{P}_b \approx \frac{1}{2k} a_{d_{\text{min}}} f(d_{\text{min}}) e^{-R_c d_{\text{min}} \mathcal{E}_b / N_0} \quad (9.7.21)$$

For hard-decision decoding, the basic procedure follows the above derivation. The only difference is the bound on  $P_2(d)$ . It can be shown that (see Problem 9.49)  $P_2(d)$  can be bounded by

$$P_2(d) \leq [4p(1-p)]^{d/2} \quad (9.7.22)$$

where  $p$  is the crossover probability of the binary symmetric channel. Using this result, it is straightforward to show that in hard-decision decoding, the probability of error is upperbounded as

$$\bar{P}_b \leq \frac{1}{k} \left. \frac{\partial T_2(D, N)}{\partial N} \right|_{N=1, D=\sqrt{4p(1-p)}} \quad (9.7.23)$$

A comparison of hard-decision decoding and soft-decision decoding for convolutional codes shows that here, as in the case for linear block codes, soft-decision decoding outperforms hard-decision decoding by a margin of roughly 2 dB in additive white Gaussian noise channels.

**Convolutional Codes with Good Distance Properties.** From the analysis carried out above it is obvious that  $d_{\text{free}}$  plays a major role in the performance of convolutional codes. For a given  $n$  and  $k$ , the free distance of a convolutional code depends on the constraint length of the code. Searching for convolutional codes with

**TABLE 9.2** RATE  $\frac{1}{2}$  MAXIMUM FREE DISTANCE CODES

Constraint length $L$	Generators in octal		$d_{\text{free}}$
3	5	7	5
4	15	17	6
5	23	35	7
6	53	75	8
7	133	171	10
8	247	371	10
9	561	753	12
10	1167	1545	12
11	2335	3661	14
12	4335	5723	15
13	10533	17661	16
14	21675	27123	16

Odenwalder (1970) and Larsen (1973).

**TABLE 9.3** RATE  $\frac{1}{3}$  MAXIMUM FREE DISTANCE CODES

Constraint length $L$	Generators in octal			$d_{\text{free}}$
3	5	7	7	8
4	13	15	17	10
5	25	33	37	12
6	47	53	75	13
7	133	145	175	15
8	225	331	367	16
9	557	663	711	18
10	1117	1365	1633	20
11	2353	2671	3175	22
12	4767	5723	6265	24
13	10533	10675	17661	24
14	21645	35661	37133	26

Odenwalder (1970) and Larsen (1973).

good distance properties has been extensively carried out in the literature. Tables 9.2 and 9.3 summarize the result of computer simulations carried out for rate  $\frac{1}{2}$  and rate  $\frac{1}{3}$  convolutional codes. In these tables, for each constraint length, the convolutional code that achieves the highest free distance is tabulated. For this code, the generators  $\mathbf{g}_i$  are given in octal form. The resulting free distance of the code is also given in these tables.

## 9.8 COMPLEX CODES BASED ON COMBINATION OF SIMPLE CODES

As we have seen in the preceding sections, the performance of block and convolutional codes depends on the distance properties of the code and, in particular, the minimum distance in block codes and the free distance in convolutional codes. In order to design

block codes with a given rate and with high minimum distance, we have to increase  $n$ , the block length of the code. Increasing  $n$  increases the complexity of the decoding. In most decoding algorithms the complexity of the decoding increases exponentially with increasing the block length of the code.

For convolutional codes, increasing the free distance at a given rate requires increasing the constraint length of the code. But increasing the constraint length of the code increases the number of states in the code trellis, which in turn, increases the decoding complexity. Again, here the decoding complexity increases exponentially with the constraint length of the convolutional code.

Various methods have been proposed to increase the effective block length of the code but at the same time keeping the complexity tractable. Most of these methods are based on combining simple codes to generate more complex codes. The decoding of the resulting code is performed by using methods for decoding the simple component codes. The resulting decoding is a suboptimal decoding scheme, which in most cases performs satisfactorily. Here, we discuss three widely used methods for combining simple codes to generate more complex codes. These techniques generate *product codes*, *concatenated codes*, and *turbo codes*.

### 9.8.1 Product Codes

The structure of product codes (or array codes) is very similar to a crossword puzzle. Product codes are generated by using two linear block codes arranged in a matrix form. Two linear block codes, one with parameters  $n_1, k_1, d_{\min 1}$  and another with parameters  $n_2, k_2, d_{\min 2}$ , are used in a matrix of the form shown in Figure 9.35. The resulting code is an  $(n_1 n_2, k_1 k_2)$  linear block code. It can be shown that the minimum distance of the resulting code is the product of the minimum distances of the component codes; i.e.,  $d_{\min} = d_{\min 1} d_{\min 2}$ , and is capable of correcting  $\lfloor \frac{d_{\min 1} d_{\min 2} - 1}{2} \rfloor$ , using complex optimal decoding. But one can also decode this code using the properties of the component codes, similar to how a crossword puzzle is solved. Using the row codes, we can come up with the best guess for the bit values and, then, using the column codes improve these

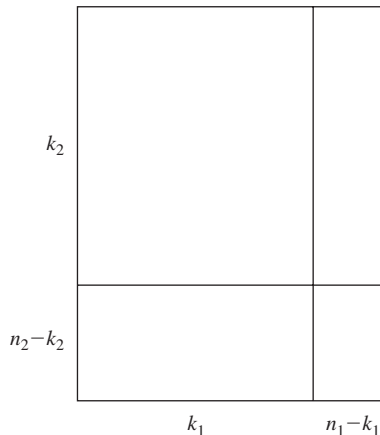


**Figure 9.35** The structure of a product code.

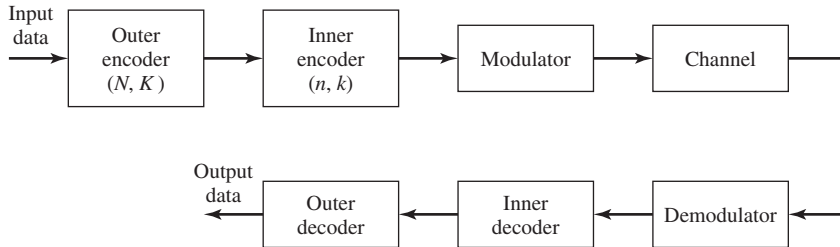


**Figure 9.36** Block diagram of a communication system with concatenated coding.

guesses. This process can be repeated in an iterative fashion, improving the quality of the guess in each step. This process is known as *iterative decoding* and is very similar to the way a crossword puzzle is solved. To employ this decoding procedure, we need decoding schemes for the row and column codes that are capable of providing *guesses* about each individual bit. In other words, decoding schemes with soft outputs (usually, the likelihood values) are desirable. We will describe in Section 9.8.4, such decoding procedures in our discussion of turbo codes.

### 9.8.2 Concatenated Codes

A concatenated code consists of two codes, an inner code and an outer code, connected serially as shown in Figure 9.36. The inner code is a binary block or convolutional code and the outer code is typically a Reed-Solomon code. If the inner code is an  $(n, k)$  code, the combination of the inner encoder, digital modulator, waveform channel, digital demodulator, and the inner decoder can be considered as a channel whose input and output are binary blocks of length  $k$ , or equivalently, elements of a  $q$ -ary alphabet where  $q = 2^k$ . Now the Reed-Solomon code (the outer code) can be used on this  $q$ -ary input,  $q$ -ary output channel to provide further error protection. It can easily be seen that if the rates of the inner and the outer codes are  $r_c$  and  $R_c$ , respectively, the rate of the concatenated code will be

$$R_{cc} = R_c r_c \quad (9.8.1)$$

Also, the minimum distance of the concatenated code is the product of the minimum distances of the inner and the outer codes. In concatenated codes, the performance of the inner code has a major impact on the overall performance of the code. That is why usually convolutional codes with soft decoding using the Viterbi algorithm are commonly employed for the inner code.

### 9.8.3 Turbo Codes

Turbo codes are a special class of concatenated codes where there exists an interleaver between two parallel or serial encoders. The existence of the interleaver results in very large code word lengths with excellent performance, particularly at low SNRs. Using these codes, it is possible to get as close as 0.7 dB to the Shannon limit at low SNRs.

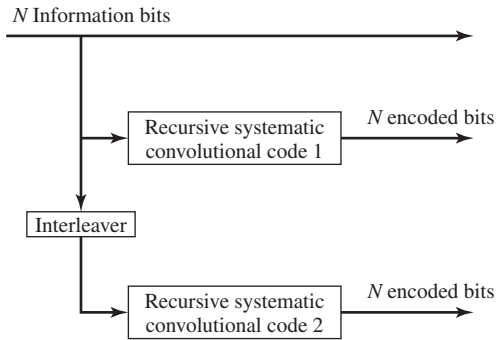


**Figure 9.37** Block diagram of a turbo encoder.

The structure of a turbo encoder is shown in Figure 9.37. The turbo encoder consists of two constituent codes separated by an interleaver of length  $N$ . The constituent codes are usually *recursive systematic convolutional codes (RSCC)* of rate  $\frac{1}{2}$ , and usually the same code is employed as the two constituent codes. Recursive convolutional codes are different from the nonrecursive convolutional codes by the existence of feedback in their shift-register realization. Therefore, unlike the nonrecursive convolutional codes which are realized as finite impulse response (FIR) digital filters, recursive convolutional codes are infinite impulse response (IIR) filters. An example of a recursive systematic convolutional encoder is shown in Figure 9.38.

In the encoder structure shown in Figure 9.37,  $N$  information bits enter the first encoder. The same information bits are interleaved and applied to the second encoder. Because the encoders are systematic, each encoder generates the  $N$ -information bits applied to its input followed by  $N$  parity check bits. After the encoding, the  $N$  information bits and the  $2N$  parity check bits of the two encoders; i.e., a total of  $3N$  bits, are transmitted over the channel. Therefore, the overall rate is  $R = N/3N = 1/3$ . If higher rates are desirable, the parity check bits are punctured; i.e., only some of parity check bits, according to a regular pattern, are transmitted.

The interleaver in turbo codes is usually very long, in the order of thousands

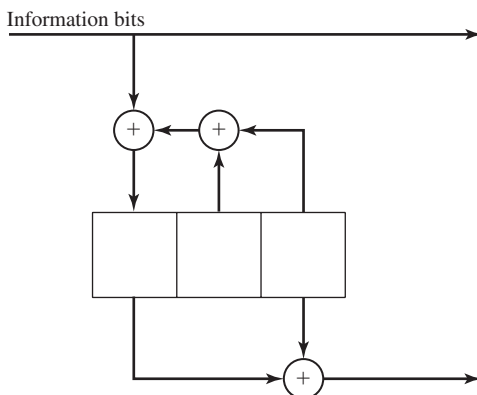


**Figure 9.38** A recursive systematic convolutional encoder.



of bits. Pseudorandom interleavers perform well, although some improvement in the performance of the code can be obtained by clever choice of the interleaver. This improvement is more noticeable at short interleaver lengths. Also note that unlike nonrecursive convolutional codes in which a sequence of zeros padded to the message sequence guarantees that the encoder returns to the all-zero state, here returning a component code to the all-zero state requires padding the information sequence with a particular nonzero sequence. Due to the existence of the interleaver, it is, in most cases, impossible to return both codes to the all-zero state.

Since turbo codes have two constituent-code components, an iterative algorithm is appropriate for their decoding. Any decoding method that yields the likelihood of the bits as its output can be used in the iterative decoding scheme. One such decoding scheme is the *maximum a posteriori* (MAP) decoding method of *Bahl, Cocke, Jelinek, and Raviv* (BCJR) (see Bahl et al. (1974)) and variations of it. Another popular method with lower complexity (and degraded performance) is the soft-output Viterbi algorithm (SOVA) due to Hagenauer and Hoher (1989). Using either method, the likelihoods of different bits are computed and passed to the second decoder. The second decoder computes the likelihood ratios and passes them to the first decoder; this process is repeated until the likelihoods suggest high probability of correct decoding for each bit. At this point, the final decision is made. The iterative decoding procedure is shown in Figure 9.39. In this figure,  $y_s$ ,  $y_{1p}$ , and  $y_{2p}$  represent the received data corresponding to the systematic bits, parity check bits for encoder 1 and parity check bits for encoder 2, respectively,  $L_{12}^e$  and  $L_{21}^e$  represent the information passed between the two decoders.

#### 9.8.4 The BCJR Algorithm

The BCJR algorithm is a trellis-based decoding algorithm that decodes *each information bit* in a convolutional code based on the MAP criteria. This is in contrast to the Viterbi algorithm that makes a maximum-likelihood decision on a *sequence* of information bits based on the maximum-likelihood criterion. As a by-product, the BCJR algorithm generates the probabilities, or likelihoods, for the transmitted bits that can be used in

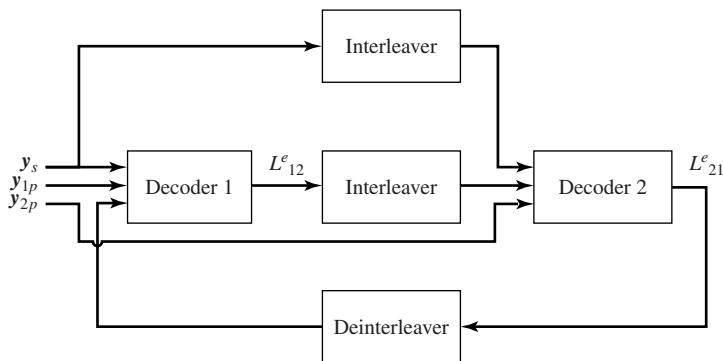


**Figure 9.39** The iterative decoding scheme for turbo codes.

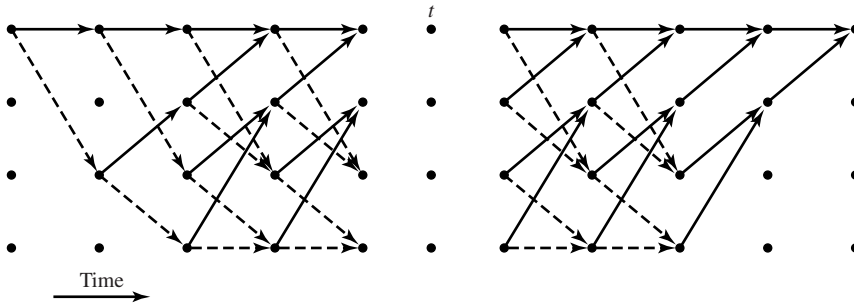


Figure 9.40 The trellis for the BCJR algorithm.

the iterative decoding of the turbo codes.

Let us assume that the code is described by a trellis shown in Figure 9.40, where we are assuming that the depth of the trellis for the received sequence is  $N$  stages and we are considering stage  $i$ . The number of states is denoted by  $M$  and the total received sequence is  $\mathbf{y}_{[1,N]}$ . Denote the received sequence up to time  $i$  by  $\mathbf{y}_{[1,i]}$  and from time  $i$  to time  $N$  by  $\mathbf{y}_{[i,N]}$ . Let us denote three  $M$ -dimensional vectors, defined as

$$\boldsymbol{\lambda}(i) = P[s(i) | \mathbf{y}]$$

$$\boldsymbol{\alpha}(i) = P[s(i) | \mathbf{y}_{[1,i]}]$$

$$\boldsymbol{\beta}(i) = P[s(i) | \mathbf{y}_{[i,N]}]$$

and let for any two  $M$ -dimensional vectors  $\mathbf{a}$  and  $\mathbf{b}$ , the  $M$ -dimensional vector  $\mathbf{c} = \mathbf{a} \wedge \mathbf{b}$  be defined as

$$\mathbf{c} = \mathbf{a} \wedge \mathbf{b} = (a_1 b_1, a_2 b_2, \dots, a_M b_M)$$

The BCJR algorithm states that

1.  $\boldsymbol{\lambda}(i)$ ,  $\boldsymbol{\alpha}(i)$ , and  $\boldsymbol{\beta}(i)$  are related by

$$\boldsymbol{\lambda}(i) \sim \boldsymbol{\alpha}(i) \wedge \boldsymbol{\beta}(i)$$

where  $\sim$  denotes proportionality. It means that the right-hand side should be appropriately normalized to make it a probability mass function equal to the left-hand side.

2. Defining

$$\gamma_{m'm}(i) = P[s(i) = m, y(i) | s(i-1) = m']$$

and the  $M \times M$  matrix  $\boldsymbol{\Gamma}(i) = [\gamma_{m'm}(i)]$ , we have the following recursions

$$\boldsymbol{\alpha}'(i) \sim \boldsymbol{\alpha}'(i-1) \boldsymbol{\Gamma}(i)$$

$$\boldsymbol{\beta}(i) \sim \boldsymbol{\Gamma}(i+1) \boldsymbol{\beta}(i+1)$$

3. Using the boundary conditions,  $\boldsymbol{\alpha}(0) = \boldsymbol{\beta}(N) = (1, 0, \dots, 0)$ , with the recursive relations in part 2, provide the forward and backward relations for the computation

of  $\alpha$  and  $\beta$ , and hence  $\lambda$ .

The boundary conditions in part 3 are based on the assumption that the path starts and ends in the all-zero state of the trellis.

Computation of  $\gamma$ 's requires knowledge of the channel characteristics because

$$\begin{aligned}\gamma_{m'm}(i) &= P[s(i) = m, y(i) | s(i-1) = m'] \\ &= P[s(i) = m | s(i-1) = m'] P[y(i) | s(i) = m, s(i-1) = m'] \\ &= P[s(i) = m | s(i-1) = m'] P[y(i) | x(i)] \\ &= P(u(i)) P[y(i) | x(i)]\end{aligned}$$

where  $u(i)$  is the input bit and  $x(i)$  is the channel symbol that cause a transition from  $s(i-1) = m'$  to  $s(i) = m$ . The term  $P[y(i) | x(i)]$ , depends on the channel characteristics. In an AWGN channel

$$P[y(i) | x(i)] = \frac{1}{\sqrt{2\pi}\sigma} e^{-\frac{(y(i)-x(i))^2}{2\sigma^2}}$$

and an estimate of the channel SNR is required.

In summary, the BCJR algorithm can be carried out as outlined next.

1. Initialize the algorithm with the boundary conditions  $\alpha(0) = \beta(N) = (1, 0, \dots, 0)$  (trellis termination condition).
2. Given prior probabilities of  $u(i)$  (usually assumed equiprobable to be 0 or 1), the channel characteristics, and the received sequence, compute the  $\gamma$ 's.
3. Use the forward recursion to compute the  $\alpha$ 's.
4. Use the backward recursion to compute the  $\beta$ 's.
5. Compute  $\lambda$ 's.
6. Compute the posterior probabilities of  $u(i)$ 's and make the decision.

Note that, in the BCJR algorithm, we have to pass the trellis once in the forward direction and once in the backward direction. Therefore, the complexity of this algorithm is roughly twice the complexity of the Viterbi algorithm. Also, because in the forward pass the values of  $\alpha$  have to be stored, the storage requirements of the algorithm are quite demanding.

Because the BCJR algorithm provides the likelihood ratios for the transmitted bits, it can be employed in the iterative decoding of turbo codes as shown in Figure 9.39.

### 9.8.5 Performance of Turbo Codes

Turbo codes are characterized by excellent performance at low SNRs. The performance of turbo codes improves with increasing the length of the interleaver and the number of iterations. The original turbo code studied by Berrou et al. (1993) used the recursive systematic convolutional encoder shown in Figure 9.41. It is seen that in this code the forward connections to the code can be represented by  $\mathbf{g}_1 = [1 \ 0 \ 0 \ 0 \ 1]$  and the feedback connection can be described by  $\mathbf{g}_2 = [1 \ 1 \ 1 \ 1 \ 1]$ . These vectors can be represented in octal form as 21 and 37, respectively. It is customary to refer to such a code as a 21/37

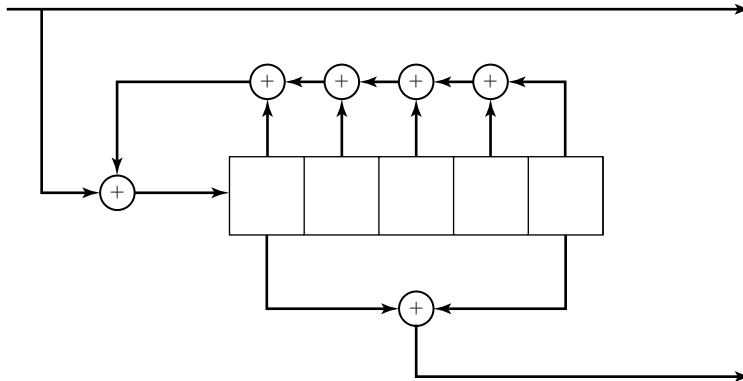


**Figure 9.41** The 21/37 recursive systematic convolutional code.

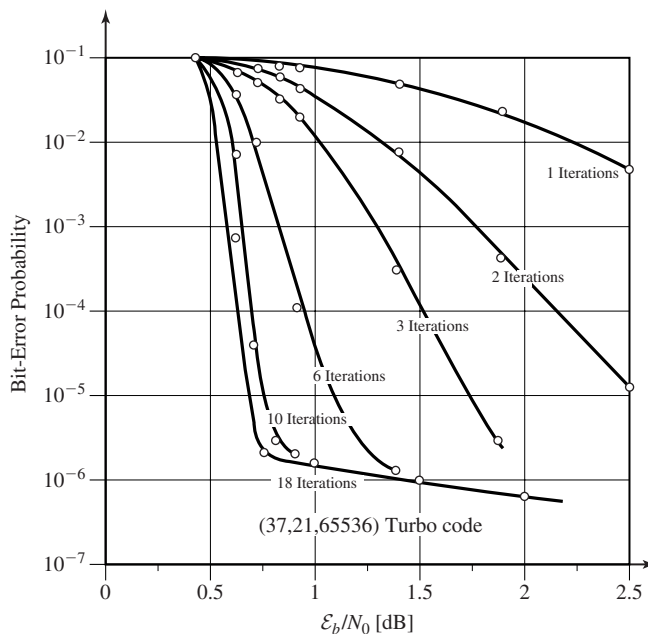


**Figure 9.42** The performance plots for the (37,21,65536) turbo code for different number of iterations.

recursive systematic convolutional code. This code was employed in a turbo code with a constraint length of  $N = 65536$  and puncturing was used to increase its rate to  $1/2$ . The performance of the resulting code using the BCJR decoding algorithm is shown in Figure 9.42. After 18 iterations, the performance of this code is only 0.7 dBs from the Shannon limit.

One problem with the turbo codes is the existence of the error floor. As seen in Figure 9.42, the probability of error decreases sharply with increasing  $E_b/N_0$  up

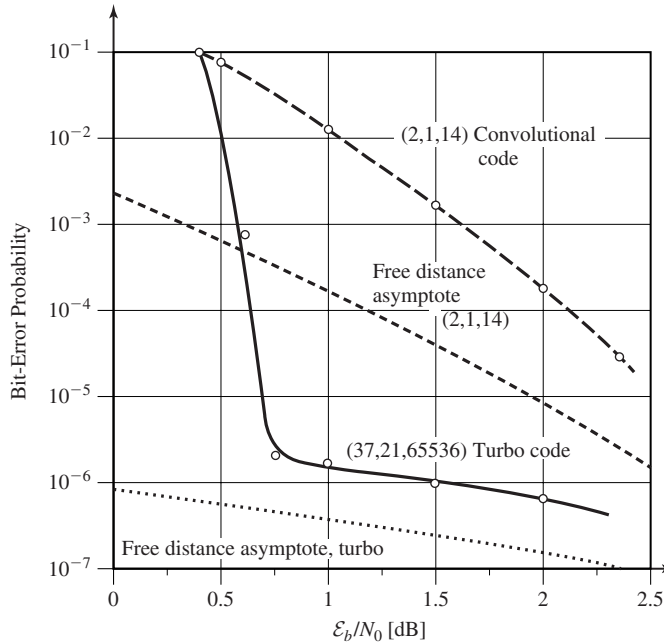


**Figure 9.43** Comparison of performance of a turbo code and a convolutional code.

to a certain point. After this point, the error probability decreases very slowly. The existence of the error floor is a consequence of the distance properties of turbo codes. It turns out that, although turbo codes have excellent performance, they have rather poor minimum distance. The reason they can perform well is that, although the distance properties are poor, the number of paths at low distance (called the *multiplicity* of that distance) is very low. In ordinary convolutional codes, one can design codes with much better minimum distance but the multiplicity of the low distances is much higher. Now referring to Equation (9.7.21), we see that for low SNRs the effect of multiplicity ( $a_{d_{\min}}$ ) is more important on the performance of the code, whereas at high SNRs, the minimum distance of the code plays a major role and, thus, the performance of turbo codes at high SNRs sharply degrades.

Figure 9.43 compares the performance of the 37/21 turbo code described above with a rate 1/2 convolutional code with constraint length 14, and soft-decision Viterbi decoding. In the same plot performance bounds (using the union bound) for both codes are also plotted.

## 9.9 CODING FOR BANDWIDTH-CONSTRAINED CHANNELS

In the two major classes of codes studied so far; i.e., block and convolutional codes, an improvement in the performance of the communication system is achieved by expanding bandwidth. In both cases the Euclidean distance between the transmitted

coded waveforms is increased by use of coding, but at the same time the bandwidth is increased by a factor of  $\frac{n}{k} = \frac{1}{R_c}$ . These type of codes have wide applications in cases where there exist enough bandwidth and the communication system designer is not under tight bandwidth constraints. Examples of such cases are deep-space communication systems. However, in many practical applications we are dealing with communication channels with strict bandwidth constraints and the bandwidth expansion due to coding may not be acceptable. For example, in transmission of digital data over telephone channels (modem design), we are dealing with a channel that has a restricted bandwidth, and the overhead due to coding imposes a major restriction on the transmission rate. In this section, we will discuss an integral coding and modulation scheme called *trellis-coded modulation* that is particularly useful for bandwidth-constrained channels.

### 9.9.1 Combined Coding and Modulation

Use of block or convolutional codes introduces redundancy that, in turn, causes increased Euclidean distance between the coded waveforms. On the other hand, the dimensionality of the transmitted signal will increase from  $k$ -dimensions/transmission to  $n$ -dimensions/transmission, if binary PSK modulation is employed. This increase in dimensionality results in an increase in bandwidth since bandwidth and dimensionality are proportional. If we want to reap the benefits of coding and, at the same time, not increase the bandwidth, we have to use a modulation scheme other than binary PSK; i.e., a scheme that is more bandwidth efficient. This means that we have to employ a multilevel/multiphase-modulation scheme to reduce the bandwidth. Of course using a multilevel/multiphase-modulation scheme results in a more “crowded” constellation and, at a constant power level, decreases the minimum Euclidean distance within the constellation. This certainly has a negative effect on the error performance of the overall coding-modulation scheme. But, as we will see next, this reduction of the minimum Euclidean distance within the constellation can be well compensated by the increase in the Hamming distance due to coding such that the overall performance shows considerable improvement.

As an example, let us assume that, in the coding stage, we want to use a rate  $\frac{2}{3}$  code. If the rate of the source is  $R$  bits/sec, the number of encoder output binary symbols/sec will be  $\frac{3}{2}R$ . If we want to use a constellation such that the bandwidth requirement is equal to the bandwidth requirement of the uncoded signal (no bandwidth expansion), we must assign  $m$  dimensions for each output binary symbol such that the resulting number of dimensions/sec is equal the number of dimensions/sec of the uncoded data, which is  $R$ . Therefore, we must have

$$R = \frac{3}{2}Rm \quad (9.9.1)$$

and, hence,

$$m = \frac{2}{3} \quad \text{dimension/binary symbol} \quad (9.9.2)$$

This means that the constellation should be designed in such a way that we have two dimensions for each three binary symbols. But three binary symbols are equivalent

to eight points in the constellation and therefore we can achieve our goal with an eight-point constellation in the two-dimensional space. One such constellation is, of course, an 8-PSK modulation scheme. Therefore, if we use a rate  $\frac{2}{3}$  code in conjunction with an 8-PSK modulation scheme, there will be no bandwidth expansion.

Now, let us examine how much coding gain we can obtain from such a scheme. Assuming that the available power is  $P$ , with no coding we have

$$\mathcal{E}_b = \frac{P}{R} \quad (9.9.3)$$

and, therefore, for the minimum Euclidean distance between two sequences, we have

$$d^2 = \frac{4P}{R} \quad (9.9.4)$$

If two information bits are mapped into a point in an 8-PSK constellation, the energy of this point is

$$\mathcal{E}_s = \frac{2P}{R} \quad (9.9.5)$$

From this, we can derive an expression for the minimum Euclidean distance within the constellation (see Figure 9.44) as

$$d_{\min}^2 = 4 \frac{2P}{R} \sin^2 \frac{\pi}{8} = 2(2 - \sqrt{2}) \frac{P}{R} \quad (9.9.6)$$

Obviously, the minimum Euclidean distance has been decreased. To see this effect we derive the loss due to using this constellation

$$\frac{d_{\min}^2}{d^2} = \frac{2}{2 - \sqrt{2}} = 2 + \sqrt{2} = 3.141 \sim 5.33 \text{ dB} \quad (9.9.7)$$

This loss has to be compensated by the code. Of course, the rate  $\frac{2}{3}$  code employed here should not only compensate for this loss but should also provide additional gain to justify

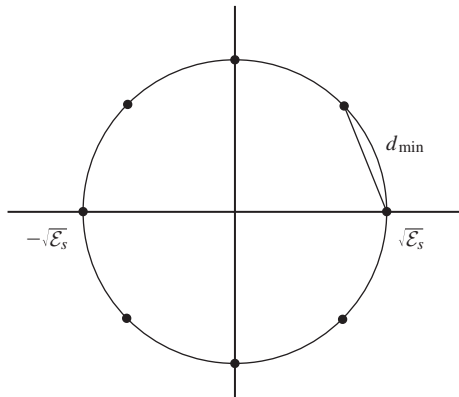


**Figure 9.44** The 8-PSK constellation used for bandwidth-efficient coding.

its use of the overall coding-modulation scheme. We can use any block or convolutional code that can provide the minimum distance required to achieve a certain overall coding gain. For example, if we need an overall coding gain of 3 dB, the code must provide a coding gain of 8.33 dB to compensate for the 5.33-dB loss due to modulation and to provide an extra 3-dB coding gain. A code that can provide such a high coding gain is a very complex (long constraint length) code requiring a sophisticated encoder and decoder. However, by interpreting coding and modulation as a single entity as shown in Section 9.9.2, we see that a comparable performance can be achieved using a much simpler coding scheme.

### 9.9.2 Trellis-Coded Modulation

*Trellis-coded modulation*, or TCM, is a simple method for designing coded-modulation schemes that can achieve good overall performance. This coding-modulation scheme is based on the concept of *mapping by set partitioning* developed by Ungerboeck (1982). Mapping by set partitioning can be used in conjunction with both block and convolutional codes, but due to the existence of a simple optimal soft-decision decoding algorithm for convolutional codes (the Viterbi algorithm), it has been mostly used with convolutional codes. When used with convolutional codes, the resulting coded-modulation scheme is known as *trellis-coded modulation*.<sup>†</sup>

**Set Partitioning Principles.** The key point in partitioning of a constellation is to find subsets of the constellation that are similar and the points inside each partition are maximally separated. To do this starting from the original constellation, we partition it into two subsets that are congruent and the points within each partition are maximally separated. Then, apply the same principle to each partition and continue. The point at which the partitioning is stopped depends on the code that we are using and will be discussed shortly.

An example of set partitioning is shown in Figure 9.45. We start with an 8-PSK constellation with power  $\mathcal{E}_s$ . The minimum distance within this constellation is

$$d_0 = \sqrt{(2 - \sqrt{2})\mathcal{E}_s} \quad (9.9.8)$$

This constellation is partitioned into two subsets denoted by  $B_0$  and  $B_1$ . Note that  $B_0$  and  $B_1$  are congruent. There are many ways that the original 8-PSK constellation can be partitioned into two congruent subsets, but  $B_0$  and  $B_1$  provide the maximum inner-partition distance. This distance is easily seen to be

$$d_1 = \sqrt{2\mathcal{E}_s} \quad (9.9.9)$$

Now, we further partition  $B_0$  and  $B_1$  to obtain  $C_0$ ,  $C_1$ ,  $C_2$  and  $C_3$ . The inner partition distance now has increased to

$$d_2 = 2\sqrt{\mathcal{E}_s} \quad (9.9.10)$$

<sup>†</sup>To be more precise, the term trellis-coded modulation is used when a general trellis code is employed.



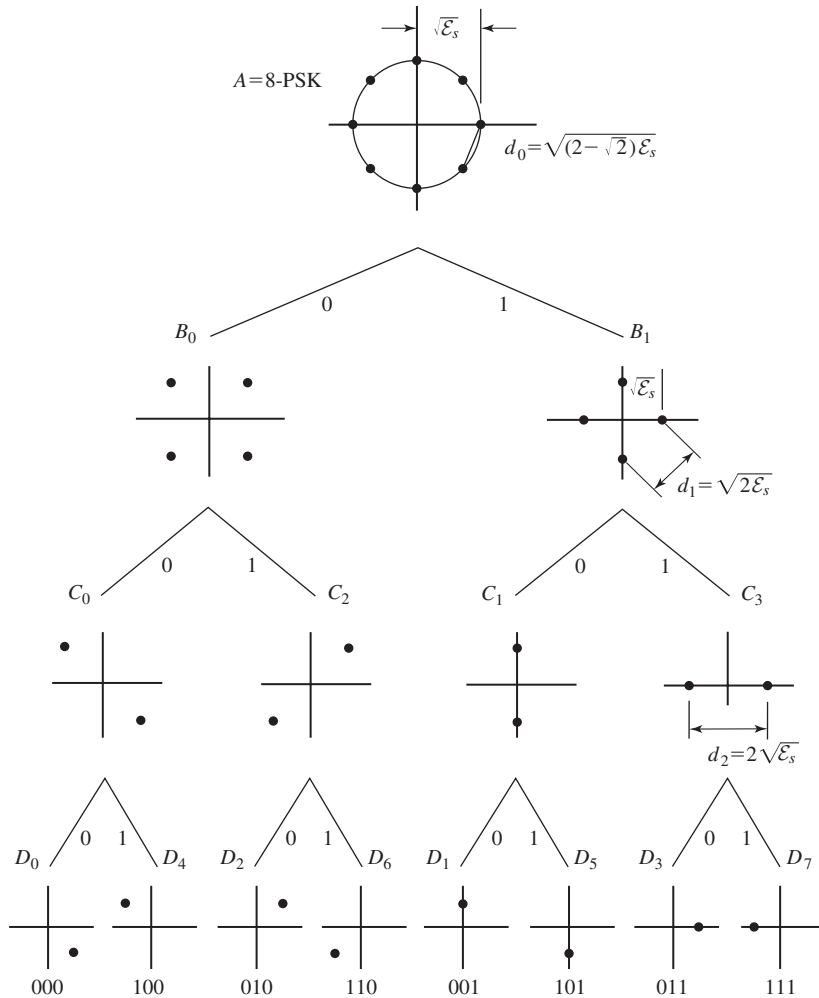


**Figure 9.45** Partitioning of an 8-PSK constellation.

We can still go one step further to obtain eight partitions each containing a single point. The corresponding subsets are denoted by  $D_0$  through  $D_7$ . Another example of set partitioning applied to a QAM constellation is given in Figure 9.46. The reader can verify that this partitioning follows the general rules for set partitioning as described above.

**Coded Modulation.** The block diagram of a coded-modulation scheme is shown in Figure 9.47. A block of length  $k$ -input bits is broken into two subblocks of lengths  $k_1$  and  $k_2$ , respectively. The first  $k_1$  bits are applied to an  $(n_1, k_1)$  binary encoder.

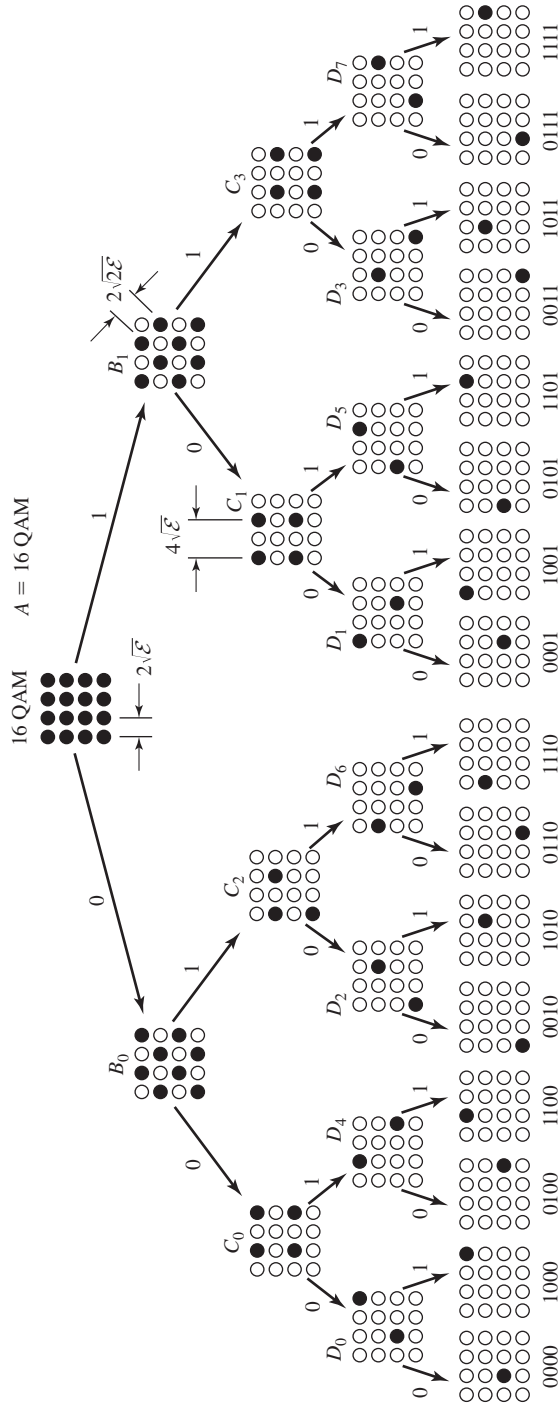


**Figure 9.46** Set partitioning of a 16-QAM constellation.

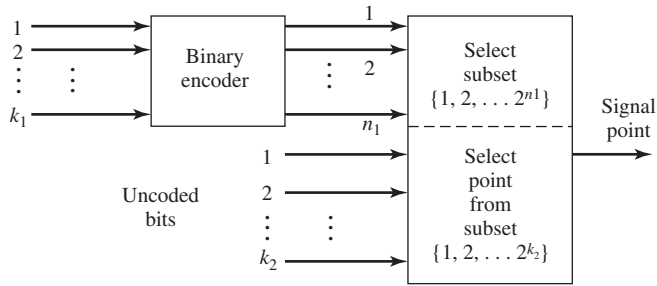


**Figure 9.47** The block diagram of a coded-modulation system.

The output of the encoder consists of  $n_1$  bits. These bits are used to choose one of  $2^{n_1}$  partitions in the constellation. This means that the constellation has been partitioned into  $2^{n_1}$  subsets. After the constellation is chosen the remaining  $k_2$  bits are used to choose one of the points in the chosen constellation. This means that there exist  $2^{k_2}$  points in each partition. Therefore, the partitioning that is used contains  $2^{n_1}$  subsets and each subset contains  $2^{k_2}$  points. This gives us a rule for how large a constellation is required and how many steps in partitioning of this constellation must be taken.

Ungerboeck (1982) has shown that by choosing  $n_1 = k_1 + 1$  and  $k_2 = 1$  and using simple convolutional codes we can design coded modulation schemes that achieve an overall coding gain between 3 and 6 dB. One such scheme is shown in Figure 9.48. In this coding scheme  $k_1 = 1$ ,  $n_1 = 2$  and  $k_2 = 1$ . The constellation contains  $2^{n_1+k_2} = 8$

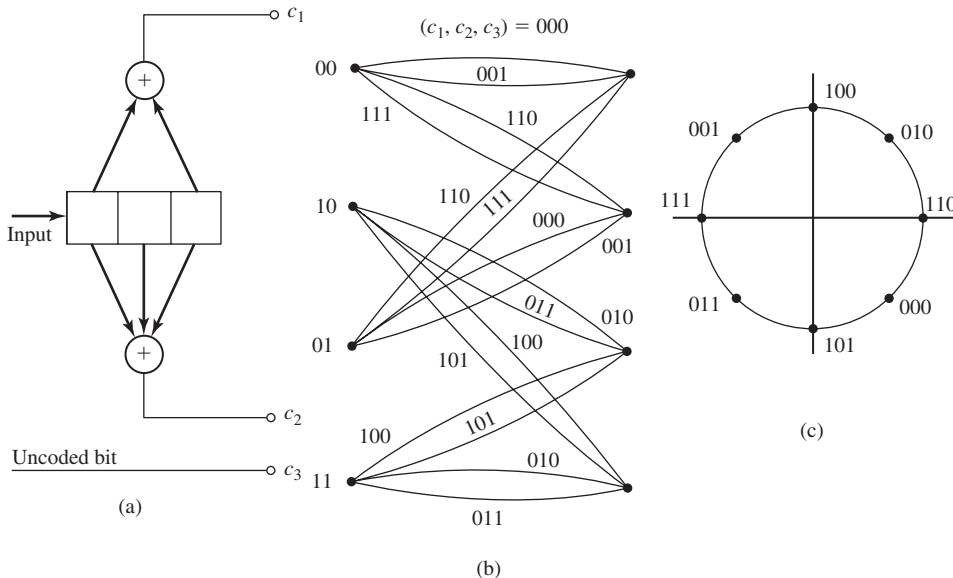


**Figure 9.48** A simple TCM scheme.

points which are partitioned into  $2^{n_1} = 4$  subsets each containing  $2^{k_2} = 2$  points. The constellation chosen here is an 8-PSK constellation and it is partitioned as shown in Figure 9.45. The convolutional code employed here can be any rate  $\frac{k_1}{n_1} = \frac{1}{2}$  code. The constraint length of this code is a design parameter and can be chosen to provide the desired coding gain. Higher constraint lengths, of course, provide higher coding gains at the price of increased encoder-decoder complexity. In this very simple example, the constraint length has been chosen to be equal to 3. The (one-stage) trellis diagram of this code is also shown in Figure 9.48.

The trellis diagram shown in Figure 9.48 is the trellis diagram of an ordinary convolutional code. The main difference is that here we have two paths connecting two states. The reason for this is the existence of the extra  $k_2 = 1$  bit, which chooses a point in each partition. In fact, the two parallel paths connecting two states correspond to a partition, and any single path corresponds to a point in the partition. One final question remains to be answered: what is the optimal assignment of the constellation points to the branches of the code trellis? Extensive computer simulations as well as heuristic reasoning result in the following rules.

1. Parallel transitions, when they occur, correspond to signal points in a single partition at the last stage of partitioning (thus providing the largest Euclidean distance). In the above example  $C_0 = \{D_0, D_4\}$ ,  $C_2 = \{D_2, D_6\}$ ,  $C_1 = \{D_1, D_5\}$  and  $C_3 = \{D_3, D_7\}$  correspond to parallel transitions. These points are separated by the maximum Euclidean distance of  $d_2 = 2\sqrt{\mathcal{E}_s}$ .
2. The transitions originating from, or merging into, any state are assigned partitions, in the last stage of partitioning, that have a single parent partition in the preceding stage. In the above example  $\{C_0, C_2\}$  and  $\{C_1, C_3\}$  are such partitions, having parents  $B_0$  and  $B_1$ , respectively. The maximum distance in this case is  $d_1 = \sqrt{2\mathcal{E}_s}$ .
3. The signal points should occur with equal frequency.

To see how the trellis-coded modulation scheme of Figure 9.48 performs, we have to find the minimum Euclidean distance between two paths originating from a node and merging into another node. This distance, known as the *free Euclidean distance* and denoted by  $D_{\text{fed}}$ , is an important characteristic of a trellis-coded modulation scheme. One obvious candidate for  $D_{\text{fed}}$  is the Euclidean distance between two parallel transitions. The Euclidean distance between two parallel transitions is  $d_2 = 2\sqrt{\mathcal{E}_s}$ . Another candidate path is shown in Figure 9.49. However, the Euclidean distance between these two paths is  $d^2 = d_0^2 + 2d_1^2 = 4.58\mathcal{E}_s$ . Obviously, this is larger than the distance between two parallel transitions. It is easily verified that for this code the free Euclidean distance is  $D_{\text{fed}} = d_2 = 2\sqrt{\mathcal{E}_s}$ . To compare this result with an uncoded scheme, we note that in an uncoded scheme

$$d_{\text{uncoded}}^2 = 4\mathcal{E}_b = 4\frac{P}{R} \quad (9.9.11)$$

and in the coded scheme

$$d_{\text{coded}}^2 = 4\mathcal{E}_s = 8\mathcal{E}_b \quad (9.9.12)$$

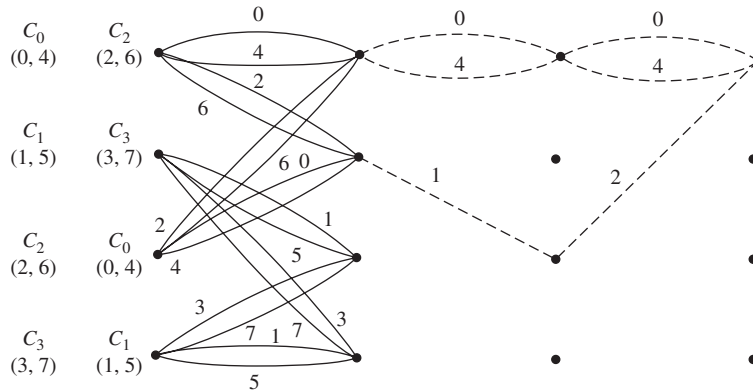


Figure 9.49 Two candidate minimum distance paths.

Therefore, the coding gain is given by

$$G_{\text{coding}} = \frac{d_{\text{coded}}^2}{d_{\text{uncoded}}^2} = 2 \sim 3 \text{ dB} \quad (9.9.13)$$

Thus, this simple coding scheme is capable of achieving a 3-dB coding gain without increasing bandwidth. Of course, the price paid for this better performance is increased complexity in encoding and decoding.

Instead of a 8-state trellis, a trellis with a higher number of states yields higher coding gains. Extensive computer simulations by Ungerboeck indicate that with 8, 16, 32, 64, 128, and 256 states coding gains in the range of 3.6–5.75 dB can be achieved. The trellis diagram for an 8-state trellis is shown in Figure 9.50

**Decoding of Trellis-Coded Modulation Codes.** The decoding of trellis-coded modulation is performed in two steps. Because each transition in the trellis corresponds to a partition of the signal set, and each partition generally corresponds to a number of signal points, the first step is to find the most likely signal point in each partition. This is accomplished by finding the point in each partition that is closest in Euclidean distance to the received point. This first step in decoding of a trellis-coded modulation scheme is called *subset decoding*. After this step, corresponding to each transition in the trellis there exists only one point (the most likely one), and only one Euclidean distance (the distance between the received point and this most likely point). The second step of the decoding procedure is to use this Euclidean distance to find a path through the trellis whose total Euclidean distance from the received sequence is minimum. This is done by applying the Viterbi algorithm.

Trellis-coded modulation is now widely used in high-speed telephone line modems. Without coding, high-speed modems achieved data rates up to 14,400 bits/sec with a 64-QAM signal constellation. The added coding gain provided by trellis-coded modulation has made it possible to more than double the speed of transmission.

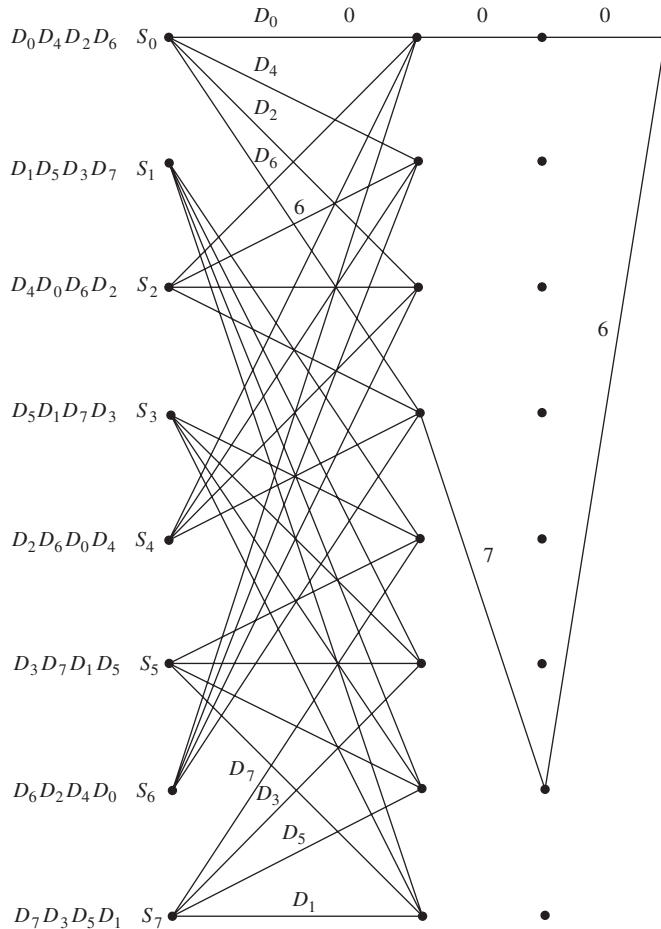


Figure 9.50 An 8-state Ungerboeck encoder.

### 9.10 PRACTICAL APPLICATIONS OF CODING

In the previous sections, we have seen that coding can be employed to improve the effective SNR and, thus, enhance the performance of the digital communication system. Block and convolutional codes and combinations of them in the form of concatenated and turbo codes as discussed earlier, have been applied to communication situations where bandwidth is not a major concern and, thus, some bandwidth expansion due to coding is allowed. On the other hand, in cases where bandwidth is a major concern, as in digital communication over telephone channels, coded modulation can be employed. By using coding, performance of practical digital communication systems has been improved by up to 9 dB, depending on the application and the type of the code employed. In this section, we discuss applications of coding to three digital communication cases.

These include deep-space communications, telephone-line modems, and coding for compact discs (CDs).

### 9.10.1 Coding for Deep-Space Communications

Deep-space communication channels are characterized by very low SNRs and practically no bandwidth limitations. The transmitter power is usually obtained from on-board solar cells and, therefore, is typically limited 20–30 W. The physical dimensions of the transmitting antenna are also quite limited and, therefore, its gain is limited too. The enormous distance between the transmitter and the receiver and lack of repeaters results in a very low SNR at the receiver. The channel noise can be characterized by a white Gaussian random process. These channels are very well modeled as AWGN channels. Because bandwidth is not a major concern on these channels both block and convolutional codes can be applied.

In the Viking orbiters and landers mission to Mars, a (32, 6) block code (Reed-Muller code) was employed that provided a coding gain a gain of approximately 4 dB with respect to an uncoded PSK system at an error rate of  $10^{-6}$ . Later, in the Voyager space mission to outer planets (Mars, Jupiter, and Saturn), convolutional codes with Viterbi decoding were employed. Two codes that were designed at the Jet Propulsion Laboratory (JPL) for that mission were a (2, 1) convolutional code with a constraint length of  $L = 7$  with

$$\mathbf{g}_1 = [1 \quad 1 \quad 0 \quad 1 \quad 1 \quad 0 \quad 1]$$

$$\mathbf{g}_2 = [1 \quad 0 \quad 0 \quad 1 \quad 1 \quad 1 \quad 1]$$

and a (3, 1) convolutional code with  $L = 7$  and

$$\mathbf{g}_1 = [1 \quad 1 \quad 0 \quad 1 \quad 1 \quad 0 \quad 1]$$

$$\mathbf{g}_2 = [1 \quad 0 \quad 0 \quad 1 \quad 1 \quad 1 \quad 1]$$

$$\mathbf{g}_3 = [1 \quad 0 \quad 1 \quad 0 \quad 1 \quad 1 \quad 1]$$

The first code has a free distance of  $d_{\text{free}} = 10$  and for the second code  $d_{\text{free}} = 15$ . Both codes were decoded using the Viterbi algorithm and a soft-decoding scheme in which the output was quantized to  $Q = 8$  levels. The first code provides a coding gain of 5.1 dB with respect to an uncoded PSK system operating at an error rate of  $10^{-5}$ . The second code provides a gain of 5.7 dB. Both codes operate about 4.5 dB above the theoretical limit predicted by Shannon's formula.

In subsequent missions of the Voyager to Uranus, in 1986, the (2, 1) convolutional code with  $L = 7$  was used as an inner code in a concatenated coding scheme where a (255, 223) Reed-Solomon code served as the outer code. Viterbi decoding followed by a Reed-Solomon decoder at the Earth terminal provided a total coding gain of 8 dB at an error rate of  $10^{-6}$ . This system operated at a data rate of approximately 30 Kbits/sec.

Other decoding algorithms for convolutional codes have also been applied to certain deep-space communication projects. For NASA's Pioneer 9 mission a (2, 1) convolutional code with a constraint length of  $L = 21$  was designed with generator

sequences (in octal representation)

$$\mathbf{g}_1 = [4 \ 0 \ 0 \ 0 \ 0 \ 0 \ 0]$$

$$\mathbf{g}_2 = [7 \ 1 \ 5 \ 4 \ 7 \ 3 \ 7]$$

which employed Fano's algorithm with a soft-decision decoding scheme and eight levels of output quantization. Pioneers 10, 11, and 12 and also in Helios A and B German solar orbiter missions employed a (2, 1) convolutional code with a constraint length of  $L = 32$ . The generator sequences for this code (in octal representation) are given below.

$$\mathbf{g}_1 = [7 \ 3 \ 3 \ 5 \ 3 \ 3 \ 6 \ 7 \ 6 \ 7 \ 2]$$

$$\mathbf{g}_2 = [5 \ 3 \ 3 \ 5 \ 3 \ 3 \ 6 \ 7 \ 6 \ 7 \ 2]$$

This code has a free distance of  $d_{\text{free}} = 23$ . For decoding, again, the Fano decoding algorithm with eight-level output quantization was employed. Majority logic decoding has also been used in a number of coding schemes designed for the INTELSAT communication satellites. As an example a (8, 7) code with  $L = 48$  designed to operate at 64 Kbits/sec on an INTELSAT satellite was capable of improving the error rate from  $10^{-4}$  to  $5 \times 10^{-8}$ . In the Galileo space mission a (4, 1, 14) convolutional code was used, resulting in a spectral-bit rate of  $\frac{1}{4}$ , which at  $\mathcal{E}_b/N_0$  of 1.75 dB, achieved an error probability of  $10^{-5}$ . This code performed 2.5 dB from the Shannon limit. Using an outer (255, 223) Reed-Solomon code improves the coding gain by another 0.8 dB, resulting in a concatenated code operating 1.7-dB from the Shannon limit. Turbo codes performing at a spectral-bit rate of 0.5 and operating only 0.7-dB from the Shannon limit, compare quite favorably with all systems described above.

### 9.10.2 Coding for Telephone-Line Modems

Telephone-line channels are characterized by a limited bandwidth, typically between 300–3000 Hz, and a rather high SNR, which is usually 28 dB or more. Therefore, in designing coding schemes for telephone-line channels, we are faced with bandwidth limitation. This is in direct contrast to the deep-space communication channel which is primarily power limited. This corresponds to the case of  $r \gg 1$  in Figure 9.11. Because bandwidth is limited, we have to use low dimensional signaling schemes, and since power is rather abundant, we can employ multilevel modulation schemes. As we have already seen in Section 9.9, trellis-coded modulation is an appropriate scheme to be employed in such a case.

Historically, the first modems on telephone channels (prior to 1960s) employed frequency-shift keying with asynchronous detection and achieved bit rates in the range of 300–1200 bits/sec. Later, in the early 1960s, the first generation of synchronous modems employing 4-PSK modulation achieved bit rates of up to 2400 bit/sec. Advances in equalization techniques allowed for more sophisticated constellations which resulted in higher bit rates. These included 8-PSK modems achieving a bit rate of



4800 bit/sec and 16-point QAM modems that increased the bit rate to 9600 bits/sec. In the early 1980s, modems with a bit rate of 14,400 bits/sec were introduced that employed a 64-point QAM signal constellation. All these improvements were results of advances in equalization and signal-processing techniques and also improvements in the characteristics of telephone lines.

The advent of trellis-coded modulation made it possible to design coded-modulation systems that improved overall system performance without requiring excess bandwidth. Trellis-coded modulation schemes based on variations of the original Ungerboeck's codes and introduced by Wei (1984) were adopted as standard by the CCITT standard committees. These codes are based on linear or nonlinear convolutional codes to guarantee invariance to  $180^\circ$ - or  $90^\circ$ -phase rotations. This is crucial in applications where differential encoding is employed to avoid phase ambiguities when a PLL is employed for carrier-phase estimation at the receiver. These codes achieve a coding gain comparable to Ungerboeck's codes with the same number of states but, at the same time, provide the required phase invariance. In Figure 9.51 we have shown the combination of the differential encoder, the nonlinear convolutional encoder, and the signal mapping for the 8-state trellis-coded modulation system that is adopted in the CCITT V.32 standard.

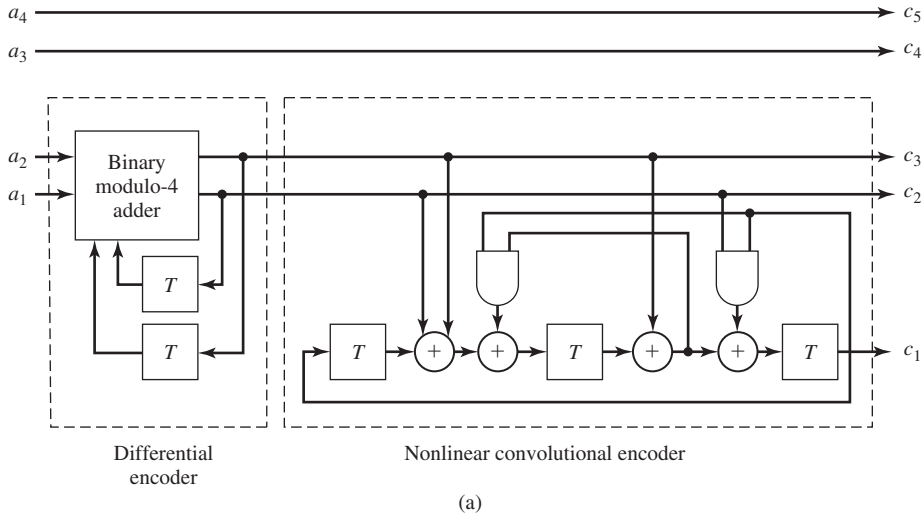
### 9.10.3 Coding for Compact Discs

In Chapters 6 and 8, the problems of source coding and modulation codes for compact discs were addressed. In this section we consider error correcting techniques that are employed for compact disc digital audio recording.

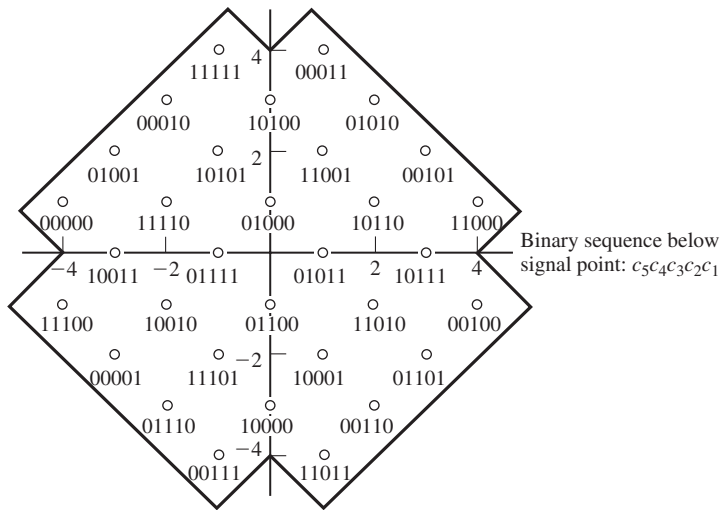
The storage medium for digital audio recording on a compact disc is a plastic disc with a diameter of 120 mm, a thickness of 1.2 mm and a track pitch of  $1.6 \mu\text{m}$ . At playing time, this disc is read by a laser beam at a velocity of 1.25 m/s. Inside the spiral track on the disc, there are depressions called "pits" and flat areas between pits called "lands." The digital audio is stored by the length of these pits and lands. A 1 is represented by a transition from a pit to a land or vice versa, whereas a 0 corresponds to no transition (NRZI modulation). As we have seen in Chapter 8, constraints on the physical length of pits and lands make it necessary to employ runlength-limited (RLL) codes. The eight-to-fourteen modulation (EFM) code with  $d = 2$  and  $\kappa = 10$  is used in compact-disc recording.

The main source of errors in a compact disc is imperfections in the manufacturing of the disc, such as air bubbles in the plastic material or pit inaccuracies; and damages to the disc, such as fingerprints or scratches, dust, dirt, and surface abrasions. Since each pit is almost  $0.5 \mu\text{m}$  wide and between  $0.9$  and  $3.3 \mu\text{m}$  long, these sources of errors result in error bursts, affecting many adjacent information bits. This means that a good model for this storage channel is a channel with bursts of error, and well-known techniques for correcting bursts of errors can be employed. As we have discussed in Section 9.6.1, Reed-Solomon codes are particularly attractive for such applications.

Recall from Chapter 6, that the left and the right channel are sampled at a rate of 44.1 KHz and then each sample is quantized to 16 levels. Therefore, at each sampling



(a)



(b)

**Figure 9.51** (a) Differential encoder, nonlinear convolutional encoder, and (b) signal constellation adopted in the V.32 standard.

instant there are 32 bits, or four 8-bit sequences to be encoded. Each 8-bit sequence is called a “symbol.”

For error correction and detection, two Reed-Solomon codes are employed,<sup>†</sup> as shown in Fig. 9.52. The first code, denoted by  $C_1$ , is a (28, 24) RS code and the second

<sup>†</sup>These are in fact, *shortened* Reed-Solomon codes, obtained from Reed-Solomon codes by putting some information bits equal to zero, and therefore reducing both  $k$  and  $n$  by a constant, while keeping the minimum distance intact.

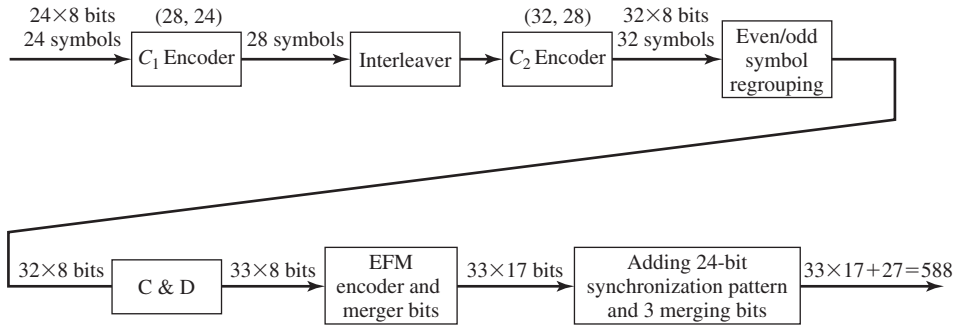


Figure 9.52 Encoding for compact-disc recording.

code,  $C_2$ , is a  $(32, 28)$  RS code. The alphabet on which these codes are defined consists of binary sequences of length 8, which coincides with our definition of a symbol.

The input sequence to the  $C_1$  encoder consists of 24 symbols (usually known as a “frame”), which are encoded into 28 symbols. The 28 symbols at the output of the  $C_1$  encoder are *interleaved* (see Section 9.5.2) to reduce the effect of error bursts and spread them over a longer interval, making them look more “random.” These are encoded by the  $C_2$  encoder to 32 symbols. At the output of the  $C_2$  encoder, the odd-numbered symbols of each frame are grouped with the even-numbered symbols of the next frame to form a new frame. At the output of the  $C_2$  encoder corresponding to each set of six audio samples, we have 32 eight-bit symbols. One more 8-bit symbol is added that contains the control and display (C & D) information, bringing the total to 33 symbols/frame.

The output is then applied to the eight-to-fourteen (EFM) runlength-limited encoder, which maps each symbol into a binary sequence of length 14. We have seen in Chapter 8 that three more bits, called “merger” bits, are added for each symbol to make sure that the merger of code words satisfies the runlength constraint. These bring the length of each sequence to 17. Next, a frame is completed by adding a 24 synchronization pattern and 3 additional “merger” bits to guarantee the runlength constraint after a merger. This brings the total number of encoded bits/frame (six samples, or  $6 \times 2 \times 16 = 192$  audio bits) to

$$33 \times 17 + 24 + 3 = 588$$

channel bits (see Figure 8.29). This means that an expansion of, roughly, three times has taken place. These extra bits are used to protect the digital audio information bits from errors (the RS codes) and also make sure that the runlength constraint is satisfied (the EFM code).

On the playback, first synchronization and merger bits are separated, and then the 32 symbols are deinterleaved. The result then enters the decoder for the code  $C_2$ . This code has a minimum distance of 5 and, therefore, is capable of correcting up to 2 errors. The decoder, however, is designed to correct only 1 error. Then according to

the relation in Equation (9.5.37)

$$e_c + e_d = d_{\min} - 1$$

it can detect up to 3 errors with certainty and 4 or more errors with high probability. If a single error is encountered, it is corrected, if multiple errors are detected, then all 28 symbols are flagged as “unreliable.” After deinterleaving, these symbols are passed to the decoder for the code  $C_1$ . Decoder  $C_1$  tries single error, or 2 erasure corrections. If it fails, all output symbols are flagged; if there are more 3 or more flags at its input, it copies them to its output.

At the output of the second decoder, the symbol corresponding to “unreliable” positions are filled in by interpolation of the other positions. Using this rather complex encoding–decoding technique together with the signal processing methods, burst errors of up to 12,000 data bits, which correspond to a track length of 7.5 mm on the disc, can be concealed.

## 9.11 FURTHER READING

The noisy channel-coding theorem, which plays a central role in information theory, and the concept of channel capacity were first proposed and proved by Shannon (1948). For detailed discussion of this theorem and its several variations the reader may refer to standard books on information theory such as Gallager (1968), Blahut (1987), and Cover and Thomas (1991).

Golay (1949), Hamming (1950), Hocquenghem (1959), Bose and Ray-Chaudhuri (1960a,b), and Reed and Solomon (1960) are landmark papers in the development of block codes. Convolutional codes were introduced by Elias (1955) and various methods for their decoding were developed by Wozencraft and Reiffen (1961), Fano (1963), Zigangirov (1966), Viterbi (1967), and Jelinek (1969). Trellis-coded modulation was introduced by Ungerboeck (1982) and later developed by Forney (1988a,b). Product codes were introduced by Elias (1954) and concatenated codes were developed and analyzed by Forney (1966). Berrou, Glavieux, and Thitimajshima (1993) introduced turbo codes. The interested reader is referred to books on coding theory including Berlekamp (1968), Peterson and Weldon (1972), MacWilliams and Sloane (1977), Lin and Costello (1983), and Blahut (1983). The reader is referred to the book by Heegard and Wicker (1999) on turbo codes.

## PROBLEMS

- 9.1 Find the capacity of the channel shown in Figure P-9.1.
- 9.2 The channel shown in Figure P-9.2 is known as the *binary erasure channel*. Find the capacity of this channel and plot it as a function of  $\epsilon$ .
- 9.3 Find the capacity of the cascade connection of  $n$  binary-symmetric channels with same crossover probability  $\epsilon$ . What is the capacity when the number of channels goes to infinity.

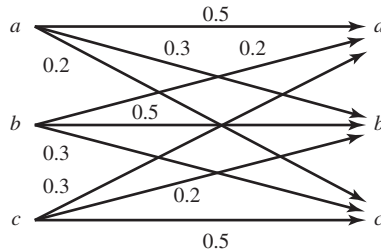


Figure P-9.1

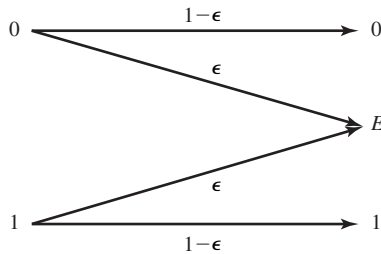


Figure P-9.2

9.4 Using Stirling's approximation  $n! \approx n^n e^{-n} \sqrt{2\pi n}$ , show that

$$\binom{n}{n\epsilon} \approx 2^{nH_b(\epsilon)}$$

9.5 Show that the capacity of a binary-input, continuous-output AWGN channel with inputs  $\pm A$  and noise variance  $\sigma^2$  (see Example 9.1.2) is given by

$$C = \frac{1}{2} f\left(\frac{A}{\sigma}\right) + \frac{1}{2} f\left(-\frac{A}{\sigma}\right)$$

where

$$f(x) = \int_{-\infty}^{\infty} \frac{1}{\sqrt{2\pi}} e^{-(u-x)^2/2} \log_2 \frac{2}{1 + e^{-2xu}} du$$

9.6 The matrix whose elements are the transition probabilities of a channel; i.e.,  $p(y_i | x_j)$ 's, is called the channel probability transition matrix. A channel is called *symmetric* if all rows of the channel probability transition matrix are permutations of each other, and all its columns are also permutations of each other. Show that in a symmetric channel the input probability distribution that achieves capacity is a uniform distribution. What is the capacity of this channel?

9.7 Channels 1, 2, and 3 are shown in Figure P-9.7.

1. Find the capacity of channel 1. What input distribution achieves capacity?
2. Find the capacity of channel 2. What input distribution achieves capacity?

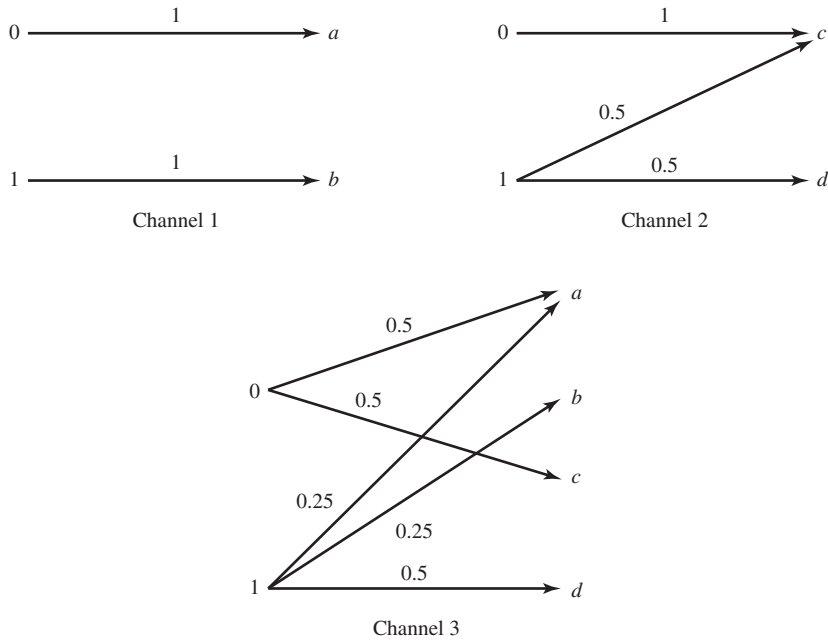


Figure P-9.7

3. Let  $C$  denote the capacity of the third channel and  $C_1$  and  $C_2$  represent the capacities of the first and second channel. Which of the following relations holds true and why?

- (a)  $C < \frac{1}{2}(C_1 + C_2)$ .
- (b)  $C = \frac{1}{2}(C_1 + C_2)$ .
- (c)  $C > \frac{1}{2}(C_1 + C_2)$ .

9.8 Let  $C$  denote the capacity of a discrete-memoryless channel with input alphabet  $\mathcal{X} = \{x_1, x_2, \dots, x_N\}$  and output alphabet  $\mathcal{Y} = \{y_1, y_2, \dots, y_M\}$ . Show that  $C \leq \min\{\log M, \log N\}$ .

9.9 The channel  $C$  is (known as the Z channel) shown in Figure P-9.9.

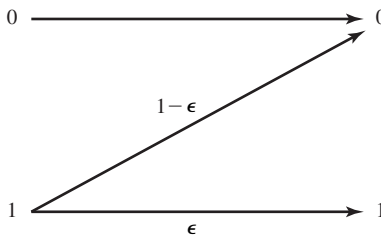
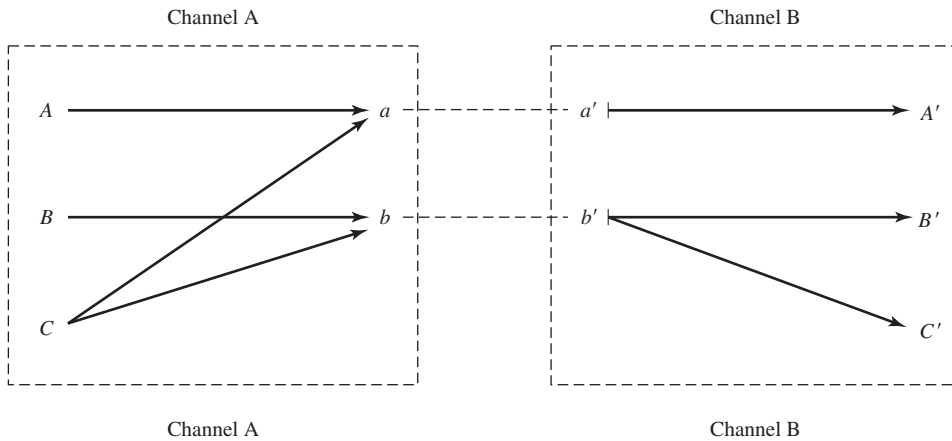


Figure P-9.9

1. Find the input probability distribution that achieves capacity.
  2. What is the input distribution and capacity for the special cases  $\epsilon = 0$ ,  $\epsilon = 1$ , and  $\epsilon = 0.5$ ?
  3. Show that if  $n$  such channels are cascaded, the resulting channel will be equivalent to a  $Z$  channel with  $\epsilon_1 = \epsilon^n$ .
  4. What is the capacity of the equivalent  $Z$  channel when  $n \rightarrow \infty$ .
- 9.10** Find the capacity of the channels A and B as shown in Figure P-9.10. What is the capacity of the cascade channel AB? (Hint: Look carefully at the channels and avoid lengthy math.)



**Figure P-9.10**

- 9.11** Find the capacity of an additive white Gaussian noise channel with a bandwidth of 1 MHz, power of 10 W, and noise power-spectral density of  $\frac{N_0}{2} = 10^{-9}$  W/Hz.
- 9.12** Channel  $C_1$  is an additive white Gaussian noise channel with a bandwidth of  $W$ , transmitter power of  $P$  and noise power-spectral density of  $\frac{N_0}{2}$ . Channel  $C_2$  is an additive Gaussian noise channel with the same bandwidth and power as channel  $C_1$  but with noise power-spectral density  $S_n(f)$ . It is further assumed that the total noise power for both channels is the same, that is

$$\int_{-W}^W S_n(f) df = \int_{-W}^W \frac{N_0}{2} df = N_0 W$$

Which channel do you think has a larger capacity? Give an intuitive reasoning.

- 9.13** A discrete-time memoryless Gaussian source with mean 0 and variance  $\sigma^2$  is to be transmitted over a binary-symmetric channel with crossover probability  $\epsilon$ .
1. What is the minimum value of the distortion attainable at the destination? (Distortion is measured in mean-squared-error.)

2. If the channel is a discrete-time memoryless additive Gaussian noise channel with input power  $P$  and noise power  $\sigma_n^2$ , what is the minimum attainable distortion?
  3. Now assume that the source has the same basic properties but is not memoryless. Do you expect that the distortion in transmission over the binary-symmetric channel to be decreased or increased? Why?
- 9.14** For the channel shown below, find the channel capacity and the input distribution that achieves capacity.

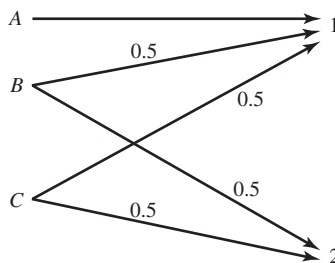


Figure P-9.14

- 9.15** Consider two discrete-memoryless channels represented by  $(\mathcal{X}_1, p(y_1 | x_1), \mathcal{Y}_1)$  and  $(\mathcal{X}_2, p(y_2 | x_2), \mathcal{Y}_2)$  with corresponding (information) capacities  $C_1$  and  $C_2$ . A new channel is defined by  $(\mathcal{X}_1 \times \mathcal{X}_2, p(y_1 | x_1)p(y_2 | x_2), \mathcal{Y}_1 \times \mathcal{Y}_2)$ . This channel is referred to as the “product channel” and models the case where  $x_1 \in \mathcal{X}_1$  and  $x_2 \in \mathcal{X}_2$  are simultaneously transmitted over the two channels with no interference. Prove that the capacity of this new channel is the sum of  $C_1$  and  $C_2$ .
- 9.16** Let  $(\mathcal{X}_1, p(y_1 | x_1), \mathcal{Y}_1)$  and  $(\mathcal{X}_2, p(y_2 | x_2), \mathcal{Y}_2)$  represent two discrete-memoryless communication channels with inputs  $\mathcal{X}_i$ , outputs  $\mathcal{Y}_i$ , and conditional probabilities  $p(y_i | x_i)$ . Further assume that  $\mathcal{X}_1 \cap \mathcal{X}_2 = \emptyset$  and  $\mathcal{Y}_1 \cap \mathcal{Y}_2 = \emptyset$ . We define the *sum* of these channels as a new channel with input alphabet  $\mathcal{X}_1 \cup \mathcal{X}_2$ , output alphabet  $\mathcal{Y}_1 \cup \mathcal{Y}_2$  and conditional probability  $p(y_i | x_i)$ , where  $i$  denotes the index of  $\mathcal{X}$  to which the input to the channel belongs. This models a communication situation where we have two channels in parallel, and at each transmission interval we can use one and only one of the channels, the input and output alphabets are disjoint and, therefore, at the receiver there is no ambiguity which channel was being used.
1. Show that the capacity of the *sum* channel satisfies  $2^C = 2^{C_1} + 2^{C_2}$  where  $C_1$  and  $C_2$  are the capacities of each channel.
  2. Using the result of part 1 show that if  $C_1 = C_2 = 0$  we still have  $C = 1$ ; that is, using two channels with zero capacity we are able to transmit one bit/transmission. How do you interpret this result?
  3. Find the capacity of the channel shown in Figure P-9.16.



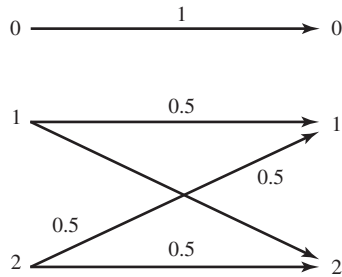


Figure P-9.16

**9.17**  $X$  is a binary memoryless source with  $P(X = 0) = 0.3$ . This source is transmitted over a binary-symmetric channel with crossover probability  $\epsilon = 0.1$ .

1. Assume that the source is directly connected to the channel; i.e., no coding is employed. What is the error probability at the destination?
2. If coding is allowed, what is the minimum possible error probability in reconstruction of the source.
3. For what values of  $\epsilon$  is reliable transmission possible (with coding, of course)?

**9.18** Each sample of a Gaussian memoryless source has a variance equal to 4 and the source produces 8000 samples/sec. The source is to be transmitted via an additive white Gaussian noise channel with a bandwidth equal to 4000 Hz. It is desirable to have a distortion/sample not exceeding 1 at the destination (assume squared-error distortion).

1. What is the minimum required signal-to-noise ratio of the channel?
2. If it is further assumed that, on the same channel, a binary PSK scheme is employed with hard-decision decoding, what will be the minimum required channel signal-to-noise ratio?

(Hint: The SNR of the channel is defined by  $\frac{P}{N_0 W}$ .)

**9.19** A certain source can be modeled as a stationary zero-mean Gaussian process  $X(t)$  with power-spectral density

$$\mathcal{S}_x(f) = \begin{cases} 2 & |f| < 10 \\ 0, & \text{otherwise} \end{cases}$$

The distortion in reproducing  $X(t)$  by  $\hat{X}(t)$  is  $D = E|X(t) - \hat{X}(t)|^2$ . This source is to be transmitted over an additive Gaussian noise channel, in which the noise power-spectral density is given by

$$\mathcal{S}_n(f) = \begin{cases} 1 & |f| < 4 \\ 0, & \text{otherwise} \end{cases}$$

1. What is  $D_{\max}$  in the compression of the source?
  2. Find the rate-distortion function for the source.
  3. If we want to reproduce  $X(t)$  with a distortion equal to 10, what transmission rate is required?
  4. Find the channel capacity-cost function, where cost is assumed to be the power. What is the required power such that the source can be transmitted via the channel with a distortion not exceeding 10?
- 9.20** It can be shown that the capacity of a discrete-time power constrained additive noise channel described by  $Y = X + Z$ , where  $X$  and  $Y$  are the input and the output and  $Z$  is the noise, satisfies the inequalities

$$\frac{1}{2} \log \left( 1 + \frac{P}{N} \right) \leq C \leq \frac{1}{2} \log[2\pi e(P + N)] - h(Z)$$

where  $P$  is the input power constraint,  $N$  is the variance (power) of the noise process, and  $h(\cdot)$  denotes the differential entropy as defined in Chapter 6. Using the result of Problem 6.36, plot the lower and upper bounds to the capacity for a channel with Laplacian noise (see Problem 6.36) as a function of the noise variance (noise power).

- 9.21** Plot the capacity of an AWGN channel that employs binary antipodal signaling, with optimal bit-by-bit detection at the receiver, as a function of  $\frac{E_b}{N_0}$ . On the same axis, plot the capacity of the same channel when binary orthogonal signaling is employed.
- 9.22** In Example 9.5.1, find the minimum distance of the code. Which code word(s) is(are) minimum weight?
- 9.23** In Example 9.5.3, verify that all code words of the original code satisfy

$$\mathbf{cH}^t = \mathbf{0}$$

- 9.24** By listing all code words of the (7, 4) Hamming code verify that its minimum distance is equal to 3.
- 9.25** Find the parity check matrix and the generator matrix of a (15, 11) Hamming code in the systematic form.
- 9.26** Show that the minimum Hamming distance of a linear block code is equal to the minimum number of columns of its parity check matrix that are linearly dependent. From this conclude that the minimum Hamming distance of a Hamming code is always equal to 3.
- 9.27** A simple repetition code of blocklength  $n$  is a simple code consisting of only two code words one  $\underbrace{(0, 0, \dots, 0)}_n$  and the other  $\underbrace{(1, 1, \dots, 1)}_n$ . Find the parity check matrix and the generator matrix of this code in the systematic form.
- 9.28**  $\mathbf{G}$  is the generator matrix of a (6, 3) linear code. This code is *extended* by adding an overall parity check bit to each code word so that the Hamming weight of each

resulting code word is even.

$$\mathbf{G} = \begin{bmatrix} 1 & 0 & 0 & 1 & 1 & 0 \\ 0 & 1 & 0 & 1 & 0 & 1 \\ 0 & 0 & 1 & 0 & 1 & 1 \end{bmatrix}$$

1. Find the parity check matrix of the extended code.
  2. What is the minimum distance of the extended code?
  3. Find the coding gain of the extended code?
- 9.29** Compare the block error probability of an uncoded system with a system that uses a (15, 11) Hamming code. The transmission rate is  $R = 10^4$  bps and the channel is AWGN with a received power of  $1 \mu\text{W}$  and noise power-spectral density of  $\frac{N_0}{2}$ . The modulation scheme is binary PSK and soft-decision decoding is employed. Answer the question when hard decision is employed.
- 9.30** Generate the standard array for a (7, 4) Hamming code and use it to decode the received sequence (1, 1, 1, 0, 1, 0, 0).
- 9.31** For what values of  $k$  does an  $(n, k)$  cyclic code exist? List all possible  $k$ 's with corresponding generator polynomial(s).
- 9.32** Find a generator polynomial and the corresponding code words for a (7, 3) cyclic code. What is the minimum distance of this code?
- 9.33** Design an encoder for a (15, 11) cyclic code.
- 9.34** Using the generator polynomial  $g(p) = 1 + p + p^4$ , find the generator matrix and the parity check matrix (in systematic form) of a (15, 11) cyclic code.
- 9.35** Let  $g(p) = p^8 + p^6 + p^4 + p^2 + 1$  denote a polynomial over the binary field.
1. Find the lowest rate cyclic code whose generator polynomial is  $g(p)$ ; what is the rate of this code?
  2. Find the minimum distance of the code found in part 1.
  3. What is the coding gain for the code found in part 1?
- 9.36** The polynomial  $g(p) = p + 1$  over the binary field is considered.
1. Show that this polynomial can generate a cyclic code for any choice of  $n$ . Find the corresponding  $k$ .
  2. Find the systematic form of  $\mathbf{G}$  and  $\mathbf{H}$  for the code generated by  $g(p)$ .
  3. Can you say which type of code this generator polynomial generate?
- 9.37** Design a (6, 2) cyclic code by choosing the shortest possible generator polynomial.
1. Determine the generator matrix  $\mathbf{G}$  (in the systematic form) for this code and find all possible code words.
  2. How many errors can be corrected by this code?
  3. If this code is used in conjunction with binary PSK over an AWGN channel with  $P = 1$  W,  $N_0 = 2 \times 10^{-6}$  W/Hz, and  $W = 6 \times 10^4$  Hz and the

information is transmitted at the maximum theoretically possible speed, while avoiding ISI, find the upper bound on the block error probability assuming the receiver employs a soft-decision scheme.

- 9.38** The Golay code is a cyclic  $(23, 12)$  code with  $d_{\min} = 7$ . Show that if this code is used with interleaving/deinterleaving of depth 5, the resulting block of length 115 can correct single bursts of error of length up to 15.
- 9.39** Let  $C_1$  and  $C_2$  denote two cyclic codes with the same block length  $n$ , with generator polynomials  $g_1(p)$  and  $g_2(p)$  and with minimum distances  $d_1$  and  $d_2$ . Define  $C_{\max} = C_1 \cup C_2$  and  $C_{\min} = C_1 \cap C_2$ .
1. Is  $C_{\max}$  a cyclic code? Why? If yes, what are its generator polynomial and minimum distance?
  2. Is  $C_{\min}$  a cyclic code? Why? If yes, find its generator polynomial. What can you say about its minimum distance?
- 9.40** In a coded-communication system,  $M$  messages  $1, 2, \dots, M = 2^k$  are transmitted by  $M$  baseband signals  $x_1(t), x_2(t), \dots, x_M(t)$ , each of duration  $nT$ . The general form of  $x_i(t)$  is given by

$$x_i(t) = \sum_{j=0}^{n-1} \varphi_{ij}(t - jT)$$

where  $\varphi_{ij}(t)$  can be either of the two signals  $\phi_1(t)$  or  $\phi_2(t)$ , where  $\phi_1(t) = \phi_2(t) \equiv 0$  for all  $t \notin [0, T]$ . We further assume that  $\phi_1(t)$  and  $\phi_2(t)$  have equal energy  $\mathcal{E}$  and the channel is ideal (no attenuation) with additive white Gaussian noise of power-spectral density  $\frac{N_0}{2}$ . This means that the received signal is  $r(t) = x(t) + n(t)$ , where  $x(t)$  is one of the  $x_i(t)$ 's and  $n(t)$  represents the noise.

1. With  $\phi_1(t) = -\phi_2(t)$ , show that  $N$ , the dimensionality of the signal space, satisfies  $N \leq n$ .
2. Show that in general  $N \leq 2n$ .
3. With  $M = 2$ , show that for general  $\phi_1(t)$  and  $\phi_2(t)$

$$P(\text{error} | x_1(t) \text{ sent}) \leq \int \cdots \int_{R^N} \sqrt{p(\mathbf{r} | \mathbf{x}_1) p(\mathbf{r} | \mathbf{x}_2)} d\mathbf{r}$$

where  $\mathbf{r}$ ,  $\mathbf{x}_1$ , and  $\mathbf{x}_2$  are the vector representations of  $r(t)$ ,  $x_1(t)$ , and  $x_2(t)$  in the  $N$ -dimensional space.

4. Using the result of part 3, show that for general  $M$ ,

$$P(\text{error} | x_m(t) \text{ sent}) \leq \sum_{\substack{1 \leq m' \leq M \\ m' \neq m}} \int \cdots \int_{R^N} \sqrt{p(\mathbf{r} | \mathbf{x}_m) p(\mathbf{r} | \mathbf{x}_{m'})} d\mathbf{r}$$

5. Show that

$$\int \cdots \int_{R^N} \sqrt{p(\mathbf{r} | \mathbf{x}_m) p(\mathbf{r} | \mathbf{x}_{m'})} d\mathbf{r} = e^{-\frac{\|\mathbf{x}_m - \mathbf{x}_{m'}\|^2}{4N_0}}$$

and, therefore,

$$P(\text{error} | x_m(t) \text{ sent}) \leq \sum_{\substack{1 \leq m' \leq M \\ m' \neq m}} e^{-\frac{\|\mathbf{x}_m - \mathbf{x}_{m'}\|^2}{4N_0}}$$

9.41 A convolutional code is described by

$$\mathbf{g}_1 = [1 \ 0 \ 0]$$

$$\mathbf{g}_2 = [1 \ 0 \ 1]$$

$$\mathbf{g}_3 = [1 \ 1 \ 1]$$

1. Draw the encoder corresponding to this code.
2. Draw the state-transition diagram for this code.
3. Draw the trellis diagram for this code.
4. Find the transfer function and the free distance of this code.
5. Verify whether this code is catastrophic or not.

9.42 Show that in the trellis diagram of a convolutional code,  $2^k$  branches enter each state and  $2^k$  branches leave each state.

9.43 The block diagram of a binary convolutional code is shown in Figure P-9.43.

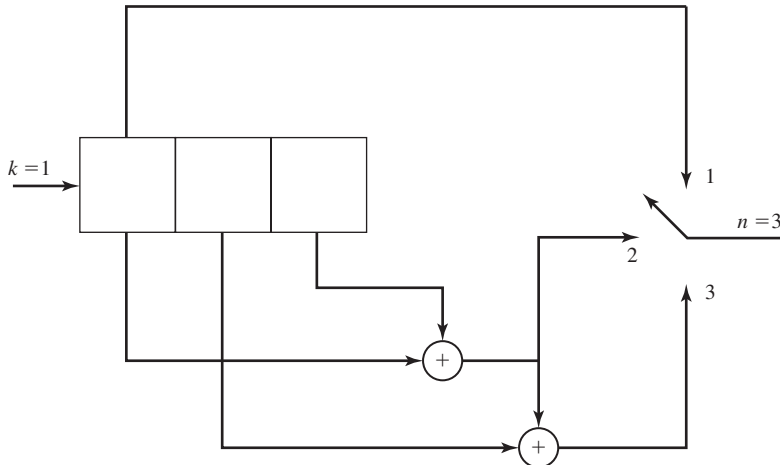


Figure P-9.43

1. Draw the state diagram for the code.
2. Find  $T(D)$ , the transfer function of the code.
3. What is  $d_{\text{free}}$ , the minimum free distance of the code?
4. Assume that a message has been encoded by this code and transmitted over a binary-symmetric channel with an error probability of  $p = 10^{-5}$ . If the received sequence is  $\mathbf{r} = (110, 110, 110, 111, 010, 101, 101)$ , using the Viterbi algorithm find the transmitted bit sequence.
5. Find an upper bound to bit-error probability of the code when the above binary-symmetric channel is employed. Make any reasonable approximations.

9.44 The block diagram of a (3, 1) convolutional code is shown in Figure P-9.44.

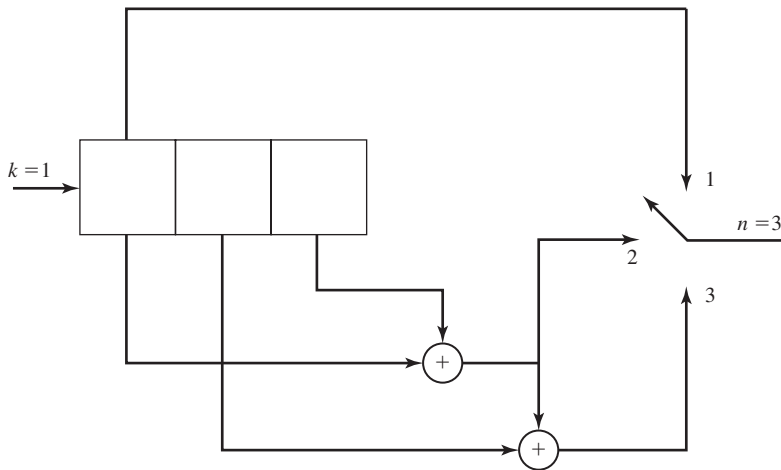


Figure P-9.44

1. Draw the state diagram of the code.
2. Find the transfer function  $T(D)$  of the code.
3. Find the minimum free distance ( $d_{\text{free}}$ ) of the code and show the corresponding path (at distance  $d_{\text{free}}$  from the all-zero code word) on the trellis.
4. Assume that four information bits,  $(x_1, x_2, x_3, x_4)$ , followed by two zero bits, have been encoded and sent via a binary-symmetric channel with crossover probability equal to 0.1. The received sequence is (111, 111, 111, 111, 111, 111). Use the Viterbi decoding algorithm to find the most likely data sequence.

- 9.45** The convolutional code of Problem 9.41 is used for transmission over a AWGN channel with hard-decision decoding. The output of the demodulator-detector is (101001011110111...). Using the Viterbi algorithm, find the transmitted sequence.
- 9.46** Repeat Problem 9.41 for a code with

$$\mathbf{g}_1 = [1 \ 1 \ 0]$$

$$\mathbf{g}_2 = [1 \ 0 \ 1]$$

$$\mathbf{g}_3 = [1 \ 1 \ 1]$$

- 9.47** Show the paths corresponding to all code words of weight 6 in Example 9.7.3.
- 9.48** In the convolutional code generated by the encoder shown in Figure P-9.48.

1. Find the transfer function of the code in the form  $T(N, D)$ .
2. Find  $d_{\text{free}}$  of the code.
3. If the code is used on a channel using hard-decision Viterbi decoding, assuming the crossover probability of the channel is  $p = 10^{-6}$ , use the hard-decision bound to find an upper bound on the average bit-error probability of the code.

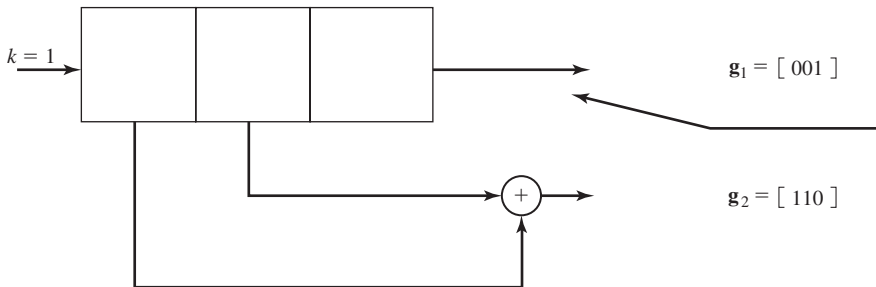


Figure P-9.48

- 9.49** Let  $\mathbf{x}_1$  and  $\mathbf{x}_2$  be two code words of length  $n$  with distance  $d$ , and assume that these two code words are transmitted via a binary-symmetric channel with crossover probability  $p$ . Let  $P(d)$  denote the error probability in transmission of these two code words.
1. Show that

$$P(d) \leq \sum_{i=1}^{2^n} \sqrt{p(\mathbf{y}_i | \mathbf{x}_1)p(\mathbf{y}_i | \mathbf{x}_2)}$$

where the summation is over all binary sequences  $\mathbf{y}_i$ .

2. From above, conclude that

$$P(d) \leq [4p(1-p)]^{\frac{d}{2}}$$

- 9.50 The complementary error function  $\operatorname{erfc}(x)$  is defined by

$$\operatorname{erfc}(x) = \frac{2}{\sqrt{\pi}} \int_x^{\infty} e^{-t^2} dt$$

1. Express  $Q(x)$  in terms of  $\operatorname{erfc}(x)$ .
2. Using the inequality

$$\operatorname{erfc}(\sqrt{x+y}) \leq \operatorname{erfc}(\sqrt{x}) e^{-y} \quad x \geq 0, \quad y \geq 0$$

prove the following bound on the average bit-error probability of a convolutional code, assuming that soft-decision decoding is employed.

$$P_b \leq \frac{1}{2k} \operatorname{erfc}(\sqrt{d_{\text{free}} R_c \rho_b}) e^{d_{\text{free}} R_c \rho_b} \left. \frac{\partial T(D, N)}{\partial N} \right|_{N=1, D=e^{-R_c \rho_b}}$$

- 9.51 A trellis-coded modulation system uses an 8-ary PAM signal set given by  $\{\pm 1, \pm 3, \pm 5, \pm 7\}$  and the 4-state trellis encoder shown in Figure 9.48(a).

1. Using the set partitioning rules, partition the signal set into four subsets.
2. If the channel is additive white Gaussian noise, and at the output of the matched filter the sequence  $(-.2, 1.1, 6, 4, -3, -4.8, 3.3)$  is observed, what is the most likely transmitted sequence?



# *Wireless Communications*

In Chapters 7 and 8, we described digital modulation and demodulation methods for transmission of information over two types of channels, namely, an additive Gaussian noise channel and a linear filter channel. Such channel models are appropriate for characterizing physical channels that are relatively static; i.e., the channel transmission characteristics are generally modeled as time invariant. In this chapter we treat modulation and demodulation techniques that are appropriate for wireless communication channels, such as radio and acoustic communication channels, whose transmission characteristics are time varying.

## 10.1 DIGITAL TRANSMISSION ON FADING MULTIPATH CHANNELS

Physical channels with time-varying transmission characteristics may be characterized as time-varying linear filters. Such linear filters are described by a time-varying impulse response  $h(\tau; t)$ , where  $h(\tau; t)$  is the response of the channel at time  $t$  due to an impulse applied at time  $t - \tau$ . Thus,  $\tau$  denotes the “age” (elapsed time) variable. The time-varying linear filter model of the channel with additive noise was previously shown in Figure 1.10. We cite the following examples of wireless communication channels that can be modeled in this manner.

**Signal Transmission via Ionospheric Propagation in the HF Band.** We recall from our discussion in Chapter 1 that sky-wave propagation, as illustrated in Figure 1.6, results from transmitted signals (in the HF frequency band) being bent or refracted by the ionosphere, which consists of several layers of charged particles ranging in altitude from 30–250 miles above the surface of the earth. As a consequence

of these ionospheric layers, the signal arrives at the receiver via different propagation paths at different delays. These signal components are called *multipath components*. The signal multipath components generally have different carrier-phase offsets and, hence, they may add destructively at times, resulting in a phenomenon called *signal fading*. Hence, signal fading is a result of multipath signal propagation. To characterize such channel behavior, we adopt a time-varying impulse response model.

**Mobile Cellular Transmission.** In mobile cellular radio transmission between a base station and a mobile telephone, the signal transmitted from the base station to the mobile receiver is usually reflected from surrounding buildings, hills, and other obstructions. As a consequence, we observe multiple propagation paths arriving at the receiver at different delays. Hence, the received signal has characteristics similar to those for ionospheric propagation. The same is true of transmission from the mobile telephone to the base station. Moreover, the speed that the mobile (automobile, train, etc.) is traveling results in frequency offsets, called *Doppler shifts*, of the various frequency components (see Problem 10.1) of the signal.

**Line-of-sight Microwave Radio Transmission.** In line-of-sight (LOS) radio transmission of signals, the transmitting and receiving antennas are generally mounted on high towers, in order to avoid obstructions, such as buildings and hills, in the path of signal propagation. However, when there are tall obstructions or hilly terrain in the path of propagation, it is likely that signals will be reflected from the ground to the receiving antenna as illustrated in Figure 10.1. This is especially a problem under severe weather conditions. In this case, there is a received signal component that arrives via the direct path and an ensemble of secondary paths that are reflected from the ground terrain. The latter arrive at the receiver with various delays and constitute multipath propagation. Relatively narrow-beamwidth antennas are employed in microwave LOS transmission to reduce the occurrence of secondary reflections. Nevertheless, some secondary signal reflections are frequently observed in practice. Such secondary signal reflections generally vary with time, so the channel may be characterized by a time-varying impulse response.

**Airplane-to-Airplane Radio Communications.** In radio communications between two aircraft, it is possible for secondary signal components to be received from ground reflections, as illustrated in Figure 10.2. This is especially the case when omnidirectional antennas are employed in the communication system. The ensemble of

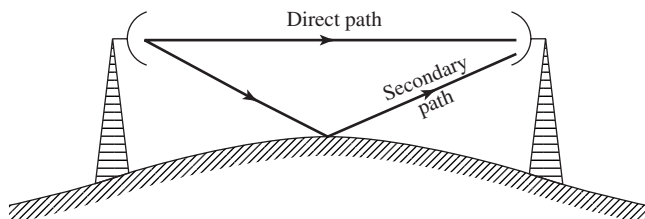


**Figure 10.1** Illustration of multipath propagation in LOS microwave transmission.

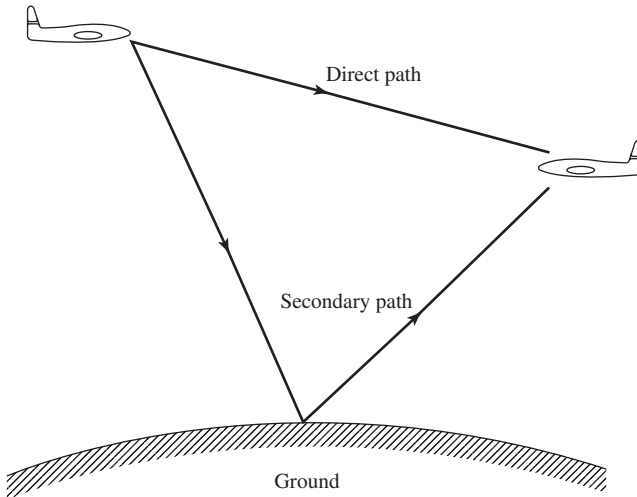


**Figure 10.2** Illustration of multipath propagation in airplane-to-airplane communications.

ground-reflected signal components generally arrive at the receiver with different delays and different attenuations. In addition, the motions of the aircraft result in Doppler frequency offsets in the various signal components. In many respects, this situation is similar to that in mobile cellular communications.

**Underwater Acoustic Signal Transmission.** A shallow-water acoustic channel is generally characterized as a multipath channel due to acoustic signal reflections from the surface and the bottom of the sea. Because of wave motion, the signal multipath components undergo time-varying propagation delays which result in signal fading. In addition, there is frequency-dependent attenuation, which increases proportionally as the square of the signal frequency.

The channels briefly described above may be generally characterized as linear systems with time-varying impulse responses. Since it is generally difficult, if not impossible, to characterize the microscopic effects of signal transmission on channels as the ones described above in a deterministic fashion, it is logical to adopt a statistical characterization. Such an approach is described below.

### 10.1.1 Channel Models for Time-Variant Multipath Channels

As we have observed, there are basically two distinct characteristics of the types of radio channels described above. One characteristic is that the transmitted signal arrives at the receiver via multiple propagation paths, each of which has an associated time delay. For example, if we transmit an extremely short pulse, the channel response due to multiple scatterers (such as ionized particles in the ionosphere) might appear as shown in Figure 10.3. Because the received signal is spread in time due to the multiple scatterers at different delays, we say that the channel is time dispersive.

A second characteristic of the types of radio channels described above is concerned with the time variations in the structure of the medium. As a result of such

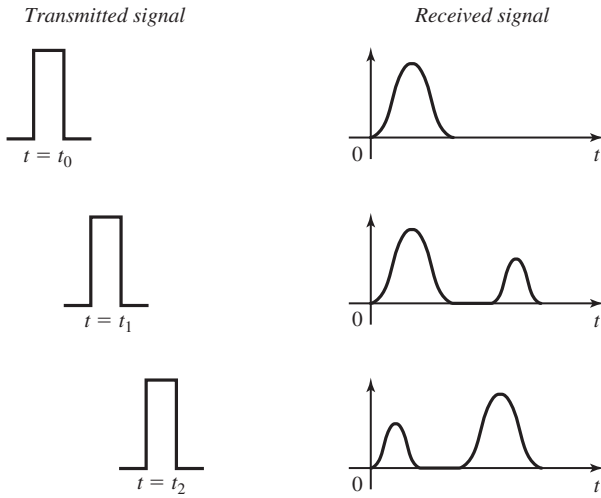


**Figure 10.3** Illustration of time-variant channel response characteristics.

time variations, the response of the channel to any signal transmitted through it will change with time. Hence, if we repeat the short pulse transmission experiment over and over, we would observe changes in the received signal, which are due to physical changes in the medium. Such changes include variations in the relative delays of signals from the multiple scatterers. Hence, the received signal might appear as illustrated in Figure 10.3. In other words, the impulse response of the channel is varying with time. In general, the time variations in the received signal appear to be unpredictable to the user of the channel. This leads us to characterize the time-variant multipath channel statistically.

To obtain a statistical description of the channel, let us consider the transmission of an unmodulated carrier

$$c(t) = A \cos 2\pi f_c t \quad (10.1.1)$$

The received signal in the absence of noise may be expressed as

$$\begin{aligned} x(t) &= A \sum_n \alpha_n(t) \cos[2\pi f_c(t - \tau_n(t))] \\ &= A \operatorname{Re} \left[ \sum_n \alpha_n(t) e^{-j2\pi f_c \tau_n(t)} e^{j2\pi f_c t} \right] \end{aligned} \quad (10.1.2)$$

where  $\alpha_n(t)$  is the time-variant attenuation factor associated with the  $n$ th propagation path and  $\tau_n(t)$  is the corresponding propagation delay. The complex-valued signal

$$\begin{aligned} z(t) &= \sum_n \alpha_n(t) e^{-j2\pi f_c \tau_n(t)} \\ &= \sum_n \alpha_n(t) e^{-j\phi_n(t)} \end{aligned} \quad (10.1.3)$$

represents the response of the channel to the complex exponential  $\exp(j2\pi f_c t)$ . We note that, although the input to the channel is a monochromatic signal; i.e., a signal at a single frequency, the output of the channel consists of a signal that contains many different frequency components. These new components are generated as a result of the time variations in the channel response. The r.m.s. (root-mean-square) spectral width of  $z(t)$  is called the *Doppler frequency spread* of the channel and is denoted as  $B_d$ . This quantity is a measure of how rapidly the signal  $z(t)$  is changing with time. If  $z(t)$  changes slowly, the Doppler frequency spread is relatively small, while if  $z(t)$  changes rapidly, the Doppler frequency spread is large.

We may view the received complex-valued signal  $z(t)$  in Equation (10.1.3) as the sum of a number of vectors (phasors) each of which has a time-variant amplitude  $\alpha_n(t)$  and phase  $\phi_n(t)$ . In general, it takes large dynamic changes in the physical medium to cause a large change in  $\{\alpha_n(t)\}$ . On the other hand, the phases  $\{\phi_n(t)\}$  will change by  $2\pi$  radians whenever  $\{\tau_n(t)\}$  change by  $1/f_c$ . But  $1/f_c$  is a small number and, hence, the phases  $\{\phi_n(t)\}$  change by  $2\pi$  or more radians with relatively small changes of the medium characteristics. We also expect the delays  $\{\tau_n(t)\}$  associated with the different signal paths to change at different rates and in an unpredictable (random) manner. This implies that the complex-valued signal  $z(t)$  in Equation (10.1.3) can be modeled as a random process. When there are a large number of signal propagation paths, the central limit theorem can be applied. Thus,  $z(t)$  can be modeled as a complex-valued Gaussian random process.

The multipath propagation model for the channel, embodied in the received signal  $x(t)$  or, equivalently,  $z(t)$  given by Equation (10.1.3), results in signal fading. The fading phenomenon is primarily a result of the time-variant phase factors  $\{\phi_n(t)\}$ . At times, the complex-valued vectors in  $z(t)$  add destructively to reduce the power level of the received signal. At other times, the vectors in  $z(t)$  add constructively and, thus, produce a large signal value. The amplitude variations in the received signal due to the time-variant multipath propagation in the channel are usually called *signal fading*.

**Tapped Delay Line Channel Model.** A general model for a time-variant multipath channel is illustrated in Figure 10.4. The channel model consists of a tapped delay line with uniformly spaced taps. The tap spacing between adjacent taps is  $1/W$ , where  $W$  of the signal transmitted through the channel. Hence,  $1/W$  is the time resolution that can be achieved by transmitting a signal of bandwidth  $W$ . The tap coefficients, denoted as  $\{c_n(t) \equiv \alpha_n(t)e^{j\phi_n(t)}\}$  are usually modeled as complex-valued, Gaussian random processes which are mutually uncorrelated. The length of the delay line corresponds to the amount of time dispersion in the multipath channel, which is usually called the *multipath spread*. We denote the multipath spread as  $T_m = L/W$ , where  $L$  represents the maximum number of possible multipath signal components.

#### Example 10.1.1

Determine an appropriate channel model for two-path ionospheric propagation, where the relative time delay between the two received signal paths is 1 msec and the transmitted signal bandwidth  $W$  is 10 kHz.

**Solution** A 10-kHz signal can provide a time resolution of  $1/W = 0.1$  msec. Since the relative time delay between the two received signal paths is 1 msec, the tapped delay line

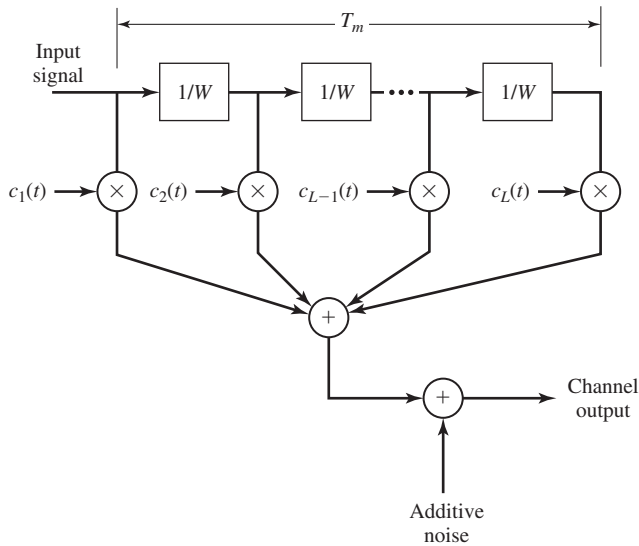


**Figure 10.4** Model for time-variant multipath channel.

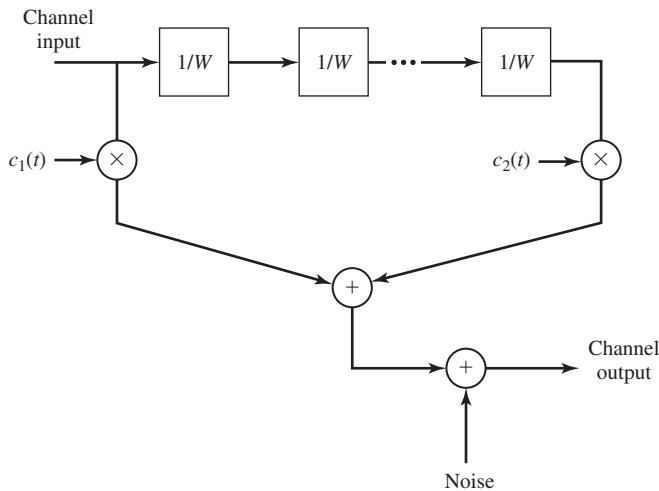


**Figure 10.5** Channel model for two-path channel in Example 10.1.1.

model consists of 10 taps, with only the first tap and the last tap having non-zero, time-varying coefficients, denoted as  $c_1(t)$  and  $c_2(t)$ , as shown in Figure 10.5. Because  $c_1(t)$  and  $c_2(t)$  represent the signal response of a large number of ionized particles from two different regions of the ionosphere, we may characterize  $c_1(t)$  and  $c_2(t)$  as complex-valued, uncorrelated Gaussian random processes. The rate of variation of the tap coefficients determine the value of the Doppler spread for each path.

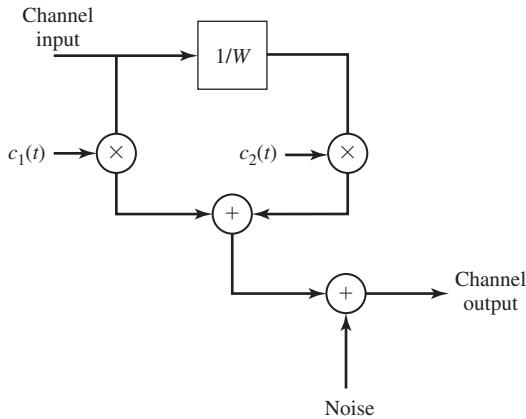


**Figure 10.6** Channel model for two-path channel in Example 10.1.2.

### Example 10.1.2

Determine an appropriate channel model for an airplane-to-airplane communication link in which there is a direct signal propagation path, and a secondary propagation resulting from signal scattering due to the surrounding ground terrain. The secondary path has a propagation delay of  $\tau_0 = 10 \mu\text{sec}$  relative to the propagation delay of the direct path. The signal bandwidth is  $W = 100 \text{ kHz}$ .

**Solution** A 100-kHz signal provides a time resolution of  $1/W = 10 \mu\text{sec}$ . Consequently, the secondary signal path is resolvable, since its relative time delay is  $10 \mu\text{sec}$ . In this case, a channel model that has two taps with tap coefficients  $c_1(t) = \alpha_1(t) e^{j\phi_1(t)}$  and  $c_2(t) = \alpha_2(t) e^{j\phi_2(t)}$ , as shown in Figure 10.6, is appropriate. The direct path may be modeled as having a fixed (time-invariant) attenuation  $\alpha_1$ , but a time-varying phase shift. The secondary path, which results from ground terrain, is modeled as having a time-varying attenuation and phase shift, since the ground terrain is changing with time due to the motion of the airplanes. In this case, it is appropriate to model  $c_2(t)$  as a complex-valued, Gaussian random process. The rates of variation of the tap coefficients,  $c_1(t)$  and  $c_2(t)$ , determine the value of the Doppler frequency spreads for these paths. Note that, in both the direct and the reflected signal paths, there will be Doppler frequency shifts resulting from motion of the aircraft.

### Example 10.1.3

Determine the appropriate channel model for the airplane-to-airplane communication link described in Example 10.1.2, but now assume that the transmitted signal bandwidth is 10 kHz.

**Solution** A 10-kHz signal provides a time resolution of  $100 \mu\text{sec}$ . Since the relative delay between the two signal components is  $10 \mu\text{sec}$ , the two signal paths are not resolvable in time. Consequently, the channel appears as a single path channel with tap coefficient  $c(t)$  that includes the direct path and the secondary path. Since the secondary path results from signal scattering from a large number of scatterers, we may characterize  $c(t)$  as a complex-valued Gaussian random process with a mean value of  $\alpha_1 e^{j\phi_1(t)}$ , which is due to the direct path.

**Rayleigh and Ricean Fading Models.** In the channel models described in Examples 10.1.2 and 10.1.3, the tap coefficients in the tapped-delay line model were characterized as complex-valued Gaussian random processes. We may express each of the tap coefficients as

$$c(t) = c_r(t) + jc_i(t) \quad (10.1.4)$$

where  $c_r(t)$  and  $c_i(t)$  represent real-valued Gaussian random processes. We assume that  $c_r(t)$  and  $c_i(t)$  are stationary and statistically independent. This assumption generally holds for the tapped delay model of physical channels.

We may also express  $c(t)$  in the form as

$$c(t) = \alpha(t) e^{j\phi(t)} \quad (10.1.5)$$

where

$$\begin{aligned} \alpha(t) &= \sqrt{c_r^2(t) + c_i^2(t)} \\ \phi(t) &= \tan^{-1} \frac{c_i(t)}{c_r(t)} \end{aligned} \quad (10.1.6)$$

In this representation, if  $c_r(t)$  and  $c_i(t)$  are Gaussian with zero-mean values, the amplitude  $\alpha(t)$  is characterized statistically by the Rayleigh probability distribution and  $\phi(t)$  is uniformly distributed over the interval  $(0, 2\pi)$ . As a consequence, the channel is called a *Rayleigh fading channel*. The Rayleigh fading signal amplitude is described by the PDF

$$f(\alpha) = \frac{\alpha}{\sigma^2} e^{-\alpha^2/2\sigma^2}, \quad \alpha \geq 0 \quad (10.1.7)$$

and  $f(\alpha) = 0$  for  $\alpha < 0$ . The parameter  $\sigma^2 = E(c_r^2) = E(c_i^2)$ .

On the other hand, if  $c_r(t)$  and  $c_i(t)$  are Gaussian with nonzero mean as in the airplane-to-airplane communication link described in Example 10.1.3, the amplitude  $\alpha(t)$  is characterized statistically by the Rice probability distribution and the phase  $\phi(t)$  is also nonzero mean. In this case the channel is called a *Ricean fading channel* and the PDF of the amplitude is given as

$$f(\alpha) = \frac{\alpha}{\sigma^2} e^{-(\alpha^2+s^2)/2\sigma^2} I_0\left(\frac{s\alpha}{\sigma^2}\right), \quad \alpha \geq 0 \quad (10.1.8)$$

where the parameter  $s^2$  represents the power of the received nonfading signal component and  $\sigma^2 = \text{VAR}(c_r) = \text{VAR}(c_i)$ .

**Propagation Models for Mobile Radio Channels.** In the link budget calculations that were described in Section 7.7.2, we had characterized the path loss of radio waves propagating through free space as being inversely proportional to  $d^2$ , where  $d$  is the distance between the transmitter and the receiver. However, in a mobile radio channel, propagation is generally neither free space nor LOS. The mean path loss encountered in mobile radio channels may be characterized as being inversely proportional



to  $d^p$ , where  $2 \leq p \leq 4$ , with  $d^4$  being a worst-case model. Consequently, the path loss is usually much more severe compared to that of free space.

There are a number of factors affecting the path loss in mobile radio communications. Among these factors are base-station antenna height, mobile antenna height, operating frequency, atmospheric conditions, and presence or absence of buildings and trees. Various mean path loss models have been developed that incorporate such factors. For example, a model for a large city in an urban area is the Hata model, in which the mean path loss is expressed as

$$\begin{aligned} \text{Loss in dB} = & 69.55 + 26.16 \log_{10} f - 13.82 \log_{10} h_t - a(h_r) \\ & + (44.9 - 6.55 \log_{10} h_t) \log_{10} d \end{aligned} \quad (10.1.9)$$

where  $f$  is the operating frequency in MHz ( $150 < f < 1500$ ),  $h_t$  is the transmitter antenna height in meters ( $30 < h_t < 200$ ),  $h_r$  is the receiver antenna height in meters ( $1 < h_r < 10$ ),  $d$  is the distance between transmitter and receiver in km ( $1 < d < 20$ ), and

$$a(h_r) = 3.2(\log_{10} 11.75h_r)^2 - 4.97, \quad f \geq 400 \text{ MHz} \quad (10.1.10)$$

In mobile radio communications we often encounter the effect of shadowing of the signal due to large obstructions, such as large buildings, trees, and hilly terrain between the transmitter and the receiver. Shadowing is usually modeled as a multiplicative and, generally, slowly time-varying random process; i.e., the received signal may be characterized mathematically as

$$r(t) = A_0 g(t) s(t) \quad (10.1.11)$$

where  $A_0$  represents the mean path loss,  $s(t)$  is the transmitted signal, and  $g(t)$  is a random process that represents the shadowing effect. At any time instant, the shadowing process is modeled statistically as lognormally distributed. The PDF for the lognormal distribution is

$$f(g) = \begin{cases} \frac{1}{\sqrt{2\pi\sigma^2}g} e^{-(\ln g - \mu)^2/2\sigma^2} & (g \geq 0) \\ 0, & (g < 0) \end{cases} \quad (10.1.12)$$

If we define a new random variable  $X$  as  $X = \ln g$ , then

$$f(x) = \frac{1}{\sqrt{2\pi\sigma^2}} e^{-(x-\mu)^2/2\sigma^2}, \quad -\infty < x < \infty \quad (10.1.13)$$

The random variable  $X$  represents the path loss measured in dB,  $\mu$  is the mean path loss in dB and  $\sigma$  is the standard deviation of the path loss in dB. For a typical cellular environment,  $\sigma$  is in the range of 5–12 dB.

**The Coherence Time and Coherence Bandwidth of the Channel.** Besides the multipath (time) spread  $T_m$  and the Doppler (frequency) spread  $B_d$ , there are two other parameters that are useful in characterizing fading, multipath channels. One parameter is the reciprocal of the Doppler spread. This quantity is a measure of the time interval over which the channel characteristics will change very little. We call this

parameter the *coherence time* of the channel, and define it as

$$T_{ct} = \frac{1}{B_d} \quad (10.1.14)$$

The other useful parameter is the reciprocal of the multipath spread, which has units of frequency. This quantity is a measure of the bandwidth over which the channel characteristics (magnitude  $\alpha(t)$  and phase  $\phi(t)$ ) are highly correlated. In other words, all frequency components of a signal within this bandwidth will fade simultaneously. We call this parameter the *coherence bandwidth* of the channel and define it as

$$B_{cb} = \frac{1}{T_m} \quad (10.1.15)$$

#### Example 10.1.4

Consider the communication link described in Example 10.1.1. Determine the coherence bandwidth of this channel.

**Solution** The multipath spread for this channel is  $T_m = 1$  msec. Hence, the coherence bandwidth of the channel is  $1/T_m = 1000$  Hz. Within this bandwidth, all frequency components of a signal will be affected similarly by the channel. For example, all frequency components of a signal that fall within the coherence bandwidth will fade simultaneously.

Examples 10.1.1, 10.1.3, and 10.1.4 provide some indication on the role that the signal bandwidth plays in relation to the characteristics of the channel model. For example, if the transmitted signal has a bandwidth  $W$  that is larger than the coherence bandwidth  $B_{cb}$  of the channel ( $W > B_{cb}$ ), as is the case in Example 10.1.1 and 10.1.2, the multipath components are resolvable and, as a consequence, frequency components of the transmitted signal that are separated by more than  $B_{cb}$  are affected (attenuated and phase shifted) differently by the channel. In such a case we say that the channel is *frequency selective*. On the other hand, if the signal bandwidth  $W$  is smaller than  $B_{cb}$  ( $W < B_{cb}$ ), as is the case in Example 10.1.3, all the frequency components in the signal are affected (attenuated and phase shifted) similarly by the channel at any instant in time. In such a case, we say that the channel is *frequency nonselective*.

**The Channel Spread Factor.** The product  $T_m B_d = T_m / T_{ct}$  is usually called the *channel spread factor*. If  $T_m B_d < 1$ , the channel is called *underspread* and if  $T_m B_d > 1$ , the channel is said to be *overspread*. The spread factor usually provides some indication on whether or not phase-coherent demodulation is possible at the receiver. In general, if the channel is overspread, due either to a large multipath spread or a large Doppler spread or both, the estimation of the carrier phase is extremely difficult because of the rapid time variations ( $T_{ct} \ll T_m$ ) in the channel that occur in the time interval  $T_m$ . On the other hand, if the channel is underspread, the channel-time variation is slow relative to the multipath spread ( $T_{ct} \gg T_m$ ) and, hence, the carrier phase of the received signal can be estimated with good precision. Fortunately, most physical time-varying channels encountered in practice are underspread.

Next, we describe how these channel parameters are used in the design of modulation signals for transmitting digital information over the channel. Table 10.1 lists the

**TABLE 10.1** MULTIPATH SPREAD, DOPPLER SPREAD, AND SPREAD FACTOR FOR SEVERAL TIME-VARIANT MULTIPATH CHANNELS

Type of channel	Multipath duration (s)	Doppler spread (Hz)	Spread factor
Shortwave ionospheric propagation (HF)	$10^{-3} - 10^{-2}$	$10^{-1} - 1$	$10^{-4} - 10^{-2}$
Ionospheric propagation under disturbed auroral conditions	$10^{-3} - 10^{-2}$	10 – 100	$10^{-2} - 1$
Ionospheric forward scatter (VHF)	$10^{-4}$	10	$10^{-3}$
Tropospheric scatter	$10^{-6}$	10	$10^{-5}$
Mobile cellular (UHF)	$10^{-5}$	100	$10^{-3}$

values of these channel parameters for several multipath channels. Although we focus our treatment on binary modulation, the basic concepts carry over to  $M$ -ary modulation without exceptions.

### 10.1.2 Signal Design for Fading Multipath Channels

There are different approaches that one can take in the design of signals for transmitting digital information through a fading multipath channel. Although, in principle, any of the carrier-modulation methods (PAM, QAM, PM, and FSK) are applicable, signal fading generally causes large fluctuations in the received signal amplitude and, consequently, it is extremely difficult to discriminate among multiple-amplitude levels in the received signal. For this reason, PAM and QAM are often avoided for digital communications through fading channels. In our discussion, we shall focus our attention on digital-phase modulation (PSK) and frequency-shift keying (FSK).

As indicated in the previous section, the available channel bandwidth plays an important role in the design of the modulation. If the bandwidth that is allocated to the user exceeds the coherence bandwidth  $B_{cb}$  of the channel, we have basically two options. One option is to transmit the information on a single sinusoidal carrier, using a signal that occupies the entire available channel bandwidth. In this case, the multipath signal components are resolvable to within a time resolution of  $1/W$ . Hence, signal propagation paths that differ in time-of-arrival at the receiver by a time interval greater than or equal to  $1/W$  will be distinguishable as separate propagating signal components. The number of distinct signal components depends on the channel characteristics. For example, in the airplane-to-airplane communication link, we would expect to see the direct path and the ground-reflected path. In radio-signal transmission via ionospheric propagation in the HF frequency band, the number of received signal components depends on the number of ionospheric reflecting layers and the possibility of paths arriving by multiple skips.

We observe that, when  $W > B_{cb}$ , the received signal may be corrupted by inter-symbol interference, unless the symbol rate is selected to be significantly smaller than the multipath spread  $T_m$ . We recall that the symbol rate  $1/T$  satisfies the condition

$$\frac{1}{T} \leq 2W \quad (10.1.16)$$

For example, if we select the symbol rate  $1/T = W$ , then, since  $T_m > 1/W$ , it follows that  $T_m > T$ . In this case, the receiver encounters intersymbol interference (ISI) and must employ some type of equalization, as previously described in Section 8.6. On the other hand, if the symbol rate is selected to be very small; i.e.,  $T \gg T_m$ , then the ISI becomes insignificant and no equalization is necessary. Such signal design is usually accomplished by the use of spread-spectrum signals, as described in Section 10.3. Further discussion on this topic is deferred to Section 10.3.2.

#### Example 10.1.5 Single Carrier Signal Transmission

Suppose that an HF channel with a nominal bandwidth allocation of 3200 Hz is to be used for transmitting digital information at a rate of either (1) 4800 bits/sec or (2) 20 bits/sec. The channel multipath spread is  $T_m = 5$  msec. Specify a modulation method for achieving the desired data rates and indicate whether or not an equalizer is necessary at the receiver for the intersymbol interference.

**Solution** For the 4800-bps system, we select a symbol rate of 2400 symbols/second and four-phase modulation (either coherent PSK or DPSK). A symbol rate of 2400 can be accommodated in a channel bandwidth of 3200 Hz, since there is an excess bandwidth of 800 Hz. A transmitting filter with a raised cosine spectral characteristic may be used to obtain the desired signal shaping. The symbol rate  $1/T = 2400$  means that the received signal will be corrupted by intersymbol interference ( $T_m \gg T$ ), which will require the use of an equalizer to reduce its effect on performance.

For the low rate of 20 bits/sec we may again employ four-phase modulation (PSK or DPSK). Thus, the symbol rate is 10 symbols/sec and, hence,  $T = 100$  msec. Since  $T \gg T_m$ , the effect of the multipath spread is negligible and no equalization is necessary at the receiver. To use the entire channel bandwidth, we may employ a phase-modulated spread-spectrum signal as described in Section 10.3.

#### Example 10.1.6 Multicarrier OFDM Signal Transmission

Consider an HF channel which has a nominal bandwidth of 3200 Hz and a multipath spread of  $T_m = 1$  msec. Design a multiple-carrier OFDM signal that achieves a data rate of 4800 bits/sec.

**Solution** We may select the number  $N$  of subcarriers to be as large as we like so as to achieve the desired condition that  $T_{sc} \gg T_m$ , where  $T_{sc}$  is the symbol duration for each subcarrier. However, the complexity of the demodulator increases, as  $N \log_2 N$  (computational complexity of FFT algorithm) and the demodulation delay for delivering the information to the user increases (linearly) with  $N$ . Therefore, it is desirable to keep  $N$  as small as possible. Suppose we select  $N$  such that  $T_{sc} = 100$  msec. Then, each subchannel may be as narrow<sup>†</sup> as  $W_{ac} \approx \frac{1}{T_{sc}} = 10$  Hz. Note that  $W_{sc} \ll B_{cb} = 1000$  Hz as desired. If we employ four-phase (PSK or DPSK) modulation in each subchannel, we achieve a bit rate of 20 bits/sec, per subchannel. With  $N = 240$  subchannels, we achieve the desired data rate of 4800 bps.

As previously indicated in Section 8.7, a disadvantage of multicarrier OFDM modulation is the relatively high peak-to-average ratio (PAR) that is inherent in the

<sup>†</sup>In practice, it will be necessary to have some excess bandwidth in each subchannel. The excess bandwidth may be in the range of 25–50%.

transmitted signal. In general, large peaks occur in the transmitted signal when the signals in many of the subchannels add constructively in phase. Such large signal peaks may saturate the power amplifier and, thus, cause intermodulation distortion in the transmitted signal. One way to avoid intermodulation distortion is to reduce the power in the transmitted signal and, thus, operate the power amplifier at the transmitter in its linear operating range. However, this power reduction or “power backoff” results in inefficient operation of the communication system. For this reason, alternative methods have been developed to reduce the PAR in OFDM systems. The interested reader is referred to the references cited at the end of Chapter 8.

In the above discussion, we assumed that the available channel bandwidth exceeds the coherence bandwidth  $B_{cb}$  of the channel. On the other hand, if the channel bandwidth is much smaller than  $B_{cb}$ , there is no point in designing a multicarrier system. A single-carrier system can be designed using the entire bandwidth, with a symbol rate of  $W \leq 1/T \leq 2W$ . In this case  $T \gg T_m$ , so that the effect of intersymbol interference on the performance of the system is negligible.

Next, we evaluate the performance of the demodulator and detector for a PSK, DPSK, and FSK modulations in a Rayleigh fading channel under the condition that intersymbol interference is negligible.

### 10.1.3 Performance of Binary Modulation in Frequency Nonselective Rayleigh Fading Channels

In this section, we determine the probability of error at the receiver of a binary digital communication system that transmits information through a Rayleigh fading channel. The signal bandwidth  $W$  is assumed to be much smaller than the coherence bandwidth  $B_{cb}$  of the channel, as in Example 10.1.3. Since the multipath components are not resolvable, the channel is frequency nonselective and, hence, the channel impulse response is represented as

$$h(\tau; t) = \alpha(t)\delta(\tau - \tau_0(t)) \quad (10.1.17)$$

where  $\alpha(t)$  has a Rayleigh distribution at any instant in time.

We assume that the time variations of  $\alpha(t)$  and  $\tau_0(t)$  are very slow compared to the symbol interval, so that within the time interval  $0 \leq t \leq T$ , the channel impulse response is constant; i.e.,

$$h(\tau; t) \equiv h(\tau) = \alpha\delta(\tau - \tau_0) \quad (10.1.18)$$

where the amplitude  $\alpha$  is Rayleigh distributed; i.e.,

$$f(\alpha) = \begin{cases} \frac{\alpha}{\sigma^2} e^{-\alpha^2/2\sigma^2}, & \alpha > 0 \\ 0, & \text{otherwise} \end{cases} \quad (10.1.19)$$

Now, suppose that binary antipodal signals; e.g., binary PSK, are used to transmit the information through the channel. Hence, the two possible signals are

$$u_m(t) = \sqrt{\frac{2\mathcal{E}_b}{T}} \cos(2\pi f_c t + m\pi) + n(t), \quad m = 0, 1 \quad (10.1.20)$$

The received signal in the interval  $0 \leq t \leq T$  is

$$r(t) = \alpha \sqrt{\frac{2\mathcal{E}_b}{T}} \cos(2\pi f_c t + m\pi + \phi) + n(t) \quad (10.1.21)$$

where  $\phi$  is the carrier-phase offset. Let us assume that  $\phi$  is known to the demodulator, which crosscorrelates  $r(t)$  with

$$\psi(t) = \sqrt{\frac{2}{T}} \cos(2\pi f_c t + \phi), \quad 0 \leq t \leq T \quad (10.1.22)$$

Hence, the input to the detector at the sampling instant is

$$r = \alpha \sqrt{\mathcal{E}_b} \cos m\pi + n, \quad m = 0, 1 \quad (10.1.23)$$

For a fixed value of  $\alpha$ , the probability of error is the familiar form

$$P_b(\alpha) = Q\left(\sqrt{\frac{2\alpha^2\mathcal{E}_b}{N_0}}\right) \quad (10.1.24)$$

We view  $P_b(\alpha)$  as a conditional probability of error for a given value of the channel attenuation  $\alpha$ . To determine the probability of error averaged over all possible values of  $\alpha$ , we compute the integral

$$P_b = \int_0^\infty P_b(\alpha) f(\alpha) d\alpha \quad (10.1.25)$$

where  $f(\alpha)$  is the Rayleigh PDF given by Equation (10.1.19). This integral has the simple closed form expression

$$P_b = \frac{1}{2} \left[ 1 - \sqrt{\frac{\bar{\rho}_b}{1 + \bar{\rho}_b}} \right] \quad (10.1.26)$$

where, by definition,

$$\bar{\rho}_b = \frac{\mathcal{E}_b}{N_0} E(\alpha^2) \quad (10.1.27)$$

Hence,  $\bar{\rho}_b$  is the average received SNR/bit and  $E(\alpha^2) = 2\sigma^2$ .

If the binary signals are orthogonal, as in orthogonal FSK, where the two possible transmitted signals are given as

$$u_m(t) = \sqrt{\frac{2\mathcal{E}_b}{N_0}} \cos \left[ 2\pi \left( f_c + \frac{m}{2T} \right) t \right], \quad m = 0, 1, \quad (10.1.28)$$

the received signal is

$$r(t) = \alpha \sqrt{\frac{2\mathcal{E}_b}{T}} \cos \left[ 2\pi \left( f_c + \frac{m}{2T} \right) t + \phi \right] + n(t) \quad (10.1.29)$$

In this case, the received signal is crosscorrelated with the two signals

$$\begin{aligned} \psi_1(t) &= \sqrt{\frac{2}{T}} \cos(2\pi f_c t + \phi) \\ \psi_2(t) &= \sqrt{\frac{2}{T}} \cos \left[ 2\pi \left( f_c + \frac{1}{2T} \right) t + \phi \right] \end{aligned} \quad (10.1.30)$$

If  $m = 0$ , for example, the two correlator outputs are

$$\begin{aligned} r_1 &= \alpha \sqrt{\mathcal{E}_b} + n_1 \\ r_2 &= n_2 \end{aligned} \quad (10.1.31)$$

where  $n_1$  and  $n_2$  are the additive noise components at the outputs of the two correlators. Hence, the probability of error is simply the probability that  $r_2 > r_1$ . Since the signals are orthogonal, the probability of error for a fixed value of  $\alpha$  has the familiar form

$$P_b(\alpha) = Q \left( \sqrt{\frac{\alpha^2 \mathcal{E}_b}{N_0}} \right) \quad (10.1.32)$$

As in the case of antipodal signals, the average probability of error over all values of  $\alpha$  is determined by evaluating the integral in Equation (10.1.25). Thus, we obtain

$$P_b = \frac{1}{2} \left[ 1 + \sqrt{\frac{\bar{\rho}_b}{2 + \bar{\rho}_b}} \right] \quad (10.1.33)$$

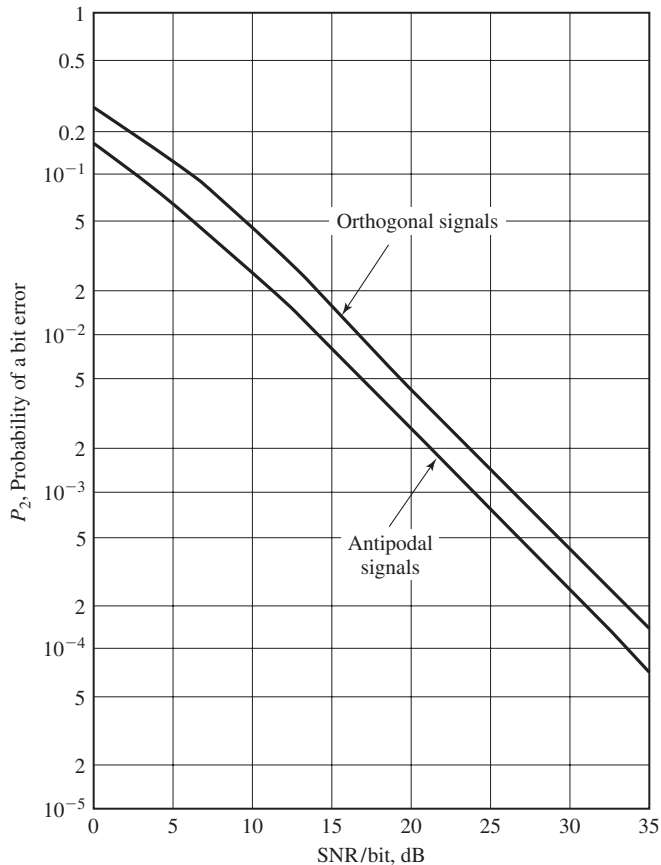
where  $\bar{\rho}_b$  is the average SNR/bit defined by Equation (10.1.27).

Figure 10.7 illustrates the average probability of error for binary antipodal and orthogonal signals. The striking aspects of these graphs is the slow decay of the probability of error as a function of SNR. In fact, for large values of  $\bar{\rho}_b$ , the probability of error for binary signals is

$$\begin{aligned} P_b &\approx \frac{1}{4\bar{\rho}_b}, & \text{antipodal signals} \\ P_b &\approx \frac{1}{2\bar{\rho}_b}, & \text{orthogonal signals} \end{aligned} \quad (10.1.34)$$

Hence the probability of error in both cases decreases only inversely as the SNR. This is in contrast to the exponential decrease in the case of the AWGN channel. We also note that the difference in SNR between antipodal signals (binary PSK) and orthogonal signals (binary FSK) is 3 dB.

Two other types of signal modulation are DPSK and noncoherent FSK. For completeness, we state that the average probability of error for these signals (see



**Figure 10.7** Performance of binary signaling on a Rayleigh fading channel.

Problem 10.3) is

$$P_b = \frac{1}{2(1 + \bar{\rho}_b)}, \quad \text{DPSK} \quad (10.1.35)$$

$$P_b = \frac{1}{2 + \bar{\rho}_b}, \quad \text{noncoherent FSK} \quad (10.1.36)$$

#### 10.1.4 Performance Improvement Through Signal Diversity

The basic problem in digital communication through a fading channel is that a large number of errors occur when the channel attenuation is large; i.e., when the channel is in a deep fade. If we can supply to the receiver two or more replicas of the same information signal transmitted through independently fading channels, the probability that all the signal components will fade simultaneously is reduced considerably. If  $p$



is the probability that any one signal will fade below some critical value, than  $p^D$  is the probability that all  $D$  independently fading replicas of the same signal will fade below the critical value. There are several ways that we can provide the receiver with  $D$  independently fading replicas of the same information-bearing signal.

One method for achieving  $D$  independently fading versions of the same information-bearing signal is to transmit the same information on  $D$  OFDM carrier frequencies, where the separation between successive carriers equals or exceeds the coherence bandwidth  $B_{cb}$  of the channel. This method is called *frequency diversity*.

A second method for achieving  $D$  independently fading versions of the same information-bearing signal is to transmit the same information in  $D$  different time slots, where the time separation between successive time slots equals or exceeds the coherence time  $T_{ct}$  of the channel. This method is called *time diversity*.

Another commonly used method for achieving diversity is via use of multiple receiving antennas, but only one transmitting antenna. The receiving antennas must be spaced sufficiently far apart so that the multipath components in the signal have significantly different propagation paths, as illustrated in Figure 10.8. Usually, a separation of a few wavelengths is required between a pair of receiving antennas in order to obtain signals that fade independently.

Other diversity transmission and reception techniques that are used in practice, are angle-of-arrival diversity and polarization diversity.

Given that the information is transmitted to the receiver via  $D$  independently fading channels, there are several ways that the receiver may extract the transmitted information from the received signal. The simplest method is for the receiver to monitor the received power level in the  $D$  received signals and to select for demodulation and detection the strongest signal. In general, this approach results in frequent switching from one signal to another. A slight modification that leads to a simpler implementation is to use a signal for demodulation and detection as long as the received power level in that signal is above a preset threshold. When the signal falls below the threshold, a switch is made to the channel which has the largest received power level. This method of signal selection is called *selection diversity*.

For better performance, we may use one of several more complex methods for combining the independently fading received signals as illustrated in Figure 10.9. One

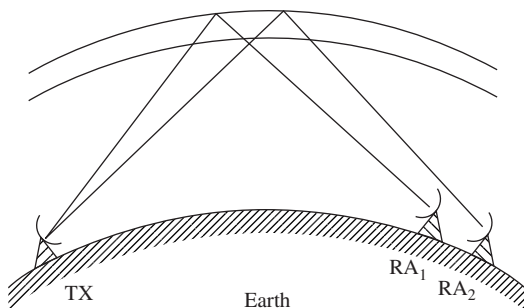
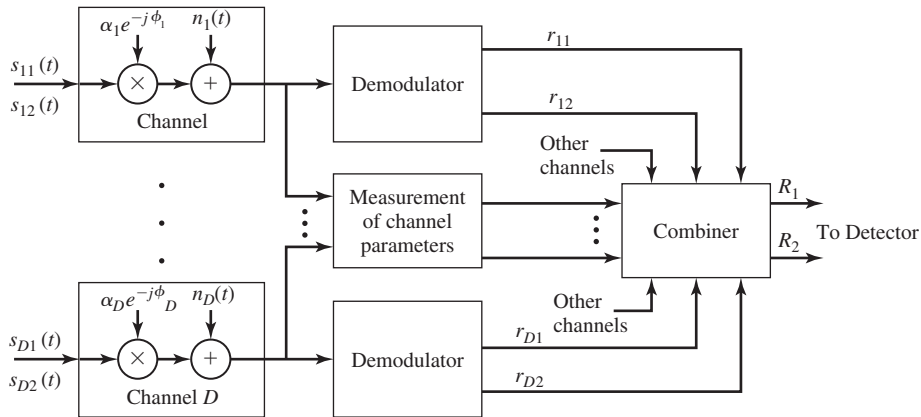


**Figure 10.8** Illustration of diversity reception using two receiving antennas.



Equal gain combiner : 
$$R_m = \sum_{k=1}^D r_{km} e^{j\phi_k}, m = 1, 2$$

Maximal ratio combiner: 
$$R_m = \sum_{k=1}^D \alpha_k r_{km} e^{j\phi_k}, m = 1, 2$$

Square law combiner: 
$$R_m = \sum_{k=1}^D |r_{km}|^2, m = 1, 2$$

**Figure 10.9** Model of binary digital communication system with  $D$ -order diversity.

that is appropriate for coherent demodulation and detection requires that the receiver estimate and correct for the different phase offsets on each of the  $D$  received signals after demodulation. Then, the phase-corrected signals at the outputs of the  $D$  demodulators are summed and fed to the detector. This type of signal combining is called *equal-gain combining*. If, in addition, the received signal power level is estimated for each of the  $D$  received signals, and the phase-corrected demodulator outputs are weighted in direct proportion of the received signal strength (square-root of power level) and then fed to the detector, the combiner is called a *maximal-ratio combiner*. On the other hand, if orthogonal signals are used for transmitting the information through  $D$  independently fading channels, the receiver may employ noncoherent demodulation. In such a case the outputs from the  $D$  demodulators may be squared, summed, and then fed to detector. This combiner is called a *square-law combiner*.

All these types of combining methods lead to performance characteristics that result in a probability of error which behaves as  $K_D/\bar{\rho}^D$  where  $K_D$  is a constant that depends on  $D$ , and  $\bar{\rho}$  is the average SNR/diversity channel. Thus, we achieve an exponential decrease in the error probability. Without providing a detailed derivation, we simply state that for antipodal signals with maximal ratio combining, the probability

of error has the general form

$$P_b \approx \frac{K_D}{(4\bar{\rho})^D}, \quad \bar{\rho}_b \gg 1 \quad (10.1.37)$$

where  $K_D$  is defined as

$$K_D = \frac{(2D-1)!}{D!(D-1)!} \quad (10.1.38)$$

For binary orthogonal signals with square-law combining, the probability of error has the asymptotic form

$$P_b \approx \frac{K_D}{\bar{\rho}^D}, \quad \bar{\rho} \gg 1 \quad (10.1.39)$$

Finally, for binary DPSK with equal gain combining, the probability of error has the asymptotic form

$$P_b \approx \frac{K_D}{(2\bar{\rho})^D}, \quad \bar{\rho} \gg 1 \quad (10.1.40)$$

These error probabilities are plotted in Figure 10.10 for  $D = 1, 2, 4$  as a function of the SNR/bit  $\bar{\rho}_b = D\bar{\rho}$ . It is apparent that a large reduction in SNR/bit is achieved in having  $D = 2$  (dual diversity) compared to no diversity. A further reduction in SNR is achieved by increasing the order of diversity to  $D = 4$ , although the additional gain from  $D = 2$  to  $D = 4$  is smaller than going from  $D = 1$  to  $D = 2$ . Beyond  $D = 4$ , the additional reduction in SNR is significantly smaller.

These performance results illustrate that efficient use of transmitter power in a Rayleigh fading channel can be achieved by using some form of diversity to provide the receiver with several independently fading signals all carrying the same information. The types of diversity that we described (time or frequency) are a form of channel coding usually called *repetition coding* where the code rate is  $1/D$ . Thus, if each information bit is transmitted twice in two widely separated time slots or in two widely separated frequency bands, we have a dual diversity ( $D = 2$ ) system obtained with a repetition code of rate  $R_c = 1/2$ . However, in general, a nontrivial code of rate  $1/2$  will yield significantly better performance if the coded bits are interleaved prior to transmission, as described in Chapter 9, so that the fading on each bit of a code word is statistically independent. In particular, a binary linear  $(n, k)$  code with minimum Hamming distance  $d_{\min}$  results in a performance that is equivalent to a repetition code of diversity  $d_{\min}$  when soft-decision decoding is used and  $d_{\min}/2$  when hard-decision decoding is used. Therefore, for any code rate  $1/D$ , a nontrivial code can be selected which has a minimum Hamming distance  $d_{\min} > D$  and, thus, provides a larger order of diversity than the corresponding repetition code of the same rate.

#### Example 10.1.7

Compare the error-rate performance of binary orthogonal FSK with dual diversity with the performance of the rate  $1/2$ ,  $d_{\min} = 8$ , extended Golay (24, 12) code in which binary

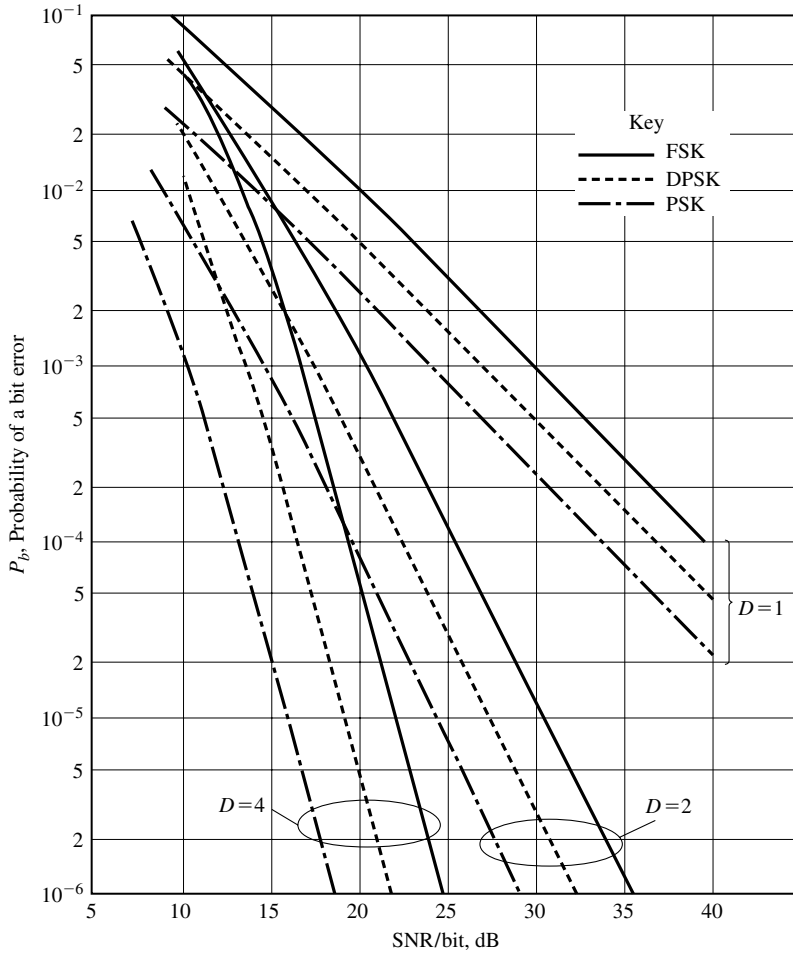


**Figure 10.10** Performance of binary signals with diversity.

orthogonal FSK is used to transmit each code bit. The channel is a Rayleigh fading channel and the receiver employs square-law combining and detection for both types of signals.

**Solution** Let us assume that signal diversity is obtained by interleaving the coded bits so that we have statistically independent fading among the coded bits for both signals. Note that, the repetition code and the Golay (24, 12) code, are rate 1/2 codes. For the repetition code, we combine the square-law detected FSK signals in the two (interleaved) signal intervals. Hence, if a zero is transmitted, the two metrics at the combiner output corresponding to a 0 and a 1, respectively, are

$$r_0 = |\alpha_1 \sqrt{\mathcal{E}} e^{j\phi_1} + n_{01}|^2 + |\alpha_2 \sqrt{\mathcal{E}} e^{j\phi_2} + n_{02}|^2$$

$$r_1 = |n_{11}|^2 + |n_{12}|^2$$

where the  $\{n_{ij}\}$  are statistically i.i.d. complex-valued, zero-mean Gaussian random variables. The probability of error is simply the probability that  $r_2 > r_1$ , and is given as

$$P_b \approx \frac{K_2}{\bar{\rho}^2} = \frac{3}{(\bar{\rho}_b/2)^2}, \quad \bar{\rho} \gg 1$$

where the average SNR/bit is  $\bar{\rho}_b$ . In the Golay code, there are  $2^{12} = 4096$  code words, so that there are 4096 metrics at the output of the square-law combiner. To compute the probability of error, we may assume that the all-zero code word is transmitted. Then the combiner output corresponding to the all-zero code word is the metric

$$r_0 = \sum_{k=1}^{24} |\alpha_k \sqrt{\mathcal{E}} e^{j\phi_k} + n_{0k}|^2$$

In the Golay (24, 12) code, there are 759 code words having distance  $d_{\min} = 8$  from the all-zero code words. Since any one of these code words differs in 8 bits from the all-zero code word and is identical with the all-zero word in 16 bits, the combiner output corresponding to any one of these 759 code words is statistically equivalent to the metric

$$r_1 = \sum_{k=1}^8 |n_{1k}|^2 + \sum_{k=9}^{24} |\alpha_k \sqrt{\mathcal{E}} e^{j\phi_k} + n_{0k}|^2$$

Hence, the difference between  $r_0$  and  $r_1$  is

$$r_0 - r_1 = \sum_{k=1}^8 [|\alpha_k \sqrt{\mathcal{E}} e^{j\phi_k} + n_{0k}|^2 - |n_{1k}|^2]$$

We observe that this difference is a function of summing the received signal over eight independently fading bits and, consequently, the code provides an order of diversity of  $d_{\min} = 8$ . This implies that the error rate for the Golay code decays inversely as  $\bar{\rho}^8$ ; i.e., the bit-error rate is

$$P_2 \approx \frac{K}{\bar{\rho}^8} = \frac{K}{(\bar{\rho}_b/2)^8}$$

where  $K$  is a constant independent of SNR,  $\bar{\rho}_b = \bar{\rho}/R_c$  is the SNR/bit and  $R_c$  is the code rate. Figure 10.11 illustrates the error probability for the two types of signals. Note that the Golay code outperforms the repetition code by over 8 dB at a bit-error probability of  $10^{-4}$ . The difference is even greater at lower error rates. In conclusion, a nontrivial code with interleaving generally provides more signal diversity than a repetition code of the same code rate.

### 10.1.5 Modulation and Demodulation on Frequency Selective Channels—The RAKE Demodulator

Let us consider the case in which the available channel bandwidth  $W$  exceeds the coherence bandwidth  $B_{cb}$  of the channel, and we transmit digital information at a symbol rate  $1/T$  by modulating a single carrier frequency. We assume that the symbol duration  $T$  satisfies the condition  $T \ll T_{cr}$ . Consequently, the channel characteristics change very slowly in time, so that the channel is slowly fading, but it is frequency selective because  $W \gg B_{cb}$ . Furthermore, we assume that  $T \gg T_m$  so that ISI is negligible.

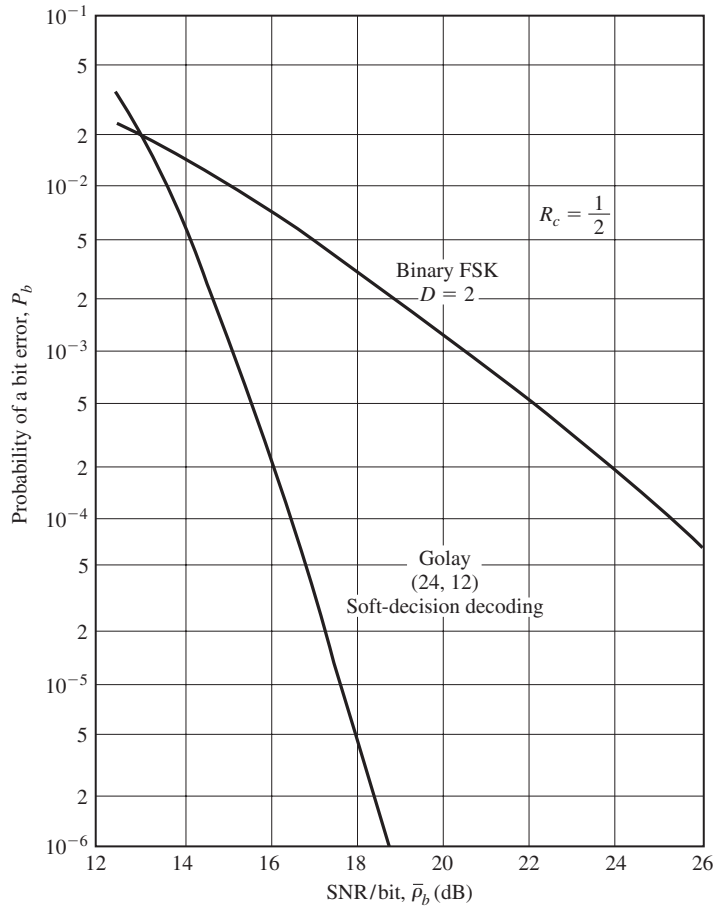


**Figure 10.11** Comparison of performance of repetition code with Golay (24, 12) code.

Since  $W$  is the bandwidth of the bandpass signal, the bandwidth occupancy of the equivalent lowpass signal is  $W/2$ . Hence, we employ a band-limited lowpass signal  $s(t)$ . Using the channel model for the frequency, selective channel shown in Figure 10.4, we may express the received signal as

$$r(t) = \sum_{n=1}^L c_n(t)s(t - n/W) + n(t) \quad (10.1.41)$$

where  $n(t)$  represents the AWGN. Therefore, the frequency-selective channel provides the receiver with up to  $L$  replicas of the transmitted signal, where each signal component is multiplied by a corresponding channel tap weight  $c_n(t)$ ,  $n = 1, 2, \dots, L$ . Based on

the slow fading assumption, the channel coefficients are considered as constant over the duration of one or more symbol intervals.

Since there are up to  $L$  replicas of the transmitted signal  $s(t)$  in  $r(t)$ , a receiver that processes the received signal in an optimum manner will achieve the performance that is equivalent to that of a communication system with diversity equal to the number of received (resolvable) signal components.

Let us consider binary signaling over the channel. Suppose we have two equal energy signals  $s_1(t)$  and  $s_2(t)$ , which are orthogonal, with a time duration  $T \gg T_m$ . Since the ISI is negligible, the optimum receiver consists of two correlators or two matched filters that are matched to the received signals. Let us use the correlator structure that is illustrated in Figure 10.12. The received signal is passed through a tapped

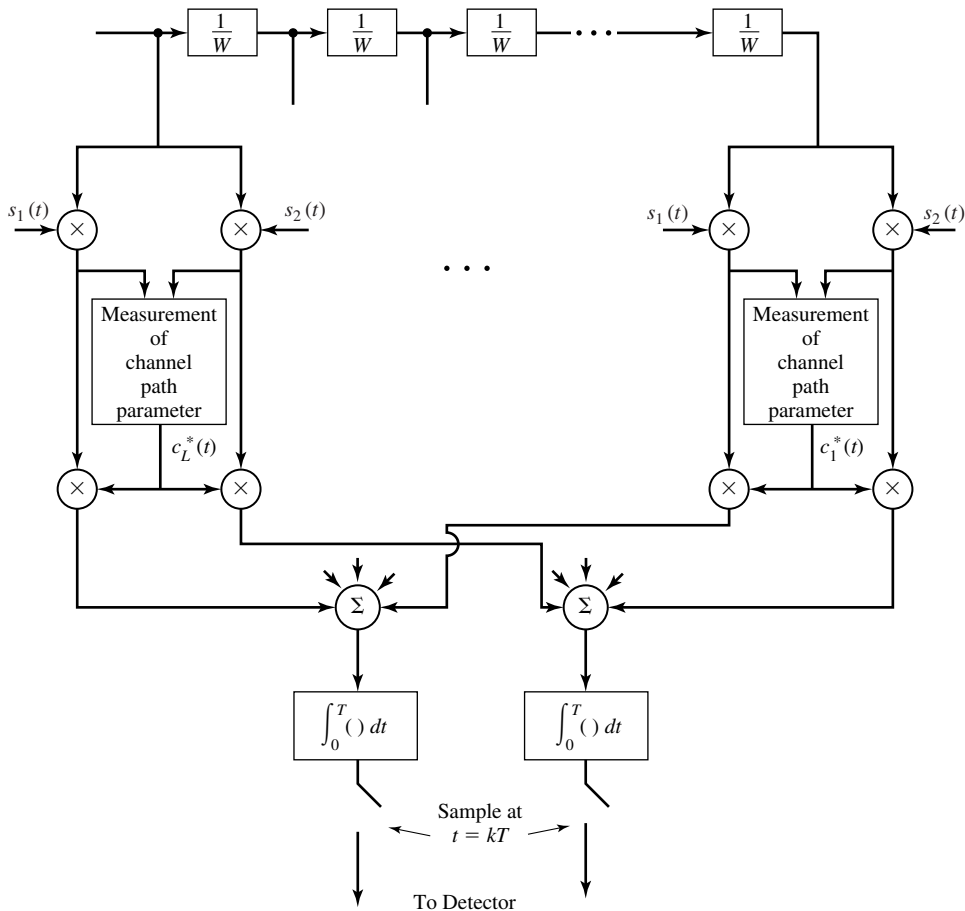


**Figure 10.12** RAKE demodulator for signal transmitted through a frequency selective channel.

delay-line filter with tap spacing of  $1/W$ , as in the channel model. The number of taps is selected to match the total number of resolvable signal components. At each tap, the signal is multiplied with each of the two possible transmitted signals  $s_1(t)$  and  $s_2(t)$ , and, then, each multiplier output is phase corrected and weighted by multiplication with  $c_n^*(t)$ ,  $n = 1, 2, \dots, L$ . Then, the corresponding phase-aligned and weighted signal components are integrated over the duration of the symbol interval  $T$  and the two integrator outputs are sampled periodically every  $T$  seconds. Their outputs are then sent to the detector. Thus, we have crosscorrelated the received signal with each of the two possible transmitted signals at all possible delays introduced by the channel. Note that the multiplication of the signal at each tap with the corresponding tap coefficient  $c_n^*(t)$  results in weighting the signal components by the corresponding signal strengths. Hence, the combining of the phase-corrected and weighted signal components corresponds to maximal ratio combining.

In order to perform maximal ratio combining, it is necessary to estimate the channel-tap coefficients  $c_n(t)$  from the received signal. Since these coefficients are time varying, it is necessary for the estimator to be adaptive; i.e., to be able to track the time variations.

The demodulator structure shown in Figure 10.12 is called a *RAKE demodulator*. Because this demodulator has equally spaced taps with tap coefficients that essentially collect all the signal components in the received signal, its operation has been likened to that of an ordinary garden rake.

Assuming that there are  $L$  signal components in the received signal, with corresponding signal strengths that are distinct and Rayleigh distributed, the probability of error for binary signals is well approximated as

$$P_b = K_L \prod_{k=1}^L \frac{1}{[2\bar{\rho}_k(1 - \gamma_r)]} \quad (10.1.42)$$

where  $\bar{\rho}_k$  is the average SNR for the  $k$ th-signal component; i.e.,

$$\bar{\rho}_k = \frac{\mathcal{E}_b}{N_0} E(\alpha_k^2) \quad (10.1.43)$$

where  $\alpha_k = |c_k|$  is the amplitude of the  $k$ th-tap coefficient,  $\gamma_r = -1$  for antipodal signals and  $\gamma_r = 0$  for orthogonal signals, and  $K_L$  is the constant defined in Equation (10.1.38). In the special case where all the signal components have the same strength, the error probability in Equation (10.1.42) reduces to that given by Equation (10.1.37) with  $D = L$ .

### 10.1.6 Multiple Antenna Systems and Space-Time Codes

The use of two or more antennas at the receiving terminal of a digital communication system is a commonly employed method for achieving spatial diversity to mitigate the effects of signal fading. Typically, the receiving antennas must be separated by one or more wavelengths to ensure that the received signal undergoes statistically independent fading. Spatial receiver diversity is especially attractive because the signal diversity is achieved without expanding the signal transmission bandwidth.



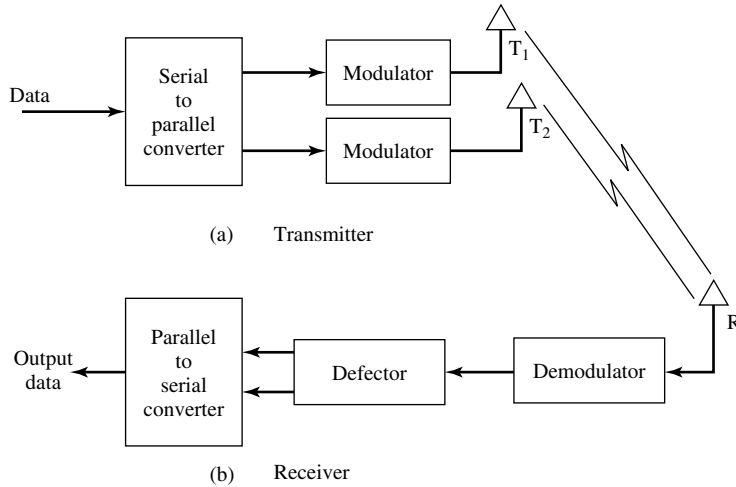


**Figure 10.13** Communication system employing two transmit antennas and one receive antenna.

Spatial diversity can also be achieved by using multiple antennas at the transmitter terminal of the communication system. For example, suppose we employ two antennas at the transmitter (T1 and T2) and one antenna at the receiver, as shown in Figure 10.13. Two information symbols are transmitted in each symbol interval. In the  $k$ th-symbol interval, antenna T1 transmits the signal  $s_{1k}g_T(t)$  and antenna T2 simultaneously transmits the signal  $s_{2k}g_T(t)$ , where  $g_T(t)$  is some basic signal pulse and  $s_{1k}$  and  $s_{2k}$  are symbols selected from some signal constellation; e.g., QAM or PSK. The signal at the receiving antenna may be expressed as

$$r(t) = c_1s_{1k}g_T(t) + c_2s_{2k}g_T(t) + n(t) \quad (10.1.44)$$

where the fading channel is assumed to be slowly fading and frequency nonselective with complex valued channel coefficients  $c_1$  and  $c_2$ , and  $n(t)$  denotes the additive noise. The receiver processes the received signal by passing it through a filter matched to  $g_T(t)$ . Hence, at the sampling instant, the matched-filter output may be expressed as

$$r_k = c_1s_{1k} + c_2s_{2k} + n_k \quad (10.1.45)$$

In the following symbol interval, T1 transmits the signal  $s_{2k}^*g_T(t)$  and T2 transmits  $-s_{1k}^*g_T(t)$  where the asterisk denotes complex conjugate. Hence, the output of the matched filter may be expressed as

$$r_{k+1} = c_1s_{2k}^* - c_2s_{1k}^* + n_{k+1} \quad (10.1.46)$$

It is assumed that the receiver has knowledge of the channel coefficients  $c_1$  and  $c_2$ , which is obtained by periodically transmitting pilot signals through the channel and measuring the channel coefficients  $c_1$  and  $c_2$ . Thus, it is possible for the receiver to recover  $s_{1k}$  and  $s_{2k}$  and, thus, achieve dual diversity. The recovery of  $s_{1k}$  and  $s_{2k}$  from

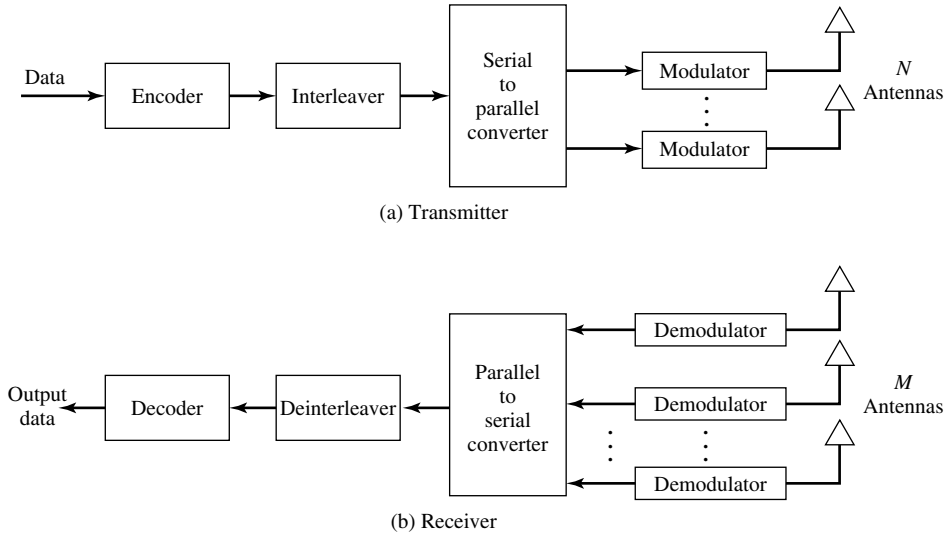


**Figure 10.14** A digital communication system with multiple transmit and receive antennas.

$r_k$  and  $r_{k+1}$  is left as an exercise for the reader. The scheme for achieving dual transmit diversity is especially suitable when the receiving terminal is a small mobile platform where it may be difficult more than one receiving antenna on the platform.

In addition to providing signal diversity, multiple transmit antennas can be used to create multiple spatial channels for the purpose of increasing the data transmission rate. In particular, suppose that we employ  $N$  transmit antennas and  $M$  receive antennas, where each of the  $N$  transmit antennas is used to transmit a different symbol in every symbol interval. Figure 10.14 illustrates the block diagram of a digital communication system that employs  $N$  transmit antennas and  $N$  receive antennas. The system shown in this figure includes an encoder and an interleaver at the transmitter and a deinterleaver and a decoder at the receiver. In the system all signals from the  $N$  transmit antennas are transmitted synchronously through the common channel. Thus, we achieve an  $N$ -fold increase in data rate compared to a system that uses a single transmit antenna. Assuming that the channel is frequency nonselective and slowly fading, so that the channel coefficients can be accurately measured, we can achieve  $M$ th-order spatial diversity by using  $M$  receive antennas, where  $M \geq N$ . Additional diversity, equal to the minimum distance of the code, can be achieved by encoding the data, provided that we employ a sufficiently long interleaver to ensure statistically independent channel fading.

#### Example 10.1.8

Consider a communication system that employs two transmit and two receive antennas. The encoder implements a rate  $1/2$  convolutional code with free distance  $d_{\text{free}} = 6$ . The interleaver is sufficiently long to assure that successive code symbols are separated in time

by at least the coherence time of the channel. The channel is slowly fading and frequency nonselective. The decoder employs the Viterbi algorithm to recover the data.

1. Express mathematically the signal that is transmitted through the channel by the two antennas, the signal received at each of the received antennas, and the signal at the output of the demodulator (input to the decoder).
2. What is the order of diversity achieved by the receiver if the decoder performs soft-decision decoding?
3. What is the order of diversity achieved by the receiver if the decoder performs hard-decision decoding?

### Solution

1. The signal at the input to the channel at the  $k$ th-symbol interval is

$$x(t) = s_{1k}g_T(t) + s_{2k}g_T(t), \quad 0 \leq t \leq T$$

The signal received at the two receive antennas are

$$r_1(t) = c_{11}s_{1k}g_T(t) + c_{12}s_{2k}g_T(t) + n_1(t)$$

$$r_2(t) = c_{21}s_{1k}g_T(t) + c_{22}s_{2k}g_T(t) + n_2(t)$$

where the  $\{c_{ij}\}$  are the channel coefficients,  $s_{1k}$  and  $s_{2k}$  are the channel symbols and  $n_1(t)$  and  $n_2(t)$  are the additive noise terms at the input to the receiver. The demodulator (matched filter) outputs are

$$r_1 = c_{11}s_{1k} + c_{12}s_{2k} + n_1$$

$$r_2 = c_{21}s_{1k} + c_{22}s_{2k} + n_2$$

These two signals are fed to the decoder.

2. With ideal interleaving, all the coded symbols fade independently so the received signal at each antenna provides a diversity order equal to  $d_{\text{free}} = 6$ . If the decoder is a soft-decision decoder; the total order of diversity for the two antennas is  $2d_{\text{free}} = 12$ .
3. With hard-decision decoding, the order of signal diversity from each antenna is  $d_{\text{free}}/2$ . Hence, the total order of diversity for the two antennas is reduced to  $d_{\text{free}} = 6$ .

An alternative approach to coding for multiple antenna systems is to employ a new class of codes, called *space-time codes*. A space-time code may be either a block code or a trellis code that is especially designed for multiple transmit and receive antennas to achieve diversity and an increase in data rate.

We consider a trellis code to illustrate the encoding process. A block diagram of the transmitter and the receiver is illustrated in Figure 10.15 for the case of two transmit and receive antennas. We assume that the data is binary and a signal constellation of  $2^k$  signal points is selected. Thus, any  $k$ -input data bits are mapped into one of  $2^k$  signal points. As an example, suppose that the modulation is 4-PSK and the encoder is represented by the 4-state trellis shown in Figure 10.16. This trellis generates a rate  $\frac{1}{2}$  code, where each input symbol, represented by the possible phase values 0, 1, 2, 3 is encoded into two output symbols, as specified by the trellis code. Each of the two output symbols is passed to (identical) interleavers. The symbol (phase) sequence at the output of each interleaver modulates a basic pulse shape  $g_T(t)$  and the

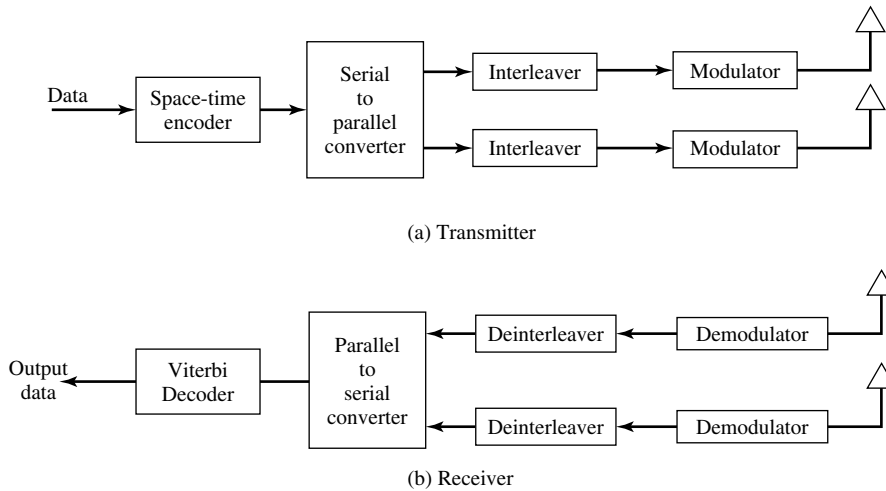


**Figure 10.15** Block diagram of communication system employing a space-time code for two transmit and two receive antennas.

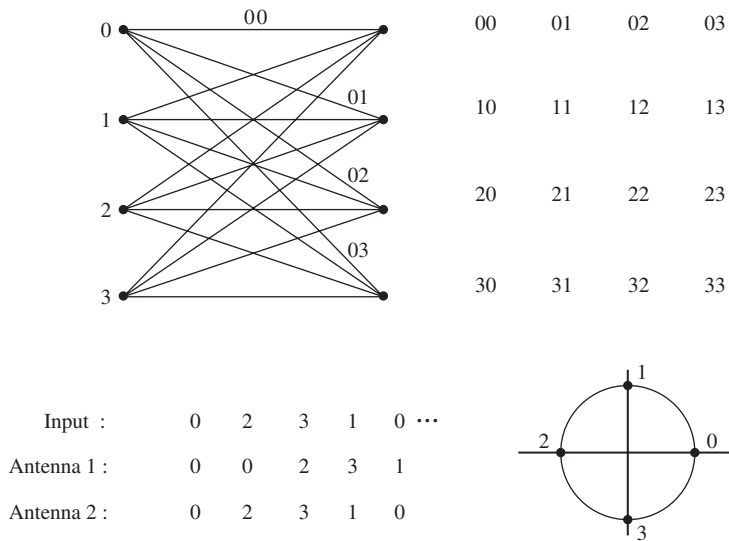


**Figure 10.16** 4-PSK, 4-state, space-time code.

two symbols are transmitted synchronously through the channel. At the receiver, the signals received at the antennas are passed through matched filters, deinterleaved, and fed to the trellis (Viterbi) decoder. The 4-state trellis code can be shown to provide dual diversity and the use of two antennas at the receiver results in fourth-order diversity for the communication system.

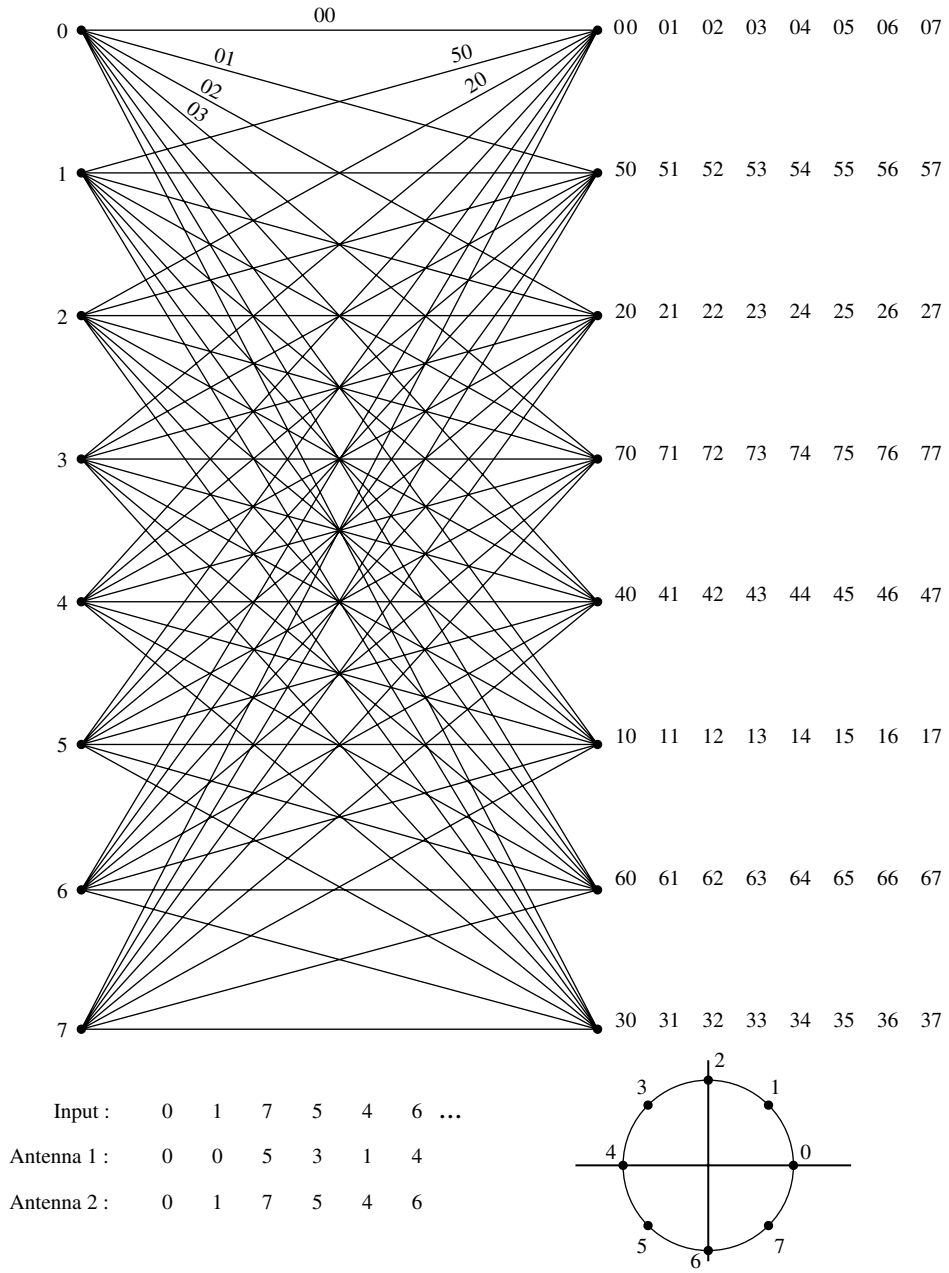


**Figure 10.17** 8-PSK, 8-state, space-time code.

As a second example, we consider a rate  $1/2$ , 8-state trellis code which is used with 8-PSK modulation, as shown in Figure 10.17. In this case, we transmit 3 bits/symbol, so that the throughput is 50% higher compared with the rate  $1/2$ , 4-state trellis code. With two transmit and two receive antennas, the code also results in fourth-order diversity.

For the sake of brevity, we will not discuss methods for designing space-time codes. For the interested reader, we cite the papers by Tarokh, et al. (1998, 1999) which describe the design of trellis codes and block codes.

## 10.2 CONTINUOUS CARRIER-PHASE MODULATION

The radio spectrum is a precious commodity that is shared by many users. For example, in the 900 MHz- and 1800 MHz-frequency bands used for digital cellular communications, the available licenses to use this spectrum are sold by the government licensing authorities—such as the FCC in the U.S.—to the cellular telephone operators, by means of an auction. In other words, the licenses to use certain parts of the spectrum are sold to the highest bidder. Therefore, it is important that the modulation used to transmit information over these radio channels be bandwidth efficient, so that more subscribers can be accommodated in any given frequency band.

In the case of FSK and PSK modulation, the bandwidth of the transmitted signal can be narrowed further by imposing the condition that the carrier phase of the transmitted signal be continuous from one signal interval to the next. This is in contrast to conventional FSK and PSK, where the carrier phase may change instantaneously at the beginning of each symbol interval.

In Sections 10.2.1 and 10.2.2, we describe both continuous-phase FSK and, more generally, continuous-phase modulation. After describing the characteristics of these modulations, we present their spectral characteristics and describe their demodulation and detection. We will observe that the inherent memory provided by the phase continuity of the signal not only results in a narrower spectrum, but it also allows us to employ a demodulator that exploits this memory. We begin by describing continuous-phase FSK.

### 10.2.1 Continuous-Phase FSK (CPFSK)

Ordinary FSK signals may be generated by having  $M = 2^k$  separate oscillators tuned to the desired frequencies  $f_c + m\Delta f \equiv f_m$ , and selecting one of the  $M$  frequencies according to the particular  $k$ -bit symbol that is to be transmitted in a signal interval. However, such abrupt switching from one oscillator output to another in successive signaling intervals results in relatively large spectral sidelobes outside of the main spectral band of the signal, which decay slowly with frequency separation. Consequently, this method is wasteful of bandwidth.

To avoid the use of signals having large spectral sidelobes, we may use the information-bearing signal to frequency-modulate a single carrier whose frequency is changed in a continuous manner. The resulting frequency-modulated signal is phase continuous and, hence, it is called *continuous-phase* FSK (CPFSK).

In order to represent a CPFSK signal, we begin with a PAM signal

$$v(t) = \sum_n a_n g_T(t - nT) \quad (10.2.1)$$

where the amplitudes are obtained by mapping  $k$ -bit blocks of binary digits from the information sequence into the amplitude levels  $\pm 1, \pm 3, \dots, \pm(M - 1)$ , and  $g_T(t)$  is a rectangular pulse of amplitude  $1/2T$  and duration  $T$ . The signal  $v(t)$  is used to frequency modulate the carrier. Consequently, the frequency-modulated carrier is

$$u(t) = \sqrt{\frac{2\mathcal{E}_s}{T}} \cos \left[ 2\pi f_c t + 4\pi T f_d \int_{-\infty}^t v(\tau) d\tau + \phi_0 \right] \quad (10.2.2)$$

where  $f_d$  is the *peak-frequency deviation* and  $\phi_0$  is an arbitrary initial phase of the carrier. Note that the instantaneous frequency of the carrier is  $f_c + 2T f_d v(t)$ .

We observe that, although  $v(t)$  contains discontinuities, the integral of  $v(t)$  is continuous. We may denote the phase of the carrier as

$$\theta(t; \mathbf{a}) = 4\pi T f_d \int_{-\infty}^t v(\tau) d\tau \quad (10.2.3)$$

where  $\mathbf{a}$  denotes the sequence of signal amplitudes. Since  $\theta(t; \mathbf{a})$  is a continuous function of  $t$ , we have a continuous-phase signal.

The phase of the carrier in the interval,  $nT \leq t \leq (n+1)T$ , is determined by the integral in Equation (10.2.3). Thus,

$$\begin{aligned} \theta(t; \mathbf{a}) &= 2\pi f_d T \sum_{k=-\infty}^{n-1} a_k + 2\pi(t - nT) f_d a_n \\ &= \theta_n + 2\pi h a_n q(t - nT) \end{aligned} \quad (10.2.4)$$

where,  $h$ ,  $\theta_n$  and  $q(t)$  are defined as

$$h = 2f_d T \quad (10.2.5)$$

$$\theta_n = \pi h \sum_{k=-\infty}^{n-1} a_k \quad (10.2.6)$$

$$q(t) = \begin{cases} 0, & t < 0 \\ t/2T, & 0 \leq t \leq T \\ \frac{1}{2}, & t > T \end{cases} \quad (10.2.7)$$

The parameter  $h$  is called the *modulation index*. We observe that  $\theta_n$  represents the phase accumulation (memory) from all symbols up to time  $(n-1)T$ . The signal  $q(t)$  is simply the integral of the rectangular pulse, as illustrated in Figure 10.18.

It is instructive to sketch the set of all phase trajectories  $\theta(t; \mathbf{a})$  generated by all possible values of the information sequence  $\{a_n\}$ . For example, with binary symbols,  $a_n = \pm 1$ , the set of phase trajectories beginning at time  $t = 0$  are shown in Figure 10.19.

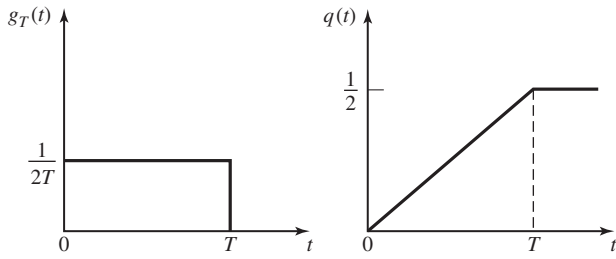


**Figure 10.18** The signal pulse  $g_T(t)$  and its integral  $q(t)$ .

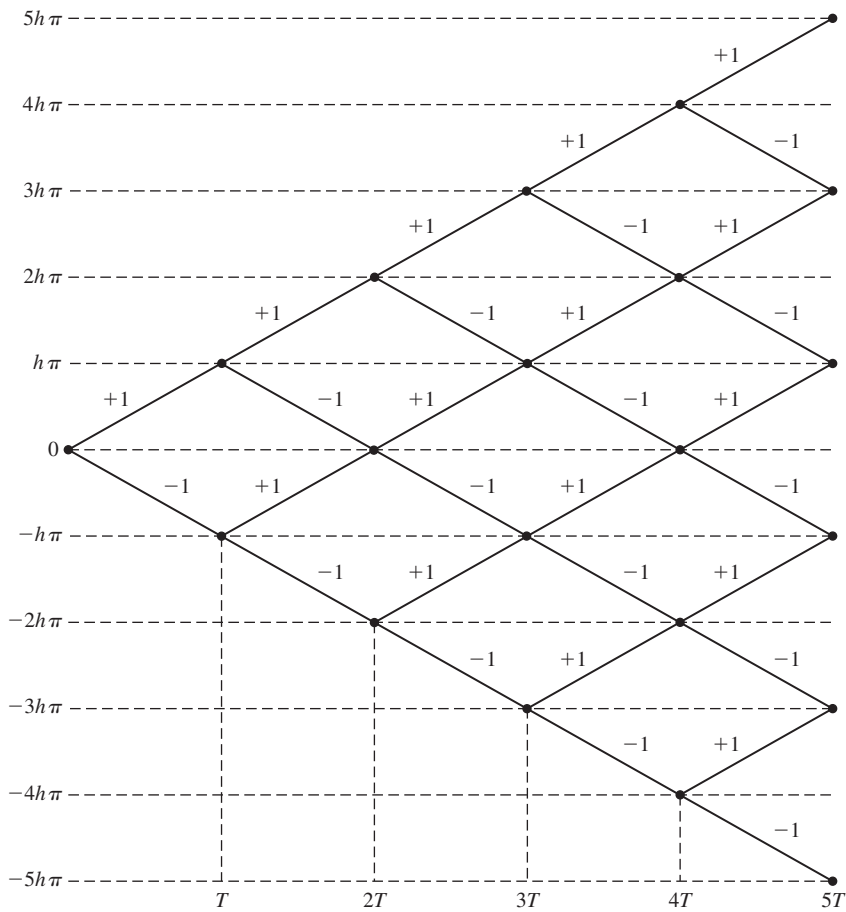


**Figure 10.19** Phase trajectory for binary CPFSK.



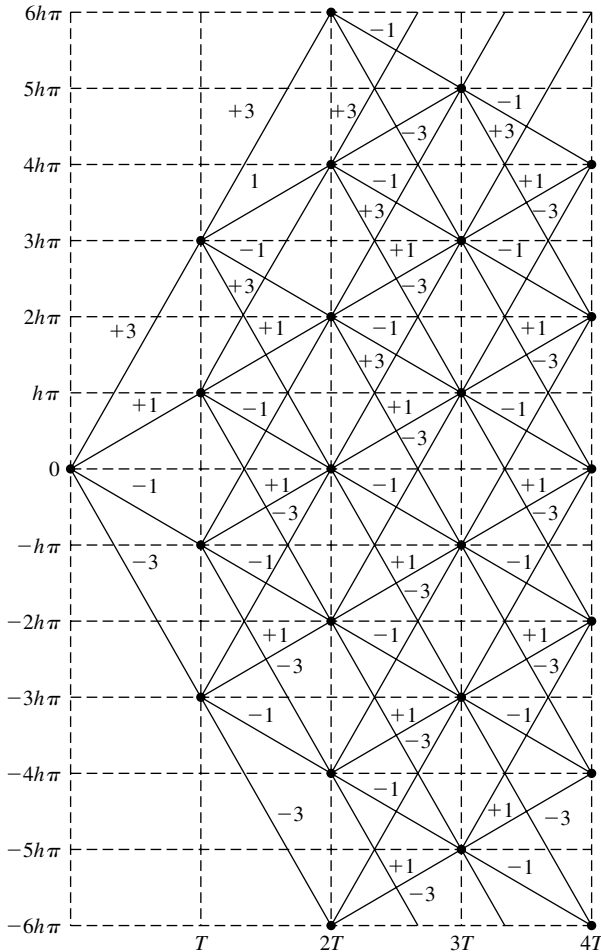


**Figure 10.20** Phase trajectory for quaternary CPFSK.

For comparison, the phase trajectories for quaternary CPFSK ( $a_n = \pm 1, \pm 3$ ) are illustrated in Figure 10.20. These phase diagrams are called *phase trees*. We observe that the phase trees are piecewise linear as a consequence of the fact that the pulse  $g_T(t)$  is rectangular. Smoother phase trajectories and phase trees may be obtained by using pulses that do not contain discontinuities.

The phase trees shown in these figures grow with time. However, the phase of the carrier is unique only in the range  $\theta = 0$  to  $\theta = 2\pi$ , or equivalently, from  $\theta = -\pi$  to  $\theta = \pi$ . When the phase trajectories are plotted modulo  $2\pi$ , say in the range  $(-\pi, \pi)$ , the phase tree collapses into a structure called a *phase trellis*. One way to view the phase trellis as a function of time is to plot the two quadrature components  $x_c(t; \mathbf{a}) = \cos \theta(t; \mathbf{a})$  and  $x_s(t; \mathbf{a}) = \sin \theta(t; \mathbf{a})$  as  $(x, y)$  coordinates and to let time vary in a third dimension.

Since  $x_c^2 + x_s^2 = 1$  at any time instant, the three-dimensional plot generated by  $x_c(t; \mathbf{a})$  and  $x_s(t; \mathbf{a})$  appears as a trajectory on the surface of a cylinder of unit radius.

Simpler representations for the phase trajectories can be obtained by displaying only the terminal values of the signal phase at the time instants  $t = nT$ . In this case, we restrict the modulation index  $h$  to be rational. In particular, let us assume that  $h = m/p$ , where  $m$  and  $p$  are relatively prime integers. Then, at the time instants  $t = nT$ , the terminal phase states for  $m$  even are

$$\Theta_s = \left\{ 0, \frac{\pi m}{p}, \frac{2\pi m}{p}, \dots, \frac{(p-1)\pi m}{p} \right\} \quad (10.2.8)$$

and for  $m$  odd are

$$\Theta_s = \left\{ 0, \frac{\pi m}{p}, \frac{2\pi m}{p}, \dots, \frac{(2p-1)\pi m}{p} \right\} \quad (10.2.9)$$

Hence, there are  $p$  terminal phase states when  $m$  is even and  $2p$  terminal phase states when  $m$  is odd. For example, binary CPFSK with  $h = 1/2$  has four terminal phase states. The *state trellis* for this signal is illustrated in Figure 10.21. We emphasize that the phase transitions from one state to another are not true phase trajectories. They represent phase transitions to the terminal states at the time instants  $t = nT$ .

An alternative representation to the state trellis is the *state diagram*, which also illustrates the state transitions at the time instants  $t = nT$ . This is an even more compact representation of the CPFSK signal. Only the possible terminal phase states and their transitions are displayed in the state diagram. Time does not appear explicitly as a variable. For example, the state diagram for the CPFSK signal with  $h = 1/2$  is shown in Figure 10.22.

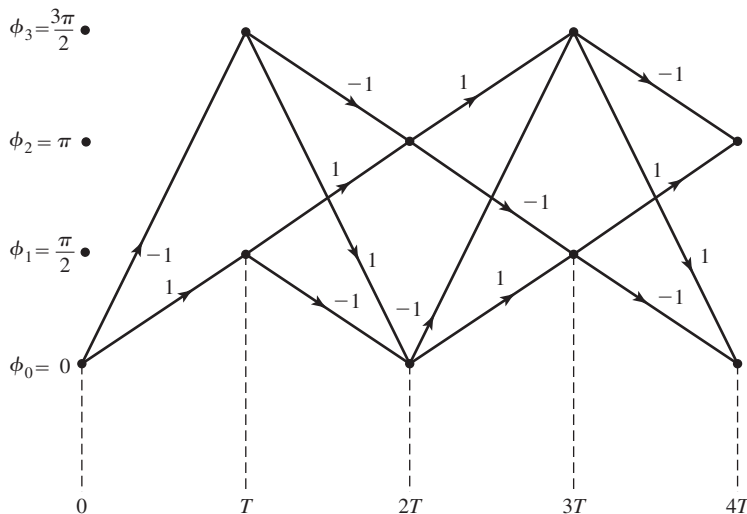


**Figure 10.21** State trellis for binary CPFSK with  $h = 1/2$ .

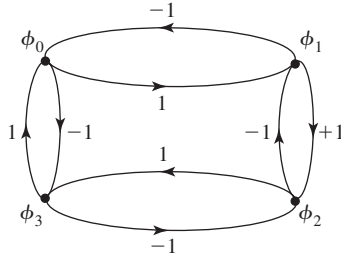


**Figure 10.22** State diagram for binary CPFSK with  $h = 1/2$ .

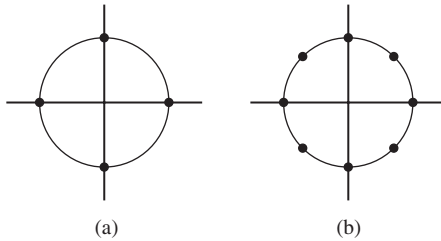


**Figure 10.23** Signal-space diagrams for binary FSK with (a)  $h = 1/2$  and (b)  $h = 1/4$ .

We should emphasize that a CPFSK signal cannot be represented by discrete points in signal space as in the case of PAM, PSK, and QAM, because the phase of the carrier is time-variant. Instead, the constant amplitude CPFSK signal may be represented in two-dimensional space by a circle, where points on the circle represent the combined amplitude and phase trajectory of the carrier as a function of time. For example, Figure 10.23 illustrates the signal space diagrams for binary CPFSK with  $h = 1/2$  and  $h = 1/4$ . The four dots at  $\theta = 0, \pi/2, \pi, 3\pi/2$  and  $\theta = 0, \pm\pi/4, \pm\pi/2, \pm3\pi/4, \pi$  for  $h = 1/2$  and  $h = 1/4$ , respectively, represent the terminal phase states previously shown in the state diagram.

**Minimum-Shift Keying (MSK).** MSK is a special form of binary CPFSK in which the modulation index  $h = 1/2$ . Thus, the phase of the carrier for the MSK signal is

$$\begin{aligned}\theta(t; \mathbf{a}) &= \frac{\pi}{2} \sum_{k=-\infty}^{n-1} a_k + \pi a_n q(t - nT_b) \\ &= \theta_n + \frac{\pi}{2} \left( \frac{t - nT_b}{T_b} \right) a_n, \quad nT_b \leq t \leq (n+1)T_b\end{aligned}\quad (10.2.10)$$

which follows from Equation (10.2.4). The corresponding carrier-modulated signal is

$$\begin{aligned}u(t) &= \sqrt{\frac{2\mathcal{E}_b}{T_b}} \cos[2\pi f_c t + \theta_n + \pi(t - nT_b)a_n/2T_b] \\ &= \sqrt{\frac{2\mathcal{E}_b}{T_b}} \cos \left[ 2\pi \left( f_c + \frac{1}{4T_b} a_n \right) t - \frac{n\pi}{2} a_n + \theta_n \right]\end{aligned}\quad (10.2.11)$$

The expression in Equation (10.2.11) indicates that the MSK (binary CPFSK) signal is basically a sinusoid consisting of one of two possible frequencies in the interval  $nT_b \leq t \leq (n+1)T_b$ , namely,

$$\begin{aligned} f_1 &= f_c - \frac{1}{4T_b} \\ f_2 &= f_c + \frac{1}{4T_b} \end{aligned} \quad (10.2.12)$$

Hence, the two sinusoidal signals may be expressed as

$$u_i(t) = \sqrt{\frac{2\mathcal{E}_b}{T_b}} \cos \left[ 2\pi f_i t + \theta_n + \frac{n\pi}{2} (-1)^{i-1} \right], \quad i = 1, 2 \quad (10.2.13)$$

The frequency separation is  $\Delta f = f_2 - f_1 = 1/2T_b$ . Recall that this is the minimum-frequency separation for orthogonality of the two sinusoids, provided the signals are detected coherently. This explains why binary CPFSK with  $h = 1/2$  is called *minimum-shift keying* (MSK). Note that the phase of the carrier in the  $n$ th signaling interval is the phase state of the signal that results in phase continuity between adjacent intervals.

It is interesting to demonstrate that MSK is also a form of four-phase PSK. To prove this point, let us begin with a four-phase PSK signal which has the form

$$\begin{aligned} u(t) &= \sqrt{\frac{2\mathcal{E}_b}{T_b}} \left\{ \left[ \sum_{n=-\infty}^{\infty} a_{2n} g_T(t - 2nT_b) \right] \cos 2\pi f_c t \right. \\ &\quad \left. + \left[ \sum_{n=-\infty}^{\infty} a_{2n+1} g_T(t - 2nT_b - T_b) \right] \sin 2\pi f_c t \right\} \end{aligned} \quad (10.2.14)$$

where  $g_T(t)$  is a sinusoidal pulse defined as

$$g_T(t) = \begin{cases} \sin \frac{\pi t}{2T_b}, & 0 \leq t \leq 2T_b \\ 0, & \text{otherwise} \end{cases} \quad (10.2.15)$$

and illustrated in Figure 10.24. First, we observe that the four-phase PSK signal consists of two quadrature carriers,  $\cos 2\pi f_c t$  and  $\sin 2\pi f_c t$ , which are amplitude modulated at a rate of one bit/ $2T_b$  interval. The even-numbered information bits  $\{a_{2n}\}$  are transmitted

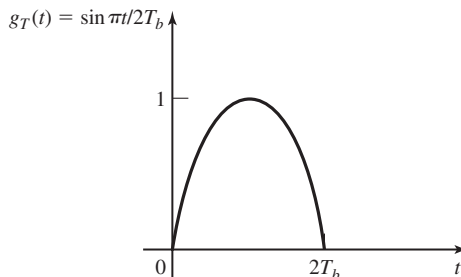


**Figure 10.24** Sinusoidal pulse shape.

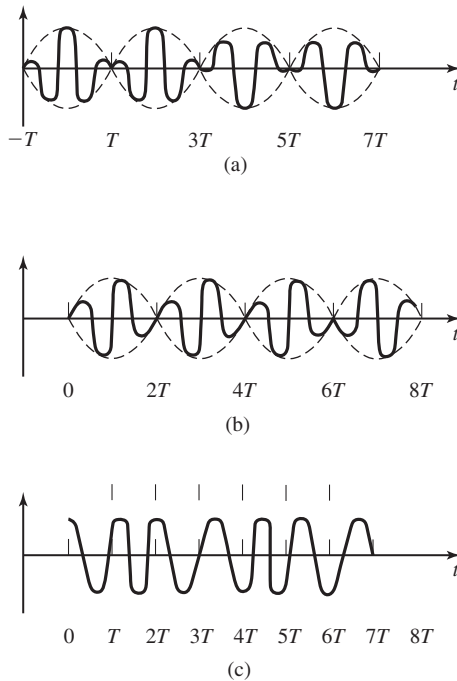


**Figure 10.25** Representation of MSK signal as a form of two staggered binary PSK signals, each with a sinusoidal envelope. (a) In-phase signal components, (b) quadrature signal component, and (c) MSK signal ( $a + b$ ).

by modulating the cosine carrier, while the odd-numbered information bits  $\{a_{2n+1}\}$  are transmitted by amplitude modulating the sine carrier. Note that the modulation of the two quadrature carriers is staggered in time by  $T_b$  and that the transmission rate for each carrier is  $1/2T_b$ . This type of four-phase modulation is called *offset quadrature PSK (OQPSK)* or *staggered quadrature PSK (SQPSK)*.

Figure 10.25 illustrates the SQPSK signal in terms of the two staggered quadrature-modulated binary PSK signal. The corresponding sum of the two quadrature signals is a constant-amplitude, continuous-phase FSK signal, as shown in Figure 10.25.

It is also interesting to compare the waveforms for MSK with the waveforms for staggered QPSK in which the pulse  $g_T(t)$  is rectangular for  $0 \leq t \leq 2T_b$ , and with conventional quadrature PSK (QPSK) in which the baseband pulse is rectangular in the interval  $0 \leq t \leq 2T_b$ . We emphasize that all three of these modulation methods result in identical data rates. The MSK signal is phase continuous. The SQPSK signal with a rectangular baseband pulse is basically two binary PSK signals for which the phase transitions are staggered in time by  $T_b$  seconds. Consequently, this signal contains phase jumps of  $\pm 90^\circ$  that may occur as often as every  $T_b$  seconds. On the other hand, in conventional QPSK with constant envelope, one or both of the information symbols may cause phase transitions as often as every  $2T_b$  seconds. These phase jumps may be  $\pm 180^\circ$  or  $\pm 90^\circ$ . An illustration of these three types of four-phase PSK signals is shown in Figure 10.26.

From the description given above, it is clear that CPFSK is a modulation method with memory. The memory results from the phase continuity of the transmitted carrier

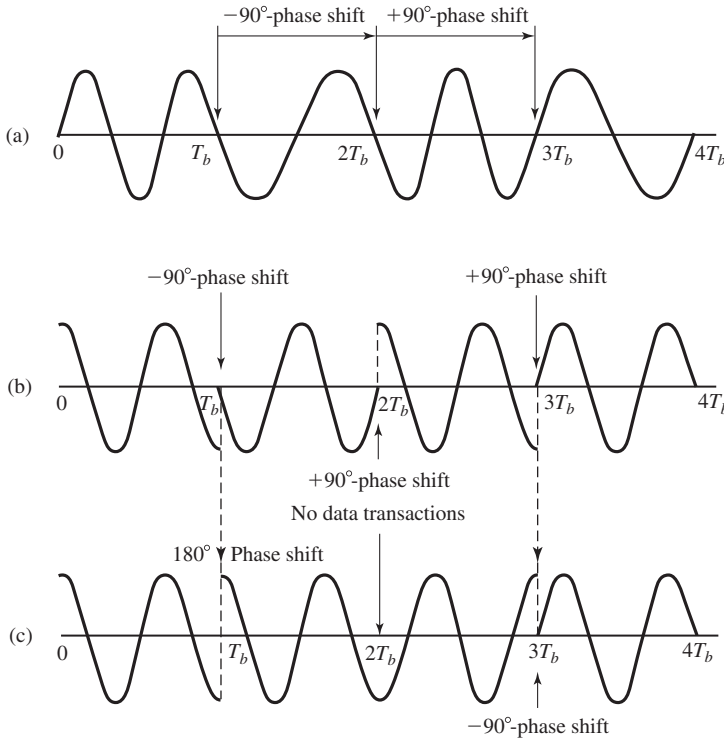


**Figure 10.26** Signal waveforms for (a) MSK, (b) offset QPSK (rectangular pulse), and (c) conventional QPSK (rectangular pulse). (From Gronemeyer and McBride; © 1976 IEEE.)

phase from one symbol interval to the next. As a consequence of the continuous phase characteristics, the power spectra of CPFSK signals are narrower than the corresponding FSK signals in which the phase is allowed to change abruptly at the beginning of each symbol interval. The spectral characteristics of CPFSK signals are given in Section 10.2.3. The demodulation and detection of CPFSK are described in Section 10.2.4, which deals with the demodulation and detection of the more general class of continuous-phase modulated signals.

### 10.2.2 Continuous-Phase Modulation (CPM)

When the phase of the carrier is expressed in the form of Equation (10.2.4), CPFSK becomes a special case of a general class of continuous-phase modulated (CPM) signals in which the carrier phase is

$$\theta(t; \mathbf{a}) = 2\pi \sum_{k=-\infty}^n a_k h_k q(t - kT), \quad nT \leq t \leq (n+1)T \quad (10.2.16)$$

where  $\{a_k\}$  is the sequence of  $M$ -ary information symbols with possible values  $\pm 1, \pm 3, \dots, \pm(M-1)$ ,  $\{h_k\}$  is a sequence of modulation indices, and  $q(t)$  is some arbitrary normalized waveform. Recall that for CPFSK,  $q(t) = t/2T$  for  $0 \leq t \leq T$ ,  $q(t) = 0$  for  $t < 0$ , and  $q(t) = 1/2$  for  $t > T$ .

When  $h_k = h$  for all  $k$ , the modulation index is fixed for all symbols. When the modulation index varies from one symbol to another, the CPM signal is called *multi-h*. In such a case the  $\{h_k\}$  are usually selected to vary in a cyclic pattern through the set of indices.

The waveform  $q(t)$  is the integral of a pulse  $g_T(t)$  of arbitrary shape; i.e.,

$$q(t) = \int_0^t g_T(\tau) d\tau \quad (10.2.17)$$

If  $g_T(t) = 0$  for  $t > T$ , the CPM signal is called a *full-response CPM signal*. If the signal pulse  $g_T(t)$  is nonzero for  $t > T$ , the modulated signal is called *partial-response CPM*. In Figure 10.27 we illustrate several pulse shapes for  $g_T(t)$  and the corresponding  $q(t)$ . It is apparent that there is an infinite number of CPM signals that can be obtained by selecting different pulse shapes for  $g_T(t)$  and by varying the modulation index  $h$  and the number of symbols  $M$ .

The primary reason for extending the duration of the pulse  $g(t)$  beyond the time interval  $0 \leq t \leq T$  is to further reduce the bandwidth of the transmitted signal, as it is demonstrated in Section 10.2.3. We note that, when the duration of the pulse  $g_T(t)$  extends over the time interval  $0 \leq t \leq LT$ , where  $L > 1$ , additional memory is introduced in the CPM signals and, hence, the number of phase states increases.

Three popular pulse shapes are given in Table 10.2. LREC denotes a rectangular pulse of duration  $LT$ , where  $L$  is a positive integer. In this case,  $L = 1$  results in a CPFSK signal, with the pulse as shown in Figure 10.27(a). The LREC pulse for  $L = 2$  is shown in Figure 10.27(c). LRC denotes a raised cosine pulse of duration  $LT$ . The LRC pulses corresponding to  $L = 1$  and  $L = 2$  are shown in Figure 10.27(b) and (d), respectively.

**TABLE 10.2** SOME COMMONLY USED CPM PULSE SHAPES

LREC

$$g(t) = \begin{cases} \frac{1}{2LT} & (0 \leq t \leq LT) \\ 0, & \text{otherwise} \end{cases}$$

LRC

$$g(t) = \begin{cases} \frac{1}{2LT} \left(1 - \cos \frac{2\pi t}{LT}\right) & (0 \leq t \leq LT) \\ 0, & \text{otherwise} \end{cases}$$

GMSK

$$g(t) = \left\{ Q \left[ 2\pi B \left( t - \frac{T}{2} \right) / (\ln 2)^{1/2} \right] - Q \left[ 2\pi B \left( t + \frac{T}{2} \right) / (\ln 2)^{1/2} \right] \right\}$$

$$Q(t) = \frac{1}{2\pi} \int_t^\infty e^{-x^2/2} dx$$

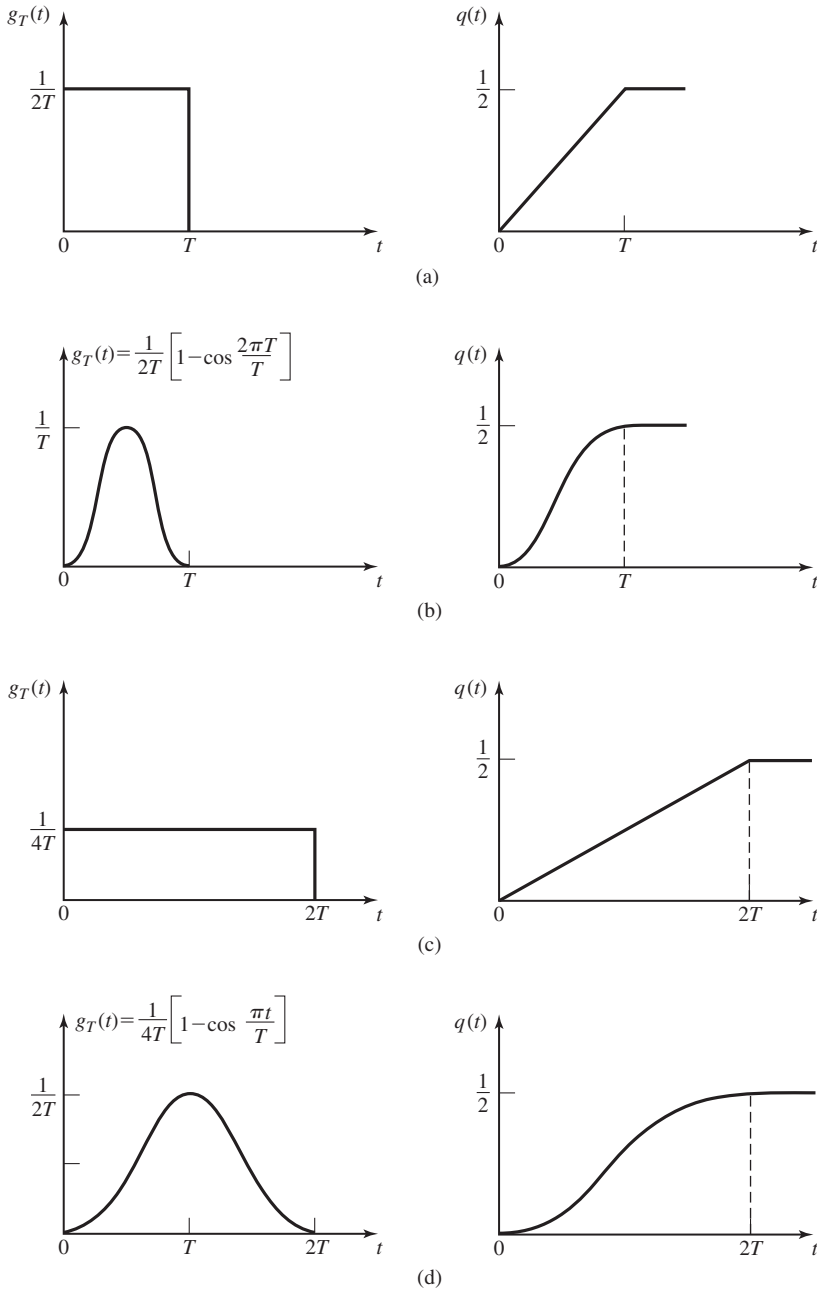


**Figure 10.27** Pulse shapes for full-response (a, b) and partial response (c, d) CPM.



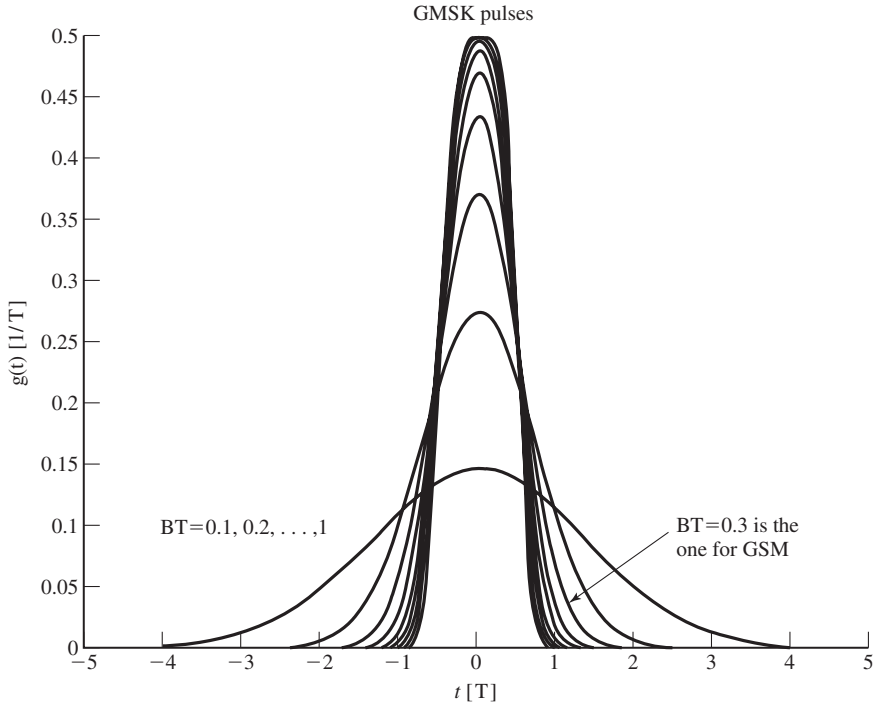


**Figure 10.27** (continued) (e) GMSK pulse shape.

The third pulse given in Table 10.2 is called a Gaussian minimum-shift keying (GMSK) pulse with bandwidth parameter  $B$ , which represents the  $-3$ -dB bandwidth of the Gaussian pulse. Figure 10.27(e) illustrates a set of GMSK pulses with time-bandwidth products  $BT$  ranging from 0.1–1. We observe that the pulse duration increases as the bandwidth of the pulse decreases, as expected. In practical applications, the pulse is usually truncated to some specified fixed duration. GMSK with  $BT = 0.3$  is used in the European digital cellular communication system, called GSM. From Figure 10.27(e) we observe that when  $BT = 0.3$ , the GMSK pulse may be truncated at  $|t| = 1.5T$  with a relatively small error incurred for  $t > 1.5T$ .

In general, CPM signals cannot be represented by discrete points in signal space as in the case of PAM, PSK, and QAM, because the phase of the carrier is time-variant. As we observed in the case of CPFSK, we may employ phase trajectories (or phase trees) to illustrate the signal phase as a function of time. Alternatively, we may use a state trellis or a state diagram to illustrate the terminal phase states and the phase transitions from one state to another. Finally, as in the case of CPFSK, we may represent a CPM signal in signal space by a circle, where the points on the circle correspond to the combined amplitude and phase of the carrier as a function of time. The terminal phase states are usually identified as discrete points on the circle. For example, Figure 10.28 illustrates the signal space diagrams for binary CPFSK with  $h = 1/4, 1/3$ , and  $2/3$ . Note that the

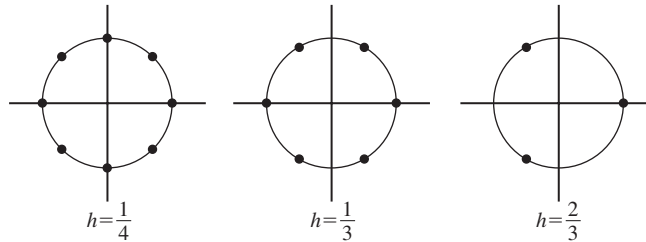


**Figure 10.28** Signal-space diagram for CPFSK.

length of the phase trajectory (lengths of the arc) between two terminal phase states increases with an increase in  $h$ . An increase in  $h$  also results in an increase of the signal bandwidth, as shown in Section 10.2.3.

### 10.2.3 Spectral Characteristics of CPFSK and CPM Signals

In this section, we consider the spectral characteristics of CPFSK and CPM signals and present some results on their power-spectral density. The derivation of these results may be found in more advanced digital communication textbooks; e.g., Anderson et al. (1986) and Proakis (2001).

A CPM signal may be expressed in the general form

$$\begin{aligned} u(t; \mathbf{a}) &= \sqrt{\frac{2\mathcal{E}_s}{T}} \cos[2\pi f_c t + \theta(t; \mathbf{a})] \\ &= \operatorname{Re} \left\{ \sqrt{\frac{2\mathcal{E}_s}{T}} e^{j[2\pi f_c t + \theta(t; \mathbf{a})]} \right\} \end{aligned} \quad (10.2.18)$$

where the carrier phase  $\theta(t; \mathbf{a})$  is given by Equation (10.2.16). Since the complex exponential  $e^{j2\pi f_c t}$  serves as a frequency translation of the complex-valued baseband signal

$$v(t) = \sqrt{\frac{2\mathcal{E}_s}{T}} e^{j\theta(t; \mathbf{a})} \quad (10.2.19)$$

it is sufficient to focus our attention on the spectral characteristics of the information-bearing signal  $v(t)$ .

Unlike the computation of the power-spectral density for linear modulation methods such as PAM, PSK, and QAM, which was relatively straightforward, the computation of the power-density spectrum of a CPM signal is much more tedious and involved. The difficulties are due to the memory in the continuous-phase signal and to the exponential relationship between  $v(t)$  and  $\theta(t; \mathbf{a})$ . Nevertheless, the general procedure used in the derivation for the power-density spectrum of PAM, given in Section 8.2, may be followed.

The general procedure begins with the computation of the autocorrelation function of the random process  $V(t)$ , denoted as  $R_V(t + \tau, t)$ . As in the case of linear modulation methods, the random process  $V(t)$  is cyclostationary and, hence, the autocorrelation function is periodic with period  $T$ ; i.e.,  $R_V(t + T + \tau, t + T) = R_V(t + \tau, t)$ . By averaging  $R_V(t + \tau, t)$  over a single period, we eliminate the time dependence  $t$  and, thus, we obtain the average autocorrelation function

$$\bar{R}_V(\tau) = \frac{1}{T} \int_0^T R_V(t + \tau, t) dt \quad (10.2.20)$$

Finally, we compute the Fourier transform of  $\bar{R}_V(\tau)$  to obtain the power-spectral density  $\mathcal{S}_V(f)$  of the signal. The power-spectral density of the real-valued signal  $u(t; \mathbf{a})$  is then found by translating  $\mathcal{S}_V(f)$  in frequency by the carrier  $f_c$ . Thus, we obtain

$$\mathcal{S}_U(f) = \frac{1}{4} [\mathcal{S}_V(f - f_c) + \mathcal{S}_V(f + f_c)] \quad (10.2.21)$$

In the case of the CPFSK signal, this procedure yields the following expression for the power-spectral density

$$\mathcal{S}_V(f) = T \left[ \frac{1}{M} \sum_{n=1}^M A_n^2(f) + \frac{2}{M^2} \sum_{n=1}^M \sum_{m=1}^M B_{nm}(f) A_n(f) A_m(f) \right] \quad (10.2.22)$$

where

$$\begin{aligned} A_n(f) &= \frac{\sin \pi [fT - (2n - 1 - M)h/2]}{\pi [fT - (2n - 1 - M)h/2]} \\ &= \text{sinc} \left( fT - \frac{h(2n - 1 - M)}{2} \right) \end{aligned} \quad (10.2.23)$$

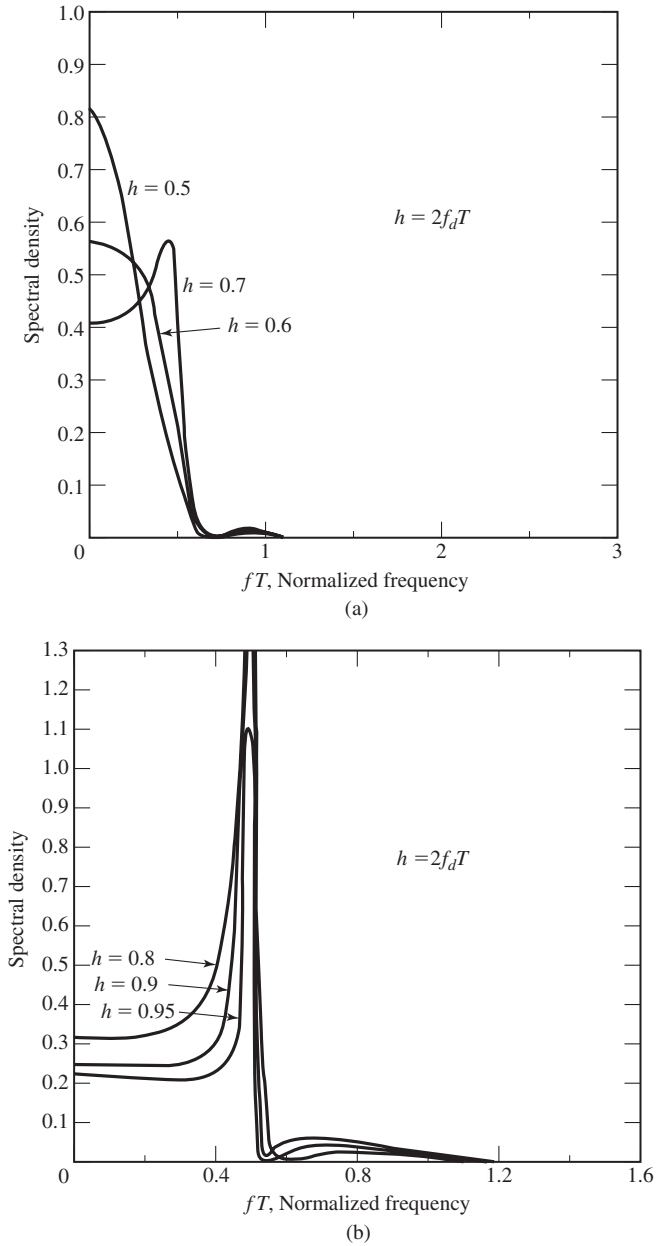
$$B_{nm}(f) = \frac{\cos(2\pi fT - \alpha_{nm}) - \beta \cos \alpha_{nm}}{1 + \beta^2 - 2\beta \cos 2\pi fT} \quad (10.2.24)$$

$$\alpha_{nm} = \pi h(m + n - 1 - M) \quad (10.2.25)$$

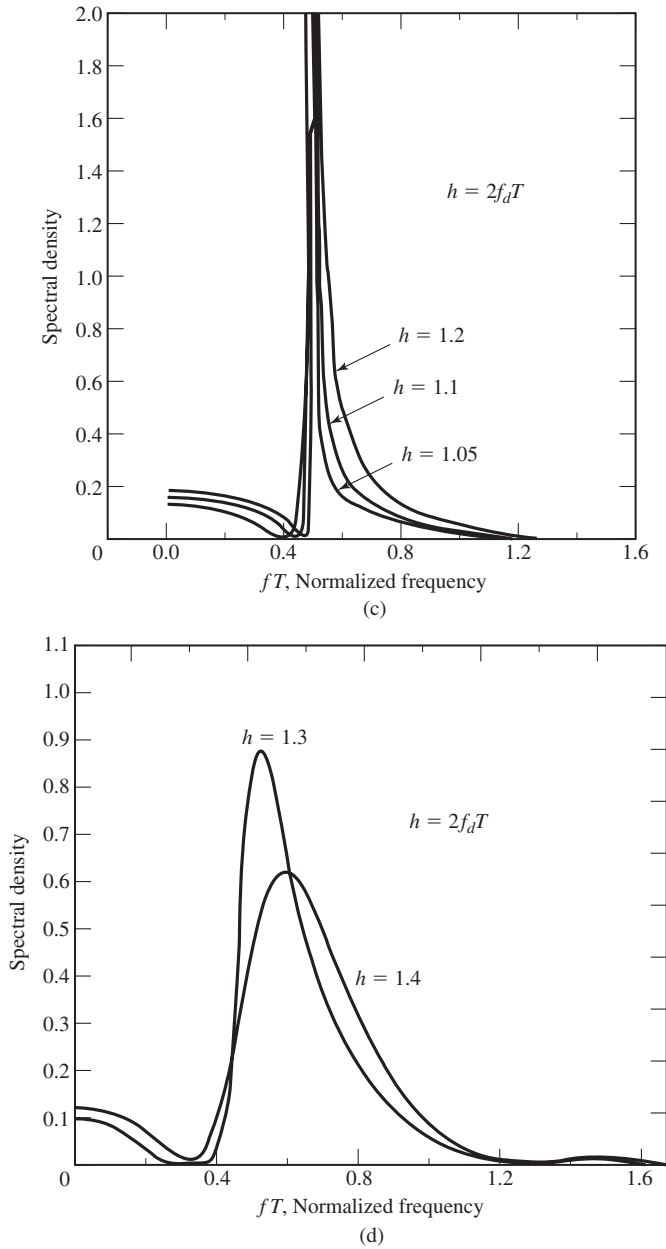
$$\beta = \frac{\sin M\pi h}{M \sin \pi h} \quad (10.2.26)$$

The power-spectral density of CPFSK for  $M = 2$  is plotted in Figure 10.29 as function of the normalized frequency  $fT$ , with the modulation index  $h = 2f_d T$  as a parameter. Note that only one-half of the spectrum is shown in these graphs, because the spectrum is symmetric in frequency. The origin  $fT = 0$  corresponds to the carrier frequency  $f_c$  in the spectrum of the real-valued signal.

These graphs show that the spectrum of the CPFSK signal is relatively smooth and well-confined for  $h < 1$ . As  $h$  approaches unity, the spectra become very peaked and, for  $h = 1$ , where  $|\beta| = 1$ , we find that impulses occur at  $M$  frequencies. When



**Figure 10.29** Power-density spectrum of binary CPFSK. (From *Digital Communications*, 2nd Ed., by J. G. Proakis; © 1989 McGraw-Hill. Reprinted with permission of the publisher.)

**Figure 10.29** (continued)

$h > 1$ , the spectrum becomes much broader. In communication systems that employ CPFSK, the modulation index is selected to conserve bandwidth, so that  $h < 1$ .

The special case of binary CPFSK with  $h = 1/2$  (or  $f_d = 1/4T_b$ ) and  $\beta = 0$ , corresponds to MSK. In this case, the power-spectral density obtained from Equation (10.2.22) through Equation (10.2.26) is

$$\mathcal{S}_V(f) = \frac{32\mathcal{E}_s}{\pi^2} \left[ \frac{\cos 2\pi f T}{1 - 16f^2 T^2} \right]^2 \quad (10.2.27)$$

In contrast, the power-density spectrum of SQPSK with a rectangular pulse  $g_T(t)$  of duration  $T = 2T_b$  is

$$\mathcal{S}_V(f) = 4\mathcal{E}_s \left( \frac{\sin 2\pi f T_b}{2\pi f T_b} \right)^2 \quad (10.2.28)$$

The power-density spectra in Equations (10.2.27) and (10.2.28) are illustrated in Figure 10.30. Note that the main lobe of MSK is 50% wider than that of SQPSK. However, the sidelobes of MSK fall off considerably faster. As a consequence, MSK is significantly more bandwidth efficient than SQPSK.

In the more general case of CPM signals, the use of smooth pulses such as raised cosine pulses (LRC) of the form given in Table 10.2, where  $L = 1$  for full response and  $L > 1$  for partial response, result in smaller bandwidth occupancy and, hence, in greater bandwidth efficiency than the use of rectangular pulses. For example, Figure 10.31

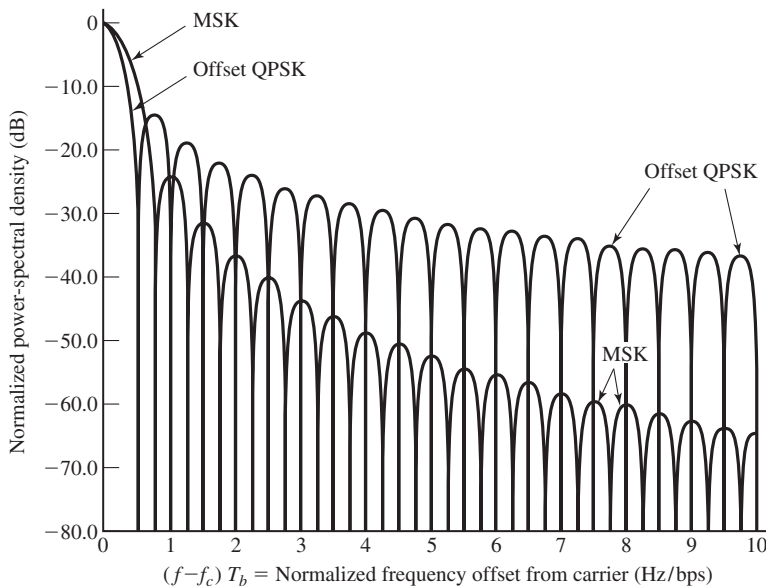


**Figure 10.30** Power-density spectra of MSK and QPSK. (From Gronemeyer and McBride; © 1976 IEEE.)

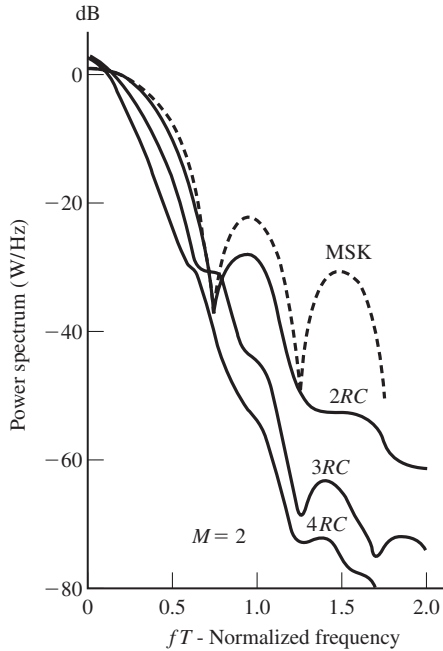


**Figure 10.31** Power-spectral density for binary CPM with  $h = 1/2$  and different pulse shapes (From Aulin et al.; © 1981 IEEE.)

illustrates the power-spectral density for binary CPM with different partial-response raised cosine (LRC) pulses and  $h = 1/2$ . For comparison, the spectrum of binary CPFSK with  $h = 1/2$  (MSK) is also shown. We note that, as  $L$  increases, the pulse  $g_T(t)$  becomes smoother and the corresponding spectral occupancy of the signal is reduced.

The effect of varying the modulation index in a CPM signal is illustrated in Figure 10.32 for the case of  $M = 4$  and a raised cosine pulse of the form given with  $L = 3$ . Note that these spectral characteristics are similar to the ones for CPFSK, except that the power spectra for CPM are narrower due to the smoother raised cosine pulse shape.

#### 10.2.4 Demodulation and Detection of CPM Signals

The transmitted CPM signal may be expressed as

$$u(t) = \sqrt{\frac{2\mathcal{E}_s}{T}} \cos[2\pi f_c t + \theta(t; \mathbf{a})] \quad (10.2.29)$$

where  $\theta(t; \mathbf{a})$  is the carrier phase. The filtered received signal for an additive Gaussian noise channel is

$$r(t) = u(t) + n(t) \quad (10.2.30)$$

where

$$n(t) = n_c(t) \cos 2\pi f_c t - n_s(t) \sin 2\pi f_c t \quad (10.2.31)$$

The optimum receiver for this signal consists of a correlator followed by a ML

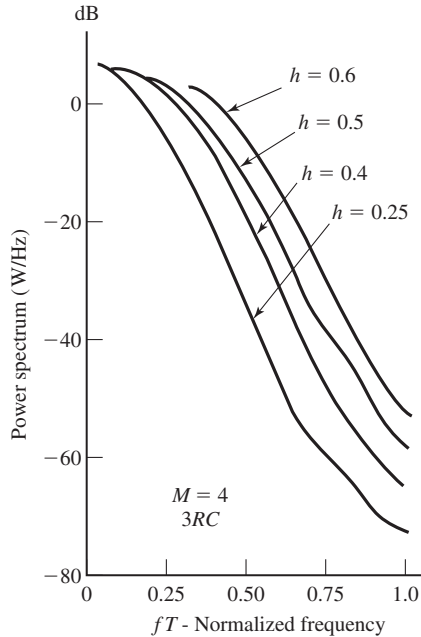


**Figure 10.32** Power-spectral density for  $M = 4$  CPM for 3RC different modulation indices (From Aulin et al.; © 1981 IEEE.)

sequence detector that searches the paths through the state trellis for the minimum Euclidean distance path. The Viterbi algorithm is an efficient method for performing this search. Let us establish the general state trellis structure for CPM and then describe the metric computations.

The carrier phase for a CPM signal having a fixed modulation index  $h$  may be expressed as

$$\begin{aligned}
 \theta(t; \mathbf{a}) &= 2\pi h \sum_{k=-\infty}^n a_k q(t - kT), \quad nT \leq t \leq (n+1)T \\
 &= \pi h \sum_{k=-\infty}^{n-L} a_k + 2\pi h \sum_{k=n-L+1}^n a_k q(t - kT) \\
 &= \theta_n + \phi(t; \mathbf{a}), \quad nT \leq t \leq (n+1)T
 \end{aligned} \tag{10.2.32}$$

where, by definition,

$$\theta_n = \pi h \sum_{k=-\infty}^{n-L} a_k \tag{10.2.33}$$

$$\phi(t; \mathbf{a}) = 2\pi h \sum_{k=n-L+1}^n a_k q(t - kT) \tag{10.2.34}$$



and  $q(t) = 0$  for  $t < 0$ ,  $q(t) = 1/2$  for  $t \geq LT$ , and

$$q(t) = \int_0^t g_T(\tau) d\tau \quad (10.2.35)$$

where  $L$  is a positive integer. The signal pulse  $g_T(t) = 0$  for  $t < 0$  and  $t \geq LT$ . For  $L = 1$  we have a full response CPM signal and for  $L > 1$ , we have a partial response CPM signal. Note that  $\theta_n$  represents the phase of the carrier at  $t = nT$  and  $\phi(t; \mathbf{a})$  represents the additional phase accumulation in the interval  $nT \leq t \leq (n+1)T$ .

When  $h$  is rational; i.e.,  $h = m/p$ , where  $m$  and  $p$  are relatively prime integers, the phases of the CPM signal at  $t = nT$  may be represented by a trellis. The number of terminal phase states for  $L = 1$  is  $p$  for  $m$  even and  $2p$  for  $m$  odd, as previously indicated by Equations (10.2.8) and (10.2.9). However, for  $L > 1$  we have additional phase states due to the partial-response characteristic of the signal pulse  $g_T(t)$ . These additional terminal phase states can be determined by expressing the phase  $\phi(t; \mathbf{a})$  in Equation (10.2.34) as

$$\phi(t; \mathbf{a}) = 2\pi h \sum_{k=n-L+1}^{n-1} a_k q(t - kT) + 2\pi h a_n q(t - nT) \quad (10.2.36)$$

The first term on the right-hand side of Equation (10.2.36) is a function of the information symbols  $(a_{n-1}, a_{n-2}, \dots, a_{n-L+1})$ , which is called the *correlative state vector*, and represents the phase contribution of signal pulses that have not reached their final value. The second term on the right-hand side of Equation (10.2.36) represents the phase contribution due to the most recent symbol  $a_n$ . Therefore, the state of the CPM signal at  $t = nT$  may be expressed as the combined phase state  $\theta_n$  and the correlative state vector  $(a_{n-1}, a_{n-2}, \dots, a_{n-L+1})$ , which we denote as

$$S_n = \{\theta_n, a_{n-1}, \dots, a_{n-L+1}\} \quad (10.2.37)$$

for the partial-response signal of length  $LT$ . Thus, the number of states is

$$N_s = \begin{cases} pM^{L-1} & m \text{ even} \\ 2pM^{L-1} & m \text{ odd} \end{cases} \quad (10.2.38)$$

when  $h = m/p$ .

The state transition from  $S_n$  to  $S_{n+1}$  can be determined by determining the effect of the new symbol  $a_n$  in the time interval  $nT \leq t \leq (n+1)T$ . In general, we have

$$S_{n+1} = \{\theta_{n+1}, a_n, a_{n-1}, \dots, a_{n-L+2}\} \quad (10.2.39)$$

where

$$\theta_{n+1} = \theta_n + \pi h a_{n-L+1} \quad (10.2.40)$$

### Example 10.2.1

Determine the terminal states of a binary signal having a modulation index  $h = 3/4$  and a partial response pulse of  $L = 2$ . Also, sketch the state trellis.

**Solution** Since  $p = 4$ ,  $m$  is odd ( $m = 3$ ) and  $M = 2$ , we have  $N_s = 16$  phase states. The  $2p$  phase states corresponding to  $\theta_n$  are

$$\Theta_s = \left\{ 0, \pm \frac{\pi}{4}, \pm \frac{\pi}{2}, \pm \frac{3\pi}{4}, \pi \right\}$$

For each of these phase states, there are two states that result from the memory due to the partial response signal. Hence, the sixteen states  $S_n = (\theta_n, a_{n-1})$  are

$$\begin{aligned} &(0, +1), (0, -1), (\pi/4, 1), (\pi/4, -1), (-\pi/4, 1), (-\pi/4, -1), \\ &(\pi/2, 1), (\pi/2, -1), (-\pi/2, 1), (-\pi/2, -1), (3\pi/4, 1), (3\pi/4, -1), \\ &(-3\pi/4, 1), (-3\pi/4, -1), (\pi, 1), (\pi, -1) \end{aligned}$$

Suppose the system is in phase state  $\theta_n = 3\pi/4$  and  $a_{n-1} = -1$ . Then  $S_n = (3\pi/4, -1)$  and

$$\begin{aligned} \theta_{n+1} &= \theta_n + \pi h a_{n-1} \\ &= 3\pi/4 + (3\pi/4)(-1) = 0 \end{aligned}$$

Hence,  $S_{n+1} = (\theta_{n+1}, a_n) = (0, a_n)$ . If  $a_n = 1$ , then  $S_{n+1} = (0, 1)$ . If  $a_n = -1$ , then  $S_{n+1} = (0, -1)$ . The state trellis is illustrated in Figure 10.33. A path through the state trellis corresponding to the data sequence  $(1, -1, -1, -1, 1, 1)$  is illustrated in Figure 10.34.

Let us now focus on the demodulation and detection of CPM signals. Since all signal waveforms have the same energy, we may base decisions at the detector on correlation metrics. The crosscorrelation of the received signal  $r(t)$  with each of the possible transmitted signals yields the metrics

$$\begin{aligned} C_n(\mathbf{a}, \mathbf{r}) &= \int_{-\infty}^{(n+1)T} r(t) \cos[2\pi f_c t + \theta(t; \mathbf{a})] dt \\ &= C_{n-1}(\mathbf{a}, \mathbf{r}) + \int_{nT}^{(n+1)T} r(t) \cos[2\pi f_c t + \theta_n + \phi(t; \mathbf{a})] dt \quad (10.2.41) \end{aligned}$$

In the ML sequence detector, the term  $C_{n-1}(\mathbf{a}, \mathbf{r})$  represents the metrics of the surviving sequences up to time  $nT$ . The term

$$C_n(\theta_n; \mathbf{a}, \mathbf{r}) = \int_{nT}^{(n+1)T} r(t) \cos[2\pi f_c t + \theta_n + \phi(t; \mathbf{a})] dt \quad (10.2.42)$$

represents the additional increments to the correlation metrics contributed by the received signal in the time interval  $nT \leq t \leq (n+1)T$ . We observe that there are  $M^L$  possible sequences  $\mathbf{a} = (a_n, a_{n-1}, \dots, a_{n-L+1})$  of symbols and either  $p$  or  $2p$  possible phase states  $\{\theta_n\}$ . Therefore, there are either  $pM^L$  or  $2pM^L$  different values of the correlation metrics  $C_n(\theta_n; \mathbf{a}, \mathbf{r})$  computed in each signal interval and each value is used to increment the metrics corresponding to the surviving sequences from the previous

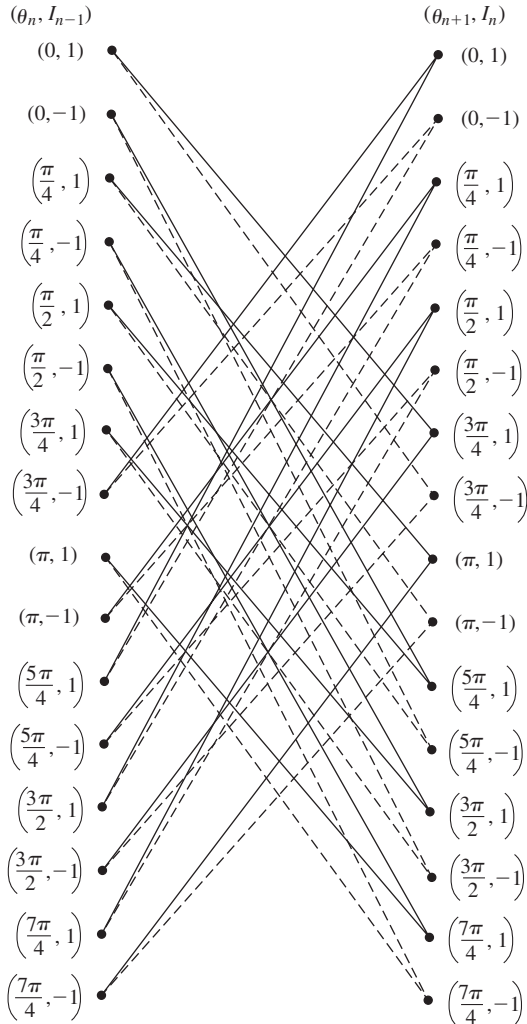


**Figure 10.33** State trellis for partial-response ( $L = 2$ ) CPM with  $h = 3/4$ .

signal interval. A general block diagram that illustrates the computations of  $C_n(\theta_n; \mathbf{a}, \mathbf{r})$  for the Viterbi detector is shown in Figure 10.35.

In the ML sequence detector, the number of surviving sequences at each state of the Viterbi search process is either  $pM^{L-1}$  or  $2pM^{L-1}$ . For each surviving sequence, we have  $M$  new correlation increments  $C_n(\theta_n; \mathbf{a}, \mathbf{r})$  that are added to the existing metrics to yield either  $pM^L$  or  $2pM^L$  sequences with corresponding metrics. However, this number is then reduced back to either  $pM^{L-1}$  or  $2pM^{L-1}$  survivors with corresponding metrics by selecting the most probable sequence of the  $M$  sequences merging at each node of the trellis and discarding the other  $M - 1$  sequences.

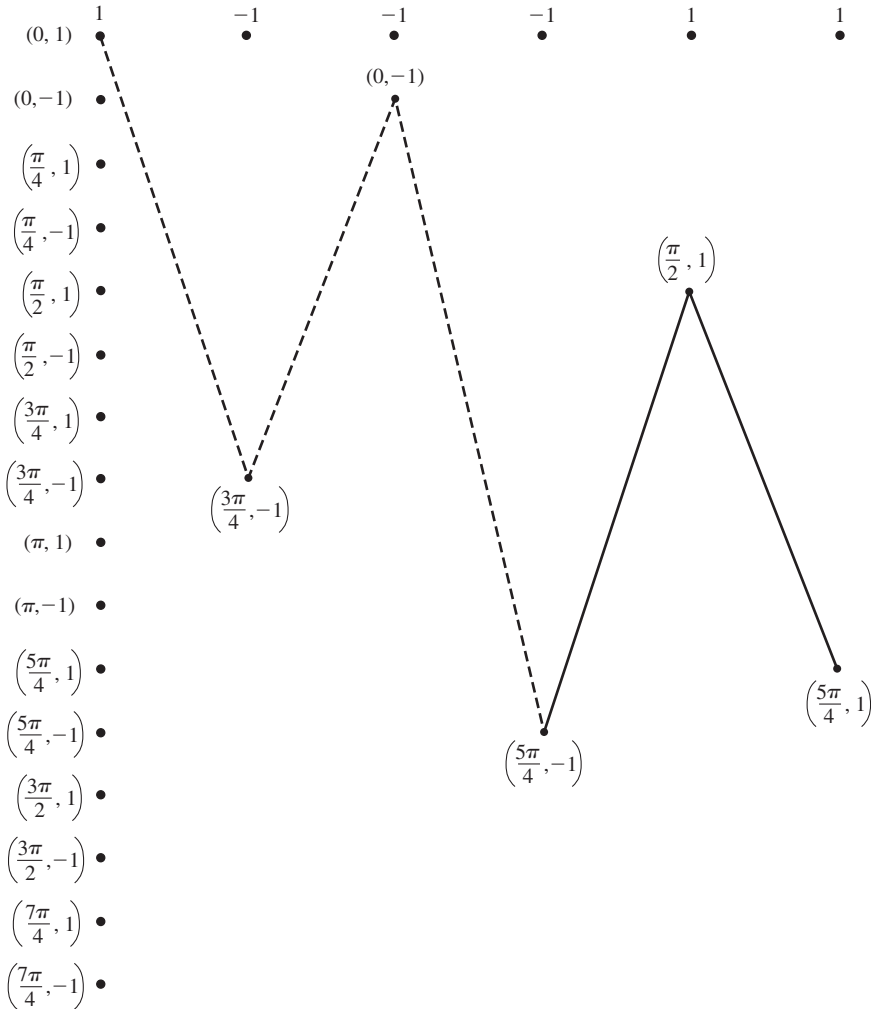


**Figure 10.34** A signal path through the trellis.

Although we have described the ML sequence detector for exploiting the memory inherent in the CPM signal, it is also possible to design symbol-by-symbol detection algorithms based on the maximum a posteriori probability (MAP) criterion that also exploit the signal memory. MAP-type detection algorithms have been devised for CPM signals and can be found in the technical literature. The interested reader may refer to the paper by Gertsman and Lodge (1997) for the derivation of the MAP algorithm for CPM and the evaluation of its performance. In essence, the MAP algorithm is designed to minimize the symbol (bit) error probability and, consequently, it results in a slightly smaller symbol (bit) error probability than the ML sequence detector. More importantly,

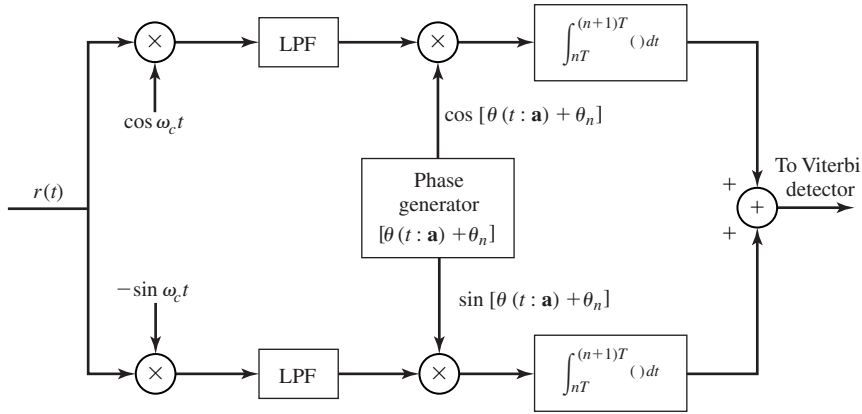


Figure 10.35 Computation of metric increments  $C_n(\theta_n; \mathbf{a}, \mathbf{r})$ .

in the case of coded CPM, the MAP algorithm can be employed for both signal detection and decoding, thus, making it possible to perform iterative demodulation and decoding. In such a case, the performance of the iterative MAP demodulation and decoding algorithms is significantly better than that of a conventional ML sequence detector and decoder.

### 10.2.5 Performance of CPM in AWGN and Rayleigh Fading Channels

In determining the probability of error for the Viterbi detector of CPM signals, we must determine the minimum Euclidean distance of paths through the trellis that separate at a node and remerge at a later time at the same node. The distance between two paths through the trellis depends on the phase difference between the paths, as we now demonstrate.

Suppose that we have two signals  $u_i(t)$  and  $u_j(t)$  corresponding to two phase trajectories  $\theta(t; \mathbf{a}_i)$  and  $\theta(t; \mathbf{a}_j)$ . The sequences  $\mathbf{a}_i$  and  $\mathbf{a}_j$  must be different in their first symbol. Then, the Euclidean squared distance between the two signals over an interval of length  $NT$ , where  $1/T$  is the symbol rate, is defined as

$$\begin{aligned}
 d_{ij}^2 &= \int_0^{NT} [u_i(t) - u_j(t)]^2 dt \\
 &= \int_0^{NT} u_i^2(t) dt + \int_0^{NT} u_j^2(t) dt - 2 \int_0^{NT} u_i(t)u_j(t) dt \\
 &= 2N\mathcal{E}_s - 2 \left( \frac{2\mathcal{E}_s}{T} \right) \int_0^{NT} \cos[2\pi f_c t + \theta(t; \mathbf{a}_i)] \cos[2\pi f_c t + \theta(t; \mathbf{a}_j)] dt \\
 &= \frac{2\mathcal{E}_s}{T} \int_0^{NT} \{1 - \cos[\theta(t; \mathbf{a}_i) - \theta(t; \mathbf{a}_j)]\} dt \tag{10.2.43}
 \end{aligned}$$

Since the symbol energy is related to the energy/bit by the expression  $\mathcal{E}_s = \mathcal{E}_b \log_2 M$ , the squared Euclidean distance  $d_{ij}^2$  may also be expressed

$$d_{ij}^2 = \frac{2\mathcal{E}_b \log_2 M}{T} \int_0^{NT} \{1 - \cos[\theta(t; \mathbf{a}_i) - \theta(t; \mathbf{a}_j)]\} dt \quad (10.2.44)$$

The probability of error for the Viterbi detector in an AWGN channel is dominated by the term corresponding to the minimum Euclidean distance, which is defined as

$$d_{\min}^2 = \lim_{N \rightarrow \infty} \min_{i,j} [d_{ij}^2] \quad (10.2.45)$$

Then, the symbol error probability is approximated as

$$P_M \simeq N_{\min} Q \left( \sqrt{\frac{d_{\min}^2}{2N_0}} \right) \quad (10.2.46)$$

where  $N_{\min}$  is the number of minimum-distance paths. We note that for conventional binary PSK with no memory,  $N = 1$  and  $d_{\min}^2 = d_{12}^2 = 4\mathcal{E}_b$ . Hence, Equation (10.2.46) agrees with our previous result.

In general,  $d_{\min}^2$  is a function of the modulation index  $h$ , the number of symbols  $M$ , and the pulse shape  $g_T(t)$ . The choice of the modulation index  $h$  and the pulse shape have a significant impact in determining the bandwidth occupied by the transmitted signal. The class of raised cosine (LRC) pulses are especially suitable for use in the design of bandwidth efficient CPM signals.

The value of  $d_{\min}^2$  has been evaluated for a variety of CPM signals, including full response and partial response, by Aulin and Sunberg (1981, 1984). For example, Figure 10.36 illustrates the value of  $d_{\min}^2$  normalized by  $4\mathcal{E}_b$  as a function of the time-bandwidth product  $2WT_b$ , where  $W$  is the 99% in-band power bandwidth. Since MSK results in a  $d_{\min}^2 = 4\mathcal{E}_b$ , the MSK signal serves as a point of reference (0 dB) in this graph. Along any curve in Figure 10.36, the bandwidth  $W$  increases as the modulation index  $h$  increases and the SNR gain increases as  $h$  increases. Furthermore, the bandwidth efficiency increases with an increase in the symbol size  $M$  for fixed LRC pulse shape. We observe from this figure, that there are several decibels to be gained by using partial response signals and higher signal alphabets. The major price paid for this performance gain is the added exponentially increasing complexity in the implementation of the Viterbi detector for searching for the most probable path through the trellis. However, reduced complexity Viterbi-type detectors can be implemented with a relatively small loss in performance.

The performance results in Figure 10.36 illustrate that 3–4-dB gain relative to MSK can be easily obtained with relatively no increase in bandwidth by use of raised cosine partial response CPM and  $M = 4$ . Although these results are for raised cosine signal pulses, similar gains can be achieved with other partial response signal shapes. We emphasize that this gain in SNR is achieved by introducing memory into the signal modulation and exploiting this memory in the detection of the signal.

In a fading channel, the performance of CPM is no longer a function of the Euclidean distance between pairs of merging phase trajectories as described above.

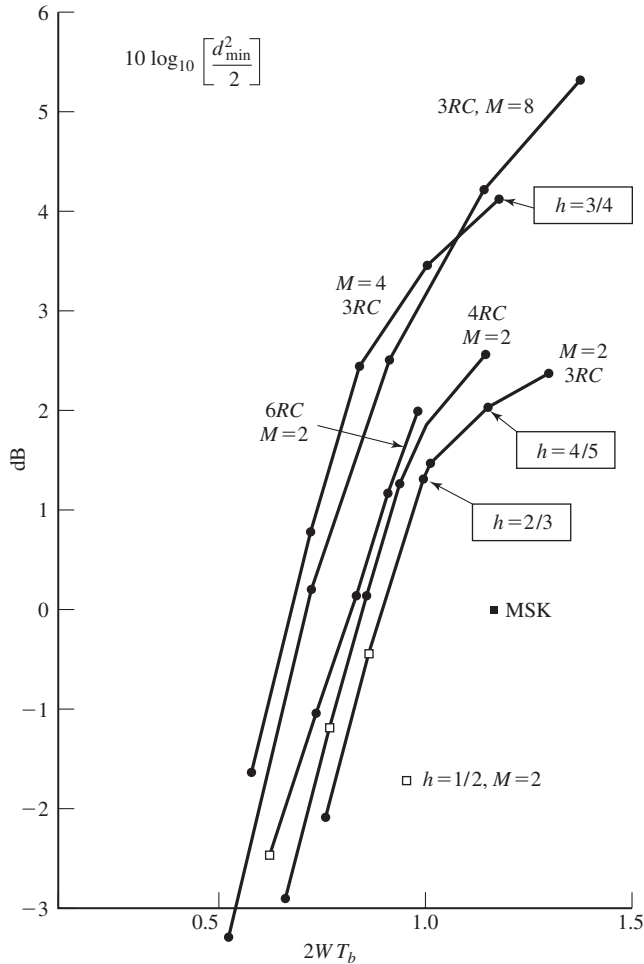


**Figure 10.36** Power bandwidth trade-off for partial-response CPM signals with raised cosine pulses;  $W$  is the 99% in-band power bandwidth. (From Sundberg; © 1986 IEEE.)

In fact, uncoded CPM in a Rayleigh fading channel has performance characteristics similar to conventional uncoded PSK, in which the error probability decays inversely as the received SNR.

To improve the performance of CPM in the presence of fading, we must provide signal diversity, which is most efficiently obtained through coding and interleaving the coded symbols. Toward this goal, we may employ a linear block code or a convolutional code followed by an interleaver prior to the continuous-phase modulator. The interleaver must be sufficiently long so that any pair of coded symbols from the same code word in a block code are separated in time by an amount that exceeds the coherence time

$T_{ct}$  of the channel. Similarly, in the case of a convolutional code, two coded symbols that fall within the constraint length of the code must be separated by the interleaver by at least  $T_{ct}$ . Thus, we achieve independent fading of the coded symbols and a level of diversity equal to  $d_{\min}^H$  or  $d_{\text{free}}^H$  with soft-decision decoding and  $d_{\min}^H/2$  or  $d_{\text{free}}^H/2$  with hard-decision decoding. Consequently, the resulting error probability decays inversely as the SNR raised to the power  $d_{\min}^H$  ( $d_{\text{free}}^H$ ) or  $d_{\min}^H/2$  ( $d_{\text{free}}^H/2$ ) for soft-decision decoding and hard-decision decoding, respectively.

### 10.3 SPREAD-SPECTRUM COMMUNICATION SYSTEMS

In our treatment of signal design for digital communication over an AWGN channel, the major objective has been the efficient utilization of transmitter power and channel bandwidth. As we observed in Chapter 9, channel coding allows us to reduce the transmitter power by increasing the transmitted signal bandwidth through code redundancy and, thus, to trade off transmitter power with channel bandwidth. This is the basic methodology for the design of digital communication systems for AWGN channels.

In practice, one encounters other factors that influence the design of an efficient digital communication system. For example, in multiple-access communication when two or more transmitters use the same common channel to transmit information, the interference created by the users of the channel limits the performance achieved by the system. The system designer must take into account the existence of such interference in the design of a reliable digital communication system.

Even in this complex design problem, the basic system design parameters are transmitter power and channel bandwidth. To overcome the problems of intentional or unintentional interference, we may further increase the bandwidth of the transmitted signal, as described below, so that the bandwidth expansion factor  $B_e = W/R$  is much greater than unity. This is one characteristic of a *spread-spectrum signal*. A second important characteristic is that the information signal at the modulator is spread in bandwidth by means of a code that is independent of the information sequence. This code has the property of being *pseudorandom*; i.e., it appears to be random to receivers other than the intended receiver that uses the knowledge of the code to demodulate the signal. It is this second characteristic property that distinguishes a spread-spectrum communication system from the conventional communication system that expands the transmitted signal bandwidth by means of channel code redundancy. However, we should emphasize that channel coding is an important element in the design of an efficient spread-spectrum communication system.

Spread-spectrum signals for digital communications were originally developed and used for military communications either (1) to provide resistance to jamming (antijam protection), or (2) to hide the signal by transmitting it at low power and, thus, making it difficult for an unintended listener to detect its presence in noise (low probability of intercept). However, spread-spectrum signals are now used to provide reliable communications in a variety of civilian applications, including digital cellular communications and interoffice communications.



In this section we present the basic characteristics of spread-spectrum signals and assess their performance in terms of probability of error. We concentrate our discussion on two methods for spreading the signal bandwidth, namely, by direct sequence modulation and by frequency hopping. Both methods require the use of pseudorandom code sequences whose generation is also described. Several applications of spread-spectrum signals are presented.

### 10.3.1 Model of a Spread-Spectrum Digital Communication System

The basic elements of a spread spectrum digital communication system are illustrated in Figure 10.37. We observe that the channel encoder and decoder and the modulator and demodulator are the basic elements of a conventional digital communication system. In addition to these elements, a spread-spectrum system employs two identical pseudorandom sequence generators, one which interfaces with the modulator at the transmitting end and the second which interfaces with the demodulator at the receiving end. These two generators produce a pseudorandom or pseudonoise (PN) binary-valued sequence, which is used to spread the transmitted signal at the modulator and to despread the received signal at the demodulator.

Time synchronization of the PN sequence generated at the receiver with the PN sequence contained in the received signal is required in order to properly despread the received spread-spectrum signal. In a practical system, synchronization is established prior to the transmission of information by transmitting a fixed PN bit pattern which is designed so that the receiver will detect it with high probability in the presence of interference. After time synchronization of the PN sequence generators is established, the transmission of information commences. In the data mode, the communication system usually tracks the timing of the incoming received signal and keeps the PN sequence generator in synchronism. The synchronization of the PN sequence generators is treated in Section 10.3.7.

Interference is introduced in the transmission of the spread-spectrum signal through the channel. The characteristics of the interference depend to a large extent on its origin. The interference may be generally categorized as being either broadband or narrowband (partial band) relative to the bandwidth of the information-bearing signal, and either continuous in time or pulsed (discontinuous) in time. For example, an

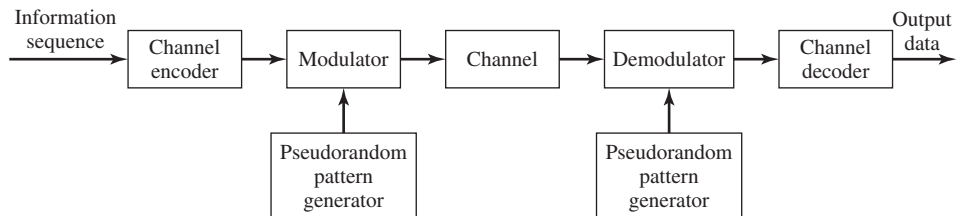


**Figure 10.37** Model of spread-spectrum digital communications system.

interfering signal may consist of a high-power sinusoid in the bandwidth occupied by the information-bearing signal. Such a signal is narrowband. As a second example, the interference generated by other users in a multiple-access channel depends on the type of spread-spectrum signals that are employed by the various users to transmit their information. If all users employ broadband signals, the interference may be characterized as an equivalent broadband noise. If the users employ frequency hopping to generate spread-spectrum signals, the interference from other users may be characterized as narrowband. We shall consider these types of interference and some others in Section 10.3.6.

Our discussion will focus on the performance of spread-spectrum signals for digital communication in the presence of narrowband and broadband interference. Two types of digital modulation are considered, namely, PSK and FSK. PSK modulation is appropriate for applications where phase coherence between the transmitted signal and the received signal can be maintained over a time interval that spans several symbol (or bit) intervals. On the other hand, FSK modulation is appropriate in applications where phase coherence of the carrier cannot be maintained due to time variations in the transmission characteristics of the communications channel. For example, this may be the case in a communications link between two high-speed aircraft or between a high-speed aircraft and a ground-based terminal.

The PN sequence generated at the modulator is used in conjunction with the PSK modulation to shift the phase of the PSK signal pseudorandomly, as described below at a rate that is an integer multiple of the bit rate. The resulting modulated signal is called a *direct-sequence (DS) spread-spectrum signal*. When used in conjunction with binary or  $M$ -ary ( $M > 2$ ) FSK, the PN sequence is used to select the frequency of the transmitted signal pseudorandomly. The resulting signal is called a *frequency-hopped (FH) spread-spectrum signal*. Although other types of spread-spectrum signals can be generated, our treatment will emphasize DS and FH spread-spectrum communication systems, which are the ones generally used in practice.

### 10.3.2 Direct-Sequence Spread-Spectrum Systems

Let us consider the transmission of a binary information sequence by means of binary PSK. The information rate is  $R$  bits/sec and the bit interval is  $T_b = 1/R$  sec. The available channel bandwidth is  $B_c$  Hz, where  $B_c \gg R$ . At the modulator, the bandwidth of the information signal is expanded to  $W = B_c$  Hz by shifting the phase of the carrier pseudorandomly at a rate of  $W$  times/sec according to the pattern of the PN generator. The basic method for accomplishing the spreading is shown in Figure 10.38.

The information-bearing baseband signal is denoted as  $v(t)$  and is expressed as

$$v(t) = \sum_{n=-\infty}^{\infty} a_n g_T(t - nT_b) \quad (10.3.1)$$

where  $\{a_n = \pm 1, -\infty < n < \infty\}$  and  $g_T(t)$  is a rectangular pulse of duration  $T_b$ . This signal is multiplied by the signal from the PN sequence generator, which may be

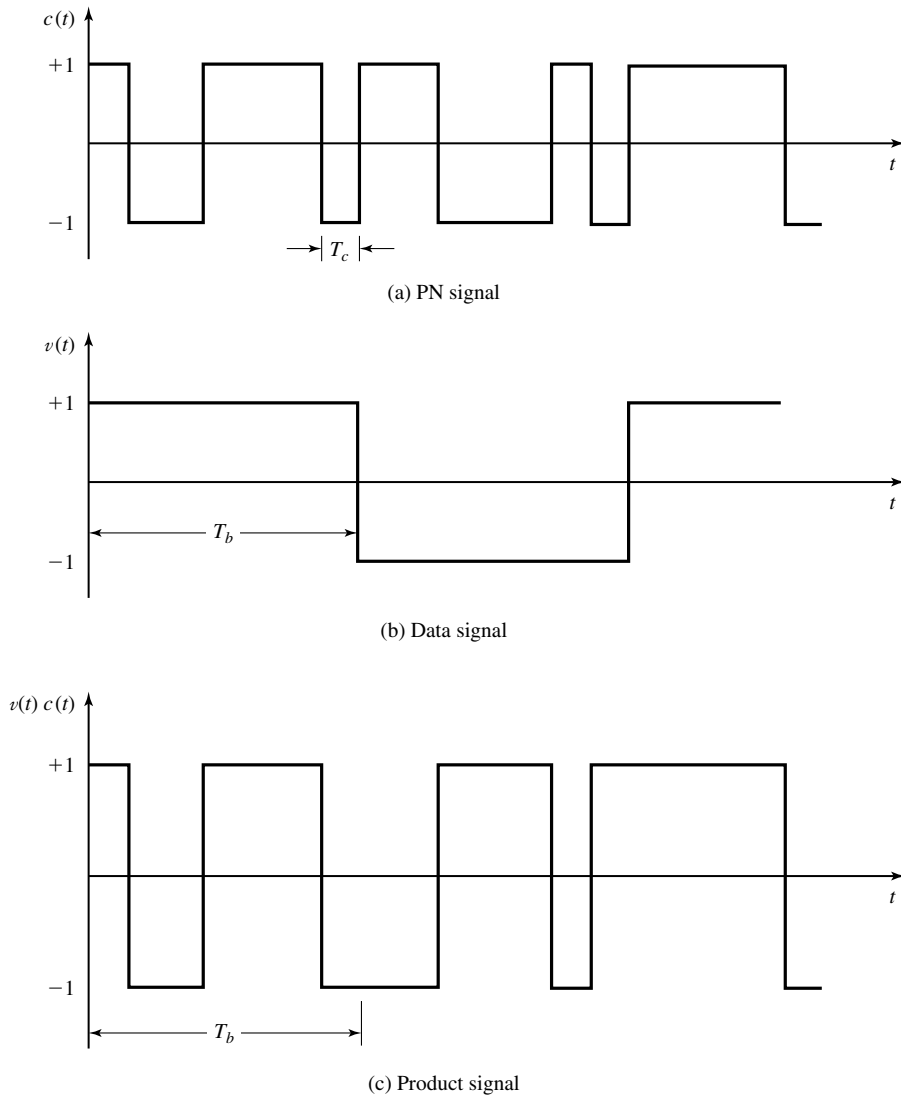


**Figure 10.38** Generation of a DS spread-spectrum signal.

expressed as

$$c(t) = \sum_{n=-\infty}^{\infty} c_n p(t - nT_c) \quad (10.3.2)$$

where  $\{c_n\}$  represents the binary PN code sequence of  $\pm 1$ 's and  $p(t)$  is a rectangular pulse of duration  $T_c$ , as illustrated in Figure 10.38. This multiplication operation

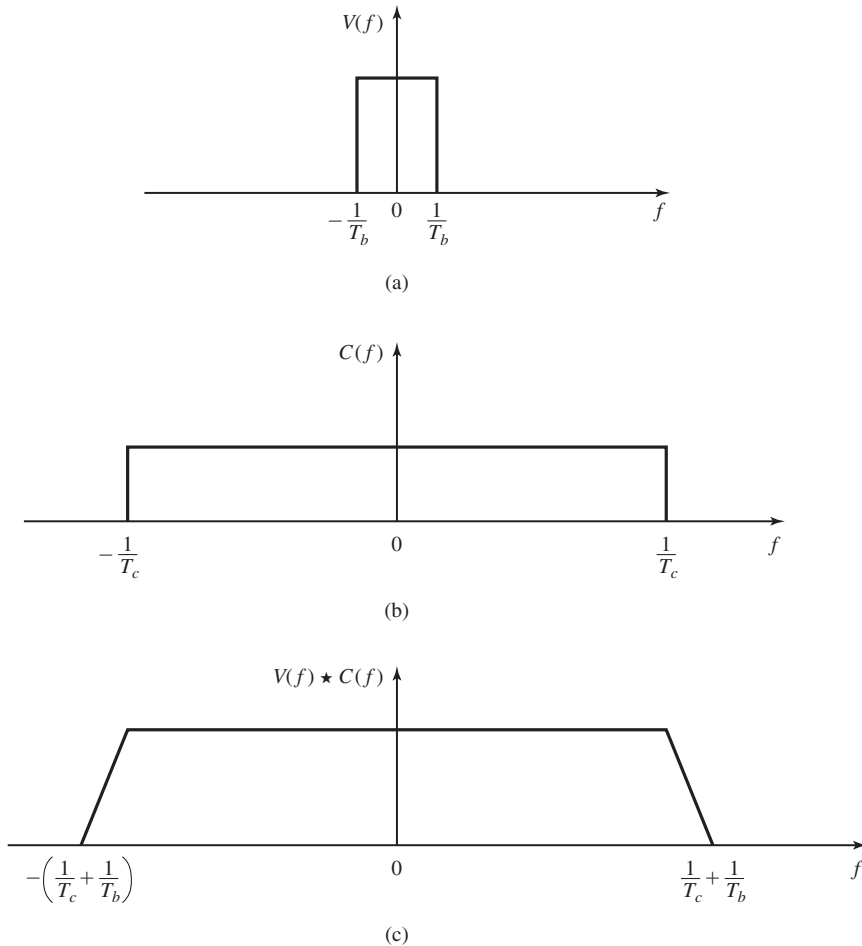


**Figure 10.39** Convolution of spectra of the (a) data signal with the (b) PN code signal.

serves to spread the bandwidth of the information-bearing signal (whose bandwidth is  $R$  Hz, approximately) into the wider bandwidth occupied by PN generator signal  $c(t)$  (whose bandwidth is  $1/T_c$ , approximately). The spectrum spreading is illustrated in Figure 10.39, which shows, in simple terms, using rectangular spectra, the convolution of the two spectra, the narrow spectrum corresponding to the information-bearing signal and the wide spectrum corresponding to the signal from the PN generator.

The product signal  $v(t)c(t)$ , also illustrated in Figure 10.39, is used to amplitude modulate the carrier  $A_c \cos 2\pi f_c t$  and, thus, to generate the DSB-SC signal

$$u(t) = A_c v(t)c(t) \cos 2\pi f_c t \quad (10.3.3)$$

Since  $v(t)c(t) = \pm 1$  for any  $t$ , it follows that the carrier-modulated transmitted signal may also be expressed as

$$u(t) = A_c \cos[2\pi f_c t + \theta(t)] \quad (10.3.4)$$

where  $\theta(t) = 0$  when  $v(t)c(t) = 1$  and  $\theta(t) = \pi$  when  $v(t)c(t) = -1$ . Therefore, the transmitted signal is a binary PSK signal.

The rectangular pulse  $p(t)$  is usually called a *chip* and its time duration  $T_c$  is called the *chip interval*. The reciprocal  $1/T_c$  is called the *chip rate* and corresponds (approximately) to the bandwidth  $W$  of the transmitted signal. The ratio of the bit interval  $T_b$  to the chip interval  $T_c$  is usually selected to be an integer in practical spread spectrum systems. We denote this ratio as

$$L_c = \frac{T_b}{T_c} \quad (10.3.5)$$

Hence,  $L_c$  is the number of chips of the PN code sequence/information bit. Another interpretation is that  $L_c$  represents the number of possible  $180^\circ$  phase transitions in the transmitted signal during the bit interval  $T_b$ .

The demodulation of the signal is performed as illustrated in Figure 10.40. The received signal is first multiplied by a replica of the waveform  $c(t)$  generated by the PN code sequence generator at the receiver, which is synchronized to the PN code in the received signal. This operation is called (spectrum) *despreading*, since the effect of multiplication by  $c(t)$  at the receiver is to undo the spreading operation at the transmitter. Thus, we have

$$A_c v(t) c^2(t) \cos 2\pi f_c t = A_c v(t) \cos 2\pi f_c t \quad (10.3.6)$$

since  $c^2(t) = 1$  for all  $t$ . The resulting signal  $A_c v(t) \cos 2\pi f_c t$  occupies a bandwidth (approximately) of  $R$  Hz, which is the bandwidth of the information-bearing signal. Therefore, the demodulator for the despread signal is simply the conventional cross correlator or matched filter that was previously described in Chapter 7. Since the demodulator has a bandwidth that is identical to the bandwidth of the despread signal, the only additive noise that corrupts the signal at the demodulator is the noise that falls within the information-bandwidth of the received signal.

**Effect of Despreading on a Narrowband Interference.** It is interesting to investigate the effect of an interfering signal on the demodulation of the desired

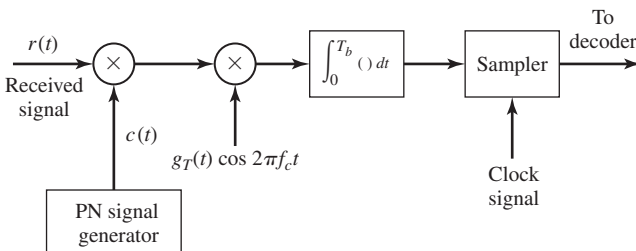


**Figure 10.40** Demodulation of DS spread-spectrum signal.

information-bearing signal. Suppose that the received signal is

$$r(t) = A_c v(t) c(t) \cos 2\pi f_c t + i(t) \quad (10.3.7)$$

where  $i(t)$  denotes the interference. The despreading operation at the receiver yields

$$r(t)c(t) = A_c v(t) \cos 2\pi f_c t + i(t)c(t) \quad (10.3.8)$$

The effect of multiplying the interference  $i(t)$  with  $c(t)$ , is to spread the bandwidth of  $i(t)$  to  $W$  Hz.

As an example, let us consider a sinusoidal interfering signal of the form

$$i(t) = A_I \cos 2\pi f_I t, \quad (10.3.9)$$

where  $f_I$  is a frequency within the bandwidth of the transmitted signal. Its multiplication with  $c(t)$  results in a wideband interference with power-spectral density  $I_0 = P_I/W$ , where  $P_I = A_I^2/2$  is the average power of the interference. Since the desired signal is demodulated by a matched filter (or correlator) that has a bandwidth  $R$ , the total power in the interference at the output of the demodulator is

$$I_0 R_b = P_I R_b / W = \frac{P_I}{W/R_b} = \frac{P_I}{T_b/T_c} = \frac{P_I}{L_c} \quad (10.3.10)$$

Therefore, the power in the interfering signal is reduced by an amount equal to the bandwidth expansion factor  $W/R$ . The factor  $W/R = T_b/T_c = L_c$  is called the *processing gain* of the spread-spectrum system. The reduction in interference power is the basic reason for using spread-spectrum signals to transmit digital information over channels with interference.

In summary, the PN code sequence is used at the transmitter to spread the information-bearing signal into a wide bandwidth for transmission over the channel. By multiplying the received signal with a synchronized replica of the PN code signal, the desired signal is despread back to a narrow bandwidth while any interference signals are spread over a wide bandwidth. The net effect is a reduction in the interference power by the factor  $W/R$ , which is the processing gain of the spread-spectrum system.

The PN code sequence  $\{c_n\}$  is assumed to be known only to the intended receiver. Any other receiver that does not have knowledge of the PN code sequence cannot demodulate the signal. Consequently, the use of a PN code sequence provides a degree of privacy (or security) that is not possible to achieve with conventional modulation. The primary cost for this security and performance gain against interference is an increase in channel bandwidth utilization and in the complexity of the communication system.

**Probability of Error.** To derive the probability of error for a DS spread-spectrum system, we assume that the information is transmitted via binary PSK. Within the bit interval  $0 \leq t \leq T_b$ , the transmitted signal is

$$s(t) = a_o g_T(t) c(t) \cos 2\pi f_c t, \quad 0 \leq t \leq T_b \quad (10.3.11)$$

where  $a_o = \pm 1$  is the information symbol, the pulse  $g_T(t)$  is defined as

$$g_T(t) = \begin{cases} \sqrt{\frac{2\mathcal{E}_b}{T_b}}, & 0 \leq t \leq T_b \\ 0, & \text{otherwise} \end{cases} \quad (10.3.12)$$

and  $c(t)$  is the output of the PN code generator which, over a bit interval, is expressed as

$$c(t) = \sum_{n=0}^{L_c-1} c_n p(t - nT_c) \quad (10.3.13)$$

where  $L_c$  is the number of chips per bit,  $T_c$  is the chip interval, and  $\{c_n\}$  denotes the PN code sequence. The code chip sequence  $\{c_n\}$  is uncorrelated (white); i.e.,

$$E(c_n c_m) = E(c_n)E(c_m) \quad \text{for } n \neq m \quad (10.3.14)$$

and each chip is  $+1$  or  $-1$  with equal probability. These conditions imply that  $E(c_n) = 0$  and  $E(c_n^2) = 1$ .

The received signal is assumed to be corrupted by an additive interfering signal  $i(t)$ . Hence,

$$r(t) = a_o g_T(t - t_d) c(t - t_d) \cos(2\pi f_c t + \phi) + i(t) \quad (10.3.15)$$

where  $t_d$  represents the propagation delay through the channel and  $\phi$  represents the carrier-phase shift. Since the received signal  $r(t)$  is the output of an ideal bandpass filter in the front end of the receiver, the interference  $i(t)$  is also a bandpass signal, and may be represented as

$$i(t) = i_c(t) \cos 2\pi f_c t - i_s(t) \sin 2\pi f_c t \quad (10.3.16)$$

where  $i_c(t)$  and  $i_s(t)$  are the two quadrature components.

Assuming that the receiver is perfectly synchronized to the received signal, we may set  $t_d = 0$  for convenience. In addition, the carrier phase is assumed to be perfectly estimated by a PLL. Then, the signal  $r(t)$  is demodulated by first despreading through multiplication by  $c(t)$  and then crosscorrelation with  $g_T(t) \cos(2\pi f_c t + \phi)$ , as shown in Figure 10.41. At the sampling instant  $t = T_b$ , the output of the correlator is

$$y(T_b) = \mathcal{E}_b + y_i(T_b) \quad (10.3.17)$$

where  $y_i(T_b)$  represents the interference component, which has the form

$$\begin{aligned} y_i(T_b) &= \int_0^{T_b} c(t) i(t) g_T(t) \cos(2\pi f_c t + \phi) dt \\ &= \sum_{n=0}^{L_c-1} c_n \int_0^{T_b} p(t - nT_c) i(t) g_T(t) \cos(2\pi f_c t + \phi) dt \\ &= \sqrt{\frac{2\mathcal{E}_b}{T_b}} \sum_{n=0}^{L_c-1} c_n v_n \end{aligned} \quad (10.3.18)$$

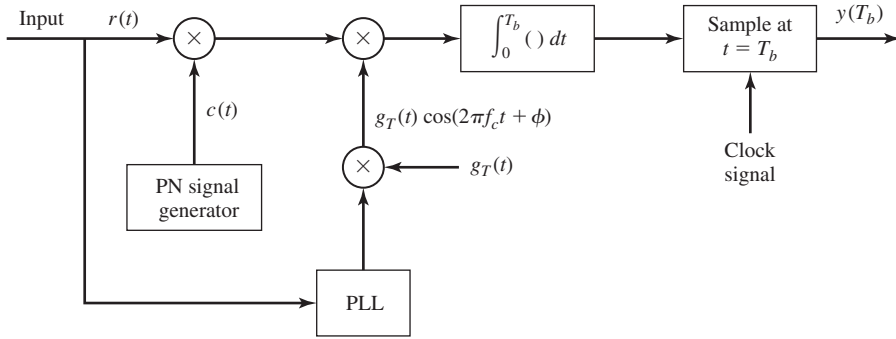


**Figure 10.41** DS spread-spectrum signal demodulator.

where, by definition,

$$v_n = \int_{nT_c}^{(n+1)T_c} i(t) \cos(2\pi f_c t + \phi) dt \quad (10.3.19)$$

The probability of error depends on the statistical characteristics of the interference component. Clearly, its mean value is

$$E[y_i(T_b)] = 0 \quad (10.3.20)$$

Its variance is

$$E[y_i^2(T_b)] = \frac{2\mathcal{E}_b}{T_b} \sum_{n=0}^{L_c-1} \sum_{m=0}^{L_c-1} E(c_n c_m) E(v_n v_m)$$

But  $E(c_n c_m) = \delta_{mn}$ . Therefore,

$$\begin{aligned} E[y_i^2(T_b)] &= \frac{2\mathcal{E}_b}{T_b} \sum_{n=0}^{L_c-1} E(v_n^2) \\ &= \frac{2\mathcal{E}_b}{T_b} L_c E(v^2) \end{aligned} \quad (10.3.21)$$

where  $v = v_n$ , as given by Equation (10.3.19). To determine the variance of  $v$ , we must postulate the form of the interference.

First, let us assume that the interference is sinusoidal. Specifically, we assume that the interference is at the carrier frequency, and has the form

$$i(t) = \sqrt{2P_I} \cos(2\pi f_c t + \Theta_I) \quad (10.3.22)$$

where  $P_I$  is the average power and  $\Theta_I$  is the phase of the interference, which we assume to be random and uniformly distributed over the interval  $(0, 2\pi)$ . If we substitute for



$i(t)$  in Equation (10.3.19), we obtain

$$\begin{aligned} v_n &= \int_{nT_c}^{(n+1)T_c} \sqrt{2P_I} \cos(2\pi f_c t + \Theta_I) \cos(2\pi f_c t + \phi) dt \\ &= \frac{1}{2} \sqrt{2P_I} \int_{nT_c}^{(n+1)T_c} \cos(\Theta_I - \phi) dt = \frac{T_c}{2} \sqrt{2P_I} \cos(\Theta_I - \phi) \end{aligned} \quad (10.3.23)$$

Since  $\Theta_I$  is a random variable,  $v_n$  is also random. Its mean value is zero; i.e.,

$$E(v_n) = \frac{T_c}{2} \sqrt{2P_I} \int_0^{2\pi} \frac{1}{2\pi} \cos(\Theta_I - \phi) d\Theta_I = 0 \quad (10.3.24)$$

Its mean-square value is

$$\begin{aligned} E(v_n^2) &= \frac{T_c^2 P_I}{2} \frac{1}{2\pi} \int_0^{2\pi} \cos^2(\Theta_I - \phi) d\Theta_I \\ &= \frac{T_c^2 P_I}{4} \end{aligned} \quad (10.3.25)$$

We may now substitute for  $E(v^2)$  into Equation (10.3.21). Thus, we obtain

$$E[y_i^2(T_b)] = \frac{\mathcal{E}_b P_I T_c}{2} \quad (10.3.26)$$

The ratio of  $\{E[y(T_b)]\}^2$  to  $E[y_i^2(T_b)]$  is the SNR the detector. In this case we have

$$(\text{SNR})_D = \frac{\mathcal{E}_b^2}{\mathcal{E}_b P_I T_c / 2} = \frac{2\mathcal{E}_b}{P_I T_c} \quad (10.3.27)$$

To see the effect of the spread-spectrum signal, we express the transmitted energy  $\mathcal{E}_b$  as

$$\mathcal{E}_b = P_S T_b \quad (10.3.28)$$

where  $P_S$  is the average signal power. Then, if we substitute for  $\mathcal{E}_b$  in Equation (10.3.27), we obtain

$$(\text{SNR})_D = \frac{2P_S T_b}{P_I T_c} = \frac{2P_S}{P_I / L_c} \quad (10.3.29)$$

where  $L_c = T_b / T_c$  is the processing gain. Therefore, the spread-spectrum signal has reduced the power of the interference by the factor  $L_c$ .

Another interpretation of the effect of the spread-spectrum signal on the sinusoidal interference is obtained if we express  $P_I T_c$  in Equation (10.3.29) as follows. Since  $T_c \simeq 1/W$ , we have

$$P_I T_c = P_I / W \equiv I_0 \quad (10.3.30)$$

where  $I_0$  is the power-spectral density of an equivalent interference in a bandwidth  $W$ . Therefore, in effect, the spread-spectrum signal has spread the sinusoidal interference over the wide bandwidth  $W$ , creating an equivalent spectrally flat noise with

power-spectral density  $I_0$ . Hence,

$$(\text{SNR})_D = \frac{2\mathcal{E}_b}{I_0} \quad (10.3.31)$$

### Example 10.3.1

The SNR required at the detector to achieve reliable communication in a DS spread-spectrum communication system is 13 dB. If the interference-to-signal power at the receiver is 20 dB, determine the processing gain required to achieve reliable communication.

**Solution** We are given  $(P_I/P_S)_{\text{dB}} = 20$  dB or, equivalently,  $P_I/P_S = 100$ . We are also given  $(\text{SNR})_D = 13$  dB, or equivalently,  $(\text{SNR})_D = 20$ . The relation in Equation (10.2.29) may be used to solve for  $L_c$ . Thus,

$$L_c = \frac{1}{2} \left( \frac{P_I}{P_S} \right) (\text{SNR})_D = 1000$$

Therefore, the processing gain required is 1000 or, equivalently, 30 dB.

As a second case, let us consider the effect of an interference  $i(t)$  that is a zero-mean broadband random process with a constant power-spectral density over the bandwidth  $W$  of the spread-spectrum signal, as illustrated in Figure 10.42. Note that the total interference power is

$$P_I = \int_{-\infty}^{\infty} \mathcal{S}_{ii}(f) df = WI_0 \quad (10.3.32)$$

The variance of the interference component at the input to the detector is given by Equation (10.3.21). To evaluate the moment  $E(v^2)$ , we substitute the bandpass representation of  $i(t)$ , given by Equation (10.3.16), into Equation (10.3.19). By neglecting the double frequency terms (terms involving  $\cos 4\pi f_c t$ ) and making use of the statistical properties of the quadrature components, namely  $E[i_c(t)] = E[i_s(t)] = 0$ , and

$$\begin{aligned} R_{i_c}(\tau) &= E[i_c(t)i_c(t+\tau)] = E[i_s(t)i_s(t+\tau)] \\ &= I_0 \frac{\sin \pi W \tau}{\pi \tau} \end{aligned} \quad (10.3.33)$$

we obtain the result

$$E(v^2) = \frac{1}{4} \int_0^{T_c} \int_0^{T_c} R_{i_c}(t_1 - t_2) dt_1 dt_2 \quad (10.3.34)$$

This is an integral of the autocorrelation function over the square defined by the region  $0 \leq t_1 \leq T_c$  and  $0 \leq t_2 \leq T_c$ , as shown in Figure 10.43. If we let  $\tau = t_1 - t_2$ ,  $E(v^2)$

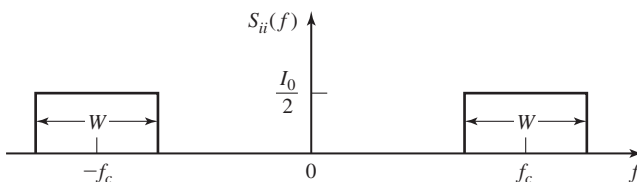


**Figure 10.42** Power-spectral density of broadband interference.

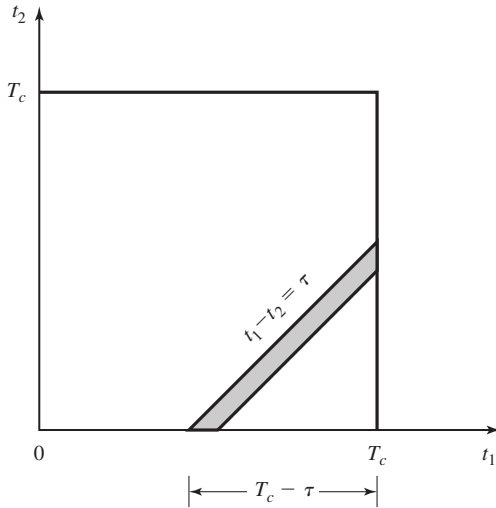


**Figure 10.43** Region of integration of the autocorrelation function  $R_{cc}(t_1, t_2)$ .

can be reduced to the single integral (see Figure 10.43)

$$\begin{aligned}
 E(v^2) &= \frac{1}{4} \int_{-T_c}^{T_c} (T_c - |\tau|) R_{nc}(\tau) d\tau \\
 &= \frac{I_0 T_c}{4} \int_{-T_c}^{T_c} \left(1 - \frac{|\tau|}{T_c}\right) \frac{\sin \pi W \tau}{\pi \tau} d\tau \\
 &= \frac{P_I T_c}{4W} \int_{-T_c}^{T_c} \left(1 - \frac{|\tau|}{T_c}\right) \frac{\sin \pi W \tau}{\pi \tau} d\tau \quad (10.3.35)
 \end{aligned}$$

Since  $T_c \approx \alpha/W$ , where  $\alpha > 0$ , the above integral may be expressed as

$$J(\alpha) = 2 \int_0^{\alpha} \left(1 - \frac{x}{\alpha}\right) \frac{\sin \pi x}{\pi x} dx \quad (10.3.36)$$

and it can be numerically evaluated for any value of  $\alpha$ . Figure 10.44 illustrates  $J(\alpha)$ . Note that  $J(\alpha) \leq 1$  for any value of  $\alpha$  and that  $J(\alpha) \rightarrow 1$  as  $\alpha \rightarrow \infty$ .

By combining the results in Equations (10.3.21), (10.3.35) and (10.3.36), we conclude that the variance of the interference component  $y_i(T_b)$  for the broadband interference is

$$E[y_i^2(T_b)] = \frac{\mathcal{E}_b P_I T_c}{2} J(\alpha) \quad (10.3.37)$$

Therefore, the SNR at the detector is

$$(\text{SNR})_D = \frac{2\mathcal{E}_b}{I_0 J(\alpha)} \quad (10.3.38)$$

If we compare Equation (10.3.31) with Equation (10.3.38) we observe that the SNR for the case of the broadband interference is larger due to the factor  $J(\alpha)$ . Hence, the

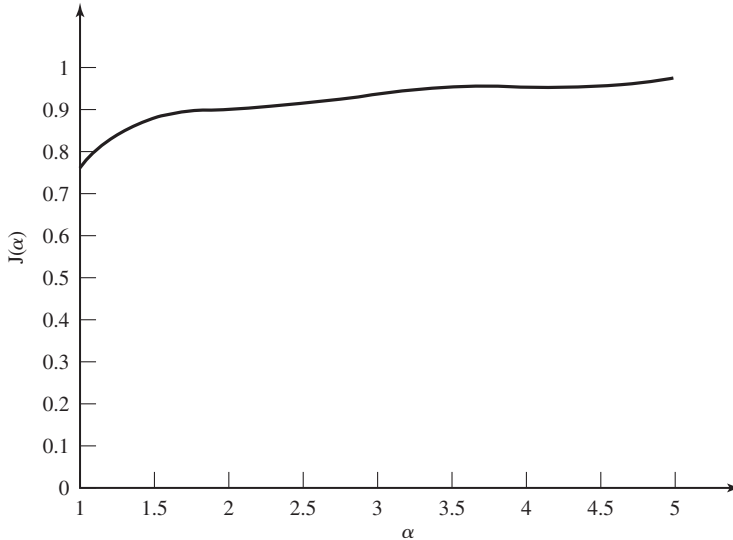


**Figure 10.44** Plot of the function  $J(\alpha)$  given in (10.3.30).

sinusoidal interference results in a somewhat larger degradation in the performance of the DS spread-spectrum system compared to that of a broadband interference.

The probability of error for a DS spread-spectrum system with binary PSK modulation is easily obtained from the SNR at the detector, if we make an assumption on the probability distribution of the sample  $y_i(T_b)$ . From Equation (10.3.18) we note that  $y_i(T_b)$  consists of a sum  $L_c$  uncorrelated random variables  $\{c_n v_n, 0 \leq n \leq L_c - 1\}$ , all of which are identically distributed. Since the processing gain  $L_c$  is usually large in any practical system, we may use the Central Limit Theorem to justify a Gaussian probability distribution for  $y_i(T)$ . Under this assumption, the probability of error for the sinusoidal interference is

$$P_b = Q\left(\sqrt{\frac{2\mathcal{E}_b}{I_0}}\right) \quad (10.3.39)$$

where  $I_0$  is the power-spectral density of an equivalent broadband interference. A similar expression holds for the case of a broadband interference, where the SNR at the detector is increased by the factor  $1/J(\alpha)$ .

**The Interference Margin.** We may express  $\frac{\mathcal{E}_b}{I_0}$  in the  $Q$ -function in Equation (10.3.39) as

$$\frac{\mathcal{E}_b}{I_0} = \frac{P_S T_b}{P_I / W} = \frac{P_S / R}{P_I / W} = \frac{W / R}{P_I / P_S} \quad (10.3.40)$$

Also, suppose we specify a required  $\mathcal{E}_b/I_0$  to achieve a desired level of performance. Then, using a logarithmic scale, we may express Equation (10.3.40) as

$$10 \log \frac{P_I}{P_S} = 10 \log \frac{W}{R} - 10 \log \left( \frac{\mathcal{E}_b}{I_0} \right) \quad (10.3.41)$$

$$\left( \frac{P_I}{P_S} \right)_{\text{dB}} = \left( \frac{W}{R} \right)_{\text{dB}} - \left( \frac{\mathcal{E}_b}{I_0} \right)_{\text{dB}}$$

The ratio  $(P_I/P_S)_{\text{dB}}$  is called the *interference margin*. This is the relative power advantage that an interference may have without disrupting the communication system.

### Example 10.3.2

Suppose we require an  $(\mathcal{E}_b/I_0)_{\text{dB}} = 10$  dB to achieve reliable communication. What is the processing gain that is necessary to provide an interference margin of 20 dB?

**Solution** Clearly, if  $W/R = 1000$ , then  $(W/R)_{\text{dB}} = 30$  dB and the interference margin is  $(P_I/P_S)_{\text{dB}} = 20$  dB. This means that the average interference power at the receiver may be 100 times the power  $P_S$  of the desired signal and we can still maintain reliable communication.

**Performance of Coded Spread-Spectrum Signals.** As shown in Chapter 9, when the transmitted information is coded by a binary linear (block or convolutional) code, the SNR at the output of a soft-decision decoder is increased by the coding gain, defined as

$$\text{coding gain} = R_c d_{\min}^H \quad (10.3.42)$$

where  $R_c$  is the code rate and  $d_{\min}^H$  is the minimum Hamming distance of the code. Therefore, the effect of coding is to increase the interference margin by the coding gain. Thus, Equation (10.3.41) may be modified as

$$\left( \frac{P_I}{P_S} \right)_{\text{dB}} = \left( \frac{W}{R} \right)_{\text{dB}} + (CG)_{\text{dB}} - \left( \frac{\mathcal{E}_b}{I_0} \right)_{\text{dB}} \quad (10.3.43)$$

where  $(CG)_{\text{dB}}$  denotes the coding gain.

### 10.3.3 Some Applications of DS Spread-Spectrum Signals

In this subsection, we briefly describe the use of DS spread-spectrum signals in three applications. First, we consider an application in which the signal is transmitted at very low power, so that a listener trying to detect the presence of the signal would encounter great difficulty. A second application is multiple-access radio communications. A third application involves the use of a DS spread-spectrum signal to resolve the multipath in a time-dispersive radio channel.

**Low-detectability Signal Transmission.** In this application, the information-bearing signal is transmitted at a very low power level relative to the background channel noise and thermal noise that is generated in the front end of a receiver. If the DS spread-spectrum signal occupies a bandwidth  $W$  and the power-spectral density of the additive noise is  $N_0$  W/Hz, the average noise power in the bandwidth  $W$  is  $P_N = WN_0$ .

The average received signal power at the intended receiver is  $P_R$ . If we wish to hide the presence of the signal from receivers that are in the vicinity of the intended receiver, the signal is transmitted at a power level such that  $P_R/P_N \ll 1$ . The intended receiver can recover the weak information-bearing signal from the background noise with the aid of the processing gain and the coding gain. However, any other receiver which has no knowledge of the PN code sequence is unable to take advantage of the processing gain and the coding gain. Consequently, the presence of the information-bearing signal is difficult to detect. We say that the transmitted signal has a *low probability of being intercepted* (LPI) and it is called an *LPI signal*.

The probability of error given in Section 10.3.2 applies as well to the demodulation and decoding of LPI signals at the intended receiver.

### Example 10.3.3

A DS spread-spectrum signal is designed so that the power ratio  $P_R/P_N$  at the intended receiver is  $10^{-2}$ ; (a) if the desired  $\mathcal{E}_b/N_0 = 10$  for acceptable performance, determine the minimum value of the processing gain; and (b) suppose that the DS spread-spectrum signal is transmitted via radio to a receiver at a distance of 2000 Km. The transmitter antenna has a gain of 20 dB, while the receiver antenna is omnidirectional. The carrier frequency is 3 MHz, the available channel bandwidth  $W = 10^5$  Hz and the receiver has a noise temperature of 300 K. Determine the required transmitter power and the bit rate of the DS spread-spectrum system.

**Solution** (a) We may write  $\mathcal{E}_b/N_0$  as

$$\frac{\mathcal{E}_b}{N_0} = \frac{P_R T_b}{N_0} = \frac{P_R L_c T_c}{N_0} = \left( \frac{P_R}{W N_0} \right) L_c = \left( \frac{P_R}{P_N} \right) L_c$$

Since  $\mathcal{E}_b/N_0 = 10$  and  $P_R/P_N = 10^{-2}$ , it follows that the necessary processing gain is  $L_c = 1000$ .

(b) The expression for the received signal power is

$$P_{R\text{dB}} = P_{T\text{dB}} - L_{s\text{dB}} + G_{T\text{dB}}$$

where  $L_{s\text{dB}}$  is the free-space path loss and  $G_{T\text{dB}}$  is the antenna gain. The path loss is

$$L_{s\text{dB}} = 20 \log \left( \frac{4\pi d}{\lambda} \right)$$

where the wavelength  $\lambda = 100$  meters. Hence,

$$L_{s\text{dB}} = 20 \log(8\pi \times 10^4) = 108 \text{ dB}$$

Therefore,

$$\begin{aligned} P_{T\text{dB}} &= P_{R\text{dB}} + 108 - 20 \\ &= P_{R\text{dB}} + 88 \end{aligned}$$

The received power level can be obtained from the condition  $P_R/P_N = 10^{-2}$ . First of all,  $P_N = W N_0$ , where  $N_0 = kT = 4 \times 10^{-21}$  W/Hz and  $W = 10^5$  Hz. Hence,

$$P_N = 4.1 \times 10^{-16} \text{ W}$$

and

$$P_R = 4.1 \times 10^{-18} \text{ W}$$

or, equivalently,  $P_{R\text{dB}} = -174$  dBW. Therefore,

$$P_{T\text{dB}} = P_{R\text{dB}} + 88 = -86 \text{ dBW}$$

or, equivalently,  $P_T = 2.5 \times 10^{-9}$  W. The bit rate is  $R = W/L_c = 10^5/10^3 = 100$  bps.

**Code Division Multiple Access.** The enhancement in performance obtained from a DS spread-spectrum signal through the processing gain and the coding gain can be used to enable many DS spread-spectrum signals to occupy the same channel bandwidth provided that each signal has its own pseudorandom (signature) sequence. Thus, it is possible to have several users transmit messages simultaneously over the same channel bandwidth. This type of digital communication in which each transmitter-receiver user pair has its own distinct signature code for transmitting over a common channel bandwidth is called *code division multiple access (CDMA)*.

In the demodulation of each DS spread-spectrum signal, the signals from the other simultaneous users of the channel appear as additive interference. The level of interference varies as a function of the number of users of the channel at any given time. A major advantage of CDMA is that a large number of users can be accommodated if each user transmits messages for a short period of time. In such a multiple access system, it is relatively easy either to add new users or to decrease the number of users without reconfiguring the system.

Next, we determine the number of simultaneous signals that can be accommodated in a CDMA system. For simplicity, we assume that all signals have identical average powers. In many practical systems, the received signal power level from each user is monitored at a central station and power control is exercised over all simultaneous users by use of a control channel that instructs the users on whether to increase or decrease their power level. With such power control, if there are  $N_u$  simultaneous users, the desired signal-to-noise interference power ratio at a given receiver is

$$\frac{P_S}{P_N} = \frac{P_S}{(N_u - 1)P_S} = \frac{1}{N_u - 1} \quad (10.3.44)$$

From this relation, we can determine the number of users that can be accommodated simultaneously. The following example illustrates the computation.

#### Example 10.3.4

Suppose that the desired level of performance for a user in a CDMA system is an error probability of  $10^{-6}$ , which is achieved when  $\mathcal{E}_b/I_0 = 20$  (13 dB). Determine the maximum number of simultaneous users that can be accommodated in a CDMA system if the bandwidth-to-bit-rate ratio is 1000 and the coding gain is  $R_c d_{\min}^H = 4$  (6 dB).

**Solution** From the relationships given in Equations (10.3.43) and (10.3.44), we have

$$\frac{\mathcal{E}_b}{I_0} = \frac{W/R}{N_u - 1} R_c d_{\min}^H = 20$$

If we solve for  $N_u$  we obtain

$$N_u = \frac{W/R}{20} R_c d_{\min}^H + 1$$

For  $W/R = 1000$  and  $R_c d_{\min}^H = 4$ , we obtain the result that  $N_u = 201$ .

In determining the maximum number of simultaneous users of the channel, we implicitly assumed that the pseudorandom code sequences used by the various users are uncorrelated and that the interference from other users adds on a power basis only. However, orthogonality of the pseudorandom sequences among the  $N_u$  users is generally difficult to achieve, especially if  $N_u$  is large. In fact, the design of a large set of pseudorandom sequences with good correlation properties is an important problem that has received considerable attention in the technical literature. We shall briefly treat this problem in Section 10.3.5.

CDMA is a viable method for providing digital cellular telephone service to mobile users. In Section 10.4 we describe the basic characteristics of the North American digital cellular system that employs CDMA.

**Communication Over Channels with Multipath.** In Section 10.1, we described the characteristics of fading multipath channels and the design of signals for effective communication through such channels. Examples of fading multipath channels include ionospheric propagation in the HF frequency band (3–30 MHz) where the ionospheric layers serve as signal reflectors, and in mobile radio communication systems, where the multipath propagation is due to reflection from buildings, trees, and the other obstacles located between the transmitter and the receiver.

Our discussion on signal design in Section 10.1.5 focused on frequency selective channels, where the signal bandwidth  $W$  is larger than the coherence bandwidth  $B_{cb}$  of the channel. If  $W > B_{cb}$ , we considered two approaches to signal design. One approach is to subdivide the available bandwidth  $W$  into  $N$  subchannels such that the bandwidth per channel  $\frac{W}{N} < B_{cb}$ . In this way, each subchannel is frequency nonselective and the signals in each subchannel satisfy the condition that the symbol interval  $T \gg T_m$ , where  $T_m$  is the multipath spread of the channel. Thus, intersymbol interference is avoided. A second approach is to design the signal to utilize the entire signal bandwidth  $W$  and transmit it on a single carrier. In this case, the channel is frequency selective and the multipath components with differential delays of  $\frac{1}{W}$  or greater become resolvable.

DS spread spectrum is a particularly effective way to generate a wideband signal for resolving multipath signal components. By separating the multipath components, we may also reduce the effects of fading. For example, in LOS communication systems where there is a direct path and a secondary propagation path resulting from signal reflecting from buildings and surrounding terrain, the demodulator at the receiver may synchronize to the direct-signal component and ignore the existence of the multipath component. In such a case, the multipath component becomes a form of interference (ISI) on the demodulation of subsequent transmitted signals.

ISI can be avoided if we are willing to reduce the symbol rate  $\frac{1}{T}$  such that  $T \gg T_m$ . In this case, we employ a DS spread-spectrum signal with bandwidth  $W$  to resolve the



multipath. Thus, the channel is frequency selective and the appropriate channel model is the tapped-delay-line model with time-varying coefficients as shown in Figure 10.4. The optimum demodulator for this channel is a filter matched to the tapped-delay channel model called the RAKE demodulator, as previously described in Section 10.1.5.

### 10.3.4 Effect of Pulsed Interference and Fading

In Section 10.3.2, we evaluated the effectiveness of a DS spread-spectrum system in the presence of narrowband and broadband interference. We observed that the processing gain and the coding gain provide the means for suppressing the detrimental effects of these types of interference. In this section, we consider the effect of pulsed interference and the effect of fading on the performance of a DS spread-spectrum system.

Let us consider an interfering signal that consists of short bursts of spectrally flat Gaussian noise that covers the entire signal bandwidth. We call this type of an interfering signal *pulsed interference*. It may occur in a CDMA digital cellular system in which a mobile transmitter located near a base station is transmitting at a high power; i.e., operating without power control. Suppose that the interferer is average-power limited, with an average power  $P_I$  in the signal bandwidth  $W$ . Hence,  $I_0 = P_I/W$ . The interferer transmits pulses at a power level  $P_I/\beta$  for  $\beta$  percent of the time. Thus, the probability that the interferer is transmitting at a given instant is  $\beta$ . For simplicity, we assume that an interference pulse spans an integer number of bits (or symbols). When the interferer is not transmitting, the transmitted bits are assumed to be received error-free, and when the interferer is transmitting, the probability of error for an uncoded DS spread-spectrum system is

$$\begin{aligned} P(\alpha) &= \frac{\beta}{2} Q\left(\sqrt{\frac{2\mathcal{E}_b}{I_0/\beta}}\right) \\ &= \frac{\beta}{2} Q\left(\sqrt{\frac{2\beta W/R}{P_I/P_S}}\right) \end{aligned} \quad (10.3.45)$$

where  $W/R$  is the processing gain and  $P_I/P_S$  is the interference-to-signal power ratio.

Let us consider the value of the duty cycle  $\beta$  that maximizes the probability of error for the communication system. Upon differentiating Equation (10.3.45) with respect to  $\beta$ , we find the worst-case pulse interference occurs when

$$\beta^* = \begin{cases} \frac{0.71}{\mathcal{E}_b/I_0} & \frac{\mathcal{E}_b}{I_0} \geq 0.71 \\ 1, & \frac{\mathcal{E}_b}{I_0} < 0.71 \end{cases} \quad (10.3.46)$$

and the corresponding probability of error is

$$P_2 = \begin{cases} \frac{0.082}{\mathcal{E}_b/I_0} = \frac{0.082P_I/P_S}{W/R}, & \frac{\mathcal{E}_b}{I_0} \geq 0.71 \\ Q\left(\sqrt{\frac{2\mathcal{E}_b}{I_0}}\right) = Q\left(\sqrt{\frac{2W/R}{P_I/P_S}}\right), & \frac{\mathcal{E}_b}{I_0} < 0.71 \end{cases} \quad (10.3.47)$$

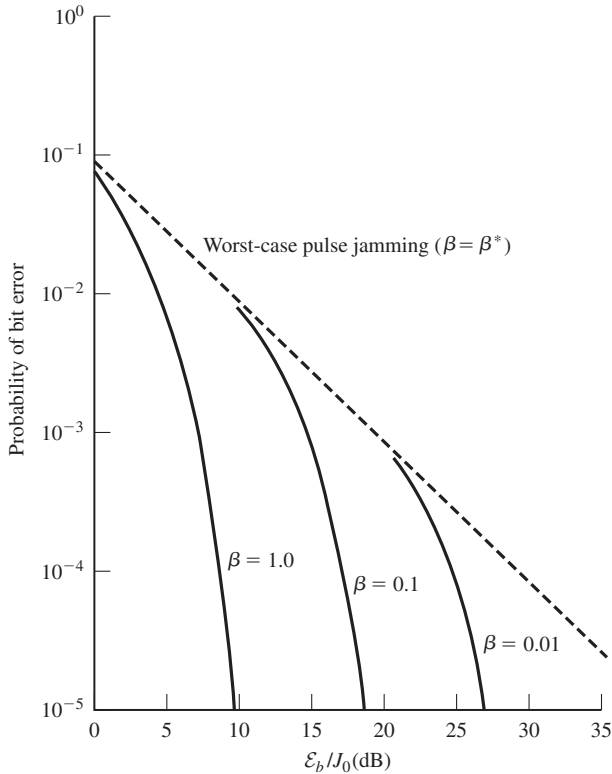


**Figure 10.45** Performance of DS binary PSK with pulse interference.

The error rate performance given by (10.3.45) for  $\beta = 1.0, 0.1$ , and  $0.01$  along with the worst-case performance based on  $\beta^*$  is plotted in Figure 10.45. When we compare the error rate for continuous wideband Gaussian noise interference ( $\beta = 1$ ) with worst-case pulse interference, we find a large difference in performance; e.g., approximately 40 dB at an error rate of  $10^{-6}$ . This is, indeed, a large penalty.

We should point out that practical consideration may prohibit an interferer from achieving small values of  $\beta$  at a high peak power. Nevertheless, the error probability given by Equation (10.3.47) serves as an upper bound on the performance of uncoded binary PSK with worst-case pulse interference. Clearly, the performance of the DS spread-spectrum system in the presence of pulse interference is poor.

If we simply add coding to the DS spread-spectrum system, the performance in SNR is improved by an amount equal to the coding gain, which in most cases is limited to less than 10 dB. The reason that the addition of coding does not improve the performance significantly is that the interfering signal pulse duration (duty cycle) may be selected to affect many consecutive coded bits. Consequently, the code word error probability is high due to the burst characteristics of the interference.

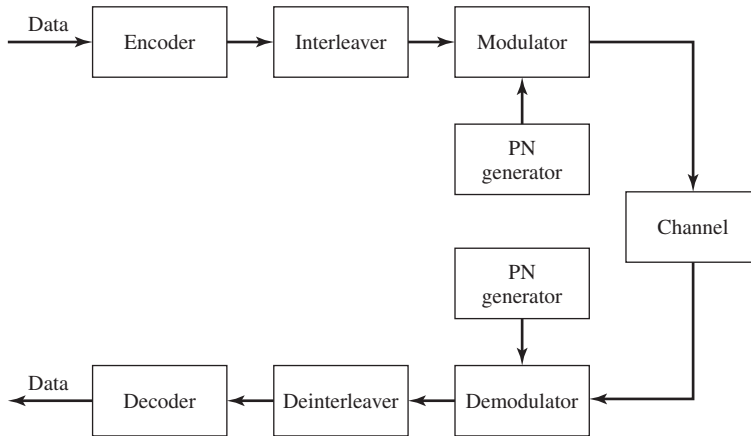


**Figure 10.46** Block diagram of communication system.

In order to improve the performance of the coded DS spread-spectrum system, we should interleave the coded bits prior to transmission over the channel. The effect of interleaving is to make the coded bits that are affected by the interferer statistically independent. Figure 10.46 illustrates a block diagram of a DS spread-spectrum system that employs coding and interleaving. By selecting a sufficiently long interleaver so that the burst characteristics of the interference are eliminated, the penalty in performance due to pulse interference is significantly reduced; e.g., to the range of 3–5 dB for conventional binary block or convolutional codes.

Signal fading has a similar effect on the performance of the DS spread-spectrum system. In a frequency nonselective channel, when the signal is in a deep fade, the communication system experiences a burst of errors. By use of coding and interleaving the coded bits so that the fading on the bits in any code word is statistically independent (through interleaving, the bits in a burst of errors belong to different code words), the error-rate performance of the system decreases as the inverse of the SNR raised to the power of the diversity provided by the code. This order of diversity is equal to the Hamming distance  $d_{\min}^H$  of the block code (or  $d_{\text{free}}^H$  of the convolutional code) for soft-decision decoding and  $d_{\min}^H/2$  for hard-decision decoding.

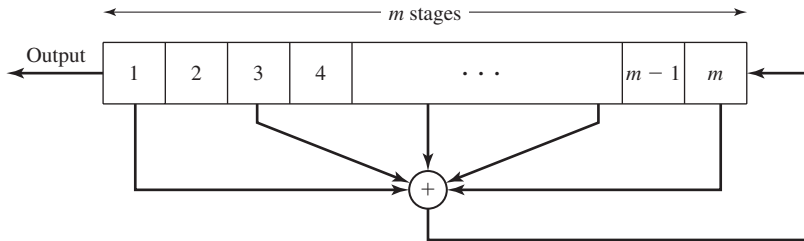
### 10.3.5 Generation of PN Sequences

A pseudorandom or pseudonoise (PN) sequence is a code sequence of 1's and 0's whose autocorrelation has the properties similar to those of white noise. In this section, we briefly describe the construction of some PN sequences and their autocorrelation and crosscorrelation properties. For a comprehensive treatment of this subject, the interested reader may refer to the book by Golomb (1967) and the paper by Sarwate and Pursley (1980).

By far the most widely known binary PN code sequences are the maximum-length shift-register sequences. A maximum-length shift-register sequence, or  $m$ -sequence for

**TABLE 10.3** SHIFT-REGISTER CONNECTIONS FOR GENERATING ML SEQUENCES

$m$	Stages connected to modulo-2 adder	$m$	Stages connected to modulo-2 adder	$m$	States connected to modulo-2 adder
2	1, 2	13	1, 10, 11, 13	24	1, 18, 23, 24
3	1, 3	14	1, 5, 9, 14	25	1, 23
4	1, 4	15	1, 15	26	1, 21, 25, 26
5	1, 4	16	1, 5, 14, 16	27	1, 23, 26, 27
6	1, 6	17	1, 15	28	1, 26
7	1, 7	18	1, 12	29	1, 28
8	1, 5, 6, 7	19	1, 15, 18, 19	30	1, 8, 29, 30
9	1, 6	20	1, 18	31	1, 29
10	1, 8	21	1, 20	32	1, 11, 31, 32
11	1, 10	22	1, 22	33	1, 21
12	1, 7, 9, 12	23	1, 19	34	1, 8, 33, 34

**Figure 10.47** General  $m$ -stage shift register with linear feedback.

short, has a length  $L = 2^m - 1$  bits and is generated by an  $m$ -stage shift register with linear feedback as illustrated in Figure 10.47. The sequence is periodic with period  $L$ . Each period has a sequence of  $2^{m-1}$  ones and  $2^{m-1} - 1$  zeros. Table 10.3 lists shift register connections for generating maximum-length sequences.

In DS spread-spectrum applications, the binary sequence with elements  $\{0, 1\}$  is mapped into a corresponding binary sequence with elements  $\{-1, 1\}$ . We shall call the equivalent sequence  $\{c_n\}$  with elements  $\{-1, 1\}$  a *bipolar sequence*.

An important characteristic of a periodic PN sequence is its autocorrelation function which is usually defined in terms of the bipolar sequences  $\{c_n\}$  as

$$R_c(m) = \sum_{n=1}^L c_n c_{n+m}, \quad 0 \leq m \leq L - 1 \quad (10.3.48)$$

where  $L$  is the period of the sequence. Since the sequence  $\{c_n\}$  is periodic with period  $L$ , the autocorrelation sequence  $\{R_c(m)\}$  is also periodic with period  $L$ .

Ideally, a PN sequence should have an autocorrelation function that has correlation properties similar to white noise. That is, the ideal autocorrelation sequence for  $\{c_n\}$  is  $R_c(0) = L$  and  $R_c(m) = 0$  for  $1 \leq m \leq L - 1$ . In the case of  $m$ -sequences, the

autocorrelation sequence is

$$R_c(m) = \begin{cases} L, & m = 0 \\ -1, & 1 \leq m \leq L - 1 \end{cases} \quad (10.3.49)$$

For long  $m$ -sequences, the size of the off-peak values of  $R_c(m)$  relative to the peak value  $R_c(0)$ ; i.e., the ratio  $R_c(m)/R_c(0) = -1/L$ , is small and, from a practical viewpoint, inconsequential. Therefore,  $m$ -sequences are very close to ideal PN sequences when viewed in terms of their autocorrelation function.

In some applications, the crosscorrelation properties of PN sequences are as important as the autocorrelation properties. For example, in CDMA each user is assigned a particular PN sequence. Ideally, the PN sequences among users should be mutually uncorrelated so that the level of interference experienced by one user from transmissions of other users adds on a power basis. However, the PN sequences used in practice by different users exhibit some correlation.

To be specific, let us consider the class of  $m$ -sequences. It is known that, the periodic cross correlation function between a pair of  $m$ -sequences of the same period, can have relatively large peaks. Table 10.4 lists the peak magnitude  $R_{\max}$  for the periodic crosscorrelation between pairs of  $m$ -sequences for  $3 \leq m \leq 12$ . Also listed in Table 10.4 is the number of  $m$ -sequences of length  $L = 2^m - 1$  for  $3 \leq m \leq 12$ . We observe that the number of  $m$ -sequences of length  $L$  increases rapidly with  $m$ . We also observe that, for most sequences, the peak magnitude  $R_{\max}$  of the crosscorrelation function is a large percentage of the peak value of the autocorrelation function. Consequently,  $m$ -sequences are not suitable for CDMA communication systems. Although it is possible to select a small subset of  $m$ -sequences that have relatively smaller crosscorrelation peak value than  $R_{\max}$ , the number of sequences in the set is usually too small for CDMA applications.

Methods for generating PN sequences with better periodic crosscorrelation properties than  $m$ -sequences have been developed by Gold (1967, 1968) and by

**TABLE 10.4** PEAK CROSSCORRELATIONS OF  $m$  SEQUENCES AND GOLD SEQUENCES

$m$ sequences					Gold sequences	
$m$	$L = 2^m - 1$	Number	Peak cross-correlation $R_{\max}$	$R_{\max}/R(0)$	$R_{\max}$	$R_{\min}/R(0)$
3	7	2	5	0.71	5	0.71
4	15	2	9	0.60	9	0.60
5	31	6	11	0.35	9	0.29
6	63	6	23	0.36	17	0.27
7	127	18	41	0.32	17	0.13
8	255	16	95	0.37	33	0.13
9	511	48	113	0.22	33	0.06
10	1023	60	383	0.37	65	0.06
11	2047	176	287	0.14	65	0.03
12	4095	144	1407	0.34	129	0.03

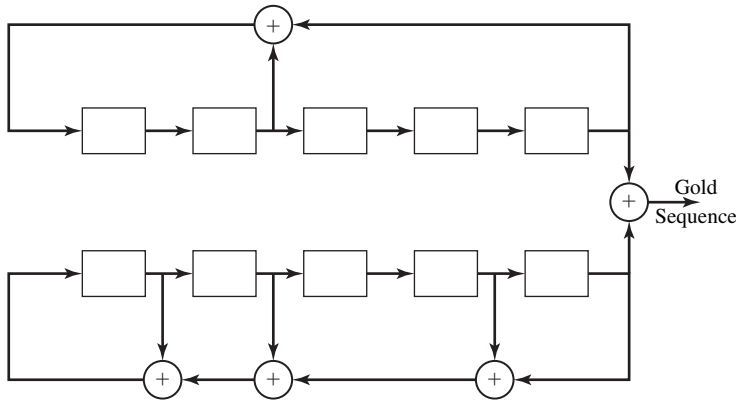


**Figure 10.48** Generation of Gold sequences of length 31.

Kasami (1966). Gold sequences are constructed by taking a pair of specially selected  $m$ -sequences, called *preferred  $m$ -sequences*, and forming the modulo-2 sum of the two sequences, for each of  $L$  cyclicly shifted versions of one sequence relative to the other sequence. Thus,  $L$  Gold sequences are generated as illustrated in Figure 10.48. For  $m$  odd, the maximum value of the crosscorrelation function between any pair of Gold sequences is  $R_{\max} = \sqrt{2L}$ . For  $m$  even,  $R_{\max} = \sqrt{L}$ .

Kasami (1966) described a method for constructing PN sequences by decimating an  $m$ -sequence. In Kasami's method of construction, every  $2^{m/2} + 1$  bit of an  $m$ -sequence is selected. This method of construction yields a smaller set of PN sequences compared with Gold sequences, but their maximum crosscorrelation value is  $R_{\max} = \sqrt{L}$ .

It is interesting to compare the peak value of the crosscorrelation function for Gold sequences and for Kasami sequences with a known lower bound for the maximum crosscorrelation between any pair of binary sequences of length  $L$ . Given a set of  $N$  sequences of period  $L$ , a lower bound on their maximum crosscorrelation is

$$R_{\max} \geq L \sqrt{\frac{N-1}{NL-1}} \quad (10.3.50)$$

which, for large values of  $L$  and  $N$ , is well approximated as  $R_{\max} \geq \sqrt{L}$ . Hence, we observe that Kasami sequences satisfy the lower bound and, hence, they are optimal. On the other hand, Gold sequences with  $m$  odd have a  $R_{\max} = \sqrt{2L}$ . Hence, they are slightly suboptimal.

Besides the well-known Gold sequences and Kasami sequences, there are other binary sequences that are appropriate for CDMA applications. The interested reader is referred to the papers by Scholtz (1979), Olsen (1977), and Sarwate and Pursley (1980).

Finally, we should point out that although we discussed the periodic crosscorrelation function between pairs of periodic sequences, many practical CDMA systems use an information bit duration that encompasses only a fraction of a periodic sequence. In

such a case, it is partial-period crosscorrelation between two sequences that is important. The partial-period crosscorrelation properties of periodic PN sequences has been widely investigated and discussed in the technical literature.

### 10.3.6 Frequency-Hopped Spread Spectrum

In frequency-hopped (FH) spread spectrum, the available channel bandwidth  $W$  is subdivided into a large number of nonoverlapping frequency slots. In any signaling interval the transmitted signal occupies one or more of the available frequency slots. The selection of the frequency slot ( $s$ ) in each signal interval is made pseudorandomly according to the output from a PN generator.

A block diagram of the transmitter and receiver for an FH spread-spectrum system is shown in Figure 10.49. The modulation is either binary or  $M$ -ary FSK (MFSK). For example, if binary FSK is employed, the modulator selects one of two frequencies, say  $f_0$  or  $f_1$ , corresponding to the transmission of a 0 for a 1. The resulting binary FSK signal is translated in frequency by an amount that is determined by the output sequence from a PN generator, which is used to select a frequency  $f_c$  that is synthesized by the frequency synthesizer. This frequency is mixed with the output of the FSK modulator and the resultant frequency-translated signal is transmitted over the channel. For example, by taking  $m$  bits from the PN generator, we may specify  $2^m - 1$  possible carrier frequencies. Figure 10.50 illustrates an FH signal pattern.

At the receiver, there is an identical PN sequences generator, synchronized with the received signal, which is used to control the output of the frequency synthesizer. Thus, the pseudorandom frequency translation introduced at the transmitter is removed at the demodulator by mixing the synthesizer output with the received signal. The resultant signal is then demodulated by means of an FSK demodulator. A signal for maintaining synchronism of the PN sequence generator with the FH received signal is usually extracted from the received signal.

Although binary PSK modulation generally yields better performance than binary FSK, it is difficult to maintain phase coherence in the synthesis of the frequencies used in the hopping pattern and, also, in the propagation of the signal over the channel

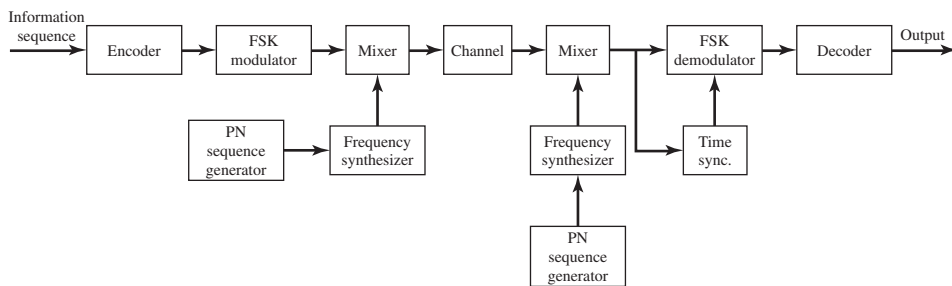


**Figure 10.49** Block diagram of an FH spread-spectrum system.

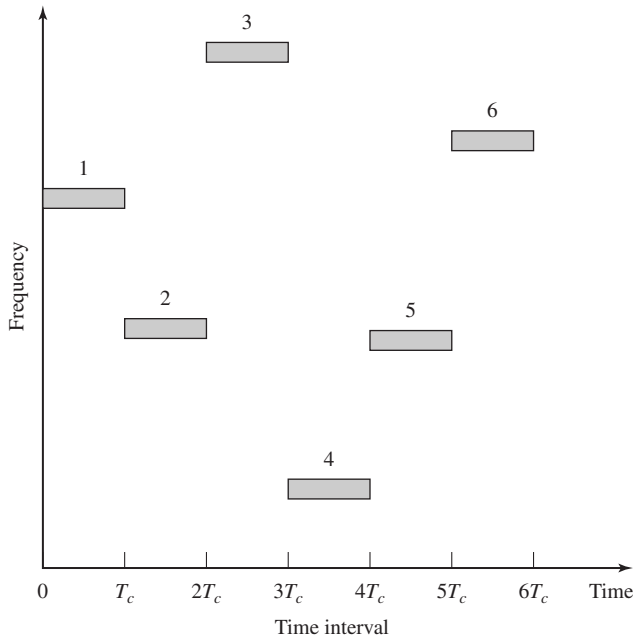


**Figure 10.50** An example of an FH pattern.

as the signal is hopped from one frequency to the another over a wide bandwidth. Consequently, FSK modulation with noncoherent demodulation is usually employed in FH spread-spectrum systems.

The frequency-hopping rate, denoted as  $R_h$ , may be selected to be either equal to the symbol rate, or lower than the symbol rate, or higher than the symbol rate. If  $R_h$  is equal to or lower than the symbol rate, the FH system is called a *slow-hopping* system. If  $R_h$  is higher than the symbol rate; i.e., there are multiple hops/symbol, the FH system is called a *fast-hopping* system. However, there is a penalty incurred in subdividing an information symbol into several frequency-hopped elements, because the energy from these separate elements is combined noncoherently.

FH spread-spectrum signals may be used in CDMA where many users share a common bandwidth. In some cases, an FH signal is preferred over a DS spread-spectrum signal because of the stringent synchronization requirements inherent in DS spread-spectrum signals. Specifically, in a DS system, timing and synchronization must be established to within a fraction of a chip interval  $T_c = 1/W$ . On the other hand, in an FH system, the chip interval  $T_c$  is the time spent in transmitting a signal in a particular frequency slot of bandwidth  $B \ll W$ . But this interval is approximately  $1/B$ , which is much larger than  $1/W$ . Hence, the timing requirements in an FH system are not as stringent as in a DS system.

Next, we shall evaluate the performance of FH spread-spectrum systems under the condition that the system is either slow hopping or fast hopping.



**Slow Frequency-Hopping Systems.** Let us consider a slow frequency-hopping system in which the hop rate  $R_h = 1$  hop/bit. We assume that the interference on the channel is broadband and is characterized as AWGN with power-spectral density  $I_0$ . Under these conditions, the probability of error for the detection of non-coherently demodulated binary FSK is

$$P_b = \frac{1}{2} e^{-\rho_b/2} \quad (10.3.51)$$

where  $\rho_b = \mathcal{E}_b/I_0$  is the SNR/bit.

As in the case of a DS spread-spectrum system, we observe that  $\mathcal{E}_b$ , the energy/bit, can be expressed as  $\mathcal{E}_b = P_S T_b = P_S/R$ , where  $P_S$  is the average transmitted power and  $R$  is the bit rate. Similarly,  $I_0 = P_I/W$ , where  $P_I$  is the average power of the broadband interference and  $W$  is the available channel bandwidth. Therefore, the SNR  $\rho_b$  can be expressed as

$$\rho_b = \frac{\mathcal{E}_b}{I_0} = \frac{W/R}{P_I/P_S} \quad (10.3.52)$$

where  $W/R$  is the processing gain and  $P_I/P_S$  is the interference margin for the FH spread-spectrum signal.

Slow FH spread-spectrum systems are particularly vulnerable to partial-band interference that may result in FH CDMA systems. To be specific, suppose that the partial-band interference is modeled as a zero-mean Gaussian random process with a flat power-spectral density over a fraction of the total bandwidth  $W$  and zero in the remainder of the frequency band. In the region or regions where the power-spectral density is nonzero, its value is  $S_I(f) = I_0/\beta$ , where  $0 < \beta \leq 1$ . In other words, the interference average power  $P_I$  is assumed to be constant.

Let us consider the worst-case partial-band interference by selecting the value of  $\beta$  that maximizes the error probability. In an uncoded slow-hopping system with binary FSK modulation and noncoherent detection, the transmitted frequencies are selected with uniform probability in the frequency band  $W$ . Consequently, the received signal will be corrupted by interference with probability  $\beta$ . When the interference is present, the probability of error is  $1/2 \exp(-\beta\rho_b/2)$  and when it is not, the detection of the signal is assumed to be error free. Therefore, the average probability of error is

$$\begin{aligned} P_b(\beta) &= \frac{\beta}{2} e^{-\beta\rho_b/2} \\ &= \frac{\beta}{2} \exp\left(-\frac{\beta W/R}{2P_I/P_S}\right) \end{aligned} \quad (10.3.53)$$

Figure 10.51 illustrates the error rate as a function of  $\rho_b$  for several values of  $\beta$ . By differentiating  $P_b(\beta)$ , and solving for the value of  $\beta$  that maximizes  $P_b(\beta)$ , we find that

$$\beta^* = \begin{cases} 2/\rho_b, & \rho_b \geq 2 \\ 1, & \rho_b < 2 \end{cases} \quad (10.3.54)$$

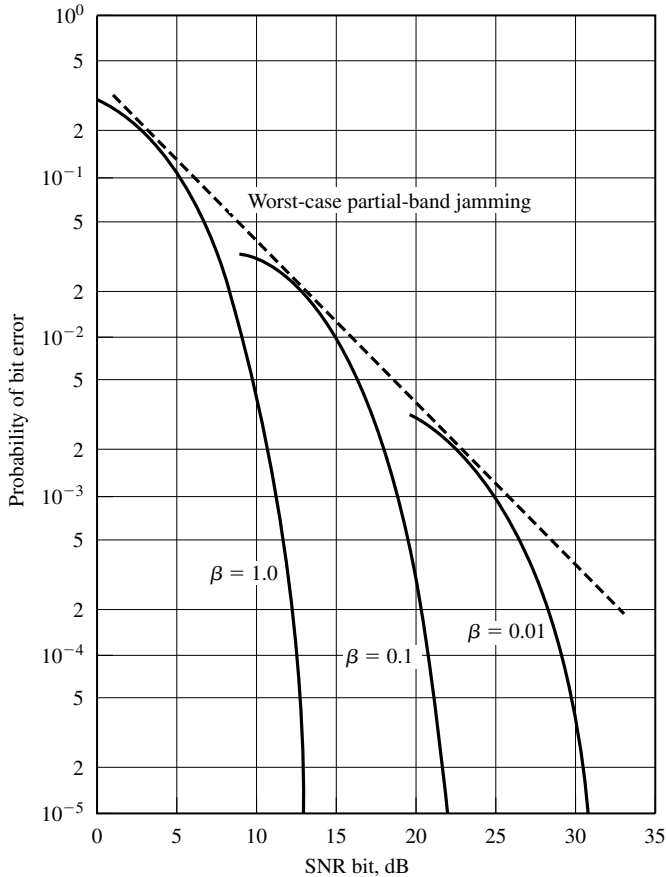


**Figure 10.51** Performance of binary FSK with partial-band interference.

The corresponding error probability for the worst-case partial-band interference is

$$P_b = \begin{cases} e^{-1/\rho_b}, & \rho_b \geq 2 \\ \frac{1}{2}e^{-\rho_b/2}, & \rho_b < 2 \end{cases} \quad (10.3.55)$$

which is also shown in Figure 10.51. Whereas the error probability decreases exponentially for full-band interference as given by Equation (10.3.51), the error probability for worst-case partial-band interference decreases only inversely with  $\mathcal{E}_b/I_0$ . This result is similar to the error probability for DS spread-spectrum signals in the presence of pulse interference. It is also similar to the error probability for binary FSK in a Rayleigh fading channel.

In our discussion of signal design for efficient and reliable communication over a fading channel in Section 10.1, we found that diversity, which can be obtained by simple

repetition of the transmitted information bit on different frequencies (or by means of block or convolutional coding), provides a significant improvement in performance relative to uncoded signal transmission. It should not be surprising that the same type of signal coding is also effective on partial-band interference channels. In fact, it has been shown by Viterbi and Jacobs (1975) that by optimizing the code design for the partial-band interference, the communication system can achieve an average bit-error probability of

$$P_b = e^{-\rho_b/4} \quad (10.3.56)$$

Therefore, the probability of error achieved with the optimum code design decreases exponentially with an increase in SNR and is within 3 dB of the performance obtained in an AWGN channel. Thus, the penalty due to partial-band interference is reduced significantly.

**Fast Frequency-Hopping Systems.** In fast FH systems, the frequency-hop rate  $R_h$  is some multiple of the symbol rate. Basically, each ( $M$ -ary) symbol interval is subdivided into  $N$  subintervals, which are called *chips* and one of  $M$  frequencies is transmitted in each subinterval. Fast frequency-hopping systems are particularly attractive for military communications. In such systems, the hop rate  $R_h$  may be selected sufficiently high so that a potential intentional interferer does not have sufficient time to detect the presence of the transmitted frequency and to synthesize a jamming signal that occupies the same bandwidth.

To recover the information at the receiver, the received signal is first de-hopped by mixing it with the hopped carrier frequency. This operation removes the hopping pattern and brings the received signal in all subintervals (chips) to a common frequency band that encompasses the  $M$  possible transmitted frequencies. The signal in each subinterval is then passed through the  $M$  matched filters (or correlators) tuned to the  $M$  possible transmitted frequencies which are sampled at the end of each subinterval and passed to the detector. The detection of the FSK signals is noncoherent. Hence, decisions are based on the magnitude of the matched filter (or correlator) outputs.

Since each symbol is transmitted over  $N$  chips, the decoding may be performed either on the basis of hard decisions or soft decisions. The following example illustrates the decoding based on hard decisions.

**Example 10.3.5**

Suppose that binary FSK is used to transmit binary symbols, and each symbol is transmitted over  $N$  frequency hops, where  $N$  is odd. Determine the probability of error for an AWGN channel if hard-decision decoding is used.

**Solution** The probability of error for noncoherent detection of binary FSK for each hop is

$$p = \frac{1}{2} e^{-\rho_b/2N} \quad (10.3.57)$$

where

$$\frac{\rho_b}{N} = \frac{\mathcal{E}_b/N}{N_0} \quad (10.3.58)$$

is the SNR/chip and  $\mathcal{E}_b$  is the total bit energy. The decoder decides in favor of the transmitted frequency that is larger in at least  $(N + 1)/2$  chips. Thus, the decision is made on the basis of a majority vote given the decisions on the  $N$  chips. Consequently, the probability of a bit error is

$$P_b = \sum_{m=(N+1)/2}^N \binom{N}{m} p^m (1-p)^{N-m} \quad (10.3.59)$$

where  $p$  is given by Equation (10.3.57). We should note that the error probability  $P_b$  for hard-decision decoding of the  $N$  chips will be higher than the error probability for a single hop/bit FSK system, which is given by Equation (10.3.51), when the SNR/bit  $\rho_b$  is the same in the two systems (see Problem 10.20).

The alternative to hard-decision decoding is soft-decision decoding in which the magnitudes (or magnitudes squared) of the corresponding matched-filter outputs are summed over the  $N$  chips and a single decision is made based on the frequency giving the largest output. For example, if binary orthogonal FSK is used to transmit the information, the two soft-decision metrics for the  $N$  chips based on square-law combining are

$$\begin{aligned} DM_1 &= \sum_{k=1}^N \left| \frac{\mathcal{E}_b}{N} + v_{1k} \right|^2 \\ DM_2 &= \sum_{k=1}^N |v_{2k}|^2 \end{aligned} \quad (10.3.60)$$

where  $\{v_{1k}\}$  and  $\{v_{2k}\}$  are the noise components from the two matched filters for the  $N$  chips. Since frequency  $f_1$  is assumed to have been transmitted, a decision error occurs when  $DM_2 > DM_1$ . The probability of this event error for additive Gaussian noise may be obtained in closed form, although its derivation is cumbersome. The final result is (see Appendix A)

$$P_b = \frac{1}{2^{2N-1}} e^{-\rho_b/2} \sum_{i=0}^{N-1} K_i \left( \frac{\rho_b}{2} \right)^i \quad (10.3.61)$$

where the set  $\{K_i\}$  are constants, which may be expressed as

$$K_i = \frac{1}{i!} \sum_{r=0}^{N-1-i} \binom{2N-1}{r} \quad (10.3.62)$$

The error probability for soft-decision decoding given by Equation (10.3.61) is lower than that for hard-decision decoding given by Equation (10.3.59) for the same  $\mathcal{E}_b/N_0$ . The difference in performance is the loss in hard-decision decoding. However, Equation (10.3.62) is higher than the error probability for single-hop FSK, which is given by Equation (10.3.51) for the AWGN channel. The difference in performance between Equation (10.3.51) and Equation (10.3.61) for the same SNR is due to the

noncoherent (square-law) combining at the decoder. This loss is usually called the *noncoherent combining loss* of the system.

If soft-decision decoding is used in the presence of partial-band interference, it is important to scale (or normalize) the matched-filter outputs in each hop, so that a strong interference that falls within the transmitted signal band in any hop does not dominate the output of the combiner. A good strategy in such a case is to normalize, or clip, the matched-filter outputs from each hop if their values exceed some threshold that is set near (slightly above) the mean of the signal-plus-noise power level. Alternatively, we may monitor the noise power level and scale the matched filter outputs for each hop by the reciprocal of the noise power level. Thus, the noise power levels from the matched filter outputs are normalized. Therefore, with proper scaling, a fast FH spread-spectrum system will not be as vulnerable to partial-band interference because the transmitted information/bit is distributed (or spread) over  $N$  frequency hops.

**Applications of FH Spread Spectrum.** FH spread spectrum is a viable alternative to DS spread spectrum for protection against narrowband and broadband interference that is encountered in CDMA. In CDMA systems based on frequency hopping each transmitter-receiver pair is assigned its own pseudorandom frequency-hopping pattern. Aside from this distinguishing feature, the transmitters and receivers of all users may be identical; i.e., they have identical encoders, decoders, modulators, and demodulators.

CDMA systems based on FH spread-spectrum signals are particularly attractive for mobile (land, air, sea) users because timing (synchronization) requirements are not as stringent as in a DS spread-spectrum system. In addition, frequency-synthesis techniques and associated hardware have been developed that make it possible to frequency-hop over bandwidths that are significantly larger, by one or more orders of magnitude, than those currently possible with DS spread-spectrum signals. Consequently, larger processing gains are possible by FH, which more than offset the loss in performance inherent in noncoherent detection of the FSK-type signals.

FH is also effective against intentional interference. As we have described above, an FH  $M$ -ary ( $M \geq 2$ ) FSK system that employs coding, or simply repeats the information symbol on multiple hops (repetition coding), is very effective against a partial-band interference. As a consequence, the interferer's threat is reduced to that of an equivalent broadband noise interference whose transmitter power is spread across the channel bandwidth  $W$ .

### 10.3.7 Synchronization of Spread-Spectrum Systems

Time synchronization of the receiver to the received spread-spectrum signal may be separated into two distinct phases. There is an initial acquisition phase, during which time the receiver establishes time synchronization by detecting the presence of a special initial acquisition sequence. The initial acquisition phase is followed by the transmission of data, during which period the receiver must track the signal timing.

**Acquisition Phase.** In a DS spread-spectrum system, the PN code sequence must be synchronized in time to within a small fraction of the chip interval  $T_c = 1/W$ .

The problem of initial synchronization may be viewed as one in which we attempt to synchronize the receiver clock to the transmitter clock. Usually, extremely accurate and stable time clocks are used in spread-spectrum systems in order to reduce the time uncertainty between the receiver clock and the transmitter clock. Nevertheless, there is always an initial timing uncertainty that is due to propagation delay in the transmission of the signal through the channel. This is especially a problem when communication is taking place between two mobile users. In any case, the usual procedure for establishing initial synchronization is for the transmitter to send a known pseudorandom sequence to the receiver. The receiver is continuously in a search mode looking for this sequence in order to establish initial synchronization.

Suppose that the initial timing uncertainty is  $T_u$  seconds and the chip duration is  $T_c$ . Since initial synchronization takes place in the presence of additive noise and, perhaps other interference, it is necessary to dwell for  $T_d = NT_c$  sec in order to test synchronism at each time instant, where  $N$  is some positive integer. If we search over the time uncertainty interval in (coarse) time steps of  $T_c/2$ , then the time required to establish initial synchronization is

$$T_{\text{init sync}} = \frac{T_u}{T_c/2} T_d = 2NT_u$$

Clearly, the synchronization sequence transmitted to the receiver must be at least as long as  $2NT_c$  sec in order for the receiver to have sufficient time to perform the necessary search in a serial fashion.

In principle, matched filtering or crosscorrelation are optimum methods for establishing initial synchronization in the presence of additive Gaussian noise. A filter matched to the known data waveform generated from the known pseudorandom sequence continuously compares its output with a predetermined threshold. When the threshold is exceeded, initial synchronization is established and the demodulator enters the “data receive” mode.

Alternatively, we may implement a *sliding correlator* as shown in Figure 10.52. The correlator cycles through the time uncertainty, usually in discrete-time intervals of  $T_c/2$  seconds or less. The crosscorrelation is performed over the time interval  $NT_c$ , where  $N$  is the number of chips in the synchronization sequence, and the correlator

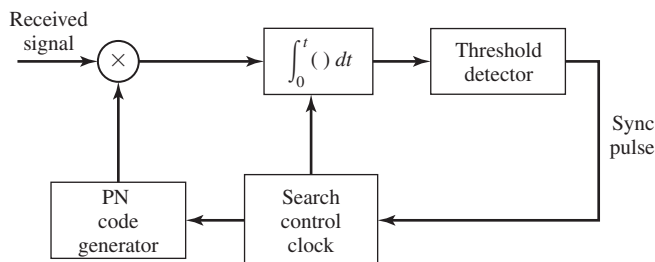


**Figure 10.52** A sliding correlator for DS signal acquisition.

output is compared with a threshold to determine if the known signal sequence is present. If the threshold is not exceeded, the known reference sequence is advanced by  $T_c/2$  sec and the correlation process is repeated. These operations are performed until a signal is detected or until the search has been performed over the time uncertainty interval  $T_u$ . In the case of the latter outcome, the search process is repeated.

A similar procedure may be used for FH signals. In this case, the problem is to synchronize the PN code sequence generated at the receiver that controls the hopped-frequency pattern. To accomplish this initial synchronization, a known frequency-hopped signal is transmitted to the receiver. The initial acquisition system at the receiver looks for this known FH signal pattern. For example, a band of matched filters tuned to the transmitted frequencies in the known pattern may be employed. Their outputs must be properly delayed, envelope or square-law detected, weighted, if necessary, and added to produce the signal output which is compared with a threshold. A signal present (signal acquisition) is declared when the threshold is exceeded. The search process is usually performed continuously in time until a threshold is exceeded. A block diagram illustrating their signal acquisition scheme is given in Figure 10.53. As an alternative, a single matched-filter and envelope detector may be used preceded by a frequency-hopping pattern generator and followed by a threshold detector. This configuration,

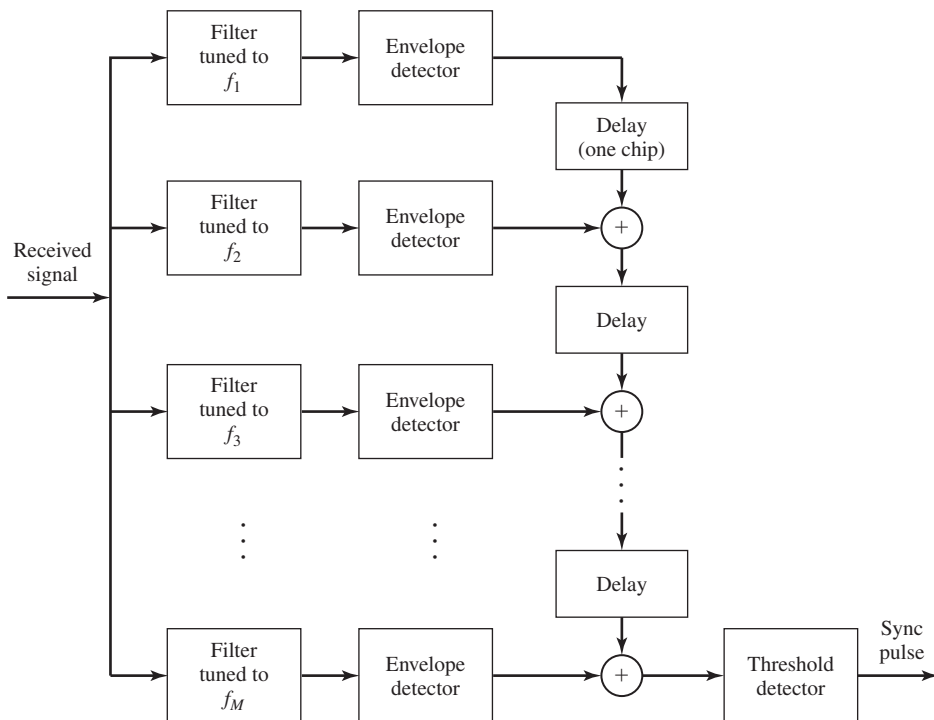


**Figure 10.53** System for acquisition of an FH signal.

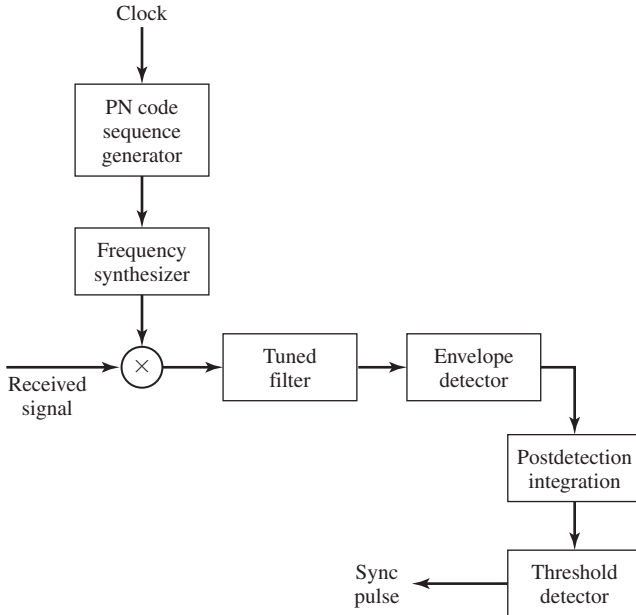


**Figure 10.54** Alternative system for acquisition of an FH signal.

which is shown in Figure 10.54, is based on a serial search and is akin to the sliding correlator for DS spread-spectrum signals.

The sliding correlator for DS signals and its counterpart shown in Figure 10.54 for FH signals basically perform a serial search that is generally time consuming. As an alternative, one may employ some degree of parallelism by having two or more such correlators operating in parallel and searching over nonoverlapping time slots. In such a case, the search time is reduced at the expense of a more complex and costly implementation.

During the search mode, there may be false alarms that occur occasionally due to additive noise and other interference. To handle the occasional false alarms, it is necessary to have an additional method or circuit that checks to confirm that the received signal at the output of the correlator remains above the threshold. With such a detection strategy, a large noise pulse that causes the matched-filter output to exceed the threshold will have only a transient effect on synchronization, since the matched-filter output will fall below the threshold once the large noise pulse passes through the filter. On the other hand, when a signal is present, the correlator or matched-filter output will remain above the threshold for the duration of their transmitted signal. Thus, if confirmation fails, the search for signal synchronization is resumed.

In the above discussion, we considered only time uncertainty in establishing initial synchronization. However, another aspect of initial synchronization is frequency uncertainty. If the transmitter and, or, the receiver are mobile, the relative velocity between them results in a Doppler frequency shift in the received signal relative to the transmitted signal. Since the receiver does not know the relative velocity, a priori, the Doppler



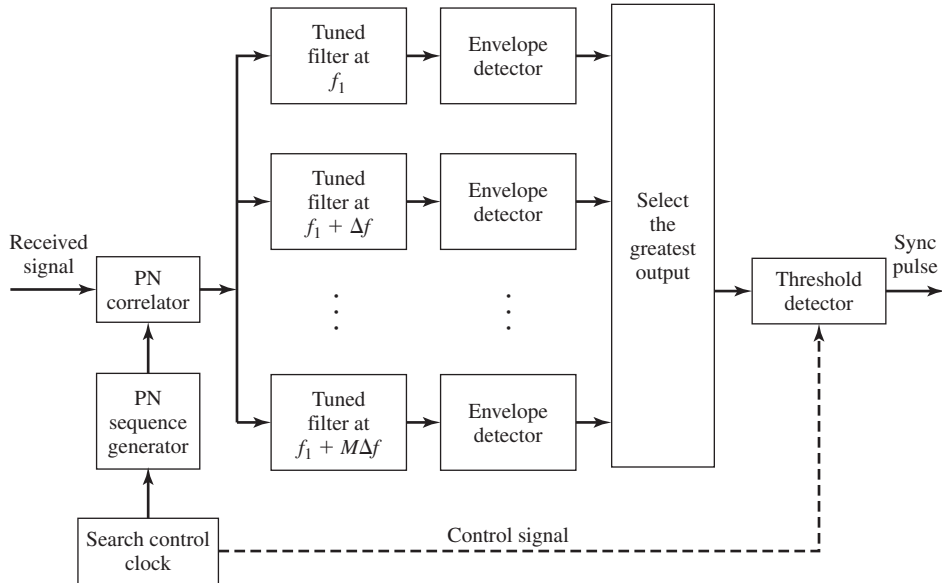


**Figure 10.55** Initial search for the Doppler frequency offset in a DS system.

frequency-shift is unknown and must be determined by means of a frequency-search method. Such a search is usually accomplished in parallel over a suitably quantized frequency uncertainty interval and serially over the time uncertainty interval. A block diagram of this scheme for DS spread-spectrum signals is shown in Figure 10.55. Appropriate Doppler frequency-search methods can also be devised for FH signals.

**Tracking.** Once the signal is acquired, the initial synchronization process is stopped and fine synchronization and tracking begins. The tracking maintains the PN code generator at the receiver in synchronism with the received signal. Tracking includes fine-chip synchronization.

For a DS spread-spectrum signal, tracking is usually performed by means of a tracking loop, called a *delay-locked loop* (DLL), as shown in Figure 10.56. In this tracking loop, the received signal is applied to two multipliers, where it is multiplied by two outputs from the local PN code generator which are delayed relative to each other by an amount of  $2\delta \leq T_c$ . Thus, the product signals are the crosscorrelations between the received signal and the PN sequence at the two values of delay. These products are bandpass filtered, envelope (or square-law) detected, and then subtracted. This difference signal is applied to the loop filter that drives the voltage-controlled clock (VCC). The VCC output serves as the clock for the PN code signal generator.

If the synchronism is not exact, the filtered output from one correlator will exceed the other and the VCC will be appropriately advanced or delayed. At the equilibrium point, the two filtered-correlator outputs will be equally displaced from the peak value, and the PN code generator output will be exactly synchronized to the received signal

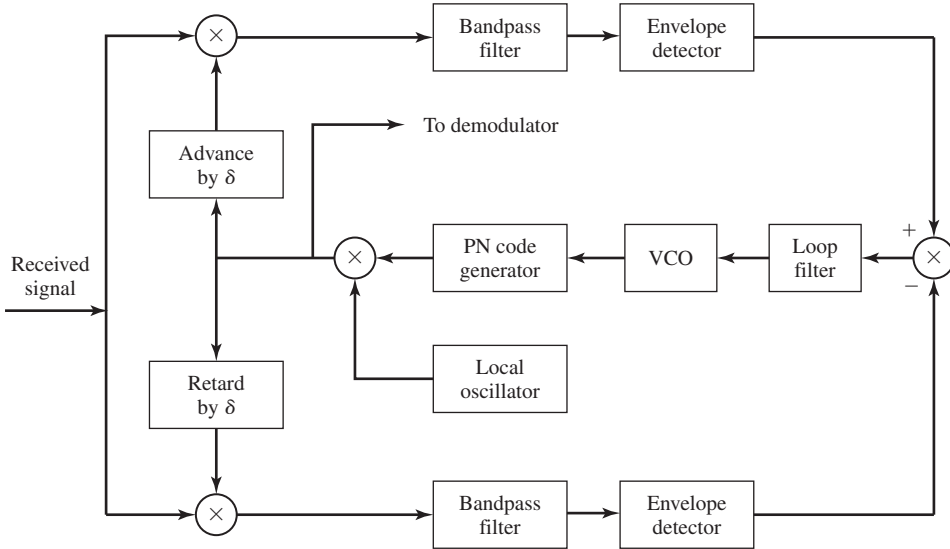


**Figure 10.56** DLL for PN code tracking.

which is fed to the demodulator. We observe that this implementation of the DLL for tracking the DS signal is equivalent to the early-late gate bit-tracking synchronizer previously described in Section 7.8.1.

An alternative method for time tracking a DS signal is to use a tau-dither loop (TDL), which is illustrated by the block diagram in Figure 10.57. The TDL employs only a single “arm” instead of the two “arms” shown in Figure 10.56. By providing a suitable gating waveform, it is possible to make this single “arm” implementation appear to be equivalent to the two “arm” realization. In this case, the crosscorrelator output is regularly sampled at two values of delay, by stepping the code clock forward and backward in time by an amount  $\delta$ . The envelope of the crosscorrelation that is

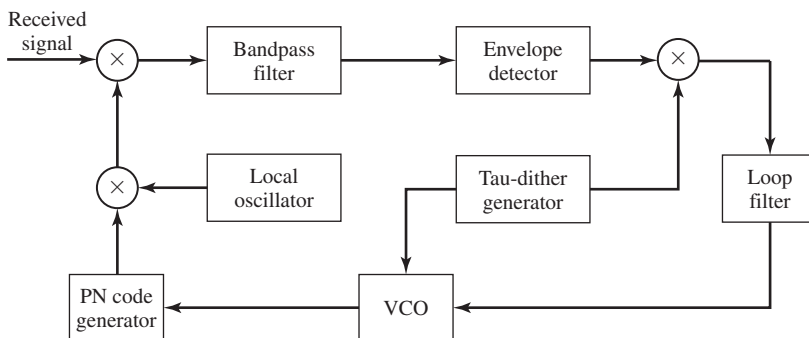


**Figure 10.57** Tau-dither loop.

sampled at  $\pm\delta$  has an amplitude modulation whose phase relative to the tau-dither modulator determines the sign of the tracking error.

One advantage of the TDL is the less costly implementation resulting from elimination of one of the two arms that are employed in the conventional DLL. A second and less apparent advantage is that the TDL does not suffer from performance degradation that is inherent in the DLL when the amplitude gain in the two arms is not properly balanced.

Both the DLL and the TDL generate an error signal by sampling the signal correlation function at  $\pm\delta$  off the peak, as shown in Figure 10.58(a). This generates an error signal as shown in Figure 10.58(b). The analysis of the performance of the DLL is similar to that for the PLL, previously described in Section 5.2. If it were not for the envelope detectors in the two arms of the DLL, the loop resembles a Costas loop. In general, the variance of the time-estimation error in the DLL is inversely proportional to the loop SNR, which depends on the input SNR to the loop and on the loop bandwidth. Its performance is somewhat degraded as in the squaring PLL by the nonlinearities inherent in the envelope detectors, but this degradation is relatively small.

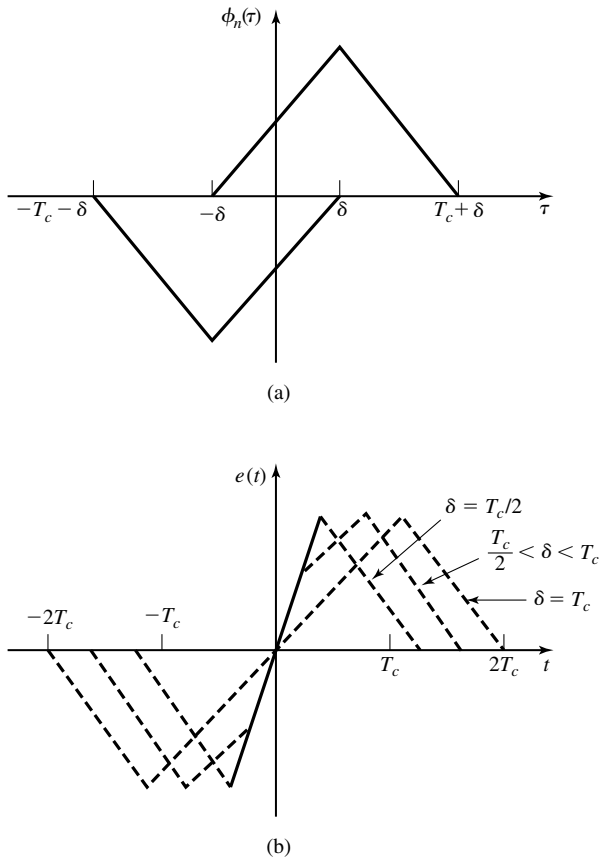


**Figure 10.58** Autocorrelation function (a) and tracking error signal (b) for DLL.

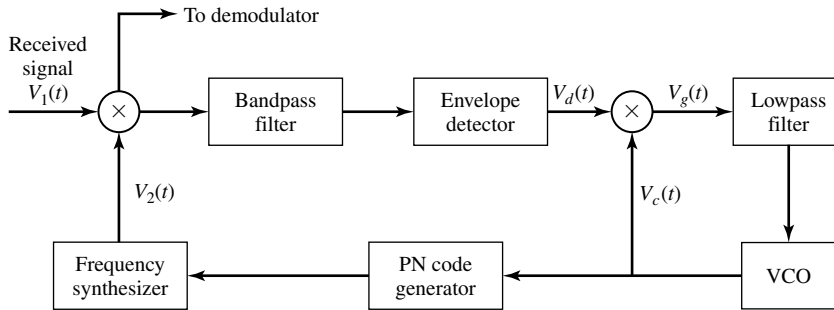


**Figure 10.59** Tracking method for FH signals. (From paper by Pickholtz et al.; © 1992 IEEE. Reprinted with permission.)

A tracking method for FH spread-spectrum signals is illustrated in Figure 10.59. This method is based on the premise that, although initial acquisition has been achieved, there is a small timing error between the received signal and the received clock. The bandpass filter is tuned to a single intermediate frequency and its bandwidth is of the order of  $1/T_c$ , where  $T_c$  is the chip interval. Its output is envelope detected and then multiplied by the clock signal to produce a three-level signal, as shown in Figure 10.60,

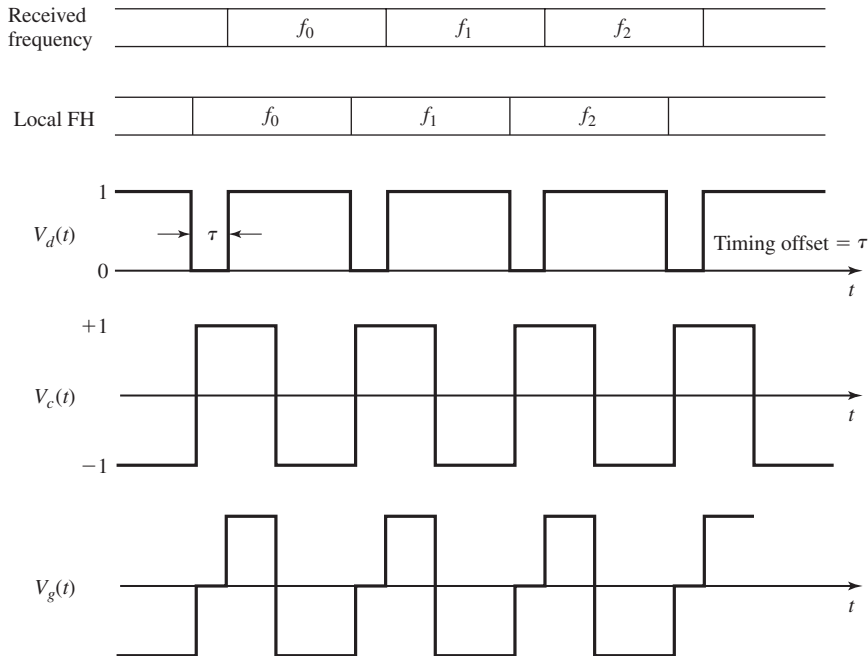


**Figure 10.60** Waveforms for the tracking method of FH signals shown in Figure 10.59.

which drives the loop filter. Note that when the chip transitions from the locally generated sinusoidal waveform do not occur at the same time as the transitions in the incoming received signal, the output of the loop filter will be either negative or positive, depending on whether the VCC is lagging or advanced relative to the timing of the input signal. This error signal from the loop filter will provide the control signal for adjusting the VCC timing signal so as to drive the frequency synthesized FH signal to proper synchronism with the received signal.

## 10.4 DIGITAL CELLULAR COMMUNICATION SYSTEMS

In this section, we present an overview of two types of digital cellular communication systems that are currently in use. One is the GSM (Global System for Mobile Communication) system that is widely used in Europe and other parts of the world. It employs time-division multiple access (TDMA) to accommodate multiple users. The second is the CDMA system based on Interim Standard 95 (IS-95) that is widely used in North America and some countries in the Far East.

### 10.4.1 The GSM System

GSM was developed in Europe for the purpose of providing a common digital cellular communication system that would serve all of Europe. It is now widely used in many parts of the world. The GSM system employs the frequency band 890–915 MHz for signal transmission from mobile transmitters to base-station receivers (uplink or reverse link) and the frequency band 935–960 MHz for transmission from the base stations to the mobile receivers (downlink or forward link). The two 25 MHz-frequency bands are each subdivided into 125 channels, where each channel has a bandwidth of 200 KHz. To reduce interference from transmissions in adjacent cells, different sets of frequencies are assigned to adjacent base stations and frequencies are reused according to some

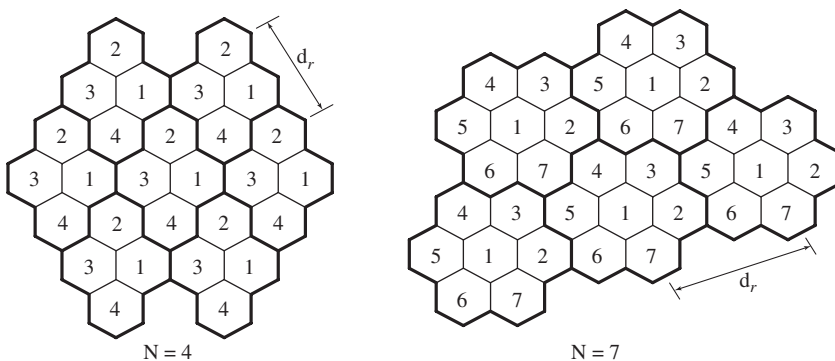


**Figure 10.61** Frequency reuse in cellular system with reuse factor  $N = 4$  or  $N = 7$ .

design plan, such as the frequency plans shown in Figure 10.61, where the frequency reuse factor is either  $N = 4$  or  $N = 7$ . We observe that larger values of  $N$  increase the distance  $d_r$  between two base stations using the same set of frequencies, thus, reducing co-channel interference. On the other hand, a large value of  $N$  reduces the spectral efficiency of the cellular system, since fewer frequencies are assigned to each cell. The maximum radius for a cell is 35 Km.

Each 200 KHz-frequency band accommodates 8 users by creating 8 TDMA nonoverlapping time slots, as shown in Figure 10.62. The eight time slots constitute a frame of duration 4.615 msec, and each time slot has a time duration of  $576.875 \mu\text{sec}$ . The information data from the users is transmitted in bursts at a rate of 270.833 Kbps. Figure 10.63 illustrates the basic GSM frame structure, in which 26 frames are grouped

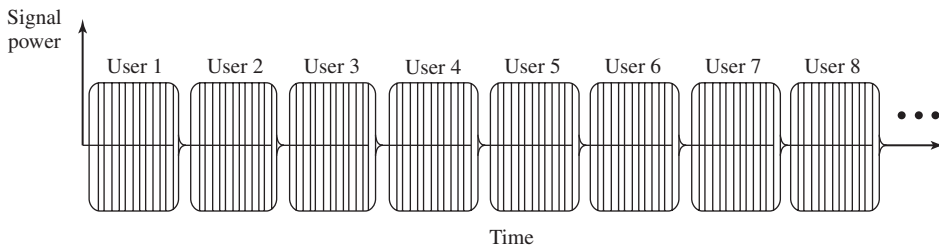


Figure 10.62 TDMA frame in GSM.

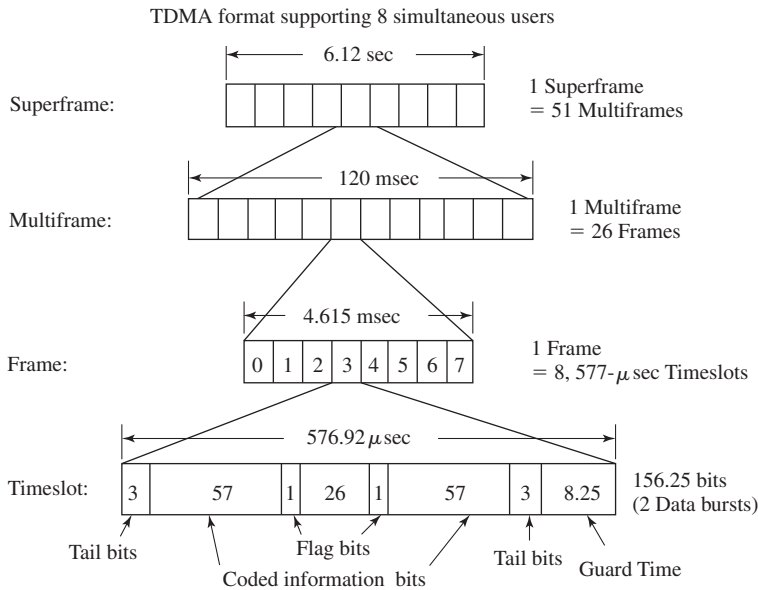
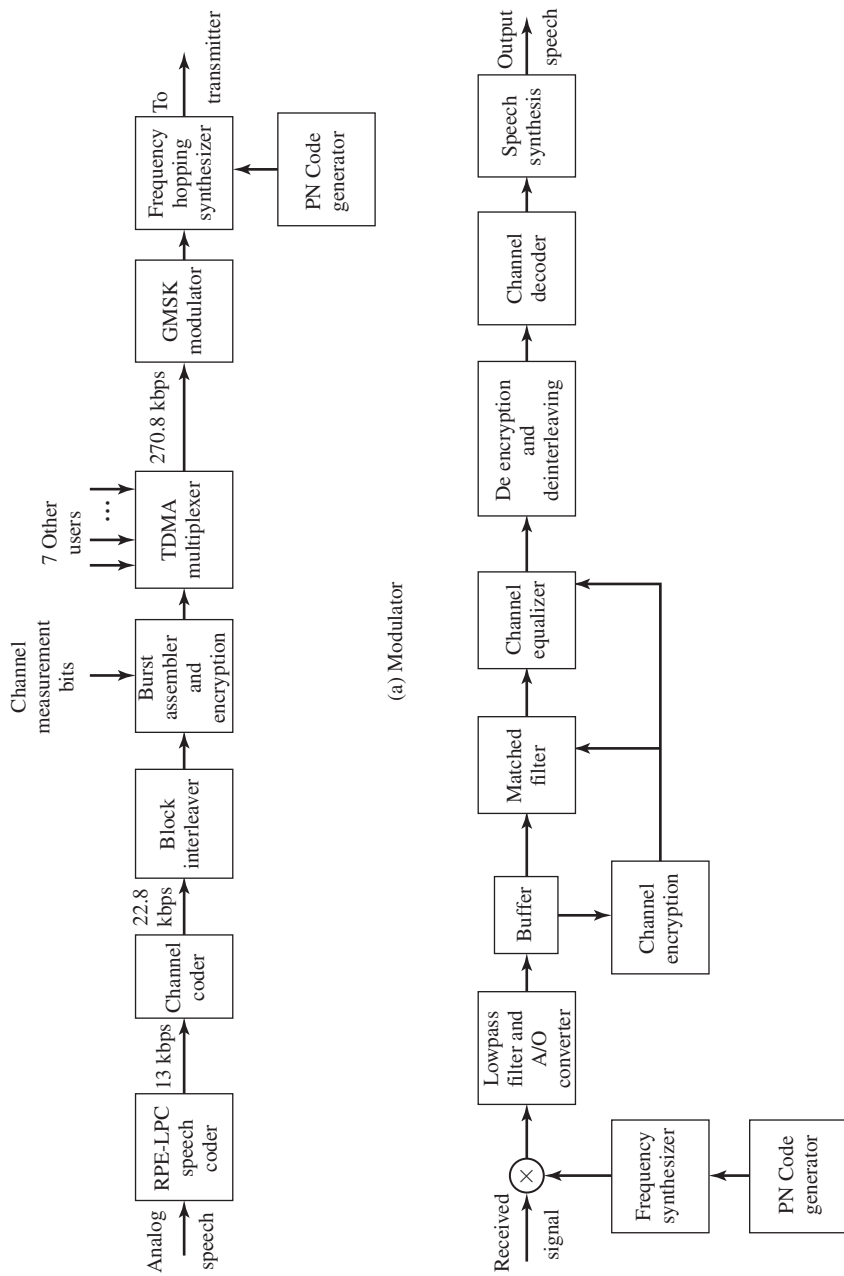


Figure 10.63 GSM frame structure.



**Figure 10.64** Functional block diagram of modulator and demodulator for GSM.

to form a multiframe and 51 multiframes are grouped to form a superframe. The framing hierarchy is convenient in facilitating synchronization and network control. To reduce the effect of fading and interference and, thus, provide signal diversity, the carrier frequency is hopped at the frame rate of (nominally) 217 hops/sec.

The functional block diagram of the transmitter and receiver in the GSM system is shown in Figure 10.64. The speech coder is based on a type of linear predictive coding (LPC) called residual pulse-excited (RPE) linear-predictive coding (RPE-LPC). RPE-LPC delivers 260 bits in each 20 msec time interval, hence, a bit rate of 13 Kbps. The most significant bits are encoded by a rate  $1/2$ , constraint length  $L = 5$  convolutional encoder, and the coded and uncoded bits are block interleaved to produce data at a rate of 22.8 Kbps. Thus, the 260 information bits are transformed into 456 coded bits in each 20 msec time interval. The coded bit stream is encrypted and, then, organized for burst transmission in time slots that carry 114 coded bits and some overhead bits, as shown in Figure 10.63, including a sequence of 26 bits which is used to measure the characteristics of the channel in each time slot. Therefore, the 456 coded bits are transmitted in four consecutive bursts, where each burst contains 114 coded bits and occupies one time slot.

The modulation used to transmit the bits in each time slot is GMSK with  $BT = 0.3$ , which is a signal pulse that is illustrated in Figure 10.27(e). The output of the GMSK modulator is translated in frequency to the desired carrier frequency, which is hopped to a different frequency in each frame.

At the receiver, the received signal is dehopped and translated to baseband, thus creating in-phase ( $I$ ) and quadrature ( $Q$ ) signal components, which are sampled and buffered. The 26 known transmitted bits are used to measure the channel characteristics and, thus, to specify the matched filter to the channel corrupted signal. The data bits are passed through the matched filter and the matched-filter output is processed by a channel equalizer, which may be realized either as a decision-feedback equalizer (DFE) or an ML sequence detector that is efficiently implemented via the Viterbi algorithm. The bits in a burst at the output of the equalizer are deassembled, decrypted, deinterleaved, and passed to the channel decoder. The decoded bits are used to synthesize the speech signal that was encoded via RPE-LPC.

In addition to the time slots (channels) that are used for transmission of the digitized speech signals, there are additional channels that are allocated to various control and synchronization functions, such as paging, frequency correction, synchronization, and requests for access to send messages. These control channels are additional time slots that contain known sequences of bits for performing the control functions.

Table 10.5 provides a summary of the basic parameters in the GSM system.

#### 10.4.2 CDMA System Based on IS-95

As described in Section 10.3, the enhancement in performance obtained from a DS spread-spectrum signal through the processing gain and coding gain can be used to enable many DS spread-spectrum signals to simultaneously occupy the same channel bandwidth, provided that each signal has its own distinct pseudorandom sequence.



**TABLE 10.5** SUMMARY OF PARAMETERS IN GSM SYSTEM

System Parameter	Specification
Uplink frequency band	890–915 MHz
Downlink frequency band	935–960 MHz
Number of carriers/band	125
Bandwidth/carrier	200 KHz
Multiple-access method	TDMA
Number of users/carrier	8
Data rate/carrier	270.8 Kbps
Speech-coding rate	13 KHz
Speech encoder	RPE-LPC
Coded-speech rate	22.8 kbps
Modulation	GMSK with $BT = 0.30$
Demodulation	Matched filter + equalizer
Interleaver	Block
Frequency-hopping rate	217 hops/sec

Direct-sequence CDMA has been adopted as one multiple-access method for digital cellular voice communications in North America. This first generation digital cellular (DMA) communication system was developed by Qualcomm, and has been standardized and designated as IS-95 by the Telecommunications Industry Association (TIA) for use in the 800 MHz- and 1900 MHz-frequency bands. A major advantage of CDMA over other multiple-access methods is that the entire frequency band is available at each base station; i.e., the frequency reuse factor  $N = 1$ .

The nominal bandwidth used for transmission from a base station to the mobile receivers (forward link) is 1.25 MHz, and a separate channel, also with a bandwidth of 1.25 MHz, is used for signal transmission from mobile receivers to a base station (reverse link). The signals transmitted in both the forward and the reverse links are DS spread-spectrum signal having a chip rate of  $1.2288 \times 10^6$  chips/sec (Mchips/s).

**Forward Link.** A block diagram of the modulator for the signals transmitted from a base station to the mobile receivers is shown in Figure 10.65. The speech coder is a code-excited linear-predictive (CELP) coder which generates data at the variable rates of 9600, 4800, 2400, and 1200 bits/s, where the data rate is a function of the speech activity of the user, in frame intervals of 20 ms. The data from the speech coder are encoded by a rate 1/2, constraint length  $L = 9$  convolutional code. For lower speech activity, where the data rates are 4800, 2400, or 1200 bits/s, the output symbols from the convolutional encoder are repeated either twice, four times, or eight times so as to maintain a constant bit rate of 9600 bits/s. At the lower speech activity rates, the transmitter power is reduced by either 3, 6, or 9 dB, so that the transmitted energy/bit remains constant for all speech rates. Thus, a lower speech activity results in a lower transmitter power and, hence, a lower level of interference to other users.

The encoded bits for each frame are passed through a block interleaver, which is needed to overcome the effects of burst errors that may occur in transmission through the channel. The data bits at the output of the block interleaver, which occur at a rate

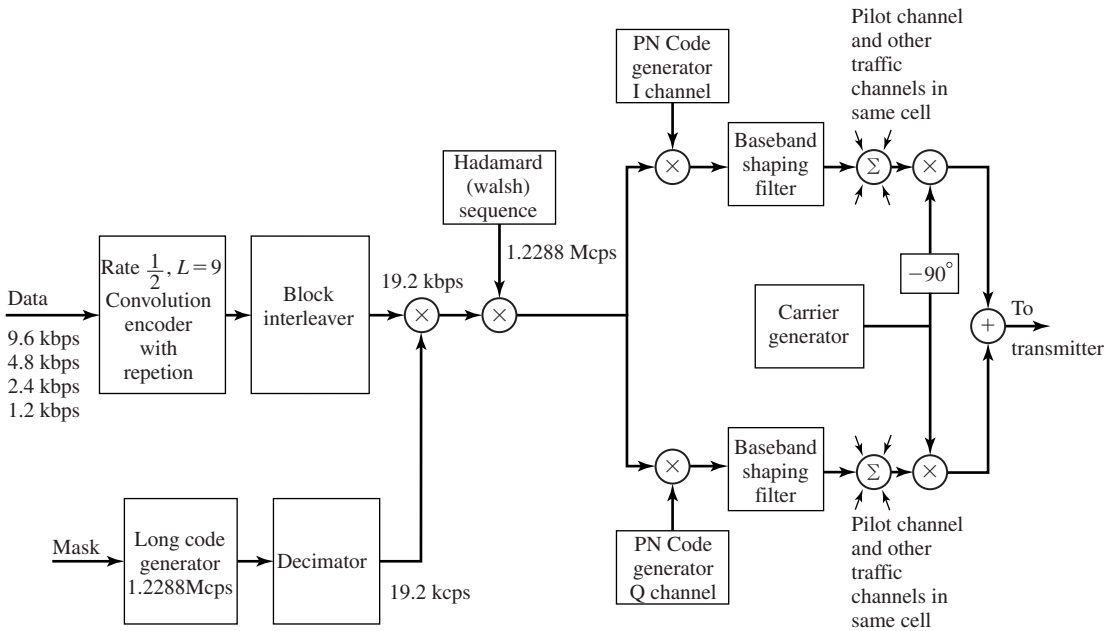


Figure 10.65 Block diagram of IS-95 forward link.

of 19.2 kbits/s, are scrambled by multiplication with the output of a long code (period  $N = 2^{42} - 1$ ) generator running at the chip rate of 1.2288 M chips/s, but whose output is decimated by a factor of 64 to 19.2 kchips/s. The long code is used to uniquely identify a call of a mobile station on the forward and reverse links.

Each user of the channel is assigned a Hadamard (also called Walsh) sequence of length 64. There are 64 orthogonal Hadamard sequences assigned to each base station, and, thus, there are 64 channels available. One Hadamard sequence (the all-zero sequence) is used to transmit a pilot signal, which serves as a means for measuring the channel characteristics, including the signal strength and the carrier phase offset. These parameters are used at the receiver in performing phase-coherent demodulation. Another Hadamard sequence is used for providing time synchronization. One channel, and possibly more if necessary, is used for paging. That leaves up to 61 channels for allocation to different users.

Each user, using the Hadamard sequence assigned to it, multiplies the data sequence by the assigned Hadamard sequence. Thus, each encoded data bit is multiplied by the Hadamard sequence of length 64. The resulting binary sequence is now spread by multiplication with two PN sequences of length  $N = 2^{15}$ , so as to create in-phase ( $I$ ) and quadrature ( $Q$ ) signal components. Thus, the binary data signal is converted to a four-phase signal and both the  $I$  and  $Q$  components are filtered by baseband spectral-shaping filters. Different base stations are identified by different offsets of these PN sequences. The signals for all the 64 channels are transmitted synchronously so that,

in the absence of channel multipath distortion, the signals of other users received at any mobile receiver do not interfere because of the orthogonality of the Hadamard sequences.

At the receiver, a RAKE demodulator is used to resolve the major multipath signal components, which are then phase-aligned and weighted according to their signal strength using the estimates of phase and signal strength derived from the pilot signal. These components are combined and passed to the Viterbi soft-decision decoder.

**Reverse Link.** The modulator for the reverse link from a mobile transmitter to a base station is different from that for the forward link. A block diagram of the modulator is shown in Figure 10.66. An important consideration in the design of the modulator is that, signals transmitted from the various mobile transmitters to the base station are asynchronous and, hence, there is significantly more interference among users. Second, the mobile transmitters are usually battery operated and, consequently, these transmissions are power limited. To compensate for these major limitations, a  $L = 9$ , rate 1/3 convolutional code is used in the reverse link. Although this code has essentially the same coding gain in an AWGN channel as the rate 1/2 code used in the forward link, it has a much higher coding gain in a fading channel. As in the case of the forward link, for lower speech activity, the output bits from the convolutional encoder are repeated either two, or four, or eight times. However, the coded bit rate is 28.8 kbits/s.

For each 20-ms frame, the 576 encoded bits are block-interleaved and passed to the modulator. The data is modulated using an  $M = 64$  orthogonal signal set using Hadamard sequences of length 64. Thus, a 6-bit block of data is mapped into one of the 64 Hadamard sequences. The result is a bit (or chip) rate of 307.2 kbits/s at the output of the modulator. We note that 64-ary orthogonal modulation at an error probability of  $10^{-6}$  requires approximately 3.5 dB less SNR/bit than binary antipodal signaling.

To reduce interference to other users, the time position of the transmitted code symbol repetitions is randomized so that, at the lower speech activity, consecutive bursts do not occur evenly spaced in time. Following the randomizer, the signal is spread by the output of the long code PN generator, which is running at a rate of 1.2288 Mchips/s. Hence, there are only four PN chips for every bit of the Hadamard sequence from the modulator, so the processing gain in the reverse link is very small. The resulting 1.2288 Mchips/s binary sequences of length  $N = 2^{15}$ , whose rate is also 1.2288 Mchips/s, create  $I$  and  $Q$  signals (a QPSK signal) which are filtered by baseband spectral-shaping filters and then passed to quadrature mixers. The  $Q$ -channel signal is delayed in time by one-half PN chip relative to the  $I$ -channel signal prior to the baseband filter. In effect, the signal at the output of the two baseband filters is an offset QPSK signal.

Although the chips are transmitted as an offset QPSK signal, the demodulator employs noncoherent demodulation of the  $M = 64$  orthogonal Hadamard waveforms to recover the encoded data bits. A computationally efficient (fast) Hadamard transform is used to reduce the computational complexity in the demodulation process. The output of the demodulator is then fed to the Viterbi detector, whose output is used to synthesize the speech signal.

Table 10.6 provides a summary of the basic parameters in the IS-95 system.

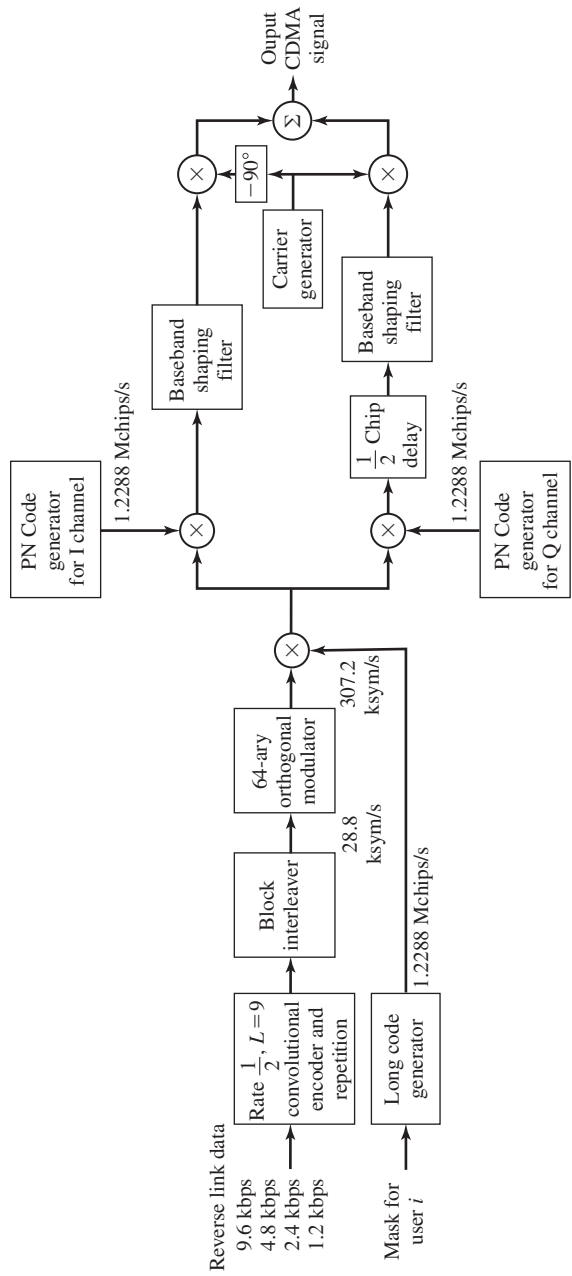


**Figure 10.66** Block diagram of IS-95 reverse link.

**TABLE 10.6** SUMMARY OF PARAMETERS IN IS-95 SYSTEM

System Parameter	Specification
Uplink frequency band	824–849 MHz
Downlink frequency band	869–894 MHz
Number of carriers/band	20
Bandwidth/carrier	1.25 MHz
Multiple-access method	CDMA
Number of users/carrier	60
Chip rate	1.2288 Mcps
Speech coder	Variable rate CELP
Speech rate	9600, 4800, 2400, 1200 bps
Interleaver	Block
Channel encoder	$R = 1/2, L = 9(D)$ $R = 1/3, L = 9(U)$
Modulation	BPSK with QPSK Spreading (D) 64-ary Orthogonal with QPSK Spreading (U)
Demodulation	RAKE matched filter with maximal-ratio combining
Signature sequences	Hadamard (Walsh) of length 64
PN sequence	$N = 2^{42} - 1$ (Long code) $N = 2^{15}$ (Spreading codes)

## 10.5 FURTHER READING

In this chapter, we focused our topics dealing with wireless communications. First, we treated digital transmission on fading multipath channels. Our treatment of this topic was indeed very brief and focused primarily on the Rayleigh fading channel model. For the most part, this is due to the wide acceptance of this model for describing the fading effects on many radio channels and to its mathematical tractability. Although other statistical models, such as the Ricean fading model, may be more appropriate for characterizing fading on some real channels, such as microwave LOS, the general approach for providing reliable communications by means of signal diversity is still applicable.

More extensive and advanced treatments on fading channels are found in books by Schwartz et al. (1966) and Proakis (2001). The pioneering work on the characterization of fading multipath channels and on signal and receiver design for reliable digital communications over such channels was done by Price (1954, 1956). This early work was followed by additional significant contributions from Price and Green (1958, 1960), Kailath (1960, 1961), and Green (1962). Diversity transmission and diversity-combining techniques under a variety of channel conditions have been treated in the papers by Pierce (1958), Brennan (1959), Turin (1961, 1962), Pierce and Stein (1960), Barrow (1963), Bello and Nelin (1962a,b, 1963), Price (1962a,b), and Lindsey (1964).

CPFSK and CPM are especially suitable for wireless digital communications because these types of digital modulations are bandwidth efficient and have the additional desirable property of having a constant envelope. Therefore, high efficiency nonlinear

power amplifiers can be used in transmission of the signals. CPFSK and CPM have been treated extensively in the technical journals and in textbooks. A thorough treatment of CPM can be found in the book by Anderson et al. (1986). The journal papers by Aulin and Sundberg (1981, 1982a,b, 1984) and by Aulin et al. (1981) provide detailed analysis of the performance characteristics of CPM. The tutorial paper by Sundberg (1986) gives a very readable overview of CPM, its demodulation and its performance characteristics. This paper also contains a comprehensive list of references.

Our third topic of this chapter was a brief, introductory treatment of spread-spectrum modulation and demodulation and the performance evaluation of this type of signaling in the presence of several different types of interference. Historically, the primary application of spread-spectrum modulation has been in the design of secure digital communications systems for military use. However, in the last two decades we have seen a trend toward commercial use of spread-spectrum modulation, especially its use in mobile cellular communications, in multiple-access communications via satellites, and in interoffice radio communications.

A historical account on the development of spread-spectrum communications covering the period 1920–1960 is given in a paper by Scholtz (1982). Tutorial treatments of spread-spectrum modulation that deal with basic concepts are found in papers by Scholtz (1977) and Pickholtz et al. (1982). These papers also contain a large number of references to the previous work. Two tutorial papers by Viterbi (1979, 1985) contain a basic analysis of the performance characteristics of DS and FH spread-spectrum signals.

Comprehensive treatments of various aspects concerning the analysis and design of spread-spectrum signals and systems, including synchronization techniques, are found in books by Simon et al. (1985), Ziemer and Peterson (1985), and Holmes (1982). Also, special issues of the *IEEE Transactions on Communications* (August 1977, May 1982) are devoted to spread-spectrum communications. These special issues contain a collection of papers devoted to a variety of topics, including multiple-access techniques, synchronization techniques, and performance analysis with various types of channel interference. A number of important papers that have been published in IEEE journals have been reprinted in book form by the IEEE press, (see Dixon, ed. (1976) and Cook et al. (1983)).

In the last section of this chapter, we presented two examples of digital cellular communication systems designed for voice transmission. One system, called GSM, is based on TDMA to accommodate multiple users, while the second system employs CDMA.

## PROBLEMS

- 10.1** In the transmission and reception of signals to and from moving vehicles, the transmitted signal frequency is shifted in direct proportion to the speed of the vehicle. The so-called *Doppler frequency shift* imparted to a signal that is received in a vehicle traveling at a velocity  $v$  relative to a (fixed) transmitter is given by

the formula

$$f_D = \pm \frac{v}{\lambda}$$

where  $\lambda$  is the wavelength, and the sign depends on the direction (moving toward or moving away) that the vehicle is traveling relative to the transmitter. Suppose that a vehicle is traveling at a speed of 100 km/hr relative to a base station in a mobile cellular communication system. The signal is a narrowband signal transmitted at a carrier frequency of 1 GHz.

1. Determine the Doppler frequency shift.
  2. What should be the bandwidth of a Doppler frequency tracking loop if the loop is designed to track Doppler frequency shifts for vehicles traveling at speeds up to 100 km/hr?
  3. Suppose the transmitted signal bandwidth is 1 MHz centered at 1 GHz. Determine the Doppler frequency spread between the upper and lower frequencies in the signal.
- 10.2** A multipath fading channel has a multipath spread of  $T_m = 1$  s and a Doppler spread  $B_d = 0.01$  Hz. The total channel bandwidth at bandpass available for signal transmission is  $W = 5$  Hz. To reduce the effect of intersymbol interference, the signal designer selects a pulse duration of  $T = 10$  sec.
1. Determine the coherence bandwidth and the coherence time.
  2. Is the channel frequency selective? Explain.
  3. Is the channel fading slowly or rapidly? Explain.
  4. Suppose that the channel is used to transmit binary data via (antipodal) coherently detected PSK in a frequency diversity mode. Explain how you would use the available channel bandwidth to obtain frequency diversity and determine how much diversity is available.
  5. For the case in (4), what is the approximate SNR required/diversity to achieve an error probability of  $10^{-6}$ ?
- 10.3** The probability of error for binary DPSK and binary FSK with noncoherent detection in an AWGN channel is

$$P_b = \frac{1}{2} e^{-c\rho_b}$$

where  $c = 1$  for DPSK and  $c = \frac{1}{2}$  for FSK, and  $\rho_b = \frac{\alpha^2 \mathcal{E}_b}{N_0}$ , where  $\alpha$  is the attenuation factor. By averaging  $P_b$  over the Rayleigh distributed variable  $\alpha$ , as indicated by Equation (10.1.25), verify the expression for the probability of error for DPSK and FSK in a Rayleigh fading channel.

- 10.4** A communication system employs dual antenna diversity and binary orthogonal FSK modulation. The received signals at the two antennae are

$$\begin{aligned} r_1(t) &= \alpha_1 s(t) + n_1(t) \\ r_2(t) &= \alpha_2 s(t) + n_2(t) \end{aligned}$$

where  $\alpha_1$  and  $\alpha_2$  are statistically i.i.d. Rayleigh random variables, and  $n_1(t)$  and  $n_2(t)$  are statistically independent, zero-mean white Gaussian random processes with power-spectral density  $N_0/2$  W/Hz. The two signals are demodulated, squared, and then combined (summed) prior to detection.

1. Sketch the functional block diagram of the entire receiver including the demodulator, the combiner, and the detector.
  2. Plot the probability of error for the detector and compare the result with the case of no diversity.
- 10.5** A binary communication system transmits the same information on two diversity channels. The two received signals are

$$\begin{aligned} r_1 &= \pm\sqrt{\mathcal{E}_b} + n_1 \\ r_2 &= \pm\sqrt{\mathcal{E}_b} + n_2 \end{aligned}$$

where  $E(n_1) = E(n_2) = 0$ ,  $E(n_1^2) = \sigma_1^2$  and  $E(n_2^2) = \sigma_2^2$ , and  $n_1$  and  $n_2$  are uncorrelated Gaussian variables. The detector bases its decision on the linear combination of  $r_1$  and  $r_2$ ; i.e.,

$$r = r_1 + kr_2$$

1. Determine the value of  $k$  that minimizes the probability of error.
  2. Plot the probability of error for  $\sigma_1^2 = 1$ ,  $\sigma_2^2 = 3$  and either  $k = 1$  or  $k$  is the optimum value found in (1). Compare the results.
- 10.6** Suppose the binary antipodal signals  $\pm s(t)$  are transmitted over a fading channel and the received signal is

$$r(t) = \pm\alpha s(t) + n(t), \quad 0 \leq t \leq T$$

where  $n(t)$  is zero-mean white Gaussian noise with autocorrelation function  $\frac{N_0}{2}\delta(\tau)$ . The energy in the transmitted signal is  $\mathcal{E} = \int_0^T |s(t)|^2 dt$ . The channel gain  $\alpha$  is specified by the PDF  $p(\alpha) = 0.1\delta(\alpha) + 0.9\delta(\alpha - 2)$ .

1. Determine the average probability of error  $P_e$  for the demodulator which employs a filter matched to  $s(t)$ .
2. What value does  $P_e$  approach as  $\frac{\mathcal{E}}{N_0}$  approaches infinity?
3. Suppose the same signal is transmitted over two statistically *independently*



*fading* channels with gains  $\alpha_1$  and  $\alpha_2$ , where

$$p(\alpha_k) = 0.1\delta(\alpha_k) + 0.9\delta(\alpha_k - 2), \quad k = 1, 2$$

The noises on the two channels are statistically independent and identically distributed. The demodulator employs a matched filter for each channel and simply adds the two filter outputs to form the decision variable. Determine the average  $P_e$ .

4. For the case in (c) what value does  $P_e$  approach as  $\frac{\mathcal{E}}{N_0}$  approaches infinity?
- 10.7 In a MSK signal, the initial state for the phase is either 0 or  $\pi$  radians. Determine the terminal phase state for the following four input pairs of input data: (a) 00, (b) 01, (c) 10, (d) 11.
- 10.8 A continuous-phase FSK signal with  $h = 1/2$  is represented as

$$s(t) = \pm \sqrt{\frac{2\mathcal{E}_b}{T_b}} \cos\left(\frac{\pi t}{2T_b}\right) \cos 2\pi f_c t \pm \sqrt{\frac{2\mathcal{E}_b}{T_b}} \sin\left(\frac{\pi t}{2T_b}\right) \sin 2\pi f_c t$$

$$0 \leq t \leq 2T_b$$

where the  $\pm$  signs depend on the information bits transmitted.

1. Show that this signal has a constant amplitude.
  2. Sketch a block diagram of the modulator for synthesizing the signal.
  3. Sketch a block diagram of the demodulator and detector for recovering the information.
- 10.9 Sketch the phase-tree, the state trellis, and the state diagram for partial-response CPM with  $h = \frac{1}{2}$  and

$$g(t) = \begin{cases} \frac{1}{4T}, & 0 \leq t \leq 2T \\ 0, & \text{otherwise} \end{cases}$$

- 10.10 Determine the number of terminal phase states in the state trellis diagram for (a) a full response binary CPFSK with either  $h = \frac{2}{3}$  or  $\frac{3}{4}$  and (b) a partial response  $L = 3$  binary CPFSK with either  $h = \frac{2}{3}$  or  $\frac{3}{4}$ .
- 10.11 A rate  $1/2$  convolutional code with  $d_{\text{free}} = 10$  is used to encode a data sequence occurring at a rate of 1000 bits per second. The modulation is binary PSK. The DS spread spectrum sequence has a chip rate of 10 MHz.
1. Determine the coding gain.
  2. Determine the processing gain.
  3. Determine the interference margin assuming an  $\mathcal{E}_b/I_0 = 10$ .
- 10.12 Demonstrate that a DS spread-spectrum signal without coding provides no improvement in performance against additive white Gaussian noise.
- 10.13 A total of 30 equal-power users are to share a common communication channel by CDMA. Each user transmits information at a rate of 10 kbps via DS spread

spectrum and binary PSK. Determine the minimum chip rate in order to obtain a bit-error probability of  $10^{-5}$ . Additive noise at the receiver may be ignored in this computation.

- 10.14** A CDMA system is designed based on DS spread spectrum with a processing gain of 1000 and binary PSK modulation. Determine the number of users, if each user has equal power and the desired level of performance is an error probability of  $10^{-6}$ . Repeat the computation if the processing gain is changed to 500.
- 10.15** A DS spread-spectrum system transmits at a rate of 1000 bps in the presence of a tone interference. The interference power is 20 dB greater than the desired signal and the required  $\mathcal{E}_b/I_0$  to achieve satisfactory performance is 10 dB.
1. Determine the spreading bandwidth required to meet the specifications.
  2. In the case of a pulse interference, determine the pulse duty cycle that results in worst-case performance and the corresponding probability of error.
- 10.16** A DS spread-spectrum system is used to resolve the multipath signal component in a two-path radio signal propagation scenario. If the path length of the secondary path is 300 m longer than that of the direct path, determine the minimum chip rate necessary to resolve the multipath component.
- 10.17** A CDMA system consists of 15 equal-power users that transmit information at a rate 10,000 bps each using a DS spread-spectrum signal operating at a chip rate of 1 MHz. The modulation is binary PSK.
1. Determine the  $\mathcal{E}_b/I_0$ , where  $I_0$  is the spectral density of the combined interference.
  2. What is the processing gain?
  3. How much should the processing gain be increased to allow for doubling the number of users without affecting the output SNR?
- 10.18** An FH binary orthogonal FSK system employs a  $m = 15$  stage linear feedback shift register that generates a maximal length sequence. Each state of the shift register selects one of  $N$  nonoverlapping frequency bands in the hopping pattern. The bit rate is 100 bits/sec and the hop rate is once/bit. The demodulator employs noncoherent detection.
1. Determine the hopping bandwidth for this channel.
  2. What is the processing gain?
  3. What is the probability of error in the presence of AWGN?
- 10.19** Consider the FH binary orthogonal FSK system described in Problem 10.18. Suppose that the hop rate is increased to two hops/bit. The receiver uses square-law combining to combine the signal over the two hops.
1. Determine the hopping bandwidth for the channel.
  2. What is the processing gain?
  3. What is the error probability in the presence of AWGN?

- 10.20** In a fast FH spread-spectrum system, the information is transmitted via FSK, with noncoherent detection. Suppose there are  $N = 3$  hops/bit, with hard-decision decoding of the signal in each hop.
1. Determine the probability of error for this system in an AWGN channel with power-spectral density  $\frac{N_0}{2}$  and an SNR = 13 dB (total SNR over the three hops).
  2. Compare the result in (1) with the error probability of an FH spread-spectrum system that hops once/bit.
- 10.21** A slow FH binary FSK system with noncoherent detection operates at an  $\mathcal{E}_b/I_0 = 10$ , with a hopping bandwidth of 2 GHz, and a bit rate of 10 Kbps.
1. What is the processing gain for the system?
  2. In the case of a partial-band interference, what is the bandwidth occupancy for worst-case performance?
  3. What is the probability of error for the worst-case partial-band interference?
- 10.22** A DS binary PSK spread spectrum has a processing gain of 500. What is the interference margin against a continuous tone interference if the desired error probability is  $10^{-5}$ ?
- 10.23** Repeat Problem 10.22 for a pulsed noise interference with a duty cycle of 1%.
- 10.24** Consider the DS spread-spectrum signal

$$c(t) = \sum_{n=-\infty}^{\infty} c_n p(t - nT_c)$$

where  $c_n$  is a periodic  $m$ -sequence with a period  $L = 127$  and  $p(t)$  is a rectangular pulse of duration  $T_c = 1 \mu\text{sec}$ . Determine the power-spectral density of the signal  $c(t)$ .

- 10.25** Suppose that  $\{c_{1i}\}$  and  $\{c_{2i}\}$  are two binary (0, 1) periodic sequences with periods  $L_1$  and  $L_2$ , respectively. Determine the period of the sequence obtained by forming the modulo-2 sum of  $\{c_{1i}\}$  and  $\{c_{2i}\}$ .
- 10.26** An  $m = 10$  maximum-length shift register is used to generate the pseudorandom sequence in a DS spread-spectrum system. The chip duration is  $T_c = 1 \mu\text{sec}$ , and the bit duration is  $T_b = LT_c$ , where  $L$  is the length (period) of the  $m$ -sequence.
1. Determine the processing gain of the system in dB.
  2. Determine the interference margin if the required  $\mathcal{E}_b/I_0 = 10$  and the interference is a tone interference with an average power  $I_{av}$ .
- 10.27** Figure P10-27 illustrates the average power multipath delay profile for (a) suburban and urban areas and (b) hilly terrain area, in cellular communication. In a GSM system, the bit rate is 270.8 Kbps and in IS-95 system (forward link) the bit rate is 19.2 Kbps. Determine the number of bits affected by intersymbol interference in the transmission of the signal through the channels (a) and (b) for each cellular system.

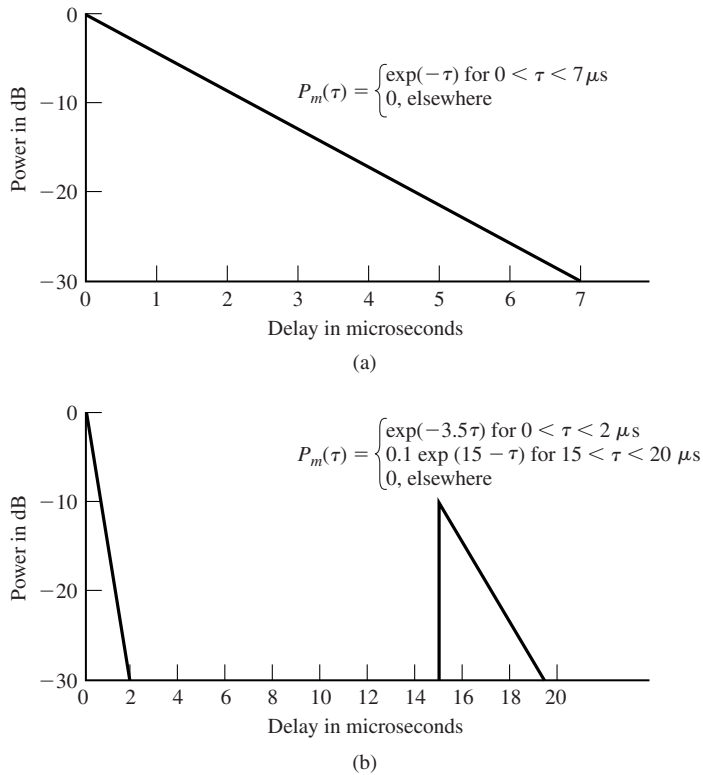


**Figure P-10.27**

- 10.28** For the multipath delay problem shown in Figure P10-27, determine the number of taps in a RAKE demodulator that would be needed to span the multipath for channels (a) and (b). Of the total number of RAKE taps, how many will contain signal components and how many will have no signal for channel (b)?
- 10.29** A widely used model for the Doppler power spectrum of a mobile radio channel is the so-called *Jake's model*, given as

$$S(f) = \begin{cases} \frac{1}{\pi f_m} \frac{1}{\sqrt{1-(f/f_m)^2}}, & |f| \leq f_m \\ 0, & \text{otherwise} \end{cases}$$

where  $f_m = vf_0/c$  is the maximum Doppler frequency,  $v$  is the vehicle speed in m/s,  $f_0$  is the carrier frequency, and  $c$  is the speed of light ( $3 \times 10^8$  m/s). Determine  $f_m$  for an automobile traveling at 100 Km/hr, for a train traveling at 200 Km/hr and plot  $S(f)$  for the two vehicles for a cellular communication system with a carrier frequency of 900 MHz. What are the spread factors of the channel for the two vehicles if the multipath delay profile is the one shown in Figure P10-27?

# Appendix A

## *The Probability of Error for Multichannel Reception of Binary Signals*

In multichannel communication systems that employ binary signals for transmitting information over an AWGN channel, the decision metric can be expressed as a special case of the general quadratic for

$$Q = \sum_{k=1}^N (A|X_k|^2 + B|Y_k|^2 + CX_kY_k^* + C^*X_k^*Y_k) \quad (\text{A.1})$$

in complex-valued Gaussian random variables. A, B, and C are constants satisfying the condition  $|C|^2 - AB > 0$ ;  $X_k$  and  $Y_k$  are a pair of (possibly) correlated, complex-valued Gaussian random variables of the form  $X_k = X_{kr} + jX_{ki}$  and  $Y_k = Y_{kr} + jY_{ki}$ ; and  $N$  represents the number of independent channels over which the signal is received.

For example, in binary DPSK detection, which is described in Section 7.6.4, the decision metric is given as

$$\text{Re}(r_k r_{k-1}^*) = \frac{1}{2}(r_k r_{k-1}^* + r_k^* r_{k-1}) \quad (\text{A.2})$$

where  $r_k$  is the output of the demodulation filter. We note that Equation (A.2) is a special case of Equation (A.1) which is obtained from Equation (A.1) by setting  $N = 1$ ,  $A = B = 0$ ,  $X_k = r_k$ ,  $Y_k = r_{k-1}$ , and  $C = 1/2$ .

As another example, we have the case of fast frequency-hopped, binary FSK, in which case the output of the two square-law combiners is given by Equation (10.3.60), where  $N$  is the number of frequency-hopped chips/symbol. The probability of error, is

simply the probability that  $DM_1 - DM_2 < 0$ , where

$$DM_1 - DM_2 = \sum_{k=1}^N \left[ \left| v_{1k} + \frac{\mathcal{E}_b}{N_0} \right|^2 - |v_{2k}|^2 \right] \quad (\text{A.3})$$

where  $v_{1k}$  and  $v_{2k}$  are complex-valued Gaussian random variables that represent the noises of the outputs of the correlators. We again note that Equation (A.3) is a special case of the general quadratic form in Equation (A.1), where  $A = -B = 1$ ,  $C = 0$ ,  $X_k = (v_{1k} + \frac{\mathcal{E}_b}{N_0})$  and  $Y_k = v_{2k}$ .

The probability of error is just the probability that  $Q < 0$ ; i.e.,

$$P_2 = P(Q < 0) = \int_{-\infty}^0 f_Q(q) dq \quad (\text{A.4})$$

where  $f_Q(q)$  is the PDF of  $Q$ .

The derivation for the error probability  $P_2$  may be found in the technical literature and in the book by Proakis (2001). This derivation is lengthy and is not repeated here. The expression for the probability of error resulting from this derivation is

$$\begin{aligned} P_2 = & Q(a, b) - I_0(ab) \exp\left(-\frac{a^2 + b^2}{2}\right) \\ & + \frac{I_0(ab) \exp[-(a^2 + b^2)/2]}{(1 + v_2/v_1)^{2N-1}} \sum_{k=0}^{N-1} \binom{2N-1}{k} \left(\frac{v_2}{v_1}\right)^k \\ & + \frac{\exp[-(a^2 + b^2)/2]}{(1 + v_2/v_1)^{2N-1}} \sum_{n=1}^{N-1} I_n(ab) \\ & \times \left\{ \sum_{k=0}^{N-1-n} \binom{2N-1}{k} \left[ \left(\frac{b}{a}\right)^n \left(\frac{v_2}{v_1}\right)^k - \left(\frac{a}{b}\right)^n \left(\frac{v_2}{v_1}\right)^{2N-1-k} \right] \right\} \quad N > 1 \end{aligned} \quad (\text{A.5})$$

$$P_2 = Q(a, b) - \frac{v_2/v_1}{1 + v_2/v_1} I_0(ab) \exp\left(-\frac{a^2 + b^2}{2}\right) \quad N = 1$$

where the parameters  $a, b, v_1, v_2$  are defined as

$$\begin{aligned} a &= \left[ \frac{2v_1^2 v_2 (\alpha_1 v_2 - \alpha_2)}{(v_1 + v_2)^2} \right]^{1/2} \\ b &= \left[ \frac{2v_1 v_2^2 (\alpha_1 v_1 + \alpha_2)}{(v_1 + v_2)^2} \right]^{1/2} \\ v_1 &= \sqrt{w^2 + \frac{1}{(\mu_{xx}\mu_{yy} - |\mu_{xy}|^2)(|C|^2 - AB)}} - w \\ v_2 &= \sqrt{w^2 + \frac{1}{(\mu_{xx}\mu_{yy} - |\mu_{xy}|^2)(|C|^2 - AB)}} + w \end{aligned}$$

$$\begin{aligned}
w &= \frac{A\mu_{xx} + B\mu_{yy} + C\mu_{xy}^* + C^*\mu_{xy}}{2(\mu_{xx}\mu_{yy} - |\mu_{xy}|^2)(|C|^2 - AB)} \\
\alpha_{1k} &= (|C|^2 - AB)(|\bar{X}_k|^2\mu_{yy} + |\bar{Y}_k|^2\mu_{xx} - \bar{X}_k^*\bar{Y}_k\mu_{xy} - \bar{X}_k\bar{Y}_k^*\mu_{xy}^*) \\
\alpha_{2k} &= A|\bar{X}_k|^2 + B|\bar{Y}_k|^2 + C\bar{X}_k^*\bar{Y}_k + C^*\bar{X}_k\bar{Y}_k^* \\
\bar{X}_k &= E(X_k); \quad \bar{Y}_k = E(Y_k) \\
\mu_{xx} &= E[(X_k - \bar{X}_k)^2], \quad \mu_{yy} = E[(Y_k - \bar{Y}_k)^2] \\
\mu_{xy} &= E[(X_k - \bar{X}_k)(Y_k - \bar{Y}_k)] \\
\alpha_1 &= \sum_{k=1}^N \alpha_{1k}, \quad \alpha_2 = \sum_{k=1}^N \alpha_{2k} \tag{A.6}
\end{aligned}$$

The function  $Q(a, b)$ , is defined as

$$Q(a, b) = \int_b^\infty x e^{-\frac{x^2+a^2}{2}} I_0(ax) dx \tag{A.7}$$

We note that in the special case where  $a = 0$ ,

$$Q(0, b) = \frac{1}{2} e^{-b^2/2} \tag{A.8}$$

Finally,  $I_n(x)$  is the modified Bessel function of order  $n$ .

# References

- ADLER, R. L., COPPERSMITH, D., AND HASSNER, M. (1983), "Algorithms for Sliding Block Codes," *IEEE Trans. Inform. Theory*, vol. IT-29, pp. 5–22, January.
- ANDERSON, J. B., AULIN, T., AND SUNDBERG, C. W. (1986), *Digital Phase Modulation*, Plenum, New York.
- AULIN, T., RYDBECK, N., AND SUNDBERG, C. W. (1981), "Continuous Phase Modulation—Part II: Partial Response Signaling," *IEEE Trans. Commun.*, vol. COM-29, pp. 210–225, March.
- AULIN, T., AND SUNDBERG, C. W. (1981), "Continuous Phase Modulation—Part I: Full Response Signaling," *IEEE Trans. Commun.*, vol. COM-29, pp. 196–209, March.
- AULIN, T., AND SUNDBERG, C. W. (1982a), "On the Minimum Euclidean Distance for a Class of Signal Space Codes," *IEEE Trans. Inform. Theory*, vol. IT-28, pp. 43–55, January.
- AULIN, T., AND SUNDBERG, C. W. (1982b), "Minimum Euclidean Distance and Power Spectrum for a Class of Smoothed Phase Modulation Codes with Constant Envelope," *IEEE Trans. Commun.*, vol. COM-30, pp. 1721–1729, July.
- AULIN, T., AND SUNDBERG, C. W. (1984), "CPM—An Efficient Constant Amplitude Modulation Scheme," *Int. J. Satellite Commun.*, vol. 2, pp. 161–186.
- BAHAI, A. R. S., AND SALTZBERG, B. R. (1999), *Multi-Carrier Digital Communications—Theory and Applications of OFDM*, Kluwer, Plenum, New York.
- BAHL, L. R., COCKE, J., JELINEK, F., AND RAVIV, J. (1974), "Optimal Decoding of Linear Codes for Minimizing Symbol Error Rate," *IEEE Trans. Inform. Theory*, vol. IT-20, pp. 284–287, March.
- BARROW, B. (1963), "Diversity Combining of Fading Signals with Unequal Mean Strengths," *IEEE Trans. Commun. Sys.*, vol. CS-11, pp. 73–78, March.
- BELLO, P. A., AND NELIN, B. D. (1962a), "Predetection Diversity Combining with Selectively Fading Channels," *IRE Trans. Commun. Sys.*, vol. CS-10, pp. 32–44, March.



- BELLO, P. A., AND NELIN, B. D. (1962b), "The Influence of Fading Spectrum on the Binary Error Probabilities of Incoherent and Differentially Coherent Matched Filter Receivers," *IRE Trans. Commun. Sys.*, vol. CS-11, pp. 170–186, June.
- BELLO, P. A., AND NELIN, B. D. (1963), "The Effect of Frequency Selective Fading on the Binary Error Probabilities of Incoherent and Differentially Coherent Matched Filter Receivers," *IEEE Trans. Commun. Sys.*, vol. CS-11, pp. 170–186, June.
- BENEDETTO, S., BIGLIERI, E., AND CASTELLANI, V. (1987), *Digital Transmission Theory*, Prentice-Hall, Englewood Cliffs, N.J.
- BERGER, T., AND TUFTS, D. W. (1967), "Optimum Pulse Amplitude Modulation, Part I: Transmitter-Receiver Design and Bounds from Information Theory," *IEEE Trans. Inform. Theory*, vol. IT-13, pp. 196–208.
- BERGER, T. (1971), *Rate Distortion Theory: A Mathematical Basis for Data Compression*, Prentice-Hall, Englewood Cliffs, N.J.
- BERLEKAMP, E. R. (1968), *Algebraic Coding Theory*, McGraw-Hill, New York.
- BERROU, C., GLAVIEUX, A., AND THITIMAJSHIMA, P. (1993), "Near Shannon Limit Error Correcting Coding and Decoding: Turbo Codes," *Proc. IEEE Int. Conf. Commun.*, pp. 1064–1070, May, Geneva, Switzerland.
- BINGHAM, J. A. C. (1990), "Multicarrier Modulation for Data Transmission: An Idea Whose Time Has Come," *IEEE Commun. Mag.*, vol. 28, pp. 5–14, May.
- BLAHUT, R. E. (1983), *Theory and Practice of Error Control Codes*, Addison-Wesley, Reading, Mass.
- BLAHUT, R. E. (1987), *Principles and Practice of Information Theory*, Addison-Wesley, Reading, Mass.
- BLAHUT, R. E. (1990), *Digital Transmission of Information*, Addison-Wesley, Reading, Mass.
- BOSE, R. C., AND RAY-CHAUDHURI, D. K. (1960a), "On a Class of Error Correcting Binary Group Codes," *Inform. Control*, vol. 3, pp. 68–79, March.
- BOSE, R. C., AND RAY-CHAUDHURI, D. K. (1960b), "Further Results in Error Correcting Binary Group Codes," *Inform. Control*, vol. 3, pp. 279–290, September.
- BOYD, S. (1986), "Multitone Signals with Low Crest Factor," *IEEE Trans. Circ. Sys.*, vol. CAS-33, pp. 1018–1022.
- BRACEWELL, R. (1965), *The Fourier Transform and Its Applications*, 2nd Ed., McGraw-Hill, New York.
- BRENNAN, D. G. (1959), "Linear Diversity Combining Techniques," *Proc. IRE*, vol. 47, pp. 1075–1102, June.
- CARLSON, A. B. (1986), *Communication Systems*, 3rd Ed., McGraw-Hill, New York.
- CHANG, R. W. (1966), "Synthesis of Bandlimited Orthogonal Signals for Multichannel Data Transmission," *Bell Sys. Tech. J.*, vol. 45, pp. 1775–1796, December.
- CHOW, J. S., CIOFFI, J. M., AND BINGHAM, J. A. C. (1995), "A Practical Discrete Multitone Transceiver Loading Algorithm for Data Transmission over Spectrally Shaped Channels," *IEEE Trans. Commun.*, vol. 43, pp. 357–363, October.
- CLARKE, K. K., AND HESS, D. T. (1971), *Communication Circuits: Analysis and Design*, Addison-Wesley, Reading, Mass.
- COOK, C. E., ELLERSICK, F. W., MILSTEIN, L. B., AND SCHILLING, D. L. (1983), *Spread Spectrum Communications*, IEEE Press, New York.

- COUCH, L. W., II (1993), *Digital and Analog Communication Systems*, 4th Ed., Macmillan, New York.
- COVER, T. M., AND THOMAS, J. A. (1991), *Elements of Information Theory*, Wiley-Interscience, New York.
- DAVENPORT, W. B., Jr., AND ROOT, W. L. (1958), *Random Signals and Noise*, McGraw-Hill, New York.
- DELLER, J. P., PROAKIS, J. G., AND HANSEN, H. L. (2000), *Discrete-Time Processing of Speech Signals*, IEEE Press, Piscataway, N.J.
- DIXON, R. C. (1976), *Spread Spectrum Techniques*, IEEE Press, New York.
- DOELTZ, M. L., HEALD, E. T., AND MARTIN, D. L. (1957), "Binary Data Transmission Techniques for Linear Systems," *Proc. IRE*, vol-45, pp. 656–661, May.
- ELIAS, P. (1954), "Error-Free Coding," *IRE Trans. Inform. Theory*, vol. IT-4, pp. 29–39, September.
- ELIAS, P. (1955), "Coding for Noisy Channels," *IRE Conv. Rec.*, vol. 3, pt. 4, pp. 37–46.
- FANO, R. M. (1963), "A Heuristic Discussion of Probabilistic Decoding," *IEEE Trans. Inform. Theory*, vol. IT-9, pp. 64–74, April.
- FORNEY, G. D., Jr. (1966), *Concatenated Codes*, MIT Press, Cambridge, Mass.
- FORNEY, G. D., Jr. (1972), "Maximum-Likelihood Sequence Estimation of Digital Sequences in the Presence of Intersymbol Interference," *IEEE Trans. Inform. Theory*, vol. 18, pp. 363–378, May.
- FORNEY, G. D., Jr. (1988a), "Coset Codes I: Introduction and Geometrical Classification," *IEEE Trans. Inform. Theory*, vol. IT-34, pp. 671–680, September.
- FORNEY, G. D., Jr. (1988b), "Coset Codes II: Binary Lattices and Related Codes," *IEEE Trans. Inform. Theory*, vol. IT-34, pp. 671–680, September.
- FRANASZEK, P. A. (1968), "Sequence-State Coding for Digital Transmission," *Bell Sys. Tech. J.*, vol. 27, p. 143.
- FRANASZEK, P. A. (1969), "On Synchronous Variable Length Coding for Discrete Noiseless Channels," *Inform. Control*, vol. 15, pp. 155–164.
- FRANASZEK, P. A. (1970), "Sequence-State Methods for Run-Length-Limited Coding," *IBM J. Res. Dev.*, pp. 376–383, July.
- FRANKS, L. E. (1969), *Signal Theory*, Prentice-Hall, Englewood Cliffs, N.J.
- FRANKS, L. E. (1980), "Carrier and Bit Synchronization in Data Communication—A Tutorial Review," *IEEE Trans. Commun.*, vol. COM-28, pp. 1107–1121, August.
- FREIMAN, C. E., AND WYNER, A. D. (1964), "Optimum Block Codes for Noiseless Input Restricted Channels," *Inform. Control*, vol. 7, pp. 398–415.
- GABOR, A. (1967), "Adaptive Coding for Self Clocking Recording," *IEEE Trans. Elect. Comput.*, vol. EC-16, p. 866.
- GALLAGER, R. G. (1968), *Information Theory and Reliable Communication*, Wiley, New York.
- GARDNER, F. M. (1979), *Phaselock Techniques*, Wiley, New York.
- GERSHO, A., AND GRAY, R. M. (1992), *Vector Quantization and Signal Compression*, Kluwer, Boston.
- GERST, I., AND DIAMOND, J. (1961), "The Elimination of Intersymbol Interference by Input Pulse Shaping," *Proc. IRE*, vol. 53, July.
- GIBSON, J. D. (1993), *Principles of Digital and Analog Communications*, 2nd Ed., Macmillan, New York.

- GIBSON, J. D., BERGER, T., LOOKABAUGH, T., LINDBERG, D., AND BAKER, R. L. (1998), *Digital Compression for Multimedia: Principles and Standards*, Morgan Kaufmann, San Francisco, Calif.
- GOLAY, M. J. E. (1949), "Notes on Digital Coding," *Proc. IRE*, vol. 37, p. 657, June.
- GOLD, R. (1967), "Maximal Recursive Sequences with 3-Valued Recursive Cross Correlation Functions," *IEEE Trans. Inform. Theory*, vol. IT-14, pp. 154–156, January.
- GOLOMB, S. W. (1967), *Shift Register Sequences*, Holden-Day, San Francisco, Calif.
- GRAY, R. M., AND DAVISSON, L. D. (1986), *Random Processes: A Mathematical Approach for Engineers*, Prentice-Hall, Englewood Cliffs, N.J.
- GREEN, P. E., Jr. (1962), "Radar Astronomy Measurement Techniques," MIT Lincoln Laboratory, Lexington, Mass., Tech. Report No. 282, December.
- GRONEMEYER, S. A., AND MCBRIDE, A. L. (1976), "MSK and Offset QPSK Modulation," *IEEE Trans. Commun.*, vol. COM-24, pp. 809–820, August.
- GUPTA, S. C. (1975), "Phase-Locked Loops," *Proc. IEEE*, vol. 63, pp. 291–306, February.
- HAGENAUER, J., AND HOEHER, P. (1989), "A Viterbi Algorithm with Soft Decision Outputs and Its Applications," *Proc. IEEE Globecom Conf.*, pp. 1680–1686, November, Dallas, Tex.
- HAMMING, R. W. (1950), "Error Detecting and Error Correcting Codes," *Bell Sys. Tech. J.*, vol. 29, pp. 147–160, April.
- HARTLEY, R. V. (1928), "Transmission of Information," *Bell Sys. Tech. J.*, vol. 7, p. 535.
- HAYKIN, S. (2000), *Communication Systems*, 4th Ed., Wiley, New York.
- HEEGARD, C., AND WICKER, S. B. (1999), *Turbo Coding*, Kluwer, Boston.
- HELLER, J. A. (1975), "Feedback Decoding of Convolutional Codes," in *Advances in Communication Systems*, vol. 4, A. J. Viterbi (Ed.), Academic, New York.
- HELSTROM, C. W. (1991), *Probability and Stochastic Processes for Engineers*, Macmillan, New York.
- HOCQUENGHEM, A. (1959), "Codes Correcteurs d'Erreurs," *Chiffers*, vol. 2, pp. 147–156.
- HOLMES, J. K. (1982), *Coherent Spread Spectrum Systems*, Wiley-Interscience, New York.
- HUFFMAN, D. A. (1952), "A Method for the Construction of Minimum Redundancy Codes," *Proc. IRE*, vol. 40, pp. 1098–1101, September.
- JACOBY, G. V. (1977), "A New Look-Ahead Code for Increased Data Density," *IEEE Trans. Magnetics*, vol. MAG-13, pp. 1202–1204.
- JAYANT, N. S., AND NOLL, P. (1984), *Digital Coding of Waveforms*, Prentice-Hall, Englewood Cliffs, N.J.
- JELINEK, F. (1969), "Fast Sequential Decoding Algorithm Using a Stack," *IBM J. Res. Dev.*, vol. 13, pp. 675–685, November.
- JONES, A. E., WILKINSON, T. A., AND BARTON, S. K. (1994), "Block Coding Schemes for Reduction of Peak-to-Mean Envelope Power Ratio of Multicarrier Transmission Systems," *Elect. Lett.*, vol. 30, pp. 2098–2099, December.
- KAILATH, T. (1960), "Correlation Detection of Signals Perturbed by a Random Channel," *IRE Trans. Inform. Theory*, vol. IT-6, pp. 361–366, June.
- KAILATH, T. (1961), "Channel Characterization: Time-Variant Dispersive Channels," in *Lectures on Communication Theory*, Chapter 6, E. Baghdadi (Ed.), McGraw-Hill, New York.

- KARABED, R., AND SIEGEL, P. H. (1991), "Matched-Spectral Null Codes for Partial-Response Channels," *IEEE Trans. Inform. Theory*, vol. IT-37, pp. 818–855, May.
- KASAMI, T. (1966), "Weight Distribution Formula for Some Class of Cyclic Codes," Coordinated Science Laboratory, University of Illinois, Urbana, Ill., Tech. Report No. R-285, April.
- KOTELNIKOV, V. A. (1947), "The Theory of Optimum Noise Immunity," Ph.D. Dissertation, Molotov Energy Institute, Moscow. Translated by R. A. Silverman, McGraw-Hill, New York, 1959.
- KRETZMER, E. R. (1966), "Generalization of a Technique for Binary Data Communication," *IEEE Trans. Commun. Tech.*, vol. COM-14, pp. 67–68, February.
- LARSON, K. J. (1973), "Short Convolutional Codes with Maximal Free Distance for Rates 1/2, 1/3, 1/4," *IEEE Trans. Inform Theory*, vol. IT-19, pp. 371–372, May.
- LENDER, A. (1963), "The Duobinary Technique for High Speed Data Transmission," *AIEE Trans. Commun. Elect.*, vol. 82, pp. 214–218.
- LEON-GARCIA, A. (1994), *Probability and Random Processes for Electrical Engineering*, 2nd Ed., Addison-Wesley, Reading Mass.
- LIN, S., AND COSTELLO, D. J., Jr. (1983), *Error Control Coding: Fundamentals and Applications*, Prentice-Hall, Englewood Cliffs, N.J.
- LINDE, J., BUZO, A., AND GRAY, R. M. (1980), "An Algorithm for Vector Quantizer Design," *IEEE Trans. Commun.*, vol. COM-28, pp. 84–95, January.
- LINDSEY, W. C. (1964), "Error Probabilities for Ricean Fading Multichannel Reception of Binary and  $N$ -ary Signals," *IEEE Trans. Inform. Theory*, vol. IT-10, pp. 339–350, October.
- LINDSEY, W. C. (1972), *Synchronization Systems in Communications*, Prentice-Hall, Englewood Cliffs, N.J.
- LINDSEY, W. C., AND CHIE, C. M. (1981), "A Survey of Digital Phase-Locked Loops," *Proc. IEEE*, vol. 69, pp. 410–432.
- LINDSEY, W. C., AND SIMON, M. K. (1973), *Telecommunication Systems Engineering*, Prentice-Hall, Englewood Cliffs, N.J.
- LLOYD, S. P. (1957), "Least Square Quantization in PCM," Reprinted in *IEEE Trans. Inform. Theory*, vol. IT-28, pp. 129–137, March 1982.
- LUCKY, R. W. (1965), "Automatic Equalization for Digital Communication," *Bell Sys. Tech. J.*, vol. 45, pp. 255–286, April.
- LUCKY, R. W. (1966), "Techniques for Adaptive Equalization for Digital Communication," *Bell Sys. Tech. J.*, vol. 45, pp. 255–286.
- LUCKY, R. W., SALZ, J., AND WELDON, E. J., Jr. (1968), *Principles of Data Communication*, McGraw-Hill, New York.
- LYON, D. L. (1975a), "Timing Recovery in Synchronous Equalized Data Communication," *IEEE Trans. Commun.*, vol. COM-23, pp. 269–274, February.
- LYON, D. L. (1975b), "Envelope-Derived Timing Recovery in QAM and SQAM Systems," *IEEE Trans. Commun.*, vol. COM-23, pp. 1327–1331, November.
- MACWILLIAMS, F. J., AND SLOANE, J. J. (1977), *The Theory of Error Correcting Codes*, North Holland, New York.
- MARKEL, J. D., AND GRAY, A. H., Jr. (1976), *Linear Prediction of Speech*, Springer-Verlag, New York.
- MASSEY, J. L. (1963), *Threshold Decoding*, MIT Press, Cambridge, Mass.

- MAX, J. (1960), "Quantizing for Minimum Distortion," *IRE Trans. Inform. Theory*, vol. IT-6, pp. 7–12, March.
- McMAHON, M. A. (1984), *The Making of a Profession—A Century of Electrical Engineering in America*, IEEE Press.
- MENGALI, U., AND D'ANDREA, A. N. (1997), *Synchronization Techniques for Digital Receivers*, Plenum Press, New York.
- MEYR, H., AND ASCHEID, G. (1990), *Synchronization in Digital Communication*, Wiley-Interscience, New York.
- MILLMAN, S., Ed. (1984), *A History of Engineering and Science in the Bell System—Communications Sciences (1925–1980)*, AT&T Bell Laboratories.
- MUELLER, K. H., AND MULLER, M. S. (1976), "Timing Recovery in Digital Synchronous Data Receivers," *IEEE Trans. Commun.*, vol. COM-24, pp. 516–531, May.
- NELSON, R. (1995), *Probability, Stochastic Processes and Queueing Theory: The Mathematics of Computer Modeling*, Springer Verlag.
- NORTH, D. O. (1943), "An Analysis of the Factors Which Determine Signal/Noise Discrimination in Pulse-Carrier Systems," RCA Tech. Report No. 6, PTR-6C.
- NYQUIST, H. (1924), "Certain Factors Affecting Telegraph Speed," *Bell Sys. Tech. J.*, vol. 3, p. 324.
- NYQUIST, H. (1928), "Certain Topics in Telegraph Transmission Theory," *AIEE Trans.*, vol. 47, pp. 617–644.
- ODENWALDER, J. P. (1970), "Optimal Decoding of Convolutional Codes," Ph.D. Dissertation, Dept. of Systems Sciences, UCLA, Los Angeles.
- OLSEN, J. D. (1977), "Nonlinear Binary Sequences with Asymptotically Optimum Periodic Cross Correlation," Ph.D. Dissertation, University of Southern California, Los Angeles.
- OMURA, J. (1971), "Optimal Receiver Design for Convolutional Codes and Channels with Memory via Control Theoretical Concepts," *Inform. Sci.*, vol. 3, pp. 243–266.
- OPPENHEIM, A. V., WILLISKY, A. S., AND YOUNG, I. T. (1983), *Signals and Systems*, Prentice-Hall, Englewood Cliffs, N.J.
- PAPOULIS, A. (1962), *The Fourier Integral and Its Applications*, McGraw-Hill, New York.
- PAPOULIS, A. (1991), *Probability, Random Variables, and Stochastic Processes*, 3rd Ed., McGraw-Hill, New York.
- PETERSON, W. W., AND WELDON, E. J., Jr. (1972), *Error Correcting Codes*, 2nd Ed., MIT Press, Cambridge, Mass.
- PETERSON, R. L., ZIEMER, R. E., AND BORTH, D. E. (1995), *Introduction to Spread Spectrum Communications*, Prentice-Hall, Englewood Cliffs NJ.
- PICKHOLTZ, R. L., SCHILLING, D. L., AND MILSTEIN, L. B. (1982), "Theory of Spread Spectrum Communications—A Tutorial," *IEEE Trans. Commun.*, vol. COM-30, pp. 855–884, May.
- PIERCE, J. N. (1958), "Theoretical Diversity Improvement in Frequency Shift Keying," *Proc. IRE*, vol. 46, pp. 903–910, May.
- PIERCE, J. N., AND STEIN, S. (1960), "Multiple Diversity with Non-Independent Fading," *Proc. IRE*, vol. 48, pp. 89–104, January.
- POPOVIC, B. M. (1991), "Synthesis of Power Efficient Multitone Signals with Flat Amplitude Spectrum," *IEEE Trans. Commun.*, vol. 39, pp. 1031–1033, July.

- PRICE, R. (1954), "The Detection of Signals Perturbed by Scatter and Noise," *IRE Trans. Inform. Theory*, vol. PGIT-4, pp. 163–170, September.
- PRICE, R. (1956), "Optimum Detection of Random Signals in Noise with Application to Scatter Multipath Communication," *IRE Trans. Inform. Theory*, vol. IT-2, pp. 125–135, December.
- PRICE, R. (1962a), "Error Probabilities for Adaptive Multichannel Reception of Binary Signals," MIT Lincoln Laboratory, Lexington, Mass., Tech. Report No. 258, July.
- PRICE, R. (1962b), "Error Probabilities for Adaptive Multichannel Reception of Binary Signals," *IRE Trans. Inform. Theory*, vol. IT-8, pp. 308–316, September.
- PRICE, R., AND GREEN, P. E., Jr. (1958), "A Communication Technique for Multipath Channels," *Proc. IRE*, vol. 46, pp. 555–570, March.
- PRICE, R., AND GREEN, P. E., Jr. (1960), "Signal Processing in Radio Astronomy—Communication via Fluctuating Multipath Media," MIT Lincoln Laboratory, Lexington, Mass., Tech. Report No. 2334, October.
- PROAKIS, J. G. (2001), *Digital Communications*, 4th Ed., McGraw-Hill, New York.
- RABINER, L. R., AND SCHAFFER, R. W. (1978), *Digital Processing of Speech Signals*, Prentice-Hall, Englewood Cliffs, N.J.
- REED, I. S., AND SOLOMON, G. (1960), "Polynomial Codes over Certain Finite Fields," *SIAM J.*, vol. 8, pp. 300–304, June.
- RYDER, J. D., AND FINK, D. G. (1984), *Engineers and Electronics*, IEEE Press.
- SAKRISON, D. J. (1968), *Communication Theory: Transmission of Waveforms and Digital Information*, New York, Wiley.
- SALTZBERG, B. R. (1967), "Performance of an Efficient Data Transmission System," *IEEE Trans. Commun.*, vol. COM-15, pp. 805–811, December.
- SARWATE, D. V., AND PURSLEY, M. B. (1980), "Crosscorrelation Properties of Pseudorandom and Related Sequences," *Proc. IEEE*, vol. 68, pp. 2399–2419, September.
- SCHOLTZ, R. A. (1977), "The Spread Spectrum Concept," *IEEE Trans. Commun.*, vol. COM-25, pp. 748–755, August.
- SCHOLTZ, R. A. (1979), "Optimal CDMA Codes," *1979 National Telecommunications Conf. Record*, Washington, D.C., pp. 54.2.1–54.2.4, November.
- SCHOLTZ, R. A. (1982), "The Origins of Spread Spectrum," *IEEE Trans. Commun.*, vol. COM-30, pp. 822–854, May.
- SCHOUHAMER IMMINK, K. A. (1991), *Coding Techniques for Digital Recorders*, Prentice-Hall, Englewood-Cliffs, N.J.
- SCHWARTZ, M., BENNETT, W. R., AND STEIN, S. (1966), *Communication Systems and Techniques*, McGraw-Hill, New York.
- SHANMUGAM, K. S. (1979), *Digital and Analog Communication Systems*, Wiley, New York.
- SHANNON, C. E. (1948a), "A Mathematical Theory of Communication," *Bell Sys. Tech. J.*, vol. 27, pp. 379–423, July.
- SHANNON, C. E. (1948b), "A Mathematical Theory of Communication," *Bell Sys. Tech. J.*, vol. 27, pp. 623–656, October.
- SIMON, M. K., OMURA, J. K., SCHOLTZ, R. A., AND LEVITT, B. K. (1985), *Spread Spectrum Communications vol. I, II, III*, Computer Science Press, Rockville, Md.

- SMITH, J. W. (1965), "The Joint Optimization of Transmitted Signal and Receiving Filter for Data Transmission Systems," *Bell Sys. Tech. J.*, vol. 44, pp. 1921–1942, December.
- STARK, H., AND WOODS, J. W. (1994), *Probability, Random Processes and Estimation Theory for Engineers*, 2nd Ed., Prentice-Hall, Upper Saddle River, N.J.
- STENBIT, J. P. (1964), "Table of Generators for BCH Codes," *IEEE Trans. Inform. Theory*, vol. IT-10, pp. 390–391, October.
- STIFFLER, J. J. (1971), *Theory of Synchronous Communications*, Prentice-Hall, Englewood Cliffs, N.J.
- STREMLER, F. G. (1990), *Introduction to Communication Systems*, 3rd Ed., Addison-Wesley, Reading, Mass.
- SUNDBERG, C. W. (1986), "Continuous Phase Modulation," *IEEE Commun. Mag.*, vol. 24, pp. 25–38, April.
- TANG, D. L., AND BAHL, L. R. (1970), "Block Codes for a Class of Constrained Noiseless Channels," *Inform. Control*, vol. 17, pp. 436–461.
- TAROKH, V., SESHADRI, N., AND CALDERBANK, A. R. (1998), "Space-Time Codes for High Data Rate Wireless Communications: Performance Analysis and Code Construction," *IEEE Trans. Inform. Theory*, vol. 44, pp. 744–765, March.
- TAROKH, V., JAFARKHANI, H., AND CALDERBANK, A. R. (1999), "Space-Time Block Codes from Orthogonal Designs," *IEEE Trans. Inform. Theory*, vol. IT-45, pp. 1456–1467, July.
- TAROKH, V., AND JAFARKHANI, H. (2000), "On the Computation and Reduction of the Peak-to-Average Power Ratio in Multicarrier Communications," *IEEE Trans. Commun.*, vol. 48, pp. 37–44, January.
- TAUB, H., AND SCHILLING, D. L. (1986), *Principles of Communication Systems*, 2nd Ed., McGraw-Hill, New York.
- TELLADO, J., AND CIOFFI, J. M. (1998), "Efficient Algorithms for Reducing PAR in Multicarrier Systems," *Proc. 1998 IEEE Int. Symp. Inform. Theory*, p. 191, August 16–21, Cambridge, Mass. Also in *Proc. 1998 Globecom*, Nov. 8–12, Sydney, Australia.
- TUFTS, D. W. (1965), "Nyquist's Problem—The Joint Optimization of Transmitter and Receiver in Pulse Amplitude Modulation," *Proc. IEEE*, vol. 53, pp. 248–259, March.
- TURIN, G. L. (1961), "On Optimal Diversity Reception," *IRE Trans. Inform. Theory*, vol. IT-7, pp. 154–166, March.
- TURIN, G. L. (1962), "On Optimal Diversity Reception II," *IRE Trans. Commun. Sys.*, vol. CS-12, pp. 22–31, March.
- UNGERBOECK, G. (1974), "Adaptive Maximum Likelihood Receiver for Carrier Modulated Data Transmission Systems," *IEEE Trans. Commun.*, vol. COM-22, pp. 624–636, May.
- UNGERBOECK, G. (1982), "Channel Coding with Multilevel/Phase Signals," *IEEE Trans. Inform. Theory*, vol. IT-28, pp. 55–67, January.
- VITERBI, A. J. (1966), *Principles of Coherent Communication*, McGraw-Hill, New York.
- VITERBI, A. J. (1967), "Error Bounds for Convolutional Codes and an Asymptotically Optimum Decoding Algorithm," *IEEE Trans. Inform. Theory*, vol. IT-13, pp. 260–269, April.
- VITERBI, A. J. (1979), "Spread Spectrum Communication—Myths and Realities," *IEEE Commun. Mag.*, vol. 17, pp. 11–18, May.

- VITERBI, A. J. (1985), "When Not to Spread Spectrum—A Sequel," *IEEE Commun. Mag.*, vol. 23, pp. 12–17, April.
- VITERBI, A. J., AND JACOBS, I. M. (1975), "Advances in Coding and Modulation for Noncoherent Channels Affected by Fading, Partial Band, and Multiple-Access Interference," in *Advances in Communication Systems*, vol. 4, A. J. Viterbi, (Ed.), Academic, New York.
- WEI, L. F. (1984), "Rotationally Invariant Convolutional Channel Coding with Expanded Signal Space. Part I: 180°, Part II: Nonlinear Codes," *IEEE J. Selected Areas Commun.*, vol. SAC-2, pp. 659–687, September.
- WEINSTEIN, SW. B., AND EBERT, P. M. (1971), "Data Transmission by Frequency Division Multiplexing Using the Discrete Fourier Transform," *IEEE Trans. Commun.*, vol. COM-19, pp. 628–634, October.
- WIDROW, B. (1966), "Adaptive Filters, I: Fundamentals," Tech. Report No. 6764-6, Stanford Electronic Laboratories, Stanford University, Stanford, Calif., December.
- WIENER, N. (1949), *The Extrapolation, Interpolation, and Smoothing of Stationary Time-Series with Engineering Applications*, Wiley, New York. (The original work appeared in an MIT Radiation Laboratory Report, 1942).
- WILKINSON, T. A., AND JONES, A. E. (1995), "Minimization of the Peak-to-Mean Envelope Power Ratio of Multicarrier Transmission Systems by Block Coding," *Proc. IEEE Vehicular Tech. Conf.*, pp. 825–829, July.
- WONG, E., AND HAJEK, B. (1985), *Stochastic Processes in Engineering Systems*, Springer-Verlag, New York.
- WOZENCRAFT, J. M. (1957), "Sequential Decoding for Reliable Communication," *IRE Natl. Conv. Rec.*, vol. 5, pt. 2, pp. 11–25.
- WOZENCRAFT, J. M., AND JACOBS, I. M. (1965), *Principles of Communication Engineering*, Wiley, New York.
- WOZENCRAFT, J. M., AND REIFFEN, B. (1961), *Sequential Decoding*, MIT Press, Cambridge, Mass.
- WULICH, D. (1996), "Reduction of Peak-to-Mean Ratio of Multicarrier Modulation Using Cyclic Coding," *Elect. Lett.*, vol. 32, pp. 432–433, February.
- ZIEMER, R. E., AND PETERSON, R. L. (1985), *Digital Communications and Spread Spectrum Systems*, Macmillan, New York.
- ZIEMER, R. E., AND TRANTER, W. H. (1990), *Principles of Communications: Systems, Modulation, and Noise*, Houghton Mifflin, Boston.
- ZIGANGIROV, K. S. (1966), "Some Sequential Decoding Procedures," *Problemy Peredachi Informatsii*, vol. 2, pp. 13–25.
- ZIV, J., AND LEMPEL, A. (1977), "A Universal Algorithm for Sequential Data Compression," *IEEE Trans. Inform. Theory*, vol-IT23, pp. 337–343.
- ZIV, J., AND LEMPEL, A. (1978), "Compression of Individual Sequences via Variable Rate Coding," *IEEE Trans. Inform. Theory*, vol. IT-24, pp. 530–536.



# Index

- A posteriori probability, 383
- A priori probability, 383
- Additive white Gaussian noise
  - channel (AWGN) capacity, 583–585
- Aliasing distortion, 47
- AM, 3, 5, 71–96, 217–225
  - conventional (*see* conventional AM)
  - demodulators, 93–94
  - double-sideband (*see* DSB-SC) modulators, 88–92
  - modulators, balanced, 91
  - modulators, power law, 88–89
  - modulators, ring, 91–92
  - modulators, switching, 89–90
  - radio broadcasting, 115–116
  - single-sideband (*see* SSB)
  - vestigial-sideband (*see* VSB)
- AMI code, 568–569
- Amplitude modulation (AM) (*see* AM)
- Amplitude shift keying (ASK), 349
- Analog modulation, 70–143, 217–266
- Analog-modulation systems, comparison, 251–252
- Analytic signal, 151
- Angle modulation, 96–115, 234–251
  - balanced discriminator, 110, 112, 117
  - indirect method, 108–110
  - low-index, 100
  - modulators and demodulators, 107–115
  - narrowband, 100
  - by a periodic message, 105
- Antenna, 14
  - effective area, 439
  - effective isotropically radiated power (EIRP), 439
  - gain, 438
  - illumination efficiency factor, 440
- ASK, 349
- Autocorrelation function, 41, 165
  - properties, 168
  - of random processes, 165
  - time-average, 42
- Automatic volume control (AVC), 116
- Balanced discriminator, 110, 112, 117
- Balanced modulator, 91
- Bandlimited channels, 474–482
  - signal design for, 490
- Bandlimited processes, 192
- Bandpass-lowpass translation table, 56
- Bandpass processes, 194–201
  - in-phase component, 195
  - quadrature component, 195
- Bandpass signals, 49–57, 347–349
  - analytic signal, 151
  - envelope, 53
  - in-phase component, 52
  - lowpass representation, 52
  - phase, 53
  - quadrature component, 52
  - transmission through bandpass systems, 55–57
- Bandwidth
  - conventional AM, 79
  - DSB-SC, 72–74
  - FM, 101–105
  - PCM, 304
  - SSB, 82–84
  - VSB, 86–87
- Bayes rule, 146
- BCH codes, 620–623
- BCJR algorithm, 642
- Bessel function, 101, 231, 402
- Binary antipodal signaling, 345
  - error probability, 405
  - optimal receiver, 385
- Binary-coded signals, 367
- Binary entropy function, 271
- Binary equiprobable signaling, error probability, 406
- Binary orthogonal signaling, error probability, 407

- Binary-symmetric channel (BSC), 577
  - crossover probability, 577
- Biorthogonal signaling, 353, 365
  - error probability, 428
- Black-and-white TV, 120–123
- Boltzmann's constant, 189, 253
- Broadcasting
  - AM, 115–116
  - FM, 116–119
  - TV, 120–128
- Burst error correcting codes, 614
  
- CAP, 574
- Capacity
  - of AWGN channel, 583–585
  - of channels, 579, 581
  - of DMC, 582
  - of runlength-limited codes, 512
- Carrier-amplitude modulation, 347
  - carrier-phase recovery, 387
  - demodulation and detection, 386
  - optimum detector, 388
- Carrier demodulation, 7
- Carrier-phase modulation, 354
  - carrier-phase estimation, 390
  - demodulation and detection, 388
  - differential phase modulation and demodulation, 394
- Carrier-phase recovery
  - for carrier-amplitude modulation, 387
  - for carrier-phase modulation, 388
  - for QAM, 397
- Carrierless
  - amplitude or phase modulation (CAP), 574
  - PSK, 573
  - QAM, 573
- Carson's rule, 107
- Catastrophic convolutional codes, 628
- Cauchy–Schwartz inequality, 60, 155, 169, 378
- CDF, 147
- CDMA, 744, 753, 754, 758, 769–774
- CELP, 770
- Central limit theorem, 159
- Channel, 7
- Channel encoder, 8
- Channel equalization (see equalization)
- Channel
  - additive noise, 19–20
  - AWGN, 340, 578
  - bandlimited, 474–482
  - bandlimited bandpass, 480
  - binary symmetric (BSC), 577
  - capacity, 11, 579, 581
  - characterization, 12
  - discrete memoryless (DMC), 577
  - fading multipath, 674–703
  - fiber optic, 14
  - linear filter, 20–21
  - linear time-variant filter, 21–22
  - mathematical model, 19–22
  - modeling, 576
  - Rayleigh fading, 681
  - reliability function, 595
  - Ricean fading, 681
  - storage, 19, 508–515
  - underwater acoustic, 17–19
  - wireless, 14–17
  - wireline, 12–14
- Chebyshev inequality, 204
- Chip, 734
- Chip interval, 734
- Chip rate, 734
- Chrominance signal, 125
- Code
  - AMI, 568–569
  - BCH, 620–623
  - burst error correcting, 614
  - concatenated, 623, 640
  - Convolutional (see Convolutional codes)
  - cyclic (see Cyclic codes)
  - dual, 604
  - eight-to-fourteen modulation (EFM), 520
  - fixed-to-variable length, 276–279
  - Hamming, 605
  - linear block, 601–623
  - Miller, 515
  - Morse, 2
  - prefix, 277
  - product, 639
  - Reed-Solomon, 620–623, 640, 659–661
  - runlength-limited, 510–515
  - space-time, 700–703
  - Turbo, 640–646
  - uniquely decodable, 277
- Code division multiple access (CDMA), 744, 753, 754, 758, 769–774
- Code excited linear prediction (CELP), 770
- Coding
  - bandwidth expansion ratio, 600
  - block, 600
  - for compact discs, 520–521, 658–661
  - convolutional, 600, 623–638
  - for deep-space communication, 656
  - for reliable transmission, 591
  - for telephone-line modems, 657
- Coding for reliable communication, 591
- Coding gain, 600
  - for TCM, 654
- Coding rate, 598
- Coherence bandwidth, 683
- Coherence time, 683
- Coherent demodulator, 219
- Coherer, 3
- Color TV, 125–128
- Compact disc (CD), 319–323
  - coding for, 520–521, 658–661
- Compander
  - A-law, 305
  - $\mu$ -law, 304
  - optimal, 305
- Companding, 304
- Comparison
  - of analog modulation systems, 251–252
  - of digital modulation systems, 432–436
- Concatenated codes, 623, 640
- Conditional PDF, 155
- Conditional probability, 146
- Continuous-phase FSK (see CPFSK)
- Continuous-phase modulation (see CPM)
- Controlled ISI, 497
  - symbol-by-symbol detection, 501
- Conventional AM, 78–81, 221–226
  - bandwidth, 79
  - demodulation, 81, 92–93
  - effect of noise, 221–226
  - modulation index, 79
  - power content, 80
  - SNR, 222
  - threshold effect, 223
- Convolutional codes, 623–638
  - catastrophic, 628
  - decoding, 629–634
  - encoding, 625
  - error probability bound, 634–637
  - Fano algorithm, 634
  - feedback decoding, 634
  - first error event, 635
  - free distance, 627
  - generator sequences, 624
  - majority logic decoding, 634
  - recursive systematic, 641
  - sequential decoding, 634
  - stack algorithm, 634
  - state transition diagram, 624
  - transfer function, 626
  - trellis diagram, 625
  - Viterbi algorithm, 629–634

- Convolutional codes (*continued*)
  - with good distance
    - properties, 637
- Correlation coefficient, 155
- Correlation metrics, 384
- Correlation-type demodulator, 370
- Coset, 609
- Coset leader, 609
- Costas loop, 233
- Covariance, 155
- CPFSK, 703–711
  - modulation index, 704
  - peak-frequency deviation, 704
  - phase tree, 706
  - phase trellis, 706
  - state diagram, 707
- CPM, 711–729
  - demodulation and detection, 720–726
  - full response, 712
  - MAP demodulation, 725
  - partial response, 712
  - performance in AWGN channels, 726
  - performance in Rayleigh fading channels, 728
  - spectral characteristics, 715–720
- Cross-correlation function, 174
- Cross-spectral density, 184
- Crossover probability, 577
- Cumulative distribution function (CDF), 147
- Cyclic codes, 615–623
  - encoding, 619
  - generator matrix, 618
  - generator polynomial, 616
- Cyclostationary processes, 167, 484
- Data compression, 8, 274
  - lossy, 282
- DCT, 323
- Decoding
  - convolutional codes, 629–634
  - hard-decision, 608–612
  - soft-decision, 606–608
- Deep-space communication, coding for, 656
- Delay-locked loop (DLL), 762
- Delay modulation, 519
- Delta modulation, 310
  - adaptive, 311
  - granular noise, 310
  - slope overload distortion, 311
- Demodulation
  - AM, 93–94
  - carrier-amplitude modulation, 386
  - carrier-phase modulation, 388
  - coherent, 219
    - conventional AM, 81, 92–93
    - DSB-SC, 76–78, 93
    - FSK, 398
    - PCM signals, 720–726
    - QAM signals, 396
    - SSB, 84–85, 93
    - synchronous, 219
    - VSF, 94
- Demodulation gain, 263
- Detection
  - carrier-amplitude modulation, 386
  - carrier-phase modulation, 388
  - duobinary signaling, 526
  - PCM signals, 720–726
  - QAM signals, 396
- Deviation constant, FM, 97
- DFPLL, 392, 397, 398
- DFT, 558–560
- Differential encoding, 516
- Differential PCM, 307
- Differential PSK (DPSK), 395
- Digital audio recording, 319
- Digital audio telephony, 317
- Digital cellular communication systems, 766–774
  - GSM, 766–769
  - IS-95, 769–774
- Digital demodulator, 9
- Digital modulation systems, comparison, 432–436
- Digital modulator, 8
- Discrete cosine transform (DCT), 323
- Discrete Fourier transform (DFT), 558–560
- Discrete-memoryless channel (DMC), 577
  - capacity, 582
- Discrete-memoryless source (DMS), 269
- Discrete-multitone modulation (DMT), 560
- Distortion
  - amplitude, 534
  - delay, 534
  - phase, 534
  - slope overload, 311
  - squared-error, 286
- Distortion-rate function, 289
- DLL, 762
- DMS, 269
- DMT, 560
- Doppler frequency spread, 678
- Doppler shift, 675, 775
- Double-sideband suppressed carrier modulation (*see* DSB-SC)
- DPSK, 395
  - error probability, 417–418
- DSB, SNR, 220
- DSB-SC, 71–78, 218–220, 347
  - bandwidth, 72–74
  - demodulation, 76–78, 93
  - effect of noise, 218–220
  - power content, 74–76
- Dual code, 604
- Duobinary signaling, 497, 502–503
  - detection, 526
  - error probability, 528–530
- Early-late gate, 443
- Effective noise temperature, 255
- EFM code, 520, 658, 660
- EIRP, 439
- Encoding
  - convolutional codes, 625
  - cyclic codes, 619
  - differential, 516
- Energy-spectral density, 42
- Energy-type signals, 41–42
- Entropy, 270
  - conditional, 272
  - joint, 271
- Entropy rate, 273
- Envelope
  - of bandpass signals, 53
  - delay, 68
  - detector, 81, 92–93, 403
- Equal gain combining, 691
- Equalization, 538–556
  - adaptive, 540, 546–556
  - decision-feedback (DFE), 550–555
  - fractionally spaced, 543
  - linear, 540–550
  - MMSE, 544–546
  - preset, 540
  - symbol-spaced, 542
  - zero forcing, 541, 543–544
- Equalizers (*see* equalization)
- Equivalent discrete-time channel model, 539
- Ergodic processes, 160
- Error probability
  - bandpass PAM, 411–413
  - binary antipodal, 405
  - binary equiprobable, 406
  - binary orthogonal, 407
  - convolutional codes, 634–637
  - DPSK, 417–418
  - duobinary signaling, 528–530
  - $M$ -ary biorthogonal, 428
  - $M$ -ary orthogonal, 423–426
  - $M$ -ary PAM, 408–411
  - MLSD, 528–530

- noncoherent FSK, 430–432
- PAM with zero ISI, 500
- PCM, 726–728
- phase-coherent PSK, 413–417
- QAM, 418–423
- simplex signaling, 429–430
- spread-spectrum DS systems, 735
- symbol-by-symbol detection in
  - partial response signaling, 504
- union bound, 426
- Euclidean distance
  - metric, 523
  - minimum, 599
- Event, 145
- Excess bandwidth, 495
- Eye pattern, 490–491
- Fading channels
  - Doppler frequency spread, 678
  - Doppler shift, 675
- Fading multipath channels, 674–703
  - channel model, 676
  - coherence bandwidth, 683
  - coherence time, 683
  - equal gain combining, 691
  - frequency nonselective, 683
  - frequency selective, 683
  - maximum ratio combining, 691
  - multipath spread, 678
  - overspread, 683
  - performance in frequency
    - nonselective, 686
  - RAKE demodulation, 694, 772, 774
  - Rayleigh fading, 681
  - Ricean fading, 681
  - signal design, 684
  - spread factor, 683
  - square-law combining, 694
  - tapped delay line model, 678
  - underspread, 683
- Fast Fourier transform (FFT), 557
- FCC, 4, 5, 129
- FDM, 94, 556
- FFT, 557
- First-error-event, 635
- Fixed-to-variable length codes, 276–279
- FM, 4, 5, 96–115, 234–251, 591
  - bandwidth, 101–105
  - demodulation by balanced discriminator, 110, 112, 117
  - demodulation with feedback, 111, 113
  - deviation constant, 97
  - effect of noise, 234–251
  - modulation by indirect method, 108–110
  - modulation index, 99
  - narrowband, 100
  - pre-emphasis and de-emphasis filtering, 248–251
  - radio broadcasting, 116–119
  - representation, 97–100
  - SNR, 243
  - threshold effect, 244–247
  - threshold extension, 247
- FM stereo, 118–119
- Fourier series, 24–31
- Fourier series, theorem, 25
- Fourier series, trigonometric form, 29–31
- Fourier transform, 31–40
  - autocorrelation property, 37
  - convolution, 37
  - differentiation property, 37
  - duality, 36
  - integration property, 38
  - inverse, 32
  - linearity, 36
  - modulation property, 37
  - moments property, 38
  - Parseval's theorem, 37
  - for periodic signals, 39–40
  - properties, 36–38
  - Rayleigh's theorem, 37
  - for real signals, 35
  - scaling, 37
  - table, 38
  - theorem, 32
  - time shift, 37
- Free distance of convolutional codes, 627
- Free-space path loss, 257
- Frequency-division multiplexing (FDM), 94
- Frequency hopping (FH), 752–758
  - fast, 753, 756–758
  - slow, 753–756
- Frequency modulation (FM) (*see* FM and angle modulation)
- Frequency nonselective fading multipath channels, 683
- Frequency selective fading channels, 683
- Frequency-shift keying (*see* FSK)
- Fries formula, 256
- FSK, 363
  - demodulation and detection, 398
  - error probability in noncoherent detection, 430–432
  - noncoherent detection, 399
  - optimum detector, 401
  - orthogonality condition, 364
- Full-response CPM, 712
- Fundamental frequency, 25
- Gaussian processes, 186–188
- Gaussian random variable, 149
- Generator matrix
  - for cyclic codes, 618
  - for linear block codes, 603
- Generator polynomial for cyclic codes, 616
- GMSK, 712, 714, 769
- Gold sequences, 750
- Gram-Schmidt procedure, 341
- Granular noise, 310
- Group delay, 68
- GSM, 766–769
- Guard band, 48
- Hadamard sequences, 360, 463, 771
- Hamming
  - code, 605
  - distance, 602
  - distortion, 286
  - weight, 602
- Hard-decision decoding, 608–612
- Harmonics, 25
- Hilbert transform, 51–52, 82–84, 106
- Huffman coding, 276
- IDFT, 558–560, 575
- IF, 115–116
- Image frequency, 116
- Information source,
  - discrete-memoryless, 269
- Information
  - sources, 268
  - theory, 11
- Innovation process, 313
- In-phase component of bandpass signals, 52
- In-phase process, 195
- Interleavers, 614, 641
- Intermediate frequency (IF), 115–116
- Intersymbol interference (ISI), 480–482, 490–507, 538–555
- Ionospheric propagation, 674
- IS-95, 769–774
- ISI, 480–482, 490–507, 538–555
  - controlled, 497
- Jointly Gaussian random variables, 158
- JPEG image coding, 323–327
- Kasami sequences, 751
- Law of large numbers, 159
- Lempel-Ziv algorithm, 280

- Levinson-Durbin algorithm, 315
- Linear block codes, 601–623
  - BCH codes, 620–623
  - coset, 609
  - coset leader, 609
  - cyclic codes, 615–623
  - dual code, 604
  - error detection and correction, 612
  - generator matrix, 603
  - hard-decision decoding, 608–612
  - parity check matrix, 604
  - Reed-Solomon codes, 620–623
  - soft-decision decoding, 606–608
  - standard array, 609
  - syndrome, 610
  - systematic, 604
- Line-of-sight radio transmission (LOS), 675
- Linear predictive coding (LPC), 312, 316, 318
- Link budget analysis, 438
- Lloyd-Max conditions, 298
- LMS algorithm, 548
- Loop, Costas, 233
- LOS, 675
- Lossy data compression, 282
- Low probability of being intercepted (LPI), 743
- Lowpass representation of bandpass signals, 52
- LPC, 312, 316, 318
- LPI, 743
- Luminance signal, 12
- $M$ -ary modulation, 9
- $m$ -sequences, 748–752
- Magnetic recording, 508–515
- MAP decoding, BCJR algorithm, 642
- MAP demodulation for CPM, 725
- Matched-filter, 375
  - frequency domain interpretation, 378
  - output SNR, 378
  - properties, 376
- Maximum a posteriori (MAP) algorithm, 642
- criterion, 382
- Maximum-length shift-register sequences (MLSR), 748–752
- Maximum-likelihood (ML) criterion, 383
- sequence detector (*see* MLSD)
- Maximum ratio combining, 691
- Miller Code, 515, 517–520
- Minimum-shift keying (MSK), 708–711
- Gaussian (GMSK), 712, 714, 769
- power-spectral density, 719
- Mixers, 92
- MLSD, 521–530, 540
  - error probability, 528–530
  - for partial response signals, 525–528
  - path memory truncation, 525, 528
- MLSR sequences, 748–752
- Mobile cellular transmission, 675
- Mobile radio channels, propagation model, 681
- Mobile radio systems, 128–130
  - base station, 129
- Mobile telephone switching office (MTSO), 129
- Modems, coding for, 657
- Modified duobinary pulse, 498
- Modulation
  - $M$ -ary, 9
  - sigma-delta, 322
  - signals with memory, 508
- Modulation codes, 507, 510–525
- trellis, 515, 523–525
- Modulation index
  - conventional AM, 79
  - CPFSK, 704
  - FM, 99
- Modulators, AM, 88–92
- Monochromatic signal, 50
- Morse code, 2
- MTSO, 129
- Multicarrier modulation, 556–560
- Multidimensional signal waveforms, 360
- Multipath spread, 678
- Multiple antenna systems, 697–703
- Multiplexing, 94, 317
  - frequency-division (FDM), 94, 556
  - Orthogonal frequency-division (OFDM), 556–560
  - quadrature carrier, 95
  - time division (TDM), 318
- Mutual information, 283
- Narrowband FM, 100
- Narrowband signals (*see* bandpass signals)
- Noise
  - effect on conventional AM, 221–226
  - effect on DSB-SC, 218–220
  - effect on FM, 234–251
  - effect on SSB, 220–221
  - granular, 310
- Noise-equivalent bandwidth, 190, 231, 255
- Noise figure, 256
- Noisy channel coding
  - theorem, 579–581
- Noncoherent detection, FSK, 399
- NRZ signaling, 508, 516–518
- NRZI signaling, 508–510, 516–525
  - power-spectral density, 531–533
- NTSC, 120
- Nyquist criterion for zero ISI, 492
- Nyquist pulse shaping, 492
- Nyquist rate, 10, 48, 494
- OFDM, 556–560, 685, 690
  - based on FFT, 557–560
- Offset QPSK (OQPSK), 710
- On-off signaling, 456
- Optimum detector, 381
  - binary antipodal signaling, 385
  - for carrier-amplitude modulation, 388
  - FSK, 401
- Orthogonal signals, 352, 360
  - bound on the error probability, 592–595
- Orthogonality condition, 214
- Orthonormal basis, 342
- PAM
  - constellation, 349
  - error probability, 408–411
  - error probability with zero ISI, 500
  - optimal transmitter and receiver filters, 534–538
  - power-spectral density, 488
  - transmission through bandlimited channels, 478
- PAR, 557, 685
- Parity check matrix, for linear block codes, 604
- Parseval's relation
  - for Fourier Series, 59
  - for Fourier transform, 37
- Parseval's theorem, Fourier transform, 37
- Partial response channels, MLSD, 525, 528
- Partial response CPM, 712
- Partial response signaling, 497
  - probability of error in symbol-by-symbol detection, 504
  - symbol-by-symbol detection, 501
- Path memory truncation, 525, 528, 633
- PCM, 302
  - bandwidth, 304

- effect of transmission errors, 590–591
- nonuniform, 304
- SQNR, 303
- uniform, 302
- PDF, 147
  - conditional, 155
- Peak-frequency deviation in CPFSK, 704
- Peak-to-average power ratio (PAR), 557, 685
- Phase delay, 68
- Phase-locked loop (*see* PLL)
- Phase modulation (PM) (*see* angle modulation and FM)
- Phase of bandpass signals, 53
- Phase-shift keying (*see* PSK)
- Phase tree in CPFSK, 706
- Phase trellis in CPFSK, 706
- Planck's Constant, 189, 253
- PLL, 111, 113–115, 225–234, 388
  - decision feedback (DFPLL), 392, 397, 398
  - effect of noise, 229–231
  - linear model, 227
  - squaring loop, 231
- PM, SNR, 243
- PMF, 148
- PN sequences, 729, 748–752
- Poisson random variable, 204
- Poisson's sum formula, 63, 450
- Posterior probability, 382
- Power
  - in conventional AM, 80
  - in DSB-SC, 74–76
- Power and energy, 40–44
- Power-law modulator, 88–89
- Power-spectral density, 42
  - digitally modulated signals, 482–490
  - digitally modulated signals with memory, 530–534
  - NRZI signaling, 531–533
  - QAM, 488
  - for random processes, 177–182
- Power spectrum, 42
- Power-type signals, 41–44
- Precoding, 501, 516
- Pre-emphasis and de-emphasis filtering, 248–251
- Prefix condition, 277
- Probability
  - a posteriori, 383
  - a priori, 383
  - conditional, 146
- Probability density function (PDF), 147
  - cross-spectral density, 184
  - cyclostationary, 167, 484
  - discrete time, 161
  - ergodicity, 169
  - frequency-domain analysis, 177–186
    - Gaussian, 186–188
  - jointly wide-sense stationary, 174
  - mean, 165
  - power and energy, 171
  - power-spectral density, 177
  - sample function, 160
  - sampling theorem, 192–194
  - stationarity, 166
  - statistical description, 162
  - strictly stationary, 167
  - through linear systems, 174, 183
  - white, 188
  - wide-sense stationary (WSS), 167
- Random variables, 147
  - Bernoulli, 149
  - binomial, 149
  - CDF, 147
  - characteristic function, 154
  - continuous, 147
  - discrete, 147
  - functions of, 153, 156
  - Gaussian, 149
  - jointly Gaussian, 158
  - mean, 153
  - PDF, 147
  - Poisson, 204
  - Rayleigh, 158, 205
  - Ricean, 208
  - uniform, 149
  - variance, 154
- Rate-distortion
  - function, 285, 589
  - theorem, 287
- Rayleigh fading, 681
- Rayleigh random variable, 158, 205
- Rayleigh's relation, 44
- Rayleigh's theorem, Fourier transform, 37
- RDS, 521
- Reactance tube, 108
- Rectangular pulse, 27, 34
- Recursive systematic convolutional codes, 641
- Reed-Solomon codes, 620–623, 640, 659–661
- Reliability function, 595
- Reliable transmission, 581
- Repeaters
  - analog, 258
  - digital, 437
- Ricean fading, 681
- Ricean random variable, 208
- Probability mass function (PMF), 148
- Probability measure, 145
- Probability space, 145
- Product codes, 639
- Propagation
  - ground wave, 15–16
  - ionospheric, 674
  - line of sight (LOS), 14, 17, 675
  - sky wave, 16
- Pseudonoise sequences (PN), 729, 748–752
- PSK, 355
  - carrierless, 573
  - constellation, 356
  - differential, 395
  - error probability, 413–417
- Pulse amplitude modulation (PAM), 345
- Pulse-code modulation (*see* PCM)
- Q*-function, 151
  - bounds, 151, 206
  - table, 152
- QAM, 357
  - block diagram, 358
  - carrier-phase estimation, 397
  - carrierless, 573
  - constellation, 359
  - demodulation and detection, 396
  - error probability, 418–432
  - power-spectral density, 488
- QPSK, 355
- Quadrature amplitude modulation (*see* QAM)
- Quadrature component of bandpass signals, 52
- Quadrature filter, 52
- Quadrature phase shift keying (QPSK), 355
- Quadrature process, 195
- Quantization, 290
  - noise, 294
  - nonuniform, 297
  - scalar, 291
  - uniform, 294
  - vector, 300
- Raised cosine pulse shape, 495
  - rolloff factor, 495
- RAKE demodulation, 694, 772, 774
- Random experiment, 145
- Random processes, 159–201
  - autocorrelation function, 165
  - bandlimited, 192
  - bandpass, 194–201
  - continuous time, 161
  - cross-correlation function, 174

- Ring modulator, 91–92
- Rolloff factor, for raised cosine pulse shape waveform, 495
- Runlength-limited codes, 510–515
  - capacity, 512
- Running digital sum (RDS), 521
- Sample space, 145
- Sampling theorem, 10, 45–49
  - for random processes, 192–194
- SDM, 322
- Self-information, 270
- Sequences, 751
  - Gold, 750
  - Hadarnard, 360, 463, 771
  - $m$ , 729, 748–752
  - MLSR, 729, 748–752
  - PN, 729, 748–752
- Set partitioning principle, 649
- Shannon, C. E., 10–11, 276, 579
- Sifting property, 34
- Sigma-delta modulation (SDM), 322
- Sigma field, 145
- Signal design
  - for bandlimited channels, 490
  - for controlled ISI, 497
  - for fading multipath channels, 684
  - for zero ISI, 492
- Signal-to-noise ratio (*see* SNR)
- Signal to quantization noise ratio (*see* SQNR)
- Signals
  - bandpass, 49–57, 347–349
  - binary-coded, 367
  - biorthogonal, 353, 365
  - energy-type, 41–42
  - monochromatic, 50
  - power-type, 41–44
  - two-dimensional, 350–360
- Signum signal, 38
- Simplex signaling, 366
  - error probability, 429–430
- Sinc signal, 27, 34
- Single-sideband modulation (*see* SSB)
- Sliding correlator, 759
- Slope-overload distortion, 311
- SNR
  - bandlimited AWGN channel, 476
  - baseband, 218
  - conventional AM, 222
  - DSB, 220
  - FM, 243
  - PM, 243
  - SSB, 221
  - threshold, 244–245
- Soft-decision decoding, 606–608
- Soft output Viterbi algorithm (SOVA), 642
- Source-coding theorem, 275
- SOVA algorithm, 642
- Space-time codes, 700–703
- Spectrum
  - continuous, 31
  - discrete, 26
- Spread factor, 683
- Spread-spectrum systems, 729–766
  - direct-sequence (DS), 731–752
    - error probability for DS, 735
    - frequency-hopped (FH), 752–758
    - interference margin, 742
    - pulsed interference, 746
    - synchronization, 758–766
- SQNR
  - bounds on, 590
  - definition, 294
  - in nonuniform PCM, 338
  - in PCM, 303
- Square-law combining, 691
- Squared-error distortion, 286
- SSB, 81–85, 220–221
  - bandwidth, 82–84
  - demodulation, 84–85, 93
  - effect of noise, 220–221
  - SNR, 221
- Staggered QPSK (SQPSK), 710
- Standard array, 609
- State diagram
  - convolutional codes, 624
  - CPFSK, 707
- Stationary processes, 166
  - cyclostationary, 167, 484
  - strictly, 167
  - wide-sense (WSS), 167
- Stirling's approximation, 580
- Stochastic gradient algorithm, 548
- Stochastic processes, 159–201
- Subset decoding, 654
- Sufficient statistics, 373
- Superheterodyne receiver, 3, 115–116
  - image frequency, 116
- Switching modulator, 89–90
- Symbol-by-symbol detection in controlled ISI systems, 501
- Symbol synchronization, 442
  - for carrier-modulated signals, 451
  - early–late gate, 443
  - maximum-likelihood method, 448
  - minimum mean-square-error method, 445
  - spectral line method, 449
  - for spread-spectrum systems, 758–766
- Synchronous demodulator, 219
- Systematic linear block codes, 604
- Tau-dither loop (TDL), 763
- TCM, 646–655
  - coding gain, 654
  - decoding, 654
  - set partitioning, 649
- TDL, 763
- TDM, 318
- Television broadcasting, 120–128
- Thermal noise, 6, 12, 189, 253–256
- Threshold effect, AM, 223
  - FM, 243–244
- Threshold extension in FM, 247
- Timing recovery (*see* symbol synchronization)
- Toeplitz matrix, 315
- Total probability theorem, 146
- Transfer function of convolutional codes, 626
- Transmission losses, 257
- Trellis-coded modulation (*see* TCM)
- Trellis diagram, 515, 625
  - for convolutional codes, 625
  - for modulation codes, 515, 523–525
- Turbo codes, 640–646
  - error floor, 646
  - performance, 645–646
- Two-dimensional signals, 350–360
- Typical sequences, 274
- Underwater acoustic signal transmission, 676
- Union bound on error probability, 426
- Uniquely decodable codes, 277
- Varactor diode, 107–108
- Variance, 154
- VCC, 762
- VCO, 107, 111–114, 226–234
- Viterbi algorithm, 523–525, 554, 629–634
  - path memory truncation, 525, 528, 633
  - survivor path, 631, 632
- Voltage controlled clock (VCC), 762
- Voltage-controlled oscillator (VCO), 107, 111–114, 226–234
- VSB, 85–88, 123, 125
  - bandwidth, 86–87
  - demodulation, 94
  - filter characteristics, 86

- Walsh-Hadamard sequences, 360, 463, 771
- Waveform coding, 302
- White processes, 188
- Wide-sense stationary (WSS) random processes, 167
- Wiener filter, 11
- Wiener-Khinchin theorem, 178–193
- WSS, 167
- Yule-Walker equations, 309, 315